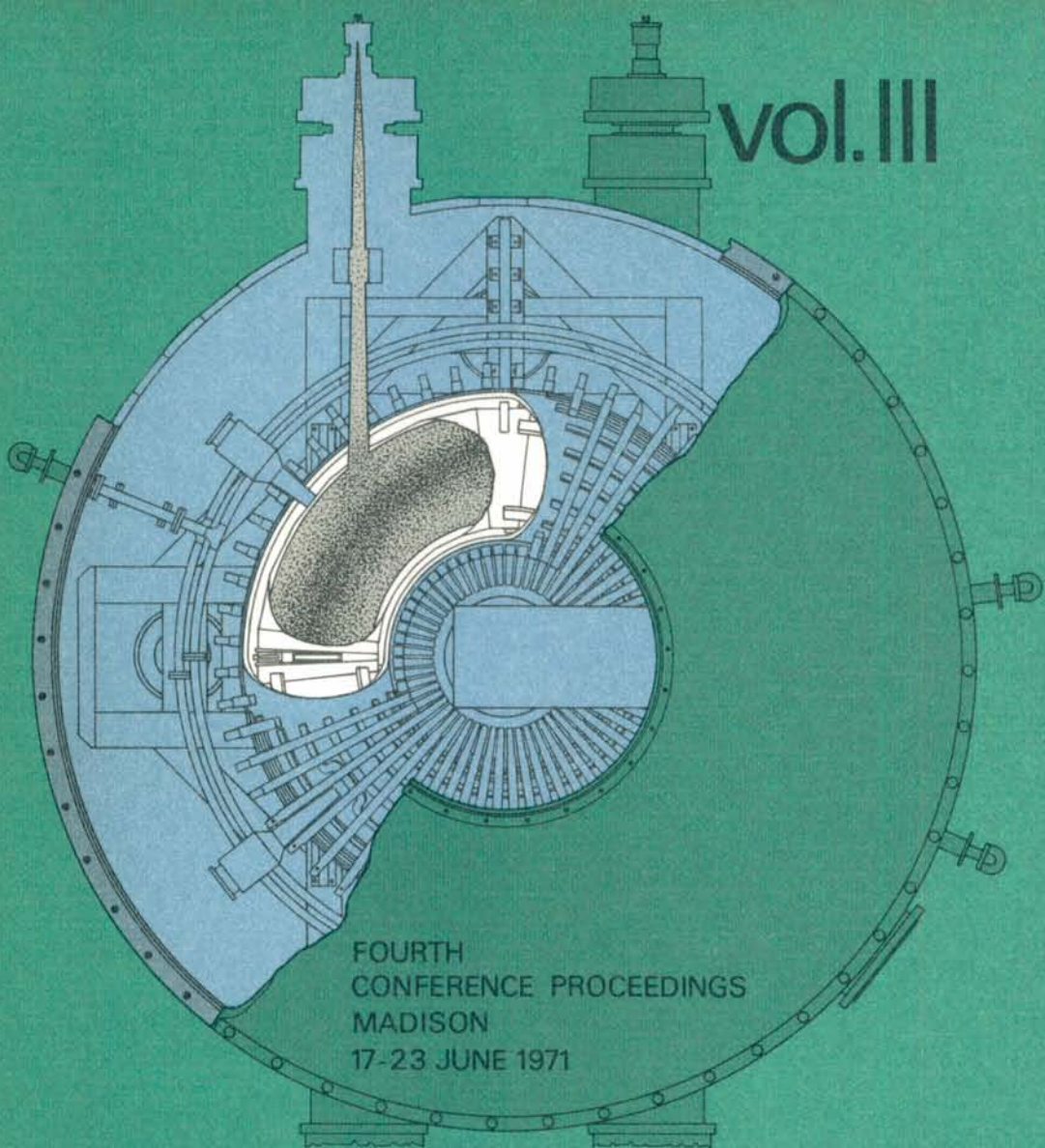


vol. III

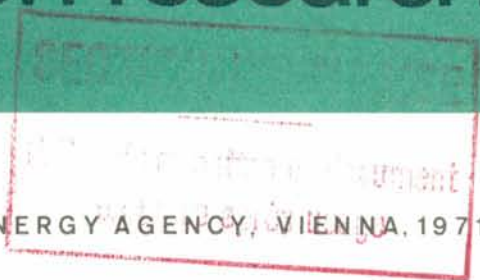


FOURTH
CONFERENCE PROCEEDINGS
MADISON
17-23 JUNE 1971

plasma physics and controlled nuclear fusion research 1971



INTERNATIONAL ATOMIC ENERGY AGENCY, VIENNA, 1971



PLASMA PHYSICS
AND CONTROLLED
NUCLEAR FUSION RESEARCH
1971

The following States are Members of the International Atomic Energy Agency:

AFGHANISTAN	GUATEMALA	PAKISTAN
ALBANIA	HAITI	PANAMA
ALGERIA	HOLY SEE	PARAGUAY
ARGENTINA	HUNGARY	PERU
AUSTRALIA	ICELAND	PHILIPPINES
AUSTRIA	INDIA	POLAND
BELGIUM	INDONESIA	PORTUGAL
BOLIVIA	IRAN	ROMANIA
BRAZIL	IRAQ	SAUDI ARABIA
BULGARIA	IRELAND	SENEGAL
BURMA	ISRAEL	SIERRA LEONE
BYELORUSSIAN SOVIET SOCIALIST REPUBLIC	ITALY	SINGAPORE
CAMEROON	IVORY COAST	SOUTH AFRICA
CANADA	JAMAICA	SPAIN
CEYLON	JAPAN	SUDAN
CHILE	JORDAN	SWEDEN
CHINA	KENYA	SWITZERLAND
COLOMBIA	KHMER REPUBLIC	SYRIAN ARAB REPUBLIC
COSTA RICA	KOREA, REPUBLIC OF	THAILAND
CUBA	KUWAIT	TUNISIA
CYPRUS	LEBANON	TURKEY
CZECHOSLOVAK SOCIALIST REPUBLIC	LIBERIA	UGANDA
DENMARK	LIBYAN ARAB REPUBLIC	UKRAINIAN SOVIET SOCIALIST REPUBLIC
DOMINICAN REPUBLIC	LIECHTENSTEIN	UNION OF SOVIET SOCIALIST REPUBLICS
ECUADOR	LUXEMBOURG	UNITED KINGDOM OF GREAT BRITAIN AND NORTHERN IRELAND
EGYPT, ARAB REPUBLIC OF	MADAGASCAR	UNITED STATES OF AMERICA
EL SALVADOR	MALAYSIA	URUGUAY
ETHIOPIA	MALI	VENEZUELA
FINLAND	MEXICO	VIET-NAM
FRANCE	MONACO	YUGOSLAVIA
GABON	MOROCCO	ZAIRE, REPUBLIC OF
GERMANY, FEDERAL REPUBLIC OF	NETHERLANDS	ZAMBIA
GHANA	NEW ZEALAND	
GREECE	NIGER	
	NIGERIA	
	NORWAY	

The Agency's Statute was approved on 23 October 1956 by the Conference on the Statute of the IAEA held at United Nations Headquarters, New York; it entered into force on 29 July 1957. The Headquarters of the Agency are situated in Vienna. Its principal objective is "to accelerate and enlarge the contribution of atomic energy to peace, health and prosperity throughout the world".

Printed by the IAEA in Austria

December 1971

PROCEEDINGS SERIES

PLASMA PHYSICS
AND CONTROLLED
NUCLEAR FUSION RESEARCH
1971

PROCEEDINGS OF THE
FOURTH INTERNATIONAL CONFERENCE ON PLASMA PHYSICS
AND CONTROLLED NUCLEAR FUSION RESEARCH
HELD BY THE
INTERNATIONAL ATOMIC ENERGY AGENCY
AT MADISON, USA, 17-23 JUNE 1971

In three volumes

VOL. III

INTERNATIONAL ATOMIC ENERGY AGENCY
VIENNA, 1971

PLASMA PHYSICS AND CONTROLLED NUCLEAR FUSION RESEARCH 1971
IAEA, VIENNA, 1971
STI/PUB/288

FOREWORD

The ultimate goal of controlled nuclear fusion research is to make a new energy source available to mankind, a source that will be virtually unlimited and that gives promise of being environmentally cleaner than the sources currently exploited. This goal has stimulated research in plasma physics over the past two decades, leading to significant advances in the understanding of matter in its most common state as well as to progress in the confinement and heating of plasma. An indication of this progress is that in several countries considerable effort is being devoted to design studies of fusion reactors and to the technological problems that will be encountered in realizing these reactors.

This range of research, from plasma physics to fusion reactor engineering, is shown in the present three-volume publication of the Proceedings of the Fourth Conference on Plasma Physics and Controlled Nuclear Fusion Research. The Conference was sponsored by the International Atomic Energy Agency and was held in Madison, Wisconsin, USA from 17 to 23 June 1971. The enthusiastic co-operation of the University of Wisconsin and of the United States Atomic Energy Commission in the organization of the Conference is gratefully acknowledged. The Conference was attended by over 500 scientists from 24 countries and 3 international organizations, and 143 papers were presented. These papers are published here in the original language; English translations of the Russian papers will be published in a Special Supplement to the journal Nuclear Fusion.

The series of conferences on Plasma Physics and Controlled Nuclear Fusion Research has become a major international forum for the presentation and discussion of results in this important and challenging field. In addition to sponsoring these conferences, the International Atomic Energy Agency supports controlled nuclear fusion research by publishing the journal Nuclear Fusion, and has recently established an International Fusion Research Council. The primary aim of this Council, which had its first meeting in conjunction with the Madison Conference, is to promote international co-operation in controlled nuclear fusion research and its application. By these activities the International Atomic Energy Agency hopes to contribute significantly to the attainment of controlled fusion power.

EDITORIAL NOTE

The papers and discussions incorporated in the proceedings published by the International Atomic Energy Agency are edited by the Agency's editorial staff to the extent considered necessary for the reader's assistance. The views expressed and the general style adopted remain, however, the responsibility of the named authors or participants.

For the sake of speed of publication the present Proceedings have been printed by composition typing and photo-offset lithography. Within the limitations imposed by this method, every effort has been made to maintain a high editorial standard; in particular, the units and symbols employed are to the fullest practicable extent those standardized or recommended by the competent international scientific bodies.

The affiliations of authors are those given at the time of nomination.

The use in these Proceedings of particular designations of countries or territories does not imply any judgement by the Agency as to the legal status of such countries or territories, of their authorities and institutions or of the delimitation of their boundaries.

The mention of specific companies or of their products or brand-names does not imply any endorsement or recommendation on the part of the International Atomic Energy Agency.

CONTENTS OF VOL. III

CLOSED CONFINEMENT SYSTEMS (Session H)

Поведение плазмы в стеллараторе при больших длинах свободного пробега электронов (IAEA-CN-28/H-1)	3
В. Н. Бочаров, В. И. Волосов, А. В. Комин, В. М. Панасюк и Ю. Н. Юдин	
Исследование удержания плазмы в стеллараторе TOP-1 (IAEA-CN-28/H-2)	21
Д. К. Акулина, Э. Д. Андрюхина, Ю. И. Нечаев, О. И. Федянин и Ю. В. Хольнов	
Particle-confinement minima in the Wendelstein II-a-Stellarator (IAEA-CN-28/H-3)	37
G. Grieger, W. Ohlendorf, H. D. Pacher, H. Wobig and G. H. Wolf	
Discussion	48
Экспериментальное исследование квазистационарных продольных потоков ионов в стеллараторе L-1 (IAEA-CN-28/H-4)	49
М. С. Бережецкий, С. Е. Гребенщиков, И. А. Косый, И. С. Сбитникова и И. С. Шпигель	
Удержание плазмы в двухзаходном стеллараторе при резонансных значениях угла вращательного преобразования (IAEA-CN-28/H-5)	63
М. А. Ивановский, С. Н. Попов, А. П. Попрядухин и М. С. Рабинович	
Discussion	77
Plasma containment in the Proto-Cleo stellarator (IAEA-CN-28/H-6)	79
R. A. E. Bolton, J. Hugill, D. J. Lees, W. Millar and P. Reynolds	
Dependence of plasma confinement on magnetic configuration and plasma properties in the J. I. P. P. stellarator (IAEA-CN-28/H-7)	93
K. Miyamoto, A. Mohri, N. Inoue, M. Fujiwara, K. Yatsu, Y. Terashima and R. Itatani	
Discussion	107
Plasma confinement experiment in the Heliotron-D machine (IAEA-CN-28/H-8)	109
K. Uo, A. Iiyoshi, Sh. Yoshioka, T. Ishida, Sh. Konoshima and M. Sato	
Электропроводность и токовый нагрев плазмы в сильном магнитном поле (IAEA-CN-28/H-9)	119
П. Я. Бурченко, Е. Д. Волков, В. А. Рудаков, В. Л. Сизоненко и К. Н. Степанов	
Discussion	130

Экспериментальные исследования магнитных поверхностей и удержания плазмы в трехзаходном стеллараторе-торсатроне "САТУРН-1" (IAEA-CN-28/H-10).....	131
В. С. Войценья, А. В. Георгиевский, В. Е. Зисер, Д. П. Погожев, А. И. Скибенко, С. И. Солодовченко, В. А. Супруненко, В. Т. Толлок, И. П. Фомин и Л. А. Душин	
Поведение высокотемпературной плазмы при токовом нагреве в стеллараторе с большим широм "УРАГАН" (IAEA-CN-28/H-11).....	151
А. Г. Дикий, Дж. Г. Горман, В. М. Залкинд, Г. В. Зеленин, В. Д. Коцубанов, А. П. Литвинов, В. Г. Коновалов, О. С. Павличенко, Н. Ф. Перепелкин, Н. П. Пономаренко, В. А. Супруненко, В. Т. Толлок и В. М. Тонкопряд	
Discussion to papers IAEA-CN-28/H-10, H-11	161
Plasma shift in fast stellarators with finite conductivity (IAEA-CN-28/H-12)	163
D. Pfirsch and K. Schlüter	
Discussion	165

THETA PINCHES; SHOCK WAVES (Session J)

Confinement of a toroidal theta-pinch plasma in a periodic caulked-cusp field (IAEA-CN-28/J-1)	169
T. Uchida, K. Sato, A. Mohri and R. Akiyama	
Discussion	178
Toroidal high- β experiments in compact axisymmetric configurations (IAEA-CN-28/J-2)	179
H. J. Belitz, L. Janicke, P. Noll, U. Plantikow, F. Sand, J. Schlüter, F. Waelbroeck and G. Waidmann	
High-beta ($\ell = 1$)-stellarator experiments (IAEA-CN-28/J-3)	189
E. Fünfer, M. Kaufmann, W. Lotz and J. Neuhauser	
Discussion	199
Theta-pinch experiments with helical equilibrium fields in a 5-meter toroidal sector and in a 3-meter linear device (IAEA-CN-28/J-4)	201
S. C. Burnett, W. R. Ellis, C. F. Hammer, C. R. Harder, H. W. Harris, F. C. Jahoda, W. E. Quinn, A. S. Rawcliffe, F. L. Ribe, G. A. Sawyer, R. E. Siemon, K. S. Thomas and E. L. Zimmermann	
Discussion	214
Survey of Scyllac theory (IAEA-CN-28/J-5)	215
J. P. Freidberg	
Toroidal high- β equilibria (IAEA-CN-28/J-6)	223
H. Weitzner	
Plasma containment in closed line systems (IAEA-CN-28/J-7)	229
H. Grad	

Plasma heating by strong shock waves (IAEA-CN-28/J-8)	241
Y.G. Chen, C.K. Chu, R.A. Gross, E. Halmoy, P. Moriette and S. Schneider	
Experimental study of collisionless shock waves (IAEA-CN-28/J-9)	251
J.W.M. Paul, C.C. Daughney, L.S. Holmes, P.T. Rumsby, A.D. Craig, E.L. Murray, D.D.R. Summers and J. Beaulieu	
Experimental study of collective dissipation in shock waves for a wide range of plasma parameters (IAEA-CN-28/J-10)	265
M. Keilhacker, M. Kornherr, H. Niedermeyer, K.-H. Steuer and R. Chodura	
Shock waves and turbulent heating in low-density plasmas (IAEA-CN-28/J-11)	277
P. Bogen, K.J. Dietz, K.H. Dippel, E. Hintz, K. Höthker, F. Siemsen and G. Zeyer	
Ion heating in a high-voltage theta pinch (IAEA-CN-28/J-12)	289
W.D. Davis, A.W. DeSilva, W.F. Dove, H.R. Griem, N.A. Krall and P.C. Liewer	
Conditions and mechanism of theta-pinch plasma heating (IAEA-CN-28/J-13)	303
S. Kiyama and K. Ogawa	
Discussion to papers IAEA-CN-28/J-8, J-9, J-10, J-11, J-12, J-13	311

REACTOR SYSTEMS (Session K)

Experimental and computational investigations of the direct conversion of plasma energy to electricity (IAEA-CN-28/K-1) ...	315
R.W. Moir, W. L. Barr, R.P. Freis and R.F. Post	
Engineering and economic aspects of mirror machine reactors with direct conversion (IAEA-CN-28/K-2)	329
R.W. Werner, G.A. Carlson, J.D. Lee, R.W. Moir, R.F. Post and C.E. Taylor	
Discussion to papers IAEA-CN-28/K-1, K-2	351
Efficient re-circulation of power in mirror reactors (IAEA-CN-28/K-3)	353
J.G. Cordey, F.B. Marcus, D.R. Sweetman and C.J.H. Watson	
Discussion	372
Economic feasibility of stellarator and tokamak fusion reactors (IAEA-CN-28/K-4)	375
A. Gibson, R. Hancox and R.J. Bickerton	
Fast neutral injection for plasma heating and reactor start-up (IAEA-CN-28/K-5)	393
D.R. Sweetman, A.C. Riviere, H.C. Cole, E. Thompson, D.P. Hammond, J. Hugill and G.M. McCracken	
Discussion to papers IAEA-CN-28/K-4, K-5	409

Влияние реакций синтеза на работу термоядерных установок (IAEA-CN-28/K-7)	411
В. С. Беликов, Я. И. Колесниченко и В. Н. Ораевский	
Thermal instability and control of fusion reactor (IAEA-CN-28/K-8)	423
M. Ohta, H. Yamato and S. Mori	
Discussion	432
Engineering design studies on the superconducting magnet system of a Tokamak fusion reactor (IAEA-CN-28/K-10)	433
M.S. Lubell, W.F. Gauster, K.R. Efferson, A.P. Fraas, H.M. Long, J.N. Luton, C.E. Parker, D. Steiner and W.C.T. Stoddart	
Discussion	444
Emergency cooling and radioactive-waste-disposal requirements for fusion reactors (IAEA-CN-28/K-11)	447
D. Steiner	
Neutronic and thermal design aspects of thermonuclear fusion reactor blankets (IAEA-CN-28/K-12)	457
H. Borgwaldt, W.H. Köhler and K.E. Schroeter	
Blanket cooling concepts and heat conversion cycles for controlled thermonuclear reactors (IAEA-CN-28/K-13)	469
S. Förster and Th. Bohn	
Discussion to papers IAEA-CN-28/K-11, K-12, K-13	487

HIGH-FREQUENCY HEATING (Session L)

Neoclassical theory of magnetic pumping in toroidal geometry (IAEA-CN-28/L-1)	491
E. Canobbio	
Nouvelle méthode de pompage magnétique pour le chauffage des plasmas (IAEA-CN-28/L-2)	505
F. Koechlin et A. Samain	
Cylindrical plasma sources with densities high above critical density excited by an RF-helix with and without magnetic field (IAEA-CN-28/L-3)	513
A.E. Aubert, A.M. Messiaen and P.E. Vandenplas	
Discussion	524
Исследования трансформации и поглощения высокочастотных волн в плазме, направленные на разработку методов нагрева плазмы (IAEA-CN-28/L-4)	525
В. И. Архипенко, А. Б. Березин, В. Н. Будников, В. Е. Голант, К. М. Новик, А. А. Обухов, А. Д. Пилия, В. И. Федоров и К. Г. Шаховец	
Исследование плазмы на установке "Туман-2" (IAEA-CN-28/L-5)	543
А. И. Анисимов, Н. И. Виноградов, В. Е. Голант, В. А. Ипатов, М. Г. Каганский, С. Г. Калмыков, А. И. Кисляков, В. А. Овсянников, Л. П. Пахомов, К. А. Подушникова, С. С. Тюльпанов и К. Г. Шаховец	

Экспериментальное исследование нагрева плазмы на частоте, близкой к нижнему гибричному резонансу (IAEA-CN-28/L-6).....	559
В. М. Глаголев, Н. А. Кривов и Ю. В. Скосырев	
Discussion to papers IAEA-CN-28/L-4, L-5, L-6	571
Исследование высокочастотного нагрева плазмы (IAEA-CN-28/L-7).....	573
Л. И. Григорьева, А. В. Лонгинов, А. И. Пятак, В. Л. Сизоненко, Б. И. Смердов, К. Н. Стеланов и В. В. Чечкин	
Эксперименты по высокочастотному нагреву плазмы в тороидальной ловушке (IAEA-CN-28/L-8).....	597
С. С. Овчинников, С. С. Калининченко, П. И. Курилко, О. М. Швец и В. Т. Толоч	

SUMMARY OF THE CONFERENCE (Session M)

Review of theory	613
T. K. Fowler	
Review of experimental work	619
R. J. Bickerton	
Review of reactor systems	627
H. K. For sen	
Chairmen of Sessions and Secretariat of the Conference	631
List of Participants	633
Author Index	661
Transliteration Index	669

CLOSED CONFINEMENT SYSTEMS
(Session H)

Chairman: G. von GIERKE

Papers H-1 and H-2 were presented by
V. I. VOLOSOV as Rapporteur

Papers H-10 and H-11 were presented by
V. S. VOITSENYA as Rapporteur

ПОВЕДЕНИЕ ПЛАЗМЫ В СТЕЛЛАРАТОРЕ ПРИ БОЛЬШИХ ДЛИНАХ СВОБОДНОГО ПРОБЕГА ЭЛЕКТРОНОВ

В.Н.БОЧАРОВ, В.И.ВОЛОСОВ, А.В.КОМИН,
В.М.ПАНАСЮК, Ю.Н.ЮДИН
Институт ядерной физики Сибирского отделения
Академии наук СССР, Новосибирск,
Союз Советских Социалистических Республик

Abstract—Аннотация

BEHAVIOUR OF A PLASMA IN A STELLARATOR FOR THE CASE OF LARGE ELECTRON FREE-PATH LENGTHS.

A study has been carried out of the characteristics of plasma behaviour in a stellarator under conditions where the electron free-path length is larger than or of the order of the longitudinal wavelength of drift oscillations. A study has been made of the relationship between the plasma decay process (decay time, density profile, etc.) and the main parameters of the experiment (magnetic field, ratio of the currents in the helical and toroidal windings, collision frequency of the plasma radius, electron temperature, etc.). An investigation has likewise been made of the structure of the oscillations (wavelength, frequency and correlative dimensions) accompanying plasma decay; measurements have also been made of the radial plasma flows caused by these oscillations. The characteristic oscillation frequencies of the potentials, electric fields and density of the plasma are close to the drift frequency, and their dependence on the magnetic field, electron temperature and other parameters coincides with drift theory predictions. Experiments have shown that plasma decay is determined by drift oscillations, while the plasma decay time increases with an increase in the size of the magnetic field, the plasma dimensions and the parameter ϵ . At a quite small value of the magnetic field a quadratic relationship is observed between the plasma decay time and the field strength; as the field increases the relationship becomes linear, the absolute decay time being 5 to 10 times greater than the Bohm time. The results obtained may be explained quantitatively if an analysis is made of the radial plasma flows caused by azimuthal drift electric fields. This process gives the characteristic time for plasma losses $\tau_p \approx \gamma^{-1}(a/x_0)$. Here γ is the increment in the drift-collisionless oscillations, a the plasma dimensions and x_0 the amplitude of the radial oscillations of the plasma. The expression for τ_p coincides with the empirical formulae for that value obtained experimentally.

ПОВЕДЕНИЕ ПЛАЗМЫ В СТЕЛЛАРАТОРЕ ПРИ БОЛЬШИХ ДЛИНАХ СВОБОДНОГО ПРОБЕГА ЭЛЕКТРОНОВ.

Проводилось изучение особенностей поведения плазмы в стеллараторе в режимах, когда свободный пробег электронов больше или порядка продольной длины дрейфовых колебаний. Изучалась зависимость процесса распада плазмы (время распада, профиль плотности и т.д.) от основных параметров эксперимента (магнитного поля, отношения токов в винтовой и тороидальной обмотках, частоты столкновений радиуса плазмы, температуры электронов и др.). Одновременно исследовалась структура колебаний (длины волны, частоты, корреляционные размеры), сопровождающих распад плазмы, а также проводились измерения радиальных потоков плазмы, вызванных этими колебаниями. Характерные частоты колебаний потенциалов, электрических полей и плотности плазмы лежат близко к дрейфовым, а их зависимость от магнитного поля, температуры электронов и других параметров совпадает с предсказаниями дрейфовой теории. Эксперименты показали, что распад плазмы определяется дрейфовыми колебаниями, время распада плазмы возрастает с увеличением магнитного поля, размеров плазмы и параметра ϵ . При достаточно малом значении магнитного поля наблюдается квадратичная зависимость времени распада плазмы от величины поля; по мере увеличения поля она переходит в линейную, при этом абсолютное время распада в 5-10 раз больше бовмского времени. Полученные результаты можно качественно объяснить, если провести анализ радиальных потоков плазмы, вызванных азимутальными дрейфовыми электрическими полями. Этот процесс дает характерное время потерь плазмы $\tau_p \approx \gamma^{-1}(a/x_0)$. Здесь γ — инкремент дрейфово-бесстолкновительных колебаний, a — размер плазмы, x_0 — амплитуда радиальных колебаний плазмы. Выражение для τ_p совпадает с эмпирическими формулами для τ_p , полученными экспериментально.

Продолжалось изучение плазмы на стеллараторе Института ядерной физики Сибирского отделения Академии наук СССР. Подробное описание экспериментальной установки было приведено в работах [1-3]. Основные параметры стелларатора: большой радиус тора — 50 см, малый радиус — 5 см, магнитное поле H — до 3-3,5 кэ, трехзаходная винтовая обмотка, ϵ^2 — до 0,2. Плазма создавалась методом стохастического нагрева [4-5], как и в опубликованных ранее экспериментах.

В отличие от прежних экспериментов, проводилось более тщательное измерение температуры электронов в процессе всего распада, что позволило уточнить зависимость времени распада от различных параметров. С помощью корреляционных методов изучались пространственные характеристики колебаний и измерены радиальные потоки плазмы, обусловленные колебаниями.

МАКРОСКОПИЧЕСКИЕ ХАРАКТЕРИСТИКИ РАСПАДА ПЛАЗМЫ

Изучалась зависимость скорости распада плазмы от основных параметров эксперимента: магнитного поля H , отношения токов в винтовой и тороидальной обмотках стелларатора (параметр ϵ), температуры электронов T_e , давления нейтрального газа p .

Основные эксперименты были выполнены на аргоне; для сравнения некоторые зависимости были измерены также на He и Xe. Чистота использованных газов была достаточно высокой, концентрация примесей молекулярных газов не превышала 10^{-2} – 10^{-3} %. Давление нейтрального газа в экспериментах менялось от $5 \cdot 10^{-6}$ до $5 \cdot 10^{-3}$ тор, при давлении остаточного газа 2 – $3 \cdot 10^{-7}$ тор. Перед измерениями поверхность камеры подвергалась тренировке разрядом в рабочем газе.

Плотность плазмы определялась с помощью открытого СВЧ-резонатора ($f = 1830$ МГц); температура электронов, потенциалы и локальная плотность плазмы измерялись лэнгмювскими зондами, установленными, как и резонатор, на прямолинейных промежутках камеры. Максимальная плотность плазмы в разряде достигала $1,5 \cdot 10^{10}$ см $^{-3}$, в процессе распада измерения велись до плотности $\sim 2 \cdot 10^6$ см $^{-3}$. Для измерения температуры электронов использовался один из вариантов зондового метода [6], который позволял быстро, без дополнительной обработки, определять T_e в любой точке вдоль распада. Размеры зонда: диаметр — 0,035 мм, длина — 5–7 мм; при этом практически всегда ларморовский радиус электронов был больше радиуса зонда (см. [7]). Остывание плазмы в процессе распада определялось, в основном, потерями энергии электронов из "хвоста" максвелловского распределения на возбуждение нейтральных атомов. На рис. 1 приведены типичные зависимости температуры электронов и плотности плазмы от времени.

Радиальные профили температуры T_e и плотности плазмы n (см. рис. 2) несколько меняют свою форму в начальной стадии распада. Длительность этого переходного процесса на Ar была обычно $< 0,5$ мсек; измерение времени распада плазмы проводилось лишь после установления профиля плотности.

При увеличении давления нейтрального газа и величины магнитного поля наблюдалось некоторое уплощение вершины радиального профиля плотности и, соответственно, уменьшение градиентного размера. Сле-

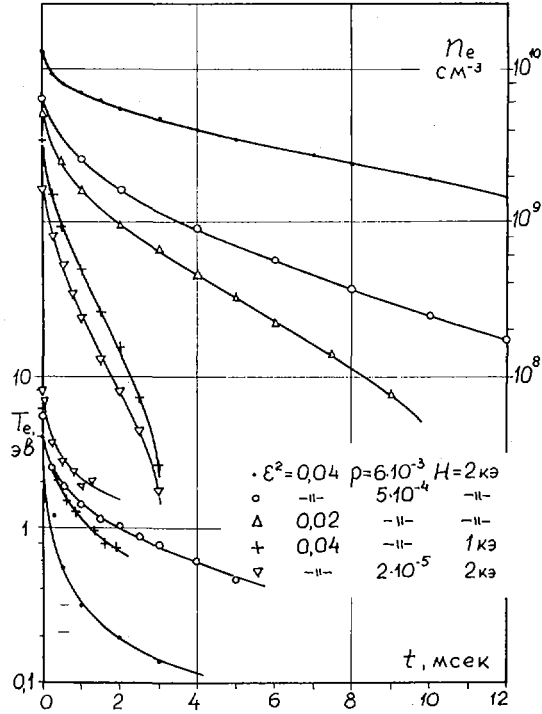


Рис. 1. Типичные кривые зависимости плотности и температуры электронов от времени для Ar.

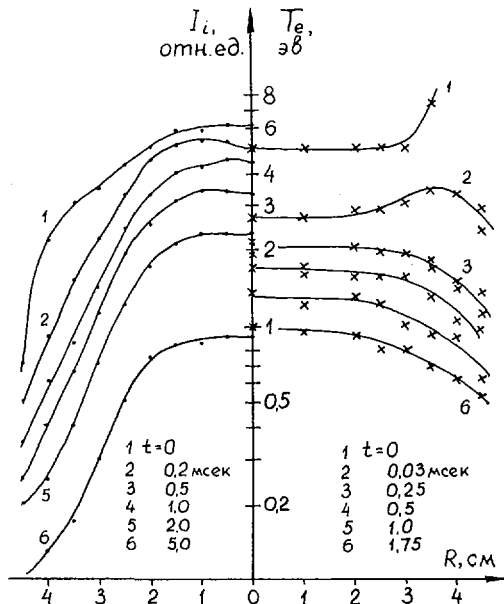


Рис. 2. Радиальные профили плотности (слева) и температуры электронов (справа) в различные моменты времени от начала распада: $H = 2 \text{кэ}$, $\epsilon^2 = 0,04$, $P = 4,0 \cdot 10^{-4}$ тор (Ar).

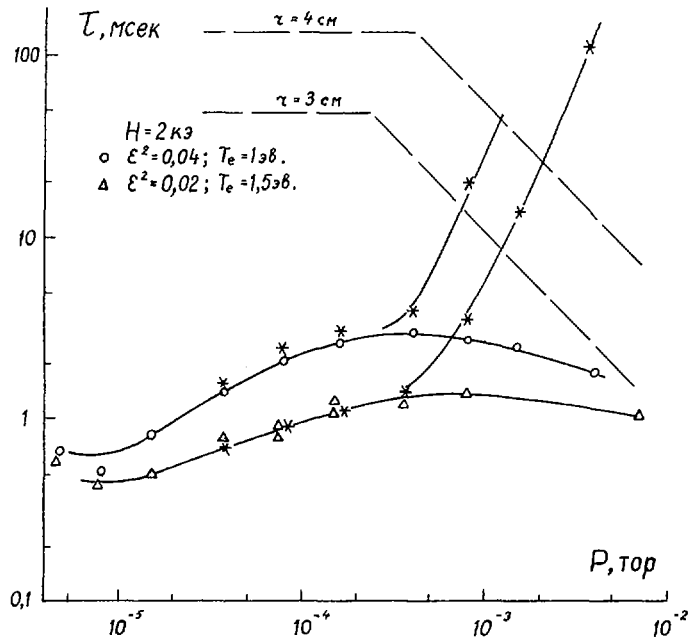


Рис.3. Зависимость времени распада плазмы τ_p от давления нейтрального газа (Ar). Значком * обозначены точки, полученные из корреляционных измерений; - - - расчетные кривые для классической диффузии.

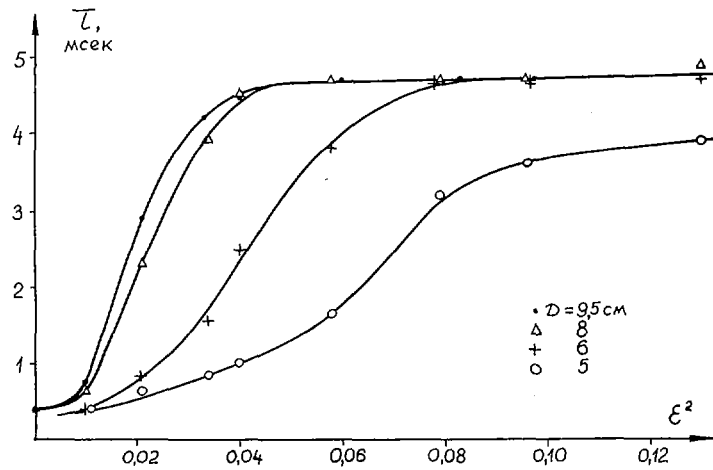


Рис.4. Зависимость $\tau_p(\varepsilon^2)$ для разных размеров диафрагмы: $H = 2 \text{ кэ}$, $P = 4,0 \cdot 10^{-4} \text{ тор (Ar)}$, $T_e = 0,5 \text{ эВ}$.

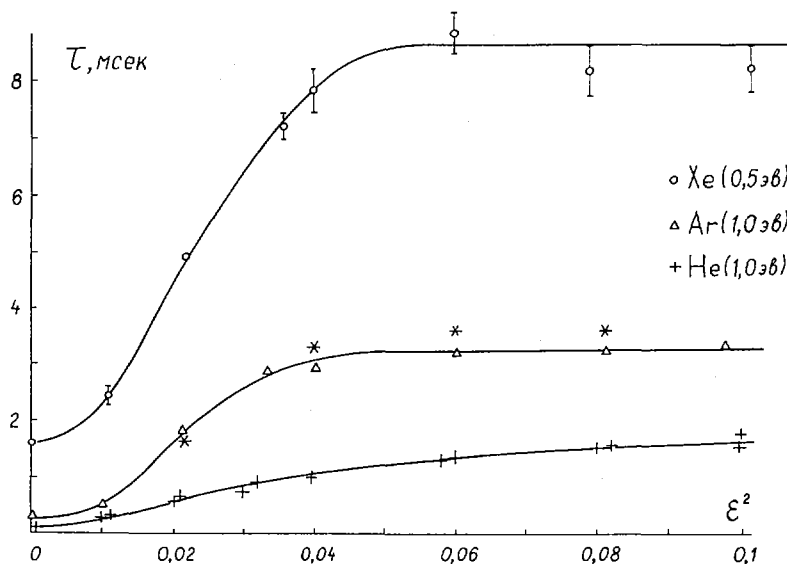


Рис. 5. Зависимость $\tau_p(\epsilon^2)$ для разных газов; $H = 2$ кэ, $P = 4,0 \cdot 10^{-4}$ тор, $T_e = 1$ эВ. Значком * обозначены точки, полученные из корреляционных измерений для Ar.

дует отметить также, что при увеличении ϵ^2 распределение плотности сужается; это согласуется с представлениями о том, что при достаточных больших ϵ^2 сепаратриса становится меньше радиуса камеры.

Эксперименты показали, что характер зависимости времени распада плазмы τ_p от параметров остается качественно подобным при различных значениях температуры электронов. Однако для определенности, а также для того, чтобы иметь возможность сравнивать абсолютные величины τ_p в разных режимах и для разных газов, измерения проводились, в большинстве случаев, при температуре электронов 1 эВ. Величина τ_p определялась по наклону кривой распада плотности $n(t)$ при этой температуре.

На рис. 3-8 приведены зависимости времени τ_p от параметров p , H , ϵ^2 .

Зависимость $\tau_p(p)$ (рис. 3) отличается от ранее опубликованной [1] лишь менее крутым увеличением времени удержания с ростом давления p (кривые в [1] были получены без контроля температуры).

Зависимость $\tau_p(\epsilon^2)$ также мало отличалась от ранее опубликованной. В данных экспериментах дополнительно изучалась зависимость $\tau_p(\epsilon^2)$ при различных размерах диафрагмы, установленной в одном из прямолинейных промежутков стелларатора. Эти измерения подтверждают высказанное в [1] предположение, что появление излома на кривых $\tau_p(\epsilon^2)$ при достаточно больших значениях параметра ϵ^2 связано с тем, что сепаратриса вписывается внутрь вакуумной камеры. Из этого эксперимента также следует, что величина $r_d^2 \epsilon_d^2 \approx \text{Const}$, где r_d — радиус диафрагмы, а ϵ_d — значение ϵ в точке перегиба кривой $\tau_p(\epsilon^2)$ при данном размере диафрагмы. Это согласуется с теоретическими представлениями о том, что на последней неразрушенной магнитной поверхности величина

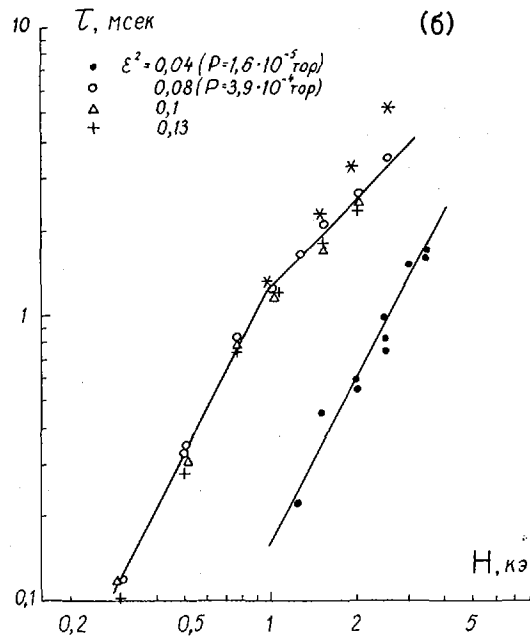
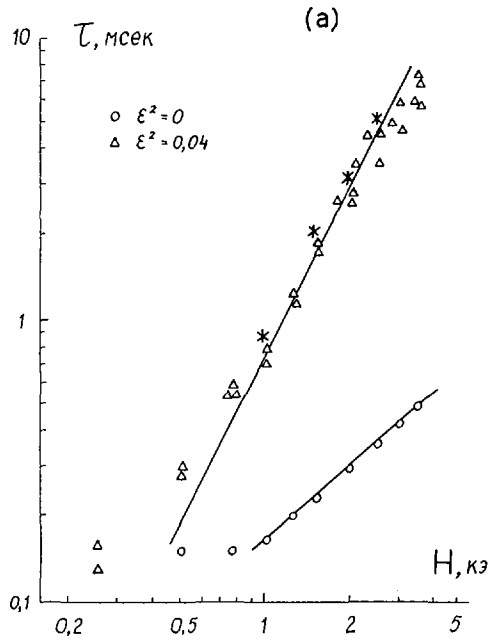


Рис. 6(а и б). Зависимость $\tau_p(H)$ для Ar: $T_c = 1$ эВ.
 Значком * обозначены точки, полученные из корреляционных измерений.

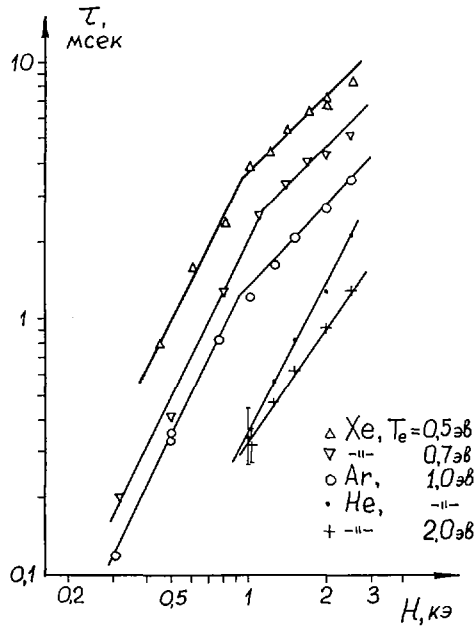


Рис. 7. Зависимость $\tau_p(H)$ для разных газов: $\epsilon^2 = 0,08$, $P = 4,010^{-4}$ тор.

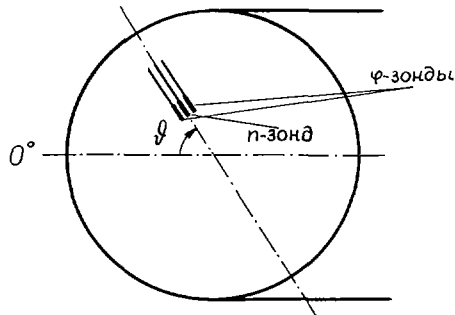


Рис. 8. Схема расположения nE-зондов в камере.

$\epsilon^2 r^2 \approx \text{Const}$ [8]. На рис. 5 приведены для сравнения зависимости $\tau_p(\epsilon^2)$ для различных газов. Качественный ход кривых подобен, хотя при больших ϵ^2 их поведение несколько отличается.

Зависимость $\tau_p(H)$ при значениях $\epsilon^2 = 0,01 \div 0,04$ и магнитных полях до 3 кэ близка к квадратичной (рис. 6 а). Для $\epsilon^2 = 0,08$ и выше и для магнитного поля более 1 кэ наблюдается линейная зависимость τ_p от магнитного поля (рис. 6 б). По-видимому, переход к линейному закону намечается также на графиках для $\epsilon^2 = 0,04$ при $H > 3$ кэ.

Кривые $\tau_p(H)$ для Хе при $\epsilon^2 = 0,04$ и $0,08$ имеют те же особенности (рис. 7). Для Не ход зависимости $\tau_p(H)$ несколько отличается; при $\epsilon^2 = 0,08$ не наблюдалось линейного участка на кривой $\tau_p(H)$. Кроме того, наклон кривых несколько зависел от электронной температуры.

Время распада плазмы при $\epsilon^2 = 0$ (рис. 6а) совпадает, по порядку величины, с бомовским временем.

В экспериментах не проводилось детального исследования зависимости времени распада от массы иона, однако измерения, проведенные при $T_e = 1$ эВ на Не, Аг и Хе при давлении $4 \cdot 10^{-4}$ тор, $H = 2$ кэ, $\epsilon^2 = 0,04$, позволяют сравнить τ_p для этих ионов. Отношение времен равно 4:3:1; соответственно $m_{\text{Хе}}^{1/2} : m_{\text{Аг}}^{1/2} : m_{\text{Не}}^{1/2} = 5,7:3,2:1$.

Сравнение кривых распада плотности и кривых остывания плазмы показало, что $\tau_p \sim T_e^{-q}$, где $2/3 \leq q \leq 3/2$. Величина зависит от условий эксперимента и несколько меняется в процессе распада. Интересно отметить, что $q = 3/2$ в случае, когда τ_p находится в окрестности максимума на кривой $\tau_p(p)$.

Зависимость времени распада от радиального размера плазмы (a) в стеллараторе исследовалась в двух режимах. В случае, когда размер сепаратрисы меньше размеров камеры, размер плазмы можно изменять, варьируя ϵ^2 . Зависимость $\tau_p(a)$, в этом случае, имеет вид $\tau_p \sim \epsilon^2 a^{2+q}$ (см. рис. 4,5). В другом случае, когда размер сепаратрисы больше размера камеры, зависимость $\tau_p(a)$ изучалась при изменении размеров диафрагмы.

Величина τ_p убывала с уменьшением a , однако сильный разброс экспериментальных точек не позволил определить зависимость $\tau_p(a)$ достаточно точно. Приблизительно $\tau_p(a) \sim a^S$, где $1 < S < 3$. Предполагается, что разброс точек связан с неоднородностью шнура плазмы вдоль большого азимута и наличием неконтролируемых процессов в плазме, находящейся в "тени" диафрагмы.

Таким образом, время распада плазмы можно представить в виде эмпирической зависимости:

$$\tau_p \sim \epsilon^2 H a^S T_e^{-q} F(p) \quad (1)$$

в сильном магнитном поле и

$$\tau_p \sim \epsilon^2 H^2 a^S T_e^{-q} F(p) \quad (2)$$

при относительно малых магнитных полях. Здесь $F(p)$ — функция давления нейтрального газа, слабо зависящая от p (см. рис. 3), $2/3 \leq q \leq 3/2$; $1 < S < 3$.

КОРРЕЛЯЦИОННЫЕ ИЗМЕРЕНИЯ

Коэффициент корреляции между двумя сигналами в наших экспериментах определялся с помощью метода диаграмм рассеяния [9-12]. Для получения диаграммы рассеяния излучавшиеся сигналы через усилители подавались на пластины осциллографа. Если время наблюдения много больше, чем характерный период изучаемых колебательных процессов, то на экране осциллографа наблюдается яркостное изображение, которое

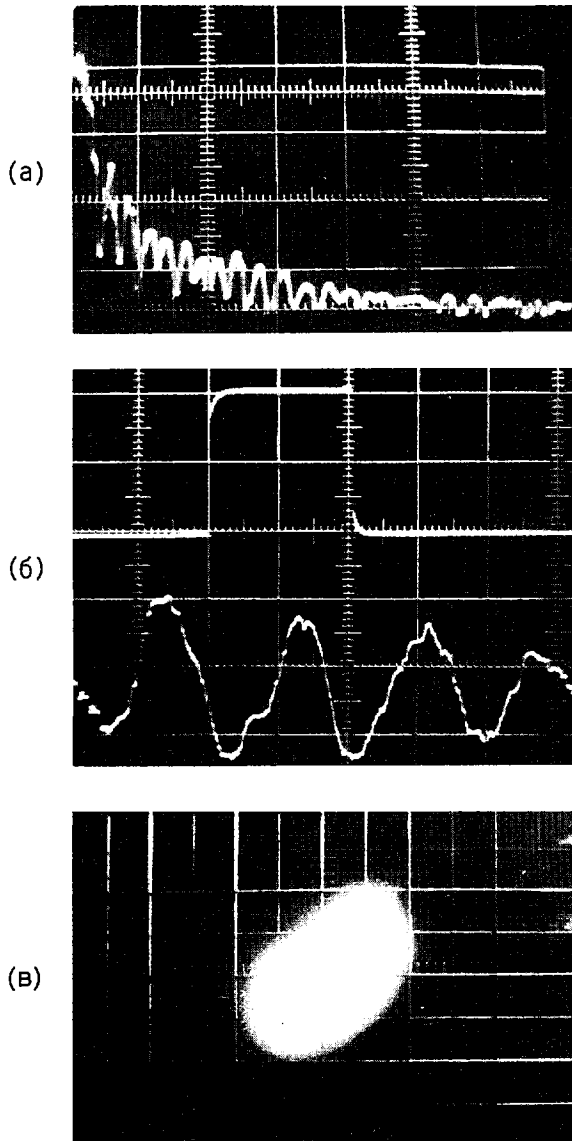


Рис.9. Характерный вид сигналов ионного тока (а), азимутального электрического поля (б) — нижний луч и диаграмма рассеяния (в) для сигналов (а) и (б). На верхнем луче (б) — импульс подсветки. Скорость развертки: (а) — 0,5 мсек/см; (б) — 0,1 мсек/см; чувствительность — 0,2 В/см; $l = 6$ мм; $H = 1,0$ кэ, $P = 4,0 \cdot 10^{-4}$ тор (Ar), $\epsilon^2 = 0,04$.

и является диаграммой рассеяния двух сигналов, причем линии равной яркости являются эквивероятностными кривыми. Следует заметить, что здесь необходимо использовать экран с большим временем послесвечения (много больше периода колебаний), либо фотографировать осциллограмму с достаточно длительной экспозицией.

В наших экспериментах эквивероятностные кривые, как правило, имели форму, близкую к эллипсу. В этом случае коэффициент корреляции определяется выражением:

$$R = \frac{1 - b^2/a^2}{(1 + b^2/a^2) \sin 2\psi} \quad (3)$$

где b и a — малая и большая полуоси эллипса, ψ — угол наклона большой оси эллипса к одной из координатных осей.

Особенность изучающихся процессов состояла в относительно быстром изменении параметров плазмы (T_e , n); в ряде случаев характерный период колебаний был соизмерим со временем распада плазмы τ_p . Измерения проводились на отрезках времени $\sim 0,2 - 0,4$ мсек, длительность которых была меньше времени распада (см. рис. 9). Для сравнения укажем, что время распада плазмы было $\sim 0,5-5,0$ мсек, период колебаний $\sim 0,05-0,5$ мсек, частота повторения импульсов, создающих плазму — 50-10 Гц. Для построения диаграмм рассеяния использовалась серия сигналов ($10^2 - 10^3$) из ряда последовательных распадов плазмы.

Измерения радиальных потоков плазмы, обусловленных колебаниями, велось с помощью "тройных" ленгмюровских зондов (nE-зондов). Схема расположения nE-зонда в камере показана на рис. 8. Крайние зонды использовались для измерения плавающих потенциалов (φ), а средний — для измерения относительной плотности плазмы по ионному току насыщения. При условии $l \ll \lambda_\varphi$ электрическое поле E_φ равно разности сигналов с потенциальных зондов ($\Delta\varphi$), деленной на расстояние между ними l . Все три зонда имели одинаковые размеры: диаметр — 0,1 мм, длина — 4 мм.

На рис. 9 представлены характерный вид сигналов ионного тока и $\Delta\varphi$, а также диаграмма рассеяния, соответствующая этим сигналам.

Выражение для потока плазмы имеет вид:

$$\Gamma = \langle \tilde{n} \tilde{v}_{op} \rangle = \frac{c}{H} \langle \tilde{n} \tilde{E}_\varphi \rangle = \frac{c}{H} n R_E (\langle \tilde{n}^2 \rangle \langle \tilde{E}_\varphi^2 \rangle)^{1/2} \quad (4)$$

Измеряя коэффициент корреляции $n R_E$ между \tilde{n} и \tilde{E}_φ и дополнительно определяя $\langle \tilde{n}^2 \rangle$ и $\langle \tilde{E}_\varphi^2 \rangle$, можно вычислить величину радиального потока плазмы.

Поскольку измерение E_φ при этом проводится не в точке, то возникает погрешность при определении $\langle \tilde{E}_\varphi^2 \rangle$, и величина потока занижается. Следует отметить, что измеренный поток может отличаться от истинного, если n-зонд установлен несимметрично по отношению к φ -зондам.

Расчет показывает, что при расстоянии между φ -зондами $l \leq \lambda_\varphi/4$, где λ_φ — длина волны по азимуту, величина ошибки составляет $\sim 10\%$. Исходя из этого, расстояние l выбиралось таким образом, чтобы коэффициент корреляции φR_φ был не менее $0,8 \div 0,9$. Это условие выполнялось при $l \sim 2 \div 6$ мм.

Для определения интегрального потока использовалось несколько одинаковых зондов, расположенных на разных углах по малому азимуту,

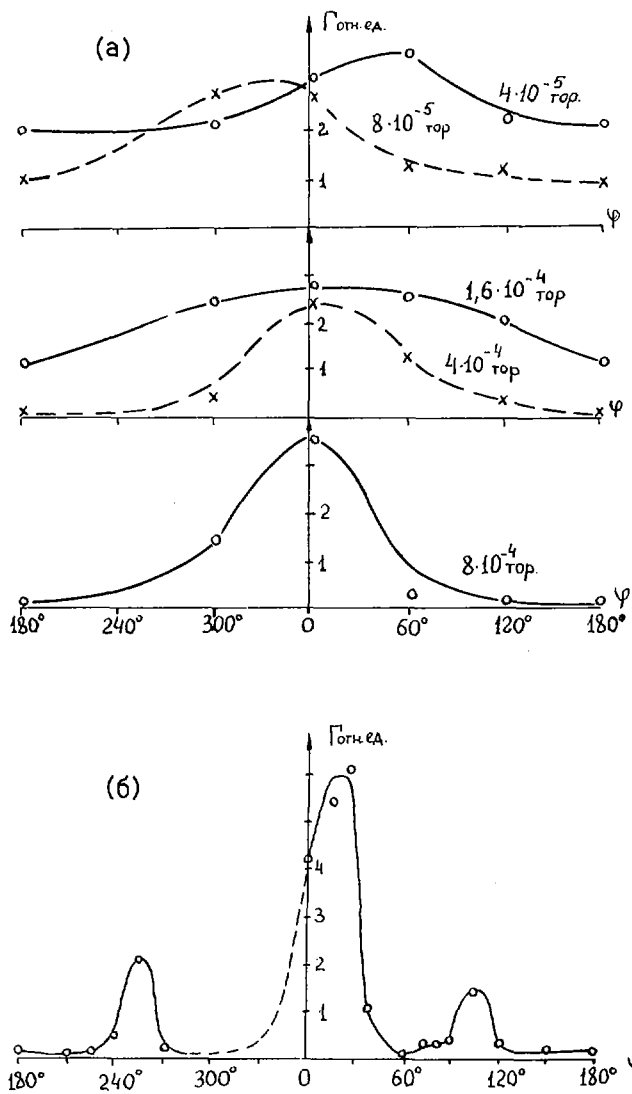


Рис.10. Зависимость радиального потока Γ от угла φ , $H = 2$ кэ, аргон: (а) $\epsilon^2 = 0,02$; (б) $\epsilon^2 = 0,08$; $P = 4,010^{-4}$ тор.

а также специальный зонд, который мог плавно перемещаться по азимуту в пределах $\sim 120^\circ$. Зонды устанавливались по радиусу в точках, соответствующих полувысоте профилей плотности. Время жизни плазмы определялось из выражения:

$$\tau_\gamma = k \frac{n(r_1) \cdot \bar{r}_1 / 2}{\int_0^{\frac{d\varphi}{2\pi}} \Gamma(\varphi) \cdot \frac{d\varphi}{2\pi}} \quad (5)$$

где: $n(r_1)$ – плотность в точке измерения,
 $\Gamma(\varphi)$ – величина потока в точке,
 \bar{r}_1 – средний радиус поверхности, на которой измеряется поток,
 k – коэффициент, связанный с формой профиля плотности:

$$k = 2 \int_0^{r_1} \frac{n(r)}{n(0)} \cdot \frac{r dr}{r_1^2}$$

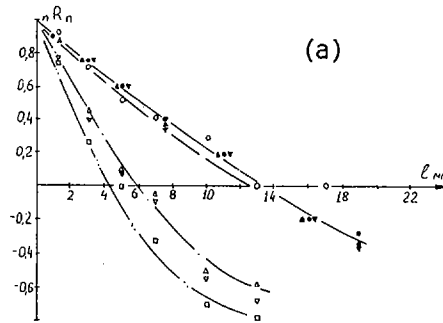
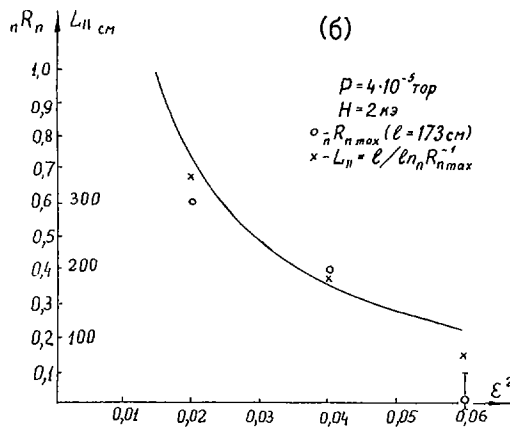
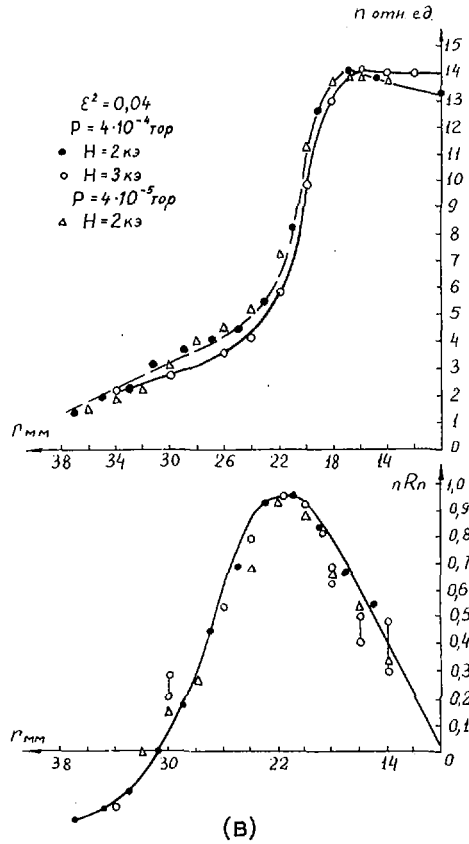


Рис. 11(а). Азимутальная пространственная корреляционная функция (ПКФ) для $\varphi = 0^\circ$.
 $\bullet \blacktriangle$ – $\epsilon^2 = 0,04$; $\circ \triangle \nabla \square$ – $\epsilon^2 = 0,08$; $\bullet \circ$ – $H = 1$ кэ; $\blacktriangle \triangle$ – $H = 1,5$ кэ; ∇ – $H = 2$ кэ;
 \square – $H = 2,5$ кэ; $P = 4,0 \cdot 10^{-4}$ тор.



(б). Зависимость максимального коэффициента корреляции вдоль магнитного поля L_{\max} от параметра ϵ^2 (сплошная линия – расчет).



(в). Распределение плотности по радиусу (вверху) и радиальная ПКФ для $\varphi = 0^\circ$ (внизу).

Если $n(r)$ — функция, для которой $\partial^2 n / \partial r^2 < 0$ и $n(r_1) = 0,5 n_{\text{max}}$, не трудно показать, что $1 \leq k \leq 2$ (для $n(r) \sim J_0(r)$ $k = 1,42$). Ниже, при вычислении γ , величина k полагается равной 1,4, поскольку в наших экспериментах профили плотности не сильно отличаются от профиля функции $J_0(r)$.

При оценке величины ошибки в этих измерениях следует учитывать, что длина волны λ_φ равна 2-6 см, т.е. по порядку величины совпадает с расстоянием между nE-зондами. Поэтому измерение потока лишь в отдельных точках по малому азимуту не может приводить к заметным ошибкам. Более существенные ошибки могут возникать за счет того, что измерения велись лишь на прямолинейном участке, без контрольных измерений на тороидальном участке.

В случаях достаточно сложной структуры распределения потока по азимуту, для получения зависимости $\Gamma(\varphi)$ использовался зонд, плавно перемещавшийся по углу. Графики $\Gamma(\varphi)$ для разных значений ϵ^2 и давления

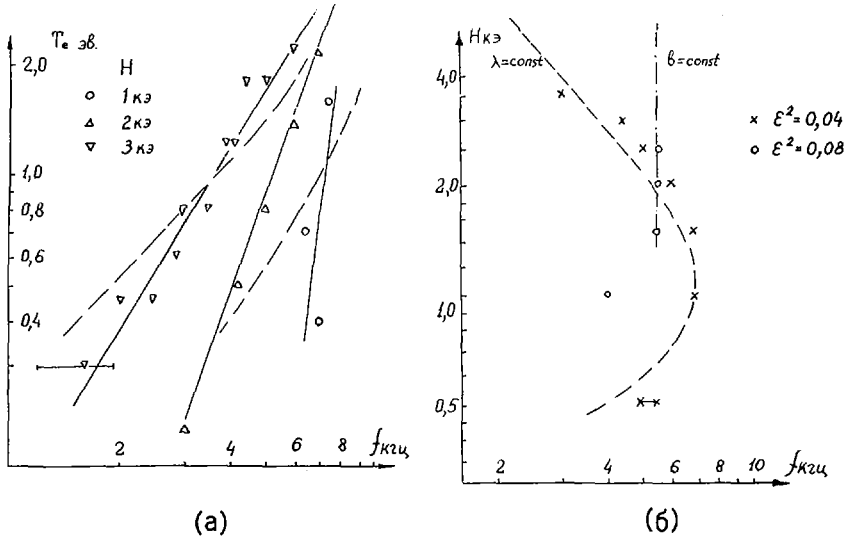


Рис. 12(а). Зависимость частоты колебаний от температуры электронов $\epsilon^2 = 0,04$; $P = 4,0 \cdot 10^{-4}$ тор; штриховые линии — расчет.

Рис. 12(б). Зависимость частоты колебаний от магнитного поля; $P = 4,0 \cdot 10^{-4}$ тор; штриховые линии — расчет.

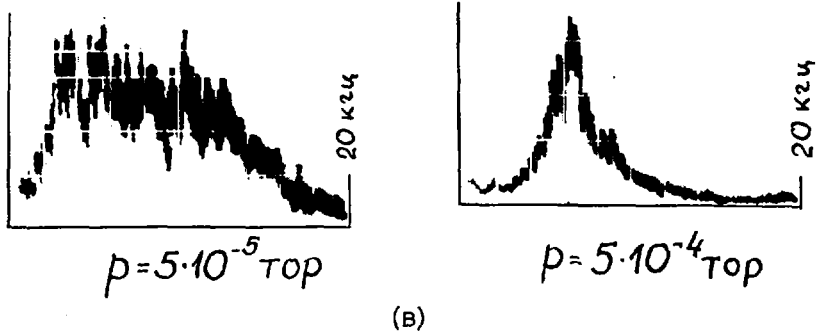


Рис. 12(в). Типичный вид спектра колебаний; $H = 2$ кэ; $\epsilon^2 = 0,04$.

приведены на рис. 10. Следует отметить, что поток плазмы возрастает на азимутах, где имеются запертые частицы.

Вычисленные по потокам времена τ_γ нанесены на рис. 3, 5 и 6. Как отмечалось выше, погрешность в определении интегрального потока может быть существенной, однако видно, что качественно ход зависимостей $\tau(p)$, $\tau(\epsilon^2)$, $\tau(H)$, полученных разными способами, совпадает. В области давлений $p > 10^{-3}$ тор, где должен наблюдаться переход к классической диффузии, поток плазмы на стенки существенно падает и τ_γ , соответственно, возрастает: $\tau_\gamma \gg \tau_p$ (см. рис. 3).

На рис. 11 приведены характерные пространственные корреляционные функции, а также зависимость продольного корреляционного размера $L_{||}$ от параметра ϵ^2 . Из вида этих кривых можно определить азимутальные (порядка 2-6 см) и радиальные (порядка 4 см) длины волн; о структуре волн вдоль магнитного поля можно судить по величине $L_{||}$.

Фазовые скорости v_{φ} при $N = 1 \div 2,5$ кэ были порядка $1 \div 6 \cdot 10^4$ см/сек, что совпадает с оценками дрейфовой теории; направление скорости также соответствовало теории. Радиальные составляющие скорости v_r были направлены наружу и по порядку совпадали с v_{φ} ; величина продольной скорости составляла $\sim 10^7$ см/сек.

Характерные частоты колебаний лежали в области 8-10 кГц. Типичный спектр колебаний приведен на рис. 12; там же приведена зависимость частоты колебаний от N и T_e .

СРАВНЕНИЕ С ДРЕЙФОВОЙ ТЕОРИЕЙ

Параметры колебаний, сопровождающих распад плазмы, являются характерными для дрейфовых волн. Оценим поток плазмы из стелларатора, обусловленный этими колебаниями. В случае, когда частота электронных столкновений ν_e меньше, чем $k_{||}v_e$, что обычно выполняется в описанных выше экспериментах, происходит раскачка дрейфово-бесстолкновительной неустойчивости. Из дисперсионного уравнения для неизотермической плазмы [13,14], предполагая $v_i \ll \omega/k_{||} \ll v_e$; $k_{\perp}^2 \rho_i^2 \ll 1$; $\omega/k_{||} \ll c_s$; $T_i \ll T_e$; $|\operatorname{Re} \omega| \gg \operatorname{Im} \omega \equiv \gamma$, получаем:

$$\operatorname{Re} \omega = \frac{\omega_e}{1+b}; \quad \gamma \approx \sqrt{\pi} \frac{\omega_e^2}{k_{||} v_e} \frac{b}{(1+b)^3} \quad (6)$$

Здесь ω_e — дрейфовая частота электронов, $b = (k_{\perp}^2 T_e)/(m_i \Omega_i^2) = (1/2 k_{\perp} \rho_i^*)^2$, а ρ_i^* — ларморовский радиус иона с электронной температурой. Заметим, что условие $k_{\perp}^2 \rho_i^2 \ll 1$ соответствует условию $0 < b < T_e/T_i$. Поправки к (6) за счет электронных столкновений приводят к возрастанию инкремента, однако при условии $\nu_e \ll k_{||}v_e$ эти поправки малы. Ион-нейтральные столкновения стабилизируют эту неустойчивость при $\nu_{i0} \sim \gamma$. Максимальный инкремент имеют волны с $k_{\perp} \rho_i^* \approx 1$, что нетрудно показать, исследуя (6) на максимум; величина k_{φ} ограничена также условием кратности периметра плазмы длине волны, т.е. $k_{\varphi} = M\Gamma^{-1}$, где M — номер азимутальной моды. Это ограничение существенно при достаточно малых M .

Рассмотрим связь τ и γ с учетом ряда особенностей дрейфового движения плазмы в азимутальных электрических полях. Уход частиц из плазмы в стеллараторе происходит или на магнитной поверхности, касающейся стенки камеры лишь в нескольких точках (при $r_c > a$), или на сепаратрисе (при $a > r_c$). Это значит, что E_{φ} на границе плазмы может существенно отличаться от E_{φ} в объеме и, соответственно, радиальная скорость частиц v_r на границе плазмы должна по порядку величины совпадать со скоростью v_r в объеме. Частица, которая пересекла крайнюю магнитную поверхность или сепаратрису, может уходить на стенку камеры, двигаясь вдоль силовых линий, на одном или нескольких периодах магнитного поля за время порядка или меньше периода колебаний. Если $k_r^{-1} \approx a_n = (1/n \cdot \partial n / \partial r)^{-1}$, то амплитуда колебаний частиц по радиусу x_0 по порядку величины совпадает с градиентным размером плазмы a_n :

$$x_0 = \int_0^{T/4} v_{\text{др}} dt \approx \beta a_n \quad (7)$$

где $\beta = e\varphi_{\text{max}}/T_e$.

Эта оценка справедлива для всех частиц с $\bar{v}_{\parallel} \leq \omega/k_{\parallel}$. В стеллараторе это условие выполнено как для ионов, так и для всех "запертых" электронов, которые составляют 30-40% от полного числа электронов в области развитых дрейфовых колебаний, при достаточно больших длинах свободного пробега.

В случае, когда свободный пробег электронов становится малым, число "запертых" электронов, для которых $\bar{v}_{\parallel} < \omega/k_{\parallel}$, должно убывать; однако одновременно появляется заметное количество пролетных электронов с относительно малой средней продольной скоростью, что связано с диффузионным характером движения электронов вдоль поля.

Число частиц, уходящих из плазмы за время $t_{\omega} = \omega^{-1}$ через единичный элемент поверхности плазмы, равно:

$$\Delta N = n_0 \Delta x \quad (8)$$

где Δx — приращение амплитуды колебаний за t_{ω} : $\Delta x \approx x_0 \cdot \gamma / \omega$ (x_0 — амплитуда радиальных колебаний).

Усредняя (8) по поверхности плазмы и учитывая регулярность колебаний во времени, получим:

$$\frac{\partial n}{\partial t} \approx n \frac{x_0 \gamma}{a}$$

откуда время распада плазмы по порядку величины равно:

$$\tau_t \approx \frac{a}{\gamma x_0} \quad (9)$$

Следует отметить, что уход частиц из плазмы в данном случае определяется не диффузией в точном смысле этого слова, а переносом частиц плазмы на стенку за счет переменного азимутального электрического поля за время порядка нескольких периодов колебаний, и поэтому коэффициент диффузии можно здесь ввести лишь условно.

Преобразуем выражение (6), учитывая, что длина волны λ_{\parallel} уменьшается за счет шира: $(\lambda_{\parallel})^{-1} = k_{\parallel} \approx k_{\phi} \theta$. Тогда:

$$\gamma \approx \left(\frac{cT}{eH} \right)^2 \left\langle \frac{1}{a_n^2(r) \cdot \lambda_{\phi}(r) \cdot \theta(r) \cdot v_e} \right\rangle \frac{\sqrt{\pi} b}{(1+b)^3} \quad (10)$$

Индекс (r) означает, что параметры определены на радиусе r . Время распада τ_t определяется выражением (9), в котором γ усредняется по объему плазмы. Пусть $a_n = a/2,4$; предположим также, что радиальная амплитуда колебаний порядка размера локализации колебаний x_1 (в рассматриваемой задаче $x_0 \approx x_1 \approx a_n$). Тогда:

$$\tau_t \approx \left(\frac{eH}{cT_e} \right)^2 \frac{3,8 \epsilon^2 \alpha^3 a^2 v_e}{2,4 \left\langle \frac{1}{\lambda(r) \cdot r^3} \right\rangle} \cdot \frac{(1+b)^3}{\sqrt{\pi} b}$$

Если $a \gg \rho_i^*$, то $\lambda_\varphi \approx \rho_i^*$ и

$$\tau_t \approx A \tau_B \theta(\bar{r}) \sqrt{m_i/m_e} \sim H \epsilon^2 a^2 T_e^{-1} m_i^{1/2} \quad (11)$$

В случае $\rho_i^* \geq a$, как отмечалось выше, $\lambda_\varphi \approx r$ и, соответственно,

$$\tau_t \approx A \tau_B \theta(\bar{r}) \sqrt{m_i/m_e} \left(\frac{a}{\rho_i^*} \right) \frac{(1+b)^3}{3,8 M \sqrt{\pi b}}$$

При $T_e \approx 1$ эВ отсюда получаем:

$$\tau_t \approx H^2 \epsilon^2 a^3 T^{-q} \quad (12)$$

Здесь A – постоянный множитель порядка 2,5; τ_B – боровское время распада $\tau_B = (a/2,4)^2 (16 \text{ eH}/cT)$; \bar{r} – радиус, в окрестности которого $\gamma(r)$ достигает максимума ($\bar{r} < a$); $q < 1$.

Очевидно, что ион-нейтральные столкновения приводят к уменьшению инкремента в (10) и, соответственно, к увеличению τ_t .

Зависимости τ_t от магнитного поля, ϵ^2 и размеров плазмы, приведенные выше, хорошо совпадают с τ_p .

Сравним абсолютное время τ_t , полученное из (11), (12), с экспериментом. В типичных условиях $a \approx 3$ см; $T_e = 1$ эВ. $H = 2$ кэ, $\epsilon^2 = 0,08$; $\bar{r} = 2$ см; $\theta(r) = 0,01$; $(m_i/m_e)^{1/2} = 270$, $\rho_i^* = 0,5$ см $< a$; таким образом, расчетное значение $\tau_t \approx 6,5 \tau_B = 3,1$ мсек с точностью до множителя ~ 1 совпадает с экспериментальным значением $\tau_p \approx 2,9$ мсек.

ОБСУЖДЕНИЕ РЕЗУЛЬТАТОВ

1. Сопоставление времени распада плазмы, измеренного по убыванию средней плотности плазмы τ_p , и времени распада, измеренного по радиальным потокам плазмы, обусловленным колебаниями потенциала, τ_γ , позволяет сделать вывод о том, что потери плазмы из стелларатора в описанных экспериментах полностью определяются колебаниями плазмы. Этот вывод дополнительно подтверждается тем фактом, что все изученные функциональные зависимости τ_p и τ_γ совпадают. Следует отметить, что при достаточно больших давлениях нейтрального газа ($p > 10^{-3}$) (рис. 3) амплитуды колебаний и связанные с ними потоки плазмы резко падают.

2. Развитые выше представления о возможности дрейфового переноса элементов плазмы по радиусу на расстояние порядка градиентного размера за период колебаний позволяют оценить время распада плазмы τ_t . Оно хорошо совпадает с экспериментальными значениями τ_p по абсолютной величине и изменяется подобно τ_p при изменении параметров.

ЛИТЕРАТУРА

- [1] БОЧАРОВ, В.Н., ВОЛОСОВ, В.И., КОМИН, А.В., ПАНАСЮК, В.М., ЮДИН, Ю.Н., Доклады III Междунар. конф. по управляемому термоядерному синтезу и физике плазмы (Новосибирск, 1968) IAEA, Vienna, I 1969, p. 561.
- [2] БОЧАРОВ, В.Н., ВОЛОСОВ, В.И., КОМИН, А.В., ПАНАСЮК, В.М., ЮДИН, Ю.Н., Доклады III Европейской конф. по управляемому термоядерному син-

- тезу и физике плазмы (Утрехт, 1969) 123, Изд. "Wolters - Noordhoff", Голландия, 1969.
- [3] БОЧАРОВ, В.Н., ВОЛОСОВ, В.И., КОМИН, А.В., ПАНАСЮК, В.М., ЮДИН, Ю.Н., Доклад на III Междунар. конф. по удержанию плазмы в замкнутых системах (Дубна, 1969) (в печати), (см. также Аннотации докладов, Москва, 1969, стр.12).
- [4] ВОЛОСОВ, В.И., КОМИН, А.В., ЖТФ 38 (1968) 846.
- [5] БОЧАРОВ, В.Н., ВОЛОСОВ, В.И., КОМИН, А.В., ПАНАСЮК, В.М., ЮДИН, Ю.Н., ЖТФ 40 (1970) 1334.
- [6] TAMAGAWA, H., TUJITA, J., J. Phys. Soc. Jap. 14 (1959) 678.
- [7] КАГАН, Ю.М., ПЕРЕЛЬ, В.И., ЖТФ 38 (1968) 1663.
- [8] GIBSON, A., Phys. Fl. 10 7 (1967) 1553.
- [9] SUGAR, G.R., J. Appl. Phys. 25 (1954) 354.
- [10] JENSEN, T.H., MOORE, R.W., Rev. Sci. Instr. 40 (1969) 772.
- [11] BURFORD, T.M., J. Appl. Phys. 26 (1955) 56.
- [12] БЕХТЕНЕВ, А.А., ВОЛОСОВ, В.И., ЭЛЛИС, Р.А., ЮДИН, Ю.Н., Препринт ИЯФ СО АН СССР 37-70, Новосибирск, 1970.
- [13] KRALL, N., ROSENBLUTH, M., Phys. Fluids 8 (1965) 1488.
- [14] КАДОМЦЕВ, Б.Б., в сб. "Вопросы теории плазмы", вып.4, Госатомиздат, М., 1964, стр.188.

ИССЛЕДОВАНИЕ УДЕРЖАНИЯ ПЛАЗМЫ В СТЕЛЛАРАТОРЕ TOR-1

Д. К. АКУЛИНА, Э. Д. АНДРЮХИНА,
Ю. И. НЕЧАЕВ, О. И. ФЕДЯНИН,
Ю. В. ХОЛЬНОВ
Физический институт им. П. Н. Лебедева
Академии наук СССР, Москва,
Союз Советских Социалистических Республик

Доклад представлен В.И. Волосовым

Presented by V.I. Volosov

Абстракт—Аннотация

AN INVESTIGATION OF PLASMA CONFINEMENT IN THE TOR-1 STELLARATOR.

Investigations have been carried out previously on the TOR-1 stellarator of the confinement of plasma in a collisionless regime. A relationship was established between the plasma lifetime and potential on the one hand and the rotational transform angle and structure of the magnetic surfaces close to the resonance value $i = 2\pi$ on the other. In the present paper plasma confinement conditions are investigated as a function of the collision frequency, the rotational transform angle and the intensity of the magnetic field. Use was made of the ultra-high-frequency method of creating and heating plasma, permitting a transition to substantially higher collision frequencies (dense plasma). When ultra-high-frequency heating was applied in the TOR-1 stellarator a plasma having the following parameters was obtained; density $n_e = 3-5 \times 10^{12} \text{ cm}^{-3}$; $T_e = 3-8 \text{ eV}$; density of neutrals $n_0 = 10^{13} \text{ cm}^{-3}$; the working gases were argon and helium. This permitted an investigation of a wide range of changes in the collision frequencies (Coulomb type collision and collisions with neutrals) with a transition to the region of hydrodynamics. An investigation was carried out of the relationship between the plasma lifetime and the rotational transform angle $0,1 \leq i/2\pi \leq 3$, the density of the magnetic field $H = 1-10 \text{ kOe}$, the temperature of the electrons and the density. The experimental results were compared with those obtained on the basis of classical diffusion theory.

ИССЛЕДОВАНИЕ УДЕРЖАНИЯ ПЛАЗМЫ В СТЕЛЛАРАТОРЕ TOR-1.

Ранее на стеллараторе TOR-1 проводились исследования удержания плазмы в бесстолкновительном режиме. Были получены зависимости времени жизни и потенциала плазмы от угла вращательного преобразования и структуры магнитных поверхностей вблизи резонансного значения $i = 2\pi$. В данной работе исследовались условия удержания плазмы в зависимости от частот столкновений, угла вращательного преобразования и напряженности магнитного поля. Для этого использовался СВЧ-метод создания и нагрева плазмы, позволивший перейти к существенно большим частотам столкновений (плотная плазма). При СВЧ-нагреве в стеллараторе TOR-1 получена плазма со следующими параметрами: плотность $n_e = 3-5 \cdot 10^{12} \text{ см}^{-3}$; $T_e = 3-8 \text{ эВ}$; рабочий газ — аргон, гелий. Это позволило проводить исследования в широкой области изменения частот столкновений (кулоновских и столкновений с нейтралами) с переходом в область гидродинамики. Исследовалась зависимость времени жизни плазмы от угла вращательного преобразования $0,1 \leq i/2\pi \leq 3$, напряженности магнитного поля $H = 1-10 \text{ кэ}$, температуры электронов и плотности. Проведено сравнение результатов экспериментов с теорией классической диффузии.

Теоретические исследования удержания плазмы в замкнутых магнитных ловушках, проведенные в последние годы, весьма расширили наши понятия о классическом механизме диффузии. Учет влияния тороидальности, наличия различных классов частиц и, соответственно, различия в траекториях движения дали существенно отличные результаты в коэффициентах переноса по сравнению с прямолинейными системами. Имеющиеся в

настоящее время теоретические модели заставляют по-новому отнестись к постановке эксперимента и трактовке накопленных экспериментальных данных. Законы диффузии плазмы существенным образом меняются в различных областях частот столкновения. С нашей точки зрения представляет несомненный интерес проведение на одной и той же экспериментальной установке исследования удержания плазмы с различными параметрами.

В данной работе представлены результаты экспериментов по исследованию удержания плазмы в области малых и больших частот соударений. Плазма создавалась двумя способами: во-первых, внешней инжекцией плазмы из искрового источника ($n_e \approx 5 \cdot 10^{10} \text{ см}^{-3}$, $T_e \approx 1 \div 2 \text{ эВ}$) и, во-вторых, методом ионизации и нагрева с помощью сверхвысокочастотного электромагнитного поля ($n_e \approx 2 \cdot 10^{12} \text{ см}^{-3}$, $T_e \approx 0,2 - 0,4 \text{ эВ}$). Если в первом случае при рассмотрении механизма ухода необходимо учитывать чисто стеллараторные эффекты: траектории различного сорта частиц (пролетных и запертых), различие в механизмах ухода электронов и ионов, то во втором случае можно ожидать чисто столкновительную диффузию, описываемую магнитной гидродинамикой.

СТЕЛЛАРАТОР TOP-1

Установка TOP-1 [1] представляет собой тороидальную магнитную ловушку с двухзаходным винтовым магнитным полем.

Продольное магнитное поле создается секционированным соленоидом, состоящим из 28 катушек. Для создания винтового магнитного поля применяется система двухзаходной винтовой обмотки. Винтовая обмотка представляет собой спираль, образованную четырьмя шинами с взаимно противоположными направлениями токов. Закон намотки спирали $\varphi = N\theta$, где φ — угол в плоскости сечения, θ — угол в плоскости тора, N — число шагов.

Питание установки осуществляется от конденсаторной батареи. При изменении отношения токов в системах продольного и винтового полей можно получать различные значения ϵ (ϵ — отношение амплитуды основной гармоники винтового поля к продольному, $\epsilon = 0 - 0,72$), которые определяют

ТАБЛИЦА I. ОСНОВНЫЕ ПАРАМЕТРЫ
УСТАНОВКИ TOP-1

Большой радиус тора	60 см
Малый радиус винтовой обмотки [a]	8,5 см
Число заходов винта [n]	2
Число шагов винта [N]	7
Закон намотки винта	$\varphi = N\theta$ (где: θ — угол в плоскости тора, φ — в плоскости сечения)
Максимальное значение угла вращательного преобразования	$i = 4,5 \pi$
Максимальное значение среднего шира [e]	$\sim \{1,5 \div 2\} \cdot 10^{-2}$
Малый радиус вакуумной камеры	5 см
Максимальная напряженность магнитного поля [H ₀]	15 кэ
Длительность постоянного уровня магнитного поля [$\pm 5\%$]	$\sim 10 \div 12$ мсек

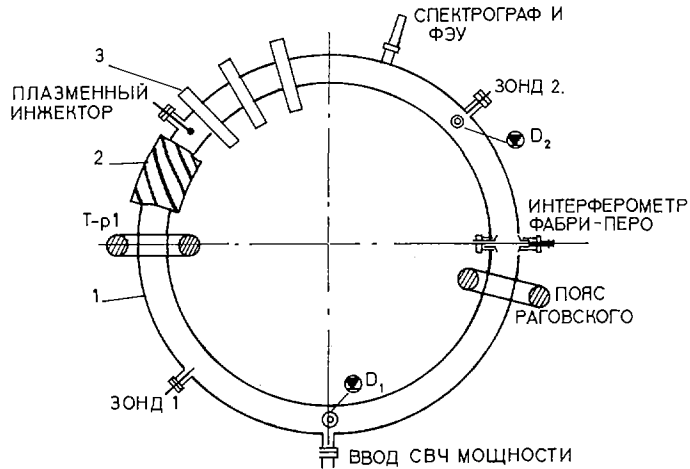


Рис. 1. Схема расположения аппаратуры на стеллараторе TOP-1: 1 - вакуумная камера, 2 - двухзаходная винтовая обмотка, 3 - катушка продольного поля (28 шт), ТР-1 - трансформатор возбуждения пробного тока, Д₁, Д₂ - детекторы СВЧ-мощности.

всю структуру магнитного поля стелларатора. Так, например, угол вращательного преобразования силовой линии в зависимости от радиуса и величины ϵ выражается следующим образом: $i/2\pi = \dot{i} \approx N\epsilon^2 \{ 1/2 + [(Nr)/R]^2 \}$.

Вакуумная камера установки, изготовленная из немагнитной нержавеющей стали, состоит из двух полуторов, разделенных изолирующими прокладками. Большой радиус тора $R = 60$ см, малый радиус камеры $r_0 = 5$ см, толщина стенки $\delta = 0,2$ см.

Основные параметры установки приведены в табл. I, а схема установки представлена на рис. 1.

МАГНИТНЫЕ ИЗМЕРЕНИЯ

Магнитные измерения [2], проведенные на установке с помощью пробного электронного пучка, показали, что структура магнитного поля достаточно совершенна. Экспериментально измеренные зависимости угла вращательного преобразования от радиуса, смещение магнитной оси относительно геометрического центра, эксцентриситет магнитных поверхностей хорошо согласуются с теоретическими расчетами структуры поля стелларатора [3]. Максимальные значения угла вращательного преобразования и шира, $\theta = [i(r) - i(o)] r / (2\pi R)$, измеренные экспериментально, соответствуют предельным значениям для кругового стелларатора [4,5]:

$$\dot{i}_{\max} \leq (0,25 \div 0,33) N = 1,75 - 2,25.$$

При проведении магнитных измерений исследована структура магнитных поверхностей в области резонансных углов вращательного преобразования $\dot{i} = 1/2, 2/2, 3/2, 4/2$. На рис. 2 приведены структуры магнитных поверхностей в резонансных случаях.

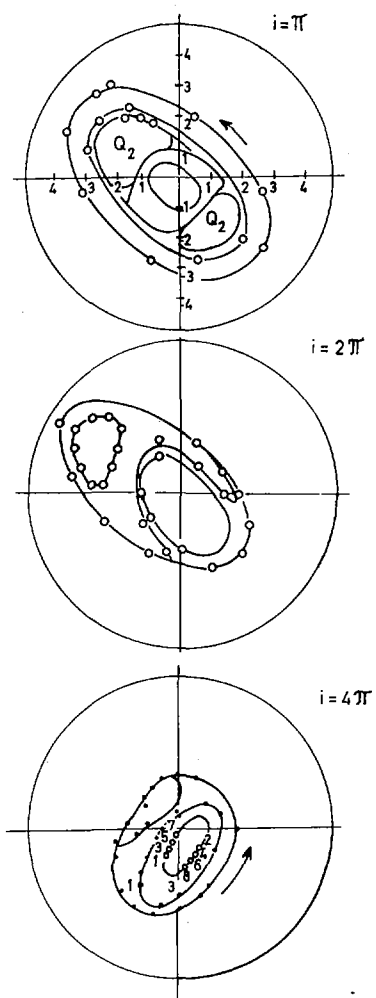


Рис. 2. Структура возмущенных магнитных поверхностей при резонансных значениях угла вращательного преобразования.

Величины полей, которые могут приводить к таким возмущениям структуры магнитных поверхностей в резонансах, согласуются с точностью изготовления магнитной системы.

Для уменьшения резонансных возмущений на установке были проведены исследования возможности компенсации возмущающего поля в области наиболее сильного резонанса $\dot{i} = 1$ [6].

Компенсация возмущающего поля проводилась путем наложения внешнего магнитного поля, потенциал которого в цилиндрических координатах имеет вид: $\Phi_k \approx \Phi_0 r \cos(\varphi - z/R + \psi)$ (однозаходный винт с шагом, равным периметру установки).

Изучение влияния компенсирующего поля на структуру магнитных поверхностей показало, что можно ликвидировать смещение магнитной оси, а также значительно уменьшить размер резонансных розеток.

Таким образом, исследование удержания плазмы проводится на установке с хорошо изученной конфигурацией магнитного поля ловушки.

ИССЛЕДОВАНИЕ УДЕРЖАНИЯ БЕССТОЛКНОВИТЕЛЬНОЙ ПЛАЗМЫ

Плазма в ловушке создавалась искровой пушкой [8], расположенной вблизи граничной магнитной поверхности ($r \sim 4$ см). Максимальное значение плотности плазмы $(0,5-1) \cdot 10^{11} \text{ см}^{-3}$, $T_e \approx 1 \div 2$ эВ, $T_i \approx 20-30$ эВ. Квазистационарное продольное распределение плотности устанавливается через 150-200 мксек после инжекции. Профиль плотности в условиях невозмущенных магнитных поверхностей носит характер обычного диффузионного распределения. С достаточной точностью граница плазмы ($n/n_{\text{max}} \sim 0,1$) совпадает с крайней замкнутой магнитной поверхностью. Изменение плотности плазмы во времени с большой степенью точности носит экспоненциальный характер при изменении плотности примерно на порядок.

Одной из основных задач наших экспериментов было выяснение влияния вращательного преобразования на время жизни плазмы. На рис. 3 приведена зависимость экспериментально измеренного времени жизни плазмы от угла вращательного преобразования. Пунктиром показана зависимость нормированного времени жизни от \dot{i} с учетом уменьшения размера плазмы при увеличении угла вращательного преобразования: $r_{\text{cp}}^2 = r_0^2 [(1 - \epsilon)/(1 + \epsilon)]$, где r_{cp} — средний радиус магнитной поверхности, r_0 — радиус камеры.

Особенностью графика $\tau(\dot{i})$ является: 1) линейный рост времени жизни в зависимости от \dot{i} ; 2) наличие провалов на кривой в области резонансных значений углов вращательного преобразования ($\dot{i}(0) = 0,25; 0,5; 1; 2$).

Можно было предположить, что такое уменьшение времени жизни обусловлено несовершенством структуры магнитного поля, т.е. изменением диффузионного размера при образовании резонансных волокон. Проверка этого предположения проводилась в области первого резонанса $\dot{i} = 1$. При этом изменялась величина возмущения и, как следствие, форма и величина магнитной розетки. Эксперименты показали, что, несмотря на то что распределение плотности плазмы по сечению камеры перестраивается в соответствии с перестройкой магнитных поверхностей, одна из основных интегральных характеристик удержания плазмы — время жизни — практически остается неизменной, и соответственно — провал в кривой $\tau(\dot{i})$ около $\dot{i} = 1$ остается. Исходя из этого, можно предположить, что резкое умень-

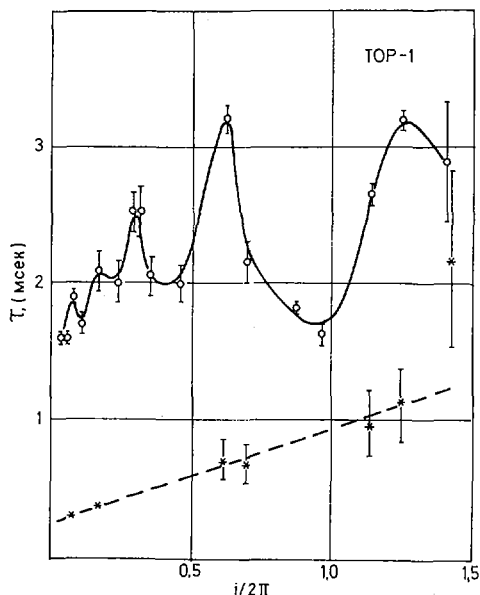


Рис. 3. Зависимость времени жизни плазмы от угла вращательного преобразования (бесстолкновительный режим); пунктирная кривая — зависимость приведенного времени жизни плазмы с учетом уменьшения радиуса плазмы с ростом угла вращательного преобразования.

шение τ вблизи резонансных значений i не обязано резонансному разрушению структуры поля [6,7]. Этот эффект имеет более глубокую физическую природу. Поскольку характерным для всех резонансов является замыкание силовых линий магнитного поля, то естественно предположить, что за быстрый уход плазмы ответственны в этом случае длинноволновые неустойчивости, условия для развития которых в данной ситуации оптимальны.

СВЧ-МЕТОД СОЗДАНИЯ ПЛАЗМЫ В СТЕЛЛАТОРЕ TOP-1

Для проведения экспериментов по изучению удержания плазмы в области высоких частот соударений (гидродинамическая область) был выбран метод СВЧ-ионизации и нагрева плазмы.

Область гидродинамики задается следующим неравенством [9] $\lambda < (2\pi R)/i$, где i — угол вращательного преобразования, $2\pi R$ — периметр ловушки, λ — длина свободного пробега. Выражая длину свободного пробега через плотность и температуру, получим для характерных параметров TOP-1 ($R = 60$ см и $i \approx 2\pi$) следующую нижнюю границу для плотности плазмы $n > 1,2 \cdot 10^{10} \text{ Т}^2$ эВ. Как показали эксперименты, это условие выполнялось с большим запасом.

Плазма в стеллаторе создавалась следующим образом. Металлическая вакуумная камера возбуждалась СВЧ-генератором на длине волны ~ 4 см. Добротность камеры — многомодового резонатора — в отсутствие плазмы составляла 10^3 . Энергия вводится в камеру через круг-

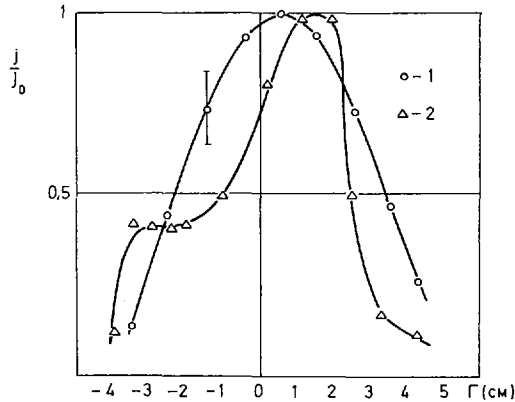


Рис. 4. Распределение плотности плазмы по радиусу для различных значений мощности СВЧ: $w_1 \sim 0,2 w_2$.

лый волновод (патрубок). Напряженность электрического поля в резонаторе в отсутствие плазмы может изменяться в широком диапазоне $E = 100-400$ В/см. Эксперименты проводились при постоянном давлении нейтрального газа (аргон или гелий) в диапазоне $5 \cdot 10^{-5} - 5 \cdot 10^{-4}$ мм рт. ст. Предварительная ионизация при работе на малых уровнях СВЧ-мощности осуществлялась искровой пушкой.

Исследования показали, что стационарный СВЧ-разряд в стеллараторе имеет ряд особенностей. Развитие разряда при широком изменении внешних параметров (давление p_0 , мощность w , напряженность магнитного поля H) происходит за относительно малое время: меньше 200 мксек.

С помощью СВЧ-разряда получается большая плотность плазмы $n_{\max} \approx 5 \cdot 10^{12}$ см $^{-3}$, причем ни при каких параметрах (p_0 , w , H) не удается получить квазистационарный разряд при плотности плазмы, ниже критической, для рабочей длины волны СВЧ ($n_c \approx 6 \div 7 \cdot 10^{11}$ см $^{-3}$).

Квазистационарная температура электронов, зависящая от уровня СВЧ-мощности ($T_e \sim w$) и давления нейтрального газа ($T_e \sim p_0^{-1}$) лежит в диапазоне 3-8 эВ. Следует отметить, что возможно существование квазистационарного состояния и при более низких усредненных значениях температуры $T_e \approx 1$ эВ.

Характеристики разряда (n_e , T_e) не зависят от способа возбуждения СВЧ-волн в камере (электрический вектор параллелен или перпендикулярен направлению магнитного поля).

Измерения уровня СВЧ-поля в камере указывают на сильную перестройку резонатора при разряде; это обстоятельство не позволяет определить величину поглощения СВЧ-мощности в плазме.

Измерения распределения плотности плазмы, точнее полного тока насыщения, указывают на то, что величина СВЧ-мощности значительно влияет на геометрию плазмы. Примеры распределения плотности по радиусу представлены на рис. 4. Наличие неоднородностей в $n(r)$, по-видимому, может указывать на локальный характер поглощения энергии.

Одной из основных особенностей СВЧ-разряда является наличие в плазме квазистационарного постоянного тока, протекающего вдоль оси тора в течение всего времени действия СВЧ. Направление тока совпада-

ет с направлением продольного магнитного поля стелларатора и изменяется с изменением его направления. Величина тока равна нескольким амперам (1-3) и возрастает при увеличении уровня СВЧ-мощности. Природа этого тока в настоящее время не выяснена, но, по-видимому, он связан с механизмом поглощения СВЧ. Косвенно на это указывает тот факт, что при циклотронном резонансе, когда $\omega = \omega_{eH}$ и циклотронное поглощение является преобладающим, постоянный ток не зависит от направления магнитного поля.

Совокупность приведенных экспериментальных данных (малое время развития разряда, наличие квазистационарного состояния при $n > n_e$, возможность создания плазмы с малым усредненным значением электронной температуры когда время ионизации больше времени жизни, заметное поглощение СВЧ-мощности, возникновение постоянного тока в плазме) позволяет сделать предположение, что нагрев плазмы носит не резистивный характер, а имеет место механизм аномального поглощения СВЧ плазмой [10]. Наличие такого аномального поглощения позволяет получить плотную плазму $n \approx 5 \cdot 10^{12} \text{ см}^{-3}$, $T_e \approx 3 \div 8 \text{ эВ}$.

Таким образом, сложность явлений, проходящих при СВЧ-разряде, не позволяет изучать диффузию плазмы в этих условиях. Поэтому активная стадия СВЧ-разряда нами рассматривалась лишь как способ создания плотной плазмы. Исследование характеристик удержания плотной плазмы в стеллараторе производилось для распадающейся плазмы после выключения СВЧ.

ИССЛЕДОВАНИЕ РАСПАДАЮЩЕЙСЯ ПЛАЗМЫ

На рис. 5 приведена временная последовательность процессов с указанием масштаба времени. СВЧ-мощность спадает за время, меньше 100 мксек, и в дальнейшем происходит распад плазмы с заданными начальными условиями, определенными активной стадией.

а. Измерение электронной температуры

Электронная температура определялась ленгмюровскими зондами (локальные измерения) и по проводимости плазмы (средняя по объему). В последнем случае в плазме возбуждался пробный высокочастотный ток с помощью воздушного трансформатора ТР-1. Измерения тока проводятся высокочувствительным поясом Роговского (см. рис. 1).

На рис. 6 приведена осциллограмма пробного тока, протекающего по плазме, и определенная из проводимости плазмы величина электронной температуры:

$$T_e(\text{эВ}) = \left[\frac{I(a)}{V(b)} \frac{R}{5r^2} \right]^{2/3}$$

где I – величина тока, V – напряжение на обходе, r – радиус плазменного столба.

С помощью одиночных ленгмюровских зондов установлено постоянство фактора r^2 , определяющего сопротивление плазменного столба. Ток – чисто активный, величина удельного сопротивления плазмы изменяется в диапазоне $(5 \cdot 10^{-3} - 1) \text{ ом} \cdot \text{см}$. Из приводимого графика $T(t)$ видно, что охлаждение электронов происходит быстро: через 1 мсек практически уста-

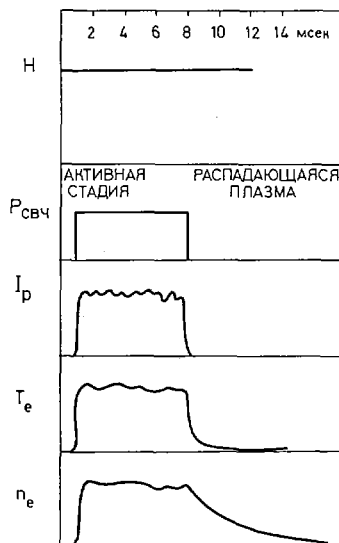


Рис. 5. Временная последовательность процессов при СВЧ-разряде: H – магнитное поле, $P_{свч}$ – мощность СВЧ, I_p – квазистационарный плазменный ток, T_e – электронная температура, n_e – плотность плазмы.

наливается квазистационарная температура $T_e \approx 0,2 \div 0,4$ эВ; скорость изменения температуры уменьшается на порядок. Скорость охлаждения, т. е. время установления квазистационарной температуры и ее величина не зависят от напряженности магнитного поля и давления нейтралов.

Охлаждение электронов может быть объяснено двумя процессами: до $T_e \approx 2$ эВ охлаждение может быть обусловлено неупругими столкновениями (ионизация и возбуждение), а при $T_e < 2$ эВ основной причиной охлаждения, помимо поперечной теплопроводности, играющей определенную роль и при $T_e > 2$ эВ, являются упругие столкновения с ионами.

Однако неясным остается вопрос об относительно высокой ($T_e \approx 0,2 \div 0,4$ эВ) квазистационарной температуре. Этот факт можно объяснить только в предположении о существовании ионной температуры $T_i \approx 0,2 \div 0,4$ эВ. Заметим, что аналогичные результаты по измерению квазистационарной температуры в распадающейся плазме $T_e \approx 0,2$ эВ получены в работе [16].

б. Исследование распада плазмы

Основные зависимости, характеризующие удержание плазмы в стеллараторе, т. е. зависимости времени жизни плазмы от величины магнитного поля и угла вращательного преобразования получены из измерения распада электронной плотности. Измерения хода плотности плазмы во времени производились с помощью открытого микроволнового резонатора Фабри-Перо [11], работающего на длине волны ~ 4 мм. Характерная ос-

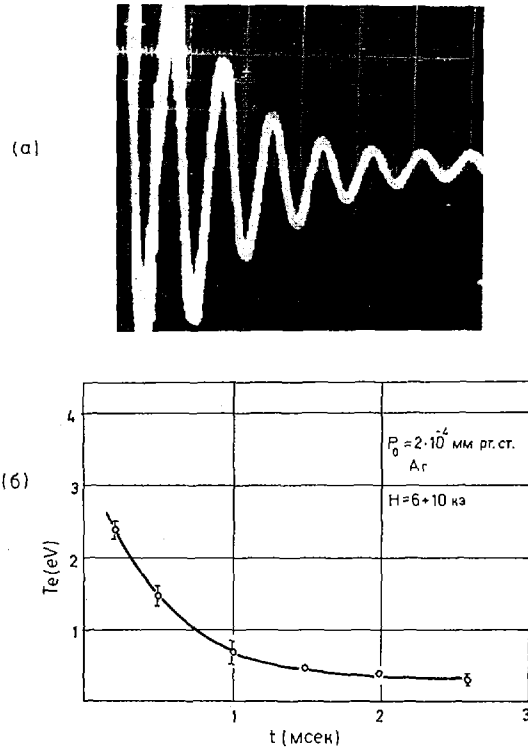


Рис. 6. Осциллограмма пробного тока в распадающейся плазме (а): $f = 3,5$ кГц. Зависимость электронной температуры распадающейся плазмы от времени (б).

циллограмма приведена на рис. 7(а). Величина горизонтального отклонения резонансного пика от нулевого значения (нулевой отсчет задается вторым опорным резонатором) пропорциональна плотности. Измерение плотности производится через дискретные интервалы времени, что на осциллограмме соответствует различным горизонтальным линиям (временное расстояние между линиями на приводимой осциллограмме — 400 мксек).

На рис. 7(б) приводится зависимость абсолютной плотности плазмы от времени (результат обработки осциллограммы, аналогичной представленной на рис. 7а). Зависимость $n(t)$ дана в двух различных системах координат: верхняя ($\ln n, t$), нижняя ($1/n, t$).

Измерение плотности плазмы во времени происходит, строго говоря, не по экспоненциальному закону; экспонента в системе ($\ln n, t$) представляется прямой линией (см. рис. 7б).

Вопрос функциональной зависимости плотности распадающейся плазмы от времени, когда коэффициент диффузии зависит от плотности и, в

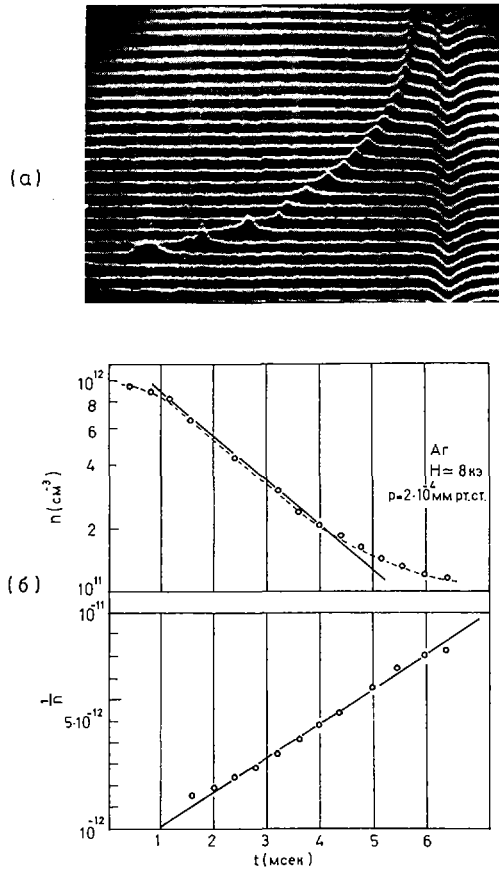


Рис. 7. Осциллограмма измерения плотности распадающейся плазмы (а). Зависимость хода плотности от времени для распадающейся плазмы, построенная в различных системах координат (б): $(\ln n, t)$ и $(1/n, t)$.

частности, определяется кулоновскими столкновениями, не рассмотрен достаточно подробно. Уравнение диффузии в этом случае получается нелинейным. В работах [12] получено частное решение для случая, когда возможно разделение переменных (время и пространство). Однако общее решение принципиально определяется начальными условиями, т. е. начальным распределением плотности.

Временная зависимость частного решения нелинейного уравнения диффузии имеет следующий вид:

$$[n_0/n(t) - 1] = [t/\tau]$$

n_0 — начальная плотность в центре, $\tau = a^2 / [(2,4)^2 D_0]$,
 D_0 — значения коэффициента диффузии при $n = n_0$.

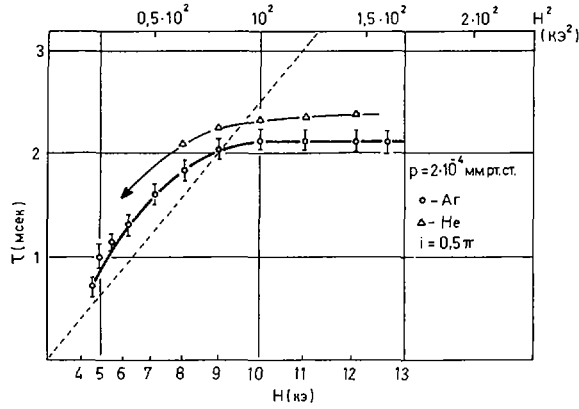


Рис. 8. Зависимость времени жизни плазмы от квадрата напряженности магнитного поля $\tau(H^2)$. Пунктиром представлена теоретическая зависимость для гидродинамической области.

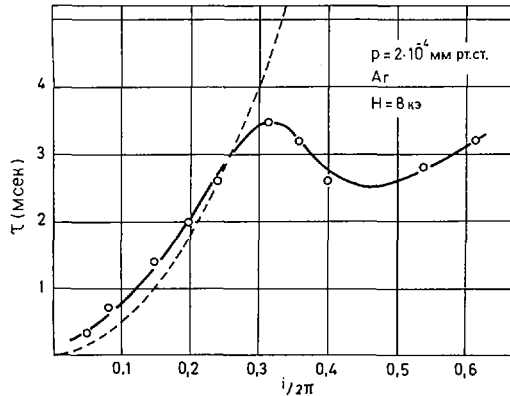


Рис. 9. Зависимость времени жизни плазмы от угла вращательного преобразования. Пунктиром представлена теоретическая кривая.

Форма кривой (см. рис. 7б) в некоторых условиях вполне удовлетворительно описывается этой зависимостью, т. е. проведение сравнения различных условий удержания (вариация напряженности магнитного поля, угол вращательного преобразования) по величине постоянной времени является не совсем корректным. За характерное время распада плазмы принималось время изменения плотности в 3 раза для фиксированного диапазона плотности ($10-3 \cdot 10^{11}$ см⁻³).

Зависимость времени жизни плазмы τ от квадрата напряженности магнитного поля H^2 приведена на рис. 8. Из графика видно, что имеются две области: при $H < 8-9$ кэ зависимость $\tau(H^2)$ близка к линейной, в области небольших полей наблюдается четко выраженное насыщение $\tau(H^2)$.

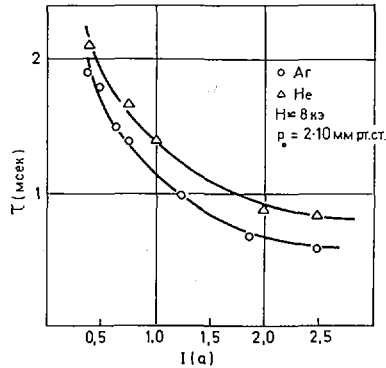


Рис. 10. Зависимость времени жизни плазмы от величины квазистационарного тока.

Измерения при малых напряженностях магнитного поля осложнены затрудненным развитием разряда; одной из возможных причин изменения картины разряда может быть малое время жизни плазмы.

Характер зависимости $\tau(H^2)$ и абсолютная величина времени жизни не зависят от массы ионов (Ar, He). В настоящее время не имеется достаточного количества экспериментальных данных для объяснения насыщения кривой $\tau(H^2)$ при больших полях.

На рис. 9 приведена зависимость времени жизни плазмы от угла вращательного преобразования. Характерной особенностью представленной кривой является более сильная зависимость от угла вращательного преобразования по сравнению с режимом бесстолкновительной плазмы. Для сравнения пунктиром показано теоретическое время жизни, определяемое коэффициентом диффузии для тороидальной системы в гидродинамической области. Теоретическая кривая [13,14] получается более крутой. Оценка времени жизни для $i = 0,25$, $r = 3$ см, $H = 10$ кэ и $T_e = 0,2$ эВ дает абсолютную величину $\tau = r^2 / [(2,4)^2 D_{кул}(1 + 8\pi^2/i^2)] = 4 \cdot 10^{-3}$ сек, по порядку совпадающую с экспериментальным временем жизни.

ОСОБЕННОСТИ УДЕРЖАНИЯ ПЛОТНОЙ ПЛАЗМЫ, СОЗДАННОЙ МЕТОДОМ СВЧ-ПРОБОЯ

Исследования распадающейся плазмы показали, что при заданных начальных условиях — напряженность магнитного поля, род газа и давление — скорость распада существенным образом зависит от активной фазы разряда, а именно от величины мощности, и, очевидно, как следствие, — от величины тока, протекающего по плазме (рис. 10). Из графика $\tau(I)$ видно, что с уменьшением тока и, соответственно, СВЧ-мощности, время жизни плазмы растет, однако, насыщения при малых токах не наблюдается, а предельные значения τ соответствуют минимальной мощности, при которой возможен пробой.

Эксперименты по исследованию характеристики удержания проводились с учетом этого факта, т. е. при минимальной мощности СВЧ, при которой возможен пробой и, следовательно, при минимальных значениях квазистационарного тока. В настоящее время нельзя утверждать однозначно, что является определяющим в установленном факте влияния активной фазы разряда на скорость диффузии распадающейся плазмы. Одной из возможных гипотез могло бы служить предположение о влиянии условий создания плазмы на ее пространственное распределение, т. е. на наличие продольного градиента плотности или на различное начальное распределение плазмы по сечению. Однако исследования продольного градиента плотности для двух различных газов (аргона и гелия) показали, что продольная неоднородность даже для аргоновой плазмы мала, т. е. меньше 20-30%. Кроме того, было показано, что основные характеристики удержания, например τ (H) (см. рис. 8) не зависят от сорта ионов.

ЗАКЛЮЧЕНИЕ

1. Более совершенная структура магнитного поля стелларатора TOP-1 позволила проследить зависимость времени жизни плазмы в бесстолкновительном режиме в существенно большем диапазоне углов вращательного преобразования (вплоть до 3π), чем это было сделано ранее [15]. Измерения показали, что полученный ранее линейный рост времени жизни продолжается и в области углов вращательного преобразования, больших 2π .

2. Точное знание структуры поля и проведение экспериментов по исследованию влияния резонансных возмущений (в области резонанса ± 1) на удержание плазмы позволяет утверждать, что изменение диффузионного размера не является определяющим в уменьшении времени жизни для областей резонансных значений углов вращательного преобразования.

3. Проведены исследования возможности получения плазмы в стеллараторе методом СВЧ-ионизации. Показано, что при взаимодействии СВЧ с плазмой наблюдается аномальное, нерезистивное поглощение энергии. Аномальное поглощение сопровождается появлением квазистационарного постоянного тока, протекающего по плазме. Параметры плазмы, получающиеся при СВЧ-ионизации, $n_{e \max} \approx 5 \cdot 10^{12} \text{ см}^{-3}$, $T_e \approx 3 \div 8 \text{ эВ}$.

Условия создания плазмы в значительной мере определяют поведение распадающейся плазмы.

4. Исследование характеристик удержания плотной плазмы показали, что полученное время удержания по величине совпадает с временем жизни, которое следует ожидать из теории гидродинамического равновесия для тороидальных систем. Зависимость от угла вращательного преобразования — более сильная, чем для бесстолкновительной плазмы, но несколько слабее теоретической для гидродинамической области частот столкновений. Зависимость времени жизни от величины магнитного поля при $H \geq 8 \text{ кэ}$ практически отсутствует.

Для детального выяснения зависимостей необходимо проведение дальнейших экспериментов с целью выяснения роли начальных распределений плотности по объему магнитной ловушки, определяемых способом создания плазмы.

Несомненный интерес представляет выяснение причины возникновения квазистационарного тока, его природы и механизма его влияния на характеристики удержания распадающейся плазмы. Весьма интересным

в дальнейшем представляется использование аномального поглощения СВЧ для нагрева плазмы, созданной в ловушке независимым образом.

Считаем своим приятным долгом выразить благодарность М. С. Рабиновичу и И. С. Шпигелю за внимание к работе и полезные дискуссии, Г. Н. Смирнову, Ю. А. Игнатьеву, В. Я. Судьенкову, И. В. Солдатскому, Д. М. Корфидову — за помощь в проведении экспериментов.

ЛИТЕРАТУРА

- [1] ЗУБКОВ, В. Л., ФЕДЯНИН, О. И., ХОЛЬНОВ, Ю. В., Препринт ФИАН СССР № 94 (1968).
- [2] АНДРЮХИНА, Э. Д., ФЕДЯНИН, О. И., ХОЛЬНОВ, Ю. В., Препринт ФИАН СССР № 118 (1969); Труды Физического института АН СССР им. П. Н. Лебедева (1971).
- [3] ДАНИЛКИН, И. С., КАРПЕНКО, И. К., Препринт ФИАН СССР № 114 (1967).
- [4] КОМИН, А. В., КРАСНИЦКАЯ, Л. С., МИНАЕВ, В. П., Препринт ИЯФ СО АН СССР № 225 (1968).
- [5] GIBSON, A., Phys. of Fluids 10 7 (1969) 1553.
- [6] АНДРЮХИНА, Э. Д., СОЛДАТСКИЙ, И. В., ФЕДЯНИН, О. И., ХОЛЬНОВ, Ю. В., Препринт ФИАН СССР № 117 (1970).
- [7] ИВАНОВСКИЙ, М. А., ПОПРЯДУХИН, А. П., Препринт ФИАН СССР № 118 (1970).
- [8] БАТАНОВ, Г. М., ГРЕБЕНЩИКОВ, С. Е., ИВАНОВСКИЙ, М. А., СБИТНИКОВА, И. С., ФЕДЯНИН, О. И., ШПИГЕЛЬ, И. С., "Труды ФИАН", Физика плазмы 32 (1965) 7.
- [9] ГАЛЕЕВ, А. А., САГДЕЕВ, Р. З., ЖЭТФ 53 (1967) 359; КОВРИЖНЫХ, Л. М., ЖЭТФ 56 (1969) 887.
- [10] БАТАНОВ, Г. М., САРКСЯН, К. А., СИЛИН, В. А., Труды IX Междунар. конф. по явлениям в ионизованных газах. Бухарест, 1969. Доклады № 4,7,9,10; ГЕККЕР, И. Р., СИЗУХИН, О. В., Письма в ЖЭТФ 9 7 (1969) 408; БАТАНОВ, Г. М., ГОРБУНОВ, Л. М., САРКСЯН, К. А., Письма в ЖЭТФ (в печати).
- [11] АКУЛИНА, Д. К., НЕЧАЕВ, Ю. И., ФЕДЯНИН, О. И., Труды III Всесоюзной конф. по диагностике плазмы, Сухуми, 1970.
- [12] ГОЛАНТ, В. Е., ЖИЛИНСКИЙ, А. П., ЖТФ XXXII 11 (1962) 1313; АЛИХАНОВ, С. Г., ЗАХАРОВ, В. Е., ХОРАСАНОВ, Г. Л., Атомная энергия 2 (1963) 137.
- [13] PFIRSCH, D., SCHLUTER, A., Report of the Max-Planck-Institute, Munich, NPI/PA/7/62.
- [14] ШАФРАНОВ, В. Д., Атомная энергия 19 (1965) 120.
- [15] БЕРЕЖЕЦКИЙ, М. С., ГРЕБЕНЩИКОВ, С. Е., КОССЫЙ, И. А., НЕЧАЕВ, Ю. И., РАБИНОВИЧ, М. С., СБИТНИКОВА, И. С., ШПИГЕЛЬ, И. С., Proc. of III Int. Conf. on Contr. Nucl. Fus. Res. 1968, D-5.
- [16] MEADE, D., YOSHIKAWA, S., Matt Q-24. Annual report, 1967, p. 71.

PARTICLE-CONFINEMENT MINIMA IN THE WENDELSTEIN II-a-STELLARATOR*

G. GRIEGER, W. OHLENDORF, H.D. PACHER, H. WOBIG, G.H. WOLF
Max-Planck-Institut für Plasmaphysik, Garching, Munich,
Federal Republic of Germany

Abstract

PARTICLE-CONFINEMENT MINIMA IN THE WENDELSTEIN II-a-STELLARATOR.

For not too large values of ι , previous experiments in contact-ionized barium plasmas have demonstrated confinement in accordance with classical theory, except in the neighbourhood of the low-order rational values of ι . The minima in confinement there observed may be understood as the result of stationary or non-stationary convection. The present experiments are concerned with the investigation of these minima. In particular, measurements of the dependencies of the peak density on the input flux, magnetic field strength, and neutral pressure have been carried out at various values of ι in order to test theoretically predicted relations. Low-frequency oscillations have been observed and the influence of shear on the position of the minima has been investigated. The conclusion is drawn that the most probable explanation for the observed minima is an unstable transition between the classical diffusive equilibrium and a stationary or non-stationary convection.

1. INTRODUCTION

As reported earlier [1] the confinement in the $\ell = 2$ Wendelstein II-a stellarator under certain conditions showed a behaviour predictable from classical theory. The dependence of the maximum ion density on various parameters, such as shear, disturbing magnetic fields etc., has been investigated. In the neighbourhood of certain values of ι ($\ell = 1/2, 1/3, 1/4 \dots^1$), minima in the traces of ion density versus ι were observed, for which until now no explanation could be found. It is the purpose of this work to obtain more information on these minima and to discuss various effects which might be responsible for their occurrence.

Theoretically, higher losses at rational values of ι can be the result of stationary or nonstationary convective motion. This motion could be initiated by one of the following effects.

- 1) Destruction of magnetic surfaces
- 2) Noncoincidence of the rational magnetic surfaces and $\oint \frac{dl}{B}$ surfaces
- 3) Inappropriate boundary conditions
- 4) Spatially localized plasma source
- 5) Instability

* This work was performed as part of the agreement between the Max-Planck-Institut für Plasmaphysik, Munich-Garching, and Euratom.

¹It should be noted that the ι scale, which one deduces from the assumption that the minima occur at rational values of ι , disagrees by 10% from the numerically calculated one. This discrepancy is thought to be due to errors in the mechanical positioning of the helical field windings and is presently being investigated by electron beam measurements.

In order to study the behaviour of the minima and their dependence on various parameters barium plasma was used as in the earlier measurements. This plasma was produced by contact ionization on a tungsten ball of 3 mm diameter which was heated by laser irradiation to a temperature of about 2500°K and suspended on 3 tungsten wires of 10 μ m diameter each. The base pressure was rather high, 10^{-6} Torr. In some cases argon was added in order to increase the neutral background.

The ion density was measured spectroscopically using resonance fluorescence [2]. The ball potential was monitored with a high impedance voltmeter and recorded. In addition the flux to an annular particle detector acting as a limiter was measured.

2. EXPERIMENTAL RESULTS

In order to study the properties of the minima the following parameters were varied:

- a) the toroidal magnetic field, B, between 3 kG and 6 kG
- b) the ion input flux, ϕ , between 5×10^{12} and 2×10^{13} sec $^{-1}$
- c) the neutral pressure between 1×10^{-6} Torr and 6×10^{-5} Torr by the addition of argon

The main object of this experiment was the plasma behaviour in the minima. The experimental conditions were not optimized specifically to achieve a close approach of the maximum density towards the classical value; at low neutral pressure agreement within a factor of 3 was typical.

2.1. Conditions for the Existence of the Minima

Most observations were made at minima No. 5 ($t \approx 1/5$) and No. 6 ($t \approx 1/6$); minima No. 4 ($t \approx 1/4$) and No. 7 ($t \approx 1/7$) have also been investigated.

In general, minima No. 5 and 6 behave in the following manner:

a) There exists a critical magnetic field above which the minimum occurs (see for example Fig. 1). Fig. 1 shows that minimum No. 5 occurs above a value of the magnetic field lying between 4 and 5 kG, whereas for minimum No. 6 the critical field lies between 5 and 6 kG. This critical magnetic field decreases with increasing neutral pressure, as shown in Fig. 2.

b) The width of the minima does not depend on neutral pressure but increases slightly with increasing magnetic field (see Fig. 1).

c) At low values of argon pressure, peaks in the middle of the minima are observed under some conditions. These peaks vanish at higher magnetic field and at higher neutral pressures.

d) As t is changed the transition between maxima and minima extends over a very small range of t ($dt \approx 0.005$). Simultaneously oscillations of the floating potential of the ball and of the flux to the particle detector are observed, with frequencies between 1 and 25 Hz.

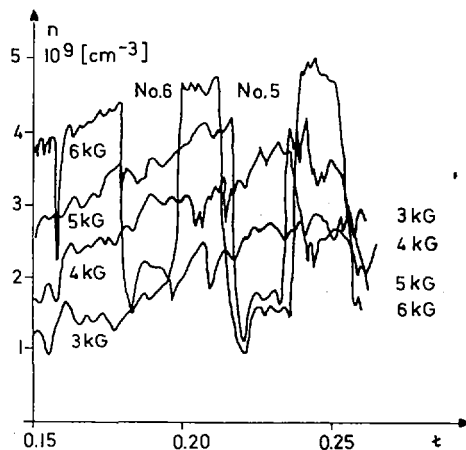


FIG. 1. Density versus ι at different magnetic fields and with constant argon pressure ($p_{Ar} = 1.0 \times 10^{-6}$ Torr, $\varphi = 1.75 \times 10^{15}$ s $^{-1}$).

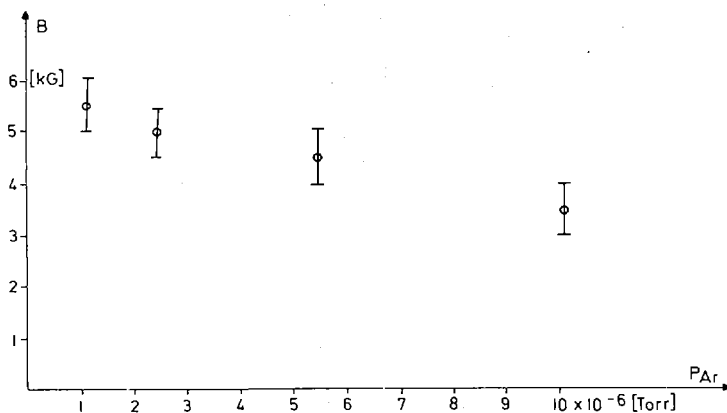


FIG. 2. Critical magnetic field for minimum No. 5 versus argon pressure ($\varphi = 5 \times 10^{12}$ s $^{-1}$).

2.2. Dependence on Magnetic Field

From the variation of the n vs ι curve with magnetic field the following results were obtained:

- a) At low pressure ($p_{Ar} < 5 \times 10^{-6}$ Torr) the density in most of the maxima appears to scale as $B^{3/2}$ (Fig. 3), while at higher argon pressure (p_{Ar} up to 10^{-5} Torr) it scales as B . The $B^{3/2}$ scaling at low argon pressure is probably a mixture of the classical B scaling and an anomalous effect which scales as B^2 .

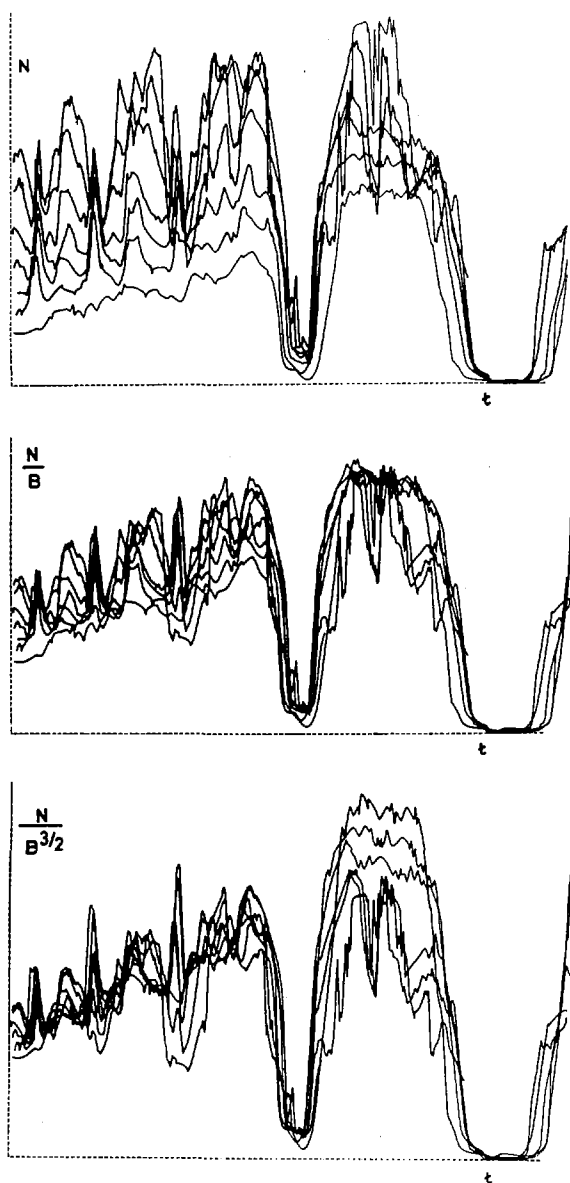


FIG. 3. N , N/B , $N/B^{3/2}$ as functions of ι for various magnetic fields ($p = 1.5 \times 10^{-6}$ Torr, $\varphi = 2 \times 10^{13}$ s $^{-1}$).

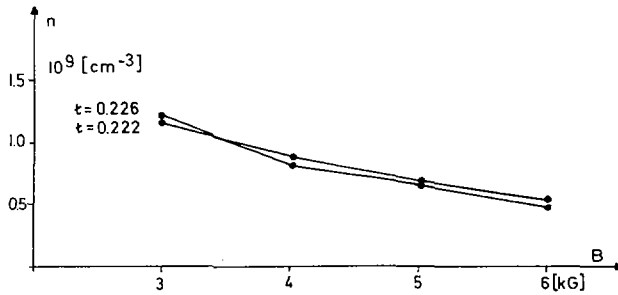


FIG.4. Density versus magnetic field in the minimum No.5 ($p_{Ar} = 1.0 \times 10^{-6}$ Torr, $\phi = 5 \times 10^{12} \text{ s}^{-1}$).

b) The density in the minima stays constant or decreases with increasing magnetic field (Fig. 4). The decrease was found at higher argon pressure (10^{-5} Torr), where the minima No. 5 and 6 were more pronounced than at low pressure.

2.3. Dependence on Ion Input Flux

For various magnetic fields, $n, \frac{n}{\sqrt{\phi}}, \frac{n}{\phi}$ were plotted versus B (Fig. 5). It is found that at low pressure the density scales as ϕ , but at higher neutral pressure a proportionality to $\phi^{1/2}$ results. With respect to the dependence on ion input flux there is no significant difference between minima and maxima.

2.4. Influence of Argon Pressure

The effect of interaction between plasma and neutral particles was studied by adding argon at pressures up to 5×10^{-5} Torr. With an increase of the pressure up to 10^{-5} Torr the plasma density in the maxima increases by approximately 100 per cent, while between 1×10^{-5} and 2×10^{-5} Torr the density decreases below its value at low pressure (Fig. 6). In the high pressure regime ion-neutral collisions begin to dominate over ion-electron collisions.

As for the minima, a distinction must be drawn between Nos. 5 and 6, and No. 4. In minima No. 5 and 6 the density is independent of neutral pressure in most cases. At high ion input flux ($2 \times 10^{13} \text{ sec}^{-1}$) and at high magnetic field an increase of the neutral pressure results in a decrease of the density (Fig. 7).

In minimum No. 4 the density first increases with increasing neutral pressure (up to 8×10^{-6} Torr) but decreases for even higher pressure. Simultaneously the minimum becomes wider. This broadening of the minimum occurs as a discontinuous process. As the neutral pressure increases, more and more minima appear in the neighbourhood of the original minimum, and at even higher neutral pressure the maxima between these minima vanish.

At high neutral pressure (2.1×10^{-5} Torr) minimum No. 4 shows the same unexpected scaling with B as the minima Nos. 5 and 6, i.e. a decrease of the density with increasing magnetic field.

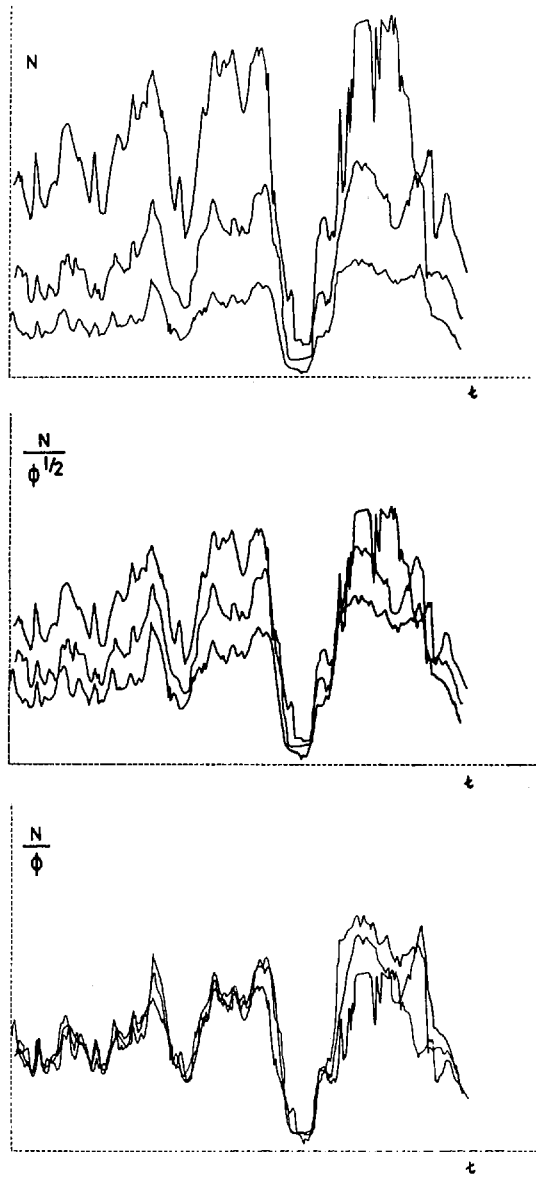


FIG. 5. N , $N/\sqrt{\phi}$, N/ϕ as a function of ι for different fluxes ($p = 1.5 \times 10^{-6}$, $B = 5.5$ kg).

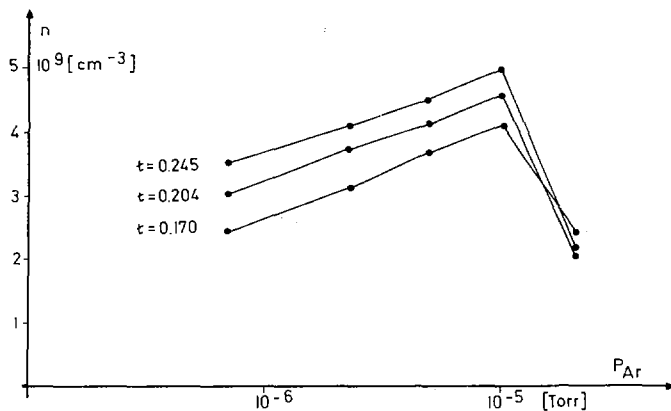


FIG. 6. Density versus argon pressure at various maxima ($\omega = 1.9 \times 10^{13} \text{ s}^{-1}$, $B = 5 \text{ kG}$).

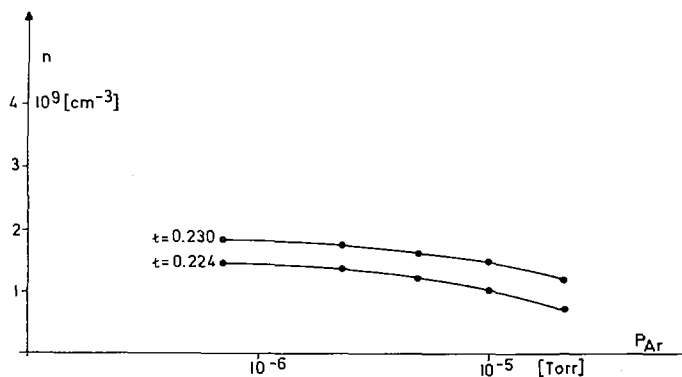


FIG. 7. Density versus argon pressure in minimum No. 5 ($\omega = 1.9 \times 10^{13} \text{ s}^{-1}$, $B = 6 \text{ kG}$).

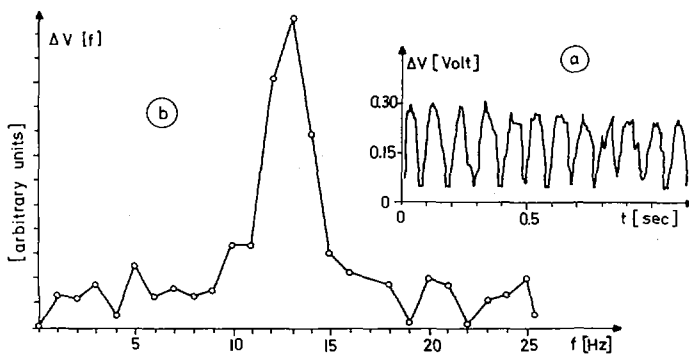


FIG. 8. Oscillation of sphere potential versus a) time, b) frequency ($\omega = 5 \times 10^{12} \text{ s}^{-1}$, $p = 1.1 \times 10^{-6} \text{ Torr}$, $B = 4.5 \text{ kG}$, $\tau = 0.194$).

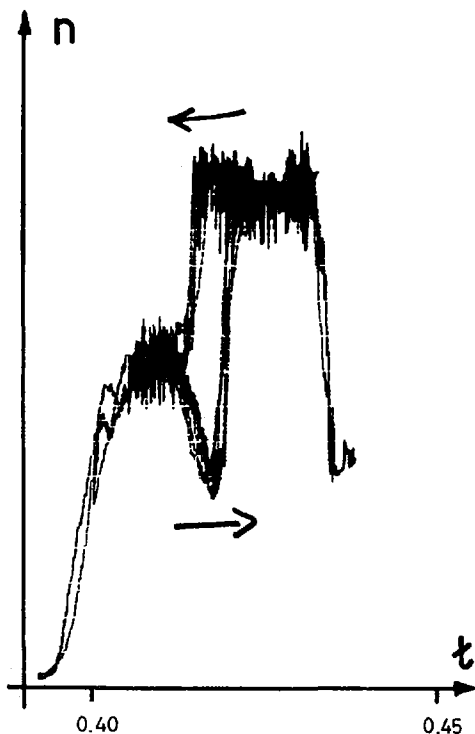


FIG. 9. Example of a hysteresis effect in the n -versus- t curve ($B = 4$ kG).

2.5. Oscillations

In the present experiment, high level, low frequency oscillations are observed under some conditions. As t is changed slowly, the onset of oscillations is followed by a transition of the density from the adjacent maximum to the density of the minimum. The oscillations show an increase in frequency (from 5-10 Hz to 11-20 Hz) and a decrease in amplitude as the center of the minimum is approached.

The main diagnostic used to investigate these oscillations in a preliminary manner was the floating potential of the hot sphere. A typical example of the oscillations is shown in figure 8 in which a frequency spectrum from 1-20 Hz is also demonstrated.

The oscillations in this example appear to be a single mode, but measurements at other values of t show a broader spectrum. Simultaneous oscillations of the flux to the particle detector and of the floating potential and the density signal of a probe are also observed. Unfortunately, lack of detailed experiments does not permit conclusions about the amplitude of the density fluctuations and their phase relation to the potential fluctuations.

A discontinuous transition between a higher density and a lower density state as t is varied can be subject to a hysteresis effect, that is, the transition occurs at a lower value of t when t is decreasing than when t is increasing (see Fig. 9). The upward as well as the downward transitions are preceded by a hard onset of oscillations.

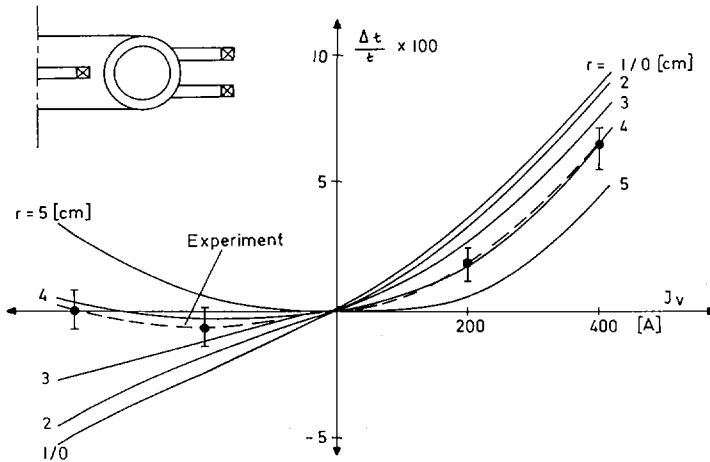


FIG. 10. Experimental and theoretical results for the relative shift in iota for minimum No.4 ($B = 4.5$ kG).

Little can be said at this point about the type of oscillations observed. However, the present data indicate that the amplitude of the oscillations increases with magnetic field. In the minima the oscillations show a decrease of frequency with increasing magnetic field, although this trend is not very definite. For all magnetic fields, an increase in frequency of oscillations at the edges of the minima with increasing argon pressure is observed.

In summary, the low frequency oscillations that are observed are strongly correlated with the transition between the maxima and the minima in density. The presence of oscillations of comparable amplitude in adjacent maxima and minima makes it possible that the oscillations are not directly responsible for the observed particle loss but rather accompany the transition from one state to another.

2.6. Influence of Shear on the Position of the Minima

To decide whether the occurrence of the minima results from the coincidence of a particular value of iota with a certain plasma radius, the magnetic shear was changed by superimposing a quadrupole magnetic field. For several plasma radii the variation of the relative change of the local iota with the shear producing currents was calculated numerically (Fig. 10), and was found to be markedly different on the axis ($r = 0$) and in the outer plasma region. In the latter, the sign of the shift of iota is independent of the direction of the "shear current", J_V , while on and near the axis a reversal of the "shear current" changes the sign of the shift of iota. Therefore, if the minima can only occur when a particular value of iota lies on some radius in the inner plasma region, the experimentally observed shift of a minimum should change sign on reversal of the shear current, while for the outer region the sign should remain constant. The experimental data are shown in figure 10 by the dotted line. They demonstrate that one may exclude the region with $r \lesssim 3$ cm as a possible origin of the observed minima. However, from this result one cannot decide which effect near the plasma boundary, determined by the limiter, is responsible for the poor confinement in the minima.

An additional experimental result is that the width of the minima does not vary with the applied shear ($\frac{\Delta \iota}{\iota} < 10$ %).

3. DISCUSSION

The possible causes for the occurrence of the minima, as stated in the introduction, will now be discussed on the basis of the experimental results.

3.1. Destruction of Magnetic Surfaces

Numerical calculations, starting from an ideal current distribution, showed the existence of magnetic surfaces, but also islands of relatively small radial extent were found at rational values of $iota$ ($\iota = 1/2, 1/3, \dots$). Besides, it could not yet be ruled out that the magnetic surfaces in the device are destroyed by unknown magnetic field perturbations. If, however, the plasma were to stream freely along the field lines to the boundary, an addition of neutral gas should inhibit the flow and therefore increase the plasma density. On the contrary, a decrease of plasma density with neutral pressure is observed in some cases (see section 2.4). For the same reason enhanced radial transport by parallel flow along the islands is also considered to be unlikely.

3.2. $\oint \frac{dl}{B} \neq \text{const. on Rational Surfaces}$

A theoretical model [3] which was developed for this case predicts a stationary convection at rational values of $iota$. But the asymmetries in the magnetic field needed to explain the experimental results are much larger than those possibly present in the machine. Furthermore, again, the theory predicts increasing density with increasing neutral pressure. In some cases, this dependence is apparently not observed (see 2.4).

3.3. Boundary conditions

If the outer boundary does not coincide with a magnetic surface, a static equilibrium with $n = \text{const.}$ on this surface is no longer possible. The more closely the $iota$ on this surface approaches a rational value of low order, the larger is the stationary convection which might occur. This convection, again, should be inhibited by increasing the neutral pressure. Although some of the experiments show a decrease of the density with increasing neutral pressure, the boundary conditions cannot be excluded as a possible cause for the minima. However, their description by a continuous variation of an unique equilibrium state seems to be implausible.

3.4. Spatially Localized Plasma Source

This cause can be ruled out by the result of the shear experiment (2.6), since there the region near the axis was excluded.

3.5. Non-stationary Processes

The experimental results clearly indicate that the transition between a maximum and a minimum is correlated with an instability (2.5). This conclusion is supported by the existence of a critical magnetic field and a critical neutral pressure (2.1). The results reported above show a great similarity to the nonstationary convection of a fluid heated from below [4]. Here also saw-tooth-like oscillations and hysteresis effects are predicted. As for the critical field and anomalous scaling with B , an analogous situation exists in the case of the instability of a positive column [5,6].

4. CONCLUSIONS

From these results it can be concluded that the most probable explanation for the minima in particle confinement time is an unstable transition between the classical diffusive equilibrium and a stationary or nonstationary convection. Although the experimental observations give no clear indications, the shear experiment gives some hint that the convective state might be determined by the conditions at the plasma boundary.

ACKNOWLEDGEMENTS

The authors would like to thank Dr. J. Hugill for his significant contributions in conducting the experiments as well as to the discussions. The help of J. Eisert in the computer evaluation of the experiments has been invaluable. The voluminous calculations of S. Rehker, as well as the calculations of B. Streibl and Miss I. Horn on the magnetic field structure have been necessary for the interpretation. Furthermore, the capable and untiring help of D. Köhler and the technical staff and of Miss H. Rupprecht is greatly appreciated.

REFERENCES

- 1 e.g. BERKL, E., ECKHARTT, D.E., V.GIERKE, G., GRIEGER, G., HINNOV, E., V.HAGENOW, K.U., and OHLENDORF, W., in *Plasma Physics and Controlled Nuclear Fusion Research*, p. 513, International Atomic Energy Agency, Vienna (1969).
- 2 HOFMANN, F.W., *Phys. Fluids* 7 (1964) 532.
- 3 WOBIG, H., to be published.
- 4 BUSSE, F.H., *J. Fluid Mechanics Pt. 2*, 28 (1967) 223.
- 5 GOLANT, V.E., DANILOV, O.B., and ZHILINSKII, A., P., *Zhur. Tekh. Fiz.* 33 (1963) 1043.
- 6 KADOMTSEV, B.B., *Plasma Turbulence*, Academic Press, London (1965).

APPENDIX:

OHMIC HEATING IN THE WENDELSTEIN STELLARATOR W II b

G. Grieger, R. Jaenicke, I. Katsumata, H. Renner, G. Schilling, J.-G. Wegrowe, G. H. Wolf

Max-Planck-Institut für Plasmaphysik, EURATOM-Association, 8046 Garching, Red. Rep. of Germany

In order to expand the barium plasma experiments on the W II a stellarator to hydrogen plasmas of higher temperatures and densities, another apparatus with similar constructional features was built: it is an $\ell = 2$ stellarator with major radius $R = 50$ cm, minor radius $r = 9$ cm. The internal limiter restricts the plasma radius to 6.5 cm. The toroidal magnetic field can achieve 7.5 kG in a stationary state, 15 kG pulsed.

The preionized plasma is subject to ohmic heating applied in two steps. For the preheating stage the energy of capacitor bank of 30 kJ is discharged into an air core transformer. The loop voltage induced in the torus reaches 40 V over 0,3 msec. The subsequent heating pulse applied by a second air core transformer should allow for quasistationary operation with a loop voltage of up to 3 V over 50 msec. Estimates yield expected temperatures of $T_i \approx T_e \sim 40$ eV and densities of $n \approx 10^{13}$. Preionization is accomplished with an RF discharge or ECRH, supplemented by an electron emitting filament.

The first test runs were used to obtain some information on the build-up and properties of the preheated plasma. Initial parameters are: filling pressure of H_2 of 10^{-4} Torr, toroidal magnetic field 7.3 kG and $\epsilon_0 \approx 0.1$. The plasma current thus achieved is about 1.5 kA. An estimate based on classical resistivity gives for the electron temperature $T_e \lesssim 20$ eV. A five-beam microwave interferometer operating at 70 GHz shows peak plasma densities of $5 \times 10^{12} \text{ cm}^{-3}$, assuming a plasma radius of 5 cm, and a decay time of typically 1.5 msec. The density reaches its maximum in 0.3 msec, in correlation with the time dependence of the plasma current, the latter decaying during 0.5 msec.

An x-ray energy analyzer pointed at the limiter shows a bremsstrahlung spectrum with energies up to about 40 keV, the maximum of its intensity occurring at the characteristic iron line. The emission of the bremsstrahlung is restricted to the build-up phase of the plasma density. Additional diagnostics as laser scattering, particle energy analyzers, spectroscopic and photographic methods, magnetic probes, etc. are installed and will be put into operation in the near future.

ACKNOWLEDGEMENTS

The authors gratefully acknowledge the help and stimulation of their colleagues who prepared the diagnostic methods to be used in the near future and who will participate in the above experiment as for instance Drs. J. Brown, J. Hugill, A. Gondhalekar, C. Mahn, W. Ohlendorf, A. van Oordt, H. Pacher, H. Ringler and W. Wobig; they are thankful for scientific discussions with Dr. v. Gierke. They are further indebted to the technical staff for its unflagging support. The leading contributions were made by: J. Kolos, K. Freudenberger, H. Goss and H. Ihmann, design; M. Zippe and H. Holitzner, electronics; U. Weber and E. Würsching, microwave techniques; W. Spensberger, J. Böhmerl, A. Gronmayer and G. Preißer, construction.

DISCUSSION

A. GIBSON: Can you rule out the possibility that the observed resonances may be associated with effects due to the ball support wires?

W. OHLENDORF: Yes, because we got the same qualitative features using photo-ionized Ba-plasma and ECRH-argon.

K. MIYAMOTO: You conclude that the resonant losses are connected with instability. Do you have any idea what kind of instability is involved?

W. OHLENDORF: The experiments give no definite indications as regards the nature of the instability, but it seems to be macroscopic.

ЭКСПЕРИМЕНТАЛЬНОЕ ИССЛЕДОВАНИЕ КВАЗИСТАЦИОНАРНЫХ ПРОДОЛЬНЫХ ПОТОКОВ ИОНОВ В СТЕЛЛАРАТОРЕ Л-1

М. С. БЕРЕЖЕЦКИЙ, С. Е. ГРЕБЕНЩИКОВ,
И. А. КОССЫЙ, И. С. СБИТНИКОВА, И. С. ШПИГЕЛЬ
Физический институт им. П. Н. Лебедева
Академии наук СССР, Москва,
Союз Советских Социалистических Республик

Abstract—Аннотация

EXPERIMENTAL INVESTIGATION OF QUASISTATIONARY LONGITUDINAL ION STREAMS IN THE L-1 STELLARATOR.

The results are presented of an experimental investigation of a quasistationary longitudinal ion stream detected in the L-1 stellarator. The possibility of the existence of closed ion and electron streams is predicted by the theory of plasma equilibrium in toroidal traps formulated by Pfirsch, Schlüter, Sagdeev, Galeev and others. However, the directed ion and electron motion superposed on the random thermal movement of charged particles in toroidal systems had not until recently been investigated experimentally. An attempt to study experimentally streams of this kind was made using the L-1 stellarator. With the help of a specially developed technique, the motion of the ion component in one direction along the axis of the toroidal chamber was recorded. The experimental results indicate an absence of either qualitative or quantitative agreement with the conclusions of the existing theory of plasma equilibrium in toroidal traps. In particular, the measured directed velocities considerably exceed the values predicted by the theory; the longitudinal stream detected in the experiment does not change its direction in the transverse cross-section of the chamber; the radial dependence of the directed velocities and their dependence on the rotational transform angle of the magnetic field lines — relationships which were found in the experiment — contradict the theoretical relationships. To explain the observed effect, the authors advance a hypothesis based on the existence of "blocked" particles in the toroidal trap. In the presence of radial electric fields, the longitudinal velocity distribution function of the particles becomes asymmetric, which leads to the appearance of an effective ion stream directed along the axis of the toroidal chamber. The relationships found in the experiment confirm the unique connection between the electric field and longitudinal ion stream values. Comparison of the experimental results with calculations performed on the basis of the suggested hypothesis confirms the validity of the explanation given of the mechanism whereby the ion stream occurs.

ЭКСПЕРИМЕНТАЛЬНОЕ ИССЛЕДОВАНИЕ КВАЗИСТАЦИОНАРНЫХ ПРОДОЛЬНЫХ ПОТОКОВ ИОНОВ В СТЕЛЛАРАТОРЕ Л-1.

В докладе приведены результаты экспериментального исследования квазистационарного продольного потока ионов, обнаруженного на стеллараторе "Л-1". Возможность существования замкнутых потоков ионов и электронов предсказывается теорией равновесия плазмы в тороидальных ловушках, развитой Пфиршем, Шлютером, Сагдеевым, Галеевым и др. Однако направленное движение ионов и электронов, накладывающееся в тороидальных системах на хаотическое тепловое перемещение заряженных частиц, не исследовалось до последнего времени экспериментально. На стеллараторе Л-1 была предпринята попытка экспериментального изучения потоков такого рода. С помощью специально разработанной методики удалось зарегистрировать движение ионного компонента в одном из направлений вдоль оси тороидальной камеры. Совокупность экспериментальных данных свидетельствует об отсутствии как качественного, так и количественного согласия с выводами развитой к настоящему времени теории равновесия плазмы в тороидальных ловушках. В частности, измеренные величины направленных скоростей существенно превосходят величины, предсказываемые теорией; экспериментально обнаруженный продольный поток сохраняет неизменное направление в поперечном сечении камеры; радиальная зависимость величин направленных скоростей, а также зависимость от угла вращательного преобразования магнитных силовых линий, полученные в эксперименте, противоречат теоретическим зависимостям. Для объяснения наблюдаемого эффекта в докладе выдвигается гипотеза, основанная на наличии в тороидальной ловушке "запертых" частиц. В присутствии радиальных электрических полей функция распределения частиц по продольным скоростям становится

асимметричной, что приводит к появлению эффективного потока ионов, направленного вдоль оси тороидальной камеры. Экспериментально полученные зависимости подтвердили однозначную связь между величинами электрического поля и продольного потока ионов. Сравнение результатов эксперимента с расчетами, выполненными в рамках предлагаемой гипотезы подтверждает справедливость выдвинутого в докладе объяснения механизма возникновения ионного потока.

ВВЕДЕНИЕ

Экспериментальное исследование удержания бесстолкновительной плазмы в стеллараторе Л-1 привело к обнаружению квазипостоянных потоков ионов, направленных вдоль оси тороидальной камеры (ось Z на рис. 1). Результаты первых экспериментов сообщались в докладе [1] на IV Европейской конференции по управляемому синтезу и физике плазмы (Рим, 1970 год). В этом же докладе было выдвинуто предположение о возможном механизме возникновения такого рода аксиального движения ионов. Явление, обнаруженное на стеллараторе Л-1, связывалось с наличием "резонансных" ионов, образующих "конус потерь" на функции распределения по продольным скоростям.

В данной работе подробно описываются измерения направленного движения ионов и приводятся результаты новых экспериментов, поставленных с целью проверки предполагаемого механизма формирования ионного потока. В ходе экспериментов определены факторы, влияющие на направление потока. Найдены зависимости аксиальных скоростей ионов от величины угла вращательного преобразования магнитных силовых линий, от напряженности тороидального магнитного поля H_z , а также от величины радиального электрического поля E_r .

Результаты измерений находятся в хорошем согласии с гипотезой, выдвинутой ранее [1]. Это позволяет рассматривать данную работу как экспериментальное подтверждение (по-видимому, одно из первых) существования "запертых" или "резонансных" ионов в тороидальных магнитных ловушках и как доказательство определяющей роли этих частиц в формировании направленного потока ионов. В работе отмечается, что подобного рода потоки с аналогичным механизмом их возникновения не являются специфическими для стеллараторов, а должны, по-видимому, существовать и в аксиально-симметричных системах.

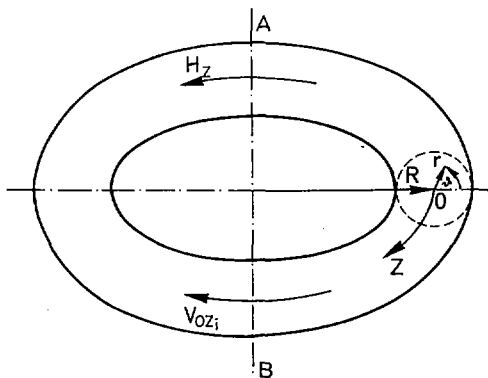


Рис. 1. Общий вид тороида.

1. "РЕЗОНАНСНЫЙ" МЕХАНИЗМ ВОЗНИКНОВЕНИЯ ПРОДОЛЬНЫХ ИОННЫХ ПОТОКОВ

Бишоп и Смит впервые обратили внимание [2] на то, что радиальные электрические поля в замкнутых ловушках при наличии стенок вакуумной камеры могут приводить к появлению ионных потоков вдоль оси Z. Однако расчет траекторий заряженных частиц и их отклонений от магнитных поверхностей был выполнен в [2] не корректно. Более строгий анализ движения заряженных частиц в тороидальных ловушках содержится в теоретических работах А.П. Попрядухина [3], А.А. Галеева, Р.З. Сагдеева и Г.Л. Берка [4]. В соответствии с данными работами в разряженной плазме при наличии радиального электрического поля E существует группа так называемых "резонансных" ионов и электронов. К категории "резонансных" относятся частицы, движущиеся в одном из направлений вдоль магнитного поля с продольными скоростями $v_{||}$, близкими к:

$$v_{||res} = \frac{v_E}{\theta} \quad (1)$$

где $v_E = c \cdot (E_r / H_z)$ – скорость азимутального дрейфа, а $\theta = (i_m r) / (2\pi R)$. i_m – угол вращательного преобразования магнитных силовых линий на периметре системы $2\pi R$. Физическое условие резонанса означает равенство нулю полного угла азимутального прокручивания заряженных частиц: $i = i_m + i_E = 0$, где i_E – угол вращательного преобразования, связанный с дрейфом в E_r и H_z полях: $i_E = (2\pi \cdot R \cdot v_E) / (v_{||} \cdot r)$.

С точки зрения описываемых в дрейфовом приближении траекторий резонансные частицы аналогичны частицам, "запертым" тороидальностью магнитного поля в отсутствие электрического. Резонансные частицы движутся по траекториям, проекция которых на плоскость, перпендикулярную оси Z, представляет те же "бананы", что и для запертых частиц. Отклонения траекторий резонансных частиц от магнитных поверхностей (Δr) существенно превосходят отклонения нерезонансных или "пролетных" частиц. Величину отклонения ионов для случая точного резонанса (расстройка $\Delta v = |v_{||} - v_{||res}| = 0$) можно оценить из соотношения:

$$\Delta r_i \approx \frac{1}{\theta} \sqrt{\frac{2r \cdot v_{gi}}{\omega_{ci}}} \quad (2)$$

где $v_{gi} = (v_r^2 + 1/2v_i^2) / (\omega_{ci} \cdot R)$ – скорость тороидального дрейфа, а ω_{ci} – ларморовская частота ионов.

Приближенное выражение для полуширины резонансной области имеет вид:

$$\Delta v_{res} \approx 2 \cdot \sqrt{v_{gi} \cdot r \cdot \omega_{ci}} \quad (3)$$

Повышенный уход резонансных ионов из тороидальной ловушки должен (при $E_r \neq 0$) приводить к асимметрии функции распределения по продольным скоростям. Этот эффект выражен особенно сильно в том случае, когда Δr_i больше размера системы и траектория резонансного иона пересекает стенку камеры. Попадая в резонансную область, ион покидает ловушку, и в пространстве скоростей формируется "конус потерь". Функция распределения по продольным скоростям при этом приобретает

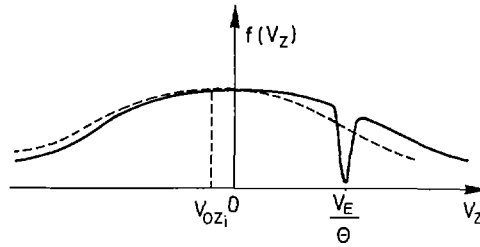


Рис. 2. Распределение ионов по продольным скоростям при наличии "конуса потерь" (сплошная кривая) и смещенное (в результате заполнения "конуса") распределение (пунктир).

вид, указанный на рис. 2 (сплошная линия). Поток ионов в "конус потерь", связанный со столкновениями, а также с развитием неустойчивостей [4], должен приводить к сглаживанию "ям" и, в результате, — к эффективному смещению максвелловской функции распределения по продольным скоростям на некоторую величину v_{0z1} (смещенное распределение показано на рис. 2 пунктирной линией). Смещение функции распределения равносильно появлению ионного потока с плотностью $S_z \approx n v_{0z1}$, направленного вдоль оси тороидальной камеры.

Следует отметить, что для возникновения "конуса потерь" необходимо выполнение соотношения:

$$\frac{a}{v_{gi}} < \tau_{0\text{эфф}} \quad (4)$$

означающего, что резонансный ион успевает достичь стенок камеры за время пребывания в резонансной области. $\tau_{0\text{эфф}}$ — соответствует наименьшей из величин $1/Y_{ie} \left(\frac{2 \cdot \sqrt{a/R}}{\pi} \right)^2$; $1/Y_{ii} \left(\frac{2 \cdot \sqrt{a/R}}{\pi} \right)^2$; $1/Y_{in}$. a — поперечный размер камеры, Y_{ie} , Y_{ii} , Y_{in} — частоты соударений ион-электрон, ион-ион и ион-нейтрал, соответственно.

В стеллараторе Л-1, в котором магнитные поля сравнительно невелики (2-10 кэ), а плазма, созданная методом внешней инжекции, имеет относительно горячие ионы ($T_i \approx 10-40$ эВ), отклонения Δr_i оказываются сравнимыми с размерами системы a ($\Delta r_i \approx a$). Для типичных условий эксперимента, как правило, выполняется и соотношение (4). Резонансная скорость близка к тепловой скорости ионов ($E_r \approx 3-10$ В/см; $\theta \approx 1/30$). Таким образом, из этих оценок следует, что в условиях нашего эксперимента весьма вероятно возникновение "конуса потерь" и образования "ям" на функции распределения $f(v_z)$ так, как это показано на рис. 2.

Описанный механизм не существенен для электронного компонента плазмы, в частности, из-за малости отклонения траекторий от магнитных поверхностей: $\Delta r_e \ll a$.

Оценки потока в "конус потерь", аналогичные проведенным для прямолинейных ловушек, можно выполнить и для стелларатора в предположении, что $E_r = 0$. Величина потока оказывается вполне достаточной для объяснения наблюдаемого аксиального движения уходом резонансных ионов (и соизмерима с полным потоком ионов на стенку камеры, определяемым по времени жизни распадающейся плазмы). Отсутствие решения с $E_r \neq 0$ не позволяет найти количественную зависимость продольного потока от по-

ложения резонансной скорости (1) на функции распределения ионов по продольным скоростям. Тем не менее, приближенный характер изменения v_{0zi} с изменением параметров плазмы и характеристик стеллараторного поля может быть установлен из следующих соображений.

Продольный импульс, приобретаемый ионами плазмы, равен импульсу, уносимому из плазмы резонансными частицами. Определим направленную скорость ионов плазмы v_{0zi} из соотношения:

$$n_{0i} \cdot v_{0zi} = B \cdot v_{||res} \cdot n_{resi} \quad (5)$$

Здесь n_{0i} — плотность нерезонансных ионов, n_{resi} — плотность резонансных ионов, а B — коэффициент, величина которого должна, по-видимому, определяться трением между нерезонансными ионами и нейтралами, степенью заполнения "ямы" на распределении по продольным скоростям и т.д. (и не зависит от положения резонансной области на функции распределения по продольным скоростям).

Определяя n_{resi} , как

$$n_{resi} = n_i \left(\frac{M_i}{2\pi k T_i} \right)^{1/2} \cdot \int_{v_{||res} - \Delta v_{res}}^{v_{||res} + \Delta v_{res}} e^{-\frac{M_i v_{||}^2}{2k T_i}} dv_{||} \quad (6)$$

где Δv_{res} находится из соотношения (2), получаем окончательное выражение для v_{0zi} :

$$v_{0zi} = B \cdot v_{res} \frac{\Phi(t_1) - \Phi(t_2)}{1 - \frac{\Phi(t_1) - \Phi(t_2)}{2}} \quad (7)$$

$t_{1,2} = \frac{1}{v_{T_i}} (v_{||res} \pm \Delta v_{res}) \Phi(t)$ — функция ошибок.

Из соотношения (7) можно определить характер зависимости продольного потока от E_r , i_m , N_z и T_i . Ниже приводятся результаты экспериментов и дано их сравнение с расчетами.

2. РЕЗУЛЬТАТЫ ЭКСПЕРИМЕНТА И ОБСУЖДЕНИЕ

Основные измерения направленных ионных потоков осуществлялись на установке Л-1 — двухзаходном ($\ell=2$) стеллараторе с плазмой, инжектируемой извне искровым источником. (Параметры и конструкция Л-1 приведены в работе [5]). Некоторые эксперименты проводились на стеллараторе "Тор-2" [6], обладающем рядом конструктивных особенностей по сравнению с "Л-1".

Методика, развитая нами для измерения направленных скоростей, подробно описана в работе [7]. Направленный поток ионов регистрировался с помощью электростатических зондов. Расчеты, проведенные в предположении существования смещенного на величину v_{0zi} максвелловского распределения ионов по скоростям и учитывающие возмущения, вносимые зондом в замагниченную плазму, позволили связать вид вольтамперных характеристик многосеточного зонда, работающего в режиме сбора ионного тока, с величиной отношения v_{0zi} / \bar{v}_{T_i} . Существование направленного потока приводит к появлению асимметрии в показаниях зонда при

двух взаимнопротивоположных положениях его. Вольтамперные характеристики при этом отличаются как величиной тока насыщения I_{i0} , так и наклоном в области тормозящих ионы потенциалов. Для количественных оценок величины v_{0zi} вводятся два коэффициента асимметрии: $k \equiv I_{i0\uparrow} / I_{i0\downarrow}$ и $\xi \equiv (T_{i\uparrow} - T_{i\downarrow}) / T_{i\text{ср}}$, однозначно зависящие от отношения направленной скорости к тепловой ($T_{i\uparrow}$ и $T_{i\downarrow}$ — эффективные температуры, соответствующие наклону характеристик при противоположных положениях зонда; значком \uparrow обозначается положение, при котором вектор потока ионов направлен на зонд, значком \downarrow — положение, при котором поток идет от зонда; $T_{i\text{ср}} = (T_{i\uparrow} + T_{i\downarrow}) / 2$). Коэффициенты k и ξ сложным образом связаны с отношением v_{0zi} / v_{Ti} и напряженностью магнитного поля H_z [7]. В сильных магнитных полях зависимость коэффициента k от v_{0zi} / v_{Ti} становится слабой и для характеристики этого отношения и его функциональной связи с H_z , i_m и другими параметрами удобно использовать коэффициент температурной асимметрии ξ . Ниже в ряде случаев для простоты в качестве относительной величины отношения v_{0zi} / v_{Ti} приводятся значения коэффициента температурной асимметрии.

Основные результаты проведенных измерений заключаются в следующем:

1) Вольтамперные характеристики многосеточного зонда, ориентированного так, что плоскость его коллектора перпендикулярна магнитному полю, свидетельствуют о существовании продольной скорости ионов. Экспериментально найденная величина v_{0zi} / v_{Ti} . Приблизненные оценки в рамках рассмотрения, приведенного в [7], показывают, что в зависимости от условий эксперимента величина отношения v_{0zi} / v_{Ti} колеблется в интервале $0,1 \div 0,5$. Оцененная плотность аксиального ионного тока, соответствующая такого рода направленным скоростям, примерно равна $1-4 \text{ мА/см}^2$.

2) Исследовано радиальное распределение величины v_{0zi} / v_{Ti} (типичная зависимость приведена на рис. 3). Направление вектора скорости неизменно по сечению камеры (так что средний ионный ток по сечению шнура не равен нулю). Величина продольной направленной скорости возрастает

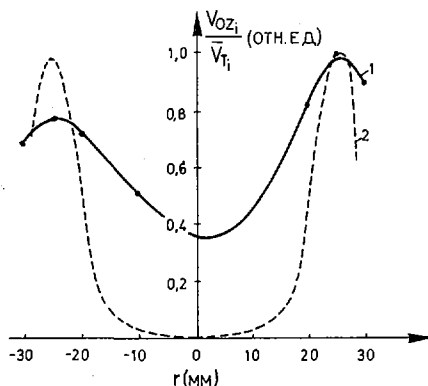


Рис. 3. Радиальное распределение продольной направленной скорости ионов (отнесенной к тепловой). $H_z = 2,0 \text{ кэ}$; $i_m = 4/3 \text{ л}$; $t = 400 \text{ мксек}$. (t — время, отсчитываемое от момента инъекции плазмы). 1 — эксперимент; 2 — расчет.

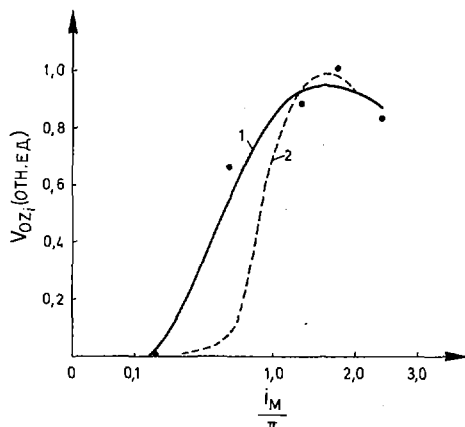


Рис. 4. Зависимость направленной продольной скорости ионов от величины угла вращательного преобразования магнитных силовых линий. $H_z = 2,0$ кэ; $r = 15$ мм; $t = 400$ мсек. 1 - эксперимент; 2 - расчет.

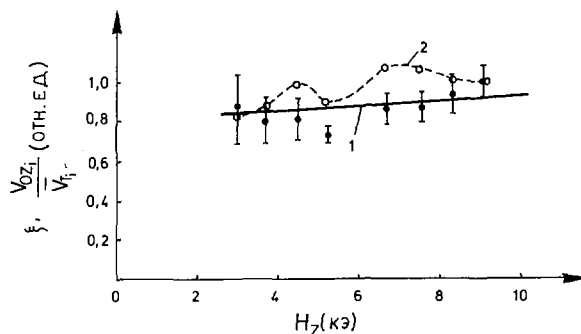


Рис. 5. Зависимость экспериментально определенного коэффициента температурной асимметрии ζ (кривая 1) и расчетных величин отношения v_{0z} / v_{T1} (кривая 2) от магнитного поля H_z . $i_m = 4/3 \pi$; $r = 15$ мм, $t = 400$ мсек.

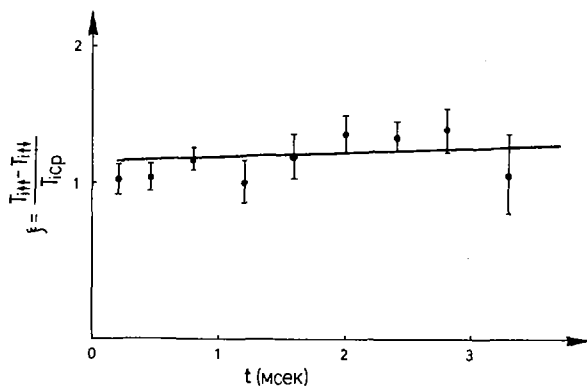


Рис. 6. Изменение во времени коэффициента температурной асимметрии ζ вольтамперных характеристик. $H_z = 6,0$ кэ; $i_m = 4/3 \pi$; $r = 15$ мм.

к периферии. Наблюдается некоторая асимметрия распределения v_{0zi} на внешней и внутренней сторонах тора.

3) Направление ионного потока однозначно определяется двумя факторами:

- а) направлением тороидального магнитного поля H_z и
- б) направлением прокручивания магнитных силовых линий (задаваемого направлением винтовой обмотки в стеллараторе). Изменение любого из этих факторов меняет направление потока на противоположное.

При известном направлении E_z , H_z и i_m легко определить направление резонансной скорости ионов $v_{||res}$. Знак v_{0zi} в рамках предложенной выше гипотезы должен быть противоположен знаку $v_{||res}$ (см. рис. 2). Экспериментально определенное направление аксиального движения ионов совпадает с тем, которое следует ожидать при "резонансном" механизме формирования ионного потока.

4) Наблюдается существенная зависимость величины направленного потока от угла вращательного преобразования i_m (рис. 4). В измерениях, проведенных на "Тор-2" (при использованной чувствительности зондов), не удалось зарегистрировать аксиальных направленных скоростей v_{0zi} при $i_m < 0,2\pi$. С ростом угла вращательного преобразования (в интервале $2\pi > i_m > 0,2\pi$) v_{0zi} заметно растет.

5) Экспериментально полученная зависимость коэффициента температурной асимметрии ξ от величины магнитного поля изображена на рис. 5. Данные эксперимента свидетельствуют о незначительных изменениях направленного потока при вариации магнитного поля от 3 до 9 кэ.

6) Аксиальный поток квазипостоянен и регистрируется в течение интервала, большего времени релаксации для ионного компонента. Характерная зависимость коэффициента ξ от времени приводится на рис. 6. Постоянство коэффициента температурной асимметрии во временном интервале 0,1-3,2 мсек свидетельствует о незначительных изменениях направленного ионного потока. (Время t отсчитывается от момента инъекции плазмы в ловушку).

На рис. 3, 4 и 5 приведены пунктирные кривые, соответствующие значениям v_{0zi}/v_{Ti} , полученным по формуле (7). При построении расчетных кривых использовались экспериментально определенные зависимости ионной температуры T_i и радиального электрического поля E_r от i_m , H_z и r [8,9]. Как следует из рис. 3-5, расчетные результаты не противоречат данным эксперимента.

Согласно (1), при постоянном i_m отношение резонансной скорости иона к тепловой пропорционально: $(v_{||res}/v_{Ti}) \sim (E_r/H_z \sqrt{T_i})$. Из проведенных ранее измерений следует, что с ростом H_z происходит рост как E_r , так и T_i . Существующая в экспериментальных условиях зависимость радиального электрического поля и ионной температуры от напряженности магнитного поля приводит к тому, что величина $v_{||res}/\bar{v}_{Ti}$ (а следовательно, и относительное положение резонансной скорости на функции распределения ионов по продольным скоростям) практически не меняется с изменением H_z во всем используемом в работе интервале. Это означает, что остается почти неизменным относительное число резонансных частиц. Следовательно, близка к постоянной и величина v_{0zi}/v_{Ti} , определяемая из выражения (7) (что объясняет слабую зависимость ξ от H_z - рис. 5). Наблюдаемая на эксперименте зависимость $T_i(H_z)$ приводит к незначительному изменению величины отклонения траектории резонансного иона от магнитной поверхности (Δr_i).

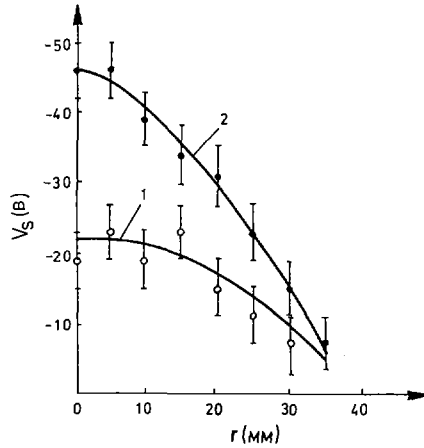


Рис. 7. Радиальное распределение плазменного потенциала. $N_2 \approx 3,0$ кэ; $i_m \approx 4/3 \pi$; $t = 400$ мксек. 1 – распределение, полученное в отсутствие электронного пучка ($V_{эл.п} = 0$). 2 – распределение, полученное с введением на ось камеры электронного пучка ($V_{эл.п} = -100$ В).

Отсутствие заметной временной зависимости коэффициента ζ (рис. 6) также может быть объяснено неизменностью величины $v_{||res}/v_{Ti}$ (со временем уменьшается как E_r , так и T_i , таким образом, что $v_{||res}/v_{Ti}$ меняется несущественно). Несмотря на уменьшение T_i , величина Δr_i остается соизмеримой с поперечным размером системы вплоть до времен $t \sim 3$ мсек.

В предложенном объяснении природа наблюдаемого аксиального потока определяется наличием E_r . Ввиду этого представляет несомненный интерес изменить E_r , не меняя ионную температуру, и проследить при этом характер изменения скорости продольного движения ионов. Если справедлив "резонансный" механизм формирования аксиального потока, то с ростом радиального электрического поля следует ожидать заметное уменьшение аксиальной направленной скорости ионов (см. (1)).

Дополнительный источник электронов (электронная пушка), помещенный на ось камеры, позволил существенным образом изменить величину радиального электрического поля. Характеристики пушки: ток эмиссии $I_{эм.} \approx 10-20$ мА, ускоряющее электроны напряжение $V_{эл.п} \approx -50-200$ В.

Механизм заполнения ловушки эмитируемыми электронами и формирования нового радиального поля не изучался достаточно подробно. Однако проведены измерения энергетического распределения электронов в различных точках по радиусу, показавшие, что в условиях эксперимента происходит весьма быстрое рассеяние пучка (за времена, много меньшие времен кулоновского рассеяния τ_{ei}) как по сечению камеры, так и в пространстве скоростей. Такое сильное "размытие" пучка приводит к изменению плазменного потенциала, характерное радиальное распределение которого показано на рис. 7 (кривая 2). Как следует из рис. 7, введение электронного пучка приводит к заметному изменению E_r . Экспериментально установлено, что величина радиального электрического поля однозначно определяется ускоряющим напряжением на электронной пушке.

Электрические поля определялись по распределению плазменного потенциала V_S , измеряемого горячим одиночным зондом [10]. Данные по

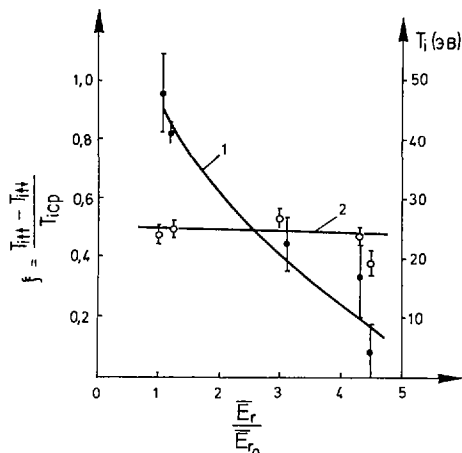


Рис. 8. Зависимость коэффициента температурной асимметрии вольтамперных характеристик ξ и ионной температуры T_i от величины радиального электрического поля. $N_z = 6,0$ кэ; $i_m = 4/3\pi$; $r = -10$ мм; $t = 400$ мксек.

температуре электронов и ионов, а также по величине продольного ионного потока получены с помощью многосеточного зонда. Экспериментально установлено, что введение электронного пучка, сопровождаемое существенным увеличением E_r , не приводит к заметному изменению T_e и T_i . Результаты измерения T_i приведены на рис. 8 (кривая 2).

На рис. 8 (кривая 1) изображена зависимость коэффициента температурной асимметрии ξ от величины среднего по радиусу электрического поля \bar{E}_r , приведенного к \bar{E}_{r0} — полю в отсутствие электронного пучка. Из рис. 8 следует, что с увеличением E_r , как и следовало ожидать по "резонансной" гипотезе, наблюдается заметное уменьшение направленного аксиального потока ионов. Распределения величины ξ по радиусу, полученные при $V_{эл.п.} = 0$ и $V_{эл.п.} = -100$ В, и приведенные на рис. 9, свидетельствуют о том, что эффект уменьшения направленной вдоль оси Z скорости ионов заметно сильнее на периферии камеры.

Все приведенные выше расчеты носят качественный характер и могут только описывать функциональные зависимости потока от ряда характеристик магнитного поля стелларатора и параметров плазмы. Для более строгой количественной оценки величины направленного потока необходимо учесть ряд дополнительных факторов. К числу наиболее очевидных следует отнести трение ионов о нейтралы и электроны. Уход "резонансных" ионов приводит к возникновению импульса отдачи у всей оставшейся плазмы. Поскольку потери резонансных ионов длятся все время, можно было бы ожидать непрерывного ускорения плазмы. Однако трение ионов о нейтральный газ должно приводить к установлению некоторой квазистационарной скорости. При достаточно высокой частоте соударений электрон-ион электроны увлекаются в направлении ионного потока, причем скорость направленного движения электронного компонента при малой плотности нейтралов достаточно близка к скорости ионов. Однако чрезвычайно малая величина отношения направленной скорости

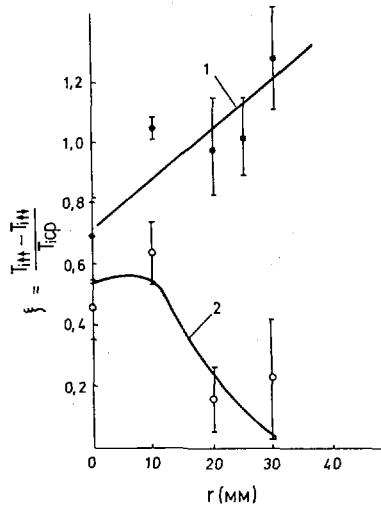


Рис.9. Радиальное распределение коэффициента ξ . $N_z = 6,0$ кэ; $i_m = 4/3 \pi$; $t = 400$ мсек. 1 - $V_{эл.п} = 0$. 2 - $V_{эл.п} = -100$ В.

к тепловой затрудняет применение методики электростатического зонда для обнаружения факта продольного движения электронов. По-видимому, именно появлением электронных аксиальных потоков и объясняется то, что в специально поставленных на Л-1 измерениях не удалось зарегистрировать магнитное поле, связанное с движением ионного компонента (при чувствительности метода ≈ 10 мА ионного тока).

ЗАКЛЮЧЕНИЕ

Достаточно хорошее соответствие экспериментальных результатов и расчетных зависимостей свидетельствует о том, что наблюдаемый в стеллараторах Л-1 и Тор-2 аксиальный ток ионов может быть объяснен в рамках предложенной модели – существования "резонансной" группы ионов. Поскольку рассматриваемый механизм обусловлен тороидальностью удерживающего магнитного поля в присутствии радиального электрического, очевидно, что продольный поток должен существовать не только в стеллараторах, но и в аксиально-симметричных тороидальных ловушках (токамак и др.). Отметим, что подобного рода потоки должны возникать всегда, когда существует повышенная диффузия "резонансных" частиц. Наличие "конуса потерь" приводит лишь к наиболее сильному проявлению эффекта. Подробный теоретический анализ причин, вызывающих направленный поток при диффузии плазмы в аксиально-симметричных системах, выполнен недавно Л.М. Коврижных [11].

Безусловно, роль "резонансных" ионов не ограничивается формированием аксиального потока. Оценки, проведенные нами, показывают, что поток "резонансных" ионов на стенку камеры близок к полному потоку ионов, определяемому по времени жизни плазмы. Возможно, что учет

ухода "резонансных" ионов позволит объяснить корреляцию между радиальным электрическим полем и временем жизни, наблюдаемую в эксперименте [8]. Кроме того, не исключено, что наличие продольной скорости у электронного компонента плазмы может сказаться на величине коэффициентов переноса в стеллараторах и, в частности, на величине коэффициента диффузии. В настоящее время нет еще достаточно ясного представления о роли обсуждаемых потоков в формировании макроскопических характеристик плазмы, таких, как электрическое поле, скорость диффузии частиц и т.д. Поэтому представляет определенный интерес продолжение изучения направленных потоков в стеллараторах и постановка аналогичных экспериментов на аксиально-симметричных системах.

Авторы признательны М.С.Рабиновичу за поддержку данной работы и постоянный интерес к ней, а также благодарны Л.М.Коврижных, А.П.Попрядухину и И.С.Данилкину — за ценные замечания и полезные дискуссии.

ЛИТЕРАТУРА

- [1] БЕРЕЖЕЦКИЙ, М.С., ГРЕБЕНЩИКОВ, С.Е., КОССЫЙ, И.А., ШПИГЕЛЬ, И.С., Доклад на IV Европейской конф. по управляемому синтезу и физике плазмы. Рим, 1970.
- [2] BISHOP, A.S., SMITH, C.G., Phys. Fl. 9 (1966) 1380.
- [3] ПОПРЯДУХИН, А.П., ЖТФ XL, вып.9 (1970) 1839.
- [4] BERK, H.L., GALEEV, A.A., Phys. Fl. 10 (1967) 441; ГАЛЕЕВ, А.А., САГДЕЕВ, Р.З., Доклады АН СССР 189 (1969) 1204.
- [5] БЕРЕЖЕЦКИЙ, М.С., ГРЕБЕНЩИКОВ, С.Е., ЗВЕРЕВ, Н.М., ШПИГЕЛЬ, И.С., Труды ФИАН 32 (1966) 7.
- [6] ИВАНОВСКИЙ, М.А., ПОПОВ, С.Н., ПОПРЯДУХИН, А.П., "Удержание плазмы в стеллараторах", препринт ФИАН СССР, № 94 (1968) Т-08865.
- [7] БЕРЕЖЕЦКИЙ, М.С., ГРЕБЕНЩИКОВ, С.Е., КОССЫЙ, И.А., ШПИГЕЛЬ, И.С., препринт ФИАН СССР, № 62 (1970) Т-08407.
- [8] БЕРЕЖЕЦКИЙ, М.С., ГРЕБЕНЩИКОВ, С.Е., КОССЫЙ, И.А., НЕЧАЕВ, Ю.И., РАВИНОВИЧ, М.С., СБИТНИКОВА, И.С., ШПИГЕЛЬ, И.С., Доклад CN-24/D-5. III Международ. конф. по физике плазмы и управляемому синтезу, Новосибирск, 1968.
- [9] БЕРЕЖЕЦКИЙ, М.С., ГРЕБЕНЩИКОВ, С.Е., КОВРИЖНЫХ, Л.М., КОССЫЙ, И.А., СБИТНИКОВА, И.С., ШПИГЕЛЬ, И.С., Доклад на III Европейской конф. по управляемому синтезу и физике плазмы. Утрехт, 1969.
- [10] БЕРЕЖЕЦКИЙ, М.С., ГРЕБЕНЩИКОВ, С.Е., КОССЫЙ, И.А., ЖТФ, XL, вып. 8 (1970) 1618.
- [11] КОВРИЖНЫХ, Л.М., Доклад CN-28/C-5. IV Международ. конф. по физике плазмы и управляемому синтезу, Мэдисон, США, 1971.

DISCUSSION

G. GRIEGER: The effect described is a resonance effect and I wonder if the shear present in your machine might not be sufficient to reduce the effect considerably or at least to restrict it to the outer edge of the plasma. I think there are signs of this in one of your slides.

S.E. GREBENSHCHIKOV: The dimensions of the resonance-particle bananas depend of course on both magnetic and electric shear. Quantitatively, the stream may vary with increasing shear, but qualitatively everything will be the same for large values of shear. The longitudinal move-

ment of the ions is due to the asymmetry of the diffusion coefficient in velocity space. With a radial electric field this asymmetry will always exist in the case of weak-collision plasmas.

E. K. MASCHKE: Is the asymmetry of the longitudinal velocity as a function of the major radius related to toroidal effects?

S. E. GREBENSHCHIKOV: Yes, it apparently is.

E. K. MASCHKE: Do your measurements permit you to estimate the number of particles in the loss cone and to make a comparison between the theoretical superbanana diffusion and the experimental life-time?

S. E. GREBENSHCHIKOV: All theoretical work on plasma diffusion in toroidal machines is based on the assumption of just a slight deviation of the particles from the magnetic surfaces. It is therefore difficult to make a comparison between theory and experiment in the case of large deviations or loss cones.

F. F. CHEN: How can you tell that this is a resonant-particle effect rather than a fluid effect such as that of the bootstrap Tokamak?

S. E. GREBENSHCHIKOV: To confirm the postulated mechanism of stream formation we studied the functional dependence on the parameters of the stellarator and plasma. All our measurements are in qualitative agreement with the proposed model. We cannot explain the observed dependences on the basis of any other theoretical works that we are acquainted with.

УДЕРЖАНИЕ ПЛАЗМЫ В ДВУХЗАХОДНОМ СТЕЛЛАРАТОРЕ ПРИ РЕЗОНАНСНЫХ ЗНАЧЕНИЯХ УГЛА ВРАЩАТЕЛЬНОГО ПРЕОБРАЗОВАНИЯ

М. А. ИВАНОВСКИЙ, С. Н. ПОПОВ,
А. П. ПОПРЯДУХИН, М. С. РАБИНОВИЧ
Физический институт им. П. Н. Лебедева
Академии наук СССР, Москва,
Союз Советских Социалистических Республик

Доклад представлен С.Е.Гребенщиковым

Presented by S.E.Grebenshchikov

Abstract—Аннотация

CONFINEMENT OF A PLASMA IN A TWO-TURN STELLARATOR AT RESONANCE VALUES OF THE ROTATIONAL TRANSFORM ANGLE.

In a stellarator with high shear the existence of resonance magnetic surfaces with magnetic field lines which close after a small number of revolutions ($i/2\pi = q/p$) is inevitable. The decrease in the plasma lifetime in the event of resonances, which has been observed in a number of devices, may be connected both with the enhanced sensitivity of the structure of magnetic surfaces to resonance perturbations (the magnetic surfaces acquire an island-type structure and consequently the dispersion length for the electrons decreases) and with the influence of closing of the magnetic field lines on stability and dispersion (the development of oscillations, the formation of convective cells and the mixing of trajectories which is associated with these phenomena). In the TOR-2 two-turn stellarator a field of resonance harmonics with a relative magnitude of the order of 10^{-4} has a highly destructive effect on the magnetic surfaces. However, with the help of a special compensation system it was possible to take these harmonics to the 10^{-6} - 10^{-7} level and to obtain magnetic surfaces of a satisfactory shape. At the resonances $1/2$ and $3/2$ the magnetic islands were compensated by fields with one spatial harmonic: $(q, p) = (1, 2)$ and $(3, 2)$ respectively. However, at the resonances $i/2\pi = 1$ and 2 it proved necessary to use two types of compensating harmonic: $(1, 1)$ and $(2, 2)$ for the resonance $i/2\pi = 1$ and $(2, 1)$ and $(4, 2)$ for the resonance $i/2\pi = 2$, their amplitude and phase being selected in the appropriate manner. A detailed study is made of the influence of perturbation compensation on the lifetime, the oscillation type and other confinement characteristics of a plasma in a stellarator. It is found that the dependence of plasma lifetime on the degree of compensation is complex, indicating the simultaneous influence of several of the factors noted above. However, the best magnetic field compensation does not destroy the plasma confinement time minima in the event of resonances, in spite of the fact that the density distribution over the cross-section of the device becomes symmetric. Study of the density distribution, potential and oscillation type shows that there is an increase in the transfer coefficients within the resonance surface. On the basis of the experimental data an attempt is made to explain the observed phenomena within the framework of existing theoretical conceptions.

УДЕРЖАНИЕ ПЛАЗМЫ В ДВУХЗАХОДНОМ СТЕЛЛАРАТОРЕ ПРИ РЕЗОНАНСНЫХ ЗНАЧЕНИЯХ УГЛА ВРАЩАТЕЛЬНОГО ПРЕОБРАЗОВАНИЯ.

В стеллараторе с большим широм неизбежно существование резонансных магнитных поверхностей с замыкающимися после небольшого числа оборотов магнитными силовыми линиями ($i/2\pi = q/p$). Уменьшение времени жизни плазмы при резонансах, которое наблюдалось на ряде установок, может быть связано как с повышенной чувствительностью структуры магнитных поверхностей к резонансным возмущениям (возникновение розеточной структуры поверхностей и, как следствие, уменьшение диффузионной длины для электронов), так и с влиянием замыкания силовых линий на устойчивость и диффузию (развитие колебаний, образование конвективных ячеек и связанное с ними перемешивание траекторий). На двухзаходном стеллараторе TOR-2 поле резонансных гармоник с относительной величиной порядка 10^{-4} сильно разрушает магнитные поверхности. Однако с помощью специальной системы компенсации можно было довести эти гармоники до уровня 10^{-6} - 10^{-7} .

и получить удовлетворительную форму магнитных поверхностей. Компенсация розеток при резонансах $1/2$ и $3/2$ могла осуществляться полями одной пространственной гармоники $(q, p) = (1, 2)$ и $(3, 2)$, соответственно. Однако при резонансах $i/2\pi = 1$ и 2 оказалось необходимо использовать два типа компенсирующих гармоник $(1, 1)$ и $(2, 2)$ для резонанса $i/2\pi = 1$ и $(2, 1)$ и $(4, 2)$ для резонанса $i/2\pi = 2$, соответствующим образом подбирая их амплитуду и фазу. В работе подробно изучено влияние компенсации возмущений на время жизни, характер колебаний и на другие характеристики удержания плазмы в стеллараторе. Оказалось, что зависимость времени жизни от степени компенсации имеет сложный характер, что указывает на одновременное действие целого ряда отмеченных выше причин. Однако самая лучшая компенсация магнитного поля не уничтожает минимумы времени удержания плазмы при резонансах, несмотря на то, что распределение плотности по сечению установки приобретает симметричный вид. Изучение распределения плотности, потенциала и характера колебаний свидетельствует о повышенных коэффициентах переноса внутри резонансной поверхности. На основе экспериментальных данных делается попытка объяснить наблюдаемые явления в рамках существующих представлений теории.

ВВЕДЕНИЕ

Как показали исследования последних лет [1, 2], в тороидальных магнитных ловушках с вращательным преобразованием топологии магнитных поверхностей может быть весьма сложной. Магнитные поверхности невозмущенного поля, для которых число вращения рационально $i/2\pi = q/p$ (i — угол вращательного преобразования), являются вырожденными, т. е. все силовые линии на таких поверхностях замыкаются сами на себя после p -обходов тора. При воздействии малой резонансной винтовой гармоники возмущения магнитного поля (гармоники с p -периодами по малому и q -периодами по большому обходу тора) вырождение снимается. При этом силовые линии, вообще говоря, не замыкаются на себя с образованием при этом розетки. Как показали экспериментальные исследования [3], особую опасность представляют случаи резонансов при небольших p . При $p = 1; 2$ размер розеток даже при высокой точности изготовления магнитной системы [4] может составлять значительную часть апертуры ловушки. Одновременно с ухудшением геометрии магнитного поля при основных резонансах $p = 1; 2$ наблюдалось также уменьшение времени удержания плазмы [5].

В этой связи возникла задача осуществления компенсации резонансных гармоник возмущений для основных типов резонансов. Решение этой задачи представляет самостоятельный интерес для развития экспериментальных работ по удержанию плазмы в замкнутых ловушках, так как даже в случае полной устойчивости плазмы в них сложная розеточная структура магнитных поверхностей может приводить к ухудшению удержания. В системах с большим широм присутствие резонансных поверхностей с малыми p в пределах апертуры ловушки неизбежно. Поэтому основные резонансы для них особенно опасны.

Представляет большой интерес также исследование эффекта замыкания силовых линий и в проблеме устойчивости плазмы. В работе [6] обнаружена связь между модами наблюдающихся колебаний и величиной $i/2\pi$. В работе [7] было показано, что имеет место возрастание амплитуды колебаний плазмы при резонансных значениях угла вращательного преобразования. Поэтому уменьшение времени жизни при выполнении условия $i/2\pi = q/p$ (особенно при больших значениях p [8]) может быть также связано с неустойчивостью плазмы.

На установке TOP-2 [4] осуществлялась компенсация резонансов $i/2\pi = 1/2$ и 1 .¹ Основные параметры установки приведены в табл. I.

¹ Первые экспериментальные данные по компенсации получены в работах [9], [10].

ТАБЛИЦА I. ПАРАМЕТРЫ СТЕЛЛАРАТОРА ТОР-2

Магнитное поле B_{0max}	25 кгс ($i \leq \pi/s$)
Число заходов винтового магнитного поля	2
Число шагов М.....	$1/2 \div 13$
Большой радиус тора R	62,5 см
Малый радиус камеры.....	3,6 см
Максимальный шир ν_B	$3 \cdot 10^{-2}$ ($B_{0max} = 4$ кгс)

Значения параметров установки, при которых производились измерения в данной работе:

$$\begin{aligned} B_0 &= 6 \div 8 \text{ кгс} \\ M &= 8 \\ \nu_B &= 1 \div 4 \cdot 10^{-3} \end{aligned}$$

МЕТОДИКА КОМПЕНСАЦИИ

1. При резонансе первого рода $i/2\pi = 1$ к появлению розеточной структуры магнитных поверхностей приводят гармоники возмущений, у которых $q/p = 1/1; 2/2; 3/3; \dots$, аналогично при резонансе второго рода $i/2\pi = 1/2$ — гармоники $q/p = 1/2; 2/4; \dots$ [2]. Поэтому для компенсации необходимо создать те же пространственные гармоники так, чтобы их амплитуды b_{pq} совпадали с амплитудами гармоник возмущений \tilde{b}_{pq} , а фазы были противоположны. Вообще говоря, для каждого рационального значения $i/2\pi$ ряд опасных гармоник возмущений бесконечен. Однако, благодаря его сходимости, при заданной точности компенсации достаточно скомпенсировать конечное число гармоник.

Амплитуды и фазы компенсирующих гармоник могут быть определены из экспериментально полученной структуры магнитных поверхностей при резонансе. В случае, когда резонанс имеет место вблизи поверхности со средним радиусом r_0 , и r_0 не слишком мало [2], отклонения \tilde{r} поверхностей от невозмущенных связаны с возмущениями магнитного поля формулой:

$$\frac{1}{2} \nu_B \left(\frac{\tilde{r}}{r_0} \right)^2 + \frac{r_0}{R} \left[\frac{i(r_0)}{2\pi} - \frac{q}{p} \right] \frac{\tilde{r}}{r_0} + \frac{q}{p} \sum_q \frac{\tilde{b}_{pq}}{q} \cos q(\theta + \theta_{pq}) = \text{const} \quad (1)$$

где $\nu_B = \frac{r_0^2}{2\pi R} \frac{di}{dr}$ — шир,

R — большой радиус тора,

\tilde{b}_{pq} — определяется из соотношения $\tilde{E}_r/B_0 = \tilde{b}_{pq} \sin q(\theta + \theta_{pq})$ (\tilde{E}_r — радиальная компонента pq -й гармоники, $\theta = (p/q)\varphi - (z/R)$; θ_{pq} — начальная фаза), $q/p = \text{const}$.

Если выбрать r_0 так, чтобы $i(r_0)/2\pi = q/p$, нетрудно определить \tilde{b}_{pq} , $\tilde{\theta}_{pq}$ из гармонического состава $(\tilde{r}/r_0)^2$. При таком способе определения

² При этом надо учитывать, что \tilde{r} и θ в формуле (1) представляют собой усредненное отклонение и усредненную фазу.

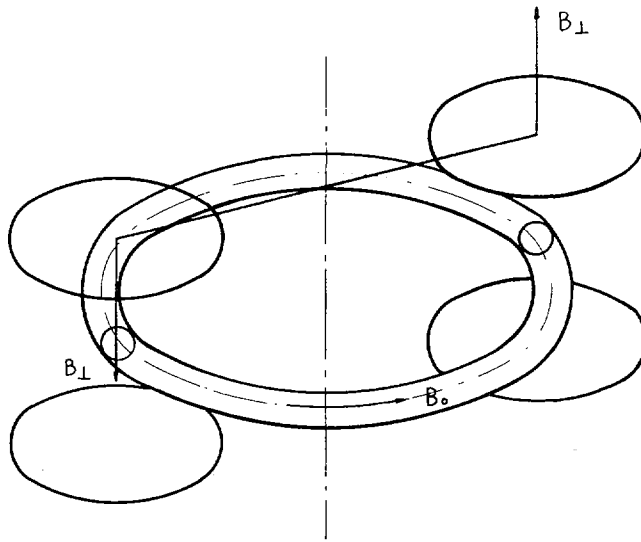


Рис. 1. Система компенсационных обмоток.

$\bar{b}_{r\varphi}, \theta_{r\varphi}$, однако, трудно достичь необходимой точности. Поэтому более приемлемой является последовательная компенсация отдельных гармоник, начиная с низшей $p = q = 1$, с контролем формы поверхностей на каждом этапе.

2. Для компенсации гармоники $q/p = 1/1$ была использована система обмоток (рис. 1), ток в которой изменялся во времени синхронно с основным магнитным полем. Компенсирующее поле создавалось двумя круговыми катушками, укрепленными на поворотной ферме так, что их плоскости были параллельны экваториальной плоскости тора, а центры находились на противоположных азимутах тора ψ и $\psi + \pi$. Имелась возможность включать также вторую пару катушек, расположенных в плоскости, симметричной относительно экваториальной плоскости (нижние катушки). Обмотки создают в основном компоненту магнитного поля B_{\perp} , перпендикулярную магнитной оси. Направление поля в катушках на противоположных азимутах противоположно. Возникающую при этом первую линейно-поляризованную гармонику поля можно представить в виде суммы винтовых гармоник с равными амплитудами и противоположным вращением. Одна из этих гармоник является лишней, но она практически не влияет на форму поверхностей, так как не является резонансной, а величина компенсирующего поля мала. Из расчета выполненного с учетом зависимости B_{\perp} от азимута ψ следует, что амплитуда винтовой гармоники $q/p = 1/1$ составляла $0,26 B_{\perp \max}$. Данная система обмоток создавала также и другие "лишние" гармоники: $q/p = 3/1$ с амплитудой $0,13 B_{\perp \max}$, $q/p = 1/2$; $3/2$; $1/3$; $3/3$ и т. д. Из них резонансной при $i/2\pi = 1$ является только гармоника $3/3$, но ее амплитуда весьма мала: $3 \cdot 10^{-3} B_{\perp \max}$. Четные по p гармоники, например $1/2$, не возникают, если включается нижняя пара катушек, а азимуты верхних и нижних катушек совпадают.

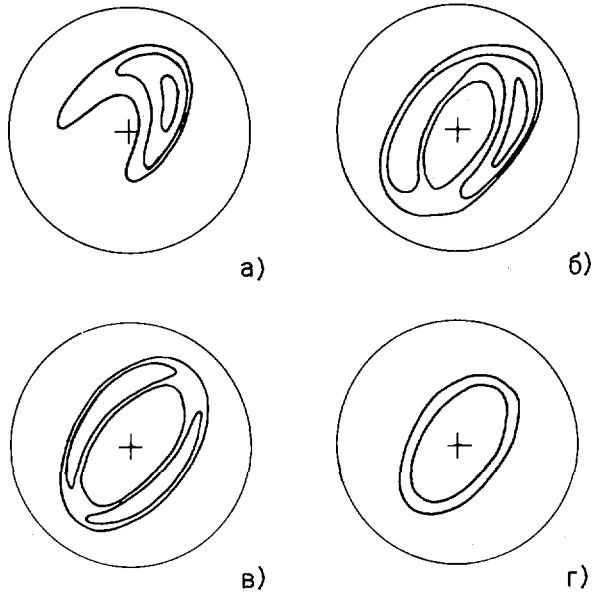


Рис. 2. Магнитные поверхности при резонансе $i/2\pi = 1$ при различной амплитуде гармоник $1/1$ и $2/2$:

- а) до компенсации $b_{11} \neq 0$, $b_{22} \neq 0$;
 б) гармоника $1/1$ частично скомпенсирована, $b_{22} \neq 0$;
 в) $b_{11} = 0$, $b_{22} \neq 0$;
 г) полная компенсация двух гармоник $b_{11} = 0$, $b_{22} = 0$.

Средний радиус резонансной поверхности — 1,6 см,
 окружность — камера с радиусом 3,5 см.

3. На установке TOP-2 винтовое магнитное поле создается системой эллиптических катушек [11], повернутых друг относительно друга на одинаковый угол $\Delta\gamma = \gamma_i^0 - \gamma_{i-1}^0$ (γ_i — угол ориентации отдельной катушки). Поэтому имеется простая возможность создавать компенсирующую гармонику с $p = 2$ за счет небольшого изменения ориентации некоторых катушек (изменения γ_i). При повороте одной катушки возникает спектр гармоник:

$$p = 2, q = 1, 2, 3 \dots \quad (2)$$

При резонансе $i/2\pi = 1/2$ из этого спектра для компенсации используется гармоника $q/p = 1/2$. Гармоника $2/2$ может быть использована при компенсации резонанса $i/2\pi = 1$. Поворотом нескольких катушек можно было исключать некоторые лишние гармоники, например, при симметричном повороте двух катушек, расположенных на азимутах ψ и $\psi + \pi$, возникают только четные или нечетные гармоники по q и т. д. Амплитуда компенсирующей гармоники пропорциональна углу расстройки $\gamma_i - \gamma_i^0$ катушки относительно исходного положения γ_i^0 , фаза определяется азимутом катушки ψ_i и ее первоначальной ориентацией $\theta_{2,q}^{(i)} = \gamma_i^0 - (q/2)\psi_i$. Ввиду того что азимуты ψ_i дискретны, для точного подбора фазы компенсирующего поля производилась дополнительная коррекция при помощи поворота катушки, для которой $\theta_{2,q}^{(i)} = \theta_{2,q}^{(i)} + (\pi/2)$.

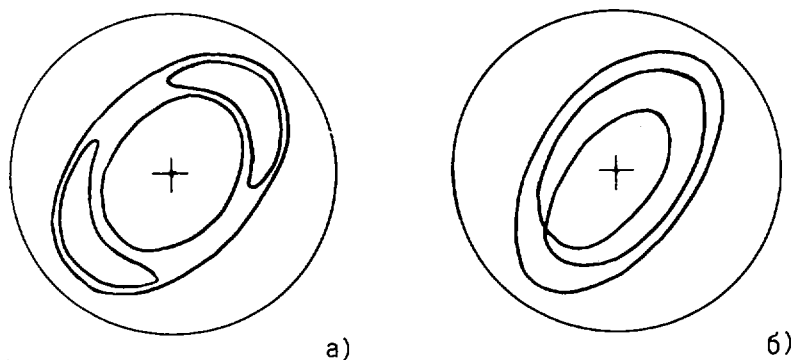


Рис. 3. а) Поверхности при резонансе $i/2\pi=1/2$, $r_c = 2$ см, $b_{21} = 1,5 \cdot 10^{-4}$.
 б) Поверхности при резонансе $i/2\pi = 1$, $r_0 = 1,6$, $b_{11} = 5 \cdot 10^{-5}$, $b_{22} = 0$.

4. Перейдем теперь к описанию экспериментальных результатов, полученных при компенсации.

Структура розеток при резонансе первого рода показана на рис. 2(а). Необходимую амплитуду b_{11} и фазу θ_{11} компенсирующего поля, благодаря применению быстродействующей сеточной методики измерения магнитных поверхностей [12], оказалось удобным определять подбором. Последовательные изменения формы розеток при компенсации показаны на рис. 2(б) и (в). Можно видеть, что при компенсации гармоники 1/1 наряду с уменьшением ширины розетки происходит также топологическое изменение структуры поверхностей: одна розетка разбивается на две. О правильном выборе b_{11} , θ_{11} можно судить из симметрии получающейся картины. Структура поверхностей на рис. 2(б) аналогична случаю резонанса второго рода $i/2\pi = 1/2$, см. рис. 3(а). Разница состоит в том, что при $i/2\pi = 1/2$ одна силовая линия образует обе розетки, в то время как при $i/2\pi = 1$ — только одну.

Чтобы достичь дальнейшего уменьшения ширины резонансной области при резонансе $i/2\pi = 1$ необходимо скомпенсировать гармонику $q/p = 2/2$. Компенсация осуществлялась методом подбора b_{22} , θ_{22} ; окончательная картина поверхностей, полученных после компенсации гармоник 1/1 и 2/2, приведена на рис. 2(г), где изображены две поверхности, между которыми расположена резонансная поверхность. Структуру поверхностей внутри резонансной полосы измерить не удалось из-за недостаточности длины свободного пробега электронов при имевшемся вакууме (10^{-6}) (по мере уменьшения ширины розетки уменьшается скорость ее обхода).

При резонансе второго рода $i/2\pi = 1/2$ компенсация осуществлялась таким же способом, как и для гармоники 2/2. В спектре (2) в этом случае использовалась гармоника $q/p = 1/2$. Структура магнитных поверхностей, полученная после компенсации, аналогична показанной на рис. 2(г). Ширина оставшейся резонансной области составляла ≈ 3 мм.

УДЕРЖАНИЕ ПЛАЗМЫ В ОБЛАСТИ РЕЗОНАНСОВ $i/2\pi = 1/2$ и 1

1. Плазма в установке создавалась инъекцией поперек магнитного поля из 8-ми искровых плазменных пушек, расположенных на равных расстояниях по внешней образующей тора. Пушки работали синхронно и инжектировали плазму в момент максимума магнитного поля.

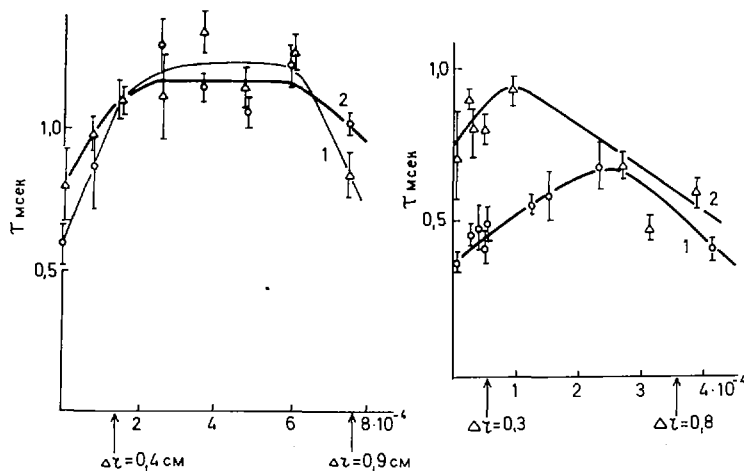


Рис. 4. Зависимости τ от амплитуды резонансных гармоник:
 а) Резонанс $1/2$, $B_0 = 8$ кэ, b_{21} — амплитуда гармоники $1/2$ при $g_0 = 2$ см; 1) $g_c = 2$ см, 2) $g_0 = 1,3$ см. Указана полуширина розеток на радиусе 2 см.
 б) Резонанс $1/1$, $B_0 = 6$ кэ; 1) $g_0 = 1,8$ см, 2) $g_0 = 1,2$ см. Полуширина розеток на радиусе 1,8 см.

Плотность плазмы в ловушке определялась микроволновым методом по сдвигу резонансной частоты открытого резонатора [13], работавшего на длине волны 4 мм. Ось зеркал резонатора была перпендикулярна магнитной оси стелларатора и направлена по малой оси эллиптического сечения магнитной поверхности, т. е. определялась средняя плотность вдоль малого диаметра эллипса (см. рис. 6).

Отсчеты плотности производились через 100 мксек, начиная от плотности $\sim 3 \cdot 10^{11}$ см $^{-3}$ до уровня $1 \cdot 10^9$ см $^{-3}$. Скорость распада плазмы $1/\tau = -(1/n)(dn/dt)$ была непостоянная во времени, τ изменялось от 0,2–0,3 мсек в начале распада до 1–2 мсек при уровне плотности 10^9 . В дальнейшем для характеристики удержания плазмы приводится τ среднее в интервале плотности $1,6 \cdot 10^{10}$ – $4 \cdot 10^9$.

Исследование влияния резонансных гармоник на удержание плазмы производилось путем определения зависимостей $\tau(\bar{b}_{pq})$ от амплитуды данной гармоники при некоторых выбранных значениях i вблизи резонансов и зависимостей $\tau(i)$ в окрестности резонансного значения при некоторой фиксированной амплитуде гармоники и в режиме компенсации.

Зависимости $\tau(\bar{b}_{pq})$, полученные для резонанса $i/2\pi = 1/2$, рис. 4(а), и для резонанса $i/2\pi = 1$, рис. 4(б), при изменении амплитуды нижней гармоники качественно подобны друг другу. Максимальная величина \bar{b}_{pq} на графиках рис. 4 приблизительно соответствует тому уровню возмущений, который был получен в установке TOP-2 после геометрической юстировки системы ($4 \div 7 \cdot 10^{-4}$). Ширина резонансных розеток при этом составляет около половины размера апертуры поверхностей.

Как видно из графиков на рис. 4, при уменьшении ширины розетки τ сначала несколько возрастает, а затем при более точной компенсации снова падает. Таким образом, в двух крайних случаях полной компенсации и большей розетки значения времени жизни плазмы оказались близки друг к другу.

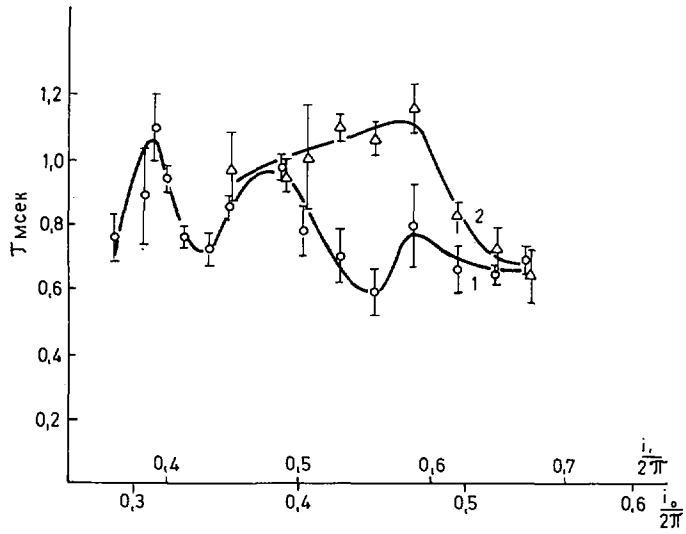


Рис. 5. Зависимость τ от i_0 - вращательное преобразование на оси, i_1 - на радиусе $r_0 = 2,6$ см, 1) $b_{21} = 0$, 2) $b_{21}(r_0 = 2 \text{ см}) = 4,5 \cdot 10^{-4}$.

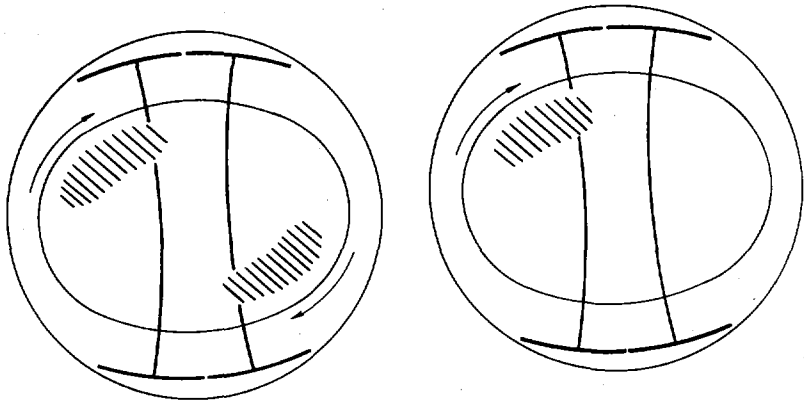


Рис. 6. Расположение открытого микроволнового резонатора в сечении вакуумной камеры. Схематически показано пересечение микроволнового луча неоднородностями плотности плазменного шнура, соответствующими модам $m = 2$ и $m = 1$ при резонансах $i/2\pi = 1/2$ и 1.

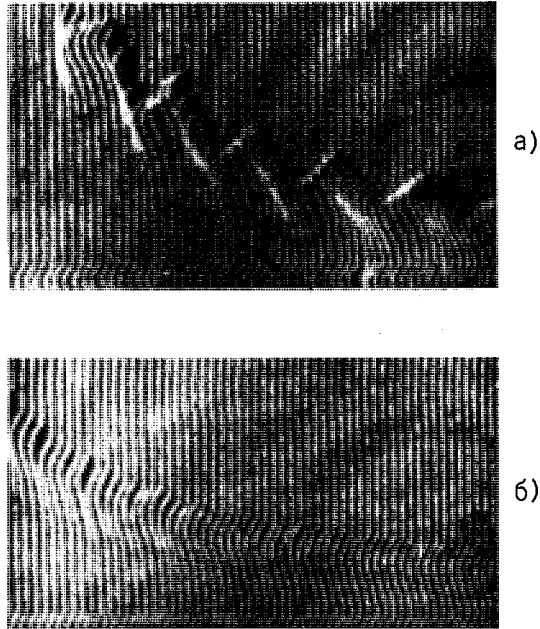


Рис. 7(а) и (б). Осциллограммы микроволновых измерений плотности ($i/2\pi = 1/2$): (а) полная компенсация; (б) без-компенсации.

На рис. 5 приведена зависимость τ от i при точной компенсации гармоники $1/2$ (кривая 1) и та же зависимость при амплитуде, равной $4 \cdot 10^{-4}$ при $\tau_0 = 2$ см, что соответствует максимуму τ на кривой $\tau(b_{12})$. Провал τ в области $i/2\pi = 0,4 \div 0,5$ при точной компенсации соответствует резонансу $i/2\pi = 1/2$ и исчезает при введении оптимальной амплитуды гармоники $1/2$ (кривая 2). Вне указанной области i влияние гармоники $1/2$ не существенно. Вид кривых распада плазмы $n(t)$ в резонансной области меняется при изменении амплитуды гармоники $1/2$. При плотности $n > 10^{10}$ см $^{-3}$ обе кривые практически совпадают. Дальнейший ход распада существенно различный. Если при $\tilde{b}_{21} = 0$ распад продолжается по экспоненте, то в случае $\tilde{b}_{21} = 4 \cdot 10^{-4}$ распад существенно неэкспоненциальный: τ растет со временем.

Для резонанса $i/2\pi = 1$ наблюдаются аналогичные закономерности, однако максимальное τ при некоторой оптимальной ширине розетки первого рода остается меньше τ в соседней нерезонансной области, т. е. провал сохраняется при любых амплитудах b_{11} . Отметим также, что уменьшение τ в этом случае ($i \approx 2\pi$) наблюдается в более широком интервале i , чем для резонанса $i/2\pi = 1/2$, и продолжается в область, где $i > 2\pi$ и геометрическое искажение поверхностей за счет гармоники b_{11} пренебрежимо мало.

2. Исследования колебаний плазмы показали, что имеется сильное влияние степени компенсации на их амплитуду.

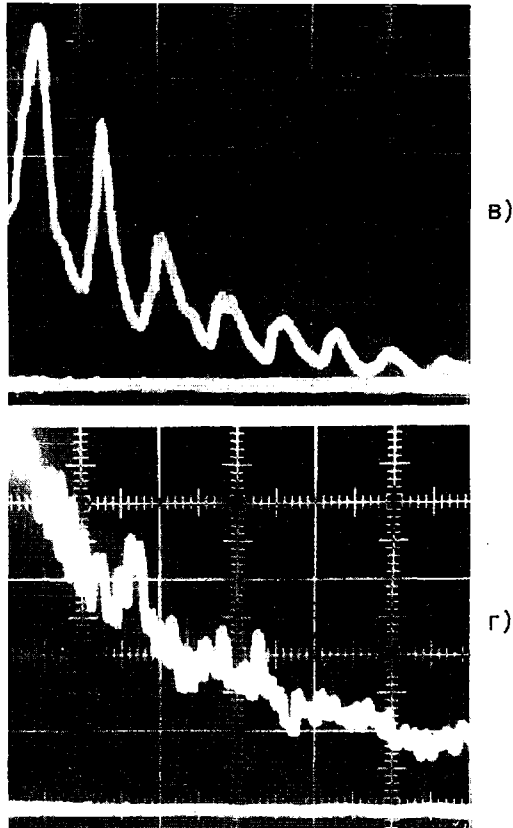


Рис. 7(в) и (г). Осциллограммы зондового сигнала ($i/2\pi = 1$):
(в) полная компенсация; (г) без компенсации.

Измерения производились двумя методами. С помощью микроволновой диагностики (рис. 6) исследовались колебания средней по длине луча плотности плазмы. Зондовый метод позволял производить измерения распределения амплитуды колебаний по радиусу. На рис. 7 приведены осциллограммы хода плотности во времени при резонансах $i/2\pi = 1/2$ и 1 для случая полной компенсации и при наличии розеток. Видно, что компенсация приводит к значительной раскочке колебаний. На графиках рис. 8 приведена зависимость амплитуды колебаний плотности плазмы $\Delta n/n$ от величины резонансной розетки при резонансах $i/2\pi = 1/2$ и 1, для разных моментов времени после инжекции плазмы. Зонд располагался на таком расстоянии от магнитной оси, при котором колебания максимальны.

На рис. 9 приведено радиальное распределение амплитуды колебаний. При изменении радиуса резонансной поверхности качественно наблюдалось соответствующее перемещение точки максимальной амплитуды колебаний.

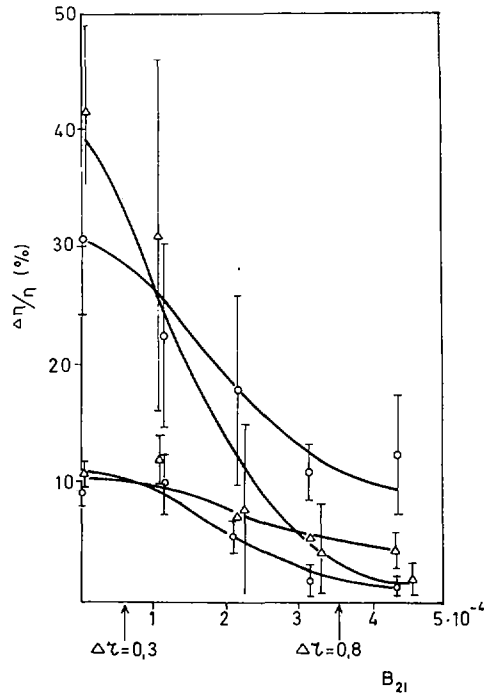


Рис. 8(а). Зависимость относительной амплитуды $\Delta n/n$ колебаний от амплитуды гармоники $1/2$:

(b_{21} — амплитуда при $r_0 = 2$ см)

- | | | |
|---|------------------------------------|---------------------------|
| ○ | через 1 мсек после инъекции плазмы | } зондовые измерения |
| △ | "- 1,8 мсек "- "- "- "- | |
| ● | через 0,8 мсек "- "- "- "- | } микроволновые измерения |
| ▲ | "- 1,4 мсек "- "- "- "- | |

Из рис. 8 видно, что при увеличении размера розеток происходит значительное уменьшение амплитуды колебаний, причем это ослабление сильнее для более поздних моментов времени после инъекции.

При полной компенсации колебания плотности носят весьма регулярный характер (рис. 7). Период колебаний T составлял приблизительно 100 мсек при резонансе $i/2\pi = 1/2$ (по зондовым и микроволновым измерениям). При резонансе $i/2\pi = 1$ зондовые измерения давали длительность периода колебаний около 200 мсек, а микроволновые измерения в два раза меньшую величину. Эти данные легко понять, если предположить, что при $i/2\pi = 1/2$ в сечении плазменного шнура образуются два сгустка, которые вращаются вокруг магнитной оси с частотой $\Omega = 2\pi/2T$ (мода $m = 2$). Изменение средней плотности во времени, фиксируемое микроволновым методом, понятно из рис. 6. При резонансе $i/2\pi = 1$ в сечении шнура образуется один сгусток (пространственная мода $m = 1$), который при своем вращении дважды пересекает микроволновый луч. Подобное предположение о пространственной структуре неоднородности плотности подтверждается одновременными измерениями колебаний двумя зондами, проведен-

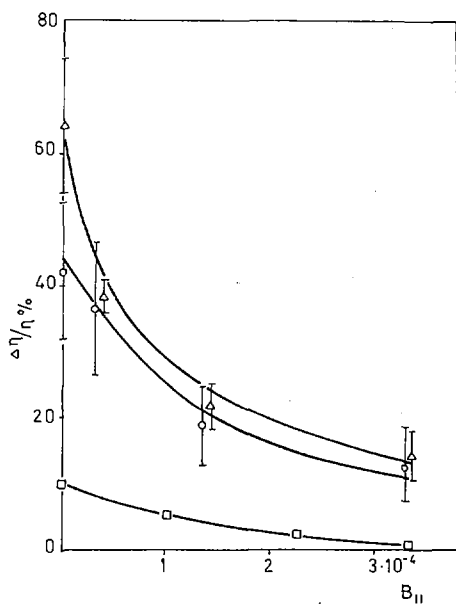


Рис. 8(б). Зависимость относительной амплитуды $\Delta n/n$ от амплитуды гармоники 1/1:
 ○ через 1 мсек после инжекции плазмы } зондовые
 Δ или 1,8 мсек -"- -"- } измерения
 □ через 0,8 мсек после инжекции плазмы } микроволновые
 } измерения

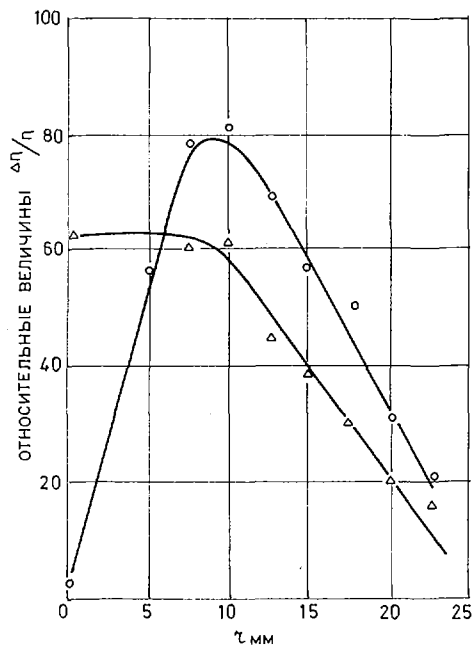


Рис. 9. Радиальные распределения амплитуды Δn колебаний (○) и плотности n плазмы (Δ).

ными при резонансе $i/2\pi = 1$. Сдвиг фаз между регистрируемыми ими колебаниями приблизительно соответствовал рассчитанному, исходя из предположения о наличии моды $m = 1$. При перемещении одного из зондов в пределах $0,5 < x < 2$ см от магнитной оси частоты колебаний, фиксируемых обоими зондами, оставались одинаковыми, что свидетельствует о вращении неоднородности плотности как целого.

Радиальное электрическое поле, определенное по зондовым измерениям плавающего потенциала при $i/2\pi = 1/2$, составляло $E_2 = 5$ В/см при $r_0 = 1,5$ см. Частота вращения неоднородности плотности плазмы приблизительно соответствует скорости дрейфа sE_r/V_0 ($V_0 = 8$ кэ). При резонансе $i/2\pi = 1$ распределение электрического поля имело параболический характер, и в области, где регистрировались колебания $\Omega_E = sE_r/r_0V_0$ сильно изменялось. Поэтому трудно говорить о соответствии частоты колебаний и частоты вращения из-за электрического дрейфа.

3. Сопоставляя уменьшение времени жизни плазмы при приближении к точной компенсации с одновременным ростом амплитуды колебаний, естественно сделать вывод о том, что причиной повышенного ухода плазмы является развивающаяся в этих условиях неустойчивость. При большом радиальном размере розеток время жизни плазмы, очевидно, уменьшается просто из-за уменьшения эффективного поперечного размера плазмы.

Представляет интерес выяснить механизм подавления неустойчивости при увеличении размера розеток.

Нарастание амплитуды колебаний в резонансных областях, соответствии пространственной моды неоднородности плотности числу вращения $i/2\pi$ при резонансах $i/2\pi = 1/2, 1$ и другие данные о колебаниях, приведенные в разделе 2, указывают на то, что они являются локализованными вблизи вырожденной поверхности $r = r_0$. Тогда, очевидно, розетки не должны влиять на характер колебаний, если их ширина $\Delta r \ll x$, где x — ширина области локализации. Если же $\Delta r \sim x$, то можно ожидать подавления колебаний.

Известен целый ряд неустойчивостей, локализованных вблизи вырожденных поверхностей [14,15]. В условиях данного эксперимента речь может идти только о потенциальных колебаниях, поскольку величина $\beta = [8\pi n(T_e + T_i)] / V_0^2$ была крайне мала ($\beta \sim 10^{-7}$, $T_i = 10 \div 15$ эВ, $T_e = 2 \div 4$ эВ). Произведем в качестве примера оценку ширины области локализации для дрейфоводиссипативной и конвективной неустойчивости. Согласно работе [15], для этих типов неустойчивости мы можем написать:

$$\frac{x}{r_0} < \frac{1}{v_B} \sqrt{\frac{P_d}{m\lambda_e}} \left(\frac{m_e}{m_i}\right)^{1/4} \quad (3)$$

где v_B — шир,

P_d — ларморовский радиус ионов,

m — номер моды колебаний,

λ_e — длина свободного пробега электронов.

Подставляя в эту формулу значения $P_{d1} = 7 \cdot 10^{-2}$ см; $m = 2; 1$ $\lambda_e = 2 \cdot 10^3$ см; $v_B = 1-2 \cdot 10^{-3}$, при $r_0 = 1,5$ см, мы получим $x \approx 1$ см, что согласуется с приведенным выше условием подавления локальной моды колебаний $\Delta r \sim x$. Выражение (3) для ширины области локализации, поскольку $x \sim 1/\sqrt{\lambda_e}$, дает также качественное согласие с тем фактом, отмеченным в разделе 2, что влияние розеток на колебания больше при меньших уровнях плотности (в более далекие от инжекции моменты времени).

Для строгой идентификации типа наблюдаемой неустойчивости нужны специальные исследования. Как это видно из полученных экспериментальных данных, при таких исследованиях влияние структуры магнитных поверхностей может быть весьма существенным.

КРАТКИЕ ВЫВОДЫ

1. Разработана методика компенсации резонансных возмущений магнитных поверхностей. Осуществлена компенсация для наиболее опасных основных резонансов $i/2\pi = 1/2$ и 1. В случае резонанса $i/2\pi = 1$ для достижения точности $b \sim 10^{-6}$ потребовалась компенсация двух гармоник $q/p = 1/1$ и $2/2$.

2. Исследования влияния возмущений на удержание плазмы при резонансах $i/2\pi = 1/2$ и 1 показали, что существует некоторая оптимальная ширина розеток Δr_0 , когда время жизни плазмы максимально. При больших размерах розеток и при полной компенсации время жизни меньше.

3. Обнаружено значительное нарастание колебаний при улучшении степени компенсации. Одновременное уменьшение времени жизни плазмы можно связать с этим явлением.

4. Обнаруженные колебания носят локализованный характер. Независимо от конкретного типа колебаний ширина области их локализации x должна уменьшаться при увеличении магнитного поля B_0 и ширины ν_B . Поэтому, если $\Delta r \sim x$, оптимальная для удержания плазмы степень точности компенсации должна повышаться с ростом этих параметров в тороидальных магнитных ловушках.

В заключение авторы считают своим приятным долгом поблагодарить И. С. Данилкина, А. А. Рухадзе и И. С. Шпигеля за ценные обсуждения и В. А. Дрындина — за помощь при проведении измерений.

ЛИТЕРАТУРА

- [1] МОРОЗОВ, А. И., СОЛОВЬЕВ, Л. С., Вопросы теории плазмы, вып. 2, Госатомиздат, М., 1963.
- [2] СОЛОВЬЕВ, Л. С., ШАФРАНОВ, В. Д., Вопросы теории плазмы, вып. 5, Госатомиздат, М., 1967.
- [3] БЕРЕЖЕЦКИЙ, М. С., ГРЕБЕНЩИКОВ, С. Е., ПОПРЯДУХИН, А. П., ШПИГЕЛЬ, И. С., ЖТФ 35 12 (1965) 2167.
- [4] ИВАНОВСКИЙ, М. А., ПОПОВ, С. Н., ПОПРЯДУХИН, А. П., Сб. "Удержание плазмы в стеллараторах". Препринт №94 ФИАН, Москва, 1968, стр. 42.
- [5] АКУЛИНА, Д. К., БАТАНОВ, Г. М., БЕРЕЖЕЦКИЙ, М. С., ГРЕБЕНЩИКОВ, С. Е., РАБИНОВИЧ, М. С., СВИТНИКОВА, И. С., ШПИГЕЛЬ, И. С., Plasma Physics and Controlled Nuclear Fusion Research II (Conf. Proc., Culham, 1965) IAEA, Vienna, 1966, p. 733.
- [6] БЕРЕЖЕЦКИЙ, М. С., ГРЕБЕНЩИКОВ, С. Е., КОССЫЙ, И. А., НЕЧАЕВ, Ю. И., РАБИНОВИЧ, М. С., СВИТНИКОВА, И. С., ШПИГЕЛЬ, И. С. Plasma Physics and Controlled Nuclear Fusion Research I (Conf. Proc., Novosibirsk, August 1968) IAEA, Vienna, 1969, p. 529.
- [7] YOUNG, K. M., Phys. Fl. 10 (1967) 213.
- [8] BERKL, E., ECKHARTT, D., v. GIERKE, G., GRIEGER, G., HINNOV, E., v. HAGENOV, K. U., OHLONDORF, W.; Plasma Physics and Controlled Nuclear Fusion Research I (Conf. Proc., Novosibirsk, August 1968) IAEA, Vienna, 1969, p. 513.

- [9] ИВАНОВСКИЙ, М.А., ПОПРЯДУХИН, А.П., Компенсация резонансных возмущений магнитного поля стелларатора. Препринт №118, ФИАН, Москва, 1970.
- [10] АНДРЮХИНА, Э.Д., СОЛДАТСКИЙ, И.В., ФЕДЯНИН, О.И., ХОЛЬНОВ, Ю.В., "Влияние резонансной структуры магнитного поля на удержание бесстолкновительной плазмы в стеллараторе TOP-1". Препринт №117 ФИАН, Москва, 1970.
- [11] ПОПОВ, С.Н., ПОПРЯДУХИН, А.П., ЖТФ, вып. 2 (1966) 390.
- [12] ПОПРЯДУХИН, А.П., ЖТФ (в печати); также Препринт №108 ФИАН, Москва, 1969.
- [13] АКУЛИНА, Д.К., НЕЧАЕВ, Ю.И., ФЕДЯНИН, О.И., Доклад на Международ. конф. по диагностике плазмы. Сухуми, 1970.
- [14] РУХАДЗЕ, А.А., СИЛИН, В.П., УФН 96 вып. 1 (1968) 87.
- [15] КАДОМЦЕВ, Б.Б., ПОГУЦЕ, О.П., Вопросы теории плазмы, вып. 5, Госатомиздат, М., 1967.

DISCUSSION

R. M. SINCLAIR: There are a number of perturbations in a real stellarator that can perturb the surfaces and form islands. How closely did your calculations of the amount of correcting harmonics required for complete correction agree with the observed amount of corrections required?

S. E. GREBENSHCHIKOV: After measuring the size of the magnetic islands one can calculate the necessary magnitude of the compensating harmonic. Conversely, having compensated the excitations in an actual machine, one can then superimpose the resonance excitation and measure the dimensions of the magnetic islands. The experimental data are in good quantitative agreement with theory.

G. GRIEGER: Is it not true that magnetic field components lying within the plane of the torus are the most dangerous ones for a stellarator field? Why have you chosen correction field which are mainly perpendicular to the plane of the torus?

S. E. GREBENSHCHIKOV: The most dangerous magnetic surface excitations are resonance excitations. For every rational angle of rotation of the lines of force it is necessary to estimate what excitations may contain resonance harmonics. From the point of view of compensation of the excitations it is of no importance how the corresponding harmonic is set up. This may be done in different ways.

G. GRIEGER: I should just like to add that in our experiments with the Wendelstein stellarator we found that correction fields strongly affect the maxima of the confinement time but there were only slight effects on the minima.

A. J. LICHTENBERG: It is possible for resonance between a harmonic of the island frequency and the rotational frequency to break up the main island into second-order islands, thereby giving rise to stochastic regions of field lines and, hence, enhanced fluctuations. Did you observe any region of stochastic field lines near the islands? I am suggesting that the compensating fields might strengthen the second-order resonances.

S. E. GREBENSHCHIKOV: In this experiment no stochastic destruction of magnetic surfaces was observed. Apparently, the amplitudes of the excitations were relatively small.

PLASMA CONTAINMENT IN THE PROTO-CLEO STELLARATOR

R. A. E. BOLTON, J. HUGILL, D. J. LEES,
W. MILLAR, P. REYNOLDS
UKAEA, Culham Laboratory,
Abingdon, Berks,
United Kingdom

Abstract

PLASMA CONTAINMENT IN THE PROTO-CLEO STELLARATOR.

Measurements are reported of the confinement of plasma in the Proto-Cleo $\ell = 3$ stellarator. The plasma has been produced in this machine by a variety of methods, including the irradiation of a metallic target by a laser beam, and covers a density range from 10^9 to 10^{13} cm^{-3} and electron temperatures from 2 to 10 eV. With the rotational transform of up to 2π radians used in the experiment, the plasma conditions embrace both the collisionless and the collisional regimes.

A comparison of the observed confinement times and those derived from recent theories is given. The enhanced diffusion predicted for the intermediate and collisionless regimes has been shown by various authors to be explicable theoretically in terms of a unidirectional current flowing along the minor axis of the torus. The experimental evidence for the existence of this current is summarized.

1. INTRODUCTION

Proto-Cleo is a small $\ell=3$ stellarator in which the scaling of plasma containment times with magnetic field, collision frequency and rotational transform has previously been studied in the Galeev and Sagdeev intermediate regime [1,2,3]. In the present paper experiments are described where the containment studies have been extended into the collisionless and into the collisional regimes by developments in plasma production methods. Also, an attempt has been made to detect the presence of the unidirectional current flowing along the minor axis of the torus predicted by several authors for axisymmetric systems.

2. APPARATUS

The machine, plasma parameters and methods of injection are summarized in Table I.

The design of the stellarator is described in detail in References [1] and [3]. It is unusual in that the helical winding is placed inside the vacuum tank so giving good access to the plasma and, by virtue of the titanium layer coated on the winding and the walls remote from the plasma, high pumping speed for neutral gas. Two helical windings have been used in turn. The first with a 30° pitch angle has a medium amount of magnetic shear and the second with a 45° pitch angle, high magnetic shear. The helical winding is connected in series with the toroidal magnetic field winding across a large electro-

TABLE I. PARAMETERS OF THE PROTO-CLEO $\ell = 3$ STELLARATOR

Parameter		Medium Shear	High Shear
Major radius R (true toroid)	(cm)	40	40
Helical winding mean radius	(cm)	9	10
Separatrix radius (to apex of trefoil) r_m	(cm)	5	5
Vacuum vessel cross section	(cm)	40 X 40	40 X 40
Number of field periods on torus		7	13
Maximum toroidal field B_ϕ	(kG)	3	5
Computed maximum rotational transform at plasma boundary ι_0	(radians)	1.24π	2.1π
Mean shear length $\bar{L}_S = \frac{2\pi R}{\iota_0}$	(cm)	130	76
Maximum shear parameter $\theta = \frac{r_m}{\bar{L}_S} \min$		0.26	0.52
Useful time duration of fields	(ms)	10	10
Plasma density	(cm^{-3})	$10^9 - 10^{13}$	$10^{10} - 10^{11}$
Electron temperature	(eV)	2-10	2-10
Ion temperature	(eV)	4-30	4-30
Confinement time	(ms)	1-10	1-10
Base pressure	(Torr)	10^{-8}	10^{-8}

lytic capacitor bank which gives a useful time duration of the magnetic field of about 10 ms.

3. PLASMA PRODUCTION

In the previous work [1,2,3], the plasma was produced by hydrogen loaded titanium guns based on the Ashby design [4] which limited the plasma density to the range 10^{10} to 10^{11}cm^{-3} . Since then a combination of a titanium gun working near its point of exhaustion, followed by E C R H to reduce the density still further to $\sim 10^9 \text{cm}^{-3}$ and at the same time increase the electron temperature to about 10eV, has enabled the collisionless regime to be attained.

An increase in density up to 10^{12}cm^{-3} has been found possible by the use of the Ashby gun with pulsed gas feed and the beginning of the collisional regime has thereby been achieved. Further extension into this regime to a density of 10^{13}cm^{-3} has been gained by the use of a plasma produced by

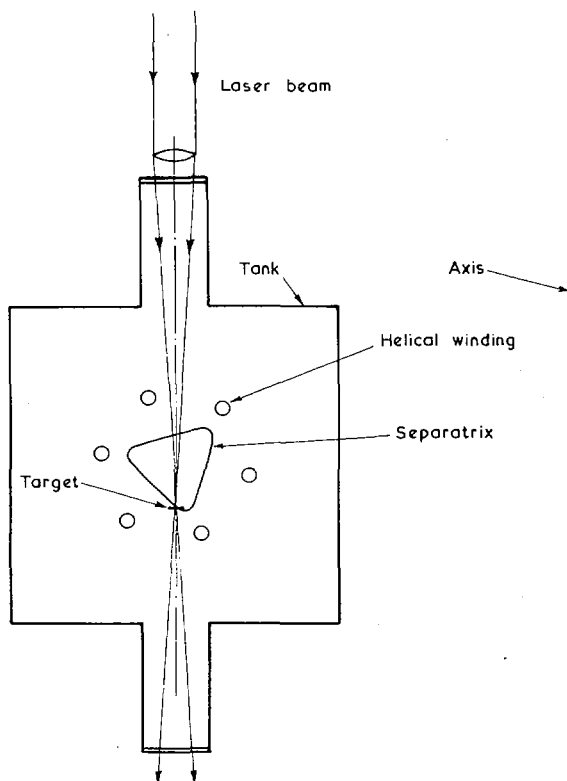


FIG.1. Layout of apparatus for laser beam production of plasma.

the irradiation of a solid target placed near the separatrix by the beam from a Q spoiled neodymium glass laser, as described in detail in the next section.

3.1. Laser method of plasma production

Fig. 1. shows the experimental arrangement of wire target and laser beam in relation to the vacuum vessel and helical winding. The wire target is held on a larger diameter rod which can be adjusted accurately in position inside the vacuum vessel by external screws.

The laser has a pulse width of 25 nanosec and delivers up to 15J at the target over a focal spot diameter of 0.5mm.

The optimum position for the target was found to be just outside the separatrix as shown in Fig.1. When the target was inserted into the confinement region a reduction in plasma density was observed which was not due to the presence of the target in the plasma as was shown by inserting a similar obstacle in the plasma. The fact that the

optimum position for the target is outside the separatrix can be attributed to the plasma coming off the target as a "plume" in a direction opposite to that of the laser beam. With the target in the optimum position there is, therefore, the whole of the separatrix diameter available for capture of the plasma. Various targets have been used ranging from thin beryllium wire to beryllium or lithium rods of up to 1.5mm diameter.

4. DIAGNOSTICS

Comparison of experimental results for the containment time of the plasma with predictions of theory involves a knowledge of plasma density, electron and ion temperature, plasma dimensions and rotational transform. Where possible these quantities have been measured by several different methods and good agreement between them obtained.

Plasma density determinations have been made by means of a microwave interferometer and a double Langmuir probe on which the applied voltage is swept. The electron temperature has been measured by the same probe as a function of time, by microwave noise emission, and by the retarding potential energy analyser used for the determination of the ion temperature. This analyser was of the type used by Eubank [5] and was usually placed just outside the plasma boundary, although a miniature version of it (9mm cube) was also used in the plasma in order to establish that the ion energy measured from the ions escaping from the containment region was the same as that of the confined ions. All these diagnostic methods are described in greater detail in Reference [3].

The following additional diagnostic methods have been used in recent work.

The plasma impedance and hence the electron temperature has been determined by a method used by the Princeton group [6,7], of two Rogovsky coils encircling the minor circumference of the plasma. One coil was energized by an audio oscillator and the resulting current induced in the plasma was determined by the voltage induced in the second coil. These coils were positioned in the vacuum system and within the helical winding assembly. They were very uniformly wound to minimize pick-up from the high pulsed currents flowing in the neighbouring helical winding conductors. One of the coils was electro-statically screened by a split copper shell and this coil was also used in the search for a unidirectional current flowing in the direction of the minor axis of the torus. (Section 5.5.1).

Directed fluxes of ions and electrons were also measured. For this, a "Janus" [8] probe was used consisting of two equal area single probes spaced 7mm apart and each surrounded by a cylindrical screening electrode of outside diameter 2mm so that each probe could collect particles over only a small angle of

incidence, either upstream or downstream. By suitably biasing the probes to collect either electrons or ions and balancing off the signals from them, a measure of the directed flux can be obtained. The difference in the floating potential of the two probes was also used as an indication of a directed flux of ions.

5. EXPERIMENTAL RESULTS

5.1. Plasma production by guns

Plasma guns have been found satisfactory for filling the Proto-Cleo stellarator with plasma over a density range 3×10^9 to 10^{12}cm^{-3} , with a corresponding electron temperature range of 8 to 2eV and initial ion energy of 30-10eV.

In passing it is worth noting, however, that these guns may not be suitable for filling all designs of small stellarators. It had been hoped to fill the Clasp stellarator by means of this type of hydrogen loaded titanium gun to enable comparative containment measurements to be made. Clasp [9,10] is a stellarator of approximately the same dimensions as the high shear version of Proto-Cleo, but it is constructed in the conventional way with a helical winding wound on the outside of a toroidal vacuum vessel. This vessel has only about $\frac{1}{14}$ of the volume of that in Proto-Cleo and the pumping speed for neutral gas is much smaller due to the smaller area of wall that can be gettered with titanium. Table II compares the electron and ion temperatures in Proto-Cleo and in Clasp at times of 0.2ms and 1ms after gun injection. For this comparison a somewhat smaller version of the normal gun was used and this gun was transferred between the two machines. It can be seen that the rate of cooling is much greater in Clasp than in Proto-Cleo. This difference was found to be due to a much higher neutral

TABLE II. COMPARISON OF PROTO-CLEO AND CLASP

Time	<u>Proto-Cleo</u>		<u>Clasp</u>	
	T_i	T_e	T_i	T_e
0.2ms	26	4.7	11	2.7
1ms	14	4.0	1.5	1.0

T_i and T_e in eV

$B_\phi = 1.8 \text{ kG}$

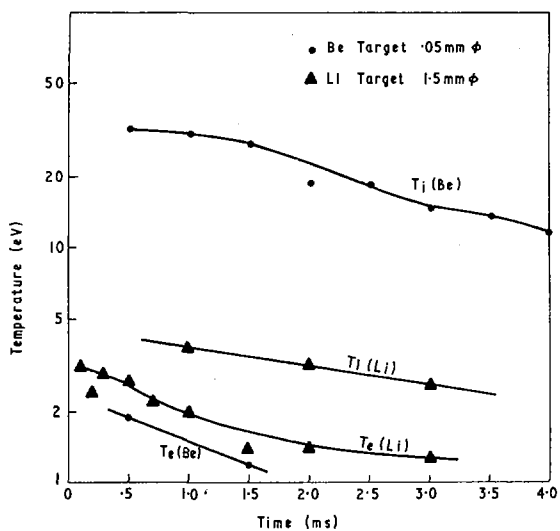


FIG. 2. Ion and electron temperatures as a function of time for laser-plasma production from a thin beryllium and a thick lithium target. $B_\phi = 3 \text{ kG}$, $\tau = 0.3$.

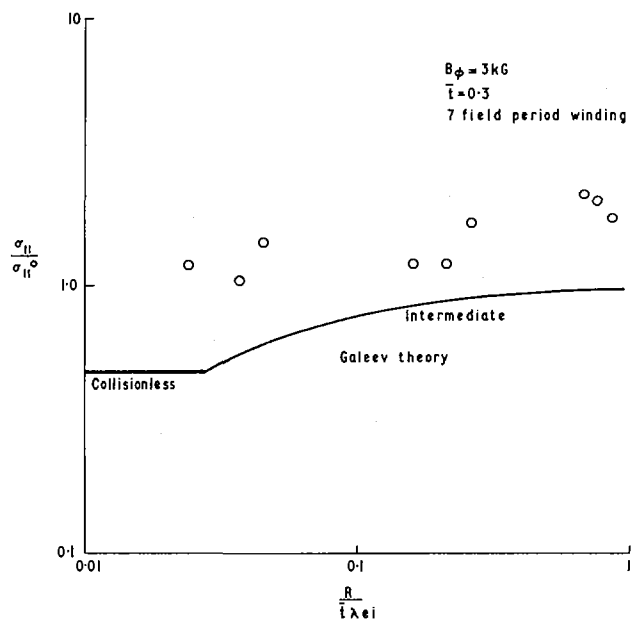


FIG. 3. Experimental points and theoretical curve for the variation of the ratio of the plasma conductivity to Spitzer conductivity with the ratio of connection length to electron-ion mean free path.

gas pressure in Clasp than in Proto-Cleo after gun injection and it indicates the advantage of the Proto-Cleo design when plasma sources evolving a large proportion of neutral molecules are used.

5.2. Plasma production using a Laser

A considerable range of plasma density and ion energy has been obtained by the use of various sized targets and laser energies.

With a thin target consisting of a beryllium wire 0.05 mm diameter and with a laser energy of 15J on a 0.5 mm focal spot diameter, a trapped plasma with an initial ion energy of 30eV and electron temperature of 2eV and an initial density of $2 \times 10^{11} \text{cm}^{-3}$ can be produced. Figure 2 shows the variation of T_i and T_e with time after injection.

When the target size is increased to a 1.5mm diameter lithium or beryllium rod and with a laser energy of 5J a much denser plasma of up to 10^{13}cm^{-3} is obtained but with a lower initial ion energy of 4eV (Fig.2).

The signal on a Langmuir probe positioned 180° around the major circumference from the point of laser injection shows a time delay between injection and arrival of the plasma at the probe consistent with the ion energy of 4eV given by the analyser. A proportional delay was also shown in the time of arrival of plasma at the microwave interferometer 90° from the injection point.

5.3. Plasma conductivity measurements

Using the double Rogovsky coil method described in Section 4 the plasma conductivity was determined over a range of frequency. In the results given below a frequency of applied signal of 6.5 kHz was used as this gave adequate power transfer from the coil to the plasma, small inductive reactance of the plasma compared with its resistive component and negligible skin effect in the plasma.

Fig. 3 shows the ratio of the measured conductivity to the Spitzer conductivity as a function of the ratio of connection length to electron-ion mean free path. In this, the Spitzer conductivity is derived from double probe measurements of electron temperature. Shown as a full line is the calculated value obtained from the theory of Galeev [11]. There is a tendency for the measured value of $\sigma_{11}/\sigma_{11}^0$ to fall with $R/t\lambda_{ei}$ as predicted theoretically, although the spread in the measured points is too large to be certain of this fact. The observed values are about a factor 2 larger than those calculated which is about as good agreement as could be expected taking into account that this conductivity is an average value across the column.

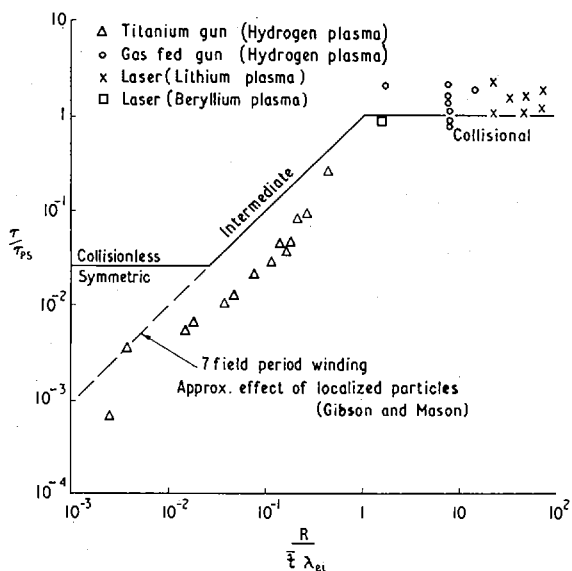


FIG.4. Experimental points and theoretical curve for the plasma containment time in terms of the Pfirsch and Schlüter time as a function of the ratio of connection length to electron ion mean free path. 7 and 13 field period windings.

5.4. Plasma loss rate and comparison with diffusion theory

Over the range of parameters studied, plasma containment times of from 1 to 10 ms have been observed. A preliminary comparison of these experimental results with neo-classical diffusion theory for the Proto-Cleo and Clasp stellarators was given by Hugill et al [10]. Fig.4 shows this comparison for Proto-Cleo only, plotted in the same way as in [10] but extended over a greater range by means of the improved plasma production. The containment time is expressed in terms of the Pfirsch-Schlüter containment time and is plotted against the dimensionless parameter $R/\tau\lambda_{ei}$, the ratio of connection length to electron-ion mean free path. Expressed in this way the theoretical curve for containment time covering the range from the collisional Pfirsch & Schlüter regime through the Galeev & Sagdeev intermediate to the collisionless regime is shown by the full line.

It is assumed in evaluating the theoretical value of τ that the plasma has a Bessel function density distribution so that $\tau_{ps} = D_{ps}^{-1} (\frac{R}{2.4})^2$ and $D_{ps} = \frac{1.66 \times 10^{-5} n \log \Lambda (T_e + T_i)}{T_e^{\frac{3}{2}} B^2 \tau^2}$ where τ is the mean value of the rotational transform across the plasma radius, and T_e and T_i are in eV. The value of λ_{ei} is taken as $\frac{2.23 \times 10^{13} T_e^2}{n \log \Lambda}$.

The agreement with theory is good in the collisional regime, but deteriorates in the intermediate regime where the containment time is about a factor of 4 shorter than the theoretical value.

In the collisionless regime the indication is that the dimensionless containment time continues to decrease with $R/\tau\lambda_{ei}$ instead of becoming constant as in the Galeev-Sagdeev theory for an axisymmetric system. This may be an indication that non-axisymmetric effects due to the field of the helical winding are coming into play. The dashed lines on the figure show the containment time to be expected when these effects are taken into account for the medium shear windings of Proto-Cleo using the theory of Gibson and Mason [12] for localized particles. It has not yet been possible to extend the experimental measurements further into the collisionless regime due to difficulties in making temperature and density measurements in the rare plasma.

It should be noted that over the whole range of conditions studied the containment time exceeds the Bohm time. At the largest value of $R/\tau\lambda_{ei}$, $\frac{\tau}{T_B} = 4$ and at the smallest value $\frac{\tau}{T_B} = 25$.

5.5. Diffusion driven plasma currents

It has been pointed out by Bickerton et al, [13], Galeev [11] and Hinton [14] that the enhanced diffusion in the low collisional frequency regime in an axisymmetric system is accompanied by a current which flows parallel to the magnetic field. Galeev [11] and Stringer [15] have shown that this current also flows in the intermediate regime and Stringer [15] has predicted its value for the collisional regime. The current should exist in the absence of any external driving electric field and therefore if the theory is also applicable to non-axisymmetric systems, the current should flow in a gun-fed stellarator. The absence of any Ohmic heating current in this case will make the detection of the current easier. Figure 5 shows the calculated value of the current for the various regimes as a function of density for typical Proto-Cleo conditions. The current rises linearly with density for the collisional regime because of the rise in the pressure gradient term with increase in density.

5.5.1. Measurement of current by a Rogovsky coil

The predicted levels of current for Proto-Cleo are of the order of 1A. To measure such small currents in the presence of the neighbouring helical winding currents of 15kA rising in 15 ms required careful winding of the coil and balancing out of the residual signal. In this

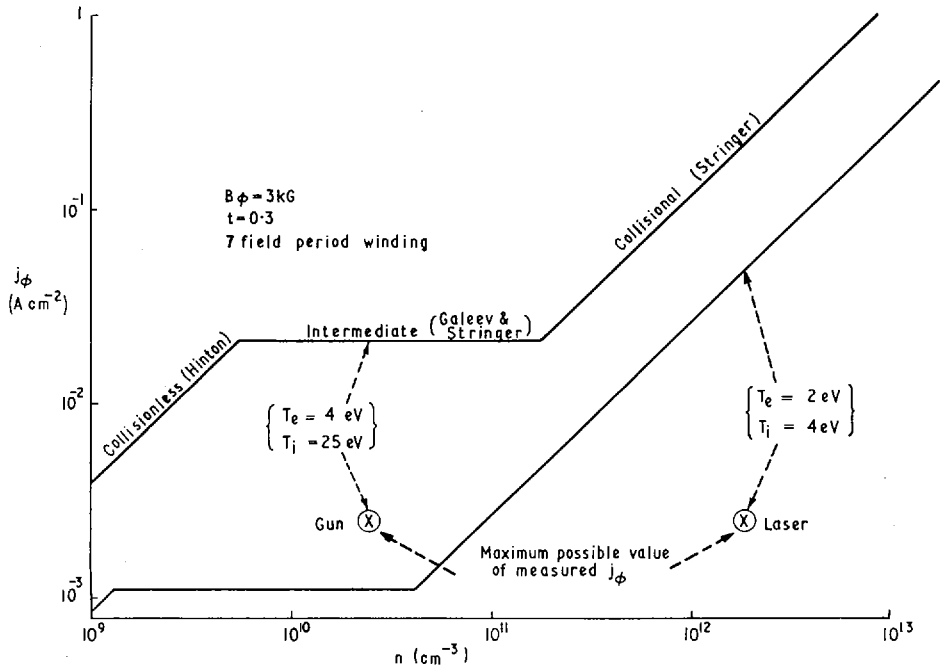


FIG. 5. Comparison of calculated value of current in the ϕ direction with that measured for Proto-Cleo.

way it was found possible to attain adequate sensitivity for currents in the plasma building up in 1 ms. For the gun plasma in the intermediate regime the limit of detection was 10^{-1} of the current predicted and for the laser plasma in the collisional regime it was 5×10^{-2} . Measurements in these two regions showed, however, no detectable signal which could be attributed to a diffusion driven current.

5.5.2. Indication of current by probes

Using the "Janus" double probe described in section 4, preliminary measurements have been made of the directed fluxes of electrons and ions. Although in both cases there was an indication of a particle drift which was in a direction dependent on the direction of B_ϕ , the evidence is not considered very reliable. In both cases there appear to be shadowing effects and further work will have to be done to assess their importance. A measurement of the difference of floating potential of the two probes also indicated an electron drift, but no quantitative work has yet been done.

6. DISCUSSION

6.1. Laser produced plasma

The mean ion energy of the trapped plasma (4-30eV) is very much lower than would be expected in the laser-produced plume from the target. Data reported by Langer et al, [16] of detailed measurements of plasma from beryllium targets with a similar power density shows the ion yield to be mostly Be^+ with a mean energy of several hundred eV. The large yield of 2×10^{17} ions at 5eV in the confined plasma of Proto-Cleo is therefore rather surprising. There are three possibilities. Firstly, there could be a slow component in the laser plasma as has been reported by several authors [17,18]. Secondly, charge exchange could be occurring between the high energy ions and neutrals of a few eV ejected from the target. The ejection of plasma as a narrow plume and the relatively slow drift of this plume across the magnetic field could combine to retain the ions long enough in the vicinity of the target for charge exchange to occur. Thirdly, there is the possibility of ionization of background neutrals by fast electrons.

6.2. Comparison of containment results with theory

The very similar shape of the experimental and theoretical curves shown in Fig. 4. for the containment time τ_{ps} as a function of $R/\bar{\tau}\lambda_{ei}$ strongly suggest that the plasma is being lost according to neo-classical diffusion theory.

In the intermediate regime the experimental results are however a factor of 4 smaller than the theoretical ones. This could be due to the fact that the theory is for an axisymmetric system where the magnetic surfaces have an approximately circular cross section, whereas in the stellarator the system is nonaxisymmetric and the surfaces have a trefoil cross section.

The possibilities that the extra dissipation implied by the enhanced loss rate could be due to an anomalously high plasma resistivity is eliminated by the direct measurement of plasma resistivity described in section 5.3.

Furthermore, the unidirectional current predicted by theory to account for the enhanced loss of plasma in the intermediate and collisionless regimes above the Pfirsch and Schlüter value has not been found. The direct method of measuring the current by means of a Rogovsky coil showed that the current present did not exceed 10% of the expected value in the intermediate regime and 5% in the collisional regime.

There are, however, at least two reasons which could be given for the non-appearance of this current. Firstly

the theory is for an axisymmetric system where there is everywhere a poloidal B_θ field, as in the tokamak. In the stellarator, however, there is only an average B_θ field brought about by currents in the helical windings. Thus at points around the minor circumference under the conductors there are much larger local B_θ fields alternating in direction. Under these circumstances, the theory may not apply.

Secondly the theory is for a steady state and in this pulsed experiment there may not be time for this state to be reached.

It is also possible that the agreement of scaling between theory and experiment in Fig. 4. is fortuitous and that the plasma loss is due to an effect unrelated to neo-classical diffusion. One possibility is that fluctuations in electric field and density lead to plasma loss. Previous measurements in Proto-Cleo [1] in the intermediate regime at points along a minor radius in the equatorial plane showed that the loss estimated from the magnitude of fluctuations in E_θ and n , even assuming a correlation factor of unity, was insufficient by a factor of ten to account for the observed plasma loss. It should be emphasized however, that only these local measurements of fluctuations were made.

7. CONCLUSIONS

(1) Proto-Cleo has been successfully filled with plasma over a wide range of density by transverse injection from plasma guns and by irradiation of a solid target by a laser beam. The latter method gives up to a ten-fold increase in density over that produced by plasma guns.

(2) The containment time of plasma has been studied over values of $R/t\lambda_{ei}$ covering five orders of magnitude and has been found to scale with this parameter in the way predicted by neo-classical diffusion theory. The absolute value of the containment time is however a factor of 4 less than expected from theory and the unidirectional current predicted by theory was not detectable. It is possible that both these anomalies are due to applying a theory for axisymmetric systems to a non-axisymmetric stellarator system.

A unidirectional current has been detected by a magnetic probe in the Model C stellarator by Yoshikawa and Yamato [19] but this current appears to be about 100 times larger than the value predicted theoretically for a diffusion driven current and its presence was attributed to the effect of the ion cyclotron waves used for heating the plasma.

Berezhetskii et al [20] have reported directional ion fluxes in the Lebedev stellarators using a gridded ion detector.

They attribute the directed flux to resonant loss of particles due to the presence of a radial electric field in the plasma. A radial field of sufficient magnitude is not however observed in Proto-Cleo.

Local measurements of the fluctuations suggest that they are not responsible for the plasma loss. However more measurements would be needed to prove this conclusively.

8. ACKNOWLEDGMENTS

The authors are grateful to Dr. R.J. Bickerton for his help and encouragement throughout this work, and to the members of CLASP and PROTO-CLEO teams for their experimental work.

REFERENCES

- [1] ADLAM, J.H., et al., "Plasma physics and Controlled Nuclear Fusion Research". (IAEA, Vienna, 1969) Vol. I, p.573.
- [2] LEES, D.J., et al., Fourth European Conference on Controlled Fusion and Plasma Physics, Rome 1970 (CNEN) Paper No.25.
- [3] BOLTON, R.A.E., et al., Plasma containment in medium and high shear stellarators. Physics of Fluids (in press).
- [4] ASHBY, D.E.T.F., Plasma Physics 10 (1968) 665
- [5] EUBANK, H.P. MATT Q22 (1965) 63
- [6] COOR, T., CUNNINGHAM, S.P., ELLIS, R.A., HEALD, M A. KRANZ, A.Z. Physics of Fluids 1 (1958) 411.
- [7] GROVE, D.J., MESERVEY, E.B., STODIEK, W., YOUNG, K.M., "Plasma Physics and Controlled Nuclear Fusion Research". (IAEA, Vienna, 1969) Vol.I, p. 479.
- [8] ANDERSON, O.A., BIRDSALL, D.H., HARTMAN, C.W., LAUER, E.J., "Plasma Physics and Controlled Nuclear Fusion Research" (IAEA, Vienna, 1969) Vol.I. p.443.
- [9] GIBSON, A., et al. "Plasma Physics and Controlled Nuclear Fusion Research. (IAEA Vienna, 1969) Vol.I, p.465.
- [10] HUGILL, J., et al., Fourth European Conference on Controlled Fusion and Plasma Physics, Rome 1970 (CNEN) Paper No. 26.
- [11] GALEEV, A.A., Zhur. Exp. Teor. Fiz. 59 (1970) 1378.
- [12] GIBSON, A., and MASON, D.W., Plasma Physics 11, (1969) 121.
- [13] BICKERTON, R.J., CONNOR, J.W., TAYLOR, J.B., Nature Physical Science, 229 (1971) 110.
- [14] HINTON, F., (1970), private communication.
- [15] STRINGER, T.E., Fourth Conference on Plasma Physics and Controlled Nuclear Fusion Research. Madison, 1971. Paper No. CN-28/F-3.
- [16] LANGER, P., TONON, G., GURAND, Y., BUGES, J.C., C.E.A. R 3296 (1967).
- [17] DAVID, C.D., and WEICHEL, H., Journal of Applied Physics 40 (1969) 3674.

- [18] NAMBA, S., KIM, P.H., ITOH, T., ARAI, T., SCHWARZ, H.,
I.E.E.E. Conference on Electron, Ion and Laser Beam
Technology, Berkeley, 1967.
- [19] YOSHIKAWA, S., and YAMATO, H., Physics of Fluids 9 (1966)
1814
- [20] BEREZHETSKY, M.S., GREBENTSHIKOV, S.E., KOSSY, I.A.,
SHPIGEL, I.S., Fourth Conference on Controlled Fusion &
Plasma Physics, Rome 1970 (CNEN) Paper No. 31.

NOTE ADDED IN PROOF

Immediately before the conference it was pointed out by T.E.Stringer that the derivation of the Galeev-Sagdeev diffusion rate assumes that the ion Larmor radius in the B_θ magnetic field is less than the density scale length, whereas in Proto-Cleo their ratio is everywhere greater than 4. In this condition, the radial drift due to the azimuthal electric field becomes important and decreases the confinement time in the intermediate regime. For Proto-Cleo the confinement time relative to the Galeev and Sagdeev time is reduced by this effect by a factor of 3.5 which brings the theoretical and experimental times into good agreement. Nevertheless, there still remains the difficulty that the unidirectional diffusion current predicted by the theory has so far eluded observation.

DISCUSSION

S. E. GREBENSHCHIKOV: The equilibrium currents measured experimentally in your work differ from the theoretical calculations by about a factor of ten. How, then, can you explain the very good agreement between the theoretically and the experimentally determined plasma lifetime?

P. REYNOLDS: We cannot at present explain this very good agreement.

S. YOSHIKAWA: How is τ_{ps} determined?

P. REYNOLDS: It is determined from the Bessel function density distribution with an average rotational transform and an average radius.

S. YOSHIKAWA: So the theoretical value may be off by a factor of 3 to 4?

P. REYNOLDS: Yes.

DEPENDENCE OF PLASMA CONFINEMENT ON MAGNETIC CONFIGURATION AND PLASMA PROPERTIES IN THE J. I. P. P. STELLARATOR

K. MIYAMOTO, A. MOHRI, N. INOUE, M. FUJIWARA,
K. YATSU*, Y. TERASHIMA, R. ITATANI**
Institute of Plasma Physics, Nagoya University, Nagoya,
Japan

Abstract

DEPENDENCE OF PLASMA CONFINEMENT ON MAGNETIC CONFIGURATION AND PLASMA PROPERTIES IN THE J. I. P. P. STELLARATOR.

The dependence of plasma confinement on the properties of the stellarator field as well as on the plasma parameters is studied using the J. I. P. P. stellarator with several kinds of plasma sources. The observed diffusion coefficients of helium plasmas are 1/20-1/30 times the Bohm coefficient, which is one order of magnitude larger than the neoclassical case. In the case of argon plasma produced by electron cyclotron resonance heating the observed diffusion coefficient is 1/100 times of Bohm value and agrees with the neoclassical value within a factor of 2.

A circular $\ell = 3$ stellarator with a vertical field is constructed with good geometrical accuracy using numerically controlled machines. The helical winding has a minor radius of 10.6 cm and major radius of 50 cm with eight field periods. Two halves of the stainless-steel vacuum vessel with inner radius of 8.4 cm are insulated by ceramic spacers to make Ohmic heating possible. The stationary (5s) magnetic field is 4 kG at maximum, the angle of rotational transform ι is up to 1.7π , and the shear parameter is up to 0.15. The well depth is variable from -5% to 10%. This device can be used in the torsatron configuration. The plasma sources used are a J \times B-type gun with a fast-acting valve ($T_e = 0.2 - 3$ eV, $n = 10^9 - 10^{10}$ cm $^{-3}$), electron cyclotron resonance heating (ECRH) ($T_e \approx 2$ eV, $n \approx 10^{10}$ cm $^{-3}$) and Ohmic heating by an air-core coil ($T_e \approx 3$ eV, $n \approx 10^{10-12}$ cm $^{-3}$). The winding of the air-core coil is arranged so that the disturbance due to the stray field is negligibly small within the plasma region. These plasma parameters cover the range of intermediate collisional and collisional regions.

It is observed that the diffusion coefficients D estimated from the decay times and the plasma radius a are proportional to the first and second powers of the angle of rotational transform ι . The profile of the density distribution is similar to $\cos [1.57(r/a)^2]$ or $(r/a)^2 J_{-2/3} [1.25(r/a)^3]$ which are solutions of the diffusion equation with diffusion coefficients $D \propto r^{-2} (\propto \iota^{-1})$ or $D \propto r^{-4} (\propto \iota^{-2})$ (r is the radial co-ordinate). The confinement times do not substantially depend on the properties of the magnetic well (and antiwell), and the dependence of confinement on the magnitude of the magnetic field is linear in our experimental conditions.

The two-dimensional distributions of the plasma densities and potentials produced by the J \times B-type gun and by ECRH show the existence of convective motion due to electric fields, which are possibly caused by trapped electrons and the toroidal drift. The plasma near the central regions is transported across the field towards the boundary, where a density gradient exists and fluctuations due to drift waves are observed. The transport by convection and the fluctuations can roughly explain the observed confinement time.

1. INTRODUCTION AND EXPERIMENTAL ARRANGEMENTS

In stellarator configurations, plasma equilibrium and stability are satisfied without any close connection with plasma production and heating. Studies of plasma confinement in the stellarator field have been carried

* Tokyo University of Education, Tokyo, Japan.

** Kyoto University, Kyoto, Japan.

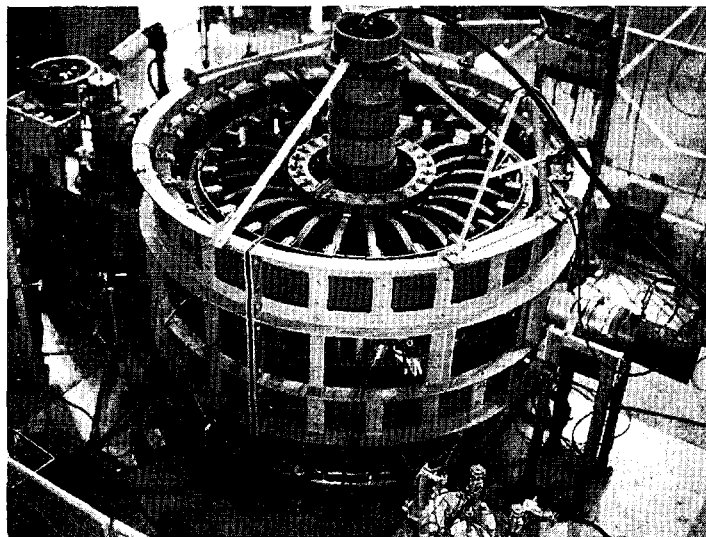


FIG. 1. The J.I.P.P. stellarator device.

out in many laboratories [1-6]. However, the diffusion or transport phenomena across the stellarator fields are not yet fully understood, and the results obtained so far are not always consistent with each other. In this paper, the dependence of plasma confinement on the properties of the stellarator field as well as on the plasma parameters is studied in relation with the convective transport and fluctuations in the J. I. P. P. stellarator.

This device is circular in shape and has $\ell = 3$ helical windings (Fig. 1). The major radius is 50 cm and the maximum toroidal field is 4 kG (the coil current $I_T = 1.6$ kA) in quasi-stational operation (5 s per minute). The inner radius of the stainless steel vacuum vessel is 8.4 cm, and the two halves of the vessel are insulated by ceramic spacers of 1 cm thickness, so that r. f. stochastic heating and Ohmic heating can be applied. The helical winding has a minor radius of 10.6 cm with eight field periods. The helical current is up to 22 kAT (= 2.5 kA \times 9 turns) and is fed through coaxial current feeders. The helical coils are wound by using helical grooves which are machined by a numerically controlled method. The geometrical accuracy of the helical coil is better than 0.5 mm. The magnetic surfaces are checked with the pulsed-electron-beam method [7], the measurements agree well with the results of computation. The parameters of the magnetic configuration of the J. I. P. P. stellarator are shown in Table I. The well depth is variable from -5% to +10%. This device can be used in the torsatron-type configuration. The plasma sources used are a quasi-steady $J \times B$ -type gun with a fast acting valve, ECRH of 2.45 GHz and Ohmic heating by an air-core coil.

Movable probes are arranged for scanning purposes inside the vessel. A sensitive micro-wave 8-mm-interferometer is used. Multi-grid-type energy analysers are used for measuring the ion energy.

TABLE I. PARAMETERS OF MAGNETIC CONFIGURATION

I_T , I_H and I_V are currents of the toroidal coil, the helical coil and the vertical-field coil, respectively

I_H/I_T	2		3.2	
I_V/I_T	0	0.02	0	0.02
R/a	9.5	11.5	14	16
ι (outside)	1.5π	π	1.7π	1.1π
ι (axis)	0	0.4π	0	0.5π
shear	0.15	0.05	0.12	0.03
well depth	3%	10%	3%	7%

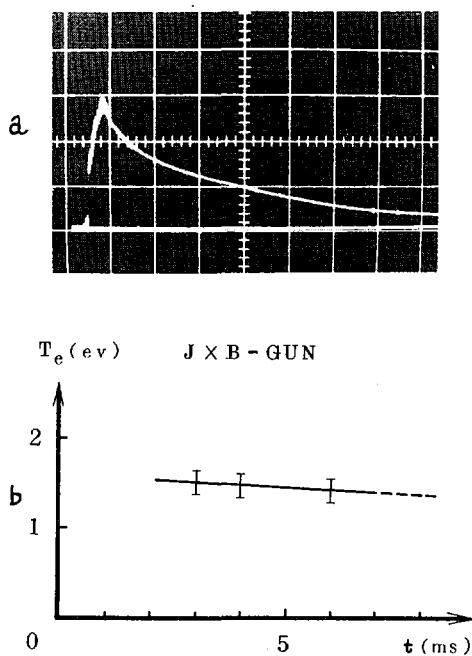


FIG. 2. a) Typical signal of the ion-saturation current of the $J \times B$ -type gun ($1 \mu\text{A}/\text{div.}$, $1 \text{ms}/\text{div.}$); b) time variation of the electron temperature.

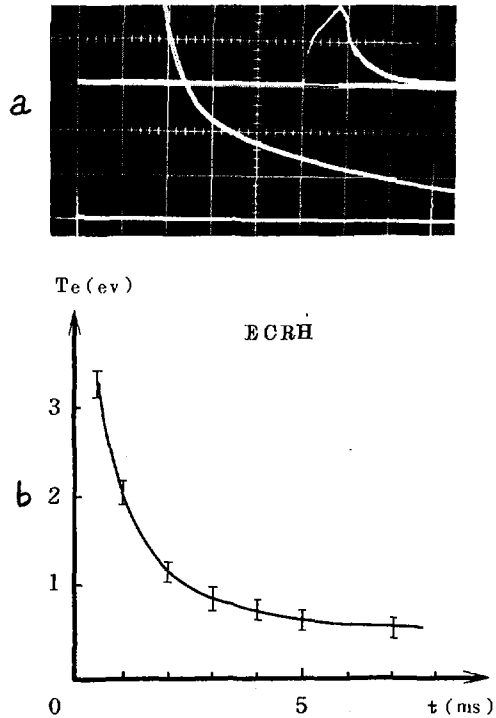


FIG. 3. a) Typical signal of the ion-saturation current of an ECRH-plasma with different sensitivities and time sweeps (upper trace: $200 \mu\text{A}/\text{div.}$, $2 \text{ ms}/\text{div.}$; lower trace: $10 \mu\text{A}/\text{div.}$, $1 \text{ ms}/\text{div.}$); b) time variation of the electron temperature.

2. DEPENDENCE OF PLASMA CONFINEMENT ON THE FIELD CONFIGURATION

Figure 2a shows a typical signal of the ion saturation current of the helium plasma produced by the $J \times B$ -type gun. The gun is fired $260 \mu\text{s}$ after triggering the fast-acting valve; it is short-circuited at $800 \mu\text{s}$. The electron temperature in the standard condition is 1.5 eV (Fig. 2b); the density is $0.7 \times 10^{10} \text{ cm}^{-3}$. The degree of ionization is $\sim 0.7\%$. This plasma is in the intermediate collisional region. The electron temperature varies from 0.2 to 3 eV . The cooling time of electrons by helium gas is about 0.1 s , but the cooling of ions by charge exchange with the helium atoms is estimated to be 0.4 ms . So, the ion temperature during the observed period is low, although the ion energy at the injection stage is high.

The ECRH-plasma is produced by using a magnetron of 2.45 GHz ($B_{ce} \sim 0.87 \text{ kG}$) with helium gas of 10^{13} cm^{-3} . The microwave power of about 300 W is fed through a coaxial cable and a loop antenna during about 3 ms . Figure 3a shows a typical signal of the ion saturation current of a

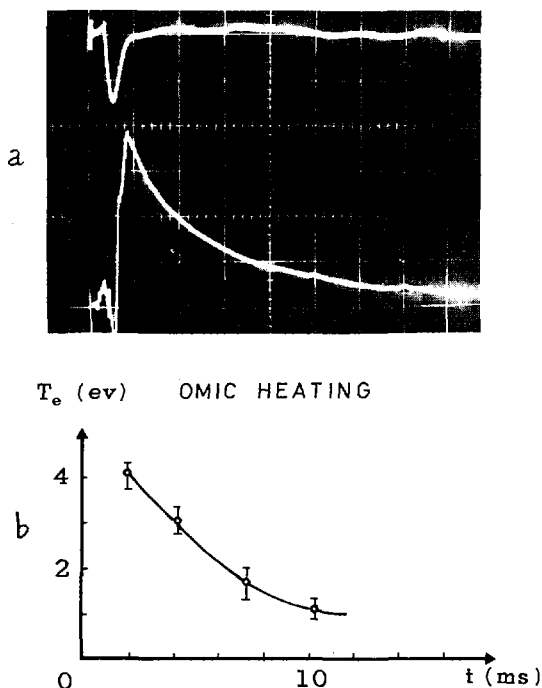


FIG.4. a) Upper trace: induced current in the plasma produced by Ohmic heating (130 A/div.). Lower trace: typical signal of the ion-saturation current of afterglow plasma. The sensitivity of the lower trace is 100 μ A/div.; the time sweep is 2 ms/div. b) Time variation of the electron temperature.

Langmuir probe. After the power is turned off, the density decreases with two different decay-time constants. During about 2 ms after that, the density decays rapidly and then decreases slowly with a decay time of 2-5 ms in the later period. As will be shown later, very strong convective cells are observed in the early period. The time variation of the electron temperature measured by a swept Langmuir probe is also shown in Fig. 3b. Typical ECRH-plasma has $T_e \approx 1$ eV and $n \approx 1.5 \times 10^{10}$ cm^{-3} . The degree of ionization is about 0.2%. The electrons are in the intermediate collisional region while the ions are in the collisional region. In the case of a neutral density of $\sim 10^{13}$ cm^{-3} and an applied power of 300 W, no X-rays are observed by a detector with scintillator and photomultiplier combination or by a proportional counter with a mylar window of 6 μ thickness; hot electrons do not exist during the afterglow period.

Figure 4a shows the typical signal of helium plasma produced by Ohmic heating, using the air-core coil whose winding consists of a homogeneous coil and mirror coils so that the disturbance due to the stray field is negligibly small within the plasma region. R. f. stochastic heating or $J \times B$ -type gun are used for pre-ionized plasma sources. One-turn loop voltage of about 10 V is applied during 1.5 ms. The afterglow plasma has an electron temperature of 3 eV and a density of 0.4×10^{12} cm^{-3} .

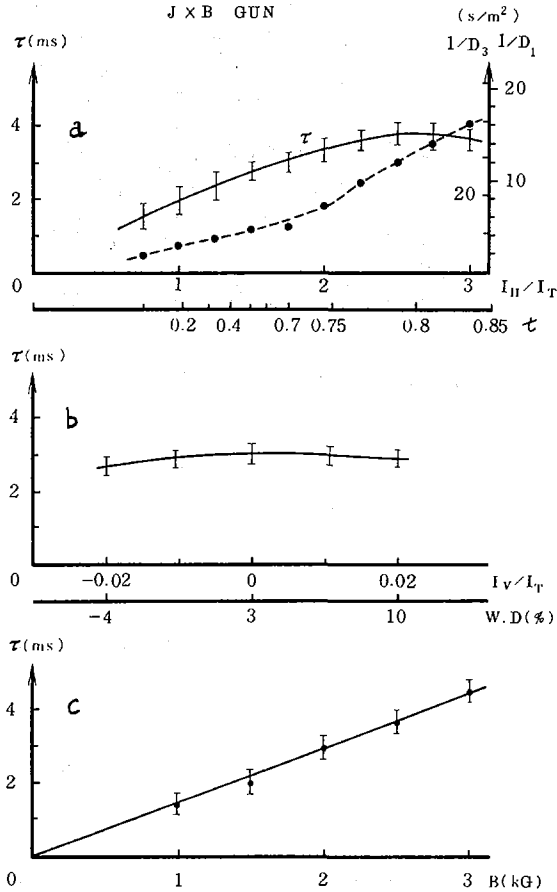


FIG. 5. a) $1/D_1 = 5.8 \tau/a^2$, $1/D_3 = 14 \tau/a^2$; b) confinement time τ of gun plasma versus angle of rotational transform and well depth (W.D.) for a toroidal field of 2 kG; c) τ versus magnitude B of toroidal field for helical-coil to toroidal-field-coil current ratio of 2.

The degree of the ionization is 20 ~ 100%. This plasma is in the collisional region.

Figure 5 shows the dependence of the confinement time τ of helium plasma by the J × B-type gun on the angle of rotational transform ι , the well depth W. D. and the magnetic field B. Figure 6 shows the dependence of τ on ι and W. D. in the case of the ECRH-plasma; Figure 7 shows the dependence of τ on ι and B in the case of Ohmic heating. The confinement times τ depend linearly on B in the cases of the J × B type gun and the Ohmic heating. The dependence of τ on the well depth as well as antiwell depth is weak. The diffusion coefficient D can be estimated from the decay time, as the dependences of the angle of rotational transform, the shear and the plasma radius are known from the ratio of currents of the helical coil to that of toroidal coil. The dependence of D on the helical current

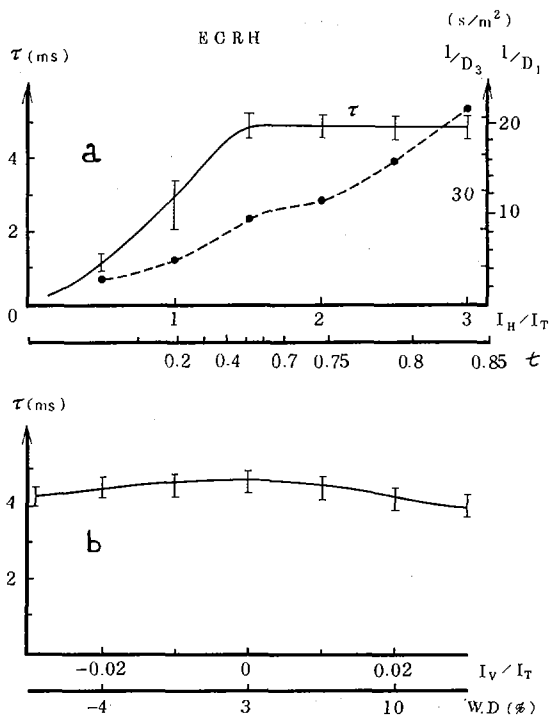


FIG. 6. a) Dependence of confinement time τ for the ECRH-plasma on the ratio of helical-coil and toroidal-field-coil currents (the angle of rotational transform); b) dependence of confinement time τ on magnetic well depth (W. D.).

indicates that the diffusion coefficient appears to be related to the angle of rotational transform and not to the shear parameter. The inverse diffusion coefficients $1/D$ are proportional to the first and second powers of ι (Fig. 8). The solutions of the diffusion equation with assumed forms of D become as follows; $n_1(r) = J_0(2.4 r/a)$ for $D_1 = \text{const}$, $n_2(r) = \cos[1.57(r/a)^2]$ for $D_2 \propto r^{-2}$ and $n_3(r) = 1.95 (r/a)^2 J_{2/3}[1.25 (r/a)^3]$ for $D_3 \propto r^{-4}$. They are plotted in the lower part of Fig. 8. The measured density profiles of the ECRH- and gun plasmas are plotted; they are similar to the $n_3(r)$ -distribution in the outer region of the torus. The ratio of the estimated diffusion coefficient D_1 to the Bohm coefficient D_B is $D_1/D_B = [a^2/5.8 \tau_{\text{exp}}]$ [16 eB/T_e] which corresponds to the zero-order Bessel distribution and the ratio D_3/D_B is $D_3/D_B = [a^2/14 \tau_{\text{exp}}]$ [16 eB/T_e] which corresponds to the $n_3(r)$ -distribution. The values of D_1/D_B are 1/8, 1/13 and 1/11 for the $J \times B$ -type-gun, the ECRH and the Ohmic-heating plasmas, respectively, and the ratios of D_3/D_B are 1/20, 1/30 and 1/27, for the respective cases. In the case of the ECRH-plasma using argon gas, this ratio becomes 1/100 ($T_e \sim 1.2$ eV, $\tau = 8$ ms).

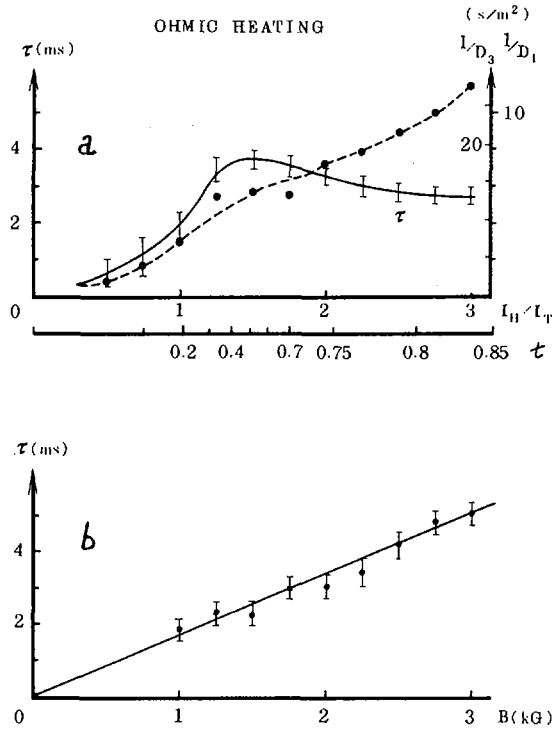


FIG. 7. a) Dependence of confinement time τ for Ohmic-heating plasma on angle of rotational transform for a toroidal field of 2 kG; b) dependence of τ on the toroidal field B is for helical-current to toroidal-current ratio of 2.

3. CONVECTIVE TRANSPORT AND FLUCTUATIONS

The experimental results show that convective transport and the enhanced diffusion due to fluctuations take place. The distributions of densities and floating potentials over the plasma cross-section in the case of the $J \times B$ -type gun are measured at different times using a single probe with a scanning mechanism (Fig. 9). The reproducibility of the floating potential signals is within a few percents and that of the ion-saturation-current signals is within several percents. The difference between the floating potential and the plasma potential can be considered constant over the plasma cross-sections since the electron temperature does not change except at the boundary. The direction of the $E \times B$ -drift is approximately parallel to the equi-potential lines, as the magnetic field is almost perpendicular to the cross-section. The deviation of the equi-potential lines from the magnetic surfaces shows the existence of convective motions [8, 9] across the field. The magnetic field is weaker at the corners of the $\ell = 3$ stellarator magnetic surfaces as is shown in Fig. 11, where the profile of the constant- $|B|$ -surfaces is mapped at the position of the different

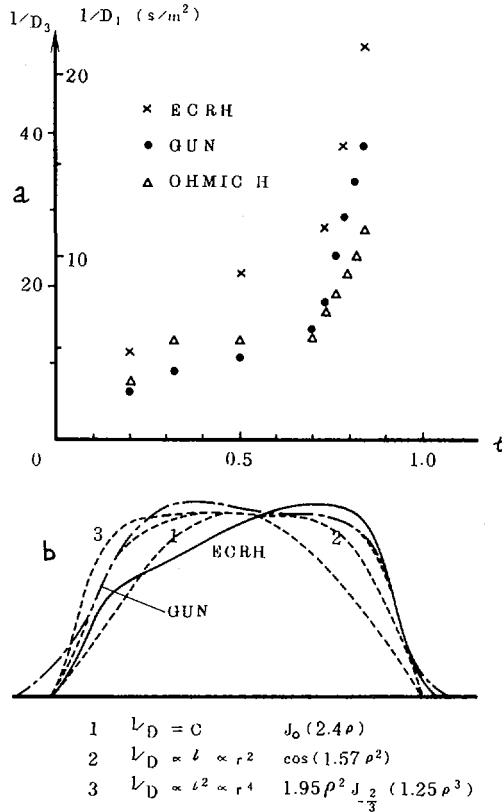


FIG. 8. a) Dependence of diffusion coefficients on angle of rotational transform for ECRH-plasma ($B = 0.87$ kG, $T_e \sim 0.8$ eV), gun plasma ($B = 2$ kG, $T_e \sim 1.5$ eV) and Ohmic-heating plasma ($B = 2$ kG, $T_e \sim 3$ eV). The inverse of the diffusion coefficient $1/D_1 = \tau(5.8/a^2)$ of the zero-order Bessel density distribution, and $1/D_3 = \tau(14/a^2)$ for the n_3 -distribution are shown; b) profiles of $n_1(r)$, $n_2(r)$ and observed density profiles in cases of the ECRH and $J \times B$ -type-gun plasmas are also shown ($\rho = r/a$).

phases of the helical coils [10]. The potential is more negative locally, in correlation with the constant- $|B|$ -surfaces. The direction of the convective motion is clockwise in these figures; its effect is observed in the corresponding density profiles.

Similar measurements are carried out in the case of ECRH-helium plasma (Fig. 10). The reproducibility of ion-saturation currents and floating potentials is within a few percents. Again, similar convective motions are observed. At the other phase of the helical pitch, similar results are observed. These observations show that the convective cells are related to the stellarator field. It may be considered that the electrons are trapped during the electron cyclotron resonance heating at the corners of the magnetic surfaces where the magnetic field is weaker. These convective cells then decay by ion-ion and ion-neutral collisions [9]. The electric field due to the toroidal drift [11] remains without cancellation since the angle of rotational transform ι of the $\ell = 3$ -stellarator is small near the minor axis

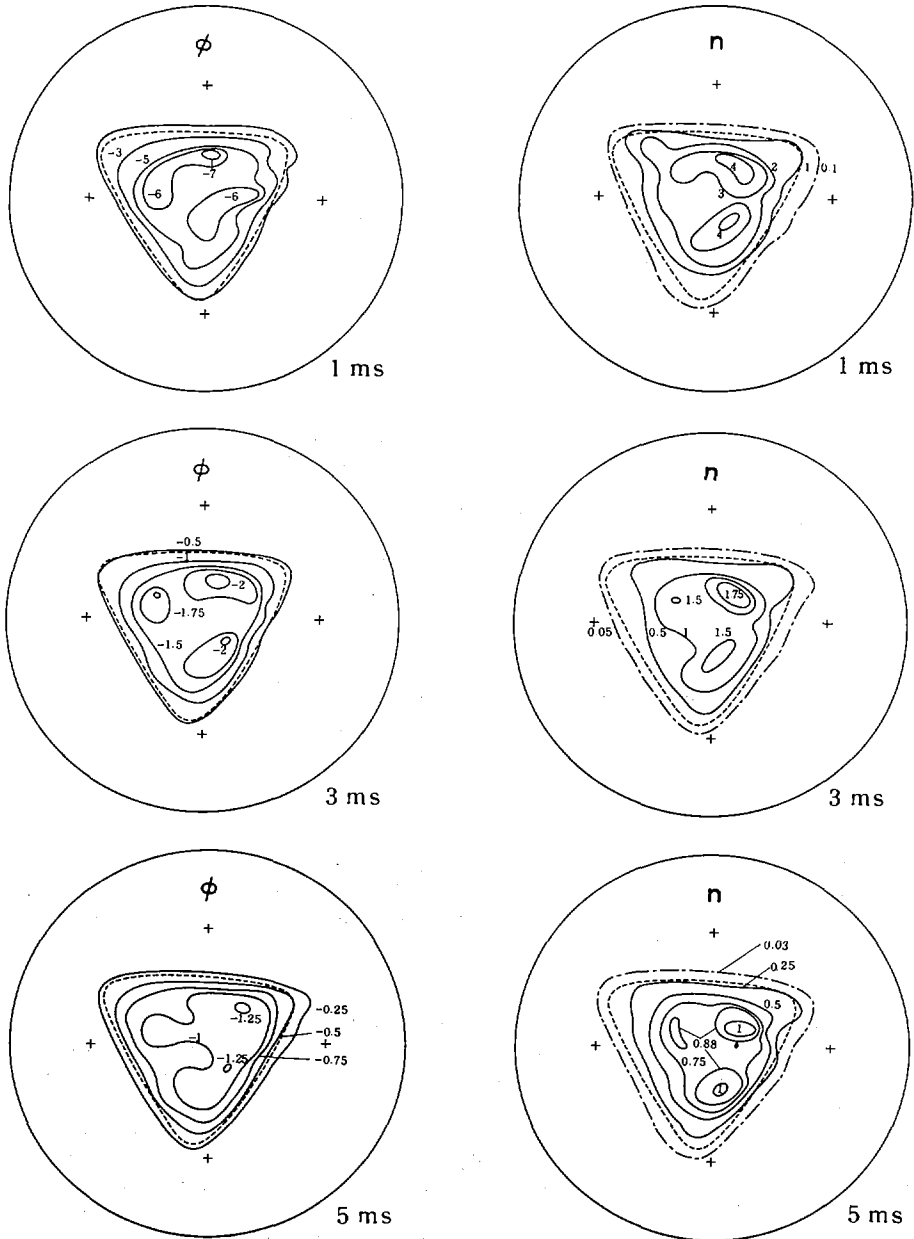


FIG. 9. Two-dimensional distributions of floating potentials (left-hand side) and densities (right-hand side) at different times (1 ms, 3 ms and 5 ms after triggering the fast-acting valve) observed for the gun plasma. The numbers in the figures showing the potential distributions are in volts; the enclosing circle is the inner wall of the vacuum vessel with a diameter of 16.8 cm. The number in the figures showing the density distributions are in arbitrary units; the value of 1 approximately corresponds to the value of $n \sqrt{T_e} \sim 3 \times 10^9 \sqrt{eV} \text{ cm}^{-3}$. The direction of the magnetic field is into the figure.

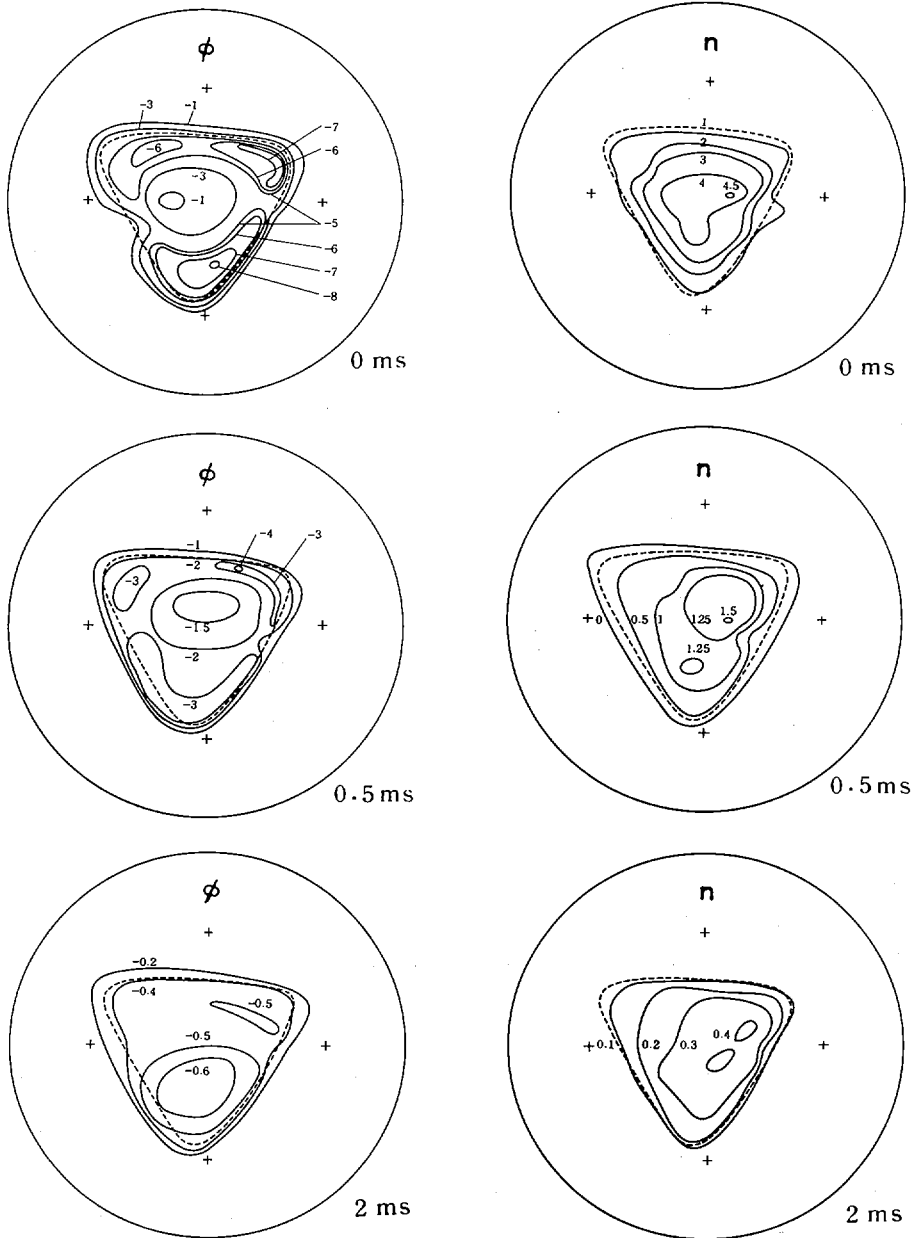


FIG. 10. Two-dimensional distributions of floating potentials (left-hand side) and densities of ECRH-plasma at different times (0 ms, 0.5 ms and 2 ms after switching off the ECRH-power) (right-hand side). The numbers in the figures have the same meaning to those in Fig. 9. The value of 1 approximately corresponds to the value of $n \sqrt{T_e} \sim 5 \times 10^{10} \text{ veV cm}^{-3}$.

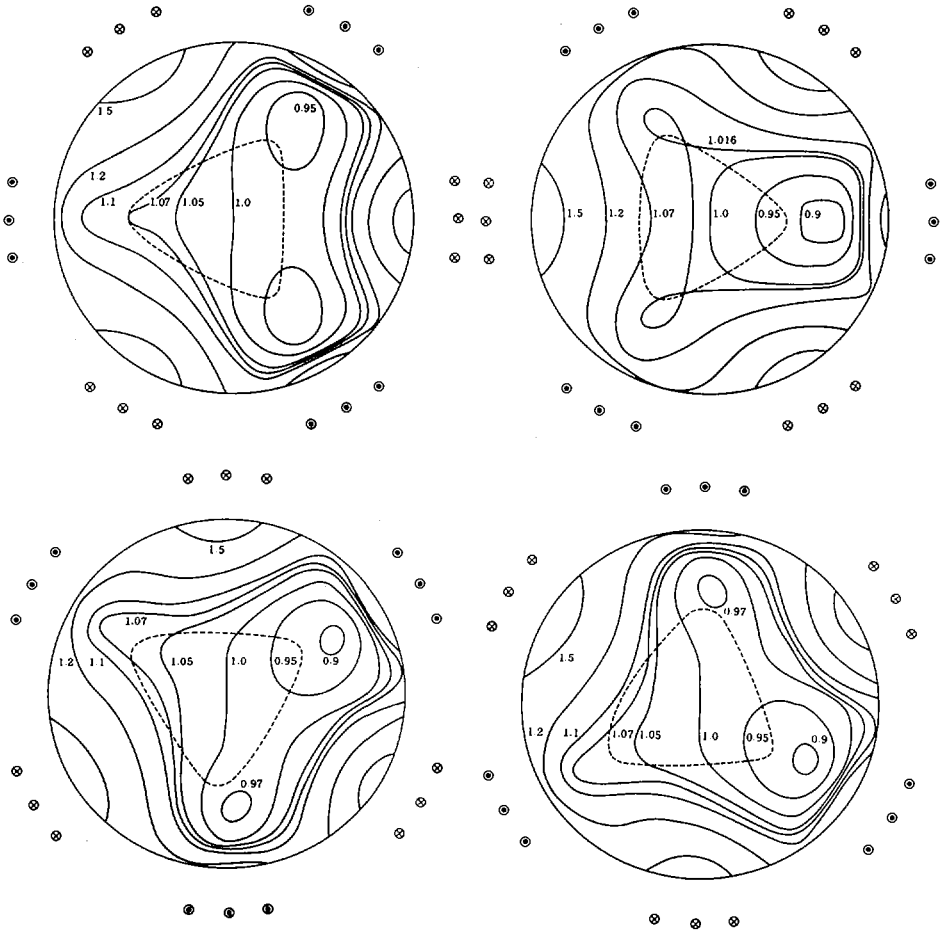


FIG. 11. Constant- $|B|$ -surfaces of the $\ell = 3$ -stellarator field with the magnetic surface (dotted line). The angle of rotational transform on the magnetic surface is 1.7π .

($\nu \propto r^2$). The convection stream-lines cross the outmost magnetic surface during the early phase of rapid decay. In the later phase of slow ECRH-plasma decay and in the case of $J \times B$ -type gun, the deviation of the stream lines in the boundary is small at the outmost magnetic surface, but the density-profile shapes are nearly flat top since the plasma near the central region is transported across the magnetic field to the boundary region, where density and electric-field fluctuations are observed.

Convective motions have been treated theoretically before [12]. When the inertia term $(\vec{v} \cdot \nabla) \vec{v}$, pressure anisotropy and collision terms are introduced into the fluid equations for the electrons and ions, the deviation of a perturbed potential ϕ_1 from the equilibrium potential $\phi_0(\Phi)$ can be deduced (Φ is a flux function of the magnetic surface). These studies are being carried out for the interpretation of the experimental results.

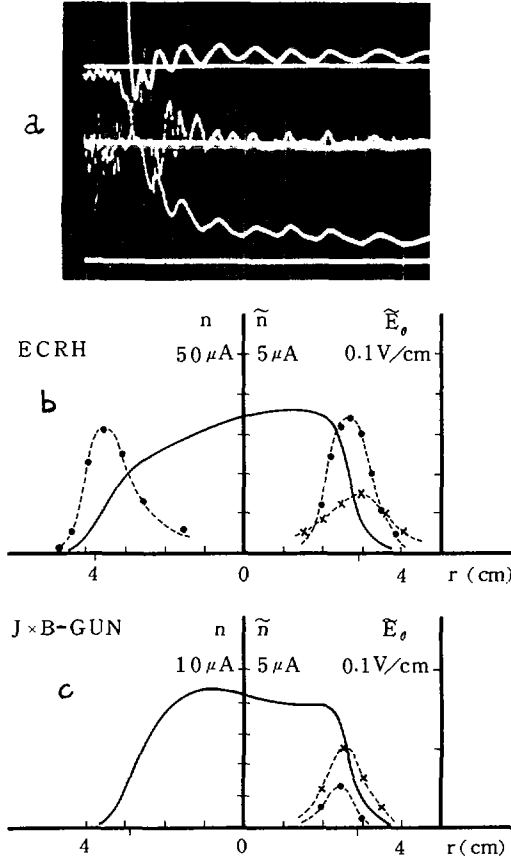


FIG. 12. a) Fluctuation of azimuthal electric field \tilde{E}_θ (0.2 V/cm/div.), product $\tilde{n} \cdot \tilde{E}_\theta$ (arbitrary units) and the signal of ion-saturation current n (20 μA /div.) for ECRH-plasma. The time sweep is 0.2 ms/div. b) Distributions of density n , fluctuations of \tilde{n} and \tilde{E}_θ for ECRH; c) J x B-type gun (--- x ---; \tilde{E}_θ , --- \bullet ---; \tilde{n}).

As described before, fluctuations of density and potential are observed in the boundary region. The fluctuations of the density \tilde{n} and the fluctuations of the azimuthal electric field \tilde{E}_θ are measured for ECRH and the J x B-type gun. The flux of transport Γ due to fluctuations is calculated as $\Gamma = \langle \tilde{n} \times E_\theta \rangle / B$ (the brackets $\langle \dots \rangle$ denote time average). If the confinement time is determined by the flux, it is given by $\tau_f = n_0 a / 2\Gamma = (aB/2) \langle (\tilde{n}/n_0) \times E_\theta \rangle$ where n_0 is the average density. In the slowly decaying stage of the ECRH plasma, we have $\tilde{n}/n_0 \approx 0.12$ and $\tilde{E}_\theta \approx 0.03$ V/cm, and they are in phase (Fig. 12). The estimated time τ_f is 7 ms, while the observed confinement time is 4.5 ms. In the case of the J x B-type gun, we have $\tilde{n}/n_0 \approx 0.13$ and $\tilde{E}_\theta \approx 0.06$ V/cm. The estimated time τ_f is 7 ms, while the observed confinement time is 3.5 ms. The phase velocity of the fluctuations along the azimuthal direction on a magnetic surface is measured

by shifting the probe position with reference to a fixed probe. The direction of propagation of the fluctuations is the same as the direction of the diamagnetic electron drift. The phase velocity of the fluctuations changes with time, but its typical value is 1.0×10^5 cm/s for the ECRH-plasma. On the other hand, the phase velocity of the drift wave v_d in the laboratory frame can be estimated as $v_d = (T_e/eB)\nabla n/n + E_r/B$. When the observed values are used, we have $v_d = 1.4 \times 10^5$ cm/s. The frequency of n is 5 kHz; this result reduces to the wavelength of 20 cm, which is approximately equal to $2\pi a$. In the case of the J × B-type gun, the estimated value of v_d is 1.5×10^5 cm/s. The frequency of n is 4.8 kHz; this reduces the velocity of drift wave to 1.1×10^5 cm/s. These results show that the observed fluctuations are due to drift waves. Although the condition of shear stabilization [13] is difficult to satisfy in the stellarator, there is evidence that shear decreases the amplitude of the fluctuations [14]. In the case of an argon plasma produced by ECRH, the fluctuations become weaker, and the convective cells are weaker than for the helium plasma.

4. CONCLUSION

The observed diffusion coefficients are 20-30 times smaller than the Bohm coefficient in the case of helium plasmas and they are one order of magnitude smaller than those suggested by neoclassical transport theories [15-17]. In the case of argon plasma produced by ECRH, the observed diffusion coefficient is about 1/100 of the Bohm coefficient, and it agrees with the neoclassical value within a factor of 2. The scaling of the confinement time τ is $\tau \propto Ba^2/T_e \iota^\alpha$, ($\alpha = 1-2$). The observed distributions of the plasma densities and potentials show that the equipotential surfaces deviate from the magnetic surfaces, because of the inhomogeneity of the magnitude of stellarator field. These electric fields cause convective motions and transport the plasma close to the centre towards the boundary region where a density gradient exists and fluctuations due to drift waves are observed. The plasma losses caused by the observed convective motions and the fluctuations due to drift waves can roughly explain the decay times of the plasmas.

Finally, the authors wish to express their sincere gratitude to Professors K. Husimi and K. Takayama for their continuous encouragement.

REFERENCES

- [1] BERKL, E. et al., in Plasma Physics and Controlled Nuclear Fusion Research (Proc. Conf., Novosibirsk, 1968) 1, IAEA, Vienna (1969) 513.
- [2] BROWN, I.G. et al., *ibid.*, 1, 497.
- [3] ADLAM, J.H. et al., *ibid.*, 1, 573.
- [4] BEREZHETSKY, M.S. et al., *ibid.*, 1, 529.
- [5] BURCHENKO, P.Ya. et al., *ibid.*, 1, 543.
- [6] BOCHAROV, V.N. et al., *ibid.*, 1, 61.
- [7] BERKL, E., von GIERKE, G., GRIEGER, G., IPP 2/69, Garching (Juni 1968).
- [8] HARRIES, W.L., *Physics Fluids* 13 (1970) 140.
- [9] SCHMIDT, J.A., SCHMIDT, G.L., *Physics Fluids* 13 (1970) 1351.
- [10] MIYAMOTO, K., *Physics Fluids* 14 (1971) 722.

- [11] PFIRSCH, D., SCHLÜTER, A., Max-Planck-Institut Report MPI-PA-7/62; ECKHART, D., GRIEGER, G., *ibid.*, MPI-PA-29/64.
- [12] YOSHIKAWA, S., BARRAULT, M. R., *Physics Fluids* 12 (1969) 1858.
- [13] KRALL, N. A., ROSENBLUTH, M. N., *Physics Fluids* 6 (1963) 254.
- [14] STOTT, P. E., LITTLE, P. F., BURT, J., *Phys. Rev. Letts* 25 (1970) 996.
- [15] GALEEV, A. A., SAGDEEV, R. Z., *Sov. Phys. JETP* 26 (1968) 233.
- [16] STRINGER, T. E., *Physics Fluids* 13 (1970) 810.
- [17] KOVRIZHNYKH, L. M., *Sov. Phys. JETP* 29 (1969) 475.

DISCUSSION

N. K. WINSOR: In Figs 9 and 10, where is the major toroidal axis?

K. MIYAMOTO: The major axis is on the left in Figs 9 and 10.

N. K. WINSOR: Near the upper right-hand corner of each density plot, there is a local region of steep radial density gradient with local ripples in the density contours near the outside. This may indicate the presence of a stationary shock and associated increases in local convection and dissipation.

K. MIYAMOTO: We tried to explain the contour of equipotential and equidensity surfaces using stationary-state fluid equations for two components. We have qualitative but not quantitative agreement with the experimental results. We should take account of time-dependent terms.

A. V. GEORGIEVSKY: Have you studied the magnetic field configuration and the plasma confinement for the torsatron regime? If so, what were the main results?

K. MIYAMOTO: We spent so much time investigating potential and density distribution that we were unable to consider the torsatron configurations in detail.

A. V. GEORGIEVSKY: How can you explain the fact that τ is practically independent of the ratio I_V/I_T ? A change in I_V/I_T causes changes in many of the magnetic field parameters ϵ , θ , V'' , $\iota(0)$, etc.

K. MIYAMOTO: When the ratio I_V/I_T is changed, the magnetic-field parameters you mention also change, along with the well depth. It is not easy to determine the dependence of τ on the well depth, but it may be that this depth does not greatly affect the confinement time under our experimental conditions.

C. W. HARTMAN: Have you compared potential and density contours with symmetric reversal of the winding currents and, if so, do the contours also show a symmetric reversal?

K. MIYAMOTO: We measured the contours for different phases of helical pitch, changing the direction of the current in the helical coil. The contours rotate according to the helical pitch, but the components of the perturbation due to the toroidal drift remain without rotation.

R. M. SINCLAIR: In Fig. 5 of the preprint you show a smooth dependence of confinement time on rotational transform, with no maxima or minima reflecting rational transform values. When $L = 2\pi(p/q)$, do your measurements of the field itself show break-up of the magnetic surfaces into islands?

K. MIYAMOTO: We followed the magnetic lines of force by a pulsed electron beam method in several cases. The agreement between measured and computed results is within a few percent. Since our stellarator has an $\ell = 3$ helical winding, we did not measure the magnetic surface for $L = 2\pi(p/q)$ with particular care.

S. YOSHIKAWA: Would you comment on why the confinement time of the argon plasma is longer than that of the helium plasma by a factor of 4?

K. MIYAMOTO: We have not yet done the detailed experimental investigations, but there are a number of possible reasons. The large ion/electron mass ratio reduces the growth rate of the collisional drift mode. We observed a decrease in density fluctuations. Owing to the larger ion Larmor radius, the viscosity becomes greater than in the case of the helium plasma. The vortex of convection can be damped more quickly and this might result in the suppression of convective loss. The electron mean free path is longer and the short circuit effect of the perturbed electric fields is greater. Observed convective cells are actually weak in the case of argon plasma.

PLASMA CONFINEMENT EXPERIMENT IN THE HELIOTRON-D MACHINE

K. UO, A. IYOSHI, Sh. YOSHIOKA, T. ISHIDA,
Sh. KONOSHIMA
Plasma Physics Laboratory, Faculty of Engineering,
Kyoto University,
Gokasho, Uji, Japan
M. SATO
Keio University,
Tokyo, Japan

Abstract

PLASMA CONFINEMENT EXPERIMENT IN THE HELIOTRON-D MACHINE.

The Heliotron-D is a toroidal machine with the helical heliotron field as confining magnetic field. By varying the combination of the three kinds of fields produced by the helical, toroidal and vertical field coils various kinds of helical heliotron field are obtained. The maximum rotational transform angle of the field is more than 9π and the shear parameter is over 2.0. It is possible to form a shallow magnetic well or an anti-well by changing $\alpha = B(\text{toroidal})/B(\text{helical})$. Plasma with $n_e = 10^8 \sim 10^{10} \text{ cm}^{-3}$ and $T_e = 1 \sim 20 \text{ eV}$ is produced by electron cyclotron resonance heating and a gun. The neutral particle density is typically $5 \times 10^{12} \text{ cm}^{-3}$ for the ECRH-plasma and 10^{11} cm^{-3} for the gun plasma. The plasma is weakly ionized. The effect of the vertical field on confinement is examined and the optimum $\beta = B(\text{vertical})/B(\text{helical})$ is determined. The equi-density curve nearly coincides with the calculated magnetic surface, and the density profile has a sharp boundary. Under optimum conditions, the confinement time is about 40 Bohm times. For the gun plasma, the observed confinement time is a few tenths of the value predicted by the "neo-classical" theory in an asymmetric toroidal system.

1. THE HELICAL HELIOTRON MAGNETIC FIELD

The helical heliotron field [1-3] is one of the new axially asymmetric external conductor systems [4] similar to the torsatron field [5, 6]; it is composed of three kinds of fields, the helical, the toroidal, and the vertical field. The helical field is produced by the current-carrying single helical conductor, which is $m + 1/\ell$ times wound around the minor axis of the torus and closes itself after ℓ circuits around the torus, where m and ℓ are integers. The equation of the helix of the helical conductor is given by $r_0 = a$, and $\theta_0 = \kappa \varphi_0$ in the (r, θ, φ) -quasi-toroidal co-ordinate system, where $\kappa = 2\pi R/p = m + 1/\ell$ with R being the major radius of the torus, a the minor radius and p the helical pitch. In the Heliotron-D machine, we have $m = 12$ and $\ell = 2$.

The field characteristics are determined by the parameters R , a , κ , α and β , where α and β are, respectively, the ratios of the magnetic flux density of the toroidal and the vertical field to that of the longitudinal helical-field component on the minor axis. An adequate choice of β gives the closed magnetic surfaces of a wide cross-section inside the helical conductor as shown in Fig. 1. The rotational transform, $\iota/2\pi$, the shear parameter $\Theta = (r^2/2\pi R)(d\iota/dr)$, and the average magnetic well $\langle B \rangle^2$ for various α are shown in Figs 2, 3, and 4, respectively. The field has a shallow magnetic well for $\alpha < -1$ and an anti-well for $\alpha > -1$. The rotational transform near the magnetic axis increases as $|\alpha + 1|$ decreases. The

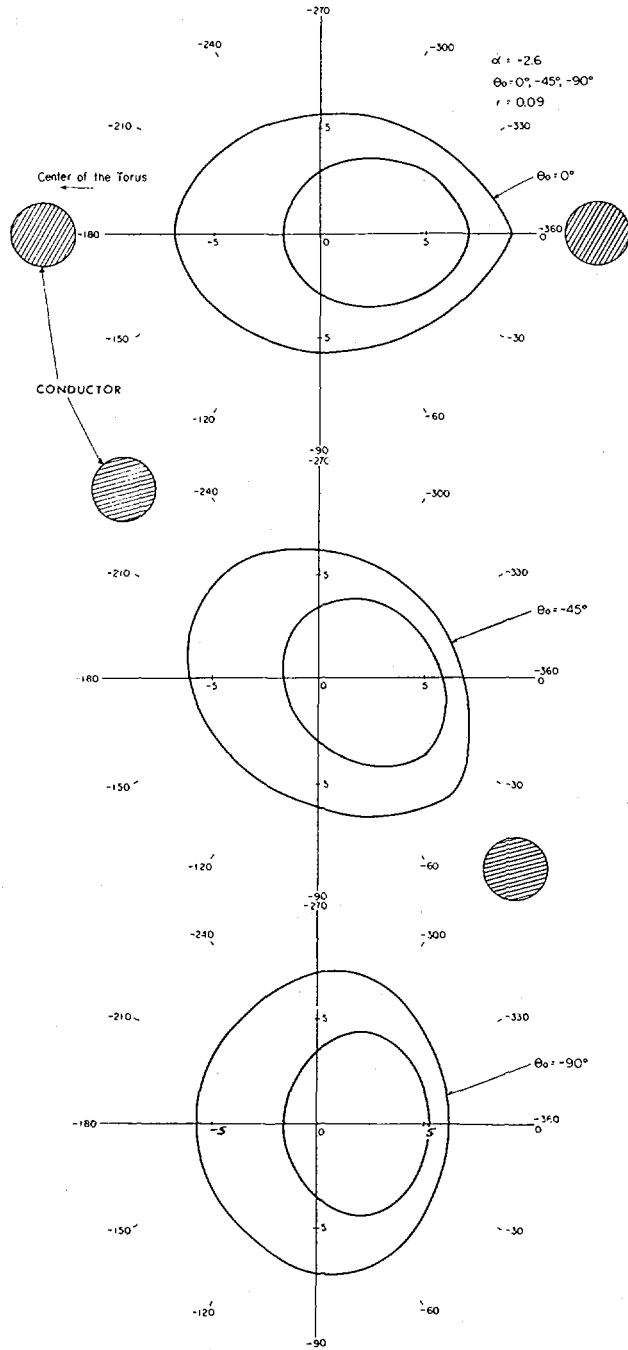


FIG.1. Examples of closed magnetic surfaces for $\alpha = -2.6$. Hatched circles are cross-sections of the helical conductor. Radial distance in centimetres.

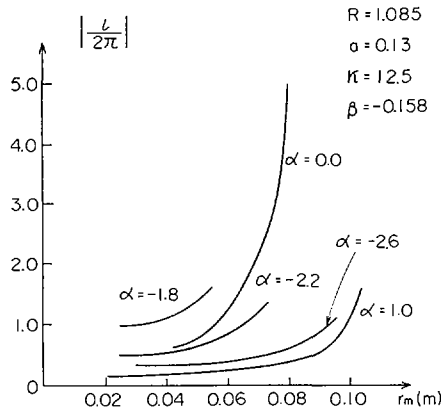


FIG.2. Rotational transform as a function of r_m . r_m is the average radius of the magnetic surfaces.

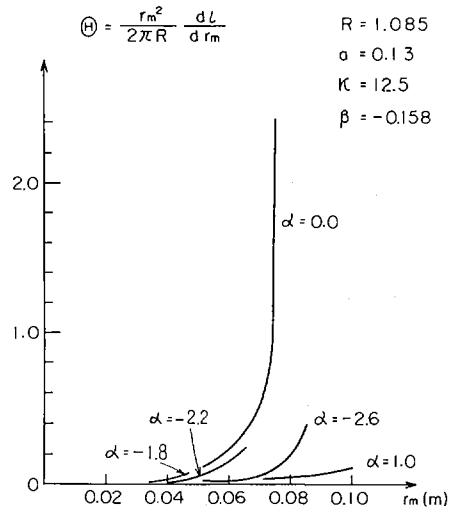


FIG.3. Shear parameter as a function of r_m .

maximum values of $l/2\pi$ and Θ at the outermost closed magnetic surface are obtained for $\alpha = 0$. The larger cross-sectional area of the outermost closed magnetic surface inside the helical conductor is provided by the larger $|\alpha + 1|$. The magnetic axis rotates about a circle on the median plane concentric with the minor axis. For $\alpha = -1$, the field becomes a helical quadrupole, and for $\alpha > -1$, it becomes a hybrid field of both the internal and the external conductor systems.

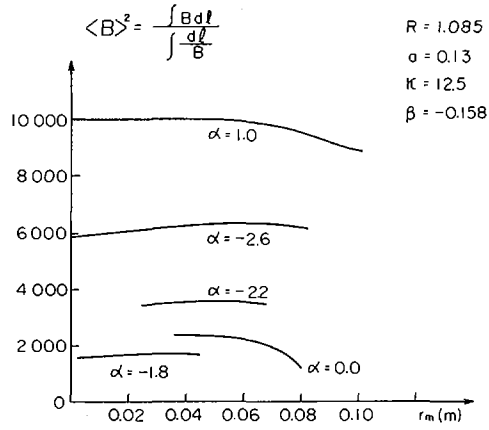


FIG. 4. Average magnetic well $\langle B \rangle^2$ as a function of r_m .

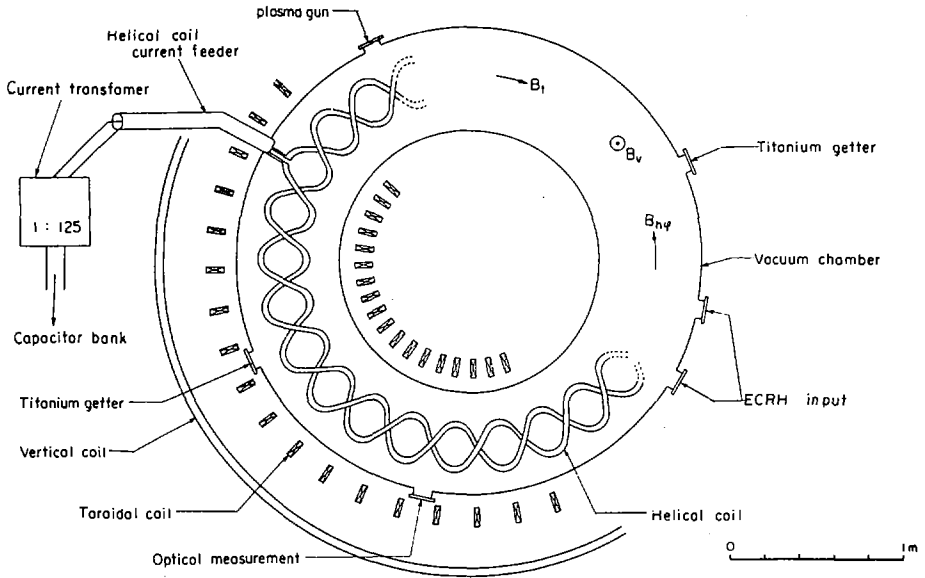


FIG. 5. Schematic view of the Heliotron-D machine. Major radius of vacuum vessel, $R_0 = 1.05$ m. Major radius of helical coil, $R = 1.085$ m. Minor radius of helical coil, $a = 0.13$ m. Inner radius of vacuum vessel, $r_0 = 0.3$ m. Helical coil thickness, $d = 0.04$ m. Helical coil pitch, $p = 2\pi R/\kappa$, $\kappa = 12.5$.

2. THE HELIOTRON-D MACHINE

The general structure of the Heliotron-D machine is shown in Fig. 5. A current-carrying helical conductor of radius 0.13 m, thickness 0.04 m and pitch $2\pi R/12.5$, is suspended with thin inconel wires inside a vacuum vessel. It is designed to be exchangeable with other helical conductors of different geometries. The maximum magnetic flux densities of the toroidal, helical, and vertical field are 5 kG, 3 kG, and 0.5 kG, respectively; ninety percent flat top of the magnetic field lasts normally 25 ms. By varying the combinations of the three kinds of fields, we obtain the various kinds of magnetic field configuration. The field configurations used for the experiment are $\alpha = -2.6$, -2.2 , -1.8 , and 0. The configuration with $\alpha = -2.65$ is used as a standard in this paper. The base pressure is 5×10^{-7} Torr; helium is the gas used.

3. PLASMA PRODUCTION AND DIAGNOSTICS

The plasma is produced by electron cyclotron resonance heating (ECRH) and by a rail-type plasma gun. The peak microwave power of 2.45 GHz is 5 kW, and the pulse width varies between $50 \mu\text{s}$ and 2 ms. The pressure of neutral helium is between 5×10^{-5} Torr and 3×10^{-3} Torr. The plasma density of the experiment ranges between 10^8 cm^{-3} and 10^{10} cm^{-3} , and electron temperature in the afterglow is 2 eV to 20 eV. The neutral density is typically 10^{12} to 10^{13} cm^{-3} . The degree of ionization is between 10^{-3} and 10^{-4} . Electron density and electron temperature are measured by double and single probes.

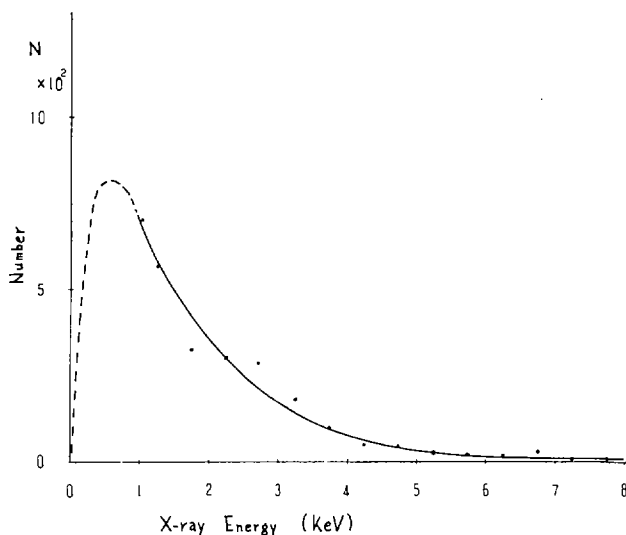


FIG.6. Energy distribution of X-rays observed during ECRH. Average energy is 1.1 keV, under the assumption of Maxwell distribution. The ECRH-power is about 2.5 kW and the pulse width is 2 ms. $\alpha = -2.2$.

X-rays from the ECRH-plasma are observed by a proportional counter with Mylar window. The observed energy distribution of high-energy electrons during the ECRH-pulse is shown in Fig. 6, where a correction due to the transmission characteristics of the window film is taken into account. The average energy is about 1 keV. We cannot, however, observe any X-ray signal in the afterglow. This implies that the hot electrons cannot survive in rather high-density neutral gas of density 10^{12} to 10^{13} cm^{-3} . Thus, we can neglect the strong re-cycling effect due to high-energy electrons in the afterglow.

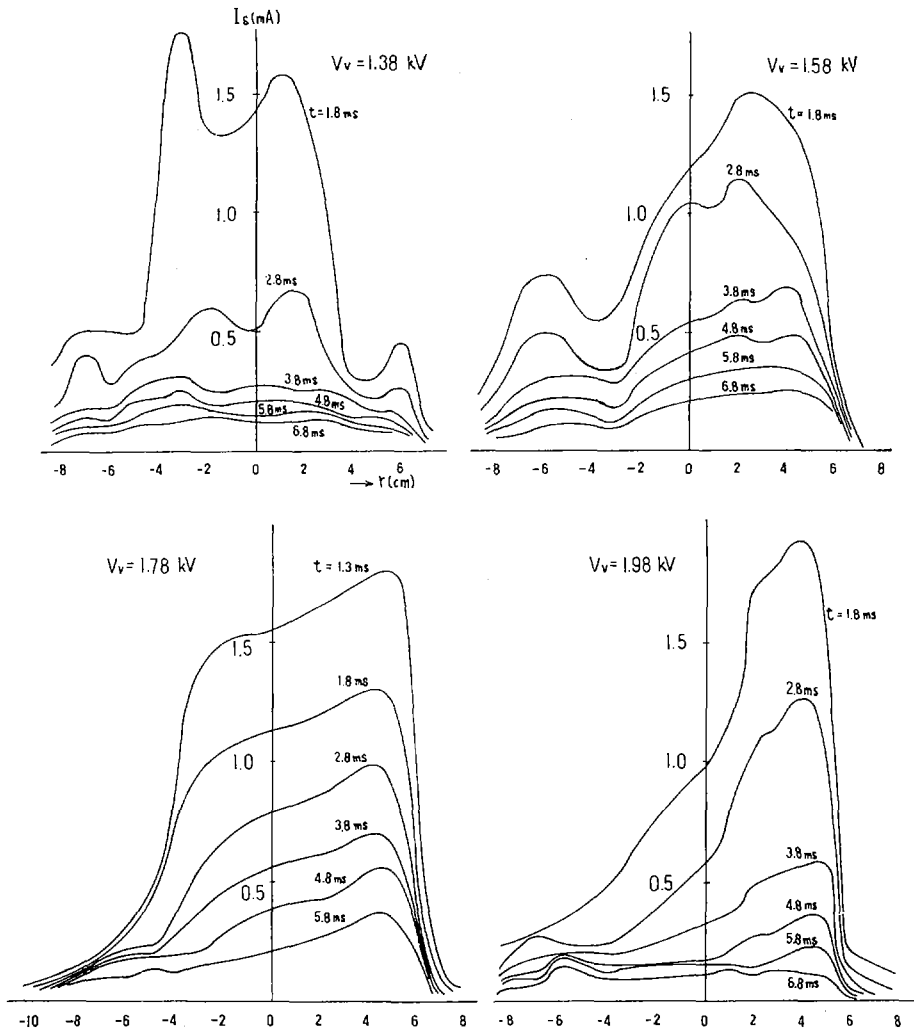


FIG. 7. Density profiles for different β . $V_v = 1.78$ kV (50 G/kV) corresponds to $\beta = -0.15$. $T_e \approx 20$ eV immediately after ECRH.

The gun produces a plasma of $T_e < 20$ eV and $n_e < 10^{11}$ cm $^{-3}$. The neutral density changes slightly during the afterglow, but is typically 10^{11} cm $^{-3}$. We have not obtained any definite information on ions. The ion temperature estimated by measuring the time of flight is higher than several tens of eV at the initial stage, and it is cooled down to several eV in a few ms, owing to charge exchange with neutral atoms. The Ohmic-heating current, which could be induced in the plasma owing to a time-varying magnetic flux interlinked with the plasma ring, is measured by a Rogowski coil and a directional probe. Near the flat top of the magnetic field, the loop voltage is less than 0.1 V and the current strength is about 0.05 A in the case of $\alpha = -2.6$ and $|B| \sim 0.9$ kG. This result indicates that the plasma resistivity is by about a factor of 3 larger than that of the calculated value for the weakly ionized plasma. The discrepancy could be attributed to the rather strong mirror effect of the helical heliotron field and/or the anomalous resistivity due to ion acoustic instability.

4. CONFINEMENT EXPERIMENT AND DISCUSSION

(a) ECRH plasma

Figure 7 shows the density profiles for different β . We can see that the density profiles and the decay rates vary as β varies. The dependence of τ on β is shown in Fig.8. Optimum β is close to the calculated value. Figure 7 also shows that the density has a sharp boundary which corresponds to the calculated outermost closed magnetic surface. The density distribution $n(r, \theta)$ is measured to check the equilibrium condition $p(\psi) = \text{const.}$ Both equi-density contours measured and the calculated outermost closed magnetic surfaces are shown in Fig.9. It is found that at an earlier stage of the afterglow ($t = 1$ ms) the plasma almost reaches the equilibrium state. Equi-floating potential contours are also shown in Fig.9. The convective-cell effect is not observed to an appreciable extent. Since the plasma is

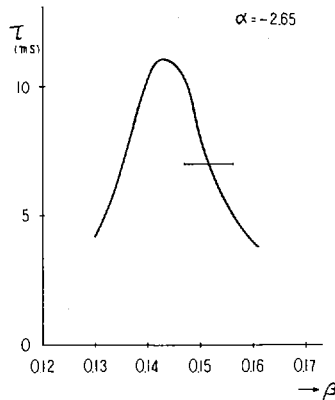


FIG.8. The dependence of τ on β for $\alpha = -2.65$, $n_e = 10^9$ cm $^{-3}$, $T_e = 6$ eV.

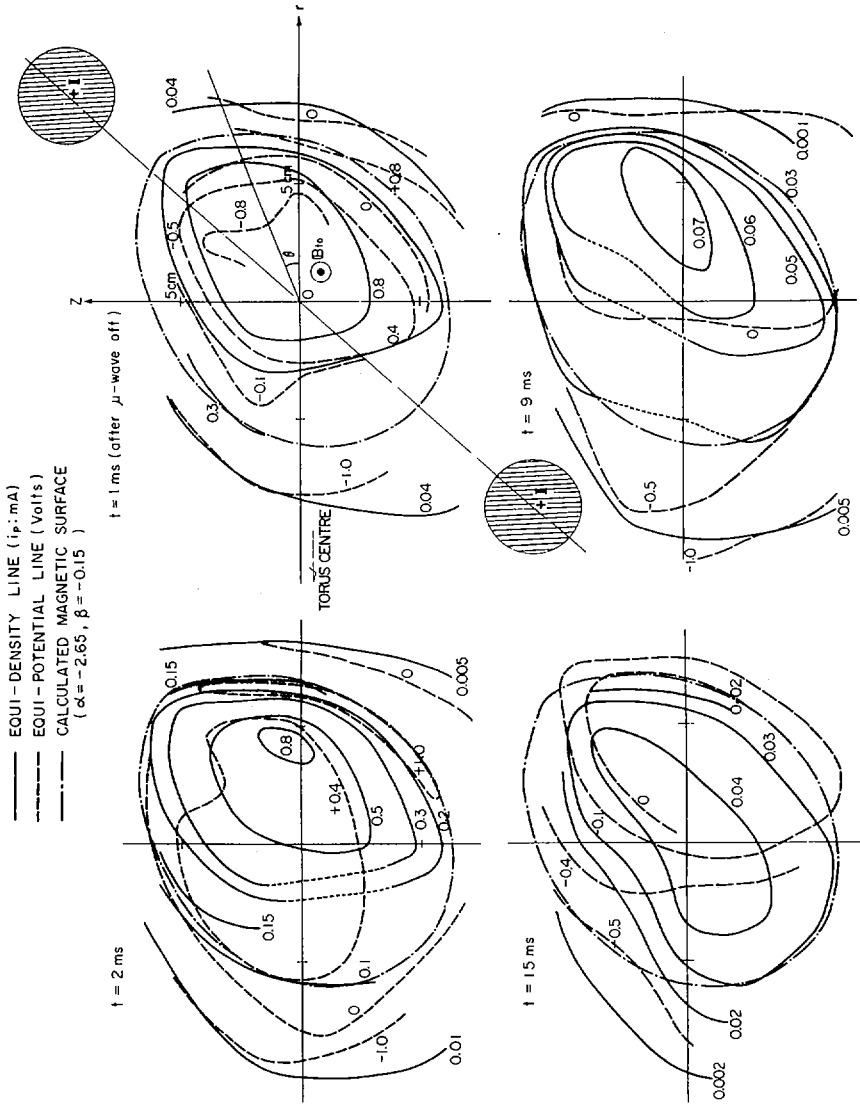


FIG. 9. Equi-density contours and equi-floating potential contours at different times, $\alpha = -2.65$ and $\beta = -0.15$. The calculated outermost magnetic surface is shown in chain line.

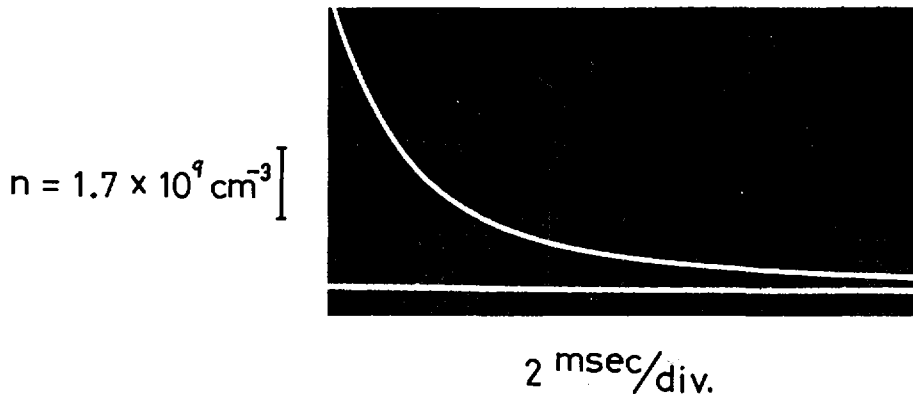


FIG.10. Ion saturation current of the double probe. $\alpha = -2.65$, $\beta = -0.14$, $T_e \cong 10 \text{ eV}$ and $|B| \cong 1.7 \text{ kG}$.

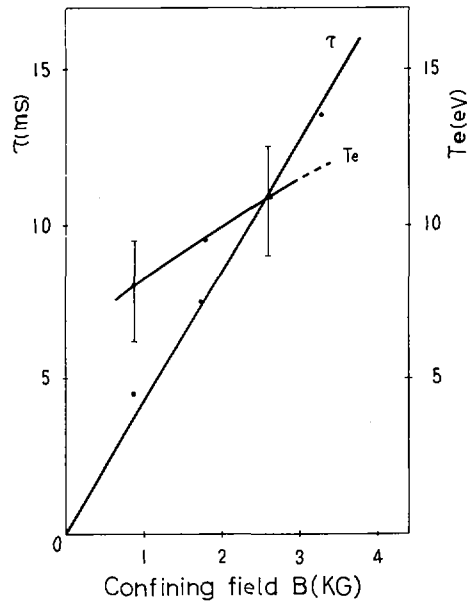


FIG.11. Confinement time and electron temperature as a function of confining field. $\alpha = -2.65$.

positively charged, the electric field is in the positive r -direction. The electron temperature drops rapidly from about 20 eV to several eV and then decays slowly. The electron cooling can be attributed to inelastic collisions with neutral atoms. To avoid an ambiguity of the confinement time resulting from both the variation of the electron temperature and the ionization effect, we measure the decay time in the region of slow temperature variation several microseconds after the ECRH-pulse. Since the neutral density is not low enough in our experiment, we cannot neglect the

ionization effect due to hot electrons in the Maxwellian tail of the electrons of 4 eV. After correcting for this effect, we obtain $\tau \approx 17$ ms for $T_e = 4$ eV, $n_e \approx 10^9$ cm⁻³, and $|B| \approx 0.9$ kG, which is about $40 \tau_B$. The change of the neutral pressure from 10^{-5} Torr to 10^{-3} Torr gives no drastic change in τ . Fluctuations which might have a serious effect on confinement are not observed.

(b) Gun plasma

The density decay with two different time constants are shown in Fig. 10. The shorter time constant of a few microseconds may be ascribed to the filling process of the plasma into the confining magnetic field and/or to the higher ion and electron temperatures; it does not seem to depend on the magnetic flux density B . As shown in Fig. 11, the longer time constant of 5 to 30 ms depends on B . The plasma parameters obtained in this experiment satisfy the conditions of the theory of trapped-particle diffusion in an axially asymmetric system as given by Kovrizhnykh [7]. The observed confinement time is somewhat shorter than the theoretically predicted value, i. e. a few tenths of the predicted value.

ACKNOWLEDGEMENTS

The authors wish to express their indebtedness to Prof. C. Uenosono for his constant encouragement and are grateful to Prof. I. Sakisaka, Dr. K. Hirano, Dr. Y. Sakamoto, and Dr. S. Ohi for their kind help in plasma production and diagnostics. They would also like to thank Messrs. I. Ohtake and K. Sazuki for their help in the experiment.

REFERENCES

- [1] UO, K., *J. Phys. Soc. Japan* **16** (1961) 1380.
- [2] UO, K., ITATANI, R., MOHRI, A., OSHIYAMA, H., ARIGA, S., UEDE, T., in *Plasma Physics and Controlled Fusion Research (Proc. Conf. Novosibirsk, 1968)* **1**, IAEA, Vienna (1969) 217.
- [3] UO, K., *Plasma Physics* **13** (1971) 243.
- [4] Final Report of the IAEA Panel, *Nucl. Fusion* **10** (1970) 413.
- [5] GOURDON, C., MARTY, D., MASCHKE, E., DUMONT, J.P., in *Plasma Physics and Controlled Fusion Research (Proc. Conf. Novosibirsk, 1968)* **1**, IAEA, Vienna (1969) 847.
- [6] GOURDON, C., MARTY, D., MASCHKE, E., TOUCHE, J., *Controlled Fusion and Plasma Physics (Proc. 4th Europ. Conf. Rome, 1970)* 35.
- [7] KOVRIZHNYKH, L.M., *Sov. Phys. JETP* **26** (1969) 475.

ЭЛЕКТРОПРОВОДНОСТЬ И ТОКОВЫЙ НАГРЕВ ПЛАЗМЫ В СИЛЬНОМ МАГНИТНОМ ПОЛЕ

П. Я. БУРЧЕНКО, Е. Д. ВОЛКОВ, В. А. РУДАКОВ,
 В. Л. СИЗОНЕНКО, К. Н. СТЕПАНОВ
 Физико-технический институт
 Академии наук Украинской ССР,
 Харьков,
 Союз Советских Социалистических Республик

Abstract—Аннотация

THE ELECTRICAL CONDUCTIVITY AND CURRENT HEATING OF PLASMA IN A STRONG MAGNETIC FIELD.

The results are given of a study, with electric fields from $E = (0.01-100) E_k$, of the electrical conductivity of a plasma in a strong magnetic field $H_0 > (4\pi m_e c^2 n_e)^{1/2}$. Here $E_k = 1.36 \times 10^{-12} n_e / T_e$ is the Dreicer critical field, n_e the plasma density, m_e the electron mass, T_e the electron temperature of the plasma and c the speed of light. It is shown that when the electric fields $E = (0.1-0.7) \text{ V/cm}$ and the plasma density $n_e = (2-4) \times 10^{12} \text{ cm}^{-3}$, the electrical conductivity of the plasma σ is inversely proportional to E . The current velocity of the electrons u in the region $10 < E/E_k < 100$ tends to saturation. At the same time a linear relationship is observed between the current and thermal velocities of the electrons $u \approx 0.1 v_{Te}$. The relationship between the resistance anomaly σ_{CT}/σ and E/E_k is also linear in the region $0.1 < E/E_k < 100$. Here σ_{CT} is the Coulomb conductivity calculated on the basis of the temperature determined from measurements of the plasma diamagnetism. The electrical conductivity anomaly reaches values of the order of 10^3 when $E/E_k = 100$. When such an anomaly exists the plasma temperature $T = T_e + \xi T_i$ amounts to 500-600 eV at a density $n_e = (2-4) \times 10^{12} \text{ cm}^{-3}$. A comparison is made with data obtained during previous experiments carried out in a narrower range of E/E_k in various closed magnetic traps. An explanation is offered for the data obtained on the basis of assumptions regarding the build-up of ion-acoustic instability. It is assumed that the stabilization of unstable ion-acoustic oscillations occurs when the movement of resonance electrons in the field of these oscillations becomes strongly non-linear, namely when their oscillation velocity attains the order of the wave phase velocity. In that case the energy of the oscillations $W = 1/8\pi \langle (\Delta\varphi)^2 \rangle \sim (U/v_{Te})^4 n_e T_e$. Deceleration of the greater part of the non-resonance electrons and, consequently, the occurrence of an anomalous resistance, may be caused by the scattering of the electrons by oscillations, the phase of which undergoes arbitrary changes in a non-linear régime. On the assumption that the correlation time of the Fourier components of the oscillational electric field is of the order of the inverse non-linear decrement of attenuation, an expression has been obtained for the conductivity of the plasma.

ЭЛЕКТРОПРОВОДНОСТЬ И ТОКОВЫЙ НАГРЕВ ПЛАЗМЫ В СИЛЬНОМ МАГНИТНОМ ПОЛЕ.

Приведены результаты изучения электропроводности плазмы в сильном магнитном поле $H_0 > (4\pi m_e c^2 n_e)^{1/2}$, полученные при электрических полях $E = (0,01 \div 100) E_k$. Здесь $E_k = 1,36 \cdot 10^{-12} n_e / T_e$ — критическое поле Драйзера, n_e — плотность плазмы, m_e — масса электрона, T_e — электронная температура плазмы, c — скорость света. Показано, что при электрических полях $E = (0,1 \div 0,7) \text{ В/см}$ и плотности плазмы $n_e = (2 \div 4) \cdot 10^{12} \text{ см}^{-3}$ электропроводность плазмы σ обратно пропорциональна E . Величина токовой скорости электронов U в области $10 < E/E_k < 100$ стремится к насыщению. При этом наблюдается линейная связь между токовой и тепловой скоростями электронов $U \approx 0,1 v_{Te}$. Зависимость аномалии сопротивления σ_{CT}/σ от E/E_k также линейна в области $0,1 < E/E_k < 100$. Здесь σ_{CT} — кулоновская проводимость, вычисленная по температуре, определенной из измерений диамагнетизма плазмы. Величина аномалии электропроводности достигает значений порядка 10^3 при $E/E_k \approx 100$. Температура плазмы $T = T_e + \xi T_i$ составляет при наличии такой аномалии 500-600 эВ при плотности $n_e \approx (2 \div 4) \cdot 10^{12} \text{ см}^{-3}$. Проведено сравнение полученных данных с более ранними экспериментами, проведенными в более узкой области E/E_k на различных замкнутых магнитных ловушках. Предлагается объяснение полученных данных на основе предположения о расщепе ионно-звуковой неустойчивости. Предполагается, что стабилизация неустойчивых ионно-звуковых колебаний происходит, когда движение резонансных электронов в поле этих колебаний становится сильно нелинейным, а именно, когда

их осцилляционная скорость становится порядка фазовой скорости волны. В этом случае энергия колебаний $W = 1/8\pi <(\Delta\varphi)^2> \sim (U/v_{Te})^4 n_e T_e$. Торможение основной массы нерезонансных электронов и, следовательно, появление аномального сопротивления могут быть обусловлены их рассеянием колебаниями, фаза которых в сильно нелинейном режиме изменяется случайно. В предположении, что время корреляции компонент Фурье электрического поля колебаний порядка обратного нелинейного декремента затухания, получено выражение для проводимости плазмы.

Экспериментальные исследования токового нагрева плазмы, выполненные на замкнутой магнитной ловушке Токамак [1,2], а также на стеллараторах "С" [3,4] и "Сириус" [5,6], показали, что в случае сильных магнитных полей $H_0 > (4\pi m_e c^2 n)^{1/2}$ наблюдается значительная аномалия сопротивления при электрических полях, меньших или сравнимых с критическим полем Драйзера $E_k \approx 1,4 \cdot 10^{-12} n_e / T_e$ [7]. Здесь n — плотность электронов плазмы, T_e — температура ее электронной компоненты в электрон-вольтах, m_e — масса электрона, c — скорость света.

Существующая теория аномальной электропроводности для случая слабых магнитных полей [8-10] не дает объяснения результатов указанных выше работ.

Было предложено два механизма [11,12] для интерпретации данных, полученных на токамаке, но их детальное сравнение с экспериментом пока затруднительно из-за ограниченности области изменения параметров плазмы в этой установке. Кроме того, в работе [13] была предпринята попытка объяснить аномалию сопротивления замагниченной плазмы применительно к экспериментам на стеллараторах [3-6], в которых исследовался режим слабых электрических полей $E < E_k$.

С целью исследования изучаемого эффекта и его макроскопических характеристик на стеллараторе "Сириус" [14] была выполнена серия экспериментов, отдельные результаты которых и их сравнение с имеющимися теоретическими представлениями приводятся в данном докладе.

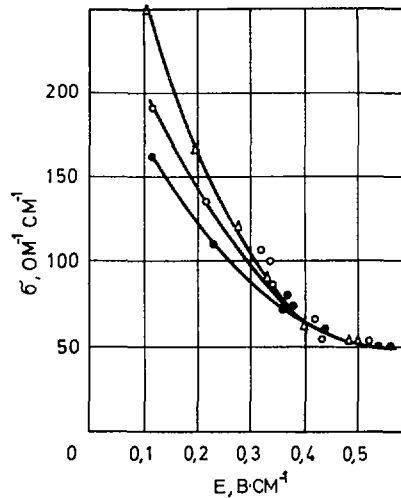


Рис. 1. Зависимость проводимости плазмы от напряженности электрического поля. $H_0 = 16$ кэ. Δ $n = 4 \cdot 10^{12}$ см⁻³, \square $n = 3 \cdot 10^{12}$ см⁻³, \bullet $n = 2 \cdot 10^{12}$ см⁻³.

Исследовалось сопротивление гелиевой плазмы с плотностью электронов $n = (2 \div 6) \cdot 10^{12} \text{ см}^{-3}$. Напряженность магнитного поля изменялась при этом в пределах от 8 до 16 кэ, напряженность электрического поля, параллельного магнитному, — от 0,1 до 0,7 В/см. Величина отношения электронной циклотронной ω_{He} и ленгмювской ω_{pe} частот изменялась в исследуемой области от 0,8 до 3,6.

Проводились измерения разрядного тока в камере стелларатора, напряжения на ее обходе, изменения продольного магнитного потока, обусловленного диамагнетизмом плазмы и поведения плотности плазмы во времени.

При обработке результатов экспериментов предполагалось, что ток равномерно распределен по сечению плазменного шнура (прямоугольное распределение).

Обнаружено, что при повышении напряженности электрического поля плазменный ток стремится к насыщению, а скорость нарастания диамагнитного сигнала увеличивается. При этом определенная по диамагнитным измерениям сумма электронной и ионной температур значительно превосходит ту, которая соответствует измерениям по проводимости в приближении чисто кулоновских столкновений.

На рис. 1 показана зависимость проводимости плазмы $\sigma = j/E$, измеренная при напряженности магнитного поля $H_0 = 16 \text{ кэ}$ и трех различных значениях плотности электронов, от напряженности продольного электрического поля. При $E > 0,2 \text{ В/см}$ она очень близка к зависимости типа $\sigma \sim 1/E$. Обработка данных экспериментов показала, что величина токовой скорости $U = j/en$ быстро нарастает с ростом напряженности электрического поля в диапазоне $0 < E/E_k < 10$ и стремится к насыщению в области $10 \leq E/E_k \leq 80$. Следует отметить, что E_k рассчитывалось в этом случае по температуре, вычисленной из измерений диамагнетизма плазмы, в предположении, что температура ее ионной компоненты $T_i = 0$.

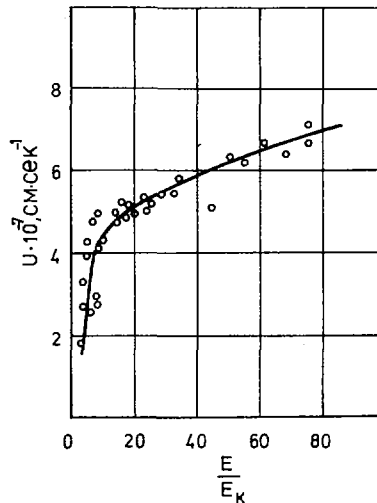


Рис. 2. Зависимость токовой скорости электронов от отношения приложенного электрического поля к критическому полю Драйзера. $H_0 = 16 \text{ кэ}$.

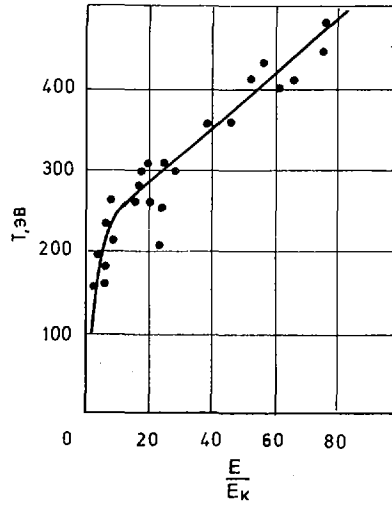


Рис. 3. Зависимость температуры плазмы $(T_e + \zeta T_i) = T$ от отношения приложенного электрического поля к критическому полю Драйзера. $H_0 = 16$ кэ.

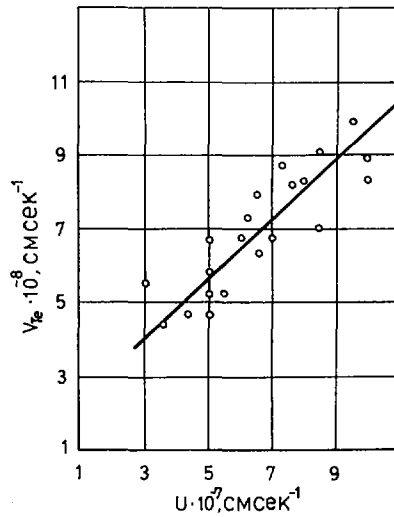


Рис. 4. Зависимость тепловой скорости электронов плазмы от их токовой скорости $H_0 = 16$ кэ.

Скорость роста температуры плазмы с увеличением напряженности электрического поля также претерпевает изменение при $E/E_k \approx 10$. Обе эти зависимости показаны на рис. 2 и 3.

Из данных, приведенных на рис. 2 и 3, непосредственно следует линейная зависимость тепловой скорости электронов плазмы $v_{Te} = \sqrt{T_e/m_e}$ от U (рис. 4). Как видно, в этом случае, так же как и на стеллараторе "С",

$U \approx 0,1 v_{Te}$. Для токамака эта величина оказывается несколько большей, а именно $U \approx 0,3 v_{Te}$.

Интересно было определить величину аномалии электропроводности и ее зависимость от отношения приложенного электрического поля к критическому полю Драйзера. На рис. 5 представлены результаты исследования зависимости отношения проводимостей, вычисленной по формуле Спитцера [15] σ_{cT} и измеренной экспериментально σ , от E/E_k . Эта зависимость остается линейной в довольно широком диапазоне изменения E/E_k . Вместе с тем, величина σ_{cT}/σ примерно в 6 раз превосходит ту, которая была получена на установке токамак при одинаковых значениях E/E_k . Столь существенная разница может быть связана с различными предположениями о распределении плотности тока по сечению плазменного шнура, использованными в данной работе и на установке токамак при вычислениях U и σ , а также отчасти тем, что при вычислениях σ_{cT} и E_k здесь использовалась температура, определенная из измерений диамагнетизма, в предположении $T_i = 0$.

Разница может быть обусловлена величиной напряженности магнитного поля и количеством нейтрального газа и примесей в плазме. Контрольные измерения показали, что величина σ_{cT}/σ возрастает с увеличением количества нейтралов и H_0 .

Сравнительный анализ количества примесей в обеих установках и определение эффективного заряда ионов пока невозможны из-за отсутствия экспериментальных данных.

Используя ранее полученные данные [5,6], можно проследить зависимость аномалии электропроводности в широкой области изменения параметров. Графики зависимости σ_{cT}/σ от E/E_k приведены на рис. 6. Для сравнения на этом же графике нанесены точки, полученные на установке

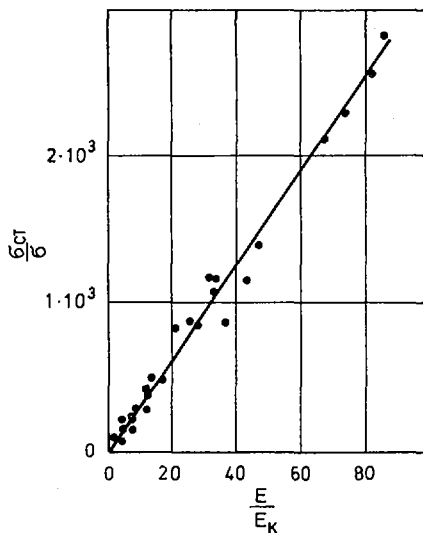


Рис. 5. Зависимость аномалии проводимости σ_{cT}/σ от отношения приложенного электрического поля к критическому полю Драйзера. $H_0 = 16$ кэ, $n = (2 \div 4) \cdot 10^{12} \text{ см}^{-3}$.

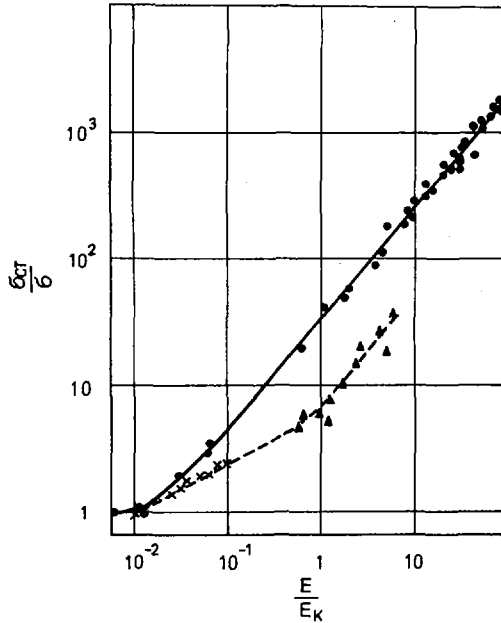


Рис. 6. Зависимость аномалии проводимости $\sigma_{ст}/\sigma$ от отношения приложенного электрического поля к критическому полю Драйзера. Пунктирной линией показана эта же зависимость, построенная по данным, полученным на стеллараторе "С" (X) и токамаке (\blacktriangle).

токамак и стеллараторе "С". Как видно, разница между данными, полученными на различных установках, сводится, в основном, к множителю порядка $2 \div 5$. Причины этого расхождения были уже указаны выше.

Наблюдаемая аномалия сопротивления замагниченной плазмы с продольным током может быть объяснена в предположении развития ионно-звуковой неустойчивости. Теория должна при этом ответить на два основных вопроса:

- 1) Каким механизмом обусловлена стабилизация ионно-звуковой неустойчивости и каков уровень турбулентных пульсаций?
- 2) Если стабилизация имеет место, то каков механизм передачи импульса от электронов ионам, обеспечивающий появление аномального сопротивления, и какова величина эффективной частоты рассеяния электронов на турбулентных пульсациях электрического поля?

В плазме при $\omega_{He}/\omega_{pe} \gg 1$ электроны совершают в поле ионно-звуковых колебаний почти одновременное движение вдоль магнитного поля.

Движение резонансных электронов, ответственных за возбуждение колебаний и имеющих скорость вдоль магнитного поля $v_{||} \sim \omega_k^2/k_{||}$, становится сильно нелинейным, когда потенциал колебаний $\varphi(\vec{r}, t)$ достигает значения, при котором осцилляционная скорость

$$\tilde{v}_z \sim \frac{ek_{||}\varphi}{m_e(k_{||}v_{||} - \omega_k^2)} \quad (1)$$

становится равной по порядку величины фазовой скорости волны $\omega_k^*/k_{||} = v_f \sim U$. Здесь $\omega_k^* \sim \omega_{pi}$ — частота ионно-звуковых колебаний, $k \sim 1/r_D$ — характерный волновой вектор, $k_{||}$ — проекция волнового вектора на направление магнитного поля, U — направленная скорость электронов. Отсюда получаем оценку для энергии ионно-звуковых колебаний.

$$W \approx \frac{k^2 \varphi^2}{8\pi} \sim \left(\frac{U}{v_{Te}} \right)^4 n T_e \quad (2)$$

При уровне шумов (2) резонансный электрон в течение времени $1/\omega_k^*$ смещается под действием поля колебаний на расстояние порядка продольной длины волны $1/k_{||}$ и изменяет свою фазу по отношению к волне на величину порядка π . Естественно ожидать, что в этом случае обмен энергией между резонансными частицами и волнами в среднем прекратится, т.е. ионно-звуковая неустойчивость стабилизируется. Оценку (2) можно также получить на основе теории слабой турбулентности, приравнявая нелинейный декремент заглушения $\gamma_{NL} \sim \omega_{pi} (v_{Te}/U)^3 W/nT_e$, учитывающий нелинейное рассеяние ионно-звуковых колебаний на резонансных электронах, линейному инкременту нарастания $\gamma_L \sim \omega_{pi} U/v_{Te}$ [15].

Основная масса электронов имеет скорость $|v_{||}| \sim v_{Te}$, значительно большую фазовой скорости волны в системе отсчета, движущейся со средней скоростью U , $(\omega_k^* - k_{||} U)/k_{||} \sim v_s \equiv \sqrt{T_e/m_i}$, так что их взаимодействие с колебаниями является адиабатическим и в квазилинейном приближении они должны были бы непрерывно ускоряться внешним электрическим полем. (Асимптотическое поведение функций распределения электронов и ионов и спектральной интенсивности колебаний при $t \rightarrow \infty$ на основе квазилинейной теории было найдено Векштейном, Ржотовым и Сагдеевым [16]).

Торможение электронов и ионов в электрическом поле в отсутствие столкновений может осуществляться за счет нелинейных эффектов. Рассеяние электронов на "биениях" ионно-звуковых колебаний с фазовой скоростью $|(\omega_k^* - \omega_k^*)/(k_{||} - k_{||}^*)| \sim v_{Te}$ приводит к появлению эффективной частоты рассеяния электронов [15].

$$v_{eff} \sim \omega_{pi} \frac{U}{v_{Te}} \left(\frac{W}{nT_e} \right)^2 \sim \omega_{pi} \left(\frac{U}{v_{Te}} \right)^9 \quad (3)$$

Кроме рассеяния на "биениях", возможно существование более сильного механизма торможения электронов и ионов, связанного со случайным сбоем фаз и конечностью времени корреляции компонент Фурье колебаний вследствие их нелинейного взаимодействия.

Так как осциллирующая часть функции распределения электронов при $|v_{||}| \sim v_{Te}$ мала по сравнению с усредненной (фоновой) частью функции распределения f_{0e} ($f \sim U/v_{Te} f_{0e} \ll f_{0e}$), то для f_0 можно воспользоваться уравнением типа квазилинейного уравнения диффузии [17]:

$$\frac{\partial f_0}{\partial t} = \frac{e^2}{m_e^2} \frac{\partial}{\partial v_{||}} \int d\vec{k} k_{||}^2 |\varphi_{\vec{k}}|^2 \frac{\partial f_0}{\partial v_{||}} \frac{v}{(\omega_{\vec{k}}^* - k_{||} v_{||})^2 + \nu^2} \quad (4)$$

При получении (4) корреляционная функция была выбрана для простоты в виде:

$$R_{\vec{k}}(\tau) = \frac{1}{2T} \int_{t-T}^{t+T} \frac{\varphi_{\vec{k}}^*(t') \varphi_{\vec{k}}(t' - \tau)}{|\varphi_{\vec{k}}(t)|^2} dt' \sim e^{-\nu\tau}$$

Время корреляции $1/\nu$ порядка времени нелинейного затухания колебаний, т.е. $\nu \sim \gamma_{NL} \sim \gamma_L$. Умножая (4) на $m_e v_{||}$ и интегрируя по скоростям, получим для скорости изменения импульса электронов в единице объема плазмы:

$$\begin{aligned} \dot{P}_z^{(\text{перез})} &= \frac{\partial}{\partial t} \int m_e v_{||} f_{0e} dv_{||} = -m_e n_0 \nu_{\text{eff}} U \\ &\approx -\frac{e^2}{m_e} \iint d\vec{k} dv_{||} k_{||}^2 |\varphi_{\vec{k}}|^2 \frac{\partial f_{0e}}{\partial v_{||}} \frac{\nu}{(\omega_{\vec{k}} - k_{||} v_{||})^2} \sim \nu m_e n_0 U \frac{W}{n T_e} \end{aligned} \quad (5)$$

Отсюда находим эффективную частоту столкновений:

$$\nu_{\text{eff}} \sim \omega_{pi} \left(\frac{U}{v_{Te}} \right)^5 \quad (6)$$

При наличии электрического поля в стационарном состоянии $m_e \nu_{\text{eff}} U \sim eE$ и

$$U = \eta v_{Te} \left(\frac{eE}{m_e v_{Te} \omega_{pi}} \right)^{1/6} \quad (7)$$

где η — коэффициент порядка единицы. Соотношение (7) можно также представить в виде:

$$\sigma = \frac{e n v_{Te}}{\eta_1 E} \left(\frac{eE}{m_e v_{Te} \omega_{pi}} \right)^{1/6} \quad (8)$$

$$\frac{\sigma_{\text{CT}}}{\sigma} = 2\eta_1 \frac{E}{E_k} \left(\frac{E_k \omega_{pi}}{E \nu_{\text{CT}}} \right)^{1/6} \quad \eta_1 \sim 1 \quad (9)$$

Несмотря на малость по сравнению с единицей параметра $(eE)/(m_e v_{Te} \omega_{pi})$ из-за наличия корня шестой степени в (7)-(9) можно считать, что U не зависит от E , а σ — обратно пропорционально E .

Остановимся на вопросе о законе сохранения импульса. Импульс, приобретаемый в единицу времени электронами от ионно-звуковых колебаний, $\dot{P}_z^{(e)}$, должен в конечном счете передаваться ионам.

Величину $\dot{P}_z^{(i)}$ можно оценить, используя уравнение диффузии для фоновой функции распределения ионов:

$$\frac{\partial f_{0i}}{\partial t} = \frac{e^2}{m_i^2} \frac{\partial}{\partial v} \int d\vec{k} k (\vec{k} \frac{\partial f_{0i}}{\partial v}) |\varphi_{\vec{k}}|^2 \frac{\nu}{(\omega_{\vec{k}} - \vec{k} \vec{v})^2 + \nu^2}$$

Умножая это уравнение на $m_i v_z$ и интегрируя, получим, учитывая малость величин $k v \sim k v_{Ti}$ и ν по сравнению с $\omega_{\vec{k}}$, что

$$\begin{aligned}
 \langle \dot{P}_z \rangle^{(i)} &= \frac{\partial}{\partial t} \int m_i v_z f_0 dv_z = - \frac{e^2}{m_i} \iint d\vec{k} d\vec{v} k_z |\varphi_{\vec{k}}|^2 \left(\vec{k} \frac{\partial f_{0i}}{\partial \vec{v}} \right) \frac{\nu}{(\omega_{\vec{k}} - \vec{k} \cdot \vec{v})^2 + \nu^2} \\
 &\approx - \frac{e^2}{m_i} \iint d\vec{k} d\vec{v} k_z |\varphi_{\vec{k}}|^2 \left(\vec{k} \frac{\partial f_{0i}}{\partial \vec{v}} \right) \frac{2\nu (\vec{k} \cdot \vec{v})}{\omega_{\vec{k}}^3} \sim \omega_{pi} \frac{W}{n T_e} \frac{v_{Te}}{U} U m_e n
 \end{aligned} \quad (10)$$

Сравнивая (10) с (5), находим, что импульс, получаемый ионами, в $(v_{Te}/U)^2$ раз превосходит импульс, получаемый нерезонансными электронами. Однако, поскольку суммарный импульс электронов и ионов должен сохраняться, то изменение импульса ионов должно компенсироваться изменением импульса резонансных электронов. Действительно, для изменения импульса резонансных электронов ($v_{\parallel} \leq U$) получим из (4), полагая в резонансной области

$$\frac{\nu}{(\omega_{\vec{k}} - k_{\parallel} v_{\parallel})^2 + \nu^2} \approx \pi \delta(\omega_{\vec{k}} - k_{\parallel} v_{\parallel})$$

что

$$\begin{aligned}
 \langle \dot{P}_{ze} \rangle^{(рез)} &\sim - \frac{e^2}{m_e} \iint d\vec{k} d\vec{v} k_{\parallel}^2 |\varphi_{\vec{k}}|^2 \frac{|v_{\parallel}|}{v_{Te}^2} \delta(\omega_{\vec{k}} - k_{\parallel} v_{\parallel}) \\
 &\sim \omega_{pi} \frac{W}{n T_e} \cdot \frac{v_{Te}}{U} m_e n U
 \end{aligned} \quad (11)$$

Установившееся турбулентное состояние, по-видимому, не будет стационарным. Характерные времена пульсаций можно оценить, используя уравнения переноса:

$$\begin{aligned}
 \frac{\partial}{\partial t} m_{\alpha} n_{\alpha} U_{\alpha i} + \frac{\partial}{\partial x_k} m_{\alpha} n_{\alpha} \langle (v_i - U_{\alpha i})(v_k - U_{\alpha k}) \rangle \\
 = e_{\alpha} n_{\alpha} E_0 - e_{\alpha} n_{\alpha} \nabla \varphi
 \end{aligned}$$

Произведя усреднение, получим:

$$\frac{\partial}{\partial t} P_{z\alpha} = \frac{\partial}{\partial t} (m_{\alpha} n_{\alpha} U_{\alpha 0} + m_{\alpha} \langle \tilde{n} \tilde{U}_{\alpha z} \rangle) = e_{\alpha} E_0 n - e_{\alpha} \langle \tilde{n}_{\alpha} \nabla \varphi \rangle \quad (12)$$

где $\tilde{A} = A - \langle A \rangle$.

Умножая уравнение Пуассона

$$\Delta \varphi = 4\pi e (\tilde{n} - \tilde{n}_i)$$

на $\nabla \varphi$ и усредняя, получим с учетом однородности турбулентности, что

$$\langle \tilde{n} \nabla \varphi \rangle = \langle n_i \nabla \varphi \rangle$$

Это означает, что сила трения $E_e = e \langle \tilde{n} \nabla \varphi \rangle$, действующая на электроны, равна по абсолютной величине и противоположна по знаку силе трения, действующей на ионы $F_i = -e \langle \tilde{n}_i \nabla \varphi \rangle$. Используя это, получаем из (12) закон сохранения импульса $\dot{P}_{ze} + \dot{P}_{zi} = 0$.

Учитывая (1) и используя линеаризованные уравнения движения и уравнения непрерывности, можно получить следующие оценки пульсаций плотности и скорости электронов и ионов:

$$\begin{aligned}\tilde{U}_i &\sim \frac{eE_{\perp}}{m_i \omega} \sim \sqrt{\frac{m_e}{m_i}} \frac{U^2}{v_{Te}} \\ \tilde{U}_{iz} &\sim \frac{m_e}{m_i} U \quad \tilde{U}_{ez} \sim U \left(\frac{U}{v_{Te}} \right)^2 \\ \tilde{n} &\sim \tilde{n}_i \sim n \left(\frac{U}{v_{Te}} \right)^2\end{aligned}\quad (13)$$

Оценим, учитывая (13), величину силы трения F_i . Если бы время корреляции было бесконечным, то величины \tilde{n}_R и $E_R = ik_{\parallel} \phi_R$ совершали бы колебания в противофазе и величина $\langle \tilde{n} \nabla_{\parallel} \phi \rangle$ была бы равна нулю. При учете конечности времени корреляции получаем:

$$F_i = -e \tilde{n} k_{\parallel} \phi \frac{\nu}{\omega_R} \sim \omega_{pi} \left(\frac{U}{v_{Te}} \right)^3 m_e n U \quad (14)$$

что совпадает с оценкой (10).

Учитывая (7) в уравнении движения для ионов (12), можно пренебречь действием постоянного электрического поля, так что

$$\frac{\partial}{\partial t} m_i \langle \tilde{n}_i \tilde{U}_{iz} \rangle \approx -e \langle \tilde{n} \nabla_{\parallel} \phi \rangle$$

Отсюда и из (14) следует, что характерная частота пульсаций величины $\langle \tilde{n}_i \tilde{U}_{iz} \rangle$ должна быть порядка ν . Действительно, в этом случае, левая часть этого уравнения порядка

$$\frac{\partial}{\partial t} m_i \langle \tilde{n}_i \tilde{U}_{iz} \rangle \sim m_i \nu \tilde{n}_i \tilde{U}_{iz} \sim F_i$$

В уравнении движения для электронов (12) также можно пренебречь $e n E_0$ по сравнению с $F_e = -F_i$. Величина $e n E_0$ компенсируется изменением импульса электронов, в который главный вклад дают нерезонансные электроны. Оценим теперь \dot{P}_{ze} . В резонансной области

$$\tilde{f}_e \sim \frac{e E_{\parallel}}{m(\omega_R - k_{\parallel} v_{\parallel})} \frac{\partial f_0}{\partial v_{\parallel}} \sim \frac{v_{\parallel} U}{v_{Te}^2} f_{0e}$$

Отметим, что изменение производной f_e по скорости в резонансной области

$$\left| \frac{\partial \tilde{f}_e}{\partial v_{\parallel}} \right| \sim \left| \frac{\partial f_0}{\partial v_{\parallel}} \right|$$

Отсюда находим вклад резонансных электронов в пульсации плотности:

$$n_{\text{рез}} \sim \tilde{f}_e U \sim \left(\frac{U}{v_{Te}} \right)^3 n$$

Пульсации скорости этих электронов $\tilde{U}_{\text{рез}} \sim U$. Величины \tilde{f} , $\tilde{n}_{\text{рез}}$, $\tilde{U}_{\text{рез}}$ колеблются с частотой $\sim \omega_{\text{pi}}$. Значит

$$\dot{P}_{\text{ze}}^{(\text{рез})} \sim \frac{\partial}{\partial t} m_e \tilde{n}_{\text{рез}} \tilde{U}_{\text{рез}} \sim \omega_{\text{pi}} m_e \tilde{n}_{\text{рез}} U \sim F_e$$

Наконец, если величина $\langle \tilde{n} \tilde{U}_e \rangle$ также колеблется с характерной частотой порядка ν , то для левой части (5) получаем оценку:

$$\frac{\partial}{\partial t} P_{\text{ez}}^{(\text{нерез})} \sim \nu m_e \tilde{n} \tilde{U}_{\text{ie}} \sim \omega_{\text{pi}} \left(\frac{U}{v_{\text{Te}}} \right)^5 n m_e U$$

которая порядка правой части уравнения (5).

Полученные выше оценки ν_{eff} и силы трения F_i справедливы лишь по порядку величины, так как уравнения диффузионного типа для усредненных функций распределения $f_{0e,i}$ также справедливы в рассматриваемом случае сильной турбулентности лишь по порядку величины.

Вместе с тем, полученные таким образом функциональные зависимости $\sigma_{\text{ст}}/\sigma$ (E/E_k) и $U(v_{\text{Te}})$ совпадают с экспериментально полученными зависимостями. Количественное расхождение между экспериментальными значениями $\sigma_{\text{ст}}/\sigma$ и U и их теоретическими оценками не превышает множителя ~ 3 .

ЛИТЕРАТУРА

- [1] АРЦИМОВИЧ, Л.А., БОБРОВСКИЙ, Г.А., ГОРБУНОВ, Е.П., ИВАНОВ, Д.П., КИРИЛЛОВ, В.Д., КУЗНЕЦОВ, Э.И., МИРНОВ, С.В., ПЕТРОВ, М.П., РАЗУМОВИЧ, К.А., СТЕЛКОВ, В.С., ШЕГЛОВ, Д.А., Plasma Physics and Controlled Nuclear Fusion Research, IAEA, Vienna 1 1969, p.157.
- [2] PEACOCK, N.I., ROBINSON, D.S., FORREST, M.I., WILCOCK, P.D., SANNIKOV, V.V., Nature 224 (1969) 488.
- [3] DIMOCK, D., MAZZUCATO, E., Phys. Rev. Letters 20 (1968) 713.
- [4] BROWN, I., DIMOCK, D.L., MAZZUCATO, E., ROTHMAN, M.A., SINCLAIR, R.M., YOUNG, K.M., Plasma Physics and Controlled Nuclear Fusion Research, IAEA, Vienna 1 1969, p.497.
- [5] БУРЧЕНКО, П.Я., ВАСИЛЕНКО, Б.Т., ВОЛКОВ, Е.Д., ПАВЛИЧЕНКО, О.С., ПОТАПЕНКО, В.А., РУДАКОВ, В.А., ТЕРЕЩЕНКО, Ф.Ф., ТОЛОК, В.Т., ЗЫКОВ, В.Г., РУДНЕВ, Н.И., ЗАЛКИНД, В.М., КАРПУХИН, В.И., Plasma Physics and Controlled Nuclear Fusion Research, IAEA, Vienna 1 1969, p.543.
- [6] БУРЧЕНКО, П.Я., ВАСИЛЕНКО, Б.Т., ВОЛКОВ, Е.Д., ПОТАПЕНКО, В.А., ТОЛОК, В.Т., Атомная энергия 27 2 (1969) 164.
- [7] DREISER, H., Phys. Rev. 115 (1959) 238.
- [8] РУДАКОВ, Л.И., КОРАБЛЕВ, Л.В., ЖЭТФ 50 (1966) 220.
- [9] КОВРИЖНЫХ, Л.М., ЖЭТФ 51 (1966) 1735.
- [10] СИЗОНЕНКО, В.Л., СТЕПАНОВ, К.Н., Письма ЖЭТФ 9 (1969) 468.
- [11] КАДОМЦЕВ, Б.Б., ПОГУЦЕ, О.П., ЖЭТФ 53 (1967) 2025.
- [12] СИЗОНЕНКО, В.Л., СТЕПАНОВ, К.Н., УФЖ 16 (1971) 429.
- [13] CORPI, V., MAZZUCATO, E., Princeton University, Matt-617 (1968).
- [14] БИРЮКОВ, О.В., БУРЧЕНКО, П.Я., ВАСИЛЕНКО, Б.Т., ВОЛКОВ, Е.Д., ГЕОРГИЕВСКИЙ, А.В., ЛОГИНОВ, А.С., НИКОЛАЕВ, Р.М., САШЕНКО, Ю.В., СУПРУНЕНКО, В.А., ТОЛОК, В.Т., Атомная энергия 23 (1967) 99.
- [15] СИЗОНЕНКО, В.Л., СТЕПАНОВ, К.Н., УФЖ 12 (1970) 15.
- [16] ВЕДЕНОВ, А.А., РЮТОВ, Д.Д., Квазилинейные эффекты в токовых неустойчивостях. Лекция на Европейской школе по физике плазмы, Тбилиси, 12-22 октября 1970 г.
- [17] БАСС, Ф.Г., ФАЙНБЕРГ, Я.Б., ШАПИРО, В.Д., ЖЭТФ 49 (1965) 329.

DISCUSSION

B. COPPI: Have you any new experimental information on the $E/E_{\text{crit}} < 1$ regime, in addition to that presented at the Dubna conference?

K.N. STEPANOV: No. The weak-field regime was not further considered in this work.

S.E. GREBENSHCHIKOV: Have you any new experimental evidence that ion-sound instabilities are excited in the case considered?

K.N. STEPANOV: Yes. Measurements with a dual high-frequency probe showed high-frequency fluctuations with a frequency close to the ion Langmuir frequency. As the current was increased and, at the same time, the density, the frequency of the fluctuations in the plasma also increased. The measured fluctuation frequencies were somewhat higher (by a factor of 1.2) than the ion Langmuir frequency. This may be due to excitation of the plasma by the probe.

ЭКСПЕРИМЕНТАЛЬНЫЕ ИССЛЕДОВАНИЯ МАГНИТНЫХ ПОВЕРХНОСТЕЙ И УДЕРЖАНИЯ ПЛАЗМЫ В ТРЕХЗАХОДНОМ СТЕЛЛАРАТОРЕ-ТОРСАТРОНЕ "САТУРН-1"

В. С. ВОЙЦЕНЯ, А. В. ГЕОРГИЕВСКИЙ, В. Е. ЗИСЕР,
Д. П. ПОГОЖЕВ, А. И. СКИБЕНКО, С. И. СОЛОДОВЧЕНКО,
В. А. СУПРУНЕНКО, В. Т. ТОЛОК, И. П. ФОМИН,
Л. А. ДУШИН

Физико-технический институт Академии наук
Украинской ССР, Харьков,
Союз Советских Социалистических Республик

Abstract—Аннотация

EXPERIMENTAL RESEARCH ON MAGNETIC SURFACES AND PLASMA CONFINEMENT IN THE "SATURN-1" THREE-TURN STELLARATOR-TORSATRON.

The "Saturn-1" toroidal trap is designed for the investigation of the properties of a magnetic field of various configurations and their effect on the plasma confinement. The design of the device allows the creation of two types of magnetic configuration: a three-turn stellarator and three-turn torsatron configuration. The main parameters of the trap are as follows: magnetic field strength $H_0 \leq 6$ kOe; major radius of the torus $R = 35.6$ cm; minor radius of the spiral winding $a = 10$ cm; inside radius of the vacuum chamber $r = 8.6$ cm; number of periods of the magnetic field $m = 8$. Experimental investigations of the magnetic surfaces were carried out with the help of pulsed low-energy electron beams. The results were compared with calculations on a BESM-6 computer. The investigations of the torsatron configuration have shown that closed surfaces exist over a wide range of changes in the components of the magnetic field:

$0.4 \leq K_\varphi = H_{\varphi b}/H_0 \leq 1$, $0.5\% \leq H_L/H_0 \leq 1.5\%$, where $H_{\varphi b}$ is the longitudinal field created by the helical winding and H_L is the vertical field for formation of a magnetic well. When a longitudinal field is produced only by a helical winding ($K_\varphi = 1$) the rotational transform angle and shear are rather high ($i_0 \sim 0.9\pi$, $S_0 \sim 0.12$). The optimum conditions, however, are realized when $K_\varphi = 0.66$ and are characterized by the following values: $i_0 = 0.8\pi$, $S_0 \sim 0.2$ and $r_0 \sim 5$ cm (r_0 is the average radius of the outermost undestroyed surface). In the stellarator regime optimum conditions these values are equal to $\sim \pi$, ~ 0.25 and ~ 4.8 , respectively. Both in the torsatron and the stellarator configurations the superposition of a small vertical field leads to the occurrence of a magnetic well ($\sim 10\%$) while a moderate shear value (~ 0.05) is maintained. The traps were filled with plasma by external injection from several titanium sources arranged near the outermost undestroyed surface. The parameters of the trapped plasma were measured approximately 0.5 ms after the triggering of the sources. The dependence was investigated of the plasma confinement time τ_n on the value of the longitudinal field and on the field ratio in both stellarator and torsatron regimes. Investigations of the radial density distribution with the help of twin electric probes showed that the plasma boundary approximately coincides with the outermost undestroyed surface. The quoted confinement time ($\tau_n^* = \tau_n \cdot r^2 / r_{pl}^2$, where r_{pl} is the plasma radius) increases with the increase in the helical harmonic of the magnetic field in both torsatron and stellarator regimes.

ЭКСПЕРИМЕНТАЛЬНЫЕ ИССЛЕДОВАНИЯ МАГНИТНЫХ ПОВЕРХНОСТЕЙ И УДЕРЖАНИЯ ПЛАЗМЫ В ТРЕХЗАХОДНОМ СТЕЛЛАРАТОРЕ-ТОРСАТРОНЕ "САТУРН-1".

Тороидальная ловушка "Сатурн-1" предназначена для исследования свойств магнитного поля различных конфигураций и их влияния на удержание плазмы. Конструкция установки позволяет создавать магнитные конфигурации двух типов: трехзаходного стелларатора и трехзаходного торсатрона. Основные параметры ловушки: напряженность магнитного поля $H_0 \leq 6$ кэ, большой радиус тора $R = 35,6$ см, малый радиус винтовой обмотки $a = 10$ см, внутренний радиус вакуумной камеры $r = 8,6$ см, число периодов магнитного поля $m = 8$. Экспериментальные исследования магнитных поверхностей проводились с помощью импульсных низкоэнергетических электронных пучков. Результаты сравнивались с расчетами, выполненными на ЭВМ БЭСМ-6. Исследования торсатронной конфигурации показали, что замкнутые поверхности существуют в широком диапазоне изменения компонентов магнитного поля: $0,4 \leq K_\varphi = H_{\varphi b}/H_0 \leq 1$, $0,5\% \leq H_L/H_0 \leq 1,5\%$, где $H_{\varphi b}$ — продоль-

ное поле, создаваемое винтовой обмоткой, H_z – вертикальное поле для получения "магнитной ямы". В том случае, когда продольное поле создается только винтовой обмоткой ($K_\varphi = 1$) значение угла вращательного преобразования и "шира" оказываются довольно высокими ($i_0 \sim 0,9\pi$, $S_0 \sim 0,12$). Однако оптимальные условия реализуются при $K_\varphi = 0,66$ и характеризуются следующими величинами: $i_0 = 0,8\pi$, $S_0 \sim 0,2$, $r_0 \sim 5$ см (r_0 – средний радиус крайней неразрушенной поверхности). В стеллараторном режиме в оптимальных условиях эти величины оказываются равными $\sim \pi$, $\sim 0,25$ и $\sim 4,8$ см, соответственно. Как в торсатронной, так и в стеллараторной конфигурациях наложение вертикального поля небольшой величины приводит к появлению "магнитной ямы" ($\sim 10\%$) при сохранении умеренной величины "ширы" ($\sim 0,05$). Заполнение ловушки плазмой осуществлялось при внешней инжекции плазмы из нескольких титановских источников, расположенных вблизи крайней неразрушенной поверхности. Параметры захваченной плазмы измерялись через $\sim 0,5$ мсек после срабатывания источников. Были исследованы зависимости времени удержания плазмы, τ_p , от величины продольного поля и от соотношений полей как в стеллараторном, так и в торсатронном режимах. Исследования радиальных распределений плотности с помощью двойных электрических зондов показали, что граница плазмы примерно совпадает с крайней неразрушенной поверхностью. Величина приведенного времени удержания ($\tau'_p = \tau_p (r^2 / r_{пл}^2)$), где $r_{пл}$ – радиус плазмы) возрастает с ростом винтовой гармоники магнитного поля как в торсатронном, так и в стеллараторном режимах.

I. ВВЕДЕНИЕ

В течение последних лет проводились систематические изучения различных модификаций стеллараторов [1-7]. Целью этих изучений была оптимизация и дальнейшее усовершенствование магнитной системы классического стелларатора, поскольку сооружение стеллараторов больших размеров в настоящее время ограничено, в основном, техническими возможностями создания в больших объемах магнитного поля значительной напряженности. Кроме того, в стеллараторах объем удерживающего поля примерно на порядок превышает объем, непосредственно занятый плазмой.

Наиболее полно рассчитанной является магнитная система "торсатрона" [3-7], позволяющая частично устранить этот недостаток. В результате расчетов было показано, что такой тип ловушки обладает хорошими стабилизирующими свойствами и рядом преимуществ по сравнению со стеллараторами.

Воплощение идеи торсатрона и экспериментальное исследование основных теоретических положений осуществлено в Харьковском физико-техническом институте АН УССР на установке "Сатурн-1" [8]. Целью данного доклада является обобщение основных результатов, полученных на этой установке.

II. ОПИСАНИЕ КОНСТРУКЦИИ

Установка "Сатурн-1" (рис.1) представляет замкнутую тороидальную магнитную ловушку с трехзаходным винтовым магнитным полем.

Основные параметры установки:

1. Максимальная напряженность продольного магнитного поля H_0 :
 - а) в квазистационарном режиме ≈ 6 кэ,
 - б) в импульсном режиме ≈ 10 кэ.
2. Большой радиус винтовой обмотки, $R = 35,6$ см.

3. Малый радиус винтовой обмотки, $a = 10,0$ см.
4. Рабочий объем вакуумной камеры, $v = 55$ л.
5. Число периодов винтового поля, $m = 8$.
6. $\beta_E \approx 3,5 \cdot 10^{-3}$.

Вакуумная камера (3) изготовлена из нержавеющей стали НН-3 толщиной 5 мм и не имеет разъемов. Винтовая обмотка (2) уложена непосредственно на камеру, предварительно обработанную и размеченную с высокой степенью точности.

Система винтового поля имеет две независимые обмотки, каждая из которых объединяет "положительные" или "отрицательные" полюсы. При работе в торсатронном режиме включается любая из них. Двухслойная обмотка продольного поля уложена на наружный каркас винтовой обмотки и выполнена в виде спиралей с взаимно противоположным направлением навивки, намотанных с шагом, позволяющим располагать патрубки для от качки, диагностической аппаратуры и систем нагрева плазмы. В каждом слое расположены 32 витка. Благодаря сдвигу обмотки относительно центра камеры на 15 мм удалось снизить "гофры" в рабочем объеме до $\pm 1\%$.

При величине тока в обмотке, равном 15 кА, напряженность продольного поля на оси камеры составляет ≈ 5 кэ.

Система вертикального поля состоит из корректирующей (4) и компенсирующей (5) обмоток и изготовлена отдельным блоком. Назначение компенсирующей обмотки состоит в том, чтобы в торсатронном режиме свести к минимуму величину вертикального поля, созданного винтовой обмоткой. Неоднородность компенсирующего магнитного поля внутри камеры составляет $\pm 2,5\%$.

Корректирующая обмотка предназначена для создания "магнитной ямы" или "антиямы" как в стеллараторном, так и в торсатронном режимах. Обе обмотки жестко связаны друг с другом, и предусмотрена регулировка их расположения по отношению к винтовой обмотке, как в вертикальной, так и в горизонтальной плоскостях.

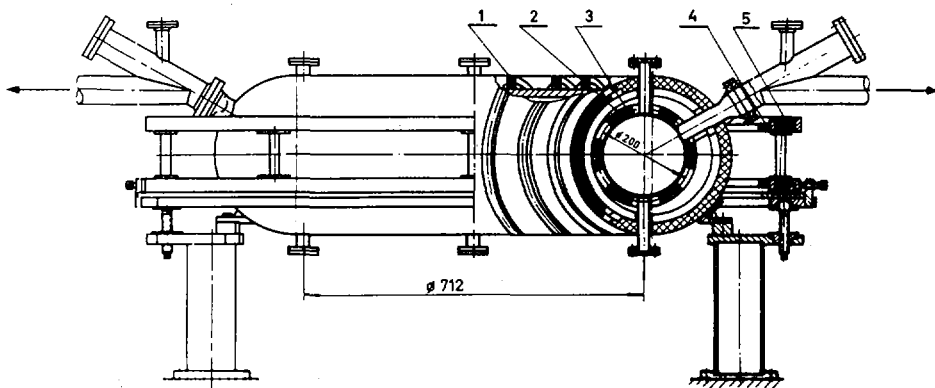


Рис. 1. Схема установки:

1 - обмотка продольного магнитного поля, 2 - винтовая обмотка, 3 - вакуумная камера, 4 - корректирующая обмотка, 5 - компенсирующая обмотка.

Все обмотки выполнены из охлаждаемой медной трубки, а в качестве изоляции применена стеклоткань, пропитанная кремнеорганическим составом, что позволяет прогревать камеру до температуры свыше 300° .

Предельный вакуум в камере $1 \cdot 10^{-7}$ мм рт. ст.

Конструкция установки обусловила высокую точность изготовления и взаимного расположения обмоток ($\Delta a/a \approx \Delta R/R \approx 10^{-3}$, непараллельность плоскостей обмоток винтового и продольного поля $\leq 1^{\circ}$), а максимально возможная близость обмоток к рабочему объему обеспечивает высокую эффективность магнитной системы.

III. ИССЛЕДОВАНИЕ СТРУКТУРЫ МАГНИТНОГО ПОЛЯ

1. Методика исследования

Исследование магнитных поверхностей было проведено с помощью электронных пучков [9]. Точечная электронная пушка инжестрировала электронный пучок с энергией 20-30 эВ, длительностью $\approx 1,5$ мксек. Время жизни электронного пучка определялось при помощи кольцевого электростатического зонда. Перемещая пушку, можно определить границы существования замкнутых магнитных поверхностей.

Для изучения топографии магнитного поля использовался вращающийся зонд, который представлял собой восемь радиально расположенных датчиков $\phi 2$ мм с осью вращения, совпадающей с центром камеры. Специальное координатное устройство позволило определять положение датчиков в рабочем объеме камеры. Таким образом, при изменении расстояния пушки от оси камеры можно построить семейство магнитных поверхностей.

Существенным недостатком этого метода является то, что дрейфовые поверхности вблизи магнитной оси для трехзаходного стелларатора значительно отличаются от вакуумных магнитных поверхностей.

Изучение магнитных поверхностей проводилось для стеллараторного и торсионного режимов работы установки в широком диапазоне изменения ϵ — отношения основной винтовой гармоники магнитного поля к продольному магнитному полю.

Первым этапом было определение области существования замкнутых поверхностей, вторым — изучение их структуры.

Основными параметрами магнитных поверхностей, которые можно было измерять экспериментально, являются углы поворота силовой линии на периоде поля i_k и на длине установки i_0 , а также средний радиус магнитной поверхности r_0 :

$$i_k = \lim_{m_0 \rightarrow \infty} \frac{1}{m_0} \sum_{j=1}^{m_0} i_{kj}$$

$$i_0 = i_k \cdot m$$

Средний радиус определяется как радиус круга, площадь которого равна площади усредненного сечения магнитной поверхности. Из зависимости $i_0 = f(r_0)$ численным методом определялось значение ширины S_0 на данной поверхности:

$$S_0 = \frac{r_0^2}{L} \frac{di_0}{dr_0}$$

где L — общая длина установки.

Величина "среднего $\min B$ " не измерялась непосредственно. Однако, как показано численным счетом [10], значение "глубины ямы", определенное как

$$v'' = -\frac{2\delta}{R}$$

(δ — смещение центра магнитных поверхностей от магнитного центра винтовой обмотки), хорошо совпадает с расчетными значениями. Напряженность продольного магнитного поля при измерениях в постоянном режиме: $H_0 = 0,5 \div 1$ кэ. Контрольные измерения проведены в полях 3 кэ в импульсном режиме.

2. Стеллараторный режим

Топография магнитных поверхностей трехзаходного стелларатора неоднократно исследовалась теоретически [11-13] и экспериментально [14-15]. Для установки "Сатурн-1" при различных ϵ были рассчитаны магнитные поверхности и определены их основные параметры. Расчеты проводились в предположении чисто тороидального продольного магнитного поля. При этом компоненты винтового магнитного поля вычислялись по закону Био-Савара для бесконечно тонкого полюса реальной ширины.

Как показывают вычисления, крайняя неразрушенная поверхность полностью вписывается в вакуумную камеру, начиная с $\epsilon = 0,48$. Для $H_0 = 5$ кэ это соответствует полному току в полюсе 32 кА^1 . Дальнейшее увеличение ϵ ведет к уменьшению объема, заключенного внутри замкнутой поверхности; при этом максимальный угол остается практически постоянным ($i_{0\max} \approx 1,3\pi$). В области $\epsilon < 0,48$ наблюдается резкое уменьшение угла вращательного преобразования, которое объясняется тем, что поверхность, ограниченная внутренним радиусом камеры, не является крайней неразрушенной. Экспериментальные измерения показали хорошее совпадение характера зависимости $i_0 = f(r_0)$ с расчетом, однако максимальные значения r_0 и, соответственно, i_0 оказываются несколько ниже расчетных значений (рис. 2).

Незначительное разрушение магнитных поверхностей вызвано различными возмущениями, обусловленными реальной конструкцией системы, которые не учитывались при расчете. Это приводит к снижению максимально допустимого шира на установке.

Максимальный измеренный угол вращательного преобразования равен $\approx \pi$ для всех $\epsilon > 0,48$. С увеличением ϵ величина шира увеличивается и достигает максимума $S_0 = 0,25$ при $\epsilon = 0,625$, а затем уменьшается вследствие уменьшения r_0 .

В отношении магнитного поля оптимальным является режим с $\epsilon = 0$, $\epsilon = 0,625$. При радиусе камеры 8,6 максимальный радиус крайней неразрушенной поверхности равен 7,25 см, т.е. поверхность достаточно "оторвана" от стенок камеры. Это обстоятельство позволяет изучать в дан-

¹ Полный ток равен утроенному току винтовой обмотки.

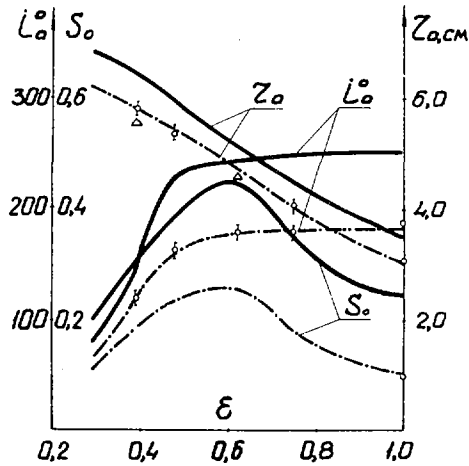


Рис. 2. Параметры поверхностей в стеллараторном режиме: (—) — расчет, (- - -) — эксперимент.

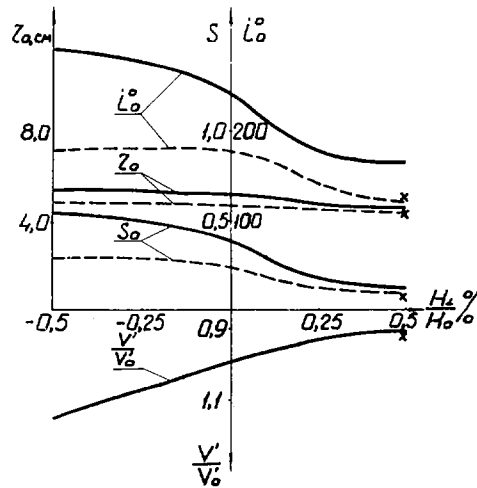


Рис. 3. Влияние поперечного поля на параметры магнитных поверхностей в стеллараторном режиме: (—) — расчет, (- - -) — эксперимент.

ном режиме влияние вертикального магнитного поля H_{\perp} на форму и параметры магнитных поверхностей.

Величина вертикального поля сильно влияет на параметры крайних магнитных поверхностей (рис. 3). Так, в режиме "антиямы" ($H_{\perp}/H_0 = -0,5\%$) объем замкнутых поверхностей увеличивается, одновременно с этим увеличиваются i_0 и S_0 . Вертикальное поле обратного знака приводит к уменьшению объема, увеличению угла на оси и снижению

скорости изменения угла по радиусу. При величине поля, равной 1% от продольного, шир во всем объеме отсутствует, но значение "магнитной ямы" достигает 15%. Эта величина вертикального поля является предельной, так как дальнейшее увеличение H_{\perp} приводит к полному разрушению магнитных поверхностей.

В интервале изменения H_{\perp}/H_0 от 0 до 0,5% можно получать магнитные поверхности, характеризующиеся наличием сравнительно большого шара ($0,05 \div 0,1$) и достаточно глубокой (до 10%) магнитной ямы одновременно, причем соотношение между этими параметрами можно легко изменять, регулируя величину вертикального поля. Средний радиус магнитной поверхности остается почти неизменным, а i_0 снижается всего на 30% (от π при $H_{\perp}/H_0 = 0$ до $2/3 \pi$).

С целью выяснения вопроса о влиянии распределения вертикального поля магнитные поверхности были рассчитаны при различных уровнях неоднородности этого поля. Как показали расчеты (и подтвердили эксперименты), колебания величины вертикального поля в объеме камеры в пределах ($0,9 \div 1,2$) H_{\perp} ($r = 0$) не сказываются заметно на структуре магнитных поверхностей². Этот факт позволяет использовать для создания вертикального поля винтовую обмотку. Как было отмечено ранее, "положительные" и "отрицательные" полюсы винтовой обмотки объединяются в две независимые ветви, каждая из которых создает собственное вертикальное поле. При равенстве токов в ветвях усредненное суммарное поле равно нулю. Однако, незначительно изменив соотношение тока, можно получить вертикальное поле необходимой величины и направления. Для случая $\epsilon = 0,625$ и $\Delta J = 0,025 J_b$ вертикальное поле достигает 0,5% H_0 .

На рис.3 этот режим отмечен х.

Как и при отсутствии вертикального поля, экспериментальные зависимости хорошо согласуются с расчетными, однако параметры крайних поверхностей несколько ниже расчетных.

3. Торсатронный режим

Во многих теоретических исследованиях [1,3-7] показано существование замкнутых магнитных поверхностей в торсатроне.

Как известно [1], в отличие от стелларатора, направление токов в полюсах винтовой обмотки торсатрона является одинаковым. С этим связаны некоторые особенности магнитного поля торсатронной конфигурации:

1. Осевая компонента винтового тока создает значительное вертикальное поле H_y , которое для получения замкнутых магнитных поверхностей необходимо компенсировать.

2. Наряду с этим, винтовой ток создает продольное поле $H_{\phi b}$. В зависимости от шага винтовой обмотки соотношение между этими полями будет меняться. Для установки "Сатурн-1" при полном токе в полюсе 45 кА величина $H_{\phi b} = 2$ кэ, а отношение $H_y/H_{\phi b} = 0,5$.

3. Результирующее продольное поле H_0 является суммой двух полей: основного поля H_{ϕ} и поля $H_{\phi b}$. Вклад винтовой обмотки в результирующее поле характеризуется коэффициентом $K_{\phi} = H_{\phi b}/H_0$.

² $H_{\perp}(r = 0)$ - значение вертикального поля в центре камеры.

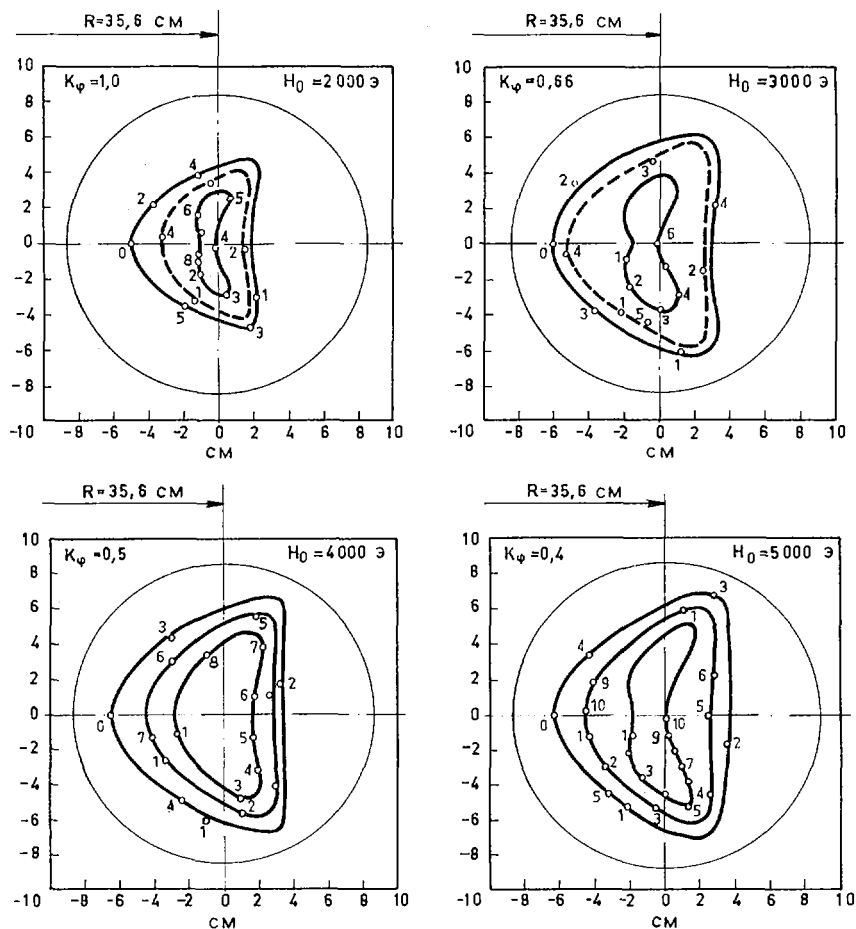


Рис. 4. Магнитные поверхности в торсатронном режиме.

4. Основная гармоника винтового поля в два раза меньше, чем в стеллараторном режиме, при равенстве токов и одинаковых винтовых обмотках в обоих режимах.

Магнитные измерения поверхностей проводились для $0,4 \geq K_\phi \geq 1$.

На рис. 4 приведены типичные магнитные поверхности для различных значений K_ϕ и полной компенсации вертикального поля винтовой обмотки. Пунктиром нанесены некоторые расчетные поверхности. Видно, что магнитные поверхности имеют, как и в стеллараторном режиме, форму искаженного треугольника.

Измеренные величины углов поворота i_0 достаточно точно совпадают с расчетными (рис. 5). На расчетные зависимости точками нанесены экспериментальные данные. Крайняя неразрушенная поверхность вписывается в камеру при $K_\phi \cong 0,57$, а i_0 и r_0 для нее равны $\approx 0,9\pi$ и 5,5 см.

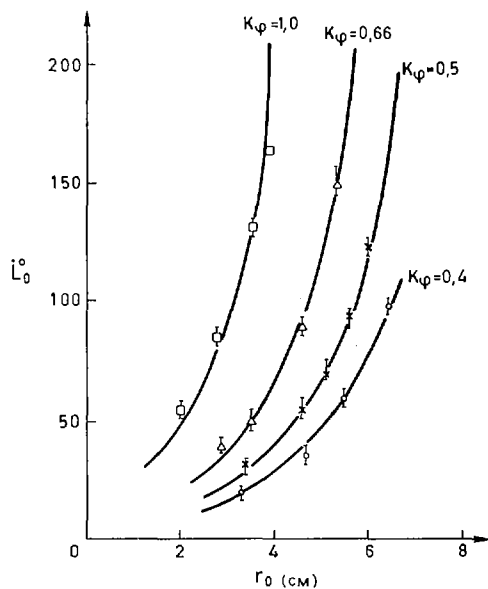


Рис. 5. Зависимость $i_0 = f(r_0)$ для различных K_ϕ .

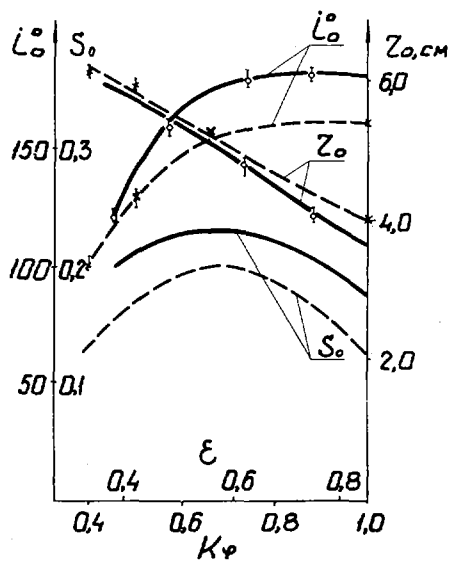


Рис. 6. Предельные параметры магнитных поверхностей в стеллараторном (—) и торсатронном (----) режимах.

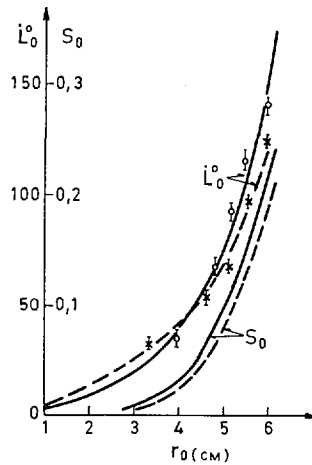


Рис. 7. Зависимости i_0 и S_0 от радиуса r_0 для стеллараторного при $\epsilon = 0,43$ (—) и торсатронного при $K_\varphi = 0,5$ (- - -) режимов.

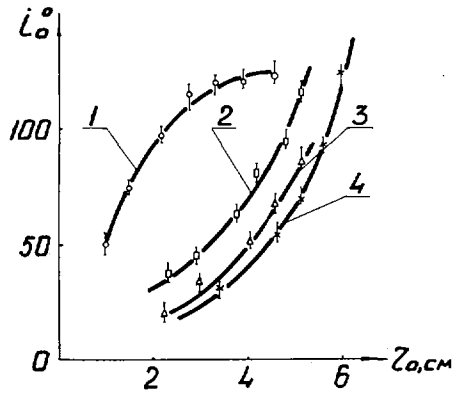


Рис. 8. Влияние поперечного поля в торсатронном режиме при $K_\varphi = 0,5$:
1 - $H_\perp/H_0 = 2,0\%$; 2 - $H_\perp/H_0 = 0,6\%$; 3 - $H_\perp/H_0 = -0,6\%$; 4 - $H_\perp/H_0 = 0$.

Дальнейшее увеличение K_φ не приводит к существенному росту i_0 , но при этом значительно уменьшается величина r_0 и, следовательно, S_0 .

Более наглядно это показано на рис. 6.

Параметры магнитных поверхностей достигают максимальных значений при $K_\varphi = 0,6 \pm 0,7$ и составляют $i_0 \approx 0,9 \pi$, $r_0 = 5$ см, $S_0 \approx 0,2$.

Наиболее экономичным для торсатрона является режим, когда продольное магнитное поле создается только винтовой обмоткой ($K_\varphi = 1$). Экспериментально было показано, что этот режим характеризуется достаточно высокими параметрами магнитных поверхностей ($i_0 \approx 0,9 \pi$; $r_0 = 4$ см; $S_0 = 0,12$). Однако напряженность магнитного поля в квазистационарном режиме не превышает 2,0 кэ, что является существенным недостатком этого режима.

ТАБЛИЦА 1. ВЛИЯНИЕ ПОПЕРЕЧНОГО МАГНИТНОГО ПОЛЯ НА ПАРАМЕТРЫ МАГНИТНЫХ ПОВЕРХНОСТЕЙ

$H_L/H_0, \%$	- 0,6	0	0,6	2
r_0 (см)	5,4	5,9	5,1	4,5
i_0	90	125	120	120
S_0	0,1	0,17	0,12	0,01
v'/v_0'	1,2	1	0,9	0,85

При сравнении экспериментальных и расчетных значений параметров выяснилось, что относительное разрушение поверхностей в торсатроне выше, чем в стеллараторе (рис. 6). Это объясняется тем, что формы и параметры магнитных поверхностей, как показали расчеты, в значительной степени зависят от компенсирующего поля. Поэтому дополнительное разрушение, вероятно, вызвано неидеальностью компенсирующей обмотки и возможным перекосом ее плоскости по отношению к обмоткам винтового и продольного поля.

Коэффициент K_φ косвенным образом характеризует отношение основной гармоники винтового поля к продольному магнитному полю. Для установки "Сатурн-1" при $\epsilon = 0,85$ K_φ поверхности в стеллараторном и торсатронном режимах имели близкие параметры. Как видно из рис. 7, в этом случае объем внутри крайней неразрушенной поверхности в торсатронном режиме несколько выше, а значения i_0 и S_0 — ниже.

Дополнительное вертикальное (корректирующее) поле в торсатроне оказывает на магнитные поверхности такое же действие, как и в стеллараторе. Однако имеются и различия:

1. В режиме "магнитной ямы" на оси $i_0 = 0$.

2. Замкнутые магнитные поверхности существуют при больших значениях H_L/H_0 , чем в стеллараторе.

Зависимость $i_0 = f(r_0)$ и экспериментальные данные для $K_\varphi = 0,5$ и для различных значений H_L/H_0 приведены на рис. 8, а параметры крайних магнитных поверхностей³ — в табл. I.

IV. ИССЛЕДОВАНИЕ УДЕРЖАНИЯ ПЛАЗМЫ

1. Создание плазмы

На первом этапе плазменных исследований на установке "Сатурн-1" плазма создавалась титановыми источниками, электроды которых насыщались водородом. Источники вводились через вертикальные патрубки (рис. 1) и располагались в области между крайней неразрушенной поверхностью и внутренней стенкой вакуумной камеры. Питание источников ($C = 0,1$ мкФ, $U = 5$ кВ, $T = 1$ мксек) осуществлялось через разрядник и активное сопротивление, благодаря которому длительность тока была

³ Размеры и параметры поверхности ограничены вакуумной камерой.

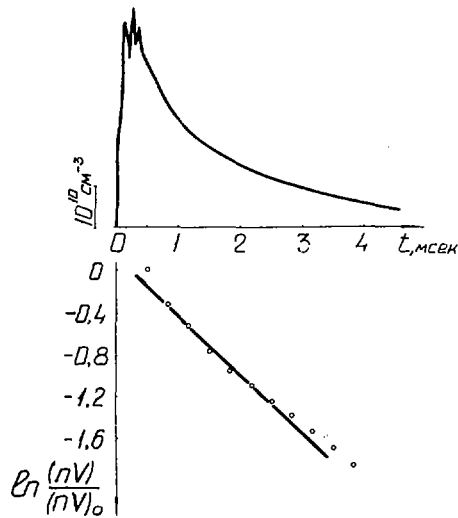


Рис.9. Типичная осциллограмма сигнала ионного тока насыщения, при использовании одного источника, и ее обработка.

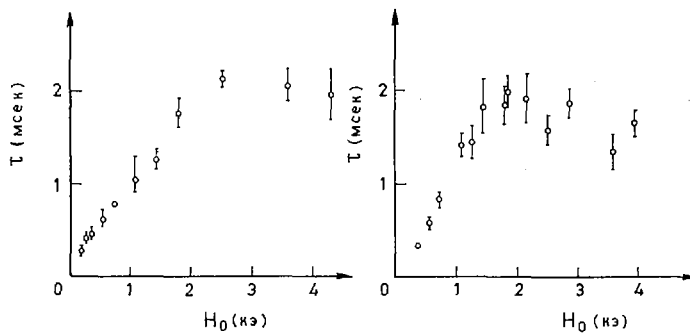


Рис.10. Зависимость времени жизни плазмы от напряженности удерживающего магнитного поля для одного источника:
а) стелларатор ($\epsilon = 0,38$), б) торсатрон ($K_{\varphi} = 0,5$).

ограничена практически только первым полупериодом. Титановые электроды располагались по отношению к продольному магнитному полю так, чтобы полярность напряжения между ними во время протекания разрядного тока обеспечивала дрейф плазмы (в скрещенных полях) внутрь камеры. Массовый и энергетический состав ионов захваченной плазмы не изучался. Однако измерения на прямой системе в отсутствие магнитных полей показали, что количество примесей могло достигать 20-30%. При этом основную долю примесей составляли (в порядке убывания интенсивностей) ионы углерода, кислорода и титана с зарядом от 1 до 3, а средняя энергия ионов, оцененная по времени пролета, была порядка 25 эВ.

2. Методы измерений

Для изучения параметров плазмы применялись двойные электрические зонды, работавшие в режиме ионного тока насыщения. Зонды изготовлялись из вольфрамовой проволоки диаметром $0,3 \pm 1$ мм и длиной 4 мм. Они были разнесены на расстояние 3 ± 6 мм и могли перемещаться по радиусу. Зонды находились под плавающим потенциалом, а с измерительной аппаратурой соединялись через разделительный трансформатор (полоса пропускания от 50 до 10^5 Гц).

Типичная осциллограмма зондового сигнала приведена на рис.9. На рис.9 показан способ усреднения спада амплитуды зондового сигнала при определении времени жизни плазмы τ . Калибровка зондов при определении плотности плазмы осуществлялась по ВЧ-методике, описанной в работе [17].

Тороидальная вакуумная камера установки служила резонатором и запитывалась сигналом с частотой $f = 37$ ГГц. По величине сдвига одного из резонансов вычислялась средняя плотность плазмы в камере в различные моменты времени. Времена жизни, определенные по ВЧ-методике и по спаду ионного тока насыщения, отличались не более чем в полтора раза.

Температура электронов, оцененная из вольт-амперных характеристик двойного электрического зонда, составляла ≈ 10 эВ и уменьшалась с постоянной времени, несколько превышающей время жизни плазмы.

Следует отметить существенный недостаток титановых источников плазмы, который заключается в следующем. Даже при малой длительности разрядного тока из электродов выделяется значительное количество нейтралов, в состав которых, кроме водорода, могут входить и различные примеси, такие как кислород, азот и пр. Этот нейтральный газ за время $\approx 0,5$ мсек (с момента срабатывания источников до начала измерения спада зондового сигнала) успевает полностью распределиться внутри вакуумной камеры. В результате этого, в наших экспериментах реальная степень ионизации к началу измерений τ не превышала $\sim 30\%$, хотя предельное давление было $1 \cdot 10^{-7}$ торр. Кроме того, поскольку разрядный ток протекал поперек основного магнитного поля, количество выделившихся нейтралов не оставалось постоянным, а несколько увеличивалось с ростом напряженности поля.

3. Удержание плазмы

Все измерения с плазмой в торсатронном режиме проводились при полной компенсации H_z (включая и магнитное поле Земли), в стеллараторном режиме магнитное поле Земли не компенсировалось. Однако, как следует из специальных измерений, наложение H_z , менее $0,3\%$ от величины H_0 , заметно не изменяет времени жизни плазмы.

Экспериментальные данные зависимости τ от напряженности удерживающего магнитного поля для стелларатора, $\epsilon = 0,38$ и торсатрона $K_\phi = 0,5$, представлены на рис.10. Видно, что в обоих режимах в области малых магнитных полей с ростом поля время жизни плазмы увеличивается. Обращает на себя внимание тот факт, что как в стеллараторном, так и в торсатронном режимах при полях, больших 2 кэ, время жизни почти не меняется и остается на уровне около 2 мсек. Обсуждение этого результата будет проведено ниже.

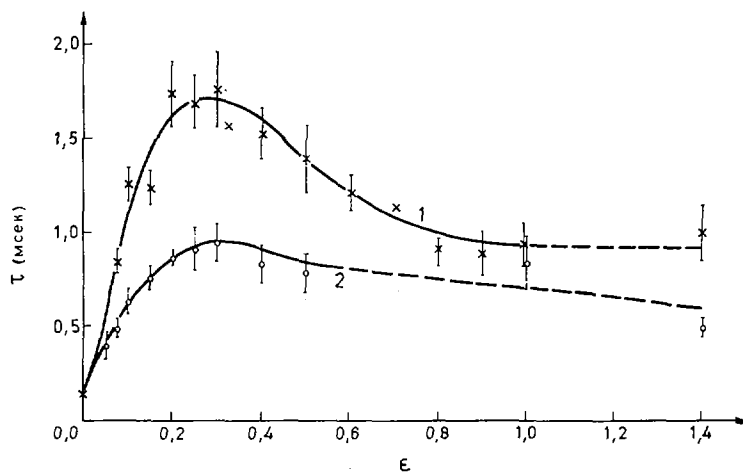


Рис.11(а). Зависимость τ от ϵ для стелларатора $H_0 = 1,8$ кэ:
1 – один источник, 2 – четыре источника.

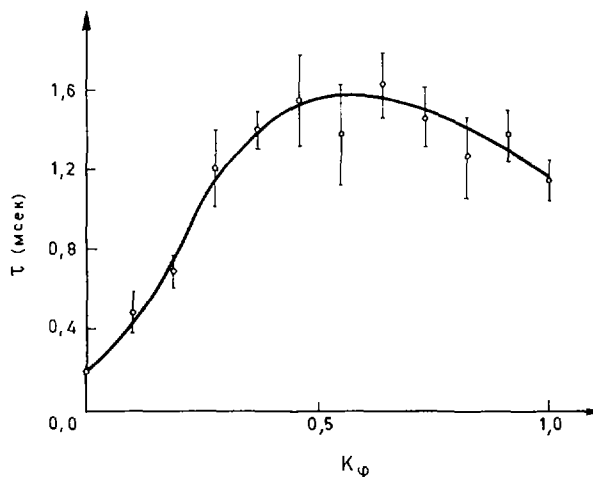


Рис.11(б). Зависимость τ от K_ϕ для торсатрона. $H_0 = 1,8$ кэ. Один источник.

Измерение τ при изменении ϵ и K_ϕ для стеллараторной и торсатронной конфигураций, соответственно, показано на рис.11(а) и (б). Величина основного магнитного поля H_0 составляла $\approx 1,8$ кэ. Как видно, результаты в обоих случаях качественно подобны. Наличие максимумов связано с изменением радиуса крайней неразрушенной магнитной поверхности (при изменении ϵ или K_ϕ). Однако положение максимума ($\epsilon \approx 0,3$) на кривой 1 (рис.10 а) является не очень понятным, поскольку крайняя поверхность начинает вписываться в камеру только для $\epsilon \geq 0,48$. Следовательно, с увеличением ϵ до этого значения происходит (рис.2) непрерывное

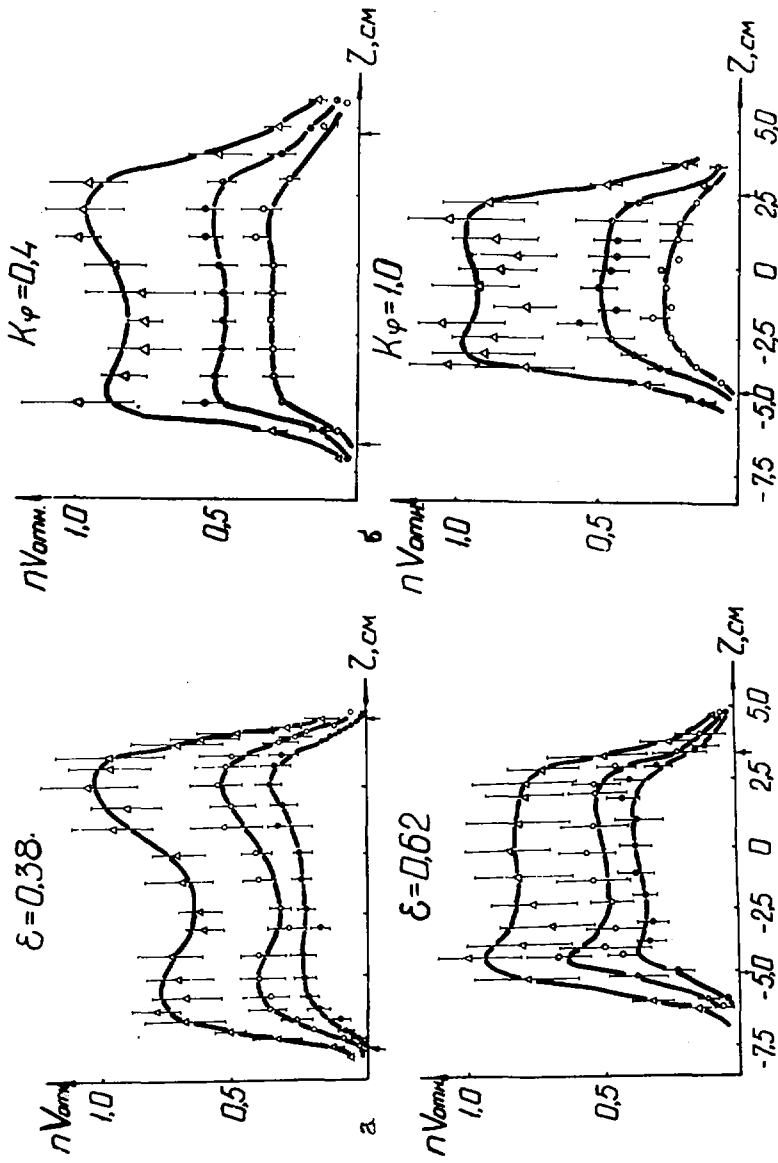


Рис. 12. Радиальное распределение (nV) для моментов времени 0,5 мсек, 0,9 мсек, 1,3 мсек (считая сверху). а) стелларатор $H_0 = 1,8$ кэ, б) торсатрон $H_0 = 2$ кэ.

возрастание как угла вращательного преобразования, так и величины ширины на последней неразрушенной поверхности при незначительном уменьшении ее радиуса.

То, что изменение радиуса плазмы обусловлено изменением r_0 , видно из рис. 12 (а) и (б), на которых представлены радиальные распределения ионного тока насыщения для стеллараторного и торсатронного режимов в горизонтальной плоскости. Стрелками указаны измеренные с помощью электронного пучка положения крайних поверхностей на радиусе, вдоль которого перемещался зонд. Уменьшение плотности плазмы вблизи центра наблюдалось и на других установках [18-19] и, по-видимому, не связано со способом создания плазмы, а объясняется характерными для трехзаходного стелларатора зависимостями i_0 и S_0 от радиуса.

4. Рекомбинационные эффекты

Ранее уже отмечалось, что время жизни плазмы при $H_0 \approx 2$ кэ не зависит от напряженности магнитного поля (или даже несколько уменьшается с ростом последнего, рис. 10(б)). Это означает, что при достаточно больших магнитных полях потери плазмы определяются не диффузией поперек магнитного поля, а каким-то иным механизмом. Возможными причинами, ограничивающими время жизни плазмы в наших экспериментах, являются рекомбинация и процессы взаимодействия заряженных частиц с нейтральными частицами плазмы.

К сожалению, в литературе отсутствуют данные о рекомбинации в диапазоне плотностей и температур, близких к нашим. Однако, как следует из обзора Хастеда [20], коэффициент рекомбинации для гелия зна-

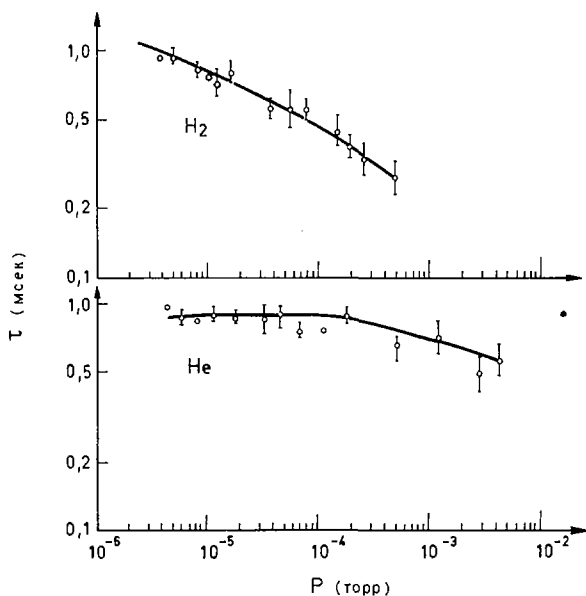


Рис. 13. Зависимость τ (при срабатывании четырех источников): а) от давления водорода и примесей, выделяющихся из электродов, б) от давления гелия. Режим стеллараторный, $H_0 = 1,8$ кэ, $\epsilon = 0,38$.

чительно ниже, чем для других газов. Таким образом, можно ожидать, что в одинаковых условиях время спада плотности заряженных частиц будет максимальным при использовании гелия в качестве основного газа.

Экспериментально полученные зависимости τ от давления газов, которые выделяются в момент срабатывания источников (в основном водород) и от давления гелия приведены на рис.13. В первом случае измерения проводились при полностью перекрытых клапанах, соединяющих вакуумную камеру с диффузионными насосами, так что давление в камере постепенно повышалось за счет газовой выделения из электродов источника; во втором случае осуществлялся непрерывный проток гелия через вакуумную камеру. Режимы работы плазменных источников были одинаковы.

Как видно из графиков, заметное уменьшение τ в случае гелия начинается при давлении $(2 \div 3) \cdot 10^{-4}$ торр, что хорошо совпадает с данными других авторов [19,21]. Эта величина давления почти на два порядка выше соответствующих значений для верхней кривой.

Максимальные времена жизни плазмы для обеих кривых на рис.13 ограничиваются газовой выделением у титановых электродов при каждом срабатывании источников. С увеличением числа источников происходит возрастание плотности как заряженных частиц, так и нейтралов. Это ведет к резкому уменьшению времени жизни плазмы, как видно из рис.11(a), где кривая 1 получена при использовании только одного, а кривая 2 — четырех источников.

Максимальная плотность, оцененная по ВЧ-методике, составляла $\approx 5 \cdot 10^{10} \text{ см}^{-3}$ и $\approx 4 \cdot 10^{11} \text{ см}^{-3}$, а изменение давления при каждом импульсе инжекции $\approx 1,6 \cdot 10^{-6}$ торр и $\approx 8 \cdot 10^{-6}$ торр для одного и четырех источников, соответственно.

Таким образом, возможно, что наличие нейтральных частиц в плазме является одной из основных причин, ограничивающих удержание плазмы.

Кроме того, было замечено, что ввод дополнительного зонда (при $H_0 \approx 2$ кэ) также уменьшает τ примерно на 30%. Следовательно, прекращение роста τ с увеличением H_0 (рис.10) частично может быть объяснено потерями плазмы на подводах измерительного зонда [22].

5. Сравнение с теорией

Оценки показывают, что поток частиц на стенки, обусловленный флуктуациями плотности и потенциала, слишком мал, чтобы объяснить наблюдаемые потери плазмы в области $H_0 < 2$ кэ. В то же время длина свободного пробега электронов значительно превышает длину установки, так что при изучении диффузии необходимо учитывать эффекты захваченных частиц. Причем, в условиях наших экспериментов частоты соударений ν_{ei} и ν_{en} таковы, что основную роль должны играть частицы, захваченные за счет тороидального, а не винтового магнитного поля. Поэтому при обосновании результатов мы будем пользоваться расчетами Галеева и Сагдеева [23] для промежуточной области частот соударений.

В целях сравнения с теорией изучалась зависимость времени жизни плазмы от давления гелия, напускаемого в систему, при использовании только одного источника плазмы. На рис.14 вместе с экспериментальными точками приведена кривая, рассчитанная на основании работы [23] из соотношения:

$$\tau = \frac{\pi \cdot r^2 \cdot n}{2\pi \cdot r \cdot D_1 \left(\frac{\partial n}{\partial r} \right)}$$

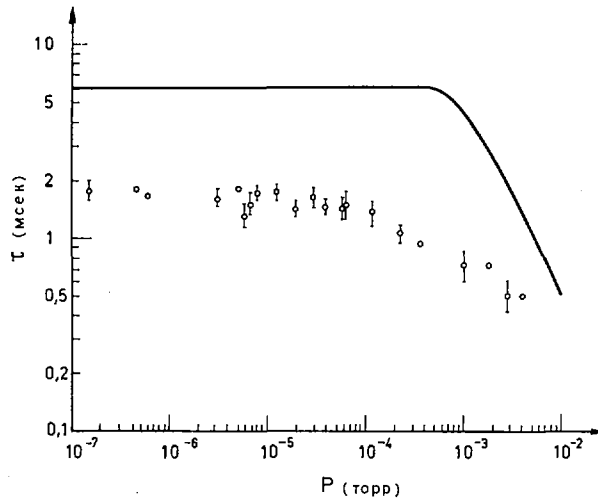


Рис. 14. Зависимость времени жизни плазмы от давления гелия. Стеллараторный режим, $H_0 = 1,8$ кэ. (—) — расчет, (·) — эксперимент.

При этом предполагалось, что $T_e = 10$ эВ во всем диапазоне давлений гелия, а величины $(1/n \cdot \partial n / \partial r)^{-1}$ и r принимались равными 1 см и 6 см (рис. 12 а).

Экспериментальные точки получены при $H_0 = 1,8$ кэ, т.е. в области, где еще наблюдается рост τ с увеличением напряженности магнитного поля.

Из сравнения измеренной зависимости с расчетной видно их удовлетворительное совпадение в широком диапазоне давлений за исключением того участка, где происходит переход к гидродинамической зависимости D_{\perp} от ν_{eff}^e .

Различие, наблюдаемое в этой области давлений, связано с предположением о постоянстве электронной температуры, которая при этом не измерялась. Учет уменьшения температуры с ростом давления гелия приведет к сужению той области давлений, где D_{\perp} не зависит от ν_{eff}^e .

Таким образом, в области $H_0 \leq 2$ кэ потери плазмы определяются, в основном, запертыми частицами.

V. ВЫВОДЫ

Из проведенных экспериментов можно сделать следующие выводы:

1. Полученные в торсатронном режиме параметры магнитных поверхностей ($r_0 \approx 5$ см, $i_0 \approx 0,9 \pi$, $S_0 \approx 0,2$) близки по значению к результатам, полученным в стеллараторном режиме ($r_0 = 5$ см, $i_0 \approx \pi$, $S_0 \approx 0,23$).

2. В наиболее экономичном режиме торсатрона ($K_{\varphi} = 1$) магнитные поверхности имеют достаточно высокие параметры ($r_0 = 4$ см, $i_0 \approx 0,9 \pi$, $S_0 = 0,12$).

3. В отношении одновременного получения "магнитной ямы" и шира торсатрон не имеет преимуществ перед стелларатором, так как в стел-

лараторе при $N_1/N_0 = 0,5\%$ глубина "ямы" могла достигать 10% при значении шира $S_0 \approx 0,1$.

4. Вся сумма экспериментальных результатов свидетельствует о том, что с точки зрения удержания плазмы торсатронная конфигурация мало отличается от стеллараторной. В то же время, по простоте изготовления и удобству эксплуатации торсатрон намного превосходит стелларатор.

5. При $N < 2$ кэ зависимость времени жизни плазмы от давления согласуется с неоклассической теорией, хотя абсолютное значение τ при этом в несколько раз меньше, чем можно ожидать на основании этой теории.

ЛИТЕРАТУРА

- [1] GOURDON, C., VUILLEMIN, M., EUR-CEA-FC (1966) 391.
- [2] ALEKSIN, V.F., SEBKO, V.P., Nuclear Fusion 8 3 (1968) 145.
- [3] GOURDON, C., MARTY, D., MASHKE, E.K., DUMOUT, J.P., Третья конф. по исследованиям в области физики плазмы и управляемого термоядерного синтеза (Новосибирск, СССР, 1968) доклад CN-24/F-2.
- [4] MIYAMOTO, K., J. Phys. Soc. Japan 27 (1969) 1925.
- [5] GOURDON, G., MARTY, D., TOUCHÉ, J., VI Symp. on Fusion Technology, 1970.
- [6] HUBERT, P., EUR-CEA-FC (1970) 533.
- [7] МОНРИ, А., J. Phys. Soc. Japan 28 (1970) 1549.
- [8] СУПРУНЕНКО, В.А., Атомная энергия 29 вып.6 (1970).
- [9] БЕРЕЖЕЦКИЙ, М.С., ГРЕБЕНЩИКОВ, С.Е., ПОПРЯДУХИН, А.П., ШПИГЕЛЬ, И.С., ЖТФ 35 вып. 12 (1965) 2167.
- [10] GIBSON, A., Phys. of Fluids 10 (1967) 1553.
- [11] КОВРИЖНЫХ, Л.М., ЖТФ 33 (1964).
- [12] АЛЕКСИН, В.Ф., Физика плазмы и проблемы управляемого термоядерного синтеза, вып.3, Изд-во АН УССР, Киев (1963) 216.
- [13] КОМИН, А.В., КРАСИЦКАЯ, Л.С., МИНАЕВ, В.П., Атомная энергия 27 вып.3 (1969).
- [14] БУРЧЕНКО, П.Я., ВАСИЛЕНКО, Б.Т., ВОЛКОВ, Е.Д., НИКОЛАЕВ, Р.М., ПОТАПЕНКО, В.А., СЕБКО, В.П., Атомная энергия 23 вып.2 (1967).
- [15] АЛЕКСИН, В.Ф., БИРЮКОВ, О.В., ГЕОРГИЕВСКИЙ, А.В., ГРОТ, Ю.И., ЗИСЕР, В.Е., КИТАЕВСКИЙ, Л.Х., ПОГОЖЕВ, Д.П., СЕРГЕЕВ, Ю.Ф., СУПРУНЕНКО, В.А., ТОЛОК, В.Т., Атомная энергия 27 вып.3 (1969).
- [16] SINCLAIR, R.M., HOSEA, T.C., SHEFFIELD, G.V. RSI 41 1552 (1970).
- [17] АКУЛИНА, Д.А., НЕЧАЕВ, Ю.И., ТВТ 6 (1969) 1061.
- [18] ВИШНЕВЕЦКИЙ, В.Н., ДИКИЙ, А.Г., ЗАЛКИНД, В.М., КОНОТОП, П.И., КУЗНЕЦОВ, Ю.К., МОИСЕЕВ, С.С., ПАВЛИЧЕНКО, О.С., СУПРУНЕНКО, В.А., ТОЛОК, В.Т., ТЕРЕЩЕНКО, Ф.Ф., ТОНКОПРЯД, В.М., ТАРАСЕНКО, В.П., Международ. конф. по удержанию плазмы в замкнутых ловушках, Дубна, СССР, 1969.
- [19] BOLTON, R.A.E., HOFFMAN, C.R.I., LEES, P.J., MEDLEY, S.S., REYNOLDS, P., SHATFORD, P.A., WHITE, V.M., CLM-P243 (1970).
- [20] ХАСТЕД, Дж., Физика атомных столкновений, Изд-во "Мир", М., (1965) 345.
- [21] KUCKES, A.F., MOTLEY, R.W., HINNOV, E., HIRSCHBERG, J.G., Phys. Rev. Lett. 6 (1961) 337.
- [22] FREEMAN, R., OKABAYASHI, M., PASKER, G., YOSHIKAWA, S., MATT-Q-27 (1970) 1.
- [23] ГАЛЕЕВ, А.А., САГДЕЕВ, Р.З., ЖЭТФ 53 (1967) 349.

ПОВЕДЕНИЕ ВЫСОКОТЕМПЕРАТУРНОЙ ПЛАЗМЫ ПРИ ТОКОВОМ НАГРЕВЕ В СТЕЛЛАРАТОРЕ С БОЛЬШИМ ШИРОМ "УРАГАН"

А. Г. ДИКИЙ, Дж. Г. ГОРМАН, В. М. ЗАЛКИНД,
Г. В. ЗЕЛЕНИН, В. Д. КОЦУБАНОВ, А. П. ЛИТВИНОВ,
В. Г. КОНОВАЛОВ, О. С. ПАВЛИЧЕНКО,
Н. Ф. ПЕРЕПЕЛКИН, Н. П. ПОНОМАРЕНКО,
В. А. СУПРУНЕНКО, В. Т. ТОЛОК, В. М. ТОНКОПРЯД
Физико-технический институт Академии наук
Украинской ССР, Харьков,
Союз Советских Социалистических Республик

Доклад представлен В. С. Войценой

Presented by V. S. Voitsenya

Abstract—Аннотация

BEHAVIOUR OF A HIGH-TEMPERATURE PLASMA UNDER CURRENT HEATING IN THE HIGH-SHEAR STELLARATOR "URAGAN".

In this paper the results are presented of an investigation into the behaviour of plasma produced by ohmic discharges in the high-shear stellarator "Uragan" ("Hurricane"). During the past year the magnetic system of the stellarator has undergone changes: new rectilinear cylinder elements have been installed. Measurements conducted with an electron beam have shown that with the new cylinder elements operation is possible with a magnetic system of the following parameters: maximum shear and rotational transform angle of 0.12 and 1.8 respectively on magnetic surfaces having a radius of 6 cm. Ohmic discharges were produced by means of a discharge from a capacitor bank via a corresponding transformer directly on a metal discharge chamber having an insulating ceramic section. Preliminary ionization was effected with the help of a high-frequency generator having a frequency of 100 kc/s and an output of up to 200 kW. The following plasma parameters were measured: electron density, by means of a phase meter, and electron temperature, on the basis of the plasma conductivity and the ratio of the intensities of the spectral lines of helium. The radial distribution of the electron density and temperature was measured with the help of electric probes. Under some conditions control measurements were made of the radial distributions of the electron temperature and concentration on the basis of the Thomson scattering of light from a ruby laser. The results are given of measurements of the energy lifetime and the charged particle lifetime as a function of the configuration of the magnetic field in the stellarator. When measuring the charged particle lifetime account was taken of the effect of ionization by the spectroscopic method. In typical operating régimes the electron density attained 10^{19} cm⁻³ and the electron temperature up to 100 eV. The results are discussed of attempts to separate the effect of shear and of the rotational transform angle using the specific behaviour of the shear and rotational transform values when the increase $\epsilon = h_3 / H_z$ (h_3 is the fundamental harmonic of the helical field and H_z the strength of the longitudinal magnetic field).

ПОВЕДЕНИЕ ВЫСОКОТЕМПЕРАТУРНОЙ ПЛАЗМЫ ПРИ ТОКОВОМ НАГРЕВЕ В СТЕЛЛАРАТОРЕ С БОЛЬШИМ ШИРОМ "УРАГАН".

В докладе приводятся результаты исследования поведения плазмы, создаваемой омическими разрядами в стеллараторе с большим широм "Ураган". В течение прошедшего года магнитная система стелларатора претерпела изменения: были установлены новые прямолинейные цилиндры. Измерения с электронным пучком показали, что с новыми цилиндрами возможна работа с магнитной системой со следующими параметрами: максимальный шир и угол вращательного преобразования, соответственно 0,12 и 1,8 на магнитных поверхностях с радиусом 6 см. Омические разряды создавались путем разрядки конденсаторной батареи через согласующий трансформатор непосредственно на металлическую

разрядную камеру, имевшую изолирующий керамический участок. Предварительная ионизация осуществлялась с помощью высокочастотного генератора с частотой 100 кГц и мощностью до 200 кВт. Измерялись следующие параметры плазмы: плотность электронов — фазометром, электронная температура — по проводимости плазмы и по отношению интенсивностей спектральных линий гелия; радиальное распределение плотности и температуры электронов измерялось с помощью электрических зондов. В некоторых режимах производились контрольные измерения радиальных распределений электронной температуры и концентрации по томсоновскому рассеянию света рубинового лазера. В работе приводятся результаты измерений энергетического времени жизни и времени жизни заряженных частиц в зависимости от конфигурации магнитного поля в стеллараторе. При измерениях времени жизни заряженных частиц производился учет влияния ионизации спектроскопическим методом. В типичных режимах работы плотность электронов достигала 10^{13} см⁻³, электронная температура — до 100 эВ. Обсуждаются результаты попыток разделения влияния шира и угла вращательного преобразования, использовавших специфическое поведение величины шира и вращательного преобразования при увеличении $\epsilon = h_3/H_z$ (h_3 — основная гармоника винтового поля, H_z — напряженность продольного магнитного поля).

За последнее время наблюдается существенный прогресс в изучении процессов переноса плазмы в стеллараторах. На стеллараторах "Вендельштейн" (Гарчинг) [1] в экспериментах с щелочной плазмой время жизни частиц в гидродинамическом режиме находится в количественном согласии с классической теорией диффузии плазмы в стеллараторе [2]. На стеллараторе "Протоклео" (Калэм) [3] время жизни частиц в бесстолкновительном режиме, соответствующем "плато" в теории процессов переноса плазмы в тороидальных ловушках [4], находится в качественном согласии с предсказываемым теорией. В этом сообщении приводятся результаты измерений времени жизни энергии и частиц в бесстолкновительной плазме стелларатора "Ураган", приготавливаемой с помощью токового нагрева на аномальном сопротивлении.

В стеллараторе "Ураган" после экспериментов, доложенных в Дубне [5], произошли изменения: были установлены новые прямолинейные цилиндрические и удалена диафрагма. Магнитная система стелларатора была настроена с помощью электронно-пучковой методики [6]; полученные параметры системы приведены в табл. I.

Изучалось поведение гелиевой плазмы в диапазоне давлений $5 \cdot 10^{-5} \div 1 \cdot 10^{-4}$ торр; нагрев плазмы, полученной с помощью высокочастотной предиионизации, производился путем приложения на обход системы импульса напряжения длительностью 10 мсек.

Измерялись следующие параметры плазмы: напряжение на обходе и ток в плазме, средняя по диаметру плотность плазмы — с помощью 8-мм-интерферометра Уортона, поперечная энергия плазмы $n \cdot (T_e + T_i)$ — с помощью диамагнитной петли, доплеровская температура ионов — с помощью сканируемого электромеханически интерферометра Фабри-Перо. Локальные измерения электронной температуры и плотности производились с помощью томсоновского рассеяния света рубинового лазера (энергия импульса ≈ 4 Дж, длительность ~ 25 нсек). Измерялись также абсолютные интенсивности спектральных линий He I и He II и микроволновое излучение плазмы вблизи частот $\omega \approx \omega_{0e}$. На рис. 1 приведены типичные осциллограммы сигналов.

Во всех оценках использовались соответствующие данному ϵ ($\epsilon = h_3/H_0 \sim I_{\text{винт}}/H_0$; h_3 — основная гармоника винтового поля. H_0 — удерживающее магнитное поле) значения среднего радиуса сепаратрисы a , угла преобразования $t = L/2\pi$ и шира θ , полученные с помощью электронных пучков.

ТАБЛИЦА I. ОСНОВНЫЕ ПАРАМЕТРЫ СТЕЛЛАТОРА "УРАГАН"

1. Удерживающее магнитное поле	$H_0 = 10 \text{ кЭ}$
2. Максимальный угол вращательного преобразования	$\ell = 1,8 \pi$
3. Максимальный шир	$\theta = 0,12$
4. Аксиальная длина вакуумной камеры	$L = 1035 \text{ см}$
5. Большой радиус тороидальных участков	$R = 110 \text{ см}$
6. Радиус камеры	$b = 10 \text{ см}$
7. Максимальное значение β_e	$\beta_{e \text{ max}} = 4 \cdot 10^{-3}$

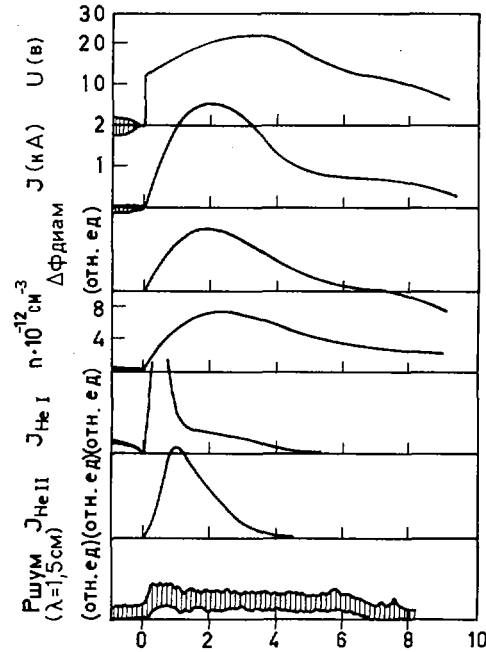


Рис. 1. Осциллограммы сигналов различных датчиков:

- 1) напряжение на обходе камеры,
- 2) сила тока в плазме,
- 3) диамагнитный сигнал,
- 4) плотность плазмы,
- 5) интенсивность линии He I ($\lambda = 5015 \text{ \AA}$),
- 6) интенсивность линии He II ($\lambda = 4686 \text{ \AA}$),
- 7) интенсивность шумового излучения из плазмы ($\lambda = 1,6 \text{ см}$).

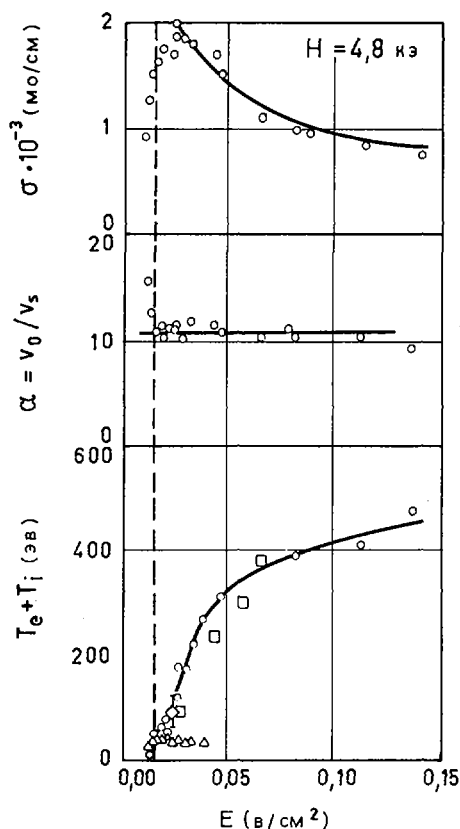


Рис. 2. Зависимость от электрического поля:

- а) проводимость плазмы,
 б) отношения дрейфовой скорости электронов к скорости ионного звука,
 в) температуры плазмы (○ - диамагнитные измерения, □ - измерения шумового излучения, ◇ - рассеяние света лазера).

1. ЭЛЕКТРОПРОВОДНОСТЬ И НАГРЕВ ПЛАЗМЫ

Измерения средней по сечению проводимости плазмы в зависимости от напряженности электрического поля (при $\epsilon = 0,58$; $H_0 = 5$ кЭ) показали, что, начиная с полей $E/E_{cr} \geq 0,05$ (E_{cr} - поле Драйсера), проводимость плазмы значительно ниже кулоновской, вычисленной в предположении $Z = 2$ с использованием диамагнитной температуры (рис. 2 а). В этих же условиях токовая скорость электронов стабилизировалась на уровне: $v_{0e} \approx 10 v_s$ (где $v_s = \sqrt{(Z \cdot T_e)/M_i}$ - скорость неизотермического ионного звука) (рис. 2 б) и наблюдался сильный нагрев плазмы (рис. 2 в). Измерения микроволнового излучения вблизи $\omega \approx \omega_{pe}$ на оси разряда показали, что его временное поведение и уровень удовлетворительно соответствуют тепловому, т.е. не наблюдается "убегающих" электронов.

Одновременные измерения электронной температуры по томсоновскому рассеянию света и диамагнитной температуры ($T_e + T_i$) показали, что

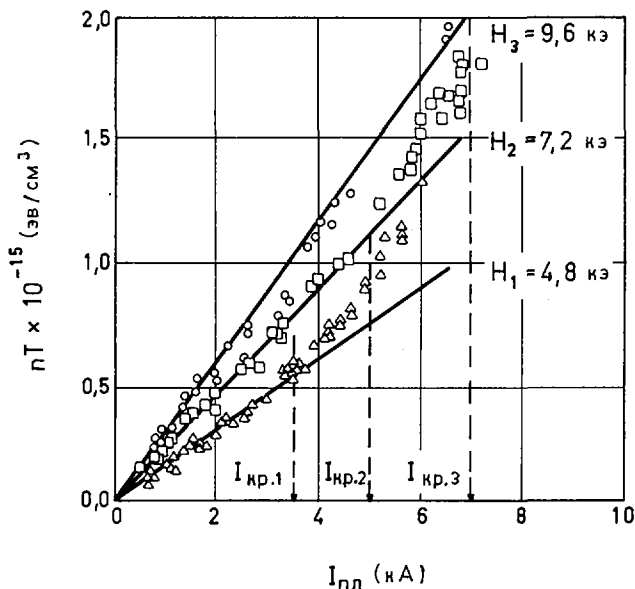


Рис.3. Зависимость диамагнитного сигнала от силы тока в плазме для трех значений магнитного поля H_0 .

в пределах ошибок методов они совпадают, а прямые измерения ионной температуры T_i показали, что она находится в диапазоне $10 \div 20$ эВ и слабо зависит от параметров разрядов.

Изучение зависимости $n \cdot (T_e + T_i) \approx n \cdot T_e$ от разрядного тока и напряженности магнитного поля H_0 (при значении $\epsilon = 0,58$, близком к оптимальному) показало, что существует диапазон величин тока ($I \leq I_{кр}$), в котором выполняется соотношение (рис.3):

$$n \cdot T_e = 2 \cdot 10^{13} \cdot I \text{ (кА)} \cdot H_0 \text{ (кЭ)} \left(\frac{\text{эВ}}{\text{см}^3} \right) \quad (1)$$

Таким образом, так же как и на установках "Токамак", величины электронной температуры и плотности связаны между собой; различие состоит в том, что для "Токамаков" $n \cdot (T_e + T_i) \sim I^2$ и не зависит от H_0 . Критический ток $I_{кр}$ зависит от величины удерживающего магнитного поля, так что выполняется соотношение $I_{кр}/H_0 \approx 0,7$ (при $\epsilon = 0,58$). При токах, больших критического, исчезает зависимость $n \cdot T_e$ от магнитного поля H_0 и выполняется соотношение $n \cdot T_e \sim I^2$.

Природа критического тока не очень ясна, поскольку при токах, равных критическим,

$$\beta_{равнов} = \frac{8\pi \cdot nT}{H_0^2} = \frac{8\pi \cdot 2 \cdot 10^7 \cdot I \cdot H_0}{H_0^2} \approx 6 \cdot 10^{-4}$$

а угол преобразования $l_{ток}$, связанный с током,

$$\ell_{\text{ток}} = \frac{L}{5 a^2} \cdot \left(\frac{I_{\text{кр}}}{H_0} \right) \approx \pi$$

так что суммарный угол преобразования ($\epsilon = 0,58$) равен

$$\ell = \ell_{\text{винт}} + \ell_{\text{ток}} = 1,5\pi + \pi = 2,5\pi$$

2. ЭНЕРГЕТИЧЕСКОЕ ВРЕМЯ ЖИЗНИ

Энергетическое время жизни плазмы τ_E (без учета потерь на излучение) находилось обычным способом из измерений полной энергии плазмы с помощью диамагнитной петли и вводимой мощности. Зависимость энергетического времени жизни от электронной температуры показана на рис. 4. Здесь можно видеть две области: область I, где τ_E растет с ростом T_e , и область II, где τ_E падает при дальнейшем увеличении T_e примерно пропорционально $T_e^{-1/2}$.

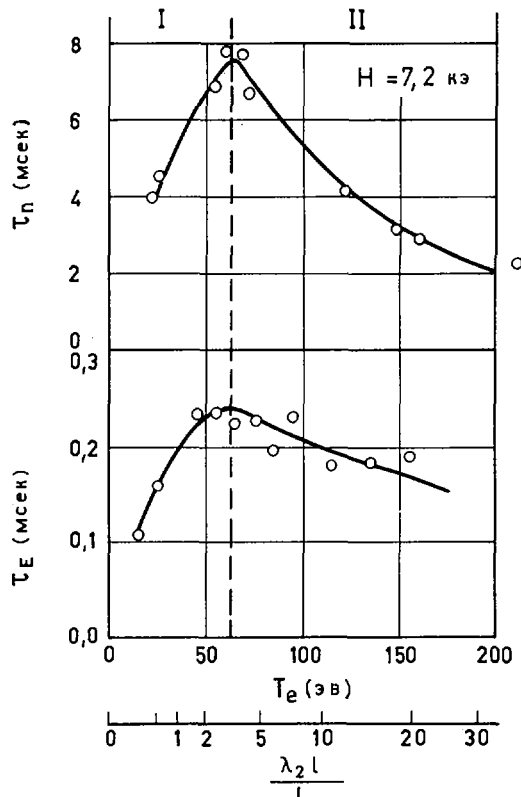


Рис. 4. Зависимость времени жизни частиц и энергетического времени жизни плазмы от температуры.

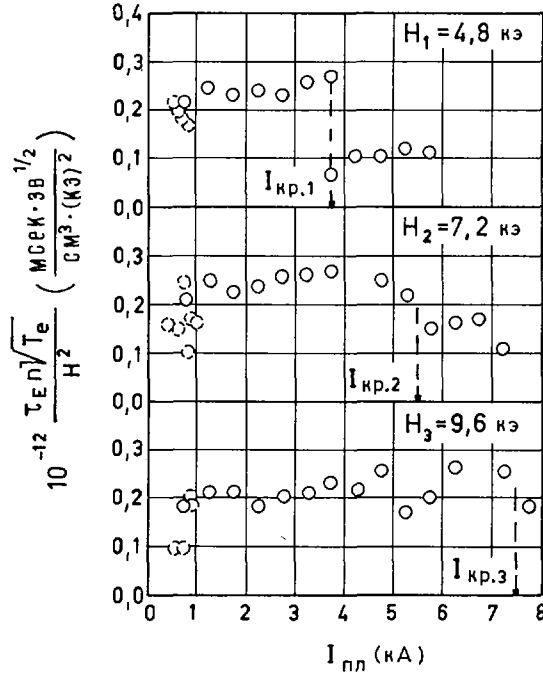


Рис. 5. Зависимость приведенного энергетического времени жизни плазмы от силы тока в плазме.

Более подробно зависимость τ_E от параметров плазмы в области I не изучалась, однако обращает на себя внимание факт, что переход из области I в область II происходит при частотах электронных столкновений, соответствующих границе между гидродинамическим режимом Пфирша и Шлютера [2] и "плато" Галеева и Сагдеева [4] (в предварительном докладе была сделана попытка увязать этот переход с существованием критического тока, меньшего $I_{кр} \approx 0,7 H_0$).

Анализ данных, полученных при постоянном ϵ , показал, что в области II для τ_E выполняется соотношение:

$$\tau_E \sim \frac{H_0^2}{n \cdot \sqrt{T_e}} \quad (2)$$

независимо от величины тока в плазме вплоть до тока $I_{кр}$ (рис. 5). Изучение зависимости нормированной в соответствии с (2) τ_E от величины угла вращательного преобразования t и радиуса плазмы a (при увеличении ϵ средний радиус сепаратрисы уменьшался от 7,8 см до 5,2 см) показало (рис. 6), что в области II эта зависимость удовлетворительно описывается выражением:

$$\tau_E \approx (3 \div 5) \cdot 10^{10} \cdot \frac{H_0^2 (кЭ) \cdot a \cdot \sqrt{t}}{n \cdot \sqrt{T_e} (эВ)} \quad (3)$$

Абсолютная величина τ_E достигала $(5 \div 6) \cdot \tau_B$.

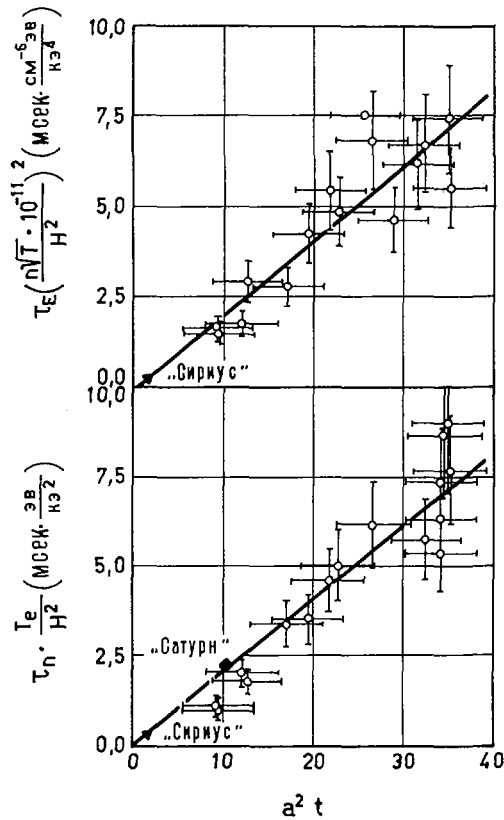


Рис. 6. Зависимость квадрата приведенного энергетического времени жизни и приведенного времени жизни частиц от $a^2 t$.

Обнаруженный экспериментально факт зависимости $n \cdot T_e \sim I \cdot H_0$ позволяет сделать вывод, что во всем диапазоне изменения T_e энергетическое время жизни $\tau_E \sim H_0^2$. Действительно, если из уравнения баланса энергии электронов $I^2 / [\sigma \cdot (\pi a^2)^2] = [3/2 n T_e] / \tau_E$ исключить ток, используя выражение (1), то можно получить следующую функциональную зависимость $\tau_E \sim H_0^2 \cdot \sigma / n \cdot T_e$ (4). Зависимость σ от параметров плазмы в области I подробно не исследовалась, однако совпадение диамагнитной температуры с температурой, измеренной по проводимости, при $T_e \leq 20$ эВ, позволяет считать, что в этом диапазоне $\sigma \sim T_e^{3/2}$ и $\tau_E \sim H_0^2 \cdot \sqrt{T_e} / n$. В области II ($50 \text{ эВ} \leq T_e \leq 200 \text{ эВ}$) σ продолжает увеличиваться с ростом температуры, однако закон возрастания более слабый: $\sigma \sim \sqrt{T_e}$, что дает в сочетании с (4)

$$\tau_E \sim \frac{H_0^2}{n \cdot \sqrt{T_e}}$$

Учитывая тот факт, что $T_e \gg T_i$ и $\tau_E \ll \tau_{eq}$ (τ_{eq} — время кулоновского обмена энергии между электронами и ионами), можно сделать вывод, что

потери энергии из плазмы происходят за счет электронов. Абсолютная величина времени жизни энергии примерно на два порядка ниже теоретической для области II, вычисленной в соответствии с [4].

3. ВРЕМЯ ЖИЗНИ ЧАСТИЦ

Время жизни частиц τ_n определялось из уравнения баланса заряженных частиц путем измерения электронной плотности и вклада ионизации атомов и однократно ионизированных ионов гелия (подробно соответствующие расчеты будут описаны позже). Зависимость определенного таким способом τ_n от электронной температуры, как это можно видеть, подобна зависимости $\tau_e = f(T_e)$, за исключением того, что уменьшение τ_n во II области происходит приблизительно пропорционально T_e^{-1} . Время жизни частиц оказалось не зависящим от n_e (в диапазоне $n_e = (2 \div 8) \cdot 10^{12} \text{ см}^{-3}$) и возрастающим пропорционально H_0^2 ($2,4 \text{ кЭ} \leq H_0 \leq 9,6 \text{ кЭ}$).

Зависимость нормированного времени жизни $(\tau_n \cdot T_e) / H_0^2$ от величины $t \cdot a^2$ показана на рис. 6; видно, что результаты этих измерений можно представить в виде выражения:

$$\tau_n \approx (0,2 \div 0,5) \cdot \frac{H_0^2 \cdot (a^2 t)}{T_e} \text{ (ms)}$$

Абсолютная величина времени жизни частиц достигает $(40 \div 50) \cdot \tau_B$, но в то же время примерно на порядок ниже неоклассического.

Основным результатом данной работы является экспериментальное исследование функциональной зависимости времени удержания плазмы в стеллараторе в достаточно широком диапазоне изменения электронной температуры. Обнаружены две области с различной функциональной зависимостью времени жизни от электронной температуры плазмы. Первая область ($T_e \leq 50 \text{ эВ}$), вероятно, соответствует гидродинамической области, вторая область ($T_e \geq 50 \text{ эВ}$) соответствует "плато".

В этой области было экспериментально исследовано в стеллараторе энергетическое время жизни плазмы с достаточно высокой электронной температурой. Показано, что потери энергии здесь определяются электронной компонентной плазмы; энергетическое время жизни существенным образом отличается от времени удержания частиц как по абсолютной величине, так и по функциональной зависимости от параметров плазмы.

Результаты экспериментов по удержанию плазмы в стеллараторах "Сатурн" и "Сириус" находятся в хорошем согласии с эмпирическими соотношениями, полученными в данной работе.

ЛИТЕРАТУРА

- [1] BERKEL, E., ECKHART, D.E., GIERKE, G.von, GRIEGER, G., Phys. Rev. Lett. 17 (1966) 906.
- [2] PFIRSCH, D.von, SCHLÜTER, A., Preprint MPI/PA/7/62. Max-Planck Institut für Physik und Astrophysik (1962).
- [3] LEES, D.J., BOLTON, R.A.E., HOFFMAN, C.R.J., MEDLEY, S.S., REYNOLDS, P., WHITE, S.M., IIIrd European Conference on Controlled Fusion and Plasma Physics. Report No. 4.

- [4] ГАЛЕЕВ, А.А., САГДЕЕВ, Р.З., ЖЭТФ 53 (1967) 348.
- [5] ВИШНЕВЕЦКИЙ, В.Н., ВОЛКОВ, Е.Д., ДИКИЙ, А.Г., ЗАЛКИНД, В.М., КОНОТОП, П.И., МОИСЕЕВ, С.С., ПАВЛИЧЕНКО, О.С., СУПРУНЕНКО, В.А., ТАРАСЕНКО, В.П., ТЕРЕЩЕНКО, Ф.Ф., ТОЛОК, В.Т., ТОНКОПРЯД, В.М., ЖТФ 40 (1970) 1615.
- [6] ГЕОРГИЕВСКИЙ, А.В., ДИКИЙ, А.Г., ЗИСЕР, В.Е., МИРАНСКИЙ, М.А., ПЕЛЕТМИНСКАЯ, В.Г., ПОГОЖЕВ, Д.П., ТАРАН, В.М., УФЖ 15 (1971) 680.

DISCUSSION

TO PAPERS IAEA-CN-28/H-10, H-11

A. GIBSON: You indicated that the energy confinement time (τ_E) and particle confinement time (τ_c) show different scaling with plasma radius (a), i. e. $\tau_E \propto a$ but $\tau_c \propto a^2$. How was " a " varied in these measurements, and over what range?

V. S. VOITSENYA: It has been shown previously that without a limiter the plasma cross-section is approximately the same as the cross-section of the last intact surface. In these experiments, therefore, the authors varied the plasma radius by varying the value of ϵ . The relations shown in Fig. 6 were obtained by varying the mean plasma radius " a " in the range 5.2-7.8 cm.

PLASMA SHIFT IN FAST STELLARATORS WITH FINITE CONDUCTIVITY

D. PFIRSCH, A. SCHLÜTER

Max-Planck-Institut für Plasmaphysik, Euratom Association
Garching, Munich
Federal Republic of Germany

Abstract

PLASMA SHIFT IN FAST STELLARATORS WITH FINITE CONDUCTIVITY.

The magnetohydrodynamic theory of low- β stellarator and Tokamak equilibria shows that finite electrical conductivity demands rather large plasma flows. In a fast-compression stellarator, the question arises whether these flows can be set up fast enough to avoid the plasma hitting the walls. One can distinguish two cases:

- (1) There is a vacuum between the plasma and the wall and the plasma has already shifted out of the magnetic surfaces such that in the most pessimistic idealization no secondary currents can flow along the lines of force. The plasma is then accelerated in radial direction until the necessary plasma flows are established. An estimate of the resulting plasma shift δr_1 is given.
- (2) The same finite conductivity exists throughout the volume inside the walls. An optimistic assumption would be that the radial flow of the plasma already exists, permitting the secondary currents to flow. Due to this radial flow the plasma moves until the plasma flow in toroidal direction is achieved. Also in this case the shift, δr_2 , is estimated.

The truth might be somewhere between δr_1 and δr_2 . The relations derived make it desirable to use configurations with small secondary currents only. This could be attained, for example, by corrugating the magnetic lines of force to a certain extent.

The magnetohydrodynamic theory of low- β stellarator and Tokamak equilibria [1] shows that finite electrical conductivity demands rather large plasma flows. In a fast-compression stellarator, the question arises whether these flows can be set up fast enough to prevent the plasma from hitting the walls. The largest component of the flow velocity is that parallel to the magnetic fields. Its value is given by the expression

$$v_{\parallel} = v_D \left(\frac{2\pi}{\iota} \right)^3 \left(\frac{R}{r_p} \right)^2$$

There v_D is the classical diffusion velocity without any torus corrections, ι the angle of rotational transform, R the major torus radius, and r_p the minor plasma radius. This relation had been derived assuming an axially symmetric magnetic field whose rotational transform is due to curl $B \neq 0$ in a non-selfconsistent way (so-called mock-up stellarator). It is a valid approximation for a real stellarator, at least, if the main component of the field is the toroidal $1/R$ -vacuum field. The plasma has to be accelerated parallel to the fields in order for the plasma to reach this velocity. Such an acceleration can only be achieved by a pressure gradient, parallel to the magnetic field, which is not larger than the total pressure

$p = 2nkT$ divided by the connection length $2\pi/R\iota$. The time t after which v_{\parallel} is obtained is thus given by

$$t \approx \frac{n m_i v_{\parallel}}{|\text{grad}_{\parallel} p|} \approx \frac{m_i v_{\parallel}}{2 kT} \frac{2\pi R}{\iota} = \frac{1}{2} \frac{v_{\parallel}}{v_i^2} \frac{2\pi R}{\iota}$$

where m_i is the ion mass and $v_i = (kT/m_i)^{1/2}$ the thermal ion velocity.

We can now distinguish two limiting cases:

1) There is a vacuum between the plasma and the wall and the plasma has already shifted out of the magnetic surfaces so that in the most pessimistic idealization no secondary currents can flow along the lines of force. The plasma is then accelerated in the radial direction by the centrifugal force $m_i v_i^2/R$. After the time t , the plasma has covered a distance of

$$\delta r_1 = \frac{1}{2} \frac{v_i^2}{R} t^2$$

Substituting the above expression for t we obtain

$$\delta r_1 = \frac{1}{8} \frac{v_D^2}{v_i^2} \left(\frac{2\pi}{\iota} \right)^8 \left(\frac{R}{r_p} \right)^5 r_p$$

2) The same finite conductivity exists throughout the volume inside the walls. An optimistic assumption would be that the radial flow of the plasma already exists, thus permitting the secondary currents to flow. The radial flow velocity is given by

$$v_R = v_D \left(\frac{2\pi}{\iota} \right)^2 \frac{R}{r_p}$$

Owing to this velocity, the plasma moves during the time t given by the above formula through a distance of

$$\delta r_2 = v_R t = \frac{1}{2} \frac{v_D^2}{v_i^2} \left(\frac{2\pi}{\iota} \right)^6 \left(\frac{R}{r_p} \right)^4 r_p$$

The actual distance might be somewhere between δr_1 and δr_2 . For practical purposes δr_1 and δr_2 can be expressed more conveniently as

$$\frac{\delta r_1}{r_p} = \frac{1}{4} \times 10^{-20} \left(\frac{m_e c^2}{kT} \right)^4 \beta^2 \left(\frac{2\pi}{\iota} \right)^8 \left(\frac{R}{r_p} \right)^5$$

$$\frac{\delta r_2}{\delta r_1} = 4 \frac{r_p}{R} \left(\frac{\iota}{2\pi} \right)^2$$

$$\beta = 8 \pi p / B^2$$

Anomalous resistivity would increase δr quadratically. We would expect this formula to give the correct order of δr for finite values of β , as well. An example is the "Spinne" experiment in Garching with $R/r_p = 25$, $\iota = 2\pi = 0.1$, $T = 50\text{eV}$, $\beta \sim 1$. These data give

$$\delta r_1/r_p = 10^4, \quad \delta r_2/r_p = 10.$$

Thus, for this particular experiment it is doubtful whether equilibrium can be attained.

The results obtained in this paper, therefore, suggest the use of configurations with only small secondary currents. This could be achieved, for instance, by suitably corrugating the magnetic lines of force.

REFERENCE

- [1] PFIRSCH, D., SCHLÜTER, A., MPI Report, MPI/PA/7/62 (1962).

DISCUSSION

M. N. ROSENBLUTH: Did you consider radial electric fields? These could completely change the assumed mass motion, and there seems to be no reason to equate them to zero. The real question is transfer of angular momentum between surfaces.

D. PFIRSCH: We did not consider radial electric fields. I agree that these could change the mass motion.

THETA PINCHES; SHOCK WAVES
(Session J)

Papers J-5 to J-7 were presented by
H. GRAD as Rapporteur

Papers J-8 to J-13 were presented by
R. A. GROSS as Rapporteur

CONFINEMENT OF A TOROIDAL THETA-PINCH PLASMA IN A PERIODIC CAULKED-CUSP FIELD

T. UCHIDA, K. SATO, A. MOHRI, R. AKIYAMA
 Institute of Plasma Physics, Nagoya University, Nagoya,
 Japan

Abstract

CONFINEMENT OF A TOROIDAL THETA-PINCH PLASMA IN A PERIODIC CAULKED-CUSP FIELD.

It has been established with a toroidal theta-pinch experiment that a periodic caulked cusp field is effective in the suppression of the toroidal drift of a high-beta plasma as well as in the stabilization. This caulked cusp field is generated from currents induced by the theta-pinch magnetic field in the metal rings placed, perpendicularly to the main field, inside the discharge tube. The current in the ring is simply inductive and a closed line of null field lies inside each ring. Owing to the skin effect of the ring conductor, the null field line remains during the discharge.

Experiments are carried out on a toroidal machine with a theta-pinch coil of 50 cm major diameter and 13 cm minor diameter, equipped with 24 ceramic-coated metal rings inside.

In the implosion phase, the plasma sheath contracts uniformly in space except for the ring planes, and the axial inhomogeneity of the produced plasma that might result from the insertion of rings is hindered fairly well by a negative bias field applied to pre-heated plasma. The plasma is located at several millimetres outside of the tube axis at the final stage of contraction.

To obtain a favourable result for the confinement of the pinch plasma, there should be a region in which a magnetic-field minimum exists on the midplane between neighbouring rings, and the region should correspond to the plasma location at the maximum contraction. The number "24" for the rings is chosen so as to satisfy these conditions, and the plasma is really observed to stay at this location. Some flute-like instabilities are observed when 12 rings are used, in which case there is no region of field minimum.

The dynamics of the implosion phase is studied by magnetic probes, spectroscopy and laser techniques. The plasma behaviour in a periodic caulked cusp field is discussed for a plasma with Doppler temperature of several tens of eV, a density of $1 \times 10^{16} \text{ cm}^{-3}$ and a beta-ratio of 0.1-0.2.

1. INTRODUCTION

Several attempts have been proposed for the confinement of high-beta toroidal plasma and they are being studied experimentally in many laboratories [1-4]. It was established that a series of caulked cusp fields was successful in suppressing the toroidal drift of a theta-pinch plasma with a curved, but open-ended machine [5]. Here, we give experimental evidence of the realization of this idea in a full toroidal machine.

Experiments are carried out on a simple toroidal theta-pinch machine equipped with hi-alumina coated copper rings inside a pyrex glass tube, which are set perpendicularly to the main field along the tube axis at regular intervals. When the rings are removed, the theta-pinch plasma drifts outward, accompanied by radial oscillation; it is observed to hit the wall after about $1 \mu\text{s}$ (Fig. 1a). With the appropriate number of rings in place, the plasma does not drift and the streak photograph indicates the plasma to be stable for about $20 \mu\text{s}$ (Fig. 1b and 1d).

2. EXPERIMENTAL ARRANGEMENTS

A capacitor bank of 20 kV and 45 kJ in full charge is used for the main theta-pinch discharge. The electric field induced azimuthally by the

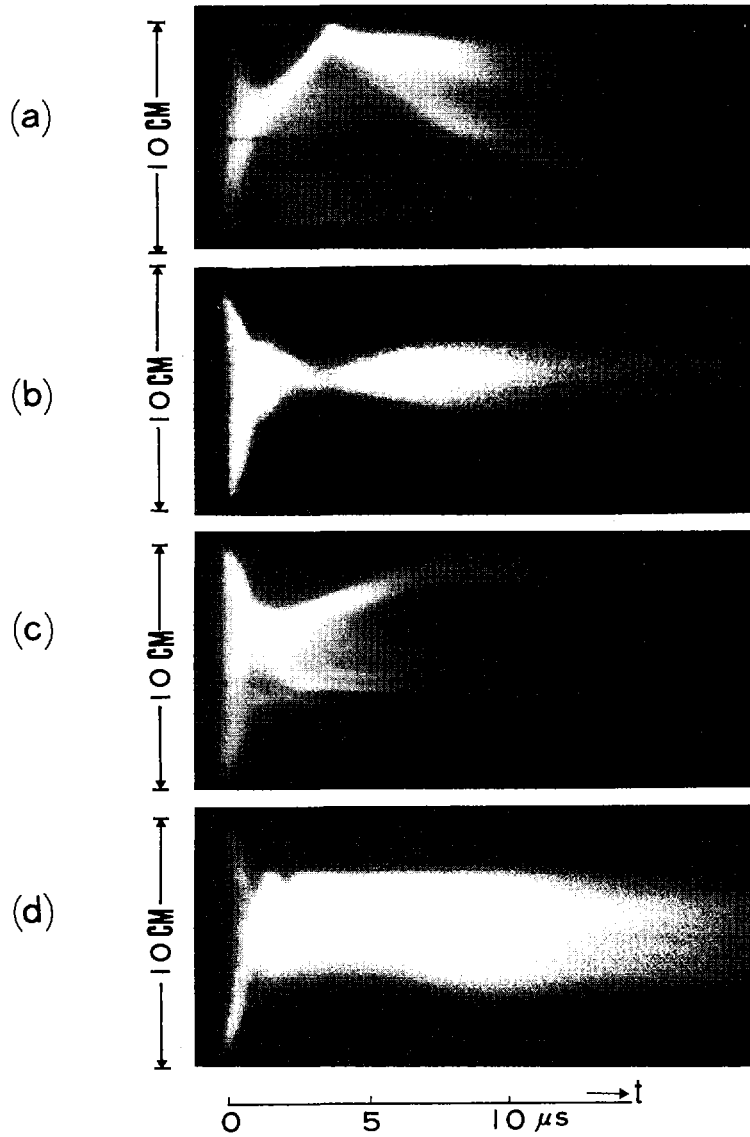


FIG. 1. (a) Without rings: the plasma drifts outward and is observed to hit the tube wall. (b) With 24 rings: such a drift is suppressed. (c) With 12 rings: the plasma is not observed to be stable. (d) The plasma boundary is well-defined even at the bad region outside the ring in the case of 24 rings. Black line at the centre represents the tube axis. These photographs are taken through a slit of the coil (a), at the midplane of neighbouring rings (b, c) and in the vicinity of the ring (d).

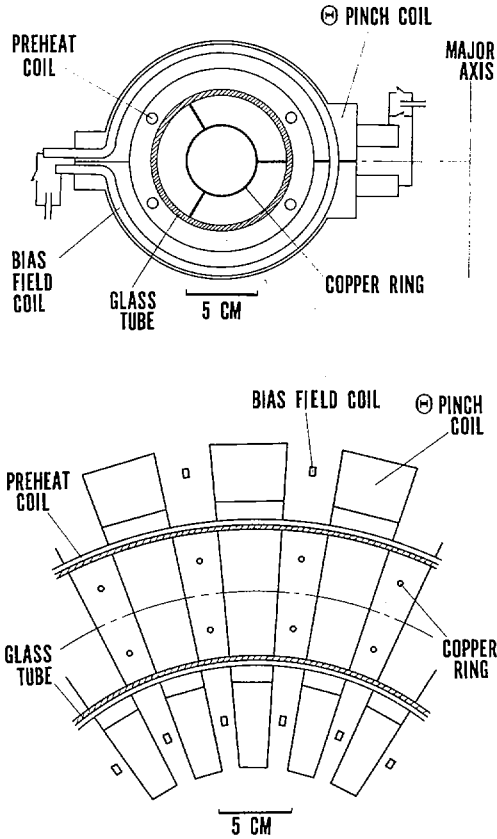


FIG. 2. Schematic drawing of the cross-sectional views of the machine on the meridian plane (a) and the equatorial plane (b).

discharge is around 100 V/cm along the inner surface of the tube so that the plasma temperature to be obtained is relatively low and 100 eV, at most. The major diameter of the machine is 50 cm, and the minor diameters of the coils and the glass tube are 13 cm and 10 cm, respectively. Each ring of 5 cm in diameter is supported by three thin Be-Cu wires coated with hi-alumina (Fig. 2).

A negative bias field of up to 600 G is applied prior to the plasma pre-heating by an axial current of pulse up to 10 kA; a few ten μ s later, the main discharge is fired. In the case of a simple torus, the main magnetic field reaches 13 kG on the minor axis at 4 μ s. When 24 rings are used, its maximum values change to 10 kG in the midplane of neighbouring rings and 6 kG beneath the ring. The coil current is crow-barred at the maximum of 1.6 MA and decays with a time constant of 70 μ s.

Figure 3 shows the computed magnetic lines of force and the wells of potential $U = - \int dl/B$ for the cases of 12 rings and 24 rings, neglecting the plasma pressure (here B is the magnetic flux density and dl is the

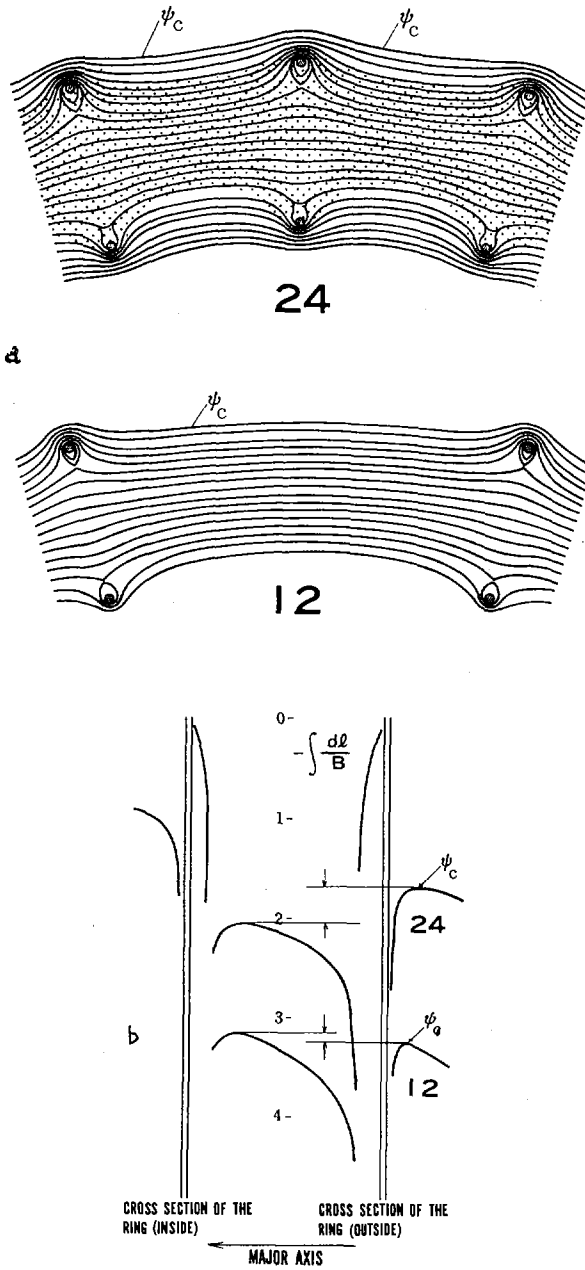


FIG. 3. Magnetic field lines of force (a) and the wells of potential $U = -d\ell/B$ (b), neglecting plasma pressure. Written figure means the number of rings. Shaded portion in (a) represents the plasma location deduced from photographs.

line element along the magnetic line of force). When low-beta plasma is contained in these configurations, equilibrium is established [6], and the magnetic wells seem to be effective in the stabilization of magnetohydrodynamic instabilities. A significant difference in the containment of the theta-pinch plasma appears between the cases of 12 rings and 24 rings. To obtain a favourable result, it is essential that a region exists in which the magnetic field has a minimum in the midplane between neighbouring rings. The number "24" for the rings is chosen so as to satisfy this condition, and there is a place on the outer side where the magnetic pressure is 15% higher than that at the minor axis. Such a difference in magnetic pressure gives a measure for the allowable beta ratio of the plasma to be confined. This configuration is called a periodic caulked-cusp field.

3. PLASMA PRODUCTION

Computation by a snow-plow model for the simple toroidal theta-pinch indicates that the central position of the pinched plasma column deviates from the axis by 15% of the tube radius towards the outside, for the

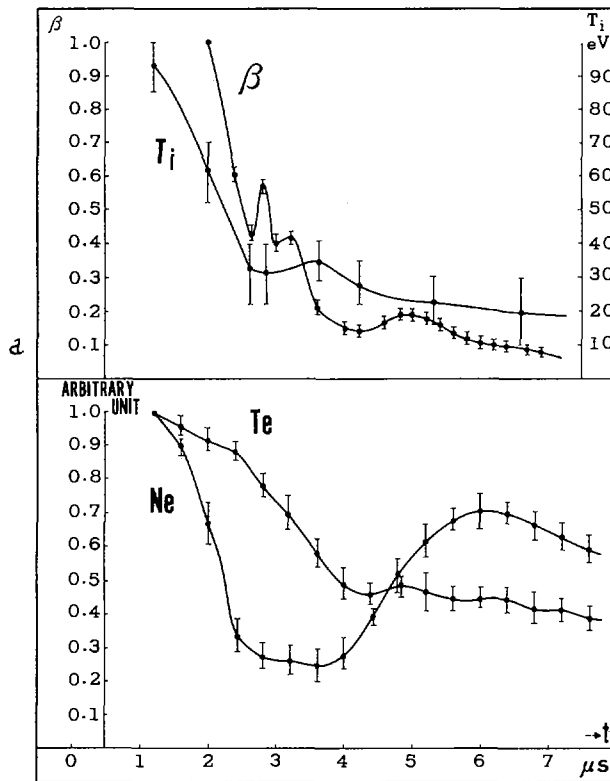


FIG. 4. Time variations of the beta-ratio, the Doppler temperature, the line density and the electron temperature in the case of 24 rings and 600 G negative bias field, observed at the midplane (a) and in the vicinity of the ring (b). Intensities of He II (4686 Å) and O II (4661, 6 Å) are compared, referring to the field variation, at the midplane (c) and in the vicinity of the ring (d). Figs 4 b, c, d are to be found on the following page.

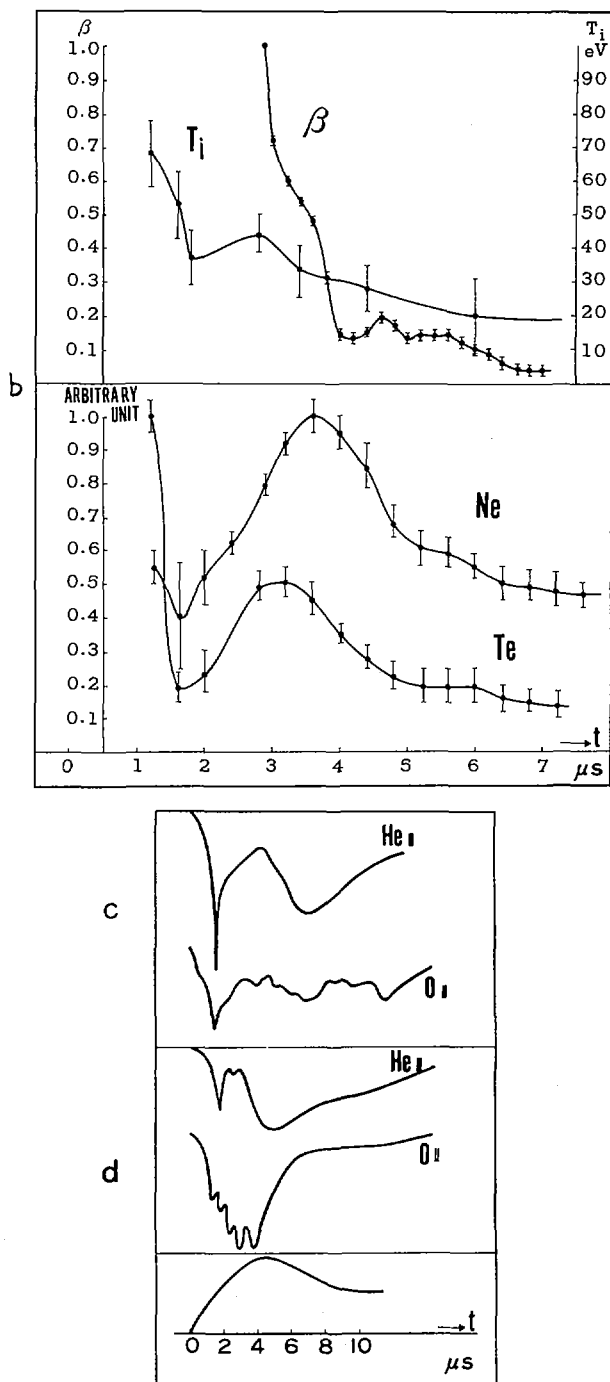


FIG. 4 b, c, d. See caption on preceding page.

present case with an aspect ratio of 5 [7]. When helium gas of 40-50 mTorr filling pressure is used, the plasma contracts at a position of 5-7 mm outside, and the diameter is 2 cm at the maximum contraction. The temperature as deduced from the drift speed is 60-90 eV, on the assumption that it is caused by the toroidal effect, and the density is estimated to be $2 \times 10^{16} \text{ cm}^{-3}$, from the period of the radial oscillation.

Even when 24 rings are present, similar pinch phenomena are observed, and the contraction speed is almost equal to that occurring in the case without the rings. The plasma appears also at several millimetres outside the axis at the final stage of contraction, and this location corresponds to the minimum-field region in the midplane. The plasma stays at this location (Fig. 1b).

The maximum electron density is deduced to be of the order of 10^{16} cm^{-3} with a He-Ne laser interferometer, and the maximum ion temperature of several tens of eV is estimated from Doppler broadening of O II (4661.6 Å) with an echelle monochromator [8]. Then the self-collision time for the ions is around 0.1 μs , and the relaxation time of the ions with electrons is a few microseconds.

In the implosion phase, the plasma sheath contracts uniformly in space except for the ring plane (width of 2.5-3 mm). It is observed, using streak photographs and diamagnetic probe signals, that the pinch time at the position immediately adjacent to the rings is the same as that observed in the midplane between the rings. However, some differences in the measured plasma parameters are present between the midplane and the vicinity of the rings, as is seen in Fig. 4. Such differences are inevitable in the present experiment.

4. PLASMA BEHAVIOUR AFTER THE PINCH

4.1. Photographs

The plasma behaviour in the case of 12 rings is different from that in the case of 24 rings (Figs 1b and 1c). The photographs suggest that there is no equilibrium in the case of 12 rings, in which case there is no region of field minimum in the midplane. When 24 rings are present, the plasma seems to be stable and neither the drift nor the $m = 1$ -instability are seen even in the midplane. The luminosity, however, increases on the exterior side of the plasma (Fig. 5). After having become quiescent, the plasma is located in the region shown by the shading in Fig. 3a. There should be an equilibrium state.

4.2. Magnetic-field distribution

The annihilation of the trapped reverse field in the midplane occurs about 1 μs earlier than that in the ring-plane. Diamagnetic probe signals suggest that the reverse-field region in the ring plane is shifted, and its shape is deformed in a complicated way after maximum contraction. It may, then, be possible for the plasma to touch the rings in this phase. However, spectral lines of Al I (3961.5 Å) and Al II (4666.8 Å) and Al III (4701.7 Å) are scarcely observed during the discharge. The principal caulked-cusp field is achieved at about 3 μs . The beta ratio is reduced from the signals

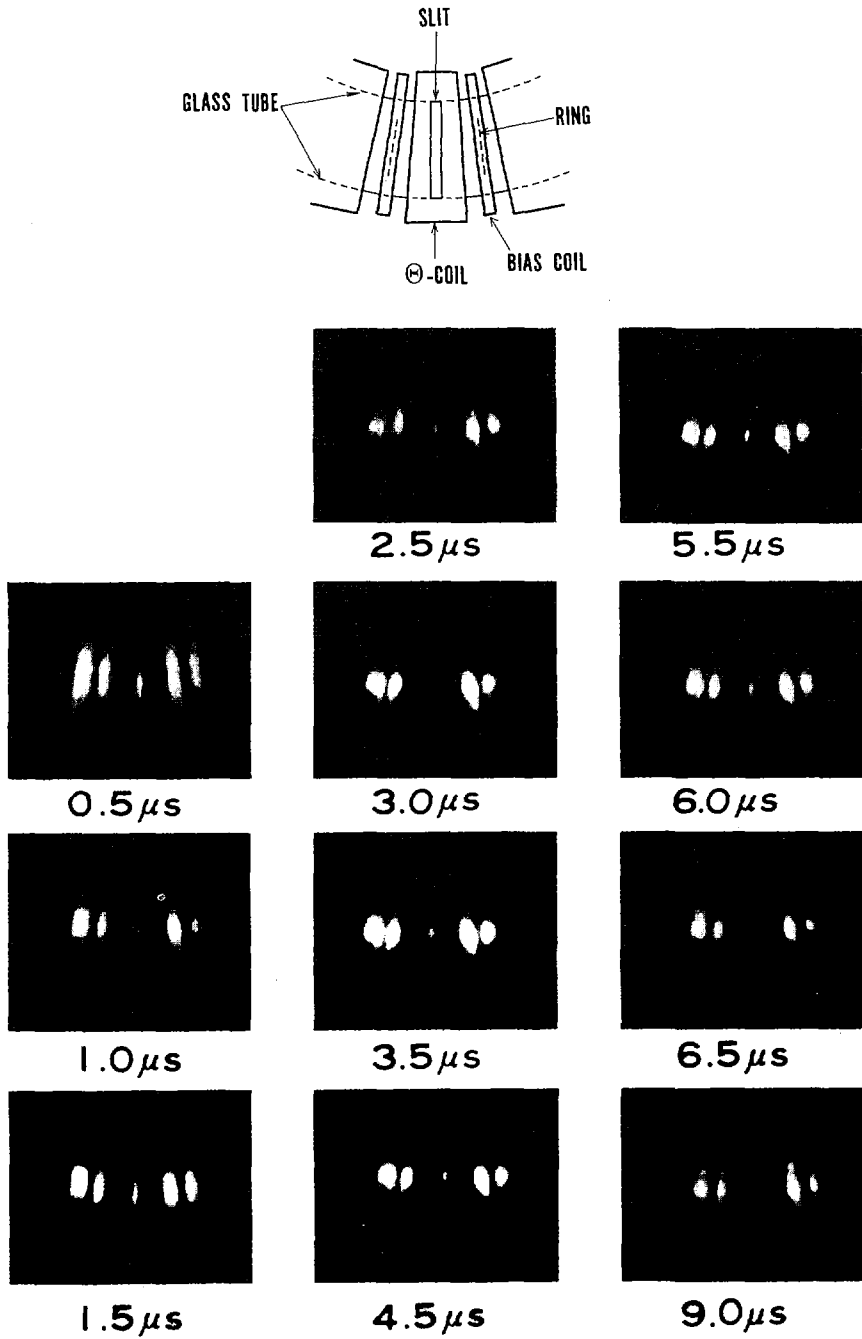


FIG. 5. Framing photographs on a caulked-cusp-field region taken from the up-side of the machine.

of the diamagnetic probes located 5 mm outside of the tube axis. The value of the beta ratio is determined to be 0.1-0.2 at the time of the field maximum; its decay-time constant is 5-6 μs , which agrees well with those values estimated from the Doppler temperature and the density measurements.

4.3. Time variations of plasma parameters

Time variations of the electron line density and the electron temperature are estimated from the signals of the continuum intensity and the relative line-to-continuum intensities [9], respectively. By the time of the field maximum, the line density in the midplane decreases to a minimum and the density in the ring plane reaches a maximum. These signals imply an axial plasma motion, toward the ring plane and back to the midplane (Fig. 4). Such an axial motion should be expected from the corrugated-field configuration whose mirror-ratio is 1.6 : 1 on the axis since it is also observed when no bias field is applied. The decay-time constant of the electron temperature is about 10 μs , and the line density decays with a time constant of about 20 μs . The intensity of a spectral line of the main impurity O II (4661.6 Å) varies roughly in phase with that of the plasma ion He II (4686 Å), but in addition of 0.5% oxygen has a dominant influence on the plasma parameters.

4.4. Induced ring current

The induced ring current is determined by the use of a small Rogowski coil surrounding the ring conductor. The decay-time constant of the induced ring current is about one half of that of the main field, independent of plasma production. This seems to be caused by the proximity effect on the current distribution in the ring conductor.

Then, the location of the stagnation point approaches almost the inside of the ring, after about 20 μs , owing to the differences in decay speed between the coil current and the ring current. Accordingly, the caulked-cusp field is no longer formed after the time of about 20 μs , and then the outside boundary of the plasma becomes diffuse.

5. CONCLUSION

It is experimentally established that the periodic caulked-cusp field with 24 current-induced rings is effective in the suppression of toroidal drift of the theta-pinch plasma with a beta ratio of about 0.1, as well as in the stabilization of the $m = 1$ -instability. As a contrary evidence, it is recognized that there is no equilibrium in the case of 12 rings in which case there is no region of field minimum in the midplane between neighbouring rings. Braginskii and Kadomtsev suggested theoretically that this field configuration should not only stabilize the $\beta = 1$ -plasma but also make the equilibrium state itself possible [10].

The results obtained imply that minimum-B field property is necessary for the containment of high-beta collision-dominated plasma.

Although the confinement times have been limited by some inherent technical factors of this configuration, the values obtained are all prolonged

about twice, as long as those obtained previously in the curved but open-ended machine. Thus, we can say that plasma confinement is improved in the toroidal configuration, compared with that in the open-ended configuration.

If the conductivity of the ring is increased by its cooling down and a super-fast theta-pinch bank is used with some positive bias field, the produced plasma might be stable for a longer time.

ACKNOWLEDGEMENTS

The authors would like to thank Professors K. Husimi, K. Takayama and H. Yoshimura for their encouragement and Drs K. Miyamoto and Y. Hamada for valuable discussions. They are also indebted to Mr. S. Hirabayashi for technical assistance and to Messrs K. Adati, K. Hayase and N. Inoue for helpful assistance in measuring the plasma parameters.

The authors would also like to thank Drs A. W. DeSilva and J. Fujita for a critical reading of the manuscript.

REFERENCES

- [1] BODIN, H. A. B., BUTT, E. P., EVANS, D. E., JUNKER, J., NEWTON, A. A., ROBINSON, D. C., Bull. Amer. Phys. Soc., Ser. II 15 11 (1970) 1423.
- [2] WILHELM, R., ZWICKER, H., Z. Physik 240 4 (1970) 295.
- [3] QUINN, W. E., RIBE, F. L., SIEMON, R. E., in Controlled Fusion and Plasma Physics (Proc. 4th. Europ. Conf., 1970) 40.
- [4] DE VRIES, R. F., VAN HEIJNINGEN, R. J. J., BOBELDIJK, C., GOEDBLOED, J. P., VAN DER LAAN, P. C. T., SCHUURMAN, W., in Controlled Fusion and Plasma Physics (Proc. 3rd Europ. Conf., 1969) 88.
- [5] UCHIDA, T., AKIYAMA, R., Phys. Rev. Letts 24 21 (1970) 1157.
- [6] MOHRI, A., INOUE, M., to be published in Physics Letters A.
- [7] ITOH, S., FUJISAWA, N., YAMAMOTO, K., Physics Fluids 12 1 (1969) 220.
- [8] MIYAMOTO, K. et al., Jap. J. appl. Phys. 5 10 (1966) 970.
- [9] GRIEM, H. R., Plasma Spectroscopy, McGraw-Hill, New York, (1964) 279.
- [10] BRAGINSKII, S. L., KADOMTSEV, B. B., "Stabilization of a Plasma by the Use of Guard Conductors", in Plasma Physics and the Problem of Controlled Thermonuclear Reactions 3, (LEONTOVICH, M. A., Ed.) Pergamon Press, London (1959) 356.

DISCUSSION

F. L. RIBE: How do you account for the decrease of beta with time?

T. UCHIDA: The beta-ratio is deduced from the signals of a diamagnetic probe located 5 mm off the tube axis. The rapid decrease from the value of one could be caused by destruction of the trapped reverse field.

TOROIDAL HIGH- β EXPERIMENTS IN COMPACT AXISYMMETRIC CONFIGURATIONS

H. J. BELITZ, L. JANICKE, P. NOLL, U. PLANTIKOW, F. SAND,
 J. SCHLÜTER, F. WAELEBROECK, G. WAIDMANN
 Institut für Plasmaphysik der Kernforschungsanlage Jülich,
 Assoziation EURATOM-KFA,
 Federal Republic of Germany

Abstract

TOROIDAL HIGH- β EXPERIMENTS IN COMPACT AXISYMMETRIC CONFIGURATIONS.

The confinement of plasmas heated by fast-rising ($B/\dot{B} \approx 1 \mu\text{s}$) and confined by slowly decaying ($|B/\dot{B}| > 1 \text{ ms}$) magnetic fields is studied in axisymmetric toroidal configurations. Small aspect ratios R/a (R = major radius, a = characteristic minor dimension) are chosen to reach relatively high current densities and to confine plasmas of higher β below the Kruskal-Shafranov (K. S.) limit.

In a first experiment (Helical Hard-core Thetapinch), plasmas with temperatures $T \approx 20 \text{ eV}$, densities $n > 10^{16} \text{ cm}^{-3}$ and strongly elliptical (typically $b/a = 3$) cross-sections are produced at the end of the fast compression. By adjusting the voltages and currents of the hard-core and the theta coil, and the time-delay between switching the banks, R can be varied and the net plasma momentum in r direction can be made ≈ 0 at the end of the dynamic phase. Slower variations of R , resulting from the diffusion of the toroidal field into the plasma (β decreases to 15% in a few μs) and from the contraction of the plasma cross-section in the z -direction occur later. They can be controlled by programming the hard-core current. Theoretical results on the equilibrium plasma configuration agree with the result of magnetic-probe and optical measurements which further indicate some triangular deformation of the plasma cross-section. Outside the plasma, a vacuum magnetic field configuration is observed. The angle of rotational transform ι was varied by changing R and the ellipticity; the plasma appears hydromagnetically stable when $q = 2 \pi/\iota > 2.5$. The observed confinement time ($\approx 30 \mu\text{s}$) agrees then with the decay time of the toroidal plasma current and can be explained by the relatively low plasma temperature. A second experiment is being built to study the high- β stability limit in a torus with circular cross-section and larger dimensions ($R = 25 \text{ cm}$, $r_w = 10 \text{ cm}$). The toroidal magnetic field ($\approx 10 \text{ kG}$) and the discharge current rise simultaneously in $1.6 \mu\text{s}$. It will be attempted to reach temperatures $\approx 200 \text{ eV}$ at densities $n_e = 3 \times 10^{14}$ to 10^{15} cm^{-3} . The r. f. pre-ionization and the preheat stage of this experiment were studied using a similar coil system and a small capacitor bank ($T = 11 - 30 \mu\text{s}$). At the required small gas pressures of typically 1 mTorr , optimum breakdown occurs at voltages of $\approx 1.5 \text{ kV}$ per turn; at higher voltages, runaway electrons are indicated. The preheat discharge then produces plasmas with $T_e = 2$ to 4 eV , n_e (spatially resolved) = 10^{13} to $\approx 6 \times 10^{13} \text{ cm}^{-3}$ and a toroidal current of several kA.

1. INTRODUCTION

In the last few years, considerable progress has been achieved in experiments aiming at plasma confinement. Results obtained in axisymmetric toroidal devices of the Tokamak family [1] have received particular attention since containment times significantly longer than the Bohm time were achieved at densities, temperatures and magnetic field strengths which do not differ too much from the thermonuclear requirements. In the present Tokamak experiments, the β -values are still about 50 times smaller than the "reactor- β ". Stable plasma confinement in these geometries at $\beta \gtrsim 0.1$ has still to be demonstrated. In linear systems, the thetapinch technique produces high-temperature plasma with relatively high β -values. It seems, therefore, appropriate to adapt this technique to the production of plasmas with moderately high β in toroidal configurations and study their stability.

We report here on two experiments designed to reach this goal. The geometries investigated are axisymmetric. In contrast to most screw pinch experiments carried out as yet, the angle of rotational transform is $< 2\pi$. This is a serious limit to the β -value which can be contained and the current density unless the aspect ratio of the plasma is small. In the first experiment (TESI), a particularly low equivalent aspect ratio is achieved by producing plasmas where the magnetic surfaces have elliptic cross-sections. In the second experiment, the cross-section of the torus is circular; the use of compact geometry and very fast magnetic compression to shockheat the plasma, (with almost no adiabatic compression phase) make us hope that plasmas with relatively high β -values - lower, however, than in the TESI experiment - can be confined.

2. THE TESI EXPERIMENT

In axisymmetric toroidal configurations with circular magnetic surfaces, the ballooning-mode instability is cancelled out [2, 3] by the deepening of the well resulting from the ballooning itself. The corresponding stability criterion is independent of the plasma pressure. The confinable β is essentially limited by equilibrium considerations. The K.S. condition imposes, however, a severe limitation on the current density j_φ , and the achievement of thermonuclear temperatures by means of Joule heating alone appears to be difficult.

For a purely elliptical plasma boundary, the maximum β -value compatible with the equilibrium condition was calculated to be [4]

$$\beta \leq \frac{\iota^2}{4\pi^2} \frac{d^2 + 3b^2}{4aR} - \frac{b^2}{4R^2} \quad (1)$$

where r , φ , z are cylindrical co-ordinates; ι is the angle of rotational transform, R the major torus radius, and a and b are elliptic semi-axes parallel to r and z , respectively. Equation (1) assumes that p and $(B_\varphi^2 - B_{\varphi \text{ surface}}^2)$ are proportional to the poloidal flux function ψ , (i. e. a flat current distribution if effects of toroidicity are ignored). If the stability criterion were simply $\iota < 2\pi$, large β -values would appear to be possible according to Eq. (1) for $b > a$. It was, however, shown that for these cross-sections the stability criteria for localized flute modes and ballooning modes becomes pressure-dependent. The resulting maximum β is not larger than that for circular cross-sections. Moreover, the maximum permissible current density for a given aspect ratio R/a decreases with b/a .

For $\beta = 1$ -plasmas with sharp boundaries, equilibrium can be obtained with $\iota < 2\pi$ for moderate values of b/a (Fig. 1). This has been calculated numerically for the $\beta = 1$ -equilibrium in the TESI geometry [5].

In the case of elliptical cross-sections with small triangular corrections, the average magnetic well can be deeper by an order of magnitude than for strictly elliptic cross-sections [2, 6]. Therefore, the limiting β - and j_φ -values compatible with the criteria for equilibrium and for stability against flute and ballooning modes can even be larger than the corresponding limits for circular cross-sections (see, e. g. Fig. (5) in [7]). In the case $b > a$, the favourable orientation of the triangular deformation is just that

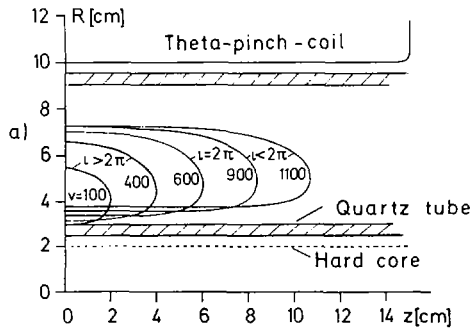


FIG. 1. Equilibrium configurations of $\beta = 1$ -plasmas in the TESI-coil system. Parameter is the plasma volume v .

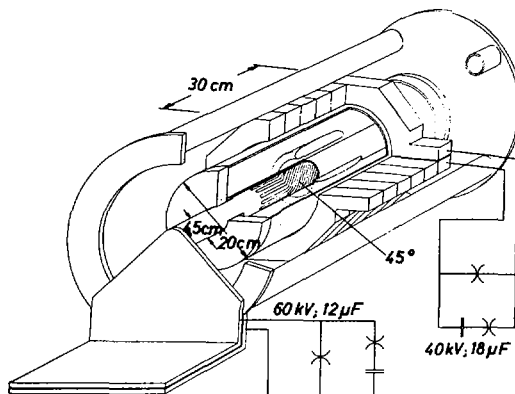


FIG. 2. The helical hard-core theta-pinch experiment TESI.

indicated in Fig. 1. The effect of a non-circular magnetic surface on kink instabilities has not yet been fully investigated. These instabilities become more dangerous with increasing ellipticity [8].

To build a toroidal device producing plasma cross-sections of variable ellipticity, the cylindrically symmetric geometry of a hard-core thetapinch was used (Fig. 2). The thetapinch coil (20 cm diameter, 30-60 cm length) is connected to a 40kV/15kJ-capacitor bank. The hard core consists of 16 current conductors in parallel, distributed over the surface of a tube of 4.5 cm diameter. Within the theta coil these conductors have a pitch angle of 45°. Four conductors outside the theta coil provide the return connection to a 60kV-15kJ bank. Both currents, clamped by metal-to-metal crowbar switches, decay with an e-folding time of 1.6 ms. The filling gas deuterium, contained in a hollow cylindrical quartz vessel, is ionized and pre-heated by a pre-discharge.

The plasma is confined and heated by fast magnetic compression techniques; therefore, no limiter is used to determine the plasma dimensions. Numerical computations show (Fig. 1) that for a given

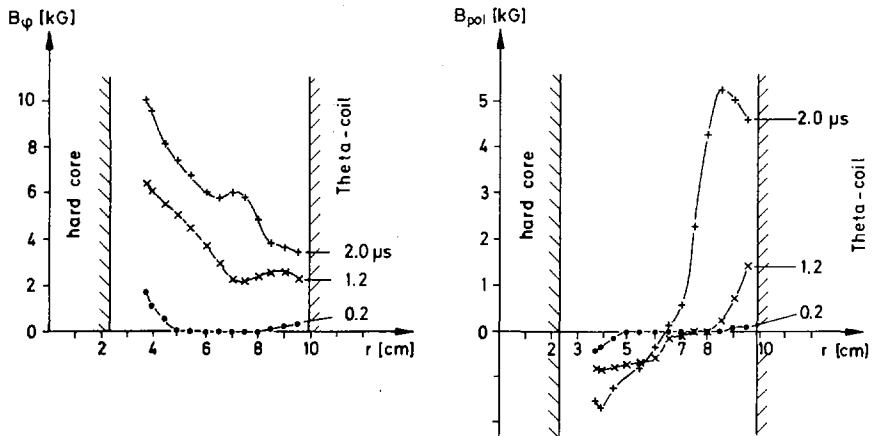


FIG. 3. Toroidal field B_ϕ and poloidal field B_{pol} at the equatorial plane $z = 0$ as functions of r and t (for probe measurements, the hard-core voltage was reduced from 60 kV to 40 kV; therefore, a net force directed to the hard-core results from the poloidal fields).

current ratio in the hard core and the theta coil, a continuous sequence of equilibrium plasma configurations exists; the nearly elliptical cross-section exhibits a small triangular deformation. R and a are nearly constant; b can be increased up to almost the coil length without jeopardizing the existence of the equilibrium. Thereby, the volume varies by more than an order of magnitude, and the pressure decreases by a factor of about two.

The main experimental problem lies in the appropriate control of the transition from the initial pre-ionized plasma state via the fast magnetic compression to the final stable equilibrium configuration. The radial equilibrium can be controlled through the firing time of the crow-bar switches (not necessarily at current maximum). The net outward plasma momentum, at the end of the implosion phase, can be made negligibly small by adjusting the voltages of the two main banks. A fifth parameter, the time delay between firing the two banks, can finally be varied. At the end of the compression, the plasma cross-section should, moreover, have roughly the shape which corresponds to the equilibrium configuration for the experimental case (plasma volume and pressure). A strong axial compression (reduction of b) has indeed a disastrous effect on the plasma confinement: this compression is accompanied by a reduction of R (as is expected if flux is assumed constant); the plasma boundary reaches the hard core. The case of a too large plasma volume is less dangerous. This occurs when the quartz vessel is longer than the coil length. Here, a plasmoid is emitted at each end of the coil and a plasma toroid of nearly maximum ellipticity remains confined within the coil. A variation of the ellipticity is most easily achieved by changing the ratio of the theta coil length to that of the quartz vessel.

Another consequence of the non-circular cross-section is that, during the dynamic phase, the projections of the current and magnetic field lines in the r - z -plane are not necessarily congruent; the resulting volume force

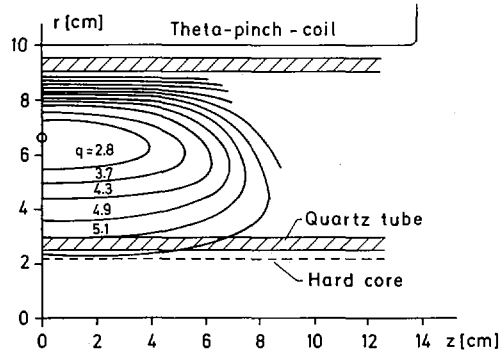


FIG. 4. Magnetic surfaces derived from local magnetic-probe measurements at $t = 2 \mu\text{s}$; $\Delta\psi = 30 \text{ kG} \times \text{cm}^2$; $q = 2.7 \pm 0.5$.

$(j_z B_r - j_r B_z)$ can lead to toroidal plasma rotations [9] which are anti-symmetric with respect to the equatorial plane. In the case of TESI, two factors reduce the importance of this effect: the rapid decay of the poloidal current [10] and the short connection length within the ellipse. The poloidal current decays much faster than the toroidal current. Characteristic times calculated for $R = 7 \text{ cm}$, $a = 1 \text{ cm}$, $b \gg a$, $T \approx 20 \text{ eV}$ are 3 and $30 \mu\text{s}$, respectively. This agrees reasonably well with local magnetic-probe measurements (Fig. 3) which show that, after about $2 \mu\text{s}$, the toroidal current is large whereas the diamagnetic dip in the B_ϕ -field has already disappeared. The B_ϕ -field diffusion results in a slow variation of R , which can be controlled by programming the hard-core current. The magnetic surfaces, deduced from a three-dimensional set of magnetic probe measurements, at $t = 2 \mu\text{s}$ are plotted on Fig. 4. The shape of the magnetic surfaces clearly exhibits a triangular component. From the field distribution, one derives a nearly homogeneous plasma current density of about 1.6 kA/cm^2 . The value of $N = (2\pi jR/B) \approx 1.1$ on the magnetic axis is similar to that obtained in Tokamak experiments. Outside the plasma, a vacuum magnetic field is observed; most of the field lines in this region cross the wall.

The following values have been obtained: $\beta \approx 15\%$, $\beta_{\text{pol}} \approx 1$, $T \approx 20 \text{ eV}$, $n_e = 1.3 \times 10^{16} \text{ cm}^{-3}$ at the magnetic axis, $\epsilon = b/a \approx 3$. Even with strongly reduced filling pressures (down to $p_0 = 5 \text{ mTorr}$), it was not possible to rise the temperature above 30 eV , presumably because of the low β -value of $4 \times 10^9 \text{ G/s}$; the radiation-cooling barrier due to the impurity ions could not be crossed.

The MHD-stability behaviour has been examined as a function of different parameters. The reciprocal rotational transform, $q = \Delta\chi/\Delta\psi$ ($\Delta\chi$ toroidal, $\Delta\psi$ poloidal flux between two adjacent magnetic surfaces) has been obtained from the probe measurements. For the case considered, $q = 2.7 \pm 0.5$ has been measured. The limiting value of N for stability against flutes or ballooning is, for $\epsilon = b/a > 1$, not much larger than unity [11], the corresponding q is about $(1 + \epsilon^2)/(2\epsilon N)$. For the experimental conditions $\epsilon \approx 4$ near the magnetic axis, a limiting q of ≈ 2 is predicted. We have never observed a stable plasma, which would allow reproducible probe measurements, with q -values smaller than 2.2.

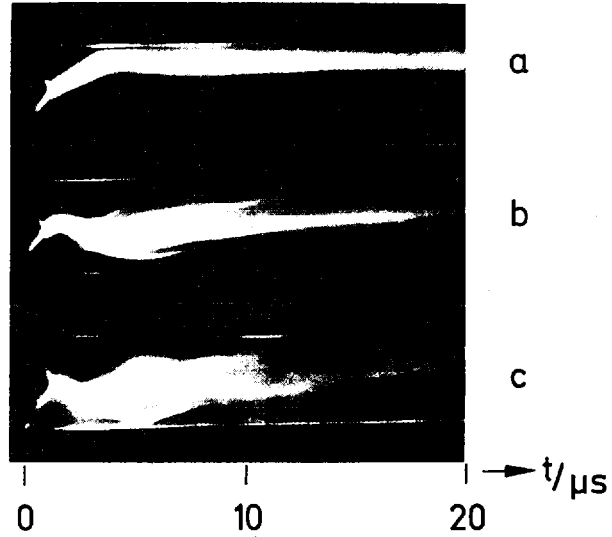


FIG. 5. End-on streak pictures at a) $\Delta\tau = 1.2 \mu\text{s}$, b) $\Delta\tau = 1.0 \mu\text{s}$ and c) $\Delta\tau = 0.4 \mu\text{s}$. $\Delta\tau$ is the delay between switching the hard-core bank and the theta bank.

An important experimental parameter concerning stability was the time $\Delta\tau$ between firing the hard-core bank and the theta bank. If the hard-core bank is switched on $1.2 \mu\text{s}$ before the theta bank, the plasma seems from streak pictures¹ (Fig. 5a) to be stable for more than $20 \mu\text{s}$. If $\Delta\tau$ is decreased (Fig. 5 b, c) the plasma becomes less and less stable. A violation of the condition ($B_\varphi \approx B_{\varphi\text{vacuum}}$) for absence of rotation or of a maximum β compatible with stability may explain this behaviour. The latter possibility is somewhat favoured by the side-on observations under conditions of Fig. 5b, which shows that plasma is lost relatively early in the region of bad curvature; the plasma which remains in the central region of the coil appears thereafter to be confined in a stable way.

Finally, we want to mention that the observed triangular deformation of the elliptical cross-section has the orientation which gives optimal deepening of the magnetic well.

3. FAST AXISYMMETRIC TORUS EXPERIMENT

In this experiment, which is being built, we aim at significantly higher temperatures than in TESI, in the density domain $n = 3$ to $10 \times 10^{14} \text{cm}^{-3}$. The volume is larger and the torus cross-section is circular. The stability of plasmas of small ellipticity can thus be compared with that of the TESI plasmas.

¹ The radial deviation ($R = 6.5 \rightarrow 7.5 \text{cm}$), which does not result in a contact with the wall, is due to an unprecise switching of the crow-bar switches.

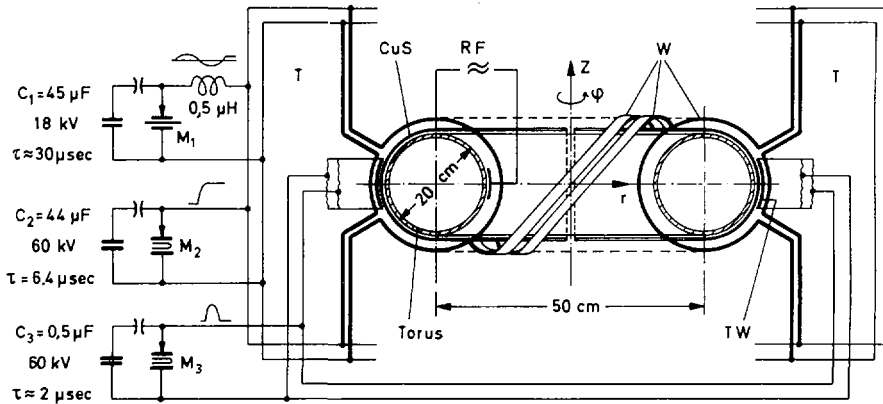


FIG. 6. Schematic diagram of the fast axisymmetric torus experiment.

The maximum permissible β , consistent with ideal MHD-equilibrium and stability, is here of the order of a/Rq^2 (a = plasma radius, $q = 2\pi/l > 1$). For the containment of plasma with high β it is therefore necessary to choose a compact torus and to avoid a strong compression ratio. Different calculations, assuming diffuse or sharp boundary plasmas inside a flux-conserving conducting torus of dimensions $R = 25$ cm, $r_w = 10$ cm, have been made; they indicate that for $q \approx 1$ and a volume compression ratio of 1 : 4, the maximum β which can be confined is 0.12 to 0.16; the corresponding outward displacement of the plasma centre is 3 to 4 cm and the ellipticity ϵ is 1.2 to 1.4.

Low initial gas pressures and strong electric fields are chosen to enhance the anomalous field diffusion effects [12] during the plasma implosion. To reduce the compression ratio, the rise time of the magnetic field is short, not much longer than the implosion time. Provision is made for the addition of an initial bias magnetic field to provide a further control of the β -value and plasma volume.

The apparatus is shown in Fig. 6. After an RF-pre-ionization, the gas is ionized by discharging the bank C_1 . The firing time of the clamping switch M_1 controls the magnetization of the plasma. The main bank C_2 is connected to 36 helically wound parallel windings via a 1 : 2 step-up transformer T . The resulting current ($I_{\max} = 1.25$ MA) induces the toroidal magnetic flux and the toroidal plasma current; it can be clamped by four metal-to-metal switches M_2 . Two half copper shells CuS and an auxiliary toroidal winding $T.W.$ surround the torus. The B_z -flux penetrates into the shell through two meridional slits and can be frozen to a specified value by short-circuiting $T.W.$ with the metal-to-metal switch M_3 . The shape and pitch of the coil can be modified. For the first experiments, the angle between the entering and return leads is 100° ; the windings have such a shape that, in vacuo, a negligible B_z -field is produced within the coil; the restoring forces leading to the equilibrium result then only from image currents in the shell or additional currents in $T.W.$ Because of the small aspect ratio, the plasma is expected to have a significant outward momentum

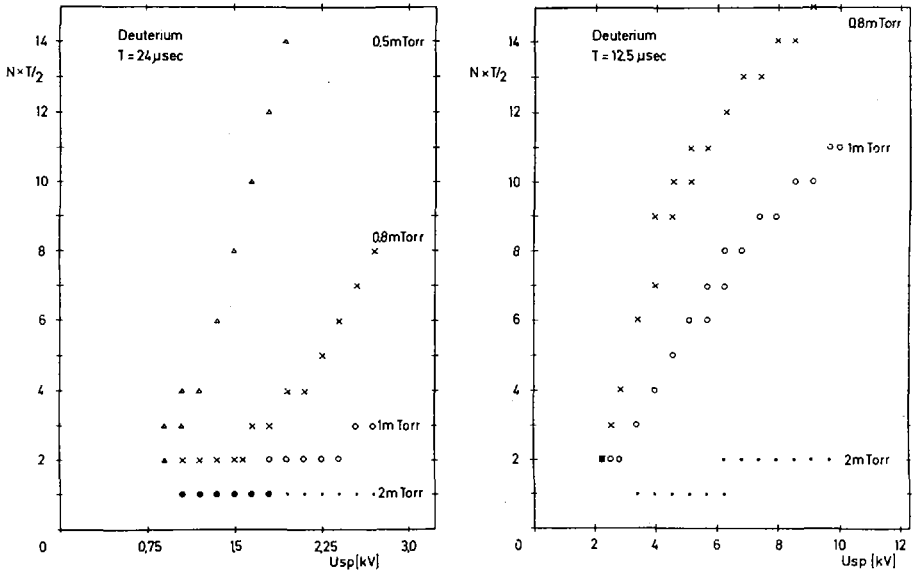


FIG. 7. Breakdown delay times versus coil voltage U_{sp} for two typical discharge periods T .

at the end of the compression phase. Resulting oscillations could bring it to the wall. Since only a partial copper shell is used, a short current pulse (with voltage doubling) launched in T.W. at the start of the main discharge can produce a compensating inward-directed force. The breakdown and ionization of the gas in the low-density domain provided for ($p \approx 1$ mTorr) have been studied in a similar set-up. The main differences are: major and minor radii 20 and 10 cm, respectively; no voltage doubling; the T.W. coil is situated close to, but outside of the main winding.

The breakdown of the pre-ionized deuterium gas depends strongly on the gas density and on the toroidal electric field; in this experiment, the poloidal field does not break down the gas at the investigated pressures of ≈ 1 mTorr. The gas desorption from the walls during the rf-pre-ionization and the pre-heat phase requires some care; an oil-free vacuum system and a prolonged discharge cleaning before each experimental run reduced the gas release to about 10% of the filling pressure. Gas breakdown was detected by the almost simultaneous appearance of the D_β -line, of the toroidal plasma current and of diamagnetic signals. It occurs during a short interval around a time when the oscillating magnetic field crosses zero. The higher the initial electric field, the later the time when breakdown is observed. For different deuterium filling pressures and two different discharge periods T , Fig. 7 shows the breakdown times, counted in half-periods of the oscillating magnetic field, as a function of the initial coil voltage U_{sp} . Above a certain pressure-dependent voltage, the breakdown no longer occurs at the end of the first half-cycle; it is delayed until the electric field has decreased by circuit damping down to the upper electric breakdown field E_{φ_B} . A reduction of E_{φ_B} with the neutral gas

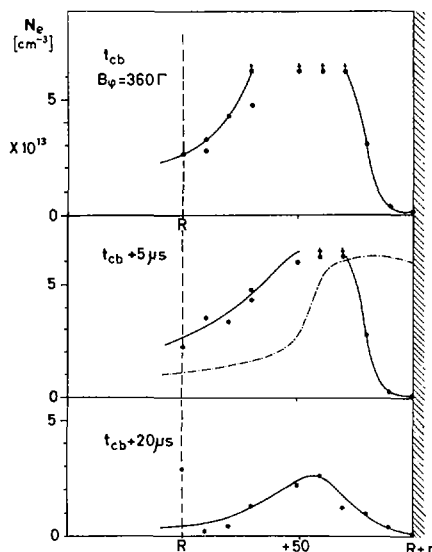


FIG. 8. Radial electron density profile at the time of crowbar and at two later times. A density profile without B_{\perp} -field is shown $5 \mu\text{s}$ after crowbar (dashed curve). $\uparrow n \cong 6.25 \times 10^{13} \text{ cm}^{-3}$.

pressure p gives for our geometry a value of $E_{\varphi B}/p = (6 \pm 1)\text{V}/\text{cm} \cdot \text{mTorr}$, which is nearly independent of the neutral gas pressure. For electric fields exceeding $E_{\varphi B}$ and pressures $p \geq 1 \text{ mTorr}$, X-ray radiation spikes are observed shortly before gas breakdown occurs. This X-ray emission, which disappears after plasma formation, is attributed to fast runaway-electrons striking the discharge wall.

The radial plasma density distribution is measured with a movable 4mm-microwave probe [13]. At the moment of a magnetic field maximum, a compressed plasma is observed and the coil current is clamped. In the decaying magnetic field, ($\tau_{1/e} = 120 \mu\text{s}$) radial motion of the plasma to the outer wall was detected. To avoid this effect, the inward-directed momentum is increased by means of an auxiliary field B_{\perp} , produced by the coil T.W. The radial motion of the plasma is stopped when $\bar{B}_{\perp}/B_{\varphi} \approx 7\%$. Toroidal plasma currents of several kA with a decay time of about $20 \mu\text{s}$ were measured by a Rogowski coil (the q -value, just after crowbar at the wall is about 4). The electron temperature, measured on the axis of the vessel by the H_{β} -line to continuum intensity ratio is 4.5 eV just after crowbar and 2.2 eV $50 \mu\text{s}$ later. Figure 8 shows the electron density profile at the moment of crowbar t_{cb} and at two later times. The electron density exceeds the cut-off density for 4mm-waves ($N_0 = 6.25 \times 10^{13} \text{ cm}^{-3}$) in the centre of the plasma column at t_{cb} . A comparison of a density profile $5 \mu\text{s}$ after crowbar with and without auxiliary magnetic field B_{\perp} is shown. The plasma density maximum with applied B_{\perp} -field is still shifted off axis; it remains, however, clearly separated from the wall and appears to be in an equilibrium position during the whole time of observation. This fact is confirmed by image converter observations.

4. CONCLUSIONS

Using the fast magnetic compression technique it was possible to produce plasmas with strong elliptic deformation ($\epsilon \approx 3$) of the magnetic surfaces. No instabilities were detected in plasmas with $\beta \lesssim 15\%$, $q \gtrsim 2$, $2\pi \cdot j_\phi R / B_\phi \lesssim 1$. These values are close to the limiting values for MHD-stability which are expected when the observed effects are taken into account, i. e., that the toroidal magnetic field has practically a vacuum distribution ($j_{r,z} = 0$) and favourable triangular deformation of the magnetic surfaces occurs. β -values larger than 15% should become possible at higher temperatures when the poloidal currents decrease more slowly. We attempt to reach such temperatures by using small initial densities for which efficient ionization was shown to be possible.

ACKNOWLEDGEMENTS

The authors would like to thank Dr. H. Kever for many fruitful discussions and Dr. P. Dokopoulos and F. Friedrich for the development of components essential for these experiments. We are also indebted to W. Kohlhaas, F. Schöngen, C. Stickelmann who designed the experiments, and to L. Grobusch, H. Korr, W. Pysik, and G. Telemann for technical assistance.

REFERENCES

- [1] See e. g. ARTSIMOVICH, L. A., GLUKHOV, A. V., GORBUNOV, E. P., PETROV, M. P., in *Controlled Fusion and Plasma Physics* (Proc. 4th Europ. Conf. Rome, 1970) 18; GROVE, D. J., DIMOCK, D. L., HINNOV, E., HOSEA, J. C., JOHNSON, L. C., MESERVEY, E. B., TOLNAS, E. L., *ibid.* 21.
- [2] SOLOVEV, L. S., SHAFRANOV, V. D., YURCHENKO, E. I., *Nucl. Fusion Suppl.* (1969) 25.
- [3] MERCIER, C., *Nucl. Fusion* 4 (1964) 213.
- [4] LAVAL, G., MASCHKE, E. K., PELLAT, R., *ICTP Rep. IC/70/110*.
- [5] JANICKE, L., *Rep. Jül-700-PP* (1970).
- [6] DAGAZIAN, R. Y., GOEDBLOED, J. P., MASCHKE, E. K., TANAKA, M., *ICTP Rep. IC/70/120* (1970).
- [7] LUC, H., *Rep. EUR-CEA-FC-569* (1970).
- [8] LAVAL, G., PELLAT, R., *Rep. EUR-CEA-FC-575* (1970).
- [9] DÜCHS, D., DIXON, R. H., ELTON, R. C., KOLB, A. C., *Bull. Am. Phys. Soc., Series II*, 13 (1968) 1551.
- [10] NOLL, P., SCHLÜTER, J., in *Controlled Fusion and Plasma Physics* (Proc. 3rd Europ. Conf., Utrecht, 1969) 85.
- [11] ZUEVA, N. M., SOLOVEV, L. S., *Atomn. Énerg.* 26 1 (1969) 35.
- [12] BODIN, H. A. B., McCARTAN, J., NEWTON, A. A., WOLF, G. H., in *Plasma Physics and Controlled Nuclear Fusion Research* (Proc. Conf. Novosibirsk, 1968) 2, IAEA, Vienna (1969) 533.
- [13] HARTWIG, H., *Rep. Jül-473-PP* (1967).

HIGH-BETA ($\ell = 1$)-STELLARATOR EXPERIMENTS

E. FÜNFER, M. KAUFMANN,
W: LOTZ, J. NEUHAUSER
Max-Planck-Institut für Plasmaphysik,
Euratom Association,
Garching, Munich,
Federal Republic of Germany

Abstract

HIGH-BETA ($\ell = 1$)-STELLARATOR EXPERIMENTS.

Recently, toroidal high-beta equilibria with rotational transform, but essentially without net toroidal current (high-beta stellarator) were proposed and subsequently refined by several authors. The experimental investigations reported here were concentrated on the ($\ell = 1$)-stellarator because of its theoretically favourable stability properties. The experiments were done in straight as well as in toroidal geometry. In all cases the plasma was heated by shock waves (theta-pinch). In straight helical geometry a 5.4 m long coil in essentially four different versions was used. In all cases the typical plasma helix was formed after the fast compression. Oscillations correlated with the helix formation could be explained by MHD-theory. At high temperatures ($T_e + T_i \approx 0.5 \dots 2.1$ keV) ($m = 1, k \approx 0$)-instabilities are observed. A reduction in β led to lower growth rates in agreement with the theory. From internal magnetic probe measurements magnetic field profiles and beta-values are derived. The field profiles indicated that longitudinal or helical currents also flow in the thin plasma ("halo") outside the dense plasma column. Such currents may influence the plasma stability. In a small toroidal pre-experiment with low aspect ratio $A=R/r_p$ (bank energy 10 kJ, major radius $R = 26$ cm, plasma radius $r_p \approx 1$ cm), effects which might not be seen in straight geometry were sought. The helical field was generated by a shaped coil. As in the linear experiment, a helix was formed and oscillations of the helix radius were observed. A net toroidal current, induced by the ($\ell = 1$)-field, could be explained by a simple model. The shape of the magnetic field was varied, and additional toroidal plasma currents were induced by external conductors. The toroidal drift motion of the plasma helix was a function of the various parameters. With a toroidal current well above the Kruskal limit, a highly unstable, screw-pinch-like equilibrium was found. These experiments will be continued with our device ISAR-1 (bank energy 2.6 MJ) with a torus of 135 cm major radius and relatively large aspect ratio.

1. INTRODUCTION

In the last few years several theoretical results have been published on toroidal high-beta equilibria with rotational transform, but essentially without a net toroidal current (high-beta stellarator) /1-6/. Equilibria and their stability were studied by expansion in a small parameter e.g. $\epsilon = kr_p \ll 1$ ($k = 2\pi/\lambda$, $\lambda =$ period length of the helical field, r_p is the plasma radius). For very large aspect ratio $A \gg 1$ (the toroidal curvature is of third order in the smallness parameter) equilibria with the simple ($\ell = 1$)-stellarator were proposed which should be nearly stable to the most dangerous ($m = 1, k = 0$)-mode /1,3/. F. Ribe /4/ has shown that the shift of the equilibrium position caused by the toroidal

curvature might be compensated by a small admixture of ($l = 0$)- and/or ($l = 2$)-fields.

In the ($l = 1$)-stellarator model of Nührenberg /2/ the toroidal curvature is of second order in the smallness parameter, thus giving a more realistic aspect ratio. But he finds a solution of his system of equations only when the pitch of the magnetic axis varies along the period.

These calculations were performed using MHD theory with infinite conductivity. In Ref. /1,3/ the sharp boundary model is used, while in Ref. /2/ a diffuse profile is assumed. Freidberg and Marder /6/ have shown that the results of Ref. /1,3/ are also essentially valid for diffuse profiles. More recent results and a survey on present theories are given in /7,8/.

In order to test the shock heating mechanism in the presence of the helical fields and to compare with the above theories, we performed experiments in linear as well as in toroidal geometry. These experiments are preparatory to a larger toroidal experiment which is now being built.

2. LINEAR ($l = 1$)-STELLARATOR EXPERIMENTS

2.1 Description of experiments

The linear experiments were done on the 2.6 MJ bank, ISAR I with a 5.4 m long coil in essentially four versions, the main differences being in the method of generating the ($l = 1$)-field and in the position and diameter of the discharge tube (see Table I).

TABLE I. EXPERIMENTAL PARAMETERS^a

experiment No.	I	II	III	IV
generation of ($l=1$) field	wires	shaped coil		
local coil diameter	19.6cm	23cm		
periods	8	9		
$B_{z,max}$	45 kG	40kG		
amplitude of magn. axis	0...2cm	1 cm		
tube diameter	8,5 cm			17cm
tube position	concentric	eccentric	concentric	

Several problems concerning plasma formation and fast growing instabilities could be solved by these experiments. The results of Experiment I have been given elsewhere /9,10/. Some further details of the linear work were presented at the European Conference on Plasma Physics /11/.

2.2 Plasma formation and helical equilibrium

If the ($\ell = 1$)-field is generated by a pair of helical conductors (Exp. I), it is possible to vary the onset time of the helical field relative to that of the B_z -field. On the other hand, if the inner surface of the coil is shaped as a magnetic surface of an ($\ell = 1$)-stellarator, there is no separatrix in the vacuum magnetic field (Exp. II ... IV).

Experimentally, we found that in general the dense plasma column formed a helix near the magnetic axis of the vacuum field. Exceptions were found when we worked with high impurity concentration or switched on the ($\ell = 1$)-field before the main field. With eccentric tube position (III) the helix formed outside the magnetic axis as demonstrated later on. In all cases the radius of the helix oscillated about a mean value, which was about equal to the radius of the helix of the magnetic axis in the vacuum field.

Starting from the theoretical treatment of Weitzner /5/ it is in fact found /12/ that these helical oscillations should be stable. Their frequency to leading order would be

$$\omega_H = \sqrt{(2 - \beta) \cdot kV_A} \quad (1)$$

V_A is an Alfvén speed calculated with the plasma density on the axis and the magnetic field outside. The calculated frequencies agreed with the measured frequencies within 20 %.

In Exp. III we worked with the tube in an eccentric position (37mm from the axis), the other parameter being the same as in Exp. II. It was found that the plasma helix was formed in this eccentric position, too, that is, concentric to the quartz tube. This can be understood by observing the topology of the vacuum

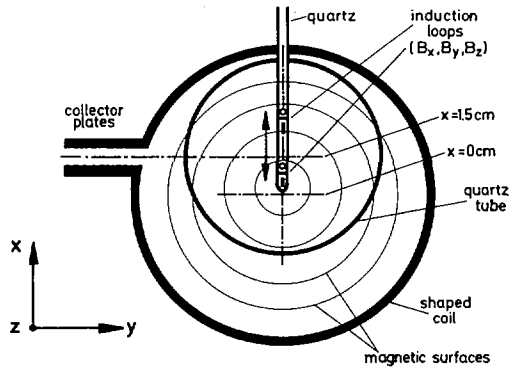


FIG. 1. Internal magnetic probe measurements (schematic).

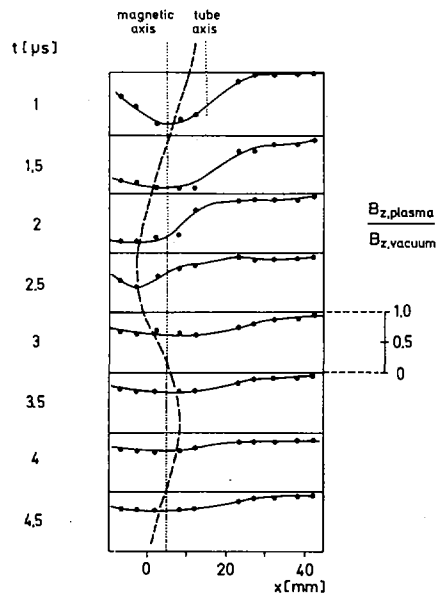


FIG. 2. Normalized profiles of the longitudinal field. The dashed line shows the plasma oscillation around the magnetic axis of the vacuum field.

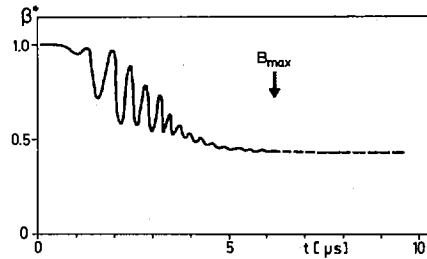


FIG. 3. β^* (see Eq. (2)) as function of time ($T_i + T_e \approx 500$ eV).

magnetic field, keeping in mind that the total rotational transform ℓ along the coil is very small ($\ell = \ell/2\pi \approx 0.05$). The plasma helix did not move towards the magnetic axis, as one might expect, but there was even a small drift motion in the opposite direction.

If the end plates were short circuited in the linear experiments net longitudinal currents were observed which could be explained by simple models (see Sect. 3.2).

2.3 Internal magnetic probe measurements

With Exp. IV and 0.5 MJ bank energy ($T_e + T_i \approx 500$ eV) we made internal magnetic probe measurements near the midplane of the coil. Figure 1 shows the geometrical arrangement. From these measurements we could derive magnetic field profiles and beta-values for early times, where plasma cooling by the probe itself could be neglected. In Fig. 2 normalized profiles of the longitudinal B_z -field are shown for various times. The helical oscillations of the plasma are readily seen and agree well with the oscillations derived from stereoscopic smear pictures taken 150 cm away from that point. In Fig. 3 the value

$$\beta^* = \frac{B_{z,vac}^2 - B_{z,min}^2}{B_{z,vac}^2} \quad (2)$$

derived from the field profiles is given. $B_{z,vac}$ is the longitudinal magnetic field measured without plasma in the discharge tube, while $B_{z,min}$ is the longitudinal field on the plasma axis. For $t \gg 3 \mu s$ the compression oscillations are damped out and to lowest order

$$\beta^* \approx \beta_{max} \approx 2 \cdot \mu_0 \cdot p_{max} / B_{z,vac}^2$$

(p = plasma pressure perpendicular to the field lines). There is no chance to derive the rotational transform inside the plasma from the field components measured only along one line. There is, however, an interesting feature in the B_y -profile. In Fig. 4 the B_z -profile and the profile of

$$\Delta B_y = B_{y,plasma} - B_{y,vac}$$

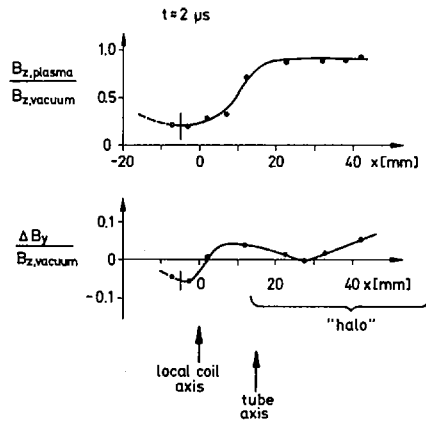


FIG. 4. Comparison of field profiles normalized to the longitudinal field measured without plasma. The range of the visible "halo" (thin plasma) is also given.

6/6 bank, i.d. tube = 17 cm

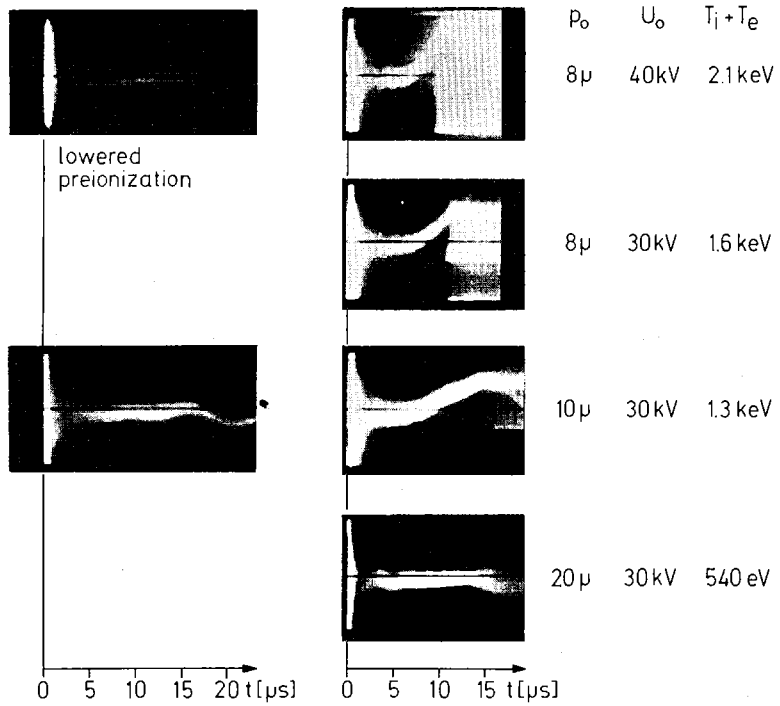


FIG. 5. ($m = 1, k \approx 0$)-instabilities for various plasma parameters.

are given for the second expansion of the plasma column ($t \approx 2\mu\text{s}$), again normalized to the longitudinal field without plasma. One finds that during the first few microseconds ΔB_y has a complicated structure in the outer region. This indicates that longitudinal or helical currents are also flowing in the relatively thin plasma (density some 10^{14} cm^{-3} /13/) well outside the dense plasma. Later on the currents are more and more concentrated near the dense plasma column. But again one cannot derive the exact current distribution. It should be noted that such currents may have an influence on plasma stability, as demonstrated experimentally and theoretically for screw-pinch-like equilibria /14,15/.

2.4 Plasma stability

In the experiments I, II, III the plasma was stable, similarly to that of the theta-pinch. The e-folding time of an ($m=1$)-instability, if present, was comparable with or greater than the transit-time of an Alfvén wave from the ends.

Only in Exp. IV, where a temperature of more than 2 keV was achieved, were ($m=1$)-instabilities observed. Examples are given in Fig. 5 (right-hand side). The plasma helix moved away like a rigid body throughout.

At first we shall compare the experimental growth rate with the analytical results of Weitzner /5/. In the theory of Weitzner /5/ the growth rate $\omega_{m=1}$ is given by

$$\omega_{m=1}^2 = k^2 \cdot v_A^2 \left(\frac{a}{r_p} \right)^2 \cdot \beta^2 \left(\left(\frac{r_p}{r_w} \right)^4 - \left(\frac{a}{r_p} \right)^2 \cdot \beta^3 / 32(2-\beta) \right) \quad (3)$$

(a = helix radius, r_p = plasma radius, r_w = radius of conducting wall).

Experimentally, r_p is small compared with r_w , and therefore the stabilizing wall-term is neglected in the following.

It is convenient to eliminate v_A by introducing ω_H from eq. (1). We then use the ratio

$$K \equiv \left(\frac{\omega_H}{\omega_{m=1}} \right)^2 \approx - \frac{32(2-\beta)^2}{\beta^5 (a/r_p)^4} \quad (4)$$

which can be determined experimentally for various parameters. One finds that K lies between 700 for low temperature ($T_e + T_i \approx 500$ eV) and small growth rate and about 70 for high temperature ($T_e + T_i \approx 2.1$ keV) and high growth rate.

It is difficult to compare these results with the sharp boundary theory, because there are many possibilities of defining the mean β and the plasma radius of a diffuse profile. If one uses a mean beta-value of 0.3 ... 0.5 and the mean plasma radius, then the calculated ratio is one order of magnitude higher than the experimental one. But if the β on the axis is used one obtains fairly good agreement.

The variation of K with temperature (plasma radius approx. constant) may be caused by a small change in β according to eq.(4). Such a small variation in β can readily be explained by the different collisional relaxation and hence different time dependence of β /16/. With small growth rate, end effects may also become important.

But β was also changed in a defined manner, the temperature remaining constant. By lowering the degree of preionization from the usual ≈ 50 % to 15%, β was reduced by about 20%. From the neutron rate and the plasma density it was found that the temperature had changed less than 10%. For a temperature of $T_e + T_i \approx 2$ keV the growth time then increased from 1.5 μ s to 3.4 μ s in good agreement with Weitzner's theory. With lower temperature no instability was observed because of end effects.

With a further small reduction in β the plasma remained stable during the time of observation even for high temperatures (Fig. 5, left-hand side). We should mention that no unstable modes with $m > 1$ were observed.

In the meantime Freidberg /7/ has developed a theory which is based on the new ordering of Weitzner/5/. If we compare the experimental growth rates of the ($m = 1$)-instability with those numerically calculated from Freidberg's theory, we find excellent agreement as far as standard preionization was used. But in this theory the growth rate depends relatively weakly on the plasma beta in contrast to the experimental results stated above.

3. A SMALL TOROIDAL PRE-EXPERIMENT

3.1. Data and general plasma behaviour

In a small toroidal experiment (bank energy 10 kJ, major radius 26 cm, local minor radius 5 cm) we looked for effects which might not be seen in a straight geometry. The ($l = 1$)-field was generated by a shaped coil (8 periods on the whole torus). The amplitude of the geometrical helix was 1 cm in a first and 1.5 cm in a second version, the rotational transform of the vacuum field around the torus being $t = 0.1$ and $t = 0.2$. The temperature was $T_e \approx T_i \approx 10 \dots 50$ eV and the density a few 10^{16}cm^{-3} .

As in the linear experiments, a plasma helix was formed during the fast compression and oscillations of the radius of the helix were seen. The total plasma helix drifted to the outer wall of the non-helical glass vessel. From present theories we could not in fact expect to have an equilibrium with a sufficiently small toroidal shift.

3.2. Toroidal plasma currents

It was found that a toroidal plasma current proportional to the total rotational transform was induced by the helical fields. This current could be explained by the following model. It is assumed that an infinitely conducting toroidal plasma loop near the magnetic axis is established during breakdown ($t \approx 0$). Afterwards a poloidal flux is set up by the helical field which is connected to the toroidal flux by the total rotational transform. From conservation of the poloidal flux one immediately finds that with a shaped coil a plasma current

$$I_{\text{plasma}} \approx I_{\theta} \cdot t \cdot \frac{L_{\text{coil}}}{L_{\text{plasma}}}$$

(I_{θ} is the main current, L is the inductance) must develop, in agreement with the experimental results.

In general, the self-induced toroidal plasma current was compensated by an externally induced current. If the externally induced current was further increased in such a direction that the total rotational transform was increased, then a small reduction of the drift motion was measured.

With an induced toroidal plasma current above the Kruskal limit a highly unstable, screw-pinch-like equilibrium was found. By observation around the torus, it was confirmed that the wave length of the helical ($m = 1$)-instability was equal to the circumference of the torus.

3.3. Modified ($\ell = 1$)-field

Subsequently, the ($\ell = 1$)-field was modified by a small admixture of ($\ell = 0$), ($B_{\min}/B_{\max} = 0.8$), and by varying the pitch angle of the magnetic axis along the period according to Ref./4/ and Ref./2/ respectively. With the right phase in both cases a reduction of the drift motion was achieved. From the drift velocity as a function of time with the pure and modified ($\ell = 1$) - fields, one might conclude that an equilibrium near the conducting wall, but partially outside the nonhelical glass vessel, should exist.

4. CONCLUSIONS

From the experiments described above, we find that starting with the well-known and effective theta-pinch, equilibria of the type wanted can be realized. Most of the problems connected with the special field configuration were solved and explained by existing theories. But there remain questions which can be answered only with a complete torus with appropriate aspect ratio and sufficiently high temperature, especially concerning the optimum modification of the ($\ell = 1$)- field, and stability and diffusion in the toroidal equilibrium.

Therefore, our linear experiment (2.6 MJ bank energy) is being converted into a torus of 135 cm major radius. Starting with the drifting theta-pinch plasma, stellarator fields will be added by currents in helical conductors and by using shaped coils.

ACKNOWLEDGEMENTS

We gratefully acknowledge helpful discussions with F. Herrnegger, W.Grossmann and J.Wesson. We also wish to thank U.Seidel, G.Schramm and M.Münich for their help with the experiments.

REFERENCES

- /1/ A.A.BLANK, H.GRAD, H.WEITZNER; "Plasma Physics and Controlled Nuclear Fusion Research", IAEA, Vienna (1969), Vol.II, p.607
- /2/ J.NÜHRENBURG; Phys.Fluids 13, 2082 (1970)
- /3/ H.GRAD, H.WEITZNER, Phys. Fluids 12, 1725 (1969)
- /4/ F.L.RIBE, Report LA-4098, Los Alamos Scientific Laboratory (1969)
- /5/ H.WEITZNER; Phys. Fluids 14, 658 (1971)
- /6/ J.P.FREIDBERG, B.M.MARDER; Phys.Fluids 14, 174 (1971)
- /7/ J.P.FREIDBERG, T.A.OLIPHANT, H.WEITZNER; paper J-5
(this conference)
- /8/ H.WEITZNER, paper J - 6 (this conference)
- /9/ M.KAUFMANN, E.FÜNFER, J.JUNKER, J.NEUHAUSER; Bull.Am. Phys.Soc. 14, 1037 (1969)
- /10/ M.KAUFMANN, E.FÜNFER, J.JUNKER, J.NEUHAUSER; Report IPP-1/111, Institut für Plasmaphysik, Garching (1970)
- /11/ M.KAUFMANN, E.FÜNFER, W.LOTZ, J.NEUHAUSER; Contributions to the "Fourth European Conference on Controlled Fusion and Plasma Physics", Rome (1970), p. 39
- /12/ J.WESSON, Culham Laboratory, private communication (Aug. 1970)
- /13/ J.FREUND; Max-Planck-Institut für Plasmaphysik, Garching (to be published)
- /14/ W.SCHURMAN, C.BOBELDIJK, R.F. de VRIES, Plasma Phys. 11, 495 (1969)
- /15/ R.WILHELM, H.ZWICKER; Z. Physik 240, 295 (1970)
- /16/ H.A.B.BODIN, D.J.DANCY; Nucl. Fusion 7, 191 (1967)

DISCUSSION

F.L. RIBE: Have any theoretical estimates been made at Garching on the stabilizing effect of the outer low-density plasma which you observe?

J. NEUHAUSER: I believe W. Grossmann of our institute has done calculations assuming an outer pressureless plasma and a net longitudinal current parallel to the magnetic field lines. The effect of these currents is essentially the same as for screw pinches; I think they have a stabilizing effect in general. However, the currents might also be helical, with the same pitch as the helical conductors, somewhat like helical mirror currents. Such currents would not be completely force-free, but we have no theoretical estimates for this case.

H. A. B. BODIN: I was not quite clear whether your explanation of instabilities observed at higher temperatures was essentially a matter of growth rates or something that went further. In some bulged M- and S-type theta-pinch experiments better stability was claimed at higher temperatures — the opposite dependence to what you find. Have you any comments on this?

J. NEUHAUSER: We find that the growth rate of the $m = 1$ -instability increases with temperature faster than one would expect, i. e., faster than the Alfvén speed. We have commented on this result in our paper. We have no explanation for the fact that it goes the other way in M and S configurations.

THETA-PINCH EXPERIMENTS WITH HELICAL EQUILIBRIUM FIELDS IN A 5-METER TOROIDAL SECTOR AND IN A 3-METER LINEAR DEVICE*

S. C. BURNETT, W. R. ELLIS, C. F. HAMMER, C. R. HARDER,
H. W. HARRIS, F. C. JAHODA, W. E. QUINN, A. S. RAWCLIFFE,
F. L. RIBE, G. A. SAWYER, R. E. SIEMON, K. S. THOMAS
Los Alamos Scientific Laboratory,
University of California,
Los Alamos, N. Mex.,
United States of America

Abstract

THETA-PINCH EXPERIMENTS WITH HELICAL EQUILIBRIUM FIELDS IN A 5-METER TOROIDAL SECTOR AND IN A 3-METER LINEAR DEVICE.

Experiments on a θ -pinch sector comprising one-third of the Scyllac torus of major radius $R = 237.5$ cm and plasma radius $a \approx 1$ cm (aspect ratio $R/a \approx 240$) are reported. Equilibrium is obtained by balancing the toroidal force by means of an $\ell = 1$ -helical field which produces a helical shift $R_0 = a\delta_1$ of the plasma column approximately equal to its radius ($\delta_1 \approx 1$) and a small admixture of $\ell = 0$ field ($\delta_0 = 0.1$). Both fields have a wavelength of 33 cm. End effects are not expected to dominate before the lapse of one Alfvén (or ion-thermal) transit time τ from the plasma ends. Hence there is sufficient time to observe the attainment of equilibrium and some of its stability properties. Related experiments on a 3-meter linear θ -pinch with superimposed $\ell = 1$ fields show that only the $m = 1$, $k \approx 0$ magnetohydrodynamic (MHD) mode occurs. No higher- m modes are seen during the time τ , even though the MHD-theory of Grad and Weitzner and Rosenbluth et al. predicts much larger growth rates γ_m for these modes. In the linear experiments, the $m = 1$ -growth rate γ_1 is measured and compared with the theoretical predictions. The magnitude of γ_1 largely determines the difficulty of feedback stabilizing the $m = 1$ -mode. On the linear device, experiments to determine the feedback coupling force $F_{1,0}$ on the $\ell = 1$ plasma column are reported which is produced by separately driven $\ell = 0$ coils, as described by Ribe and Rosenbluth. This force is also used to obtain the toroidal equilibrium of the toroidal sector. The experiments reported here are preliminary to experiments in the complete Scyllac torus of 15-meter circumference.

I. INTRODUCTION

When a straight theta pinch is bent into a torus, the plasma is no longer in equilibrium, and the magnetic pressure gradient of the longitudinal compression field B_0 and the plasma pressure force the plasma toward the outside of the torus. For a plasma of major radius R and minor radius a the force per unit length is

$$F_R = \beta B_0^2 a^2 / 4R \quad (1)$$

where β is the ratio of the plasma pressure to the external magnetic pressure $B_0^2/8\pi$. In the Scyllac experiment to be discussed here the force F_R is overcome by means of helical transverse fields [1] whose scalar potential is of the form

$$\chi_\ell = (B_0/h)[C_\ell I_\ell(hr) + D_\ell K_\ell(hr)] \sin(\ell\theta - hz). \quad (2)$$

* Work performed under the auspices of the US Atomic Energy Commission.

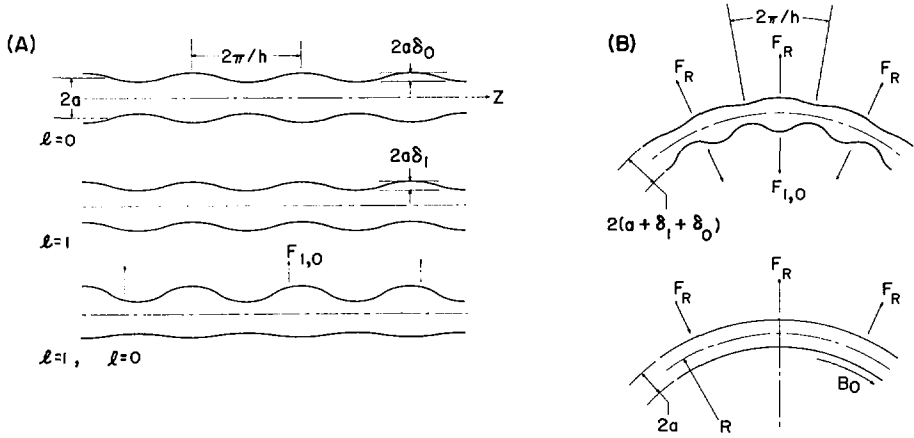


FIG. 1. (A) Illustrating the parameters involved when helical fields are applied to a plasma column to produce a body force $F_{1,0}$. (B) Illustrating the use of the $\ell = 1, 0$ -body force to produce a high- β toroidal equilibrium.

Here C_ℓ and D_ℓ are constants, and I_ℓ and K_ℓ are the modified Bessel functions. The quantity h is defined in Fig. 1. The equilibrium and stability of this system for a straight plasma column have been treated in the magnetohydrodynamic (MHD) approximation [2,3,4,5] and more recently by the use of the Vlasov equations for the ions and fluid equations for the electrons [5]. Recently Ribe and Rosenbluth [6] and Weitzner [7] showed that a combination of fields characterized by ℓ and $\ell \pm 1$ can be used to give a uniform transverse force $F_{\ell, \ell \pm 1}$ to counteract F_R and also to feedback stabilize the expected $m = 1$ instability. In this paper we report on experiments in which $\ell = 1$ and $\ell = 0$ helical fields are applied to a 3-meter-long straight theta pinch (Scylla IV-3) and to a 5-meter-long toroidal segment (Scyllac Toroidal Sector). In these experiments the main helical field has $\ell = 1$ symmetry, which is chosen because theory [2,3,4,5] predicts a growth rate for the dominant $k \approx 0$, $m = 1$ mode which vanishes to leading order. The smaller $\ell = 0$ fields produce the asymmetry in the plasma excursions $\delta_1 + \delta_0$ which is necessary to produce the force.

$$F_{1,0} = [\beta(3 - 2\beta)/8] B_0^2 h^2 a^3 \delta_1 \delta_0 \quad (ha \ll 1) \quad (3)$$

illustrated in Fig. 1(A). In the toroidal case [Fig. 1(B)] the balance of $F_{1,0}$ and F_R produces the toroidal equilibrium characterized by the relation

$$\delta_1 \delta_0 = -2/(3 - 2\beta) h^2 a R \quad (ha \ll 1) \quad (4)$$

II. EXPERIMENTS WITH THE 3-METER LINEAR THETA PINCH

1. Apparatus and Measured Plasma Properties

The experiments were performed on the Scylla IV-3 theta pinch [8] whose main capacitor bank has an energy storage of 700 kJ at 45 kV and produces a magnetic field B_0 , inside the 3-m long, 13.5-cm-diameter compression coil which rises to 42 kG in 3.7 μ sec. At maximum field the capacitor bank is

"crowbarred;" thereafter the magnetic field decays with a time constant of 120 μ sec and has an oscillatory peak-to-peak modulation of 20%.

The plasma, produced in a fused-quartz discharge tube whose inner diameter is 80 mm, has a maximum density on axis of $(2.7 \pm 0.3) \times 10^{16}$ cm $^{-3}$, in the absence of $\ell = 1$ and $\ell = 0$ fields, and a density profile which may be closely approximated by a Gaussian with an inflection-point radius of 0.7 ± 0.1 cm. The ion temperature is 900 ± 200 eV and β is 0.88 ± 0.03 . The density profile was measured by using a holographic ruby-laser interferometer [8,9] which produces interferograms at three times during a discharge. Each interference fringe (cf. Fig. 5) corresponds to an electron density of 3.2×10^{17} cm $^{-2}$, integrated along the axis of the discharge tube. The quantity β was measured both by means of Faraday rotation [10] at 6328 Å and by means of a double-magnetic-probe, excluded-flux measurement [11]. The two measurements agree to within the experimental error. The ion temperature was determined from the d-d neutron yield. The ion temperature was also calculated from pressure balance, assuming an electron temperature of approximately 350 eV, as has generally been found in the linear, zero-bias-field, Scylla-IV experiments [12], giving a somewhat higher value (~ 1100 eV).

2. Measurements with $\ell = 1$ Fields

Figure 2 shows the arrangement of $\ell = 1$ and $\ell = 0$ coils inside the Scylla IV-3 compression coil (the discharge tube is not shown). We first report experiments in which only the helical $\ell = 1$ coils (mean radius 5.25 cm) were installed and used. The currents in these coils were in the directions shown and rose to 80 kA in 2.5 μ sec. Thereafter the driving capacitor bank (40 kV, 33 μ F) was crowbarred, and the current decayed with a time constant of 30 μ sec. At 80 kA the transverse helical field B_r on axis is 2.8 kG. The currents to the $\ell = 1$ coils were fed in one-wavelength ($\lambda = 30$ cm) sections, as shown in Fig. 2, in order to keep the voltages induced by the main compression field in

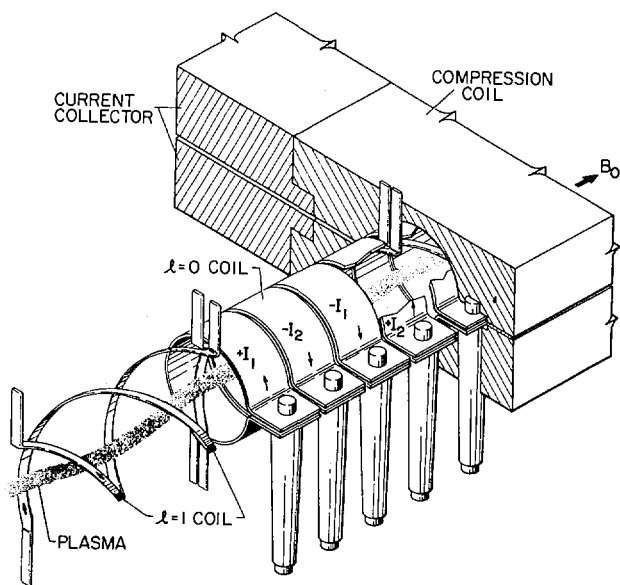


FIG. 2. Schematic view of the Scylla IV-3 compression coil and plasma with helical coils for generating the $\ell = 1$ -fields and single-loop coils for generating the $\ell = 0$ -fields.

each section to manageable levels. An important measurement was that of the transverse plasma motion by means of image-converter streak cameras (as illustrated in Fig. 2 of Ref. [13]). Three such cameras were used, each receiving an image of the plasma through slits perpendicular to the axis, located at 75, 135 and 225 cm from one end of the compression coil. At each position the equilibrium helical plasma displacement was downward.

It was necessary to analyze the interferograms for the equilibrium helical displacement $r_0 = a\delta_1$, the inflection-point radius a , and the radial density distribution $n(r')$ about the helically displaced plasma axis. This was done by a numerical inversion procedure [9,14] which converted the interferometric data from integrated end-on views of the plasma helix to the corresponding densities $n(r')$. For the 14-mtorr D_2 filling used in all discharges reported here the result at peak compression was $n(0) = (2.7 \pm 0.3) \times 10^{16} \text{ cm}^{-3}$, $a = 0.7 \pm 0.1 \text{ cm}$, $\delta_1 = 0.70 \pm 0.06$. When compared with the MHD prediction for a sharp-boundaried plasma [6],

$$\delta_1 = (B_r/B_0)[ha(1 - \beta/2)]^{-1} \quad (5)$$

it is found that $\delta_1(\text{experimental})/\delta_1(\text{sharp-boundary}) = 0.64$. This value of δ_1 was found regardless of whether the $\ell = 1$ field was applied simultaneously with B_0 or a few μsec thereafter.

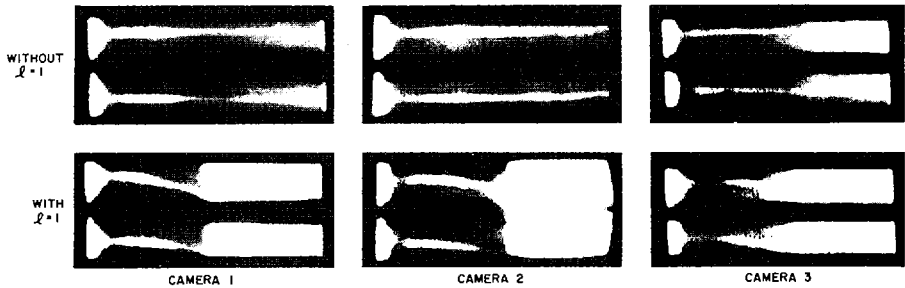


FIG. 3. Streak photographs of the Scylla IV-3 plasma at three camera positions with and without the $\ell = 1$ -coils excited. Only the $\ell = 1$ -coils were installed.

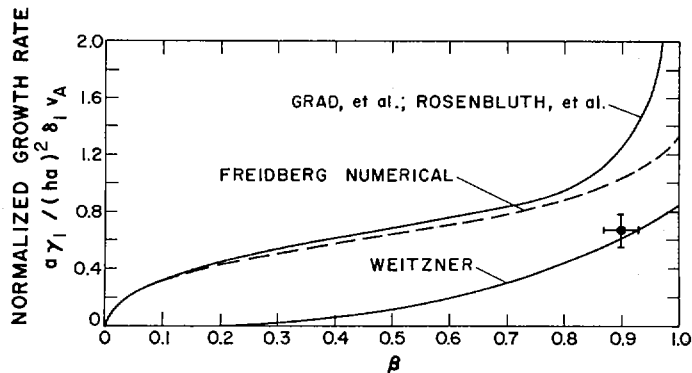


FIG. 4. Comparison of observed $m = 1$ growth rate excited by $\ell = 1$ -coils on the Scylla IV-3 plasma column with the various ordering results of the MHD, sharp-boundary theory. In the Weitzner case $\epsilon = 0.147$ and $\delta_1 = 0.7$.

After the plasma becomes helical, a $k \approx 0$, $m = 1$ instability develops with a measured growth rate $\gamma_1 = 0.54 \pm 0.09$ MHz. Typical stereoscopic streak photographs, 45° above and below horizontal, from the three image converters are shown in Fig. 3. These show an exponentiating sideward motion of the plasma column as a whole to the wall, independent of axial position. No higher- m modes are observed. Owing to a small asymmetry in the $\ell = 1$, B_0 system, this instability always develops in almost the same direction: downward and slightly away from the compression-coil feed slot. In order to compare with the various ordering results of the MHD theory we plot the observed, normalized growth rate in Fig. 4, along with the results of Rosenbluth, *et al.* [2] Grad, *et al.* [3], Weitzner [7] and Freidberg [5].

3. Measurements with $\ell = 1$ and $\ell = 0$ Fields

We next report experiments in which both the $\ell = 1$ and $\ell = 0$ coils of Fig. 2 were installed. In addition to driving the $\ell = 1$ coils as discussed above, the $\ell = 0$ coils were driven by a crowbarred capacitor bank (40-kV, 12.6- μ F, 55- μ sec decay time), which produced a maximum $|I_1| = |I_2| = 20$ kA with a rise time of 1.6 μ sec. The coils were driven in pairs as shown in order to cancel the induced voltage from the main bank. The system may be connected with I_1 and I_2 in either direction in order to vary the relative phases of the $\ell = 0$

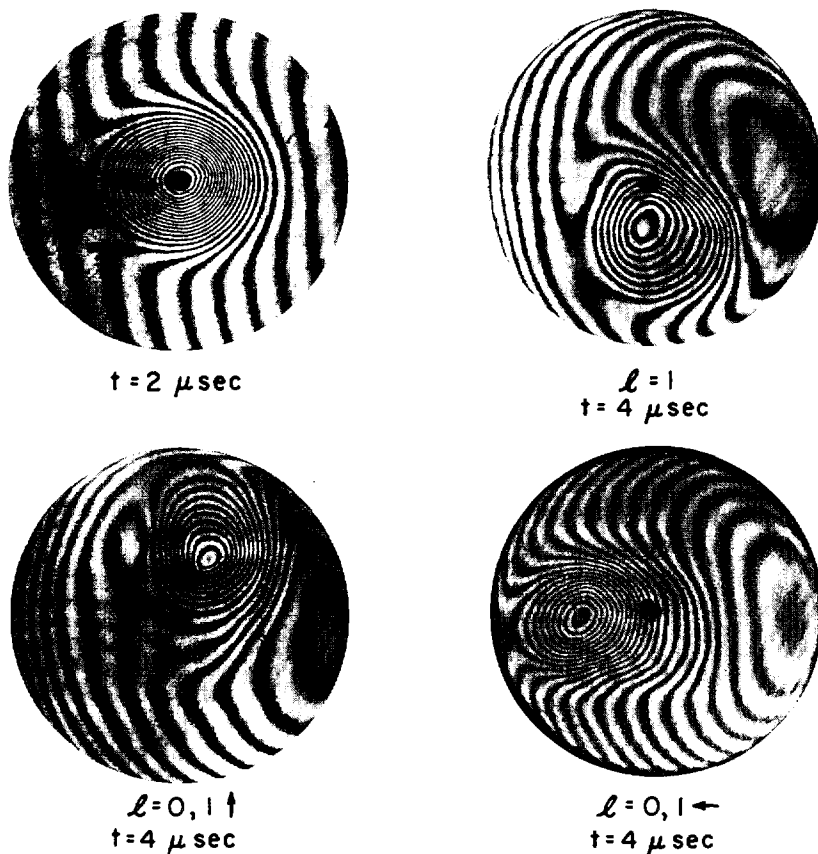


FIG. 5. Interferograms of the Scyllia IV-3 plasma under the influence of $\ell = 1$ -fields alone and for two $\ell = 1, 0$ -combinations.

and $\ell = 1$ fields and hence the direction of the $\ell = 1,0$ force. The particular arrangement shown in Fig. 2 gives an upward force. Since the present arrangement requires $I_1 = \pm I_2$ the force can be applied in only four directions, either horizontally or vertically. For a feedback system the amplitudes and phases of I_1 and I_2 would be varied independently, giving an arbitrary magnitude and direction to the $\ell = 1,0$ force. At 20-kA current, the $\ell = 0$ coils produced a first-harmonic amplitude of axisymmetric field $\delta B_z = \pm 0.70$ kG on axis. When the $\ell = 0$ coils, but not the $\ell = 1$ coils, were energized, no detectable change in plasma behavior was observed.

The result of applying both fields is shown in the end-on interferograms of Fig. 5. At $t = 2 \mu\text{sec}$ (after switch-on of B_0) the plasma has not appreciably moved for any combination of $\ell = 1,0$ fields. With $\ell = 1$ alone the 4- μsec interferogram shows the result of the $m = 1$ unstable motion. The two lower interferograms show the occurrence of the expected displacements with the $\ell = 1,0$ combinations phased to give the $F_{1,0}$ body force in the two directions indicated. The main coil feed slot is at the left.

The magnitude of the $\ell = 1,0$ force was determined by studying the plasma's dynamical behavior on stereoscopic streak photographs. In order to produce a motion which could easily be analyzed, plasma discharges were taken with the $\ell = 1$ field applied first, allowing the $m = 1$ instability to develop. Then, 1 to 2 μsec later, the $\ell = 0$ fields were applied to produce the force $F_{1,0}$ in a direction as nearly as possible opposite to that of the instability force.

The observed transverse displacement ξ was compared to that computed under the influence of the destabilizing force per unit length

$$F_1 = \pi a^2 \rho v_1^2 \xi \quad (6)$$

(ρ is the maximum plasma density) and the constant force $F_{1,0}$. Initial conditions of the computation were chosen to reproduce the unstable motion alone, assuming that the instability term had the same growth rate as that measured when the $\ell = 1$ fields were applied alone. In Fig. 6 the data points represent typical measurements of plasma displacement perpendicular to the compression-coil feed slot for the case where the applied $F_{1,0}$ was vertically upward. The computed motion represents the best fit under the assumption that $F_{1,0}$ is proportional to $(\delta B_z/B_0) \times (B_r/B_0)$. The result is

$$F_{1,0} = (0.96 \pm 0.15) \times 10^8 \frac{\delta B_z}{B_0} \frac{B_r}{B_0} \text{ dyne/cm} \quad (7)$$

We compare (7) with the theoretical expression (3), using the measured maximum value of β on axis and the value of plasma radius (corresponding to the Gaussian inflection-point) which, using the density on axis, reproduces the observed line density. When in addition we use the measured relation between δ_1 and B_r/B_z , we derive from Eqs. (3) and (7):

$$\delta_0 = (3.9 \pm 0.5) \delta B_z/B_0. \quad (8)$$

Sharp boundary theory gives

$$\delta_0 = (ha)^{-2} (I_0 K_0)^{-1} [1 - (1 - \beta) I_0 K'_0 / I'_0 K_0]^{-1} (\delta B_z/B_0) = 4.15 \delta B_z/B_0 \quad (9)$$

where the argument of the modified Bessel functions is ha . Thus we infer that the experimental and theoretical values of the $F_{1,0}$ force agree to within experimental error.

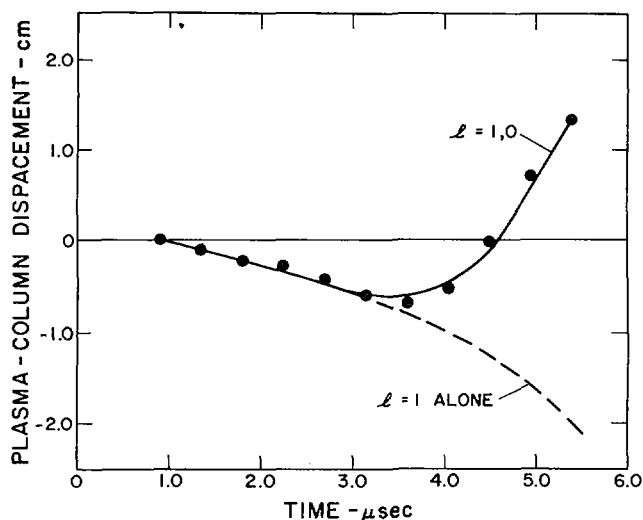


FIG. 6. Computed plasma transverse motion under the influence of $\ell = 1$ -fields alone and for the $\ell = 1, 0$ -field combination, compared with data points representing measured plasma displacement as a function of time.

III. EXPERIMENTS WITH THE 5-METER TOROIDAL THETA-PINCH SECTOR

1. Apparatus

A plan view of the toroidal-sector compression coil is shown in Fig. 7, in which the plasma measurements associated with the various viewing slots through the compression coil into the quartz discharge tube are identified. In addition, plastic-scintillation and silver-activation neutron detectors were located at four positions along the toroidal sector. Each one-meter section of the compression coil and associated collector plate is driven by a separate 700-kJ capacitor bank (called the Primary Bank) consisting of 210 1.85- μF , 60-kV capacitors, connected by means of 1,260 cables. The engineering features of the installation are described in Refs. 15 and 16, and the parameters of the θ pinch with one-half and with all of the capacitors connected are given in Table I. In the measurements reported here one-half of the primary bank was used, as well as a preionization bank consisting primarily of one 50-kV, 0.7- μF capacitor per meter which produced an oscillating longitudinal field of 0.8-kG amplitude at a frequency of 390 KHz. Each of the 1,050 spark gaps which switch the primary bank includes a "crowbar" spark gap [17,18]. At half energy the compression field B_0 rises to its maximum value in 3.6 μsec and then decays in 250 μsec with a peak-to-peak modulation of approximately 10% (see Fig. 8).

2. Measurements with a Compression Coil of Constant Minor Diameter and No Helical Fields

Control experiments were performed in order to measure the plasma heating and toroidal drift in the presence of a pure toroidal field with no helical or bumpy fields. The main bank was operated at 45 and 50 kV with deuterium filling pressures of 10, 15 and 20 mtorr. No bias field was used.

The preionized plasma electron temperature kT_e was measured with a McPherson 1-meter grating spectrometer.

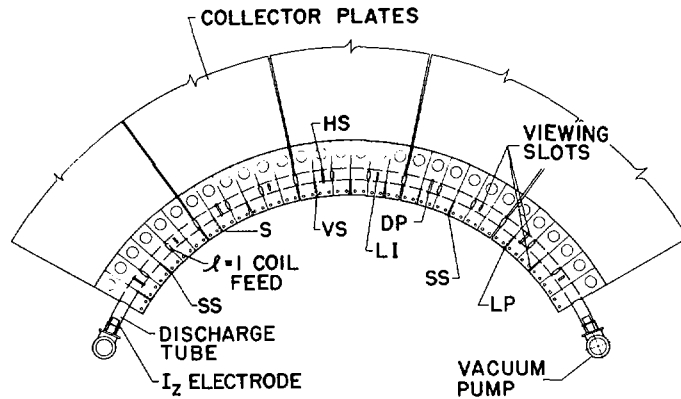


FIG. 7. The 5-metre Scyllac Toroidal Sector compression coil, with its various slots for viewing and for $\ell = 1$ -coil feeds. The plasma measurements are identified as follows: HS, streak camera for horizontal motion; VS vertical streak camera; SS, $\pm 45^\circ$ stereoscopic streak camera; LI, coupled-cavity laser interferometer; DP, double magnetic probe; LP, plasma luminosity-profile measurement.

TABLE I. SCYLLAC TOROIDAL-SECTOR PARAMETERS FOR A COMPRESSION-COIL MINOR DIAMETER OF 14.4 cm. THE MAJOR RADIUS IS 2.375 METERS AND THE COIL LENGTH IS 5.00 METERS

Fraction of Bank	One-Half	Full
V (kV)	60	60
C (μF)	971	1,942
W (MJ)	1.75	3.5
L_{source} (nH)	6.4	5.0
L_{coil} (nH)	20.5	20.5
α	0.76	0.80
E_θ ($r = 4.3$ cm) (V/cm)	600	630
$(dB/dt)_{t=0}$ (Gauss/sec)	2.46×10^{10}	2.74×10^{10}
$\tau/4$ (μsec)	3.6	4.9
I_{max} (MA)	24.0	34.5
B_{max} (kG)	59.0	86.2
$(L/R)_{\text{crowbar}}$ (μsec)	250	250

Two kT_e determinations [19] were made at 15 μsec after firing the preionization bank: (a) a measurement of the intensity ratio of the D_δ line to a 16 \AA interval of the Paschen continuum at 5400 \AA , and (b) a measurement of the relative intensities of D_δ and D_β . The results at 10 and 20 torr were $kT_e = 1.8 \pm 0.4$ and 1.3 ± 0.3 eV, respectively. The densities deduced from the filling pressures, using the Saha equation, were $7.0 \times 10^{14} \text{ cm}^{-3}$ and $1.4 \times 10^{15} \text{ cm}^{-3}$ respectively ($\sim 100\%$ ionization). A 3.4- μ He-Ne laser interferometer [20] with a rotating corner cube or a LiNbO_3 electro-optic crystal in the external cavity was used to measure the preionization electron density across a diameter

of the discharge tube. The results at 10 and 20 mtorr, 15 μsec after firing the preionization, were $6.4 \times 10^{14} \text{ cm}^{-3}$ and $1.1 \times 10^{15} \text{ cm}^{-3}$, in good agreement with the filling density. Spectrograms showed a predominant Balmer spectrum with only weak lines of C, O, and Si.

Image-converter streak photographs were made at the positions indicated in Fig. 7. Views of the horizontal and vertical plasma motion at the center of the compression coil are shown at the left of Fig. 8, for a capacitor-bank voltage of 50 kV and a filling pressure of 20 mtorr. The initial plasma implosion is followed by compressive MHD oscillations, and the plasma then drifts to the discharge-tube wall, remaining in the plane of the compression coil feed slot. (The front view shows extra luminosity from a metallic reflection in the viewing slit). Oscillograms of the main compression field and neutron emission for a 10 mtorr filling are shown at the right of Fig. 8. The neutron signal is quenched when the plasma strikes the discharge tube. Streak photographs at various positions show that the plasma strikes the wall away from the center of curvature approximately simultaneously at various axial positions.

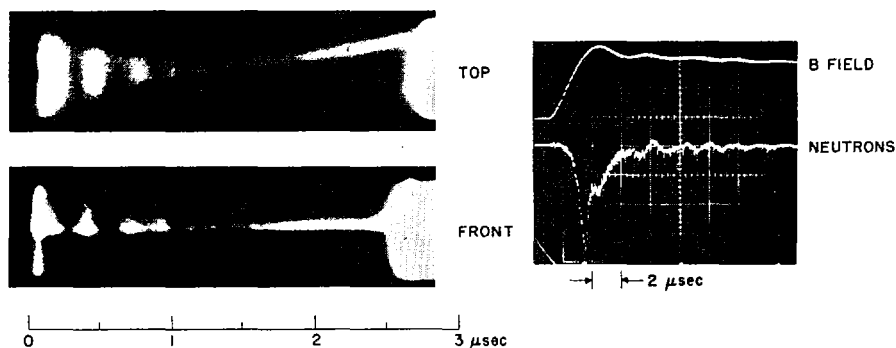


FIG. 8. Left: Streak photographs at the centre of the toroidal sector plasma without helical or bumpy fields, showing horizontal (upper photograph) and vertical (lower photograph) motions. Right: Oscillograms of main-compression field and neutron-scintillator signal.

In order to estimate the plasma temperature from the toroidal drift we set $\beta = 8\pi nk(T_e + T_i)/B_0^2$ and equate F_R of Eq. (1) to $\pi a^2 \rho k$. If b is the inner radius of the discharge tube, the time required for the plasma to move to the wall is then given by

$$\tau_R = [M_i R b / k(T_e + T_i)]^{1/2} \quad (10)$$

For the filling pressures 10, 15, and 20 mtorr and 45-kV bank voltage the observed drift times from initiation of the discharge were 2.23 ± 0.06 , 2.43 ± 0.06 , and $2.72 \pm 0.08 \mu\text{sec}$. For $b = 4.0 \text{ cm}$ one derives the corresponding mean temperatures: $k(T_e + T_i)_{\text{Av}} = 429, 361, \text{ and } 288 \text{ eV}$, respectively.

An estimate of ion temperature was obtained by normalizing the integrated scintillator signal to the absolute neutron yield given by the silver-activation counters. A plasma density of $2 \times 10^{16} \text{ cm}^{-3}$ was assumed at maximum neutron emission, and the plasma radius was taken to be $r_{1/2} = 0.72 \text{ cm}$, estimated from the multichannel luminosity data described below (cf. Fig. 9). From the Maxwellian average d-d cross section times velocity one derives $kT_i \approx 940 \text{ eV}$. This maximum ion temperature is reasonable in view of the 412-eV average of $k(T_e + T_i)$ derived from the drift and the fact that kT_e is expected to be about 300 eV near maximum compression.

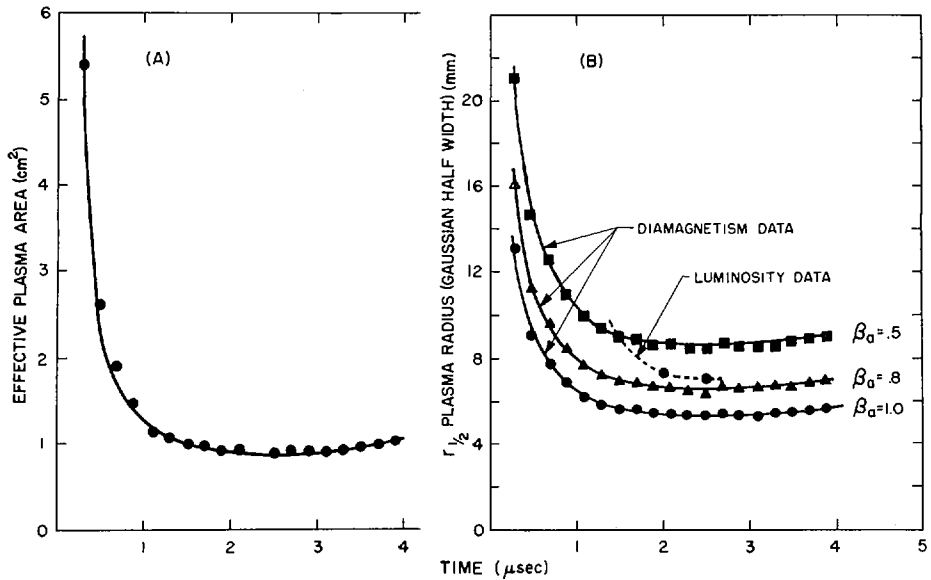


FIG. 9. (A) Effective plasma area for $\beta = 1$ as derived from double-probe measurements on the Scyllac toroidal sector. (B) Effective plasma radii corresponding to (A), on the assumption of a Gaussian $\beta(r)$ profile for various beta values β_a on axis.

The plasma diamagnetism was measured by using the double-probe technique [11] which yields the effective area of the plasma. Figure 9(A) shows the result of measurements at 10mtorr D_0 filling pressure and 45-kV primary bank voltage. On the assumption of a Gaussian profile $\beta(r)$ one can derive the half-width radii $r_{1/2}(t)$ as a function of β on axis, β_a , as shown in Fig. 9(B). An approximate determination of plasma half-width radius from multichannel luminosity measurement (whose accuracy is limited by background light) [11] yields the points so identified in Fig. 9(B). We estimate β on axis at maximum compression to be approximately 0.7.

3. Measurements with $\ell = 1$ and $\ell = 0$ Fields

Figure 10 shows the arrangement [21] for applying $\ell = 1$ and $\ell = 0$ fields to Scyllac in order to give the toroidal equilibrium depicted in Fig. 1(B). The $\ell = 1$ fields were applied by means of bifilar helical coils divided into one-period ($\lambda = 33$ cm) lengths as shown in the upper portion of Fig. 10, similar to the $\ell = 1$ coils of Fig. 2. The mean radius of the helical coils was 5.75 cm. The $\ell = 0$ fields were generated from annular grooves 1.80-cm deep in the inner surface of the compression coil, and the onset of these fields was delayed by about 0.5 μ sec by means of the annular sets of stainless-steel trapezoidal cylinders (lower portion of Fig. 10) as described in Ref. 13. The $\ell = 1$ coils were driven by crowbarred capacitors so that the current rose to its maximum value in 3.2 μ sec, thereafter decaying in 95 μ sec with 12% modulation. The $\ell = 1$ capacitor bank was switched at time delays varying from 0 to 0.6 μ sec after initiation of the primary bank.

The streak photographs of Fig. 11(A) show the vertical and horizontal plasma motions at the center of the compression coil with the $\ell = 1$ coils not excited. Note that the two streak-camera slots are 7.65 cm apart (cf. Figs.

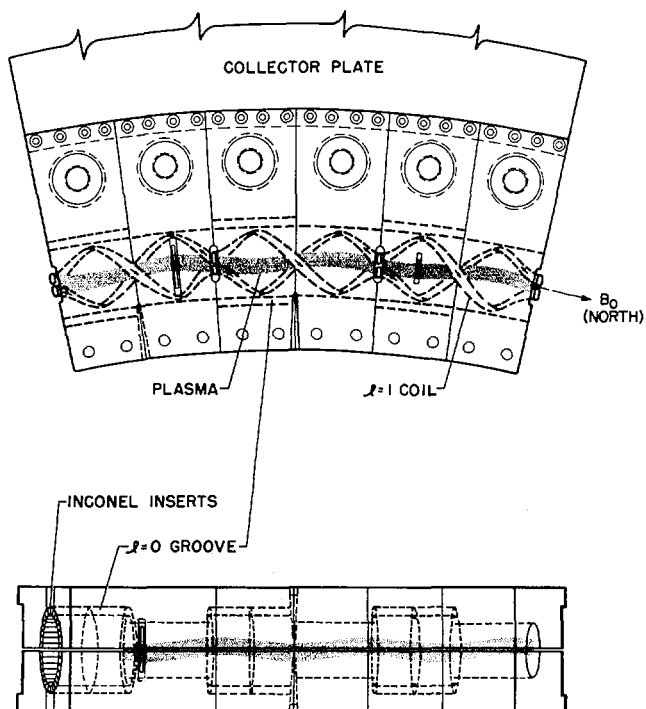


FIG.10. Arrangement of $\ell = 1$ -coils and $\ell = 0$ -grooves (with time-delay inserts) to give a toroidal equilibrium in the Scyllac 5-m toroidal sector.

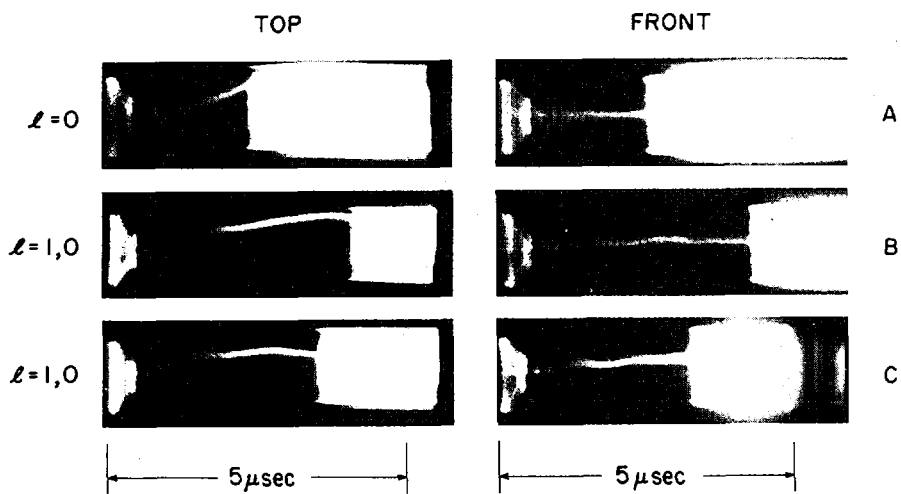


FIG.11. Streak photographs of the plasma at the centre of the Scyllac 5-metre Toroidal Sector with $\ell = 0$ -fields alone and with the $\ell = 1, 0$ -combination.

7 and 10). Even though the $\ell = 0$ fields were present because of the grooves, the motion was a simple toroidal "drift" to the walls with no observable instability induced by the bumpy fields. The streak photographs of Figs. 11(B) and 11(C) were taken with the $\ell = 1$ coils excited at maximum values of 87 kA (0.5- μ sec delay) and 75 kA (0.2- μ sec delay), respectively. The horizontal plasma motion shows that the toroidal force is overcome by the $\ell = 1, 0$ combination, and the plasma returns to the axis of the discharge tube while remaining close to the plane of the toroidal sector. These streak photographs correspond to 20-mtorr D_2 filling pressure and 45-kV primary-bank voltage. The times of observation in Figs. 11(B) and 11(C) are limited by the sudden appearance of light across the field of view. This occurs when the plasma strikes the wall at positions away from the center of the discharge tube where the balance between F_R and $F_{1,0}$ is not the same as it is near the center. Figure 12 shows the wavetforms of compression field, $\ell = 1$ current and neutron-scintillator signal for 10-mtorr filling pressure and 50-kV primary-bank voltage. The neutron signal is quenched as the plasma strikes the wall at the off-center positions.

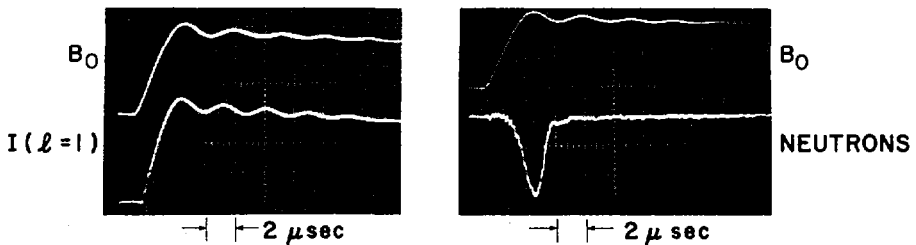


FIG. 12. Oscillograms of compression field, current through the $\ell = 1$ -coils, and neutron emission when the $\ell = 1, 0$ -combination was excited.

In these streak photographs no appreciable $m = 1$ instability is seen during the times of observation. According to the sharp-boundary, straight plasma-column, MHD theory [2,3,6] the growth rates of the $m = 1$ instabilities induced by the $\ell = 1$ and $\ell = 0$ fields separately would be approximately 0.6 and 2.6 MHz, respectively (assuming $\beta \approx 0.7$ and $n_{\max} \approx 2.4 \times 10^{16} \text{ cm}^{-3}$). Measurements have not yet been made of δ_1 and δ_0^{\max} . However, the $\ell = 1$ currents which are necessary to produce the observed toroidal equilibrium have approximately the value (≈ 80 kA) which would be estimated from Eq. (4). In this estimate the sharp-boundary theoretical value [6] of δ_0 (≈ 0.34) corresponding to the annular groove depth for $\beta \approx 0.7$ is used. The value of δ_1 is calculated from Eq. (5), using the theoretical relationship [6] between B_r and the $\ell = 1$ current and applying the experimental correction factor of 0.82 discussed in Sec. II.2 above.

IV. DISCUSSION

From the observations reported here the following main conclusions are drawn:

- (1) Within experimental error, the $m = 1$ instability on a straight plasma column with $\ell = 1$ helical fields has a growth rate not exceeding that predicted by any of the theoretical models. No higher- m modes are seen. This is in agreement with the finite-Larmor-radius effects calculated on Freidberg's Vlasov-fluid model [5].

(2) The $\ell = 1,0$ force has been observed on a straight plasma column, and it has the theoretically predicted magnitude and direction.

(3) Compensation of the toroidal force by a combination of $\ell = 1$ and $\ell = 0$ fields is observed. On the basis of preliminary estimates, the theoretical relationship among the various plasma parameters and helical fields is approximately confirmed.

(4) The $m = 1$ instability expected on sharp-boundary, MHD theory for a straight plasma column with $\ell = 0$ bumpy fields is not seen in the toroidal case during the present times of observation. This is an effect similar to that reported in Ref. 13, where a single $\ell = 0$ bump did not produce the instability in a linear hot-ion plasma.

V. ACKNOWLEDGMENTS

Essential contributions to these experiments were made by E. L. Kemp, who supervised the engineering of Scyllac, and by R. F. Gribble and D. M. Weldon. Helpful collaboration with Michael Kaufmann during an extended visit, while on leave from the Garching Institute for Plasma Physics, is also acknowledged.

REFERENCES

- [1] Blank, A. A., Grad, H., and Weitzner, H., in Plasma Physics and Controlled Nuclear Fusion Research (International Atomic Energy Agency, Vienna, 1969), Vol. II, p. 607.
- [2] Rosenbluth, M. N., Johnson, J. L., Greene, J. M., and Weimer, K. E., Phys. Fluids **12**, 726 (1969).
- [3] Grad, H. and Weitzner, H., Phys. Fluids **12**, 1725 (1969).
- [4] Freidberg, J. P. and Marder, B. M., Phys. Fluids **14**, 174 (1971).
- [5] Freidberg, J. P., Paper CN-28/J-5, these proceedings.
- [6] Ribe, F. L. and Rosenbluth, M. N., Phys. Fluids **13**, 2572 (1970).
- [7] Weitzner, H., Phys. Fluids **14**, 658 (1971).
- [8] Gribble, R. F., Little, E. M., Quinn, W. E., and Siemon, R. E., Phys. Fluids **14**, (to be published).
- [9] Siemon, R. E. and Jahoda, F. C., in Proceedings of S.P.I.E. Seminar in Depth, Holography 1971, Boston Mass. (S.P.I.E., Redondo Beach, Calif.). (to be published).
- [10] Gribble, R. F., Little, E. M., Morse, R. L., and Quinn, W. E., Phys. Fluids **11**, 1221 (1968).
- [11] Sawyer, G. A., Finlayson, V. A., Jahoda, F. C., and Thomas, K. S., Phys. Fluids **10**, 1564 (1967).
- [12] Little, E. M., Quinn, W. E., and Sawyer, G. A., Phys. Fluids **8**, 1168 (1965).
- [13] Little, E. M., Newton, A. A., Quinn, W. E., and Ribe, F. L., in Plasma Physics and Controlled Nuclear Fusion Research (International Atomic Energy Agency, Vienna, 1969), Vol. II, p. 555.
- [14] Siemon, R. E. and Weitzner, H., Bull. Am. Phys. Soc. **II-15**, 1479 (1970).
- [15] Kemp, E. L., Boicourt, G. P., Gribble, R. F., Hammer, C. F., Hanks, K. W., Quinn, W. E., and Sawyer, G. A., in Proceedings of the 6th Symposium on Fusion Technology, Aachen, September 22-25, 1970. (Euratom, CID, Luxembourg, December, 1970). p. 227.

- [16] Proceedings of Symposium on Engineering Problems of Fusion Research, Los Alamos Scientific Laboratory Report LA-4250 (1969).
- [17] Gribble, R. F., Proceedings of Symposium on Engineering Problems of Fusion Research, Los Alamos Scientific Laboratory Report LA-4250 (1969).
- [18] Gribble, R. F., Little, E. M., Quinn, W. E., and Siemon, R. E., Los Alamos Scientific Laboratory Report LA-4611-MS (1971).
- [19] Griem, H. R., Plasma Spectroscopy (McGraw-Hill, New York, 1964). Ch. 13.
- [20] Baker, D. A., Hammel, J. E., and Jahoda, F. C., *Rev. Sci. Instr.* **36**, 395 (1965).
- [21] Ribe, F. L., Borkenhagen, W. H., Ellis, W. R., and Hanks, K. S., Los Alamos Scientific Laboratory Report LA-4597-MS (1971).

DISCUSSION

H. A. B. BODIN: Could you say something further about why the $m = 1$ mode was not seen in the $\ell = 0$ and $\ell = 0, 1$ -systems, although it should have been seen at the MHD-growth times involved? One might expect MHD to be a good description of the $m = 1$ -mode. Also, the growth rates of the $\ell = 0$ system are higher than those for $\ell = 1$. If increasing proportions of $\ell = 0$ have to be added to the $\ell = 1$ -system, will the growth rates become faster?

F. L. RIBE: Perhaps the most significant observation in these experiments so far is the unexpected degree of stability of the $\ell = 0$ system. I agree with your remarks about the $m = 1$ -instability. As pointed out in the paper, at $\delta_0 = 0.2$ there should be appreciable instability. However, we were led by our observations of stability of the $\ell = 0$ -system to use this relatively large value of δ_0 in the Scyllac equilibrium configuration.

H. A. B. BODIN: In the linear bulged theta pinch experiment, where you stated that the $m = 1$ -MHD-mode was observed at low temperatures but not at high temperatures, did you — in the high temperature case — show by direct measurement that a bulge actually formed, or was this only deduced from the external fields?

F. L. RIBE: No. We did not show this by direct measurement.

R. L. MORSE: In connection with the questions asked by Dr. Bodin, it should be recalled that the $m = 1$ -instability caused by $\ell = 0, k \neq 0$ fields require $\beta < 1$ when derived from a sharp-boundary model. For $\beta = 1$ (i. e. no magnetic field in the plasma) the sharp-boundary model gives neutral stability of the $m = 1$ ballooning model, which suggests that the instability may be sensitive to the density and magnetic field profiles. The sensitivity may be responsible for the failure of the instability to appear in many experiments.

A. GIBSON: Figure 11 of your paper shows that the appearance of the light flash coincides with the time at which the $\ell = 1$ current reaches its maximum value. Do you regard this as a chance occurrence or has the coincidence some significance?

F. L. RIBE: It must be chance because when we correct the ends and delay the light flash to $7 \mu\text{s}$, coincidence is no longer observed.

SURVEY OF SCYLLAC THEORY

J. P. FREIDBERG
 University of California,
 Los Alamos Scientific Laboratory,
 Los Alamos, N. Mex.,
 United States of America

Abstract

SURVEY OF SCYLLAC THEORY.

A survey is given of both old and new theoretical results pertaining to the Scyllac experiment.

INTRODUCTION

The basic problem of the Scyllac[1] experiment is to devise a method for bending a θ pinch into a torus. The underlying principle is to use a toroidal configuration as nearly similar to linear θ pinches as possible, in order to retain the advantages of the straight geometry (i.e. neutral stability, and a tested method of plasma heating). Several methods have been proposed to achieve toroidal equilibria. The most promising of these appears to be the $\ell = 1$ helical Scyllac[2] configuration. As its name implies, equilibrium is achieved by superposing a small $\ell = 1$ helical field to the basic θ pinch field. This system has the important advantage that it is basically stable to the $m = 1$ mode in the straight geometry. The further addition of very small amounts of either $\ell = 0$ or $\ell = 2$ fields is sufficient to provide a toroidal equilibrium[3].

We proceed by briefly reviewing the early theories related to the stability of high β , $\ell = 1$ systems, and then turn to some new results.

Review of Early Theoretical Results

By and large the main theoretical effort has focussed on the equilibrium and $m = 1$ stability in the sharp boundary model. In this model, the equilibrium is described by a constant pressure plasma contained by currents flowing only on its surface. The $\ell = 1$ Scyllac configuration is illustrated in Fig. 1. δ_1 is the helical displacement of the plasma from the axis of symmetry normalized to the plasma radius a , and h is the pitch number of the helix. Figure 1 refers to a straight helix. To obtain toroidal equilibrium an additional $\ell = 0$ field is used. The corresponding toroidal configuration looks the same except that the plasma radius is now a function of z ; that is the equation for the plasma surface is given by $r(z) = a(1 + \delta_0 \sinh z)$ where δ_0 is the normalized distortion of the plasma due to the $\ell = 0$ fields.

Despite the simplifications inherent in the sharp boundary model, the theory is essentially intractable unless some expansions are used. For the toroidal configuration there are six basic dimensionless parameters; $\epsilon \equiv ha$, δ_1 , δ_0 , β , a/b , a/R . Here a/b is the ratio of plasma to wall radii, and R/a is the toroidal aspect ratio. In each of the theories of interest it is assumed that $\beta \sim 1$ and $a/b \sim 1$. In the early theories the toroidal effects are assumed to be very small so that the parameters δ_0 and a/R appeared only as high order terms in the equilibrium but do not enter explicitly into the stability calculations. Under these assumptions there evolved two stability theories whose applicability depends upon the relative size of the remaining two dimensionless parameters ϵ , δ_1 .

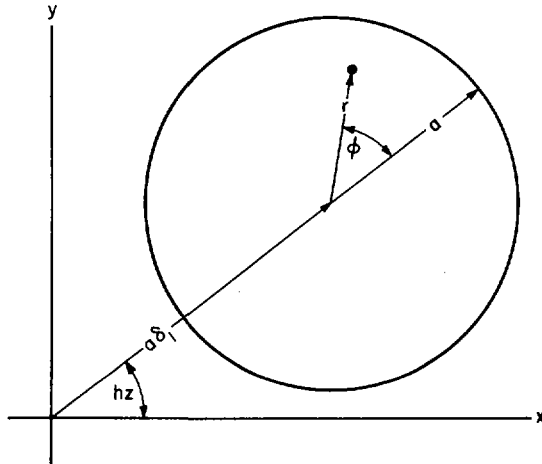


FIG. 1. Cross-section of the $l = 1$ Scyllac configuration for a fixed value of z .

In the first of these theories[4,5,6,7] it is assumed that $\delta_1 \ll \epsilon \leq 1$. This ordering corresponds to a tightly wound helix with very small helical currents. The $m = 1$ stability of this system was calculated to leading order in δ_1^2 and leading and first order in ϵ^2 . The dispersion relation is given by

$$\frac{\omega^2 a^2}{v_a^2} = \epsilon^2 \delta_1^2 \left[\beta^2 \left(\frac{a}{b}\right)^4 - \frac{\beta(4-3\beta)(2-\beta)}{8(1-\beta)} \epsilon^2 \right] \quad (1)$$

where v_a is the Alfvén velocity.

The first term on the right hand side represents a dipole wall stabilization term due to the $l = 1$ plasma currents. This term is formally larger than the second term under the ordering assumptions. However, because of the strong fourth power dependence on a/b this term is numerically small in many cases of interest. The second term represents a weakly destabilizing term arising from the $l = 1$ fields. For any $l \neq 1$ the corresponding term is $\sim 1/\epsilon^2$ larger. The vanishing of the leading order destabilizing term is one of the primary virtues of the $l = 1$ system. We see from Eq. (1) that stability is achieved by making ϵ sufficiently small; that is by making the pitch length long. This approach encounters a difficulty when attempts are made to create a toroidal equilibrium. By carrying out the equilibrium calculation to sufficiently high order a relationship is derived that determines the amount of $l = 0$ field required (expressed in terms of δ_0) to balance the toroidal drift force which is proportional to a/R . This relationship is given by

$$\delta_0 = \frac{-2}{3-2\beta} \frac{1}{\epsilon^2 \delta_1} \frac{a}{R} \quad (2)$$

We note that making ϵ small for stability purposes results in the need for large $l = 0$ fields. This effect is further magnified by the fact that the ordering requires $\delta_0 \ll \delta_1$ where δ_1 itself has been assumed small. Substituting experimental parameters into the equilibrium relation one is led to the conclusion that $\epsilon \ll \delta_1$ (i.e. $\epsilon \approx .1$, $\delta_1 \approx 1$) which is a direct violation of the original ordering.

These considerations led to the development of a new ordering [8] in which it is assumed that $\epsilon \ll \delta_1 \leq 1$. This corresponds to a configuration with moderate helical currents and a long helical pitch length. The $m = 1$ stability was calculated to leading order in ϵ^2 and leading and first order in δ_1^2 . The resulting dispersion relation is given by

$$\frac{\omega^2 a^2}{v^2 a} = \epsilon^2 \delta_1^2 \left[\beta^2 \left(\frac{a}{b}\right)^4 - \frac{\beta^5}{32(2-\beta)} \delta_1^2 \right] \quad (3)$$

The first term corresponds again to the dipole wall stabilization. The second term is a weak destabilizing term, quite small even for $\delta_1 \approx 1$ because of the small multiplying factor $\beta^5/32$. Substituting experimental parameters results in either smaller growth rates than in the original ordering or else stability. A further extension of this calculation [9] in which the plasma cross section is allowed an $l = 2$ elliptical component leads to an even more favorable result. By an appropriate choice of the ellipticity, the destabilizing term can be made to vanish identically. The amount of ellipticity required in the cross section corresponds to the condition that the external helical field be a pure sinusoidal $l = 1$ field.

In summary, two basic theories have been developed for the stability of high β $l = 1$ configurations. Each of these predicts, at worst, a very weak $m = 1$ instability as a consequence of the vanishing of the leading order destabilizing term.

The vanishing of this term is not pathological to sharp boundary models and in fact occurs for a wide class of diffuse profiles which satisfy the weak condition [10]

$$\frac{1}{B} \frac{dB}{dr} > 0 \quad (4)$$

where $B(r)$ is the θ pinch field.

Recent Results on $m = 1$ Instability

Although the early theories provide a firm foundation, they do not provide a complete picture for all experimental parameters. The second ordering discussed above, $\epsilon \ll \delta_1 \leq 1$, (hereafter referred to as the new ordering) comes close to satisfying experimental conditions and in general gives optimistic predictions as compared to the first ordering $\delta_1 \ll \epsilon \leq 1$, (hereafter referred to as the old ordering). That a difficulty arises can be seen from the fact that the destabilizing term in the old ordering, (proportional to $\epsilon^4 \delta_1^2$) is formally small compared to the destabilizing term in the new ordering (proportional to $\epsilon^2 \delta_1^4$) since we assume $\epsilon \ll \delta_1$ in the new ordering. However, because of the small numerical factor in the new ordering both of these terms are numerically comparable.

Because of this overlapping of the two ordering results a third theory has been developed, which is based on the new ordering. In this theory the expansion is carried out one term further in ϵ^2 and the restriction $\delta_1 < 1$ is removed. Thus the expansion is described by $\epsilon < 1$, δ_1 arbitrary.

The first prediction of the new theory concerns the equilibrium. The configurations of experimental interest have no net z current. This condition imposes a constraint on the range of parameters over which such equilibria exist. By assuming a circular cross section for the plasma it turns out that "no z current" equilibria are possible only if

$$\beta \delta_1 < \frac{\pi^2}{16} \quad (5)$$

that is, such equilibria are not possible with arbitrarily large β and helical shifts. A condition similar to this was found in the new ordering, [8] although in a slightly different form.

The second prediction of this theory concerns the stability of the $m = 1$ mode. A dispersion relation is derived which is of the form

$$\frac{\omega^2 a^2}{v^2} = \epsilon^2 \lambda_i \quad (6)$$

where the λ_i are numerically calculated eigenvalues of the matrix defined by

$$\delta W = - \sum_{-\infty}^{\infty} \xi_m W_{mn} \xi_n^* = - \sum_{-\infty}^{\infty} \xi_m [W_{mn}^0 + \epsilon^2 W_{mn}^1] \xi_n^* \quad (7)$$

Here δW is usual MHD energy variation, appropriately normalized; the ξ_n are arbitrary constants associated with the $m = 1$ perturbation to be chosen in such a way as to minimize δW , and the W_{mn} are matrix elements which can be calculated directly from the equilibrium $\bar{m}n$. The results presented here correspond in all cases, to the most unstable perturbations; those with the most negative λ_i . A simple way to understand the relationships between the various theories is by an examination of marginal stability. By fixing β and a/b , marginal stability as a function of ϵ and δ_1 is given by $\epsilon = \text{const}$ in the old ordering and $\delta_1 = \text{const}$ in the new ordering. Illustrated in Fig. 2 are numerically computed contours of marginal stability in the (ϵ, δ_1) plane for $\beta = .5$ and various values of a/b . The marginal values of ϵ and δ_1 from the old and new ordering are shown on the vertical and horizontal axis respectively. We note that the numerical calculation recovers both the old and new ordering results in the appropriate limits.

For present experiments where $b/a \approx 6$ values of $\epsilon \leq .02$ and $\delta \leq .55$ are required for stability. Toroidal equilibrium considerations lead to a value of $\epsilon \approx .1$. Present experiments are designed for $\epsilon \approx .1$ and consequently operate in a weakly unstable regime. Looking ahead towards reactor designs, we see that parameters change in a favorable direction. In a Scyllac reactor a large portion of the heating will be done by shock heating (as opposed to adiabatic compression) and the resulting b/a will be approximately $b/a \approx 2$. In this case, stability is achieved with $\epsilon \leq .18$ which is consistent with toroidal equilibrium requirements. A final point worth noting with regard to reactors concerns the β dependence of marginal stability. Numerical calculations of marginal stability for $b/a = 2$ in (ϵ, β) space for various values of δ_1 turn out to be independent of δ_1 . Somewhat surprisingly, the marginal condition is very accurately given by the old ordering for $\beta \leq .95$, even for values of $\epsilon \ll \delta_1 \sim 1$, which directly violates the old ordering. Using the old ordering (Eq. 1) we see that there is an optimum β for marginal stability given by $\beta \approx .75$. This also is favorable for reactor designs.

For comparison with current experiments we have numerically calculated growth rate vs β curves for $.1 < \epsilon < .2$ and $.2 < \delta_1 < 1$. The results of these computations give growth rates which are independent of b/a if $b/a > 4$. Again we find somewhat surprisingly that, despite the fact that the parameter range of interest satisfies $\epsilon \ll \delta_1$, the growth rates are accurately given, to within 15%, by the old ordering (Eq. 1) as long as $\beta < .95$ and the equilibrium condition $\beta \delta_1 < \pi^2/16$ is satisfied.

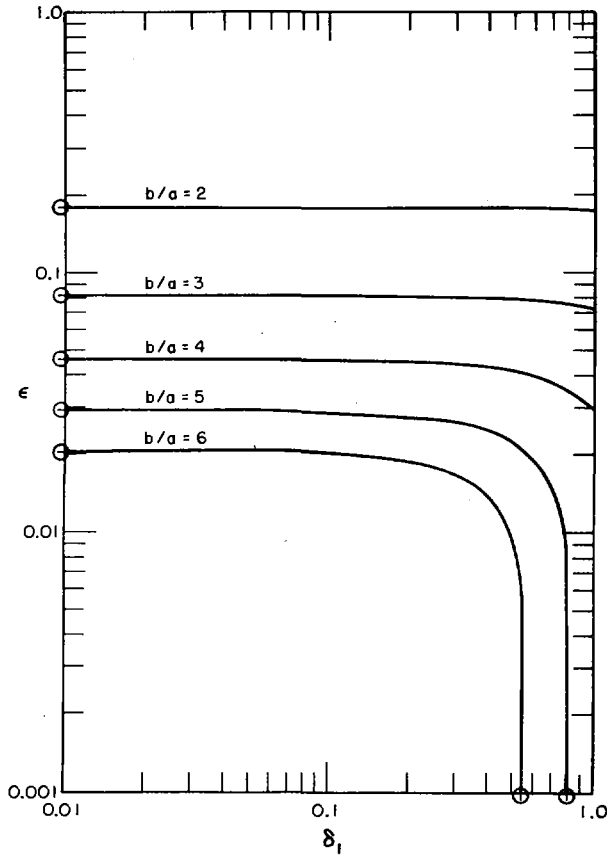


FIG.2. Contours of marginal stability in the (ϵ, δ_1) -plane for $\beta = 0.5$ and various values of b/a . The stable regions lie below the contours.

Recent Results on the $m = 2$ Instability

As we have seen, the main theoretical effort is centered around the $m = 1$ stability in the high β , $\ell = 1$ Scyllac configuration. The stability of higher m modes has not received much attention, primarily due to the fact that no such mode has ever been observed experimentally in $\ell = 0$ or $\ell = 1$ systems. However, from a theoretical viewpoint the situation has not been satisfactorily understood.

It is generally accepted that the primary virtue of the $\ell = 1$ configuration is that the $m = 1$ mode is at worst weakly unstable. This is an MHD result. However MHD also predicts growth rates of the order $1/\epsilon$ times larger than the $m = 1$ mode for any $m \geq 2$. [4,5] It is quite important to understand this discrepancy between theory and experiment, not only for current experiments, but to determine scaling laws for future large experiments.

We have attempted to answer these questions by starting with a more realistic model and then comparing the results with those of ideal MHD. The model we consider is based on the low-frequency Maxwell's equations (which neglect

displacement current and assume charge neutrality). The electrons are treated as a fluid tied to the magnetic lines. Thus their equation of motion is given by

$$\vec{E} + \vec{u}_e \times \vec{B} = 0 \quad (8)$$

and the corresponding perpendicular electron current by

$$\vec{J}_{\perp e} = -en\vec{u}_e \quad (9)$$

The ions are assumed collisionless and consequently are described by the Vlasov equation

$$\frac{\partial f}{\partial t} + \vec{v} \cdot \nabla f + \frac{e}{m_i} (\vec{E} + \vec{v} \times \vec{B}) \cdot \nabla_v f = 0 \quad (10)$$

The first question concerns equilibrium. We make the reasonable hypothesis that all equilibrium currents are carried by the electrons. This is approximately equivalent to the statement that the equilibrium is created without generating any linear or angular momentum in the plasma. In this case the ion distribution function is a function only of the energy \mathcal{E} and the ions are contained by electrostatic forces. Straightforward analysis leads to the following equilibrium equations

$$\begin{aligned} \vec{J}_0 \times \vec{B}_0 &= \nabla p_0 \\ \nabla \times \vec{B}_0 &= \mu_0 \vec{J}_0 \\ \nabla \cdot \vec{B}_0 &= 0 \end{aligned} \quad (11)$$

where

$$p_0 = \int \frac{mv^2}{3} f_0(\mathcal{E}) d\vec{v}$$

We see that the Vlasov-fluid equilibrium is identical to ideal MHD if the electrons carry all the current.

The next question considered is marginal stability through $\omega = 0$. Setting $\omega = 0$ greatly simplifies the ion distribution function and again a straightforward analysis leads to the following set of marginal stability equations

$$\begin{aligned} \nabla \times [\vec{J}_1 \times \vec{B}_0 + \vec{J}_0 \times \vec{B}_1] &= 0 \\ \nabla \times \vec{B}_1 &= \mu_0 \vec{J}_1 \\ \nabla \cdot \vec{B}_1 &= 0 \end{aligned} \quad (12)$$

Equation (12) indicates that the Vlasov-fluid marginal stability is also identical with that of MHD. This has the following important consequence. If a threshold wavenumber, β or other plasma parameter is found in ideal MHD, that same threshold applies to the Vlasov-fluid model. Finite Larmor radius effects, or other microscopic effects do not have any effect on the thresholds of instability (although they can effect the growth rates).

The final question is that of growth rates. To estimate growth rates we consider configurations which are basically θ pinches to lowest order and use a trial function approach. The basic idea is to substitute a trial function, which results in a large MHD growth rate, into the Vlasov-fluid model and to see what effects it has on the dispersion relation. This was done for the $m = 1$ and $m = 2$ modes. For the $m = 1$ mode the Vlasov-fluid model yields the following dispersion relation

$$\omega^2 = \omega_M^2 \quad (13)$$

where ω_M^2 is the growth rate obtained by substituting the trial function into the ideal MHD $\delta W(\xi, \xi)$ subject to the normalization

$$K = \frac{1}{2} \int \rho |\xi_{\perp}|^2 d\vec{r}$$

Once again - the Vlasov fluid model gives results essentially identical to ideal MHD. This situation does not prevail for $m = 2$. In this case the dispersion relation is found to be

$$\omega^2 + \frac{\omega_c}{2} \frac{r_L}{a} Z \left(\frac{a}{r_L} \sqrt{1 - \beta} \right) - \omega_M^2 = 0 \quad (14)$$

where ω_c is the ion gyro frequency, r_L/a is the ratio of gyro radius to plasma radius and Z is the plasma dispersion function. The middle term has two sources of origin. The part arising from the real Z is the familiar finite Larmor radius corrections first calculated by Rosenbluth et al [11] for low β . The contribution due to the $\text{Im } Z$ results from the action of a class of resonant particles, whose ∇B drift keeps them in phase with the perturbation. Equation (14) has been studied in various regimes. The most interesting one is one in which the $m = 2$ growth rate is greatly reduced and in fact becomes exponentially small. This regime is described by

$$1 \gg \frac{1}{(1-\beta)} \left(\frac{r_L}{a} \right)^2 \gg \frac{16 \gamma_M^2}{(v_T/a)^2} \quad (15)$$

where $\gamma_m^2 = -\omega_m^2$ and a/v_T is the ion thermal transit time across the plasma radius. In this regime the ratio of the Vlasov-fluid growth rate γ to the ideal MHD growth rate γ_M is approximately given by

$$\frac{\gamma}{\gamma_M} \approx 2\pi^{\frac{1}{2}} \frac{\gamma_M}{v_T/a} \zeta^3 e^{-\zeta^2} \quad (16)$$

where $\zeta = a\sqrt{1 - \beta}/r_L$.

We can apply these results to Scyllac. The left hand inequality in Eq. (15) is always satisfied for experimental conditions. Substituting the $m = 2$ growth rate yields the following approximate stability condition for the right hand inequality

$$\left(\frac{r_L}{a} \right)^2 > \frac{8(1-\beta)\beta^2}{2-\beta} \epsilon^2 \delta_1^2 \quad (17)$$

This condition is also satisfied for typical experimental parameters, $B = 70\text{kg}$, $T_i = 2\text{ keV}$, $a = .75\text{cm}$, $\beta = .75$, $\delta_1 = .8$ and $\epsilon = .14$. With these parameters ideal MHD predicts a growth time of $\tau = 1\ \mu\text{sec}$ for the $m = 1$ mode and $\tau = \frac{1}{3}\ \mu\text{sec}$ for the $m = 2$ mode.

The Vlasov-fluid growth time, given by Eq. (16) is much slower and is given by $\tau \approx 260\ \mu\text{sec}$. This accounts for the absence of higher m modes in the experiments.

CONCLUSION

We have presented a brief survey of high β , $\ell = 1$ Scyllac theory. The stability of the $m = 1$ mode has been studied in some detail. Recent theory indicates that growth rates and marginal stability are fairly accurately predicted by the original Scyllac ordering for present experimental parameters, despite the fact that the original ordering assumptions are violated. Recent theory also indicates that Vlasov effects are very important for the $m = 2$ mode. The Vlasov-fluid theory predicts a very small $m = 2$ growth rate thereby providing an explanation for why this mode is not seen experimentally even though its MHD growth rate is three times faster than that of the $m = 1$ mode. When Eq. (15) is satisfied the Vlasov-fluid theory in effect justifies the heretofore empirical approach of investigating gross plasma stability by studying ideal MHD equilibria and only the $m = 1$ mode.

ACKNOWLEDGMENT

This work performed under the auspices of the U. S. Atomic Energy Commission.

REFERENCES

- [1] S. C. Burnett, W. R. Ellis, C. F. Hammer, C. W. Harris, F. C. Jahoda, M. Kaufmann, W. E. Quinn, F. L. Ribe, G. A. Sawyer, R. E. Siemon, and K. S. Thomas, Fourth International Conference on Plasma Physics and Nuclear Fusion Research, Madison, Wisconsin, 17-23 June, 1971, Paper J4.
- [2] A. A. Blank, H. Grad, and H. Weitzner in Plasma Physics and Controlled Nuclear Fusion Research (International Atomic Energy Agency, Vienna, 1969), Vol. II, p 607.
- [3] F. L. Ribe and M. N. Rosenbluth, Phys. Fluids 13, 2572 (1970).
- [4] H. Grad and H. Weitzner, Phys. Fluids 12, 1725 (1969).
- [5] M. N. Rosenbluth, J. L. Johnson, J. M. Greene and K. E. Weimer, Phys. Fluids 12, 726 (1969).
- [6] F. L. Ribe "Free-Boundary Solutions for High-Beta Stellarators of Large Aspect Ratio", LA-4098, Los Alamos Scientific Laboratory Report (1969).
- [7] J. Nuhrenberg, Phys. Fluids 13, 2082 (1970).
- [8] H. Weitzner, Phys. Fluids 14, 658 (1971).
- [9] H. Weitzner, Presented at the Sherwood Theory Meeting, Princeton, New Jersey, March 1970.
- [10] J. P. Freidberg and B. M. Marder, Phys. Fluids 14, 174 (1971).
- [11] M. N. Rosenbluth, N. A. Krall, N. Rostoker, Nuclear Fusion: 1962 Supplement, Part 1, p 143.

TOROIDAL HIGH- β EQUILIBRIA

H. WEITZNER

Courant Institute of Mathematical Sciences,
New York University, New York, N. Y.,
United States of America

Abstract

TOROIDAL HIGH- β EQUILIBRIA.

The equilibrium and stability of large-aspect-ratio high-beta toroidal systems with long-wavelength helical fields are studied in an ordering that permits moderate deformations of the plasma column, includes toroidal effects in the stability analysis and yields hopeful stability criteria.

At the 1968 IAEA meeting in Novosibirsk we presented [1] an initial exploration of high beta toroidal equilibria based on the ideal magnetohydrodynamic free boundary model and appropriate to the Scyllac experiment. The equilibrium consisted of a theta pinch bent into a large aspect ratio torus with approximately helically symmetric fields added. In part to avoid the fundamental problems associated with non-existence of exact toroidal equilibria and in part from practical necessity equilibria were calculated by expansion in a small parameter. Motivated by stability properties of the equilibria obtained by us [2] and confirmed by others [3],[4] we introduced a new expansion procedure [5] closer to experimental parameters and found improved stability characteristics in some cases. Various simplifying assumptions were made in the equilibrium expansions which eliminated the effects of toroidal curvature and some of the helical fields from the stability analysis. We give here a more complete study of the equilibrium and stability problem ordering toroidal effects so that their effect on stability is present. With the new ordering, which effectively permits moderate distortions of the plasma column from a circular cross section, and with the effects of many more equilibrium fields included, there is greater freedom to try to select a stable or at least less unstable state. From the earlier results we would have concluded that a theta pinch plus $L=0$ or $L=2$ helically symmetric fields was unstable, while now we are led to speculate that the plasma can deform and adjust itself into a state with greatly reduced growth rate or possibly even a stable state. We describe the model in greater detail before proceeding.

In the free boundary model we assume that the plasma is at constant pressure and is contained within a surface in the approximate shape of a torus. The plasma-vacuum interface is a flux surface for the magnetic fields, assumed to be vacuum fields with a surface current on the interface, and we require total pressure balance across the interface. In discussions of stability we mean stability in terms of the usual energy principle and only for modes which are $m=1$ in leading order. We employ the usual approximately cylindrical toroidal

coordinate system with metric $(ds)^2 = (dr')^2 + (r'd\theta)^2 + ((1+(r'/R)\cos\theta)dz')^2$ where R is the major radius of the torus. We generate an equilibrium from approximately constant fields in the z direction, $\underline{B} = (0, 0, K/(1+(r'/R)\cos\theta))$ and various helical fields of helical wave number k . We introduce two small parameters, $\epsilon = kr_0$, where r_0 is the minor radius of the plasma column and a , a measure of the distortion of the column from the surface $r' = r_0$. In the bulk of the previous work a was the basic small parameter, but now we choose ϵ as the small parameter and $a \lesssim 1$. It is appropriate to take the toroidal curvature r_0/R to be of order $\epsilon^2 a^2$.

Since our basic expansion is not in the distortions of the column from a cylinder we may allow moderate values of the distortions, and we conclude that neither the toroidal shift, the object of many equilibrium computations, nor the index L of a helical magnetic field ($B = \nabla r' C'_L(ikr')\cos L(\theta - kz')$) are well-defined. If the plasma column may move by moderate amounts then we may determine the helical fields and the toroidal shift relative to any reasonable axis, the axis of the plasma column, the axis of the outer conducting wall, or any other such curve. For each axis, a given magnetic field will be represented differently as a superposition of helically symmetric fields and the toroidal shift also changes. When the shifts were the basic small parameters, such effects were automatically small. The correct interpretation of toroidal shifts was one of the aims of a previous note [6]. Before we can proceed we must arbitrarily choose the position of the curve $r' = 0$, and we select it as the axis of the plasma column so as to simplify subsequent computations. Hence, by convention the toroidal shift of the plasma column is identically zero. We have effectively replaced the shift by a $L=1$ helical field. Relative to the interface, the other flux surfaces will be shifted, however.

To leading order in ϵ and in dimensionless variables, $r' = r_0 r, z' = r_0 z$, we take the magnetic field outside the plasma to be

$$\begin{aligned}
 B = B_0 \nabla \cdot \left[& z - \epsilon a (D_1 r - d_1/r) \sin(\theta - \epsilon z) - \frac{\epsilon a^2}{2} (D_2 r^2 - d_2/r^2) \sin(2\theta - 2\epsilon z) \right. \\
 & - \frac{\epsilon a^2}{2} (D_3 r^2 - d_3/r^2) \sin(2\theta - \epsilon z) + \epsilon a^2 \left(\frac{r^2}{4} N + n \log \frac{\epsilon \gamma r}{2} \right) \sin \epsilon z \\
 & - \epsilon a^3 (D_4 r - d_4/r) \sin \theta + \epsilon a^3 (D_5 r - d/r) \sin(\theta + \epsilon z) \\
 & \left. + \frac{\epsilon a^3}{3} (D_6 r^3 - d_6/r^3) \sin(3\theta - \epsilon z) \right. \\
 & \left. + O(\epsilon a^4) + O(\epsilon^2) \right]
 \end{aligned}$$

We note the great variety of fields present. Many are introduced to improve stability properties and in special cases can be ignored. We take a similar magnetic field inside the plasma with all terms singular at the origin dropped, B_0 replaced by $B_0 \sqrt{1-\beta}$ and D_1 and N replaced by \bar{D}_1 and \bar{N} . The

plasma vacuum interface is

$$r = 1 - a\bar{D}_1 \cos(\theta - \epsilon z) + a^2 \left\{ \left(\frac{\bar{D}_1^2}{4} - \frac{\bar{D}_2}{2} \right) \cos(2\theta - 2\epsilon z) - \bar{D}_3 \cos(2\theta - \epsilon z) - \frac{\bar{N}}{2} \cos \epsilon z + \zeta \cos 2\theta \right\} + O(z^3)$$

Among the more pertinent equilibrium relations are the following.

$$D_1 = (1 - \beta/2)\bar{D}_1 \quad D_3 = (1 - \beta/2)\bar{D}_3 \quad N = (1 - \beta)\bar{N}$$

$$d_1 = (\beta/2)\bar{D} \quad d_3 = (\beta/2)\bar{D}_3 \quad n = (\beta/2)\bar{N}$$

$$D_4 + d_4 = (1 - \beta)(\bar{D}_3 + \bar{N}/4) \quad D_5 = (1 - \beta/2)\bar{D}_5 - d_1 \zeta \quad D_6 = (1 - \beta/2)\bar{D}_6 + 3d_1 \zeta$$

$$\bar{D}_4 = D_3 + \bar{N}/4 \quad d_5 = (\beta/2)\bar{D}_5 \quad d_6 = (\beta/2)\bar{D}_6$$

and toroidal pressure balance

$$\bar{D}_1 \frac{\bar{N}}{2} (\frac{3}{2} - \beta) + \bar{D}_1 \bar{D}_3 (1 - \beta/2) = - (r_0/R) (\epsilon^2 a^3)$$

The above relations are rather insensitive to the ordering assumptions and are the appropriate limits of the formulas in [3] and [5]. The same relations apply even if we reverse the relative magnitudes of the fields and assume the L=0 and L=2 fields are $O(\epsilon a)$ and the L=1 fields is $O(\epsilon a^2)$. We may take as independent equilibrium parameters the capital letters either with or without the bars and elliptical distortion ζ , provided only that toroidal pressure balance holds. The position of the outer conductor may be any flux surface of the magnetic field outside the plasma. The equation for the surface will be of the same form as above with the addition of a term corresponding to a shift $a \cos \theta$.

The equilibrium relations indicate the great flexibility the plasma has in adjusting to different conditions. The fields generated by D_4 , d_4 , and \bar{D}_4 are the same as are used in Tokamak to center the plasma column and here they perform the same function. However even with no external centering field, $D_4=0$, the plasma can center itself by appropriate choice of the field inside the plasma, \bar{D}_4 , and the external diamagnetic field, d_4 . Similarly, if it is desirable for for stability to have non-zero ζ , corresponding to a slightly elliptical cross section, then this may be achieved with external sources D_5 and D_6 , or merely by the plasma adjusting itself, \bar{D}_5 , \bar{D}_6 , d_5 and d_6 . We shall make use of this freedom to optimize the stability properties.

The second variation analysis of the stability is intricate but basically straight forward and we shall publish the details elsewhere. We take a perturbation which is principally $m=1$ with very long wavelength z dependence and

add other small $m=1, 2, 3$ terms of order a^2 and other z -dependence. We take the wavelength of the basic $m=1$ mode to be K . After minimization of δW we find that the perturbation is purely $m=1$. We do not give the full expression for δW , but we make several equilibrium optimizations first. If we set $D_2 = 0$ the minimum of δW is increased, and so we take $D_2 = 0$. If both \bar{D}_3 and \bar{N} are non-zero then we choose ζ , D_5 , \bar{D}_5 , D_6 , \bar{D}_6 to be non-zero and of appropriate magnitude to increase the minimum of δW . Since the plasma can adjust the equilibrium to achieve this state without additional external fields we omit further details. If one of \bar{D}_3 and \bar{N} is zero then optimization of δW permits setting the above coefficients to zero. In this case other equally desirable equilibria exist without external fields. After these optimizations we find

$$\delta W = 2\pi^2 R \epsilon^2 B_0^2 \left\{ (2-\beta)K^2 + \frac{\beta^2 a^2 \bar{D}_1^2}{4} - \beta \left((1-\beta/2)\bar{D}_3^2 + \frac{\bar{N}^2}{4} \left(\frac{3-\beta}{2}\right) a^4 + O(a^6) \right) \right\}$$

where ρ is the ratio of conducting wall radius to r_0 .

The reader acquainted with the literature will find the result quite familiar. The first term in the bracket is the usual stabilizing term for kink modes. The second is the wall stabilization effect from the $L=1$ field. In contrast with earlier work on $L=1$ systems, no destabilizing terms appear. By setting $D_2=0$ we have eliminated the term previously found in this ordering [5]. Of course, the destabilizing term of the original ordering [2] is formally too small to appear. This conclusion is clear theoretically and of uncertain experimental validity. The last two terms are the destabilizing effects of $L=0$ and $L=2$ fields present in the old ordering. Indeed the above expression includes as a special case the equilibrium with no $L=1$ fields so that $\bar{D}_1 = D_1 = d_1 = 0$. The destabilizing terms from the interference of $L=0$ and $L=2$ fields proportional to $|D_3 \bar{N}|$ have been eliminated by proper choice of ζ and the associated constants. The toroidal effects are not apparent in the above formula since we have set the plasma shift to zero and expressed the answers in terms of field strengths. However, the field strengths are influenced by toroidal curvature as will be apparent below.

We may present the result in various ways. If we minimize the destabilizing term subject to the equilibrium constraint we find

$$\bar{D}_3 = \frac{\bar{N}}{2} = - (r_0/R) (2/(5-3\beta)) / \epsilon^2 a^3 \bar{D}_1$$

and

$$\delta W = 2\pi^2 R \epsilon^2 B_0^2 \left\{ (2-\beta)K^2 + \beta^2 a^2 \bar{D}_1^2 / \rho^4 - (2\beta/(5-3\beta)) (r_0/R)^2 / \epsilon^4 a^2 \bar{D}_1^2 \right\}$$

For a pure $L=2$ field \bar{N} is zero and $5-3\beta$ is replaced by $2-\beta$ and for a pure $L=0$ field \bar{D}_3 is zero and $5-3\beta$ is replaced by $3-2\beta$.

Hence, optimization on the $L=0$, $L=2$ fields cuts the destabilizing term by approximately $1/2$. Finally, we may give the stability criterion as a relation between the $L=1$ fields and β and r_0/R .

$$\epsilon a \bar{D}_1 \geq \rho \sqrt{\frac{r_0}{R} \left(\frac{2}{\beta(5-3\beta)} \right)^{1/4}}$$

where the left hand side is the magnitude of the radial component of L=1 helical field just outside the plasma. At the optimum value of β , $\beta=5/6$ we have approximately $\epsilon a \bar{D}_1 > \rho \sqrt{\frac{r_0}{R}}$. Again, higher β values are more stable than lower ones, and large deformations of the plasma surface appear to be more stable than small deformations. While the parameters of current experiments stretch the limits of reliability of the formula if indeed they do not violate it, they suggest that $\epsilon \sim 1/5$, $a \bar{D}_1 \sim 3/2$, $\rho \sim 5$, $r_0/R \sim 1/250$ may be almost stable.

It is instructive to compare the predictions of the current work and the earlier work for a toroidal theta pinch with given L=0 or L=2 fields without regard for the requirements of the ordering assumptions. In the original ordering the plasma would shift on the order of (r_0/R) divided by the square of the helical field and achieve an unstable equilibrium. In the new ordering the plasma shifts on the order of one over the square root of the helical distortion induced by the L=0 or L=2 field, adding L=1 fields to the equilibrium, and greatly reducing the growth rates. As the shift in the old ordering increases we pass over to the new result where a large shift, present in the form of a L=1 field, leads to a less unstable, if not stable configuration.

This work was supported by the U. S. Atomic Energy Commission under Contract AT(30-1)-1480.

REFERENCES

- [1] BLANK, A.A., GRAD, H., WEITZNER, H., in Plasma Physics Controlled Nuclear Fusion Research (International Atomic Energy Authority, Vienna, 1969) Vol.II 607.
- [2] GRAD, H., WEITZNER, H., Phys. Fluids 13 (1970) 1725
- [3] RIBE, F.L., Free Boundary Solutions for High-Beta Stellarators of Large Aspect Ratio, LA4098 Los Alamos Scientific Laboratory Report (1969)
- [4] ROSENBLUTH, M.N., JOHNSON, J.L., GREEN, J.M., WEIMER, K.E., Phys. Fluids 12 (1969) 726.
- [5] WEITZNER, H., Phys. Fluids 14 (1971) 658
- [6] GRAD, H., WEITZNER, H., Phys. Fluids 13 (1970) 1418, see also [2].

PLASMA CONTAINMENT IN CLOSED LINE SYSTEMS

H. GRAD

Courant Institute of Mathematical Sciences,
New York University, New York, N. Y.,
United States of America

Abstract

PLASMA CONTAINMENT IN CLOSED LINE SYSTEMS.

Plasma equilibria with exact magnetic surfaces are obtained only in configurations with an ignorable co-ordinate. Equilibria with closed magnetic lines result from a different symmetry, reflection in a plane. The appropriate analytical methods and the ensuing plasma properties differ profoundly from magnetic-surface and closed-line equilibria. The general theory is developed for scalar-pressure and guiding-centre models and calculate a number of special results for a bumpy torus with small toroidal curvature. On occasion, the toroidally perturbed pressure profile develops islands ("bananas"). Classical resistive diffusion is atypical; the standard procedures fail, and diffusion does not follow the standard $1/B^2$ formula.

1. INTRODUCTION

Most toroidal calculations postulate closed flux surfaces. They are theoretically closed only with an ignorable coordinate; but approximate surfaces can be found in systems weakly perturbed from axial symmetry (e.g. a Stellarator). Closed lines result from the more primitive symmetry of reflection in a plane. This is more flexible than the restriction to an ignorable coordinate (without regard to desirability).

We present a self-consistent, finite β theory for scalar pressure and guiding center models. Closed magnetic lines provide several unusual features. First, there are no static equilibria on the drift time scale. Second, the assumption inherent in any perturbation theory, that the equilibrium varies continuously with parameters (such as current in a coil, wall shape, weak toroidal curvature, etc.) does not hold. A certain condition, marginal equilibrium, implies no neighboring states with the given topology. In this case, a "vertical field" (Tokamak terminology) does not induce a simple radial shift of the plasma column. Mathematically, marginal equilibrium results from a continuous spectrum reaching the origin. This implies a singular perturbation, in the present case a change in topology, with islands; but this does not herald instability. In special cases we calculate the toroidal perturbation, the marginal criterion, the effect of the vertical field, and estimate the island thickness.

Classical diffusion is described as a slow progression through perfectly conducting equilibria. This assumption, plus $\text{curl } E \sim 0$, leads to the Pfirsch-Schlüter formulas, banana diffusion, etc. Both assumptions can be violated in sheared systems but are always violated in closed line systems. At arbitrarily small plasma β and resistivity, fast MHD waves are automatically generated, coupling to the "slow" diffusion.

An estimate of the scaling for large aspect and low β shows no classical $1/B^2$ factor (although a quick standard calculation would incorrectly give a standard formula).

2. GENERAL FORMULATION

With respect to a given plane, S , we introduce two symmetry classes for vectors (Fig. 1):

axial: normal component even, tangential odd

polar: normal component odd, tangential even

This terminology is suggested by our assumption that the magnetic field, B , has the first symmetry and $J = \text{curl } B$ the second. B is normal to S and J lies within S . The symmetry guarantees that if B intersects S twice, it is a closed curve. J -lines are not necessarily closed (nor is $J \cdot B = 0$), but if a surface contains J , then J -lines also close. In a bumpy torus there may be several planes of symmetry. External coils are bound by the same symmetry as J . An arbitrary coil can be given on one side of S if its image is put on the other (Fig. 1b). For scalar fields, we also have two symmetry classes, viz. even and odd under reflection. We see that $\nabla\phi$ is axial if ϕ is odd and polar if ϕ is even; ϕA preserves the symmetry of A if ϕ is even and reverses it if ϕ is odd; $A \times \text{curl } A$ and $A \cdot \nabla A$ are polar for either symmetry of A .

The static equilibrium of a perfectly conducting, scalar pressure plasma is governed by the system

$$J \times B = \nabla p, \quad J = \text{curl } B, \quad \text{div } B = 0 \quad (2.1)$$

The mathematical theory follows from the presence of one elliptic characteristic plus the field lines, counted twice, as degenerate real characteristics. This is more evident in the following formulation

$$\begin{aligned} B \cdot \nabla p &= 0, & B \cdot \nabla \zeta &= 1 & \text{curl } B &= J \\ J &= \nabla \zeta \times \nabla p & \text{div } B &= 0 \end{aligned} \quad (2.2)$$

where the elliptic cone is visible on the right and the real characteristics on the left. The characteristics suggest an iteration process [1]: given a field B , calculate p and ζ , then J on the left; then recalculate B on the right, given J . For certain low β closed line configurations, this procedure has recently been shown to converge [2]. It is the real characteristics which give nonexistence of solutions in asymmetric sheared geometries [3]. They integrate out explicitly with an ignorable coordinate [1]. Only in the present closed line theory is the full significance of the combination of characteristics felt.

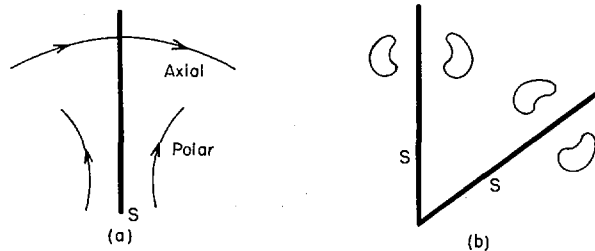


Fig. 1. Symmetry: a) axial and polar symmetry classes; b) arbitrary coil on one side of S with image put on the other.

To exploit the symmetry, we replace (2.2) by its equivalent,

$$\begin{aligned} \mathbf{B} \cdot \nabla p &= 0 & \mathbf{B} &= \nabla \phi + \zeta \nabla p \\ \mathbf{B} \cdot \nabla \zeta &= 1 & \text{div } \mathbf{B} &= 0 \end{aligned} \quad (2.3)$$

The domain is cut (e.g. at S) since ϕ and ζ are multivalued (as are $\nabla \phi$ and $\nabla \zeta$). Introducing

$$[\phi] = \oint \nabla \phi \cdot d\mathbf{x} = \oint \mathbf{B} \cdot d\boldsymbol{\ell}, \quad [\zeta] = \oint \nabla \zeta \cdot d\mathbf{x} = \oint d\boldsymbol{\ell}/B, \quad (2.4)$$

the condition that B be single-valued, viz. $\nabla[\phi] + [\zeta]\nabla p = 0$ implies that

$$[\phi] = \tau(p), \quad [\zeta] = q(p) = -\tau'(p) \quad (2.5)$$

This is the familiar condition that $\oint d\boldsymbol{\ell}/B$ be constant on each p-surface. The integrals in (2.4) are path-independent on a given surface (but not in three dimensions). Clearly p is even and ϕ and ζ are odd.

For a guiding center formulation, the pair of distribution functions, $f_{\pm}(\epsilon, \mu, \psi)$ determines the charge neutralization potential, $\Phi(B, \psi)$, thence a pressure function, $p_{\parallel} = p(B, \psi)$. Given $p(B, \psi)$, the problem reduces to a system of differential equations [4]. A convenient specialization, more easily matched to available experimental data, is $p = p_1(\psi)p_2(B)$. In this case, the formulation is

$$\begin{aligned} \mathbf{B} \cdot \nabla p_1 &= 0 & \sigma \mathbf{B} &= \nabla \phi + \zeta \nabla p_1 \\ \mathbf{B} \cdot \nabla \zeta &= p_2 & \text{div } \mathbf{B} &= 0 \end{aligned} \quad (2.6)$$

where

$$\sigma(B, \psi) = 1 - p_1(\psi)p_2'(B)/B \quad (2.7)$$

The single-valuedness condition is now

$$[\phi] = \oint \mathbf{B} d\boldsymbol{\ell} = \tau(p_1), \quad [\zeta] = \oint p_2(B) \frac{d\boldsymbol{\ell}}{B} = q(p_1) = -\tau'(p_1) \quad (2.8)$$

Note that $\oint d\boldsymbol{\ell}/B$ is a relevant quantity only for scalar pressure.

3. LARGE ASPECT EXPANSION

Introduce cylindrical coordinates (R, θ, Z) and "toroidal" coordinates (r, θ, z) as in Fig. 2.

$$\begin{aligned} R &= R_0 + r \sin \theta, & Z &= r \cos \theta, & R_0 \theta &= z \\ ds^2 &= dR^2 + R^2 d\theta^2 + dZ^2 = dr^2 + r^2 d\theta^2 + (1+r \sin \theta/R_0)^2 dz^2 \end{aligned} \quad (3.1)$$

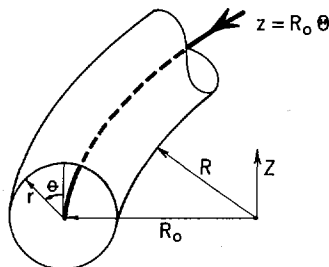


Fig. 2. Cylindrical and "toroidal" co-ordinates.

We expand in r/R_0 , both the coordinate system and the physical quantities, $\bar{p} = p_0 + p$, $\bar{B} = B_0 + B$, etc. The operator $\bar{\nabla}$ is "exact", and ∇ is the lowest order gradient, $\nabla = (\partial/\partial r, \partial/r\partial\theta, \partial/\partial z)$. We calculate

$$\begin{aligned}\bar{B} &= \bar{\nabla}\bar{\phi} + \bar{\zeta}\bar{\nabla}\bar{p} = B_0 + \nabla\phi + \zeta_0\nabla p + \zeta\nabla p_0 - \frac{r \sin\theta}{R_0} B_z^0 e_z \\ &= B_0 + \nabla f + \zeta\nabla p_0 - p\nabla\zeta_0 - \frac{r \sin\theta}{R_0} B_z^0 e_z\end{aligned}\quad (3.2)$$

where ϕ has been replaced by the single-valued function f ,

$$f = \phi + \zeta_0 p \quad (3.3)$$

Next, taking out factors $\sin\theta$ from p , ζ , f , B_r , B_z ; and $\cos\theta$ from B_θ (without changing notation, $p \rightarrow p \sin\theta$, etc.), we obtain

$$rB_\theta = f, \quad \hat{B} = \nabla f + (\zeta\nabla p_0 - p\nabla\zeta_0) - \frac{r}{R_0} B_z^0 e_z \quad (3.4)$$

where $\nabla = (\partial/\partial r, \partial/\partial z)$ and $\hat{B} = (B_r, B_z)$.

The result is a system of three equations for p , ζ , and f :

$$B_0 \cdot \nabla p + X\zeta - Yp + \nabla p_0 \cdot \nabla f = (2r/R_0) B_z^0 (\partial p_0 / \partial z) \quad (3.5)$$

$$B_0 \cdot \nabla \zeta + Y\zeta - Zp + \nabla \zeta_0 \cdot \nabla f = (2r/R_0) B_z^0 (\partial \zeta_0 / \partial z) \quad (3.6)$$

$$\Delta f - f/r^2 + \text{div}(\zeta\nabla p_0 - p\nabla\zeta_0) = (2r/R_0) (\partial B_z^0 / \partial z - B_r^0 / 2r) \quad (3.7)$$

where

$$X = |\nabla p_0|^2, \quad Y = \nabla p_0 \cdot \nabla \zeta_0, \quad Z = |\nabla \zeta_0|^2 \quad (3.8)$$

Although p , ζ , and f are coupled, the mathematical structure is such that we can interpret (3.7) as an elliptic equation in f , and (3.5) and (3.6) as a pair of ordinary differential equations for (p, ζ) along a magnetic line. Boundary conditions will be given in the next section.

Eliminating ζ from (3.5), (3.6) and treating

$$g_1 = (2r/R_0) B_z^0 (\partial p_0 / \partial z) - \nabla p_0 \cdot \nabla f, \quad g_2 = (2r/R_0) B_z^0 (\partial \zeta_0 / \partial z) - \nabla \zeta_0 \cdot \nabla f \quad (3.9)$$

as inhomogeneous terms, we obtain for p the second order equation

$$(B_0 \cdot \nabla) \left(\frac{1}{X} B_0 \cdot \nabla p \right) + \Omega_0 p = G_0 \quad (3.10)$$

$$\Omega_0 = J_0^2 / X - (B_0 \cdot \nabla) (Y/X), \quad G_0 = (B_0 \cdot \nabla + Y) (g_1/X) - g_2$$

A similar equation can be found for ζ alone, but it is less useful.

To study non-monotone pressure profiles more easily, we write $\nabla p_0 = p_0'(\psi_0) \nabla \psi_0$, and for an axially symmetric B_0 obtain

$$\frac{d}{d\ell} \left(\frac{B_0}{|\nabla \psi_0|^2} \frac{dp}{d\ell} \right) + p_0' \Omega_1 p = (p_0')^2 G_0 / B_0 \quad (3.11)$$

$$p_0' \Omega_0 / B_0 \equiv \Omega_1 = \frac{2(\kappa_0 \cdot \nabla \psi_0)}{B_0 |\nabla \psi_0|^2} \quad (3.12)$$

where κ_0 is the field line curvature. For later reference, note

$$\Omega^* = \oint \Omega_1 d\ell = p_0' \oint d\ell / B_0^3 - q_0' \quad (3.13)$$

In axial symmetry, one can verify that $\Omega^* < 0$ for any pressure profile and β (note that q_0' is v'' in a common notation).

For the guiding center formulation, a similar calculation [introducing $\bar{p}_1 = p_1 + p$, $\bar{\sigma} = \sigma_0 + \sigma$, $|\bar{B}| = |B_0| + b$, $b = B_0 \cdot B/B_0$, etc.] yields the result

$$\begin{aligned} \sigma_0 \hat{B} &= \nabla f + (\zeta \nabla p_1 - p \nabla \zeta_0) - \sigma B_0 - \frac{r}{R_0} \sigma_0 B_z^0 e_z \\ \sigma_0 r B_\theta &= \phi + \zeta_0 p_1 \equiv f \end{aligned} \quad (3.14)$$

The auxiliary variables σ and b are given in terms of p through

$$\begin{aligned} \sigma + (p_2'/B_0)p + p_1(p_2'/B_0)' b &= 0 \\ B_0^2 \sigma + p_2 p + \sigma_0 B_0 b &= B_0 \cdot \nabla f - \frac{r}{R_0} \sigma_0 (B_z^0)^2 \end{aligned} \quad (3.15)$$

The system of equations equivalent to (3.5)-(3.7) is

$$\sigma_0 B_0 \cdot \nabla p + \nabla p_1 \cdot (\zeta \nabla p_1 - p \nabla \zeta_0) + \nabla p_1 \cdot \nabla f = (2r/R_0) \sigma_0 B_z^0 (\partial p_1 / \partial z) \quad (3.16)$$

$$\begin{aligned} \sigma_0 B_0 \cdot \nabla \zeta + \nabla \zeta_0 \cdot (\zeta \nabla p_1 - p \nabla \zeta_0) + p_2' b - p_2 \sigma + \nabla \zeta_0 \cdot \nabla f \\ = (2r/R_0) \sigma_0 B_z^0 (\partial \zeta_0 / \partial z) \end{aligned} \quad (3.17)$$

$$\begin{aligned} \text{div}(\nabla f / \sigma_0) - f/r^2 + \text{div}[(\zeta \nabla p_1 - p \nabla \zeta_0) / \sigma_0] - (B_0 \cdot \nabla)(\sigma / \sigma_0) \\ = (2r/R_0) (\partial B_z^0 / \partial z - B_r^0 / 2r) \end{aligned} \quad (3.18)$$

The toroidally perturbed particle drift surfaces¹ (which are extraneous to this theory) can be calculated, once (p, ζ, f) are known, from an equation similar to (3.17) in which $p_2(B)$ is replaced by $B(B_1 - B)^{1/2}$.

4. BOUNDARY CONDITIONS

The large aspect theory is not qualitatively different from the original. There are still elliptic and hyperbolic characteristics, but the latter are now known, and there are only two variables, r and z . Given an elliptic boundary condition for f , and a pair of boundary conditions on each magnetic line for p and ζ , we must iterate on (3.5)-(3.7), solving (3.5) and (3.6) for p and ζ , given f ; then solving (3.7) for f , given p and ζ .

For p and ζ , boundary conditions are given at $z = 0$ and $z = L$ (the basic periodic length is $L = \pi R_0 / n$). We can take $\zeta(0) = 0$. If $\bar{q}(p)$ is a fixed function, then at $z = L$ we have $\zeta = q_0'(p_0)p$. With ψ_0 as independent variable, a set of boundary conditions is

$$\zeta = 0 \text{ at } z = 0, \quad p_0'(\psi_0)\zeta = q_0'(\psi_0)p \text{ at } z = L \quad (4.1)$$

Alternatively, from symmetry alone, we require

$$\partial p / \partial z = 0 \text{ at } z = 0 \text{ and } z = L \quad (4.2)$$

Examining (3.5), we find that the alternative boundary conditions (4.1) and (4.2) are exactly equivalent.

Alternative boundary conditions to $\bar{p}(\bar{q})$ fixed (e.g. the adiabatic constraint, $\bar{p}\bar{q}'$ fixed), can be met by extending

1. Numerical orbit calculations in a vacuum field are given in [5].

the basic perturbation to include $m = 0$ as well as $m=1$ terms,

$$\bar{p} = p_0(r, z) + [p(r, z) \sin\theta + \tilde{p}(r, z)]/R_0 \quad (4.3)$$

but this will not be pursued here.

For the elliptic boundary condition, we can take $f(0) = 0$, $f(L) = 0$. If the original field, B_0 , is generated by coils, the remaining boundary condition on f is regularity at infinity. If the plasma is contained within a conducting shell, the boundary condition $B \cdot n = 0$ (together with $p = 0$) leads to the boundary condition on f ,

$$\partial f / \partial n + \zeta \partial p_0 / \partial n = (r/R_0) (B_z^0 B_r^0 / B_0) \quad (4.4)$$

5. SPECIAL CASES

First consider an expansion in r , near the magnetic axis. We solve for p and ζ considering f to be given (f cannot be obtained by expansion since it is inherently global). It suffices to consider the "inhomogeneous" terms contributed by f and r/R_0 separately.

The unperturbed equilibrium is axially symmetric:

$$\begin{aligned} \psi_0 &= \frac{1}{2} b(z) r^2 + \frac{1}{8} (c - \frac{1}{2} b'') r^4, & p_0 &= a - \frac{1}{2} b(z) c r^2, \\ B_z^0 &= b(z) + \frac{1}{2} (c - \frac{1}{2} b'') r^2, & B_r^0 &= -\frac{1}{2} b' r + \frac{1}{16} b'''' r^3 \end{aligned} \quad (5.1)$$

$$\zeta_0 = \int_0^z \frac{dz}{b(z)} - \frac{1}{2} b r^2 \int_0^z (c - \frac{1}{2} b'') \frac{dz}{b^3}, \quad q_0 = \oint \frac{dz}{b(z)} - \psi_0 \oint (c - \frac{1}{2} b'') \frac{dz}{b^3}$$

To the order kept, the free parameters are two constants, a and c (the pressure and its gradient on axis); also one function, $b(z)$ (the field strength on axis). The expansion in r is equivalent to one in ψ_0 ; to lowest order $r^2 = 2\psi_0/b(z)$, whence $p_0 = a - c\psi_0$, etc.

Taking r/R_0 first, we observe in (3.9) that $g_1 = O(r^3)$ and $g_2 = O(r)$. Ordering $p = O(r)$ and $\zeta = O(r)$, to lowest consistent order,

$$B_0 \cdot \nabla p = 0, \quad B_0 \cdot \nabla \zeta - p |\nabla \zeta_0|^2 = 2r/R_0 \quad (5.2)$$

Solving, subject to boundary conditions (4.1),

$$p = - (2rb^{1/2} p_0' / R_0 \Omega^*) \oint dz / b^{3/2} \quad (5.3)$$

$$\Omega^* = - \frac{3}{2} \oint (b'/b^2)^2 dz \quad (5.4)$$

From $\bar{p} = a - bcr^2/2 + p \sin\theta$, we calculate an inward plasma shift

$$\delta = p/rbc = - [4/3 \oint dz / b^{3/2}] / [R_0 b^{1/2} \oint (b'/b^2)^2 dz] \quad (5.5)$$

The plasma displacement is large if the mirrors are weak (b' small). This is consistent with the canted high β mirror experiments, where the shift with plasma present is smaller than in a vacuum; and where it is observed that the profile, $b'(z)$ is much steeper with plasma present [6].

For the contribution of f to δ , the inhomogeneous term in (3.7) is $O(r)$ which leads to $f = O(r^3)$; this is dominated by the homogeneous solution, $\Delta f - f/r^2 = 0$, which can be $O(r)$.

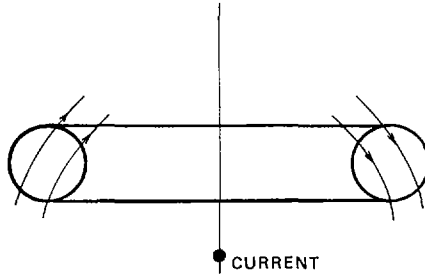


Fig.3. Vertical field.

The leading term, $f = f_0(z)r + \dots$, is influenced by coils, conducting walls, etc. and also by any explicit external coils (Fig. 3). We can calculate δ for any profile $f_0(z)$, but for simplicity take the simplest odd function, $f_0(z) = f_0 \operatorname{sgn} z$. Inserting $f = f_0 r$, $p = \hat{p}(z)r$, $\zeta = \hat{\zeta}(z)r$ (5.6)

into the lowest order system

$$B_0 \cdot \nabla p = -\nabla p_0 \cdot \nabla f, \quad B_0 \cdot \nabla \zeta - p |\nabla \zeta_0|^2 = -\nabla \zeta_0 \cdot \nabla f \quad (5.7)$$

and applying the boundary conditions (4.1) yields

$$\delta = (2/b)^{1/2} f_0 \left[\frac{\oint_0^L \left\{ (b'/b^2)^2 dz \right\} dz / b^{1/2}}{\oint (b'/b^2)^2 dz} \right] \quad (5.8)$$

In contrast to the toroidal effect, this contribution to δ is not exaggerated in a weak mirror field.

Another solvable special case is near a pressure peak, $p_0' \sim 0$. This is more interesting when q_0' is also small, of the same order as p_0' . The boundary condition (4.1) shows that $p \sim \zeta$, and the lowest order system is

$$B_0 \cdot \nabla p = 0, \quad B_0 \cdot \nabla \zeta - \zeta p = g_2 \quad (5.9)$$

The solution is easily obtained,

$$p/p_0' = \left[\oint g_2 d\ell / B_0 \right] / \left[q_0' - p_0' \oint \zeta d\ell / B_0 \right] \quad (5.10)$$

This formula is not restricted to an axially symmetric B_0 , and the denominator may vanish.

Finally consider low β in the singular guiding center limit in which $p_1 p_2''$ is kept finite as $p_1 \rightarrow 0$ (e.g. this is automatic if the mirrors become weak with β). In particular,

$$\Delta = 1 - p_1(\psi) p_2''(B) \quad (5.11)$$

may be small, but we insist that $\Delta > 0$ everywhere to avoid the mirror instability. For simplicity take $g_1 = g_2 = 0$. First, $B_0 \cdot \nabla p = 0$ or $p = p(\psi_0)$. For ζ , using only $\zeta(0) = 0$,

$$\zeta(L) = p \oint \left\{ (\nabla \zeta_0 \cdot \nabla \psi_0)^2 / |\nabla \psi_0|^2 + [p_2^2/B_0^2 - (p_2')^2] / \Delta_0 \right\} d\ell / B_0 \quad (5.12)$$

With axial symmetry, we also have

$$\nabla \zeta_0 \cdot \nabla \psi_0 = |\nabla \psi_0|^2 \int_0^L Q d\ell, \quad q_0' = \int_0^L Q d\ell \quad (5.13)$$

$$Q = (B_0^2 / \Delta_0) (p_2 / B_0^2)' (\kappa_0 \cdot \nabla \psi_0) / |\nabla \psi_0|^2 \quad (5.14)$$

An eigenvalue is reached if ζ/p from (5.12) is equal to q_0'/p_1' . This can occur if Δ_0 is small in an appropriate region of the plasma.

6. MARGINAL PERTURBATION OF EQUILIBRIUM - DISCUSSION

The (ζ, p) equations take a form which can admit eigenvalues. The displacement δ can be expected to diverge near such a flux surface. Such an occurrence signals a change in the equilibrium topology but is not related to dynamic stability (although the term stability is sometimes used to refer to singular perturbations of equilibria).

A basic question is, when do small perturbations in applied field, toroidal curvature, etc. yield equilibria which are qualitatively similar to the original? As an assumption, this is implicit in almost all theoretical calculations. A smooth perturbation, $\psi_0 + \psi_1(x, y)$, of a function $\psi_0(r)$ with a maximum at $r = 0$, also has a unique maximum near $r = 0$, with contours that are slightly shifted, approximate circles. On the other hand, a function ψ_0 which attains its maximum on a curve, say at $r = a$, is degenerate, and almost any perturbation will destroy this property. For example, a volcano with circular contours opens up into a banana region (Fig. 4). If ψ is a flux function (e.g. in a z-pinch with reversed J_z), almost any perturbation will violate the constraints implicit in perfect conductivity.

A more interesting example is a straight screw pinch with two flux functions corresponding to B_θ and B_z . This cylindrical equilibrium can be described in helical coordinates $\Phi = \theta - kz$, for any given k . The helical description assigns a unique flux function as a linear combination of the two cylindrical fluxes. The helical flux function reaches a maximum and reverses if the helical pitch (defined by k) matches the magnetic field pitch. In other words, there is a range of "resonant" values of k for which all neighboring helical equilibria have islands or "pressure bananas". In dynamic stability analysis, a resonant perturbation is stable or not depending on Suydam's criterion. But the destruction of simple flux surfaces depends on the resonance alone. In a δW stability analysis, a resonance implies that the minimum value (positive or negative) is approached but not attained.

More generally, perturbing a dynamical system whose spectrum is bounded away from the origin will give a unique neighboring equilibrium (the inhomogeneous equation can be solved).

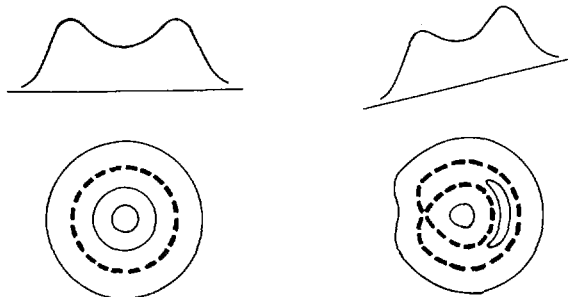


Fig.4. Volcanic bananas.

Marginal stability, with a point eigenvalue at the origin, generally separates stable from unstable equilibria; but it also indicates the existence of nonunique bifurcations, usually with a change in the symmetry of the equilibrium [7]. A continuum that reaches the origin is marginal with respect to equilibrium, but not usually with respect to stability.

The existence of a homogeneous solution (p, ζ) is local to each individual flux surface. Thus a discrete eigenvalue for (p, ζ) indicates a continuum for the complete dynamical system (i.e. for δW). We can expect, in general, that δ will diverge and reverse sign across a flux surface where a (p, ζ) eigenvalue is reached, forming a banana region. However, the actual situation is more complex.

Since (3.11) is self-adjoint, it is related to the problem of minimizing

$$U = \oint (B_0 / |\nabla \psi_0|^2) (dp/d\ell)^2 d\ell - p_0' \oint \Omega_1 p^2 d\ell \quad (6.1)$$

subject to $\oint p^2 d\ell = 1$ and the boundary conditions (4.2). We note the sign of the smallest eigenvalue λ_0 ; $\lambda_0 = 0$ is marginal. This variational problem (in particular the sign of λ_0) has no relation to the dynamic stability of the original equilibrium. Since $p = 1$ is allowed as a test function, $\Omega^* = 0$ implies $\lambda_0 < 0$. The form (4.1) of the boundary condition suggests that the two special cases $p_0' = 0$ and $q_0' = 0$ deserve special study. Clearly, $\lambda_0 = 0$ when $p_0' = 0$; also, λ_0 changes sign with p_0' ($\lambda_0 \sim -p_0' \Omega^*$ for small p_0'). However, further examination shows that the inhomogeneous terms are automatically compatible; p/p_0' is finite and there is no singularity when λ_0 vanishes with p_0' . Evidently $\lambda_0 < 0$ when $p_0' \Omega^* > 0$; also $\lambda_0 < 0$ for large p_0' of either sign. Thus, when $p_0' \Omega^* < 0$, λ_0 must change sign as $|p_0'|$ increases. From this we conclude that the Elmo experiment, with reversed pressure profile, will have a nontrivial eigenvalue (i.e. $\lambda_0 = 0$ where $p_0' \neq 0$) at sufficiently high β . Clearly, $\lambda_0 < 0$ at the edge of the plasma where $p_0' < 0$, and λ_0 reverses sign at the pressure peak. At high β (this remains to be checked quantitatively with Elmo parameters), $\lambda_0 < 0$ near the axis, which implies the existence of an interior marginal surface.

There is no implication with regard to λ_0 , when $q_0' = 0$, and $\zeta(L)/q_0'$ remains finite. However, if q_0' and p_0' vanish near one another, then the existence of a nearby marginal surface is guaranteed [cf. (5.10)]. A simple estimate of the banana thickness is

$$\delta = 2 \left[\oint g_2 d\ell / B_0 \right]^{1/2} / \left[q_0'' - (p_0' \oint z d\ell / B_0)' \right]^{1/2} |\nabla \psi_0| \quad (6.2)$$

7. CLASSICAL DIFFUSION

Classical (including "neoclassical") diffusion in systems with flux surfaces and shear is based on two assumptions: first, that the process is quasistatic, with diffusion inducing a slow progression through perfectly conducting equilibria; second, that at low β , $\text{curl } E = 0$ and $E = \nabla \phi$. Both postulates were introduced by Kruskal and Kulsrud for MHD, implemented in special geometries by Pfirsch and Schluter, and extended to

guiding center theory by Galeev and Sagdeev. The basic calculation in the MHD case proceeds from Ohm's law, $E + u \times B = \eta J$, in the averaged form

$$\langle E \cdot J \rangle - \langle u \cdot J \times B \rangle = \langle \eta J^2 \rangle \quad (7.1)$$

The term $\langle E \cdot J \rangle$ is zero for single-valued ϕ and, more generally, depends only on $\oint E \cdot dx$, not on the local distribution of ϕ . The quasistatic assumption, $J \times B = \nabla p$, gives the net diffusive flow, $\langle u \cdot \nabla p \rangle$, directly in terms of equilibrium quantities. By inspection, we see that the net diffusion velocity scales as β (this is commonly, but imprecisely, referred to as $1/B^2$ scaling).

More recent theory has shown that $\text{curl } E \sim 0$ is frequently violated even at low β [8]. In many such cases, it is possible to replace the standard theory by one which incorporates $\partial B / \partial t$ while still quasistatic. The results are non-standard, but still classical (i.e. non-turbulent). In the present problem, with closed lines, neither postulate can be kept; $\text{curl } E$ is comparable to E at low β , and the quasistatic assumption is automatically violated with arbitrarily small resistivity. The standard estimate from (7.1) is invalid because of the interference of waves ($\rho du/dt \sim \nabla p$). The non-steady convection is an unavoidable consequence of the diffusion process itself.

With shear, the Kruskal-Kulsrud postulate implies that $\langle J \cdot B \rangle = 0$ on a flux surface; in the closed line system, $\langle J \cdot B \rangle = 0$ on each line. We ask whether $\oint E \cdot dx = \oint \eta J \cdot dx$ can be zero (or the same constant) on each line. The answer is that it cannot. The equilibrium formulas allow the variation of $\oint E \cdot dx$ from line to line on a flux surface to be calculated. A more complicated argument shows that we cannot retain the quasistatic assumption, $\nabla p = J \times B$, even dropping $\text{curl } E = 0$. In other words, any slight resistivity induces plasma flow which destroys the classical estimate of diffusion based on (7.1). However, taking only the leading term in the large aspect expansion does allow a quasistatic calculation of diffusion. This is obtained as a compatibility condition relating $\partial p / \partial t$ to p , using the fact that $\partial p / \partial t$ is related to $\partial B / \partial t$, therefore to E , therefore to ηJ which is in turn related to p . In particular, the diffusion rate does not scale as β (or $1/B^2$). This calculation will be presented elsewhere.

The basic qualitative difference between diffusion in sheared systems and in closed line systems is that whereas in the former, uneven diffusion across a flux surface can be compensated by flow along the lines, in the latter it gives rise to convection of magnetic lines.

8. CONCLUSION

For a "normal" pressure profile, $p'_0 < 0$, in an axially symmetric mirror machine ($\Omega^* > 0$), λ_0 is always negative and the pressure surfaces remain simple when perturbed. At high β , a nonmonotone pressure profile can create a marginal situation in which any perturbation produces islands. The same is true at low β with a normal pressure profile if the plasma is sufficiently anisotropic or if the fields are sufficiently asymmetric (as in a magnetic well geometry).

We would expect islands to be characterized by a flat pressure distribution, possibly by a flat electrostatic potential signature, almost certainly by enhanced diffusion across

the island region. A "vertical" field, in such a situation, could be used to control the island structure and could, in theory, remove the islands to first order.

Diffusion, even in the absence of islands, is quite non-standard, not only in magnitude, but in scaling and even in concept.

The very difficult theoretical problem of the comparison between a closed line system and one with very small shear can be analyzed in special cases by studying the perturbed spectrum, but these results will be presented elsewhere.²

REFERENCES

1. Grad, H., Rubin, H., Proc. Second Int. Conf. Peaceful Uses (Geneva, 1958) 31, 190.
2. Lortz, D., Z. angew. Math. Phys., 21 (1970) 196.
3. Grad, H. Phys. Fluids, 10 (1967) 137.
4. Grad, H., Proc. Symp. Appl. Math., 18, Am. Math. Soc. (1967) 162.
5. Gibson, G., Jordan, W. C., Lauer, E. J., Woods, C. H. Phys. Fluids 7 (1964) 548.
6. Dandl, R. A., et al., Paper CN 28/G-4, These Proc.
7. Marder, B., Weitzner, H. Plasma Phys., 12 (1970) 435.
8. Grad, H., Hogan, J., Phys. Rev. Letters, 24 (1970) 1337.

This work was supported by the U. S. Atomic Energy Commission under Contract AT(30-1)-1480.

Note Added in Proof:

The compatibility condition $\langle J \cdot B \rangle = 0$ which is required by the classical diffusion calculation is automatically satisfied because of the symmetry of this geometry. The classical formulas therefore apply in this geometry, even without interference from transient skin effect. The complications discussed in Sec. 7 do not occur in this geometry.

² H. Grad, J. Marsh, and H. Weitzner, to appear.

PLASMA HEATING BY STRONG SHOCK WAVES*

Y.G. CHEN, C.K. CHU, R.A. GROSS, E. HALMOY,
P. MORIETTE, S. SCHNEIDER
Columbia University, New York, N. Y.,
United States of America

Abstract

PLASMA HEATING BY STRONG SHOCK WAVES.

About 10^4 cm³ of plasma at $T \sim 1$ keV, $n \sim 1 \times 10^{16}$ cm⁻³, were created by fast collisional shock waves in an electromagnetic shock tube. The speed of these shock waves ranges up to 4×10^8 cm/s, corresponding to an acoustic Mach number of 3200 and an Alfvén-Mach number of 15. These experiments were performed in a 3-metre-long coaxial electromagnetic shock tube, employing a 60- μ f, 120-kV capacitor bank which produces a 2×10^8 -A drive current. The pre-shock hydrogen initial state was $T = 239^\circ\text{K}$, $p = 50$ mTorr. The pre-shock 7.2-kG transverse magnetic field was used to keep the shock thickness small and retard plasma interaction with the walls. Separation of the transverse ionizing shock wave from the driving current was clearly observed, and a hot dense plasma was created behind the shock wave. The state of this plasma was determined by laser interferometer measurements, X-ray bremsstrahlung spectra, a particle energy analyser, probes, and neutron detectors. The shock-created plasma contained an azimuthal magnetic field of $B \sim 22$ kG. When deuterium gas was used, neutrons were detected and we estimate a yield of about 5×10^5 neutrons per shot. The transverse ionizing shock thickness, as determined by magnetic field structure, was found to be from 5 to 80 cm thick, the larger values occurring at higher shock speeds. These thicknesses are found to agree with the calculations made from a two-fluid MHD computer code employing classical plasma transport properties. The calculated structure of these collisional shock waves predict that the ion temperature substantially exceeds the electron temperature.

1. INTRODUCTION

Shock wave heating of plasma to fusion temperatures is being studied in many laboratories and research in this field has been summarized recently by Chu and Gross [1]. We have studied strong ionizing collisional shock waves of sufficiently high speed required to produce a hot plasma with fusion reactions. Collisional shock waves are expected to have a structure in which the ion temperature exceeds the electron temperature, a condition of particular interest for pulsed fusion reactors. Elementary theory [see, e.g., ref. 2] predicts that a strong shock wave propagating with a speed u_s into a gas of density ρ_1 and transverse magnetic field B_1 , will produce a temperature

* This research was supported by contracts AF 44620-71-C-0010 and AT (30-1)-3954.

$$kT_2 \approx \frac{m_H}{16} \left(\frac{3}{2} u_s^2 - \frac{15}{2} \frac{B_1^2}{\mu_0 \rho_1} \right) \quad (1)$$

where m_H is the mass of the hydrogen atom and μ_0 is the vacuum permeability. More detailed calculations [1] indicate that for high Alfvén Mach number shocks, i.e., $u_s^2 \mu_0 \rho_1 / B_1^2 \gg 1$,

$$T_2 \approx 1.14 \times 10^{-5} u_s^2 \quad (2)$$

where T_2 is in $^{\circ}\text{K}$ and u_s is in m/sec. Consequently, a shock speed of 10^6 m/sec is expected to produce a temperature of about 1 keV. It is useful to employ a preshock transverse magnetic field B_1 so as to keep the shock thickness small and to reduce the effects of plasma contact with the walls of the device. The density ratio across a strong shock is four, and consequently such a wave propagating into 50 mTorr pressure diatomic hydrogen will produce a post-shock plasma number density of $n_2 \approx 1 \times 10^{16} \text{ cm}^{-3}$.

At Columbia University we have an electromagnetically driven coaxial shock tube which produces shock speeds in hydrogen up to 4×10^8 cm/sec. Some of the early experimental results have been described previously by Gross et al. [3]. We describe in this paper some of the experimental results obtained in that device and some computational results which help to interpret the phenomena. Results concerning shock speed, shock structure, plasma temperature, density and volume are presented.

2. THE SHOCK TUBE

The Columbia University shock tube is 3m long, has an outer diameter of 23 cm, and consists of coaxial concentric cylinder, with a 5 cm width between the tubes. The tube length was chosen to provide sufficient time for the shock wave to evolve to a steady state, thereby making possible a study of wave structure and post-shock plasma. The 5 cm gap is a compromise between wall effects and tube inductance. A conducting rod along the tube axis is used to carry current

which produces an azimuthal bias magnetic field essentially constant over the duration of the shock experiments. This bias field current, about 350kA maximum, is produced by a 1600 μ f, 20 kV capacitor bank; the magnetic field in the shock tube test region is about 7.5 kG. The shock wave drive current is produced by a 120kV, 60 μ f capacitor bank. It passes along the inner coaxial conductor, radially through the gas in the coaxial region, and back along the outer conductor, has a 2 meg. amp. current maximum and has a quarter cycle rise time of about 4 μ sec. This bank consists of six modules, each with its own low inductance SF₆ gas filled switch. The shock tube has a characteristic impedance of 34Ω , and an inductance of 114 nh/m. Further details of this device has been described by Halmoy [4] and Moriette [5]. The shock tube is initially filled with room temperature hydrogen or deuterium to a pressure $10 < p_1 \leq 200$ mTorr.

3. RESULTS

a) Shock Speed Measurements:

The propagation of the shock wave along the shock tube was detected by magnetic probes, electric probes, H β and X-ray radiation detectors. Data were observed at axial positions along the shock tube axis at the 25, 50, 100, 150, and 200 cm locations. The shock wave speed as determined from these different diagnostics was essentially the same, the very small differences being attributed to details in the shock structure itself, different response times of the different diagnostics, and boundary layer effects. The shock structure observed at early times (first 50 cm of travel) varied from shot to shot indicating that often the shock wave was still steepening and had not yet achieved a steady state structure. Beyond about 50 cm, the wave structure was sharp and steady. Shock speeds achieved in hydrogen gas are shown in table I.

The speed of sound in the preshock gas is 1.3×10^5 cm/sec and the Alfvén speed is 2.7×10^7 cm/sec, so that the shock speed over the first 50 cm corresponds to an acoustic Mach

TABLE I. SHOCK SPEED IN HYDROGEN

Average speed } over length cm/sec.	0-50 cm	0-100 cm	0-150 cm	0-200 cm
	4×10^8	2×10^8	1×10^8	7×10^7
$p_1 = 50 \text{ mTorr.}$		$T_1 = 293^\circ\text{K.}$		$B_1 = 7.2 \text{ kG.}$

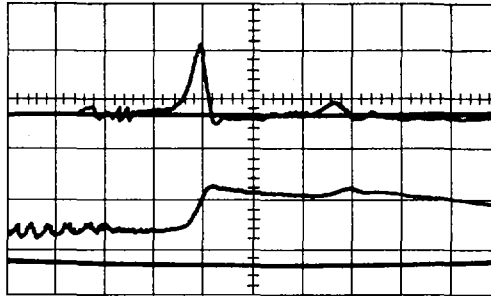


FIG.1. Measured magnetic probe signals; 150 cm location. Upper trace: $\dot{B}(t)$, un-integrated signal; lower trace: $B(t)$, integrated signal; time scale $1 \mu\text{s}$ per box, hydrogen, $p_1 = 50 \text{ mTorr}$, $T_1 = 293^\circ\text{K}$, $B_1 = 7.2 \text{ kG}$.

number of about 3000 and an Alfvén Mach number of about 15. In figure 1 are shown sample magnetic probe signals, obtained at the 150 cm axial position.

b) Shock Wave Structure:

A set of two-fluid Navier-Stokes equations employing classical plasma transport coefficients has been used to compute the detailed evolution and structure of collisional shock waves with a transverse magnetic field. The numerical method is similar to the well known Hain-Roberts code for pinches. This simulation has been helpful in understanding observed phenomena. Details of this computer code are available in ref. 6. The computer shock magnetic profiles [$B(t)$ and $\dot{B}(t)$] for a wave at the 150 cm location is shown in figure 2. Comparison with the experimental data in figure 1 shows good agreement. The temperatures, density, velocity and magnetic field

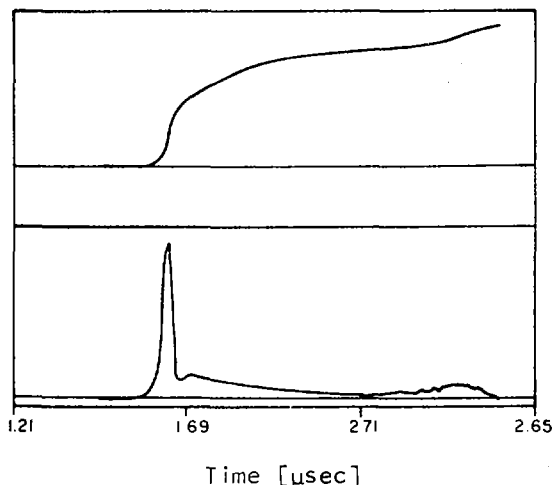


FIG. 2. Computer calculation of the magnetic field; 150 cm location. Upper trace: $B(t)$ magnetic field; lower trace: $\dot{B}(t)$, time derivative of $B(t)$.

distribution in the shock tube are also predicted by the computer code and an example of such information, for a shock traveling at $95 \text{ cm}/\mu\text{sec}$ is shown in figure 3. These shock waves invariably have $T_i > T_e$, as shown in figure 3, since the electron-ion relaxation time for the shocked plasma is long ($\tau_{ei} \approx 6 \times 10^{-5} \text{ sec}$).

Although there are several length scales associated with strong shock waves, the magnetic structure affords the most easily measured shock thickness. In figure 2, the computed $\dot{B}(t)$ gives a clear indication of the time for the shock to pass a particular location, and knowing the shock speed permits one to easily compute the magnetic shock thickness as a function of shock speed (for a constant preshock state). An identical procedure has been employed using the experimental data and the results are shown in figure 4. The mean free path is about 2 cm in the preshock gas and about 140 cm in the post-shock plasma. The shock thickness is of the order of 10 cm, so that these are indeed collisional shock waves, although the post-shock plasma is essentially collisionless. The ion gyro radius in the plasma is typically 0.2 cm. Our computations show that had we not included an initial azimuthal field, the shock thickness at corresponding speeds would be several meters, instead of the several centimeters, as in the present case.

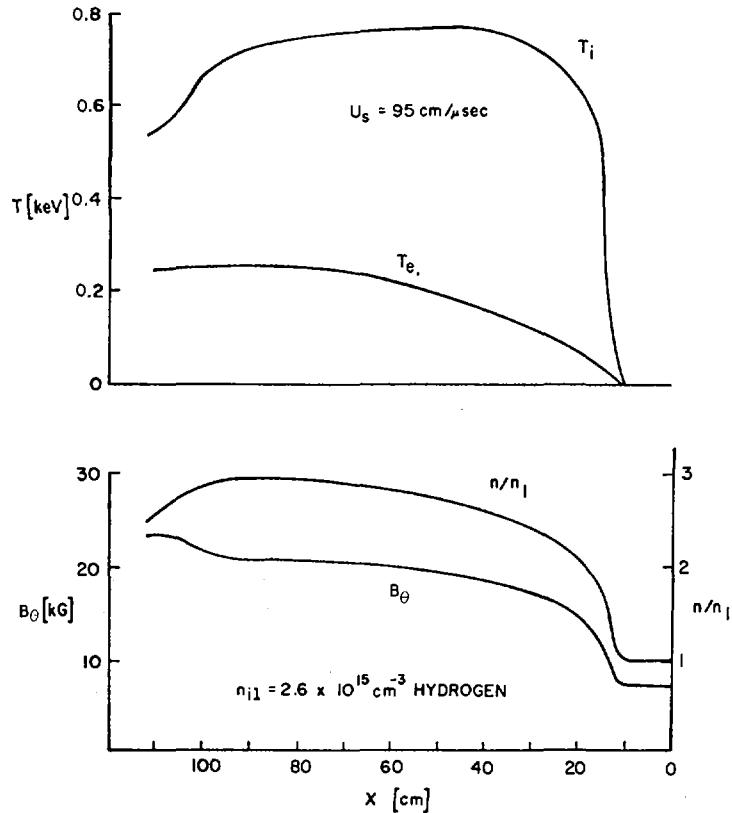


FIG. 3. Computed temperature, density and magnetic structure in the shock tube; shock speed = 95 cm/ μ s.

c) Density and Magnetic Field Compression Across the Shock Wave:

The change in electron density across the shock front was measured using a He-Ne laser interferometer, details of which are given in ref. 4. The post-shock plasma was found to have an electron density $n_{e2} = (1.4 \pm .3) \times 10^{16} \text{ cm}^{-3}$ when $p_1 = 50 \text{ mTorr H}_2$. The measured density compression ratio is therefore $n_2/n_1 \approx 4$, as expected by theory. The magnetic field compression ratios across these ionizing shock waves were found to vary from about 1.5 to 3.7, i.e., $1.5 \leq B_2 \leq 26 \text{ kG}$. For a pure MHD transverse shock, the density ratio and the field compression ratio are exactly equal. In the present case, the field compression ratios are less than the density ratios, a fact that is characteristic of ionizing shock waves [7].

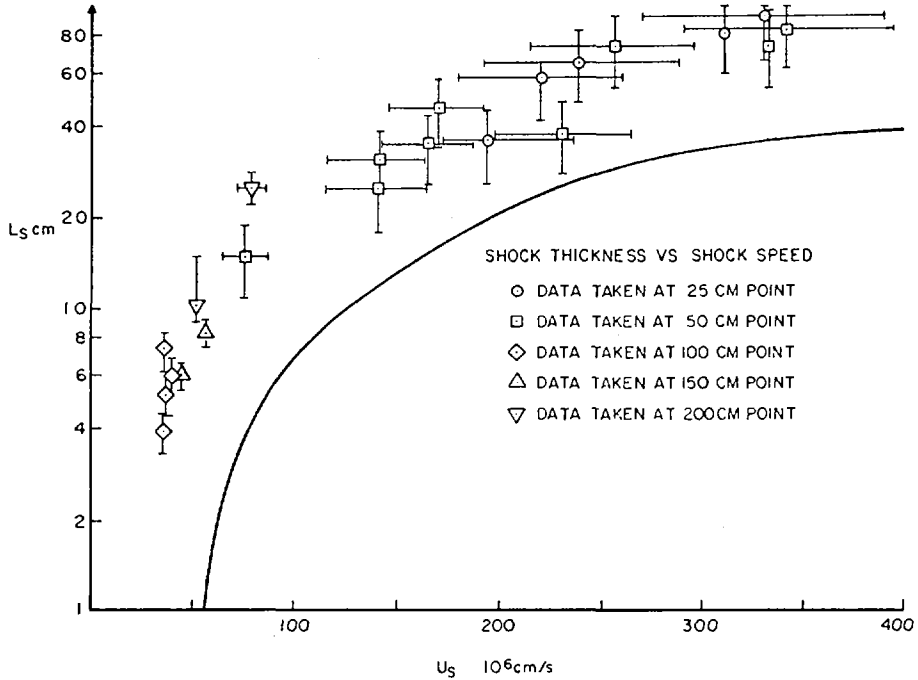


FIG. 4. Shock thickness as a function of shock speed. The solid curve is the computed thickness using classical plasma transport properties; $p_1 = 50$ mTorr, $B_1 = 7$ kG; hydrogen gas.

d) Electron and Ion Temperature:

Two x-ray detectors, each located at the 100 cm axial position, were used to obtain simultaneous measurements of the radiation transmitted through different beryllium foils. Careful collimation and shielding were employed. The bremsstrahlung energy spectrum for free-free and free-bound radiation is well known, and the fraction transmitted through various absorber foils have been computed by Elton [8]. The part of the x-ray spectrum beyond the last recombination edge when measured, can be used to determine the electron temperature. These measurements indicate that the maximum value was $T_e \approx (1 \pm 0.3)$ keV. Further details concerning these measurements are available in ref. 4.

An indication of the ion temperature was obtained by employing deuterium gas rather than hydrogen, and looking for neutron production. Geiger tubes wrapped in 10 mil silver

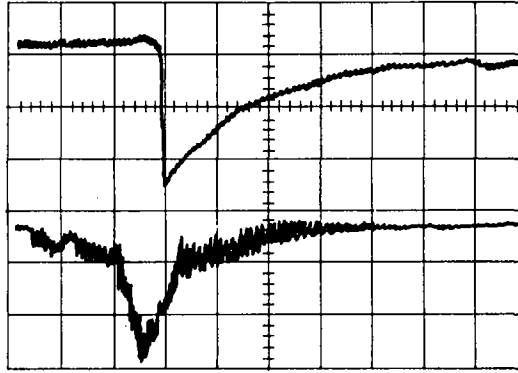


FIG. 5. Neutron flux; 75 cm location. Upper trace: H_{β} signal at 100 cm location, lower trace: Neutron flux; 75 cm location time scale, 1 μ s/cm.

foil and imbedded in a polyethylene moderator [2] were used to estimate the total production of neutrons per shot, and this value was found to be of the order of 5×10^5 neutrons. A five inch diameter Pilot B plastic scintillator with a Dumont 6364 photomultiplier, all carefully shielded by 1 inch of lead, were used to detect when the neutrons were produced. The neutrons were observed to be produced when the shock wave passed the detector which was located at about the 75 cm axial position. Figure 5 shows the neutron flux as detected by the scintillator and the H_{β} radiation from the shock wave passing the 100 cm location. The quantity of neutrons produced is the correct order of magnitude for a plasma with $T_i \approx 1$ keV, $n \approx 1 \times 10^{16}$ cm^{-3} . A plasma at 1 keV temperature and 10^{16} cm^{-3} density has an electron-electron collision time $\tau_{ee} \sim 7 \times 10^{-8}$ sec, and an ion collision time $\tau_{ii} \sim 3 \times 10^{-6}$ sec. Hence, it seems that the electrons are certainly completely Maxwellianized, but the ions may not yet have the high energy tail of their velocity distribution completely developed. Since the fusion reactions take place with these high energy ions, it is not clear whether the neutrons were produced by a thermal plasma. It is also instructive to note that the large azimuthal magnetic field makes the plasma very anisotropic. For example, the e-folding time for the relaxation of an electron temperature difference over a length of 10 cm is

2×10^{-10} sec in the azimuthal direction and 7×10^{-2} sec in the axial direction. Hence, there should be no temperature gradients in the azimuthal direction, but the post shock plasma should have an axial temperature distribution representative of the past history of the changing shock speed; i.e., between 4 keV and 100 ev.

4. ADDITIONAL REMARKS

Several operating characteristics of this high energy coaxial electromagnetic shock tube are worth mentioning. Separation of the shock wave from the driving "piston" is an important ingredient of all shock tube analysis. In the past, many electromagnetically driven shock devices have failed to observe such a separation, making it impossible to study shock structure, etc. In our device we have clear indications of such separation and the region of post-shock plasma that is essentially free of current is about 30 cm in length at the 150 cm position. Our calculations also bear out this point very clearly [6]. It is also instructive to make an energy accounting and this has been done for the first 3 μ sec of operation [5]. In this time, measurements indicate that 42% of the energy that has left the capacitor bank is delivered to the shock tube test region, 3% is dissipated by ohmic heating, 24% is stored as magnetic energy in circuit inductance outside the shock tube test region, and 31% has been transferred to the bias magnetic field circuit by inductive coupling.

REFERENCES

- [1] CHU, C.K., GROSS, R.A., *Advances in Plasma Physics*, edited by Simon, A., Thompson, W.B., (Wiley, New York 1969) Vol. 2, p. 139.
- [2] MEEHAN, R.J., Ph.D. Thesis; Columbia University 1969; *Experimental Investigation of Incident and Reflected Transverse Ionizing Shock Waves*; also, Columbia Plasma Lab., Rept. 44, 1969.

- [3] GROSS, R.A., CHEN, Y.G., HALMOY, E., MORIETTE, P., Phys. Rev. Letters. 25, 575 (c), 1970.
- [4] HALMOY, E.; Ph.D. Thesis; Columbia University, 1971; Production and Investigation of Very Strong Ionizing Shock Waves; also, Columbia Plasma Lab. Rept. 53, 1971.
- [5] MORIETTE, P.; Ph.D. Thesis; Columbia University, 1971; A Study of Strong Transverse Ionizing Shock Waves; also, Columbia Plasma Lab. Rept. 56, 1971.
- [6] SCHNEIDER, S.H.; Ph.D. Thesis, Columbia University, 1971, Numerical Simulation of Strong Plasma Shock Waves Produced in an Electromagnetic Shock Tube; also, Columbia Plasma Lab. Rept. 55, 1971.
- [7] CHU, C.K., Phys. Fluids 7, 1349 (1964).
- [8] ELTON, R.C., NRL Report 6738, Washington, D.C. (1968).

EXPERIMENTAL STUDY OF COLLISIONLESS SHOCK WAVES

J. W. M. PAUL, C. C. DAUGHNEY, L. S. HOLMES,
P. T. RUMSBY, A. D. CRAIG, E. L. MURRAY,
D. D. R. SUMMERS, J. BEAULIEU
UKAEA Research Group, Culham Laboratory,
Abingdon, Berks,
United Kingdom

Abstract

EXPERIMENTAL STUDY OF COLLISIONLESS SHOCK WAVES.

Five experiments on collisionless shock problems are described.

In the TARANTULA Z-pinch apparatus the microturbulence within a sub-critical (resistive) shock, propagating perpendicular to a magnetic field, is studied by forward scattering of light. Published and new data which reveal the frequency and wave-number spectra and the angular anisotropy of the observed turbulence are summarized. The data demonstrate the presence of current-driven ion-wave turbulence and also fit some predictions of non-linear theory. The observed turbulence is used in a stochastic model to explain the observed electron heating.

In a new apparatus, called CHARYBDIS, shock waves are produced which propagate parallel and nearly parallel to a magnetic field. These shocks are generated by applying a fast-rising radial electric field (~ 200 kV/m) to the end of a column (0.45 m diam. by 1.2 m long) of highly ionized plasma in an axial magnetic field. The steepening of a switch-on shock and its separation from the piston are observed at small radius, using magnetic probes. At larger radius an oblique shock with whistler precursor is observed.

Shock waves driven by laser-produced plasmas are also being studied. In the absence of a magnetic field, the problem of piston formation is crucial. In the PLUMES apparatus the interaction of two adjacent carbon plumes which are transversely interstreaming with Mach number $M < 4$ are observed. In the NIMBUS-I experiment, no interaction between an expanding beryllium plasma and a background hydrogen plasma with $M > 4$ is observed. The introduction of a small magnetic field, the NIMBUS-II experiment, leads to some interaction.

1. INTRODUCTION

The five experiments reported here are at different levels of development. The TARANTULA experiment has revealed the detailed structure of shocks propagating perpendicular to a magnetic field with low Alfvén Mach number ($M_A < 3$). Interest now centres on the detailed explanation of the turbulent heating and the non-linear collisionless processes. The other experiments are just beginning to reveal interesting features of shocks propagating parallel to a magnetic field (CHARYBDIS experiment) and of laser produced plasma expansion into both magnetized and unmagnetized plasmas (NIMBUS I, II, and PLUMES experiments).

2. TURBULENCE WITHIN A PERPENDICULAR MAGNETIC SHOCK WAVE

We show that the measured level and spectrum of turbulent electron density fluctuations, $\langle \delta n_e^2(\omega, k) \rangle$, within a collisionless shock can explain the observed electron heating, and furthermore they agree with some predictions of non-linear theory.

The conditions and main results of the 'TARANTULA' shock and light scattering experiments are published [1-7], and we summarize the significant features before extending our interpretation. We consider the shock with sub-critical Alfvén-Mach number ($M_A = 2.5$), propagating perpendicular to a magnetic field, through a low- β hydrogen plasma with initial parameters, $n_e = 6.4 \times 10^{20} \text{ m}^{-3}$, $T_e = T_i = 1.2 \text{ eV}$, $B_z = 0.12 \text{ T}$. The observed electron heating ($T_e \rightarrow 45 \text{ eV}$) within the shock of width $L_S = 1.4 \text{ mm}$ implies an effective resistivity $\eta^* \sim 100 \eta_S$ ($\eta_S = \text{Spitzer's binary value}$) and an effective collision frequency $\nu^* \sim 3 \text{ GHz}$.

The azimuthal current (J_θ) within the shock corresponds to an electron drift velocity (v_d) which exceeds the ion sound speed (c_s) and theory [8-12] predicts current driven ion wave turbulence with $\eta^* > \eta_S$.

We study the scattering of ruby laser light (50 MW, 40 ns, 20 mÅ) by the turbulence within the shock. As the shock passes through the laser beam, we observe a pulse (10 ns) of enhanced scattering which is over 100 times thermal. There is no resolution within the shock. We measure the average spectrum of fluctuations within the shock, $S(\omega, k) = \langle \delta n_e^2(\omega, k) \rangle / n_e$.

2.1 Spectrum $S_k(\omega) = S(\omega, \bar{k})$ for constant \bar{k} (ref. [5-7])

The scattered light spectrum, shown in Fig.1, is broader than for the incident light and the peak is shifted in frequency.

The direction of the shift shows that the scattering waves propagate in the direction of the electron current. This shift reverses sign with reversal of current (J_θ). This anisotropy shows that the waves are driven by the electron current.

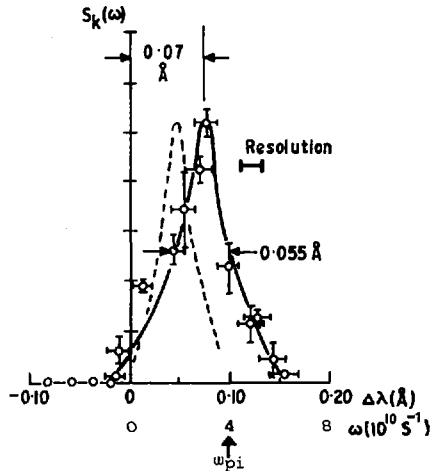


FIG. 1. Spectrum $S_k(\omega)$ with scaled $S_k(\omega)$ against $\Delta\lambda$ (dashed).

The magnitude of the shift corresponds to scattering by waves with a frequency ω_0 , which, with k , fits the ion wave dispersion curve for the mean shock conditions. By varying the shock parameter so that M_A and λ_D are constant while $\omega_{pi} \rightarrow 0.75 \omega_{pi}$ and $\omega_{ce} \rightarrow 1.3 \omega_{ce}$, we obtain the dashed spectrum of Fig.1. Clearly ω_0 scales as ω_{pi} and not ω_{ce} . The fluctuations are ion waves.

The width of the spectrum is interpreted, as a measure of the life-time ($\tau \sim 0.3$ ns) of the mode (ω_0, k). As $\tau \sim 2\pi/\omega_0$, the fluctuations have appreciable randomness of phase and constitute turbulence.

The broadened spectrum, extending to $\omega > \omega_{pi}$, cannot be explained in terms of the range of $|k|$ accepted or the range of $k\lambda_D$ within the shock. Also the scaling of the width with ω_{pi} (dashed spectrum) rules out Doppler broadening through the radial motion in the shock and the small k_R component accepted by the detector.

2.2 Spectrum $S(\bar{k}) = \int S(\omega, \bar{k}) d\omega$ (ref. [6, 7])

(a) $S(\bar{k})$, for \bar{k} parallel to \bar{J}_0 , is shown in Fig.2. It has a sharp cut-off at $k\lambda_D = 1$. (λ_D for mean shock condition). The form of the spectrum agrees with the non-linear theory of Kadomtsev [9]. Similar curves for other shock conditions confirm the dependence on k and the cut-off. The dashed curve on Fig.2, obtained for the same M_A but different n_{e1} (and B_{z1}), is $S(k)$ plotted against k/k_0 where the cut-off $k_0 = 10.5 \times 10^5 \text{ m}^{-1} \approx 1/\lambda_D$.

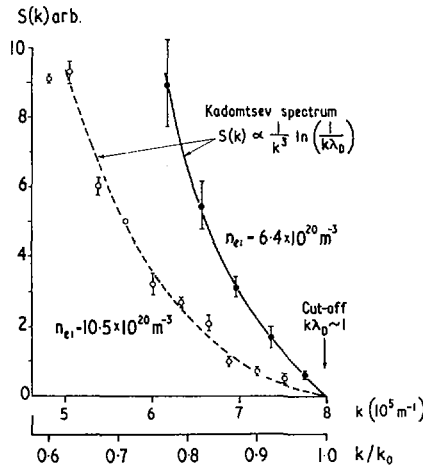
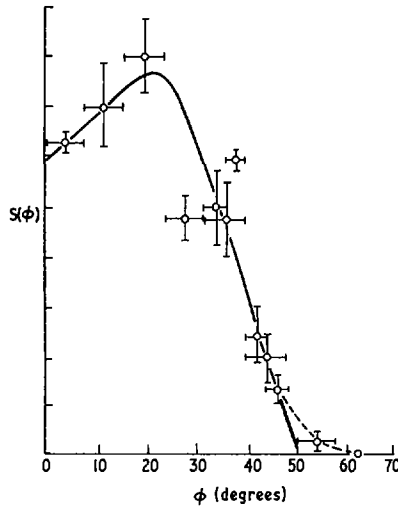


FIG.2. Spectrum $S(k)$ with scaled $S(k)$ against k/k_0 (dashed).

FIG. 3. Spectrum $S(\phi)$.

(b) $S(\phi)$, where ϕ is angle between \bar{k} and \bar{J}_θ in the plane perpendicular to B , is shown in Fig.3. The cut-off at $\phi_c = 50^\circ$, together with $S_k(\omega)$, shows that the turbulence is restricted to a cone around the electron current (assuming we can neglect magnetic effects, see Section 2.5).

2.3 Level of Turbulence (ref.[4])

Absolute calibration, by Rayleigh scattering from gases, yields $S(k) = 230$ for $k = 7.1 \times 10^6 \text{ m}^{-1}$. (This is corrected from ref.[4] by factor 0.54.) This allows a calculation of the ratio (R) of the total energy in the turbulence to the thermal energy. We assume ion wave turbulence with the Kadomtsev law (down to $k = 2\pi/L_s$) and a cone of angle $\phi_c = 50^\circ$ independent of k . We obtain $R \sim 2\%$, and the RMS electric field $E_m = 700 \text{ kV/m}$.

2.4. Measurements with $T_i > T_e$

More recently a similar study of turbulence has been made by Keilhacker et al. [13] on a super-critical shock propagating through a high- β plasma. The shock is broad with $L_s \sim 10 \text{ mm}$, comparable with (c/ω_{pi}) . Throughout the shock $T_e < 2T_i$ so ion waves should be stable. Consequently, it is surprising that the measured turbulence is almost identical with that in the TARANTULA shock ($T_e > T_i$).

2.5 Linear Stability Theory

Within the shock the magnetized electrons experience an azimuthal drift. This arises from the various driving radial

gradients $\nabla\phi, \nabla B, \nabla n_e, \nabla T_e$. Gary, Sanderson, Lashmore-Davies and Biskamp [10, 11] describe instabilities driven by E and ∇B , with the former dominating. Sanderson and Priest [12] have extended this treatment to include ∇T_e and ∇n with the former dominating. They also consider that ∇T_e should dominate the $\nabla\phi$ driven instability.

In all these cases two types of waves are involved:

- (i) Ion waves which are restricted to a cone about v_d .
- (ii) Bernstein waves which are restricted to a fan about v_d within a few degrees of perpendicular to B.

The cone of ion wave instability is well known. Two Bernstein instabilities are found; (a) Growth of negative energy (Doppler shifted) Bernstein waves when Landau damped; (b) Unstable crossing of Doppler shifted Bernstein modes with the ion wave mode.

The observed scaling of ω_o with ω_{pi} in TARANTULA favours the simple ion wave instability. It rules out the pure Bernstein mode (a) which is thought to dominate in Keilhacker's experiment [13], but does not rule out the ion wave/Bernstein mode (b). However there appears to be no reason for invoking the restricted instability when most of k-space is unstable to ion waves. Consequently we shall neglect magnetic effects.

The theoretical cone of ion wave instability depends on ion Landau damping. For $T_i = 0$, $\phi_c = 85^\circ$, the Cerenkov cone. However, the observed $\phi_c = 50^\circ$ is possible if we assume one dimensional adiabatic ion heating within the shock.

2.6 Non-Linear Processes

First order non-linear effects are analyzed in terms of the three-wave processes, wave decay, and wave scattering on particles. Current driven ion wave turbulence was first analyzed by Kadomtsev [9]. He balanced the linear growth against wave scattering on ions and obtained the spectrum $S(k) \propto k^{-3} \ln(1/k \lambda_D)$, and this form is observed (Fig.2). We previously [4,5] calculated $S(k)$ from Kadomtsev's formula using a cone angle $\phi \sim \pi/2$. If we now put $\phi = \pi/4$ we obtain $S(k) = 200$ ($k = 7.1 \times 10^5 \text{m}^{-1}$) which is in reasonable agreement with experiment. However the scaling of $S(k)$ with n_e shown in Fig.2 does not agree.

Sloan and Drummond [14] show that scattering on electrons dominates. Tsytovich [15], who dismisses scattering by electrons, notes that, for the observed broad $S_k(\omega)$ wave, decay is possible and he shows that, as the resonant process, it should dominate. He also states that the observed gross anisotropy of $S(\vec{k})$ is inconsistent with scattering on ions but is consistent with wave decay. The time scale for scattering on ions (τ_s) and decay (τ_d) derived by Tsytovich, are such that for the observed level of turbulence $R \sim 2\%$:

- (i) $\tau_s > t$ the shock transit time (6 ns);
 (ii) $\tau_d \sim 0.2$ ns ($< t$) which is comparable to the observed life time of the mode, (0.3 ns).

(These figures appear inconsistent with the fit of $S(k)$ to Kadomtsev's formula.) Thus, according to Tsytovich, the turbulence measurements favour the decay process. On the other hand the effective resistivity within such shocks scales with T_e/T_i [2,5] in agreement with wave scattering on ions and not wave decay.

2.7 Stochastic Heating of Electrons

We consider the random deflection of electrons by the fluctuating electric field of the turbulence. Large angle deflection (trapping) is neglected because $eE_m \lambda_D / kT_e \sim 3\%$. The mean electron thermal velocity $v_e \gg c_s$, the wave speed, and consequently the field is effectively static, with a coherence length $c_s \tau$. An electron experiences this as a coherence time, $\tau_e = c_s \tau / v_e$, which is much less than the effective collision time ($1/v^* \sim 40 \tau_e$). This justifies the 'random phase approximation' of a stochastic model.

Our earlier stochastic model [4,5] defined $v^* = (1/v_e^2) D_{\perp}(v_e)$ and gave:

$$v_1^* = \frac{1}{4\pi^2} \left(\frac{e}{m}\right)^2 \frac{1}{v_e^3} \int_0^{k_{\max}} E^2(k) k dk$$

We have extended this model by integrating over a cone of turbulence $(\varphi_c)_{\perp}$ and over isotropic Maxwellian electrons down to $v = (eE_m \lambda_D / m)^{1/2}$. This yields

$$v_2^* = 1.4 (2\pi)^{-1/2} (1 - \cos \varphi_c) v_1^*$$

Substituting the observed Kadomtsev form of $S(k)$, extrapolated down to $k = 2\pi/L_s$, and the measured level and cone ($\varphi_c = 50^\circ$) of turbulence yields, $v_2^* = 1$ GHz compared with the observed 3 GHz (about 2 GHz when corrected for adiabatic heating).

This treatment involves the perpendicular diffusion coefficient (D_{\perp}) and hence momentum transfer. An alternative approach, Gary and Paul [16], involves the coefficient of dynamical friction and hence energy transfer. For a non-thermal plasma these need not give the same effective collision time. The second approach yields:

$$v_3^* = (2\pi)^{-1/2} (1 - c_s/v_d) (1 - \cos \varphi) v_1^*$$

which is in general lower than v_2^* .

3. NEAR PARALLEL PROPAGATION - CHARYBDIS EXPERIMENT

The aim of this new experiment is to produce fast shocks propagating through a magnetized plasma in a direction parallel to a magnetic field in the 'switch-on' regime. This requires a

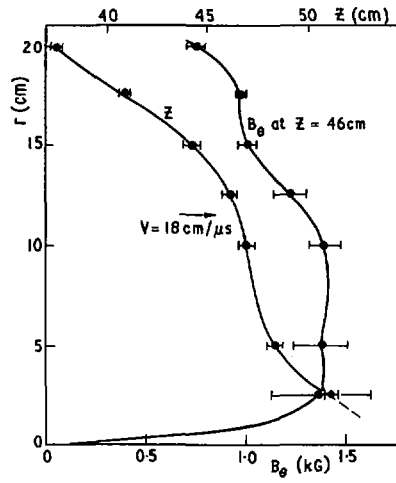


FIG. 4. Profile $B_\theta(R)$ and position $Z(R)$ of peak B_θ ($B_{z1} = 0.1$ T).

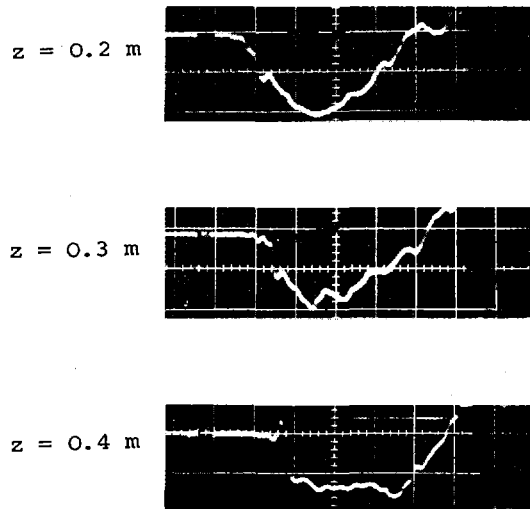


FIG. 5. Steepening of B_θ front ($B_{z1} = 0.2$ T, $R = 95$ mm, $1 \mu\text{s}/\text{div}$, 0.13 T/div).

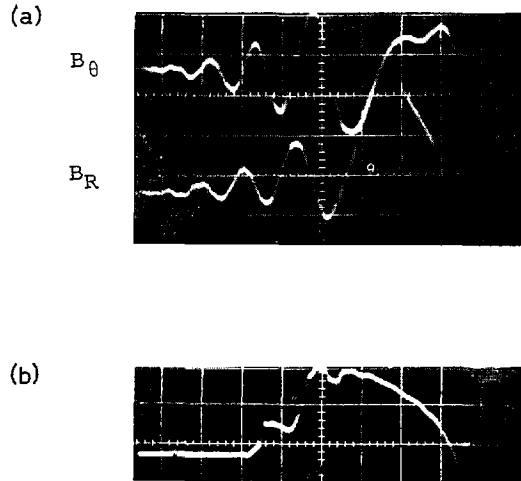


FIG. 6. (a) Whistler precursor: ($B_{z1} = 0.1$ T, $R = 95$ mm, $0.2 \mu\text{s}/\text{div}$, 0.015 T/div).
 (b) Separation of current fronts: ($B_{z1} = 0.2$ T, $R = 25$ mm, $1 \mu\text{s}/\text{div}$, 0.09 T/div).

piston with both transverse magnetic field and motion, and with an Alfvén Mach number $M_A < 2$.

The experiment is performed in a pyrex glass tube, 1.25 m long by 0.45 m diameter. The initial hydrogen plasma is similar to that in the TARANTULA experiment ($n_e \sim 6 \times 10^{20} \text{ m}^{-3}$, $T_e = T_i = 1.2$ eV, $B_z \sim 0.05$ to 0.2 T). The piston is produced by applying a radial electric field of 200 kV/m, between a central and an annular electrode at one end. The plasma current of 180 kA produces the 'transverse' field B_θ and rotation ($J_R \times B_z$) and also the axial piston ($J_R \times B_\theta$). The rotating plasma requires a centripetal force $J_\theta \times B_z$ (B_z increases with R).

Magnetic probe studies show that although 10% of the plasma current remains on the end insulator, two successive current sheets, propagate down the tube with velocities around 200 km/s. The first we interpret as a shock front and the second as the piston, although there is good separation over only a limited range of radii. The current paths for these sheets is through a central pinch or focus ($r \lesssim 0.1$ m) and an outer annulus ($\Delta R \sim 20$ mm) near the wall. Some of the irreproducibility of the experiment may arise in this focus.

Outside the pinch the magnetic pressure falls, and the propagation becomes oblique; there is, nevertheless, a region of almost parallel propagation (Fig. 4) at moderate radii. The shock involves jumps in all three components, B_θ , B_z , B_R , and these jumps all steepen as the front propagates (Fig. 5). The B_θ and B_z components are comparable while B_R is smaller.

For oblique propagation (outer region) the fast wave components (B_Z, B_R) lead the intermediate wave component (B_θ). There is a small amplitude precursor of whistler oscillations - rotating field (B_θ, B_Z, B_R) with $\omega \sim 2\omega_{ci}$ (Fig.6a). The separation of piston and shock is poor.

For parallel and near parallel propagation, a well separated double jump of B_θ is observed (Fig.6b) and now all three components change together. The two jumps in B_θ separate as they propagate along the tube and we interpret the first as a switch-on shock.

We propose an interpretation which is dependent on the geometry of the experiment. In the outer region a fast oblique shock (B_Z, B_R) is formed and is followed almost immediately by an intermediate wave (B_θ). The two structures overlap and become equivalent to a switch-on shock as parallel propagation is approached. The intermediate wave is necessary for continuity of current from the inner switch-on shock. Even for parallel propagation components other than B_θ arise from rotation and diamagnetic effects.

We conclude that the theoretical models of switch-on shocks [17, 18], are difficult to realize in finite geometry where the 'uniqueness' of the situation is removed.

4. THE NON-MAGNETIC SHOCK WAVES ($B = 0$)

A non-magnetic piston is desirable for producing a non-magnetic shock. Electrostatic pistons have been used successfully for Mach numbers $M < 1.5$ [19,20]. For higher M reflection of ions from the shock front is thought to destroy the shock. The expansion of a laser produced plasma into another plasma has also been used but the published evidence [21] for shock or piston formation is unconvincing.

The collisionless non-magnetic piston requires a strong ion-ion interstreaming instability to provide sufficient momentum transfer for compression to occur. Stringer [8] has obtained the condition for instability in hydrogen for one dimension; $v_i < 2c_s$ and $T_i/T_e < 0.3$, where v_i = interstreaming velocity, c_s = ion sound speed. We have extended this to species with charge Ze and mass AM_H . While the condition on T_e/T_i is relaxed, that on v_i is almost unchanged (N.B. $c_s \propto \sqrt{Z/A}$). A 2-D computation by Forslund and Shonks [22] suggests that the presence of oblique waves relaxes the condition to $v_i < 4c_s$. Thus, this mechanism cannot produce shocks or pistons with $M > 4$.

4.1 PLUMES Experiment - Symmetrical Plasma

We have produced a collisionless interaction between two symmetrical laser produced carbon plasmas for $M < 4$. The pulse from a Nd-laser (15J, 25 ns) is split by a prism and focused to two spots on a graphite plate in vacuum, producing two plasma

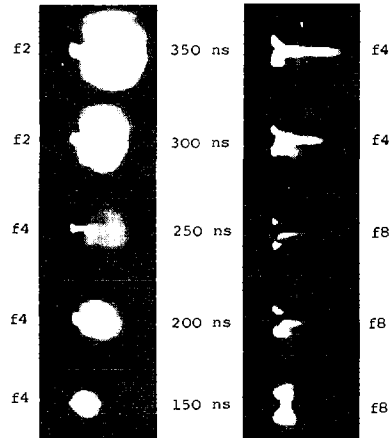


FIG. 7. Framing pictures of single and interacting plumes (Time from laser pulse) - 10 mm focal spot separation.

plumes. The transverse interstreaming of the plumes has $M < 4$ (assuming $Z \sim 6$, $T_e > 10$ eV). Fig. 7 shows framing pictures of a single plume and an interacting pair.

With greater separation (40 mm) between the plumes, the interaction zone becomes an expanding dark region 'eating' into the plumes. This is probably because the interacting plasma is hotter and radiating mainly in the UV.

As yet no attempt has been made to diagnose the nature of the strong interaction which is observed.

4.2 NIMBUS I Experiment - Asymmetrical Plasma

We have also studied the expansion of laser produced beryllium plasma into a background hydrogen plasma. The beryllium plasma is produced by focusing a ruby laser pulse (10 J, 15 ns) on to a $90 \mu\text{m}$ beryllium wire. The expansion velocity is measured by photography, spectroscopy (Be III), electric probes and ion energy analyzers, and is typically 300 km/s. The background plasma is either, the afterglow of a high current discharge (as in TARANTULA) with $n_e \sim 10^{18} - 10^{21} \text{ m}^{-3}$ or a glow discharge with $n_e \sim 10^{16} \text{ m}^{-3}$ to simulate the conditions of reference [21].

The time of arrival of the front of the beryllium plasma at various radii, is independent of the presence of any background plasma. If the expansion formed a piston, sweeping up the background plasma, there would be a detectable change. Simultaneous records of Be III and H-continuum emission show no evidence of compression of the background plasma in front of the beryllium plasma. Thus, there is no evidence of piston or shock formation.

The magnitude of the fast jump of electric potential at the front (Fig.9a) decreases with increasing plasma density and in no case is this sufficient to reflect ions. If the jump represents the change of electron pressure across the front, this decrease shows that the expanding electron gas is being cooled by the background plasma.

Although there is no theory of asymmetric interstreaming (Be-H), the fact that for any reasonable Z and T_e for both plasmas, $M > 4$ makes the lack of interaction not surprising. But these results throw some doubt on ref.[21].

5. LASER PRODUCED MAGNETIC COMPRESSION - NIMBUS II Experiment

Recently an axial magnetic field has been added to the NIMBUS experiment. In the plane perpendicular to the field the expansion of the beryllium plasma is unaffected by fields of up to 0.03 T either with or without the background plasma. The electric potential jump is appreciably reduced by small field (≈ 5 mT).

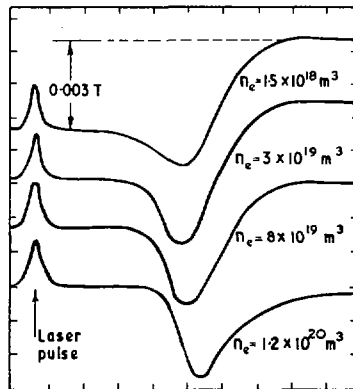


FIG. 8. $B_{z1}(t)$ for expansion perpendicular to B into different background plasma densities ($B_{z1} = 0.003$ T, $R = 50$ mm, 50 ns/div).

In vacuum the magnetic field is totally excluded from the beryllium plasma for a long time (> 500 ns). However the presence of background plasma allows some of this field back into the beryllium plasma very rapidly. The amount that gets back increases with increasing background density until for $n_e \sim 10^{20} \text{ m}^{-3}$ there is no exclusion after 100 ns. The piston becomes porous (Fig.8).

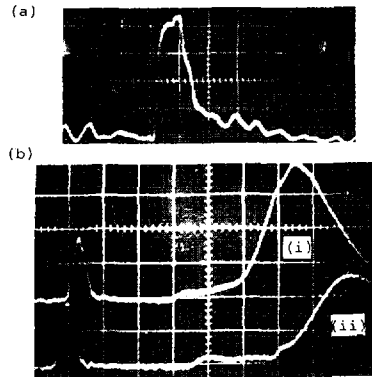


FIG.9. (a) Typical electric probe trace with background plasma (50 ns/div, 2 v/div).
 (b) Separation of precursor magnetic compression at 15° off perpendicular to B. ($B_{z1} = 0.03$ T, 0.005 T/div, 50 ns/div). Laser pulse marker delayed 100 ns. (i) $R = 70$ mm (ii) $R = 80$ mm.

At 15° off perpendicular to the field, there is clear evidence for the steady separation of a precursor compression (shock?) as shown in Fig.9b. This only occurs for $B > 0.02$ T and high $n_e \sim 10^{20} \text{ m}^{-3}$. This critical field corresponds to the value for which the maximum whistler velocity equals the interstreaming velocity but identification with the whistler interaction must depend on future scaling experiments.

REFERENCES

- [1] PAUL, J.W.M., HOLMES, L.S., PARKINSON, M.J., & SHEFFIELD, J. Nature, 208, (1965) 133; 7th Int. Conf. on Phenomena in Ionized Gases, Belgrade (1965) II, 819.
- [2] PAUL, J.W.M., GOLDENBAUM, G.C., IIYOSHI, A., HOLMES, L.S. and HARDCASTLE, R.A., Nature, 216, (1967) 363.
- [3] PAUL, J.W.M., 'Physics of Hot Plasmas' Eds. Rye, B.J. and Taylor, J.C.; Oliver & Boyd, pp.302-345.
- [4] PAUL, J.W.M., DAUGHNEY, C.C. and HOLMES, L.S., Nature, 223 (1969) 822; 9th Int. Conf. on Phenomena in Ionized Gases, Bucharest, (1969), p.650.
- [5] PAUL, J.W.M., ESRIN Study Group on Collisionless Shocks, ESRIN SP-51, (1969).
- [6] DAUGHNEY, C.C., HOLMES, L.S. and PAUL, J.W.M., Phys. Rev. Letters, 25, (1970) 497.
- [7] DAUGHNEY, C.C., HOLMES, L.S., PAUL, J.W.M., and SUMMERS, D.D.R. 4th European Conf. on Fusion and Plasma Physics (1970) p.57; Bull. Amer. Phys. Soc., II, 15, (1970), 1456.

- [8] STRINGER, T.E., J. Nucl. Energy C, 5, (1963) 89.
- [9] KADOMTSEV, B.B. Plasma Turbulence, Academic Press, London, (1965).
- [10] GARY, S.P. and SANDERSON, J.J., J. Plasma Phys., 4, (1970), 739; GARY, S.P., J. Plasma Phys., 4, (1970), 753; GARY, S.P. and BISKAMP, D. J. Phys. A, (1971) L27.
- [11] LASHMORE-DAVIES, C.N., J. Phys. A, 3, (1970) L40.
- [12] SANDERSON, J.J. and PRIEST, E.R. Accepted for publication in (a) 10th Int. Conf. on Phenomena in Ionized Gases, Oxford, 1971; (b) J. Phys. A, (1971).
- [13] KEILHACKER, M. and STEUER, K.-H., Phys. Rev. Letters, 26, (1971) 694.
- [14] SLOAN, M.L. and DRUMMOND, W.E., Phys. Fluid, 13, (1970) 2554.
- [15] TSYTOVICH, V.N. Culham Laboratory Preprint CLM - P 244 (1970) (Submitted for publication to Plasma Physics)
- [16] GARY, S.P. and PAUL, J.W.M. Phys. Rev. Letters, 26, (1971) 1097.
- [17] KEMP, N.H. and PETSCHKE, H.E., Phys. Fluids, 2, (1959) 599.
- [18] BICKERTON, R.J., LENAMON, L. and MURPHY, R.V.W., J. Plasma Phys., 5, (1971) 177.
- [19] ALIKHANOV, S.G. et al. 3rd IAEA Conf. on Plasma Physics and Fusion Research, 1, Novosibirsk (1968) 1.
- [20] TAYLOR, R.J. et al. Phys. Rev. Letters, 24, (1970) 206.
- [21] KOOPMAN, D.W. and TIDMAN, D.A., Phys. Rev. Letters, 18 (1967) 533.
- [22] FORSLUND, D.W. and SHONKS, C.R., Phys. Rev. Letters, 25, (1970) 281.

EXPERIMENTAL STUDY OF COLLECTIVE DISSIPATION IN SHOCK WAVES FOR A WIDE RANGE OF PLASMA PARAMETERS

M. KEILHACKER, M. KORNHERR, H. NIEDERMEYER,
K. -H. STEUER, R. CHODURA
Max-Planck-Institut für Plasmaphysik,
Euratom Association,
Garching, Munich,
Federal Republic of Germany

Abstract

EXPERIMENTAL STUDY OF COLLECTIVE DISSIPATION IN SHOCK WAVES FOR A WIDE RANGE OF PLASMA PARAMETERS.

Collective dissipation in collisionless shock waves was investigated in two theta-pinch experiments. These investigations are complementary in that the plasma parameters governing the onset of certain instabilities leading to micro-turbulence and collective dissipation can be varied over a wide range.

In the "Turbulent Heating Experiment" (coil diameter 16 cm) the shock waves propagate into an initial deuterium plasma of density $n \sim 3 \times 10^{14} \text{ cm}^{-3}$ produced by a fast theta pinch. The characteristic parameters are $\beta \sim 1$, $T_e/T_i \sim 0.2$, $\omega_{pe}/\omega_{ce} \sim 100$. Quasi-stationary shock waves can be generated for Mach numbers M ranging from 1.5 to 5.

Time-resolved light-scattering measurements (ruby and pulsed CO_2 lasers) show strong collisionless electron heating accompanied by density fluctuations that are up to 250 times the thermal value. The frequency and wave number spectra as well as the angular distribution of this turbulence are measured. The turbulence seems to originate from electron cyclotron waves driven by the diamagnetic current in the shock front. The ion heating is measured by collective scattering from thermal fluctuations. For $M > M_{\text{crit}}$ non-adiabatic ion heating is observed.

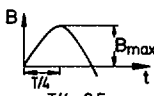
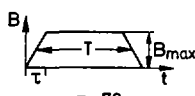
In the "Minimax" device (coil diameter 43 cm), a trapezoidal magnetic field pulse (rise time 70 ns) is generated by a Blumlein line. The UV-radiation of two Z-pinch in xenon pre-ionizes the working gas (H_2 , D_2 or a rare gas, $n = 10^{12} - 5 \times 10^{13} \text{ cm}^{-3}$). The characteristic parameters can be varied: $\beta \sim 10^{-2}$, $T_e/T_i = 1 - 10$, $\omega_{pe}/\omega_{ce} = 5 - 100$, $M = 1 - 6$.

Fast magnetic miniature probes and the observation of satellites of forbidden lines are used to investigate electric and magnetic field fluctuations occurring in the piston region during fast compression of the plasma. The amplitude of the fluctuating electric fields is about 5 kV/cm corresponding to an energy density of about 0.5% of the thermal energy of the electrons. Coherent magnetic fluctuations near the ion plasma frequency with amplitudes up to 10 G are correlated with the electric fluctuations. The results are consistent with the assumption of an electron cyclotron drift instability. - At supercritical Mach numbers a "foot" develops in the magnetic field profile.

1. INTRODUCTION

This paper, a continuation of work first published at the Novosibirsk Conference in 1968 [1], deals with the investigation of collective dissipation in collisionless shock waves. In two experiments ("Turbulent Heating Experiment" and "Mini-max") shock waves are produced by radial compression of a preionized plasma column by a fast theta pinch. As shown in Table I, the two experiments differ in the diameter of the theta-pinch coil, the pulse form and amplitude of the magnetic field, and the kind of pre-ionization used to form the initial plasma. The two types of pre-ionization are complementary in that the plasma- β and the plasma parameters decisive

TABLE I. CHARACTERISTIC PARAMETERS OF SHOCK EXPERIMENTS

	"Turbulent Heating Experiment"	"Minimax"
<u>Theta Pinch Coil:</u>		
Diameter	15,8 cm	43 cm
Length	60 cm	100 cm
<u>Magnetic Field:</u>		
Pulse Form		
Rise Time	$T/4 = 0.5 \mu\text{s}$	$\tau = 70 \text{ ns}$
Pulse Length	$T/2 = 10 \mu\text{s}$	$T = 230 \text{ ns}$
Amplitude B_{max}	12 kG	15 kG
Charging Voltage	$2 \times 40 \text{ kV}$	125 kV
<u>Preionization:</u>	Theta-Pinch	UV-Radiation
Density	$1 \div 5 \times 10^{14} \text{ cm}^{-3}$	$10^{12} \div 5 \times 10^{13} \text{ cm}^{-3}$
Plasma " β "	~ 1	$\ll 1$
T_e/T_i	< 1	≥ 1
ω_{pe}/ω_{ce}	~ 100	$5 \div 100$

for the onset of certain instabilities, such as the ratio of the electron and ion temperatures T_e/T_i and the ratio of the plasma and cyclotron frequencies ω_{pe}/ω_{ce} , can be varied over a wide range.

The first experiment, working at initial plasma densities of a few times 10^{14} cm^{-3} , produces quasi-stationary high- β shock waves with Mach numbers up to 5. Light-scattering measurements yield the electron and ion heating in the shock front and allow careful analysis of the micro-turbulence causing the observed anomalous electron heating.

In the second experiment, non-stationary compression waves propagate into a low- β plasma of density $10^{12} - 10^{13} \text{ cm}^{-3}$. Strong electric and magnetic fluctuations are observed in the piston region during compression.

2. HIGH- β SHOCK WAVES

2.1. The "Turbulent Heating Experiment"

In the "Turbulent Heating Experiment" [1] the fast-rising magnetic field (12 kG in $0.5 \mu\text{s}$) is generated in a double-fed coil of 60 cm length and 15.8 cm diameter by two 40-kV capacitor banks.

An initial deuterium plasma of density $n_1 = 2 - 5 \times 10^{14} \text{ cm}^{-3}$ is formed by a fast theta-pinch pre-ionization. Owing to the shock heating, the ion temperature¹ in the initial plasma is larger ($T_{i1} = 10 - 40 \text{ eV}$) than the

¹ The initial ion temperature, which has previously been determined spectroscopically [2], has now been measured by collective light scattering (see Fig. 5).

electron temperature ($T_{e1} = 2 - 9$ eV) and the plasma- β is about 1 [2]. The fact that $T_{e1}/T_{i1} < 1$ has important implications for possible instabilities that can develop in the shock waves.

By properly balancing the initial plasma conditions and the charging voltage of the shock bank, almost stationary shock waves with magnetosonic Mach numbers M ranging from 1.5 to 5 can be produced.

2.2. Anomalous resistivity and electron heating

In a previous experiment we have shown [2] that the electron heating observed in low-Mach-number shocks ($M \leq M_{crit}$) implies a resistivity in the shock front that is about two orders of magnitude larger than the "classical" value. To measure the level and spectrum of the turbulence causing this "anomalous" resistivity, a laser forward-scattering experiment was set up.

In this experiment [3, 4] the light pulse of a 500 MW ruby laser is timed to hit the shock wave while it traverses the laser beam. Pulse width (12 ns) and divergence of the laser beam make it possible to resolve the structure of the shock wave. The light scattered in the forward direction ($\theta = 2^\circ - 6^\circ$) is detected by a photomultiplier, either directly or after spectral resolution (resolution 3×10^{-2} Å) using a double Fabry-Perot interferometer. The geometry of the incident and scattered light paths is such that the scattering plasma waves have a wave vector \vec{k} collinear with the azimuthal current in the shock front (except for a divergence $\theta/2 = 1^\circ - 3^\circ$ in the $v_d - B_1$ plane) and with $|\vec{k}|$ of order $1/D$ ($\alpha \sim 1/|\vec{k}| \cdot D \geq 1$), D being the Debye length.

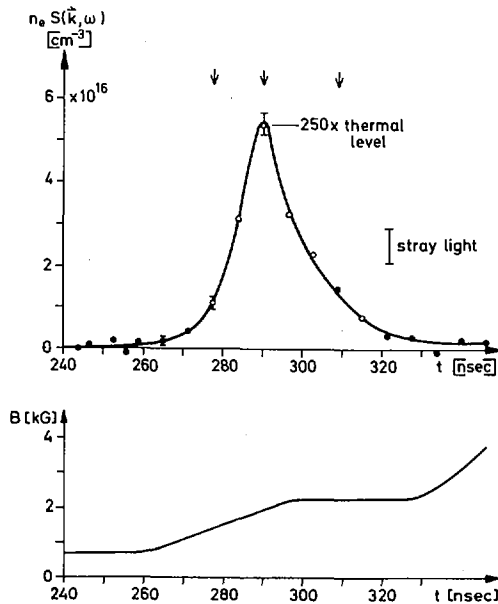


FIG. 1. Intensity of density fluctuations $n_e S(\vec{k}, \omega)$ and magnetic field B in a collisionless shock wave with Mach number 2.5 in deuterium.

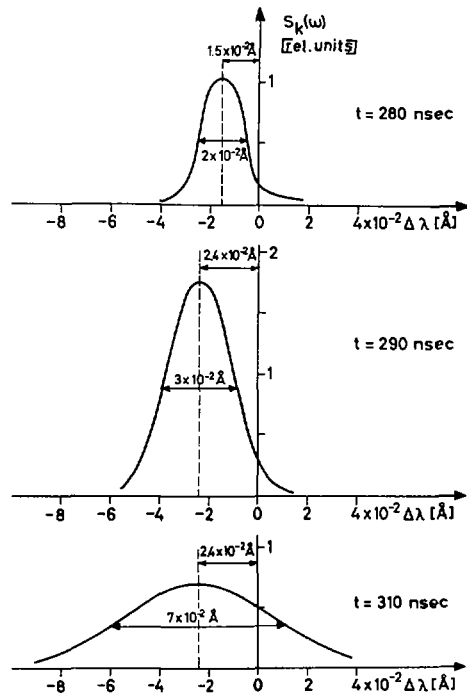


FIG. 2. Frequency spectra $S_k(\omega)$ of enhanced fluctuations at three points of time indicated by arrows in Fig. 1.

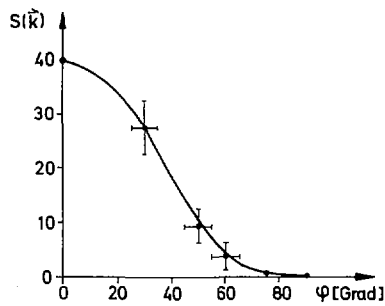


FIG. 3. Cone of propagation of enhanced fluctuations $S(\vec{k})$ with respect to the drift velocity \vec{v}_d . φ is the angle between \vec{k} and \vec{v}_d in the plane perpendicular to B_1 .

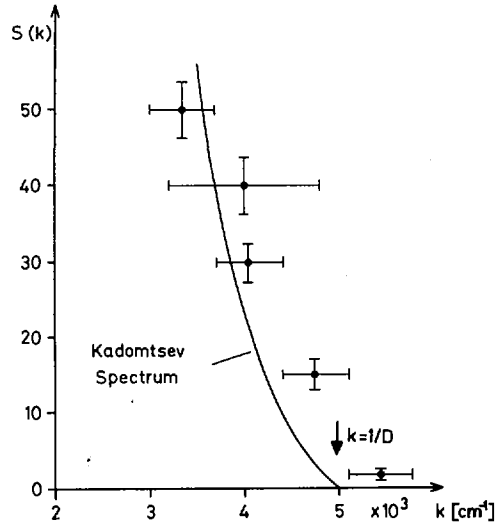


FIG. 4. Wave number spectrum $S(k)$ of enhanced fluctuations at time of maximum turbulence.

Simultaneously with the forward-scattering measurements, the density and electron temperature in the shock are determined by 90° -scattering ($\alpha \ll 1$).

Figure 1 shows the measured total level of density fluctuations $n_e S(\vec{k}, \omega)$ for $\theta = 2.5^\circ \pm 0.5^\circ$ ($|\vec{k}| = 4 \times 10^3 \text{ cm}^{-1}$) in a deuterium shock wave with Mach number 2.5 together with the magnetic field profile B . In the shock front, the level of fluctuations is strongly suprathermal, reaching at its maximum about 250 times the thermal value. At the back of the shock, the fluctuations decay to the thermal level.

Figure 2 shows the frequency spectra $S_k(\omega)$ of these fluctuations (corrected for instrumental width) at the three points of time indicated by arrows in Fig. 1. The spectra are shifted to the red with respect to the laser line. The absolute value of the shift corresponds to scattering from plasma waves with frequency $\omega \sim 0.5 \omega_{pi}$, ω_{pi} being the ion plasma frequency. Furthermore, the direction of shift shows that the waves propagate in the same direction as the electrons that carry the diamagnetic current in the shock front. This and the further result that the direction of shift reverses if the current is reversed indicate that the electron current drives the instability [5].

Figure 3 is a plot of the intensity of enhanced fluctuations at the time of maximum turbulence versus φ , the angle between wave vector \vec{k} and electron drift velocity \vec{v}_d in the plane perpendicular to B_1 . It shows that in this plane the turbulence is spread out through a cone, with half-intensity at about 40° to the drift velocity.

Figure 4 finally shows the short-wavelength part of the wave-number spectrum $S(\vec{k})$ of enhanced fluctuations at the time of maximum turbulence. The spectrum was measured by scattering ruby laser light and varying the scattering angle θ between 2° and 4° . Horizontal bars through the experimental points indicate the finite angle of acceptance of the scattered light.

At short wavelengths the measured spectrum shows a logarithmic cut-off for $|\vec{k}| > 1/D$, as predicted by Kadomtsev's theory of ion-wave turbulence [6], but the dependence on $|\vec{k}|$ is weaker than predicted. To investigate the long-wavelength part of the spectrum a scattering experiment using a pulsed CO₂ laser is currently under way. Until now the experiment suffers from stray light that is probably enhanced by deflection of the laser beam within the shock front.

We now briefly discuss the possible mechanism of the observed turbulence (for a more detailed discussion, see Ref. [4]). The observation that the frequency shift of the fluctuation spectrum reverses when the current in the shock front is reversed indicates that the electron drift drives the turbulence. The question therefore is: which waves become unstable under the conditions existing in our shock wave, viz. $v_d \sim 0.1 v_e$ ($v_e = (2 T_e/m_e)^{1/2}$) and $T_e \sim T_i$ as averages over the shock front. While ion-acoustic waves, most frequently enlisted to explain observed plasma turbulence, should be stable [7], electron cyclotron waves (Bernstein waves) propagating perpendicularly to a magnetic field can become unstable for $T_e \sim T_i$ and $v_d \ll v_e$ [8-10]. This drift instability results from the fact that the Doppler-shifted Bernstein waves "see" a positive slope of the ion distribution function and therefore undergo inverse Landau damping.

According to Ref. [10] the maximum growth rate of this electron cyclotron drift instability is

$$\frac{\gamma_{\max}}{\omega_{ce}} \sim 0.368 \frac{T_e}{T_i} \frac{v_d - v_i}{v_e} [(1 + k^2 D^2) - 0.075 \frac{T_e}{T_i}]^2 + 0.425 \left(\frac{T_e}{T_i}\right)^2]^{-1}$$

For our mean shock conditions (see above) and $kD = 0.8$, corresponding to the wave vector for which the level of turbulence has been measured, this yields $\gamma_{\max} \sim 2.5 \times 10^8 \text{ s}^{-1}$ ($\omega_{ce} = 2.5 \times 10^{10} \text{ s}^{-1}$).²

For a rough estimate of the growth rate γ needed for the waves to grow to the observed level (250 times thermal) in 30 ns we set $\exp 2\gamma t = 250$ and get $\gamma \sim 1 \times 10^8 \text{ s}^{-1}$. Thus the growth rate of the electron cyclotron drift instability seems sufficient to account for the observed level of fluctuations, and we believe that it is this instability which leads to the observed turbulence.

To get some insight into the process of dissipation by this electron cyclotron drift instability we have run a particle-in-cell simulation code for a set of parameters similar to experimental conditions. The model was the same as that used by Forslund et al. [8] except that ions were treated as unmagnetized. The following parameters were used: $\omega_{ce}/\omega_{pe} = 0.015$, $m_e/m_i = 0.001$, $T_{i1}/T_{e1} = 1$, system length = 256 initial Debye lengths, with 250 electrons and ions per Debye length.

The results (see Fig. 6) can be summarized as follows: The fluctuation energy $\langle E^2 \rangle / 8\pi$ starts to rise at $800 \omega_{pe}^{-1}$ and continues to rise during the whole computation time but exhibits a reduction in growth rate at $1500 \omega_{pe}^{-1}$. The ratio of the relative ion-electron mean velocity $\langle v_i - v_e \rangle$ (which is kept constant during the run) to the r. m. s. electron velocity $\langle v_e^2 \rangle^{1/2}$ starting from 0.7 drops off to 0.165 at the end of the run. The

² Computer calculations of the dispersion relation for electron cyclotron waves that were made for our shock conditions give roughly the same growth rates. They further show that for the first harmonic of Bernstein waves γ_{\max} is at $kD \sim 0.23$, but for the fourth harmonic at $kD \sim 0.8$.

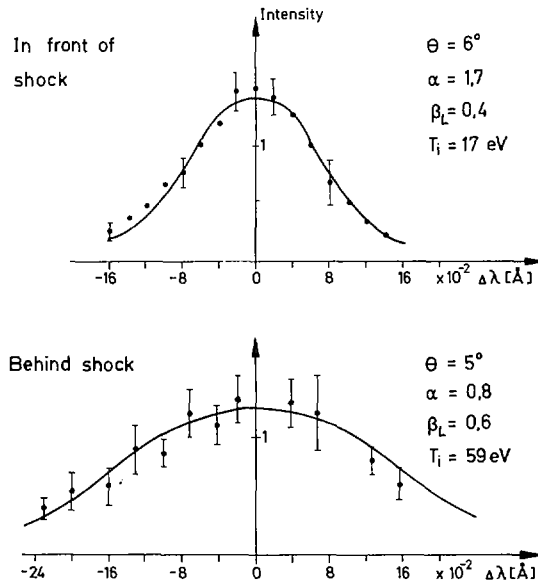


FIG. 5. Spectrum of thermal ion fluctuations in front of and behind a shock wave with Mach number $M = 2.5$ in deuterium.

mean electron velocity distribution shows a nearly symmetrical broadening. The ions form large vortices in phase space. The effective collision-frequency ν_{eff} rises up to ω_{pi} in accordance with experimental observations [2, 11].

2.3. Ion heating

Previous indirect determination of the ion heating in these shock waves using extended Rankine-Hugoniot relations [11] has shown that in shocks with Mach numbers $M < M_{\text{crit}}$ ³ the ions are only heated adiabatically, but for $M > M_{\text{crit}}$ non-adiabatic heating takes place that increases with Mach number (see Fig. 3 in Ref. [11] or Fig. 4 in Ref. [3]).

We now carried out a direct measurement of the ion temperature in such a shock by collective scattering of laser light at wavelengths shorter than the Debye length ($\alpha < 1$), where the fluctuation level is thermal (see previous section). Figure 5 shows the spectrum of thermal ion fluctuations behind the shock front of a Mach 2.5 shock, together with the corresponding spectrum in front of the shock. By comparison with theoretical profiles one gets for the ion temperatures $T_{i1} = 17$ eV and $T_{i2} = 59$ eV, while the corresponding electron temperatures (from 90° scattering) are $T_{e1} = 4$ eV and $T_{e2} = 100$ eV. These measured temperatures fit the extended Rankine-Hugoniot relations very well. Furthermore, one can show that the ion heating due to adiabatic compression in the shock front would yield $T_{i2\text{ad}} = 35$ eV. Thus most of the ion heating in this super-critical shock

³ M_{crit} , the "critical" Mach number, is 2.8 for $\beta = 0$ and decreases with increasing β .

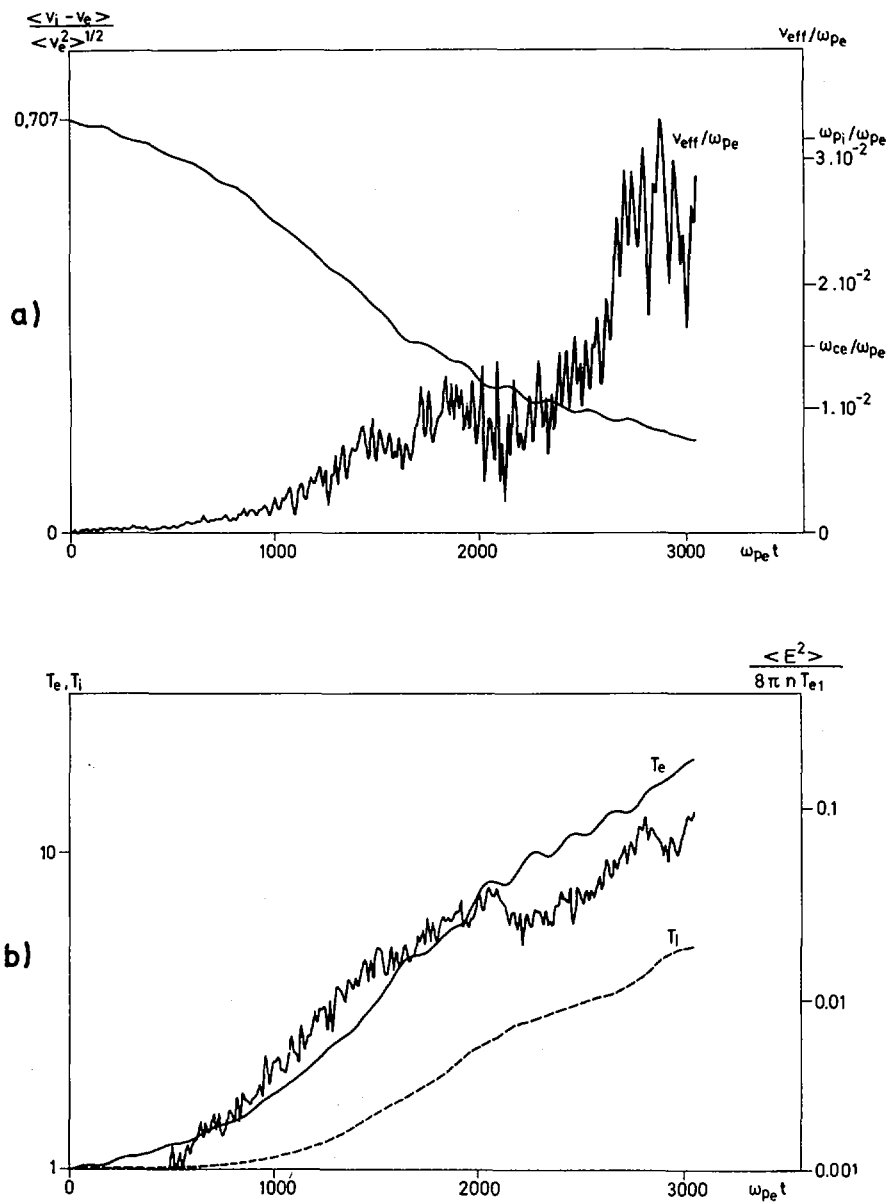


FIG. 6. Results of computer simulation for $\omega_{ce}/\omega_{pe} = 0.015$, $m_e/m_i = 0.001$, $T_{e1}/T_{i1} = 1$.

- a) Ratio of the current and r.m.s. electron velocities $\langle v_i - v_e \rangle / \langle v_e^2 \rangle^{1/2}$, and effective collision frequency ν_{eff} .
- b) Second moment of mean electron and ion distributions, T_e and T_i , and normalized fluctuation energy $\langle E^2 \rangle / 8\pi n T_{e1}$.

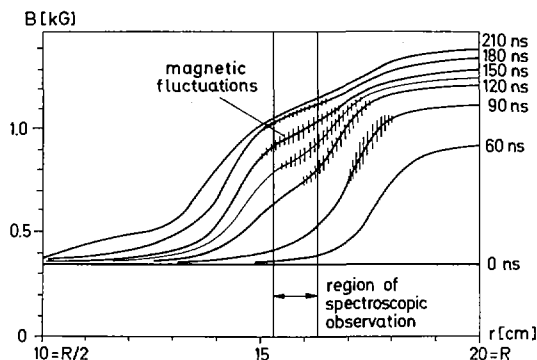


FIG.7. Magnetic field profiles $B(r)$ of non-stationary compression wave in deuterium ($n_1 = 3 \times 10^{12} \text{ cm}^{-3}$) showing "anomalous" diffusion in the piston region. The occurrence of magnetic fluctuations is indicated schematically.

wave ($M_{\text{crit}} = 1.8$) must be attributed to collisionless dissipation, which confirms our previous more indirect findings [3,11].

3. LOW- β COMPRESSION WAVES

3.1. The experiment "Minimax"

For the investigation of shock waves at lower plasma densities, where broader shock structures are to be expected, a theta pinch ("Minimax") with a larger coil diameter of 43 cm is used. In this coil, a trapezoidal magnetic field pulse (rise time 70 ns, peak field 1.5 kG) is generated by a Blumlein-type transmission line which is pulse-charged to 125 kV.

The working gas (H_2 , D_2 or a rare gas) is pre-ionized by UV-radiation emitted by two Z-pinchs, one at each end of the shock tube [1]. This UV-pre-ionization (for details see Ref. [12]) produces a radially homogeneous plasma of density $10^{12} - 10^{13} \text{ cm}^{-3}$ ($\beta \ll 1$) with electron temperatures of a few eV and with $T_e/T_i \geq 1$. Bias fields up to 500 G can be applied.

3.2. Macroscopic properties of compression waves

Figure 7, which is a plot of the magnetic field B versus the tube radius r at different points of time, shows the time evolution of a compression wave propagating into a deuterium plasma ($n_1 = 3 \times 10^{12} \text{ cm}^{-3}$, $B_1 = 350 \text{ G}$). For the applied piston field of 1.4 kG a stationary shock would have a Mach number $M = 3.5 (> M_{\text{crit}})$, and one would expect a magnetic field jump of about 2 (for one degree of freedom). The latter indicates that it is the flat part at the front of the wave (the "foot") where a shock develops, while the steep part is the piston.

These and similar magnetic field profiles for other Mach numbers agree very well with numerical calculations which explicitly take the ion distribution function into account (Vlasov description of ions) [13]. The calculations show that the "foot" in supercritical compression waves is due to the

dynamics of the ions: the overturning ion stream flushes electrons with it which in turn compress some magnetic flux ahead of the magnetic piston.

In the compression waves discussed here "anomalous" effects are only observed in the piston region. The flattening of the magnetic field profile in the piston region that starts to show up at about 120 ns in Fig. 7 is probably caused by anomalous field diffusion. To verify this conjecture the piston region was investigated in more detail.

3.3. Electric and magnetic field fluctuations

For this purpose a very fast miniature magnetic probe that can be used for frequencies up to 500 MHz was developed [14]. This probe shows strong coherent magnetic fluctuations with amplitudes up to 10 G and characteristic frequencies of about $0.5 \omega_{pi}$ to exist in the piston region (see Fig. 7) that later decay into random noise.

Simultaneously, the amplitude of fluctuating electric fields was measured spectroscopically. As pointed out in Ref. [15], strong oscillating electric fields can cause satellite lines of forbidden atomic lines, their intensity (relative to the allowed line) being proportional to $\langle E^2 \rangle$.

In our experiment the spectrum near the He I line at 4922 \AA (20% He admixture) was recorded with high time resolution using an 8-channel photomultiplier arrangement [14]. The plasma was viewed end-on and light from a section of a hollow plasma cylinder 1 cm wide was collected, as indicated in Fig. 7.

As an example Fig. 8 shows measured line profiles for two points of time during plasma compression. The two satellites merge into one line that is clearly enhanced at $t = 120 \text{ ns}$ (the slight blue-shift is due to quadratic Stark effect). Figure 9 shows the amplitude of the fluctuating electric fields as deduced from these measurements. The maximum amplitude of 5 kV/cm corresponds to an energy density of about 1% of the thermal energy of the electrons.

It can be shown [14] that the measured amplitude of magnetic fluctuations is consistent with the assumption that the fluctuations are "electrostatic" waves propagating parallel to the azimuthal current in the compression pulse.

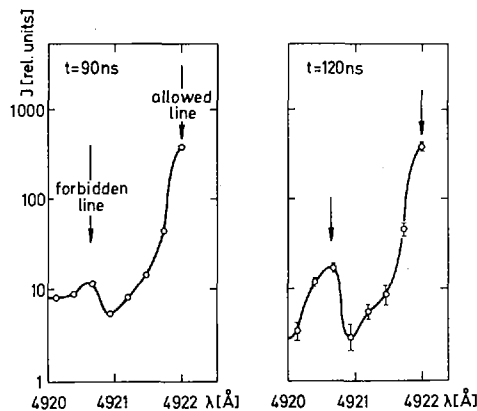


FIG. 8. Spectrum near the He I line at 4922 \AA . The intensity of the forbidden line is a measure of the energy density of fluctuating electric fields.

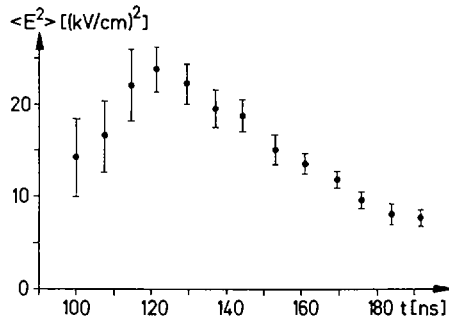


FIG. 9. Amplitude of electric fluctuations $\langle E^2 \rangle$ in the piston region of the compression wave shown in Fig. 7.

For the conditions existing in the piston region ($v_d \sim 0.2 v_e$ and $T_e \gg T_{i\theta}$, $T_{i\theta}$ being the azimuthal ion temperature) both ion acoustic [7] and electron cyclotron waves [9, 16] should be unstable. The latter only exist within a small angle to the plane perpendicular to the magnetic field, but for propagation in this direction their growth rate is substantially larger than that of the ion acoustic instability. We therefore expect the electron cyclotron waves to dominate the turbulence. The frequency ($\omega \sim 0.5 \omega_{pi}$) and growth rate ($\gamma \sim 0.5 \omega$) of these waves as calculated for our plasma parameters agree very well with the time evolution of the observed magnetic fluctuations [14].

4. SUMMARY

Summarizing these results we may speculate that in perpendicular collisionless shock waves and, in general, in a plasma with electric currents flowing perpendicularly to magnetic field lines the electron cyclotron drift instability may give rise to turbulence and collective dissipation, both under $T_e \sim T_i$ and $T_e \gg T_i$ conditions.

REFERENCES

- [1] CHODURA, R. et al., in Plasma Physics and Controlled Nuclear Fusion Research (Proc. Conf. Novosibirsk, 1968) 1, IAEA, Vienna (1969) 81.
- [2] KEILHACKER, M., KORNHERR, M., STEUER, K.-H., Z. Physik 223 (1969) 385.
- [3] CHODURA, R. et al., in Controlled Fusion and Plasma Physics (Proc. 4th Europ. Conf. 1970), Rome, (1970) 56.
- [4] KEILHACKER, M., STEUER, K.-H., Phys. Rev. Letts 26 (1971) 694.
- [5] STEUER, K.-H., KEILHACKER, M., Bull. Amer. Phys. Soc. 15 (1970) 1410.
- [6] KADOMTSEV, B. B., Plasma Turbulence, Academic Press, London (1965).
- [7] STRINGER, T. E., J. Nucl. Energy, Part C 6 (1964) 267.
- [8] FORSLUND, D. W., MORSE, R. L., NIELSON, C. W., Phys. Rev. Letts 25 (1970) 1266.
- [9] LASHMORE-DAVIES, C. N., J. Phys. A. 3 (1970) L 40.
- [10] GARY, S. P., BISKAMP, D., J. Phys. A 4 (1971) L 27.
- [11] KORNHERR, M., Z. Physik 233 (1970) 37.

- [12] KEILHACKER, M., PECORELLA, F., VLASES, G. C., *Physics Fluids* 13 (1970) 2253.
- [13] CHODURA, R., v. FINCKENSTEIN, K., Institut für Plasmaphysik, Garching, Report IPP 1/113 (1970).
- [14] NIEDERMEYER, H., Institut für Plasmaphysik, Garching, Report IPP 1/118 (1971).
- [15] BARANGER, M., MOZER, B., *Phys. Rev.* 123 (1961) 25.
- [16] GARY, S. P., SANDERSON, J. J., *J. Plasma Physics* 4 (1970) 739;
GARY, S. P., *J. Plasma Physics* 4 (1970) 753.

SHOCK WAVES AND TURBULENT HEATING IN LOW-DENSITY PLASMAS

P. BOGEN, K. J. DIETZ, K. H. DIPPEL, E. HINTZ,
K. HÖTHKER, F. SIEMSEN, G. ZEYER
Institut für Plasmaphysik der Kernforschungsanlage Jülich,
Association EURATOM-KFA,
Federal Republic of Germany

Abstract

SHOCK WAVES AND TURBULENT HEATING IN LOW-DENSITY PLASMAS.

Shock heating and shock structures are studied in theta-pinch-like devices in a wide range of plasma parameters n_{e1} , B_1 , m_i , and of wave speeds u_1 ($3 \times 10^6 \text{ cm s}^{-1} \leq u_1 \leq 10^8 \text{ cm s}^{-1}$). Densities and temperatures were determined locally by interferometry and by Thomson scattering. Magnetic and electric fields were measured with small high-frequency probes.

Previous investigations of perpendicular, hydromagnetic shocks at $\beta_1 \ll 1$ and $M_A < M_{A, \text{critical}}$ at densities above 10^{14} cm^{-3} are extended to densities close to 10^{13} cm^{-3} and to other mass ratios m_e/m_i . Shocks are nearly collision-free even with respect to the initial state. A scaling law is obtained for the effective collision frequency ν_{eff} , deduced from measured turbulent-heating rates and current densities. Results show that $\nu_{\text{eff}} \approx 10^{-3} (T_e/T_i) (v_d/c_s) \omega_{pi}$.

Studies are extended to small Alfvén-Mach numbers, where shock structures are still collision-dominated. Comparison with theory shows good agreement.

In the same density range, shocks are generated at $\beta_1 \approx 0.3$, and with $M_A \gg M_{A, \text{critical}}$. From the observed electron heating rates and the electron density jump, together with the shock relations, estimates for turbulent ion-heating rates are obtained.

Investigation of the structure of collision-dominated shocks in magnetic field-free plasma shows that electron temperature and density front are well separated; the width of separation agrees with theoretical estimates.

Attempts are made to heat low-density ($n \leq 10^{13} \text{ cm}^{-3}$), magnetic-field-free plasma by fast magnetic compression. In deuterium, an anomalously broad current sheath is observed. Nevertheless, deuteron temperatures of $\approx 10 \text{ keV}$ and relatively high values of the local β ($\beta \approx 10$) are achieved in a low-energy theta-pinch ($\approx 10 \text{ kJ}$). Electric and magnetic field fluctuations of large amplitude occur. In argon, at large radii, a stationary electromagnetic sheath is found with a width of a few c/ω_{pe} and an electric potential jump as required by theory. Ion energies and compression ratios observed at maximum compression are in accordance with implosion velocities.

I. INTRODUCTION

In the last few years, the study of collisionless low- β shocks by means of co-operative light scattering [1] has considerably advanced our understanding of collisionless energy dissipation by turbulent resistivity. A satisfactory theoretical description of the processes has, however, not yet been achieved. This implies that reliable prediction of the value of the effective conductivity for given plasma parameters is not possible. To improve this situation, an attempt was made to determine effective collision frequencies over a wide density range and for different mass ratios m_e/m_i and to compare them with proposed scaling laws [2].

For the initial conditions normally used, shocks which are collisionless at higher Alfvén-Mach numbers M_A become collision-dominated at small M_A . For such shocks, however, a theoretical description based on the

Boltzmann transport equation has been developed. Experimental investigations were therefore extended to shock waves of low strength in order to examine whether agreement between theory and experiment does exist, and whether a continuous transition from laminar to turbulent shocks can be achieved.

High- β , high Alfvén-Mach number shocks have previously been investigated at our laboratory [3] for various conditions. Results were mainly based on magnetic probe measurements, and conclusions on heating rates were rather indirect. Identification of dissipation mechanisms was not possible. It was believed that anomalous ion viscosity is responsible for the formation of the shock. Some progress was expected by measuring densities and electron temperatures by means of Thomson scattering. Assuming that the Rankine Hugoniot relations are fulfilled, estimates of ion energy can then be obtained from the pressure balance equation.

For relatively high initial pressures and using special methods of pre-heating, fast magnetic compression of nearly magnetic field free plasma has proved to be a very efficient method of heating plasmas to thermonuclear temperatures [4]. Again the basic dissipative mechanism is poorly understood. Since the theta-pinch is considered a very promising method for containment devices [5] basic studies were started to learn more about the responsible dissipation mechanism and to examine existing scaling laws at low densities [6]. The possibility of applying theta-pinch techniques to low densities may enable us to study confinement at low densities and correspondingly low magnetic fields, i. e. with modest expenditure.

2. EXPERIMENTAL ARRANGEMENT AND DIAGNOSTIC METHODS

Shock waves were generated in three theta-pinch devices with the following characteristic parameters:

	coil length	coil diam.	bank energy	voltage	density
I.	45 cm	20 cm	4 kJ	40 kV	$10^{13} - 10^{14} \text{ cm}^{-3}$
II.	40 cm	20 cm	5 kJ	25 kV	$10^{14} - 10^{15} \text{ cm}^{-3}$
III.	80 cm	40 cm	15 kJ	120 kV	$10^{12} - 5 \times 10^{13} \text{ cm}^{-3}$

All machines were operated in basically the same way [3]. A highly ionized plasma is produced by an electrodeless ring discharge, which is short-circuited at a suitable time. A slowly rising magnetic field (15 - 20 μs rise time) can then be applied and penetrates into the afterglow plasma; the corresponding electrical circuit is crowbarred at current maximum. The magnetic piston field can be switched on at any time. For all three devices the inductance of the external circuit is small compared to the coil inductance. In I. and II. low inductance resistors of such magnitude could be introduced that a magnetic field pulse of relatively small amplitude, small rise time, and long decay time was produced in the compression coil.

Electron densities were measured space-resolved by means of microwave probes in combination with a 2-mm or a 4-mm microwave interferometer [6] (mainly in the pre-heating phase) or by Thomson scattering, using high power Q-switched ruby lasers (with the beam directed along the coil axis).

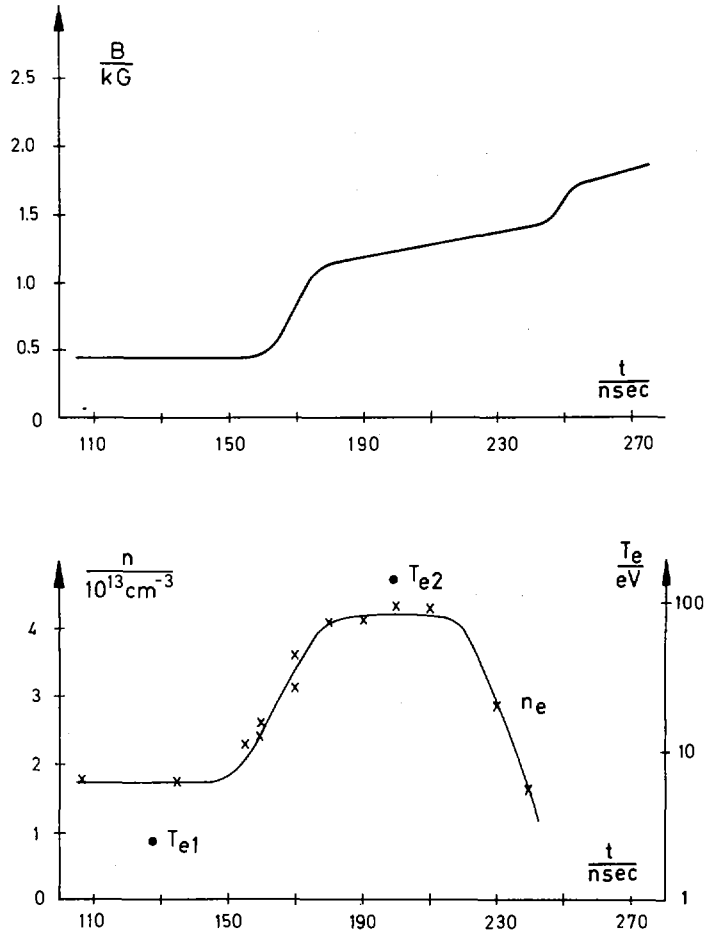


FIG. 1. Measured profiles of B and n_e ; T_e ahead of and behind the shock (case 2 of Table I).

TABLE I. CHARACTERISTIC PARAMETERS OF SHOCKS USED TO OBTAIN ν_{eff} AND ν^* IN Fig. 2

Gas	n_{e1} [cm^{-3}]	α_1	M_A	T_{e2} [eV]	T_e/T_1	v_d/c_s	ω_{pi} [Hz]
1. D_2	9×10^{13}	2.2×10^{-4}	1.7	11.6	2.26	17.4	1.06×10^{10}
2. D_2	1.7×10^{13}	1.1×10^{-3}	2.4	140	21.6	13.8	4.75×10^9
3. A	5×10^{13}	4.0×10^{-4}	?	100	17.1	68.4	2.08×10^9
4. D_2	4.4×10^{13}	3.4×10^{-4}	3.2	55	11.4	14.9	7.79×10^9

$\alpha_1 = (\omega_{ce}/\omega_{pe})^2$, ω_{ce} - electron cyclotron frequency, ω_{pe} , ω_{pi} - electron and ion plasma frequency; M_A - Alfvén-Mach number; v_d - drift velocity; c_s - ion sound speed. The subscripts 1, 2 refer to the states ahead of and behind the shock, the subscripts e, i to electrons and ions, respectively.

In the latter case, stray light levels could be reduced below values equivalent to electron densities of $2 \times 10^{12} \text{ cm}^{-3}$. At electron densities above $2 \times 10^{14} \text{ cm}^{-3}$, an optical Mach-Zehnder interferometer with the line of sight along the coil axis was employed. Electron temperatures were derived from Thomson scattering measurements. Magnetic and electric fields were measured with probes consisting of open loops of glass-insulated wire, and with double probes of high frequency response, respectively.

3. EXPERIMENTAL RESULTS

3.1. Perpendicular hydromagnetic shocks

We shall first report on results obtained on low- β shocks with the main dissipation mechanism being anomalous resistivity ($\beta \ll 1$; $M_A < M_{A, \text{critical}}$). Figure 1 shows typical profiles of the magnetic field B and of the electron density n_e as well as the electron temperature T_e ahead of and behind the shock front. Further characteristic plasma and shock parameters are given in Table I, case 2. The initial magnetic field was parallel to the compressing field. (No significant differences were noticed for antiparallel fields).

Comparing the rise time τ_s of the shock with the electron-ion collision time $(1/\nu_{ei})_1$, we obtain $\tau_s \cdot \nu_{ei,1} = 2, 2$, i. e. binary collisions contribute to the formation of the shock only in the very early phase. Magnetic field and density compression ratios are in good agreement with the shock relations. This is also true for the electron temperature, assuming that only electrons are heated. The effective collision frequency as determined from the energy balance equation, is $\nu_{\text{eff}} \approx 0.8 \times 10^9 \text{ s}^{-1}$ whereas the calculated collision frequency for binary collisions behind the front is $\nu_{ei,2} = 4.8 \times 10^5 \text{ s}^{-1}$, i. e. $\nu_{\text{eff}}/\nu_{ei,2} \approx 2 \times 10^3$ ($\nu_{\text{eff}}/\nu_{ei,1} \approx 10$).

To obtain information on the scalings of ν_{eff} , shock profiles were determined and evaluated for various other plasma parameters and shock strengths.

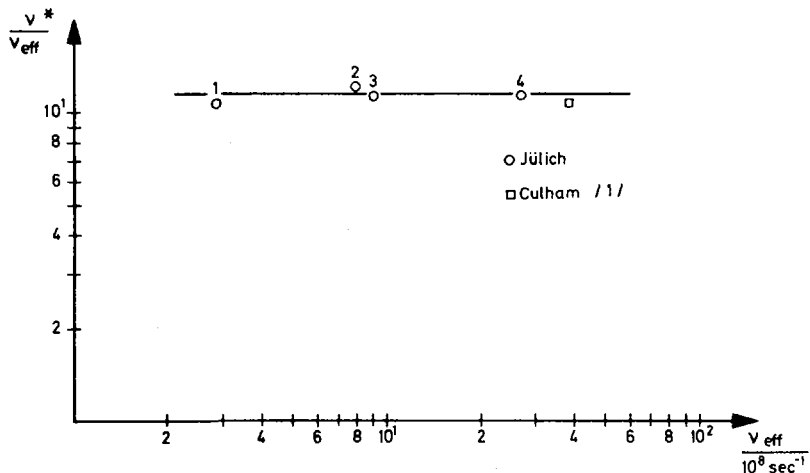


FIG. 2. Measured effective collision frequencies ν_{eff} compared with $\nu^* = 10^{-2} (T_e/T_i) (v_d/c_s) \omega_{pi}$.

The more significant parameters are summarized in Table I. In the argon case, the Alfvén-Mach number could not be determined reliably because the stage of ionization was unknown.

For the determination of T_e/T_i , v_d/c_s , and ω_{pi} the mean values of n , T , and B between initial and final state were used. The ion temperature was obtained by assuming adiabatic heating with $\gamma = 5/3$. For the above cases the effective collision frequencies were determined, and their values compared with the theoretical estimates ν^* obtained for ν_{eff} by Sagdeev [7] and by Sizonenko and Stepanov [8] who both assume that interaction of the electrons with electric field fluctuations due to ion sound turbulence is responsible for the anomalous resistivity. Concerning the magnitude of ν_{eff} , Sagdeev predicts values roughly an order of magnitude too high, while Sizonenko's and Stepanov's values are an order of magnitude too low. With regard to the scaling we find good agreement with Sagdeev, as shown in Fig. 2.

A discussion of the question whether other types of microinstabilities [9, 10] may be responsible for the observed anomalous resistivity is published elsewhere [11].

By reducing the piston field it was possible to lower the shock strength to such values that shock waves in the parameter range which was accessible to us and in which most of the shock experiments discussed in the literature have been performed become collision-dominated. We have compared our results with a theory of the shock structure by Hu [12] which is based on the Boltzmann equations for electrons and ions and on Maxwell's equations. For weak shocks the following expression for the shock profile is found: $\delta B \sim \tanh(\epsilon x/L)$. The dependence is the same as that, e.g. for the density, in weak gas-dynamic shocks. ϵ , a measure of the shock strength, is defined as $\epsilon = \Delta u / 2u_s$, where Δu is the velocity jump across the shock, and $u_s = (c_s^2 + v_A^2)^{1/2}$ is the magneto-sonic speed of the plasma. The scaled shock thickness L is a complex expression depending on the dimensionless parameters $(\omega_{ce} \tau_{ee})_1$, β_1 , and m_e/m_i .

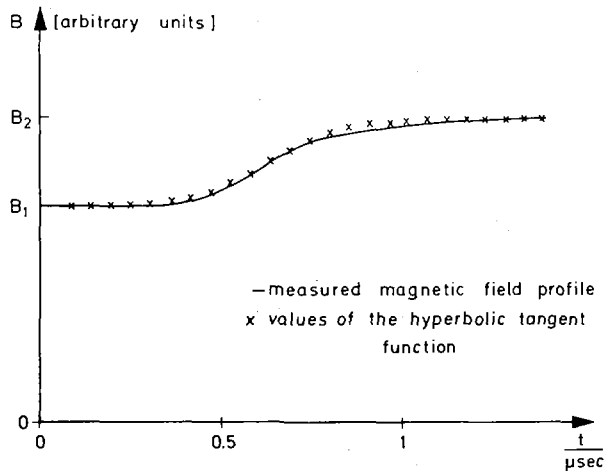


FIG. 3. Comparison of experimental profile with tanh-function.

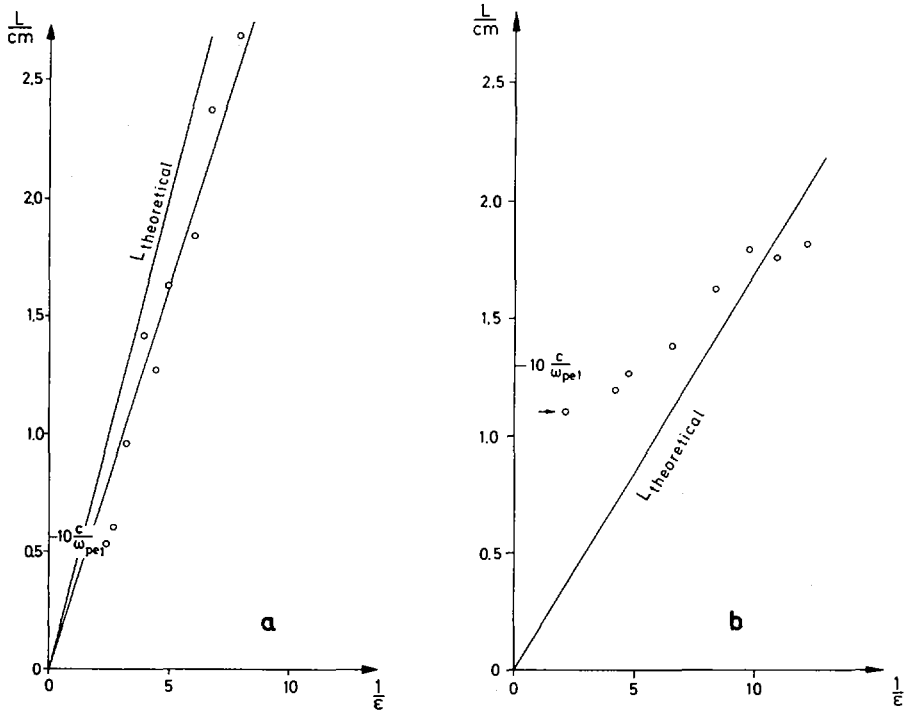


FIG. 4. a) (case 2 of Table II),

b) (case 1 of Table II).

Measured and calculated shock widths as functions of the reciprocal shock strength $1/\epsilon$.

Good agreement between measured profiles of the magnetic field in the shock and the expected hyperbolic tangent dependence is demonstrated by Fig. 3.

Figure 4 shows a comparison of numerically calculated shock thicknesses, most of which were taken from Ref. [13], with measured values plotted against $1/\epsilon$. Figure 4a corresponds to the conditions of case 2 in Table II. Within the experimental errors quantitative agreement with the theoretically expected shock thickness exists. (The maximum errors in the determination of the experimental shock thickness L and the theoretical shock thickness L_{theor} are estimated to be 20%, in the determination of $1/\epsilon$, 15%. Similarly, good agreement is obtained for the cases 3 and 4 of Table II. The situation is different in Fig. 4b, corresponding to case 1 of Table II. For small ϵ again good agreement is found; however, significant deviations appear at values $\epsilon \approx 0.1 - 0.2$. The supposition that in this case ion sound turbulence develops in the shock front is supported by the fact that the instability conditions for the ion acoustic instability are fulfilled ($v_d/c_s > 1$, $T_e/T_i > 1$), and that the growth rate, in contrast to the other cases investigated, is large compared to the electron-ion collision frequency. Furthermore, the experimental curve can well be extrapolated to the one point in Fig. 4b, marked by an arrow, which is identical with point 2 of Fig. 2, and which fits well to the Sagdeev scaling for ion sound turbulence.

TABLE II. INITIAL CONDITIONS AND CHARACTERISTIC LENGTHS OF THE LOW-MACH-NUMBER SHOCKS INVESTIGATED

	n_{e1} [cm^{-3}]	T_{e1} [eV]	B_1 [G]	β_1	$(\omega_{ce} \tau_{ee})_1$	λ_s [cm]	c/ω_{pe} [cm]	ν_{ce} [cm]
1.	1.7×10^{13}	2.5	450	0.017	61	0.46	0.13	0.0145
2.	9.0×10^{13}	2.2	450	0.079	9.5	0.087	0.056	0.0136
3.	8.3×10^{13}	1.0	225	0.131	1.57	0.015	0.059	0.0183
4.	1.9×10^{14}	1.0	450	0.075	1.36	0.0066	0.039	0.0091
5.	1.8×10^{14}	1.4	110	1.67	0.59	0.014	0.040	0.0440

λ_s = mean free path for electron-electron collisions

ν_{ce} = electron cyclotron radius

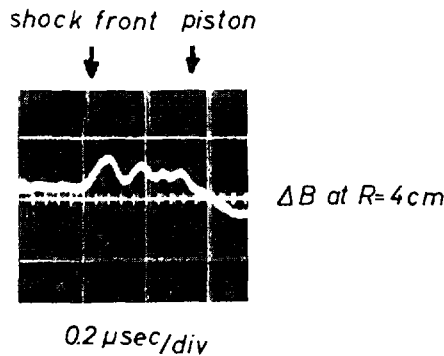


FIG. 5. Oscillatory structure for a shock at low density, with $\Delta B/B_1 \approx 0.2$. (Wave field and piston field are antiparallel).

A detailed discussion of the question of which dissipation mechanism is dominant for the different plasma conditions, together with statements about the range of applicability of the low-shock-strength approximation will be found in Ref. [15]. In addition, the last case of Table II (with $\beta > 1$), where deviations between experimental values and theory occur, will also be discussed there.

By including electron inertia into the low-shock-strength theory, Grad and Hu [14] arrived at a condition for the appearance of oscillatory structures behind the shock front. This condition is fulfilled for $\epsilon > 0.1$ in case 1, but oscillations could not be observed in the shock profiles. This again indicates enhanced resistivity. By reducing the initial density further (with the existing equipment n_e could not be measured), an oscillatory structure showed up behind the front, as can be seen from Fig. 5. Theoretical and experimental values of the oscillation period are in reasonable agreement.

For shocks with $\beta \leq 1$ and $M_A \gg M_{A, \text{critical}}$ [3] only preliminary investigations have been performed. Figure 6 shows measured profiles of n_e , and B , and the electron temperature ahead of and behind the front. The characteristic plasma parameters and the Alfvén-Mach number are: $\beta_1 \approx 0.33$;

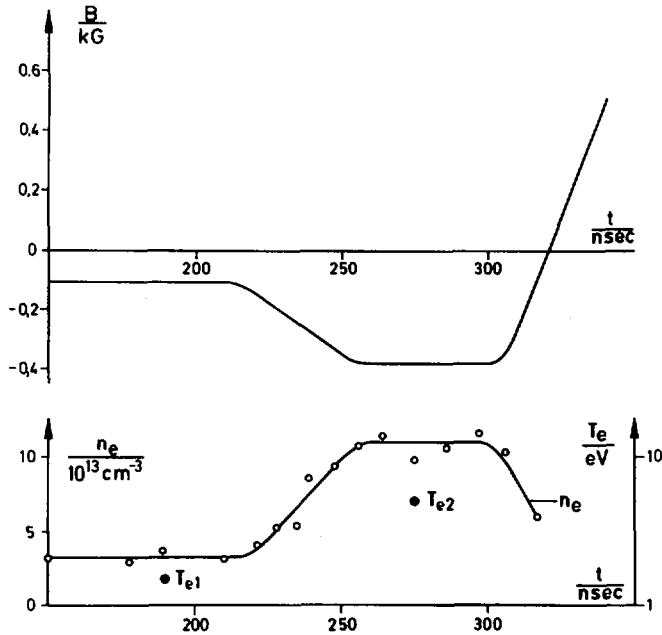


FIG. 6. Measured profiles of n_e and B for a shock with $M_A \gg M_{A, \text{crit.}}$ and $\beta_1 \approx 0.3$; T_e ahead of and behind the shock front.

$(\omega_{ce} \tau_{ei})_1 = 5.4$; $M_A \approx 7$; $T_{e1} = 1.5$ eV, $n_{e1} = 3.3 \times 10^{13}$ cm $^{-3}$, $T_{e1}/T_{i1} = 1$.

The ratios n_2/n_1 , B_2/B_1 , and u_1/u_2 all give the value expected from the shock relations: $\eta \approx 3.5$. The electron temperature increases, however, only to $T_e \approx 5$ eV, a value slightly above that expected from adiabatic heating, while from the shock relations one expects $T_e + T_i \approx 100$ eV. The ion temperature should therefore achieve $T_i \approx 100$ eV. With this value pressure balance across the piston would also be satisfied. From the density profile we obtain for the shock width $\Delta \approx 0.8$ cm $\approx 9 c/\omega_{pe}$; on the other hand, the ion-ion mean free path for binary collisions in the downstream plasma should be of the order 100 cm.

3.2. Shock structure and plasma heating in plasma with low internal magnetic field

In case of strong collision-dominated plasma shocks with $B_1 \approx 0$, the basic dissipation mechanism limiting the steepening of the wave is ion viscosity. For stationary shocks, energy transfer from the ions to the electrons has to be considered, which results in an equalization of ion and electron temperatures. Because of the high thermal conductivity of the electrons, the electron temperature propagates ahead of the density and ion temperature jump [16]. The balance equation for the heat flux: $\kappa \cdot \text{grad } T_e = 3 n_e K T_e u_1/2$ yields a separation between the electron temper-

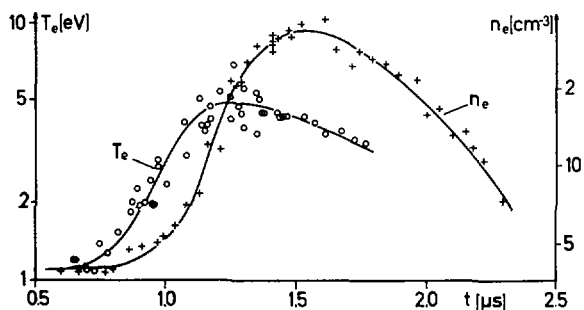


FIG. 7. Measured profiles of T_e and n_e for a collision-dominated viscous shock at $M \approx 4$.

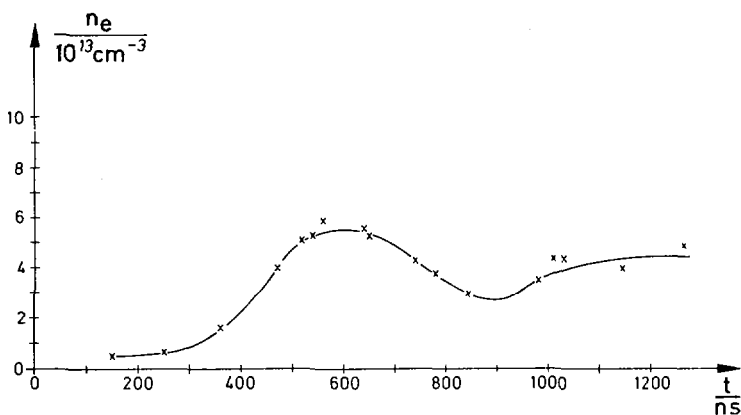


FIG. 8. Temporal development of n_e on the axis for a fast theta pinch with deuterium at the initial density $n_{e1} = 5 \times 10^{12} \text{cm}^{-3}$.

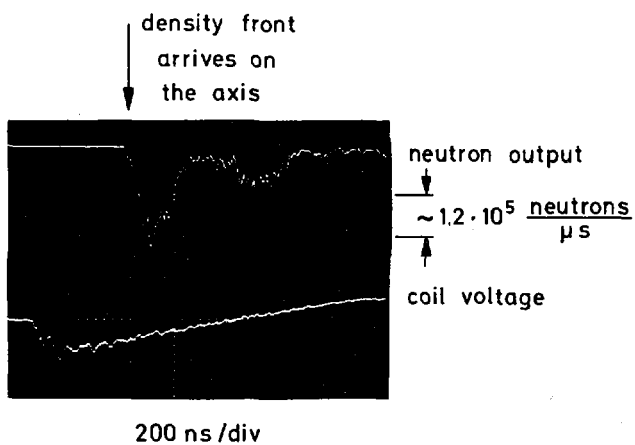


FIG. 9. Neutron emission as function of time in deuterium at $n_{e1} = 5 \times 10^{12} \text{cm}^{-3}$.

ature and density front [16] $\Delta T_e = 4 (\kappa_2 - \kappa_1) / 15 n_e K u_1$, where κ is the electron thermal conductivity. The separation width ΔT_e should scale with the Mach number as $\Delta T_e \sim M^4$.

Density and temperature behind the front are determined by the standard shock relations. For an experimental verification of the theoretical model on plasma shock structures, it is essential that the plasma has a sufficiently high degree of ionization, because otherwise even for strong shocks ($M \approx 4$) energy losses due to ionization and radiation play an important part and must be taken into account in the conservation relations. Figure 7 shows measured electron density and temperature profiles for a plasma shock with: $n_{e1} = 7 \times 10^{14} \text{ cm}^{-3}$, $T_1 = 1.3 \text{ eV}$, $M \approx 4$ (generated in device II). The observed separation is in reasonable agreement with the theoretical prediction ($\approx 0.15 \mu\text{s}$). Since the plasma is not in local equilibrium with respect to ionization the degree of ionization does not follow from the electron temperature. The observed compression ratio $\eta \approx 5$ indicates that energy losses are significant. Taking into account ionization in the conservation laws, one obtains an estimate of the degree of ionization ($n_e/n_{\text{total}} \approx 70\%$). More details about this work will be found in Ref. [17].

Irreversible heating of low-density, magnetic-field-free plasmas by fast magnetic compression was studied in device III. Previous investigations [6] of the implosion of highly ionized deuterium and argon plasmas at electron densities between 10^{13} cm^{-3} and 10^{12} cm^{-3} had shown that the observed piston velocities varied with the coil voltage and mass density as theoretically expected. In deuterium, the measured compression ratios $n_{e \text{ final}} / n_{e1}$ were too high and particle energies therefore too low; the width of the sheath Δ was anomalously broad ($\Delta \approx$ coil radius R ; compression ratio $\eta \approx 10$). The sheath was studied meanwhile in more detail with electric and magnetic probes. Field measurements were performed along the radius in the central plane of the coil; magnetic fields were measured simultaneously at the same radius and at two azimuthal positions; angles between them were varied from $0 - \pi/2$. Large electric and magnetic field fluctuations were measured in the whole current sheath with amplitudes of $E = 1 - 2 \text{ kV/cm}$ and $\vec{B} \approx 500 \text{ G}$, respectively, both electric and magnetic field fluctuations contained frequencies up to 50 MHz, the limit for our detecting equipment. An important result was that magnetic field fluctuations at different azimuthal positions were almost identical, proving that flute-like instabilities had not developed. The temporal development of the electron density on the axis was measured by Thomson scattering. The result is shown in Fig. 8. The compression ratio is indeed $\eta \approx 10$ [6]. From the observed period of the density oscillation we conclude that the line density N is approximately constant during the implosion ($\tau = 2\pi (m_1 N)^{1/2} / B_{\text{ext}}$). Initially, the electron temperature on the axis is $T_e \approx 1 \text{ eV}$. At the time of maximum compression, its value is about 5 eV, i. e. electrons are only heated adiabatically. During the next $0.5 \mu\text{s}$ pressure equilibrium is reached and the electron temperature rises to about 20 eV. Since pressure balance for $B_{\text{ext}} = 4.3 \text{ kG}$ requires $T_e + T_i \approx 10^8 \text{ }^\circ\text{K}$ ($\beta_{\text{axis}} \approx 10$), it is concluded that $T_1 \approx 10^8 \text{ }^\circ\text{K}$. This is confirmed by the measured values of the neutron output (Fig. 9) from which mean ion energies of $\approx 10 \text{ keV}$ are derived. According to X-ray measurements with the foil absorption technique (side on), electron temperatures in the sheath exceed 1.5 keV. Hard X-rays are not observed.

Previous measurements [6] in argon at maximum compression had yielded energies of about 10 keV and a plasma diameter of about 18 cm, as

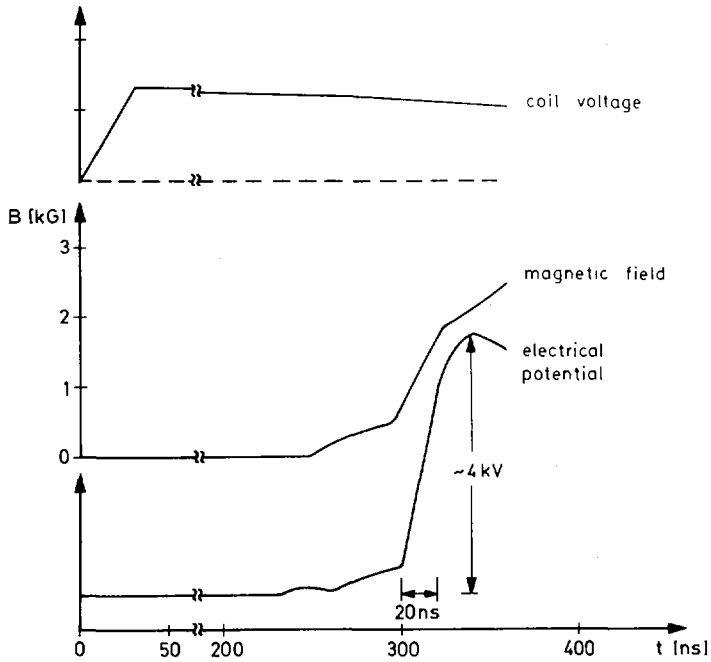


FIG.10. Stationary electromagnetic sheath during the fast magnetic compression of argon at $n_{e1} = 1 \times 10^{13} \text{ cm}^{-3}$.

expected from observed implosion velocities. Electric probe measurements showed now that fluctuation amplitudes were, at least, a factor of 50 lower than in the deuterium case. In the early phase of the implosion a stationary electromagnetic sheath is observed with properties as predicted by theory [18]. The corresponding magnetic field signal and the integrated electric field signal are shown in Fig.10. The sheath width is about $2 c/\omega_{pe}$, the potential jump is $\approx 4 \text{ keV}$ corresponding to A III ions at velocities of $\approx 2 \times 10^7 \text{ cm/s}$.

4. CONCLUSIONS

Studies of the scaling of effective collision frequencies in collisionless, resistive shocks show $\nu_{\text{eff}} \approx 10^{-3} (T_e/T_i) (v_d/c_s) \cdot \omega_{pi}$; i.e. there is good agreement with the scaling proposed by Sagdeev; however, concerning the magnitude of ν_{eff} , his formula gives values a factor of ten too high. At low Alfvén-Mach number, where shocks get collision-dominated, a detailed comparison with theory is performed. For sufficiently small shock strength the measured shock structures agree with theory, confirming in particular the values of the transport coefficients used. At low β , the transition from laminar to turbulent shock structure is observed by increasing the shock strength. At medium β , collisionless shocks at $M_A \gg M_{A,\text{critical}}$ are generated with a width $\Delta \approx 9 c/\omega_{pe}$; from pressure balance and shock relations $T_i \approx 100 \text{ eV}$ is obtained.

A detailed investigation of the structure of viscous shocks in collision-dominated, magnetic-field-free plasmas shows well separated electron density and electron temperature fronts; the width of separation is in agreement with theory.

Heating of magnetic-field-free plasmas by fast magnetic compression is extended to low particle densities. In deuterium and in argon ion "temperatures" of ≈ 10 keV are achieved, showing that thermonuclear temperatures are not necessarily only obtained with Mega-Joule capacitor banks. In deuterium a turbulent plasma-magnetic field boundary layer is observed during the implosion. In argon, an almost stationary electro-magnetic sheath is formed with a potential jump of ≈ 4 keV and a width of $\approx 2 c/\omega_{pe}$. Electrostatic shocks have not been found.

ACKNOWLEDGEMENTS

We would like to thank Dr. H. Kever for valuable advice and helpful discussions, and Dr. P. Cloth and Dr. H. Conrads for assisting with the neutron measurements. Technical assistance of D. Belitz, E. Brandt, W. Cremerius, E. Noczinski, A. Scholl, and W. Wiegmann is gratefully acknowledged.

REFERENCES

- [1] DAUGHNEY, C. C., HOLMES, L. S., PAUL, J. W. M., Phys. Rev. Letts 25 (1970) 49; PAUL, J. W. M., GOLDENBAUM, G. C., HIYOSHI, A., HOLMES, L. S., HARDCASTLE, R. A., Nature 216 (1967) 363.
- [2] DIPPEL, K. H., HÖTHKER, K., HINTZ, E., in Controlled Fusion and Plasma Physics (Proc. 4th Europ. Conf., Rome, 1970) 55.
- [3] HINTZ, E., Plasma Physics and Controlled Fusion Research (Proc. Conf. Novosibirsk, 1968) 1, IAEA, Vienna (1969) 69.
- [4] See, for example, Pulsed High Density Plasmas (Proc. APS Top. Conf. Los Alamos, 1970), Springfield, Virginia, USA.
- [5] Papers IAEA-CN-28/J-2, J-3 and J-4 of these Proceedings.
- [6] DIETZ, K. J., HINTZ, E., in Controlled Fusion and Plasma Physics (Proc. 4th Europ. Conf., Rome, 1970), Rome (1970) 60.
- [7] SAGDEEV, R. Z., Applied Mathematics (Proc. Symp. New York, 1965) 18 (1967) 281.
- [8] SIZONENKO, V. L., STEPANOV, K. N., Nucl. Fus. 10 (1970) 155.
- [9] GARY, S. P., SANDERSON, J. J., J. Plasma Physics 4 (1970) 739.
- [10] LASHMORE-DAVIES, C. N., Culham Lab. Progr. Rep. CLM-P 253 (1970).
- [11] DIPPEL, K. H., HÖTHKER, K., HINTZ, E., "Thomson Scattering Measurements on Collisionless MHD Shock Waves at Low Densities" (to be published).
- [12] HU, P. N., Physics Fluids 9 (1966) 89.
- [13] GRAD, H., in Collision-Free Shocks in the Laboratory and in Space (Proc. Study Group, Frascati, Italy, 1969) 47.
- [14] GRAD, H., HU, P. N., Physics Fluids 10 (1967) 2596.
- [15] DIPPEL, K. H., HINTZ, E., ZEYER, G., Experimental Results on the Structure of Low-Amplitude Perpendicular MHD-Shocks (to be published).
- [16] ZEL'DOVICH, Ya., RAIZER, Yu. P., Physics of Shock Waves and High Temperature Hydrodynamic Phenomena 2, Academic Press, New York (1967) 515.
- [17] BOGEN, P., DIPPEL, K. H., HINTZ, E., SIEMSEN, F., Structure of Collision-Dominated Shocks in Highly Ionized Deuterium Plasma with Low Internal Magnetic Field, in Phenomena in Ionized Gases (Proc. 10th Int. Conf. Oxford, 1971) (to be published).
- [18] LONGMIRE, C. L., Elementary Plasma Physics, Interscience Publishers, New York (1967).

ION HEATING IN A HIGH-VOLTAGE THETA PINCH*

W.D. DAVIS, A.W. DeSILVA, W.F. DOVE,
 H.R. GRIEM, N.A. KRALL, P.C. LIEWER
 Department of Physics and Astronomy,
 University of Maryland,
 College Park, Md.,
 United States of America

Abstract

ION HEATING IN A HIGH-VOLTAGE THETA PINCH.

The interaction of a low-beta, $10^{12} \text{cm}^{-3} \lesssim n_e \lesssim 3 \times 10^{13} \text{cm}^{-3}$, $kT_e \approx kT_i \lesssim 2 \text{ eV}$ highly, but not completely ionized plasma with a fast-rising magnetic field ($B(0) \approx 2 \times 10^4 \text{ G}/\mu\text{s}$) has been studied in a large theta pinch with 100 cm coil length and 46 cm inside diameter of the discharge tube. Depending on initial plasma conditions, the magnetic field penetrates into the plasma either by anomalous diffusion, collision-free compression, or a combination of both modes of penetration. Doppler-broadened and shifted line emission from charge-exchange neutrals is used to determine the ion dynamics in $6 \lesssim \text{Mach} \lesssim 26$ flows. Large Doppler shifts show that ions are accelerated up to twice the magnetic piston speeds, while Doppler broadening gives large ion heating rates ($\lesssim 10 \text{ keV}/\mu\text{s}$), leading to temperatures of $\sim 5 \text{ keV}$ at about half the design voltage on the fast energy storage. Much of this ion heating is seen behind the "leaky" piston. These ion heating rates and temperatures are supported by space- and time-resolved neutron observations. The latter further suggest that ion temperatures increase at least linearly with the stored electrical energy, and that an increase of a factor ~ 2 can be obtained by optimizing the initial plasma parameters. Maximum electron temperatures tend to be below, or nearly equal to, the ion temperatures. These measurements, together with electric-field fluctuation measurements, help to distinguish among the various theoretical models for acceleration and heating mechanisms which contribute to the large efficiency of conversion from electrical to plasma energy obtained in this experiment.

I. INTRODUCTION

In the presence of large current densities in low density plasma, ions can be heated in times far shorter than the binary ion-ion collision time [1,2,3,4]. Ion dynamics and collisionless (turbulent) ion heating in a fast theta pinch device [5,6] and direct evidence for the existence of micro-instabilities are therefore of great interest. Instabilities of interpenetrating ion beams, and of electrons streaming through ions, seem the most likely candidates for producing the observed ion heating. We will show that a significant fraction of the available electrical energy stored in the capacitor bank may be converted into quasi-random ion kinetic energy.

Our theta pinch [5,6] was designed to investigate the collisionless coupling of a high Mach number magnetic disturbance with a low density ($n_e \sim 10^{12} - 10^{13} \text{cm}^{-3}$) plasma. Two different modes of behavior were produced, depending on the relative direction of the initial "bias" magnetic field and the "piston" driving magnetic field [6].

In the "parallel" configuration (bias and piston fields directed in the same sense) the large amplitude magnetic pulse penetrates very rapidly through over half the plasma volume by diffusion, producing very little acceleration of the plasma. As shown in Fig. 1 for a hydrogen plasma with initial electron

* Supported by the Office of Naval Research.

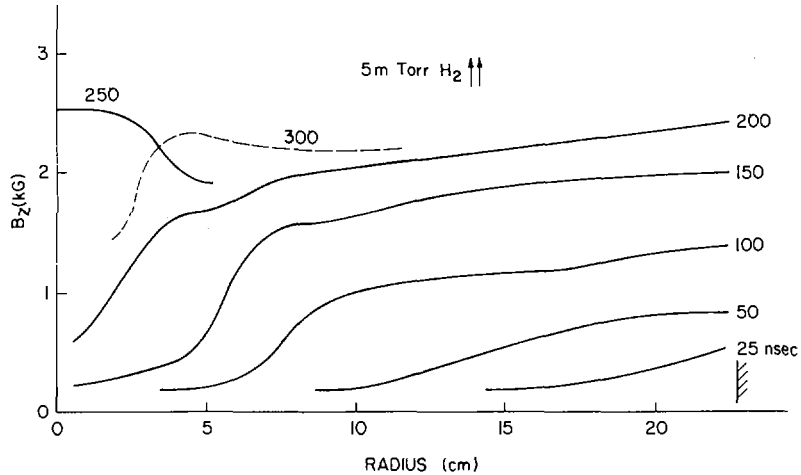


FIG. 1. Radial profiles of magnetic field B_z in hydrogen parallel bias and piston fields.

density $n_e \approx 10^{13} \text{cm}^{-3}$ and temperature $T_e \approx 0.6 \text{ eV}$, the field reaches a radius of 9 cm in the first 100 nsec, and interferometric density measurements indicate little compression during this time. Such a diffusive penetration requires an effective resistivity orders of magnitude larger than the classical resistivity, implying a rapid instability mechanism. At later times a snow-plow-like magnetic piston forms and begins to drive plasma ahead, but no detached shock wave is observed. A shock wave does form rather quickly, however, when the bias and piston fields are oppositely directed (antiparallel configuration) [6].

These differences may be transient effects due to the different initial plasma configurations, i.e., stability properties at early times. For example, the field at the wall must initially decrease in the antiparallel case, while it is always increasing in the parallel case. Given a time sufficiently longer than the experimental time of ~ 300 nsec, both might evolve into a common steady state. One suggestion that this is happening is that at late times the plasma accelerates also in the parallel case.

II. MEASUREMENTS AND RESULTS

Evidence for ion dynamics was gathered from a number of diagnostic methods, of which the most informative were Doppler broadening observations [4], measurements of turbulent electric fields by the Stark effect on the emission lines of helium ions [7] or neutrals [8,9] and the usual magnetic probe measurements. These techniques were supplemented by measurements of neutron emission, x-ray electron temperature, electric potential, electron density by means of a microwave probe [10], and neutral particle density by means of an ionizing probe [11]. Neutral particle densities were somewhat larger though of the same order as the electron density.

a. Ion Dynamics and Heating

Direct evidence for plasma motion was sought in Doppler measurements [4] of emission lines of ions and charge-exchange neutrals, in both the r and

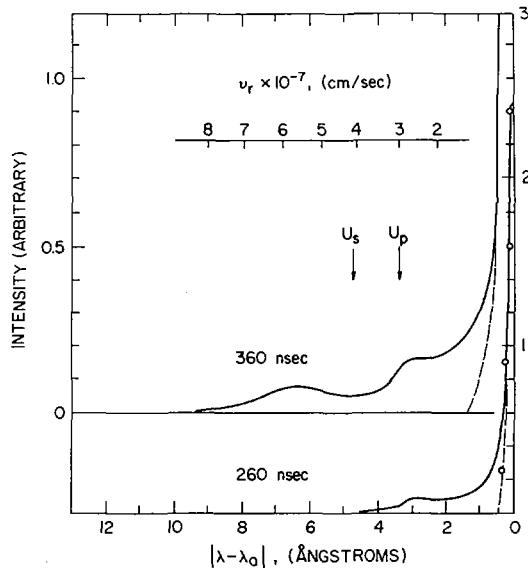


FIG. 2. Doppler profile of AII λ 4806 Å at two times after initiation of the discharge, measured from $r=0$ cm, antiparallel fields. The red wing (dashed) has been folded about the line centre onto the blue wing (solid). A velocity scale corresponding to $\Delta\lambda/\lambda = v \sin 45^\circ/c$ is shown at top.

z directions. In order to avoid seeing the plasma along a full diameter, and as a result being unable to distinguish heating from bulk flow, the plasma was viewed from a point near the tube axis, looking outward toward the wall. Lines emitted by ions moving toward the axis are then blue-shifted. The light was collimated by a lens and focal plane stop and conducted out axially by a light pipe. The volume viewed was a truncated cone with minimum diameter 2.5 cm and divergence angle 0.1 radians. The cone axis was set at 45° to the tube axis, so that light collected would originate mainly from plasma well removed from the perturbation caused by the collection lens and support. Measurements made parallel to the tube axis failed to show any significant Doppler shifts, so that the shifts seen are mostly due to radial motion.

The axial measurements also showed that no significant line emission occurred prior to the arrival of the front of the magnetic disturbance in the field of view of the optical system. Any radiation seen by the 45° system therefore originates between the tube wall and the leading edge of the magnetic disturbance.

An AII line, λ 4806 Å, was chosen to monitor the ion motions in an argon plasma. In hydrogen plasmas, we observed the H_α line of neutral hydrogen, assuming that any neutrals with velocities near shock or piston velocities could only result from single charge exchange events of ions with background neutrals, and would thus represent ion speeds. The profile of the AII line measured at two times after initiation of the discharge in an argon plasma with initial condition $n_e \approx 10^{13} \text{ cm}^{-3}$, $T_e = 1.8 \text{ eV}$, and antiparallel field configuration is given in Fig. 2. A considerable excess of emitting atoms moving radially inward (blue shifted) is evident, and at 360 nsec there are beams with speeds about equal to the piston speed (from magnetic field measurements) and to twice the piston speed.

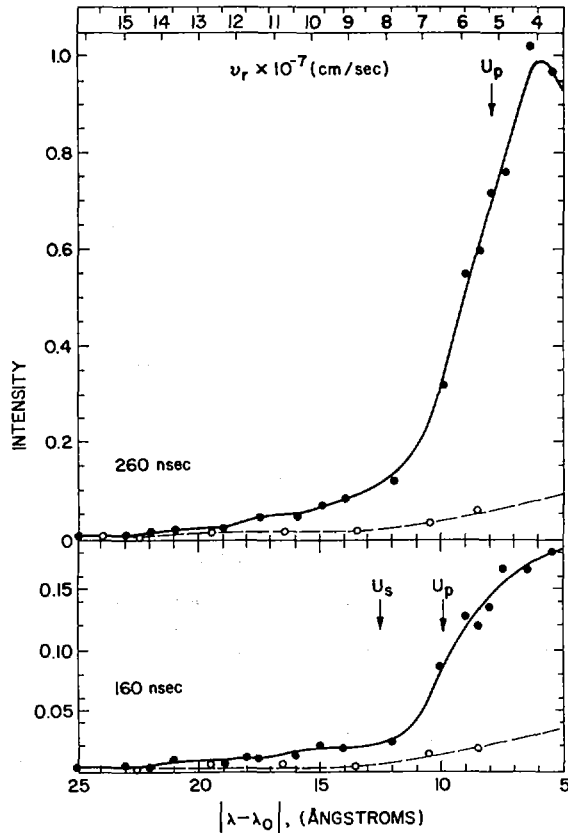


FIG. 3. Doppler profile of H_{α} -wings, showing structure at relatively large Doppler shifts, for two times, measured from $r = 0$ cm. Solid line is blue wing and dashed line red wing. u_p (u_s) are piston (shock) speeds determined from magnetic probes. Antiparallel fields.

Figure 3 shows Doppler profiles for the hydrogen plasma (antiparallel). Figures 4 and 5 are taken in a hydrogen plasma with the same initial conditions but with parallel fields. In Fig. 4 the light collecting lens was placed at a radius of 10 cm so as to see only the outer half of the plasma. Little excess of blue over red is noticeable, in accord with B_z and microwave density measurements showing that little plasma motion occurs in the outer half of the tube. Figure 5 shows the result with the collecting lens on axis. Since the excess of blue over red was small in the outer 13 cm of the tube, we conclude that most of the blue shifted radiation originates in the region between a radius of 10 cm and the front of the magnetic field step.

Ion temperatures as determined from the red wings of these Doppler profiles reveal strong ion heating, 4eV/nsec and 8eV/nsec in the parallel and antiparallel cases respectively. The temperature history is summarized in Fig. 6.

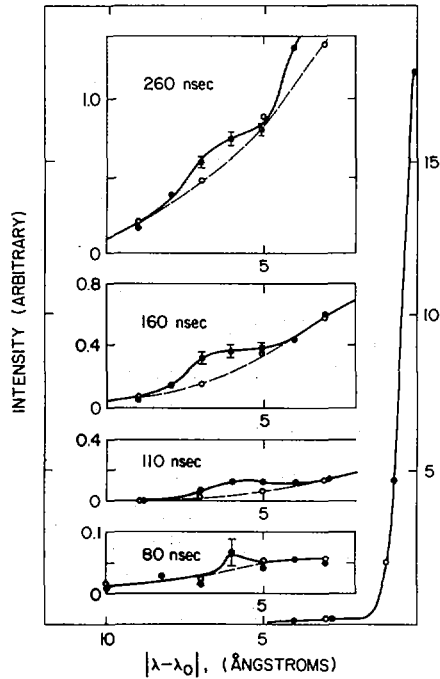


FIG.4. Doppler profile H_{α} at four times, measured from $r = 10$ cm. Dashed line is red wing, solid line is blue wing. Parallel fields.

Additional evidence for the existence of significant ion energies comes from the measurement of neutrons emitted from a deuterium plasma, with $n_e \approx 2 \times 10^{13} \text{cm}^{-3}$ at $r = 0$. Neutron emission begins when the shock is at a radius of 2 cm, and measurements using a collimator show the neutrons originate also at positions removed from the tube axis. Ions reflected from the piston in this case have energy of ~ 20 keV, while the DeHoffman-Teller temperature ($\gamma = 3$) is 10keV. The temperature derived from neutron emission, assuming isotropic emission and a 3-dimensional Maxwellian velocity distribution is 7keV, while the assumption of a 2-dimensional distribution gives ~ 10 keV. Errors in these measurements are large enough to preclude an attempt to distinguish between two-beam and random distributions of ions on this basis.

b. Electron Heating

Electron temperatures were determined from the foil-absorption technique using a 4-channel instrument that could provide either temperatures at two different spatial locations, or at the same location but using different foil thickness ratios. Channels were collimated to view a conical volume parallel with the tube axis and ~ 2 cm in diameter. Electron heating in the diffusive phase of the parallel case is small: no x-ray emission in hydrogen, helium or argon was observed from the plasma at $r \approx 16$ cm. This implies that the electron temperature was below 300 eV. The impurity line CV $\lambda 2279 \text{ \AA}$ was observed, indicating that the electron temperature was at least 100eV in the diffusive front. This low electron temperature coupled with some space and

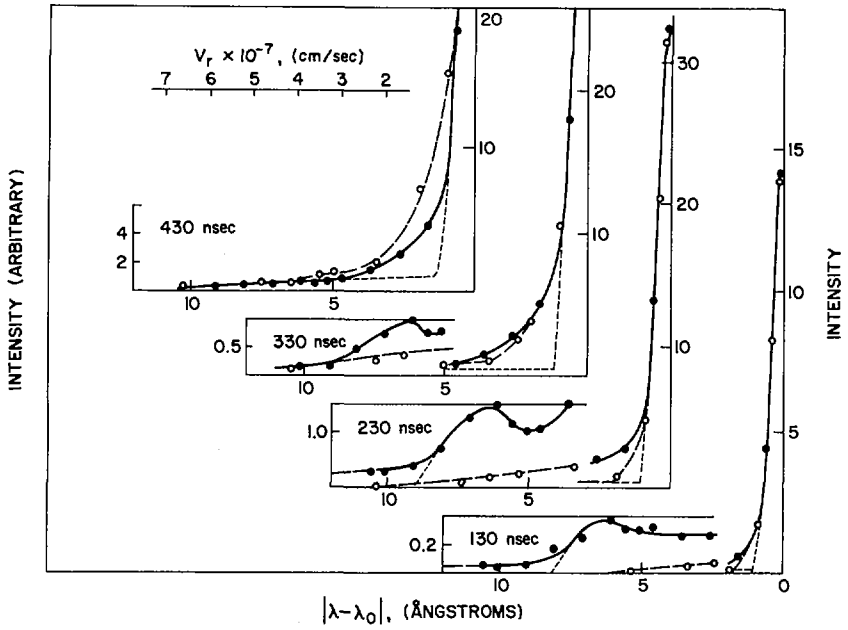


FIG. 5. Doppler profile H_{α} at four times, measured from $r = 0$ cm. Dashed line is red wing, solid line is blue wing. Dotted lines are Gaussian fits to data. Parallel fields.

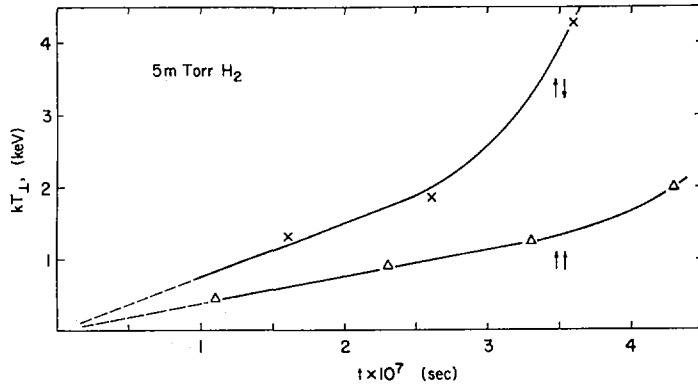


FIG. 6. Ion temperature history from Doppler wings in hydrogen for parallel (\uparrow) and antiparallel (\downarrow) field configurations. Heating rates for linear rise are 4.2 and 7.7 eV/nsec, respectively.

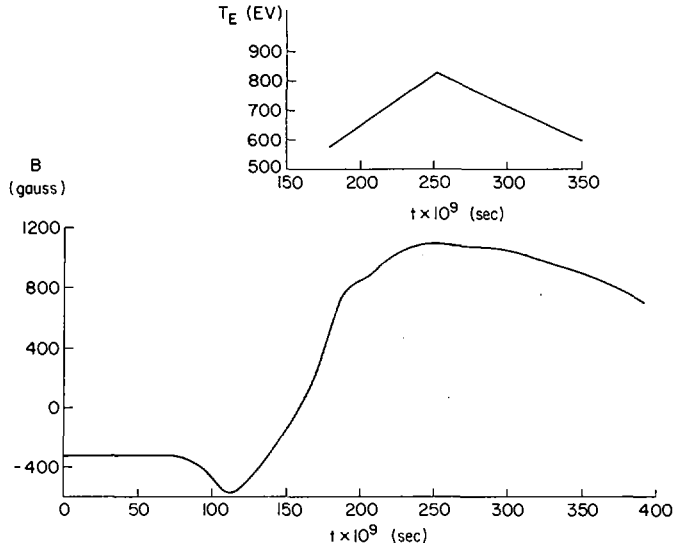


FIG. 7. Electron temperature history at $r = 14.5$ cm in helium plasma, 6 mTorr fill and antiparallel fields. Magnetic probe trace is shown below at the same radius for comparison.

time resolved ion temperature measurements in helium indicate that $T_e/T_i \lesssim 1$ late in the diffusion front. Early in the front the ratio of T_e/T_i is uncertain.

In antiparallel cases (see Fig. 7), x-ray emission corresponding to $T_e \approx 1$ keV was observed in hydrogen, helium, and argon at $r \approx 16$ cm. The x-ray emission begins near the field reversal point, i.e., behind the shock. From helium ion temperature ($T_{i||}$) measurements, $T_e/T_i \gtrsim 1$ for most of the piston with a maximum temperature ratio of 4. The electron temperatures in the antiparallel cases increase at radii less than 14 cm above the 1 keV temperature found at $r = 16$ cm.

c. Turbulent Electric Fields

The frequency spectrum of the turbulence was measured [8] in both parallel and antiparallel cases using the plasma satellite lines of He I $\lambda 4922 \text{ \AA}$ in a helium plasma, including approximate determination of the polarization. In the parallel case, turbulence near ω_{pe} as well as low frequency turbulence was evident. The turbulence at ω_{pe} can be explained by either electron-electron streaming or by the wave-wave coupling of lower frequency turbulence to ω_{pe} . The low frequency turbulence must be associated with an instability that heats ions at least as rapidly as it heats electrons. Measurements of the time of appearance of the helium satellite lines imply that the low frequency turbulence must grow at least as fast as ω_{LH} .

The frequency spectrum of turbulence in the antiparallel case consists mainly of frequencies between ω_{ce} and ω_{pe} , along with the possibility of frequencies below ω_{ce} . In most cases, total rms field strengths were of the order 10 kV/cm.

III. DISCUSSION

a. Antiparallel Fields

The magnetic field and density measurements indicate that the magnetic piston begins to drive a compressional disturbance before it by the time (~ 50 nsec) it has reached a point a few centimeters from the tube wall[6]. The initial effect upon the ions is to reflect them in a beam traveling at twice the piston speed obtained from magnetic probes. This is most clearly seen in argon data (Fig. 2) for 360 nsec, where the reflected beam appears at $\Delta\lambda \approx 6.3 \text{ \AA}$. This type of motion constitutes an essentially one-dimensional motion of ions. In the case of argon, where the beam persists for most of the experimental time, a fairly steady-state shock-like structure develops in B_z . Applying the DeHoffman-Teller conservation relations to this case ($M_A \approx 19$), we see that the observed compression ratio $\eta \approx 2$ fits the prediction for a large Mach number shock in a one-dimensional ($\gamma=3$) gas. Of course the electron motion must be at least two dimensional, since their gyroperiod is small. However, x-ray measurements of electron temperature show that T_e in the shocked gas is less than 300 eV, i.e., negligible compared with the DeHoffman-Teller "temperature".

This is then a shock only in the simplest sense: the ions are reflected at a potential barrier set up by charge separation in the magnetic gradient, and stream out front at twice the piston velocity, while the electrons serve only to carry the necessary currents and to neutralize ionic charges. The electrons remain cold while the ion beam tends to "thermalize", as is shown by the appearance of the beam at the piston speed. (The spread in the beam velocities is also partially due to an instrumental broadening of 0.5 \AA .) The potential barrier has been observed by floating electric probes in hydrogen, and reaches an amplitude sufficient to reflect the ions.

In deuterium, the magnetic profiles[6] show a tendency to remain at $\eta \approx 2$ for an interval before growing to the final state where $\eta \approx 4$, while in hydrogen the $\eta \approx 2$ state is passed through quickly. It appears that the one-dimensional behavior gives way during the experimental period to two- or three-dimensions in the lighter gases. The Doppler profiles in hydrogen (Fig. 3) show evidence of only a residual beam at $2 u_p$. There is a beam somewhat below u_p , with emitting atoms spread on down to the minimum observable velocity ($2 \times 10^7 \text{ cm sec}^{-1}$). The ions overrun by the advancing front must therefore be swept up by an incoherent interaction (as distinct from simple reflection) within the compressed gas slug. This implies a direct, stochastic interaction of ions with fields in the gas, and requires that the pressure exerted by the piston is transferred through the gas to the incoming plasma.

Such an interaction must be mediated by the electric fields of unstable ion waves, because it is difficult to suggest any other source for the required fields.

The interaction time for ions to attain some degree of random motion is clearly longer in the heavier gases. In hydrogen the time taken by an ion to pass through the shocked gas slug is $\lesssim 50$ nsec, which is also the order of time interval required for the shocked gas to exhibit more-than-one dimensional behavior, as seen in the time development of η . Therefore the instability responsible for generating ion waves must have a growth time < 50 nsec in hydrogen. On the other hand, in argon, thermalization is not far advanced after 350 nsec. In deuterium, Doppler measurements were not attempted, but the development of compression ratios as seen in B_z indicates a time of < 200 nsec for instability growth.

b. Parallel Fields

During the diffusion phase Doppler profiles [4] were obtained with the viewing volume restricted to the region between the tube wall and a radius of 10 cm. Before 80 nsec, light levels were too low for meaningful measurements. Afterward (Fig. 4) we see little gross plasma motion in this region, which is consistent with microwave density measurements and with overall dynamics. In spite of this lack of radial flow there is significant ion heating, and by 260 nsec the wings of the line may be fitted with a Gaussian profile with $T_i \approx 1$ keV. The very small gradient in B_z appearing in this region as the field rises at the tube wall shows that the resistivity is very high. An estimate based on a purely resistive diffusion model gives the effective collision frequency for electrons in this region to be $\approx 10^{10}$ sec⁻¹, about equal to $0.1 \omega_{pe}$. This ion heating along with the rapid magnetic diffusion is strong evidence of plasma instability.

Satellite measurements at $r = 17$ cm also indicate enhancement of turbulence in the magnetic piston with frequencies ranging up to include ω_{pe} . The enhancement of fluctuations about ω_{pe} in the parallel case may be the result of much lower electron temperatures with the effect that the electron-electron streaming instability becomes more likely.

For times later than about 100 nsec, when the current sheath passes around $r = 10$ cm, plasma flow is seen (Fig. 5). Here we have a situation very like the antiparallel one, with plasma moving at about the piston velocity and below, and no beam apparent at $2u_p$. We are again forced to the conclusion that the ions interact within the volume of moving gas, rather than at the potential barrier that follows.

IV. THEORETICAL INTERPRETATION

Several features of the θ -pinch dynamics can only be the result of instabilities and the turbulence they generate. These features are

1. Thermalization of ion beams generated in the antiparallel bias case.
2. Heating of ions during magnetic diffusion in the parallel bias case.
3. High resistivity at all times for parallel bias, and greater than classical resistivity for antiparallel bias.

In addition, direct evidence for plasma turbulence is obtained from the Stark broadening and forbidden line satellite measurements, which show fluctuating fields of magnitude $\delta E \gtrsim 10$ kV/cm both in and behind the magnetic piston.

A variety of instabilities [12 - 17] are expected to grow during both the shock and the magnetic diffusion phase of the θ -pinch implosion. Some basic types which we believe play a role in this experiment are

a. Counter streaming ion beams instability

In the antiparallel bias case ions are reflected from the magnetic piston as discussed above. As they penetrate the undisturbed plasma they stream through ions at rest leading to instability if [12] the ion beams have drift velocity v_b greater than C_s (the ion acoustic speed). The initial effect of this instability is to heat the electrons. This is followed by ion heating if the ion beam velocity satisfies $v_b < V_A$ and $T_e > T_i$. V_A is the Alfvén speed,

and T_e the local electron temperature. This mode grows with rate $\gamma \approx \omega_{LH}/2(2)^{1/2}$, where $\omega_{LH} = eB/c(m_e m_i)^{1/2}$. Comparing with our observations, we see that $\gamma^{-1} \sim 10$ nsec in hydrogen, 15 nsec in deuterium and 70 nsec in argon within the piston. The observed growth times are consistent with these times.

In the shocked gas slug itself $v_b > V_A$. However, V_A is quite large in the piston region. The potential barrier that accelerates ions lags the magnetic piston, so there is an overlap region of high T_e , large V_A , and reflected ions, which may therefore be the source region of instability.

b. High frequency ion and cyclotron instabilities

A number of higher frequency instabilities [14,15] have fast growth [$\gamma = \frac{v_c}{v_{T,e}} \omega_{ce}$, for $v_c > v_{T,i}$ and $k\lambda_D < 1$], corresponding to their higher frequency $\omega \approx eB/m_e c$. Although the conditions for instability are easily met, these high frequency and short wavelength modes quickly saturate and they are unlikely to heat the ions, but may provide the initial electron heating required to trigger the more ion oriented instabilities.

c. Electron-ion streaming instabilities

In the parallel bias case observations show no reflected ions at early times, so the counterstreaming ion beams instability is irrelevant except perhaps near the axis. Further, it is unlikely that waves which resonate with electron cyclotron rotation [14,15] will significantly influence the ions. In this case we believe that low frequency drift waves driven unstable by azimuthal electron currents can account for both the anomalously large resistivity observed in the experiment and for the ion heating. In addition, they may play a role in the early time development of both the parallel and antiparallel bias experiments.

Although previous calculations of ion acoustic-drift waves [13,15,16] required $T_e \gg T_i$ (which is certainly not the situation throughout the parallel bias case) a recent calculation [17] has demonstrated that a non-resonant branch remains unstable with sizeable growth rates even when $T_e < T_i$. This ion wave grows in a low β plasma in a geometry which has an axial magnetic field $\vec{B} = B\hat{z}$, "radial" electric fields $\vec{E} = E\hat{x}$ which help drive the "azimuthal" current $4\pi\vec{J}_y/c = \nabla \times \vec{B}$, and density gradients $\nabla n = |\nabla n|\hat{x}$ which are induced by the magnetic penetration. The dielectric function for these electrostatic waves of intermediate frequency ($eB/m_i c < \omega < eB/m_e c$) propagating perpendicular to \vec{B} in this geometry is

$$\epsilon(k_{\perp}, \omega) = 1 - \frac{\omega_p^2}{\omega^2} + \frac{1}{k^2 \lambda_D^2} \left[1 - I_0(k^2 a_e^2 / 2) e^{-k^2 a_e^2 / 2} \frac{\omega - k v_c}{\omega + k E c / B} \right] \quad (1)$$

where I_0 is the Bessel function of imaginary argument, λ_D is the Debye length, a_e the electron gyroradius and v_c the velocity of the azimuthal electron stream, $v_c = -c \nabla \times B / 4\pi n$. Theory predicts that if the plasma has a density gradient, so that $|v_c| > |Ec/B|$, the plasma will be unstable to an electrostatic oscillation $\phi = \bar{\phi} e^{i(\omega t - k_{\perp} r_{\perp})} e^{\gamma t}$ with

$$\omega_{\text{real}} \sim \omega_{LH}, \quad k \lesssim (1/a_e), \quad \gamma \sim \omega_{LH} \quad \text{if } 4\pi n m_e c^2 > B^2$$

The instability persists even if $T_e < T_i$ with comparable growth rates. The time scale $(\omega_{LH})^{-1}$ for this instability is easily short enough to make it relevant to the θ pinch.

A more detailed relation of the experimental results to instability growth can be made from fluid equations in which averages over fluctuating field quantities appear in place of the conventional transport coefficients. For example, the momentum transport equation for electrons is [13]

$$n_e m_e \left(\frac{\partial \vec{V}}{\partial t} + \vec{V}_e \cdot \nabla \vec{V}_e \right) = -en_e \left[\vec{E} + \frac{\vec{V}_e \times \vec{B}}{c} \right] - \nabla p_e - e \langle \delta \vec{E} \delta n_e \rangle \quad (2)$$

where $\delta \vec{E}$ and δn_e are the fluctuating electric field and electron density associated with the instability and $\langle \rangle$ denotes an average over the rapid fluctuations. The effective electron collision frequency is then defined by

$$\nu_{\text{eff}} = \frac{e \langle \delta n \delta E \rangle}{n_e m_e v_c} \quad (3)$$

and can be evaluated for any instability. For the instability derived from Eq. (1) we deduce

$$\nu_{\text{eff}} = \frac{1}{2} \frac{v_{Te}}{v_c} \sqrt{\frac{8\pi n m_e c^2}{B^2}} \left\langle \frac{\delta E^2}{8\pi n T_e} \right\rangle \omega_{pe} \quad (4)$$

in the unstable region when $B^2 < 4\pi n m_e c^2$. The resistivity according to (4) is expressed in terms of $\langle \delta E^2 \rangle / 8\pi$, the energy in electric fields produced by the instability. An estimate of this quantity is obtained from the idea that total energy in the waves, $\frac{d}{d\omega} \omega \epsilon(\omega) \left\langle \frac{\delta E^2}{8\pi} \right\rangle$, will not be more than the energy in the feature which drives the instability, in this case the electron drift. Using Eq. (1) for $\epsilon(\omega)$ we predict

$$\left\langle \frac{\delta E^2}{8\pi n T_e} \right\rangle \lesssim \left(\frac{v_c}{v_{T,e}} \right)^2 \left[\frac{B^2}{8\pi n m_e c^2} \right], \quad \text{for } B^2 / 8\pi n m_e c^2 < 1 \quad (5)$$

The experiment determines both $\langle \delta E^2 \rangle$ and ν_{eff} , and the measurements are consistent with the theoretical estimates. For example, at 5 cm from the wall and after 100 nsec the measurements in helium show $\langle \delta E^2 / 8\pi \rangle \sim 1-10\% n T_e$. At the same time, the current is weak, $v_c \sim v_{T,e}$ and $B^2 \sim \pi n m_e c^2$, so that (5) also yields $\langle \delta E^2 / 8\pi \rangle$ a few percent of the electron thermal energy. The effective electron collision frequency at the time is estimated from (4) to be $\omega_{pe} / 10$ which is consistent with the experimental estimate $\nu \sim e E_\theta / m_e v_c$.

A similar exercise can be performed to estimate the ion heating, giving (for the instability described by Eq. (1) with $4\pi n m_e c^2 > B^2$) in the unstable region

$$\frac{d(nT_i)}{dt} \sim \frac{\omega_{pi}^2}{\omega_{LH}} \left\langle \frac{\delta E^2}{8\pi} \right\rangle \quad (6)$$

This expression, along with Eq. (5) predicts an ion heating rate of about 25 eV/nsec in hydrogen for piston conditions, i.e., for a magnetic field of 2000 gauss, a density of $5 \times 10^{12} \text{ cm}^{-3}$ and field strength of 7 kV/cm. This heating rate is consistent with the experimental heating rate as shown in Fig. 6. This rate is actually an upper bound, since δE^2 will include the energy from other instabilities, which may not heat ions, as well as the energy in the mode discussed here. The heating stops when the driving instability ceases, in this

case [17] when $T_i \approx m_i v_C^2$. Comparing the maximum ion temperature in hydrogen with that in helium, the lower value of T_i in helium corresponds closely to the reduced value of $m_i v_C^2$ measured in that experiment.

The results given here are not universal transport coefficients, i.e., they assume that the plasma is unstable to the particular mode described by Eq. (1). Other instabilities would not only have different frequencies or wave numbers, but would have a different relation between δn and δE , leading to different formulae for ν . In particular, the unstable wave described here has a wave energy much larger than the electrostatic field energy, giving a large resistivity and heating rate for a fairly low field energy. This is consistent with the relatively low values of $\delta E^2/8\pi n T_e$ and contrastingly large ion heating observed in the present experiment.

d. Ballistic resistivity in the stable region

Even in stable regions well behind either the diffusion or shock front we would not expect the resistivity to be classical. This is because the electron distribution "remembers" the perturbation it suffered when it passed through an unstable region at an earlier time. This direct transport of early information to later times by particles has been termed ballistic (or free streaming) transport [13,18]. Assuming that the unstable regions are dominated by the mode described in Eq. (1), we find

$$\nu_{\text{eff}} = \omega_{pe} \left(\frac{2v_{T,e}}{v_c} \right) \left\langle \frac{\delta E^2}{8\pi n T_e} \right\rangle \sqrt{\frac{B^2}{8\pi n m_e c^2}} \quad (7)$$

for the ballistic resistivity, which is to be found far enough behind the unstable region that the waves have damped away. The ballistic resistivity in this case is smaller than the instability-produced local effect by the factor $B^2/2\pi n m_e c^2$.

We conclude that the beam thermalization, the ion heating and the resistivity can all be understood in connection with well known instabilities. Also, at early times the ion drift-hybrid instability described by Eq. (1) is expected to be much faster and more effective in the parallel bias case, where the magnetic and initial density gradient are oppositely directed near the wall, than in the antiparallel case, where $\nabla n/\nabla B > 0$. This suggests a tendency of parallel bias fields to resist the formation of a reflected ion beam, consistent with the experimental result.

V. FINAL COMMENTS

a. Scaling

Figure 8 shows how the observed neutron temperature, electron temperature, shock speed, and piston speed vary with the main bank voltage for a deuterium case with an initial density $n_e \approx 10^{12} \text{ cm}^{-3}$. Both the directed ion energy, assuming that the ions travel at the piston speed, and the ion thermal energy increase significantly with increased main bank voltage. The electron temperature does not seem to be as strongly affected by the increased voltage; however, these measurements were taken near the wall ($r \approx 16 \text{ cm}$) where the magnetic field is still somewhat diffusive for these conditions. If the ion temperature would continue to vary with voltage as shown in Fig. 8, it would reach 60 keV at the design (500 kV) voltage of the line.

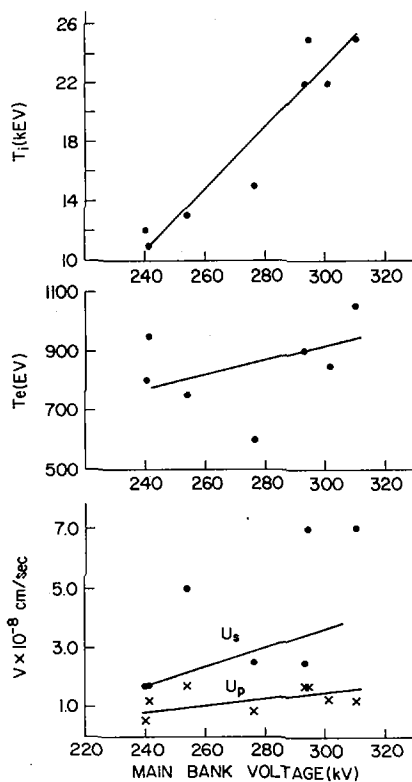


FIG. 8. Temperatures, shock and piston speeds versus main bank voltage. $n_e \approx 10^{12} \text{ cm}^{-3}$ initial density deuterium plasma and antiparallel fields. u_p (u_s) are piston (shock) speeds determined from magnetic probes.

The dependence of ion temperature on bank voltage for a higher (initial) density deuterium case ($n_e \approx 10^{13} \text{ cm}^{-3}$) is similar, but temperatures are down by a factor ~ 2.5 . It is probable that this type of heating would exist even for densities as high as 10^{15} cm^{-3} , provided that the plasma remained collisionless.

b. Efficiency

In the case of hydrogen, with antiparallel fields, the plasma ion temperature obtained from Doppler profiles (see Fig. 6) after the collapse (at about 360 nsec) approaches 5 keV, and $T_e \approx 2$ keV. The plasma has a diameter of about 10 cm at the time, and the magnetic field compression indicates about 70% of the plasma has been picked up by the piston. Assuming the plasma is uniform over the one-meter coil length, we have a plasma volume of $8 \times 10^3 \text{ cm}^3$ containing ions at 5 keV and electrons at ≈ 2 keV, with density $n_e \approx 10^{14} \text{ cm}^{-3}$. This gives an energy content of about 1 kJ. The initial stored capacitor energy was ~ 5 kJ, so we obtain an overall efficiency of $\sim 20\%$ in this case.

In the case of parallel fields the energy content is generally smaller. We find 0.3 kJ in particle energies (see Figs. 1 and 6) and an efficiency of 6%.

REFERENCES

- [1] ESKOV, A. G. , KURTMULLAEV, R. Kh., MALYNTIN, A. I., PILSKII, B. I., and SEMINOV, V. N. in ESRO SP-51 European Space Research Corp. Frascati, Italy (1969).
- [2] KEILHACKER, M., KORNHERR, M., STEUER, M. H., Z. Physik 223,385 (1969).
- [3] KAWABE, T., IANNUCCI J., EUBANK, H., Phys. Rev. Lett. 25, 642 (1970).
- [4] DOVE, W. F., Phys. Fluids 14, in press (1971).
- [5] DESILVA, A. W., DUCHS, D. F., GOLDENBAUM, G. C., GRIEM, H. R., HINTZ, E. A., KOLB, A. C., KUNZE, H.-J., VITKOVITSKY, I. M., in Plasma Physics and Controlled Nuclear Fusion Research (International Atomic Energy Agency, Vienna, 1969) Vol. I, p. 143.
- [6] DESILVA, A. W., DOVE, W. F., GOLDENBAUM, G. C., SPALDING, I. J., Phys. Fluids 14, 42 (1971).
- [7] GRIEM, H. R., KUNZE, H.-J., Phys. Rev. Letters 23, 1279 (1969).
- [8] DAVIS, W. D.(to be published).
- [9] KUNZE, H.-J., GRIEM, H. R., DESILVA, A. W., GOLDENBAUM, G. C., SPALDING, I. J., Phys. Fluids 12, 2669 (1969).
- [10] HARTWIG, H., Berichte der Kernforschungsanlage Jülich GmbH, Jul-473-pp (1967).
- [11] COMMISSO, R. J., DAVIS, W. D. (to be published).
- [12] PAPADOPOULOS, K., DAVIDSON, R. C., DAWSON, J. M., HABER, I., HAMMER, D. A., KRALL, N. A., SHANNY, R,Phys. Fluids 14, 849 (1971).
- [13] TIDMAN, D., KRALL, N. A., Shock Waves in Collisionless Plasma [Wiley & Sons, New York, 1971].
- [14] FORSLUND, D. W., MORSE, R. L., NIELSON, C. W., Phys. Rev. Letters 25, 1266 (1970); LAMPE, M., MANHEIMER, W., MCBRIDE, J., ORENS, J., SHANNY, R., SUDAN, R., Phys. Rev. Letters 26, 1221 (1971).
- [15] GARY, S. P., SANDERSON, J. Plasma Physics, 4, 4, 739 (1970); GARY, S.P., J. Plasma Physics 4 (1970) 753.
- [16] KRALL, N. A., BOOK, D., Phys. Rev. Letters 23, 574 (1969).
- [17] KRALL, N. A., LIEWER, P., Univ. of Md. Plasma Physics Preprint #71-106, Phys. Rev. (to be published).
- [18] KRALL, N. A., TIDMAN, D. A., Phys. Fluids 12, 607 (1969).

CONDITIONS AND MECHANISM OF THETA-PINCH PLASMA HEATING

S. KIYAMA, K. OGAWA
Electrotechnical Laboratory,
Tanashi, Tokyo,
Japan

Abstract

CONDITIONS AND MECHANISM OF THETA-PINCH PLASMA HEATING.

The heating rate of plasma at the initial compression phase of the theta-pinch is obtained for various conditions, and its heating mechanism is investigated by using a newly constructed 8-kJ fast theta-pinch device. The magnetic field of this theta-pinch device can rise to very high values and the rise is variable over a wide range (5×10^{10} G/s - 2×10^9 G/s) keeping the maximum magnetic field and the other parameters at fixed values. The theta-pre-heating in this device is almost perfect, employing a transmission energy storage system; it is able to fire even in the very-low-pressure regime below 10^{-3} Torr.

The plasma is substantially heated in the region where the magnetic field rise is larger than a certain value (2×10^{10} G/s which corresponds to the maximum induced electric field of 400 V/cm in the discharge tube). The value of magnetic-field rise where the heating rate changes markedly and the total energy absorbed by the plasma which is a fairly large fraction of the storage energy of the capacitor bank (up to 30%), are over a wide range (3-300 mTorr) almost independent of the initial gas pressure. Then the plasma temperature is very high (over 1 keV) in the low-pressure regime, and sharp shock structure is not always observed in this theta-pinch. For the heating mechanism of the theta-pinch plasma, it is suggested that turbulent heating, shock heating and adiabatic heating should be separately treated in the different regions of the compression stage and the magnetic-field rise. Particularly in the low-pressure regime and at high magnetic-field rise, turbulent heating by anomalous resistance is an important mechanism. This fact is closely related to collective plasma phenomena and has an important effect on the formation and the structure of the shock immediately following. Experimental and theoretical investigations are being performed in an attempt to understand these phenomena.

1. INTRODUCTION

Many investigations of plasma production have been performed in various types of θ -pinch devices — fast and slow θ -pinches, high-frequency θ -pinch, etc. Especially in the low-pressure regime the plasma temperature of the fast θ -pinch is known to be very high.

But consistent understanding of plasma production and heating mechanisms over various parameters of the θ -pinch has not yet been established. In this paper we shall try to solve this problem by using a θ -pinch device with a variable magnetic-field rise. Since crow-barring has not yet been employed so far, this experiment is of the high-frequency θ -pinch type.

2. EXPERIMENTAL PROCEDURE

The magnetic-field rise of the θ -pinch device used is varied by using a current transformer and a variable inductance as shown in Fig.1 [1]. In this paper, only the variable inductance is used and the charging voltage of the capacitor bank is 60 kV throughout the experiment.

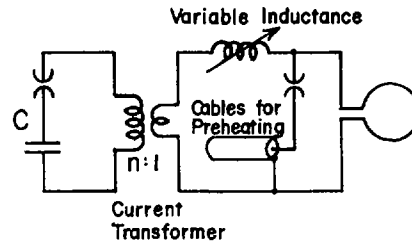


FIG.1. A simplified circuit diagram of a θ -pinch with variable \dot{B} .

TABLE I. PARAMETERS OF MAIN BANK AND PRE-HEATING DISCHARGE

Coil diameter: 10 cm, coil length: 40 cm

	Main bank 0.3 $\mu\text{F} \times 8$	Pre-heating discharge 35 Ω cable 20 m \times 48
Charging voltage	80 kV	60 kV
Capacitance	2.7 μF	0.15 μF
Energy	8.7 kJ	0.27 kJ
Period	2.4 μs	0.5 μs
Maximum current	630 kA	160 kA
B_{max}	19 kG	5.3 kG
\dot{B}_{max}	$2 \times 10^9 \sim 5 \times 10^{10}$ G/s	3.5×10^{10} G/s
E_{max}	1200 V/cm	850 V/cm

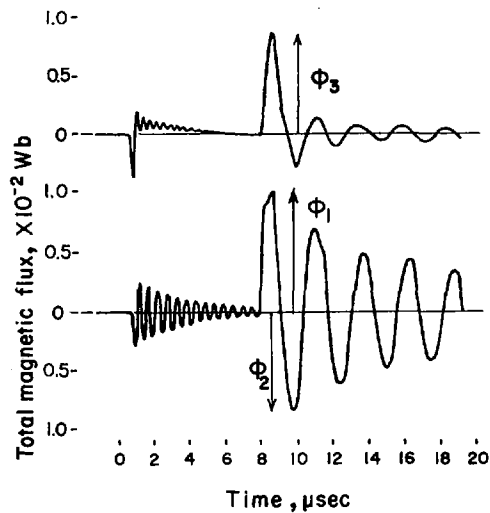


FIG.2. A typical oscillograph trace of total magnetic flux variation with plasma (upper trace) and without plasma (lower trace), 100 mTorr D_2 .

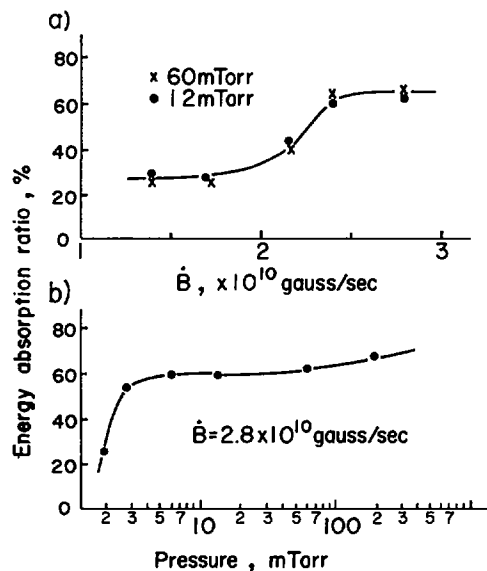


FIG. 3. Energy absorption ratio defined as $\frac{\phi_2^2 - \phi_1^2}{\phi_1^2}$, as a function of \dot{B} and pressure.

The plasma is completely θ -pre-heated by the discharge of the transmission-line storage of electrical energy. In the pre-heating phase the plasma is slightly compressed and gradually expands completely in the discharge tube which has no trapped field (< 100 G) after $8 \mu\text{s}$, when the main discharge is started.

The other parameters of the device are given in Table I. The gas mainly used is D_2 . The plasma behaviour is measured by magnetic probes inside and outside the plasma and by several other alternative methods (streak photographs, laser interferometer and spectroscopy).

3. TOTAL MAGNETIC FLUX

Figure 2 shows the wave form of the magnetic flux obtained by the external magnetic loop placed sufficiently far from the compression coil, so that the quantity measured is proportional to the total magnetic flux. The oscillation is strongly damped in the second and third half cycles, while it is not so strongly damped in the case of low magnetic-field rise. The oscillation is strongly damped in the case of low magnetic-field rise. This phenomenon indicates absorption of energy by the plasma. This absorption energy up to the middle of the second half cycle is shown in Fig. 3 as a function of the magnetic-field rise \dot{B} ; it seems to be of a transitional character. In Fig. 3, the pressure dependence of this absorption rate is also shown. It seems to be independent of the pressure, but from the observation by the streak photograph and the magnetic probe we may distinguish three characteristic regions of the pressure from each other, typically represented by 12 mTorr, 60 mTorr and 120 mTorr in D_2 ,

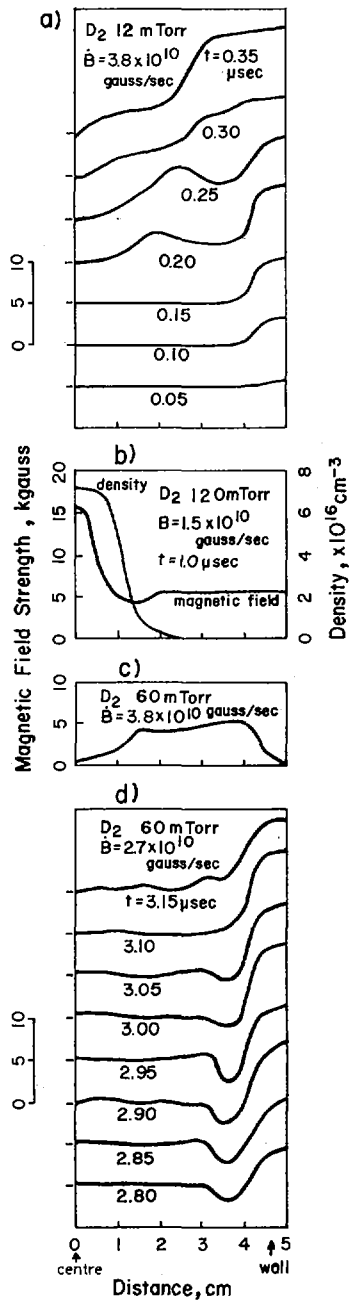
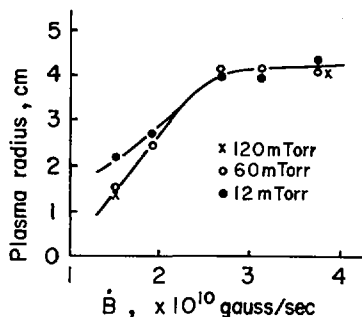


FIG. 4. Several typical configurations of magnetic field strength and an example of density profile (a-d). At $t=0$, the main discharge starts.

FIG. 5. Plasma radius as a function of \dot{B} .

respectively. In the low-pressure regime (< 40 mTorr), the plasma has no sharp structure whereas there is a sharp structure in high-pressure regime (> 90 mTorr). The plasma does not expand rapidly after compression in the high-pressure regime because collisional relaxation may occur.

These apparent reductions of the total flux are considered due to the following three reasons:

- 1) A large fraction of the magnetic field is anomalously trapped in the plasma in the first half cycle.
- 2) Completely diamagnetic hot plasma of large diameter is produced.
- 3) The coil current is strongly coupled with the large-diameter plasma current and damped by plasma anomalous resistance.

4. TRAPPED FIELD

The sharp structure of the magnetic field is destroyed at maximum compression and, at the same time, the magnetic flux penetrates rapidly toward the centre as shown in Fig. 4a. In the region of low pressure and large \dot{B} this penetration of the magnetic flux occurs at the early stage of compression; the speed of penetration exceeds 4×10^7 cm/s, while in the region of high pressure and small \dot{B} remarkable paramagnetic behaviour is seen in the central region in Fig. 4b. These phenomena may be explained by penetration of outside plasma (which traps the magnetic field) into the central region of the plasma, or by anomalous diffusion of magnetic field due to some sort of instabilities. Thus a large fraction of the magnetic field (up to 25%) is almost uniformly trapped at the end of the first half cycle as in Fig. 4c, and this rate is large in the region of large \dot{B} , which suggests an anomalous skin effect in the plasma. This trapped field diffuses rapidly in the earlier stage of the second half cycle, in the same way as in the first half cycle, which may heat the plasma. Therefore, there is nearly no trapped magnetic field ($\sim 1\%$) at the end of the second half cycle.

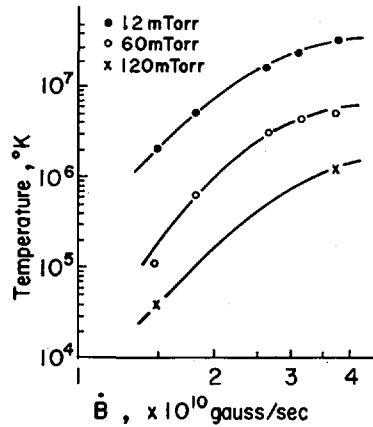


FIG. 6. Plasma temperature as a function of \dot{B} .

5. PLASMA RADIUS AND TEMPERATURE

In the third half cycle, the structure of the magnetic field is clear and sharp as shown in Fig. 4d, which indicates the existence of a sharp plasma boundary. This may be due to the fact that almost no magnetic field is trapped inside the plasma and the ordered motion of plasma is thermalized. Thus the plasma radius is easily estimated from the values at maximum magnetic field and plotted as a function of \dot{B} in Fig. 5.

Moreover, in the third half cycle, there is a sufficiently long period in which the sharp magnetic-field structure seems to be steady. In this period, the plasma temperature is obtained by assuming the plasma pressure to balance the magnetic field, the electron temperature to be equal to the ion temperature and all particles to be confined in the magnetic field. The temperature is shown as a function of \dot{B} in Fig. 6.

6. DISCUSSION

The reduction of the total magnetic flux as in Fig. 1 is partly explained by the reverse trapped field, partly by the diamagnetic current in the second half cycle, and, in the third half cycle, entirely by the diamagnetism of plasma with a large diameter because high-temperature plasma is produced.

In the region of low pressure and large \dot{B} , the plasma is thought to be very strongly heated during three stages:

- 1) The stage in which the magnetic field penetrates very rapidly in the first half cycle,
- 2) the compression stage, and
- 3) the stage in which the trapped field diffuses in the second half cycle.

The first stage is very important for heating the low-density plasma because half of the thermal energy of plasma is produced at this stage and its mechanism is very interesting from the physical point of view.

ACKNOWLEDGEMENT

The authors would like to express their gratitude to Mrs. H. Shimahara and other members of the Plasma Section of the Electrotechnical Laboratory for valuable discussions. The research work reported in this paper was supported by the Science and Technology Agency.

REFERENCE

- [1] KIYAMA, S., OGAWA, K., "A transformer-coupled fast θ -pinch device with variable rise time", 6th Symposium on Fusion Technology, Aachen (1970).

DISCUSSION

TO PAPERS IAEA-CN-28/J-8, J-9, J-10, J-11, J-12, J-13

B. D. FRIED: Could you please summarize the evidence for the statement in Paper J-10 that electron cyclotron rather than ion acoustic instabilities are responsible for the observed turbulence?

R. A. GROSS: I think Mr. Keilhacker will answer this.

M. M. K. KEILHACKER: For our shock-wave conditions and initial conditions in front of the shock, with T_i 4 times greater than T_e and drift velocities which are about one tenth of the electron thermal velocity, the ion-acoustic waves should be stable and the only instabilities we know of at the moment are electron cyclotron waves. Experimentally, it is very difficult to distinguish between ion acoustic instabilities and electron cyclotron wave instabilities since the latter are Doppler shifted. The frequency of the unstable modes should be more or less the same as for the ion acoustic instabilities, about $0.5 \omega_{pi}$ and that is what we actually observe. The only experimental method I know of to distinguish between those two instabilities would be to measure the fluctuation level not in the plane perpendicular to the magnetic field, as done by Paul and by ourselves, but to measure it in the plane which includes the magnetic field; this is very difficult technically but we are now working on it.

R. N. SUDAN: In this same connection, I should like to point out that the turbulence levels quoted in Paper J-10 are sufficient to broaden the electron cyclotron resonances, so that the drift cyclotron instability will be modified to an ion acoustic type of instability. It is then difficult to understand why such an instability will not saturate at a low level for $T_i \geq T_e$.

R. L. GULLICKSON: What was the magnitude of the neutron production in the Maryland theta-pinch experiment?

R. A. GROSS: About 10^5 to 10^6 neutrons/shot.

F. L. RIBE: In the experiments reported in Paper J-12, I assume that the 200 nsec neutron duration is fixed by the duration of the Blumlein line pulse. Is this correct?

R. A. GROSS: Yes.

F. L. RIBE: In the Jülich experiments described in Paper J-11, the piston apparently projects the ions forward to high energy, which seems to imply that the piston is not porous.

R. A. GROSS: Perhaps Mr. Hintz can comment on this.

E. A. K. HINTZ: I would say that with respect to most of the ions the piston is not porous. We do not know exactly what proportion diffuses through the piston, but we know that the total line density is coupled to the magnetic field.

REACTOR SYSTEMS

(Session K)

Chairman: E. R. VELIKHOV

Papers K-1 and K-2 were presented by
R. F. POST as Rapporteur

Papers K-4 and K-5 were presented by
R. J. BICKERTON as Rapporteur

Papers K-11 to K-13 were presented by
H. FORSEN as Rapporteur

EXPERIMENTAL AND COMPUTATIONAL INVESTIGATIONS OF THE DIRECT CONVERSION OF PLASMA ENERGY TO ELECTRICITY*

R. W. MOIR, W. L. BARR, R. P. FREIS, R. F. POST
Lawrence Radiation Laboratory, University of California,
Livermore, Calif.,
United States of America

Abstract

EXPERIMENTAL AND COMPUTATIONAL INVESTIGATIONS OF THE DIRECT CONVERSION OF PLASMA ENERGY TO ELECTRICITY,

Studies of direct conversion of plasma energy to electricity show that efficient direct conversion would permit a considerable improvement in the power balance in mirror machines. The use of fuel cycles having a high fraction of charged reaction products, such as the D-³He fuel cycle is suggested. Energy is recovered from mirror end losses by expansion in static magnetic fields (to convert perpendicular energy components to parallel), separation of ions from electrons, and, finally, deceleration and selective collection of the particles after each has lost most of its original kinetic energy. Analysis indicates that overall efficiencies of about 90% might be attainable.

The heart of the converter is the structure within which deceleration and collection take place. In the system being investigated, the energy-dependent focusing property of periodic electrostatic lenses aids the separation. Computer-derived designs were tested in scaled laboratory experiments, in which we used variable-energy ion beams to study a 22-cell collector system in detail. Under one set of operating conditions the measured efficiency averaged at constant current density over a range of 2 in energy was 88%, whereas computer-simulation calculations for the same case gave 92%; the ideal theoretical maximum efficiency under these conditions would be 97%. Implicit in obtaining the observed efficiencies was the assumption that "retrograde" particles (a few percent of the total) would in practice be re-reflected by the mirrors, be returned to the collector system, and be captured on their second try. If these assumptions had been invalid, the observed efficiencies would have dropped to 83%. Designs aimed at minimizing retrogrades are under investigation. While ultimate limits on power will be set by space charge, computer studies of this problem already indicate (scaled) power values roughly compatible with reactor requirements. Further work to optimize the collector efficiency in the presence of space charge is indicated.

A second aspect of direct conversion, also of importance for reactors with neutral beam injection, is the recovery of energy from unconverted and untrapped beams in the injectors. Experiments with 2-keV ion beams have yielded recovery efficiencies as high as 95% at low-power densities.

1. INTRODUCTION

The prospects for a successful fusion reactor based on the mirror confinement concept are enhanced if the importance of end losses are reduced by efficiently and economically recovering the energy of the charged particles that are scattered out the ends. A concept for accomplishing this energy recovery was presented in 1969 [1,2].

The purpose of this paper is to assess direct conversion in the light of this concept, from the point of view of determining attainable efficiencies and space-charge-limited power levels. Economic aspects of a mirror reactor with direct conversion are discussed in Ref. 3. A number of aspects and alternatives of direct conversion not discussed here are given in Ref. 4.

* Work performed under the auspices of the US Atomic Energy Commission.

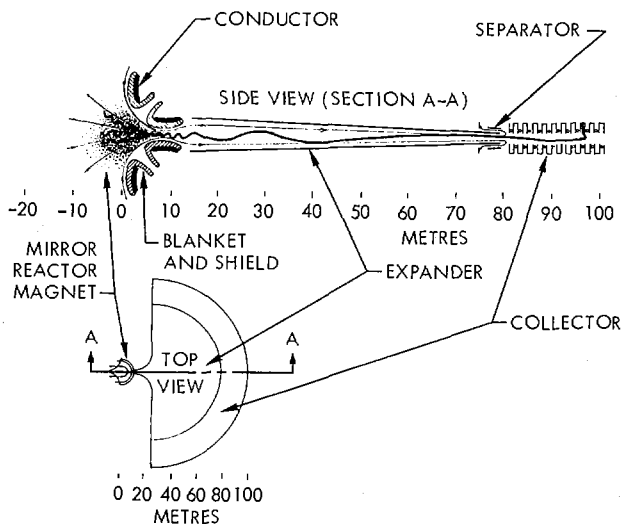


FIG. 1. Arrangement of mirror fusion reactor with direct conversion.

2. GENERAL DESCRIPTION OF THE PROCESSES AND THE CONFIGURATION

The functions of the direct conversion process can be seen by following a typical particle (Fig. 1). A fuel ion will move back and forth between mirror points in the reactor until the particle diffuses by coulomb collisions into the loss cone. Then it passes over the maximum field (≈ 150 kg), where its energy is essentially transverse to \vec{B} . As it moves outwardly in the expander, whose field may drop to a few hundred gauss, the perpendicular energy will drop linearly with $|B|$ according to the principle of adiabaticity ($\frac{W_{\perp}}{B} = \text{const}$), so that, by the conservation of total energy, the velocity, which started out perpendicular to \vec{B} , is now nearly parallel to \vec{B} . Now the outwardly directed ion passes out of the guide field with a slight deflection perpendicular to the plane of Fig. 1 and enters the collector. The electrons that must accompany the ions through the expansion phase in equal numbers follow the field lines and are thus removed from the ion stream. Since the number density and current density of ions and electrons are equal, it follows that the electrons carry away negligible energy. In the collector, the ion beam is electrostatically decelerated and kept from spreading out by the focusing effect of periodic electrostatic lenses. When the ion loses most of its energy this focusing becomes unstable (overfocused) and the ion is driven into a collector cup, where it is caught on a high-voltage electrode. The dc current from this electrode could be used to supply the current at a high voltage for one of the injectors or can be converted by inverters and rectifiers to a common dc potential for connection to high-voltage dc transmission lines, for example.

The inefficiencies of each of the above processes is analyzed in section 5. Since the collection process is thought to be the most difficult and uncertain, it has received the bulk of our attention.

The design philosophy to date has been 1) to optimize the system at low density, 2) to examine the limitation of efficiency imposed by finite density, and 3) to reoptimize at finite density. The third step has yet to be accomplished.

Section 3 discusses experiments and computations for the collector structure at densities low enough that trajectories are not affected by space charge. Section 4 describes computer simulation of space-charge effects.

3. LOW-DENSITY COLLECTION

We have analyzed one particular kind of deceleration and focusing field given by Eq. (1):

$$\frac{V}{V_0} = \frac{x}{L} + \frac{A}{2\pi} \sin\left(\frac{2\pi x}{L}\right) \cosh\left(\frac{2\pi y}{L}\right) + \frac{C}{2\pi} \sin\left(\frac{2\pi x}{L}\right) \sinh\left(\frac{2\pi y}{L}\right) \quad (1)$$

The cosh term gives weak focusing, whereas the sinh term gives strong focusing, which allows higher densities to be handled in the presence of space-charge blowup. From Fig. 2 one can see that a collector is located every $L/2$, whereas for the cosh term a collector is located every L ; thus the direct converter overall length is effectively halved by the use of strong focusing for the same number of collectors, N .

Other potential functions could be investigated in order to optimize the collection process. However, for the present discussion we take the form of Eq. (1) with $A = 0$. In this case, there are three parameters (V_0 , L , and C) whose values can be adjusted in searching for the most efficient collection compatible with practical dimensions and electric field values.

The effects of varying these parameters were studied (in the absence of space charge) with two computer programs. One program calculates trajectories of ions with a range of energies and initial positions and directions, using the analytic expression [Eq. (1)] for the potentials. This program is used to determine the parameter values to maximize the apparent collection efficiency ("apparent" because the details of the individual collectors are not included in this program). Certain qualitative features emerge from this parameter search. For C greater than optimum, efficiency declines because of particles being collected too soon (at too low a potential). On the other hand, for C less than optimum, efficiency loss is mainly caused by so-called "retrograde" particles, those particles that turn around and escape without being collected. Increasing the number of collectors raises the efficiency somewhat, but it still falls well below the ideal theoretical maximum. For example, increasing the number of collectors from 24 to 36 raises the efficiency from 84 to 88%, still about 10% below the ideal maximum of 98%. Next, using the parameters found with the first program, a second program is used to calculate individual ion trajectories all the way to actual collection. This second program, which uses analytic fields in the channel and tables generated by relaxation techniques in the collector region, is used to determine the optimum design of the individual collector assemblies.

In studies to date, the largest loss of energy has been that due to retrograde ions. The number that turn around near the central plane is studied with the first program and is minimized by adjusting the focus fields. The

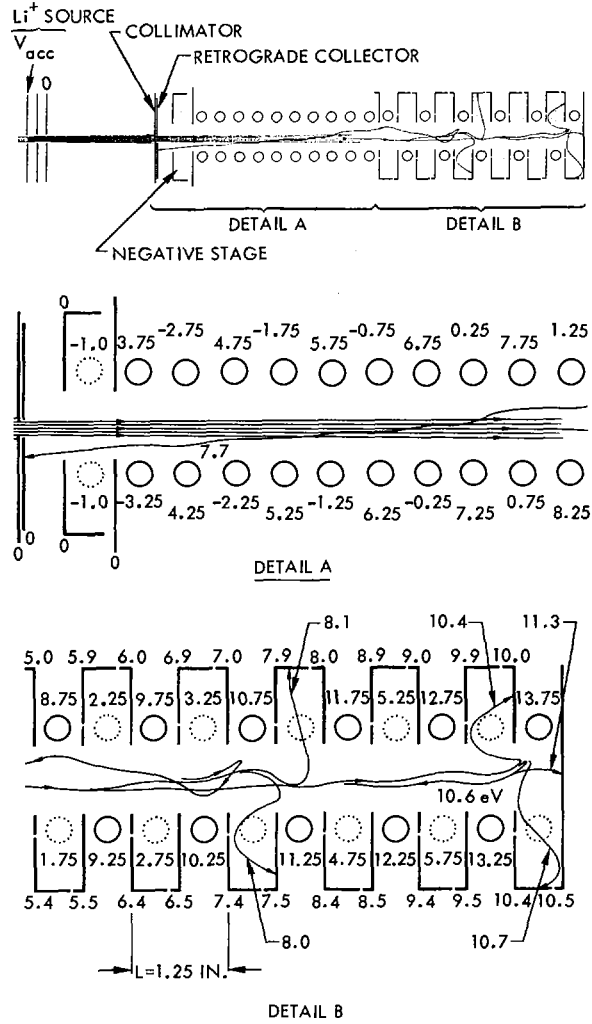


FIG. 2. Cross-section of experimental device. Typical trajectories are shown for the energies indicated. In Detail B, high-potential rods are shown as solid circles; low-potential grids are shown as dotted circles; and cups are shown bounded by solid lines.

number that turn around inside a collector cup is determined by the electric field configuration inside the cup, and is studied with the second program. The total number of retrograde particles has been reduced to less than 7% by the proper choice of parameters in the geometry studied.

Computer-derived designs are being tested in scaled laboratory experiments, using a variable-energy ion beam as a particle source. A 22-cell collector system has been studied in detail with one particular design for the collector cups. This collector structure is shown in Fig. 2; the numbers

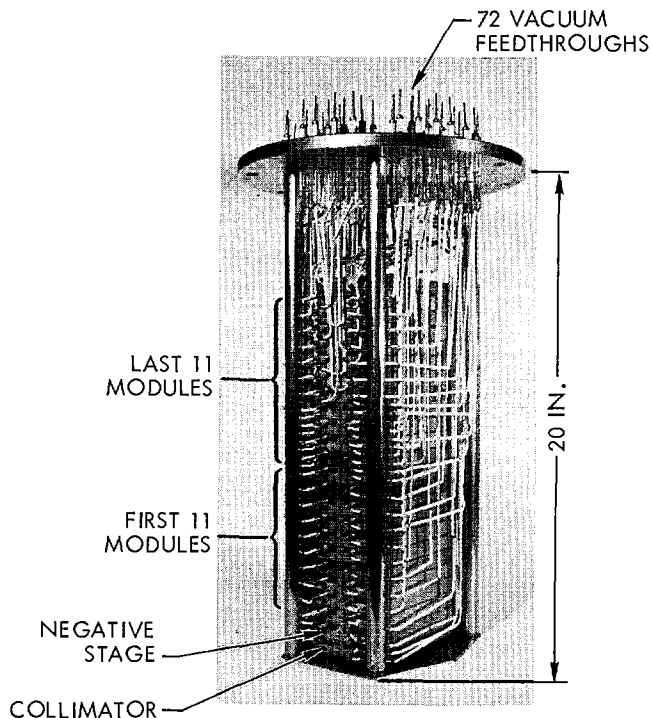


FIG. 3. Photograph of modular collector assembly.

represent the relative potentials applied to the different electrodes, and typical computed trajectories are shown. The decelerating electric field is produced by the increasing average potential as the ions go from left to right. The periodic focus field, which finally drives the particles into a collector when they become slowed sufficiently, is produced by the high-potential rod opposite a low-potential grid. The perpendicular field thus produced deflects the ions through the grid and directs them into a cup. Figure 3 is a photograph showing the modular assembly. Each of the last 11 modules contains a rod, a grid, a fin, and a cup, thus requiring four electrical connections. The first 11 modules contain only rods, so the potential is correctly established in the channel region, but at present there is no facility for recovering energy efficiently. This simplification was necessary to keep the total number of external electrical connections down to the available number of feedthroughs. A few of the 72 vacuum feedthroughs can be seen in the photo. A simple variable-energy lithium ion source was mounted 9 cm in front of the collimating aperture contained in the first module (see Fig. 2). The second module contains a negative stage to prevent secondary electrons that might be produced at the collimator from entering the collector region.

Figure 2 shows that the collimator is followed by another, similar electrode with a slightly larger aperture. This extra electrode was also maintained at ground potential and was used to monitor the retrograde-ion current.

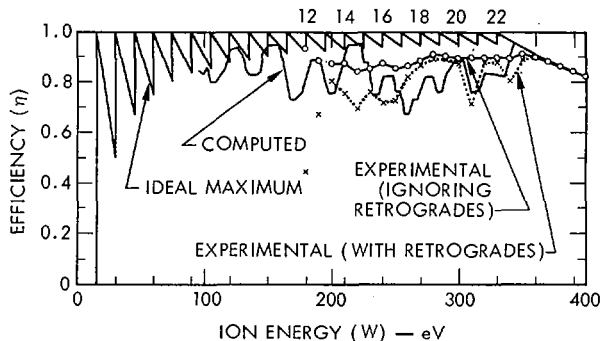


FIG. 4. Calculated and measured efficiency for $C = 3.0$ and $V_{cup} = V_{fin} + 0.4$.

Efficiency at ion energy eV_{acc} is given by

$$\eta(V_{acc}) = \frac{\sum_j V_j I_j(V_{acc})}{V_{acc} I_{total}(V_{acc})}$$

where V_j and $I_j(V_{acc})$ are the potential of, and the current to, collector j . The retrograde collector allows us to check that all current is accounted for [i.e., to see that $\sum_j I_j(V_{acc}) = I_{total}(V_{acc})$]. Also, it allows us to measure the loss in efficiency due to retrograde ions.

Figure 4 shows a plot of measured efficiency vs ion energy, for the case where $C = 3.0$ and where $V_{cup} = V_{fin} + 0.4$. The efficiency predicted, if it is assumed that the retrograde ions re-enter the collector after reflection at the reactor and are subsequently caught, is also shown as "Experimental (Ignoring Retrogrades)." The saw-tooth curve shows, for comparison, the maximum efficiency possible with 22 collectors with equal increments in potential. Also shown is the computed efficiency after averaging over a small spread in injection angle (-0.02 to $+0.02$ radians) and over a spread in energy (-0.2 to $+0.2$ units of energy). In the experiment, one unit of potential (or energy) is 30 V.

Measured efficiency, when averaged over a flat current distribution having a 2:1 range in energy (i.e., the average efficiency of the last 11 of the 22 cells) was 83% including retrogrades and 88% if retrogrades are assumed to be collected at the average efficiency (see Fig. 4). These average efficiencies are in close agreement with the results from the computer calculations as shown in Table I. The detailed comparison at specific energies (in particular where retrogrades occur) of the measured and the computed efficiency is not as close, for reasons that are not yet clear.

TABLE I. COMPUTED AND MEASURED EFFICIENCY AVERAGED OVER A 2:1 RANGE OF ENERGY, C = 3.0

	Initial Slope	Including Retrogrades	Ignoring Retrogrades
Computed	-0.02	0.822	0.907
	0	0.846	0.923
	+0.02	0.857	0.936
	+0.04	0.857	0.930
	+0.06	0.800	0.922
Experimental	~ ±0.02	0.83	0.88

4. FINITE DENSITY EFFECTS

The ions entering the direct converter produce a space-charge electric field $E_{sc} = \frac{eZnd}{2\epsilon_0}$, which acts in the direction opposite to the focus electric field $E_{focus} = \frac{CV_0}{L}$ (see Fig. 5); loss of focusing results in reduced collection efficiency. A space-charge limitation, then, is

$$E_{sc} \ll E_{focus} \quad \text{or} \quad n \ll \frac{2\epsilon_0 CV_0}{Ze dL} \quad (2)$$

For $d = 1$ m, $L = 2.67$ m, and $V_0 = 100$ kV, then,

$$n \ll 4.1 \times 10^6 \text{ C cm}^{-3} \quad (3)$$

From Eq. (2) we see the functional dependence of n on C , V_0 , d , and L . Since $C \approx 2$, Eq. (3) indicates n of the order of 10^6 cm^{-3} , as found in Ref. 1.

A dimensionless parameter useful for scaling density, energy, and size for systems that are identical in shape but not size is the relationship

$$\omega_p \tau = \text{constant}, \quad \omega_p^2 = \frac{Z^2 n e^2}{M \epsilon_0}, \quad \tau = \frac{L}{v^*}, \quad v^* = \left(\frac{2\bar{W}}{M} \right)^{1/2}$$

where:

$$\bar{W} = \int_0^\infty \frac{dJ}{dW} W dW / \int_0^\infty \frac{dJ}{dW} dW = \text{mean energy per ion coming into the collector,}$$

J = current density.

Then,

$$\omega_p \tau = \left(\frac{Z^2 e^2}{2\epsilon_0} \right)^{1/2} \left(\frac{n}{\bar{W}} \right)^{1/2} L \quad (4)$$

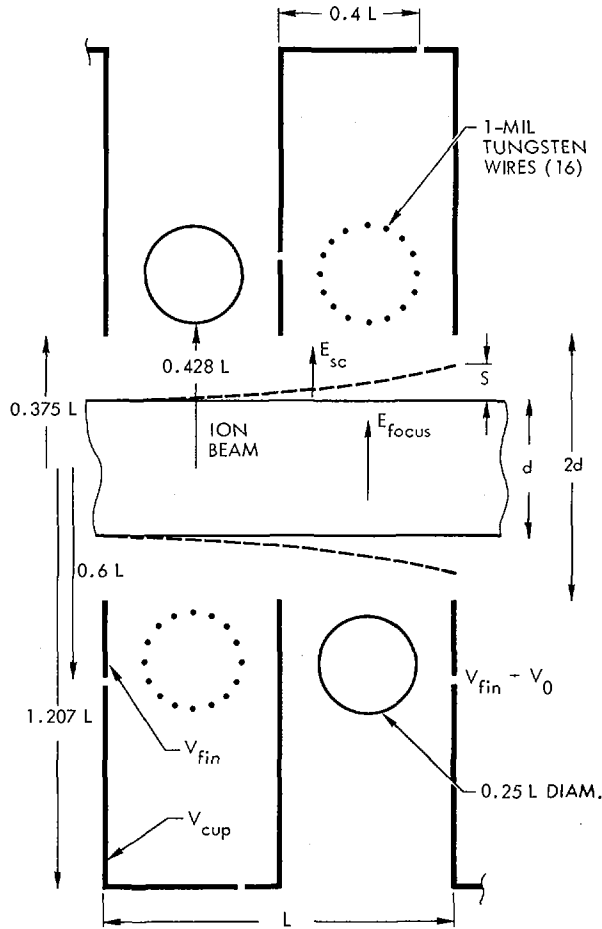


FIG. 5. Electrode structure.

Solving for n ,

$$n = \frac{2\epsilon_0}{Z^2 e^2} (\omega_p \tau)^2 \frac{\bar{W}}{L^2} \tag{5}$$

For 800 keV deuterons, $L = 2.67$ m, and $d = 1$ m, we get

$$n = 1.2 \times 10^7 (\omega_p \tau)^2 \text{ cm}^{-3} \tag{6}$$

Reference 1 discussed a case in which the density was $2.6 \times 10^6 \text{ cm}^{-3}$ and all other relevant parameters were the same as above. This would correspond to an $\omega_p \tau$ of 0.46.

The Z^2 in Eq. (5) implies a penalty for other than singly charged particles. For example, in the use of direct conversion, for the D- ^3He cycle this effect would amount to a reduction by a factor of approximately 2 in the overall power-handling capability (assuming typical D and ^3He concentrations) relative to singly charged ions. In assessing the direct converter for use with a mirror reactor, one wants the power flux

$$\frac{P}{A} = J \frac{\bar{W}}{eZ} \quad (7)$$

where J is the current density in A/m^2 .

$$J = eZn \bar{v}$$

where \bar{v} is the mean velocity. If we approximate \bar{v} by $\left(\frac{2\bar{W}}{M}\right)^{1/2}$, then

$$\frac{P}{A} = n \left(\frac{2\bar{W}}{M}\right)^{1/2} \bar{W} \quad (8)$$

Putting in n from Eq. 5, we get

$$\frac{P}{A} = 2\epsilon_0 \left(\frac{2}{M}\right)^{1/2} \frac{(\omega_p \tau)^2}{e^2 Z^2} \frac{\bar{W}^{5/2}}{L^2} \quad (9)$$

Using the same parameters as in Eq. (6), we find

$$\frac{P}{A} = 14.0 \frac{(\omega_p \tau)^2}{Z^2} \frac{\text{MW}}{\text{m}^2} \quad (10)$$

Using the $\omega_p \tau$ of 0.46 derived above, we get

$$\frac{P}{A} = 3.0 \text{ MW}/\text{m}^2 \quad (11)$$

for singly charged ions.

The power density should be maximized to minimize the capital cost per kilowatt handled. The finite density effects then reduce to determining the allowable value of $(\omega_p \tau)$ in one system and then using Eq. (9) to scale to other systems.

Space-charge effects were analyzed by a numerical simulation technique [5] that computes particle trajectories acted upon by applied external electrostatic fields and self-consistent internal space-charge fields. The space-charge fields are obtained by solving Poisson's equation with a steady-state particle distribution by iteration. This process has the advantage of obtaining rapidly computed self-consistent solutions, and the disadvantage of overlooking any dynamic instabilities which might be present.

For the collector discussed in section 3, space-charge effects are shown in Fig. 6, again assuming that current distribution is flat. The curve

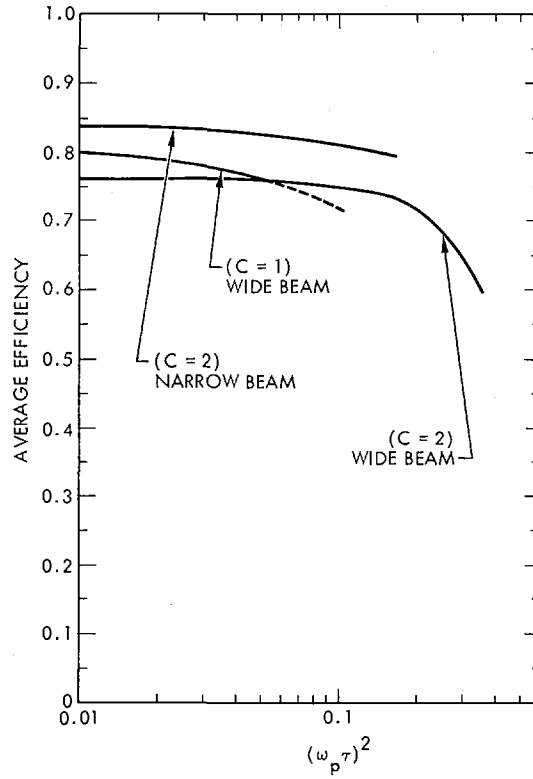


FIG. 6. Average efficiency versus $(\omega_p \tau)^2$ for a 24-fin collector.

labeled "narrow beam" has an energy spread of 2 and a physical width equal to $1/6$ of the channel width, thus corresponding to the experimental case. We see that the efficiency (with retrogrades counted as a loss) has dropped by 4% at $\omega_p \tau = 0.35$. The wide beam has an energy spread of 4 and a physical width equal to $1/2$ of the channel width, which is more like a reactor situation. This results in decreased efficiency, part of which can be regained in the low-density regime by lowering C from 2 to 1. However, for $(\omega_p \tau)^2 > 0.055$, $C = 2$ is still optimum. For the wide beam, the efficiency has dropped by 4% (76% to 73%) at $\omega_p \tau = 0.42$. This corresponds to [using Eqs. (6) and (9)]

$$n = 2.24 \times 10^6 \text{ cm}^{-3}$$

$$\frac{P}{A} = 2.46 \text{ MW/m}^2$$

The efficiency at low density is 84% for the narrow beam and 76% for the wide beam. The lower efficiency is due to the larger energy spread, rather than the increased beam width. This is seen in results that show markedly declining efficiency for the additional (lower) energies of the wide beam.

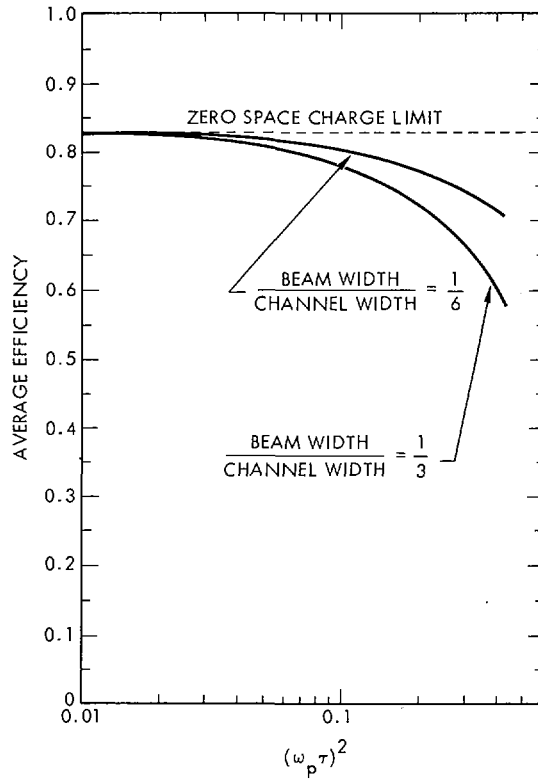


FIG. 7. Average efficiency versus $(\omega_p \tau)^2$ for a 12-fin collector.

This conclusion is further supported in Fig. 7, in which two beams with the same energy spread, differing by a factor of 2 in their physical width, have equal efficiencies at low density. At high densities the beams are in agreement with Eq. (2) in that, for a given efficiency, the ratio of beam densities is approximately equal to the inverse ratio of their widths.

To check the simulation code, a problem that could be solved analytically was run: a parallel monoenergetic slab beam of width d and density n will expand to some width $d + 2S$ in a distance L along the beam because of the space-charge field (see Fig. 5). The analytical result is that $S/L = \frac{1}{4} \frac{d}{L} (\omega_p \tau)^2$, for $S/L \ll 1$. The value of S/L found from the simulation code agreed with the calculated value to within $\pm 3\%$, in the range $S/L \ll 1$.

5. ANALYSIS OF INEFFICIENCIES

To estimate the efficiency of direct conversion, we have listed a number of losses or inefficiencies in Table II. The three columns are intended only to indicate a possible range and to call attention to individual identifiable losses. The first is appropriate to our experiment or computer model; the second and third are more speculative and are partly based on parameter scaling.

TABLE II. ESTIMATES OF DIRECT CONVERTER INEFFICIENCIES

	Present Capabilities, %	High Estimates, %	Low Estimates, %
1. Finite number of collectors (N): N = 25, 3%; N = 40, 2%.	3.0	3.0	2.0
2. Lack of ideal collection	13.0*	4.0	2.0
3. Residual transverse energy, assuming adiabaticity: $\frac{W_{\perp}}{W} = \frac{B_{\text{exit}}}{B_{\text{mirror}}} \approx 0.3\%$	0.3	0.3	0.3
4. Lack of adiabaticity: $\frac{W_{\perp}}{W} > \frac{B_{\text{exit}}}{B_{\text{mirror}}}$	0.1	0.1	0.1
5. Nonadiabatic kick at the expander exit $\left(\frac{\overline{W}_{\perp}}{W} = \frac{eZ (Bd)^2}{24M} \right)$	1.0	1.0	0.4
6. Finite space charge	4	2	0.5
7. Charge-exchange ionization (10^{-6} Torr) and secondary emission	1.0	1.0	0.1
8. Column interception [4]	2.0	2.0	0.2
9. Coupling the reactor to the direct converter	5.0	5.0	0.5
10. Inverter-rectifier [1]	0.3	0.3	0.3
11. Power for vacuum pumps [4]	0.2	0.2	0.1
	29.9	18.9	6.5

* If retrograde particles were recovered at the average efficiency, this 13% would drop to 8%.

6. SOME CONSIDERATIONS IN EXPECTED REACTOR SITUATIONS

To increase power-handling ability, several direct converters can, in principle, be stacked one on top of the other. N units will handle N times the power of one unit, unless each unit is scaled down. If all dimensions are reduced by a factor N , then the new L is the old L divided by N , in which case the power is proportional to N^2 . In practice, each unit will be made as small as possible [notice $(P/A) \propto L^{-2}$ (Eq. 9)], consistent with finite Larmor orbits in the expander and maximum tolerable electric-field strengths, wherein subdividing increases power linearly with N .

The maximum tolerable electric field, E_{MAX} , will be set by vacuum-breakdown considerations. The maximum electric field will occur on the negative grids and is approximately $150 \frac{CV_0}{L}$. For the same conditions as used in Eq. (6), the maximum E field is 1.7×10^5 V/cm, and the potential drop from the grid to nearest electrode is 250 kV.

The height of the ion stream d , which in turn sets the value of L , is $d = h + 2 a_L$, where h is the height at the collector of field lines that guide the particles from the reactor, and a_L is $\frac{Mv_L}{ZeB}$. If the trajectories in the expander are adiabatic, then $a_L = a_{Lmirror} \sqrt{\frac{B_{mirror}}{B}}$ (a_L can be less, depending on whether thermalization of reaction products is important or not). The proton resulting from the D- ^3He reaction has $a_L \leq 64$ cm for $B = 500$ G, and 45 cm for $B = 1$ kG. These values of a_L imply larger values of d than were used in the examples above [Eq. (11)] and, hence, lower power fluxes. The ^4He resulting from the D-T reaction has $a_L \leq 31$ cm for $B = 500$ G, and 22 cm for 1 kG. Thus we see that the stream height, d , can be about a factor of 2 smaller for D-T than for D- ^3He . Separating unthermalized reaction products from the ion stream before they reach the collector would relieve these dimensional constraints from either the D-T or D- ^3He reactions.

If unthermalized reaction products are to be recovered with high efficiency, electrodes must have voltages up to 1.76 MV for the $^4\text{He}^{++}$ from D-T, and up to 14.76 MV for the $^1\text{H}^+$ from the D- ^3He reaction. In some cases it might be advantageous to prevent thermalization of the $^1\text{H}^+$ by a field design that would cause this proton to be nonadiabatic and thus lost immediately; a single electrode near 14 MV would be needed, if this proves to be technically feasible.

It appears feasible to couple several direct converters onto any of a variety of different mirror magnets as shown in Ref. 6, and in some cases it is necessary for economic reasons.

In addition to the direct conversion of end losses in mirror systems, the direct conversion of the energy in monoenergetic ion beams is important in order to achieve high injection efficiency with neutral beam injection. In principle, the efficiency of this conversion could be made very high. Experiments with 2-keV ion beams have yielded recovery efficiencies as high as 95% at low-power densities, as discussed in Ref. 7.

7. CONCLUSIONS

Experiments began about 1 yr ago. At that time the collection efficiency was 40% for one collector, 46% for two collectors, and 54% for 11 collectors [8]. Progressive improvements have pushed that efficiency successively

higher to the present result of 83% with 22 collectors (88% if retrograde particles are recovered). In practice, the overall efficiency will be reduced by a number of loss processes, particularly space-charge limitations not investigated in the present experiments. Computer simulation of space-charge effects for a reactor-like case indicate a power flux of 2.5 MW/m^2 at an efficiency of 73%, for the particular case investigated. Further improvements in understanding and in achieving higher efficiencies in this very young field can surely be expected.

8. ACKNOWLEDGMENTS

We thank T. N. Haratani for assistance with the numerical calculations, J. D. Lee for engineering assistance, W. J. Gould for assistance in assembling and running the experimental apparatus, and J. A. Byers for valuable advice in numerical simulation techniques.

REFERENCES

- [1] POST, R. F., *Mirror Systems: Fuel Cycles, Loss Reduction and Energy Recovery*, Lawrence Radiation Laboratory, Livermore, Rep. UCRL-71753 (1969); Proc. Brit. Nucl. Energy Soc. Conf. Nucl. Fusion Reactors, UKAEA, Culham Laboratory, Culham, England, September 17-19, 1969 (UKAEA, 1970) 88-111.
- [2] POST, R. F., *Direct Conversion of Fusion Energy to Electricity*, Lawrence Radiation Laboratory, Livermore, Rep. UCRL-72411 (1970); in *Fusion Technology*, Proc. Energy 70 Conf., Las Vegas, Nevada, September 21-25, 1970 (Energy 70, Albuquerque, New Mexico, 1970) 1-19 — 1-28.
- [3] WERNER, R. W., CARLSON, G. A., LEE, J. D., MOIR, R. W., POST, R. F., TAYLOR, C. E., Lawrence Radiation Laboratory, Livermore, Rep. UCRL-72883 (1971); Paper CN-28/K-2, these Proceedings.
- [4] Preliminary Report of Direct Recovery Study, Lawrence Radiation Laboratory, Livermore, Rep. UCID-15650 (1970).
- [5] FREIS, R. P., BYERS, J. A., Bull. Am. Phys. Soc. 15 (1970) 1432.
- [6] MOIR, R. W., TAYLOR, C. E., *Magnets for Open-Ended Fusion Reactors*, Lawrence Radiation Laboratory, Livermore, Rep. UCRL-72399 (1970); Proc. Energy 70 Conf., Las Vegas, Nevada, September 21-25, 1970 (Energy 70, Albuquerque, New Mexico, 1970) 1-80 — 1-89.
- [7] MOIR, R. W., BARR, W. L., HAMILTON, G. W., OSHER, J. E., Bull. Am. Phys. Soc. 15 (1970) 1431.
- [8] BARR, W. L., MOIR, R. W., POST, R. F., Bull. Am. Phys. Soc. 15 (1970) 1431.

ENGINEERING AND ECONOMIC ASPECTS OF MIRROR MACHINE REACTORS WITH DIRECT CONVERSION*

R. W. WERNER, G. A. CARLSON, J. D. LEE,
R. W. MOIR, R. F. POST, C. E. TAYLOR
Lawrence Radiation Laboratory,
Livermore, Calif.,
United States of America

Abstract

ENGINEERING AND ECONOMIC ASPECTS OF MIRROR MACHINE REACTORS WITH DIRECT CONVERSION.

Reactor design studies are presented based on the use of mirror confinement zones fed by neutral beam injectors and utilizing direct converters for charged-particle-energy recovery. Designs considered include Yin-Yang and axially symmetric coil configurations, D-T and D-³He fuel cycles, and net electrical outputs ranging from one hundred to one thousand megawatts, the latter being the base case.

The operating power level of each reactor component is determined as a function of component efficiencies, Q (defined as the ratio of fusion power to trapped injected power), and other relevant variables. Then approximate cost-power scaling relationships are used to calculate component costs. Results for overall cost and system efficiency are presented as functions of Q for a variety of component efficiency sets.

The results indicate that the D-T system with direct conversion is economically attractive for expected Q -values and component efficiencies. In comparison, the D-³He system is characterized by high sensitivity to system changes at expected Q -values, and very high component efficiencies are required in order to make it economical. The disadvantage of the D-T system is that it is basically a heat engine and has little potential for overall system efficiencies greater than 45% at blanket temperatures usually considered. In contrast, D-³He has a potential for operating economically at system efficiencies greater than 80%. Such a system could be achieved if Q -values for D-³He near unity become possible and sufficient ingenuity in the design of efficient reactor components is exercised.

1. INTRODUCTION

Direct conversion of charged-particle energy to electricity has been proposed to improve the power balance in mirror systems [1]. Direct conversion may be utilized both in the injection system and in the recovery of the energy of the particles escaping through the loss cone. The potentially high efficiency of direct conversion minimizes losses and permits consideration of fuel cycles in which most of the reaction products are charged particles.

Both the capital cost per net electrical kilowatt and the overall system efficiency of mirror reactors using direct conversion can vary widely, depending on the power level, component efficiencies, reactor configuration, fuel cycle, and Q . The parameter Q is defined as the ratio of fusion power to trapped injected power. Q is a complicated function of plasma species, temperatures, ambipolar potential, and magnetic confinement field, particularly the mirror ratio. Although there is considerable uncertainty in the exact values of Q which may be obtained, there is general agreement

* This work was performed under the auspices of the United States Atomic Energy Commission.

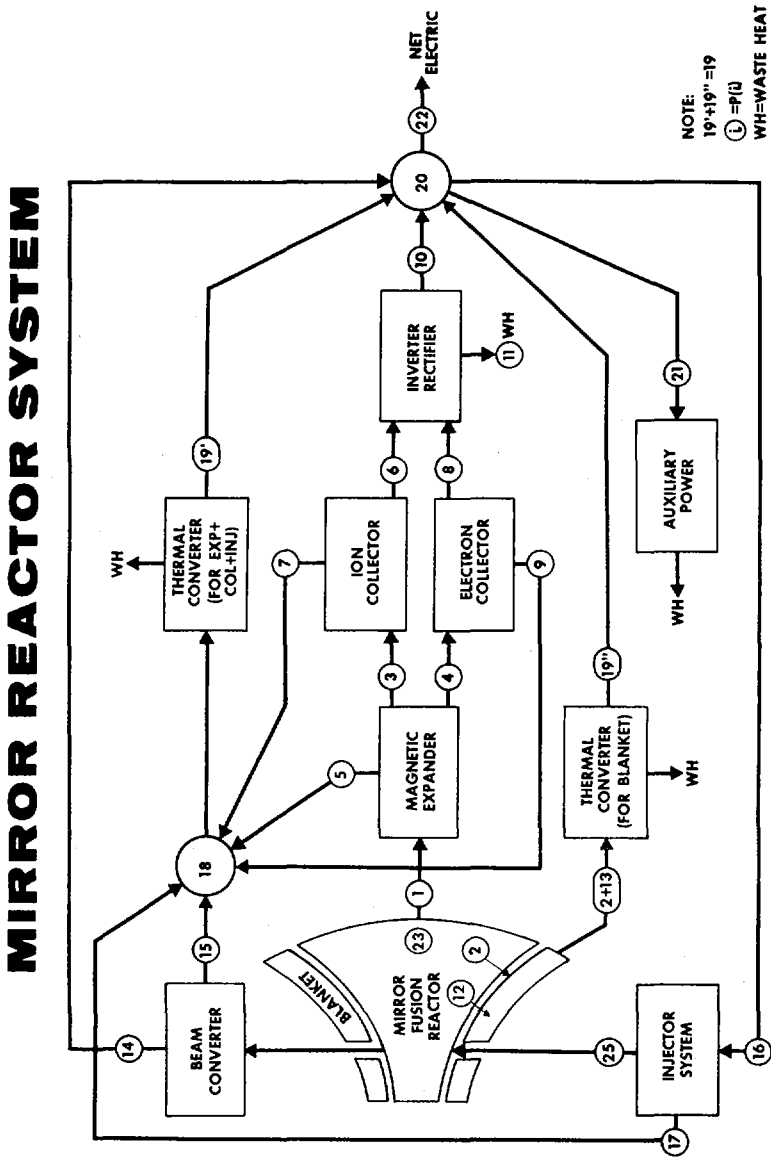


FIG. 1. Block diagram of mirror reactor system with direct conversion.

that Q should be within the range 1.0 to 2.0 for DT systems assuming collisional end losses and mirror ratios appropriate to a high- β reactor [2-4]. The value of Q for D-³He has been calculated to be ~ 0.2 [4] with prospects of 0.4 or greater under reactor conditions. Because of the potentially low values of Q , a mirror fusion reactor is necessarily a rather low-gain power amplifier. To be attractive as a commercial reactor, such a system must re-circulate energy efficiently and inexpensively.

This paper presents reactor design studies based on the use of mirror confinement zones fed by neutral beam injectors and utilizing direct converters for charged-particle-energy recovery. Designs considered include Yin-Yang [5] and axially symmetric simple mirror coil configurations, D-T and D-³He fuel cycles, and net electrical outputs ranging from one hundred to one thousand megawatts. Results for overall cost and system efficiency are presented as functions of Q for a variety of component efficiency sets.

2. SYSTEM ANALYSIS

System analysis is performed with a computer program developed for mirror reactor systems with direct conversion [6]. A block diagram of this system is displayed in Fig. 1.

Very briefly, the program logic first calculated the operating power level of each system component based on input data including the desired output power, Q , and component efficiencies. Component geometries and/or component costs are then determined based on their power levels and cost factor input data.

Since magnet costs increase with ion energy and direct converter and injector costs decrease with ion energy, the option of automatically varying mean ion energy to find its optimum value is available. The optimum energy is that which gives minimum total system cost. In this paper, this option of optimizing is always exercised. In all cases, the optimum ion energies were found to be in the range 300 - 500 KeV.

Three different fuel cycles were considered. These were the deuterium-tritium (DT) cycle, a deuterium-helium-3 (D-³He) cycle and also a combination deuterium-deuterium-helium-3-tritium (D-D-³He-T) cycle. For the D-T cycle a lithium breeding blanket was assumed. But for the D-³He and the D-D-³He-T cycles breeding is not required. The important point here is that in these two cases the necessary helium-3 and tritium is provided entirely by recovery and reinjection of the equilibrium fraction of the fusible reaction products of D-D reactions going on in the same plasma. These two cycles are therefore really D-D cycles with reaction product burn-up, an idea that goes back to the earliest days of fusion research.

Although the two D-D cycles do not require a breeding blanket, they do involve the handling of tritium and this point deserves some comment. For the D-D-³He-T cycle the problem is a straightforward one. The tritium could presumably be quickly recycled, keeping the inventory low and minimizing handling problems. But the D-D-³He-T cycle poses a different problem. What to do with the D-D tritium yield? One possibility is to use it to help fuel another reactor, either on-site or off-site. But among other possibilities, there is one that, while it does not involve the off-site transportation of tritium, does involve its storage. If the D-D tritium is

TABLE I. INPUT VARIABLES FOR MIRROR REACTOR STUDIES

	Optimistic	Nominal	Pessimistic
Trapping fraction F(3) [fraction of injected power trapped in plasma]	1.0	0.975	0.95
D- ³ He charged-particle fraction F(2) [fraction of fusion power carried by charged reaction products]	0.90	0.85	0.80
Ion expansion E(1) [mirror-leakage efficiency times expansion efficiency]	0.96	0.94	0.92
Ion sep. and coll. E(3) [ion-electron separation efficiency times collection efficiency]	0.95	0.90	0.85
Neutral beam coll. E(7) [neutral beam collector conversion efficiency]	0.95	0.925	0.9
Injection E(8) [injection system efficiency]	0.95	0.90	0.85
Thermal conv. E(9 and 10) [thermal conversion efficiencies]	0.50	0.45	0.40
Reactor leakage area CF(4) m ² [mirror leakage area (Fig. 13)]	2.1	3.15	4.2
Magnetic expansion ratio CF(5)	100	200	300
Space-charge limit CF(7) MW/m ² [space charge limited energy flux for reference expander (beam height = 1 m and ave. ion energy = 800 keV)]	6	3	1.5

recovered and immediately absorbed in a metal such as tritium, and if this metal is then stored on-site in a number of separate containers, then these containers could be periodically milked for the helium-3 resulting from the decay of the tritium. In a steady state, this procedure will allow the benefits of increased helium-3 concentration in the plasma using only on-site chemical processing.

Tables II and III-B display required code input data and results.

3. SYSTEM COMPONENTS

Figure 1 shows the flow diagram for a mirror reactor with direct conversion. As is evident from the figure, there are a large number of reactor components whose individual efficiencies will greatly affect overall performance of the system. Using Fig. 1 the flow of energy through the system can be traced and component design and performance discussed.

TABLE II. MIRROR REACTOR INPUT DATA FOR NOMINAL COMPONENT PERFORMANCE

	Fuel cycle	
	D- ³ He	D-T
Plasma data		
Q - fusion power/trapped injected power F(1)	0.4	1.0
Fraction of fusion power in charged-particle kinetic energy F(2)	0.9	0.2
Fraction of injected power trapped in plasma F(3)	0.975	0.975
Radiation fraction of fusion ions + trapped injection power F(4)	0.02	0.02
Ion fraction of expanded leakage power F(5)	1.0	1.0
Average ion energy in reactor (keV) F(6)	435	420
Average ion energy entering collector (keV) F(7) (ion energies optimized)	594	575
Beta - fuel ion pressure/magnetic pressure	0.8	0.8
Fuel - 1.0 = D-T, 2.0 = D- ³ He	2.0	1.0
Component efficiency data		
Ion expansion E(1)	0.94	0.94
Electron Expansion E(2)	0.94	0.94
Ion separation and collection E(3)	0.90	0.90
Electron collector E(4)	0.90	0.90
Inverter-rectifier (I-R) E(5)	0.99	0.99
Fusion neutron blanket energy multiplication E(6)	2.00	2.00
Neutral beam collector E(7)	0.95	0.95
Injector system E(8)	0.90	0.90
Thermal conversion of blanket heat E(9)	0.45	0.45
Thermal conversion of collector and injector heat E(10)	0.45	0.45
Auxiliary power fraction of fusion power E(11)	0.01	0.01
Desired output power level (MWe-net)	1000	1000
Cost factor data		
Blanket and shield thickness (M) CF(1)	1.0	1.5
Cost per unit area of blanket (\$/M ²) CF(2)	1000	7000
Minimum expander radius for 800 keV ave. ion energy (M) CF(3)	25	25
Mirror leakage area per hole of base reactor (M ²) CF(4)	3.15	3.15
Expander expansion ratio CF(5)	200	200
Ratio of collector length to ion beam height in collector CF(6)	25	25
Space charge limited col. flux (H = 1M, E = 800 keV) (MW/M ²) CF(7)	3	3
Expander/collector structural cost (\$/M ²) CF(8)	600	600
Expander magnet cost (\$/M ²) CF(9)	425	425
Collector element cost (\$/M ²) CF(10)	640	640
Injector system unit cost (\$/kWe into system) CF(11)	30	30
Waste heat disposal cost (\$/kW) CF(12)	5	5
Inverter-rectifier cost (\$/kWe) CF(13)	3	3
Blanket thermal conversion cost (\$/kWe) CF(14)	86	86
Injector-collector thermal conversion cost (\$/kWe) CF(15)	86	86

TABLE III-A. INPUT DATA AT Q 0.2 AND 0.4 FOR D-³He AT HIGH COMPONENT PERFORMANCE

Plasma data	
Q - fusion power/trapped injected power F(1)	0.2, 0.4
Fraction of fusion power in charged particle kinetic energy F(2)	0.9
Fraction of injected power trapped in plasma F(3)	1.00
Radiation fraction of fusion ions + trapped injection power F(4)	0.02
Ion fraction of expanded leakage power F(5)	1.0
Average ion energy in reactor (keV) F(6)	480
Average ion energy entering collector (keV) F(7) (ion energies optimized independent of Q)	652
Beta - fuel ion pressure/magnetic pressure F(8)	0.8
Fuel - 1.0 = D-T, 2.0 = D- ³ He F(9)	2.0
Component efficiency data	
Ion expansion E(1)	0.96
Electron expansion E(2)	0.96
Ion separation and collection E(3)	0.95
Electron collector E(4)	0.95
Inverter-rectifier (I-R) E(5)	0.99
Fusion neutron blanket energy multiplication E(6)	2.00
Neutral beam collector E(7)	0.95
Injector system E(8)	0.95
Thermal conversion of blanket heat E(9)	0.5
Thermal conversion of exp. + coll. + inj. heat E(10)	0.5
Auxiliary power fraction of fusion power E(11)	0.01
Desired output power level (MWe-net) E(12)	1000
Cost factor data	
Blanket + shield thickness (M) CF(1)	1.0
Cost per unit area of blanket (\$/M ²) CF(2)	1000
Minimum expander radius for 800 keV ave. ion energy (M) CF(3)	25
Mirror leakage area per hole of base reactor (M ²) CF(4)	2.1
Expander expansion ratio CF(5)	100
Ratio of collector length to ion beam height in collector CF(6)	25
Space charge limited col. flux (H = 1M, E = 800 keV) (MW/M ²) CF(7)	6
Expander-collector structural cost (\$/M ²) CF(8)	600
Expander magnet cost (\$/M ²) CF(9)	425
Collector element cost (\$/M ²) CF(10)	640
Injector system unit cost (\$/kWe at 300 keV) CF(11)	30
Waste heat disposal cost (\$/kW) CF(12)	5
Inverter-rectifier cost (\$/kWe) CF(13)	3
Blanket thermal conversion cost (\$/kWe) CF(14)	86
Exp. + coll. + inj. thermal conversion cost (\$/kWe) CF(15)	86

TABLE III-B. SYSTEM CHARACTERISTICS FOR THE D-³He CYCLE USING HIGH COMPONENT PERFORMANCE CRITERIA COUPLED WITH A LOW Q = 0.2 AND A HIGH Q = 0.4

Results - system element powers	Q = 0.2		Q = 0.4		Q = 0.2		Q = 0.4	
Mirror reactor leakage P(1)	11 745		4672		240		95	
Collector ions P(3)	11 276		4485		0		0	
Expander heat P(5)	470		187		10 712		4261	
Ion coll. heat P(7)	564		224		0		0	
Electron coll. heat P(9)	0		0		10 605		4218	
I-R heat P(11)	107		43		203		140	
Neutron induced blanket P(13)	406		280		0		0	
Untrapped beam thermal P(15)	0		0		10 691		3690	
Injector heat P(17)	535		184		1 568		596	
Thermal to Electric P(19)	1 107		486		11 712		4704	
Auxiliary (assumed) P(21)	20		14		1 000		1 000	
Fusion power P(23)	2 031		1402		1 234		542	
Neutral beam power P(25)	10 157		3505		11		5.1	
System efficiency	0.448		0.648					
Cost results with optimized expander collector (\$/kWe-net)								
Reactor magnet	94		42		0.74		0.37	
Thermal converters	95		42		15		7	
Expander magnet	9		4		4		2	
Collector elements	8.58		4		148		69	
Waste heat disposal	6.2		3		32		13	
					413		186	
System geometry with optimized expander-collector								
Plasma radius (M)	4.2		2.9		70		70	
Number of leakage beams	3		3		0.403		0.3	
Expander radius (M)	101		66		10		7.7	
Expander angle (radians)	4.2		4.2					

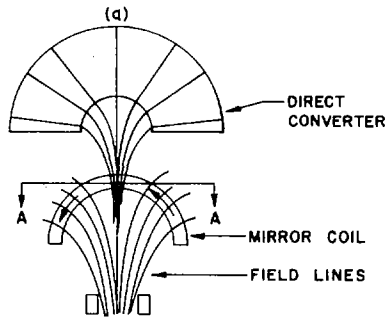


FIG. 2. Direct converter, mirror coil and field lines.

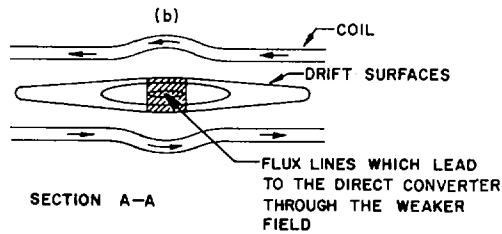


FIG. 3. Drift surfaces and flux lines leading to direct converter.

The primary reactor design discussed in this paper uses the Yin-Yang magnetic-coil geometry. This coil produces a minimum- $|B|$ mirror field with a deep well and a nearly spherical plasma volume. The magnet dimensions and cost are based on a design by Moir and Taylor for a Yin-Yang reactor [7]. An alternate reactor design uses a simple axially-symmetric-coil configuration with implied feedback stabilization [8].

The reactor blanket and shield thickness is specified and cost is calculated based on a specified cost per unit area. The D-T system blanket is taken to be both thicker and more expensive than the D- ^3He blanket because of the requirements for 14-MeV-neutron moderation and tritium breeding.

In the design of the direct converter, the charged particles are caused to preferentially leave the mirror region through a small total area [7]. This is to be accomplished by weakening the mirror field in a local region causing predominant losses at that point through small-angle scattering. One or more preferred leakage areas can be developed in this way and, therefore, one or more direct converters can be coupled to the reactor. Figures 2 and 3 illustrate the technique. It is estimated that using this method more than 95% of the particles can be caused to flow through the area(s) selected.

As the particles (e, p, D, T, ^3He , ^4He) leave the mirror region and escape from the reactor, they are guided through the expander on magnetic

field lines. Losses in the expander area arise from charge exchange with background gases and from collision with any structure required. If the structure is designed using present nominal vacuum standards (base pressures $\sim 10^{-5}$) then charge exchange losses would be less than one percent [9]. Losses from collisions with structural members, e. g. support columns, depend on engineering design, i. e. acceptable capital costs versus minimum interference. We consider a beam loss by collision of $2\frac{1}{2}\%$ to be quite reasonable with economy of construction. This energy loss is assumed recoverable thermally at efficiencies of approximately 40%.

The particles upon emerging from the expander field are subject to two additional loss mechanisms. The first of these arises from residual rotational energy because of incomplete magnetic expansion. This loss can be shown to be proportional to the ratio of the field at the expander exit to the mirror field. Typical ratios of fields are $\sim 1000/150\,000$ G so that losses are $< 1\%$.

The second loss at emergence from the expander is due to ions crossing the expander field lines. It is assumed that electrons are separated from the ions at the expander terminus by abruptly folding back field lines. The electrons continue on the field lines adiabatically but the ions, because of their higher mass, continue on a straight path and cross field lines as a consequence. The resultant transverse ion energy is of the order of 0.5%.

The ions now enter the collector region where determination of net efficiency is at present more difficult. Here, losses can occur due to space charge, charge exchange, finite number of collectors, retrograde particles and secondary emission. The Laboratory has presently underway a program on direct conversion within which these collection efficiencies are being evaluated. In the experiments to date a 22 element collector has been used and a recovery efficiency of 83% obtained [10]. If it is assumed that the retrograde particles in this experiment were recovered, then the efficiency rises to 88%. Reflection and collection of retrogrades appears quite possible in a reactor situation. We consider an assumption of 85% for collection as pessimistic and 95% as possibly achievable but optimistic.

High-efficiency direct recovery of the electron energy should not be necessary because the electron-to-ion energy ratio is calculated to be $\approx m_e/m_i$ at the expander exit. The predicted low electron energy arises because reactor equilibrium requires that electron and ion currents be equal, and charge neutrality in the expander requires that electron and ion densities also be equal. It follows that the velocity along the field lines, V_{\parallel} , be the same for electrons and ions throughout the expander (assuming no additional electrons are available). At the expander exit, almost all of the particle velocity is in the direction of the field lines; so $E_e/E_i \approx m_e/m_i$.

The expander-collector vacuum structure is based on the design described in Ref. [9]. The structure is fan-shaped and made up of hexagonal modules, the top and bottom surface of which are thin metal membranes loaded in tension. The superconducting expander magnet, the collector elements, and the collector vacuum system are also described in Ref. [9].

The efficiency of the inverter-rectifier system used to bring the potentials produced by particle collection to a common value is assumed to be 99% based on the performance of commercially available HVDC-equipment.

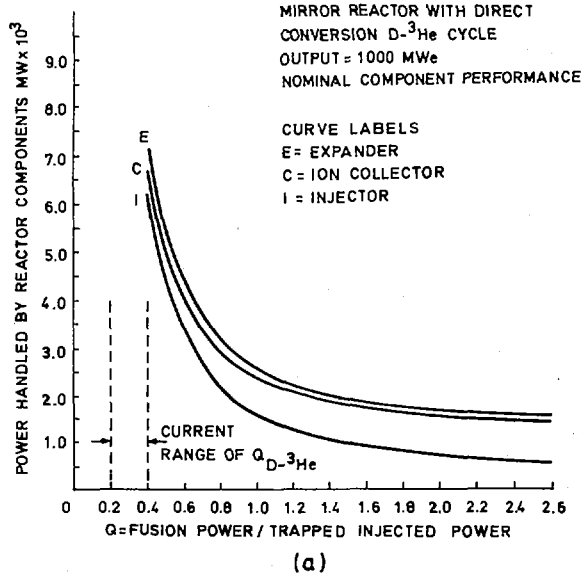


FIG. 4a. Power handled by principal reactor components as a function of Q for the D-³He-cycle.

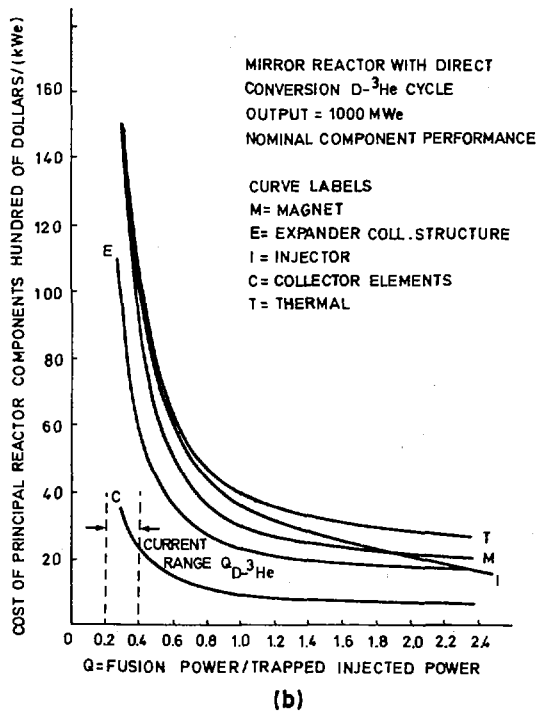


FIG. 4b. Cost of principal reactor components as a function of Q for the D-³He-cycle.

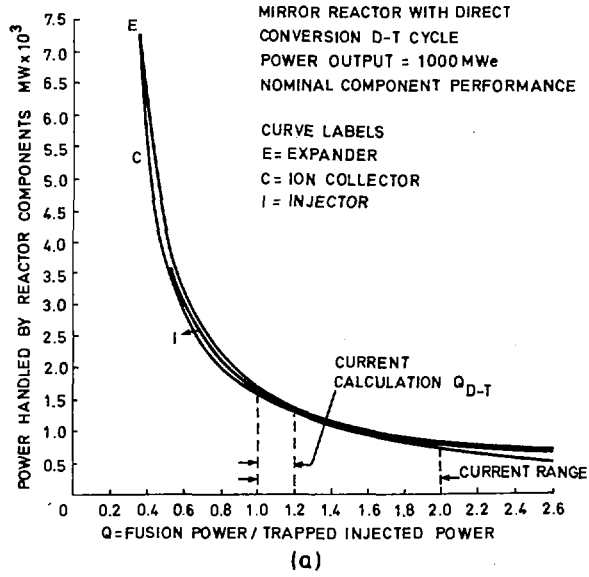


FIG. 5a. Power handled by principal reactor components as a function of Q for D-T-cycle.

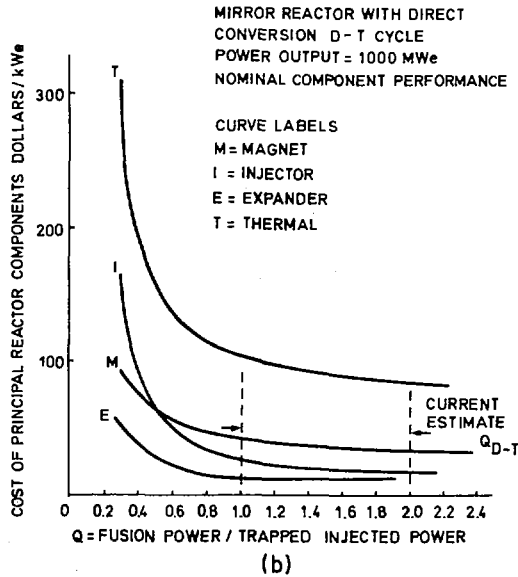


FIG. 5b. Cost of principal reactor components as a function of Q for D-T-cycle.

Thermal conversion systems are used to convert both blanket heat and direct conversion waste heat (from expander, collector, and injector losses) into electricity. For such systems we consider 40% efficiency as easily realizable and 50% within current technology.

Since, as was mentioned previously, re-circulating power in mirror machines is quite high for small values of Q , it is very important that high injection efficiencies be obtained. Injection systems require ion sources, particle accelerators and beam neutralizers as principal components. Ions are first accelerated to the desired energy level. The ions are then neutralized by passing them through a chamber containing gas or vapour. Particle neutrality is necessary for injection across the B-field. Since beam neutralization is always an incomplete process, a beam direct converter is used to recover the energy of unneutralized particles. The beam direct converter should be less complicated than the mirror-leakage direct converter because each injector is monoenergetic. Using beam direct conversion, the overall injection efficiency can possibly be as high as 95%. There is much work remaining to be done to develop injectors and beam handling systems capable of delivering high total currents (>100 A) at current densities of ≈ 50 mA/cm². The injector system cost (\$30/kW injector input) used in this study is only a crude first estimate.

Table I summarizes the various component performances just discussed. We have elected to specify performance by range; the minimum values we consider pessimistic and the maximum values to be obtainable but optimistic.

4. VARIATION OF COMPONENT EFFICIENCIES AND Q

Table II lists the variables used as input in the computer program. All component performance data, all component cost bases and all pertinent plasma data including Q are stipulated. The values specified

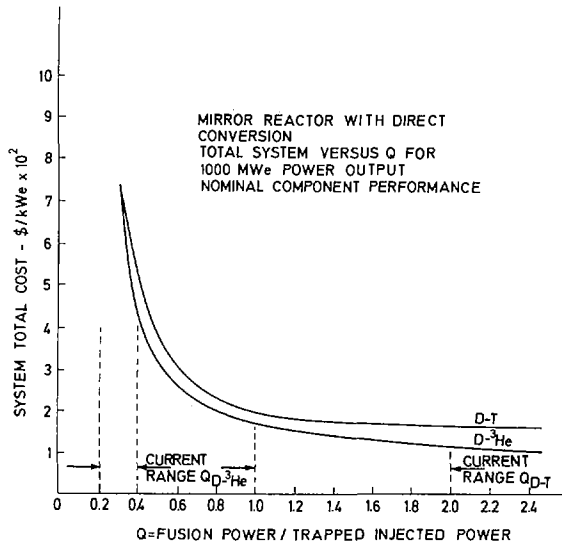


FIG. 6. Total system cost as a function of Q for D-T and D-³He-reactor.

in this particular table are for a representative analysis for D-T and D-³He in which the performances specified were those we consider "reasonable" or nominal; that is, halfway between pessimistic and optimistic for the efficiencies shown in Table I. Using these input data, Q was varied over a range from 0.2 to ~ 3.0. Figures 4a and 4b illustrate a portion of the calculated results for the D-³He cycle and Figs 5a and 5b for the D-T cycle in terms of the power handled by the principal components and in terms of costs. Figure 6 compares the total system cost for the two cycles as a function of Q.

Several observations can be made by inspection of these figures. It is evident that for values < 0.8, Q is a very sensitive parameter in the economics of fusion reactors with direct conversion. Fortunately, as noted above, the expected value of Q for D-T is 1.0 or greater and economically attractive systems are predicted. The Q for D-³He, however, is both low and presently more uncertain than that for D-T, present predictions indicating a range ~ 0.2 to 0.4. Clearly, major economic gains would result from increases in Q_{D-^3He} . As can be seen from Fig. 6 even moderate increases in Q would have a substantial effect. The cost curves shown can shift up and down by uncertainty in the cost base for each component. The right to left shift, which is more significant since it allows lower Q, is possible by improvement in component performance.

Figure 7 illustrates the consequence to the total D-³He system cost of allowing the input variables to range from the lowest anticipated values shown in Table I to the highest. If we assume that \$400/kWe is reasonably competitive with other power systems, then with the optimistic input the value of Q for D-³He which is economically acceptable is about 0.2. With the pessimistic input Q would have to be ~ 1.0. Figure 8 illustrates the same effect for the DT-cycle. Using the same criterion of \$400/kWe for a reasonable competitive cost, it can be seen that Q for D-T can be ~ 0.2 with the optimistic component performance criteria and still somewhat

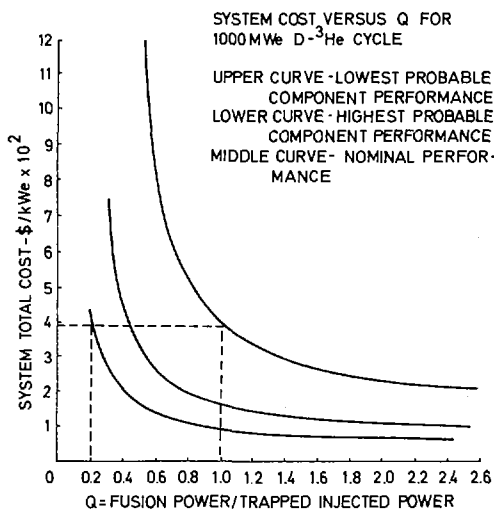


FIG. 7. System cost versus Q and component performance for D-³He-cycle.

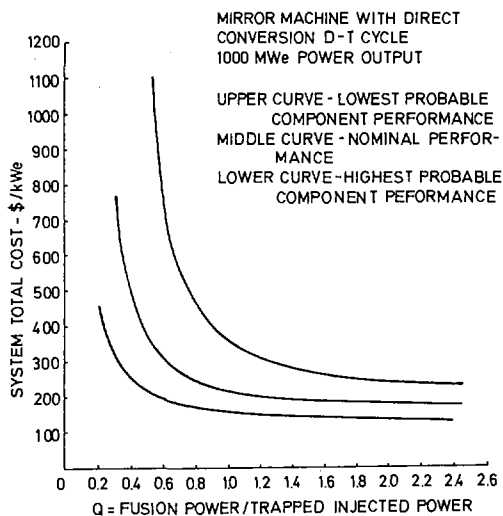


FIG. 8. System cost versus Q and component performance for D-T-cycle.

less than 1.0 with the low component performance criteria. Thus for the D-³He cycle to be of engineering and economic interest, either the component performance must be quite high or some means must be made available to increase Q . The D-T-cycle, however, is consistently attractive.

If we assume high component performances are indeed realizable, admittedly an optimistic outlook at the present time, then Tables III-A and III-B are of interest. Table III-A shows the input data at a Q of both 0.2 and 0.4 for D-³He at the high component performance and Table III-B shows the system characteristics that emerge as a consequence. Perhaps the most interesting points to observe are that the system efficiency is quite high, around 47% when $Q = 0.2$ and the system cost is around \$400/kWe. For a Q -value of 0.4, the system efficiency is 65% and the total cost \$186/kWe. The area where $Q \approx 0.2$ is an ultra-sensitive one where very small changes in component performance can mean the difference between success and failure for D-³He. For instance, at nominal component performance (those in Table II) the efficiency at $Q = 0.2$ was only 3% and the system cost \$7665/kWe compared to the 47% and the \$400/kWe. Thus a change in performance levels from those which we consider reasonable and within current technology to performances that are presently optimistic has produced an order-of-magnitude improvement in both system efficiency and system cost. The gains realized by increasing Q from 0.2 to 0.4 are not as dramatic as the effects of component performance changes but are quite evident and encouraging.

Table III-B also provides a reasonable clear idea of what a 1000 MWe-reactor might look like in terms of physical size and in terms of power handled by the individual components.

Figure 9 shows the system efficiencies plotted as a function of Q for both D-³He and D-T at the "nominal" component performances and for D-³He

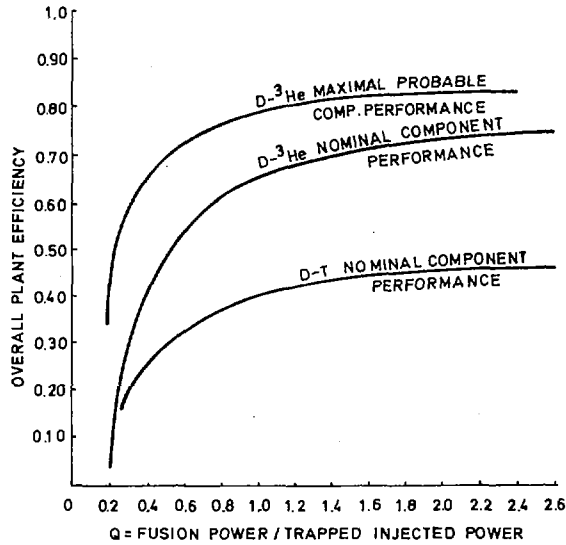


FIG. 9. Mirror reactor overall efficiency as a function of Q.

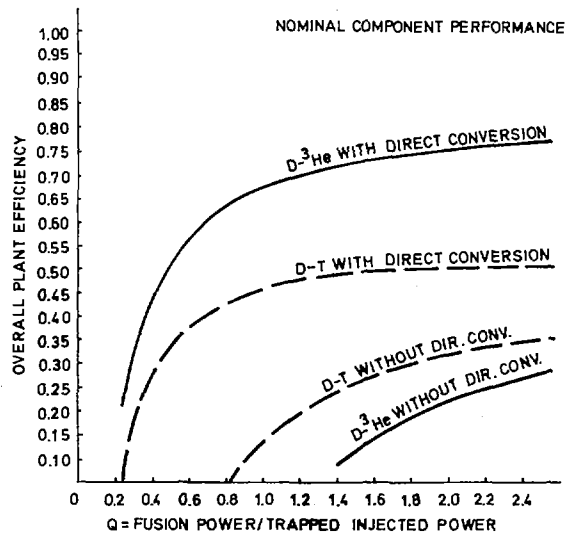


FIG. 10. Effect of direct conversion on overall efficiency of mirror machines.

at the highest probable component performance. It is clear from this figure why a mirror machine using the D-³He fuel cycle is of great interest. The best power plant systems in operation in the world today have efficiencies of about 40%. The average is more like 30%. If means can be found to increase Q_{D-^3He} or if the higher component efficiencies can be obtained, then the D-³He systems would be more efficient than any other system presently known. Figure 10 shows what the application of

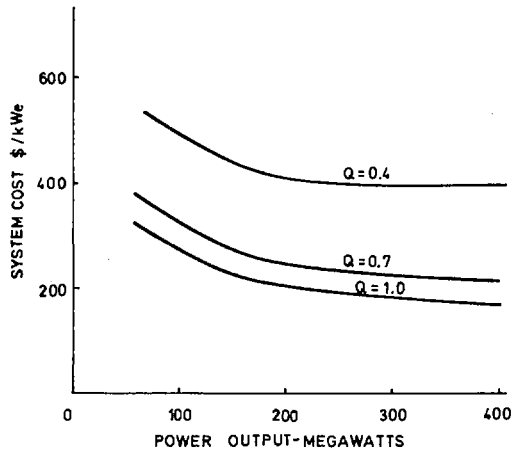


FIG. 11. System cost as a function of power output, D-³He-cycle, and nominal component performance.

direct conversion did to the efficiency of mirror reactors for both D-³He and D-T. The lower curves are those without direct conversion and the upper curves were calculated using direct conversion.

5. VARIATION OF OTHER PARAMETERS

The effect of output power level

In the next set of figures, Figs 11 and 12, the power output has been allowed to range from 100 MWe to 400 MWe for Q values of 0.4, 0.7, and 1.0. It can be seen that at ~200 MWe and higher, the cost of a mirror reactor with direct conversion with either D-T or D-³He is a weak function of power output. As also discussed by Golovin [8] this result, that mirror reactors are capable of operating economically at low power levels, is in rather striking contrast to the prediction for other fusion reactors using conventional energy recovery.

D-T system with sub-critical fast-fission blanket

If one is willing to accept the known difficulties of handling fissionable materials and their waste products, a possible method of improving the performance of fusion systems employing fuel cycles that produce neutrons (such as the D-T-cycle) is to enhance fusion-neutron-induced blanket energy generation with fast fission. Preliminary studies [11] indicate that sub-critical fast fission blankets can greatly increase blanket energy generation. For example, analysis of a blanket containing uranium depleted to 0.4% ²³⁵U plus lithium depleted to 4% Li-6 for tritium breeding and heat transfer plus niobium for structure gave energy generation of ~100 MeV per incident 14-MeV neutron. This is over three times higher

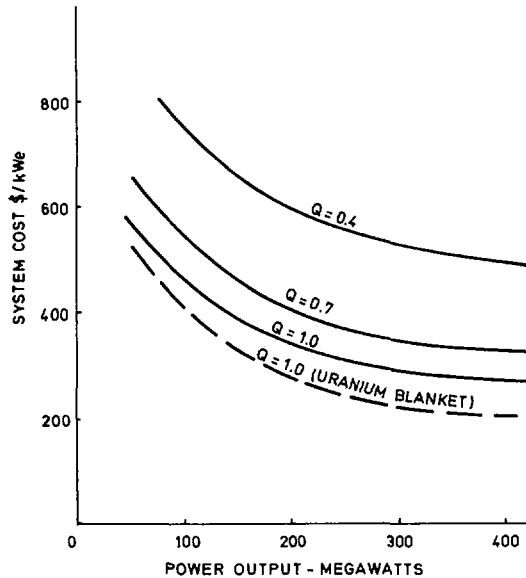


FIG. 12. System cost as a function of power output for mirror reactors with D-T-cycle and nominal component performance.

than the best non-fission blankets we have devised. Figure 12 displays the effect of the sub-critical fast fission blanket on system cost, a 25% reduction in cost at output power levels greater than ~ 300 MW.

Another important advantage of such a blanket is that it makes possible economic D-T systems at lower Q's. For example, with the fission blanket, a Q of 0.2 gives the same system cost as a Q of 0.7 with our best non-fission blanket. The systems employ nominal performance components and the cost is $\sim \$280/\text{kWe-net}$. At a system cost of $\$400/\text{kWe-net}$ the nominal components with the fission blanket require a Q of only 0.14, and the optimistic components with the fission blanket require a Q of only 0.07. These Q's are a factor of 7 to 28 below the values of Q heretofore assumed (1 to 2). Hence, tolerable anomalous losses could be a factor of 7 to 28 greater than losses resulting from collisional processes alone.

The D-D- ^3He -T fuel cycle

If we consider a D-D system with the reinjection of both the ^3He and the tritium produced in the D-D reaction together with the use of a non-breeding blanket, then the resultant fuel cycle is one in which the value of the parameter Q lies between $Q_{\text{D-}^3\text{He}}$ and $Q_{\text{D-T}}$.

For this cycle, another important plasma parameter is the fraction of fusion power released as charged particle kinetic energy. The D-D- ^3He -T-cycle's fraction is $\sim 65\%$ compared with 20% for the D-T-cycle and $\sim 85\%$

SYSTEM COST VS FUEL CYCLE & Q

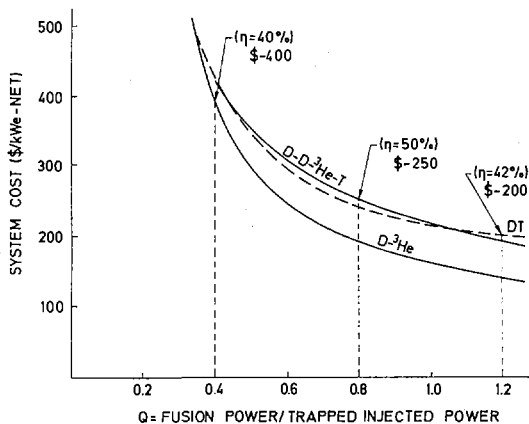


FIG. 13. Comparison of total system cost for D-T, D-³He-cycle and a cycle in which all ³He and T is re-injected. Nominal component performance.

for the D-D with only ³He-reinjection (which we call the D-³He cycle). The determination of which fuel cycle will finally make the optimum system must wait until Q-values under reactor conditions are better known.

The cost for the D-D-³He-T system as a function of Q is shown in Fig. 13. For comparison, the costs for D-T and D-³He are shown in the same figure. All are at nominal component performance. It can be seen that costs closely parallel those for D-T. If it is assumed that a reasonable maximum Q for this hybrid cycle is ~0.8, then there is a cost penalty when it is compared with the D-T cycle at Q = 1.2 and a cost benefit when compared with D-³He at a Q = 0.4. The overall plant efficiency for this cycle is ~50% as compared with 42% and 40% for D-T and D-³He at their maximum Q's. This efficiency gain is significant.

Another advantage of this cycle is that tritium breeding is not required which means that tritium inventory and hold-up problems are minimized. There is a gain in Q at a nominal price penalty over D-T but operation is in a region where sensitivity to system changes is substantially lower than is the case for D-³He.

Axially symmetric (simple mirror) coils

The axially symmetric coil, because of its relatively simple geometry, is significantly lower in cost than the Yin-Yang. The reference cases used as a basis for our calculations show the axially symmetric coil to cost \$32 million compared to \$120 million. This factor of four, while seemingly large, does not play as strong a role in influencing total reactor costs as might have been expected. In example calculations that were made using

TABLE IV. COMPARISON OF TOTAL SYSTEM COST USING YIN-YANG AND AXIALLY SYMMETRIC COILS

Coil geometry	D- ³ He (Q = 0.4)		D-T (Q = 1.0)	
	Magnet cost	Total cost	Magnet cost	Total cost
Yin Yang	\$84/kWe	\$420/kWe	\$42	\$220
Symmetric	\$58	\$379	\$19	\$188

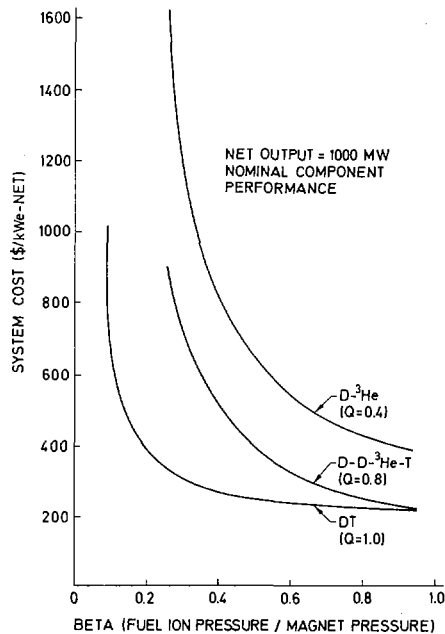


FIG. 14. System cost versus beta.

the axially symmetric coil, the total costs were reduced only about ten percent below those for a comparable Yin-Yang. However, it is likely that part of the cost saving would be utilized in providing stabilization of the flute modes likely to occur in simple mirror systems.

Since superconductor costs can represent a major part of magnet costs, some comment about the assumptions made about costs in this paper is in order. The costs are based on the studies in Ref. [7]. An index of these costs is given by the costs taken there for two conductor types, Nb₃Sn and NbTi. Costs evaluated for 100-kG operation were taken to be 0.011 \$/ampere-metre, to be compared to an estimated present-day "large-order" cost of 0.015 \$/ampere-metre, i. e. about a reduction of 40%. For NbTi present-day large-order costs were taken, as 0.0005 \$/ampere-metre at 60kG. Since it is possible that the superconductor

costs taken are conservative, considering likely advances in superconductor technology, the magnet costs we have obtained might be somewhat too high, at least as far as the superconductor costs are concerned.

Table IV illustrates the cost comparison between the Yin-Yang and simple mirror geometry.

The effect of beta

The value of beta (fuel ion pressure/magnetic pressure) that we have consistently used in this analysis has been taken to be 0.8. The effect on total system cost of varying beta (insofar as it is reflected in power density consideration alone) from 0.2 to its limit of 1.0 is shown in Fig. 14 for D-T and D-³He and the D-D-³He-T cycle for the specific assumed values of Q. The D-³He-cycle is quite sensitive to this parameter with a strong indication that $\beta \geq 0.8$ is desirable. The D-T-cycle is relatively insensitive to decreases in beta at constant Q until a value of $\beta \sim 0.3$ is reached. The cycle where all the ³He and T is re-injected has the same slope as the D-³He and therefore the same sensitivity. However, it is possible to use this particular cycle down to a $\beta = 0.45$ with a resulting system cost less than the D-³He system cost at $\beta = 0.8$.

6. CONCLUSIONS

It is interesting that mirror reactors with direct conversion do not require high output power levels in order to be competitive with other systems. Power levels as low as 2000 MWe are predicted to be almost as economic as those at 1000 MWe or higher. This suggests that mirror-fusion power plants could be introduced into the economy at considerably reduced risk capital outlays for first generation systems as compared to higher-power systems.

The studies show that within the assumptions made, the D-T-cycle using direct conversion is almost always an economically attractive system. Furthermore, a survey of the results over a broad range of component performance leads one to conclude that the sensitivity of the D-T-cycle to system changes is usually low. For this cycle and its variants an economic case can be made even in the face of end losses appreciably above those calculated from collisional effects alone. But in the final analysis D-T is basically a heat engine and although it performs well, it is at the same time difficult to make it perform in an astounding way. The maximum system efficiency of around 45% at blanket temperatures usually considered gives weight to this conclusion. This efficiency is susceptible to improvement, however, by adding a topping cycle. The topping cycle could be MHD or a high-temperature metal vapour turbine. In comparison, the D-³He cycle at this time is characterized by high sensitivity to system changes at the currently estimated values of Q and it takes a very high component performance to make it economic. But the potential is there. Given even moderate improvements in Q's, D-³He can perform in an astounding way and system efficiencies greater than 80% seem possible. With the increasing consumption of energy in the United States, high efficiency would be a very important attribute. It seems evident that despite its added difficulty, D-³He cycles should be investigated since this

particular cycle with its potentially high performance could play a very important role in the fusion power impact on the environment. Furthermore, a realization of an efficient D-³He cycle should be immediately reflected in the economics of the overall reactor system, owing to the potentially low cost of direct conversion equipment relative to conventional steam plants.

REFERENCES

- [1] POST, R.F., "Mirror systems: fuel cycles, loss reduction and energy recovery", Lawrence Radiation Laboratory, Livermore, Calif., UCRL-71753 (1969) Presented at Nuclear Fusion Reactor Conf., Culham, England.
- [2] FOWLER, T.K., RANKIN, M., "Fusion energy balance in mirror machines", Plasma Physics (Journal of Nuclear Energy Part C) (1966).
- [3] KUO-PETRAVIĆ, L.G., PETRAVIĆ, M., WATSON, C.J.H., "Alpha particle heating and energy balance in a mirror reactor." Abingdon, Berkshire, United Kingdom (Proc. Nuclear Fusion Conf., 1969).
- [4] FUTCH, A.H., HOLDREN, J.P., KILLEEN, J., MIRIN, A.A., "Multispecies Fokker-Planck calculation for DT and DHe³ mirror reactor", Lawrence Radiation Laboratory, Livermore, Calif., (unpublished).
- [5] MOIR, R.W., POST, R.F., "Yin-Yang minimum-B magnetic field coil", Nucl. Fusion 9 (1969) 253.
- [6] LEE, J.D., "Mirror fusion reactor system code No. 1", UCID-15837, Lawrence Radiation Laboratory, Livermore, Calif. (1971).
- [7] MOIR, R.W., TAYLOR, C.E., "Magnets for fusion reactors", Lawrence Radiation Laboratory, Livermore, Calif., UCRL-72399 (1970) Presented at the IECEC Energy 70 Conf., Las Vegas.
- [8] GOLOVIN, I.N., "Mirror reactor feasibility and comparison with tokamak reactor," Moscow, USSR, Kurchatov Institute of Atomic Energy, Presented at the IECEC Energy 70 Conf., Las Vegas (1970).
- [9] "Preliminary report of direct recovery study", Lawrence Radiation Laboratory, Livermore, Calif., UCID-15650 (1970).
- [10] MOIR, R.W., BARR, W.L., POST, R.F., FREIS, R.P., these Proceedings.
- [11] LEE, J.D., LRL thermonuclear reactor memorandum No. 20, "Sub-critical fast fission blanket", November 23 (1970).

DISCUSSION

TO PAPERS IAEA-CN-28/K-1, K-2

D. J. ROSE: I should like to congratulate your group on their fine work in direct energy conversion and on the progress they have made. Have you any information on the sensitivity of the system cost (\$/kW(e)) to changes in the cost of the ion expander system?

R. F. POST: The effect on cost depends, of course, on the recirculated power function. As an example, consider the data of Fig. 4 B (paper K-2) for the D-³He reactor: here, the combined costs of the direct converter are about \$80/kW(e) output but, as the figure shows, higher values of Q reduce this cost substantially. A further breakdown can be deduced from the data in Table III A (ibid). Generally, direct conversion is much cheaper than thermal conversion, per kilowatt handled.

D. J. ROSE: You mention that 2-3% of the escaping ions can be intercepted by structural members. Is this not a very serious matter, considering that there is only about 1% burn-up per pass and, hence, a need for much recycling?

R. F. POST: The particles burned out in the structure of the supports would certainly have to be recovered. We have considered several possibilities, but only superficially. One method would be to diffuse them through a metal at elevated temperatures. This problem deserves further study, which should include the possibility of magnetically diverting the particle fluxes around the support columns.

A. GIBSON: You quoted a recovery efficiency of 83% for the ion-beam system. Is this the efficiency without plasma and space-charge effects?

R. F. POST: The measurements were performed for relatively low space-charge levels ($\omega_p \tau \approx 0.2$). The information we have on space-charge effects is at present derived solely from computer simulation.

A. GIBSON: How does the unit cost of \$400/kW(e), which you used as a reference, compare with projected end-of-the-century costs for fission-reactor systems?

R. F. POST: The cost figure I quoted is substantially higher, but we regard it merely as a kind of upper limit. For a system to be of interest its cost must be lower than this figure.

H. HARRISON: Have you had an opportunity to analyse the voltage-current output of your direct-conversion system? How will the output voltage change with varying load currents?

R. F. POST: We have not analysed this in detail. However, it is clear that the direct converter will act somewhat like a constant-current device, having a short-circuit current characteristic dominated for short times by the capacitive discharge of the electrodes, and a long-term characteristic of strongly limited current. The analysis is complicated by the inverter-rectifier system and its control characteristics.

M. K. ROMANOVSKY: What was the true particle density in the beam used for the experiment on direct energy recovery?

R. F. POST: The particle density in the collector experiments was rather small ($\omega_p \tau)^2 \approx 0.05$), i. e. it was about a factor of 2 to 4 less than the $(\omega_p \tau)^2$ values we suggest for a reactor direct converter. The computer shows that the values used were about a factor 2 below the value at which space-charge effects should begin.

M. K. ROMANOVSKY: Are you aware of the work carried out at the Moscow Engineering and Physical Institute, where an experimental efficiency of 90-95% was obtained using a beam in which the particle energy was modulated from 1 to 4 keV?

R. F. POST: Yes. I have been informed during this present conference of the very interesting work performed in Moscow on different types of collector structures for use in direct conversion.

EFFICIENT RE-CIRCULATION OF POWER IN MIRROR REACTORS

J.G. CORDEY, F.B. MARCUS, D.R. SWEETMAN,
C.J.H. WATSON
UKAEA, Research Group,
Culham Laboratory,
Abingdon, Berks,
United Kingdom

Abstract

EFFICIENT RE-CIRCULATION OF POWER IN MIRROR REACTORS.

A model of a mirror reactor system has been developed which permits the overall cost of the system to be minimized with respect to the mirror ratio, mirror magnetic field and injection energy. The model is based upon calculations of the maximum- β and the density distribution of the plasma, and incorporates a number of assumptions about limiting technological parameters and costs. Both minimum- β and simple mirror systems have been considered, and both D-T and D-³He fuel cycles. Using the best present estimates of Q, the D-³He reactors are found to be considerably more expensive than the D-T systems. The use of a simple mirror system reduces the nuclear 'boiler' component of the costs by a factor of about two.

The minimum overall cost is found to occur when the mirror ratio is such that the maximum wall loading criterion and maximum- β criterion are simultaneously satisfied, and the optimum mirror fields are comparatively modest - in the range of 140-180 kG. The optimum cost is found to be rather insensitive to the maximum permissible wall loading and to the mirror magnetic field. However, the cost is sensitive to the injection energy - the optimum energy being approximately 100 keV - and there is a considerable cost penalty in working at energies at which external re-circulation schemes become practicable.

To avoid these high injection energies, a new mirror-reactor geometry is proposed which employs direct neutralization and re-injection of the flux of ions escaping through the mirrors. This scheme uses the fact that the particles emerge through the mirrors with their velocity vector nearly perpendicular to the field lines; they are then reinjected with high efficiency in a re-entrant axisymmetric mirror trap. Such a system would operate at low energy (e.g. ~ 100 keV) and can approach the self-sustaining condition.

I. Introduction

Existing calculations of the particle loss rate from mirror machines^(1,2) suggest that the prospects of a mirror reactor depend upon the development of some means of increasing its effective energy amplification factor Q. A recent addition to the list of proposed methods - a list which includes a range of schemes for reducing the losses (eg. RF stopping or multiple mirrors) or for enhancing the energy production (eg. the addition of neutron multiplying or fissile nuclei to the blanket) - is the suggestion of Post⁽³⁾ that the energy of the escaping particles should be recirculated with high efficiency. In the evaluation of any such scheme, economic considerations are of primary importance. In the first part of this paper we give a comparatively general discussion of the interaction of physical

and economic constraints in the design of mirror reactor systems which incorporate a substantial power recirculation loop. This is based on a model of the reactor system which permits an optimisation of the physical parameters of its various components with respect to the total cost. This analysis indicates that for optimum performance the system would recirculate rather large currents ($\sim 10,000$ amps) at relatively low energies ($\lesssim 100$ keV). By contrast, the Post recirculation scheme appears to work best when recirculating comparatively small currents (~ 1000 amps) at high energies ($\gtrsim 500$ keV) because of space charge limitations in the direct converter. Consequently, in Section IV of the paper we propose an alternative recirculation scheme, in which the energy is recirculated in the form of energetic neutral atoms. This scheme has the advantage that it operates best at energies in the region of 100 keV (ie. close to the optimum regime): it also provides an economically attractive means of injecting large currents of neutral atoms.

II. Reactor Model and Basic Scalings

Our model of a mirror reactor system⁽⁴⁾ is represented schematically in Figure 1. The costs of the injector, thermal converter and direct converter per KW(e) of power handled (I, T and D respectively) are all assumed (in view of the absence of costable designs) to be independent of the injection energy and mirror

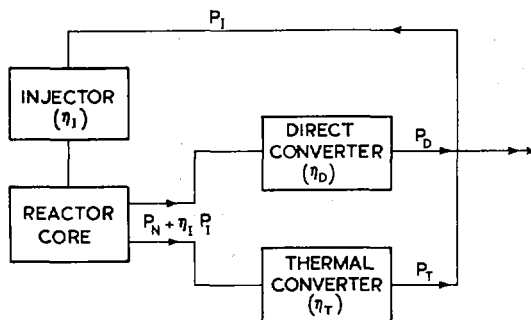


FIG.1. Schematic diagram of system model used.

magnetic field design. The cost of the reactor 'boiler' is made up of a blanket component scaling with its surface area A_B , and a magnet component scaling with the area of the windings A_w and with an empirical function of the magnetic field strength B at them, which includes the cost of windings, superconductor, refrigeration and insulation and is of the form

$$f(B) = k_1 + k_2 B + (k_3 + k_4 r_w) B^2$$

(where the k_i are constants and r_w is the winding radius). This function is assumed to be applicable up to a certain B_{max} , beyond which the cost rises much more rapidly with B .

A given reactor design is specified by a set of functions and parameters. The functions, which specify the shape of the magnetic surfaces and of the blanket, and the profiles of magnetic field strength and plasma density, are determined by the optimisation procedure described below. The parameters fall into two groups. There are first the quantities for which C , the total capital cost of the system per KW(e) of output, can only decrease monotonically as they are increased. In this category come the efficiencies $\eta_I \eta_D \eta_T$, the total power output P_{out} , the limiting field strength B_{max} and the maximum permissible thermonuclear power output per unit area of vacuum wall area (the 'wall loading limit') P_{wmax} . These parameters are fixed at maximum values which could in principle be determined by technological and economic considerations which are outside the scope of the present work. We simply assume $\eta_I = \eta_D = 0.9$, $\eta_T = 0.5$, $P_{out} = 1 \text{ GW(e)}$, $B_{max} = 180 \text{ kG}$ and $P_{wmax} = 1.5 \text{ KW(th)/cm}^2$ as representative values and examine how the total cost C scales as these values are varied. The second group of parameters are those which affect the cost C in a manner which is not a priori obvious, so that optimum values might exist. In this category come the length L , the midplane plasma radius r_p and winding radius r_w , the central density n_o , pressure p_o , vacuum field strength B_{vo} and actual field strength B_o , the mirror field strength B_m , the actual wall loading P_w , and the energy of injection ϵ_o . Four of these quantities can be calculated from the remaining six, and in fact it proves convenient to work with

$$\beta, \epsilon_o, \alpha, r_p, R, B_m \quad (1)$$

as the six independent parameters, where $\beta = \frac{8\pi P_{\perp 0}}{B_{v0}^2}$, $\alpha = L/r_p$ (the 'aspect ratio' of the plasma configuration), and $R \equiv B_m/B_0$ (the actual mirror ratio, related to the vacuum mirror ratio $R_0 \equiv B_m/B_{v0}$ by $R = R_0/(1-\beta)^{\frac{1}{2}}$).

To perform the optimisation of these parameters with respect to the total cost C we have considered two confinement configurations - I) a macroscopically stable minimum-B quadrupole configuration with a sufficiently large aspect ratio α for the analytic field expressions derived in⁽⁵⁾ to be valid, and II) a simple axisymmetric mirror stabilised by some unspecified but inexpensive means. We have also considered two fusion fuel cycles - A) a 50:50 D-T mixture with neutron capture and Tritium breeding in the blanket and B) a self-maintaining 80:20 D-He³ mixture.

The determination of the optimum parameters for a reactor proceeds in three stages. First, the vacuum magnetic field configuration is represented (following Ref.(5)) in terms of two scalar functions - $B_v(z)$, the profile of the vacuum field strength along the magnetic axis, and $C(z)$, a measure of the vacuum field line curvature - and the profiles of the actual magnetic field $B(z)$ and the plasma density $n(z)$ along any field lines are calculated from Maxwell's equations and the Fokker-Planck collisional distribution function. Secondly, optimum profiles $B_v(z)$ and $C(z)$ are determined by maximising the total thermonuclear power (proportional to $\iiint n^2 d\tau$ divided by the cost of the magnetic field windings (proportional to $\iint f(B_v) ds$, where f is the empirical cost function, subject to the constraint that the field possesses the necessary adiabaticity or stability properties. This fixes the density, pressure and vacuum field profiles $n(z)$, $p_{\perp}(z)$ and $B_v(z)$ (but not their central values, n_0 , $p_{\perp 0}$, B_{v0}) and determines the shape of the limiting flux surface within which the plasma is confined (but not its midplane radius r_p). Likewise the geometry of the blanket and magnetic windings is determined (by taking the vacuum wall at $\sqrt{2} r_p$, and adding $d = 160$ cm of blanket) apart from r_p and L . If the vacuum field is required to possess a minimum in the longitudinal direction, to ensure stability

TABLE I. ASSUMED COST PARAMETERS

$k_1 = 0.45 \text{ £ cm}^{-2}$ (refrigeration + insulation)	$I = 10 \text{ £/kWe handled}$
$k_2 = 2 \cdot 10^{-6} \text{ £ cm}^{-2} \text{ G}^{-1}$ (winding)	$D = 10 \text{ £/kWe handled}$
$k_3 = 8 \cdot 10^{-11} \text{ £ cm}^{-2} \text{ G}^{-2}$ (superconductor)	$T = 29 \text{ £/kWe handled}$
$k_4 = 5 \cdot 10^{-14} \text{ £ cm}^{-2} \text{ G}^{-2} \text{ cm}^{-1}$ (support)	Blanket cost = 0.013 £/cm^3 (including first wall)

against the 'mirror instability', a maximum value of β is obtained, expressible for reasonably large (actual) ratios R as

$$\beta_{\max} = 1/[1 + 1/(2 \ln 4R - 10/3)] \quad (2)$$

Further details of this stage of the analysis are given in Ref. (6)

In the third stage, the six remaining system parameters (1) are optimised with respect to the total cost C subject to the constraints

- (i) $P_{\text{out}} = \text{constant}$
- (ii) $\beta \leq \beta_{\max}$
- (iii) $P_w \leq P_{w\max}$
- (iv) $B_m \leq B_{\max}$
- (v) $\alpha \geq \alpha_{\min}$

The last of these constraints results from the limitations of the theory used to calculate the field and plasma profiles, which involved a large aspect ratio expansion. Fortunately our results are extremely insensitive to the value of α_{\min} , the lower limit of applicability of the theory, and for definiteness we have taken $\alpha_{\min} = 8$. A detailed study of the consequences of these constraints has been made by computer⁽⁷⁾ on the following basis. The total cost C per KW(e) of output was taken as:

$$C = 1.15 (I.P_I + D.P_D + T.P_T + N.P_N) \quad (3)$$

where the normalised powers⁽⁴⁾ are shown in Fig.1 and specific costs are as shown in Table I, and 15% 'on costs' were added. In these formulae, all absolute costs are expressed in 'notional pounds' (£) to emphasise the provisional nature of these figures: we attach much more significance to the ratios of such quantities, and to the optimised physical parameters derived from them.

Using the efficiency definitions, Eq.(3) can be written as

$$C = \frac{1.15}{\eta_e} (C_o + C_1/Q + N) \frac{Q}{Q - Q_c} \quad (4)$$

where $\eta_e = h \eta_T + (1-h) \eta_D$ is an effective efficiency of electrical generation, $Q = Q_o \log_{10} R$ is the basic energy amplification of the system in the absence of recirculation,

$$Q_c \equiv (1 - \eta_I \eta_D) / \eta_I \eta_e \quad (5)$$

is the critical Q below which there is no net output,

$$C_o \equiv \eta_T hT + \eta_D (1-h)D \quad (6)$$

and

$$C_1 \equiv (I + \eta_I \eta_D D) / \eta_I \quad (7)$$

are fixed parameters, and

$$N = \frac{(d C_B + C_w) A_w}{P_c V_p F} \quad (8)$$

where C_B is the mean cost per unit volume of the blanket materials and their fabrication,

$$C_w = \iint f(E_v) ds / \iint ds$$

is the cost of the windings and their fabrication per unit area, averaged over the previously determined field profile (where h is the fraction of the gross power output handled by the thermal plant, V_p is the volume of the plasma, P_c is the thermonuclear power density in kW(th)/cm³ at the centre of the machine, and F is the factor relating the average power density over the plasma volume to the central value, a factor which lies between $\frac{1}{4}$ and 1 for the various optimised systems).

The central thermonuclear power density P_c appearing in (8) is given by

$$P_c = 1.4 \times 10^9 (B_m/R)^4 [\beta/(1-\beta)]^2 \langle \sigma v W \rangle / [\epsilon_o^2 (1 + p_e/p_i)^2] \text{ kW(th)/cm}^3 \quad (9)$$

where $\langle \sigma v W \rangle$ is the total fusion power per unit plasma density in kW(th)-cm³ (eg. $\frac{1}{4} \overline{\sigma v} \epsilon_N$ for the D-T case, with $\epsilon_N = 22.4$ MeV), ϵ_o is the injection energy in MeV and p_e/p_i is the ratio of the electron and alpha-particle pressure to the ion pressure (taken as 0.32).

Of the four concepts obtained by combining one confinement system with one fuel cycle, only one - the D-T minimum-B reactor I(A) - can be evaluated fully, since the limiting plasma pressure

in a stabilised axisymmetric mirror, and the precise value of Q for the D-He³ fuel cycle, have not yet been determined. However, by making plausible estimates for these quantities some interesting comparisons can be made.

Although the actual optimisation was performed by computer, the results for the minimum-B reactor can be interpreted by the following heuristic arguments. We first consider the parameter β . It is clear from (4), (8) and (9) that the optimum is at $\beta = \beta_{\max}$, which we take as given by (2). As regards α , it is necessary to use constraint (i), which gives $P_{\text{out}} \sim r_p^3 = \text{const}$ and hence

$$N \sim \left(\frac{1}{P_{\text{out}} \alpha} \right)^{1/3} \left(\frac{1 - \beta}{\beta} \right)^{4/3} \frac{R^{8/3}}{B_m^{2/3}}$$

Consequently constraint (v) applies and the system should have the minimum allowed aspect ratio α_{\min} . This quantity is probably fixed by engineering design considerations outside the scope of the present study: however, the very weak dependence of N on α shows that its precise value is rather unimportant. The remaining parameters (since r_p is now determined through the relation between P_c and P_{out}) are R and B_m . For fixed B_m , there is always a minimum in C as R is varied, since C goes to infinity both as $R \rightarrow \infty$ (when $C \sim R^{8/3}$) and as $R \rightarrow R_c$, the critical value at which $Q = Q_c$. For small values of B_m , the value of C at this minimum decreases as B_m is increased. However for fixed α and P_{out} the wall loading scales as $(B_m/R)^{8/3}$, so very small values of R will always be excluded by constraint (iii), and as B_m is increased the situation is eventually reached where even the value of R at which the minimum of $C(R)$ occurs is just excluded by constraint (iii). This critical point may constitute the absolute optimum: however, depending on the value of P_{wmax} , there may exist a still cheaper design. This situation is illustrated in Figure 2 where C is plotted as a function of R for various values of B_m , with P_{wmax} taken as 1.5 KW(th)/cm². The minima of these curves are plotted in Figure 3, which shows C as a function of B_m at the optimum mirror ratio R for three different energies.

It will be seen that with this wall loading limit there is an advantage in increasing B_m somewhat past the point A, the value at which the wall loading limit and the minimum of $C(R)$

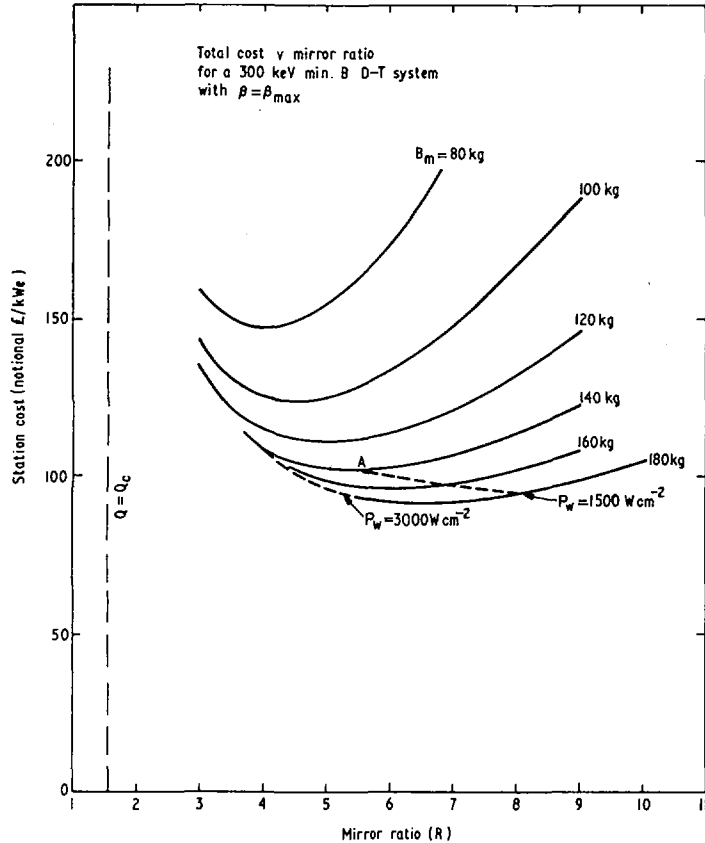


FIG. 2. Total station cost versus mirror ratio for a 300-keV minimum-B D-T system. β is assumed to be β_{\max} . In subsequent graphs the system is taken to be constrained by a wall loading limit of 1500 W/cm^2 :

occur simultaneously, but there is no advantage in going to very high magnetic fields since (as Fig.3 shows) the constrained minimum becomes insensitive to B_m and may even start to rise again. Since the wall loading limit is just reached in the optimum case, it is easy to show that the cost scales as $(P_{w\max})^{-1/4}$, so there is little advantage in pressing wall loading technology. Likewise, the cost is insensitive to further advances in the peak field attainable by superconductors, since the optimum B_m is already almost within the existing attainment and the minima of Figure 3 are in any case rather flat. The real cost advantage would accrue from a substantial reduction in the cost of superconductors at currently available field

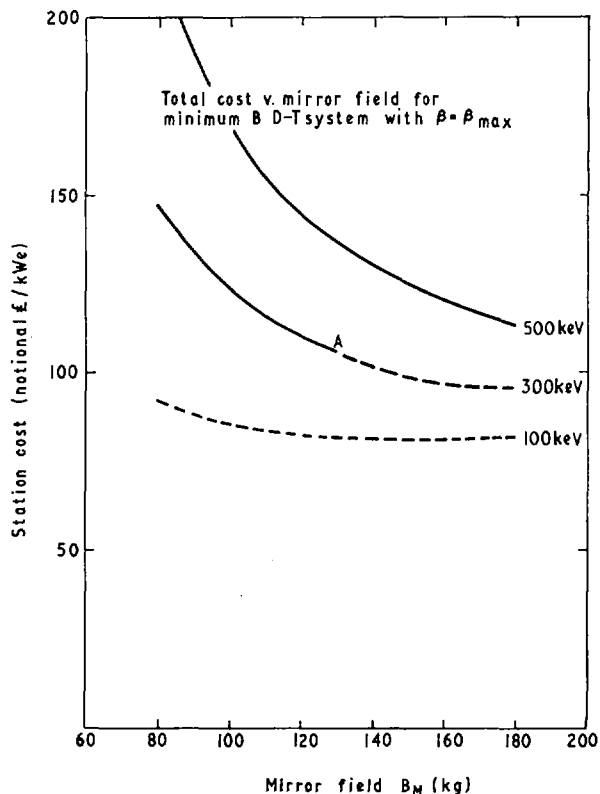


FIG. 3. Total station cost versus mirror field for minimum-B systems with $\beta = \beta_{max}$ for three injection energies. In the broken portion of the curves the reactor is wall-loading-limited.

strengths. The comparatively modest optimum mirror ratio R results from the fact that the favourable effects of high mirror ratios - the $\log R$ dependence of Q and β_{max} - are more than offset by the unfavourable effect - the $R^{8/3}$ scaling of the magnet cost, attributable to the β constraint.

By contrast with the insensitivity to the wall loading and magnetic field parameters, the cost C is sensitive to the values of ϵ_0 , β_{max} and Q_0 . To illustrate this, we show in Figures 4, 5 and 6 the dependence of C on ϵ_0 , β and Q_0 . Clearly it is important that the β values allowed by the theoretical limit (2) should actually be attained, and an improvement in Q_0 which might perhaps result from more accurate Fokker-Planck calculations would definitely be beneficial.

TABLE II. OPTIMIZED 1000-MW(e) REACTORS

	D-T (50 : 50)				D- ³ He (80 : 20)	
	Min-B			S. mirror	Min-B	S. mirror
	100	300	5500	300	500	500
Injection energy (keV)†						
Mirror field (kG)	160	180.	180	180	180	180
β (= β_{\max})	0.83	0.78	0.73	0.79	0.78	0.81
Wall loading (W/cm^2)	1500	1500	1500	1200	370	180
R (vacuum)	6.6	3.8	2.7	4.0	3.8	4.9
R (actual)	16.1	8.1	5.2	8.8	8.1	11.2
Central density ($10^{14} cm^{-3}$)	1.4	1.7	1.9	1.5	1.0	0.63
Central power density (W/cm^3)	16	16	15	13	1.7	0.66
Q_0	2	2	2	2	0.45	0.45
Q	2.41	1.82	1.43	1.88	0.41	0.47
Plasma radius (cm)	280	273	275	263	616	745
Wall radius (cm)	396	386	390	372	870	1050
Length (cm)	2250	2180	2200	1340	4930	3040
Straight section length (cm)				526	-	1490
Net output power (MW(e))	1000	1000	1000	1000	1000	1000
Injector power (MW(e))	970	1360	1870	1310	7470	5470
Direct converter power (MW(e))	1080	1420	1860	1380	8390	6410
Thermal plant power (MW(e))	880	940	1010	930	70	60
Total thermonuclear output (MW)	2100	2230	2400	2210	2750	2320
Total waste heat (MW)	1100	1230	1400	1210	1750	1320
Injector current (A)	8730	4080	3370	3930	13400	9700
Magnet cost (£/kWe out)	11	15	18	6.7	70	26
Blanket cost (£/kWe out)	14	13	14	8.5	61	45
Injector cost (£/kWe out)	10	14	19	13	75	55
Direct Converter cost (£/kWe out)	11	14	19	14	84	64
Thermal plant cost (£/kWe out)	26	27	29	27	2	1
Total cost (£/kWe out)	82	95	113	79	336	219

III. Comparison of Reactor Systems using External Recirculation

The numerical and analytic calculations of Section II were repeated for the D-He³ minimum-B reactor and then for the simple mirror for both D-T and D-He³ fuel cycles. In the absence of precise Fokker-Planck solutions for D-He³ cycles, we have assumed that Q still scales as log R, but with the constant Q_0 .

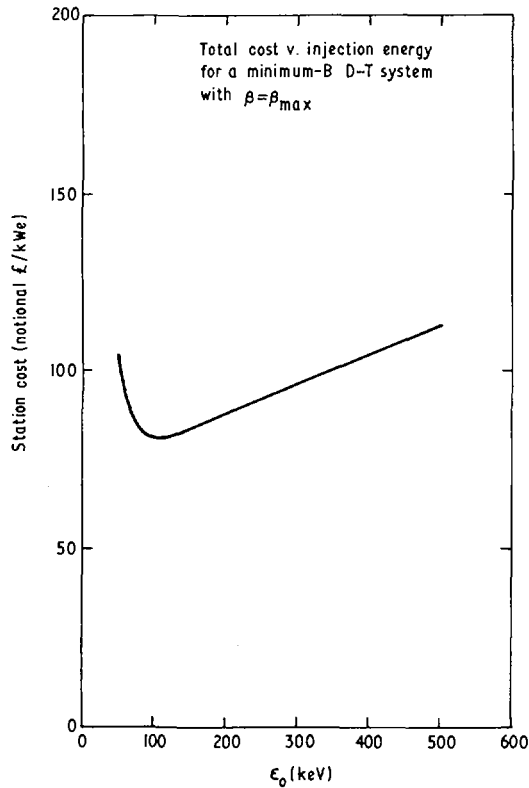


FIG. 4. Total station cost versus injection energy (ϵ_0) for a minimum-B D-T system with $\beta = \beta_{\max}$. Fokker-Planck calculations [2] suggest that the mean plasma energy is approximately equal to ϵ_0 .

in the range 0.2-0.5 and we have taken values for the average reaction rates $\langle \sigma v w \rangle$ from Post's tables⁽³⁾. Otherwise the optimisation proceeds as before, and the optimum parameters are presented in Table II. The optimisation of the simple mirror reactor proceeds in much the same manner as for the minimum-B system, but one has more freedom in the choice of magnetic field profiles; in particular one can have a section of uniform field in the centre. The length of this section was optimised taking into account the minimum length of the mirror sections necessary for adiabaticity of the reaction products.

The optimised costs of the four reactors are given in Table II. Although the simple mirror costs for both D-T and D-He³ are less than the corresponding minimum-B costs, the difference in total costs between the two field geometries is quite

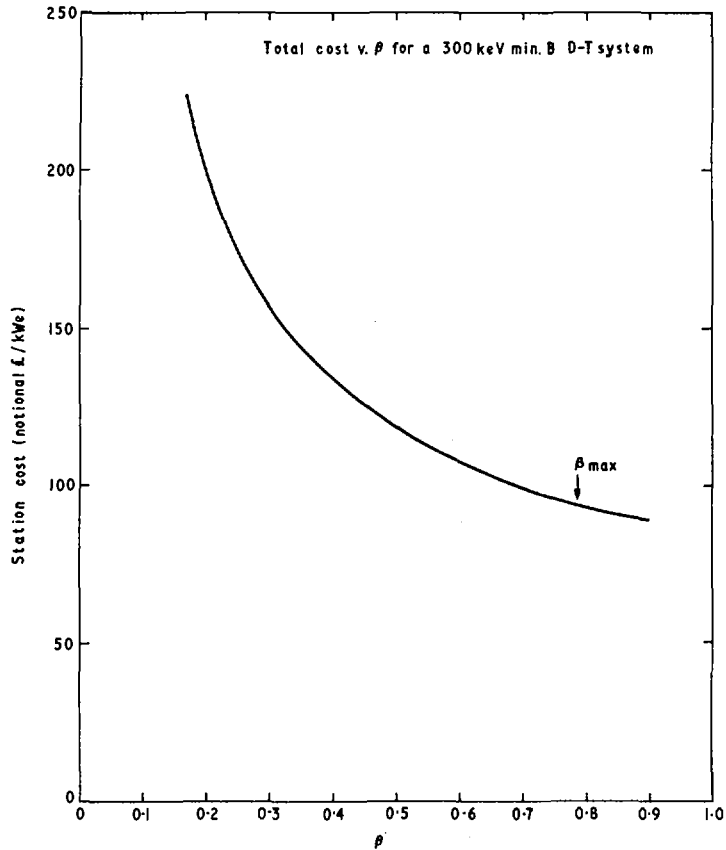


FIG. 5. Total station cost versus β for a 300-keV minimum-B system. The constraint imposed by β_{\max} for this case is indicated.

small. This is because, with the large recirculating powers required in all these reactor designs, the economics of the reactor are dominated by the cost of the direct converter and injector. The D-T fuel cycle is considerably cheaper than the D-He³ fuel cycle for both mirror geometries. However, the costs of both the D-T and D-He³ reactors are very sensitive to the value of Q_0 as is shown in Figures 6 and 7. Although the value of Q_0 for the D-T system has been moderately accurately determined⁽²⁾ the value of Q_0 for D-He³ is still uncertain, and as one can see from Figure 7 a small increase in Q_0 can lead to a considerable cost benefit.

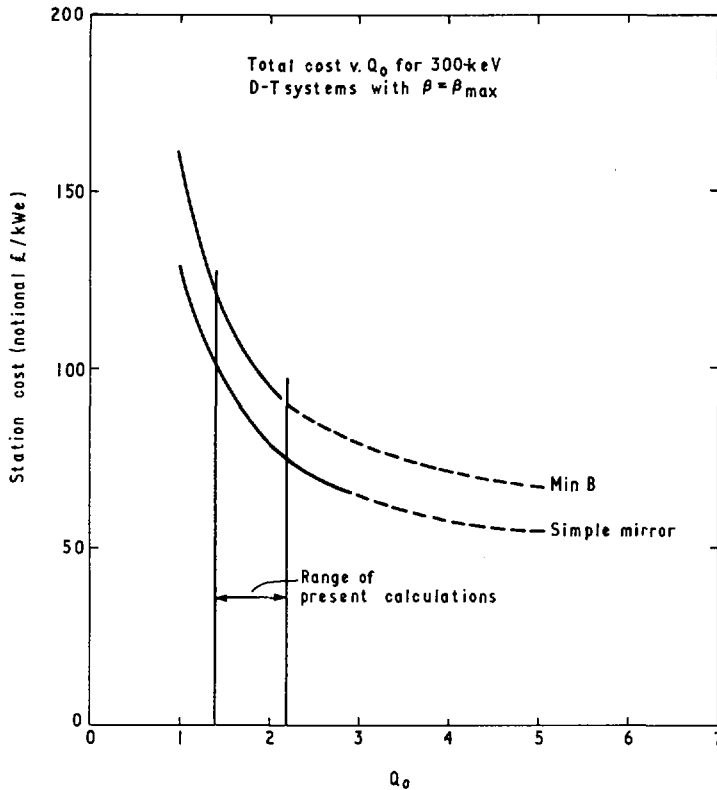


FIG. 6. Total station cost versus Q_0 for 300-keV D-T systems. The range of present calculations of Q_0 ($= Q/\log_{10}R$) is indicated.

A common feature of all these reactor systems is the uncomfortably large neutral atom injection current required - e.g. 9000 amp for case IA. Furthermore the optimum particle D-T energy (~ 100 keV) is substantially below the minimum energy at which any presently conceivable direct convertor could handle such currents. Admittedly, both of these problems can be eased by working at injection energies well in excess of the optimum but as Figure 4 shows this entails a considerable economic penalty. It follows that one should seek a system which achieves the effect of Post's scheme - the efficient reinjection of the escaping particles - without being subject to the same limitations. A possible solution to this problem is the 'auto-injection' mirror.

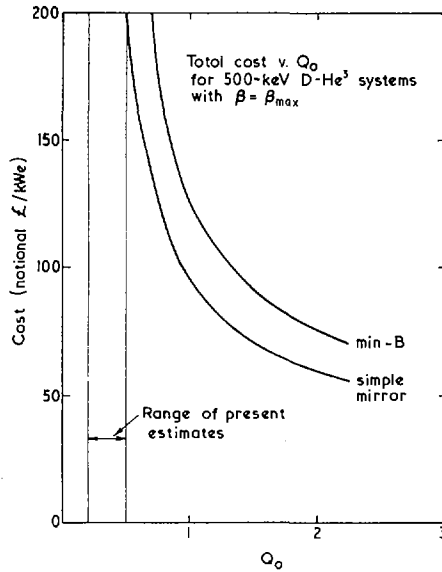


FIG. 7. Total station cost versus Q_0 for 500-keV D-³He systems. The range of present estimates for $Q_0 (= Q/\log_{10} R)$ is indicated.

IV. The Auto-Injection Mirror

In this scheme, ions emerging through the mirrors are neutralised and reinjected directly with high efficiency. The system is not subject to space charge limitations on escaping ions, so that a relatively low operating energy may be used. The system is capable of approaching the self-sustaining condition if fairly modest criteria on recirculation efficiency are met.

The scheme depends on the fact that the particles emerging through the mirror have their energy mostly in the perpendicular direction. As the magnetic field beyond the mirror falls, so some of this energy is converted to energy parallel to the field lines, but by arranging for the particles to adiabatically enter a second mirror with a field strength equal to that of the first, the energy may be converted back into perpendicular energy again. If this second mirror is made into a particle neutralisation region, neutral atoms emerge with a rather narrow angular spread on either side of the plane perpendicular to the magnetic field lines.

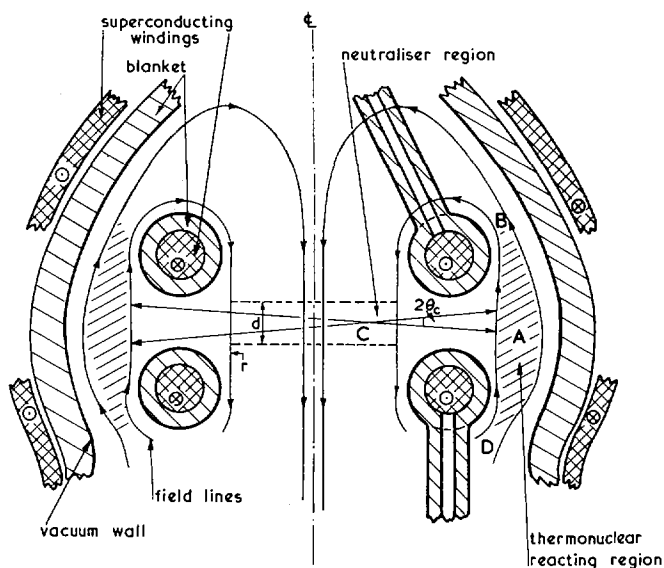


FIG. 8. Schematic diagram of an 'auto-injection mirror'. The annular thickness of the reactor plasma is somewhat exaggerated in this drawing.

In the present scheme these fast atoms are reinjected into the original reacting volume by arranging for the field lines to be re-entrant. Fig.8 shows a schematic arrangement to achieve this for simple mirror geometry. The system is essentially axisymmetric about the centre line and ions are confined and react in the annular region A. The top mirror (at B) of this reacting region is made slightly weaker than at the bottom (at D) so that essentially all the escaping ion flux emerges at the top. Those escaping through the mirror (at B) are conveyed to the region C where for each flux tube the field is arranged to be the same as at B. A high gas pressure is maintained in region C such that the probability of neutralisation is of order unity. Those particles that are neutralised emerge at a small angle to the normal to the field and are recaptured in the reacting region with high probability.

The magnetic field geometry required for the system may be generated by a system of windings similar to those shown in Fig.8. A particularly simple version which has very nearly the required field configuration is provided by a double Helmholtz

coil arrangement with opposing equal currents, the outer pair being at approximately twice the radius of the inner pair. Access to the top coil for supports, current leads, cooling etc. is made through the magnetic field as shown. Particle bombardment of the supports is avoided by arranging for the mirror magnetic field to be slightly non-uniform around the toroidal azimuth. The inner windings are surrounded by blanket sufficient to absorb neutrons.

A discussion of the physics of the auto-injection mirror is given in a separate publication⁽⁸⁾. The following principle conclusions may be drawn.

1. The angular spread about the perpendicular plane is small for ions escaping through the mirror of the reacting region⁽⁹⁾.
2. The angular spread of fast atoms emerging from the neutralisation region is small if the magnetic field and potential in regions B and C are matched to within 1%. The necessary magnetic matching can be achieved by using something like the Helmholtz coil configuration.
3. The efficiency of the neutraliser may exceed 90%. This is made possible by the fact that the path length of an ion in the neutraliser is much longer than the length of the neutraliser parallel to the magnetic field. However, the charge exchange and ionization cross sections are such that deuteron energies should be of the order of 100 keV or less.
4. It is necessary to ensure that gas from the neutraliser does not cause fast ion loss from the reacting volume by charge exchange. The hot plasma may, in fact, shield itself by forming a layer of relatively cold plasma. However, if necessary the gas flux back into the reactor can also be reduced by collimation of the injected gas or by an arc screen around the neutraliser.
5. Cold plasma will be formed in the neutraliser through ionization and charge exchange, and it will tend to stream along the field lines to the reacting plasma.

The interaction of this cold plasma with the reacting plasma and escaping hot particles is an important question needing further investigation. Certain undesirable conditions might occur.

- a) If the electron temperature became too large, runaway ionization in the neutraliser might result, though this should be inhibited by the consequent increase in the cold plasma loss rate.
 - b) The hot ions might lose energy to the cold plasma during the transit to the neutraliser; for the expected plasma densities this should be small.
 - c) Hot ions might undergo charge exchange on cold ions before reaching the neutraliser. This can be eliminated by using deuterium as the gas, which dissociates to D^+ , with no electrons.
 - d) Electron thermal conduction from the hot plasma to the cold plasma, might drain energy from the reacting plasma and heat the cold plasma. The evaluation of this effect requires a self-consistent Fokker-Planck calculation for the complete reactor system.
6. The presence of cold plasma may, in fact, have the advantage of permitting the stabilisation of the reacting plasma in a simple mirror by line tying or by feedback stabilisation with electrons. However, if the cold plasma does create major difficulties, it should be possible to remove it preferentially as it is created. One method is to produce a radial electric potential in the neutraliser, so that the $E \times B$ drift carries the plasma onto the supports for the upper magnetic coil.
7. The system could be made minimum-B by superposing an external multipole magnetic winding on the outside of the reacting volume and using favourable field curvature on the inside. It should alternatively be possible to construct an axisymmetric minimum-B system of the type described by Andreoletti⁽¹⁰⁾ and Furth⁽¹¹⁾.

The auto-injection mirror has significant advantages over other mirror systems. The effective Q of the system is given by $Q_{\text{eff}} = Q / \{1 - \eta(1 + \varepsilon Q)\}$, where η is the ion recirculation efficiency, and ε is the ratio of the thermonuclear output appearing in the ions emerging through the mirrors to total thermonuclear output. ε is determined by alpha heating and electron loss. Thus the Q value is substantially enhanced, and the reactor may even approach the self-sustaining condition before 100% particle recirculation is achieved. The externally injected power becomes correspondingly small. External injection can be accomplished either in a conventional manner, or (with very high efficiency) in the reactor neutraliser itself by injecting ions at the appropriate angle down the central flux tube. Because of the large recirculating currents, even small fractional losses may imply a considerable injection current. However, the injected power and cost will be very low, and because of the large Q_{eff} at the envisaged energy, there is less need to inject with very high efficiency. Also, there is less economic pressure to recover with high efficiency the charged particle energy escaping from the reactor (e.g. by direct conversion).

The main reactor parameters may be derived from the above conceptual model. The minimum size of the reactor is determined by the need for a neutron blanket around each of the inner windings, which must itself have a large enough winding radius to keep the self-magnetic field within acceptable bounds. Allowing a reasonable injection geometry, this leads to a reactor with an overall radius of order 10 metres. The energy of the reacting plasma is a compromise between a need for reasonable confinement time at high injection energy, and a good neutralisation efficiency at low injection energy: the optimum energy is approximately 100 keV. With the dimensions decided by the above considerations and a β rather arbitrarily chosen as 0.6 a typical design has a power output of 1000 MWe, a Q of ~ 1.5 and a recirculation current of order 10 kA. With a recirculation efficiency of 0.9 the effective Q is raised to greater than 10 and the required injection current is reduced to ~ 1000 amps.

V. Conclusions

Consideration of the above reactor model has shown that certain parameters which are otherwise only weakly restricted, such as the mirror ratio (R), are in fact strongly constrained by economic factors. For optimised systems the cost is always sensitive to the value of β_{\max} , and the system always operates at this value, whereas it is relatively insensitive to the assumed maximum wall loading and indeed is sometimes not wall loading limited.

The station cost is also relatively insensitive to the maximum mirror field B_m and indeed in some cases there is an optimum mirror field below the limit set by superconducting technology. Thus from this point of view the technological emphasis should be on developing cheaper windings for these fields rather than extending the working range above 200 kgauss.

The total cost is sensitive to the value of Q since increasing this decreases both the 'boiler' cost and the recirculating power. This is particularly so for D-He³ systems where only estimates of Q are available at present. Although these suggest that D-He³ systems are not economic compared with D-T systems Figures 6 and 7 show that this situation could be reversed by revised Q values. Simple mirror systems show substantially reduced boiler costs but still require expensive recirculation equipment.

For D-T systems the minimum cost occurs near 100 keV injection energy and because of the β constraint there is a substantial cost penalty in raising the working energy significantly.

The model assumes the existence of recovery systems whose cost depends only on the power handled. In practice external direct recovery schemes have space charge limitations on the current handling capacity which scale as $\epsilon_0^{3/2}$, i.e. a power handling capacity proportional to $\epsilon_0^{5/2}$, and thus need to work at 500 keV or above.

The auto-injection scheme discussed in this paper avoids these conflicting requirements by direct reinjection of the particles emerging through the mirrors. It thus works at an energy of 100 keV or lower where the β constraint is less

severe. There are many factors still to be evaluated in such a scheme (in particular the interaction of the neutraliser plasma with the main reactor plasma) but the prospect of an order of magnitude increase in the effective Q and the consequent reduction in the injected power make it worthy of further study.

REFERENCES

- [1] FOWLER, T.K. and RANKIN, M. Plasma Physics, (J. of Nucl. Energy Part C), 8, 121 (1966).
- [2] KUO-PETRAVIC, L.G., PETRAVIC, M. and WATSON, C.J.H., Paper 2.4 B.N.E.S. Nuclear Fusion Reactor Conference, Culham Laboratory, 1969.
- [3] POST, R.F. Paper 2.1 B.N.E.S. Nuclear Fusion Reactor Conference, Culham Laboratory 1969.
- [4] SWEETMAN, D.R. Paper 2.2 B.N.E.S. Nuclear Fusion Reactor Conference, Culham Laboratory 1969.
- [5] CORDEY, J.G. and WATSON, C.J.H. Paper 2.3 B.N.E.S. Nuclear Fusion Reactor Conference, Culham Laboratory 1969.
- [6] CORDEY, J.G. and WATSON, C.J.H. "Optimised Magnetic Field Profiles and a β -Limitation in Minimum-B Mirror Reactors" To be published.
- [7] SWEETMAN, D.R. To be published.
- [8] MARCUS, F.B., SWEETMAN, D.R., CORDEY, J.G. and CHUYANOV, V.A. Submitted for publication to Phys. Rev. Letters.
- [9] CORDEY, J.G. and WATSON, C.J.H. 'The Plasma Distribution Function near the Loss Cone of a Mirror Machine'. To be published.
- [10] ANDREOLETTI, J., C.R. Acad. Sci. (France) 257, 1235 (1962).
- [11] FURTH, H.P. Phys. Letters 11, 308 (1963).

DISCUSSION

R. F. POST: I should like to make a few comments concerning differences between our work and that reported here. The first point relates to the ion energies in the direct converter, which are actually higher than the usual mean contained ion energy by a factor depending on the plasma potential. While high energies are helpful, we do not believe that they have to be above 500 keV for economical operation. With proper design of the direct converter, we think substantially lower energies should be satisfactory.

My second comment concerns the Q values for D-³He. As stated in paper K-2, we consider a value of 0.4 possible, without enhancement, and we do not think it is necessary to achieve as much as a factor of 2 increase by enhancement in order to improve the D-³He economics by a major factor.

D. G. SAMARAS: I noticed that you had optimum plasma energies of about 100 keV. In similar calculations which we did more than 10 years ago, the optima that we got considering only bremsstrahlung and gyromagnetic radiation losses were similar to yours, but we later found that the Cherenkov radiation losses were very high so that the aforementioned optima had to be reduced. Some of these results were published in the Proceedings of the 16th International Astronautical Congress held in Athens in 1965. Did you consider Cherenkov radiation losses in your work?

D. R. SWEETMAN: No. We did not take account of radiation due to collective effects of the Cherenkov type or other collective effects such as radiation due to microinstabilities; the estimation of these effects would require a more detailed knowledge of non-linear behaviour in plasmas than we at present possess.

Synchrotron radiation was certainly estimated and it is not serious at the lower operating energies. It may well become serious at energies of 500 keV or more.

J. L. TUCK: For years I have felt, subjectively, that mirror machines are pretty hopeless as reactors, because their densities are so low and their mirror escape rates and ion temperatures so high. However, I am bound to acknowledge that Dr. Post's extremely ingenious idea of expanding the escape plasma isentropically, and directly converting, dispels many of the objections: in particular, the upper temperature of the Carnot cycle is the plasma temperature not the temperature of the boiler, as in some old-fashioned boiler-turbine combinations.

However, the point should be made that mirror-machine reactors can survive only by keeping a very low T_e in the presence of an enormous T_i (100 keV and more), a thermodynamic disequilibrium which is threatening in that a very small increase of electron-ion interaction rate will produce a lethal level of magnetic radiation. Even on Tokamaks, where T_e and T_i tend to be the same, the magnetic radiation is not trivial (M.N. Rosenbluth, Nucl. Fusion 10 (1970) 340). In conclusion, I think it is astonishing that 13 years after the Kondratsyev and Trubnikov calculation of magnetic radiation (Geneva 1958), this effect, which is destined to be of considerable importance, has still not been observed. Let us hope that by the next international conference, it will have been.

D. R. SWEETMAN: I am not sure that these comments require an answer. However, this is a quantitative matter, not an emotional one, and it should be pointed out that the drain of energy from the hot ions to the electron path is the problem that has been troubling us for a number of years (since the Fowler-Rankin calculations were published), and this is precisely the reason why the Q is reduced from approximately 10 to approximately unity.

Synchrotron radiation has been observed in a number of experiments and in our own PHOENIX II experiments it was used to measure the electron temperature.

H. LASHINSKY: The auto-injection mirror system described here appears to consist of a number of elements whose behaviour depends on geometric and physical factors that are functions of energy, density, etc.

Is it clear a priori that the overall system would be stable in the parameter range of interest?

D. R. SWEETMAN: The overall system stability has been looked into and the system appears to be stable; at operating energies of about 100 keV, if the heating from the reaction products increases the temperature, the neutralization efficiency rapidly drops and reduces the recirculating current.

ECONOMIC FEASIBILITY OF STELLARATOR AND TOKAMAK FUSION REACTORS

A. GIBSON, R. HANCOX, R.J. BICKERTON
UKAEA, Culham Laboratory,
Abingdon, Berks,
United Kingdom

Abstract

ECONOMIC FEASIBILITY OF STELLARATOR AND TOKAMAK FUSION REACTORS.

Studies of model designs of stellarator-type fusion reactors are presented. These serve to high-light key technological and plasma-physics problems which require solution. The basic conflict is between estimates of the critical β for equilibrium and stability and the cost of high magnetic fields from superconducting multipolar coils. The effect of diffusion-driven currents on the critical β and the effect of electric fields on estimates of the cross-field diffusion rate are considered.

The inclusion of a 1.5-m blanket in a system with a short-range multipolar field makes it difficult to achieve economic operation in small sizes. However, the unit cost for this type of reactor falls rapidly with increasing size. Thus if present estimates for the critical β can be realized and if low-cost superconductors can be developed, we expect a 10 000-MW(e) stellarator reactor to meet target economic costs which include a penalty for the large size.

1. Introduction

We have previously[1] considered the parameter ranges for which stellarator and tokamak reactors are likely to prove economic. In that paper we tried to avoid making detailed cost estimates by requiring, as an economic criterion, that the fusion reactor have a similar overall power density to competing systems, particularly the fast breeder reactor. This approach showed the necessity of achieving large (approaching 10%) β values for economic operation. Taking the equilibrium estimate of β as the critical value showed that economic stellarators tend to have large R/a (ratio of major to minor plasma radius) and hence large output. Tokamaks on the other hand tend to require small values of (R/a) . In this paper we try to estimate directly the costs of the main reactor components and so arrive at a cost/unit output. Again the permissible β plays a crucial role in determining the cost and we now take into account the modification of the critical β due to diffusion driven currents[2]. The size of a future fusion reactor is not likely to be a free parameter, rather it will have to be small enough to integrate into a national or regional network. Consequently cost estimates in this paper are evaluated for a reference size of 2500MW(e) or 5830MW(th) which is expected to be about 1% of the U.K. grid size at the end of the century. Cost savings from increasing this size for stellarators are examined separately.

The stellarator mainly considered in this paper is an $\ell=3$ system with a 45° winding leading to a highly sheared field. Torsatron systems, which may have advantages for diverter design, and $\ell=2$ systems, which may be more economic if less shear is necessary, are also considered.

2. The effect of diffusion driven currents on the critical β

The diffusion driven current density in the low collision rate limit is given by [2]:

$$j = - \frac{\alpha \epsilon^{\frac{1}{2}}}{B_\theta} \frac{dp}{dr} \quad (2.1)$$

where $\epsilon \approx \frac{a}{R}$

B_θ = effective poloidal magnetic field

p = Plasma pressure.

The constant α is of order one and various estimates are available. Galeev [3] gives $\alpha = 0.9$, Taylor [4] gives $\alpha = 1.6$ and Hinton [5] gives $\alpha = 2.44$.

The relation (2.1) is strictly valid only for axisymmetric systems, however it can be argued [2] that a similar current will arise in stellarators and we shall assume the same relation to apply. Then for both stellarators and tokamaks

$$B_\theta = B_0 \epsilon (t_\delta + t_\sigma) \quad (2.2)$$

where B_0 is the toroidal field on axis.

t_σ is the rotational transform due to the diffusion driven current (units of 2π)

t_δ is the rotational transform produced by external means (helical windings, injection or induction).

For the simple case of $j(r)$ constant and a linear pressure gradient (2.1) can be written approximately as:

$$\beta = 2\epsilon^{\frac{3}{2}} t_\sigma (t_\sigma + t_\delta) / \alpha \quad (2.3)$$

where β is the ratio of the maximum plasma pressure to the toroidal magnetic field on axis. If we had alternatively assumed that $\frac{dp}{dr}$ and j were restricted to a thin outer skin the same result would have been obtained. A limit to β can now be obtained from (2.3) by requiring that the diffusion driven current satisfy the Kruskal-Sharfranov condition for kink stability.

Consider first the tokamak case where the diffusion driven current permits a continuously operating tokamak [2], in this case $t_\sigma \gg t_\delta$ so that

$$\beta = 2\epsilon^{\frac{3}{2}} t_\sigma^2 / \alpha$$

TOKAMAK

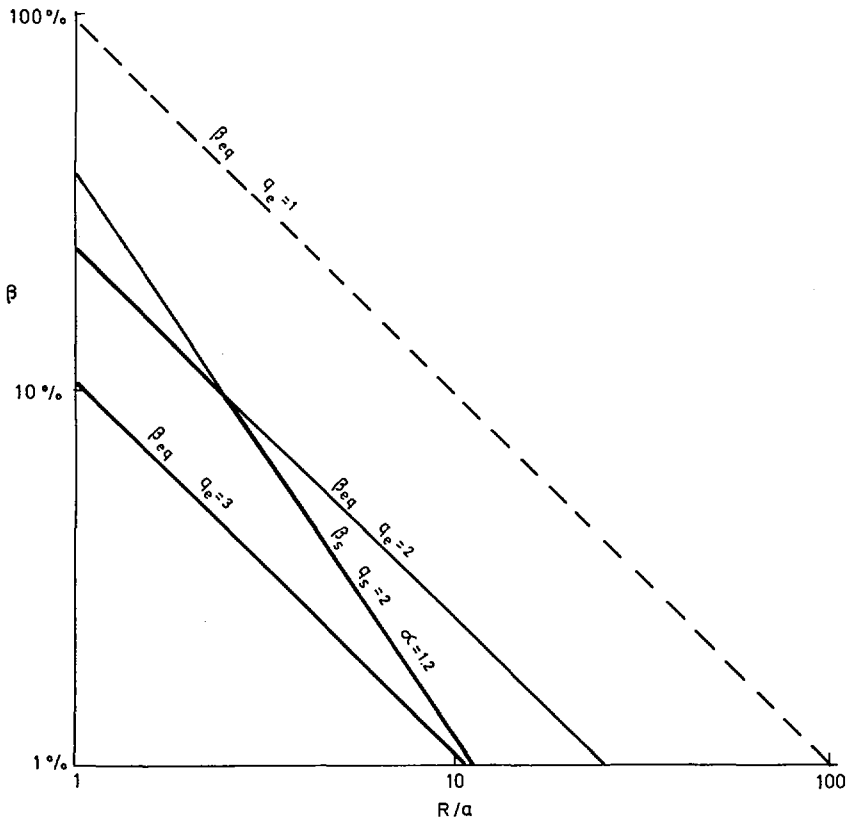


FIG. 1. Limits to the possible β in a steady-state tokamak system. The equilibrium estimates (β_{eq}) for various values of q_e are shown together with the limits (β_s) imposed, for a particular value of $\alpha (=1.2)$, by the requirement for kink stability of the diffusion driven current. To be acceptable, β must be less than both the appropriate β_{eq} and β_s .

The Kruskal-Shafranov condition is just $t_\sigma < 1$ everywhere, or in terms of a "safety factor" $q_s = t_\sigma^{-1}$ defined at the plasma edge, the stability limit to β is:

$$\beta_s = 2\epsilon^{3/2} / \alpha q_s^2 \quad (q_s > 1) \quad (2.4)$$

For bell shaped current distributions it is usually necessary to have $q_s > 3$, but the diffusion driven current will tend to occur in regions of steepest pressure gradient towards the outside, consequently smaller values of q_s will be possible.

STELLARATOR

$$\frac{\beta_s}{\alpha} = 1.2$$

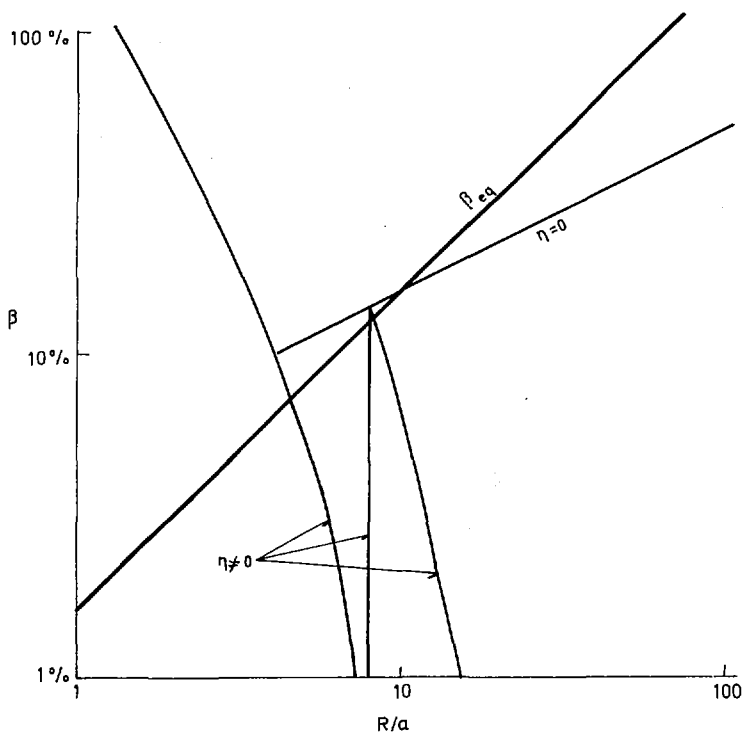


FIG. 2. Limits to the possible β in an $l=3$ -stellarator with a 45° pitch angle winding at twice the separatrix radius. The equilibrium value is shown together with stability limits imposed by the diffusion driven currents for a particular value of $\alpha (=1.2)$ and for both zero and finite resistivity.

The value of β given by (2.4) is compared, in Fig. 1., with the value allowed for equilibrium and gross stability taken [1] as:

$$\beta_\theta = R/a \quad (2.5)$$

where $\beta_\theta = 8\pi p/B_\theta^2$

and $\beta = \epsilon^2 t^2 \beta_\theta \quad (2.6)$

so that $\beta_{eq} = \epsilon/q_e^2 \quad (q_e > 1) \quad (2.7)$

We see from Fig. 1 that if α is about 1 and β_{eq} has the value corresponding to $q_e=3$ then the critical β is determined by β_{eq} . If smaller values of q_e are permitted then the diffusion driven current will limit the critical β . If α

is as large as 2.44 β_{crit} will be somewhat less than β_{eq} when $R_A > 3$ even for $q_e = 3$.

In the case of an $\ell=3$ stellarator with a superimposed uniform current distribution the stability has been examined by the Princeton group [6], results are presented in terms of t_σ and t_δ (helical transform at plasma surface). If finite resistance modes occur the conditions for stability are:

$$\begin{aligned} t_\delta + t_\sigma &\leq 1 && \text{for } t_\delta \leq 1 \\ t_\delta + t_\sigma &\leq 2 && \text{for } 1 < t_\delta \leq 2 \text{ etc.} \end{aligned}$$

If these modes are not important the system is also stable when $t_\delta > t_\sigma$

The results obtained by substituting these relations into (2.3) are displayed in Fig.2 for an $\ell=3$ stellarator having a 45° winding and assuming the winding radius to be twice the separatrix radius so that:

$$t_\delta = 3t_k/2\epsilon \quad (2.8)$$

where t_k is the transform/field period at the separatrix, taken [7] to be $1/12$. The equilibrium estimate in the absence of the diffusion driven current is also shown, from (2.5), (2.6) and (2.8) it is:

$$\beta_{eq} = [64\epsilon]^{-1}$$

We see from Fig. 2 that if α is less than about 1.2 and resistive modes are unimportant, $\beta_{crit} = \beta_{eq}$ for $R_A \leq 10$; if they are important β_{eq} is still possible for $R_A \leq 8$. If α is as large as 2.44 β_{crit} will be reduced from β_{eq} for $R_A > 3$. Stellarator reactors with $R_A > 8$ tend to have unacceptably large output. Thus provided α is not much bigger than 1.2 diffusion driven currents do not impose any further restrictions on β_{crit} than those already imposed by considerations of equilibrium and maximum acceptable output.

3. Cost Criterion

To assess whether or not a reactor is economic we take the criterion suggested by Searby and Brookes [7], of £20-25/kW(e) for the nuclear boiler component of an end of the century fusion power station. The total station cost will be of order £60/kW(e). These criteria were developed by comparison with the extrapolated cost for end of the century fission reactor systems in the context of the U.K. electrical network. Allowance was made for the cheaper fuel costs expected for a fusion reactor.

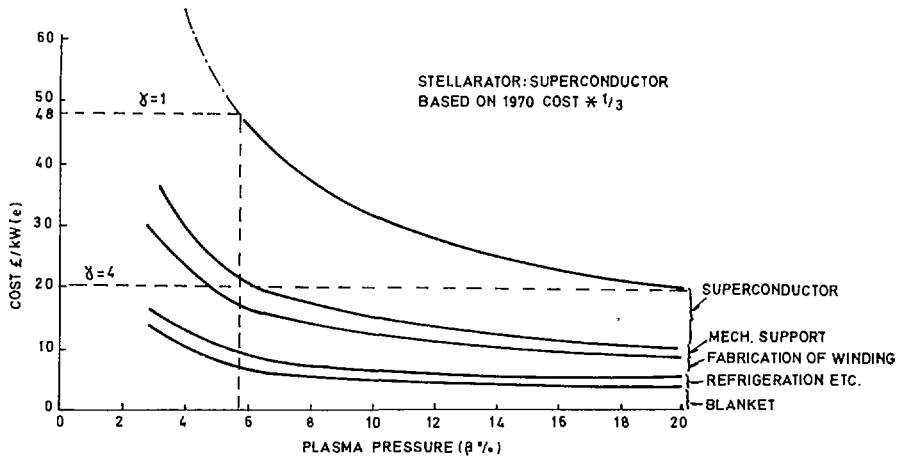


FIG. 3. Optimized cost per unit output for stellarator reactors based on superconductor cost of 10^{-2} £/kA.kG.m (i.e. $\frac{1}{3}$ 1970 costs). The maximum field is limited to 200kG on the chain dotted part of the curve and elsewhere is smaller.

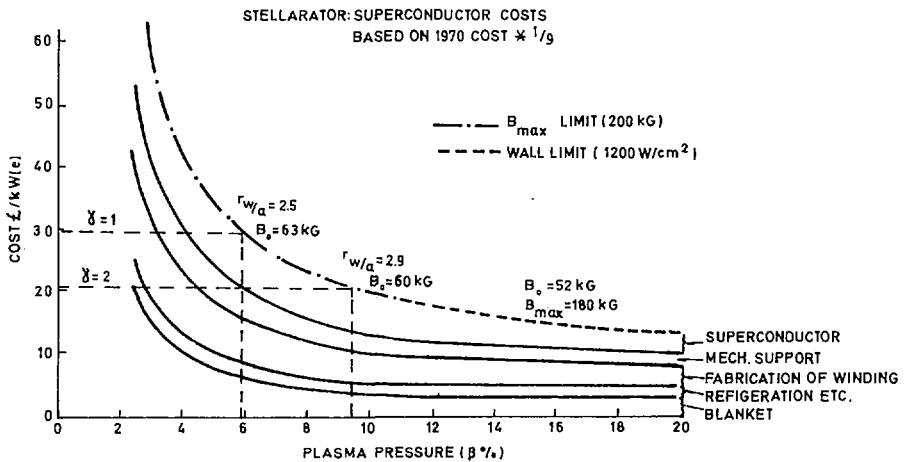


FIG. 4. Optimized cost per unit output for a stellarator reactor based on superconductor costs of 3.3×10^{-3} £/kA.kG.m (i.e. $\frac{1}{9}$ 1970 costs). As in Fig. 3, the $\ell=3$ stellarator has a 45° pitch angle and $\tau_{max} = \frac{1}{12}$. The plasma aspect ratio is 6, blanket thickness is 1.5 m, winding current density is $2000\text{A}/\text{cm}^2$ and the total output is $2500\text{MW}(e)$. The ratio (r_w/a) of winding to plasma radius is marked.

4. Method of Estimating Costs

The costs of the main reactor components are assumed as follows. The superconductor costs are extrapolated as a fraction times the 1970 N_p/T_i costs expressed as £/kA.kG.m Furthermore it is assumed that new superconductors will be developed to operate at fields approaching 200kG, at this same

reduced cost. Quoted prices for N_b/T_i multifilament superconductor in 1970 ranged from (2 to 4) $\times 10^{-2}$ £/kA.kG.m, accordingly we shall take 3×10^{-2} £/kA.kG.m as the 1970 price. Fig. 3 shows that costs of one-third this 1970 cost lead to unacceptably high £/kW(e) for stellarators and that the superconductor component of the cost is dominant. In all subsequent calculations it is assumed that by the end of the century the cost of superconductors can be reduced to one-ninth of the 1970 values. Fig. 4 shows that in this case the superconductor cost is comparable to other costs so that further cost reductions will not lead to dramatic savings. The cost of fabricating the winding is taken to be £10/litre of winding, based on winding costs for power transformers [8]. The cost of mechanical support, for the winding is taken to be $5 \times 10^{-8} B_{\max}^2 r_w$ £/cm², based upon Rose's [9] estimate using titanium, r_w is the winding minor radius in cms and B_{\max} is the maximum field anywhere in the system in kG. The blanket cost is taken to be 1.7 £/cm² based on a lithium breeding blanket with lead and borated water shielding, any dependence on wall loading is ignored. Finally insulation and refrigeration costs, which are small, are represented by $(£0.2 + £10^{-4} P_{\text{wall}})$ /cm² of winding surface, P_{wall} is the power loading, watts/cm² on the first wall.

Initially the plasma density is supposed uniform over a radius of 0.8 of the first wall radius, and rotational transform at the plasma radius in an $\ell=3$ system is taken to be $t_k = 1/2$ /field period [10]. These assumptions will be compared to the result of diffusion and configuration computations in later sections. Unless otherwise stated the acceptable power output is set to 2500MW(e). With these parameters there is an optimum in the cost near $R_a=6$ and this value is used in all the calculations(1). The current required in the helical winding is related to the field and dimensions by approximate expressions fitted to the results of filamentary conductor computations [10].

The cost of the reactor can now be calculated for given B_{\max} and P_{wall} . The blanket thickness is taken to be 1.5m, to permit tritium breeding and shielding; the current density in the winding is set at 2kA/cm², to allow sufficient copper winding protection. The wall radius is then determined from the wall loading and power output, thus the winding position is fixed and the winding current can be calculated. The various winding and blanket costs can then be evaluated. The procedure is repeated for various values of B_{\max} and P_{wall} . Each calculation leads to a cost and a β value at an assumed operating temperature of 20 keV. Further details of these cost estimates are to be published [11].

-
- (1) At large total power output the optimum occurs at larger R_a [=8 for 10,000MW(e)] but the reduction in cost from $R_a=6$ is insignificant.

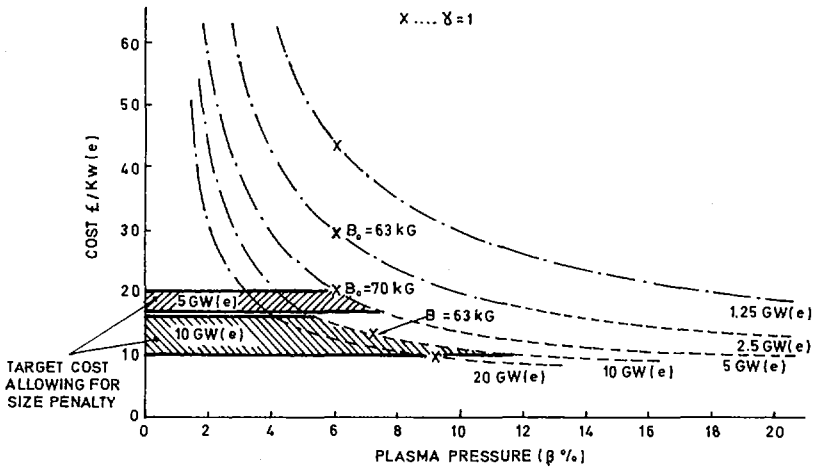


FIG. 5. The effect of increasing total output on the unit cost of a stellarator reactor. The crosses mark the points where $\gamma = 1$ and the chained and dashed parts of the curves have the same meaning as in Fig. 4. The target cost range shown for 5 GW(e) and 10 GW(e) reactor size includes a penalty for the use of large units.

5. Cost Estimates for Stellarators

Figs. 3 to 6 show the minimum cost for each β plotted against β . The minimum is chosen subject to the constraints $B_{\max} < 200\text{kG}$ and $P_{\text{wall}} < 1200\text{W/cm}^2$, if the constraints limit the cost this is indicated on the graphs. Values of γ , the ratio of β to β_{eq} defined in §2, are also indicated.

Fig. 4 shows that with the "one-ninth" superconductor cost a high shear $\ell=3$ stellarator with $\gamma=1$ has a cost of $\text{£}30/\text{kW(e)}$, just outside the allowable range. A γ value of 2 is necessary to reduce the cost to $\sim\text{£}20/\text{kW(e)}$. Fig. 3 shows that with the "one-third" superconductor cost $\text{£}20/\text{kW(e)}$ cannot be attained unless ways can be found to increase γ to 4 (corresponding to $\beta = 20\%$). Fig. 5 shows the effect on unit costs of changing the reactor output. Cost penalties have been evaluated for introducing larger reactors into the end of the century U.K. grid. These are shown as reduced target costs for larger sizes. It will be seen that for 10,000 MW(e) output, a high shear stellarator with $\gamma=1$ falls well within the target cost range. The minimum cost for the β value of 8% corresponding to $\gamma=1$ for the 10,000 MW(e) case (see Table I) occurs for a maximum field at the winding of 150 kG. The lowest costs, for given β value, in the 2500 MW(e) case are obtained when B_{\max} reaches its limit of 200 kG. However, the cost is not appreciably changed at lower values of B_{\max} , down to 150 kG, in fact for a fixed value of $\gamma=1$ the minimum cost occurs at $B_{\max}=180$ kG and is $\text{£}29/\text{kW(e)}$.

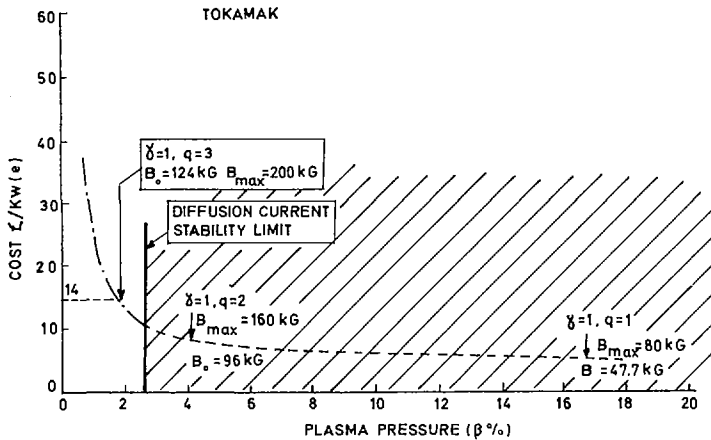


FIG. 6. Optimized unit costs for a tokamak reactor.

The field produced by the helical winding of a stellarator is essentially short range, consequently worthwhile savings in unit cost occur if the blanket thickness can be reduced. Such a reduction may be possible if breeding can be restricted to the regions between the windings so that, in front of the windings, only a shielding blanket is necessary. This solution may be particularly attractive for a Torsatron [12] which, having the same helical winding cross section, has only half the number of conductors as a stellarator. The unit cost for the $\ell=3$ stellarator we have considered for $\gamma=1$ is reduced to $\sim\pounds 24/\text{kW}(e)$ for a blanket thickness of 125 cms and to $\sim\pounds 20/\text{kW}(e)$ for a thickness of 100 cms.

6. Comparison with Tokamak

Fig. 6 shows the cost estimates for a tokamak, regarded for comparison as a stellarator with no helical winding. The unit cost at $\gamma=1, q=3$ is seen to be $\pounds 14/\text{kW}(e)$, substantially less than for a stellarator. The dimensions and costs of the two systems are compared in Table I. The diffusion driven current may make possible a steady state tokamak in which case no cost penalty for pulsed operation will be necessary. However, the separatrix of a stellarator provides a built-in magnetic diverter which is not present in a tokamak. A diverter will be necessary for a steady state tokamak reactor and will increase the cost by increasing the volume and complexity of the magnetic field.

7. Comparison with Computed Configuration

The optimisation procedure described above uses approximate expressions for the rotational transform produced by the winding and neglects the trefoil shape of the separatrix.

TABLE I. DIMENSIONS AND COSTS OF TOKAMAK AND STELLARATOR

Tokamak ($q=3$)	$\ell=3$ Stellarator 45° winding			
γ	1.0	1.0	2.0	1.0
Total Power Output MW(e)	2500	2500	2500	10 000
β	2%	6%	9%	8%
Plasma Radius (m)	1.6	1.81	1.4	2.8
Mean helical Winding Radius (m)	-	4.51	4.0	6.1
Helical Winding Current (M.A)	-	44	43	45
Major Radius (m)	7.5	10.9	8.4	16.8
Ratio of Lawson†time to Bohm time ††	210	390	400	182
Maximum Field (kG)	200	200	200	150
Confining field on axis	126	63.3	60	55
Total Power Flux at first wall W cm ⁻²	800	600	1000	1000
Cost Estimate £/kW(e)	14	30	20	13

† The Lawson time t_L is taken to be the containment time necessary for a charged particle heated self sustaining reactor, see for example reference[8].

†† The Bohm time t_B is taken to be $t_B = \frac{16eB}{ckT} \left(\frac{a}{2.4}\right)^2$ in cgs units, the symbols having their usual meaning.

Fig. 7 shows a configuration with similar parameters to the $\gamma=2$ optimised stellarator of Table I. This configuration is obtained from computations using filamentary conductors. The greatest difficulty in accommodating the blanket arises in the planes where an apex of the trefoil points inwards towards the major axis, such a plane is shown in the diagram.

First notice that because of the very tight winding aspect ratio ($R_{\text{winding}} = 2.1$) toroidal effects have reduced the maximum transform to $t \sim 1/18$ instead of $1/12$ assumed in the optimisation, this means that the γ values in the optimisation are underestimated by about a factor 2. Next notice that everywhere except on the inside horizontal plane a 1.5m blanket can be accommodated with $2kA/cm^2$ windings and a maximum field of $3B_0$ (the shape of the winding cross section will have to be suitably chosen). On the inside equatorial plane the blanket thickness in front of the winding will have to be locally

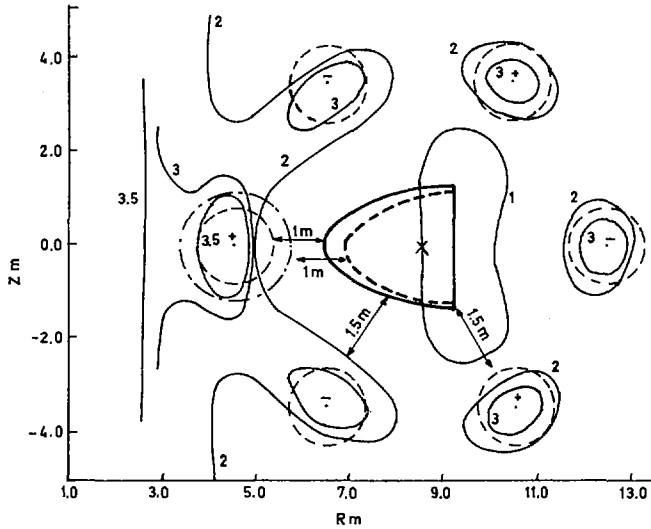


FIG. 7. The magnetic configuration of the $\gamma=2$ - stellarator of Table I. The diagram is obtained from filamentary conductor computations and is plotted in a meridional plane, the intersections of the filamentary helical winding with this plane are marked. The thin lines are contours of $|B|$ marked in units of B_0 , the field on axis. The thick curve is the magnetic separatrix and the dashed curve the separatrix when a transverse field equal to $0.005B_0$ is applied, in both cases the transform is about 20° /field period. The dashed circles represent the area of a 2 kA/cm^2 winding and the chain-dot circle of a 1 kA/cm^2 winding. The parameters are $R=8.5 \text{ m}$, $r_{\text{winding}}=4 \text{ m}$, number of field periods = 6, helical winding current = 43 MA , $B_0=60 \text{ kG}$.

reduced to 1.0 m which should be sufficient for shielding. In these circumstances a winding of about 2 kA/cm^2 can be accommodated, but with a maximum field of $3.5B_0$ and hence a further slight increase (13%) in γ over the value in Table I. The ratio of separatrix to winding volume is then 0.09 instead of 0.125 in Table I, this again will lead to an increase (18%) in γ . Introducing a transverse $B_v=0.005B_0$ moves the separatrix away from the winding so that B_0 can be increased for the same B_{max} , but this is largely compensated by a reduction in the separatrix volume.

These difficulties are reduced at larger winding aspect ratios. Thus the $\gamma=1$ case in Table I ($R/r_{\text{winding}} = 2.4$) is less affected and we find that the $10,000 \text{ MW(e)}$, $\gamma=1$ case, which has $R/r_{\text{winding}} = 2.7$ requires an increase of γ of only 40% to compensate for the small reduction in transform and volume from the approximate values used in the cost calculation. In this case it is again necessary to have a blanket thickness of 1.0 m in front of the winding where it crosses the equatorial plane at small R .

8. Other Configurations

We have applied the procedure of § 5 to $\ell=3$ torsatron systems and to $\ell=2$ stellarators. Torsatrons in which the helical winding is arranged to produce both the helical and toroidal field are especially interesting because they may lead to a simple diverter design.

The unidirectional current in the torsatron helical winding has to be approximately equal to the sum of the "go" and "return" currents in an equivalent stellarator, consequently the two systems should have similar costs. However, because there is no separately variable toroidal field the torsatron is less flexible, in particular the ratio of separatrix to winding radius tends to be undesirably large. This means that in order to accommodate a blanket with a fixed power output the wall loading is reduced. Consequently for a given γ value torsatron reactors tend to be somewhat more expensive than stellarators (by about 30%).

The greater efficiency of $\ell=2$ stellarator windings is offset by the greater distortion of the magnetic surfaces. The elliptic surfaces of the $\ell=2$ system fit less efficiently into a toroidal blanket structure than do the trefoil shaped $\ell=3$ surfaces. Consequently at β values around 6%, corresponding to $\gamma=1$, the wall loading in the $\ell=2$ system is reduced from that in $\ell=3$ and the $\ell=2$ system, despite its more efficient winding, is more expensive (by about 17%). At larger γ values where according to Fig. 4 the $\ell=3$ stellarator is wall loading limited, the $\ell=2$ system becomes slightly cheaper, the two systems have the same unit cost when $\gamma=2$.

9. Diffusion Estimates of Containment time

The diffusion loss of plasma from a stellarator has been considered by Gibson and Mason [13]. The main result is that there is a large enhancement of the diffusion in the outer regions due to the trapping (localisation) of particles in the helical field. The treatment is incomplete in a number of respects, first the effect of radial electric fields is not included and as we shall see this probably leads to an over estimate of the loss. Secondly the equilibrium and diffusion processes are not treated self-consistently. Finally, thermal conduction is considered not to increase the loss above that attributable to the slowest diffusing species (T independent of r). This is in accord with the assumed boundary condition, that near the separatrix ions and electrons drift out freely with the toroidal drift velocity. However, this model leads to ions and electrons leaving at opposite ends of the minor plasma diameter, the effect of electric fields arising from this process has not been considered.

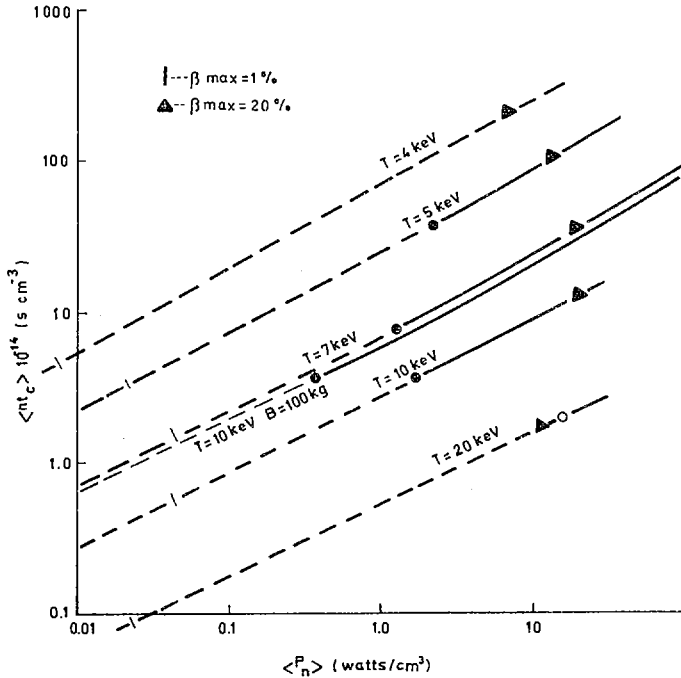


FIG. 8. The value of the density-containment time product averaged over the plasma $\langle nt_c \rangle$ versus the average thermonuclear power generated in the plasma. The model for the loss processes is that described by Gibson and Mason [13]. The curves change from dashed to solid when the requirements for a self-sustaining, charged-particle heated plasma [8] are met. The points at which the maximum β reaches 1% and 20% are marked. Curves are shown for various temperatures and $B_0=60$ kG, one curve for $B_0=100$ kG is shown for comparison. Other parameters are $R=8.5$ m, separatrix radius = 1.4 m (assumed circular), 6 field periods and $\tau_{\max} = 1/12$.

If, despite these uncertainties, we accept the treatment as it stands, we see from Fig.8 that for an operating temperature of 20keV and $B_0=60$ kG a self sustaining reactor corresponding to the $\gamma=2$ case of Table I is barely possible. The position can be improved by reducing the operating temperature (i.e. going to more collisional conditions) to reduce the effect of localised particles. From Fig.8 the optimum in this process occurs at about 7 keV. At this temperature $\beta_{\max}=20\%$ gives a margin in $\langle nt_c \rangle$ over the self sustaining condition of a factor of 5. The power density in the plasma of the $\gamma=2$ reactor in Table I is about 16w/cc and this corresponds to $\beta \sim 9\%$, for an assumed square density profile. We see from Fig.8 that with the diffusion controlled profile $\beta_{\max} \sim 18\%$ is necessary to achieve this power density, even at the optimum operating temperature. This effect increases the required γ value by a factor 2. Similar calculations for the 10,000MW(e) case show that at a temperature of 7keV the margin in $\langle nt_c \rangle$ over the self sustaining condition is increased to a factor 20 but the departure of the diffusion controlled profile from a square profile again increases the required γ by a factor 2 (to $\gamma=2$). This increase would be smaller for a larger confining field.

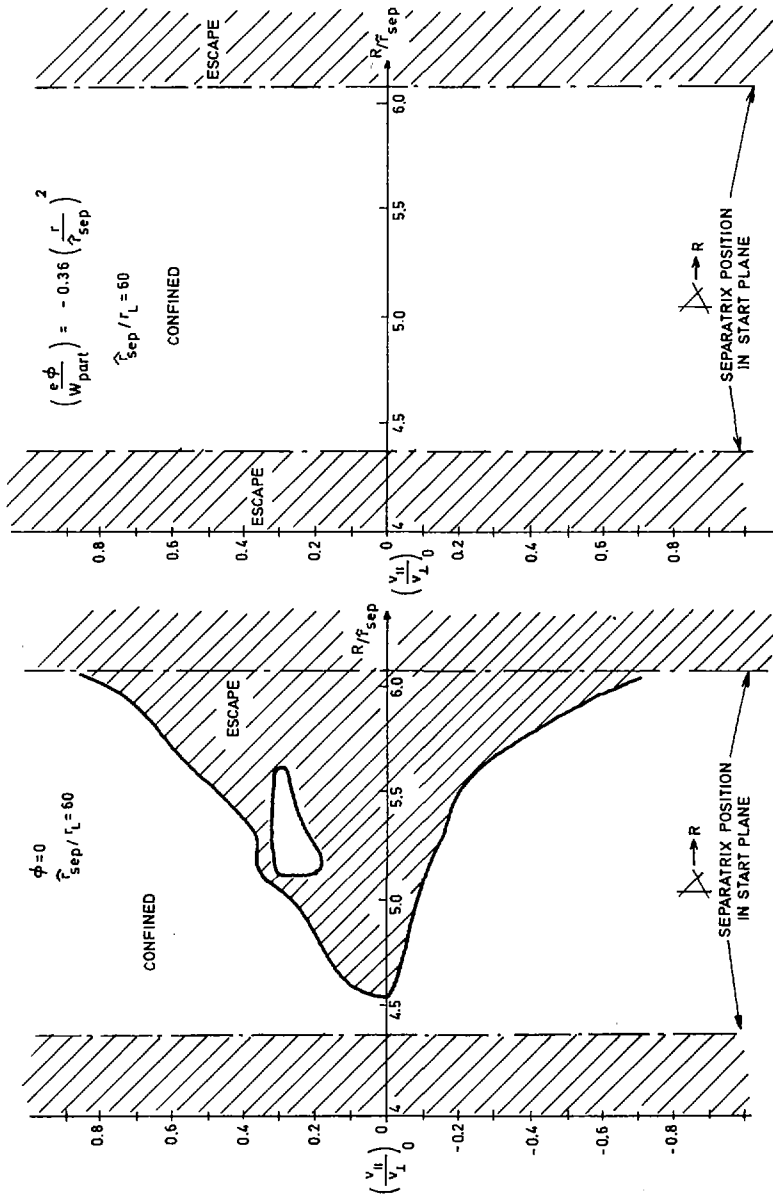


FIG. 9. The effect of a radial electric field on the confinement of particles in a stellarator. W_{part} is the particle energy, f_{sep} the maximum separatrix radius, r_L the Larmor radius and $(v_{||}/v_{\perp})_0$ the initial ratio of velocity parallel and perpendicular to \mathbf{E} . The particles originate on the intersection of an equatorial plane and a meridional plane in which the trefoil apex points outwards.

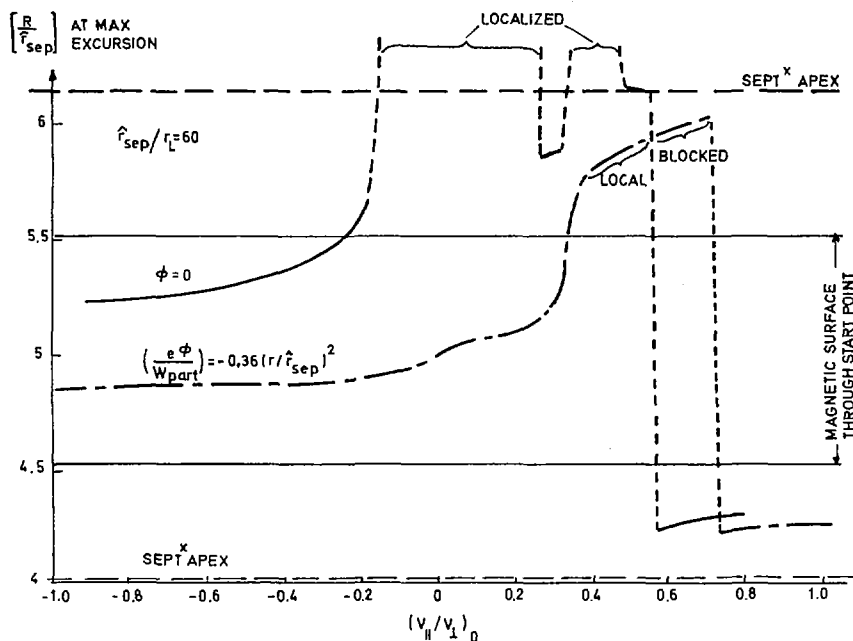


FIG. 10. The major radius of maximum excursion of particles from their initial magnetic surface. The particles all originate at the same point $(R/r_{sep}) = 5.5$ of Fig. 9, but with various $(V_H/V_L)_0$.

10. Effect of a Radial Electric Field

Plasma confined in a stellarator often shows a potential difference (ϕ), between the axis and the plasma boundary, of order $\phi = kT/e$. The corresponding radial electric field may be expected to lead to confinement of localised particles. Fig. 9 shows the result of guiding centre computations for a stellarator type field generated by a single toroidal harmonic, and having a similar topology to an $\ell=3$, 45° pitch angle stellarator. With no applied radial potential (Fig. 9a) particles in the large part of phase space shown escape beyond the separatrix, most of these are localised particles. The addition of a radial potential (Fig. 9b) leads to confinement of essentially all the particles whose start points are within the separatrix. Some of the initially localised particles are confined because the electric field converts their orbits into passing or blocked orbits [14], these orbits should have excursions, from their magnetic surface, determined by the poloidal Larmor radius. Other particles remain localised but acquire a rotational drift which keeps the orbit within the separatrix, the excursion of these particles will not depend on the Larmor radius but only on the magnitude of $(\frac{e\phi}{kT})$.

Fig. 10 shows the maximum excursion of particles originating on the equatorial plane midway between the minor axis

and the separatrix. In the computed example, although the electric field keeps the particles within the separatrix, there is a region of velocity space where large excursions, nearly to the separatrix, occur. Thus while radial potentials of order (kT/e) will result in a reduction of the diffusion, larger electric potentials may be necessary before the excursions of localised particles no longer enhance the cross field transport.

The influence of α particles, born from fusion reactions, on the electric fields and subsequent diffusion may be important. The α particles will be born isotropically and those born into the localised region of velocity space may be expected, initially, to drift freely beyond the separatrix and to the wall. This will lead to a charge imbalance in the plasma, but as we have seen this imbalance will not significantly change the α particle orbits until radial potentials of the order of the α particle energy appear. Such potentials would drastically modify the plasma behaviour.

11. Diverter Action

The helical separatrix of a stellarator forms a natural diverter, and because of toroidal effects the magnetic surfaces can be arranged only to open into diverted lines on the outside (large R) of the torus. In stellarators the diverted lines tend to pass too near to one polarity of helical winding, consequently it is difficult to position a blanket around this winding, the problem might be overcome by modifying the field near the wire. Furthermore, the toroidal field coils of a conventional stellarator would probably have to be extended to enclose the diverted lines. The torsatron does not suffer from these difficulties since the offending wire is absent and a separate toroidal winding is not essential. Gourdon [15] has examined this system and shows that the torsatron does in fact give good diverter action for the field lines.

There is a conceptual difficulty in these diverter schemes in that if, as suggested by Gibson and Mason [13], particles in the outer regions are mirrored in the helical field inhomogeneities they will be unable to stream along the diverted lines, and will instead drift across the field lines to the walls.

12. Conclusions

- 12.1 The existence of diffusion driven currents does not, for reasonable aspect ratios and values of α less than about 1.2, reduce the expected critical β for stellarators and tokamaks from the equilibrium estimate of $\beta_0 = R/a$ ($q > 2.5$ for tokamak). However if α is as large as 2.44 as suggested by Hinton the critical β for both stellarators and tokamaks will be reduced somewhat from the equilibrium value (for $R/a=6$ the reduction is about 40% for stellarators and 20% for tokamaks).

- 12.2 An economic stellarator reactor requires superconductors to operate in the range 150 to 200kG at a cost $< \text{£}3.3 \times 10^{-3} / \text{kA} \cdot \text{kG} \cdot \text{m}$ ($\frac{1}{9}$ the 1970 N_b/T_i cost).
- 12.3 When allowance is made for a non-square density profile and for the reduction in available transform at very tight aspect ratios, it seems unlikely, even with the reduced superconductor cost, that a 2500MW(e) $\ell=3$ high shear system with γ less than 4 to 8 can meet the nuclear boiler target costs of $\text{£}20\text{-}25/\text{kW(e)}$. The prospect of meeting nuclear boiler target costs of $\text{£}10\text{-}16/\text{kW(e)}$ for a 10,000MW(e) plant at $\gamma=1$ to 2 is much more promising.
- 12.4 Tokamaks are costed in this paper as equivalent to stellarators with no helical winding and consequently appear much cheaper. Provision for a diverter will increase this cost, but provided steady state operation is possible it is to be expected that tokamaks will retain an economic advantage over stellarators.
- 12.5 A number of problems which need to be solved in order to make an economic stellarator can now be identified. Some of these, other than the obvious ones of confinement and heating, are listed below.
- (a) High field, low cost superconductors will have to be developed.
 - (b) Techniques to permit thinner blankets in front of the helical winding will give a substantial cost saving.
 - (c) An understanding is required of cross field diffusion in non-axisymmetric systems, especially of the build up of electric fields in the outer regions where trapping in the helical field is important.
 - (d) The modification of electric potentials and diffusion due to α particle production needs to be studied.
 - (e) Diverter action in the presence of helical field modulations needs to be clarified.
 - (f) Methods of increasing β above the present equilibrium limit need to be examined. Possibilities include shaped minor cross sections for tokamaks, non-circular magnetic axis and generalized helical windings for stellarators.

ACKNOWLEDGMENTS

The authors wish to thank Mrs. C. Colven and W. G. Core for a number of computations.

REFERENCES

- [1] GIBSON, A., Nuclear Fusion Reactors Conf. (Proc. Conf. Culham, 1969) BNES (1970) 233.
- [2] BICKERTON, R.J., CONNOR, J.W., and TAYLOR, J.B., Nature Physical Science 229 4 (1971) 110.
- [3] GALEEV, A., Zh.Exp.Teor.Fiz. 59 4 (1970) 1378.
- [4] TAYLOR, J.B., 1971, private communication.
- [5] HINTON, F.L., 1970, private communication. (to be published Rosenbluth M.N., Hazeltine, R.D., and Hinton F.L.)
- [6] SINCLAIR, R.M., et al. Phys. Fluids 8 1 (1965) 118.
- [7] SEARBY, P.J., and BROOKES, L.G., Nuclear Fusion Reactors Conf. (Proc. Conf. Culham, 1969) BNES (1970) 20.
- [8] CARRUTHERS, E., et al. Culham Laboratory Report CLM-R-85 (1967).
- [9] ROSE, D.J., Nuclear Fusion 9 (1969) 183.
- [10] GIBSON, A., Phys. Fluids 10 7 (1967) 1553.
- [11] HANCOX, E., to be published.
- [12] GOURDON, C., et al. 3rd Int. Conf. on Nuclear Fusion Research (Proc. Conf. Novosibirsk, 1968) 1 IAEA, Vienna (1969) 847.
- [13] GIBSON, A., and MASON, D.W., Plasma Physics 11 2 (1969) 121.
- [14] GIBSON, A., and TAYLOR, J.B., Phys. Fluids 10 12 (1967) 2653.
- [15] GOURDON, C., et al. Nuclear Fusion 11 2 (1971) 161

FAST NEUTRAL INJECTION FOR PLASMA HEATING AND REACTOR START-UP

D. R. SWEETMAN, A. C. RIVIERE, H. C. COLE,
 E. THOMPSON, D. P. HAMMOND, J. HUGILL,
 G. M. McCracken
 UKAEA, Research Group,
 Culham Laboratory,
 Abingdon, Berks.
 United Kingdom

Abstract

FAST NEUTRAL INJECTION FOR PLASMA HEATING AND REACTOR START-UP.

The injection of fast neutral atoms for the heating of toroidal reactors is considered. The requirement for fast deuterons to penetrate into the plasma volume necessitates an energy of the order of 1 MeV. The basic energy transfer rates from the trapped particles are shown to be adequate though the energy reaches the plasma ions mainly via the electrons unless $E_0 \lesssim 70 T_e$ (where E_0 is the energy of the incident particles). The use of injected beams of high atomic mass does not appear to offer a significant advantage if the beam penetration is fixed.

The start-up requirements are considered for a typical 7000 MW(th) toroidal reactor system. Because of the basic scaling of diffusion rate with temperature, less than 100 MW is required to reach ignition. This power is for convenience divided into 10 MW units and the constraints on the design of one such unit are considered. Basic ion source and accelerator considerations lead to the likely further subdivision of the beam during the early acceleration stages.

The low efficiency for neutralization precludes the use of a D^+ primary beam. Various other possibilities are considered including D_2^+ , D_3^+ , and D^- . The power efficiency for D_2^+ and D_3^+ is of order 20% and this results in severe, though not insuperable, problems of beam dumping, vacuum, and cost of power supplies. The power efficiency for D^- is in the range 65 - 90% and the above problems are much less serious.

The use of the Hall accelerator as an alternative ion source is considered. Hall accelerators have been operated at potentials up to 20 kV and measurements of current output, efficiency and divergence are presented.

1. INTRODUCTION

Though the filling of mirror reactor systems by neutral injection has been accepted for a number of years, there has been little discussion of the possibilities of heating and start-up of toroidal reactor systems by fast neutral injection. This paper summarises some of the work of a recent Culham Study Group on this subject. A more detailed report is in the course of publication.

The parameter range of reactors based on Stellarator/Tokamak Systems is open to much debate at the moment. In order to sidestep these rather complex issues, for the purpose of this paper we assume a toroidal system of the general type discussed by Carruthers, Davenport and Mitchell⁽¹⁾ though expanded somewhat in major radius.

Thus as a starting point the following parameters are taken for the running reactor conditions:

Minor wall radius	=	175 cm
Mean plasma radius	=	125 cm
Major radius	=	750 cm
Power flux at wall	=	1300 watts/cm ²
Mean power density	=	30 watts/cm ³
Total power output	=	7000 MW(th)
Mean plasma temperature	=	20 keV
Mean plasma density	=	3×10^{14} cm ⁻³

The work is not however, restricted to this reactor design and where possible calculations have been performed over a wide parameter range. Injection of deuterons has been studied in some detail though comments on other mass beams are included where appropriate.

2. BASIC REQUIREMENTS AND PHYSICAL PROCESSES

In this section we discuss the constraints which define the beam power and energy, the basic neutralisation requirements and some of the dominant physical processes in the reactor plasma.

2.1 Beam power requirements

The beam power is required to overcome the difference between the power lost from the system in the form of bremsstrahlung or any additional losses, and the energy generated by thermonuclear reactions in the plasma. The additional losses have been estimated in two ways. In the first the additional power loss from the system is estimated by taking the energy containment time at 20 keV to be that required to give economic power production ($t \sim 0.6$ sec) and allowing the energy loss rate to scale with temperature according to the Bohm relationship ($\propto T_e^2$). In the second the energy loss rate due to classical scattering has been estimated for a specific system (an axisymmetric Tokamak): in this case over most of the temperature range the reactor operates in the Sagdeev-Galeev collisionless regime and the ion energy loss rate scales as $T^{1/2}$ and is thus a simple factor multiplying the bremsstrahlung loss. At low temperature the plateau regime is appropriate and the energy loss rate scales as $T^{5/2}$.

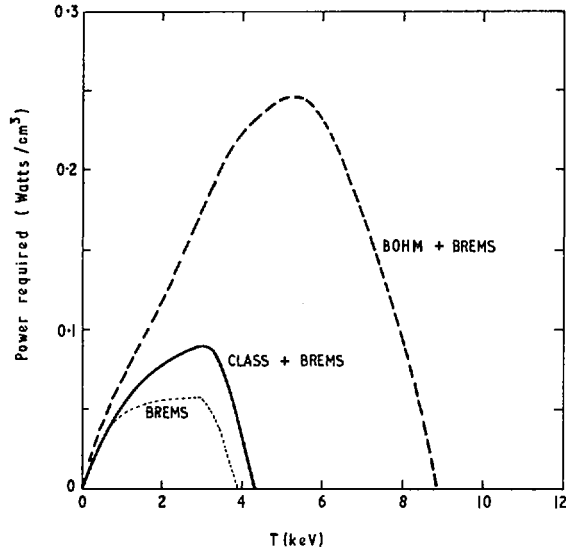


FIG. 1. Net power required to overcome losses versus plasma temperature ($T_e = T_i$). In the classical case, the particle loss component of the energy loss rate scales as T^2 in the collisionless regime (> 2 keV) and as $T^{5/2}$ in the plateau regime (< 2 keV). The curve labelled BREMS, calculated assuming only bremsstrahlung loss is operative, is shown for comparison.

The required power input at constant plasma density is shown in Fig. 1. The maximum power is estimated as 0.1 and 0.25 watts/cm³ respectively for the classical and Bohm scaling assumptions.

2.2 Beam Penetration

The penetration of a fast neutral beam into a thermonuclear plasma with $T_e = T_i$ has been calculated⁽²⁾ and the average $\langle \sigma v \rangle$ and plasma 'thickness' for $1/e$ attenuation are displayed in Fig. 2. For the injection energies of interest ($E_0 \sim 1$ MeV), charge exchange attenuation is small and for $T_e \gg (m_e/m_i)E_0$ the dominant attenuation mechanism is collisions with ions. Thus the attenuation is relatively insensitive to plasma temperature which has the important consequence that the plasma density need not be changed during the heating phase.

To achieve a reasonable radial distribution of injected particles and to minimise the loading on the far wall, approximately 2 e-folding distances are required in the plasma radius. Thus, for our standard case, the plasma thickness for an e-folding distance is required to be $2 \cdot 10^{16}$ cm⁻² and that determines a D⁰ injection energy of about 1 MeV.

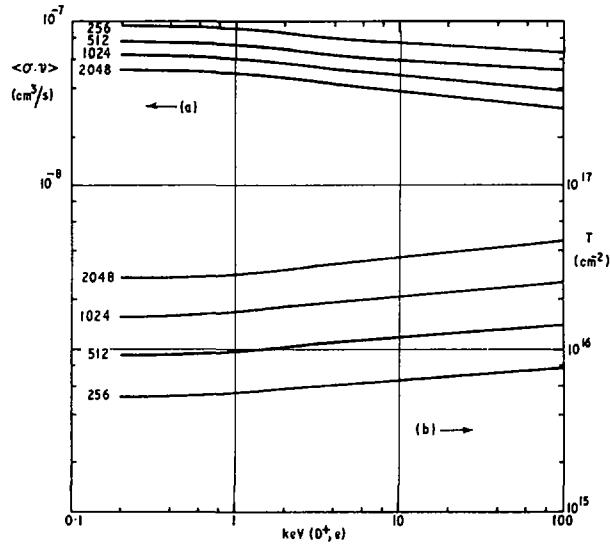


FIG. 2. Penetration of deuteron beams into reactor plasma. Ionization rates and plasma "thickness" for $1/e$ -attenuation are plotted against plasma energy ($T_e = T_i$). Four deuteron beam energies are shown (energy in keV).

As will be discussed later this choice of D^0 energy implies that heat is transferred initially to the plasma electrons. Since a lower energy would be required to transfer energy directly to the ions, the possibility of relaxing the beam penetration requirements has been considered. One possibility, open with stellarator geometry, is to use the natural drifts of energetic ions in the stellarator field to deposit the energy relatively uniformly even though the injection is only at the outside. This possibility may not be open in Tokamak geometry (or in stellarators with the diffusion current included) because of the higher rotational transform near the minor axis. Also if drifts can be invoked to transfer particles to the centre the injection of high energy ion beams is not completely excluded though we do not consider this further here.

2.3 Energy Transfer Processes

The rate of transfer of energy from a trapped ion to the electrons is given by

$$v_e \gg v_i, \quad \frac{1}{E_i} \frac{dE_i}{dt} = -3.2 \times 10^{-9} \frac{z^2 \ln \Lambda}{A T_e^{3/2}} \frac{n}{n_0} \text{ sec}^{-1} \quad (1)$$

where A , E_i are the trapped ion atomic mass (AMU) and energy (eV) and T_e is the electron temperature (eV).

The rate of transfer of energy to the ions is given approximately by

$$\frac{1}{E_i} \frac{dE_i}{dt} \approx -1.8 \times 10^{-7} \frac{(1 + A/A_p) z^2 \ell n \Lambda n}{A^{1/2} E_i^{3/2}} \quad (2)$$

where A_p is the mean plasma ion mass (AMU).

Under reactor conditions these rates of energy transfer are fast compared with the plasma loss rate. For example, if $n = 3 \times 10^{14} \text{ cm}^{-3}$, $T_e = 5 \text{ keV}$ and $A = 2$, then equation (1) gives a characteristic time constant for loss of injected particle energy of 0.07 sec which is to be compared with a plasma lifetime of greater than 1 second. However, the energy loss time may be comparable with typical drift times. For this reason the energy deposition as a function of minor radius can only be determined completely for specific systems where the detailed drifts may be calculated. Such a calculation is outside the scope of this paper.

We may set a condition for the energy transfer to be primarily to the ions by combining expressions (1) and (2) and integrating over the energy decay from the injected value E_0 . This condition is

$$E_0 < 35 [(1 + A/A_p) A^{1/2}]^{2/3} T_e \quad (3)$$

If we take $A = A_p = 2.0$ then E_0 must be less than $70 T_e$. If we take $A \gg A_p = 2$ then E_0 must be less than $22 A T_e$.

Thus with injection of deuterons at 1 MeV the energy transfer is primarily to the electrons until T_e reaches $\sim 14 \text{ keV}$. A similar condition applies to the injection of higher atomic mass beams since the penetration requirement fixes the beam velocity (assuming the ionization cross section at a given velocity varies little from element to element). Thus to first approximation the penetration required essentially fixes the ratio of energy transfer to ions and electrons (at a given electron temperature) independently of the atomic mass of the beam.

A constraint on the atomic mass of the beam may be set by the allowable impurity level (ϵ). From conservation of energy flux (in the essentially equilibrium conditions prevailing)

$$\epsilon = \frac{T_i + T_e}{E_0} \cdot \frac{\tau_i}{\tau_E}$$

where τ_i is the lifetime of the injected ions and τ_E the plasma energy containment time. If $T_i = T_e$ and this equation is combined with equation (3) then $\varepsilon > (1/11A)(\tau_i/\tau_E)$. A constraint on the impurity level is set by the need to keep the bremsstrahlung radiation within a factor of about two of that used in estimating the power requirements i.e. $\varepsilon Z^2 < 1$ (where Z is the injected ion atomic charge). Combining this with the condition for energy transfer to the ions gives $A < 44(\tau_E/\tau_i)$. Since τ_E is likely to be greater than τ_i this does not appear to be a serious constraint.

2.4 Neutralisation Efficiency

At an energy of 1 MeV the neutralisation efficiency of gaseous targets using D^+ as the primary beam has dropped to an unacceptably low value ($< 0.3\%$). The practical choice appears to be between D_3^+ , D_2^+ and D^- as the primary beam ion. The neutralisation efficiencies for beams of these species on gaseous and plasma targets have been estimated⁽³⁾ and are shown in Fig.3. D_3^+ is likely to give a neutralisation efficiency of around 20%, D_2^+ of 10-25% and D^- of 65-90% depending in each case on the degree of ionization of the neutraliser gas. It should be noted here that for D_2^+ and D^- it is an advantage to neutralise on a fully ionized plasma. For D_3^+ the relevant cross sections for an ionized neutraliser are not known.

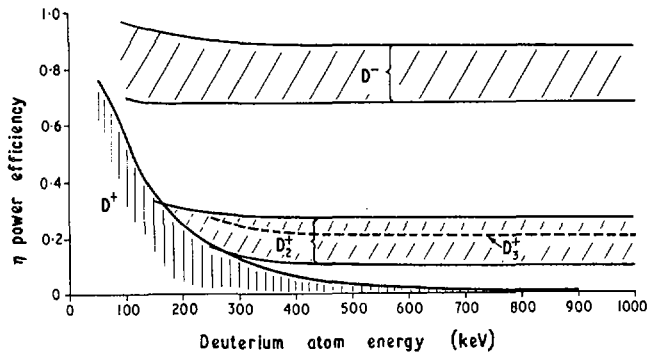


FIG. 3. Efficiency versus neutral beam energy for neutralization of D^+ , D_3^+ , D_2^+ and D^- on hydrogen. For the last three beams an optimum target thickness is taken. The range of values for D_2^+ and D^- is due to uncertainty in the degree of ionization of the target gas, a fully ionized gas giving the highest value in each case. The cross-sections for D_3^+ break-up on plasma are not known to sufficient accuracy to enable the range to be stated in this case.

2.5 Self-Consistent Electric Field and Plasma Currents

Fast ions and electrons created at the same point have a displacement of their guiding centres and this can lead to an electric field. This field (E) has been calculated⁽¹⁸⁾ and, in the plane geometry approximation, it is given by

$$E = 2 \frac{E_{\perp}}{a_i} \cdot \frac{A}{zA_p} \cdot \frac{n_i}{n} \text{ volt/cm}$$

where E_{\perp} is the trapped ion energy perpendicular to the field lines (in eV), a_i is the Larmor radius (cm), z is the atomic charge of the injected ion, A and A_p are the injected particle and plasma ion masses, and n_i and n are the trapped ion and plasma densities respectively.

This electric field results in an $E \times B$ motion of the plasma. It can be shown that the velocity of this motion is exactly that required to give conservation of momentum. Thus if the ions are injected into trapped orbits or have little velocity parallel to the field lines, essentially all the beam momentum is transferred quickly to the plasma via the electric field. If the beam ions are untrapped and have appreciable momentum along the field lines this part of the momentum remains in the fast ions and is transferred only relatively slowly by collisions.

For high injection energies the momentum parallel to the field which is transferred to the plasma by collisions, goes initially to the electrons. This gives rise to a current which is considerably greater than the beam current and which Ohkawa⁽⁴⁾ has considered in some detail. This current does not include the diffusion current⁽⁵⁾ and the derivation is presumably only valid when the latter is small. The Ohkawa current is comparable with the diffusion current at low density or when B_{θ} is high.

Thus by choosing to inject into trapped or untrapped orbits and with or without net angular momentum, extra degrees of freedom are provided which might be useful during a critical start-up phase.

2.6 Instabilities

Instabilities can arise due to the energy distribution of the injected ions and due to their anisotropy. Kolnesnichenko

and Oraevsky⁽⁶⁾ have made a start on the consideration of possible modes. The presence or otherwise of these depends very much on the energy and angular distribution of the trapped ions⁽⁷⁾: these have not been calculated for conditions appropriate to the build up phase and will be dependent on the final $n\tau$ and the geometry⁽⁸⁾.

Should instabilities prove to be present they might increase the transfer rate of energy from the fast ions to the plasma, and consequently modify the Ohkawa current. They might also introduce microturbulence which could increase the effective resistivity and possibly the diffusion rate.

3. TECHNOLOGICAL FEASIBILITY

3.1 Requirements

The considerations of Section 2.1 lead to beam power requirements in the range 0.1-0.25 watts/cm³, i.e. for our "standard" reactor 20-60 Mwatts. Since there is some uncertainty in this figure it is convenient to think in terms of a unit size of 10 MW: a number of such units being used to give the required power.

The penetration requirements of Section 2.2 lead to a neutral beam energy of order 1 MeV. Thus our standard unit becomes 10 amps equivalent at 1 MeV. By feeding in the neutralisation efficiencies discussed in Section 2.4 we may define the accelerator requirements as 17 amps of 3 MeV D₃⁺ or 25 amps of 2 MeV D₂⁺ or 12 amps of 1 MeV D⁻.

The maximum spread of the beam is decided by the reactor blanket hole size. If this is taken to be ~ 50 cm diameter through a 200 cm thick blanket this sets a requirement on neutral beam brightness⁽⁹⁾ of ~ 10⁵ which is easily achieved with existing ion source/accelerator designs. However, in a real system there are likely to be more severe constraints on the beam quality imposed by the requirements of the accelerator itself and the matching to the blanket hole.

3.2 Methods of Beam Acceleration

3.2.1 Single stage acceleration

A combination of the Child-Langmuir law and geometrical restrictions limit the ion beam current that can be obtained

from a single stage, ungridded, cylindrically symmetrical accelerator to $I_{\max} \approx 1.4 \times 10^{-7} V^{3/2} / A^{1/2}$ amps where V is the acceleration potential in volts and A is the atomic mass. This expression corresponds to an equivalent electron perveance of 6×10^{-6} . Inserting the acceleration voltages appropriate for D_3^+ , D_2^+ and D^- this relationship gives maximum currents of 300, 200 and 100 amps respectively.

However, plots of the calculated profile of an accelerating 10-20 amp beam show that space charge repulsion in the early stages requires that the plasma boundary be very large and very concave. Thus the accelerator must be carefully matched to a particular voltage and current. Also the mean plasma density at the plasma boundary is rather low and may make the achievement of high gas efficiency difficult. The latter is important to prevent excessive neutralisation of the beam in the early acceleration stages. For these reasons we favour a multi-stage system.

3.2.2 Multi-stage acceleration

The space charge effects in the early stages of acceleration can be reduced by breaking the beam up into separate shielded beams, each of which may be either circular or rectangular. The separate beams may be combined in the later stages of acceleration or after neutralisation.

Beam trajectory studies suggest that the beam requirements for the first stage are likely to be 0.1-1.0 amps at ~ 200 keV. To allow satisfactory injection into a combined beam the brightness of these individual beams must be $\approx 4 \times 10^7$ (i.e. perpendicular energy ≤ 300 eV), and to avoid too large a system the average current density at the plasma boundary must be $> 10 \text{ mA/cm}^2$.

Table I shows some of the properties of some existing ion source/accelerators for which data is available. From this table there would appear to be no difficulty in achieving the nominal requirements for first stage acceleration for D_3^+ and D_2^+ beams, though the D^- beams achieved to date are not of sufficient intensity.

Although there has been some effort devoted to negative ion sources for tandem Van de Graaff use, a most promising line has

TABLE I. PROPERTIES OF EXISTING ION SOURCES AND ACCELERATORS

Source Laboratory	Type	Beam	Beam energy (keV)	Beam [†] (A)	Emitting area (cm ²)	Current/cm ² (mA/cm ²)	Equivalent* electron perveance/hole	Brightness	Beam Power KW
Livermore	331 holes 1.5 mm diam.	H ⁺	1	0.8	32	25	3.3×10^{-6}	5×10^8	0.8
ORNL	48 holes 5 mm diam.	H ₂ ⁺	50	0.5	20	25	0.2×10^{-6}	1×10^8	87
ORNL	Expanded plasma boundary + central button	H ₂ ⁺	50	0.6	19	53	4×10^{-6}	7×10^8	30
Culham	Single hole 6 mm diam.	H ₂ ⁺	20	0.15	0.28	530	4.5×10^{-6}	4.8×10^8 5×10^8 **	0.3
Culham	13 holes 3 mm diam.	H ₂ ⁺ H ₂ ⁺ H ₂ ⁺	25 27	0.2 0.35	2 2	100 175	0.7×10^{-6} 0.5×10^{-6}	5×10^7 1.2×10^8	13
Kurchatov	Calutron	H ⁺	25	0.5	60	17		1.2×10^8	25
Sulburti	Expanded plasma boundary	H ₂ ⁺ H ₂ ⁺ H ₂ ⁺	65	0.85	80	≈11	3.3×10^{-6}	2.5×10^8	55
Rutherford	Pulsed duoplasmatron no lens	H ⁺	350	0.02	1	20	0.9×10^{-6}	1.5×10^{10} **	7
M. P. F. (LASL)	Duoplasmatron	H ⁺	200	0.02	1	20	0.42×10^{-6}	2.5×10^8 **	4
Saclay		H ⁺	300	0.1			0.8×10^{-6}	1.25×10^{10} **	30
Serpukhov		H ⁺	750	0.3			2.5×10^{-6}	6×10^8 **	225
CERN	Pulsed duoplasmatron gridded	H ⁺	540	0.5	1	500	7.2×10^{-6}	2.8×10^9 **	270
H. V. E. C.	Duoplasmatron	H ⁺	40	0.2			1.4×10^{-6}	3×10^8 **	8
Culham	Hall accelerator		1	1800	60	3×10^4		$\sim 4 \times 10^8$ **	1800
Berkeley	Calutron	H ⁺	10	0.005	3	2			

Notes: * Equivalent electron perveance is calculated using the formula $e. p = (m_i/m_e)^{1/2} V^{3/2}$, where I is the total extracted current in amps and V is the extraction potential in volts.

** In these cases the brightness has been calculated using the measured normalised emittance (9) according to the formula $b = 2I (MA)/r^2 z^2$, in the other cases the expression given in reference (9) has been used for the beam transmitted through a double stop system. Since in general stop systems are not filled, this latter method gives a lower brightness.

† This is the current obtained through a stop system at the brightness indicated. The total extracted current may be larger and is used to calculate the perveance.

not yet been exploited: the very high yield of negative ions from resonant electron capture in $\text{Cs}^{(10)}$ ($\sim 20\%$ at 1.5 keV for D^+) has not been combined with the high yield of D^+ at 1-2 keV that is obtainable from existing sources⁽¹¹⁾.

The blending of beams in the later stages of a multistage system has not, to our knowledge, been tackled seriously yet.

3.2.3 Hall Acceleration

Hall accelerators have the advantage that they are not space charge limited. They can therefore easily accelerate large currents of ions. Earlier experiments in both the spacecraft propulsion^(12,13) and fusion fields^(14,15) were performed on devices operating at 200-400 V and a few amperes in the former case and 1-2 kV and up to 3 kA in the latter.

Recent work at Culham has been aimed at designing an accelerator to operate at potential differences of tens of kilovolts and also to consider its possible application as the source of primary ions for reactor "start-up".

The present design of accelerator under investigation is shown in Fig.4. This is essentially a two stage accelerator but includes a bucking stage for reducing the strength of the magnetic field in the first stage. The characteristics obtained are shown in Fig.5. A design figure of 25 amp at 10 kV was achieved and it is interesting to note that 1 amp can be obtained at a potential difference approaching 20 kV.

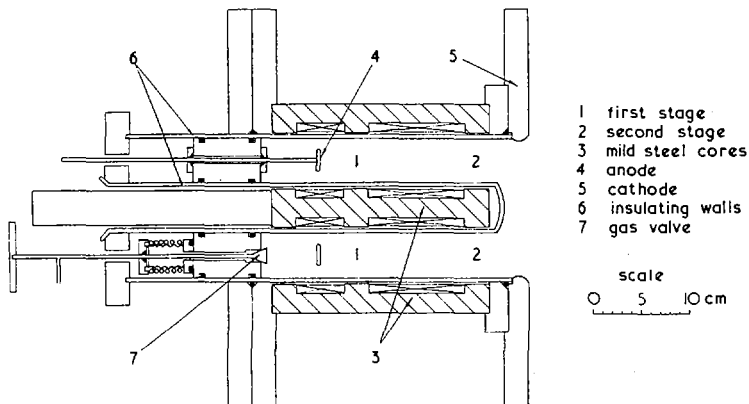


FIG.4. Schematic diagram of experimental two-stage Hall accelerator.

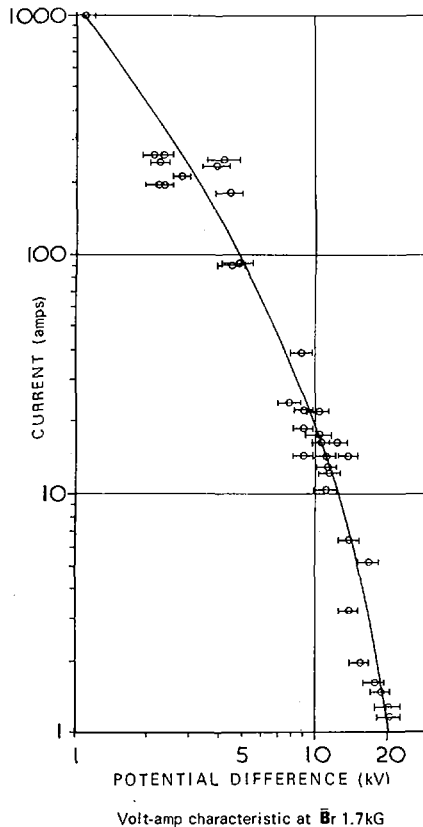


FIG. 5. Current versus applied voltage for experimental Hall accelerator.

A system of ballistic calorimeters was set up in order to measure the output and hence obtain the efficiency. Values of $> 50\%$ were obtained for the latter over the whole range measured.

We have not yet optimised the angular divergence but preliminary measurements at 230 amp, 2.2 kV indicate an angular divergence of $\pm 30^\circ$ that is a perpendicular energy of ~ 500 eV. This is well within the acceptance limit for a reactor, but it remains to be seen whether the perpendicular energy increases substantially as the parallel energy is increased.

By extrapolating the experimental results to operation at $B_r \sim 10$ kG and running the accelerator at a current density of < 1 amp/cm² a total stage length of ~ 200 cm is suggested for 2 MV operation⁽¹⁶⁾. The accelerator would then need to be

~ 400 cm long in order to accommodate the coils, and sixteen stages would be required to make the ion Larmor radius greater than a stage length. A total length of ~ 100 cm could be achieved by using superconducting coils to produce B_r fields of approximately 40 kG.

Further work is required in order to investigate the production and survival of D_2^+ or D_3^+ in the accelerator, and also the behaviour when more than two stages are used.

The Hall accelerator could become more competitive if the reactor penetration limitations could be circumvented and lower energy, higher current beams used.

3.3 Technical Problems of Injector

Some consideration has been given to the technical problems associated with X-ray loading, the neutraliser, maintenance of vacuum, beam dumping, and power supplies.

Probably one of the major problems and the least amenable to analysis is the effect of ion and electron bombardment in the accelerator and the consequent X-ray loading. These have not been considered in any detail but will clearly place very stringent conditions on the accelerator design.

A possible problem with the neutraliser is the generation of beam-plasma instabilities. Estimates of the growth times for these suggest that they are long compared with the time for the convective wave to propagate the length of the neutraliser. These could become serious however, if the wave was strongly reflected at the ends.

The vacuum problems appear to be most serious close to the ion source where there is the possibility of neutralisation in the early stages of beam acceleration. As mentioned earlier, this imposes constraints on the gas efficiency of the ion source and the configuration of sources. For primary beams of D_2^+ and D_3^+ the gas generated by dumping the unneutralised beams is serious if conventional pumping techniques are used but the problem may be diminished if the beam is deposited in a suitable solid or liquid target which traps the beam atoms and can be regenerated by heating⁽¹⁷⁾ (for example Ti, Zr, Li).

An additional problem associated with beam dumping is the magnitude of the total power deposition (~ 40 Mwatts for D_2^+ and D_3^+ beams). Conventional cooling systems restrict the power density to $100\text{-}300$ watts/cm² which implies deposition over an area of $10\text{-}40$ m². A flowing Lithium target might enable higher power densities to be used.

Both the vacuum and energy dumping problems are reduced by more than an order of magnitude by the use of D^- ions as the primary beam.

The power supplies do not appear to provide a major technical problem. Although the voltage (up to 3 MV) is rather higher than that currently used in general power transmission the power requirement is relatively modest (~ 50 Mwatts for D_3^+ , D_2^+ acceleration). Where efficiency is of prime importance a conventional transformer-rectifier set is favoured though the insulating core transformer might be competitive when somewhat lower efficiency can be tolerated. The question of protection in the case of beam collapse would require careful consideration.

Preliminary studies suggest that the cost of the power supplies might be a significant factor if D_3^+ or D_2^+ ions are used. Again this would be reduced by a factor of about four by the use of D^- ions. The cost and the beam dumping problem might also be reduced somewhat by electrostatic recovery of the energy from the unwanted beams. Preliminary studies, however, suggest that the additional voltage conversion equipment required might reduce the cost advantage to a level where the additional complexity was hardly justified.

4. CONCLUSIONS

A range of assumptions as to the scaling of the loss rate with temperature give start-up power requirements in the range $20\text{-}60$ Mwatts for a 7000 MW(th) toroidal reactor. If the discussion is limited to deuteron injection, requirements for beam penetration lead to an injection energy of about 1 MeV, at which the major fraction of the injected energy is transferred to the electrons. Neutralisation efficiency considerations lead to the production of the beam from accelerated beams of D_3^+ , D_2^+ or D^- .

The neutralisation efficiency using D_3^+ or D_2^+ is low ($\sim 20\%$) whereas for D^- it is much higher (80-90%).

Beam penetration considerations suggest that there is no general advantage in using higher mass beams though it is possible that a detailed study of the cross sections may reveal an element with specific advantages over deuterium.

A 1 MeV, 10 Mwatt unit size has been chosen for study and no in-principle overriding difficulties have been found, though it does represent a substantial extension of existing technology.

Multistage acceleration is likely to be the desirable way of achieving this aim. The current density and brightness requirements for the first stage of a multistage system working on D_3^+ or D_2^+ appear to be within the capabilities of existing types of sources; but there is a need for the development of better and more uniform plasma sources for illuminating large arrays. Single stage acceleration cannot be completely dismissed however, and the data presented here suggests that Hall accelerators might become competitive if the required acceleration energy can be reduced.

D^- sources do not appear to have been developed to their full capabilities and there is considerable technological advantage, in beam dumping, vacuum and cost, to their use.

Some progress has been made in understanding the interaction of the injected beam with the plasma though a detailed understanding will probably have to await the stimulus of results from the experiments now under construction.

ACKNOWLEDGEMENTS

The authors wish to thank J.G. Cordey, M.F.A. Harrison, A. Gibson, F.A. Julian, F.B. Marcus and C.J.H. Watson for helpful discussions during the course of this work and R.J. Bickerton and R.S. Pease for continuing encouragement.

References

- [1] CARRUTHERS, R., DAVENPORT, P.A., MITCHELL, J.T.D., CLM-R 85.
- [2] RIVIERE, A.C., Submitted to Nuclear Fusion.

- [3] RIVIERE, A.C., SWEETMAN, D.R., APS Meeting (Nov.1970), paper 4E2.
- [4] OHKAWA, T., Nuclear Fusion 10 (1970) 185.
- [5] BICKERTON, R.J., CONNOR, J.W., TAYLOR, J.B., Nature 229 (1971) 110.
- [6] KOLNESNICHENKO, Ya.I., ORAEVSKY, V.N., IV Eur. Conf. on Contr. Fusion and Plasma Physics, Rome (1970), paper 180.
- [7] KOLNESNICHENKO, Ya.I., ORAEVSKY, V.N., Atomnaya Energiya 23 (1967) 289.
- [8] OLIPHANT, T.A., Proc. Nucl. Fus. Reactors Conf., Culham (1969) 306.
- [9] KELLEY, G.G., I.E.E.E. Trans. Nucl. Sci., 14 (1967) 29.
- [10] SCHLACHTER, A.S. et al., Phys. Rev. 177 (1969) 184.
- [11] OSHER, J., Am. Phys. Soc. Meeting (Nov. 1970) paper 4E7.
- [12] PINSLEY, E.A., BROWN, C.O., Journal of Spacecraft and Rockets 1 (1964) 524.
- [13] BROWN, C.O., PINSLEY, E.A., A.I.A.A. Journal 3 (1965) 853.
- [14] MOROZOV, A.I., KISLOV, A.Y., ZUBKOV, I.D., Pisma v Redaktsiu, Zh.E.T.F. 7 7 (1968) 224 (English Trans.CTO/516).
- [15] COLE, H.C., Nuclear Fusion 10 (1970) 271.
- [16] COLE, H.C., HILL, J.W., TERRY, M.J., Symposium on Fusion Technology, Aachen (1970) paper 47.
- [17] McCracken, G.M., JEFFRIES, D.K., GOLDSMITH, P., Proc. 4th Int. Vac. Congress (1968) 149.
- [18] CORDEY, J.G., HOUGHTON, M.J., to be published.

DISCUSSION

TO PAPERS IAEA-CN-28/K-4, K-5

P. L. HUBERT: There are two reasons why I cannot share your opinion on the comparison between stellarator and torsatron: (1) For $\ell = 3$ the plasma section is triangular and the corners are pointing between the helical windings in the case of torsatron. This facilitates the installation of thick shielding, even though the magnetic surfaces may be relatively large (the same argument also holds for other values of ℓ); (2) As regards cost, it must be realized that savings can be achieved through the following features: (a) large magnetic surfaces, (b) the fact that toroidal winding can be dispensed with, (c) simplified mechanical structure through internal equilibration of constraints coupled with the advantages of the natural helicoidal diverter.

R. J. BICKERTON: We agree that the torsatron has the major advantage of providing a good magnetic diverter. In all our stellarator studies the cost of the toroidal field winding is small compared with that of the helical windings, so the saving when this winding is dispensed with in the torsatron is small. The cost of the mechanical support is also small, so the saving in the torsatron in this respect is again small. The disadvantage of the torsatron is that, to accommodate the blanket between the separatrix and the winding, it is necessary to have long-pitch windings; for a given γ -value the torsatron is then more expensive than the conventional stellarator.

H. HARRISON: Can you estimate what would be the per cent reduction in cost if ambient temperature superconductors not requiring cryogenic equipment were available?

R. J. BICKERTON: In our calculations the cost of refrigeration is £2/kW(e) or less. The cost effect of using a room-temperature superconductor thus depends mainly on whether its price is greater or less than the price of a low-temperature superconductor.

B. COPPI: Do you have a practical solution to the problem of controlling the profile of the diffusion-driven current density that you propose for a steady-state Tokamak?

R. J. BICKERTON: The current distribution in the steady-state Tokamak is controlled by the distribution of particle sources within the discharge. The only practical way of providing such sources seems to be through pellet injection.

Whatever the distribution of sources, it seems that the current density will always be greatest at the edge of the plasma, contrary to the situation in present Tokamaks. The instability of the steady-state Tokamak may thus be inevitable.

B. COPPI: Have you considered the possible impact of the development of advanced air core transformers on long-pulse Tokamaks?

R. J. BICKERTON: No. We have taken the view that long-pulse Tokamaks combine the vices of both steady-state and pulsed systems: they require refuelling and diverters and at the same time have to be ignited every pulse.

W. H. KÖHLER: When you quote target capital costs for end-of-the-century fusion reactors, do you take into account fuel-cycle costs? If so, what actual values do you use for fuel-cycle costs?

R. J. BICKERTON: We use the target costs given by Searby and Brookes (Conference on Nuclear Fusion Reactors, Culham, 1969). They assumed that the fuel-cycle costs for a fusion system might be one order of magnitude lower than those for a fission system. The estimated end-of-the-century nuclear boiler cost is $\sim \text{£}10/\text{kW(e)}$ for a fission reactor. With the lower fuel inventory and lower fuel recycling costs of the fusion system, the nuclear boiler may cost $\text{£}10/\text{kW(e)}$ more. The total target figure for the nuclear fusion boiler is thus $\text{£}20/\text{kW(e)}$.

L. M. GOLDMAN: The problem of introducing the fuel into toroidal systems has troubled investigators since 1954. Has your group considered this problem and have you any recommended solution?

R. J. BICKERTON: This is indeed the Achilles heel of all closed-line, steady-state systems. We have considered the problem but we have no new solution - only the well known pellet injection proposal.

ВЛИЯНИЕ РЕАКЦИЙ СИНТЕЗА НА РАБОТУ ТЕРМОЯДЕРНЫХ УСТАНОВОК

В.С. БЕЛИКОВ, Я.И. КОЛЕСНИЧЕНКО,
В.Н. ОРАЕВСКИЙ

Институт ядерных исследований
Академии наук Украинской ССР, Киев,
Союз Советских Социалистических Республик

Abstract—Аннотация

THE EFFECT OF FUSION REACTIONS ON THE OPERATION OF THERMONUCLEAR DEVICES.

It is shown that from some instant when the concentration of thermonuclear fusion products in the device attains a critical value, the plasma will be at the boundary of instability. The level of essentially epithermal fluctuations thus established is determined by non-linear effects. These fluctuations are due to the thermodynamic non-equilibrium of the distribution functions of the thermonuclear reaction products. Because of the large energy values of the particles formed in the fusion reactions, the critical values of their relative concentrations are very low. The paper briefly describes the linear theory of the stability of a plasma with thermonuclear reaction products; on the basis of this theory the critical values of the relative concentrations of reaction products are found for different types of instabilities. A method has been developed for calculating electromagnetic fluctuations in non-linear media located near the instability boundary. This method is used for finding the plasma oscillation spectrum when the relative concentration of the thermonuclear reaction products exceeds a value corresponding to the instability boundary. The boundaries of the different instabilities associated with the fusion reaction products are determined as a preliminary step. It is demonstrated that the energy of the reaction products is transmitted rapidly to the main plasma through the collective plasma oscillations. The corresponding relaxation times are much lower than the Coulomb collision times.

ВЛИЯНИЕ РЕАКЦИЙ СИНТЕЗА НА РАБОТУ ТЕРМОЯДЕРНЫХ УСТАНОВОК.

Показано, что, начиная с некоторого момента времени, когда концентрация продуктов термоядерного синтеза в установке достигнет критического значения, плазма будет находиться на границе неустойчивости. Устанавливающийся при этом уровень существенно над-тепловых флуктуаций определяется нелинейными эффектами. Причиной возникновения таких флуктуаций является термодинамическая неравновесность функции распределения продуктов термоядерных реакций. Вследствие большой величины энергии образующихся в реакциях синтеза частиц, критические значения их относительных концентраций весьма малы. В работе кратко изложена линейная теория устойчивости плазмы с продуктами термоядерных реакций, на основе которой найдены критические значения относительных концентраций продуктов реакций для различных типов неустойчивостей. Развита метод, позволяющий рассчитывать электромагнитные флуктуации в нелинейных средах, находящихся вблизи границы неустойчивости. Этот метод применяется для отыскания спектра колебаний плазмы, когда относительная концентрация продуктов термоядерных реакций превышает значение, соответствующее границе неустойчивости. Предварительно определяются границы различных неустойчивостей, связанных с продуктами реакций синтеза. Показано, что с помощью коллективных колебаний плазмы происходит быстрая передача энергии продуктов реакций основной плазме. Соответствующие релаксационные времена намного меньше времен кулоновских соударений.

1. ВВЕДЕНИЕ

Из проблем управляемого термоядерного синтеза важнейшей является проблема магнитной термоизоляции плазмы в течение времени, за которое успевает прореагировать значительная доля ядерного горючего. Это время (которое, как известно, определяется концентрацией и температурой реагирующих ионов) может измениться, если в результате коллективных процессов будет происходить интенсивная передача энергии от

продуктов термоядерных реакций к реагирующим ионам. Коллективные процессы, вызываемые продуктами реакций синтеза, могут также заметно увеличить коэффициенты переноса плазмы.

Коллективные процессы возникают и в отсутствие неустойчивостей. Так, при приближении плазмы к границе неустойчивости флукуационные колебания становятся аномально большими и в линейном приближении неограниченно возрастают [1]. Нелинейные эффекты (распадные процессы, затухание волн на биениях и т.п. [2-5]) приводят к установлению конечного уровня флукуаций.

В термоядерной плазме коллективные процессы могут быть существенными в связи с тем, что функция распределения продуктов реакций является термодинамически неравновесной. При этом, из-за большой величины энергии продуктов реакции, даже относительно малой концентрации этих продуктов может быть достаточно для возбуждения существенно надтепловых флукуаций. Так как процесс накопления продуктов термоядерных реакций медленный, плазма достаточно долго будет оставаться на границе неустойчивости. Уровень колебаний в течение этого периода определяется в работе с помощью нелинейной теории флукуаций. Предварительно детально исследуются границы различных неустойчивостей, вызываемых накоплением в плазме продуктов термоядерного синтеза (такие неустойчивости будем называть термоядерными).

Показано, что возникающие вблизи границ термоядерных неустойчивостей флукуации значительно сказываются на скорости передачи энергии продуктов термоядерных реакций плазме и на явлениях переноса в ней. Рассмотрение проведено на примере, когда относительно малое накопление продуктов реакций синтеза приводит плазму к границе неустойчивости по отношению к возбуждению альфвеновских волн.

2. ЛИНЕЙНАЯ ТЕОРИЯ УСТОЙЧИВОСТИ ПЛАЗМЫ С ПРОДУКТАМИ ТЕРМОЯДЕРНОГО СИНТЕЗА

2.1. Функция распределения продуктов термоядерных реакций

Для изучения влияния продуктов термоядерных реакций на работу термоядерных установок необходимо, прежде всего, знание их функции распределения $-F^\alpha(\vec{v}, r)$. Естественно, что вид этой функции зависит от закона распределения по скоростям реагирующих ионов плазмы. Вычислим функцию распределения F^α , предполагая, что термодинамическая неравновесность реагирующих ионов связана только с наличием градиента плотности. Систему координат выберем таким образом, чтобы ось z была направлена вдоль магнитного поля, а ось y — вдоль неоднородности плазмы. Тогда в приближении слабонеоднородной плазмы функцию распределения исходных ионов можно представить в виде:

$$F_i(\vec{v}, y) = n_i(y) \left[1 - \frac{k_{0i} v_x}{\omega_i} \right] \left(\frac{m_i}{2\pi T} \right)^{3/2} \exp \left\{ -\frac{m_i v^2}{2T} \right\} \quad (2.1.1)$$

где

$$k_{0i} \equiv \frac{d \ln n}{dy} \quad \omega_i = \frac{e_i H}{m_i C}$$

Для нахождения функции распределения частиц сорта, образующихся в реакции



(где Q – энергосодержание рассматриваемой реакции), поступим следующим образом. Запишем вначале выражение для интенсивности реакций, при которых скорости частиц сортов a и b лежат в элементах объемов $d\vec{v}_a$ и $d\vec{v}_b$, соответственно, а частицы сорта α попадают в элемент телесного угла $d\Omega_\alpha$:

$$\eta_{ab} F_a(\vec{v}_a, y) F_b(\vec{v}_b, y) |\vec{v}_a - \vec{v}_b| \sigma d\vec{v}_a d\vec{v}_b \frac{d\Omega_\alpha}{4\pi} \quad (2.1.3)$$

где σ – сечение ядерных реакций, зависящее от энергии относительного движения частиц; $\eta_{ab} = 1$ для реакций dt и $\eta_{ab} = 1/2$ для реакций dd; F_a и F_b даются выражением (2.1.1). Переходя к переменным:

$$\vec{v} = \frac{m_a \vec{v}_a + m_b \vec{v}_b}{m_a + m_b} \quad \vec{w} = \vec{v}_a - \vec{v}_b \quad (2.1.4)$$

получим выражение для интегральной интенсивности реакций:

$$\begin{aligned} & \eta_{ab} \left(\frac{m_a m_b}{4\pi^2 T^2} \right)^{3/2} n_a n_b \int \frac{d\Omega_\alpha}{4\pi} \int d\vec{w} \int d\vec{v} \left[1 - \frac{k_{0a}}{\omega_a} \left(v_x + \frac{m_b}{m_0} w_x \right) \right. \\ & \left. - \frac{k_{0b}}{\omega_b} \left(v_x - w_x \frac{m_a}{m_0} \right) \right] w \sigma \left(\frac{\mu w^2}{2} \right) \exp \left[- \frac{m_0 v^2}{2T} - \frac{\mu w^2}{2T} \right] \end{aligned} \quad (2.1.5)$$

где $m_0 = m_a + m_b$ $\mu = \frac{m_a m_b}{m_0}$.

Обозначив скорость частицы α в системе центра масс частиц a и b через u_α и используя закон сохранения энергии в этой системе,

$$\frac{\mu w^2}{2} + Q = \frac{m_0 m_\alpha}{2m_\alpha} u_\alpha^2 \quad (2.1.6)$$

перейдем в (2.1.5) к переменным \vec{v}_α , \vec{w} , $d\Omega_\alpha$. Затем, проинтегрировав полученное выражение по $d\Omega_\alpha$, будем иметь:

$$\begin{aligned} & \eta_{ab} \left(\frac{\sqrt{m_0 \mu}}{2\pi T} \right)^3 \int d\vec{v}_\alpha \left(1 - \frac{k_{0a} v_{\alpha x}}{\omega_a} \right) \int d\vec{w} \sigma w \\ & \times \exp \left\{ - \frac{\mu}{2T} w^2 - \frac{m_0}{2T} \left(v_\alpha^2 + u_\alpha^2 \right) \right\} \left[e^{\frac{m_b v_\alpha u_\alpha}{T}} - e^{-\frac{m_b v_\alpha u_\alpha}{T}} \right] \frac{T}{2m_0 v_\alpha u_\alpha} \end{aligned} \quad (2.1.7)$$

где $k_{0\alpha} \equiv \omega_\alpha \left(\frac{k_{0a}}{\omega_a} + \frac{k_{0b}}{\omega_b} \right)$.

Выражение, стоящее под знаком интеграла по $d\vec{v}_\alpha$, является искомой функцией распределения. Поэтому следует выполнить интегрирование по $d\vec{w}$, а для этого необходимо знание сечения ядерных реакций. Если тем-

пература реагирующих ионов мала по сравнению с энергией Q , можно воспользоваться приближенными выражениями для σ , приведенными, например, в [6,7]. Благодаря тому что $m_0 u^2 \gg T$, для вычисления интеграла по dw удобно использовать асимптотический метод Лапласа. В результате получим следующее выражение для функции распределения продуктов термоядерных реакций сорта [8]:

$$F^\alpha = n_\alpha(y) \left(\frac{m_0}{2\pi T} \right)^{1/2} \frac{1}{4\pi u_\alpha} \left(1 - \frac{k_{0\alpha} v_x}{\omega_\alpha} \right) \times \frac{1}{v} \left[\exp \left\{ -\frac{m_0(v - u_\alpha)^2}{2T} \right\} - \exp \left\{ -\frac{m_0(v + u_\alpha)^2}{2T} \right\} \right] \quad (2.1.8)$$

Здесь $u_\alpha = \sqrt{2m_\alpha Q / m_0 m_\alpha}$; $m_0 = m_a + m_b$; постоянный множитель выбран таким образом, чтобы $\int d\vec{v} F^\alpha(\vec{v}, y) = n_\alpha(y)$.

В силу того что $Q/T \gg 1$, полученная функция распределения существенно отлична от нуля лишь в точке $v = u_\alpha$, в остальных же точках она экспоненциально мала. Если полностью пренебречь тепловым разбросом в (2.1.8), то

$$F^\alpha = \frac{1}{4\pi u_\alpha^2} \left(1 - \frac{k_{0\alpha} v_x}{\omega_\alpha} \right) \delta(v - u_\alpha) \quad (2.1.9)$$

2.2. Метод нахождения обусловленных примесями поправок к собственным частотам плазмы

Исследование устойчивости высокотемпературной плазмы, в которой протекают реакции термоядерного синтеза, сводится к исследованию устойчивости системы, состоящей из электронов и двух групп ионов. Одна из групп состоит из относительно холодных ионов, концентрация которых близка к концентрации электронов. Другая группа — высокоэнергичные ионы с почти моноэнергетической функцией распределения (2.1.8). Концентрация этой группы ионов существенно меньше концентрации электронов и медленно меняется во времени (в линейной теории устойчивости термоядерной плазмы этим изменением можно пренебречь). Другими словами, продукты термоядерных реакций составляют небольшую примесь к основной плазме. Поэтому уравнения, описывающие колебания плазмы, можно представить в виде:

$$\left\{ \Lambda_{ij} + \epsilon_{ij}^\alpha \right\} E_j = 0 \quad (2.2.1)$$

где Λ_{ij} относится к основной плазме и, как хорошо известно (см., например, [1]), имеет вид:

$$\Lambda_{ij} = N^2 \left(\frac{k_i k_j}{k^2} - \delta_{ij} \right) + \epsilon_{ij} \quad (2.2.2)$$

ϵ_{ij}^α — малая добавка к тензору диэлектрической проницаемости плазмы ϵ_{ij} , обусловленная продуктами термоядерного синтеза. Эта добавка может приводить к раскату лишь слаботухающих колебаний плазмы. Исходя из этого, для решения вопроса об устойчивости применим теорию возмущений. Прежде всего, запишем ϵ_{ij} в виде:

$$\epsilon_{ij} = \epsilon_{ij}^{\prime} + i \epsilon_{ij}^{\prime\prime}$$

где $i \epsilon_{ij}^{\prime\prime}$ — антиэрмитова часть ϵ_{ij} . Тогда уравнение (2.2.1) можно записать следующим образом:

$$\begin{aligned} \Lambda_{ij}^{(0)} E_j &= - (i \epsilon_{ij}^{\prime\prime} + \epsilon_{ij}^{\alpha}) E_j \\ \Lambda_{ij}^0 &= N^2 \left(\frac{k_i k_j}{k^2} - \delta_{ij} \right) + \epsilon_{ij}^{\prime} \end{aligned} \quad (2.2.3)$$

Отсюда, в силу малости $i \epsilon_{ij}^{\prime\prime} + \epsilon_{ij}^{\alpha}$, легко получить выражение для поправок к собственным частотам магнитоактивной плазмы (для простоты считаем, что пересечение корней отсутствует):

$$\Delta \omega = -i \frac{\langle e_i^* | \epsilon_{ij}^{\prime} + \epsilon_{ij}^{\alpha} | e_j \rangle}{\langle e_i^* | \frac{\partial \Lambda_{ijk}^0}{\partial \omega} | e_k \rangle} - \frac{\langle e_i^* | \epsilon_{ij}^{\alpha} | e_j \rangle}{\langle e_i^* | \frac{\partial \Lambda_{ijk}^0}{\partial \omega} | e_k \rangle} \quad (2.2.4)$$

где e_i — вектор поляризации соответствующей волны.

Как видно из (2.2.4), вклад в мнимую часть $\Delta \omega$ дает лишь первое слагаемое, поэтому для исследования устойчивости плазмы достаточно найти антиэрмитову часть (это будет проделано в следующем разделе).

Отметим, что приведенная методика может быть использована при решении многих задач, когда к основной плазме добавляется малая группа заряженных частиц (например, при нахождении инкрементов пучковых неустойчивостей).

2.3. Антиэрмитова часть тензора диэлектрической проницаемости плазмы, связанная с продуктами реакций синтеза

Рассмотрим слабонеоднородную плазму, содержащую продукты термоядерных реакций, еще не успевшие термализоваться. Именно этот случай представляет интерес, так как с точки зрения осуществления управляемого термоядерного синтеза наиболее важными являются неустойчивости, времена развития которых малы по сравнению с характерными релаксационными временами. Ось y направим вдоль неоднородности плазмы, ось z — вдоль магнитного поля. Ограничиваясь членами, линейными по $(d/dy)(nT)$, можем записать общее выражение для компонент тензора диэлектрической проницаемости, связанных с продуктами термоядерного синтеза:

$$\epsilon_{\alpha\beta}^{\alpha} = \frac{4\pi e^2}{m\omega} \int d\vec{v} \left\{ \frac{1}{v} \frac{\partial f^0}{\partial v} - \frac{k_x}{\omega \omega_H} \frac{\partial f^0}{\partial y} \right\} \sum_{\ell=-\infty}^{\infty} \frac{q_{\alpha} q_{\beta}}{\omega - \ell \omega_H - k_z v_z + i0} \quad (2.3.1)$$

где суммирование проводится по сортам заряженных частиц, образовавшихся в результате реакций,

$$\begin{aligned} q_x &= v_{\perp} \left(\frac{\ell J_{\ell}}{\xi} \cos \psi - i J_{\ell}^{\prime} \sin \psi \right) & q_y &= v_{\perp} \left(i J_{\ell} \cos \psi + \frac{\ell J_{\ell}}{\xi} \sin \psi \right) \\ q_z &= v_z J_{\ell} & J_{\ell} &= J_{\ell}(\xi) & \xi &= \frac{k_{\perp} v_{\perp}}{\omega_H} \end{aligned}$$

Используя явный вид функции распределения продуктов термоядерных реакций (2.1.8) из (2.3.1), получим следующие выражения для компонент антиэрмитовой части тензора диэлектрической проницаемости ϵ_{ij}^α :

$$\epsilon_{ij}^\alpha \equiv \begin{matrix} \epsilon_1 & ig & \xi \\ -ig & \epsilon_2 & if \\ \xi & -if & \eta \end{matrix} \quad (2.3.2)$$

$$\begin{aligned} \text{Jm} \epsilon_1^\alpha &= \frac{\pi \Omega_\alpha^2}{2\omega |k_z| u} \sum_\ell \ell^2 \hat{\Pi}_\ell J_\ell^2 \\ \text{Jm} g^\alpha &= -\frac{\pi \Omega_\alpha^2}{2\omega |k_z| u} \sum_\ell \ell \hat{\Pi}_\ell y_\ell J_\ell J_\ell^1 \\ \text{Jm} \epsilon_2^\alpha &= \frac{\pi \Omega_\alpha^2}{2\omega |k_z| u} \sum_\ell \hat{\Pi}_\ell y_\ell^2 J_\ell^2 \\ \text{Jm} \xi^\alpha &= \frac{\pi \Omega_\alpha^2 k_\perp^2}{2\omega \omega_\alpha |k_z| k_z u} \sum_\ell \ell (\omega - \ell \omega_\alpha) \hat{\Pi}_\ell J_\ell^2 \\ \text{Jm} f^\alpha &= \frac{\pi \Omega_\alpha^2 k_\perp}{2\omega \omega_\alpha |k_z| k_z u} \sum_\ell (\omega - \ell \omega_\alpha) \hat{\Pi}_\ell y_\ell J_\ell J_\ell^1 \\ \text{Jm} \eta^\alpha &= \frac{\pi \Omega_\alpha^2 k_\perp^2}{2\omega \omega_\alpha^2 |k_z|^3 u} \sum_\ell (\omega - \ell \omega_\alpha)^2 \hat{\Pi}_\ell J_\ell^2 \end{aligned} \quad (2.3.3)$$

Здесь $\hat{\Pi}_\ell \equiv \frac{1}{y_\ell} \frac{\partial}{\partial y_\ell} + \frac{k_\perp \omega_\alpha}{k_\perp^2 \omega} \frac{d \ln n_\alpha}{dy}$, $J_\ell^1 \equiv \frac{dJ_\ell}{dy_\ell}$, J_ℓ — функция Бесселя
 $\Omega_\alpha^2 = \frac{4\pi n_\alpha e_\alpha^2}{m_\alpha}$, $y_\ell = \frac{k_\perp u}{\omega_\alpha} \sqrt{1 - \frac{(\omega - \ell \omega_\alpha)^2}{k_z^2 u^2}}$, ℓ — лежит в интервале:

$$\frac{\omega - |k_z| u}{\omega_\alpha} \leq \ell \leq \frac{\omega + |k_z| u}{\omega_\alpha}$$

2.4. Термоядерные неустойчивости плазмы

Под термоядерными неустойчивостями плазмы будем понимать такие неустойчивости, которые обусловлены реакциями синтеза.

В данном разделе приведем результаты исследования устойчивости плазмы для систем, у которых газокинетическое давление много меньше давления магнитного поля. Эти результаты могут быть получены с помощью (2.2.4) и (2.3.3), а также выражений для компонент тензора диэлектрической проницаемости локально максвелловской плазмы (часть результатов, приводимых ниже, получена в [8-11]).

2.4.1. Возбуждение продуктами реакций магнитогидродинамических волн

Как известно, запас устойчивости однородной замагниченной плазмы относительно возбуждения магнитогидродинамических волн относительно невелик. Поэтому можно ожидать, что появление в системе даже очень небольшого количества продуктов термоядерных реакций (функция распре-

деления которых существенно отличается от максвелловской) приведет к раскашке магнитогидродинамических волн. Следует также ожидать, что наиболее низкий "порог" неустойчивости будет для альфвеновских и быстрых магнитозвуковых волн.

Рассмотрим вначале условия возбуждения альфвеновских волн. Вычисления, проведенные по указанной выше схеме, приводят к следующим значениям γ_A - мнимой части поправки к частоте альфвеновской волны:

$$\gamma_A = -\frac{1}{4} \frac{\sqrt{\pi}}{2} \frac{k_z^2 c^2}{\Omega_e^2} |k_z| v_e - \frac{\pi n^\alpha \omega_\alpha^2}{4 |k_z| u n} \sum_{\ell} \frac{\ell^2}{y_\ell} \frac{\partial J_\ell^2(y_\ell)}{\partial y_\ell} \quad (2.4.1)$$

где $\Omega_e = \frac{eH}{m_e c}$, v_e - тепловая скорость электронов.

Используя (2.4.1), нетрудно получить пороговое значение для относительной концентрации продуктов реакций:

$$\frac{n_c^\alpha}{n} \sim \frac{v_A^2 v_i^2}{u^3 v_e} \quad (2.4.2)$$

при этом $k_z \sim k_\perp \sim \frac{\omega_\alpha}{u}$; $v_A < u$.

В случае, если электроны холодные ($v_A \gg v_e$), пороговое значение относительной концентрации n^α/n экспоненциально мало.

Для быстрой магнитозвуковой волны выражение для γ_M - мнимой части частоты имеет вид:

$$\gamma_M = -\frac{2\sqrt{\pi}}{4} \frac{k_\perp^2}{k_z^2} \frac{m}{M} v_e - \pi \frac{n^\alpha}{n} \frac{\omega_\alpha^2}{|k_z| u} y_0 J(y_0) J_1(y_0) \quad (2.4.3)$$

$$k_z \sim k_\perp \sim \omega_\alpha / u$$

Из этого выражения получим:

$$\frac{n_c^\alpha}{n} \sim \frac{m}{M} \frac{v_e}{u} \quad v_A < u \quad (2.4.4)$$

Наконец, для медленной магнитозвуковой волны:

$$\gamma_s = -k_z v_s \sqrt{\frac{\pi m}{8 M}} + \frac{n^i}{n} \frac{k_\perp^2 v_s^2}{\omega_i^2} k_z v_s \quad (2.4.5)$$

$$\frac{n_c^\alpha}{n} \sim \sqrt{\frac{m}{M}} \frac{\omega_i^2}{k_z^2 v_s^2} \quad k_\perp \geq \frac{\omega_i}{u}$$

Из сравнения (2.4.2), (2.4.4) и (2.4.5) следует, что при $v_A < u$ наименьший порог по относительной плотности - у альфвеновских волн. Например, при ($T_e \sim 20$ кэВ, $T_i \sim 10$ кэВ, $n \sim 10^{15}$, $H \sim 50$ кЭ)

$$\frac{n_c^\alpha}{n} \sim 2 \cdot 10^{-4} \quad (2.4.6)$$

2.4.2. Термоядерные неустойчивости на ионных циклотронных частотах

В рассмотренном примере альфвеновские волны возбуждаются при весьма малых значениях n^α/n . Однако в установках, где $v_A > u$, эти вол-

ны не возбуждаются. В этих условиях могут возбуждаться продольные колебания вблизи частот $\omega \approx \ell\omega_i$. Порог такой неустойчивости определяется выражением:

$$\frac{n_i^\alpha}{n} > \frac{\omega_i^2 u}{k_{\perp}^2 v_i^3} I_\ell(z_i) e^{-z} \chi_\ell^2 \quad (2.4.7)$$

где I_ℓ — модифицированная функция Бесселя, $z_i = \frac{k_{\perp}^2 v_i^2}{\omega_i^2}$

$$\chi_\ell^2 = \frac{(\omega - \ell\omega_i)^2}{k_z^2 v_i^2} > 1$$

2.4.3. Термоядерная неустойчивость неоднородной плазмы на частотах, близких к ионной ленгмюровской

Среди неустойчивостей неоднородной плазмы наиболее интересна неустойчивость, частота которой превышает ионную циклотронную, а ларморовский радиус велик в сравнении с длиной волны. В этом случае магнитное поле почти не нарушает прямолинейное движение быстрых ионов за время порядка периода колебаний. Поэтому в рассматриваемом случае продукты термоядерного синтеза не могут возбуждать продольные колебания пространственно однородной плазмы. Если же плазма пространственно не однородна, то, при условиях $kv_e/\omega_e \ll 1 \ll kv_i/\omega_i$; $\omega/k_z \gg v_e$; $k_z \ll k_{\perp}$; $n^\alpha/n \geq 10^{-3} \div 10^{-2}$, в ней возникает неустойчивость, время развития которой очень мало — порядка ω_i^{-1} [8]. Эта неустойчивость отличается от рассмотренных выше тем, что она не стабилизируется при повышении температуры реагирующих ионов. Для существования этой неустойчивости единственным необходимым условием по температуре ионов является условие $v_i \ll u$, которое должно всегда выполняться в термоядерных установках.

3. ТЕОРИЯ ЭЛЕКТРОМАГНИТНЫХ ФЛУКТУАЦИЙ В НЕЛИНЕЙНЫХ СРЕДАХ, НАХОДЯЩИХСЯ ВБЛИЗИ ГРАНИЦЫ НЕУСТОЙЧИВОСТИ

Коллективные колебания могут играть существенную роль в релаксационных процессах, например в том случае, когда плазма находится вблизи границы неустойчивости. Линейная теория флуктуаций предсказывает в этом случае неограниченный рост флуктуаций [1].

Покажем, что учет нелинейности среды приводит к ограничению амплитуд флуктуаций. Как известно, уравнение Максвелла для фурье-компонент электрического поля с учетом "сторонних" (не скоррелированных с полем) токов можно привести к виду:

$$\Lambda_{ij} E_j = -i \frac{4\pi}{\omega} \sum_i j_i^{\alpha 0} \quad (3.1)$$

где индекс α означает сорт частиц, а

$$\Lambda_{ij} = N^2 \left(\frac{k_i k_j}{k^2} - \delta_{ij} \right) + \epsilon_{ij}(\omega, \vec{k}, \vec{E}) \quad (3.2)$$

Используя (3.1), нетрудно получить следующее выражение:

$$\begin{aligned} & \Lambda_{ij}(\omega, \vec{k}, \vec{E}) E_i(\omega, \vec{k}) E_m^*(\omega', \vec{k}') \\ &= \frac{16\pi^2}{\omega\omega'^2} \Lambda_{m\ell}^{-1*}(\omega', \vec{k}', \vec{E}') \sum_{\alpha\beta} j_i^{\alpha 0}(k, \omega) j_j^{\beta 0*}(\omega', k') \end{aligned} \quad (3.3)$$

в (3.3) $\Lambda_{m\ell}^{-1}$ — оператор, обратный оператору $\Lambda_{\ell m}$, и равен

$$\Lambda_{m\ell}^{-1} = \frac{\Lambda_{m\ell}}{\Lambda}$$

Элементы матрицы $\Lambda_{m\ell}$ являются алгебраическими дополнениями к элементам матрицы $\Lambda_{m\ell}$, а Λ — определитель этой матрицы.

Вначале проанализируем причины возникновения в рамках линейной теории бесконечных флуктуаций на границе неустойчивости. Произведем, как обычно, усреднение по статистическому ансамблю хаотических фаз уравнения (3.3), записанного в линейном приближении. Спроектируем также полученное уравнение на направление \vec{e}^σ — собственного вектора волны σ . В результате получаем:

$$|\gamma_\sigma| I_k = \frac{16\pi^3 \text{Sp} \lambda e_m^* e_\ell}{\omega_\sigma^2 \langle e_i^* | \frac{\partial \Lambda_{ik}}{\partial \omega} | e_k \rangle | \frac{\partial \Lambda}{\partial \omega_\sigma} |} \sum_\alpha \langle j_i j_e \rangle_{k\omega}^{\alpha 0} \quad (3.4)$$

где

$$\langle E_i(\vec{k}, \omega) E_j^*(\vec{k}', \omega') \rangle e_i^* e_j = I_k \delta(\vec{k} - \vec{k}') \delta(\omega - \omega') \delta(\omega - \omega_\sigma)$$

Из (3.4) видно, что на границе неустойчивости ($|\gamma_\sigma| \rightarrow 0$) коэффициент при I_k обращается в нуль, в то время как правая часть (3.4) есть величина конечная. Это и приводит к формальному решению, дающему бесконечный рост спектральной плотности флуктуаций электромагнитного поля на границе неустойчивости. Чтобы устранить указанную некорректность, необходимо подставить в правую часть уравнения (3.3) тензор Λ_{ij} , вычисленный в нелинейном приближении. Производя ряд чисто алгебраических операций и используя известные соотношения для нелинейной части тензора диэлектрической проницаемости плазмы (см. напр. [12]), получим следующее уравнение:

$$\begin{aligned} \frac{dN_k}{dt} &= \gamma_k N_k + 4\pi \Sigma |v_{k,k',k''}|^2 \{ N_k N_{k''} - N_k N_{k'} \cdot \text{Sign}(\omega\omega') \\ &- N_k N_{k''} \cdot \text{Sign}(\omega\omega') \} \delta(\omega - \omega' - \omega'') \delta_{k, k'+k''} + \Sigma_k' \int N_k N_{k'} A(k, k' f_0) \\ &\times \delta(\omega_k - \omega_{k'} - (m - m')\omega_H - (k_{||} - k'_{||})v_{||}) d\vec{v} \\ &+ \frac{2\pi^2 \text{Sp} \lambda \Sigma_\beta \langle j_i j_k \rangle_{k\omega}^{\beta 0} e_i^* e_k}{\omega^2 | \frac{\partial \Lambda}{\partial \omega} |} \end{aligned} \quad (3.5)$$

здесь

$$N_k = I_k \frac{\langle e_i^* | \frac{\partial \Lambda_{ik}}{\partial \omega} | e_k \rangle}{\omega_k}$$

Уравнение (3.5) отличается от обычного кинетического уравнения слагаемым, учитывающим спектральную плотность флуктуационных токов, которая связана с медленно меняющейся частью функции распределения f_0^i таким же соотношением, как и в линейной теории [13]:

$$\langle j_i j_k \rangle_{\omega k}^{0i} = \sum_n \int \Pi_{ik} \delta(\omega - n\omega_H - k_{||} v_{||}) f_0^i(v) d\vec{v} \quad (3.6)$$

где

$$\Pi_{ij} = \begin{pmatrix} \frac{\ell^2 \omega_H^2}{k_{\perp}^2} J_{\ell}^2 & i v_{\perp} \frac{\ell \omega}{k_{\perp}} J_{\ell} J_{\ell}^{\dagger} & v_{||} \frac{\ell \omega_H J_{\ell}^2}{k_{\perp}} \\ i v_{\perp} \frac{\ell \omega_H J_{\ell} J_{\ell}^{\dagger}}{k_{\perp}} & v_{\perp}^2 J_{\ell}^{\dagger 2} & -i v_{||} J_{\ell} J_{\ell}^{\dagger} \\ v_{||} \frac{\ell \omega_H J_{\ell}^2}{k_{\perp}} & i v_{||} v_{\perp} J_{\ell} J_{\ell}^{\dagger} & v_{||}^2 J_{\ell}^2 \end{pmatrix} \quad (3.7)$$

Как видно из (3.5), при $\gamma = 0$ существует стационарное решение, дающее конечные значения для спектральной плотности флуктуаций электрических и магнитных полей.

4. ВЛИЯНИЕ ТЕРМОЯДЕРНЫХ НЕУСТОЙЧИВОСТЕЙ НА РЕЛАКСАЦИОННЫЕ ПРОЦЕССЫ В ПЛАЗМЕ

Рассмотрим случай, когда $v_A < u$. Тогда, как указано в разделе 2.4.1, наименьшее пороговое значение n^{α}/n формула (2.4.2), относится к альфвеновским волнам. Поскольку изменение концентрации n^{α} — процесс медленный, то функция распределения продуктов реакций F^{α} будет размазываться за счет квазилинейной релаксации достаточно быстро (за времена $\tau \approx \omega_{Hi}^{-1} (n v_A / n^{\alpha} u) \ln(n_{\alpha} \theta / w_0)$ [9], w_0 — начальный уровень шумов). Таким образом, плазма в течение достаточно большого промежутка времени будет находиться вблизи границы неустойчивости, т.е. $\gamma_A \approx 0$. Отсюда следует, что в правой части кинетического уравнения слагаемым $\gamma_A N_A$ можно пренебречь для волновых чисел $k_{\perp} \sim k_z \sim \omega_i / u$. Учитывая также, что альфвеновские волны в основном взаимодействуют с магнитогидродинамическими волнами [14], можно переписать уравнение (3.5) в виде:

$$\frac{\partial N_A}{\partial t} = \gamma_A N_A + \Sigma 4\pi |v_{k_1 k_2 k_3}|^2 (N_{k_1} N_{k_2} - N_k N_{k^*} \text{Sign}(\omega_A \omega^*)) \quad (4.1)$$

$$- N_k N_{k^*} \text{Sign}(\omega_A \omega^*) \delta(\omega - \omega' - \omega'') + 2\pi^2 \frac{n_{\alpha}^2 m_{\alpha} \omega_{H\alpha}^4}{n k_{\perp}^4 u v_A} J_1^2$$

$$\frac{\partial N_s}{\partial t} = \gamma_s N_s + \Sigma 4\pi |v_{k_s k_2 k_3}|^2 (N_{k_2} N_{k_3} - N_s N_{k_2} \text{Sign}(\omega_s \omega_3))$$

$$- N_s N_{k_3} \text{Sign}(\omega_s \omega_2) \delta(\omega_s - \omega_2 - \omega_3) \quad (4.2)$$

$$+ \sum_{k_2} \int N_s N_{k_2} A(k_s, k_2, f_0) \delta(\omega - \omega_{k_2} - (m - m')\omega_H - (k_{||} - k'_{||})v) dv$$

$$\frac{\partial N_m}{\partial t} = \gamma_M N_M + \sum 4\pi |v_{k_M k_4 k_5}|^2 (N_{k_4} N_{k_5} - N_M N_{k_4}) \text{Sign}(\omega_M \omega_5) \quad (4.3)$$

$$- N_M N_{k_5} \text{Sign}(\omega_M \omega_{k_5}) \delta(\omega_M - \omega_4 - \omega_5)$$

В квазистационарном режиме с помощью (4.1)-(4.3) можно оценить средние значения амплитуд пульсаций магнитогидродинамических волн:

$$N_m \leq N_A \approx 10^2 \frac{m_\alpha u^3}{v_A \omega_k} n_\alpha \quad (4.4)$$

$$N_s \approx 10^2 \frac{m_\alpha u v_A}{\sqrt{\beta} \omega_k} n_\alpha$$

Флуктуации, определяемые формулой (4.4), вблизи критических значений плотности (2.4.2), по порядку величины, совпадают с тепловыми. Однако при дальнейшем росте n_α эти флуктуации становятся существенно надтепловыми.

Из приведенного выше рассмотрения видно, что с помощью магнитогидродинамических волн происходит интенсивная передача энергии продуктов термоядерных реакций плазме за счет линейного затухания магнитогидродинамических волн на электронах и нелинейного — на ионах. Можно показать из (4.1)-(4.3), что нелинейное затухание на ионах становится порядка линейного затухания на электронах при $n^\alpha/n \approx 10^{-2}$. Таким образом, процесс передачи энергии продуктов реакций плазмы происходит следующим образом. Вначале греются электроны, а затем также интенсивно греются ионы. Скорость передачи энергии плазме определяется по порядку величины декрементом затухания медленных магнитозвуковых волн. Можно показать также, что диффузия плазмы вследствие развитых колебаний существенно превышает классическую.

ЛИТЕРАТУРА

- [1] СИТЕНКО, А.Г., "Электромагнитные флуктуации в плазме", Издательство Харьковского университета, Харьков, 1965.
- [2] ОРАЕВСКИЙ, В.Н., САГДЕЕВ, Р.З., ЖТФ 32 (1962) 1291.
- [3] КАДОМЦЕВ, Б.В., ПЕТВИАШВИЛИ, В.И., ЖЭТФ 43 (1962) 2234.
- [4] ГАЛЕЕВ, А.А., КАРПМАН, В.И., ЖЭТФ 44 (1963) 592.
- [5] СИЛИН, В.П., Журн. прикл. мех. техн. физ. 1 (1964) 31.
- [6] АРЦИМОВИЧ, Л.А., "Управляемые термоядерные реакции", Физматгиз, М., 1963.
- [7] POST, R.F., Revs. Modern Phys. 28 (1956) 338.
- [8] КОЛЕСНИЧЕНКО, Я.И., ОРАЕВСКИЙ, В.Н., Атомная энергия 23 (1967) 289.
- [9] КОРАБЛЕВ, Л.Л., РУДАКОВ, Л.И., ЖЭТФ 54 (1968) 818.
- [10] БЕЛИКОВ, В.С., КОЛЕСНИЧЕНКО, Я.И., ОРАЕВСКИЙ, В.Н., ЖЭТФ 55 (1968) 2210.
- [11] КОЛЕСНИЧЕНКО, Я.И., Украинский физический журнал 14 (1969) 1070.
- [12] ГАЛЕЕВ, А.А., КАРПМАН, В.И., САГДЕЕВ, Р.З., Ядерный синтез 5 (1965) 20.
- [13] СИТЕНКО, А.Г., КИРОЧКИН, Ю.А., Успехи физических наук 89 (1966) 227.
- [14] ОРАЕВСКИЙ, В.Н., Ядерный синтез 4 (1964) 263.

THERMAL INSTABILITY AND CONTROL OF FUSION REACTOR

M. OHTA, H. YAMATO*, S. MORI
 Japan Atomic Energy Research Institute,
 Tokai, Ibaraki-ken,
 Japan

Abstract

THERMAL INSTABILITY AND CONTROL OF FUSION REACTOR.

Steady-state fusion reactors will be achieved with plasmas heated by charged-particle or injection heating. Temperature and density of these plasmas can be unstable for deviations from the steady state. The stability criteria are obtained from linearized equations for deuterium-tritium plasma taking into account the difference between energy and particle confinement times. The possibilities of controlling these instabilities are also discussed in this paper.

There seems to be a critical operating temperature above which the reactor is stable. This temperature is determined from the functional dependence of the energy and particle confinement times on the temperature (T) and density (n). (1) When the energy confinement time is constant, the critical temperature corresponds to the minimum of F where F is the product of density and confinement time. (2) When the confinement time is proportional to $1/T$ as in the case of Bohm diffusion, the critical temperature is lower than in the previous case. (3) When the confinement time is proportional to $T^{1/2}n^{-1}$ as in classical diffusion, the critical temperature is higher. The temperatures for these three cases are 28 keV, 14 keV and 42 keV, respectively, in a charged-particle-heated reactor. A wider range of stable operating temperatures may be expected in an injection-heated reactor than in a charged-particle-heated reactor.

Since the operating temperature of steady-state fusion reactors probably will be in the unstable region, some kind of stabilization is indispensable to suppress this instability. Feedback stabilization by means of injection rate of fuel injection energy and radiation loss is investigated. The delay time in the process is taken into account. The stabilization is shown to be applicable when the feedback is carried out, observing the temperature deviations from a steady state. The non-linear evolution of temperature and density is analysed numerically.

1. INTRODUCTION

Fusion reactors will make use of steady-state plasmas or plasmas with successive pulses. In steady-state reactors, it will be important to keep the plasma parameters steady. We shall here discuss plasma instability with respect to density and temperature perturbations. This instability was discussed by Mills [1] in a different procedure. We shall also investigate feedback stabilization when a reactor is operated in an unstable regime. Although our discussions are restricted to D-T reactors in this paper, similar discussions can be applied to other types of reactors such as D-D reactors. The configurations are assumed to be closed-line systems in this paper. In open-ended systems, the operating temperature is higher and the instability may be less important.

* On leave from Research and Development Center, Tokyo Shibaura Electric Co., Ltd., Kawasaki, Japan.

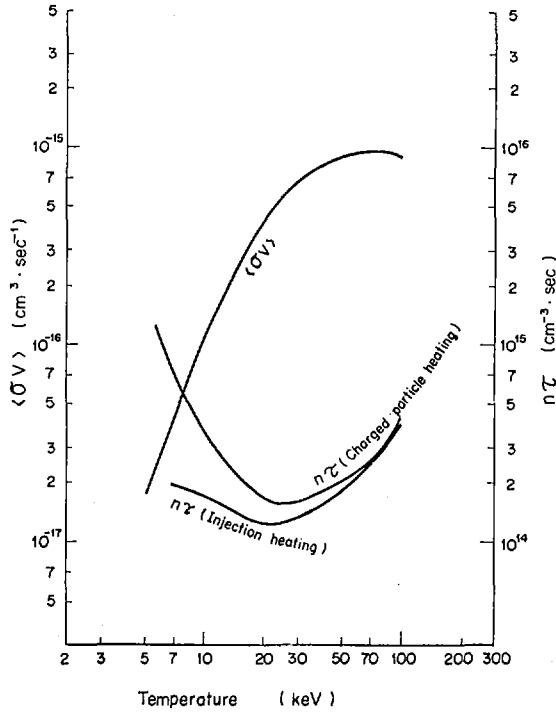


FIG.1. The reaction parameter $\langle \sigma v \rangle$ and $n\tau$ as a function of temperature. The product $n\tau$ is defined in Eq.(5) as $F(T)$, in which $R=1$ and $T_s=0$ keV are assumed in charged-particle heating and $R=10$ and $T_s=50$ keV are assumed in injection heating.

2. STEADY STATES

The density and temperature balance equations are as follows:

$$\frac{dn}{dt} = -\frac{n}{\tau_n} + S \quad (1)$$

$$\frac{dnT}{dt} = n^2 f(T) - \frac{nT}{\tau_E} + ST_s \quad (2)$$

$$f(T) = \frac{Q_c \langle \sigma v \rangle}{12} - 1.12 \times 10^{-15} T^{1/2} \quad (3)$$

where n (cm^{-3}) and T (keV) are plasma density and temperature, respectively. The ions and electrons are assumed to have the same temperature. The particle and energy confinement times are designated by τ_n and τ_E . The injected fuel rate is S ($\text{cm}^{-3} \text{s}^{-1}$), and the injected energy is $3T_s$ (keV). The function of temperature $f(T)$ consists of two terms. The first term comes from the power released in the plasma by the fusion reaction, where

Q_c is the energy carried by charged fusion products (3520 keV in the D-T reaction) and the reaction rate is given by $\frac{1}{4}n^2\langle\sigma v\rangle$. The second term in $f(T)$ designates bremsstrahlung losses. The energy loss due to cyclotron radiation is assumed to be small compared to the bremsstrahlung losses.

The steady state of a plasma is obtained by putting the left-hand sides of Eqs (1) and (2) equal to zero:

$$\frac{n_0}{\tau_{n0}} = S_0 \quad (4)$$

$$n_0\tau_{E0} = F(T_0), \quad F(T) = \frac{\xi_2 T}{f(T)} \quad (5)$$

$$\xi_2 = 1 - \frac{1}{R} \frac{T_s}{T_0}, \quad R = \frac{\tau_{n0}}{\tau_{E0}} \quad (6)$$

The subscript 0 indicates steady-state quantities.

When $T_s = 0$, a steady state is maintained by heating of charged-fusion products. To attain a steady state at lower τ_E , high-energy injection of fuel ($T_s \neq 0$) is applied. We call the former case "charged-particle heating" and the latter case "injection heating". The functions $F(T)$, as functions of temperature, are shown in Fig.1.

3. INSTABILITY

The plasma instabilities with respect to density and temperature deviations from the steady state are investigated by using linearized versions of Eqs (1) and (2); the time behaviour is obtained from the non-linear equations.

The perturbed density and temperature n' and T' are given by

$$\frac{1}{n_0} \frac{dn'}{dt} = -\left(\frac{1}{\tau_{n0}} + \frac{1}{\tau_{n1}}\right) \frac{n'}{n_0} - \frac{1}{\tau_{T1}} \frac{T'}{T_0} \quad (7)$$

$$\frac{1}{n_0} \frac{dn'}{dt} + \frac{1}{T_0} \frac{dT'}{dt} = \left(\frac{1}{\tau_1} - \frac{1}{\tau_{E0}}\right) \frac{n'}{n_0} + \left(\frac{1}{\tau_2} - \frac{1}{\tau_{E0}}\right) \frac{T'}{T_0} \quad (8)$$

$$\frac{1}{\tau_{n1}} = n_0 \left[\frac{\partial \tau_n^{-1}}{\partial n} \right]_0, \quad \frac{1}{\tau_{T1}} = T_0 \left[\frac{\partial \tau_n^{-1}}{\partial T} \right]_0 \quad (9)$$

$$\frac{1}{\tau_1} = \frac{1}{T_0} \left[2nf - nT \frac{\partial \tau_E^{-1}}{\partial n} \right]_0, \quad \frac{1}{\tau_2} = \frac{1}{n_0} \left[n^2 \frac{\partial f}{\partial T} - nT \frac{\partial \tau_E^{-1}}{\partial T} \right]_0 \quad (10)$$

where $1/\tau_n$ and $1/\tau_E$ are taken to be functions of n and T . If we assume n' and T' to be proportional to $\exp(\gamma t)$, γ is a solution of the quadratic equation

$$\gamma^2 + B\gamma + C = 0 \quad (11)$$

The parameters B and C are given by

$$B = \left(\frac{1}{\tau_{n0}} + \frac{1}{\tau_m} \right) - \left(\frac{1}{\tau_2} - \frac{1}{\tau_{E0}} \right) - \frac{1}{\tau_{T1}} \quad (12)$$

$$C = -\left(\frac{1}{\tau_{n0}} + \frac{1}{\tau_{n1}} \right) \left(\frac{1}{\tau_2} - \frac{1}{\tau_{E0}} \right) + \frac{1}{\tau_{T1}} \left(\frac{1}{\tau_1} - \frac{1}{\tau_{E0}} \right) \quad (13)$$

Therefore, plasmas are stable if the real part of τ (growth rate) is negative, or, in other words, if $B > 0$ and $C > 0$.

These are rather general stability criteria. To get on with our discussions, we must know dependence of τ_E and τ_n on n and T , which is not known at present. Here we assume

$$\tau_E \sim n^\ell T^m \quad (14)$$

τ_E and τ_n are assumed to have same dependence. From Eqs (9), (10), (12) and (13), we find the stability criteria:

$$\frac{\partial F_0}{\partial T_0} > \frac{F_0}{\xi_2 T_0} \left(m - \frac{1-\ell+m}{R} \right), \quad \frac{\partial F_0}{\partial T_0} (1-\ell) > \frac{2m F_0}{T_0} \quad (15)$$

TABLE I. STABILITY CRITERIA AND CRITICAL TEMPERATURE OF D-T FUSION REACTOR, WITH $F(T)$ GIVEN BY EQ. (5). THE REACTOR IS STABLE FOR $T > T_c$.

Dependence of τ_E	Stability Criteria	T (keV)	
		CPH*	IH**
$\tau_E = \text{constant}$	$\frac{T_0}{F_0} \frac{\partial F_0}{\partial T_0} > 0$	28	21
$\tau_E \sim T^{-1}$	$\frac{T_0}{F_0} \frac{\partial F_0}{\partial T_0} > -2, \quad -\frac{1}{\xi_2}$	14	5
$\tau_E \sim T^{1/2} n^{-1}$	$\frac{T_0}{F_0} \frac{\partial F_0}{\partial T_0} > \frac{1}{2}, \quad \frac{1}{2\xi_2} \left(1 - \frac{5}{R} \right)$	42	33

* Charged-particle heating ($T_s = 0$) $R=1$, $\xi_2=1$.

** Injection heating ($T_s \neq 0$) $T_s = 50$ keV, $R=10$.

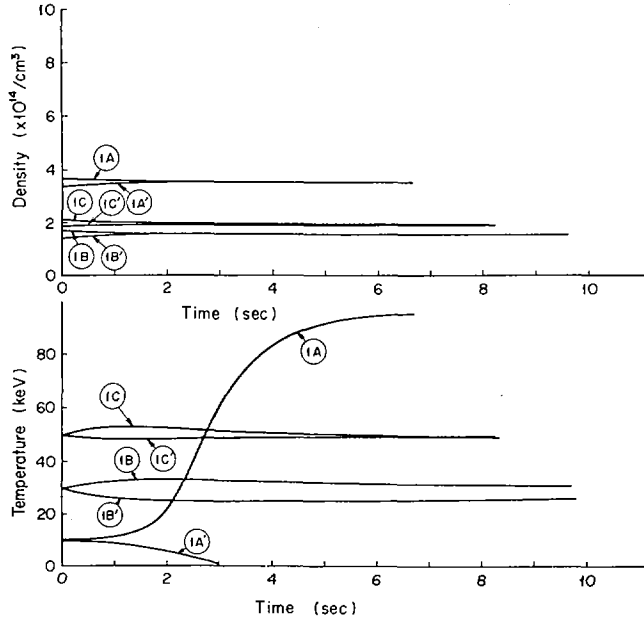


FIG. 2. Time behaviour of plasma temperature and density with constant confinement time for charged-particle heating, starting from equilibrium temperatures (10, 30 and 50 keV) and densities higher and lower than equilibrium.

We shall now give three examples: i) $\tau_E = \text{constant}$ ($\ell = 0$, $m = 0$), ii) $\tau_E \sim T^{-1}$ ($\ell = 0$, $m = -1$) as in Bohm diffusion, and iii) $\tau_E \sim n^{-1} T^{1/2}$ ($\ell = -1$, $m = 1/2$) as in classical diffusion. The stability criteria for these cases are listed in Table I.

These results show that reactor plasmas are stable when the derivative of $F(T_0)$ ($\tau_E n_0$ at an equilibrium) with respect to T_0 is greater than some constant (c) times $F(T_0)/T_0$. The function $F(T)$ has one minimum at $T = T_m$ and increasing function of T at $T > T_m$ as shown in Fig. 1. In the case i), the critical temperature T_c is equal to T_m because c is equal to zero. When c is positive, T_c is higher than T_m , while T_c is lower than T_m when c is negative. The values of T_c for cases i), ii) and iii) are also shown in Table I. A wider stable operating temperature is expected in an injection-heated reactor. As is shown in Fig. 1, T_m is lower in the case of injection heating.

If the operating temperature is stable, if the temperature increases by perturbations and even if the reaction rate increases at the same time, the temperature perturbation decreases because the change in the energy loss due to the dependence of τ_E on T overcomes the heating, and if the temperature decreases by perturbations, the energy loss decreases more rapidly than reaction rate and temperature reduction can be recovered. Thus the temperature dependence of τ_E may be considered a kind of feedback. This fact is suggestive for the problem of controlling the instabilities which will be discussed in the next chapter. Similar discussions can be made for the case of injection heating.

To demonstrate the validity of these stability criteria, we calculate density and temperature as functions of time from Eqs (1) and (2). These quantities are shown in Fig.2 for the case i). The initial temperatures are assumed to be in equilibrium, whereas the initial densities are shifted from equilibrium. When the initial temperature is 10 keV, the density approaches the equilibrium, but the temperature deviates with time. When the initial temperatures are 30 keV and 50 keV, both of them approach equilibrium. The stability criteria in Table I are supported by applying similar discussions to other cases.

4. FEEDBACK STABILIZATION

When a reactor is to be operated at an unstable operating temperature, i. e. $T < T_c$, some stabilization will be indispensable. In this chapter, we shall discuss the possibility of feedback stabilization in a simplified model, analytically with the help of linearized equations and numerically with non-linear equations.

Feedback stabilization may be applied in the following steps: (a) measurement of density or temperature deviations from the operating values, and (b) suppression of these deviations (temperature, density or both).

The controllable parameters are easily found from Eqs (1) and (2). They are 1) the particle confinement time τ_n , 2) the energy confinement time τ_E , 3) bremsstrahlung loss P_b , 4) injection rate of fuel S , and 5) injection energy $3T_s$. The confinement time may be controlled by magnetic fields or by enhanced diffusion resulting from plasma instability. Bremsstrahlung depends on impurity concentrations of plasma. Cyclotron radiation is also modulated. However, the system is probably stable without any control if cyclotron radiation is a dominant loss process because this radiation is strongly dependent on temperature. The injection rate and injection energy seem to be a good means of control. Even if these control procedures are very different from each other, the analysis of feedback stabilization is not so much different. The analysis is carried out by adding terms proportional to n'/n_0 and T'/T_0 to Eqs (7) and (8) depending upon what kind of control is adopted. The mechanism of stabilization may be considered to lie in the fact that addition of n'/n_0 , T'/T_0 terms modifies the dependence of energy loss and gain on density and temperature.

Here we shall assume τ_E and τ_n constant and discuss the stabilization of a plasma which is unstable unless any control is applied. It is easy to show that the term $\alpha(n'/n_0)$ included in Eqs (7) and (8) has no stabilizing effect. The reason is that a plasma is stable with respect to density perturbation only, whereas temperature instability can grow independently. Thus we shall investigate the following three cases by monitoring the temperature deviation:

- 1) Density control [Eq. (7) + $\alpha T'/T_0$]

Replacing B and C in Eqs (12) and (13) by

$$B = \frac{1}{\tau_{n0}} - \frac{1}{\tau_2} + \frac{1}{\tau_{E0}} + \alpha \quad (16)$$

$$C = -\left(\frac{1}{\tau_1} - \frac{1}{\tau_{E0}}\right) \alpha - \frac{1}{\tau_{n0}} \left(\frac{1}{\tau_2} - \frac{1}{\tau_{E0}}\right) \quad (17)$$

The coefficient α is given by

$$\alpha > \frac{1}{\tau_2} - \frac{1}{\tau_{n0}} \frac{1}{\tau_{E0}}, \quad \left(\frac{1}{\tau_1} - \frac{1}{\tau_{E0}}\right) \alpha < \frac{1}{\tau_{n0}} \left(\frac{1}{\tau_{E0}} - \frac{1}{\tau_2}\right) \quad (18)$$

2) Temperature control [Eq. (8) + $\alpha T'/T_0$]

Stability can be achieved when

$$\alpha < \frac{1}{\tau_{E0}} - \frac{1}{\tau_2} \quad (19)$$

3) Temperature and density control [Eqs (7) and (8) + $\alpha T'/T_0$]

We can apply feedback stabilization by means of S' which is proportional to T'/T_0 :

$$S = S_0 + S', \quad S' = \alpha_s T'(t - \Delta t) = \alpha_{n0} \frac{T'(t - \Delta t)}{T_0} \quad (20)$$

in which the delay time Δt is taken into account. Assuming T_s to be constant and $\gamma \Delta t \ll 1$, γ is obtained from

$$A\gamma^2 + B\gamma + C = 0 \quad (21)$$

$$A = 1 + (T_s/T_0 - 1) \alpha \Delta t \quad (22.1)$$

$$B = \frac{1}{\tau_{n0}} - \frac{1}{\tau_2} + \frac{1}{\tau_{E0}} - (T_s/T_0 - 1) \alpha + \frac{\alpha \Delta t \xi_2}{\tau_{E0}} \quad (22.2)$$

$$C = \frac{1}{\tau_{n0}} \left(\frac{1}{\tau_{E0}} - \frac{1}{\tau_2}\right) - \frac{\alpha \xi_2}{\tau_{E0}} \quad (22.3)$$

The system is stable if $A > 0$, $B > 0$, $C > 0$ or $A < 0$, $B < 0$, $C < 0$. The relation between the stabilizing α and the delay time Δt is shown in Fig. 3. For large Δt , feedback stabilization is not effective.

Figure 4 shows the development in time of plasma temperature in the injection-heated reactor as calculated by using the equations given above. When the operating temperature of the reactor is 15 keV, the reactor without feedback stabilization is unstable as is shown by the dotted line. On the other hand, if controlled injection is used satisfying the criteria of case 3), the plasma temperature is stabilized as shown by the solid lines. The time required for the temperature to approach the equilibrium decreases with the strength of feedback control.

In the case of a charged-particle-heated reactor with an operating temperature of 15 keV, the plasma temperature cannot be stabilized by controlling the injection rate. This case corresponds to density control in the previous analysis and the stability criterion of Eq. (18) is not satisfied.

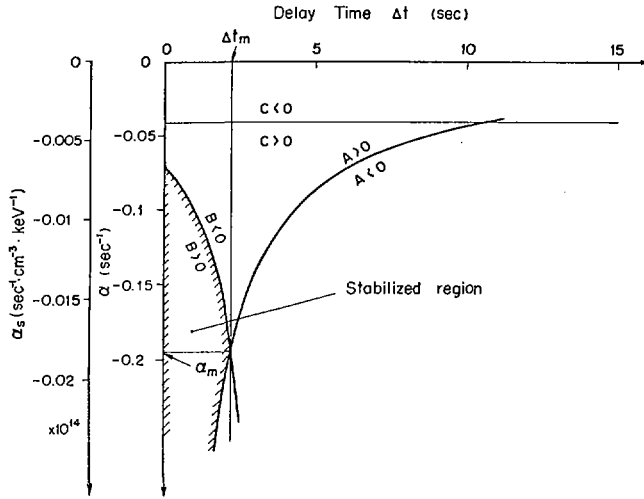


FIG. 3. Relation between coefficient α and delay time Δt satisfying Eq.(22) in an injection-heated reactor for $T_s = 50$ keV, $T_0 = 15$ keV and $R=10$. Stabilization is possible in the hatched region.

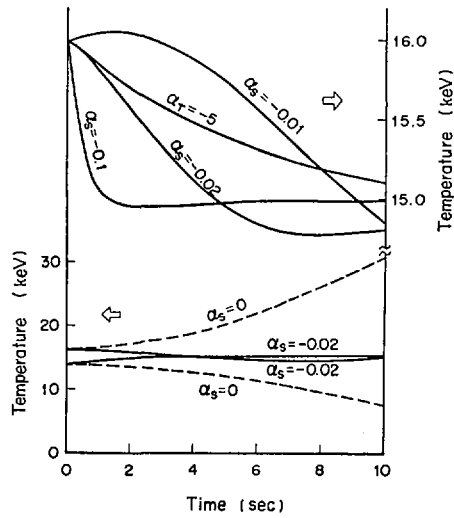


FIG. 4. Time behaviour of plasma temperature in an injection-heated reactor for $T_s = 50$ keV, $T_0 = 15$ keV, $R=10$ and $\Delta t = 0$ s. The real value of α_s used in Eq.(20) is obtained from the parameters shown in the figure multiplied by 10^{14} . The parameter α_T is given by $T_s = \alpha_T(T - T_0)$.

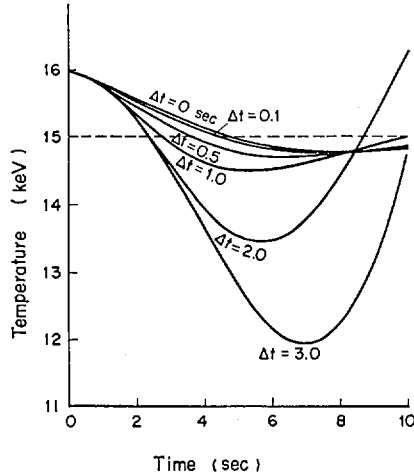


FIG. 5. Time behaviour of plasma temperature in an injection-heated reactor for $T_s = 50$ keV, $T_0 = 15$ keV, $R = 10$ and $\alpha_0 = -0.02 \times 10^{14} \text{ s}^{-1} \text{ cm}^{-3} \text{ keV}$.

Figure 5 shows the effects of the delay time Δt on the stability of plasmas in the injection-heated reactor. When the delay time Δt and the coefficient α are within the stabilized region in Fig. 3, the temperature approaches equilibrium in an oscillatory way, and the amplitude of the oscillation increases with the delay time. The temperature may be unstable for $t = 2.0$ or 3.0 s, which values are in unstable region of Fig. 3.

5. CONCLUSION

We have investigated the characteristics of the instability which modifies the temperature and density in a steady state: 1) The stability is given by critical temperatures, below which the plasma is unstable; 2) the critical temperature is determined by the dependence of the confinement times on temperature and density; 3) injection heating is favourable, as far as the instability is concerned. Feedback stabilization of this instability is shown to be applicable; 4) several kinds of feedback processes are discussed; 5) the effect of the delay time is also taken into account.

REFERENCE

- [1] MILLS, R.G., in Engineering Problems of Fusion Research (Proc. Symp. Los Alamos Scientific Laboratory) LA-4250 (1969) B1.

DISCUSSION

A. A. HUSSEINY: In Fig. 1, the difference in the behaviour of $n\tau$ for charged particle heating and injection heating is noticeable mainly for temperatures below 70 keV. Following the calculations closely, one can see that the difference is due to the use of oversimplified energy balance equations. It is assumed that fusion products heat the plasma for a period equal to the energy confinement time, while the heating time is longer in the case of injection heating. This might be true at high temperatures where the $n\tau$ values become the same for both cases. A more accurate energy balance equation than the one used here is that formulated by Rose (D. J. Rose, Nucl. Fusion 9 (1969) 183).

Another point is the invalidity of the assumption that alphas heat electrons predominantly. This assumption has been shown to be incorrect (A. A. Hussein, H. K. Forsen, Bull. Am. Phys. Soc. 15 (1970) 96).

R. G. MILLS: I would just like to comment that a very effective method of stabilizing the plasma temperature is to control the composition of the injected fuel. In the case of the D-T reactor, one should operate not at exactly 50% T, but at 45%, say. Feedback control of this percentage is then a fast and effective method.

H. P. FURTH: In your analysis of the thermal instability you did not consider the radial variation of the temperature; this means that you confined the analysis to the fundamental perturbation mode $T_1(r) \propto T_0(r)$. I should like to point out that higher radial mode numbers (for example, the mode where $T_1(r)$ is positive at $r = 0$ but negative at $r = a$) are much more difficult to stabilize by feedback; however, they tend to be stabilized by a sufficiently large thermal conductivity. This important thermal-stability problem still has to be investigated.

M. OHTA: We are now investigating the instability you mention. One method is to control the speed of the injected cold fuel. When the higher-mode instability occurs, the cold fuel injection speed will be decreased, so that the plasma surface is cooled. There would appear to be many other control methods apart from this.

ENGINEERING DESIGN STUDIES ON THE SUPERCONDUCTING MAGNET SYSTEM OF A TOKAMAK FUSION REACTOR*

M.S. LUBELL, W.F. GAUSTER, K.R. EFFERSON, A.P. FRAAS,
H.M. LONG, J.N. LUTON, C.E. PARKER, D. STEINER,
W.C.T. STODDART
Oak Ridge National Laboratory,
Oak Ridge, Tenn.,
United States of America

Abstract

ENGINEERING DESIGN STUDIES ON THE SUPERCONDUCTING MAGNET SYSTEM OF A TOKAMAK FUSION REACTOR.

A detailed engineering study has been made of a superconducting magnet system for a full-scale tokamak fusion reactor. For economic reasons, the main toroidal field must be produced by superconducting coils. We decided to employ compound conductors with twisted, thin filaments and a sufficiently high copper-to-superconductor ratio to provide both static and dynamic stability. Commercial superconductors which satisfy these criteria are NbTi compound conductors. The use of this material restricts for our design the maximum magnetic field strength (which results from the d.c. main toroidal field and the pulsed poloidal field) to about 80 kG.

We assumed a total power $P_T = 5000$ MW(th), a wall loading $P_w = 3.5$ MW/m², a vacuum chamber minor radius $r_w = 3.5$ m, a pressure ratio $\beta_\theta = 3$, and a stability margin $q = 1.4$. These values and the maximum field strength $B_M = 80$ kG yield a toroidal magnetic field $B_\phi = 37$ kG, a major radius $R = 10.5$ m, a minor coil radius $r = 5.59$ m, and a plasma aspect ratio $A = 3.75$, if we consider a blanket thickness $w = 2$ m and a ratio $\gamma = 0.8$ between plasma and vacuum chamber radii. The stored magnetic energy is about 40 000 MJ and about 1.45×10^6 m of compound conductor is required. The design of the mechanical structure is based on detailed force and stress calculations. The net radial force on each of the 48 coils is 10 580 tons, requiring massive reinforcement of the bobbins. The cryogenic calculations consider all sources of heat loads, and in the worst case about 75% of the total loss is due to the nuclear radiation. The structural design takes into consideration the assembly as well as maintenance and repair difficulties arising from radiation damage and neutron activation. Detailed cost estimates were made. We summarized the kind of major technological research and development work which is necessary for optimized realistic designs. Finally, an economic comparison is given between a 5000 MW(th) and a 1000 MW(th) reactor with the result that while the magnet system for the latter would cost only 43% as much, the unit cost is \$/kW(e) would be about double.

1. INTRODUCTION

Economic production of power by fusion will require the construction and operation of large superconducting magnet systems. The purpose of this paper is to investigate the engineering problems and economics associated with a superconducting magnet and cryogenic system for a fusion power plant. Our investigation is based on a tokamak reactor having a total output power P_T of 5000 MW(th). A discussion of the advantages and a cost estimate of smaller sized plants is also given.

* Research sponsored by the US Atomic Energy Commission under contract with the Union Carbide Corporation.

TABLE I. SYSTEM PARAMETERS

Assumed

Total output power: $P_T = 5000$ MW(th)
 Total wall loading: $P_W = 345$ W/cm²
 Vacuum chamber minor radius: $r_w = 3.5$ m
 Plasma size parameter: $y = 0.8$
 Blanket thickness: $w = 2$ m
 Pressure ratio: $\beta_\theta = 3$
 Stability margin: $q = 1.4$
 Maximum magnetic field: $B_M = 79$ kG

Calculated

Major toroid radius: $R \equiv P_T / 4\pi^2 r_w P_W = 10.5$ m
 Minor plasma radius: $r_p \equiv y r_w = 2.8$ m
 Plasma aspect ratio: $A \equiv R / r_p = 3.75$
 Inner radius of the magnet: $r = 5.6$ m
 Magnet aspect ratio: $a \equiv R / r = 1.88$
 Toroidal magnetic field: $B_\phi \equiv B_M (a - 1) / a = 37$ kG
 Poloidal magnetic field: $B_\theta \equiv B_\phi / qA = 7$ kG

2. TOROID PARAMETERS

Inasmuch as the relevant physics concerned with fusion in a toroidal machine have not been experimentally determined, the scaling of the parameters is not known, and therefore an optimum choice cannot be made. In order to get a self-consistent system, we assumed some parameters and utilized the expressions given by Golovin et al. [1] to calculate the remaining ones and the required fields. The results are listed in Table I. The toroidal magnetic field was determined from the equation

$$B_O \equiv B_\phi(r=0) = 17.4q(A^3 P_W^3 / y^3 \beta_\theta^4 P_T)^{1/8} \quad (1)$$

with the constraint that $B_M = 79$ kG. This latter condition results from our desire to avoid the use of the more costly and less reliable high field superconducting material Nb₃Sn and to construct the toroidal magnet entirely with NbTi alloy material. Using the numbers listed in Table I, we obtained $B_O = 37$ kG and the total number of amp-turns, 1.94×10^8 , from $NI = 5RB_O$. In this and all subsequent calculations, we have employed practical units, gauss, amp, cm, etc.

For a toroidal field generated by n cylindrical coils symmetrically arranged, the coil size is limited by the space available at the centermost part of the torus. If n is large, the polygonal shape of the inside contour about the major axis of symmetry can be replaced by a circle, and it is easy to obtain a general expression for the winding volume, V_w .

$$V_w = \frac{10\pi R B_0}{\langle j \rangle} \left[r + \frac{t}{2} \right]$$

(2a, b)

$$V_w = \frac{5\pi R B_0}{2 \langle j \rangle} \left[R + 3r - \frac{ng}{\pi} \pm \sqrt{\left(R - r - \frac{ng}{\pi} \right)^2 - \frac{10 R B_0}{\pi \langle j \rangle}} \right]$$

where $\langle j \rangle$ is the average overall current density, g is the bobbin end flange thickness where the coil cases just meet in the center, and t is the radial winding thickness. If we take $n = 48$, $B_0 = 37$ kG, and consider the production of the field by conventional, water-cooled copper solenoids, the power required for minimum $\langle j \rangle$ and maximum V_w is 1230 MW which clearly rules out steady state conventional coils. This solution is also invalid because the coils occupy most of the centermost space (70%) which will be needed for an iron core used for the induction of the plasma current (see Fig. 1). If we solve Eq. (2a, b) to minimize V_w and t and maximize the centermost space, the power required for a conventional coil is 3425 MW. For pulsed coils, although no precise operation cycle can be given, it is fairly certain from the estimates made of the reaction time that the capital cost and operational costs of the power supply would be significantly larger than the power needed for a superconducting magnet system.

3. SUPERCONDUCTING MAGNETS

Since the stored energy of the magnet needed for a fusion reactor is 4×10^{10} J or three orders of magnitude larger than any superconducting magnet that has been built and tested to date, extrapolation of present technology to larger size magnets must be done with extreme care. Experience has taught us that each significant increase to date was accomplished only

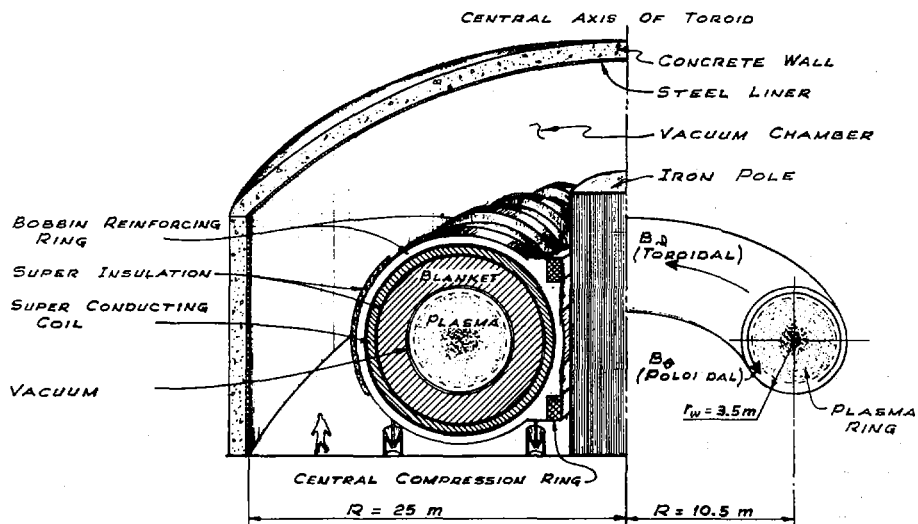


FIG.1. Schematic diagram of a tokamak fusion reactor. The structural reinforcement is not shown to scale.

TABLE II. SUPERCONDUCTING MAGNET CHARACTERISTICS

Stored energy:	$E_s = 4 \times 10^{10} \text{ J}$
Field volume:	$V = 6270 \text{ m}^3$
Amp-turns:	$2 \times 10^8 \text{ A-turns}$
Number of coils:	48
Average current density:	$\langle j \rangle = 1550 \text{ A/cm}^2$
Inductance (per coil):	$L = 67 \text{ H}$
Radial winding thickness:	$t = 51.5 \text{ cm}$
Axial winding length:	$S = 52.5 \text{ cm}$
Total compound conductor weight:	$1.2 \times 10^6 \text{ kg}$
Total magnet weight:	$3.73 \times 10^6 \text{ kg}$
Total compound conductor length:	$HF = 5.86 \times 10^5 \text{ m}$ $LF = 8.64 \times 10^5 \text{ m}$

after overcoming difficulties which were not always anticipated. In an analysis too long to present here [2], we concluded that an overall current density in the range between 1500 to 2000 A/cm² for a very large, completely stabilized magnet is compatible with extrapolation of known superconducting magnet performance.

To obtain a very high assurance of reliable magnet performance, we designed the magnet system to be completely stabilized, i.e. the superconductor is embedded in a sufficient amount of high conductivity normal material that a normal zone arising from either a local heat disturbance or exceeding the critical current will not propagate [3]. Barring failure of the cryogenic system, power supply, or some mechanical breakage, such magnets will not quench. This technique, coupled with the need for structural support to contain large hoop stresses, precludes operating at high overall current densities at least with the presently available commercial superconductors and normal matrix material. When reliability is of prime importance as in a utility application and cost and size secondary, a completely stabilized magnet is the proper choice.

Since stabilization of the compound conductor for the maximum field means that it is considerably overstabilized for the low field sections, we divided the windings into two subdivisions--one for the high fields (40 to 80 kG) at the innermost turns and one for the low fields (40 kG to almost zero). The low field material had the constraint that it carry the same current (i.e. operate in series with the high field material) and be equal in width. While it is always more economical to operate at the highest possible current density, in the present case of an inner bore very much larger than the winding thickness, it can be shown that the penalty of operating at decreased $\langle j \rangle$ is not severe. A decrease of 23% in the current density leads to an increase in conductor length of less than 1.5%. It therefore becomes worthwhile to consider current densities less than the maximum permitted if in doing so the coil dimensions and/or the compound conductor shape obtained are more convenient. The final choice made was $\langle j \rangle (HF) = 1300 \text{ A/cm}^2$ and $\langle j \rangle (LF) = 1800 \text{ A/cm}^2$, giving conductor dimensions with aspect ratio 3.2 and 2.1 to 1. The overall current density in the

magnet including stainless steel interleaving, insulation, and cooling channels is about $\langle j \rangle = 1550 \text{ A/cm}^2$. The pertinent information on the superconducting magnet system is tabulated in Table II.

The energizing losses are minimized and dynamic stability against the effects of the pulsed poloidal field is maximized by using very thin (diam. = $5 \times 10^{-3} \text{ cm}$) twisted superconducting filaments. In our system the losses are not so important, for the cryogenic system must be designed to handle the heat load after the magnet is energized and this is quite large owing to the nuclear radiation. When the magnets are being energized, no nuclear radiation is being produced, and hence the cryogenic system has ample reserve to handle the energizing losses. The effect of a pulsed poloidal field on a superconducting magnet can only be determined by experiment.

4. FORCES, STRESS, AND MECHANICAL STRUCTURE

The net force on each coil is a radial force toward the center of the torus. There is no net axial force on a coil unless one or more should quench, and then the net axial force is even larger than the radial force. In addition to these forces which must be contained by additional structural reinforcement, there is also the hoop stress and axial compression on the winding in each coil.

A computer code was used to calculate the components of the magnetic field and Lorentz force in a large number of subdivisions of the coil cross section. The summation of the components yielded a total net radial force on each coil of 10,580 tons ($9.6 \times 10^6 \text{ kg}$) toward the center of the toroid.

In the fault case of one coil quenched, the axial component on the neighboring coil is 11,630 tons. For both the standard operating and fault cases, the total forces are very large; however, since the areas are also large, the stresses remain manageable. Unfortunately, the static net radial force and bending moment require large reinforcement rings.

The force acting on the magnet coil could be supported in a number of different ways. To avoid structure on the top, bottom, and outside of the torus, which would intrude severely on the space around the reactor and make maintenance operation difficult, we decided to transfer the high radial loads to two massive rings in compression as indicated in Fig. 1. One of these rings would be just below the top of the torus and the other just above the bottom. In addition to resist the large bending moments, each bobbin also had to be reinforced with a massive outer steel ring. This outer ring can be shrink-fitted to the coil and then it might be sealed by trepanning the surface adjacent to the joint and applying a light seal weld. In this manner, the closed box formed around the coils can serve as the container for the liquid helium.

The assumption was made that the bobbin reinforcing ring could be analyzed as a circular curved beam of uniform cross section [4]. This assumption is conservative in that the minimum cross section was used in the analysis and because the coil cover rings would contact each other in the region near the torus center. The analysis indicated that the bobbin reinforcing rings would have a peak bending moment of $2.197 \times 10^8 \text{ in.-lb}$, a tensile force of $1.410 \times 10^7 \text{ lb}$, and a shear force of $4.21 \times 10^6 \text{ lb}$ at the surface closest to the torus center. The combination of bending and normal stresses amounts to 74,400 psi (52 kg/mm^2). Considering the conservative nature of the analysis, this stress should be acceptable. The axial forces induced because of the loss of a coil may be supported through compression jacks located at a number of points around the bobbin flange. This would give relatively little interference with other elements between the coils such as the cooling lines for power removal from the blanket.

TABLE III. SUMMARY OF POWER INPUT
TO CRYOGENIC SYSTEM (WATTS)

1.	Heat conduction through structural supports. (Epoxy fiberglass at 30% $\sigma_y = 75$ ksi, $\langle \kappa \rangle = 3$ mW/cm-K)	10
2.	Joule losses in coils. (Internal and external connections)	168
3.	Thermal radiation through superinsulation. (Thickness of 20 and 25 cm; $\langle \kappa \rangle$ of 0.45 and 0.35 μ W/cm-K; over toroidal surfaces 2320 m ² and 2800 m ² , respectively)	322
4.	Heat input through vapor-cooled leads. (10 W @ 5000 A per pair, refrigeration at 5 x loss)	1200
5.	Nuclear radiation. (Attenuation through blanket = 10^{-6})	5000
TOTAL		6700

The forces tending to draw the coils closer to the torus axis were assumed to be restrained by the central compression rings alone. For a radial force of 21×10^5 lb per coil and the support rings located as discussed, the average bearing stress on the ring surface is 20,000 psi, and the cross sectional area in the rings assuming a compressive hoop stress in the material [5] at half the yield value is 1600 in.² (1 m²).

We envision the whole structure installed in a circular room 165 ft in diam. and 90 ft high as indicated in Fig. 1. The room will have 4-ft thick reinforced concrete walls and floors with a stainless steel liner to permit evacuation to 10^{-4} torr. Thus, the magnets do not need to have a vacuum wall, and superinsulation can be wrapped around the magnet bobbins and their support structure. The magnets would be supported by the floor through a steel frame attached to the coils by fiberglass members in tension (much like a hammock).

5. CRYOGENICS

The heat load which determines the amount of refrigeration consists of a number of items which are listed in Table III. The total heat load using a conservative estimate for the blanket attenuation (10^{-6}) and absorption of all neutrons and gammas passing through the blanket is 6.7 kW. Eight 1 kW refrigerators (at least one spare is needed) are sufficient to handle the operating losses, and these would require about 3.6 MW of input power.

Using only the refrigeration power needed for steady state operation of the reactor will result in 60 days for the initial cool-down of the system. Once it is in operation, we anticipate that in many instances the system could be shut down and routine maintenance conducted without warming the coils to room temperature. Additional refrigeration to aid in cool-down can be supplied by units which will be used for cooling the pulsed induction field windings after the system is in operation. In this manner an occasionally used capital cost item is avoided.

6. PLASMA REQUIREMENTS

Using an expression given by Golovin et al. [1], the plasma current is $I_p = 10$ MA with inductance, if the plasma is taken as a ring of uniform current density, of 2.2×10^{-6} H. Therefore, the stored energy is 1000 MJ, and the flux produced by the plasma is 220 V-sec. Utilizing a magnetic material with a high saturation (permandur), there is sufficient area in the toroid center to produce more than 230 V-sec, if the saturation is reversed during a pulse. Unlike ORMAK, the copper current leads for the pulsed field will probably be nitrogen-cooled and placed around the iron so that the large heat dissipation will not be absorbed in the water shield. The peak joule losses are 3.8 MW at liquid nitrogen temperature. The total input power required for operating conventional nitrogen refrigerators is about ten times the heat load at 77 K. The required power depends on the duty cycle of the pulsed coil, but it will be large. This makes it worthwhile to consider superconducting winding for production of the pulsed field as well as the steady state toroidal field.

7. ECONOMICS

A realistic cost analysis which is sufficiently detailed that it may be revised periodically is useful even though complete requirements for the plasma reaction cannot be specified at this time. To avoid confusion, the term coil will be used to designate a single solenoid, and magnet will be reserved for the torus of n coils. The magnet system can be broken down into a number of components, which are enumerated in Table IV. The cost of the overall vacuum chamber housing for the reactor is included in the costs for the general structural requirements.

The cost of superconducting material, although high, has been decreasing steadily over the last five years as indicated recently by Komarek [6]. In fact, the cost has been cut in half since 1966. Shown in Fig. 2 is the field dependent unit cost $u(B)$ in mills/A-ft for NbTi compound conductor as of late 1970. The line designated normal quantities is an average value for the costs of a number of conductors obtained from a number of different manufacturers for standard quantities (10^4 to 10^5 ft). The dashed line is based in part on an estimate that the extremely long lengths required for a fusion reactor magnet will cost half the price of normal quantities and on quotations from commercial manufacturers. The cost values used by other workers for fusion reactor size magnets is also indicated in the figure. It appears that Oswald [7] was too conservative and Lee et al. [8] too optimistic in their estimates.

From Table IV, the total magnet system cost is \$70,520,000. Thus, the compound conductor cost in this example is 37%. Assuming a plant thermal efficiency of 50%, the unit cost of this magnet system is approximately \$28/kW(e).

8. MAGNET COST FOR OTHER SIZES

For a prototype plant, a smaller size than a 5000 MW(th) plant is highly desirable. For such a prototype plant, the capital cost per kilowatt would not play as important a role as either the total capital investment or the necessity of a successful demonstration.

A reactor with smaller output power and lower wall loading implies also that a lower magnetic field will suffice. A lower wall loading means a reduction in the neutron damage problem, and this is important because replacement of the vacuum wall is difficult and time consuming. Based on current tests, a 10 to 20 year life can be expected for a Nb wall in a 1000 MW(th) reactor. The lower magnetic field means a cost saving not only in superconducting material and winding but also in the structural

TABLE IV. COST ESTIMATE FOR SUPERCONDUCTING MAGNET SYSTEM (10^6 \$)

	5000 MW(th)	1000 MW(th) ^a
1. <u>Compound Conductor</u> : $I[l_{HFu}(80) + l_{LFu}(40)]$; HF + LF = 15.5 + 10.6	26.1	(10.44)
2. <u>Stainless Steel Interleaving</u> : Armco 21-6-9 ^b @ \$1/lb	4.17	(1.67)
3. <u>Insulation</u> : Epoxy fibreglass @ \$400/ft ³ ; interleaving + interpancake = 0.25 + 0.85	1.10	(0.44)
4. <u>Bobbin</u> : Armco 21-6-9 @ \$1/lb; 4 x material	6.61	(3.3)
5. <u>Winding</u> : @ \$1/ft = 4.75 @ \$2/lb = 13.64 average	9.20	(3.68)
6. <u>Structural Reinforcement</u> : Armco 21-6-9; Central compression ring, 4 x material = 2.4; bobbin reinforcement ring, 1.75 x material = 15.7	18.1	(7.24)
7. <u>Cryogenic Insulation</u> : \$215/m ² for 25 cm thick; inside + outside = 0.5 + 0.6	1.1	(1.1)
8. <u>Storage Dewars</u> : Two 30,000 gal @ \$150,000	0.3	(0.3)
9. <u>Refrigeration</u> : Eight 1 kW units @ \$380,000	3.04	(1.52)
10. <u>Power Supply</u> : Silicon control rectifiers 40 V, 5 kA; 24 units @ \$100/kW	0.5	(0.35)
11. <u>Auxiliary Items</u> : Vapor-cooled leads, protective shunts, thermal indicators, pressure regulators, switches, etc.	0.3	(0.25)
TOTAL	70.52	(30.29) ^a

^aThe numbers in this column are estimated from general formulas rather than specific calculations (see Section 8).

^bSee Reference 5.

reinforcement material needed. The cryogenic problem is also ameliorated because the nuclear radiation is the major loss component (75% in the sample studied), but even more significant is the smaller overall weight of the system which can then be cooled down in a reasonable time interval. The problems concerned with the heat transfer in the blanket and the lithium pumping system will also be significantly reduced. Whether these advantages are enough to offset the increase in the capital cost per kilowatt of capacity and the lower efficiency (some of the loss terms such as power supply, refrigeration, pulsed coil losses will not decrease as rapidly as output power), remains to be determined.

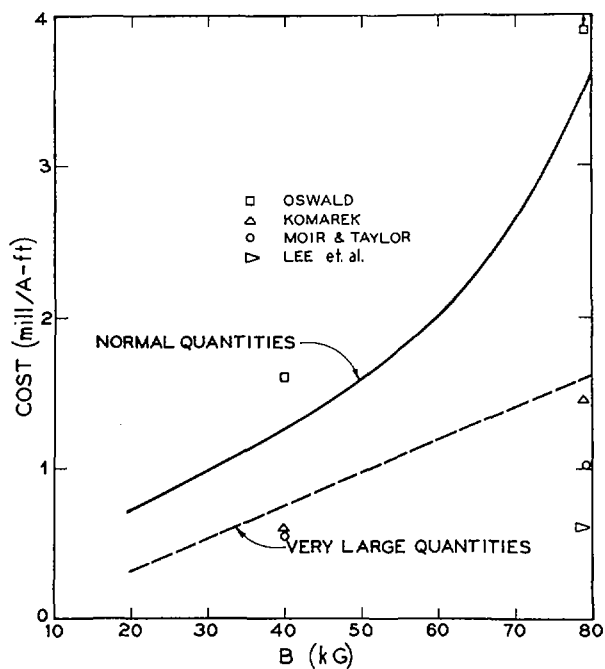


FIG.2. The unit cost of NbTi compound conductor versus magnetic field for normal lengths (10^4 - 10^5 ft) and for very long lengths ($\geq 10^6$ ft).

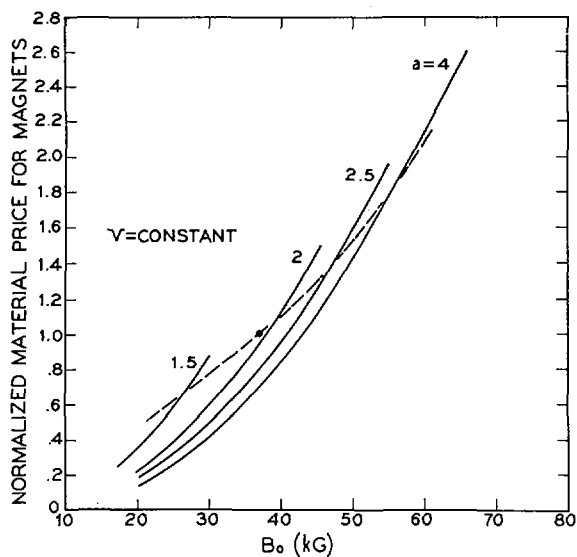


FIG.3. NbTi compound conductor price for large toroidal magnetic systems relative to our design versus toroidal magnetic field for various aspect ratios, $\alpha = R/r$. The dashed line indicates the cut-off for $B_M = 80$ kG.

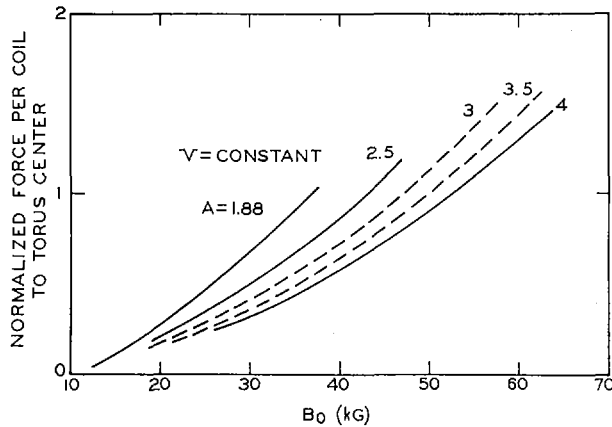


FIG. 4. Net radial force to torus centre relative to our design versus toroidal magnetic field for various aspect ratios, $a = R/r$.

For a large toroidal magnet, the total length of wire is the total number of turns times the average length of one turn which to good approximation is given as $\mathcal{L} = N 2\pi(1.05 r)$. Using the A-turn relation, $\mathcal{L} I = 10\pi B_0 R(1.05 r)$ in A-cm, and the cost in dollars is $C = 3.28 \times 10^{-5} \mathcal{L} I u(B)$, where $u(B)$ is given in Fig. 2. If the expression for $\mathcal{L} I$ is substituted in the cost along with $A = R/r$ and the constraint that the field volume remain constant, we find for the material cost

$$C = K a^{1/3} B_0 \langle u(B) \rangle \quad (3)$$

where K is a constant value equal to 5.15×10^{-4} for C in million dollars. Again, we consider the windings to consist of 41% and 59% of high and low field material, respectively. Equation (3) is shown plotted in Fig. 3 for various values of magnet aspect ratio A and central field B_0 . The cost is normalized to our design for the 5000 MW(th) reactor. It can be seen in Fig. 3 that for our design, A , the material cost, is cut in half by reducing the central field to $B_0 = 27$ kG. For the same field as our design, a doubling of A means only a reduction of the cost by 30%. These percent reductions in the cost of material can be used for the stainless steel and insulation interleaving and the winding cost.

An approximate formula for estimating the net radial force in dynes per radian on one coil tending to pull the coil toward the torus center is given by assuming a thin winding thickness. The result is $F_r/\varphi = 10^{-7} (NI)^2 [a(a^2 - 1)^{-1/2} - 1]$. With the constraint of constant volume and 48 coils, we obtain for the force per coil in tons

$$F_r = 17.5 B_0^2 a^{4/3} [a(a^2 - 1)^{-1/2} - 1] \quad (4)$$

with B_0 in kG. A graph of F also normalized is shown in Fig. 4 for various values of A and B_0 . Keeping A constant and considering a reduction of B_0 to 26 kG, the force is reduced in half. Keeping the field constant at our design value, we note that a doubling of A leads to a force of only 50%. The force varies faster with A at constant B_0 than the material cost.

Now we must analyze how a reduction in the central field affects the power output of a tokamak system. For constant plasma parameters (A , β_θ , and q), the central field is related to power according to Eq. (1) as $B_0 \propto (P_w/P_t)^{1/8}$. For a power reduction by a factor ξ , the magnetic field decreases as $\xi^{-1/4}$. Since a magnetic field reduction of 33% means a cost reduction of 60%, this corresponds to a total power reduction of 80%. Hence, by this analysis utilizing general formulas rather than specific detailed calculations, a fusion reactor with a total output of $P_T = 1000$ MW(th) and a wall loading $P_w = 69$ W/cm² would cost 43% as much as the 5000 MW(th) reactor studied in this paper. If we assume that the electrical output is fixed at 50% thermal for plants in this size range, then from the above examples we see that reducing the total power output from 5000 MW(th) to 1000 MW(th) leads to a doubling of the unit cost from \$28/kW(e) to \$60/kW(e). Whether this scaling price is economically acceptable can only be determined when the cost of all the other parts of the system are also known and when an accurate determination is made of how the operating power losses scale with output.

9. CONCLUSIONS

Large stable superconducting magnet systems operating at overall current densities in the range 1500 - 2000 A/cm² with maximum fields (in the windings) up to 80 kG appear technically feasible. The unit capital cost of a magnet system for a 5000 MW(th) fusion reactor plant was estimated to be \$28/kW(e). In magnet systems of this size, containment of the magnetic forces requires massive structural reinforcement of the bobbins. One problem introduced by this large mass is that the initial cool down time may be quite long. In our system, if we use only the refrigeration power required for the plant in normal operation, the initial cool down time is two months. In all likelihood this time can be shortened considerably by using the additional refrigeration required for the losses in the windings which produce the pulsed poloidal field. Whether the pulsed coil utilizes normal metals at either 77 or 20 K or superconductors at 4.2 K, the amount of refrigeration power needed will be large.

It appears that many of the difficulties encountered with the forces, power losses, and radiation damage are ameliorated by reducing the toroidal magnetic field and lowering both the output power and wall loading. Although the unit capital cost for the magnet system is twice as high for a 1000 MW(th) reactor as for a 5000 MW(th) reactor of equal physical dimensions, the total capital cost is less.

Finally, we would like to note that since it seems necessary to have the structural reinforcement in the cryogenic system and to avoid the use of dewars, future magnet systems for fusion applications may utilize compressed (single phase) helium flow in hollow compound conductors [10].

REFERENCES

- [1] GOLOVIN, I. N., DNESTROVSKY, Yu. N., KOSTOMAROV, D. P., Proceedings Nuclear Fusion Reactor Conf., Culham (1970) 1.
- [2] See our more detailed report, ORNL-TM-3404 (June 1971).
- [3] STEKLY, Z. J. J., ZAR, J. L., IEEE Trans. Nuclear Science NS-12 (1965) 367.
- [4] MARTIN, H. C., "Introduction to Matrix Methods in Structural Analysis," McGraw Hill Company, New York (1966).
- [5] Armco 21-6-9 stainless steel has a yield stress at 4.2 K of 196 ksi (138 kg/mm²) and a tensile stress of 245 ksi.

- [6] KOMAREK, P., 6th Symposium on Fusion Technology, Aachen (September 1970).
- [7] OSWALD, B., Int. Cryogenic Engineering Conf., Berlin (May 1970).
- [8] LEE, J. D., WERNER, R. W., MYERS, B., MOHR, P. B., CARLSON, G. A., CHRISTOFILOS, N. C., 5th Intersociety Energy Conversion Engineering Conf. Energy 70, Las Vegas, Nevada (September 1970).
- [9] MOIR, R. W., TAYLOR, C. E., 5th Intersociety Energy Conversion Engineering Conf. Energy 70, Las Vegas, Nevada (September 1970).
- [10] MORPURGO, M., Report CERN 69-25 (September 1969).

DISCUSSION

D. J. ROSE: Other papers in this session seem to call for substantially higher magnetic fields than those you refer to in your detailed example here. Could you comment on the possibility of making very large superconducting magnets for substantially higher fields? What is the limiting factor, the superconducting material or the mechanical stress?

M. S. LUBELL: We chose the upper limit of 80 kG for the magnetic field because in the present state of the art we felt that only NbTi could be reliably scaled up to fusion-reactor magnet size. Our aim was to obtain a realistic cost estimate for a large magnet system that we regarded as technically feasible.

Nb₃Sn and V₃Ga have been employed in small magnets up to 150 kG, and the latter material can be used to higher fields of perhaps 200 kG. The largest magnet built to date, with a magnetic field at the winding greater than 100 kG, had a bore of only 40 cm. No high-field fully stabilized magnet has yet been built. At each stage in the development of superconducting magnets, problems have been encountered — some of them not anticipated. Present high-field materials (Nb₃Sn and V₃Ga) cannot be reliably scaled up by a factor of 25. However, by the time fusion reactors are ready for construction, we feel that further improvements in the present superconducting materials like the commercial V₃Ga and Nb₃Sn, and the development of other materials like Nb₃Al and Nb₃(Al_xGe_{1-x}), will enable us to construct superconducting magnets with maximum fields at the windings approaching 200 kG.

At present we are limited at high fields because of inadequate material and insufficient knowledge, but we suspect that mechanical stresses will ultimately prove to be the limiting factor.

R. HANCOX: A basic assumption in your magnet design is that the maximum field does not exceed 79 kG, so that the NbTi superconductor can be used. This is because of your desire to "avoid the use of the more costly and less reliable high-field superconducting material Nb₃Sn". Since no commercial fusion reactors will be built for 30 or 40 years, I suggest that this assumption is too conservative. Indeed, the opposite situation may be true in future, since critical current densities are already a factor of five higher in Nb₃Sn than in NbTi and have a potential for further development, so that when large-scale production brings the cost of superconductors down to a level approaching the cost of basic materials it is likely that Nb₃Sn will be cheaper than NbTi.

M. S. LUBELL: I have no doubt that large magnets can be built with these materials. Our purpose was to find a system that had integrity today and to estimate its cost. Such systems will have to be up-dated continuously

in the future. I am optimistic about superconducting magnets, but if you completely stabilize a magnet the high current density will partially get washed out by the amount of normal material that you have to put in. I am waiting to see some results on coils in which completely stabilized Ni_3 is used.

F. L. RIBE: Your estimates project costs for the NbTi superconducting material using low critical fields. It seems to me that in the next 20 years or more there is time for the development of new superconducting materials, some of which show estimated critical fields near 700 kG at 4°K. Correspondingly higher temperatures should be used at fields of 100 kG to 200 kG.

M. S. LUBELL: The high critical field estimate of 700 kG to which you refer is based on an idealized set of parameters. It has not been experimentally demonstrated that such high values can be approached for present commercial superconductors. It is also possible that new superconducting materials will be found with a critical temperature T_c higher than 20.7°K, and if the upper critical field increases as T_c increases such new materials may have a very high critical field. Both of these possibilities show less promise than the development of presently known high field material into a commercial reality.

The highest measured critical field at 4.2°K is 410 kG for an $Nb_{0.79}(Al_{0.73}Ge_{0.27})_{0.21}$ alloy having a critical temperature of 20.7°K. The compound Nb_3Al also has an upper critical field of 300 kG. It has not yet been shown that these materials can carry a high transport current density at high fields and, even if they can, a suitable fabrication procedure would have to be developed for commercial production. Nevertheless, it seems worthwhile spending money on the achievement of this goal and looking for new high-field superconductors. Most likely, a successful method could be developed for the high-field materials known at present.

Any increase in the operating temperature over the boiling point of liquid helium will result in a lower cost for refrigeration. However, the cost of refrigeration is a small fraction of the total cost, and the increased material cost due to the lower current density at the higher temperature must also be considered. If a serious shortage of liquid helium should ever develop, a superconductor applicable for the hydrogen range would of course be desirable.

S. BLOW: The major cost in stellarator systems arises from the helical windings. The torsatron version of the stellarator has a "built-in" method of diversion. For a realistic comparison between Tokamak and stellarator, one must assume either (a) a pulsed Tokamak with an expensive energy storage system or (b) a d. c. Tokamak (in which case a diverter is necessary).

In case (b), do you not think that the provision of magnetic coil windings for diversion might be a major cost item, at least comparable to the cost of the normal axial windings?

M. S. LUBELL: Our primary concerns have been the economics and engineering problems of a steady-state superconducting toroidal magnet system for a pulsed Tokamak reactor power plant; we have not looked into the other necessary components in any detail and have made no cost comparisons with other possible systems. The point you raise is a good one, and you are certainly correct that a realistic cost comparison must consider all the components. Nevertheless, it may be premature to make

serious comparisons, for we lack even conceptual designs for some components, and in the final analysis we have to concentrate on the machine that proves feasible.

As regards case (b), we cannot specify costs for a diverter, if one is needed, since no convincing design is available, but we agree that it would probably be expensive; for case (a), the pulsed poloidal field will most likely also involve superconducting windings and, while this system may be relatively expensive, the energy storage system utilizing acyclical generators will not be expensive, at least its cost will be nothing like the cost of the toroidal windings.

EMERGENCY COOLING AND RADIOACTIVE-WASTE-DISPOSAL REQUIREMENTS FOR FUSION REACTORS*

D. STEINER

Oak Ridge National Laboratory, Oak Ridge, Tenn.,
United States of America

Abstract

EMERGENCY COOLING AND RADIOACTIVE-WASTE-DISPOSAL REQUIREMENTS FOR FUSION REACTORS.

The emergency cooling and radioactive waste-disposal requirements anticipated for fusion reactors are compared with those requirements posed by fission reactors. A reference fusion reactor is used as the basis for comparison. This reactor is based on the D-T fuel cycle and employs a blanket consisting of niobium as the structural material, lithium as the coolant, and graphite as the neutron moderator and reflector.

Relative to fission reactors, the reference fusion reactor exhibits the following advantages with respect to emergency cooling requirements: (1) a lower hazard potential associated with radioactive inventories, (2) lower nuclear power densities during operation and for many hours following shutdown, (3) no potential for nuclear energy insertions resulting from loss of coolant or meltdown, and (4) a more favourable coolant passage geometry. The management of radioactive wastes should require fewer operations for fusion reactors than for fission reactors, and, therefore, the associated economic penalty should be less.

The effects of alternate fusion fuel cycles and alternate blanket structural materials are summarized. Fusion reactors operating on the D-³He fuel cycle would exhibit less stringent emergency cooling and radioactive-waste-disposal requirements than would reactors operating on either the D-T or D-D fuel cycles. Of the several blanket structural materials considered, vanadium has the most desirable characteristics with regard to emergency cooling and radioactive waste disposal.

1. INTRODUCTION

Emergency cooling in the event of an accident and disposal of radioactive wastes are important economic and environmental considerations in the technology of fission reactors. The purpose of this paper is to investigate the emergency cooling and radioactive waste-disposal requirements anticipated for fusion reactors and to compare these requirements with those posed by fission reactors.

A reference fusion reactor is first described. Then, the emergency cooling and radioactive waste-disposal requirements of the reference fusion reactor are discussed in relation to the respective requirements for fission reactors. Finally, the effects of alternate fusion fuel cycles and alternate blanket structural materials are considered.

2. REFERENCE FUSION REACTOR

As the reference fusion reactor (RFR) I shall employ the conceptual reactor design proposed by Fraas [1]. This reactor design is based on the D-T fuel cycle and employs a blanket consisting of niobium as the structural material, lithium as the coolant, and graphite as the neutron moderator and

* Research sponsored by the US Atomic Energy Commission under contract with the Union Carbide Corp.

TABLE I. HAZARD POTENTIAL ASSOCIATED WITH THE PRINCIPAL RADIOACTIVE INVENTORIES OF THE RFR AND A TYPICAL PWR

	RFR		PWR		
	^3H (as HTO)	$^{93\text{m}}\text{Nb}$	^{95}Nb	^{131}I (on crops)	^{239}Pu
Activity (curies/W(th))	1.20×10^{-2}	8.76×10^{-2}	1.55×10^{-1}	3.17×10^{-2}	2.93×10^{-5}
Maximum permissible concentration ^a ($\mu\text{curies}/\text{cm}^3$)	2×10^{-6}	4×10^{-8}	3×10^{-8}	1.4×10^{-12}	6×10^{-13}
Relative biological hazard (activity \neq MPC)	6×10^3	2.2×10^6	5.2×10^{6b}	2.3×10^{10}	4.9×10^7

^aMaximum permissible air-borne concentrations for a 168 hour week as recommended by the National Committee on Radiation Protection [4].

^bWhen all the activation products of niobium are accounted for, the total relative biological hazard is about a factor of four higher than this value.

reflector. The energy flux associated with the fusion neutrons incident on the first wall of the blanket is taken as 10 MW/m^2 . Because of exothermic neutron reactions the power generated within the blanket is approximately 12.5 MW/m^2 . The neutronic behavior of fusion reactor blankets has been considered in previous studies [2,3]; the values of the operating power densities and the neutron-induced afterheat and activity reported herein are calculated by the methods described in references [2] and [3]. The tritium inventory of the reactor is assumed to be 6 kg for a 5000 MW(th) reactor. The RFR is a representative design, but, by no means, an optimized design.

2.1. Emergency cooling requirements

The emergency cooling requirements of a fission reactor are usually discussed in terms of a hypothetical reference accident, i.e., the "design basis accident". For example, the design basis accident for light-water reactors is a loss of coolant resulting from a primary system rupture of any size up to an instantaneous double-ended rupture of the largest pipe attached to the reactor pressure vessel. Since the design of fusion reactors is only in the conceptual stage, it would be premature to talk about the design basis accident for fusion reactors. Therefore, any discussion of fusion reactor safety at this time must be considered speculative. However, such speculation is instructive and, by drawing heavily on the technology of fission reactors, the emergency cooling requirements anticipated in fusion reactors can be placed in perspective.

Emergency core-cooling systems (ECCS) are employed in fission reactors because of their postulated effectiveness in preventing the release of radioactivity to the public in the event of an accident which involves the normal cooling system of the reactor. Public safety must also be the objective of emergency cooling systems for fusion reactors. Therefore, it is of interest to compare the relative hazard potential associated with the principal radioactive inventories of fusion and fission reactors. Table I shows such a comparison for the RFR and for a typical pressurized-water reactor (PWR); note that the radioactive inventories are based on one watt of reactor thermal power. As a measure of the relative biological hazard, I have employed the activity divided by the maximum permissible air-borne concentration as recommended by the National Committee on Radiation Protection. Although this is a somewhat arbitrary definition of relative biological hazard, it is useful for the comparisons presented here. The results presented in Table I indicate that the potential biological hazards of a fusion reactor are expected to be considerably less than those of a fission reactor; note particularly the factor of about 10^6 difference in relative biological hazards associated with

TABLE II. SUMMARY OF SOME CRITICAL TEMPERATURES FOR THE STRUCTURE OF THE RFR AND FOR THE CLADDING OF A PWR AND OF AN LMFBR

	<u>RFR</u>	<u>PWR</u>	<u>LMFBR</u>
Material	Niobium	Zircaloy	Stainless Steel
Operating temperature (°F)	1100-1800	600-700	1100-1300
Melting temperature (°F)	~ 4500	~ 3400	~ 2600

the volatile radioisotopes, ^3T and ^{131}I . Davies [5] proposes a reliability of one failure in every 10^8 trials for the ECCS of a liquid-metal fast-breeder reactor (LMFBR) on the basis of the the maximum possible release of the volatile radioactive inventory, i.e., total release of the ^{131}I inventory. On the same basis one could propose a reliability of one failure in every 10^2 trials for the emergency cooling system of the RFR. The preceding observations suggest that the emergency cooling system of a fusion reactor may have less stringent requirements for reliability than does the ECCS of a fission reactor.

The design requirements of the ECCS in a fission reactor are usually based on the temperature limitations of the fuel cladding. Table II summarizes some critical temperatures for the structure of the RFR and for the cladding of a PWR and of an LMFBR. Note that the margin between cladding operating temperature and cladding melting temperature is much smaller for the LMFBR than for either the RFR or the PWR.

Emergency cooling must be effective within a time scale which is consistent with both the temperature limitations of the reactor materials and the sources of thermal energy. There are three sources of thermal energy which must be considered, i.e., nuclear, stored and chemical energy.

Table III summarizes the nuclear power densities associated with the niobium structure of the RFR¹ and with the oxide fuels of a typical PWR and LMFBR. The nuclear power densities in the structure of the fusion reactor are significantly less than those characteristic of fission reactor fuels. Because the specific heats of niobium and the oxide fuels are comparable the rate-of-rise of the niobium temperature will be significantly less than the rate-of-rise of the fuel temperature in the event of a loss-of-coolant accident, e.g., at shutdown the adiabatic temperature rise associated with the average afterheat power density would be $\sim 2^\circ\text{F}/\text{sec}$ for the niobium, $\sim 10^\circ\text{F}/\text{sec}$ for the PWR fuel, and $\sim 50^\circ\text{F}/\text{sec}$ for the LMFBR fuel. However, it is also noted that the afterheat decays less rapidly for the niobium than for the fuel, and that, about one month following shutdown, the afterheat power densities in the niobium and the PWR fuel are comparable.

Two additional observations concerning sources of nuclear energy are important. First, since the fusion reaction is independent of the conditions of the coolant, loss of coolant can not lead to an insertion of nuclear energy, a situation which may arise in a fission reactor with a positive void coefficient. Second, since the fusion reaction does not depend on the configuration of the blanket, meltdown of the structure can not result in an insertion of nuclear energy, a situation which may arise in a fission reactor when the core is not designed to be in the most reactive configuration.

The stored energy, i.e., the enthalpy, of the blanket should not present a serious design requirement for emergency cooling of a fusion reactor. However, stored energy can be a significant heat source in fission reactors. For example, in a light-water reactor, redistribution of the stored energy of the fuel is a major source of energy for cladding heating following a loss-of-coolant accident and is effective within ~ 30 sec after the accident.

Table IV summarizes the principal chemical sources of energy in the RFR, a PWR and an LMFBR. For comparison this table also gives the energy in the afterheat integrated for the first 1/2 hour after shutdown. In both the RFR and the LMFBR, alkali metal-water reactions are a potential source of

¹Plasma radiation might increase the operating power densities listed in Table III by a few percent.

TABLE III. NUCLEAR POWER DENSITIES ASSOCIATED WITH THE NIOBIUM STRUCTURE OF THE RFR AND WITH THE OXIDE FUEL OF A TYPICAL PWR AND LMFBR.

	<u>RFR</u>	<u>PWR</u>	<u>LMFBR</u>
Average operating power density (watts/cm ³)	52	270	1500
Maximum to average operating power density	~ 2	~ 2	~ 2
Average afterheat power density at shutdown (watts/cm ³)	2.7	19	105
Maximum to average after-heat power density	~ 2	~ 2	~ 2

Ratio of Afterheat at Time, t, to Value at Shutdown, t=0

<u>t</u>			
1 minute	1.0	0.54	0.54
1 hour	1.0	0.20	0.20
1 day	0.90	0.08	0.08
1 month	0.35	0.03	0.03

TABLE IV. CHEMICAL SOURCES OF ENERGY AND ENERGY IN AFTERHEAT FOR THE RFR, A PWR AND AN LMFBR

	<u>RFR</u>	<u>PWR</u>	<u>LMFBR</u>
Energy in alkali metal reaction [BTU/watt(th)]	0.2	0	0.7
Energy in zirconium-water and subsequent hydrogen-oxygen reactions [BTU/watt(th)]	0	0.08	0
Energy in afterheat integrated for first 1/2 hr. after shutdown [BTU/watt(th)]	0.004	0.05	0.05

steam generator failure. The possibility of such a failure limits the dependence which can be placed on the steam generator system during an emergency cooling situation and, therefore, requires that the ECCS include reliable back-ups. In light-water reactors the zircaloy-water reaction may produce energy in excess of the afterheat if the zircaloy temperature exceeds ~ 2100°F, and therefore, imposes a limitation on the time available for activation of the ECCS [6].

TABLE V. LONG-LIVED ACTIVITIES IN THE NIOBIUM STRUCTURE OF THE RFR AND IN THE SPENT FUEL OF A FISSION REACTOR

Nuclide	Mean Life (yrs.)	Activity Generation Rate [curies/W(th)-yr]	Accumulated Activity @ 1000 yrs. [curies/W(th)]	Maximum Permissible Concentration (μ curies/cm ³)	Relative Biological Hazard (Activity @ 1000 yrs. \div MPC)
Niobium					
^{93m} Nb	19.6	8.8×10^{-3}	0.17	4×10^{-8}	4.2×10^6
⁹⁴ Nb	2.9×10^4	2.9×10^{-6}	2.9×10^{-3}	Not given	-
Spent Fuel					
⁹⁰ Sr	40.4	6.7×10^{-4}	2.7×10^{-2}	10^{-10}	2.7×10^8
¹³⁷ Cs	43.4	9.3×10^{-4}	4.0×10^{-2}	5×10^{-9}	8.0×10^6
⁹⁹ Tc	3.0×10^5	1.2×10^{-7}	1.2×10^{-4}	2×10^{-8}	6.0×10^3

^aMaximum permissible air-borne concentration for a 168-hour week as recommended by the National Committee on Radiation Protection.

In addition to the preceding observations the following points are also of interest.

(1) Both the RFR and LMFBR employ a low pressure coolant so that loss of coolant can not occur rapidly and small leaks can be detected; there is no rapid depressurization such as that which accompanies faults in light-water reactors.

(2) Fission reactor cores are characterized by a large number of narrow coolant passages; this is especially the case for the LMFBR. Since the blankets of fusion reactors should exhibit a small number of large coolant passages, the probability of a coolant passage blockage appears to be much smaller in fusion reactor blankets than in fission reactor cores.

2.2. Radioactive waste-disposal requirements

The purpose of this section is to place in perspective the radioactive waste-management problem which may accompany fusion power. Tables V and VI compare the significant long-lived activities, i.e., $T_{1/2} > 10$ years, in the niobium structure of the RFR with the most important long-lived activities in the spent fuel of a fission reactor. Table V gives the annual rate at which activity is generated, normalized to one watt of reactor thermal power, the accumulated activity resulting from 1000 years of continuous generation², and the relative biological hazard associated with this amount of activity. Table VI gives the annual rate at which afterheat is generated, as a fraction of the reactor thermal power, and the accumulated afterheat resulting from 1000 years of continuous generation.

The results presented in Tables V and VI indicate that the potential biological hazards and heat generation rates associated with long-lived activities are comparable for the activated niobium structure and the fission products. Thus, the problems associated with disposal of these long-lived activities should be comparable. However, disposal is only one aspect of radioactive waste management. It is currently envisioned that the management of the high-level liquid wastes from fuel reprocessing plants will involve a series of operations consisting of interim liquid storage, pot calcination (solidification), interim solid storage, shipment, and disposal in salt mines. The costs of such a management scheme are estimated to range between 0.03 to 0.05 mill/kwhr [7]. It seems reasonable to assume that management of the activated niobium structure would require only interim solid storage, shipment, and disposal in salt mines. These three operations together represent ~ 10 -20 percent of the estimated management costs for the high-level liquid wastes. Moreover, cladding hulls resulting from the chop-leach dissolution of spent fuel present a radiation problem which approaches that of the high-level liquid wastes. No costs have yet been ascribed to the management of the cladding hulls, however, it appears that they will require interim solid storage, shipment, and disposal in salt mines. On the basis of the preceding observations I would suggest that the management costs associated with the activated niobium structure would be less than those associated with spent fuel by an amount which approximates the management costs associated with the high-level liquid wastes, e.g., ~ 0.03 to 0.05 mill/kwhr.

3. ALTERNATE FUSION REACTOR DESIGNS

The emergency cooling and radioactive waste-disposal requirements which will accompany fusion power depend on the fuel cycle and blanket structural

²It appears more reasonable to consider the accumulated activity at 1000 years rather than at steady state which requires $\sim 10^6$ years of continuous generation for some radionuclides.

TABLE VI. LONG-LIVED AFTERHEAT IN THE NIOBIUM STRUCTURE OF THE RFR AND IN THE SPENT FUEL OF A FISSION REACTOR.

Nuclide	Afterheat Generation Rate (fraction of reactor thermal power/year)	Accumulated Afterheat @ 1000 Years (fraction of reactor thermal power)
	Niobium	
^{93m}Nb	1.6×10^{-6}	3.1×10^{-5}
^{94}Nb	3.0×10^{-8}	3.0×10^{-5}
	Spent Fuel	
$^{90}\text{Sr}^a$	3.3×10^{-6}	1.3×10^{-4}
$^{137}\text{Cs}^b$	4.3×10^{-6}	1.9×10^{-4}
^{99}Tc	6.3×10^{-11}	6.3×10^{-8}

^aAfterheats include contribution of ^{90}Y .

^bAfterheats include contribution of ^{137m}Ba .

material. Calculations [8] for alternate fusion fuel cycles indicate that, relative to the D-T fuel cycle, (1) the D-D fuel cycle exhibits an operating power density which is about a factor of two lower and an induced afterheat and activity which are comparable, and (2) the D-³He fuel cycle exhibits an operating power density which is about a factor of five lower and an induced afterheat and activity which are about 40% lower. In these calculations the blanket structural requirements are assumed to be the same for each fuel cycle.

I have been evaluating blanket designs which employ alternate structural materials, e.g., molybdenum, vanadium, iron, titanium, and tantalum. The results of this evaluation indicate that vanadium has the most desirable characteristics with regard to emergency cooling and radioactive waste disposal. If vanadium were employed as the structural material in the RFR, (1) the operating power density would be about a factor of three lower and the afterheat power density about a factor of two lower than with niobium and (2) the values of the accumulated activity, relative biological hazard and accumulated afterheat would each be between three and four orders of magnitude lower than the values of the respective quantities for niobium. Vanadium exhibits no long-lived activities as a result of its activation products, but only as a consequence of impurity activation products. Within a week after shutdown the activity of vanadium would be governed by the impurity activation products. Thus, long-term emergency cooling might not be necessary with a vanadium blanket structure. Moreover, the use of vanadium as the blanket structure might allow a totally different approach to radioactive waste management in a fusion power economy, e.g., recycle of the blanket structure. It is certainly premature to state that vanadium satisfies all the nuclear-engineering requirements of fusion blanket design, however, the results presented here suggest a strong incentive for pursuing vanadium as the blanket structural material.

As a final point I would like to note that the energy flux of fusion neutrons assumed for the RFR, i.e., 10 MW/m^2 , is a variable design parameter. Neutron radiation damage may indeed require lower incident wall loadings. Quantities normalized to one watt of thermal output are not sensitive to the value of the wall loading. However, the nuclear power densities are directly proportional to the value of the wall loading.

4. CONCLUDING REMARKS

The emergency cooling and radioactive waste-disposal requirements anticipated for fusion reactors appear to be less severe than those requirements posed by fission reactors.

Relative to fission reactors, fusion reactors should exhibit the following advantages with respect to emergency cooling requirements: (1) a lower hazard potential associated with radioactive inventories, (2) lower nuclear power densities during operation and for many hours following shut-down, (3) no potential for nuclear energy insertions resulting from loss of coolant or meltdown, and (4) a more favorable coolant passage geometry. In addition, the economic penalty for management of radioactive wastes should be less for fusion reactors than for fission reactors.

On the basis of the results presented here, vanadium emerges as an excellent choice for the structural material of fusion reactor blankets. It is indeed striking to consider that, if vanadium proves to be an acceptable blanket structural material, disposal of long-lived activities may not be a concern in a fusion power economy.

REFERENCES

- [1] FRAAS, A. P., POSTMA, H., Preliminary Appraisal of the Hazards Problems of a D-T Fusion Reactor Power Plant, ORNL-TM-2822 (Revised), Oak Ridge National Laboratory (1970).
- [2] STEINER, D., "The Nuclear Performance of Fusion Reactor Blankets," Nucl. Appl. Tech. 9 (1970) 83.
- [3] STEINER, D., The Neutron Induced Activity and Decay Power of the Niobium Structure of a D-T Fusion Reactor Blanket, ORNL-TM-3094, Oak Ridge National Laboratory (1970).
- [4] Maximum Permissible Body Burdens and Maximum Permissible Concentrations of Radionuclides in Air and in Water for Occupational Exposure, Recommendations of the National Committee on Radiation Protection, NBS Handbook 69 (1959).
- [5] An Appreciation of Fast Reactor Safety (1970), United Kingdom Atomic Energy Authority, Chapter 7.
- [6] LAWSON, C. G., Emergency Core-Cooling Systems for Light-Water-Cooled Power Reactors, ORNL-NSIC-24, Oak Ridge National Laboratory (1968).
- [7] Siting of Fuel Reprocessing Plants and Waste Management Facilities, ORNL-4451, Section 6, Oak Ridge National Laboratory (1970).
- [8] STEINER, D., "Neutron Irradiation Effects and Tritium Inventories Associated with Alternate Fuel Cycles for Fusion Reactors," to be published in Nuclear Fusion 11, 3 (1971).

NEUTRONIC AND THERMAL DESIGN ASPECTS OF THERMONUCLEAR FUSION REACTOR BLANKETS

H. BORGWALDT, W. H. KÖHLER*, K. E. SCHROETER
Institut für Neutronenphysik und Reaktortechnik,
Kernforschungszentrum Karlsruhe,
Federal Republic of Germany

Abstract

NEUTRONIC AND THERMAL DESIGN ASPECTS OF THERMONUCLEAR FUSION REACTOR BLANKETS.

Discrete ordinate transport theory calculations are presented for the tritium breeding ratio and power density profiles from neutron and γ -heating in the first wall, the blanket and the reflector of a cylindrical thermonuclear fusion reactor operating on the D-T cycle. Lithium isotopic composition and coolant (Li or flibe) are varied as parameters. Some of the breeding ratio calculations are checked with Monte-Carlo calculations. The results indicate that there should be no problem obtaining adequate tritium breeding, which is optimal at approximately the natural Li isotopic composition. Power densities in structural material are quite high and almost exclusively due to γ -heating. Switching from Li coolant to flibe increases the power produced in the blanket by about 15%, while it decreases the tritium breeding ratio between 10 and 20%.

1. INTRODUCTION

1.1 General Blanket Design Objectives and Problems

In the first generation of fusion reactors, that will, in all likelihood, operate on the D-T cycle, the two main blanket design objectives are breeding of tritium and extraction of energy from fusion neutrons. The major blanket design problems are, in increasing order of severity, in the areas of neutronics and photonics, thermohydraulics and radiation damage to materials.

Tritium breeding proceeds via the $\text{Li}_7^6(n,\alpha)\text{T}$ reaction, with a $1/v$ cross section below a few keV, and the $\text{Li}_7^6(n,\alpha')\text{T}$ reaction with a threshold of 2.47 (MeV). Because of the high energy (14.1 MeV) of the D-T reaction neutrons, the possibility of neutron multiplication by $(n,2n)$ and even fast fission reactions exists, to increase the tritium breeding by the $\text{Li}_7^6(n,\alpha)\text{T}$ reaction.

About 80% of the D-T reaction energy is fast neutron kinetic energy and only 20% α -particle kinetic energy. Hence about 80% of the power output of D-T fusion reactor will have to come from the blanket. Actually the power output of the blanket will exceed 80% of the total power output of the D-T reactor, because neutron reactions in the blanket give rise to more additional energy than the energy lost to the blanket by neutrons that penetrate the blanket and lose most of their kinetic energy in the reactor shield.

* On leave from Texas A & M University.

To give a rough idea of the thermohydraulic and radiation damage problems involved, one can say that the power density, due to neutron and γ -heating in the blanket close to the vacuum wall will be of the order of magnitude of power densities in oxide-fueled, Na cooled fast breeder reactors 0.5 (megawatt/liter) and the fast neutron fluence in the first wall will be of the order currently expected in fast reactor clads: 3×10^{23} (cm⁻²). The exact figures will depend on the neutron energy flux (megawatt/m²) through the first wall that designers will be able to accommodate.

1.2 Previous Work and Scope of This Paper

Following the initial work by ROSE [1] and co-workers [2], [3] on fusion reactor blanket design aspects, more detailed neutronics work was done by STEINER [4]. The state of the art of fusion reactor blanket design is very well documented in the proceedings of the 1969 Culham Conference; STEINER [5], Blow et al [6], and LEE [7], presented neutronics and power density calculations based on either Li or $2(\text{LiF}-\text{BeF}_2)$ called "flibe" as a coolant. Flibe is considered as an alternate coolant because of the possibly excessive pumping power requirements when the liquid metal Li flows through the strong magnetic field that contains the plasma. WERNER [8] introduced Na heat pipes into the blanket design and moved the vacuum wall outside the moderator region following the power producing and tritium breeding blanket. The heat pipes provide a surface between the plasma and the moderating fluid and distribute the energy more evenly, thus allowing more uniform coolant flow at different radial positions. This design should allow considerably higher neutron energy fluxes into the blanket than previous designs; perhaps as much as 200 (megawatt/m²) as compared to 10 (megawatt/m²) in STEINER's designs. WERNER et al [9] presented a blanket design of this type for ASTRON fusion reactors. CARLSON [10] treated some of the thermal aspects of such a blanket design.

As an alternative to liquid metal or flibe coolants gas cooling has been proposed [11] for fusion reactor blankets.

In this paper we present preliminary calculations on tritium breeding ratios and on power density profiles in the first wall, the blanket and the reflector, where both the Li isotopic abundance and the coolant (Li or flibe) are chosen as parameters.

The calculations are based on codes and cross section sets available at the present time and involve certain approximations to be spelled out in the following section.

2. CALCULATION MODEL

2.1 Geometry

One dimensional cylindrical geometry with piecewise constant reaction cross-sections was chosen for the multigroup neutron and γ -flux calculations. Region I, outer radius 100 cm, represents the plasma, region II, outer radius 220 cm is a vacuum but contains a very low density of He⁴ for calculational reasons in the S_N code, region III, outer radius 410 cm, is the tritium breeding and power generating blanket and region IV, outer radius 460 cm, represents a carbon reflector.

2.2 Plasma conditions and neutron energy flux

The plasma conditions define the neutron source. We assume a D-T plasma with the following conditions: ion temperature $T_i = 60$ (keV) and deuteron and triton densities of 10^{14} (cm^{-3}). This gives rise to a volume source of 14.1 (MeV) neutrons, S_{14} , and a volume source of $S_{2.5}$ of 2.5 (MeV) neutrons [1]:

$$S_{14} = \langle \sigma v \rangle_{DT} n_D n_T = 8.8 \times 10^{12} (\text{cm}^{-3} \text{sec}^{-1}) \quad (1)$$

$$S_{2.5} = \frac{1}{4} \langle \sigma v \rangle_{DD} n_D^2 = 4.0 \times 10^{10} (\text{cm}^{-3} \text{sec}^{-1}) \quad (2)$$

These sources, assuming an isotropic distribution, give rise to a moderate neutron energy flux of 4.48 (MW/m^2). By contrast, the rather high heat fluxes (not neutron energy fluxes) through the cladding of projected fast breeder reactors, amount to about 3 (MW/m^2).

It is, however, not clear that a neutron energy flux of 4.48 (MW/m^2) can be accommodated even with heat pipes in the blanket, especially in view of the swelling problems caused by high fast neutron fluence in the first wall and in the structural materials. The fast neutron flux at the wall for this source would be about 2×10^{14} ($\text{cm}^{-2} \text{sec}^{-1}$) leading to a neutron fluence in 20 years (with a load factor of 0.8) of about 1×10^{23} (cm^{-2}).

However, for the purposes of our calculations, the tritium breeding ratio is independent of the source strength and the power generation profile in the blanket as well as the neutron fluence are linear functions of the source, or the neutron energy flux through the first wall. We can therefore scale all these results to any acceptable value of the incident neutron energy flux.

2.3 Blanket parameters

Without going into any detail on construction, the breeding and energy conversion blanket is considered to be similar to that proposed by WERNER [8], containing Na heat pipes in the radial direction, and coolant tubes in the axial direction. Structural material is Mo and the coolant is either Li or flibe. For both coolants three values of ${}^6\text{Li}$ isotopic enrichment are considered: 7.4% (natural Li), 50% and 95%. It is assumed, for the purposes of neutronic calculations, that the blanket consists of a homogeneous mixture of 70 vol % coolant, 20 vol % Na heat pipes and 10 vol % structural material. Based on these assumptions the number densities of different nuclei are summarized in TABLE I.

2.4 Neutronics Calculations

Neutronics calculations are performed in 26 energy groups using S_4 discrete ordinate transport theory in one dimensional cylindrical geometry. Some of these calculations are also performed using Monte Carlo.

The energy structure and the cross sections for the S_4 calculations are essentially those of the BONDARENKO [12] set with the following major alternations: 1) a new first energy group covering the range from 10.5 to 14.0 (MeV) is added, 2) the old energy groups 25 and 26 are

TABLE I. NUMBER DENSITIES IN BLANKET $\times 10^{-24}$

Li Coolant		Flibe Coolant	
Mo	6.405×10^{-3}	Mo	6.405×10^{-3}
Na	2.096×10^{-4}	Na	2.096×10^{-4}
		Be	8.505×10^{-3}
		F	3.333×10^{-2}
1) Li ⁶	2.204×10^{-3}	Li ⁶	1.223×10^{-3}
Li ⁷	2.757×10^{-2}	Li ⁷	1.530×10^{-2}
2) Li ⁶	1.489×10^{-2}	Li ⁶	8.260×10^{-3}
Li ⁷	1.489×10^{-2}	Li ⁷	8.260×10^{-3}
3) Li ⁶	2.829×10^{-2}	Li ⁶	1.569×10^{-2}
Li ⁷	1.489×10^{-3}	Li ⁷	8.260×10^{-4}

condensed into a new energy group 26, 3) group cross sections in the new energy group one are based on BNL-325 [13] for the isotopes Li⁶, Li⁷, and Be⁹ and on a Karlsruhe internal evaluation [14] for Na and Mo, 4) all threshold energies were taken from HOWERTON [15] and 5) a simple evaporation model was used to calculate inelastic scattering cross sections.

The main reason for the preliminary nature of our results is that a more detailed analysis of the high energy group cross sections needs to be performed.

Cross sections for the Monte Carlo calculations are based on a similar but not identical (to the S_4 cross sections) analysis. In particular discrete levels in Na and Mo isotopes are used for the distribution of inelastically scattered neutrons and an evaporation model is used only at high energies for these isotopes. Inelastic scattering distributions for Li⁶ and Li⁷ are calculated using an evaporation model with parameters adjusted to the average energy, after scattering from the most important energy groups, from the multigroup cross section set.

Defining the tritium breeding ratio, BR, as the number of tritons produced per triton burned in the plasma, one gets, using the neutron fluxes from the S_n calculations:

$$BR = \frac{1}{4\gamma} \frac{\langle \sigma v \rangle_{DD}}{\langle \sigma v \rangle_{DT}} + \frac{2\gamma \int_{R_B}^{R_0} r \sum_i (\Sigma_6^i + \Sigma_7^i) \phi^i(r) dr}{n_T^2 \langle \sigma v \rangle_{DT} R_p^2} \quad (3)$$

where

$$\gamma = \frac{n_T}{n_D}$$

RB_i = inner radius of blanket

RB_o = outer radius of blanket

R_p = plasma radius

Σ_6^i = average macroscopic $Li^6(n,\alpha)T$ cross section in energy group i

Σ_7^i = average macroscopic $Li^7(n,n'\alpha)T$ cross section in energy group i

ϕ^i = neutron group flux in energy group i

The first term is the internal production term for tritium due to the branching of the D-D reaction and it is usually, as in the case here, negligible compared to the term arising from the blanket. The blanket contribution contains an additional term in the sum for the high energy $Be(n, Li^7)T$ reaction if flibe is used on the coolant.

In the Monte Carlo calculations the tritium breeding ratio is found by calculating the number of tritons formed per neutron entering the blanket from the plasma.

To calculate the power density due to neutron reactions, such as (n,α) , (n,p) elastic and inelastic scattering, in the vacuum wall and in the blanket, use is made of published microscopic neutron fluence to kerma conversion factors by RITTS et al [16]. Since these kerma factors are given for a 100 neutron energy group set, the 26 energy group fluxes obtained from the S_4 calculations are unfolded into the 100 group neutron energy structure of the above reference. The kerma factors for Mo are not given in the above reference and therefore the kerma factors for Nb are used as an approximation for Mo. In the blanket the error introduced by this approximation is completely negligible because the power generation from neutrons is dominated by neutron reactions on Li^6 and Li^7 . In the vacuum wall the effect of this approximation on the overall power generation is also small, because the gamma power density is much larger than the neutron induced power density.

2.5 Photonics Calculations

Photonics calculations are performed in 21 energy groups using S_4 discrete ordinate transport theory in one dimensional cylindrical geometry using the code DTF IV [17]. A P_0 approximation is used for the COMPTON scattering distribution.

To obtain the gamma sources which are assumed to be isotropic in each of the 21 energy groups use is made of secondary gamma-ray source spectra by RITTS [16] et al. Since this report gives a conversion matrix from the same 100 neutron energy groups already mentioned to 21 secondary gamma energy groups for selected isotopes, the 100 energy

group fluxes obtained from the calculated 26 energy group fluxes are used again. The report does not contain gamma-ray source spectra for molybdenum. Niobium data are substituted for the molybdenum source contribution. Although this looks like a very rough approximation, the effect should not be too large since the blanket only contains 10 Vol. % molybdenum.

Cross sections for the photonics calculations in the 21 energy group structure of reference [17] are calculated using the MUG [18] code, which in turn uses as input data the ENDF/B [19] data tape for photons.

To calculate the power density produced by photoelectric, COMPTON and pair production reactions in the vacuum wall and in the blanket, tables of 21 energy group microscopic gamma-ray fluence to kerma factors are utilized [16]. Again, Mo has to be approximated by Nb to use these tables. This approximation should be quite good since there is only a difference of about 2% in the number of electrons in Nb and Mo.

3. RESULTS

3.1 Tritium breeding ratio

TABLE II summarizes the calculated tritium breeding ratios. For the Li blanket the Monte Carlo calculations indicate that the isotopic ratio of natural Li gives the optimum breeding ratio. The numerical magnitude of this breeding ratio is in excellent agreement with STEINER's [5] results and the trend as a function of Li abundance ratio agrees with LEE [7].

The S_4 calculations for the same case are a few per cent lower than the Monte Carlo calculations with the largest discrepancy (about 9%) for the natural Li case. The S_4 calculations do not give the optimum

TABLE II. BREEDING RATIO

		Li Blanket	Flibe Blanket
S_4 Monte Carlo	Natural Li	1.24	0.789
		1.37 (3% statistical error)	--
S_4 Monte Carlo	50% Li ⁶	1.32	1.07
		1.35 (2% statistical error)	--
S_4 Monte Carlo	95% Li ⁶	1.14	1.05
		1.16 (1% statistical error)	--

breeding ratio in the close vicinity of the natural Li isotopic abundance ratio, but the difference to the 50% enriched case is quite small.

For the flibe blanket Monte Carlo calculations could not be made. It appears that the S_4 calculations give breeding ratios that are about 30% below those of STEINER [5] for similar calculations. This discrepancy could be caused by the poor approximation for the F cross sections for which Na cross sections were used. This effect will be further investigated.

The breeding ratio calculations are quite sensitive to high energy reactions, such as (n,2n) reactions in the structural material for instance.

In general, our calculations show that there will be no problem in designing blankets with a breeding ratio that can accommodate the doubling time of about 10 years for electric power generation. For exact breeding ratio calculations, say to within 5% to 10%, better knowledge of high energy cross sections is required.

3.2 Neutron Power Density

Fig. 1 shows the neutron induced power density and contributions made to it by the different isotopes in the blanket and in the reflector for the Li blanket with natural Li isotopic composition. The absolute numerical values vary linearly with the assumed incident neutron energy flux of 4.48 (MW/m²). The neutron power density shows a strong, almost exponential radial decrease until the build-up of slow neutrons in the reflector combined with the $1/v$ cross section of Li⁶ causes a rise close to the reflector interface.

Fig. 2 shows the same situation, neutron power density, for the flibe blanket again with natural Li isotopic composition. Two trends can be observed: 1) the neutron power density at the first wall interface is about 50% higher than in the Li blanket case, caused by F and Be contributions, and 2) the radial exponential decrease of the power density is much more pronounced in the flibe blanket.

It is obvious that this strong radial decrease of the power density will lead to thermohydraulic design problems and to thermodynamic inefficiencies of the power plant cycle. These large changes in the radial power density are one of the reasons why WERNER [8] introduced radial heat pipes into the blanket design, an idea that we consider promising and that was incorporated in our calculations.

We also feel that the large gradients in the neutron power density, that are, of course, reflected in the total power density, can give rise to considerable thermal stress problems in structural components of the blanket.

3.3 Gamma Power Density

Gamma induced power densities for the two cases discussed in section 3.2 are presented in Fig. 3 and Fig. 4 respectively. Two points are worth noting: 1) the gamma heating in the blanket is almost entirely due to the relatively high Z structural material Mo and 2) the

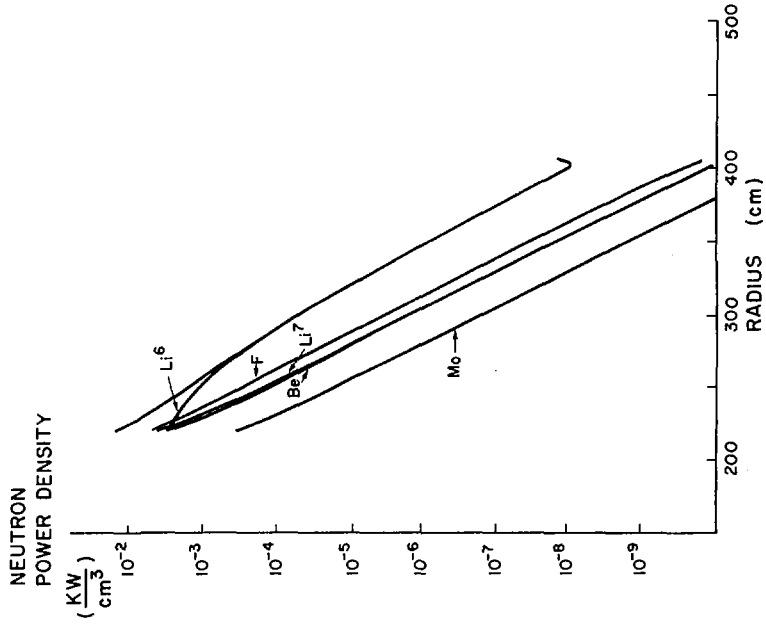


FIG. 2. Neutron power density, fibe blanket (natural lithium).

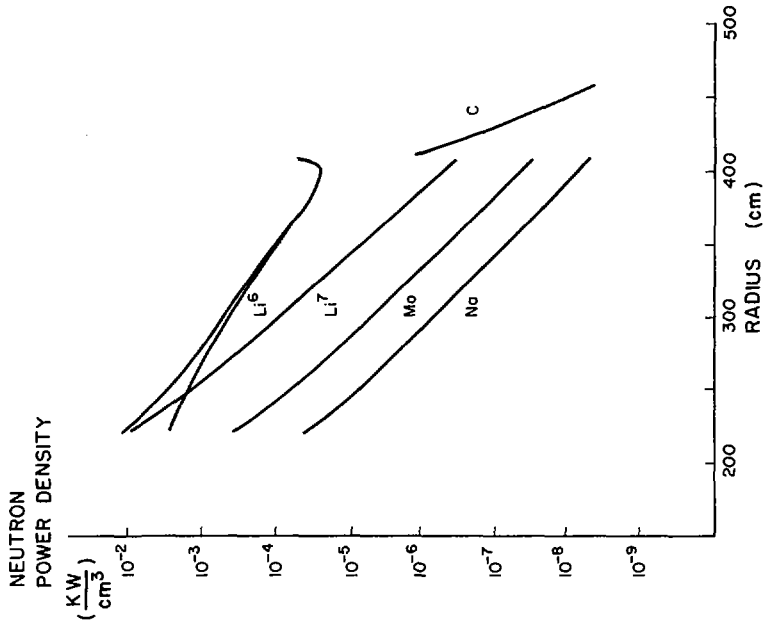


FIG. 1. Neutron power density, Li blanket (natural lithium).

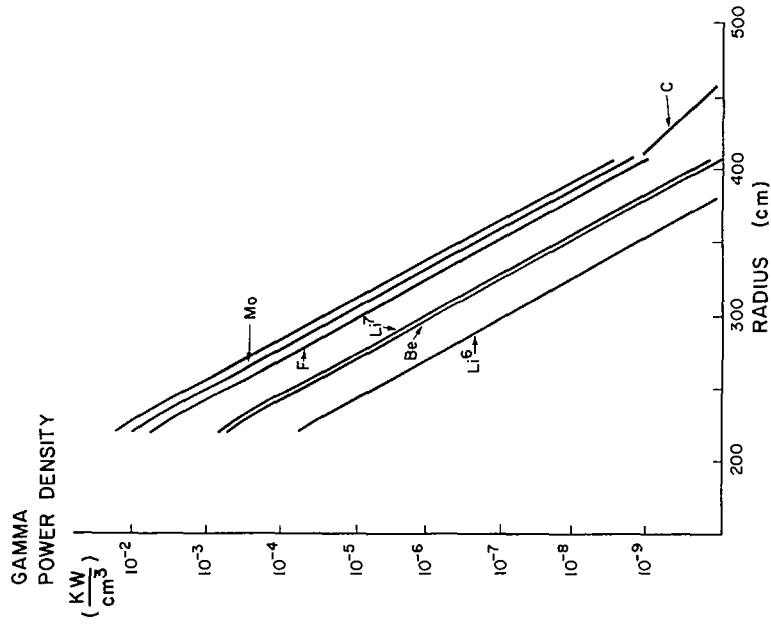


FIG. 4. Gamma power density, fibre blanket (natural lithium).

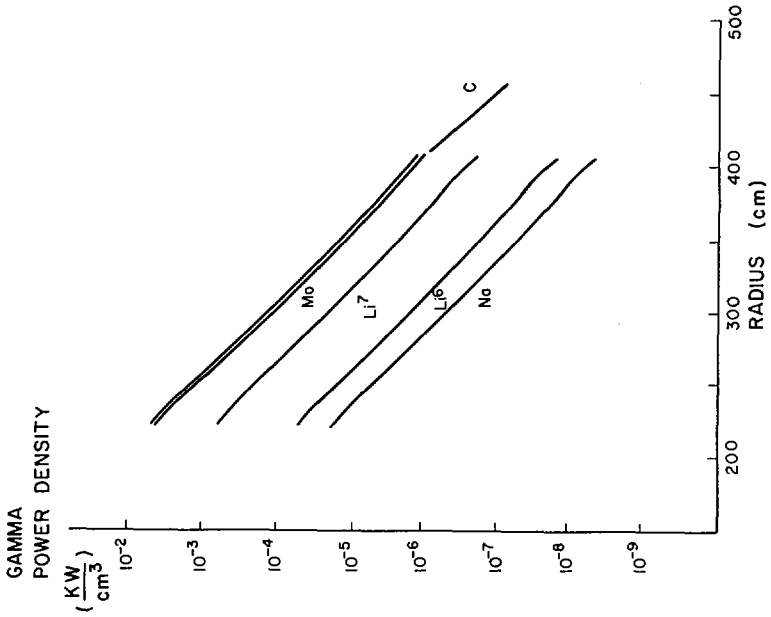


FIG. 3. Gamma power density, Li blanket (natural lithium).

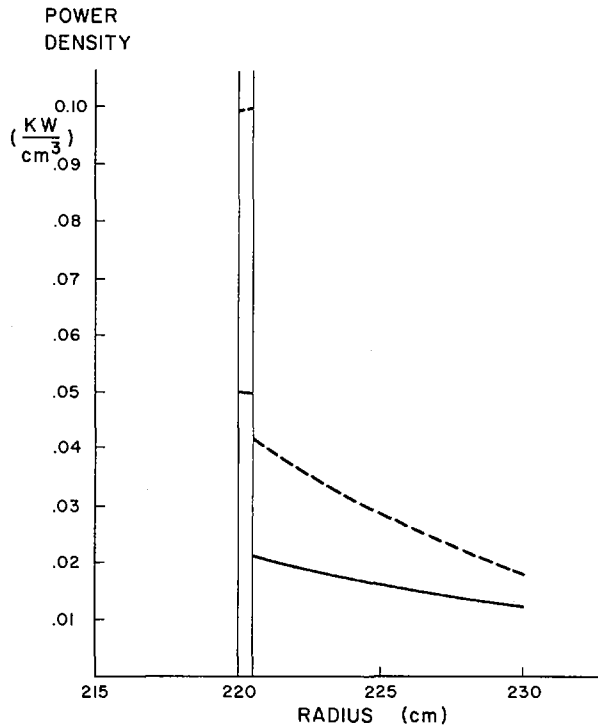


FIG. 5. Wall and blanket power densities (natural lithium). ----- flibe, ——— lithium.

TABLE III. BREAKDOWN OF HEAT SOURCES FOR NATURAL Li BLANKET

		Mo Wall	Blanket
Li Blanket	Neutron	7.3%	67.5%
	Gamma	92.7%	32.5%
Flibe Blanket	Neutron	3.5%	50.3%
	Gamma	96.5%	49.7%

γ induced power densities at the first wall are roughly 1/2 the neutron induced power density for the Li blanket and almost equal to the neutron induced power density for the flibe blanket.

3.4 Total Power density and power

To obtain the total power density the results presented in sections 3.2 and 3.3 must be added. In Fig. 5 a plot of the total power density both in the first wall (assumed to have a thickness of 0.5 cm) and in a

TABLE IV. ENERGY DEPOSITED IN BLANKET PER INCIDENT NEUTRON (MeV/NEUTRON)

		Li Blanket	Flibe Blanket	
Neutron Collisions Gamma Total	Natural Li	11.4 <u>5.49</u> 16.9	10.1 <u>10.02</u> 20.1	
	Neutron Collisions Gamma Total	50% ⁶ Li	12.5 <u>4.82</u> 17.3	11.9 <u>9.48</u> 21.4
		Neutron Collisions Gamma Total	95% ⁶ Li	12.2 <u>4.45</u> 16.7

portion of the blanket is shown for both the Li blanket and the flibe blanket. We see that in both cases the power density in the wall is about 2.5 times as high as in the surrounding blanket. The high power densities in the wall are almost entirely due to γ -heating. TABLE III gives a breakdown of the heat sources in the wall and in the blanket that illustrates this fact. These results are again in good agreement with the work of STEINER [5]. The absolute values of the power densities depend on the question of what neutron energy flux (MW/m^2) can be tolerated through the first wall, and this question has not been settled, especially in view of the fact that not only the power produced in the first wall must be removed from it, but also the heat from bremsstrahlung, and electron synchrotron radiation incident on the plasma side must be transported through and removed from the first wall. However, all magnitudes are easily scaled with the neutron source.

TABLE IV gives the total energy deposited in the blanket per fusion neutron in (MeV). These values are obtained by integrating the power densities in the blanket to obtain the linear power in (W/cm) and then multiplying by the conversion factor 2.26×10^{-5} (MeV/neutron)/(Watt/cm) characteristic of our design. Thus the power producing capability of the different blanket designs can be assessed without reference to the (arbitrary) neutron source conditions. We see that the flibe blankets produce roughly 20% more power than the Li blankets which, in part, offsets the penalty of the lower breeding ratio of these blankets.

Acknowledgement: The authors want to thank V. Brandl for work on the Monte Carlo program, M. Hardt for help with the DTF IV γ -transport calculations, R. Meyer for calculating group constants for the first neutron energy group and R. T. Perry, Jr. for calculations of neutron and γ -heating rates. Some of the calculations were performed on the IBM 360/65 at Texas A&M University.

REFERENCES

- [1] ROSE, D. J. and CLARK, M., "Plasmas and Controlled Fusion," M.I.T. Press, Cambridge (1961).
- [2] IMPINK, A.J., Neutron economy in fusion reactor blanket assemblies, M.I.T. Technical Report 434 (1965).

- [3] HOMEYER, W. G., Thermal and chemical aspects of the thermonuclear blanket problem, M.I.T. Technical Report 435 (1965).
- [4] STEINER, D., Neutronic calculations and cost estimates for fusion reactor blanket assemblies, ORNL-TM-2360 (1968).
- [5] STEINER, D., Neutronic behavior of two fusion reactor blanket designs, Proceedings of B.N.E.S. Nuclear Fusion Reactor Conference, Culham (1969) 483.
- [6] BLOW, S., CROCKER, V. S. and WADE, B. O., Neutronics calculations for blanket assemblies of a fusion reactor, Proceedings of B.N.E.S. Nuclear Fusion Reactor Conference, Culham (1969) 492.
- [7] LEE, J.D., Tritium breeding and energy generation in liquid lithium blankets, Proceedings of B.N.E.S. Nuclear Fusion Reactor Conference, Culham (1969) 471.
- [8] WERNER, R. W., Module approach to blanket design-a vacuum wall free blanket using heat pipes, Proceedings of B.N.E.S. Nuclear Fusion Reactor Conference, Culham (1969) 536.
- [9] WERNER, R. W., MYERS, B., MOHR, P. B., LEE, J.D. and CHRISTOFILOS, N.C., Preliminary design considerations for an Astron Power Reactor System, Proceedings of B.N.E.S. Nuclear Fusion Reactor Conference, Culham (1969) 449.
- [10] CARLSON, G.A., A thermal energy conversion system for a fusion reactor, presented at Symposium on Fusion Reactor Design, Lubbock, Texas (1970).
- [11] HOPKINS, G. R. and MELESE-d'Hospital, G., Direct helium cooling cycle for a fusion reactor, Proceedings of B.N.E.S. Nuclear Fusion Reactor Conference, Culham (1969) 522.
- [12] BONDARENKO, I. I. et al, Gruppenkonstanten schneller und intermediärer Neutronen für die Berechnung von Kernreaktoren, KFK-tr-144, translation from Russian (1964).
- [13] STEHN, J. R. et al, Neutron cross sections, BNL 325, Second Edition, Supplement No. 2 (1964).
- [14] MEYER, R., personal communication (1971).
- [15] HOWERTON, R. J. et al, UCRL-14000 (1967).
- [16] LATHROP, K. D., DTF-IV, a FORTRAN-IV program for solving the multigroup transport equation with anisotropic scattering. LA-3373 (1965).
- [17] RITTS, J. J., SOLOMITO, M. and STEINER, D., Kerma factors and secondary gamma-ray sources for some elements of interest in thermonuclear blanket assemblies, ORNL-TM-2564 (1970).
- [18] KNIGHT, J. R. and MYNATT, F. R., MUG, A program for generating multigroup photon cross sections, CTC-17 (1970).
- [19] HONECK, H. C., ENDF/B - Specifications for an evaluated nuclear data file for reactor applications, BNL-50066 (1966).

BLANKET COOLING CONCEPTS AND HEAT CONVERSION CYCLES FOR CONTROLLED THERMONUCLEAR REACTORS

S. FÖRSTER

Institut für Reaktorentwicklung

TH. BOHN

Institut für Technische Physik,
Kernforschungsanlage Jülich,
Jülich, Federal Republic of Germany

Abstract

BLANKET COOLING CONCEPTS AND HEAT CONVERSION CYCLES FOR CONTROLLED THERMONUCLEAR REACTORS.

The neutron energy generated in fusion plasmas produces heat in solid and liquid blanket regions which confine the fusion plasma. This heat has to be removed by cooling the blanket, and is then converted into electric energy by thermodynamic processes. Blanket cooling can directly be achieved by cycling the liquid blanket material through an outside cooler, or indirectly by leading gaseous or liquid coolants through pipes in the blanket. For the conversion of heat into electricity, single Rankine or Brayton cycles can be applied as well as binary Rankine cycles using potassium and steam as cycle fluid.

In this paper, the special features of different systems for blanket cooling and for heat conversion are described and discussed. The thermodynamic requirements for favourable operation of the different heat conversion cycles, and those for the heat removal system from the CTR are pointed out.

Also the pumping power in magnetically or unmagnetically coolant flows is considered.

Selected solutions for combining the systems of blanket cooling and of heat conversion are compared with respect to plant efficiency, lost-volume fraction in the lithium blanket region, and the expected constructional and safety features. The comparisons are made for thermal powers of the reactor between 5000 and 10 000 MW and toroidal reactor configurations.

Solutions to be preferred are pointed out.

INTRODUCTION

Fusion reactors will be applied as heat generating source for power plants with thermal reactor powers greater than 5 GW. Among the major problems for the realization of such large power plants are the heat removal from the reactor blanket and the conversion of this heat into electrical power. Both these problems are of high influence on the plant performance, on the plant costs and costs of electricity produced.

For technological reasons the maximum temperatures of structures in the blanket are restricted to values around 1000 °C. Consequently the maximum temperature for the energy conversion cycles must be lower than 1000 °C. For temperatures below 1000 °C thermodynamic cycles with turbines driving the electrical generators are well suited.

In this paper possible solutions for the lay out of the heat removal system in the fusion reactor and of the heat conversion cycle are considered and compared. Some lay out data are given for a thermal power of the reactor of 6,7 GW.

In chapters 1 and 2 the general features of the energy flow in fusion reactor power plants and of the reactor blanket region, for which the cooling system has to be adapted, are described briefly. In chapter 3 typical solutions for the combined system of blanket cooling and heat conversion cycle are selected for the further considerations.

Chapters 4 and 5 deal with the particularities of the blanket cooling and the conversion cycles. As blanket coolants Lithium, Flibe (molten salt), Potassium and Helium and as thermodynamic cycles simple He-BRAYTON and H_2O -RANKINE-cycles and binary K- H_2O -RANKINE-cycles are considered. Special attention is paid to the volume of structure and other coolants than lithium in the blanket, to the MHD forces in the coolant flow and to the performance characteristics of the cycles.

In chapter 6 the cost situation for the most interesting plant arrangements is discussed.

1. ENERGY FLOW SCHEME FOR FUSION REACTOR POWER PLANTS

To illustrate the electrical power generation from the heat of a fusion reactor, fig. 1 shows schematically the steady state energy flow distribution in the plant. Fusion reaction energy E_1 is recovered as heat E_2 by cooling the blanket which surrounds the fusion plasma. This energy is transmitted to the energy conversion system directly or through an intermediate loop (E_3). Electrical energy E_4 and E_6 is produced in the thermodynamic cycles I and II. The energy E_5 , rejected from cycle I, enters cycle II as primary energy. In the case of two power cycles as well as for only one power cycle the energy E_7 is given into the surroundings by external cooling (heat sink). A part of the electrical power (E_{int}) is consumed in the plant (for example as power supply for pumping and auxiliary systems). The remaining energy E_e leaves the plant.

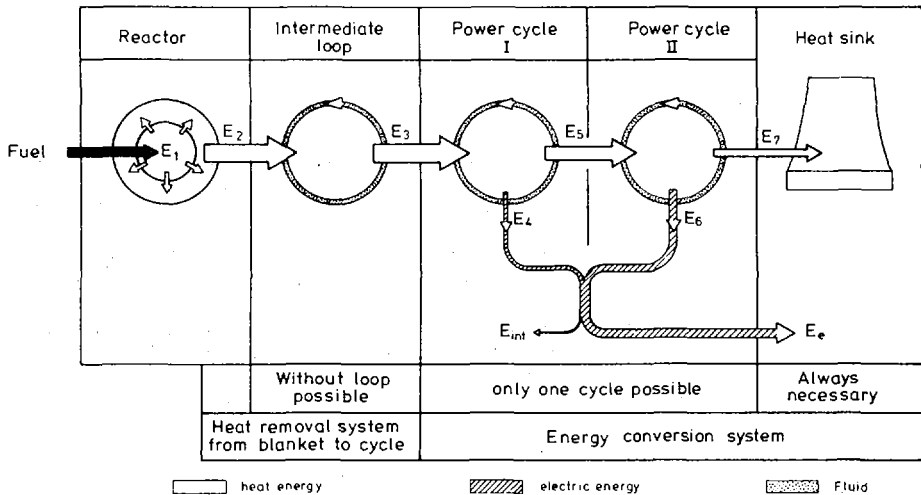


FIG. 1. Energy flow scheme for fusion power plant.

The net efficiency of the plant η is given by the relation of E_e to E_1 . This can also be expressed by

$$\eta = \underbrace{\left(1 - \frac{E_7}{E_1}\right)}_{\eta_{th}} - \frac{E_{int}}{E_1}$$

Since for a given thermal power the electrical power should be as high as possible, for economic reasons, η should be high too. This implies a high thermodynamic efficiency of the power cycle (η_{th}) i.e. a low value of E_7/E_1 and small internal electrical energy consumption, i.e. a low value of E_{int}/E_1 . With respect to these two terms the net plant efficiencies are very different for the combined heat removal and heat conversion systems considered here (see 5.1).

2. REACTOR AND BLANKET TOPICS

From the various reactor principles [1] here only two toroidal reactors are considered. Fig. 2 shows, with on scale main dimensions, on the left side a Tokamak-reactor as proposed by Golovin et al. [2] (for 6,7 GW_{th}) and on the right side a Stellarator/Torsatron-reactor as proposed by Gourdon et al. [3] (for 13,4 GW_{th}). In both cases the plasma is confined in a toroidal vacuum chamber and then surrounded first by the blanket region and then by the shielded coil region. In the case of Tokamaks the blanket and the coil regions cover the whole circumference of the torus. In the case of Stellar./Torsatrons there are arranged generally three distinct inner regions with blanket and coils and three outer regions only with blanket. Both regions are helicoidally wound around the torus.

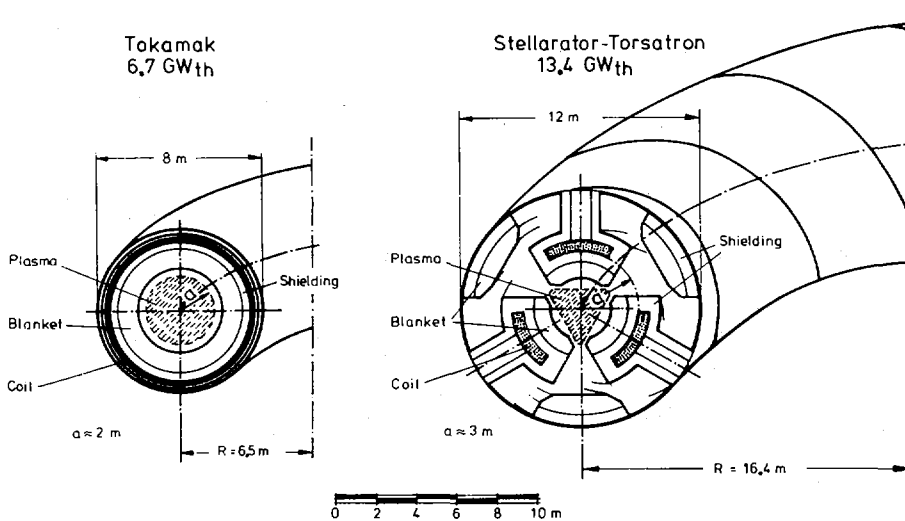


FIG. 2. Arrangements and main dimensions for toroidal fusion reactors.

From plasma physics and neutron kinetics rules for both reactor types several characteristics can be assumed to be representative for power reactors:

- The plasma diameter increases only little with increasing thermal power. The inner blanket radius is about 2 m (Tokamak) and 1,5 m (Stellarator/Torsatron).
- The blanket thickness is about 1 m, the inner region ($\approx 0,65$ m) containing Lithium or Flibe ($\text{LiF}+\text{BeF}_2$), the outer region ($\approx 0,35$ m) containing graphite.
- The coil region, including a shielding zone of about 0,45 m between blanket and coils has also a thickness of about 1 m.
- The thermal power per unit length on the torus axis is about 160 MW/m (Tokamak) and about 130 MW/m (Stell./Tors.)
- Therefore the aspect ratio (great torus radius (R)/small torus radius (a)) becomes greater with increasing thermal power.
- The minimum thermal powers are for Tokamaks about 5 GW and for Stell./Torsatrons about 10 GW.
- The radial volumetric heat distribution in the blanket decreases rapidly from values of about 120 MW/m^3 on the inner side of the blanket to less than 1 MW/m^3 at the outer side of the blanket. The heat distribution depends on the fractions of structural masses and other coolants than blanket fluids in the blanket (see for instance [4]). For Stellarator/Torsatrons the power generation in the outer blankets is lower and in the inner blankets higher than in the case of Tokamaks.
- The magnetic induction in the blanket region varies between 5 to 10 Tesla for Tokamaks and between 10 to 15 Tesla for Stell./Torsatrons. The higher values being valid near the coil.
- For technological reasons the maximum allowable temperatures of metal structures in the blanket should not exceed $1000 \text{ }^\circ\text{C}$.

The following performance requirements are to be observed for economic reactor and plant operation and for nuclear safety:

- The volume fraction of all other materials and fluids than Li and C in the blanket (lost volume fraction) should be as small as possible (for high Tritium-breeding ratios).
- The MHD pumping power for electrically conducting fluids, flowing through the blanket, should be as low as possible (to keep the net electrical power high).
- The safety against Tritium contamination of the energy conversion cycle and against chemical reactions of different fluids should be high and the activation of coolants in the blanket or of cycle fluids should be small.

The heat removal system and the conversion cycles have to meet the described reactor characteristics. The valuation of different cooling and power generation arrangements then will depend on the fulfillment of the performance requirements.

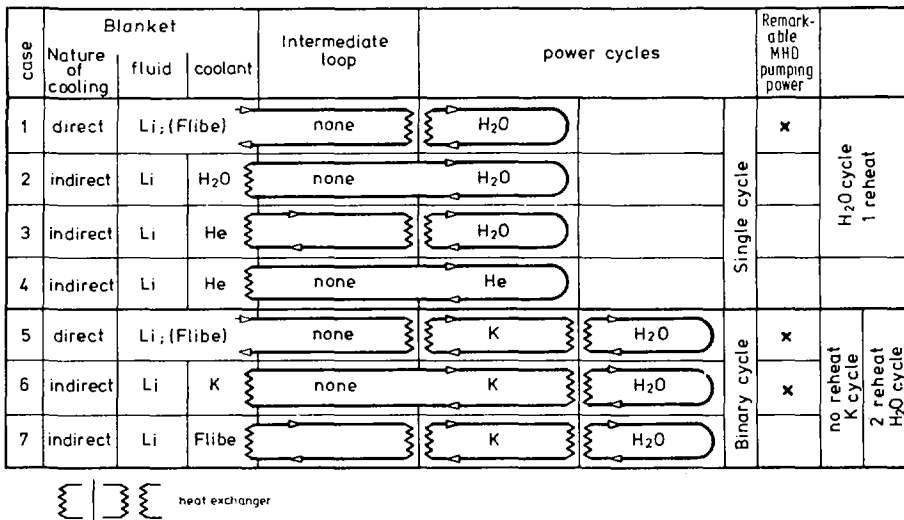


FIG. 3. Selected combinations of fusion reactor (blanket) with power cycle.

3. SELECTION OF COMBINED HEAT REMOVAL AND HEAT CONVERSION CYCLES

For a representative selection it is convenient to fix at first the heat conversion cycles, which can be operated at temperatures lower than 1000 °C. Then appropriate heat removal systems may be chosen. Fig. 3 shows schematically seven cases for combining three typical power cycles with the reactor: single cycle with H₂O- and He-turbine, binary cycle with K- and H₂O-turbines. Successively in fig. 3 are indicated: Nature of blanket cooling and coolant; intermediate loop; type of power cycle; cases with MHD pumping power. For simplicity only heat exchangers between different fluids are shown.

The three first cases have a single H₂O-RANKINE cycle. Their differences being the H₂O-steam generator located outside the reactor (1) and in the blanket (2) and an intermediate He-loop (3).

The fourth case is the only one with a He-BRAYTON cycle.

Cases 5, 6 and 7 have binary K-H₂O-RANKINE cycles. Their differences being the K-steam generator located outside the reactor (5), in the blanket (6) and an intermediate Flibe-loop (7).

The cases 1 to 4 can be compared with fission reactor power plants. The corresponding reactors are in cases 1 and 2 sodium cooled fast reactors and in the cases 3 and 4 high temperature reactors.

The binary cycle in cases 5 to 6 is proposed by Fraas [5].

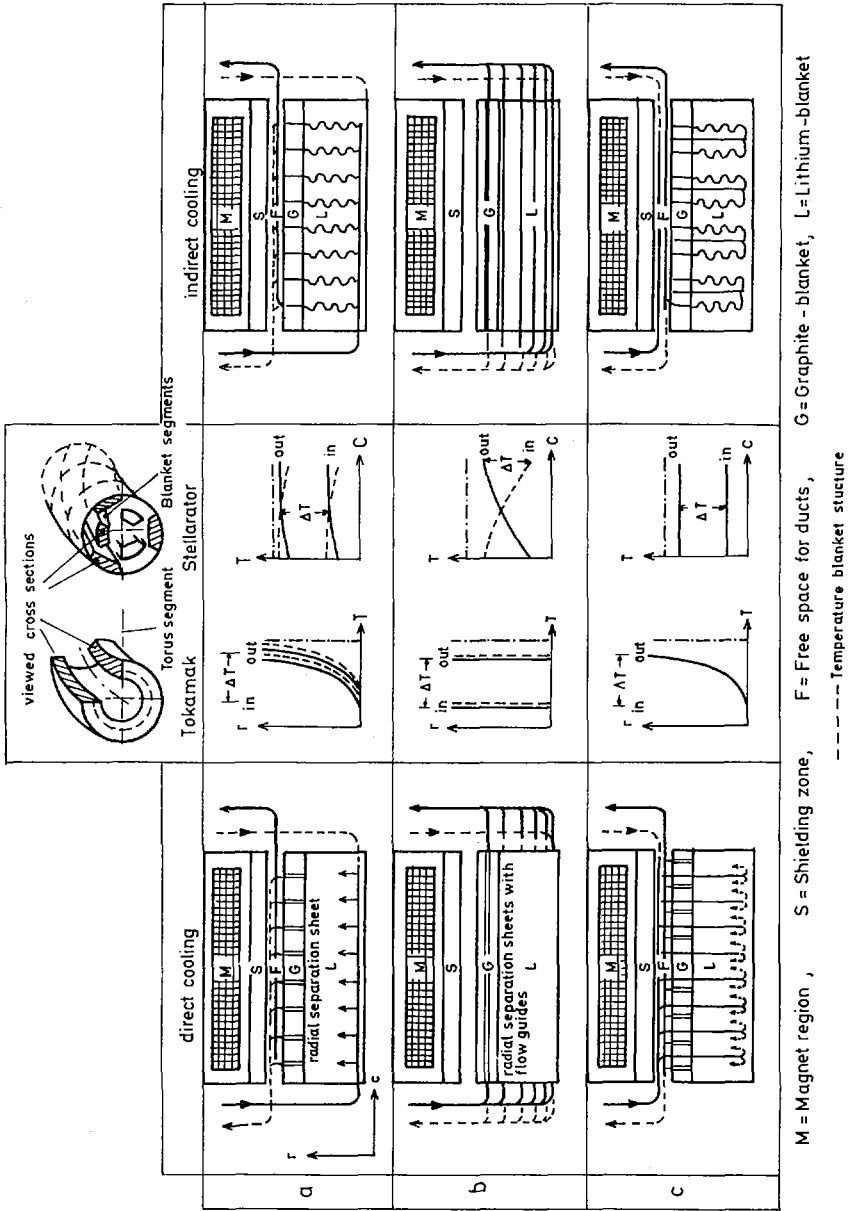


FIG. 4. Typical blanket cooling arrangements. Cases a and c radially coolant flow; case b circumferentially coolant flow. In cases b no free space (F) required.

It can be seen that only two variants for direct blanket cooling (Li and Flibe) and four variants for indirect blanket cooling (H_2O ; He; K; Flibe) have to be considered to evaluate the different cases of fig. 3.¹

4. HEAT REMOVAL SYSTEM (BLANKET COOLING)

The requirements already given in chapter 2 have to be fulfilled at best by the lay out of the heat removal system. Therefore we have to take into account the following facts:

- Nature of cooling arrangement,
- Lay out data for the cooling flow, required by the heat conversion cycle,
- Physical properties of the coolant

After the description of these facts we will discuss the lost volume fraction in the blanket and the MHD pumping effects for different cooling systems.

4.1 TYPICAL COOLING ARRANGEMENTS

In fig. 4 some typical arrangements for direct and indirect cooling are shown. They correspond to the sections viewed in the middle of fig. 4 for both types of reactors. In all cases the graphite in the blanket is cooled internally (therefore an outer Li-Blanket as proposed in [4] seems not to be necessary). The radial and circumferential temperature distributions in the coolant are indicated schematically.

For direct and indirect cooling the cases a, b and c are similar, the only difference being flow guide and separation sheets for direct cooling instead of coolant tubes for indirect cooling in the liquid blanket region. In the cases a and c the flow direction with heat loading of the coolant is radially outwards to the torus axis. In the cases b the flow direction is parallel to the torus axis (Tokamak) respectively circumferentially to the torus axis (Stell./Torsatron).

The indicated counter flow principle in the cases a and b ensures uniform mean temperature distribution in the blanket.

A segmentation of the blanket along the torus axis allows the arrangement of the inlet and outlet ducts with small spacing between two segments in the case of Tokamaks and the replacement of damaged blanket zones for both types of reactor.

4.2 LAY-OUT DATA FOR THE COOLING FLOW AND MAIN PHYSICAL DATA OF COOLANTS

According to the selected cases in fig. 3 there is a close relation of the coolant flow parameters with the corresponding

¹ Other gaseous or liquid coolants or cycle fluids than indicated were not considered here. Helium has very good heat transmission properties, it will not be activated by irradiation and is good suitable for power cycle purpose. Potassium compared with other alkaline metals is best suitable for power cycle purposes.

TABLE I. REPRESENTATIVE LAY-OUT AND PERFORMANCE DATA FOR DIFFERENT BLANKET COOLING SYSTEMS (cases as in Fig. 3); assumptions for MHD-effects see text. (Case 7 same values as case 5 with Fibre)

Case of system	Nature of cooling	State of coolant	Temperature in blanket		Required pressure for cycle operation, blanket outlet	Mass flow rate of coolant (thermal power 6.7 GW)	MHD-pressure drop	MHD-pumping power relative to therm. power	Remarks
			inlet	outlet					
1	Lithium	liquid	°C	°C	bar	10^3 kg/s	bar		
			400	700	free	5.35	710	0.128	inlet and outlet temperatures according to steam generation lay-out
5			870	930	free	26.9	710	0.64	
1	Fibre	liquid	400	700	free	9.35	< 1	1.08×10^{-3}	inlet and outlet temperatures according to steam generation lay-out
			870	930	free	46.7	< 1	5.4×10^{-3}	Same values for case 7
2	H ₂ O	liq. to superh. steam	280	540	190	2.6	negligible		Enthalpy rise water/steam 2.58×10^3 kJ/kg (one reheat)
			300	730	45(60)*	3.0	-	-	
4	He	gaseous	520	950	90(60)*	3.0	-	-	
			815	840	2	3.67	170**	0.015**	Enthalpy rise liq./steam 1.83×11^3 kJ/kg

* Values in brackets indicate pressure range.

** Only MHD-effects on inlet side; outlet side vapour.

TABLE II. MAIN PHYSICAL PROPERTIES OF DIFFERENT FLUIDS FOR BLANKET AND BLANKET COOLING.
 Fluids in brackets for comparison (informal data taken from various references)

Fluid	Melting point °C	Boiling point °C	Molecul. weight kg/kMol	Spec. heat kJ/kg/K	Density 10^3 kg/m^3	Electr. conduct. $ \Omega \text{m} ^{-1}$	Heat conduct. 10^{-3} kW/mK	Dyn. viscosity Ns/m^2	Remarks
Lithium	180.5	1338	6.94	4.14	0.398	2.22×10^6	58	1.88×10^{-4}	Specific heat, density, electrical conductivity and dynamic viscosity at 900°C
Flibe *		peritectic	33.1	2.39	1.836	3.94×10^2	1	3×10^{-3}	
Potassium	63.2	758	39.1	0.81	0.693	1.07×10^6	28	0.17×10^{-3}	Density at 60 bars 900°C; dynamic viscosity at 900°C
(Sodium)	97.8	878	23	1.29	0.737	2×10^6	53	1.7×10^{-4}	
Helium			4	5.21	2.46	negligible	0.428	0.5×10^{-4}	
(Argon)			40	0.521	24.6		0.045		
(Nitrogen)			28	1.04	17.2		0.072		
(Hydrogen)			2	14.2	1.238		0.55		

* Composition in mole %: 66 LiF + 34 BeF

energy conversion system. These flow parameters (such as temperatures, pressures and mass flow rate) which are of great influence on the lay out of the cooling system are enlisted in table 1, on the left side, for the same cases as in fig. 3. The mass flow rates correspond to a thermal power of the reactor of 6,7 GW and were calculated with the specific heat and temperature rise of the coolant respectively with the steam generation heats given in Table I.

The main physical properties for all blanket fluids (except for H₂O) and for some other fluids are enlisted in Table II.

It should be noted here, that for all cases with indirect cooling the liquid blanket temperatures are higher than the temperatures of the coolant between blanket inlet and outlet (because of additional temperature drops in the heat exchanger).

4.3 LOST VOLUME FRACTION IN THE BLANKET

For high tritium-breeding ratios the volume fraction of structure materials and coolants other than lithium or Flibe in the blanket should be as small as possible. It is evident that for direct cooling and indirect cooling with flibe this volume fraction is smaller than in all other cases of indirect cooling. Also it is clear that indirect cooling with Flibe (which might be of interest for high T-breeding lithium blanket and small MHD-pumping power) has greater volumes of structure materials than direct cooling with flibe (because of additional heat exchanger material).

For the indirect coolings with H₂O, He, K and Flibe small lost volume fractions need optimization procedures for small heat exchanger surfaces and small amounts of coolant volume in the blanket. This has to be done with respect to low pumping power due to friction. The pressures in the cooling system have to be considered too since they are of influence on the wall thicknesses.

Generally small heat exchanger surfaces will be attained with radial outwards flow cooling as shown in fig. 4, cases a and c, and as proposed for helium [6]. The reason therefore being higher mean temperature differences between coolant and wall² in the inner region of the blanket (with high volumetric power generation) than for circumferentially cooling arrangement (see temp. distributions in fig. 4).

The heat exchanger surface required for the different coolants is determined by the heat transmission coefficients of the coolant and indirectly by the temperature rise (ΔT) in the coolant, compared to the wall temperatures of the heat exchanger. If constant wall temperature is assumed the heat exchanger surface decreases with increasing ΔT .

Rough estimates show that for all indirect coolants and without MHD-forces the flow is turbulent and that the heat transmission coefficients are in the order of 20 [kW/m²K]. Then, if one assumes for all indirect coolants the heat transmission coefficients and also the temperature difference between wall temperature and max. coolant temperature as constant, smallest heat exchanger surfaces are reached for cases 3 and 4 ($\Delta T_{\text{He}} = 430$ K) followed by case 1 ($\Delta T = 300$ K) and case 2 ($\Delta T_{\text{H}_2\text{O}} = 260$ K).

² The maximum wall temperature being fixed by the lay out of the blanket, for instance at constant value.

The volume fraction of coolant in the blanket depends on the total flow cross-section (cooling tubes with const. diameter assumed) and the total length of all cooling tubes in the blanket. The individual tube lengths, for radially or circumferentially cooling arrangements, are determined by the local values of the heat transmission coefficient, the effective temperature difference and the heat to be exchanged along the coolant flow direction through the blanket. The tubes may be bends more or less corresponding either to the varying heat flux along the tubes or to the radial, circumferential or axial dimensions of a blanket section.

The diameters and numbers of tubes are to be adjusted either for the required values of heat transmission coefficients and heat exchanger surfaces or to the convenient flow velocities and the resulting heat exchanger surfaces. As a first approximation the coolant volume fractions in the blanket are, compared to this fraction in cases 3 and 4 (He), taken as 1:

case 2 (H ₂ O)	≈ 1	for water inlet velocity 1 m/s
" 6 (K)	≈ 1.5 (radial cooling)	} for 4 m/s (liquid at inlet cooling)
	≈ 3 (circumferential cooling)	
case 7 (Flibe)	≈ 5	for 8 m/s flow velocity
	≈ 2.5	for 16 m/s " "

The pressure drops in the blanket due to friction will be for the indirect coolings:

case 2 (H ₂ O)	≈ 60	bar (incl. evapor.)
" 3 (He)	at 45 bar	≈ 3.5 bar
" 4 (He)	at 90 bar	≈ 5.5 bar
" 6 (K); liq.	at 4 m/s	≈ 6 bar (incl. evapor. ≈ 2bar)
" 7 (Flibe)	at 8 m/s	≈ 4 bar
	at 16 m/s	≈ 16 bar

and for the direct coolings:

case 1 Li	(at 2 m/s)	< 2 bar
" 1 Flibe	(")	< 2 bar
" 5 Li	(")	≈ 2 bar
" 5 Flibe	(")	≈ 2 bar

Taking into account the required outlet pressures (tab. 1) and these pressure drops, the greatest wall thicknesses for the heat exchanger tubes will be necessary for case 2 and the smallest wall thicknesses for cases 6 and 7.

Resuming the heat exchanger surfaces and the volume of blanket coolant, indirect cooling with He and H₂O will have

smallest overall lost volume fractions. Indirect cooling with Flibe will be of interest, if the coolant volume fraction for other coolants reduces considerably the T-breeding ratio.

4.4 MHD-PUMPING-EFFECTS

The flow of electrically conducting fluids across magnetic fields causes pressure drops due to magneto-hydrodynamic (MHD)-forces. Thus pressure drops and pressure differences against the surroundings are produced, leading to pumping powers which might be considerably higher than for simple viscous flow. These MHD pressure drops and pumping powers are proportional to the square of the magnetic induction, the electrical conductivity and the fluid velocity perpendicular to the field lines, and to the length of the path of the fluid across the field lines. Furthermore of influence are the shape and hydraulic diameter of the flow cross section and the electrical conductivity of the wall. Generally insulating walls and small hydraulic diameters lead to smaller MHD-pressure drops.

To minimize the MHD-effects the flow of the electrically conducting fluids (Li, Flibe, K) should follow the magnetic field lines. Subsequently cooling arrangements of type b, fig.4 are recommended. (But even in this case, if the cooling tubes have to be bended for lay out reasons (optimisation of heat exchanging surface and flow velocity) MHD-forces cannot be avoided). Then the major part of the MHD-pressure drops and pumping powers arise in the radial coolant supply ducts where the flow velocity can be kept low.

Since for Li, Flibe and K the electrical conductivity and also the mass flow rates in the blanket are rather different, it is worthwhile to compare the MHD-pressure losses and MHD-pumping powers for these fluids and the corresponding cases of fig.3. In Table I the results are given, assuming for Li, Flibe and K the same values for the flow velocity (1 m/s) and for the mean magnetic induction (8 Tesla) at a constant path length in the field (1 m)³.

(The proportionality factor for the flow ducts was taken as 0.5).

For Li the MHD pressure drops and the relative MHD pumping power are extremely high and half of this pressure drop will be effective in the blanket region. For K these values are rather low and the pressure drop only is of effect on the liquid inlet side.

For Flibe the MHD pressure drop and MHD pumping power are negligible. The case with radial flow in the blanket has to be excluded. There MHD-forces will make the flow laminar and as the flow velocities are high (8 to 16 m/s) the relative pumping power will even be higher than for K.

For Helium and Water/Steam as coolant the electrical conductivity is negligible so that only thermodynamic effects are relevant for pressure drop and pumping power.

³ These assumptions are representative for radial coolant supply to the blanket, and coolant flow direction in the blanket parallel to the field lines.

5. HEAT CONVERSION CYCLES

5.1 PERFORMANCE DATA OF CYCLES

According to fig. 3 three cycles can be used for the conversion of the reactor heat into electricity:

H ₂ O-turbine cycle ⁴	Rankine	}	single cycle
He-turbine cycle 6	Brayton		
K-turbine/H ₂ O-turbine cycle ⁵ 5	Rankine-binary cycle		

For fusion reactor power plants high net efficiencies are required to reduce above all the cost of the reactor which makes about 60 % of the plant costs |6|. Therefore it is of interest to know the attainable net efficiencies for the different plant arrangements. Also for valuation purposes, the max. temperatures and max. pressures in the blanket, required for the operation of these arrangements, should be known.

In Table III a survey of the attainable cycle efficiencies (η_{th}) and net plant efficiencies as well as of the mentioned temperatures and pressures is given.

The maximum pressures in the blanket take into account both MHD- and thermodynamic pressure drops in the reactor blanket and the net plant efficiencies include the pumping power for these pressure drops. The net plant efficiencies vary within 35 % and 53 %, if one excludes case 5 (with Li) where the efficiency of ≈ 24 % only is reached by the heat conversion of the dissipated relativ pumping power.

The case 4 with He-gasturbine lies between the binary cycles with about 53 % efficiency and the single H₂O cycle with 35 to 42 % efficiency.

With respect to low blanket pressures the cases 1 (and 5) with Li-cooling and the case 2 with indirect H₂O-cooling should not be applied. For low maximum blanket temperatures case 1 with Flibe and cases 2 and 3 could be of interest. All other cases will require 200 to 300 K higher maximum temperatures in the blanket.

5.2 UNIT SIZES FOR THE TURBOMACHINES

Already in the first chapter it was mentioned that for reasons of costs of the reactor and of plasma realization the thermal power of fusion reactors must be higher than 5 to 10 GW, depending on the type of reactor. Then for net plant efficiencies of about 50 % the electrical power of the plant would be higher than 2,5 to 5 GW. Up to now only H₂O-turbine units for about 1.2 GW are installed. Units of up to 1.8 GW seem to be feasible until 1980 (Westinghouse). K-turbines have not been built yet for large power generation purpose. The same is the case for He-turbines, although from studies on such turbines, units for 1.5 GW seem to be feasible without great development expenses (see for instance |7|).

⁴ Conventional lay-out with one reheat as for fossile-fired plants.

⁵ H₂O-cycle with two reheats.

TABLE III. SURVEY OF REPRESENTATIVE CYCLE PERFORMANCE DATA, for cases as in Fig. 3.

Case of system	Nature of cooling	Cooling arrangement in blanket	Maximum blanket temperature		Blanket cooling		Efficiency		Relative pumping power due to		Remarks
			°C	°C	Maximum temperature	Maximum* pressure	net** cycle	net*** plant	MHD effects	Viscous flow	
1	dir.	rad.	700	700	700	360 (Li) < 2 (Fl)	0.42	0.35 (Li) 0.42 (Fl)	12 (Li) 0 (Fl)	< 1	
2	ind. or circ.	rad. or circ.	> 540	540	540	250	0.42	0.42	-	in η_{cycle}	H ₂ O - cycle with one reheat; multiple feed water preheating
3	ind.	rad. or circ.	> 730	730	730	45(60)	0.42	0.385	-	6	
4	ind.	rad. or circ.	> 950	950	950	90(50)	0.46	0.46	-	in η_{cycle}	One expansion; compression with one intercooling [6]
5	dir.	circ.	930	930	930	360 (Li) 2 (Fl)	0.54	≈ 0.24 (Li) 0.535 (Fl)	64 (Li) 0.5(Fl)	< 1	K-cycle no reheat, feed liq. preheating, H ₂ O-cycle two reheats according to [5]
6	ind.	circ.	> 840	840	840	5	0.54	0.585	1.5	in η_{cycle}	
7	ind.	circ.	> 870	870	870	5	0.54	0.525	0.5	1	

* including MHD- and thermodynamic pressure drops

** including MHD- and thermodynamic pressure drops

*** Dissipation heat of pumping power taken into account

circ.: circumferentially

rad.: radially

Fl: Fluibe

TABLE IV. UNIT SIZE AND NUMBER OF TURBINES FOR FUSION REACTOR POWER PLANTS OF 6.7 GW_{th}.

Case	Net efficiency %	Net Electric power GW	Turbines		
			unit size GW _e	number of units	
1 (Flibe)	0.42	2.8	1.45	2	
4	0.46	3.1	1.6	2	
6 or 7	0.53	3.55	K 1.4 (?)	1	3
			H ₂ O 1.16	2	

Including compressor

If we assume a fusion reactor-power plant with 6,7 GW_{th}, then for the most interesting cases 1 (Flibe), 4, 6 and 7th, the number and unit sizes for the turbomachines would be as given in Table IV.

5.3 SAFETY

The main safety criterions for the heat removal and energy conversion systems are the tritium contamination of the turbine cycles and chemical reactions of the blanket fluid with an indirect coolant or of liquid metal cycle fluid with H₂O.

Practically for all cases of fig. 3 the tritium contamination of the primary conversion cycle cannot be excluded because of T-diffusion phenomena. Perhaps this contamination would be lower in cases with heat exchanger between reactor coolant loop and the conversion cycle (1, 3, 5, 7) since there low T-diffusion materials can be applied as protection barrier.

Chemical reactions as indicated only are not to be feared in the cases of He-cooling (3, 4). In all other cases H₂O ingress into the blanket fluid (1, 2) or into the K-cycle (5,6,7) cannot be avoided in the case of H₂O-steam generator failures.

6. PLANT PERFORMANCE AND COST SITUATION

From the point of view of overall simplicity the combined heat removal and energy conversion systems of cases 2 and 4 are the best ones. The binary systems are very complicated. If case 2 is rejected for too high pressures in the blanket and for safety reasons, then the cases with binary system are to be compared with the case 4 (He-turbine).

The worth of plant cost differences between cases 5 to 7 and 4 for equal electricity generating costs can roughly be estimated with the help of the different electrical powers produced

by both types of systems⁶. If we assume the total specific investment costs for the plant of case 4 as 800 DM/kWe [6] then for plants of cases 5 to 7 the specific total investment costs could be lowered by the factor $3,1 \text{ GW} / 3,55 \text{ GW} \approx 0,87$. This means that for constant costs of the reactor (excluding the blanket cooling) the remaining plant costs and cost differences for the blanket cooling in the cases 5 to 7 could be higher by about 100 DM/kWe.

It is hardly imaginable that this additional sum would be sufficiently high to build the binary cycle. In comparison to case 4, for the blanket cooling system, some cost reductions seem possible in case 5 (Flibe, direct cooling) but higher costs in the cases 6 and 7 (indirect cooling).

The heat rejection from the plant must be adapted to the H₂O- or He-turbine cycles. For the later one the dry air cooling system, which itself is rather expensive is very attractive. The cost fraction of this cooling system on the plant costs can be kept smaller than in the case of H₂O-cycles (Heat rejection at temperatures between 120°C and 350°C instead of $\approx 350^\circ\text{C}$ for H₂O-cycles).

So pollution-free plant operation at economic conditions is of advantage for case 4.

SUMMARY

From the numerous technical solutions for the heat removal from the blanket region of fusion reactors and for the energy conversion cycles in fusion reactor power plants a selected number of combined systems is considered. These systems are suitable for toroidal reactor configurations such as Tokamak or Stellarator reactors.

Variants for the heat removal system are direct cooling with Li and Flibe and indirect cooling with evaporating water and Potassium, Helium and Flibe. The heat conversion cycles are single cycles with H₂O- or He-turbine and binary K-H₂O-turbine cycles.

Li as coolant requires very high MHD-pumping power which only can be kept relatively low in systems with an H₂O-turbine cycle. Flibe can be applied advantageously as indirect coolant to the binary K-H₂O-cycle. Helium as indirect coolant is suitable for a direct He-turbine cycle. Potassium may be taken as indirect coolant in the case of binary cycles, the MHD-pumping pressures and powers being sufficiently low. In the cases of indirect cooling with H₂O and K steam may be generated in the blanket.

With radial outwards cooling flow arrangements smaller heat exchanger surfaces are obtained than with coolant flows circumferentially to the vacuum wall of the reactor. For Li, Flibe and K circumferentially cooling flow arrangements must be taken to keep the MHD-effects sufficiently small. The lost volume fraction in the blanket is expected to be smallest for He-cooling and He-turbine cycle. Net plant efficiencies of about 53 % can be reached with K-H₂O-cycles. Efficiencies of 46 % with the He-turbine cycle and 42 % with single H₂O-turbine cycle are attainable. The required maximum temperatures of the blanket

⁶ The fuel costs and other running costs being neglected; the thermal power of the reactor being the same.

coolant are 580 to 770°C for single H_2O -turbine cycles. For all other cycles this temperature is 200 to 300°C higher. Lowest maximum pressures in the blanket arise in the cases with Flibe and Potassium as coolant. The highest pressures are necessary for Li as coolant (> 300 bar).

The tritium contamination of the energy conversion cycle will be smallest if external heat exchangers for the heat transmission to the power cycles are provided. Chemical reactions of water with alkaline metals (Li, K) or Flibe are to be feared in the case of H_2O -steam generator failures. No reactions will occur in the case of He-turbine cycle.

The total investment costs of the plant will be nearely the same for He-turbine and K- H_2O -turbine cycles. The economic application of the dry air cooling at the cold end of the cycle is favoured by using the He-turbine cycle.

Although the final valuation of the combined systems considered here cannot be made without more detailed studies both the direct cooled system with He-turbine and the systems with binary cycles have good chances to be adapted for fusion reactor power plants.

REFERENCES

- | 1 | R.S. Pease,
Plasma confinement by magnetic fields
BNES, Nuclear Fusion Reactor Conf., Culham
Sept. 1969
- | 2 | I.N. Golovin, et al.
Tokamak as a possible fusion reactor-comparison
with other C.T.R. devices
BNES, Nuclear Fusion Reactor Conference, Culham
Sept. 1969
- | 3 | C. Gourdon, et al.
The Torsatron without toroidal field coils as a
solution of the divertor problem
Nuclear Fusion 11; 1971, p. 161
- | 4 | D. Steiner,
Neutronic behaviour of two fusion reactor
blanket designs
USAEC Report, ORNL-TM-2648, 1969
- | 5 | A. Fraas,
Appendix 3 and 4 to: Rose D.J.
On the feasibility of power by nuclear fusion
ORNL-TM-2204, 1968

- [6] S. Förster, K.U. Schneider
Design possibilities and consequences for
the conventional parts of fusion power plants
6. Symposium on Fusion Technology, Aachen, Sept. 1970
- [7] HHT - Hochtemperatur-Reaktor mit Heliumturbine
großer Leistung
Jahrbuch 1969

DISCUSSION

TO PAPERS IAEA-CN-28/K-11, K-12, K-13

A. A. HUSSEINY: I would point out that Ref. 4 of paper K-11 gives the maximum permissible air-borne concentration for ^{131}I as $3 \times 10^{-9} \mu\text{Ci}/\text{cm}^3$, not $1.4 \times 10^{-12} \mu\text{Ci}/\text{cm}^3$, the figure given in Table I of that paper. The relative biological hazard given in Table I is meaningless and cannot be used for comparison between different systems; the method of calculating biological hazard is now well established and is taught in colleges, so there is no need to use arbitrary formulae with funny units ($\text{Ci} \cdot \text{cm}^3/\mu\text{Ci} \cdot \text{W}$). One notes in Table III that the power densities for PWR and RFR are different. Consequently, even if we accept the author's method of calculating the relative biological hazard, when we correct the misquoted figures we will end up with a fusion system as hazardous as a PWR. The attempt to promote fusion systems on grounds of safety fails. In addition, the suggestion to use vanadium instead of niobium was considered long ago in connection with fast breeders and dismissed because of embrittlement and corrosion problems (R. T. Frost, private communications (1971)).

D. STEINER: I will address myself to each point in turn. First of all, regarding Ref. 4 of the paper, if you look closely you will see that the figure listed in the Table should be corrected by a factor of 700 for iodine-131 if it appears on crops.

The problem of pathways is completely unresolved as yet and is being thoroughly studied in the AEC; although the relative biological hazard constitutes a somewhat arbitrary criterion for assessing radioactive materials, it is nevertheless very useful for comparisons.

If you read the paper carefully and note the assumptions that are made, I think you will find the figures are consistent with those reported in other studies on radiation in fission reactors.

Finally, regarding the suggested use of vanadium, I am not acquainted with the studies you mention, but work done at the Oak Ridge National Laboratory on the compatibility of vanadium with liquid metal shows that vanadium does, in fact, have better compatibility properties than niobium.

D. J. ROSE: There is much general debate about how the world's future energy needs can best be met, although the overall economics of the many options have not yet been thoroughly worked out. Up to now, decisions to exploit particular energy sources have generally been based on narrow assessments of direct costs, but recently a start has been made in various countries on cost-benefit analyses of the available energy options, including factors such as land use and the effects of effluents. If fusion energy is to be given serious consideration in these comparisons of energy sources, it will be necessary for this assembly to continue in the direction of giving more attention to the topics discussed during this session, e. g. nuclear engineering, environmental and hazard studies, present value estimates of future technology, resource economics, etc.

I congratulate the Conference on moving in this direction, and urge the continuation.

HIGH-FREQUENCY HEATING

(Session L)

Chairman: K. HUSIMI

Papers L-1 and L-2 were presented by
E. CANOBBIO as Rapporteur

Papers L-4 to L-8 were presented by
K. STEPANOV as Rapporteur

NEOCLASSICAL THEORY OF MAGNETIC PUMPING IN TOROIDAL GEOMETRY

E. CANOBBIO

Association EURATOM-CEA,

Département de la physique du plasma

et de la fusion contrôlée,

Grenoble Gare, France

Abstract

NEOCLASSICAL THEORY OF MAGNETIC PUMPING IN TOROIDAL GEOMETRY.

The heating of a low- β plasma confined in a toroidal system by Transit Time Magnetic Pumping (TTMP) is investigated in the case of an arbitrary toroidal low-frequency magnetic configuration, in the limit of low collision frequency ($\nu_{ii} < \omega$) with no restriction on both T_e/T_i (the ratio of electron to ion temperature) and $-j_z/en$ (the parallel electron drift velocity). In particular, (i) a toroidal bumpy RF-field modulation as produced by a conventional array of meridian coils, (ii) a toroidal $\ell=1$ helical RF-field obtained by properly modulating the current flowing in some helical windings, and (iii) the pure radial field produced by Koechlin-Samain coils are considered. In cases (i) and (ii), when the wavelength is comparable to the major radius of the torus, significant additional heating takes place because of the work done by the electric field on the toroidal drift when the magnetic axis is acted upon by the pumping wave. On the other hand, it is found that at relatively high current flow TTMP can be inhibited by overstability.

The heating rate is maximum in the intermediate collision frequency range $\nu_c < \nu_{ii} < \omega$ where it is independent of collisions, while it is ν_{ii}/ν_c times smaller at very low collision frequency because of the non-linear distortion of the distribution function of resonant particles. By using the same variational procedure as Rosenbluth for the toroidal diffusion coefficients in the "banana" regime, a much more precise evaluation of both the heating rate at $\nu_{ii} \ll \nu_c$ and the value of ν_c may now be given. Finally, since the heating rate even at moderate RF-power level can be made much larger than the plasma loss rate in low- β tori, it is concluded that TTMP is a powerful potential method to reach reactor temperatures in Tokamaks and Stellarators.

1. INTRODUCTION

The progress achieved in improving toroidal confinement and also the results of feasibility studies on fusion reactor systems emphasize now the urgency of producing adequate hot plasma by methods overcoming the limitations of Ohmic heating in toroidal traps.

By slightly perturbing a closed magnetic configuration at a frequency $\omega \ll \omega_{gj}$, the ion gyrofrequency, with a wave number k such that $v_\varphi \equiv \omega/k \gtrsim v_{\theta i} \equiv (2kT_i/m_i)^{1/2}$, the ion thermal speed, and $k^{-1} \gg r_{Li}$, the ion Larmor radius, direct conversion of electromagnetic energy into ion temperature occurs uniformly in a plasma volume [1]. The heating rate τ_H^{-1} which is much smaller than the ion collision frequency ν_i ($\nu_i \ll \omega$) can be made larger than the ion-energy and ion-density loss rate τ_{Ei}^{-1} and τ_n^{-1} in low- β -tori [2, 3]. As a result, this process called Transit Time Magnetic Pumping (TTMP) is an RF-method which can possibly be used to reach thermonuclear temperatures. As a matter of fact, even at very high temperatures it should not cause any such deviations from thermal equilibrium that would possibly drive instabilities and deteriorate the quality of confinement.

The purpose of this paper is (a) to generalize the neoclassical theory¹ of TTMP heating with no restriction on both T_e/T_i and $-j_z/en$ (the parallel electron drift velocity corresponding to an Ohmic current) for the most general toroidal field configuration in order to account for favourable torsional effects when the RF-wave length is comparable with the major radius of the torus, and (b), by using the same variational procedure as Rosenbluth for the transport coefficient in the "banana" regime [4], to give a much more precise evaluation of the heating rate at very low collision frequency than was given in Ref. [5]. This evaluation is of major importance for practical purposes because the heating time increases substantially when ν_i is less than a critical value ν_c .

In the next section, the characteristic dependence of TTMP on ν is clarified by simple physical arguments. The theoretical model is defined in section 3 by giving in our co-ordinates the RF-field components and the equations of motion in the drift approximation. Power absorption in the intermediate $-\nu$ regime is derived by a linear calculation in section 4. A non-linear calculation of power absorption at very low ν is presented in section 5, together with an evaluation of the critical collision frequency ν_c separating the two regimes. In section 6 the relation of TTMP heating to toroidal equilibrium is briefly discussed. An exhaustive tabulation of the results of sections 4 and 5 may be found in Ref. [6].

2. COLLISION DEPENDENCE OF TTMP

Before proceeding with precise calculations in specific physical situations it is instructive to demonstrate with simple arguments the distinguishing features of TTMP as a function of ν , by considering the equation

$$\begin{aligned} \left(\frac{\partial}{\partial t} + v \frac{\partial}{\partial z} \right) f + \frac{dv}{dt} \cdot \frac{\partial f}{\partial v} &= C(f) \approx -\nu \frac{\partial}{\partial v} \left(\frac{1}{2} v_{\theta}^2 \frac{\partial f}{\partial v} + v f \right) \\ &\approx -\nu \frac{\partial}{\partial v} \left(\frac{1}{2} v_{\theta}^2 \frac{\partial}{\partial v} (f - f_M) \right) \end{aligned}$$

(A linearized collision operator $C(f)$ can be used as long as $\tau_{Ei}, \tau_n \gg \nu^{-1}$ since f is close to the Maxwellian f_M). Here

$$dv/dt \approx -\mu \nabla B/m \approx \frac{1}{2} v_i^2 kb \sin(kz - \omega t), \quad b \equiv B_1/B_0$$

is the modulation rate. As usually, we set $f = \bar{f} + f_1$, where the perturbation f_1 has the same time and space scale as the wave while \bar{f} is a slowly varying

¹ As in the theory of toroidal diffusion, the term neoclassical is here used in the case of a stable plasma in interaction with an external wave to designate deviations of transport quantities from their classical behaviour (given by resistive/viscous-fluid equations) originating when the interaction involves trapped or slow untrapped particles.

background function, whose slope is distorted only in the interval $|v - v_\phi| \lesssim \Delta v \equiv v_\phi b^{1/2}$ where the particles are resonant:

$$dv/dt|_{v=v_\phi} \cdot \partial \bar{f} / \partial v \approx -\nu v_\phi^2 (\partial \bar{f} / \partial v - \partial f_M / \partial v) / 2\Delta v$$

As a result, $\partial \bar{f} / \partial v = (\partial f_M / \partial v) / (1 + \nu_c / \nu)$ where the critical frequency is roughly given by $\nu_c = 2\Delta v dv/dt v_\phi^2 \approx \omega b^{3/2}$. Hence $\partial \bar{f} / \partial v = \partial f_M / \partial v$ only if $\nu \gg \nu_c$. In other words, in a time of the order of the particle bounce time $\tau_B = (\omega b^{1/2})^{-1}$ in which a resonant particle reverses its velocity relative to the wave, \bar{f} will be locally distorted unless the time to scatter particles out of $\Delta v = O(b^{1/2}v)$, $\tau_c \sim b/\nu$, is shorter than τ_B : $\tau_c / \tau_B = \nu_c / \nu \ll 1$. Now, f_1 obeys a linear equation only if $|\partial f_1 / \partial v| \ll |\partial \bar{f} / \partial v|$. It is readily seen that f_1 is independent of ν if $|v - v_\phi| \gtrsim \Delta U \equiv v_\phi (v/\omega)^{1/3}$, where $f_1 = \frac{1}{2} v_\perp^2 b (\partial \bar{f} / \partial v) \cos(kz - \omega t) / (v - v_\phi)$ while it is collision-dominated within ΔU , and that the above mentioned condition on $|\partial f_1 / \partial v|$ is fulfilled only if $\nu \gg \nu_c$. However, as far as power absorption is concerned, the form of f_1 even within a range $|v - v_\phi| < v_\phi$ is immaterial. In fact, without loss of generality in the linear case we write $C(f_1) = -\nu(v) f_1$; we use complex quantities to get

$$f_1 = f_M (1 + \nu_c / \nu)^{-1} \cdot \left(d \left(\frac{1}{2} m v^2 \right) / dt \right) \times [-i\omega(1 - kv/\omega + i\nu(v)/\omega)]^{-1}$$

so that the time average of power density absorption in a uniform plasma is given by

$$\begin{aligned} \langle \dot{W} \rangle &= \left\langle \int d^3 \vec{v} \frac{d}{dt} \left(\frac{1}{2} m v^2 \right) f \right\rangle \\ &= \frac{1}{2} \int d^3 \vec{v} \frac{f_M \left| \frac{d}{dt} \frac{1}{2} m v^2 \right|^2}{\omega k T (1 + \nu_c / \nu)} \left\{ \frac{\nu(v)/\omega}{(1 - kv/\omega)^2 + (\nu(v)/\omega)^2} \right\} \end{aligned} \tag{1}$$

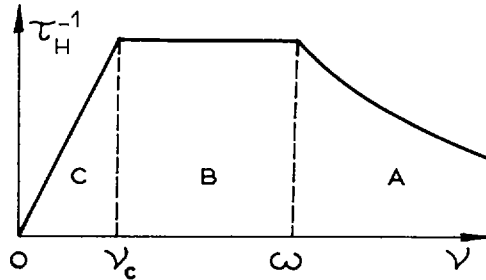


FIG.1. Collision dependency of TTMP.

From the structure of the function in the wavy brackets in Eq.(1), we find the following three ranges (see Fig.1):

$$(A) \quad \nu_c \ll \omega \ll \nu, \quad \langle \dot{W} \rangle \sim \frac{\omega^2}{\nu} b^2 nkT, \quad \tau_H^{-1} \sim \frac{\omega^2}{\nu} b^2 \ll b^2 \nu$$

$$(B) \quad \nu_c \ll \nu \ll \omega, \quad \langle \dot{W} \rangle \sim \omega b^2 nkT, \quad \tau_H^{-1} \sim \omega b^2 \ll \sqrt{b} \nu_c \ll \sqrt{b} \nu$$

$$(C) \quad \nu \ll \nu_c \ll \omega, \quad \langle \dot{W} \rangle \sim \nu b^{1/2} nkT, \quad \tau_H^{-1} \sim \sqrt{b} \nu$$

The dependence of $\langle \dot{W} \rangle$ in case (C) can also be found by using the mean value of the entropy density increase which is given by the quadratic form:

$$\begin{aligned} \langle \dot{W} \rangle &= kT \langle \dot{S} \rangle \\ &= kT \left\langle \int d^3 \vec{v} C(f) \ln f \right\rangle \approx kT \left\langle \int d^3 \vec{v} \frac{f^1}{f_M} C(f^1) \right\rangle \equiv kT \langle K(f^1, f^1) \rangle \end{aligned} \quad (2)$$

Here $f^1 = f - f_M$ is given by a non-linear collisionless equation. It has non-vanishing finite amplitude only within the resonant region $\Delta v \sim v_e b^{1/2}$, so that $\langle \dot{W} \rangle \sim \nu b^{1/2} nkT$.

Since in any case $\tau_H^{-1} \ll \nu$, there are enough collisions to redistribute to the bulk of the particles the energy given to the small number of resonant particles, so that thermal equilibrium is preserved.

In range (A) the dissipative processes in a real plasma are collisional relaxation between parallel and perpendicular degrees of freedom for the ions, heat conduction by the electrons and ion viscosity [1]. Because of the very high density involved, regime (A) is of minor practical interest. In range (B) heating results from the usual Landau absorption process which is collisionless in spite of the fact that f_1 is determined by collisions when $|v - v_\phi| \approx \Delta U$ (collisions simply interchange indistinguishable particles without increasing the entropy of the system). In range (C), where absorption involves the secular non-linear effect first calculated in Ref. [7], a very accurate collision term must be used, because any error in $C(f)$ would also be found in \dot{W} .

Finally, we observe that if a broad wave packet modulation is used with

$$\Delta \left(\frac{\omega}{k} \right) > \Delta v$$

rather than a monochromatic one, insufficient Maxwellization occurs below a critical value $\approx \omega b^2$ which is substantially lower than the value ν_c given for the monochromatic wave [5]. It has also been shown that complete Maxwellization would automatically occur at any collision rate for a pumping wave having stochastic time dependence [8]. Unfortunately, such broad band cases are of minor practical interest since it is very difficult to produce such fields at the required energy level.

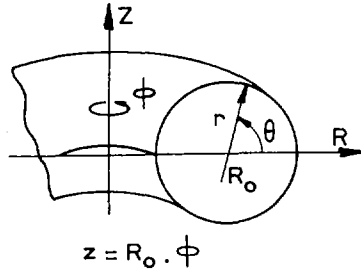


FIG. 2. The co-ordinates.

3. THE MODEL

We consider a thin toroidal plasma of radius r_p around the magnetic axis ($R = R_0 \gg r_p$, $Z = 0$) and a magnetic field $\vec{B}_\phi = \vec{e}_\phi B_0 R_0/R$ (Fig. 2). As shown in section 6, the meridian components of the static configuration are negligible in our problem. If $\beta \ll 1$, the ratio of plasma pressure to magnetic pressure, we have $\omega/k_z \approx v_{\theta i} \ll v_A$, the Alfvén speed (here $k_{||} = \vec{k} \cdot \vec{B}_\phi / B_\phi$). Then the pumping wave is essentially an evanescent vacuum wave ($k_{||}^2/k_\perp^2 + 1 = O(v_{\theta i}^2/v_A^2)$) whose attenuation is, however, irrelevant if $|k_{||} r_p| \ll 1$ both for torsional and compressional waves. Incidentally, we remember that (a) there is equipartition between kinetic and magnetic energy for both kinds of waves, (b) for a compressional wave (B_1) the perturbed pressure is $p_1 \approx \beta |B_0| |B_1| / 4\pi$ and (c) neither $nkT/(B_1^2/8\pi)$ nor $nkT/(B_0 B_1/4\pi)$ are restricted to be less than one in our problem.

The only possible electromagnetic components that are non-vanishing on the magnetic axis are B_{1R} , E_{1z} , B_{1z} , E_{1R} and B_{1z} (the last two, however, have no heating effect) as can be seen by means of the three following typical examples.

Field I: A toroidal bumpy configuration

We set $\vec{B}_1 = \nabla \phi_1$ with

$$\phi_1 = - (B_1/k) \exp i(kz - \omega t) \cdot \left[I_0(kr) (1 + r \cos \theta / R_0)^\alpha + (\alpha/kR_0)^2 \right]$$

If $1 \ll kR_0 \equiv N_\lambda$, the number of wavelengths in the torus, we take $\alpha = -1/2$ as in the usual formulation [9]. Then if $r \ll R_0$, k^{-1} close to the axis, we have in cylindrical co-ordinates $B_{1z} = 0$, $B_{1z} = iB_1 \exp i(kz - \omega t)$ and

$$B_{1R} = B_1 \exp i(kz - \omega t) \cdot (-\alpha/N_\lambda) / (1 + \alpha^2/N_\lambda^2) \approx B_1 \exp i(kz - \omega t) / 2N_\lambda$$

If $N_\lambda = O(1)$, $|B_{1R}|$ is maximum when $\alpha^2 = N_\lambda^2$. In this case, the last expression for B_{1R} holds also in the important case $N_\lambda = 1$. In all cases, we have from Faraday's law $E_{1z} = v_\phi B_{1R}/c$, $E_{1z} = E_{1R} = 0$. Clearly, this RF-configuration can be realized by a conventional array of meridian coils, unless $kR_0 = O(1)$. For example, if $N_\lambda = 1$, two new coils should be put between the two meridian coils (see Fig. 3).

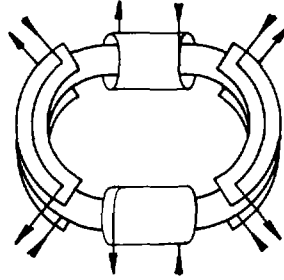


FIG. 3. Schematic RF-coil configuration for a toroidal bumpy field when $N_\lambda = 1$.

Field II: A toroidal $\ell = 1$ helical field [9]

In the limit $r \ll R_0$, k^{-1} , in cylindrical co-ordinates, we have $B_{1R} = B_1(t) \sin kz$, $B_{1z} = -B_1(t) \cos kz$; $B_{1z} = O(r) = E_{1z}$, $E_{1R} = \dot{B}_1 \sin kz / ck$, $E_{1z} = \dot{B}_1 \cos kz / ck$. This can be done by modulating the current flowing in some helical winding in such a way as to produce an essentially $\ell = 1$ field (even if the winding does not have $\ell = 1$).

Field III: A pure radial field

Assuming $\partial/\partial z = B_{1z} = 0$ on the magnetic axis, we have $B_{1R} = B_1 \exp i(kz - \omega t)$, $E_{1z} = v_\phi B_{1R} / c$, $B_{1z} = E_{1z} = E_{1R} = 0$. This can be produced by two parallel torsional coils as proposed in Ref. [10].

To all these electromagnetic components we add an electrostatic axial field as is required to ensure plasma neutrality in spite of the preferential action of TTMP on the ionic component [1, 11].

To lowest order in the RF-amplitude, the drift approximation to single particle motion gives

$$dv_z/dt = \frac{e E_{1z}}{m} + \frac{cv_z E_{1z}}{B_0 R} + \frac{p}{B_0} \left(\frac{B_{1R}}{R} - \frac{\partial B_{1z}}{\partial z} \right)$$

$$dp/dt = \frac{p}{B} \frac{dB}{dt} = \frac{p}{B_0} \left[\left(\frac{\partial}{\partial t} + v_z \frac{\partial}{\partial z} \right) B_{1z} - \frac{B_{1R}}{R} (v_z - v_\phi) \right] \quad (3)$$

$$d \left(\frac{1}{2} m v^2 \right) / dt = e \vec{V}_0 \cdot \vec{E}_1 + \mu \frac{\partial B_1}{\partial t} = e v_z E_{1z} + e V_{0z} E_{1z} + \mu \frac{\partial B_1}{\partial t}$$

where $p = \frac{1}{2} m v_1^2 = \frac{\mu B}{m}$ and $V_{0z} = (v_z^2 + p) / \omega_g R$ is the toroidal drift. Neglecting the R- and Z-dependence, the Boltzmann equation is given by

$$\frac{\partial f}{\partial t} + v_z \frac{\partial f}{\partial z} + \frac{dv_z}{dt} \frac{\partial f}{\partial v_z} + \frac{dp}{dt} \frac{\partial f}{\partial p} = C(f) \quad (4)$$

When collisions are essential, following Rosenbluth [4], we shall use the entropy equation given in section 2 together with the self-adjointness property of the quantity

$$K(g, f) = \int d^3\vec{v} C(f^1) g^1 / g_M = K(f, g)$$

where the subscript M refers to the Maxwellian portion of the function. Only like-particle collisions are considered since they give the largest contribution to power absorption. A particularly well suited form of K for treating problems with local distortions of the slope of f is the following:

$$K(g, f) = - \frac{\pi e^4 \ln \Lambda}{m^2} \int d^3\vec{v} f_M(\vec{v}) \int d^3\vec{v}' f_M(\vec{v}') \frac{\partial^2 u}{\partial v_k \partial v_l} \left(\frac{\partial \hat{g}}{\partial v'_k} - \frac{\partial \hat{g}}{\partial v_k} \right) \left(\frac{\partial \hat{f}}{\partial v'_l} - \frac{\partial \hat{f}}{\partial v_l} \right) \quad (5)$$

Here $\hat{h} = h^1 / h_M$, $u^2 = (v'_k - v_k)(v'_l - v_l)$, $\Lambda \gg 1$ is the usual ratio of the Debye length to the minimum impact parameter. The subscript on v refers to the Cartesian components.

4. THE LINEAR THEORY

For collision frequencies such that $\nu_c < \nu < \omega$, we set $C(f) = 0$ and $\partial f / \partial \vec{v} = \partial f_M / \partial \vec{v}$ in Eq.(4). Here, in general, $f_M \sim \exp[-(2p + (v_z - v_0)^2) / v_0^2]$, with $v_{0i} = 0$ for the ions and $v_{0e} = -j/ne$ for the electrons. Considering a progressive wave $B_{1R} = B_1 \exp i(kz - \omega t)$, the linear perturbations $f_{1i,e}(t, z, \vec{v})$ are easily found by means of Eqs (3) and (4). By equating n_{1e} and n_{1i} we find for

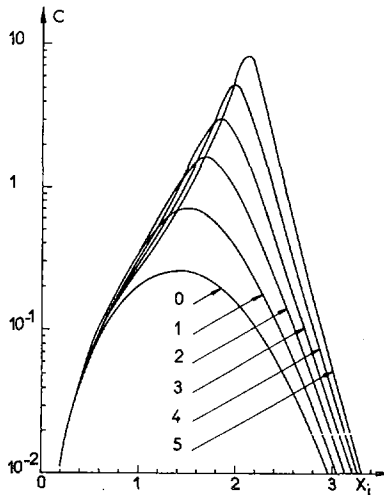


FIG.4. Power absorption by the ions against $x_i = v_\phi / v_{0i}$ for different values of T_e / T_i in regime (B) for Field I, $N_\lambda = 1$ in the case of a travelling wave:

$$\left(\langle \dot{W}_i \rangle / \langle \dot{W}_i \rangle \right)_{[s^{-1}]} = (v_{0i} / R_0)_{[s^{-1}]} |b^*|^2 C$$

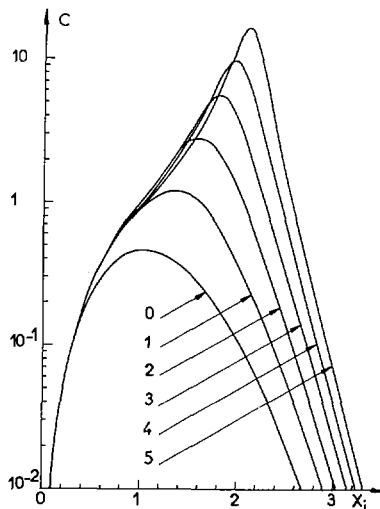


FIG. 5. The same as in Fig. 4 for $N_\lambda = 4$.

E_{1z} the expression $E_{1z} = -kT_e \times AB_{1R}\eta/(eB_0R)$ where

$$\eta = \left[\left(1 + \frac{2x_i^2}{A} \right) \dot{Z}(x_i) - \left(1 + \frac{2x_e^2}{A} \right) \dot{Z}(x_e - x_0) \right] \left[\dot{Z}(x_i) T_e/T_i + \dot{Z}(x_e - x_0) \right]^{-1} \tag{6}$$

Here $x = v_\phi/v_\theta$, $x_0 = v_0/v_\theta$; $A = 1 + 2N_\lambda^2$ for field I ($-iB_{1z} = 2N_\lambda B_{1R}$), $A = 1$ for fields II and III ($B_{1z} = 0$), and $\dot{Z}(x)$ is the derivative of the Fried-and-Conte function.

The time average of the power density absorption by one species of particle is readily seen to be given by

$$\langle \dot{W} \rangle = \left\langle \frac{d}{dt} \frac{3}{2} nkT \right\rangle = W \frac{v_\theta}{R_0} |b^*|^2 \frac{N_\lambda x}{3} \left\{ \sqrt{\pi} (x-x_0) e^{-(x-x_0)^2} \left[1 + \left| 1 + \frac{2x^2}{A} + \xi \right|^2 \right] + \frac{v_0}{v_\phi} \text{Im} [\xi] \right\} \tag{7}$$

where $b^* = AB_{1R}/N_\lambda B_0$, $\xi = \eta$ for electrons, $\xi = -T_e \eta/T_i$ for ions.

In the case of a stationary wave $B_{1R} = B_1 \cos kz \cos \omega t$, $\langle \dot{W} \rangle$ is one half of the value given by Eq. (7).

It is clear that if $v_\phi < v_{0e}$ overstability can occur resulting in power loss from the plasma if $-\langle \dot{W}_e \rangle > \langle \dot{W}_i \rangle$. Figures 4 and 5 give $\langle \dot{W}_i \rangle$ in two cases.

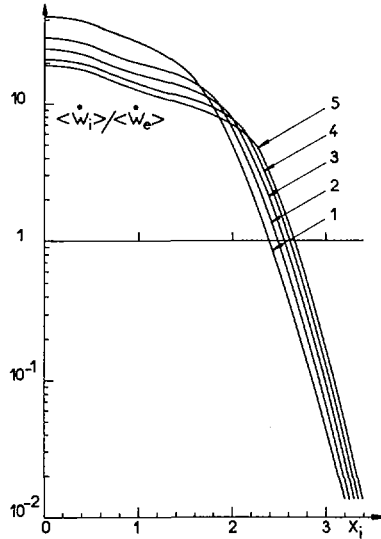


FIG.6. The ratio of ion-to-electron power absorption against $x_i = v_\phi / v_{\theta i}$ for different values of T_e / T_i for Field I, $N_\lambda = 4$, when both species are in regime (B).

It is instructive to give also the time-averaged value of $d(nv_z)/dt$:

$$\left\langle \frac{d}{dt} n_1 v_z \right\rangle = n \frac{v_{\theta 0}^2}{R_0} |b^*|^2 \frac{N_\lambda}{4} \left\{ \sqrt{\pi} (x - x_0) e^{-(x - x_0)^2} \left[1 + \left| 1 + \frac{2x^2}{A} + \xi \right|^2 \right] + \text{Im} [\xi] \right\} \quad (8)$$

The last term on the right-hand sides of both Eqs (7) and (8) is macroscopic in nature. It stems from a de-phasing between E_{1z} and the em-components due to ion Landau damping.

When also the electrons are in regime (B), above a certain x_i -value, typically $2.4 < x_i < 3$ (Fig.6), the electrons are heated preferentially. It is interesting to compare power absorption for a given RF-configuration at different N_λ -values, keeping the value of $\int dV E_1^2 / 8\pi$ constant. $N_\lambda = 1$ is the most suitable value for Fields II and III. For the Configuration I, power absorption for $N_\lambda = 1$ and $N_\lambda = 4$ are almost exactly equal. Clearly, the lowest possible ω -value for a given toroidal plasma configuration corresponds to $N_\lambda = 1$. Finally a comparison between configurations I and III, both at $N_\lambda = 1$, shows the instructive result that the former gives almost 2.6 times more heating for the same value of B_{1R} .

5. THE NON-LINEAR THEORY

If $\nu \ll \nu_c$, the full non-linear Boltzmann equation including the ion-ion collision term must be used. When the perturbation is a function of $z - v_\phi t$ only, the time can be eliminated from this equation by writing

$\partial/\partial t = -v_\varphi \partial/\partial z$, $q \equiv v_z - v_\varphi$, $d/dt = q \partial/\partial z$, $z - v_\varphi t \rightarrow z$. We write also that $E_{1z} = -\partial\phi_1/\partial z$, $B_{1R} = \partial A_{1z}/\partial z$. Then, using the integrals of motion to lowest order in the RF-amplitude, μ and

$$\epsilon = mq^2/2 + \mu B + e\phi_1 - (A_{1z}/RB_0)(\mu B_0 + mv_\varphi(v_\varphi + q))$$

Eq. (4) becomes $q \partial f(z, \epsilon, \mu)/\partial z = C(f)$. Following Ref. [7], the small collision frequency iterative solution of this equation is $f = f^0(\epsilon, \mu) + \nu f^1(z, \epsilon, \mu)$ where f^1 is given by

$$\nu q \partial f^1/\partial z = C(f^0) \quad (9)$$

while f^0 , which alone determines the power absorption, is determined by the solubility condition of Eq. (9)

$$\oint dk_z C(f^0)/q(z, \epsilon, \mu) = 0 \quad (10)$$

As has been shown by Rosenbluth [4], Eq. (10) characterizes any function of ϵ and μ which minimizes the entropy increase defined by Eq. (2). Here f^0 will be calculated by means of this variational method after transforming the integrals of Eq. (5) for $g = f$ in a convenient way for those functions which vanish except for trapped and almost resonant particles.

As a matter of fact, $C(f^0)$ (hence any transport coefficient) differs from zero only because q depends on z (Eq. (9)) and the relative changes of q as a function of z are substantial only for trapped and almost resonant particles. As a result, terms of the type $(\partial \hat{f}/\partial \vec{v})^2$ (or $(\partial \hat{f}/\partial \vec{v}')^2$) contribute to order $b^{*1/2}$ since only one of the integrations, over \vec{v} or \vec{v}' , is restricted to the localized region while the terms $(\partial \hat{f}/\partial \vec{v})(\partial \hat{f}/\partial \vec{v}')$ will contribute less, i. e. to order b^* . Since \hat{f} is localized in the angular variable $\lambda = \mu B_0/\epsilon$, only the derivatives with respect to λ must be considered:

$$\begin{aligned} \partial \hat{f}/\partial \vec{v} &\approx (\partial \hat{f}/\partial \lambda) \partial \lambda/\partial \vec{v} = (\partial \hat{f}/\partial \lambda) (-mq \vec{e}_z/\epsilon + m^2 q^2 \vec{v}/2\epsilon^2) \\ &\approx -\frac{mq}{\epsilon} \vec{e}_z \partial \hat{f}/\partial \lambda \approx \partial \hat{f}/\partial \vec{v}' \end{aligned}$$

where \vec{e}_z is the unit vector in the direction of \vec{B}_φ .

Now we perform the integrations over \vec{v}' in Eq. (5) for $g = f$ by putting $v_0 = 0$ in $f_M(\vec{v}')$. We apply $\partial^2/\partial v_z^2$ to the result, and write the integral over \vec{v} by using ϵ and λ as variables ($d^3\vec{v} = 2\pi\epsilon d\epsilon d\lambda/m^2 q$) so that:

$$\langle \dot{S} \rangle = \frac{4\pi^2 e^4 n \ln \Lambda}{m^2} \int_0^\infty d\epsilon \frac{f_M(\epsilon)}{\epsilon v(\epsilon)} \left[F'\left(\frac{v}{v_\theta}\right) + \frac{v_\theta v_\varphi^2}{v^3} F\left(\frac{v}{v_\theta}\right) \right] \int d\lambda \int \frac{dk_z}{2\pi} q \left(\frac{\partial \hat{f}}{\partial \lambda} \right)^2 \quad (11)$$

where

$$\sqrt{\pi} F(x) = \exp(-x^2) + (2x+x^{-1}) \int_0^x dy \exp(-y^2),$$

$$v^2 = v_\phi^2 + 2\epsilon/m \left(|q| \ll v_\phi \right), \text{ and } f_M(\epsilon) = n(\pi v_\theta^2)^{-3/2} \exp(-v^2/v_\theta^2).$$

To minimize $\langle \dot{S} \rangle$, we now use the trial function $f = \alpha q + h(\epsilon, \lambda)$, where the non-localized term αq (which gives $\dot{S} = 0$) is introduced to satisfy in a simple way the symmetry condition for the distribution of trapped particles at $\lambda \approx 1$, $\partial f / \partial \lambda = \partial (f_M + f_M \hat{f}) / \partial \lambda = 0$. Taking $\alpha = 2v_\phi / v_\theta^2$, we have $\partial h / \partial \lambda = 0$ for trapped particles. Since the difference between B and B_0 is unimportant to the order in which we work, except in q when $|q| \ll v_\phi$, we have $\partial q / \partial \lambda \approx -\epsilon / mq$. Now varying

$$\langle \dot{S} \rangle \sim \int \frac{dkz}{2\pi} q (\partial \hat{f} / \partial \lambda)^2 = \int \frac{dkz}{2\pi} \left(-\frac{\alpha \epsilon}{mq^{1/2}} + q^{1/2} \partial h / \partial \lambda \right)^2$$

with respect to $\partial h / \partial \lambda$ we find for passing particles the localized form

$$\partial h / \partial \lambda = (v_\phi / v_\theta^2) (2\epsilon/m)^{1/2} \int \frac{dkz}{2\pi} (mq^2/2\epsilon)^{1/2}$$

This gives

$$\int \frac{dkz}{2\pi} \frac{q}{\epsilon v} \left(\frac{\partial \hat{f}}{\partial \lambda} \right)^2 = (v_\phi / v_\theta^2)^2 2(m(1+\epsilon_\phi/\epsilon))^{1/2} \cdot^{-1} \\ \times \left\{ \int \frac{dkz/2\pi}{(mq^2/2\epsilon)^{1/2}} - \left(\int \frac{dkz}{2\pi} \left(\frac{mq^2}{2\epsilon} \right)^{1/2} \right)^{-1} \right\}$$

where $\epsilon_\phi = mv_\phi^2/2$. To perform integration over z we use now the following expression for the field of a progressive wave:

$$B_{1z}/B_0 - A_{1z}/RB_0 = -AA_{1z}/RB_0 = b^* \sin^2(kz/2), \quad b^* > 0$$

To calculate \dot{S} to lowest order in ν , E_{1z} must be taken in the limit $\nu = 0$: $e\phi_1 = kT_e AA_{1z}\eta_R/B_0R$, where η_R is obtained by setting $\text{Im}[\dot{Z}] = 0$ in Eq. (6). η_R diverges in the presence of undamped ion-sound waves. We do not give here any renormalization prescription for these isolated frequencies where our iteration procedure breaks down, for they have no real significance in practice. With these field expressions $mq^2/2\epsilon = (1-\lambda)(1-k^2 \sin^2(kz/2))$ with $k^2 = b^* (\lambda + \epsilon_\phi U/2x^2)/(1-\lambda)$ and $U = |2x^2/A + \xi_R|$ ($\xi_R = \eta_R$ for electrons, $\xi_R = -T_e\eta_R/T_i$ for ions). The integrals over z are given in terms of complete elliptic integrals by $2K(k)/\pi(1-\lambda)^{1/2}$ and $2E(k)(1-\lambda)^{1/2}/\pi$, respectively. Since at lowest order in b^* , $(1-\lambda)^{-1/2} d\lambda = 2b^{*1/2} k^2 |1 + \epsilon_\phi U/\epsilon x^2|^{1/2} dk$ by using a property of elliptic integrals, we obtain finally:

$$\langle \dot{W} \rangle_{NL} = W n v_{\theta} b^{*1/2} \ln \Lambda e^4 (kT)^{-2} \frac{8\sqrt{\pi}}{3} \times \left(1 - \frac{2}{\pi} - \frac{1}{4} \left(1 + \frac{7}{8 \times 12} + \dots \right) \right) x^2 e^{-x^2} M \tag{12}$$

where

$$M = M(x^2, U) = \int_0^{\infty} d\psi e^{-\psi} \left(\frac{\psi + U}{\psi + x^2} \right)^{1/2} \times \left[F'(\sqrt{\psi + x^2}) + \frac{x^2}{(\psi + x^2)^{3/2}} F(\sqrt{\psi + x^2}) \right]$$

M is computed in Ref. [6]. The example plotted in Fig. 7 shows the appearance of ion-sound wave divergences for $T_e > 3 T_i$.

A better estimate for the critical density separating heating regimes (C) and (B) may now be obtained by equating Eq. (12) to Eq. (7) for the same kind of wave:

$$n_{c[cm^{-3}]}^H \equiv (b^*)^{3/2} T_{[eV]}^2 D(x, A, N_{\lambda}, \xi, \xi_R) / (\ln \Lambda R_{0[cm]}) \tag{13}$$

D is plotted in Figs 8 and 9 in two ion cases.

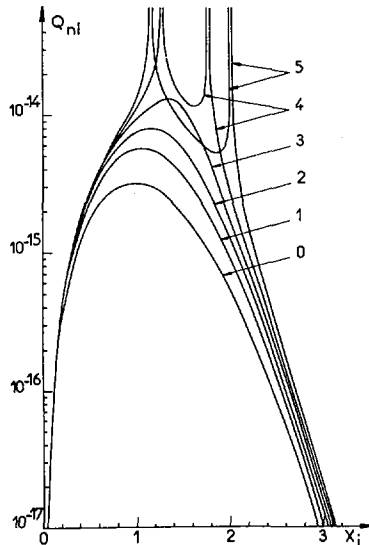


FIG. 7. Power absorption by the ions against $x_i = v_{\phi}/v_{\theta i}$ for different values of T_e/T_i in regime (C) for Field I, $N_{\lambda}=4$:

$$\left(\frac{\langle \dot{W}_i \rangle_{NL}}{\langle W_i \rangle} \right) [s^{-1}] = n_{[cm^{-3}]} v_{\theta i [cm/s]} T_{[eV]}^{-2} b^{*1/2} \ln \Lambda Q_{NL}$$

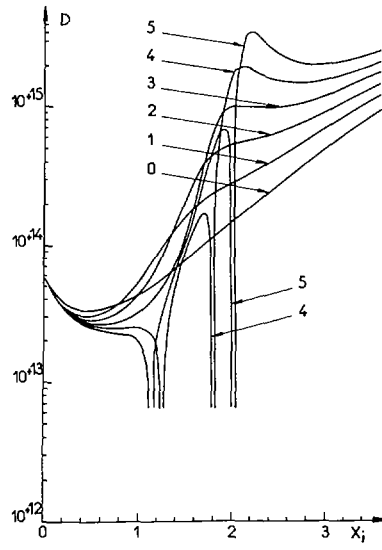


FIG. 8. The critical ion density against $x_i = v_{\phi} / v_{\theta i}$ for different values of T_e / T_i for Field I, $N_{\lambda} = 1$:

$$n_c^H [\text{cm}^{-3}] = (b^*)^{\frac{2}{3}} T_i^2 [\text{eV}] D / (\ln \Lambda R_0 [\text{cm}])$$

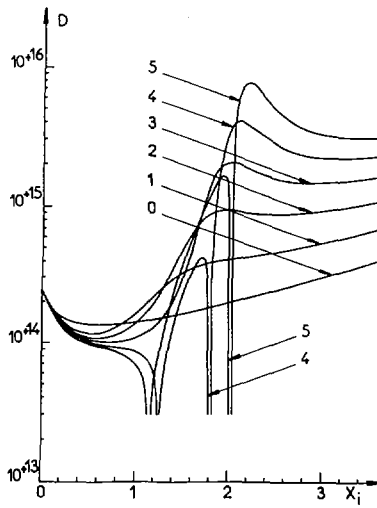


FIG. 9. The same as in Fig. 8 for $N_{\lambda} = 4$.

6. TTMP AND TOROIDAL CONFINEMENT

The main contribution to toroidal diffusion when the mean free path is less than the connection length ($v_\theta/v \ll rB/B_\theta$) arises from a velocity space region where $|v_z| \ll v_\phi$. Moreover, different from ICH, gyro-relaxation and any other RF-heating, TTMP heating acts along \vec{B}_ϕ normal to the "steady toroidal wave" $\sim B_0(1-r \cos \theta/R_0)$. On the other hand, the toroidal effect on passing particles resonating with the RF-field, $\Delta v_z/v_\theta = O(r/R_0)$, is negligible as long as $b^* \gg (r/R_0)^2$ (the Δv_z due to a displacement from a magnetic surface is of higher order).

Unless the radial temperature profile is much flatter than the density profile, $\tau_{Ei} \ll \tau_n$. The essential condition for successful heating is therefore $\tau_H \ll \tau_{Ei}$. For given $q \equiv (Br_p/B_\theta R_0)$, r_p , R_0 , and T_e/T_i values, $\tau_{Ei} \sim B_0^2 T_i^{1/2}$ (banana model) and $\tau_{Ei} \sim B_0^2 T_i^{-3/2}$ (plateau model). Thus, in the heating regime (B) where $\tau_H^{-1} \sim \omega B_i^2/B_0^2$, the increment ΔT_i can be made independent of B_0 . Comparing now n_c^D , as given by Eq.(13), to the critical density of toroidal diffusion n_c^D [12], we obtain

$$n_c^D/n_c^H = 3.6 \times 10^{13} (r_p/R b^*)^{3/2}/qD$$

If $n_c^D < n_c^H < n$, losses increase rapidly with T_i so that $\Delta T_i(t)$ saturates usually at a moderate value [3]. On the contrary, if $n_c^H < n < n_c^D$, losses diminish when T_i increases and $\Delta T_i(t)$ would exponentiate. In this case, the ratio T_e/T_i could be controlled independently from the other parameters of a Tokamak discharge.

ACKNOWLEDGEMENT

The author gratefully acknowledges Dr. S. Giuffr e's help in doing the numerical calculations.

REFERENCES

- [1] DAWSON, J.M., UMAN, M.F., Nucl.Fusion 5 (1965) 242.
- [2] WORT, D.J.H., Proc.Nucl.Fusion Reactors Conference, UKAEA, Culham Laboratory (British Nuclear Energy Society, 1970) 517.
- [3] BRAMBILLA, M., GIUFFR E, S. Report EUR-CEA-FC-595 (1971).
- [4] ROSENBLUTH, M.N., Lecture held at the International Center for Theoretical Physics, Miramare (Trieste) Italy, 1970 (unpublished).
- [5] CANOBBIO, E., in Controlled Fusion and Plasma Physics (Proc.4th.Europ.Conf. CNEN, Rome, 1970) 101.
- [6] CANOBBIO, E., GIUFFR E, S., Report EUR-CEA-FC-601 (1971).
- [7] ZAKHAROV, V.E., KARPMAN, V.I., Soviet Phys.JETP 16 (1963) 351.
- [8] NAKACH, R., Internal Report DPh.PFC-697 (1971).
- [9] MOROZOV, A.I., SOLOV'EV, L.S., in "Review of Plasma Physics" (LEONTOVICH, M.A., Ed.) 2, Consultants Bureau, New York (1967) 1.
- [10] KOEHLIN, F., SAMAIN, A., Phys.Rev.Letts 26 (1971) 490.
- [11] STEPANOV, K.N., Soviet Phys.JETP 18 (1964) 826.
- [12] FURTH, H.P. et al., Physics Fluids 13 (1970) 3020.

NOUVELLE METHODE DE POMPAGE MAGNETIQUE POUR LE CHAUFFAGE DES PLASMAS

F. KOEHLIN, A. SAMAIN
Association Euratom-CEA,
Fontenay-aux Roses, France

Abstract — Résumé

A NEW METHOD OF MAGNETIC PUMPING FOR PLASMA HEATING.

The authors propose a new method of magnetic pumping in which torsion of the static field lines is used instead of compression of the field; the oscillating magnetic field is perpendicular to the static field. The curvature of the lines of force of the static configuration plays an important part in the heating process: the force which heats the particles is the component, along the magnetic perturbation, of the centrifugal force due to thermal motion of the particles. The arrangement proposed is effective in configurations with a large aspect ratio, such as Tokamak configurations. In this case, the most efficient perturbation has the azimuthal wave number 1 around the magnetic axis and around the principal axis. The optimal pumping frequency is of the order of the inverse of the transit time around the principal axis. It is typically three times less than the optimal frequency for compressional magnetic pumping. However, heating of the particles is twice as strong, for equal magnetic perturbations. The authors estimate the increase in the heating power due to the electrostatic field accompanying the magnetic perturbation and the plasma diffusion induced by this perturbation. Particle and energy diffusion due to the perturbation are calculated under conditions where the effect of trapped particles is negligible. The diffusion coefficients have a form analogous to that of the coefficients of the mechanical theory in the intermediate range. The diffusion due to magnetic pumping is only due to the spatial harmonics created by the coils and, in a realistic example, it is assumed that its effect is negligible compared to the other causes of diffusion.

NOUVELLE METHODE DE POMPAGE MAGNETIQUE POUR LE CHAUFFAGE DES PLASMAS.

Une variante de pompage magnétique est proposée. Elle utilise une torsion des lignes de force du champ statique plutôt qu'une compression de ce champ; le champ magnétique oscillant est perpendiculaire au champ statique. La courbure des lignes de force de la configuration statique joue un rôle essentiel dans le processus de chauffage: la force qui chauffe les particules est la composante le long de la perturbation magnétique de la force centrifuge due au mouvement thermique des particules. Le schéma proposé est efficace dans les configurations à fort rapport d'aspect telles que les configurations Tokamak. Dans ce cas, la perturbation la plus efficace a le nombre d'onde azimutal 1 autour de l'axe magnétique et autour du grand axe. La fréquence optimale du pompage est de l'ordre de l'inverse du temps de transit autour du grand axe. Elle est typiquement trois fois plus faible que la fréquence optimale pour le pompage magnétique compressionnel. Cependant le chauffage des particules est deux fois plus important pour des perturbations magnétiques égales. L'augmentation de la puissance de chauffage due au champ électrostatique qui accompagne la perturbation magnétique, ainsi que la diffusion du plasma induite par cette perturbation, sont estimées. La diffusion des particules et de l'énergie introduites par la perturbation est calculée dans un régime où les particules piégées jouent un rôle négligeable. Les coefficients de diffusion ont une forme analogue à celle des coefficients de la théorie néo-classique dans le régime intermédiaire. La diffusion introduite par le pompage magnétique est seulement due aux harmoniques spatiaux créés par les bobinages, et on estime, dans un exemple réaliste, que son effet est négligeable devant les autres sources de diffusion.

I. INTRODUCTION

Le chauffage d'un plasma confiné dans une configuration magnétique fermée pourrait être réalisé au moyen du pompage magnétique par temps de transit (TTMP). La méthode proposée depuis longtemps [1, 2] utilise sur l'axe magnétique une perturbation magnétique δB parallèle au champ de confinement B : $\delta B = B_{||} \cos(k_{||} \ell) \cos(\omega t)$. Les ions de moment magnétique μ subissent

une force $F_{||} = -\mu \partial \delta B / \partial \ell$; si la vitesse de phase $\omega / k_{||}$ de la perturbation appliquée est comparable à la vitesse thermique v_{thi} des ions, un nombre important d'ions résonnants gagnent de l'énergie parallèle. Cette énergie est cédée à l'assemblée ionique si les collisions ion-ion sont suffisamment nombreuses [3].

Dans ce papier, nous montrons qu'une perturbation magnétique $\delta B = b_{\perp} \cos(k_{||} \ell) \cos(\omega t)$ dirigée suivant le grand rayon R de la configuration magnétique peut aussi transférer efficacement de l'énergie aux ions du plasma. La perturbation crée une torsion des lignes de champ dans le plan équatorial de la configuration toroidale; une force $F_{||} \approx (m v_{||}^2 / R) \delta B / B$ s'exerce sur les particules résonnantes de vitesse $v_{||}$; cette force est due à la courbure toroidale R^{-1} des lignes de champ [4]. Le mode le plus simple, $k_{||} = R^{-1}$, consiste en une translation oscillante de toute la configuration magnétique parallèlement au plan équatorial (Fig.1); si la fréquence de ce déplacement est adaptée, $\omega \sim v_{thi} / R$, les particules sont accélérées par un effet de fronde.

Nous établissons d'abord l'équation de diffusion quasi linéaire dans l'espace des phases d'une assemblée de particules sous l'action d'un pompage magnétique. Nous utilisons ensuite cette équation pour évaluer la puissance transférée au plasma dans les deux variantes du pompage magnétique, par compression et par torsion. La résonance de la perturbation avec des ondes acoustiques ou des ondes MHD de torsion est étudiée. Finalement, nous évaluons la diffusion transversale des particules et la diffusion de l'énergie induites par le champ électromagnétique oscillant.

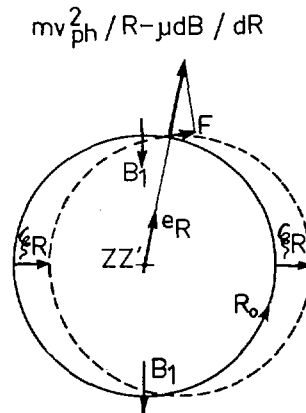


FIG. 1. Torsion de l'axe magnétique et forces agissant sur la particule, dans le cas du chauffage par ondes de torsion (Mode $M = 1$).

B_1 = perturbation magnétique; cercle en tirets = position perturbée de l'axe magnétique; v_{ph} = vitesse de phase; ξ_R = déplacement MHD.

II. DIFFUSION QUASI LINEAIRE INDUITE PAR LE POMPAGE.

Nous considérons un plasma en équilibre dans le champ magnétique B d'une configuration Tokamak. Sur chaque surface magnétique (rayon moyen r , transformée rotationnelle $i = 2\pi/q$) le potentiel électrostatique ψ est constant : $\psi = \psi(r)$ et les ions et les électrons ont une densité $n(r)$ et une température $T_{i,e}(r)$

($2T/m = v_{thi}^2$; $d \log T / d \log n = \eta$). Nous superposons au champ statique une onde électromagnétique stationnaire $\delta E = -1/c \partial \delta A / \partial t$, $\delta B = \nabla \times \delta A$ où

$$\delta A = [\exp(iM\varphi) \alpha(r, \theta) + C. C.] \exp(i\omega t) + C. C. \quad (1)$$

où θ et φ sont les coordonnées angulaires standard autour de l'axe magnétique et du grand axe (Fig.1). La fréquence de cette onde et son nombre d'onde k_{\perp} vérifient $\omega \ll \Omega_i$; $\omega \sim M v_{thi} / R$, $k_{\perp} v_{thi} \ll 1$ ($e, m =$ charge et masse d'une particule ;

$\Omega_i = -eB/mc$; $v_{thi} = v_{thi} / \Omega_i$). Nous supposons que le libre parcours moyen des particules vérifie $\lambda_c \ll q R^{3/2} / r^{1/2}$, pour pouvoir négliger les effets de trapping des électrons.

Nous utilisons le formalisme développé dans [5]. Ce formalisme est basé sur l'utilisation de 2 x 3 variables angulaires et d'action canoniquement conjuguées dont l'existence est assurée si le mouvement des particules dans le champ statique est ergodiquement périodique. Les variables d'action J_1, J_2, J_3 sont des constantes du mouvement de la particule dans le champ statique. Elles spécifient la trajectoire de la particule indépendamment de sa phase sur cette trajectoire, qui est spécifiée par les variables angulaires ϕ_1, ϕ_2, ϕ_3 . L'énergie dans le champ statique d'une particule spécifiée par J_1, J_2, J_3 est une fonction $\mathcal{E}(J_1, J_2, J_3)$. Pour des particules circulantes les dérivées $\partial \mathcal{E} / \partial J_i, \dots$ ont une interprétation simple :

$$\partial \mathcal{E} / \partial J_1 = \Omega \quad ; \quad \partial \mathcal{E} / \partial J_2 = \omega_{\theta} \quad ; \quad \partial \mathcal{E} / \partial J_3 = \omega_{\varphi} \quad (2)$$

où Ω est la fréquence cyclotronique moyenne de la particule et ω_{θ} et ω_{φ} sa fréquence de transit moyenne autour de l'axe magnétique et du grand axe, respectivement.

On peut définir à chaque instant le nombre $F(J_1, J_2, J_3, t)$ des particules de chaque assemblée par unité de volume dJ_1, dJ_2, dJ_3 au point J_1, J_2, J_3 . L'intégration au 2ème ordre de l'équation de Vlasov (utilisant les variables J_1, ϕ_1, \dots) montre que la fonction F vérifie une équation de diffusion quasi linéaire, qui dans le cas où $\omega \ll \Omega$ se réduit à :

$$\frac{\partial F}{\partial t} = 2\pi \sum_{l=-\infty}^{+\infty} \left(l \frac{\partial}{\partial J_2} + M \frac{\partial}{\partial J_3} \right) \left\{ \left(l \frac{\partial F}{\partial J_2} + M \frac{\partial F}{\partial J_3} \right) [|S_{\rho}|^2 \delta(\omega + l \frac{\partial \mathcal{E}}{\partial J_2} + M \frac{\partial \mathcal{E}}{\partial J_3}) + |S_{\rho}|^2 \delta(\omega - l \frac{\partial \mathcal{E}}{\partial J_2} - M \frac{\partial \mathcal{E}}{\partial J_3})] \right\} \quad (3)$$

où S_ℓ est la fonction de J_1, J_2, J_3 définie par :

$$S_\ell = \langle \delta H \exp [-i (\ell \omega_\theta + M \omega_\varphi) t] \rangle \quad (4)$$

$\langle \rangle$ signifie la valeur moyenne dans le temps le long de la trajectoire non perturbée spécifiée par J_1, J_2, J_3 . Si $k_\perp \rho_{thi} \ll 1$

$$\delta H = \mu (\nabla \times [\exp(iM\varphi) \mathbf{a}])_{||} - \left(\frac{e}{c} V_g a_\perp + \frac{e}{c} V_{||} a_{||}\right) \exp(iM\varphi) \quad (5)$$

où V_g et $V_{||}$ sont les vitesses de dérive du centre guide dans les directions perpendiculaire et parallèle au champ. L'équation de diffusion (3) ne concerne naturellement que les particules en résonance avec l'onde, pour lesquelles les fréquences $\omega_\theta = \partial \mathcal{E} / \partial J_2$ et $\omega_\varphi = \partial \mathcal{E} / \partial J_3$ vérifient $\omega \pm (\ell \omega_\theta + M \omega_\varphi) = 0$

Dans les calculs qui suivent, nous négligerons la variation de la vitesse des particules dans le champ statique. On peut alors spécifier la trajectoire d'une particule dans le champ statique, par son moment magnétique $\mu = m V_\perp^2 / 2B$, sa vitesse $V_{||}$ et le rayon r de la surface magnétique où elle évolue. Ces quantités sont des fonctions de J_1, J_2, J_3 . La diffusion des particules dans l'espace $V_\perp^2, V_{||}, r^2$ induite par l'onde est décrite par la transformée de (3). Cette équation de diffusion peut encore être simplifiée si la fonction de distribution des vitesses $V_{||}$ est maxwellienne ; on obtient alors :

$$\begin{aligned} \frac{\partial f}{\partial t} = 2\pi \sum_{\ell=-\infty}^{+\infty} \partial_\ell \left\{ \frac{f}{T} |S_\ell|^2 \left[\left(\omega + \frac{\ell-\lambda}{r} (V_E + V_D) \right) \right. \right. \\ \left. \left. \delta \left(\omega + \left(M + \frac{\ell}{q} \right) \frac{V_{||}}{R} + \frac{\ell-\lambda}{r} V_E \right) - \left(\omega - \frac{\ell-\lambda}{r} (V_E + V_D) \right) \right. \right. \\ \left. \left. \delta \left(\omega - \left(M + \frac{\ell}{q} \right) \frac{V_{||}}{R} - \frac{\ell-\lambda}{r} V_E \right) \right] \right\} \quad (6) \end{aligned}$$

où ∂_ℓ est l'opérateur :

$$\partial_\ell = \frac{1}{R} \left(M + \frac{\ell}{q} \right) \frac{\partial}{\partial V_{||}} + \frac{2c}{eB} (\ell - \lambda) \frac{\partial}{\partial r^2}$$

$\lambda = Mr^2 / qR^2$ et V_E, V_D sont les vitesses de dérive électrique et diamagnétique

$$V_E = \frac{c}{B} \frac{d\psi}{dr}, \quad V_D = \frac{cT}{eB} \frac{d \text{Log } n}{dr} \left[1 + \eta \left(\frac{m(V_\perp^2 + V_{||}^2)}{2T} - \frac{3}{2} \right) \right]$$

Les coefficients de couplage S_ℓ sont les fonctions de $V_\perp, V_{||}, r$, définies par (4) (5).

III. PUISSANCE FOURNIE AU PLASMA

En présence de l'onde spécifiée par (1), la puissance gagnée par les ions (ou les électrons) situés dans une surface magnétique de rayon r est donnée par :

$$W = \int_0^R 2\pi r dr \int_0^\infty dV_\perp^2 \int_{-\infty}^{+\infty} dV_\parallel \frac{\partial F}{\partial t} \varepsilon$$

Utilisant (6) on obtient la densité de puissance w que l'onde cède aux particules et le flux radial de chaleur ϕ_c qu'elle induit :

$$w = \frac{1}{R} \iint dV_\perp^2 dV_\parallel w \frac{F}{T} \sum_l |S_l|^2 \left\{ \left[\omega + \frac{l-1}{r} (V_E + V_D) \right] \delta \left(\omega + \left(M + \frac{l}{q} \right) \frac{V_\parallel}{R} + \frac{l-1}{r} V_E \right) + \left[\omega - \frac{l-1}{r} (V_E + V_D) \right] \delta \left(\omega - \left(M + \frac{l}{q} \right) \frac{V_\parallel}{R} - \frac{l-1}{r} V_E \right) \right\} \quad (7)$$

$$\phi_c = -\frac{1}{Rr} \frac{c}{eB} \iint dV_\perp^2 dV_\parallel \frac{F}{T} \varepsilon \sum_l |S_l|^2 (l-1) \left\{ \left[\omega + \frac{l-1}{r} (V_E + V_D) \right] \delta \left(\omega + \left(M + \frac{l}{q} \right) \frac{V_\parallel}{R} + \frac{l-1}{r} V_E \right) - \left[\omega - \frac{l-1}{r} (V_E + V_D) \right] \delta \left(\omega - \left(M + \frac{l}{q} \right) \frac{V_\parallel}{R} - \frac{l-1}{r} V_E \right) \right\} \quad (8)$$

Sur l'axe magnétique les coefficients S_l sont nuls si $l \neq 0$. La puissance w est due au seul terme S_0 . Ce dernier est non nul pour 2 dispositions de base :

La 1ère utilise une perturbation de compression, $\delta B_\parallel = b_\parallel \cos(\omega t) \cos(M\varphi)$. On a alors $S_0 = (m v_\perp^2 / 8) b_\parallel / B$. La densité de puissance w_i fournie aux ions devient :

$$w_i = n (M/2R) v_{thi} T_i (b_\parallel / B)^2 F(\omega R / M v_{thi})$$

$$F(u) = \pi^{3/2} u^2 \exp(-u^2) \quad (9)$$

L'onde est créée par 2 M bobines de rayon a ayant comme axe l'axe magnétique. Pour $R/a = 5$, on a $M \leq 5$ et la valeur maxima de w_i est $w_{max} = 1,6 n (v_{thi} / R) T_i (b_\parallel / B)^2$, obtenue si $\omega = 5 v_{thi} / R$.

La seconde disposition utilise une perturbation magnétique de torsion $\delta B_\perp = b_\perp \cos(\omega t) \cos(M\varphi)$

$$\left\{ \nabla \times [a \exp(iM\varphi)] \right\}_\parallel = 0 ; a_z = -i \frac{R b_\perp}{4M} ; S_0 = i \frac{m (v_\parallel^2 + v_\perp^2 / 2)}{4M} \frac{b_\perp}{B}$$

La puissance w_i est donnée par

$$w_i = n \frac{1}{2MR} v_{thi} T_i \left(\frac{b_\perp}{B} \right)^2 G \left(\frac{\omega R}{M v_{thi}} \right) \quad (10)$$

où

$$G(u) = \pi^{3/2} u^2 (1 + 2u^2 + 2u^4) \exp(-u^2)$$

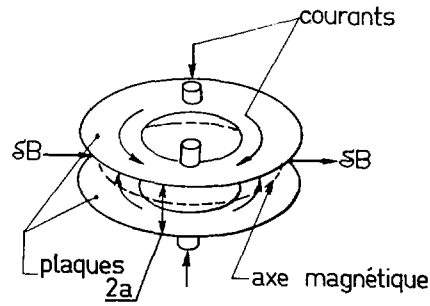


FIG. 2. Description schématique des bobinages et des courants nécessaires pour exciter le mode de torsion $M = 1$.

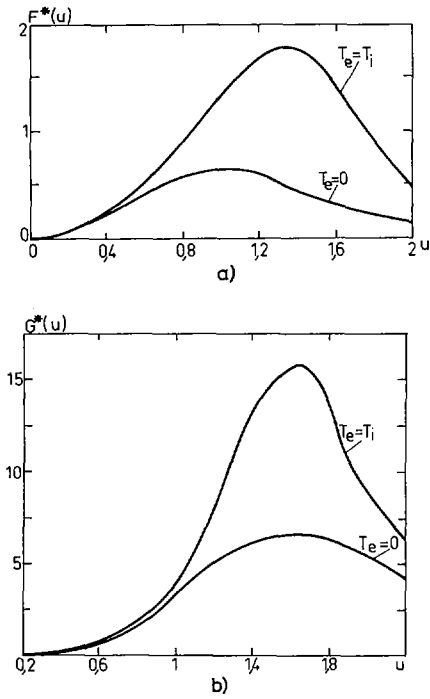


FIG. 3. Puissance cédée au plasma en fonction du rapport de la vitesse de phase de la perturbation à la vitesse thermique des ions (la résonance électrostatique est prise en compte).
 a) dans le cas d'un mode de compression
 b) dans le cas d'un mode de torsion.

La valeur maximum de ω_i^* est obtenue avec $M = 1$ (cf § I),
 $\omega = 1,7 v_{thi}/R$, vaut : $\omega_{Max}^* = 3.3 n (v_{thi}/R) T_i (b_{\perp}/B)^2$

Cette perturbation peut être créée par 2 anneaux ayant comme axe le grand axe, disposés et alimentés électriquement comme le montre la Fig.2. Ce bobinage à l'avantage de principe d'être à l'échelle du grand rayon du plasma plutôt qu'à celle du petit rayon, et éventuellement de pouvoir être éloigné du plasma.

Dans le cas où $T_e \neq 0$, le chauffage est augmenté si le pompage magnétique excite un mode propre acoustique peu amorti du plasma [6]. La puissance reçue par les ions ou les électrons dans ce cas est encore donnée par (9) (10) si les fonctions $F(u)$ $G(u)$ qui figurent dans ces formules sont remplacées par des fonctions $F^*(u)$, $G^*(u)$ qui dépendent du rapport T_i/T_e (Fig.3). Dans le cas d'une onde de torsion un autre type de résonance, de nature MHD, peut intervenir. Par exemple, le pompage induit par les bobines représentées sur la Fig.2 consiste en 2 modes MHD de torsion ayant les nombres d'ondes azimutaux $M_{\phi} = \pm 1$ et $M_{\theta} = \pm 1$. La fréquence propre au mode $M_{\phi} = 1, M_{\theta} = -1$ est $(c_A/R) (1 - q^{-1})$ (c_A est la vitesse d'Alfvén). Elle peut égaler la fréquence $\omega \sim v_{thi}/R$ du pompage au voisinage de l'axe magnétique si le facteur q y est voisin de l'unité : $q - 1 \sim v_{thi}/c_A$. De nouveau, une telle résonance augmente le chauffage du plasma.

IV. PHENOMENES DE TRANSPORT INDUITS PAR LE POMPAGE.

On obtient le flux radial ϕ de particules par unité de surface en utilisant l'équation (6). Il est donné par la formule (8) à condition d'omettre l'énergie \mathcal{E} dans le second membre. La diffusion est surtout due aux coefficients S_{ℓ} avec $\ell \neq 0$, plutôt qu'au coefficient S_0 responsable du chauffage sur l'axe magnétique. Si les bobinages présentent des dissymétries importantes autour de l'axe magnétique, on a $S_{\ell} \sim S_0 (r/a)^{\ell}$ pour certaines valeurs de ℓ ; dans ce qui suit nous prenons $\ell \sim 1$.

En l'absence d'une dérive électrique autour de l'axe magnétique ($V_E = 0$) et autour du grand axe, on a $\phi_{pi} \sim (m_i/m_e)^{1/2} \phi_{pe}$. Il se construit alors un champ radial ambipolaire, qui impose $V_E \sim V_{Di}$. Pour les perturbations de torsion et de compression considérées plus haut, si $T_e \gg T_i$, la diffusion ambipolaire résultante est de l'ordre de :

$$\phi_{pi} = \phi_{pe} \sim 2 \left(\frac{T_e}{T_i} \right)^{3/2} \left(\frac{m_e}{m_i} \right)^{1/2} \left| \frac{dn}{dz} \right| \left(1 + \frac{3}{2} \eta \right) v_{thi} \rho_{thi}^2 \frac{R}{Ma^2} \frac{\overline{\delta B^2}}{B^2}$$

où $\overline{\delta B^2}$ est l'intensité moyenne de δB sur l'axe magnétique. Le flux de chaleur transporté par les ions pour les deux types de perturbations est donné par :

$$\phi_{ci} \sim n \left| \frac{dT_i}{dr} \right| \rho_{thi}^2 v_{thi} \frac{R}{Ma^2} \frac{\overline{\delta B^2}}{B^2}$$

et

$$\phi_{ce} \sim (T_e/T_i)^{5/2} (m_e/m_i)^{1/2} \phi_{ci}$$

Comparant les temps $\tau_{\tilde{p}}$ et $\tau_{\tilde{E}}$ de diffusion des particules et de l'énergie du plasma en présence du chauffage, et le temps de chauffage des ions $\tau_{ch} = nT_i / \omega_i$, on obtient

$$\tau_{\tilde{p}} / \tau_{\tilde{E}} \sim \eta (T_i / T_e)^{3/2} (m_i / m_e)^{1/2}; \quad \tau_{\tilde{E}} / \tau_{ch} \sim \frac{M^2 a^4}{\eta R^2 c_{thi}^2}$$

Pour le plasma de T 3 on a

$$\tau_{\tilde{p}} / \tau_{\tilde{E}} \sim 10; \quad \tau_{\tilde{E}} / \tau_{ch} \sim 10^{+3} - 10^{+5}$$

REFERENCES

- [1] BERGER, J.M., NEWCOMB, W.A., DAWSON, J.M., FRIEMAN, E.A., KULSRUD, M. et LENARD, A., Phys. Fluids 1 (1958) 301.
- [2] DOLGOPOLOV, V.V. et STEPANOV, K.N., Nucl. Fusion 3 (1963) 205.
- [3] CANNOBIO, E., in Proceedings in the IVth European Conference on Controlled Fusion and Plasma Physics (C.N.E.N. Ufficio Edizioni Scientifiche, Roma, 1970) p.101.
- [4] KOECHLIN, F. et SAMAIN, A., Phys. Rev. Letters 26 (1971) 490.
- [5] REBUT, P.H. et SAMAIN, A., C.r. Acad. Sciences 268 B (1969) 607 et 268 B (1969) 783.
- [6] DAWSON, J.M. et UMAN, M.F., Nucl. Fusion 5 (1965) 242.

CYLINDRICAL PLASMA SOURCES WITH DENSITIES HIGH ABOVE CRITICAL DENSITY EXCITED BY AN RF-HELIX WITH AND WITHOUT MAGNETIC FIELD

A. E. AUBERT, A. M. MESSIAEN*, P. E. M. VANDENPLAS
 Laboratoire de Physique des Plasmas,
 Association "Euratom-Etat belge",
 Ecole Royale Militaire
 Brussels, Belgium

Abstract

CYLINDRICAL PLASMA SOURCES WITH DENSITIES HIGH ABOVE CRITICAL DENSITY EXCITED BY AN RF-HELIX WITH AND WITHOUT MAGNETIC FIELD.

It is shown that the density characteristics of plasmas created by an RF-helix are essentially determined by the low-power resonance features of the bounded system, which is constituted by the plasma column and the surrounding helix of finite axial length. The RF-power absorbed by the system is calculated using the theoretical model of a cold electron-ion collisional plasma. Whether a magnetic field is present or not, plasma densities high above critical density are obtained in agreement with the general philosophy previously developed. For each azimuthal n -mode present, the appropriate boundary conditions select discrete values of k_{\perp} (which is a function of k_{\parallel} , ω_{pe}^2/ω^2 and ω_{ce}/ω) on the dispersion curve of the infinite plasma. Experiments already performed support the theoretical predictions. When no steady magnetic field is present, very detailed comparison with experiments has been performed and shows good agreement.

I. INTRODUCTION

It has been shown [1-4] that the characteristics of RF-plasmas created by microwaves at rather high power in the presence or absence of a steady magnetic field are strongly determined by the low-power (i. e. linear) resonance features of the bounded plasma system considered (see Ref. [5] for an excellent review paper). It must be stressed that the appropriate resonances are not those of an unbounded uniform plasma (refractive index equal to infinity) but those arising from the geometrical characteristics of the bounded plasma as coupled to the external exciting microwave field. At a given frequency, the density of the plasma obtained corresponds to one of the resonances of the bounded plasma and, by appropriately choosing the resonance being excited, it is possible to obtain densities much higher than the critical density (the latter being defined by $\omega = \omega_{pe}$; $\omega_{pe}^2 = e^2 \langle N \rangle / \epsilon_0 m_e$). This has been verified in various geometries [1-4]. In Refs [1-3], Messiaen and Vandenplas considered a resonantly sustained cylindrical plasma obtained by excitation of a dipolar mode (azimuthal dependence in $\exp(in\theta)$ with $n = \pm 1$) with $k_{\parallel} \approx 0$ (k_{\parallel} is the propagation wave number along the z -axis of the cylinder). The RF-power was coupled by a waveguide perpendicular to the plasma column (wave vector \mathbf{k} and electric field \mathbf{E} perpendicular to the z -axis; steady magnetic induction B_0 parallel to the z -axis); densities greater than

* Collaborateur scientifique de l' Institut Interuniversitaire des Sciences Nucléaires.

10^{12} cm^{-3} were easily obtained (frequency: $\omega/2\pi \approx 3 \text{ GHz}$, power: 30-75 W). Good agreement was found between the densities of the resonantly sustained plasmas and those predicted on the basis of linear theory of bounded plasmas. The general nature of the results obtained was underlined.

On the other hand, RF-plasma sources have been proposed which use other devices to couple RF-energy to the plasma column [6]. More recently, plasma sources using a helicoidal excitation have been studied [7] and densities greater than 10^{13} cm^{-3} have been reported. However, the only theoretical explanation suggested was based on the characteristics of infinite plasmas since the plasmas were though not to be "resonant" in the sense used when describing bounded systems.

In accordance with the general philosophy developed in Refs [1-4], we have recently reported in a summary form [8] that the behaviour of a cylindrical plasma created by a helix depends, in fact, essentially on the properties of the bounded plasma system. In the present paper, we furthermore include the ions and the phenomenological collisions for momentum transfer (which can eventually include collisionless damping) in order to calculate the absorbed power. The resulting computations are extended into the magneto-ion domain up to the lower hybrid region. When $B_0 = 0$, the theoretical plot of absorbed power versus density is compared to experiments in the range of 1 to 3 GHz, and there is quite good agreement between theory and experiments.

When $B_0 \neq 0$, the present theoretical approach demonstrates the possibility of RF-absorption in order to create resonantly sustained plasmas for high values of ω_{ce}/ω and ω_{pe}^2/ω^2 .

2. THEORY

1. Dispersion relation of helix-plasma system

We consider the linear quasi-static cold theory (the RF-electric field $\vec{E} \cong -\nabla\phi$) of an electron-ion plasma cylinder with collisions, subjected to an axial magnetic field \vec{B}_0 . The validity of both the quasi-static and the cold-plasma approximation will be assessed carefully in Appendix A. Throughout, cylindrical co-ordinates r, θ, z will be used. We shall now show that, in accordance with the general philosophy developed in Refs [1-4], the behaviour of a cylindrical plasma column excited by a helix, in fact, only depends on the properties of this bounded system.

The column is assumed to be helicoidally excited by a surface charge density σ which is zero everywhere except along a tape helix (the width of which is vanishingly small) located at the boundary between the plasma and the outer medium. We easily obtain σ as a function of azimuthal modes

$$\begin{aligned} \sigma &= \sigma_0 \exp(i\beta_0 z) \delta\left(\theta - \frac{2\pi z}{p}\right) \delta(r - a) \\ &= \frac{\sigma_0}{2\pi} \sum_{n=-\infty}^{+\infty} \exp\left[i\left(\beta_0 - \frac{2\pi n}{p}\right)z\right] \exp(in\theta) \end{aligned} \quad (1)$$

where p is the pitch of the helix, a is the radius of the plasma column and of the helix, and β_0 is a wave number to be discussed later.

We notice that all multipolar models ($-\infty \leq n \leq \infty$) are excited simultaneously. A suitable finite solution for the RF-potential ϕ_p inside the plasma which satisfies $\nabla \cdot \vec{\epsilon}_p \cdot \nabla \phi_p = 0$ (ϵ_p being the dielectric tensor of the cold plasma) is given by

$$\phi_p = \sum_{n=-\infty}^{+\infty} A_n J_{|n|}(k_{pn}r) \exp(in\theta) \exp(ik_{||n}z) \quad (2)$$

with

$$k_{pn}^2 = -k_{||n}^2 [(1 - \Omega_e^2 - \Omega_i^2)/(1 - A_e - A_i)]$$

where

$$A_\alpha = \frac{\omega_{p\alpha}^2 \lambda_\alpha}{\lambda_\alpha^2 \omega^2 - \omega_{c\alpha}^2}; \quad \beta_\alpha = \frac{\omega_{c\alpha}}{\omega \lambda_\alpha}; \quad \lambda_\alpha = 1 + i \frac{\nu_\alpha}{\omega}$$

$$\omega_{p\alpha}^2 = \frac{\langle N \rangle e^2}{m_\alpha \epsilon_0}; \quad \Omega_\alpha^2 = \frac{\omega_{p\alpha}^2}{\omega^2 \lambda_\alpha}; \quad \omega_{c\alpha} = \frac{e B_0}{m_\alpha}; \quad \alpha = e, i$$

ν_α are effective collision frequencies for momentum transfer. The potential ϕ_{ext} outside the plasma is the solution of the Laplace equation which has the correct behaviour at infinity:

$$\phi_{\text{ext}} = \sum_{n=-\infty}^{\infty} B_n K_{|n|}(k_{||n}r) \exp(in\theta) \exp(ik_{||n}z) \quad (3)$$

To determine the constants A_n (and B_n), the boundary conditions at $r = a$ have to be imposed on every mode: first, continuity of ϕ , and secondly, discontinuity of the normal components of the electric displacement vector, the jump being equal to the surface charge density as given by Eq. (1). We obtain

$$A_n = \frac{\sigma_0}{2\pi\epsilon_0} \frac{a}{J_{|n|}(k_{pn}a)} D_n^{-1} \quad (4)$$

with

$$D_n = (1 - A_e - A_i) a k_{pn} \frac{J'_{|n|}(k_{pn}a)}{J_{|n|}(k_{pn}a)} + n(-\beta_e A_e + \beta_i A_i) - K_g a k_{||n} \frac{K'_{|n|}(ak_n)}{K_{|n|}(ak_n)} \quad (5)$$

and

$$k_{||n}^2 = \left(\beta_0 - \frac{2\pi}{p} n \right)^2 = \left[\left(\frac{S}{L} - \frac{2n}{p} \right) \pi \right]^2; \quad s = 1, 2, 3, \dots \quad (6)$$

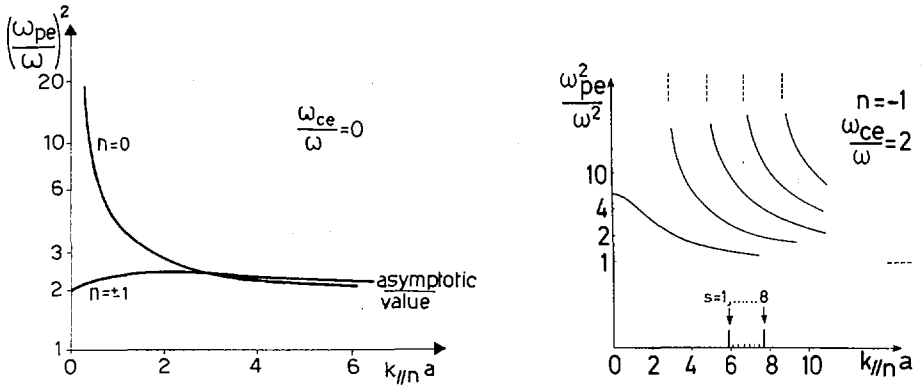


FIG. 1a) Dispersion curves of a plasma cylinder in vacuum for $n = 0$ and $n = \pm 1$ without steady magnetic field ($K_g = 1$);

1b) dispersion curve of a plasma cylinder in vacuum ($K_g = 1$) for $n = -1$ with a steady magnetic field ($B_0 = 1.7$ kG) with excitation by a helix of finite length. Discrete operating points are selected on these curves by appropriate values of $k_{||n}$. These values of $k_{||n}$ are indicated in the figure for the case of $1 \leq s \leq 8$, $a = 0.9$ cm, $p = 1$ cm and $L = 11$ cm (the dashed lines show the asymptotic values for large ω_{pe}^2/ω^2 or large $k_{||n} a$).

in which β_0 is assumed to be imposed by the finite length L of the helix. K_g is the dielectric constant of the external medium.

A given n mode of ϕ_p will be preferentially excited, in the collisionless case, when $A_n J_{|n|}$ is infinite, i. e. $D_n = 0$. These zeros correspond to points selected by the discrete values of $k_{||n}$ on the dispersion relation given by Trivelpiece and Gould [9] and more extensively discussed in Ref. [10]. These resonance values are somewhat altered when collisions are introduced. In the following theoretical discussion of the location of the resonances, we neglect these collisions.

In the absence of a steady magnetic field the picture is very clear. Figure 1a shows the dispersion curves of the infinite plasma for $n = 0$ and $n = \pm 1$ (the curves for $n = \pm 2, \pm 3, \dots$ do not differ qualitatively from those for $n = \pm 1$). The resonances of the bounded system (plasma column + helix) are given by discrete working points, corresponding to the zeros of D_n for which $k_{||n}$ is given by Eq. (6). One sees that very high values of ω_{pe}^2/ω^2 can be obtained with the $n = 0$ mode for small $k_{||0}$.

When a steady magnetic field B_0 is present, new branches will appear if $\omega_{ce}/\omega > 1$. This can be seen in Fig. 1b for $n = -1$ when $\omega_{ce}/\omega = 2$. This figure also shows that a properly chosen value of $k_{||n}$ can give rise to several resonance values of ω_{pe}^2/ω^2 . This phenomenon is perhaps clearer when examined on a CMA-diagram.

As a typical example, Fig. 2a gives the location in a CMA-diagram of the $n = -1$ mode for $k_{||} = 0$ (dashed curve 1a; this mode has been previously studied in Refs [2, 3]) together with the different branches of this $n = -1$ mode for $k_{||} a = 4$ (solid curves 1b, 2, 3, and 4). The calculation of D_n shows that for all n modes, a non-zero value of $k_{||} a$ has two effects:

(1) The shifting of the mode already existing for $k_{||} a = 0$ (1a into 1b for the case of Fig. 2a).

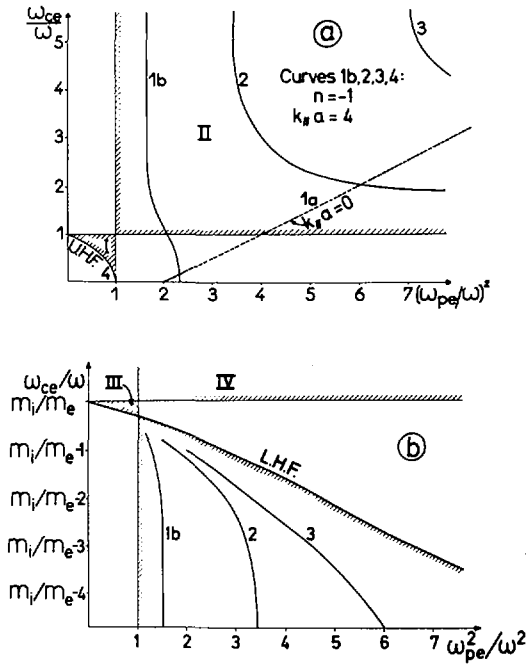


FIG. 2a) CMA-diagram of $n = -1$ mode when $k_{||}a = 0$ and $k_{||}a = 4$ for low value of ω_{ce}/ω .

2b) continuation of the CMA-diagram of Fig. 2a in the neighbourhood of the lower hybrid frequency ($\omega_{ce}/\omega \gg 1$). The curves are computed for $m_i/m_e = 7330$.

(2) The appearance of new branches as pointed out in Ref. [10]. The new branches (which become more and more numerous as $k_{||}a$ becomes larger) are located in a CMA-diagram in the region $\omega_{pe} > \omega$ when $\omega_{ce} > \omega$ (these are the "static" modes of Ref. [10] and are located in region II of Fig. 2a; in our example, they correspond to curves 2 and 3). When $\omega_{ce} < \omega$, these new branches are located in the region $(\omega^2 - \omega_{ce}^2)^{1/2} < \omega_{pe} < \omega$ (these are the "dynamic" modes of Ref. [10] and are located in region I of Fig. 2a; in our example, they form an infinite set of curves very close to curve 4 which is the upper hybrid frequency. Furthermore, in this last region the interaction with the warm Bernstein modes, near the cyclotron harmonics, is preponderant [2, 3] and this effect, which can lead to high densities, is not included in the cold theory used in the present paper. To conclude, it is clear that a large number of branches exist in region II for a given n mode permitting to obtain high densities for any value of $\omega_{ce} > \omega$.

Figure 2b indicates the behaviour of the branches of region II at high magnetic field in the immediate neighbourhood of the lower hybrid frequency. (Note that the upper and lower hybrid frequencies $\omega_{UHF}/2\pi$ and $\omega_{LHF}/2\pi$ correspond to the zeros of the expression $1 - A_1 - A_e$, i. e. to the infinities of $k_{||}^2$ given by Eq. (2)).

In Fig. 2b, two new regions, namely regions III and IV, appear in which resonances can exist in the magneto-ion domain.

2. Power absorbed by the plasma column

The RF-power absorbed by the plasma can be calculated by using Ohm's law and the RF-conductivity tensor $\vec{\sigma} = i \omega (\epsilon_0 - \vec{\epsilon}_p)$. The time-averaged power absorbed within the volume V is given by

$$P_{\text{abs}} = \frac{1}{2} \operatorname{Re} \int_V \vec{J} \cdot \vec{E}^* dV = \frac{1}{2} \operatorname{Re} \int_V (\vec{\sigma} \cdot \vec{E}) \vec{E}^* dV \quad (7)$$

where \vec{J} is the current due to the RF-field and $*$ denotes the complex conjugate. We recall that damping is introduced in $\vec{\sigma}$ by effective collision frequencies for momentum transfer (which can eventually include collisionless damping).

Introducing \vec{E} derived from Eq. (2) into Eq. (7) and using the eigenvalues of $k_{\parallel n}$ given by Eq. (6), we obtain

$$P_{\text{abs}} = \pi L \operatorname{Re} \left\{ \sum_{n=-\infty}^{+\infty} \sum_{s=1}^{\infty} \omega \epsilon_0 i A_n A_n^* F \right\} \quad (8)$$

where A_n is given by Eq. (4) and F is defined by

$$\begin{aligned} F = & \frac{4\pi a (k_{pn} k_{pn}^*) i \operatorname{Im} [k_{pn}^* J_{|n|+1} (k_{pn} a) J_{|n|}^* (k_{pn} a)]}{k_{pn}^2 - k_{pn}^{*2}} \\ & + \frac{4\pi a k_{|n|}^2 i \operatorname{Im} [k_{pn}^* J_{|n|} (k_{pn} a) J_{|n|-1}^* (k_{pn} a)]}{k_{pn}^2 - k_{pn}^{*2}} \\ & + [J_{|n|} (k_{pn} a) J_{|n|}^* (k_{pn} a)] [2\pi |n| (A_e + A_l) - 2\pi n (-\beta_e A_e + \beta_l A_l)] \end{aligned} \quad (9)$$

We now compute a normalized absorbed power

$$\mathcal{P}_{\text{abs}} = P_{\text{abs}} \left(\frac{\sigma_0^2 \omega L a^2 \pi}{\epsilon_0} \right)^{-1} \quad (10)$$

which is essentially normalized with respect to the volume $\pi a^2 L$ enclosed by the helix and to the square of the amplitude σ_0 of the RF surface charge density.

Examination of Eq. (8) shows that the absorption is due both to the discrete values of $k_{\parallel n}$ imposed by the finite dimensions of the helix, and to the excitation of the multipolar modes n . In our experimental conditions, we find that for a given n , the sum over k_{\parallel} is already well estimated when the first ten terms are taken into account. With respect to n , we find that

the terms $-6 \leq n \leq +6$ are the only ones that provide a non-negligible contribution, at least when $B_0 = 0$.

Typical results are displayed in Figs 4b, 5 and discussed in the next section.

3. DISCUSSION

1. Absorbed power versus losses

An important problem raised by the comparison of the absorbed RF-power as theoretically calculated in section 2.2 with the density obtained in a given set-up is that of the different losses occurring in the plasma. A radio-frequency resonant discharge is characterized by the equality between the RF-power P_{abs} absorbed at resonance by the plasma and the power losses in this same plasma [11]. This problem has been treated in detail in Ref. [3]: the losses are mainly due to wall heating, radiation, flow of plasma outside the interaction zone between plasma and helix, and also, in some cases, especially for the $n = 0$ mode, to propagation of waves outside the interaction zone as shown in Ref. [12]. It has also been stressed in Ref. [3] that the absorbed RF-power mostly serves to increase the electron density $\langle N \rangle$ and that the electron temperature T_e is only slightly altered. In a first approximation, this T_e is determined by the balance equation of the plasma; it is in the 1 eV - 20 eV range, depending on the gas, in a pressure range of $10^{-1} - 10^{-4}$ Torr.

The density obtained in the set-up is determined by the intersection of the curve giving the radio-frequency P_{abs} versus $\langle N \rangle$ with the curve giving P_{losses} versus $\langle N \rangle$.

2. No magnetic field

In this subsection, we compare theory to the experiments already performed.

The plasma is created in a cylindrical mercury discharge tube (neutral pressure: 3×10^{-3} Torr, $a = 0.38$ cm) surrounded by a helix ($L = 10$ cm, $p = 1$ cm), one end of which is short-circuited to the cylindrical cavity enclosing the whole in order to prevent radiation (see Fig. 3).

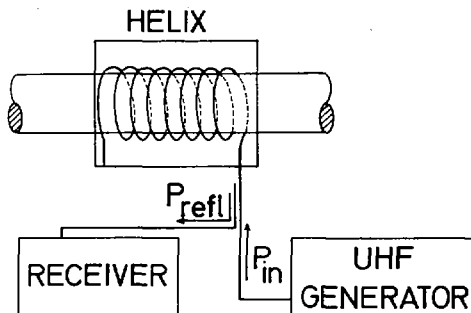


FIG. 3. Experimental setup.

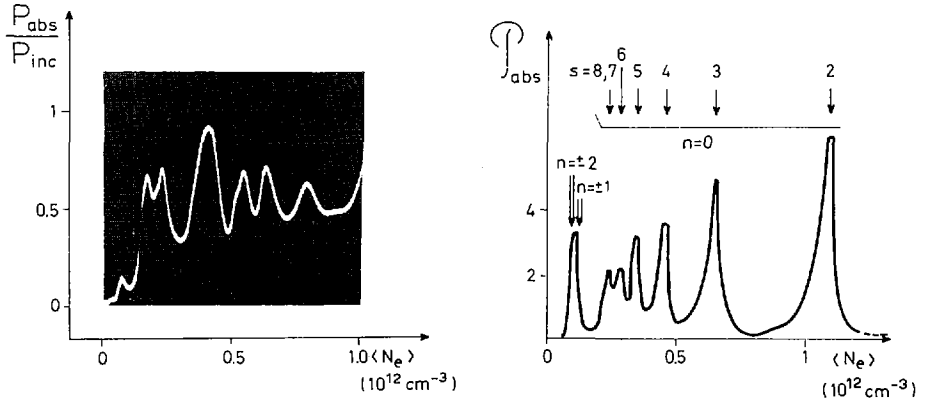


FIG. 4a) Typical experimental absorption curve at low microwave power in a Hg-discharge without magnetic field ($P_{in} \approx 20 \text{ mW}$, $\omega/2\pi = 2.0 \text{ GHz}$)

4b) computed curve for a Hg-plasma ($\nu_e = 500 \text{ MHz}$; $\nu_i = 7 \text{ kHz}$) corresponding to the experimental conditions. The contribution from the different modes are indicated in the figure.

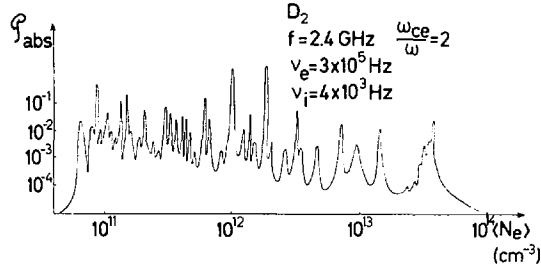


FIG. 5. Typical computed resonance curve with magnetic field.

In a first experiment at low power (20 mW), the discharge current increases linearly from a keep-alive value of 40 mA to 3 A in 100 μs while the helix is excited at a fixed frequency ω . An oscillogram exhibiting a typical resonance spectrum is shown in Fig. 4a. The time axis, is, in fact, a density axis: the plasma density increases linearly during the rise of the current. We observe:

a) Absorption maxima for $\omega_{pe} \leq \omega$ which correspond to a temperature effect not included in the cold plasma theory (see Ref. [13], chapter 5). In the oscillogram, these small peaks are situated at the foot of the left flank of the first large peak.

b) Starting from the cold dipolar resonance [$\omega_{pe}^2/\omega^2 \cong 3$ instead of 2 because of the influence of the glass wall (see Ref. [13], pp. 10-11 and 47 for the explanation of this type of resonance)], we obtain a great number of resonances up to the maximum density obtainable in our device

($\sim 10^{12} \text{ cm}^{-3}$). The densities are measured by the luminosity and cavity methods as indicated in Refs [1-4].

To be sure of the identification of the temperature modes and of the $n = \pm 1$ cold modes, these results have been compared both with scattering results [13] and with results obtained by excitation in a cylindrical cavity [14].

In a second experiment, the RF power is increased. When a minimum value is reached ($\cong 12 \text{ W}$), the dc current can be turned off because the plasma is resonantly sustained. We have checked that the densities for which these RF-sustained plasmas exist are precisely those corresponding to the various resonances excited at low power, see Fig. 2 of Ref. [8].

Figure 4b gives a theoretical curve which is in good agreement with the experimental curve of Fig. 4a. This theoretical curve for the normalized \mathcal{P}_{abs} is computed from Eqs (10) and (8) by retaining the terms $-2 \leq n \leq 2$ and $1 \leq s \leq 8$ which already give a good approximation of \mathcal{P}_{abs} .

Since $L \gg p$, the modes characterized by $n \neq 0$ are almost entirely determined by the value of the pitch p (since the contributions from high s values are negligible). The $n = \pm 2$ and $n = \pm 1$ values can be distinguished in Fig. 4b.

On the other hand, for the symmetric mode $n = 0$, $k_{\parallel 0}$ is solely determined by s/L and is thus small. Figure 1a shows that the $n = 0$ modes therefore have high values of $(\omega_{pe}/\omega)^2$; the details of their s -structure are indicated in Fig. 4b. When comparing this with the experimental curve, we must expect the greatest discrepancy to occur here since, in the experimental situation, the effective L is greater than that of the theoretical model because the plasma column created extends outside the helix of length L and leads thus to smaller $k_{\parallel 0}$ (and thus higher densities). Another cause of some numerical discrepancy is the fact that in the experiments the helix is wound around the glass cylinder while in the theoretical model it lies at the interface between the plasma and the external medium.

3. With magnetic field \vec{B}_0

The CMA-diagram of Fig. 2a helps us to understand the numerous resonances occurring in Fig. 5. With a sufficiently small magnetic field (here $\omega_{ce}/\omega = 2$), we have a single resonant operating point (on curve 1b of Fig. 2a) for a given k_{\parallel} of the $n = -1$ mode considered. Thus in the total picture (see Fig. 5) we have, in principle, one resonance peak or more for each eigenvalue of k_{\parallel} corresponding to a given n mode (here: $-2 \leq n \leq 2$). This accounts for the multiplicity of resonances in Fig. 5.

Figure 2a shows that, for a given k_{\parallel} of a given n mode, more resonances are possible when ω_{ce}/ω increases. The multiplicity of resonances thus increases with ω_{ce}/ω and this theoretical explanation indicates that the great number of possible resonances can lead, experimentally, to the misleading interpretation of a continuum of densities in the absorption spectrum. In this respect, we must bear in mind what has been said in section 3.1: the plasma will be resonantly sustained when there is equality between the losses of power P_{losses} and the absorbed RF-power. Since P_{losses} increases with $\langle N \rangle$, this explains why, at a given incident RF-power, a maximum density is reached even if resonances with higher density are still available.

It has been previously demonstrated by Messiaen and Vandenplas [2, 3] that, when $k_{\parallel} \cong 0$ and when the excitation is depolar ($n = \pm 1$), the densities obtained in a microwave-sustained plasma are those corresponding to the resonance spectrum at low power. It has furthermore been shown that the $n = -1$ resonance is followed, i. e. curve 1a of Fig. 2a when $\omega_{ce}/\omega > 1$.

A helix experiment recently performed with $B_0 \neq 0$ [15] has shown that the regions of plasma existence at high density are consistent with the location of the modes in region II of Fig. 2a. Related results have also been obtained in the cigar-shaped device of the Ioffe Institute Group [16].

4. CONCLUSION

We conclude by stressing that it is thus again clear that the various methods of creation of high-density microwave plasma in a given geometrical structure are based on the excitation of those eigenresonances of the bounded system (here helix-plasma column) for which the absorbed RF-power is sufficient to resonantly sustain the plasma even when $\omega_{pe}^2 \gg \omega^2$. The obtainment of densities high above the critical density which may seem strange from the point of view of infinite plasmas is easy to understand when bounded plasmas are considered because these bounded systems possess discrete resonance states characterized by $\omega_{pe}^2/\omega^2 \gg 1$. Indeed, the appropriate boundary conditions select, for each azimuthal n -mode present, discrete values of k_{\perp} (which is a function of k_{\parallel} , ω_{pe}^2 and ω_{ce}/ω) on the dispersion curve of the infinite plasma. The present study therefore fully confirms the general philosophy developed in Refs [1-4].

ACKNOWLEDGEMENTS

We are indebted to J. Neefs, F. Van Goethem, and F. Van Thillo for technical assistance.

APPENDIX A

The quasi-static approximation ($\vec{E} \cong -\nabla\phi$) has been made and the temperature of electrons and ions have been neglected in the present theoretical model. The validity of these approximations is assessed by comparing the results obtained here with other results obtained for the same range of parameters by using a more sophisticated approach (full electromagnetic treatment; $T_e \neq 0$ and $T_i \neq 0$) in connection with the study of resonant heating of a plasma column in the magneto-ion domain [17].

The quasi-static approximation is fully warranted, broadly speaking, when $k_0^2 \ll k_{\parallel}^2$. More precisely, the criterion for a cold plasma is given by

$$k_0^2 \ll k_{\parallel}^2 \left| \frac{2 - \Omega_e^2 - \Omega_i^2 - A_e - A_i}{(1 - A_e - A_i)^2 - (\beta_e A_e - \beta_i A_i)^2 + (1 - A_e - A_i)(1 - \Omega_e - \Omega_i)} \right|$$

and

$$k_0^4 \ll k_{\parallel}^4 \left| (1 - A_e - A_i)^2 - (\beta_e A_e - \beta_i A_i)^2 \right|^{-1}$$

The cold-plasma approximation can be examined in two distinct cases:

- 1) $\omega_{ce}/\omega < 1$, there exist supplementary temperature modes, the so-called Bernstein modes [3, 13, 15], which are strong in the vicinity of the electron cyclotron harmonics. Outside the first cyclotron harmonics, the cold-plasma approximation is valid.
- 2) $\omega_{ce}/\omega > 1$, the temperature effects can be neglected, for a given temperature, when ω_{ce}/ω is not too high. In fact, the temperature effects are strongest in the vicinity of the lower hybrid frequency. For $k_0^2 \ll k_{\parallel}^2$, the precise criterion is

$$r_{De}^2 \ll \left| \frac{1 - A_e - A_i}{k_{\parallel}^2 [\Omega_e^2 (A_i - 1) + (\Omega_e^2 - 1) A_e]} \right|$$

and

$$r_{De}^2 \ll \left| \frac{1 - \Omega_e^2 - \Omega_i^2}{k_{\parallel}^2 \Omega_e^2 (\Omega_i^2 - 1)} \right|$$

where r_{De} is the electron Debye radius.

Finally, if T_i is not greater than T_e , the ion temperature only plays a subsidiary role on the resonance pattern when $\omega \gg \omega_{L.H.F.}$

REFERENCES

- [1] MESSIAEN, A.M., VANDENPLAS, P.E., Phys. Letts 25A (1967) 339.
- [2] VANDENPLAS, P.E., MESSIAEN, A.M., Phys Letts 26A (1968) 273; 28A (1968) 59.
- [3] MESSIAEN, A.M., VANDENPLAS, P.E., Phys. Fluids 12 (1969) 2406.
- [4] MESSIAEN, A.M., VANDENPLAS, P.E., Appl. Phys. Letts 15 (1969) 30.
- [5] TAILLET, J., Am. J. Phys. 37 (1969) 423.
- [6] LISITANO, G., ELLIS, R.A., Jr., HOOKE, W.M., STIX, T.H., Rev. scient. Instrum. 39 (1968) 295.
- [7] LISITANO, G., FONTANESI, M., SINDONI, E., Appl. Phys. Letts 16 (1970) 122.
- [8] AUBERT, A.E., MESSIAEN, A.M., VANDENPLAS, P.E., Appl. Phys. Letts 18 (1971) 63.
- [9] TRIVELPIECE, A.W., GOULD, R.W., J. Appl. Phys. 30 (1959) 1784.
- [10] GRANATSTEIN, V.L., SCHLESINGER, S.P., J. Appl. Phys. 35 (1964) 2846.
- [11] TAILLET, J., Commissariat à l'Energie Atomique, Report R 2502 (1964).
- [12] AUBERT, M., LEPRINCE, P., Physics Letts 33A (1970) 7.
- [13] VANDENPLAS, P.E., Electron Waves and Resonances in Bounded Plasmas, Wiley-Interscience, New York (1968).
- [14] LEPRINCE, P., D. Sc. thesis, Report L.P.63, Faculté des Sciences d'Orsay, 1966 (unpublished).
- [15] AGNELLO, V., BERNABEI, S., COSTI, S., FONTANESI, M., Report FP-2, Istituto di Scienze Fisiche, Milano, 1970 (unpublished).
- [16] ANISOMOV, A.L., BUDNIKOV, N.N., VINOGRADOV, N.I., GOLANT, V.E., NANOBASHVILI, S.I., OBUKOV, A.A., PAKHOMOV, A.P., PILIYA, A.D., FEDOROV, V.I., Nucl. Fusion, Special Supplement (1969) 191 (Novosibirsk Conference 1968).
- [17] MESSIAEN, A.M., VANDENPLAS, P.E. (to be submitted for publication).

DISCUSSION

A. J. HATCH: The critical geometric parameters in cylindrical bounded plasmas are the diameters of the boundary and of the plasma. For a slab, they are the separation of the boundary plates and the thickness of the plasma slab. In the present work on the helical case — and in all the other similar work that I know of — these lengths are always small compared with the wavelength of the applied r. f. field. Is this a requirement of the theory?

P. E. M. VANDENPLAS: The order-of-magnitude criterion $L \ll \lambda_0$ (L is the characteristic dimension of the bounded plasma; λ_0 is the vacuum wavelength) for the validity of the quasistatic approximation is only applicable to the case $k_{\parallel} = 0$. Broadly speaking, when $k_{\parallel} \neq 0$, the criterion becomes $k_0^2 \ll k_{\parallel}^2$. A more precise criterion is given in Appendix A of the paper for the case of a cold plasma.

A. J. HATCH: Does the bounded theory apply if these critical dimensions are large, i. e. of the order of a third or half of a wavelength, and can the high plasma densities still be achieved?

P. E. M. VANDENPLAS: In the simple cases that have been studied so far ($k_{\parallel} = 0$), the resonance becomes less defined when the quasistatic approximation is no longer strictly applicable, but $\omega_{pe}^2/\omega^2 \gg 1$ remains possible. It is difficult, however, to give a general answer and, in a given situation, one should perform a full electromagnetic calculation to see whether $\omega_{pe}^2/\omega^2 \gg 1$ remains possible. It should also be emphasized that inside a metal cavity, a full electromagnetic study is essential and one obtains modes with $\omega_{pe}^2/\omega^2 \gg 1$ even when $B_0 = 0$.

H. DERFLER: In your system you introduce collisional losses and the driving frequency is real so that the wave-numbers obtained from the dispersion relation will be complex. Under these conditions, how did you manage to get a discrete spectrum of real wave-numbers?

P. E. M. VANDENPLAS: The ν_e used is a phenomenological collision frequency. For those ranges of plasma parameters in which collisionless damping could play a non-negligible role one can change the value of ν_e in order to include collisionless damping to a first approximation. The present model of a cold magnetized plasma with ν_e is all that is necessary to explain the main characteristics of these bounded r. f. plasmas with $\omega_{pe}^2 \gg \omega^2$. As is always the case, however, one could probably get a better fit from the full Vlasov equation (or Boltzmann equation) for a non-uniform plasma.

ИССЛЕДОВАНИЯ ТРАНСФОРМАЦИИ И ПОГЛОЩЕНИЯ ВЫСОКОЧАСТОТНЫХ ВОЛН В ПЛАЗМЕ, НАПРАВЛЕННЫЕ НА РАЗРАБОТКУ МЕТОДОВ НАГРЕВА ПЛАЗМЫ

В.И. АРХИПЕНКО, А.Б. БЕРЕЗИН, В.Н. БУДНИКОВ,
В.Е. ГОЛАНТ, К.М. НОВИК, А.А. ОБУХОВ,
А.Д. ПИЛИЯ, В.И. ФЕДОРОВ, К.Г. ШАХОВЕЦ
Физико-технический институт им. А.Ф. Иоффе
Академии наук СССР, Ленинград,
Союз Советских Социалистических Республик

Доклад представлен К.Н. Степановым

Presented by K.N. Stepanov

Abstract—Аннотация

RESEARCH ON THE TRANSFORMATION AND ABSORPTION OF HIGH-FREQUENCY WAVES IN A PLASMA, FOR THE PURPOSE OF DEVELOPING METHODS OF PLASMA HEATING.

The paper describes investigations on the transformation into rapidly damping longitudinal plasma waves of high-frequency waves introduced into a plasma. At the present time, the theory concerning this type of linear transformation is generalized to include the case of two-dimensional plasma inhomogeneity. It is shown that, when account is taken of the inhomogeneity, the transformation must take place in the vicinity of singular points on the constant-concentration curves. The characteristics of the transformation are investigated in a toroidal magnetic field with shear. Experiments were performed to determine the conditions of wave transformation and absorption in a uniform magnetic field (waves with wavelengths of approximately 3 cm and 10 cm were used). For the determination of the transformation region at frequencies less than the electron-cyclotron frequency, a method of local (lengthwise) perturbation was applied. A weak perturbation of the magnetic field in the region of the transformation led to a sharp reduction in absorption. The study of this effect, together with measurements of the concentration distribution, permitted a comparison of data on the transformation conditions with the non-unidimensional theory. With the help of probes an investigation was carried out of the amplitude distribution of an ultra-high-frequency field in the region of wave transformation and absorption (at frequencies close to the upper hybrid frequency). On the basis of these data it was possible to determine the localization of the transformation region and to establish the propagation regions of the plasma waves formed as a result of the transformation. For absolute measurements of the amplitude of the ultra-high-frequency field in the plasma wave transformation and propagation region, the Stark broadening of the hydrogen lines is measured. The results of determining the localization of the transformation region and the field amplitude in this region are in agreement with the theory.

ИССЛЕДОВАНИЯ ТРАНСФОРМАЦИИ И ПОГЛОЩЕНИЯ ВЫСОКОЧАСТОТНЫХ ВОЛН В ПЛАЗМЕ, НАПРАВЛЕННЫЕ НА РАЗРАБОТКУ МЕТОДОВ НАГРЕВА ПЛАЗМЫ.

В докладе описаны исследования трансформации вводимых в плазму высокочастотных волн в быстрозатухающие продольные плазменные волны. В настоящее время теория линейной трансформации такого типа обобщена на случай двумерной неоднородности плазмы. Показано, что при учете неоднородности трансформация должна происходить в окрестности особых точек кривых постоянной концентрации. Исследованы особенности трансформации в тороидальном магнитном поле с широм. Эксперименты по определению условий трансформации и поглощения волн проводились в однородном магнитном поле (использовались 3-сантиметровый и 10-сантиметровый диапазоны). Для установления области трансформации при частотах, меньших электронной циклотронной, был применен метод локального (по длине) возмущения. Слабое возмущение магнитного поля в области трансформации приводило к резкому уменьшению поглощения. Изучение этого эффекта вместе с измерениями распределения концентрации позволило сопоставить данные об условиях трансформации с неоднородной теорией. С помощью зондов исследовалось распределение амплитуды СВЧ-по-

ля в области трансформации и поглощения волн (при частотах, близких к верхней гибридной). Из этих данных можно было определить локализацию области трансформации, установить область распространения плазменных волн, образующихся в результате трансформации. Для абсолютных измерений амплитуды СВЧ-поля в области трансформации и распространения плазменных волн проводятся измерения штарковского уширения линий водорода. Результаты определения локализации области трансформации и амплитуды поля в этой области согласуются с теорией.

В последнее время в связи с успехами в получении длительного удержания плазмы в квазистационарных тороидальных магнитных ловушках усилился интерес к поискам подходящих методов нагрева. Широко обсуждаются, в частности, возможности использования высокочастотных методов. Для того чтобы эти методы в наименьшей степени влияли на удержание плазмы, желательно осуществлять их при возможно меньших величинах вводимой в плазму мощности и использовать линейные или "квазилинейные" механизмы поглощения. Как показывает анализ (см. [1,2]), наиболее эффективные условия линейного поглощения высокочастотных волн могут быть реализованы, если возбудить в плазме продольные волны с большим показателем преломления (так называемые плазменные волны). Непосредственное возбуждение плазменных волн осуществить трудно. Однако в неоднородной плазме существует линейный механизм трансформации вводимых извне поперечных электромагнитных волн в продольные плазменные волны. Этот механизм дает возможность осуществить эффективный ввод высокочастотной энергии в плазму. Обзор результатов исследования линейной трансформации и поглощения, связанного с трансформацией, был представлен в [2]. Данный доклад содержит изложение новых результатов в области теории линейной трансформации и в экспериментальном изучении условий трансформации и поглощения волн.

1. РЕЗУЛЬТАТЫ ТЕОРЕТИЧЕСКОГО РАССМОТРЕНИЯ ЛИНЕЙНОЙ ТРАНСФОРМАЦИИ

Теоретическое рассмотрение трансформации электромагнитной волны в плазменную для плазмы, параметры которой зависят от одной координаты (одномерная неоднородность), показывает, что такая трансформация происходит в окрестности точки, в которой обращается в бесконечность показатель преломления, рассчитанный, в пренебрежении тепловым движением частиц и столкновениями, для направления распространения, совпадающего с направлением градиента концентрации (см., например, [3-6]). При температуре плазмы T , равной нулю, эта точка является особой точкой волнового уравнения, в которой обращается в бесконечность электрическое поле волны; это приводит к конечному поглощению энергии даже при отсутствии столкновений. При $T \neq 0$ поле в области трансформации остается конечным, но достигает относительно очень больших значений и становится резко неоднородным, что и приводит к генерации плазменной волны. Расчеты показывают, что в широком диапазоне условий энергия, уносимая плазменной волной, равна энергии, поглощаемой в особой точке холдовой бесстолкновительной плазмы; она, следовательно, не зависит от температуры плазмы и частоты столкновений [5].

В соответствии со сказанным условия трансформации определяются тремя частотами, при которых для заданных параметров обращается в

бесконечность "холодный" показатель преломления. Верхняя и средняя частоты даются соотношениями:

$$\omega_{1,2}^2 = \frac{1}{2} \left[\omega_u^2 \pm \sqrt{\omega_u^4 - 4\omega_p^2 \omega_{He}^2 \cos^2 \alpha} \right] \quad (1)$$

$$\cos^2 \alpha \gg \frac{m_e}{m_i}$$

где ω_{He} — электронная циклотронная частота, ω_p — плазменная частота, $\omega_u = \sqrt{\omega_{He}^2 + \omega_p^2}$ — верхняя гибридная частота, α — угол между градиентом концентрации и магнитным полем. В сильно неоднородной плазме (1) определяет полосы частот, в которых возможна трансформация:

$$\omega_{He} \leq \omega \leq \omega_{1 \max} \quad \omega_{Hi} \leq \omega \leq \omega_{2 \max} \quad (2)$$

Величину поля в области трансформации можно выразить через мощность Q , поглощаемую 1 см² слоя [5]:

$$|E| = \frac{A}{\gamma} \left(\frac{8Q}{\omega \ell} \right)^{1/2} \quad (3)$$

где

$$\gamma = \left\{ \frac{v_{Te}^2}{\omega^2 \ell^2} \left[\frac{3\omega^2 \sin^4 \alpha}{\omega^2 - 4\omega_{He}^2} + \frac{6\omega^4 - 3\omega^2 \omega_{He}^2 + \omega_{He}^4}{(\omega^2 - \omega_{He}^2)^2} \sin^2 \alpha \cos^2 \alpha + \frac{3(\omega^2 - \omega_{He}^2)}{\omega^2} \cos^4 \alpha \right] \right\}^{1/3}$$

(предполагается, что $\gamma \ll 1$); A — величина порядка единицы, зависящая от α и ω ; при $\alpha = 0$ или $\pi/2$ $A \approx 1,15$; v_{Te} — тепловая скорость электронов, $\ell = \left| \frac{1}{n} \nabla n \right|^{-1}$ — характерный размер. Из формулы (3) видно, что при высоких частотах $\omega^2 \gg \omega_{He} \omega_{Hi}$ поле в области трансформации возрастает по сравнению с полем волны вне плазмы примерно в $(\ell/\rho_e)^{2/3}$ раз (ρ_e — лармовский радиус).

Выполнявшиеся до сих пор расчеты условий и эффективности трансформации относились к случаю одномерной неоднородности (рассматривались плоские или цилиндрические конфигурации в однородном магнитном поле), в то время как реально параметры плазмы зависят от 2 или 3 пространственных координат. Большой практический интерес представляет случай двумерной неоднородности, охватывающий прямые аксиально-симметричные системы и тороидальные системы типа токамака и левитрона.

Естественно думать, что в двумерном случае, как и в одномерном, трансформация волн также связана с особенностями поля при $T = 0$. Общее исследование особенностей поля при двумерной неоднородности плазмы проведено в [7]. Вкратце основные результаты этой работы сводятся

к следующему. Поскольку поле вблизи особенности является потенциальным, можно ограничиться исследованием уравнения:

$$dwD = 0 \quad D_\alpha = \epsilon_{\alpha\beta} E_\beta \quad E = -\nabla\varphi(x, z) e^{iky} \quad (4)$$

$\epsilon_{\alpha\beta}$ — тензор электрической проницаемости при $T = 0$.

Вблизи особенности эквипотенциали (линии $\varphi = \text{const}$) приближенно совпадают с характеристиками этого уравнения. Следовательно, особенности возможны только в той части плазмы, где уравнение (4) является гиперболическим (уравнение (4) принадлежит к смешанному типу, т.е. в одной части плазмы оно эллиптическое, а в другой — гиперболическое). Появление не зависящих от граничных условий особенностей связано с аномальным сгущением или пересечением характеристик. Такая ситуация, очевидно, возникает при наличии особых точек или асимптот у характеристик.

Особые точки могут возникать на одной из линий, определяемых условиями $\epsilon \sin^2\beta + \eta \cos^2\beta = 0$, $\epsilon = 0$, где

$$\epsilon = 1 - \sum_{e,i} \frac{\omega_p^2}{\omega^2 - \omega_H^2} \quad \eta = 1 - \sum_{e,i} \frac{\omega_p^2}{\omega^2} \quad (5)$$

β — угол между направлением магнитного поля и плоскостью, в которой изменяются параметры плазмы (плоскостью xz). На кривой $\epsilon = 0$ особыми являются точки, где эта кривая касается проекций силовых линий магнитного поля на плоскость xz , а на кривой $\epsilon \sin^2\beta + \eta \cos^2\beta = 0$ — точки, в которых эта проекция перпендикулярна кривой. Тип возникающей особенности определяется величиной и знаком кривизны указанных линий.

В случае ограниченной области данных асимптот у решений уравнений для характеристик быть не может. Однако может иметь место сильное сближение характеристик в "квазиодномерных" участках.

Рассмотрим теперь структуру характеристик и условия возникновения особенностей поля в ограниченных системах с однородным магнитным полем и в тороидальных системах с вращательным преобразованием магнитного поля.

В случае однородного магнитного поля ограничимся для простоты плоской геометрией. Все результаты без труда обобщаются на цилиндрические системы. Уравнение (4) при этом принимает вид:

$$\frac{\partial}{\partial x} \epsilon \frac{\partial \varphi}{\partial x} + \frac{\partial}{\partial z} \eta \frac{\partial \varphi}{\partial z} = 0 \quad (6)$$

Здесь ось z направлена вдоль магнитного поля и предполагается, что поле не зависит от y . Характеристики в этом случае определяются уравнением:

$$\frac{dx}{dz} = \pm \sqrt{\frac{-\epsilon}{\eta}} \quad (7)$$

Уравнение (6) является гиперболическим в той части плазмы, где ϵ и η разного знака ($-\epsilon/\eta > 0$), т.е. в области, лежащей между линиями $\epsilon = 0$ и $\eta = 0$. Картина характеристик имеет различный вид в трех областях частот: 1) $\omega > \omega_{He}$, 2) $\omega_{He}\omega_{Hi} < \omega^2 < \omega_{He}^2$ и 3) $\omega_{Hi}^2 < \omega^2 < \omega_{He}\omega_{Hi}$. Обсудим их в отдельности.

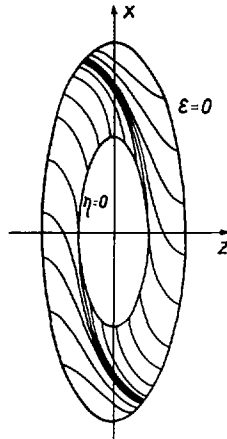


Рис. 1. Типичная картина характеристик для случая, когда на линии $\epsilon = 0$ лежит фокус и $\omega > \omega_{He}$.

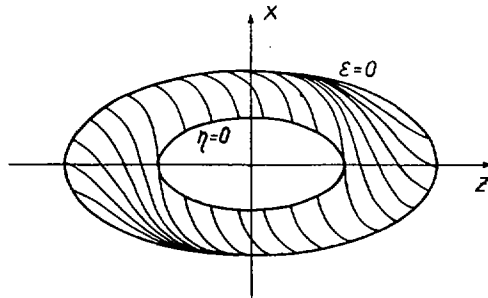


Рис. 2. Типичная картина характеристик для случая, когда на линии $\epsilon = 0$ лежит узел и $\omega > \omega_{He}$.

В области частот $\omega > \omega_{He}$ линия $\epsilon = 0$ лежит при меньших концентрациях, чем линия $\eta = 0$, и на ней возникают особые точки типа узла или фокуса.

На линии $\eta = 0$ имеются особые точки типа седла. Ход характеристик в этих случаях схематично изображен на рис. 1 (на линии $\epsilon = 0$ фокус) и на рис. 2 (на линии $\epsilon = 0$ узел). Для простоты на рис. 1 и 2 изображено только одно семейство характеристик, соответствующее знаку минус в (7). Из рис. 1 и 2 видно, что имеет место сгущение характеристик к линии, проходящее через седловую точку $x = 0$, $\eta = 0$, что приводит к особенностям поля на этой линии. Кроме того, во втором случае значительная часть характеристик сходится в узловой точке, и поле волны в этой точке тоже будет иметь особенность. В фокусе характеристики не сгущаются.

Ясно, что критерием наличия седловой особой точки является условие $\omega_p^2 / \omega^2 > 1$ (это условие требует, чтобы в плазме существовала линия $\eta = 0$). Критерий существования узловой особой точки легко получить,

воспользовавшись результатами работы [7] и предполагая для простоты, что концентрация в плазме имеет вид $n = n_{\max}(1 - x^2/a^2 - z^2/b^2)$. Он имеет вид:

$$\frac{\omega_{p\max}^2}{\omega^2} \geq 1 - \frac{\omega_{He}^2}{\omega^2} + \frac{4a^2}{b^2} \frac{\omega_{He}^2}{\omega^2} \left(1 - \frac{\omega_{He}^2}{\omega^2}\right) \quad (8)$$

Поскольку в реальных условиях размеры плазмы вдоль магнитного поля, как правило, больше поперечных размеров ($a^2/b^2 \ll 1$), условие (8) не сильно отличается от условия верхнего гибридного резонанса.

В области частот $\omega_{Hi}^2 < \omega^2 < \omega_{He}\omega_{Hi}$, соответствующей нижнему гибридне-ному резонансу, линии $\epsilon = 0$ и $\eta = 0$ меняются местами (линия $\eta = 0$ лежит теперь в области очень малых концентраций). Картина характеристик имеет, как нетрудно убедиться, такой же вид, как на рис. 1 и 2, если поменять местами оси x и z . Критерием обращения поля в бесконечность на линии, проходящей через седловую точку (седловые точки лежат на линии $\epsilon = 0$ при $z = 0$), является неравенство:

$$\frac{\omega_{p\max}^2}{\omega^2} \frac{\omega_{He}\omega_{Hi} - \omega^2}{\omega_{He}} > 1 + \frac{1}{6} \frac{a^2}{b^2} \frac{\omega_{He}^2}{\omega_{He}\omega_{Hi} - \omega^2} \quad (9)$$

В случае очень длинных систем это выражение совпадает с условием нижнего гибридного резонанса, однако для этого необходимо, чтобы выполнялось очень жесткое условие:

$$\frac{a^2}{b^2} \frac{m_i}{m_e} \ll 1$$

В промежуточной области частот $\omega_{He}\omega_{Hi} < \omega^2 < \omega_{He}^2$ ϵ в ноль не обращается, и гиперболическая область лежит внутри линии $\eta = 0$, на которой при $x = 0$ возникают особые точки типа фокуса или узла. Узел возникает при выполнении условия

$$\frac{\omega_{p\max}^2}{\omega^2} \geq 1 + \frac{4b^2}{a^2} \frac{\omega_{He}^2}{\omega_{He}^2 - \omega^2} \quad (10)$$

Кроме указанных особых точек характеристик, трансформация волн может также иметь место при более сложных распределениях концентрации, когда возникают "квазиодномерные" области, т.е. области, в которых радиус кривизны ρ линий $n = \text{const}$ много больше характерного масштаба неоднородности плазмы l . При этом условия трансформации такие же, как и в одномерном случае. Поле при этом в бесконечность не обращается, но достигает большого значения (увеличение поля пропорционально $\exp(\rho/l)$) и становится резко неоднородным в пространстве. Трансформация будет иметь место при $\rho/l \gg l \ln 1/\gamma$.

Рассмотрим теперь тороидальную систему типа "токамак", считая для простоты тороидальность слабой. Неоднородность плазмы в сечении тора связана с неоднородностью концентрации и с тороидальной неоднородностью магнитного поля. Пусть силовые линии магнитного поля составляют с плоскостью сечения угол $\beta \neq \pi/2$. В этом случае уравнение (4) является гиперболическим в области, заключенной между линиями $\epsilon = 0$ и $\epsilon \sin^2 \beta + \eta \cos^2 \beta = 0$. Наиболее сильные эффекты, связанные с двумерностью, возникают в области частот, соответствующей нижнему

гибридному резонансу, когда $|\eta| \gg 1$. В этой области частот, полагая $\omega_{\text{Hi}}^2 \ll \omega^2 < \omega_{\text{He}} \omega_{\text{Hi}}$ и учитывая, что $|\beta - \pi/2| = \beta_1 = a/qR \ll 1$ (a и R – малый и большой радиусы тора, q – запас устойчивости по критерию Крускала-Шафранова), можно записать:

$$\epsilon = 1 - \frac{\omega_p^2(r)}{\omega^2} \frac{\omega_{\text{He}} \omega_{\text{Hi}} - \omega^2}{\omega_{\text{He}}^2} - \mu \cos v \quad (11)$$

$$\epsilon \sin^2 \beta + \eta \cos^2 \beta = 1 - \frac{\omega_p^2(r)}{\omega^2} \frac{\omega_{\text{He}} \omega_{\text{Hi}} - \omega^2}{\omega_{\text{He}}^2} - \mu \cos v - \beta_1^2 \frac{\omega_{\text{He}}^2}{\omega_{\text{He}} \omega_{\text{Hi}} - \omega^2}$$

где $\omega_{\text{He}, i}$ – значения циклотронных частот электронов и ионов в центре сечения, $\omega_p(r)$ – усредненное по v значение плазменной частоты, μ – малый параметр, характеризующий тороидальную неоднородность ($\mu \sim a/R \ll 1$), v – азимутальный угол в сечении тора. В соответствии с общими результатами работы [7], особые точки характеристик возникают на линии $\epsilon = 0$ при $v = 0$ (ближайшая к оси симметрии тора точка линии $\epsilon = 0$) и при $v = \pi$. При $v = 0$ возникает седловая особая точка, а при $v = \pi$ узел или фокус. Узел имеет место при выполнении условия:

$$\frac{\omega_{\text{He}}^2}{\omega_{\text{He}} \omega_{\text{Hi}} - \omega^2} \beta_1^2 \mu \approx \frac{m_i}{m_e} \beta_1^2 \frac{a}{R} < \frac{1}{8} \quad (12)$$

Картина характеристик для случая, когда в точке $\epsilon = 0$, $v = \pi$ имеет место узел, изображена на рис. 3. Из рис. 3 видно, что часть характеристик, группируясь вблизи линии, выходящей из седла, сходится в узловую точку (для наглядности изображены только сходящиеся характеристики одного из семейств). Следовательно, наиболее сильная особенность поля будет в окрестности узловой точки, так что поглощение электромагнитных волн (и трансформация их в плазменные) будет происходить неравномерно по углу v . (Максимум поглощения при $v = \pi$). Эта неравномерность уменьшается с уменьшением параметра $m_i a^3 / m_e R^3$ и при $m_i a^3 / m_e R^3 \ll 1$ становится незначительной, так что неоднородность плазмы становится, по существу, одномерной.

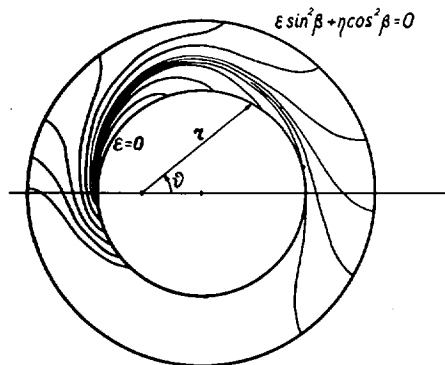


Рис. 3. Картина характеристик для случая тороидальной системы и $\omega_{\text{Hi}}^2 \ll \omega^2 < \omega_{\text{He}} \omega_{\text{Hi}}$.

В области высоких частот $\omega > \omega_{\text{He}}$ величины ϵ и $\epsilon \sin^2 \beta + \eta \cos^2 \beta$ определяются формулами:

$$\epsilon = 1 - \frac{\omega_p^2(r)}{\omega^2 - \omega_{\text{He}}^2} - \mu^1 \cos v$$

$$\epsilon \sin^2 \beta + \eta \cos^2 \beta = 1 - \frac{\omega_p^2(r)}{\omega^2 - \omega_{\text{He}}^2} - \mu^1 \cos v + \beta_1^2 \frac{\omega_{\text{He}}^2}{\omega^2 - \omega_{\text{He}}^2} \quad (13)$$

Порядок величины параметра μ^1 , входящего в эти формулы, такой же, как и параметра μ в (11) ($\mu^1 \sim a/R$). Из приведенных формул видно, что линия $\epsilon \sin^2 \beta + \eta \cos^2 \beta = 0$ идет в этом случае при больших концентрациях, чем линия $\epsilon = 0$. Это приводит к тому, что седловая особая точка располагается теперь на линии $\epsilon = 0$ при $v = \pi$, а узел или фокус — при $v = 0$ (узел при $\omega_{\text{He}}^2 / (\omega^2 - \omega_{\text{He}}^2) \beta_1^2 \mu^1 < 1/8$). Неоднородность трансформации по углу v будет определяться величиной параметра $\beta_1^2 a/R \sim a^3/R$ и, следовательно, будет значительно меньше, чем при низких частотах.

Приведенные соотношения дают возможность анализировать условия линейной трансформации волн в различных случаях. Следует при этом иметь в виду, что трансформация электромагнитных волн в плазменной должна происходить не только непосредственно в точках особенностей, но и в некоторой окрестности этих точек, в которой поле оказывается достаточно большим ($E/E_0 > \ln 1/\gamma$, где E_0 — поле в вакууме).

2. ЭКСПЕРИМЕНТАЛЬНЫЕ ИССЛЕДОВАНИЯ ТРАНСФОРМАЦИИ В ВЕРХНЕЙ ПОЛОСЕ ЧАСТОТ ($\omega > \omega_{\text{He}}$)

Проведенные ранее эксперименты [1,2,8-10] показали существование эффективного поглощения волн плазмой в полосе частот между электронной циклотронной и верхней гибридной, соответствующей верхней полосе линейной трансформации (2). Эксперименты позволили определить эффективность поглощения, которая по порядку величины и по характеру зависимости согласуется с предсказаниями одномерной теории трансформации. В частности, для широкого диапазона условий была продемонстрирована слабая зависимость эффективности поглощения от температуры, частоты столкновений электронов, напряженности высокочастотного поля. Целью исследований, представленных в данном докладе, было изучение локализации областей трансформации и распространения плазменных волн, индуцируемых по увеличению напряженности высокочастотного поля. (См. также исследования локализации поглощения в [11]).

Эксперименты проводились на установке, описанной в [12]. Плазма создавалась в стеклянном баллоне диаметром 2,5 см, помещенном в однородное магнитное поле, под действием сверхвысокочастотной мощности трехсантиметрового диапазона. Мощность подводилась по круглому волноводу, для согласования с которым концу баллона придавалась коническая форма. Рабочим газом являлся аргон при давлении около 10^{-2} мм рт.ст., концентрация заряженных частиц составляла $10^{11} - 10^{13}$ см $^{-3}$, электронная температура — 3-10 эВ. Исследования проводились с помощью зонда, состоящего из двух проводников диаметром 0,2 мм, помещенных в металлизированную керамическую трубочку диаметром 1,5 мм. Зонд мог перемещаться как в продольном, так и в радиальном направлениях в области взаимодействия СВЧ-волн с плазмой. Зонд служил как

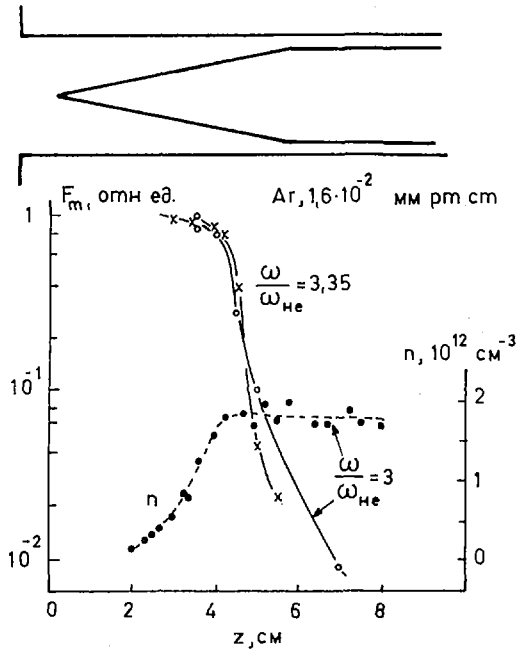


Рис. 4. Продольное распределение сверхвысокочастотного сигнала и концентрации в области взаимодействия волн с плазмой. F_m — максимальное по сечению значение сигнала.

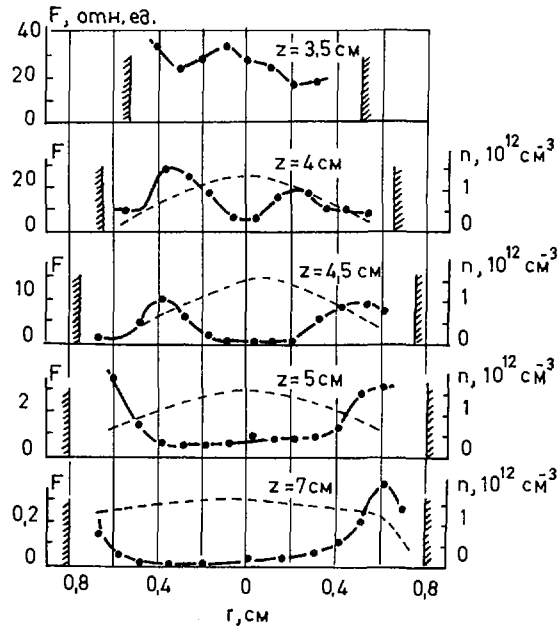


Рис. 5. Радиальное распределение сверхвысокочастотного сигнала и концентрации в различных сечениях.

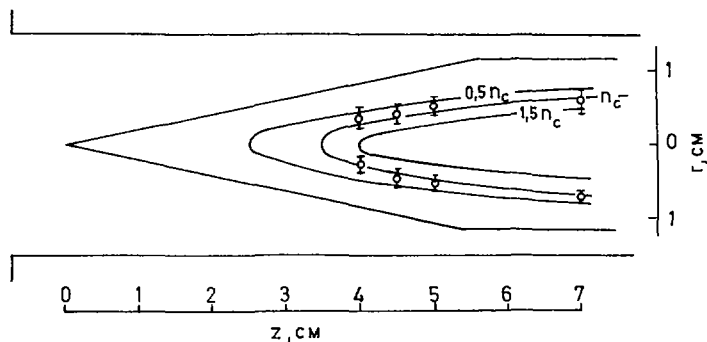


Рис. 6. Расположение линий равной концентрации и локализация сильного сверхвысокочастотного поля.

для относительных измерений напряженности высокочастотного поля, так и для измерений распределения концентрации (в режиме двойного электростатического зонда). Абсолютная градуировка зондовых измерений концентрации осуществлялась путем "просвечивания" плазмы восьмимиллиметровыми волнами с помощью интерферометра.

Типичные результаты измерений продольного и радиального распределений высокочастотного поля, а также измерений концентрации представлены на рис. 4 и 5. Из рис. 4 видно, что уже на начальном участке области взаимодействия (в конической части баллона) амплитуда высокочастотного поля быстро уменьшается в осевом направлении. При этом область сильного поля смещается от центральных областей к периферии плазмы (рис. 5). На рис. 6 представлено расположение линий равной концентрации и областей сильного поля по данным рис. 4 и 5 (точки соответствуют максимумам поля на рис. 5, отрезками обозначены длины, на которых поле падает вдвое). Полученные экспериментальные данные качественно соответствуют теоретической картине трансформации волн. В геометрии эксперимента реализуется двумерная неоднородность, связанная с зависимостью концентрации от продольной и радиальной координат. При этом, в соответствии с двумерной теорией (рис. 1), трансформация должна быть связана со сгущением характеристик к линии $\epsilon = 0$. Область сильного поля, в которой может происходить трансформация, заключена между линиями $\eta = 0$ ($\omega = \omega_p$, $n = n_c$) и $\epsilon = 0$ ($\omega = \sqrt{\omega_{He}^2 + \omega_p^2}$, $n = (1 - N^2/N_c^2)n_c$). Эта область должна смещаться от оси к периферии плазмы по мере нарастания концентрации. Такое смещение области сильного высокочастотного поля подтверждается результатами измерений — из приведенных кривых видно, что область сильного поля располагается вблизи концентраций, близких к критической.

Для определения абсолютных значений напряженности высокочастотных полей в области трансформации были проведены измерения штарковского уширения линий водорода. Этот эксперимент выполнялся на стационарной установке. Условия создания плазмы были аналогичны описанным выше. Рабочим газом в этом опыте был водород при давлении 10^{-2} мм рт. ст. Для исследования контуров спектральных линий H_β и H_γ был использован интерферометр Фабри-Перо, скрещенный с прибором предварительной дисперсии. Световое излучение принималось из окна

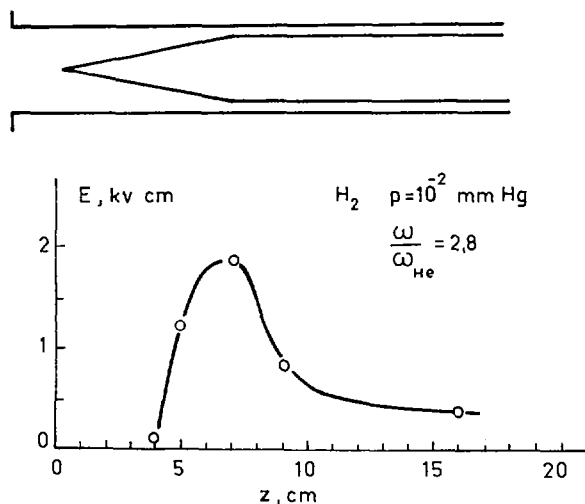


Рис. 7. Распределение амплитуды сверхвысокочастотного поля вдоль баллона.

размером 1×1 см в круглом волноводе (в области взаимодействия СВЧ-полей с плазмой). Баллон с плазмой мог перемещаться относительно волновода, и световое излучение можно было принимать из любой точки начальной части баллона.

В результате экспериментов было измерено уширение линий H_β и H_γ в различных сечениях по длине баллона. Оценки показывают, что в условиях наших экспериментов такие эффекты, как доплеровское уширение, соударения с нейтральными частицами, штарковское взаимодействие с полем заряженных частиц, не могут объяснить наблюдавшееся уширение. Поэтому, по величине уширения можно было вычислить амплитуду высокочастотного электрического поля. Типичная кривая продольного распределения поля представлена на рис. 7. Кривая получена при мощности 100 Вт, что соответствует полю в волноводе без плазмы 150 В/см. Полученную величину максимального поля в области трансформации можно сравнить с теоретической оценкой по формуле (3). Для условий, при которых получены данные рис. 7, оценка дает $E_{\max} \approx 1-2$ кВ/см, что хорошо согласуется с результатами эксперимента.

3. ЭКСПЕРИМЕНТАЛЬНЫЕ ИССЛЕДОВАНИЯ ТРАНСФОРМАЦИИ В СРЕДНЕЙ ПОЛОСЕ ЧАСТОТ ($\omega < \omega_{He}$)

Проводившиеся ранее эксперименты [13,14] позволили установить границы областей эффективного поглощения волн плазмой в полосе частот между электронной циклотронной и нижней гибридной, соответствующей средней полосе линейной трансформации (2). Положение этих границ оказалось в качественном соответствии с одномерной теорией трансформации. Однако детальное сопоставление сделать было невозможно в связи с тем, что в этой полосе частот положение границ очень сильно зависит от угла между градиентом концентрации и магнитным полем, и

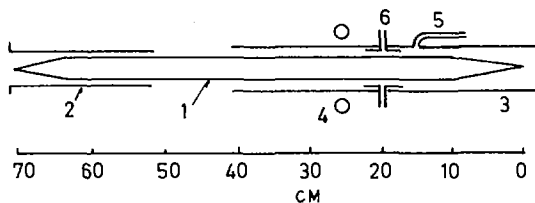


Рис. 8. Схема эксперимента: 1 - баллон с плазмой, 2 - волновод трехсантиметрового диапазона, 3 - волновод десятисантиметрового диапазона, 4 - возмущающая магнитная катушка, 5 - световод, 6 - восьмимиллиметровый интерферометр.

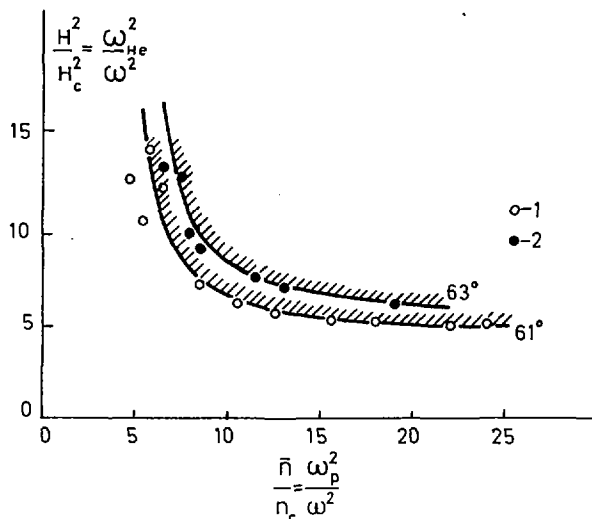


Рис. 9. Границы области поглощения: 1 - $p = 6 \cdot 10^{-3}$ мм рт.ст., 2 - $p = 2 \cdot 10^{-3}$ мм рт.ст. Сплошные линии - теоретические.

применение одномерной теории оказывается лишь очень грубым приближением. Поэтому дальнейшие эксперименты были направлены на установление соответствия экспериментальных данных с представленной в разделе 1 двумерной теорией трансформации. При этом было особенно существенным установление локализации областей трансформации.

Эксперименты выполнялись на стационарной установке по схеме, описанной в [13]. Плазма создавалась в кварцевом баллоне длиной 70 см и внутренним диаметром 2,5 см, помещенном в однородное магнитное поле (см. рис. 8). Рабочим газом являлся аргон. В большинстве экспериментов плазма формировалась в режиме электронного циклотронного резонанса под действием импульса трехсантиметровой мощности, подводимой к баллону по круглому волноводу слева. После прекращения этого импульса разряд поддерживался стационарной десятисантиметровой мощностью, подводимой по волноводу справа. В процессе экспериментов измерялось продольное распределение светового излучения. Излучение

принималось из отверстий, расположенных по оси широкой стенки волновода. В некоторых опытах с помощью восьмимиллиметрового интерферометра измерялась концентрация плазмы, находящейся в пределах десятисантиметрового волновода. Излучатели интерферометра вводились через узкую щель в широкой стенке волновода и могли перемещаться по длине.

Прежде всего были получены данные о границах области поглощения волн плазмой для более широкого диапазона условий по сравнению с предшествующими экспериментами [13]. Как и ранее, эти границы определялись по срыву стационарного разряда при изменении концентрации или магнитного поля. Некоторые результаты определения граничных значений этих величин приведены на рис.9. Экспериментальные данные хорошо соответствуют теоретической кривой границы области трансформации для одномерной модели (2), если соответствующим образом выбрать угол между градиентом концентрации и магнитным полем. Эта формула может быть записана в виде:

$$\frac{H_c^2}{H^2} = \frac{\frac{n}{n_c} - 1}{\frac{n}{n_c} \cos^2 \alpha - 1}, \quad H_c = \frac{mc\omega}{e} \quad (14)$$

При таком представлении результатов положение границ можно характеризовать соответствующим углом α или величиной $1/\cos \alpha$, которая определяет минимальное критическое поле H_{cr} при $n \cos^2 \alpha \gg n_c$. На рис.10 приведена зависимость этой величины от давления нейтрального газа. На графике представлены экспериментальные точки, полученные при различных частотах СВЧ-источников, создающих плазму (3150 МГц, 2370 МГц), а также данные работы [14], полученные при значительно более низкой частоте (116 МГц) и другом диаметре плазмы (5 см). Из этих данных следует, что положение границ трансформации (угол α) определя-

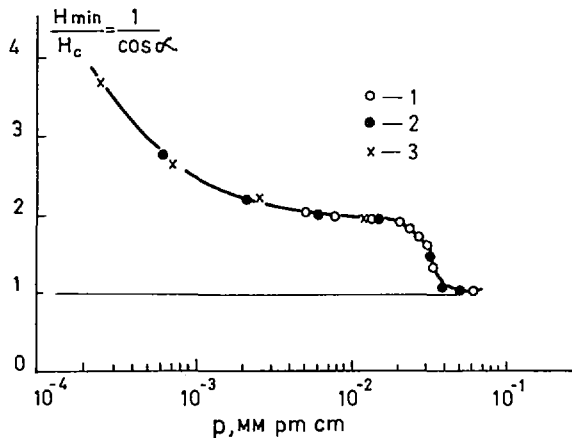


Рис.10. Зависимость угла α от давления:
 1 - данные, полученные на частоте 3150 МГц, 2 - на частоте 2370 МГц, 3 - данные работы [14].

ется в условиях проводившихся экспериментов только давлением нейтрального газа.

При интерпретации полученного результата необходимо иметь в виду, что неоднородность плазмы в экспериментах была существенно двумерной. При этом, в соответствии с излагавшейся выше теорией, трансформация в области, определяемой формулами (2) и (14), при угле α , не равном 0° и 90° , может происходить лишь при наличии "квазиодномерных" областей плазмы, которые могут образовываться при наличии перегибов на линиях равной концентрации. Вопрос о существовании таких перегибов и их роли в процессе трансформации может быть решен на основе измерений распределения концентрации и исследований локализации области трансформации.

Для определения продольной локализации областей трансформации был применен метод малых локальных возмущений магнитного поля [15]. При этом основное магнитное поле устанавливалось выше граничного значения H_{cr} , при котором происходит срыв разряда (на 1-2%). Возмущающее магнитное поле (до 10% от основного) создавалось магнитной катушкой, которая располагалась снаружи волновода и могла свободно перемещаться вдоль баллона с плазмой.

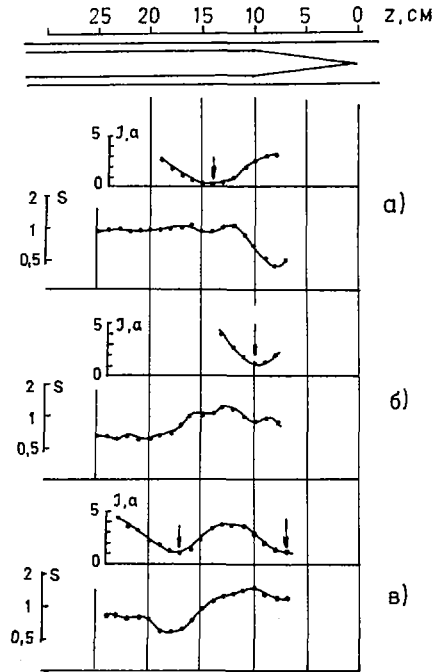


Рис. 11. Положение области трансформации и продольное световое излучение при различных давлениях. Подводимая мощность 60 Вт, S — относительная интенсивность излучения, I — ток срыва разряда:

- | | |
|---------------------------------------|------------------------------------|
| а) $p = 2 \cdot 10^{-3}$ мм рт.ст., | $H_{cr} = 2,5 H_c$, |
| б) $p = 1,6 \cdot 10^{-2}$ мм рт.ст., | $H_{cr} = 1,85 H_c (+ 1,85 H_c)$, |
| в) $p = 2,7 \cdot 10^{-2}$ мм рт.ст. | $H_{cr} = 1,6 H_c$. |

Стрелки отмечают наиболее чувствительную к возмущению точку.

В процессе экспериментов было установлено, что существуют области, помещенные в которые возмущающей катушки приводит к срыву разряда. Можно предположить, что если поглощение СВЧ-волн плазмой связано с механизмом линейной трансформации волн, то точка наибольшей чувствительности к возмущению магнитного поля (в которой срыв происходит при минимальном возмущающем токе) указывает положение области трансформации волн.

Результаты определения положения области срыва разряда при различных давлениях нейтрального газа представлены на рис.11, на котором также приведено продольное распределение интенсивности светового излучения. При низких давлениях ($p < 10^{-2}$ мм рт.ст.) область срыва разряда находится в пределах однородной части баллона. Продольное распределение света носит немонокотонный характер, причем область срыва совпадает с минимумом продольного распределения. При повышении давления область срыва разряда перемещается в коническую часть баллона. При некотором давлении, наряду с первой областью срыва, которая последовательно приближается к началу баллона, появляется вторая область срыва. Она также расположена в минимуме продольного распределения. Существенно подчеркнуть, что области срыва разряда отделены одна от другой областью, не чувствительной к возмущению магнитного поля. Интересно отметить, что положение области срыва разряда не зависит ни от начальных условий его формирования, ни от положения плазменного объема в волноводном устройстве. Это было установлено в специальных экспериментах, в которых изменялись начальные условия формирования разряда (магнитное поле, мощность), а также в опытах, в которых баллон перемещался по отношению к волноводу в продольном направлении, при этом область срыва оставалась неизменной по отношению к баллону.

Для сравнения с полученными результатами были выполнены аналогичные измерения при магнитных полях, меньших циклотронного (при $\omega_{He} < \omega$). В этой области полей существует минимальное магнитное поле $H_{cr} < H_c$ (соответствующее условию $\omega_{u\max} = \omega$), ниже которого трансформация не может происходить. Срыв разряда вблизи поля H_{cr} вызывался включением возмущающей катушки. Эксперименты показали, что в этих условиях в отличие от случая $\omega < \omega_{He}$ в области срыва разряда минимум продольного распределения отсутствует.

Приведенные экспериментальные данные показывают, что при $\omega < \omega_{He}$ области, "чувствительные" к возмущениям, совпадают с минимумами продольного распределения концентрации заряженных частиц (рис.11). Этот результат можно сопоставить с выводом двумерной теории о том, что трансформация должна быть локализована в "квазиодномерных" областях, возникающих в окрестности точек перегиба линий равной концентрации. Простое вычисление показывает, что при распределении, характеризующемся продольной модуляцией концентрации, точки перегиба кривых равной концентрации действительно существуют и располагаются вблизи минимума. При этом угол α в точках перегиба в приосевой области определяется соотношением:

$$\operatorname{tg} \alpha = \frac{1}{\sqrt{\pi}} \sqrt{\frac{\chi}{2} \left(\frac{2n_0}{\Delta n} - 1 \right)} \frac{\ell}{a} \quad (15)$$

где n_0 — среднее значение концентрации, Δn — ее продольная модуляция, ℓ — расстояние между максимумами распределения, a — радиус баллона;

соотношение (15) получено для радиального распределения концентрации $n \sim (1 - r^2/a^2)^\chi$. Оценка значений угла α из экспериментальных величин n_0 , Δn , l при $\chi \approx 1$ удовлетворительно соответствует экспериментальным данным о границах области поглощения (см. формулу (14)).

Вопрос о причинах формирования немоногоного распределения остается не вполне ясным. Можно думать, что такое распределение возникает вследствие локального выделения энергии (при этом область выделения энергии может не совпадать с областью трансформации). Если ионизация происходит вблизи области выделения энергии, то при удалении от этой области концентрация заряженных частиц должна падать вследствие поперечной диффузии. Возникающая при этом модуляция концентрации определяется отношением коэффициентов продольной и поперечной диффузии ($D_{||}$, D_{\perp}).

$$\frac{\Delta n}{n} \approx \frac{2}{\pi^2} \frac{D_{\perp}}{D_{||}} \frac{l^2}{a^2} \quad (16)$$

Подставляя (16) в (15), найдем при $\Delta n \ll n$:

$$\text{tg}^2 \alpha \approx \frac{\chi}{2} \frac{D_{||}}{D_{\perp}} \quad (17)$$

Эта формула позволяет понять наблюдавшееся на опыте отсутствие зависимости угла α от диаметра баллона. Она также дает возможность объяснить экспериментальную зависимость угла α от давления (рис.10). В частности, участок слабой зависимости объясняется постоянством отношения $D_{||}/D_{\perp}$ в соответствующем диапазоне условий.

Проведенный анализ подтверждает предположение о том, что поглощение волн в экспериментах при низких давлениях ($p < 2 \cdot 10^{-2}$ мм рт.ст.) связано с трансформацией вблизи точек перегиба кривых равной концентрации. Об этом свидетельствует положение границ областей поглощения волн и локализация точек, чувствительных к возмущению. С увеличением давления, однако, область поглощения существенно расширяется, охватывая весь диапазон $\omega \leq \omega_{\text{He}}$ (рис.10). Это сопровождается перемещением чувствительной к возмущению области в начальную коническую часть баллона (рис.11). Можно думать, что при этом поглощение определяется трансформацией, связанной с узловой особой точкой в области $\eta = 0$, $n = n_c$.

Таким образом, совокупность полученных экспериментальных данных об условиях поглощения волн в плазме в диапазоне частот $\omega > \omega_{\text{He}}$ и $\omega < \omega_{\text{He}}$ находится в согласии с двумерной теорией трансформации волн.

ЛИТЕРАТУРА

- [1] АНИСИМОВ, А.И., БУДНИКОВ, В.Н., ВИНОГРАДОВ, Н.И., ГОЛАНТ, В.Е., НАНОБАШВИЛИ, С.И., ОБУХОВ, А.А., ПАХОМОВ, Л.П., ПИЛИЯ, А.Д., ФЕДОРОВ, В.И., "Plasma Physics and Controlled Nuclear Fusion Research", Vienna 2 1969, p.399.
- [2] ГОЛАНТ, В.Е., ПИЛИЯ, А.Д., Препринт Физико-технического института им.А.Ф.Иоффе, Ленинград, № 270, 1970; Успехи физ. наук 74 вып.3 (1971).
- [3] ГИНЗБУРГ, В.Л., "Распространение электромагнитных волн в плазме", Изд. "Наука", М., 1967.
- [4] STIX, Phys. Rev. Letters 15 (1965) 878.

- [5] МОИСЕЕВ, С. С., Proceedings of the Seventh International Conference on Phenomena in Ionized Gases, Beograd 2 1966, p. 645.
- [6] ПИЛИЯ, А. Д., ФЕДОРОВ, В. И., Журн. эксп. и теор. физики 57 (1969) 1198.
- [7] ПИЛИЯ, А. Д., ФЕДОРОВ, В. И., Журн. эксп. и теор. физики 60 (1971) 389.
- [8] АНИСИМОВ, А. И., ВИНОГРАДОВ, Н. И., ГОЛАНТ, В. Е., ПАХОМОВ, Л. П., Журн. техн. физики 37 (1967) 680, 202.
- [9] БУДНИКОВ, В. Н., ВИНОГРАДОВ, Н. И., ГОЛАНТ, В. Е., ОБУХОВ, А. А., Журн. техн. физики 37 (1967) 861; 38 (1968) 28.
- [10] КРИВОШЕЕВ, М. В., Журн. техн. физики 39 (1969) 816; ГОЛАНТ, В. Е., КРИВОШЕЕВ, М. В., ФЕДОРОВ, В. И., Журн. техн. физики 40 (1970) 382.
- [11] АНИСИМОВ, А. И., ВИНОГРАДОВ, Н. И., ГОЛАНТ, В. Е., ПАХОМОВ, Л. П., Журн. техн. физики 41 (1971) 696.
- [12] BUDNIKOV, V. N., GALAKTIONOV, V. V., DJATCHENKO, V. V., NOVIK, K. M., OBUKHOV, A. A., Phenomena in Ionized Gases, Vienna, 1967, p. 173.
- [13] БУДНИКОВ, В. Н., ГОЛАНТ, В. Е., ОБУХОВ, А. А., Журн. техн. физики 38 (1968) 576; 40 (1970) 138; Phys. Lett. 31A, 2, 76.
- [14] ГАЛАКТИОНОВ, Б. В., ГОЛАНТ, В. Е., ДЬЯЧЕНКО, В. В., ЩЕРБИНИН, О. Н., Журн. техн. физики 40 (1970) 2317, 2322.
- [15] АРКНІРЕНКО, V. I., BUDNIKOV, V. N., OBUKHOV, A. A., Phys. Lett. 33A (1970) 303.

ИССЛЕДОВАНИЕ ПЛАЗМЫ НА УСТАНОВКЕ "ТУМАН-2"

А.И. АНИСИМОВ, Н.И. ВИНОГРАДОВ, В.Е. ГОЛАНТ,
В.А. ИПАТОВ, М.Г. КАГАНСКИЙ, С.Г. КАЛМЫКОВ,
А.И. КИСЛЯКОВ, В.А. ОВСЯННИКОВ, Л.П. ПАХОМОВ,
К.А. ПОДУШНИКОВА, С.С. ТЮЛЬПАНОВ,
К.Г. ШАХОВЕЦ

Физико-технический институт им. А.Ф. Иоффе
Академии наук СССР, Ленинград,
Союз Советских Социалистических Республик

Доклад представлен К.Н. Степановым

Presented by K.N. Stepanov

Abstract-Аннотация

PLASMA RESEARCH WITH THE TUMAN-2 DEVICE.

The authors describe experiments conducted in the recently constructed toroidal device Tuman-2. The toroidal discharge chamber of the device has a major radius of 80 cm and a minor radius of 20 cm. The strength of the quasi-stationary magnetic field can be varied up to 10 kOe ($T_0/2 = 10$ msec). As in Tokamak systems, the equilibrium of the plasma column is achieved by interaction of the longitudinal current with the casing and programmed transverse field. Provision is made in the device for three-stage heating of the plasma. The first stage comprises ohmic heating in conditions similar to those obtaining in the Tokamak, the second stage heating with ultra-high frequency fields, and the third stage adiabatic compression. Ultra-high frequency heating is effected by means of generators operating in the frequency ranges $f_1 \approx 10$ Gc/sec and $f_2 \approx 40$ Gc/sec, with an output of up to 100 kW for a pulse lasting 100 μ sec. Adiabatic compression is created by strengthening the longitudinal magnetic field for periods shorter than the transverse diffusion time (70-100 μ sec). The device has been used, under conditions of ohmic heating, to produce a plasma with a concentration 10^{12} - 10^{13} cm $^{-3}$ and a temperature of several tens of eV. The authors have investigated the equilibrium of the plasma column. The experimental data relating to the effect of transverse magnetic fields are in good agreement with the equilibrium theory, if it is taken into account that the conductivity of the plasma is not altered during shift of the column. Studies have been started on the absorption of ultra-high frequency energy over the 10 and 30 Gc/sec frequency ranges and on plasma heating due to this energy. In the course of these studies, it is intended to determine the effectiveness of introducing ultra-high frequency energy, localize the absorption region and determine the effect of ultra-high frequency heating on containment of the plasma. Judging by earlier experiments, absorption under the experimental conditions can be expected to be associated with transformation of the ultra-high frequency waves introduced from outside into rapidly damping plasma waves. By using two frequency ranges and varying the plasma parameters (magnetic field and density) it is possible to shift the transformation region over the whole volume and to establish the optimal conditions for introducing energy into the plasma.

ИССЛЕДОВАНИЕ ПЛАЗМЫ НА УСТАНОВКЕ "ТУМАН-2".

В докладе описываются эксперименты на недавно построенной тороидальной установке "Туман-2". Тороидальная разрядная камера установки имеет большой радиус 80 см и малый радиус 20 см. Напряженность квазистационарного магнитного поля может изменяться до 10 кЭ ($T_0/2 = 10$ мсек). Равновесие плазменного шнура обеспечивается, как и в системах "токамак", взаимодействием продольного тока с кожухом и программированным поперечным полем. В установке предусмотрен трехступенчатый нагрев плазмы. Первая стадия — омический нагрев в условиях, аналогичных "токамакам", вторая стадия — нагрев СВЧ-полями и третья стадия — адиабатическое сжатие. СВЧ-нагрев осуществляется с помощью генераторов, работающих в диапазоне частот $f_1 \approx 10$ ГГц и $f_2 \approx 40$ ГГц с мощностью до 100 кВт при длительности импульса 100 мксек. Адиабатическое сжатие проводится путем увеличения продольного магнитного поля за времена, меньшие времени поперечной диффузии (70-100 мксек). На установке в режиме омического нагрева получена плазма

с концентрацией $10^{12} \div 10^{13} \text{ см}^{-3}$ и температурой несколько десятков электронвольт. Проведены исследования равновесия плазменного шнура. Экспериментальные данные о влиянии поперечных магнитных полей оказываются в хорошем соответствии с теорией равновесия, если считать, что проводимость плазмы при смещении шнура не изменяется. Начаты исследования поглощения СВЧ-мощности в диапазонах частот 10 и 30 ГГц и нагрева плазмы под действием этой мощности. В процессе этих исследований предполагается установить эффективность ввода СВЧ-энергии, локализацию области поглощения, влияние СВЧ-нагрева на удержание плазмы. На основе проведенных ранее экспериментов можно ожидать, что поглощение в условиях эксперимента должно быть связано с трансформацией вводимых извне СВЧ-волн в медленные, быстро затухающие плазменные волны. Используя 2 диапазона частот и варьируя параметры плазмы (магнитное поле и плотность), можно перемещать по всему объему область трансформации и установить оптимальный режим ввода энергии в плазму.

ВВЕДЕНИЕ

Как известно, применяемый обычно в квазистационарных тороидальных системах нагрев плазмы продольным током трудно довести до термоядерных температур, поэтому представляет значительный интерес разработка методов нагрева, не связанных с продольным током. В установках типа "токамак" использование таких методов даст возможность разделить процессы удержания и нагрева плазмы и обеспечить независимое изменение ее параметров в более широких пределах.

Подходящими методами нагрева плазмы в тороидальных системах могут явиться нагрев высокочастотными волнами и адиабатическое сжатие. Оба эти направления в течение ряда лет исследовались в Физико-техническом институте им. А.Ф.Иоффе на установках небольшого масштаба. Исследования взаимодействия высокочастотных волн с плазмой показали существование эффективного механизма поглощения, связанного с линейной трансформацией вводимых в плазму волн в медленные быстро затухающие продольные волны (см. [1-3]). Существенной особенностью этого механизма, облегчающей его использование для нагрева плазмы, является независимость эффективности поглощения от температуры плазмы в широких пределах. Применительно к тороидальным системам механизм линейной трансформации может быть реализован в диапазонах верхних и нижних гибридных частот, причем в первом из них его можно использовать для нагрева электронов, а во втором можно ожидать также и нагрева ионов.

Исследования адиабатического сжатия плазмы проводились на малой тороидальной установке "Туман-1" с объемом плазмы ~ 15 л и максимальным магнитным полем 10 кЭ (см. [4-6]). На этой установке была показана возможность сильного сжатия тороидального плазменного шнура нарастающим магнитным полем при времени нарастания, меньшем времени поперечной диффузии плазмы. В результате сжатия удавалось получить плазменный шнур, оторванный от стенок и диафрагм разрядной камеры (концентрация плазмы в шнуре была на 2-3 порядка больше, чем на периферии). Была показана также возможность получения адиабатического нагрева плазмы при сжатии. В установке "Туман-1" нагрев был, однако, ограничен из-за малых поперечных размеров камеры.

Для дальнейшего развития экспериментов в физико-техническом институте им. А.Ф.Иоффе была недавно построена установка большего масштаба "Туман-2" с объемом плазмы ~ 50 л, рассчитанная на максимальные магнитные поля до 40 кЭ. На этой установке предполагается

совместить сверхвысокочастотный нагрев плазмы (в диапазоне верхних гибридных частот) и адиабатическое сжатие. Комбинация СВЧ-нагрева с адиабатическим сжатием плазмы представляется весьма целесообразной. Действительно, СВЧ-нагрев выгодно осуществлять при сравнительно малых магнитных полях, так как увеличение полей приведет к необходимости использования более высоких частот (при полях, больших 10 кЭ, необходимы генераторы миллиметрового диапазона волн). Применение после СВЧ-нагрева адиабатического сжатия позволит перейти к значительно более сильным полям, одновременно осуществив нагрев и увеличение плотности плазмы. При этом следует иметь в виду, что вкладываемая в плазму при сжатии энергия пропорциональна начальной температуре, т.е. она существенно возрастает при применении СВЧ-нагрева.

В данном докладе приводится описание установки "Туман-2" (разд.1) и первые результаты экспериментов (разд.2,3).

1. ОПИСАНИЕ УСТАНОВКИ "ТУМАН-2"

Установка "Туман-2" представляет собой аксиально-симметричную тороидальную магнитную ловушку с продольным током. Равновесие тороидального плазменного шнура обеспечивается, как и в установках типа "токамак", взаимодействием тока с кожухом и программированным поперечным магнитным полем. При этом величина продольного тока ограничена условием магнито-гидродинамической устойчивости Шафранова-Крускала. В установке предусмотрен трехступенчатый нагрев плазмы. Первая стадия – нагрев током в условиях, аналогичных "токамакам", вторая стадия – нагрев СВЧ-полями и третья стадия – адиабатическое

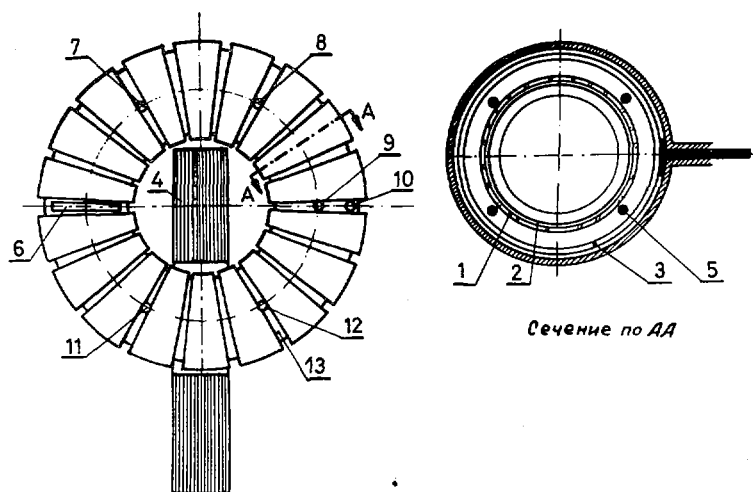


Рис.1. Эскиз установки "Туман-2":

1 – разрядная камера; 2 – лайнер; 3 – кожух; 4 – трансформатор омического нагрева; 5 – витки поперечного поля; 6 – окно для корпускулярной диагностики; 7 – окно для микроволновой диагностики; 8 – окно для спектральной диагностики; 9,10 – окна для лазерной диагностики; 11 – окно для рентгеновской диагностики; 12 – окно для ввода СВЧ-мощности; 13 – кожух.

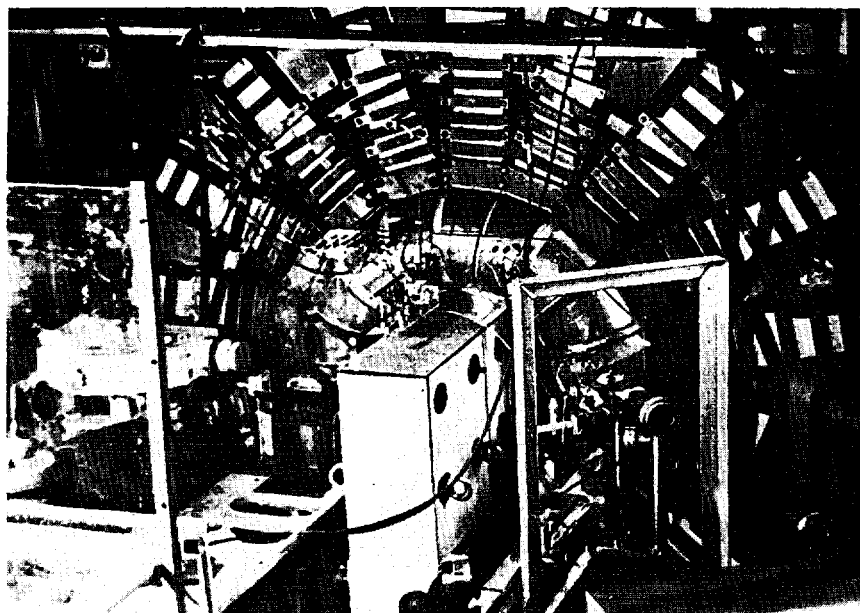


Рис. 2. Фотография общего вида установки "Туман-2".

сжатие плазмы нарастающим продольным магнитным полем. Необходимость обеспечения достаточно большой скорости нарастания поля в стадии адиабатического сжатия (большей скорости поперечной диффузии) определяет основные конструктивные особенности установки.

Эскиз установки "Туман-2" показан на рис. 1, фотография — на рис. 2. Разрядная камера изготовлена из фарфора. Она состоит из 6 секторов, склеенных с помощью эпоксидного компаунда. Камера (1) имеет большой диаметр 80 см, малый — 20 см. Внутри разрядной камеры установлен лайнер (2) из нержавеющей стали толщиной 0,02 мм (толщина ограничивается условием проникновения сжимающего магнитного поля). Внутри лайнера, для ослабления взаимодействия плазмы с ним, установлены две диафрагмы из нержавеющей стали толщиной 0,1 мм. Отверстие в диафрагме $2a = 16$ см задает максимальный диаметр плазменного шнура в период омического нагрева. Диафрагмы изготовлены из гофрированной полосы, для того чтобы увеличить эффективную толщину при сохранении достаточно большим электрического сопротивления витка. Эксперименты показали, что лайнер и диафрагмы незначительно ослабляют сжимающее магнитное поле и механические нагрузки на них малы.

Откачка вакуумной камеры производится с помощью диффузионного насоса с ловушкой, охлаждаемой жидким азотом. Система откачивается до давления $3 \cdot 10^{-7}$ мм рт. ст. Работа производится при постоянном протекании водорода. Измерениям обычно предшествует тренировка камеры разрядами. Для облегчения возникновения разряда в тени диафрагм установлена накаливаемая вольфрамовая спираль. В некоторых эксперимен-

тах предварительная ионизация осуществлялась с помощью импульсной СВЧ-мощности ($f = 10$ ГГц, $P = 20$ кВт, $\tau = 20$ мксек).

Магнитное поле создается системой (3) одновитковых катушек (18 катушек), соединенных двумя параллельными группами. Одна и та же система катушек используется для создания квазистационарного и сжимающего магнитного поля. Конструкция катушек и коммутационных шин рассчитана на очень сильные импульсные токи (до 500 кА) при очень малой составляющей магнитного поля нормальной экваториальной плоскости тора (менее 10^{-3}). Для получения магнитного поля с очень малой поперечной составляющей коммутация тока в катушках сделана с помощью симметричного подвода шин. Подводящие шины расположены в экваториальной плоскости. Коммутация катушек в группы осуществлена на некотором расстоянии от установки.

Объем магнитного поля составляет около 120 л, объем, занимаемый плазмой, 50 л. Квазистационарное поле может изменяться до 10 кЭ при полупериоде разряда батареи конденсаторов $T_0/2 = 10$ мксек. Сжатие плазмы осуществляется увеличением магнитного поля за 50-70 мксек ($T_1/4$). Амплитуда сжимающего поля на нынешнем этапе экспериментов может достигать 15 кЭ. Разработана система закорачивания витков сжимающего поля (кросс-бар), позволяющая поддерживать поле после нарастания в течение 1 мсек.

Ток омического нагрева создается трансформатором (4). При квазистационарном магнитном поле 4 кЭ и запасе устойчивости $q = 3$ он составляет 10 кА. Поскольку при адиабатическом сжатии запас устойчивости не меняется, ток в плазме должен поддерживаться постоянным в течение всех стадий нагрева. Длительность тока составляет ~ 3 мсек.

Равновесие плазменного шнура должно поддерживаться с помощью хорошо проводящего кожуха (3) и управляющих поперечных полей. Кожух имеет разрезы для ввода внутрь камеры электрического и магнитного полей. Для создания поперечного магнитного поля на поверхности разрядной камеры закреплены 4 проводника (5). Угловое расстояние между ними подобрано так, чтобы создаваемое ими (и кожухом) поперечное магнитное поле было приблизительно однородно в объеме, занятом плазмой.

Для сверхвысокочастотного нагрева плазмы созданы два генератора в диапазонах частот $f_1 \approx 10$ ГГц и $f_2 \approx 40$ ГГц. Мощность генераторов достигает 100 кВт, длительность генерации может регулироваться от нескольких микросекунд до 100 мксек. Ввод СВЧ-энергии осуществляется с помощью волноводов через специальные отверстия в камере и лайнере (12).

2. ИССЛЕДОВАНИЕ РАВНОВЕСИЯ ПЛАЗМЕННОГО ШНУРА

При нагреве плазмы с помощью СВЧ-волн и адиабатического сжатия необходимо удерживать шнур от расширения. Особенно существенно это при сжатии, так как с уменьшением диаметра шнура ослабляется стабилизирующее действие кожуха. Поэтому равновесие шнура предполагает поддерживать с помощью программированного поперечного магнитного поля.

В настоящее время мы провели изучение влияния поперечного магнитного поля на разряд в режиме омического нагрева. Исследование равновесия шнура под действием поперечного магнитного поля на установке "Токамак" описано в работе [7]. Существенное отличие наших опытов

состоит в том, что при разряде поддерживалась постоянная напряженность электрического поля. При этом оказывается возможным установить прямую связь между током и поперечным магнитным полем.

В описываемых экспериментах давление водорода изменялось от $1 \cdot 10^{-4}$ до $2 \cdot 10^{-3}$ мм рт.ст, продольное магнитное поле — от 1,5 до 6 кЭ, ток в плазме — от 1 до 8 кА. Запас устойчивости $q \geq 3$. Типичные осциллограммы разряда приведены на рис.3. Проводимость плазмы, рассчитанная по осциллограммам тока в плазме и напряжения на обходе, находится в пределах $(1 \div 4) \cdot 10^{14}$ CGSE. Концентрация заряженных частиц, измеренная по ослаблению пучка быстрых атомов водорода и по отсечке 4- и 8-миллиметровых волн, составляет $10^{12} \div 10^{13}$ см $^{-3}$. Предварительные измерения диамагнитного сигнала показали, что плазменный шнур является парамагнитным (см.рис.3). При этом в максимуме тока суммарная температура ($T_e + T_i$) составляет несколько десятков электронвольт. Отметим, что вычисленная по этой температуре проводимость значительно больше измеренной. Это, по-видимому, указывает на аномальный характер проводимости.

Известно [8,9], что малое поперечное магнитное поле, обусловленное несовершенством конструкции установки, может оказывать существенное влияние на равновесие шнура и параметры плазмы. Мы измеряли это поле $\bar{H}_{\perp \text{расс}}$ по эффекту анизотропии проводимости при изменении относительного направления E и H_0 [10]. Оказалось, что $\bar{H}_{\perp \text{расс}} = (1,0 \pm 0,3)\text{Э}$ при $H_0 = 3,5$ кЭ. Это поле было скомпенсировано с помощью специальных витков.

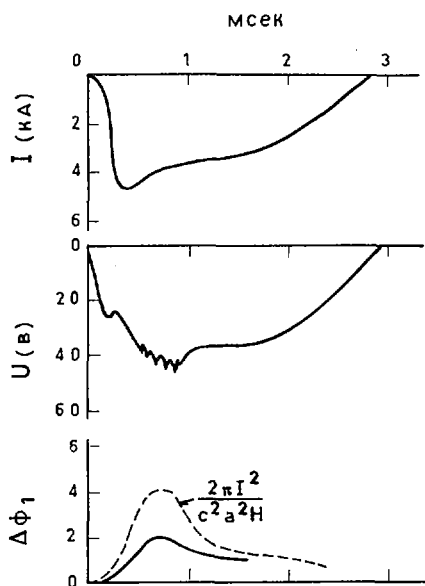


Рис.3. Осциллограммы для режима омического нагрева:
 $H_0 = 2,5$ кЭ, $E_0 = 0,15$ В/см, $r = 1,4 \cdot 10^{-4}$ мм рт.ст.
 1 — осциллограмма тока в плазме,
 2 — осциллограмма напряжения на обходе,
 3 — осциллограмма диамагнитных измерений.

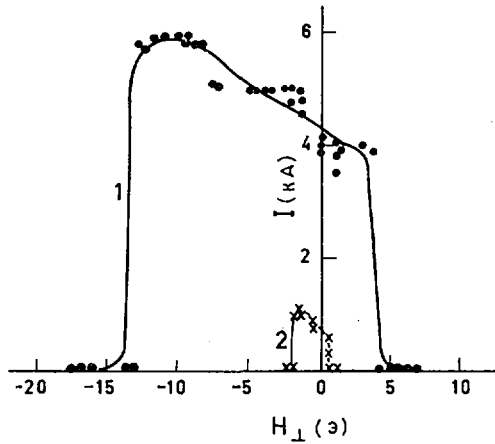


Рис. 4. Зависимость амплитуды разрядного тока от управляющего магнитного поля:
 $H_0 = 3,5$ кЭ, $p = 2,4 \cdot 10^{-4}$ мм рт.ст.
 кривая 1 - $E_0 = 0,15$ В/см,
 кривая 2 - $E_0 = 0,05$ В/см.

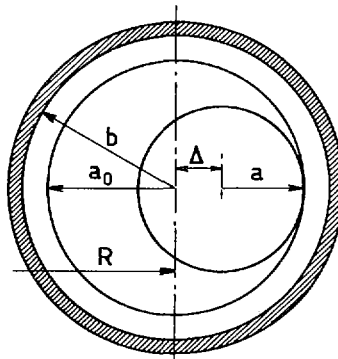


Рис. 5. Схема, поясняющая расчет зависимости $J = f(H_{\perp})$.

Управляющее магнитное поле включалось одновременно с началом омического нагрева и нарастало по синусоидальному закону, достигая максимального значения одновременно с током разряда (рис.3). На рис.4 приведены результаты измерений зависимости амплитуды разрядного тока от напряженности поперечного магнитного поля для двух значений электрического поля. Видно, что разряд существует лишь при определенных поперечных полях. Область этих поперечных полей несимметрична относительно знака поля и становится шире с ростом тока. Подбор оптимального поперечного поля позволяет увеличить амплитуду тока в плазме. Экспериментальные результаты могут быть объяснены на основе простой модели. Рассмотрим плазменный шнур (рис.5), смещенный относительно центра диафрагмы. Радиус шнура a определяется радиусом диафрагмы a_0 и смещением Δ :

$$a = a_0 - |\Delta| \quad (1)$$

Если равновесие шнура поддерживается с помощью кожуха и поперечного магнитного поля H_{\perp} , то смещение определяется соотношением [11]:

$$\Delta = \frac{b^2}{2R} \left\{ \ln \frac{b}{a} + \left(\frac{8\pi\bar{p}}{B_a^2} + \frac{l_i}{2} - \frac{1}{2} \right) \left(1 - \frac{a^2}{b^2} \right) \right\} + \frac{cb^2 H_{\perp}}{2I} \quad (2)$$

где b – радиус плазмы, R – большой радиус тора, \bar{p} – газокINETическое давление плазмы, $B_a = 2 I/c a$ – магнитное поле тока на границе шнура.

Будем предполагать, что при заданных значениях электрического поля, давления водорода и продольного магнитного поля удельная проводимость плазмы есть величина постоянная. В этом случае:

$$I = j_0 \cdot \pi a^2 \quad (3)$$

Зависимость тока от управляющего поля определяется изменением сечения шнура при его смещении. Соотношения (1)–(3) определяют зависимость $I = f(H_{\perp})$. Результаты расчета показаны на рис. 6. Максимальный ток I_0 соответствует случаю $\Delta = 0$, когда плазма заполняет все сечение внутри диафрагмы. При расчете принималось $l_i = 1/2$, что соответствует равномерному распределению плотности тока по сечению. Кривые 1–3 получены при изменении параметра $\beta_j = 8\pi\bar{p}/B_a^2$ от 0 до 1. С ростом β_j растет поле H_{\perp} , требуемое для удержания шнура в центре. Уменьшение тока соответствует смещению шнура внутрь (левая ветвь) и наружу (правая ветвь). Существенно наличие предельных управляющих полей. Вне области, определяемой предельными полями, равновесный шнур получен быть не может. Характерным также является наличие двух равновесных токов при заданном H_{\perp} . При этом малым токам (т.е. малому диаметру шнура) соответствует сильное его смещение. Наконец, отметим, что форма кривых на рис. 6 не должна зависеть от амплитуды то-

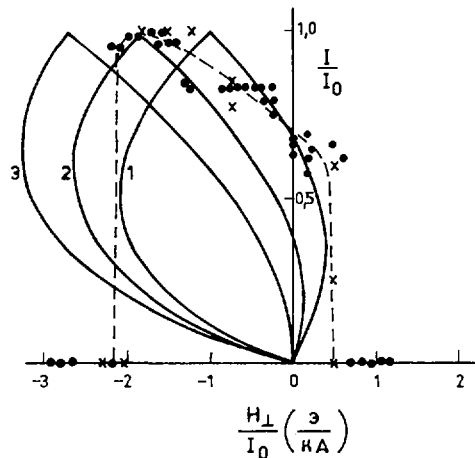


Рис. 6. Сравнение расчетной зависимости $J = f(H_{\perp})$ с экспериментальными данными: 1, 2 и 3 – расчетные кривые для $\beta_j = 0, 1/2, 1$.
 • – результаты измерений для $I_0 = 6$ кА (кривая 1 на рис. 4).
 × – результаты измерений для $I_0 = 1$ кА (кривая 2 на рис. 4).

ка I_0 , напряженности продольного поля, начального давления водорода (если $\beta_j = \text{const}$).

Сопоставление результатов измерений (рис. 4) с расчетом показано на рис. 6. Видно достаточно хорошее соответствие. Величине поперечного поля при $I = I_0$ соответствует $\beta_j \approx 1/4 \div 1/2$. Следует отметить, что в эксперименте не наблюдается амплитуд тока, соответствующих нижним участкам расчетных кривых $I = f(H_{\perp})$, т.е. малым диаметрам плазменного шнура. Такие состояния, по-видимому, не реализуются из-за неустойчивости относительно ухода шнура на диафрагму [7]. Аналогичные результаты были получены и при других давлениях. Лишь при высоких давлениях ($(1 \div 2) \cdot 10^{-3}$ мм рт.ст.) кривые $I = f(H_{\perp})$ становятся значительно шире теоретических.

Таким образом, результаты проведенных опытов хорошо согласуются с теорией равновесия в предположении, что проводимость плазмы не меняется при смещении шнура. Неизменность проводимости при усилении охлаждения шнура может быть связана с наличием аномальной проводимости.

3. ВЗАИМОДЕЙСТВИЕ СВЕРХВЫСОКОЧАСТОТНЫХ ВОЛН С ПЛАЗМОЙ

Задачи экспериментов по взаимодействию сверхвысокочастотных волн с плазмой на установке "Туман-2" состоят в определении условий поглощения волн, исследовании эффективности СВЧ-нагрева плазмы, изучении влияния СВЧ-нагрева на равновесие плазменного шнура и энергетическое время удержания. При постановке этих экспериментов имелось в виду использование для ввода энергии механизма линейной трансформации возбуждаемых в плазме волн в медленные плазменные волны [2,3]. Такая трансформация СВЧ-волн происходит в диапазоне верхних гибридных частот, определяемом равенствами:

$$\omega = (\omega_p^2 + \omega_H^2)^{1/2} \quad \text{или} \quad \frac{n}{n_c} = 1 - \left(\frac{H}{H_c}\right)^2 \quad (4)$$

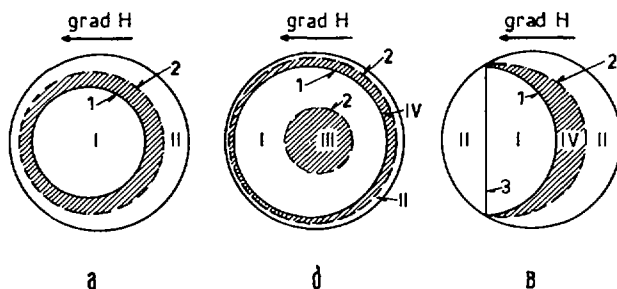


Рис. 7. Схема расположения областей распространения электромагнитных и плазменных волн в сечении тороидального плазменного шнура:

а) $H_0 = 0,7 H_c$, $n_{\text{max}} = 0,8 n_c$; б) $H_0 = 0,7 H_c$, $n_{\text{max}} = 2 n_c$; в) $H_0 = 0,9 H_c$, $n_{\text{max}} = 0,3 n_c$.

1 - линия $\omega_p^2 = \omega^2 - \omega_H^2$ (поверхность трансформации),

2 - линия $\omega_p^2 = \omega^2 \mp \omega_H^2$ (поверхность "отсечки"),

3 - линия $\omega_H = \omega$. Электромагнитные волны могут распространяться в областях I, II и затухают в областях III, IV, плазменные волны могут распространяться в областях I, III.

где ω — угловая частота поля, ω_p — плазменная, ω_H — циклотронная частоты, $n_c = (m\omega^2)/(4\pi e^2)$ — критическая концентрация (для использовавшихся в экспериментах частот $f_1 = 10$ Гц, $f_2 = 30$ Гц, $n_{c1} \approx 10^{12}$ см $^{-3}$, $n_{c2} \approx 10^{13}$ см $^{-3}$), H_c — циклотронное поле ($H_1 \approx 3,5$ кЭ, $H_2 \approx 10$ кЭ). Расположение поверхностей, определяемых равенством (4), в сечении плазменного шнура при учете тороидальной неоднородности магнитного поля иллюстрируется рис. 7. При вводе волн в плазму достижение ими поверхности трансформации определяется, в первую очередь, проникновением через область "непрозрачности", лежащую обычно между границей плазмы и поверхностью трансформации (на схеме рис. 7 эти области заштрихованы). В области "непрозрачности" поле волны экспоненциально затухает и при длинах, меньших размеров области, эффективность трансформации, определяющаяся проникновением волны, оказывается малой. Количественно эффективность трансформации для падающей на границу плазмы плоской волны может быть оценена по формуле [12]:

$$\eta = e^{-\delta} (1 - e^{-\delta}) \quad \delta = \frac{\pi \omega u^{3/4} (1 - u)}{c \ell (1 + u^{1/2})} \quad (5)$$

где $u = \omega_H^2/\omega^2$, $\ell = (1/n \cdot dn/dz)^{-1}$ при $n = n_c$. Результаты расчета для условий экспериментов на установке "Туман-2" в предположении параболического распределения концентраций представлены на рис. 8. При рассмотрении рис. 8 следует иметь в виду, что волна, не попавшая в область трансформации, отражается от плазмы, попадает к стенкам лайнера и, отражаясь от него, вновь направляется в плазму. Число возможных отражений от лайнера определяется потерями и, по-видимому, не меньше нескольких десятков. Поэтому для эффективного ввода энергии в плазму допустимы условия, при которых эффективность трансформации превышает $(1 \div 5) 10^{-2}$. Как видно из рис. 9, при соответствующих концентра-

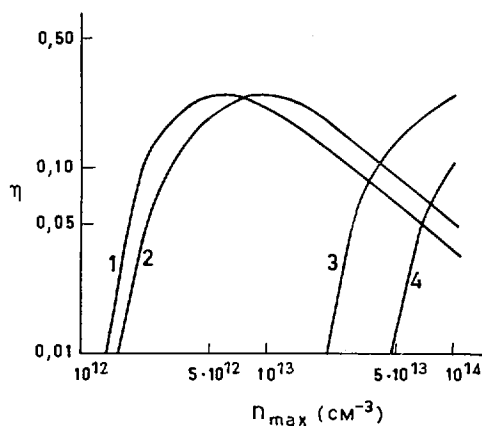


Рис. 8. Расчетная эффективность трансформации волн в плазме. При расчете принималось $n = n_{\max} (1 - r^2/a^2)$, $H = H_0 / (1 + r/R)$, $a = 8$ см, $R = 40$ см, предполагалось, что волна подводится с внешней стороны тора.
 1 - $f = 10$ ГГц, $H_0 = 1$ кЭ; 2 - $f = 10$ ГГц, $H_0 = 2,4$ кЭ; 3 - $f = 30$ ГГц, $H_0 = 2,4$ кЭ;
 4 - $f = 30$ ГГц, $H_0 = 5$ кЭ.

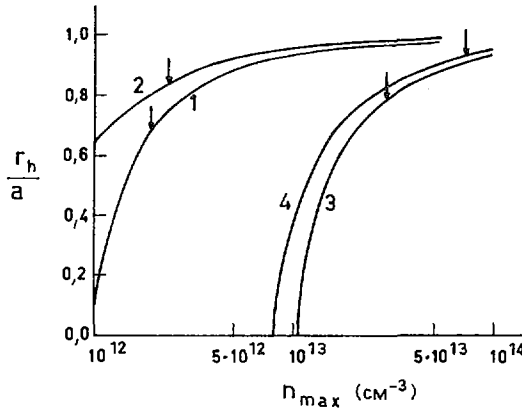


Рис.9. Положение поверхности трансформации для условий рис.8. Стрелками обозначены точки, при которых эффективность трансформации $\eta = 0,05$.

циях поверхность трансформации смещена к периферии плазменного шнура ($r/a > 0,7 \div 0,9$). Для осуществления трансформации в центральной части объема плазмы следует проводить эксперименты при условиях, когда магнитное поле вблизи одной из границ плазмы равно циклотронному, а максимальная концентрация меньше критической ($n = (0,2 \div 0,5)n_c$). В этом случае волны могут достигать поверхности трансформации, минуя область "непрозрачности" без всякого ослабления (рис.7 в).

При заданном положении поверхностей трансформации локализация областей выделения СВЧ-энергии определяется длиной поглощения плазменных волн, образующихся при трансформации. Вопрос о длине поглощения особенно важен для условий, когда трансформация происходит на периферии плазмы, так как при выделении энергии вблизи границ эффективность нагрева окажется низкой. При градиенте концентрации, перпендикулярном магнитному полю, бесстолкновительное поглощение плазменных волн по механизму Ландау отсутствует. Длина их столкновительного поглощения определяется соотношением [12]:

$$L \approx \frac{v_g}{\nu} \approx q\lambda \quad (6)$$

где v_g — групповая скорость волн, ν — частота столкновений электронов, λ — длина их свободного пробега, $q \approx 0,2 \div 0,4$ вдали от областей $\omega = N\omega_H$ и резко уменьшается вблизи этих областей. В условиях наших экспериментов величина L оказывается масштаба или больше поперечных размеров плазмы. Поэтому в отсутствие других механизмов столкновительное поглощение плазменных волн должно быть либо "размазано" по сечению плазменного шнура, либо локализовано в областях $\omega = N\omega_H$ (если они попадают в объем плазмы). Однако при наличии турбулентных колебаний концентрации эффективность поглощения плазменных волн может существенно возрасти. Поэтому вопрос о механизме их поглощения должен быть выяснен в процессе экспериментов. Для экспериментального исследования поглощения плазменных волн предполагается использовать

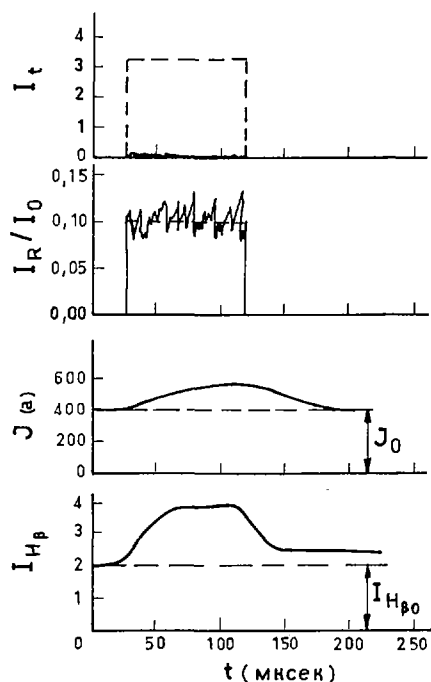


Рис. 10. Осциллограммы изменения параметров плазмы под действием СВЧ-мощности: $H_0 = 1,6$ кЭ, $p = 2 \cdot 10^{-4}$ мм рт. ст., $P = 30$ кВт. I_t - проходящий сигнал, I_R - отраженный сигнал, J - ток разряда, $I_{H\beta}$ - интенсивность линии H_β .

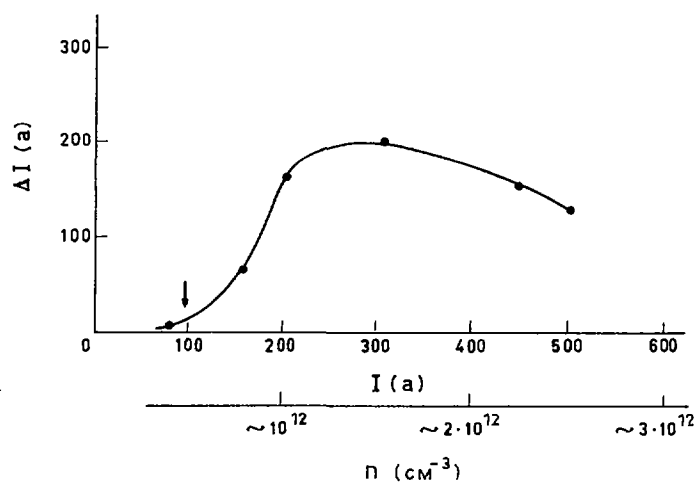


Рис. 11. Зависимость изменения тока под действием СВЧ-мощности от начального тока разряда:
 $H_0 = 1,6$ кЭ, $p = 2 \cdot 10^{-4}$ мм рт. ст., $P = 30$ кВт.

возможность перемещения поверхности трансформации и области распространения плазменных волн по объему плазмы путем изменения магнитного поля, концентрации плазмы, а также частоты вводимых волн (см. рис.8).

Первые эксперименты по взаимодействию СВЧ-волн с плазмой проводились в трехсантиметровом диапазоне длин волн. Мощность использованного генератора достигала 80 кВт при длительности импульсов до 300 мксек. Мощность вводилась в камеру с помощью круглого волновода, при этом регистрировались отраженный от камеры с плазмой сигнал и СВЧ-сигнал, принимаемый на другом участке тора ("проходящий" сигнал). Одновременно определялось влияние СВЧ-мощности на ток разряда, напряжение обхода, интенсивность излучения линии H_{β} .

Существенное влияние СВЧ-мощности на параметры плазмы было зарегистрировано лишь при относительно малых токах разряда, соответствующих малым плотностям плазмы ($J < 1$ кА, $\bar{n} < 5 \cdot 10^{12}$ см $^{-3}$). Типичные осциллограммы представлены на рис.10. Видно, что при наличии плазмы резко падает проходящий СВЧ-сигнал, и отраженная мощность не превышает 10-15%. Возрастание тока и увеличение интенсивности линии H_{β} свидетельствует о нагреве плазмы.

На рис.11 представлена зависимость изменения тока под действием

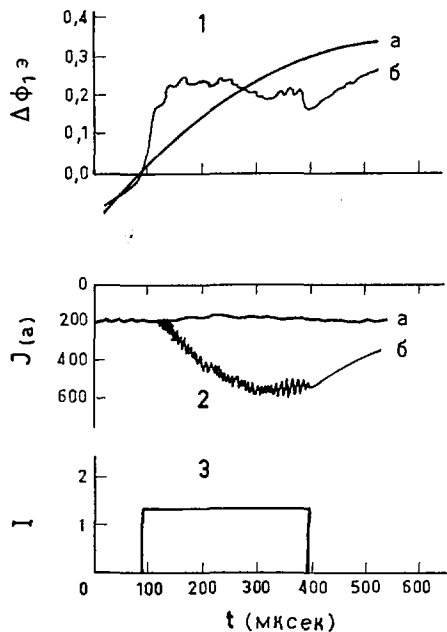


Рис.12. Влияние СВЧ-мощности на диамагнитный сигнал:

$H_0 = 1,6$ кЭ, $r = 2 \cdot 10^{-4}$ мм рт.ст., $P = 50$ кВт.

1 — осциллограммы сигнала диамагнитного зонда без СВЧ-нагрева (а) и при СВЧ-нагреве (б),

2 — осциллограммы тока в плазме без СВЧ-нагрева (а) и при СВЧ-нагреве (б),

3 — осциллограмма СВЧ-мощности, подводимой к плазме.

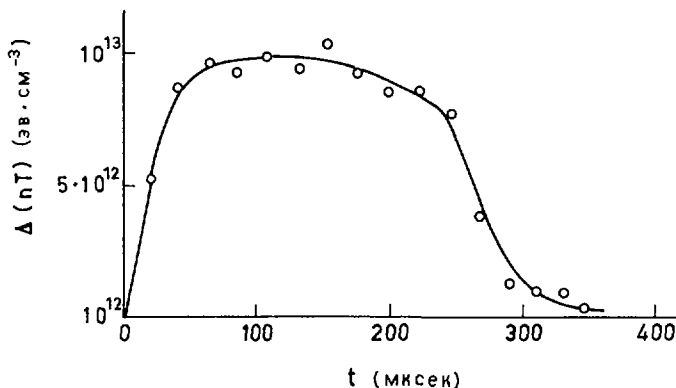


Рис. 13. Изменение энергии, запасенной в плазме под действием СВЧ-мощности: $N_0 = 1,6$ кЭ, $J_0 = 200$ А, $P = 50$ кВт, $p = 2 \cdot 10^{-4}$ мм рт.ст.

СВЧ-мощности от начального тока и, соответственно, от начальной плотности плазмы (при $n > 2 \cdot 10^{12}$ см⁻³ плотность измерялась по ослаблению пучка нейтральных атомов, при $n < 2 \cdot 10^{12}$ см⁻³ — грубо оценивалась с помощью восьмимиллиметрового интерферометра). Можно думать, что уменьшение эффекта при малых концентрациях ($n < 10^{12}$ см⁻³) связано с тем, что область трансформации $\omega = \omega_u$ удаляется от границ плазмы, при этом, как указывалось в докладе, возрастает "барьерное" затухание (см. кривую 1 на рис. 9). При дальнейшем уменьшении плотности, когда $\omega_{u \max}$ становится меньше ω , трансформация вообще оказывается невозможной (концентрация, соответствующая $\omega_{u \max} = \omega$ отмечена на рис. 11 стрелкой). Следует отметить также, что в экспериментах не обнаружено эффективного поглощения при магнитных полях, превышающих циклотронное поле ($(\omega_{He}) > \omega$). В этих условиях заметного влияния СВЧ-мощности на параметры разряда не наблюдается. Таким образом, полученные данные об условиях эффективного ввода энергии СВЧ-волн согласуются с предположением, что наблюдавшийся эффект связан с трансформацией волн в области верхнего гибридного резонанса $\omega = \omega_u$.

Для оценки эффективности нагрева плазмы под действием СВЧ-мощности были сделаны измерения диамагнитного эффекта. Осциллограммы диамагнитного сигнала и тока, полученные в условиях, когда СВЧ-мощность оказывает сильное влияние на параметры плазмы, представлены на рис. 12. Отметим, что в начальный момент нагрева β_1 достигает больших значений ($\beta_1 \approx 5$). В дальнейшем рост тока приводит, как видно из осциллограмм, к увеличению парамагнитного эффекта. На рис. 13 приведены результаты расчета изменения запасенной в плазме энергии (при вычислении учитывался парамагнитный эффект, связанный с током разряда). Полученные данные позволяют оценить эффективность ввода энергии в плазму (отношение мощности, затрачиваемой на нагрев плазмы и ионизацию, к мощности источника). В условиях, для которых получены кривые рис. 12 и 13, эта эффективность составляет несколько десятков процентов.

ЛИТЕРАТУРА

- [1] АНИСИМОВ, А.И., БУДНИКОВ, В.Н., ВИНОГРАДОВ, Н.И., ГОЛАНТ, В.Е., НАНОБАШВИЛИ, С.И., ОБУХОВ, А.А., ПАХОМОВ, Л.П., ПИЛИЯ, А.Д., ФЕДОРОВ, В.И., Plasma Physics and Controlled Nuclear Fusion Research, Vienna 2 1969, p.399.
- [2] ГОЛАНТ, В.Е., ПИЛИЯ, А.Д., Доклад на Международной конференции по замкнутым системам, Дубна, 1969.
- [3] ГОЛАНТ, В.Е., ПИЛИЯ, А.Д., Препринт №270 Физико-технического института, Ленинград, 1970; Усп. физич. наук 74 3 (1971).
- [4] ГОЛАНТ, В.Е., КАГАНСКИЙ, М.Г., ОВСЯННИКОВ, В.А., ПИЛИЯ, А.Д., Журн. техн. физ. 35 (1965) 2176.
- [5] ГОЛАНТ, В.Е., КАГАНСКИЙ, М.Г., ОВСЯННИКОВ, В.А., Plasma Physics and Controlled Nuclear Fusion Research, Vienna 2 1966, p.829.
- [6] ГОЛАНТ, В.Е., ГЛАДКОВСКИЙ, И.П., ИПАТОВ, В.А., КАГАНСКИЙ, М.Г., КАЛМЫКОВ, С.Г., КИСЛЯКОВ, А.И., ОВСЯННИКОВ, В.А., СОКОЛОВА, Л.В., ТЮЛЬПАНОВ, С.С., Plasma Physics and Controlled Nuclear Fusion Research, Vienna 1 1969, p.277.
- [7] ГРИГОРОВИЧ, Б.М., МУХАТОВ, В.С., Атомная энергия 17 (1964) 177.
- [8] АРЦИМОВИЧ, Л.А., КАРТАШЕВ, К.Б., Доклады Академии наук 146 (1962) 1305.
- [9] YOSHIKAWA, S., SINCLAIR, R.M., KESSLEAR, J.V., HARRIES, W.L., Phys. Fluids 6 (1963) 932.
- [10] КАГАНСКИЙ, М.Г., ОВСЯННИКОВ, В.А., Журн. техн. физ. 38 7 (1968).
- [11] ШАФРАНОВ, В.Д., Атомная энергия 13 (1962) 521.
- [12] ГИНЗБУРГ, В.Л., "Распространение электромагнитных волн в плазме", Изд. "Наука", М., 1967.

ЭКСПЕРИМЕНТАЛЬНОЕ ИССЛЕДОВАНИЕ НАГРЕВА ПЛАЗМЫ НА ЧАСТОТЕ, БЛИЗКОЙ К НИЖНЕМУ ГИБРИДНОМУ РЕЗОНАНСУ

В.М. ГЛАГОЛЕВ, Н.А. КРИВОВ, Ю.В. СКОСЫРЕВ

Институт атомной энергии им. И.В. Курчатова,
Москва,

Союз Советских Социалистических Республик

Доклад представлен К.Н. Степановым

Presented by K.N. Stepanov

Abstract – Аннотация

EXPERIMENTAL INVESTIGATION OF PLASMA HEATING AT A FREQUENCY CLOSE TO THE LOWER HYBRID RESONANCE.

When an electromagnetic wave excited in a plasma is slowed down as it moves along the magnetic field and propagates across the field in the direction of increasing density, it is transformed into a plasma wave. The authors study experimentally (a) the collisionless absorption of the HF power of a plasma and (b) the heating of a plasma. A plasma produced by an ultrahigh-frequency discharge or a plasma gun and having a density of $2 \times 10^{12} \text{ cm}^{-3}$ with a neutral gas pressure of $(1.5-3) \times 10^{-4} \text{ mmHg}$ is injected into a uniform magnetic field of 3 kOe. Ion-hybrid waves are excited with the help of a coil wound around a quartz tube (diameter 60 mm) which is connected with the injector. The power of the heat generator, which operates at a frequency of 140 Mc/s, is 200 kW for a pulse duration of 100 μs . The electron velocity distribution along the magnetic field and the transverse and longitudinal ion velocity distribution are studied with the help of multigrid probes and an electrostatic ion energy analyser. The probes, which move along the radius, provide data on the distribution of the hot ions and the electrons over the cross-section of the plasma. The electron distribution has a minimum at the centre of the plasma column, whereas the density of the heated ions is at a maximum. The transverse plasma energy, determined by measuring the diamagnetism of the plasma, increases with the magnetic field, beginning with a field corresponding to the hybrid resonance of a dense cold plasma. These results agree with the fully developed theory. The temperature of the plasma and its variations over time are determined by comparing the diamagnetic signal and the density of the plasma, measured with the help of 4-mm and 8-mm radiointerferometers. The maximum temperature of the heated plasma nT is $(1.5-2) \times 10^{14} \text{ eV} \cdot \text{cm}^{-3}$ for a density of $2 \times 10^{12} \text{ cm}^{-3}$. The mean transverse ion energy, found from probe measurements, is 150 eV. The energy of the electrons leaving the discharge along the magnetic field is 50-100 eV. Ions with a longitudinal energy of up to 600 eV are observed.

ЭКСПЕРИМЕНТАЛЬНОЕ ИССЛЕДОВАНИЕ НАГРЕВА ПЛАЗМЫ НА ЧАСТОТЕ, БЛИЗКОЙ К НИЖНЕМУ ГИБРИДНОМУ РЕЗОНАНСУ.

При возбуждении в плазме электромагнитной волны, замедленной вдоль магнитного поля и распространяющейся поперек поля в направлении возрастания плотности, происходит трансформация этой волны в плазменную. Экспериментально изучались явления бесстолкновительного поглощения ВЧ-мощности и нагрева плазмы. В однородное магнитное поле напряженностью до 3 кЭ инжестировалась плазма, создаваемая СВЧ-разрядом или плазменной пушкой, с плотностью до $2 \cdot 10^{12} \text{ см}^{-3}$ при давлении нейтрального газа порядка $1,5 \div 3 \cdot 10^{-4} \text{ мм рт. ст.}$ Ионногибридные волны возбуждались с помощью витка, охватывающего кварцевую трубу ($\phi 60 \text{ мм}$), соединенную с инжектором. Мощность нагревного генератора, работающего на частоте 140 МГц, составляла 200 кВт в импульсе длительностью до 100 мксек. Распределение электронов по скоростям вдоль магнитного поля и ионов по поперечным и продольным скоростям изучалось с помощью многосеточных зондов и электростатического анализатора энергии ионов. Зонды, перемещающиеся по радиусу, позволили выяснить распределение нагретых ионов и электронов по сечению плазмы. Распределение электронов имеет провал в центре, а плотность нагретых ионов в центре плазменного шнура – максимальна. Поперечная энергия плазмы, измеренная по ее диамагнетизму, возрастает с магнитным полем, начиная с поля, соответствующего гибриднему резонансу

плотной холодной плазмы. Эти результаты согласуются с развитой теорией. Температура плазмы и ее изменение во времени определялись из сравнения величины диамагнитного сигнала и плотности плазмы, измеренной с помощью четырех- и восьмимиллиметровых интерферометров. Максимальная величина nT нагретой плазмы составляет величину в $(1,5 \div 2) 10^{14}$ эВ·см⁻³ при плотности $2 \cdot 10^{12}$ см⁻³. Средняя поперечная энергия ионов, найденная из зондовых измерений, составляла 150 эВ. Энергия электронов, покидающих разряд вдоль магнитного поля, достигала 50-100 эВ. Наблюдались ионы с продольной энергией до 600 эВ.

Одним из перспективных методов нагрева ионной компоненты плазмы является метод, основанный на поглощении ионногибридных волн, возбуждаемых в плазме на частоте, близкой к нижней гибридной, соответствующей условию:

$$\omega = \frac{\omega_{0e} \omega_{He}}{\sqrt{\omega_{0e}^2 + \omega_{He}^2}} \sqrt{\cos^2 \theta + \frac{m_e}{m_i}}$$

где ω — частота нагревного генератора, ω_{0e} , ω_{He} — электронная ленгмюровская и ларморовская частоты, θ — угол между направлением распространения волны и магнитным полем.

Поглощение волн вблизи этих резонансов исследовалось в [2]. При $\omega_{Hi} < \omega < \omega_{He}$ магнитное поле слабо влияет на движение ионов, и за счет черенковского резонанса между фазовой скоростью волны и тепловой скоростью ионов возможно поглощение волн ионами. В то же время магнитное поле сильно ограничивает движение электронов перпендикулярно полю. Поглощение электронами может происходить только при приближении фазовой скорости волны вдоль магнитного поля к тепловой скорости электронов. Следовательно, в случае распространения волны под углом θ , близким к 90° , должно наблюдаться сильное ионное и слабое электронное поглощение энергии волны при условиях $v_{\phi}/\cos \theta \gg v_{Te}$ и $v_{\phi} \sim v_{Ti}$, где v_{ϕ} — фазовая скорость волны, v_{Te} и v_{Ti} — тепловые скорости электронов и ионов.

При нагреве плазмы в термоядерных установках возникает необходимость обеспечить проникновение возбуждаемой на поверхности плазмы электромагнитной волны вглубь плазменного слоя с нарастающей плотностью. В работе [1] было показано, что для этого на поверхности плазмы необходимо создать замедленную вдоль магнитного поля волну. Расчеты [1] и [2] показывают, что для этого необходимо замедлить волну в 1,5-2 раза. В этом случае при плавном нарастании плотности плазмы фронт волны поворачивается так, что в области плотной плазмы волна распространяется почти перпендикулярно магнитному полю. Фазовая скорость волны падает, при некоторой критической плотности волна трансформируется в плазменную [2-4]. После отражения от точки трансформации плазменная волна поглощается ионами черенковским механизмом [2]. Расчеты показывают [2], что электронное поглощение волны осуществляется при меньшей плотности в периферийный слой плазмы.

Полная трансформация электромагнитной волны в плазменную осуществляется только при достаточно сильном магнитном поле, когда $\omega < \sqrt{\omega_{He} \omega_{Hi}}$ [2]. Трансформация осуществляется в области $\omega \sim \omega_{0i}$ (ω_{0i} — ионная ленгмюровская частота). Целью работы являлось: экспериментальное выяснение величины и условий поглощения электромагнитной энергии плазмой на частоте, близкой к нижней гибридной; определение

распределения нагретых ионов и электронов по скоростям и сечению плазмы; изучение зависимости нагрева от параметров плазмы.

Эксперименты проводились на улучшенном варианте установки [5], имевшей два участка однородных магнитных полей общей длиной 3,5 м (рис. 1). В первом участке с напряженностью 1 кЭ помещался инжектор плазмы, работающий по принципу СВЧ-ионизации при электронно-циклотронном резонансе. Создаваемая им в кварцевой трубе с внутренним диаметром 48 мм плазма с плотностью $2 \cdot 10^{12} \text{ см}^{-3}$, распространяясь вдоль магнитного поля, инжектировалась в кварцевую трубу с внутренним диаметром 65 мм, которую охватывал виток связи ("Н"-ввод) электромагнитной ВЧ-энергии (частота 140 МГц). Магнитное поле в этом участке изменялось в пределах 300-3000 Э. Переход на трубу большего диаметра улучшал вакуумные условия в области нагрева. Виток связи являлся частью нагревного ВЧ-резонатора, представлявшего из себя полуволновую (длиной ~ 1 м) двухпроводную линию с коротким замыканием на концах. Виток связи, находившийся на одном из концов линии, имел диаметр 150 мм. Ширина витка (200 мм) определяла структуру переменного магнитного ВЧ-поля волны (продольное замедление). Радиальные электрические поля "Е"-волны получались в плазме за счет связи между "Е"- и "Н"-волнами при конечных продольных размерах витка. Две катушки создавали пробочную конфигурацию поля в области "Н"-ввода с пробочным отношением 1,5. ВЧ-генератор (длительность импульса 100 мксек) имел мощность 150 кВт. Добротность ненагруженного резонатора равнялась 550. Приближенная оценка добротности ВЧ-резонатора, нагруженного плазмой при давлении нейтрального газа $3 \cdot 10^{-4}$ тор, составляла 60.

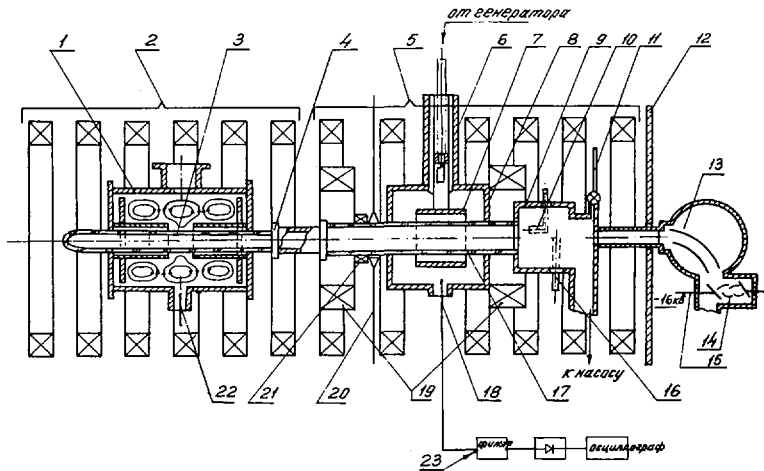


Рис. 1. Схема установки:

1 - СВЧ-инжектор (резонатор H_{013}), 2 - секция катушек продольного поля инжектора, 3 - кварцевая труба инжектора, 4 - переходная муфта, 5 - секция катушек продольного поля нагревного резонатора, 6 - петля ввода ВЧ-мощности, 7 - виток связи (Н-ввод), 8 - стенки кожуха ВЧ-резонатора, 9 - вакуумный объем с откачкой, 10 - боковой односеточный зонд, 11 - напуск газа, 12 - магнитный экран, 13 - электростатический анализатор, 14 - ФЭУ, 15 - ускоряющий электрод, 16 - многосеточный зонд, 17 - кварцевая труба ВЧ-генератора, 18 - петлевая антенна ВЧ-полей, 19 - пробочные катушки, 20 - линзы радиинтерферометра, 21 - датчик диамагнитного сигнала, 22 - петлевая антенна СВЧ-полей, 23 - фильтр СВЧ.

Нагрев плазмы фиксировался по возрастанию диамагнитного сигнала, регистрируемого с помощью датчика-многовитковой катушки, охватывающей кварцевую трубу, интегрирующего усилителя и осциллографа. Временная погрешность схемы регистрации (удлинение переднего фронта прямоугольного импульса напряжения) составляла 5 мксек.

Распределение ионов и электронов по скоростям, направленным вдоль основного продольного магнитного поля, определялось с помощью многосеточного зонда, подробно описанного в [6]. Зонд имел три расположенные перпендикулярно магнитному полю сетки и коллектор. Зонд перемещался поперек плазменного шнура.

Для анализа распределения ионов по поперечным скоростям применялся боковой односеточный зонд. Собирающий электрод зонда в виде лепестка размером 1×10 мм помещался в цилиндрический экран из нержавеющей стали с внутренним диаметром 10 мм. Экран имел щель размером 7×10 мм, расположенную параллельно образующей. Эта щель закрывалась сеткой с ячейкой (37 микрон), размер которой был меньше дебаевского радиуса. К торцам цилиндрического экрана приваривались диски $\phi 15$ мм. Зонд перемещался поперек плазменного шнура так, что щель и коллектор оставались все время параллельными магнитным силовым линиям. Торцевые диски ограничивали попадание электронов на коллектор. Электроны, имевшие значительно меньший ларморовский радиус, чем ионы, давали в десятки раз более слабый вклад в ток, идущий из плазмы на зонд. Подача положительного потенциала на коллектор позволяла по уменьшению тока, идущего на зонд, судить о поперечной энергии ионов плазмы. Измерение плотности плазмы осуществлялось с помощью четырех- и восьми-миллиметровых радиоинтерферометров по изменению фазы сигнала прошедшей сквозь плазму электромагнитной волны. Напряжение фазового детектора изменялось "пилообразно" в зависимости от увеличения фазы. Удвоенная амплитуда пилы (f) на рис.3 соответствует изменению фазы восьмимиллиметрового интерферометра на 180° . Увеличение фазы на 180° соответствует увеличению средней плотности плазмы на $2,6 \cdot 10^{12} \text{ см}^{-3}$.

Полная энергия ионов, покидающих плазму в направлении основного магнитного поля, измерялась с помощью электростатического анализатора с фотоумножителем, располагавшегося в области рассеянного магнитного поля [7]. После прохождения изогнутых по радиусу параллельных пластин конденсатора, ионы попадали на медный электрод, рис.1 (13), находившийся под потенциалом -16 кВ. Возникающие при этом вторичные электроны регистрировались при помощи ФЭУ. Энергия ионов определялась по величине потенциала на пластинах анализатора. Первоначально запускался СВЧ-инжектор (длительность импульса 1 мсек), который создавал плазму с плотностью $\sim 10^{12} \text{ см}^{-3}$ при температуре 10-20 эВ. Затем включался ВЧ-генератор с длительностью импульса 100 мксек на частоте 140 МГц. Момент включения ВЧ-генератора регулировался в широких пределах, но обычно составлял 500-600 мксек от начала работы инжектора. Эксперименты проводились в однородном магнитном поле и в поле пробочной геометрии. Давление нейтрального газа (водорода) составляло $(1,6-4) \cdot 10^{-4}$ тор. На рис.2 приводятся типичные осциллограммы, характеризующие развитие процессов во времени: огибающая ВЧ-полей в резонатора (а), диамагнетизм плазмы (b), ионный (с) и электронный (d) ток многосеточного зонда и ионный ток бокового зонда (е), а также плотность плазмы (g). Видно, что после включения ВЧ-полей диамагнитный

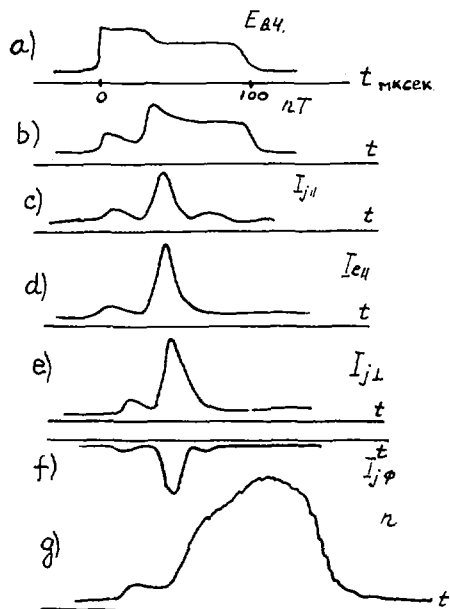


Рис. 2. Развитие во времени процессов, сопровождающих нагрев плазмы: а) огибающая ВЧ-полей в резонаторе, б) сигнал диамагнетизма плазмы, с) ионный ток на многосеточный зонд, d) электронный ток на многосеточный зонд, е) ионный ток на боковой зонд, f) ионный ток вдоль магнитного поля (сигнал ФЭУ), g) изменение плотности во времени.

сигнал увеличивался и достигал максимума спустя 20-30 мксек, а затем уменьшался, несмотря на наличие ВЧ-полей.

Рост диамагнитного сигнала происходил неравномерно. На рис. 3 даны осциллограммы диамагнитного сигнала (а, с, е) ионного тока бокового зонда (b, d) и интерферометра (f), когда величина однородного поля в области "H"-ввода составляла 3 кЭ. Осциллограммы а, b сняты при давлении нейтрального газа (водород) $1,6 \cdot 10^{-4}$ тор, а остальные осциллограммы — при давлении $2 \cdot 10^{-4}$ тор. Видно, что возникновение ВЧ-полей в резонаторе сопровождалось ростом диамагнитного сигнала, который при низком давлении в течение 20-30 мксек оставался неизменным, а затем вновь возрастал до максимума (наблюдалась "ступенька" на осциллограмме диамагнитного сигнала). При более высоком давлении длительность "ступеньки" сокращалась до 3-5 мксек. Вторичный подъем диамагнитного сигнала сопровождался резким увеличением ионного тока на боковой зонд и электронного и ионного токов вдоль плазмы. После выключения ВЧ-генератора диамагнитный сигнал спадал за время 300-400 мксек. Ионный ток на боковой зонд достигал максимума одновременно с диамагнитным сигналом, после чего спадал за время 10-20 мксек, в течение которых диамагнитный сигнал еще существенно не изменялся. При низком давлении ($2 \cdot 10^{-4}$ тор) небольшое уменьшение диамагнитного сигнала в конце "ступеньки" сопровождалось уменьшением начальной плотности плазмы. При более высоком давлении плотность плазмы во время первой "ступеньки" практически не менялась. Возрастание плотности плазмы начиналось одновременно со вторым подъемом диамагнитного сигнала.

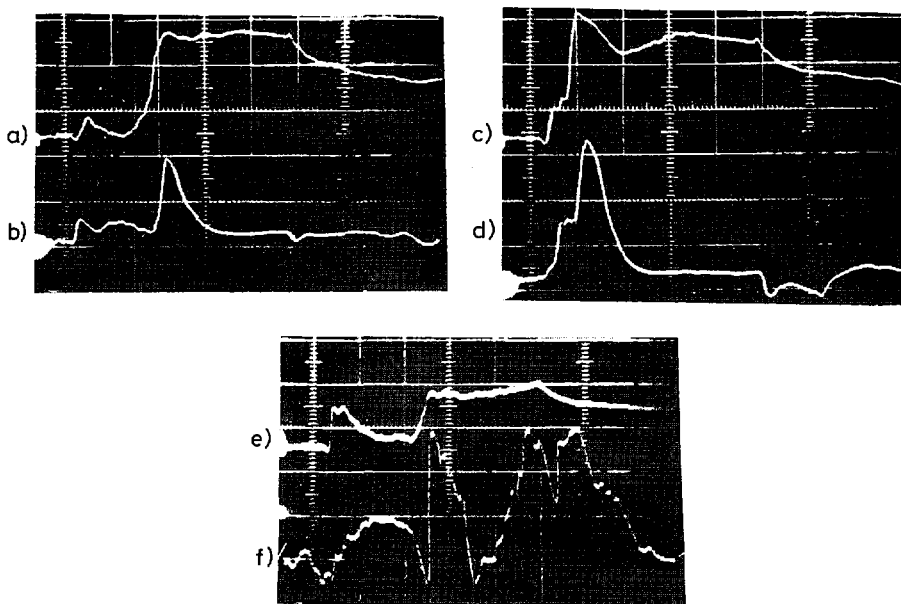


Рис. 3. Осциллограммы процессов:

a) осциллограмма диамагнитного сигнала, b) осциллограмма ионного тока бокового зонда (давление $1,6 \cdot 10^{-4}$ тор), c) осциллограмма диамагнитного сигнала, d) осциллограмма ионного тока бокового зонда (давление $2 \cdot 10^{-4}$ тор), e) осциллограмма диамагнитного сигнала, f) изменение фазы восьмимиллиметрового сигнала радиоинтерферометра.

Размах пилообразного напряжения соответствует изменению плотности $2,8 \cdot 10^{12} \text{ см}^{-3}$. Масштаб по оси ординат на всех осциллограммах диамагнитного сигнала: 10 делений — $0,6 \cdot 10^{14} \text{ эВ} \cdot \text{см}^{-3}$. Ионный ток бокового зонда приведен в относительных единицах. Развертка — 20 мксек/10 делений.

Все осциллограммы сняты при поле $H = 3 \text{ кЭ}$.

Существенно, что рост плотности происходил значительно медленнее роста диамагнитного сигнала. Это следует из рис. 4, где даны результаты обработки осциллограмм напряжения фазового детектора интерферометра, подобных рис. 3 (f), совмещенные во времени с диамагнитным сигналом, а также изменение во времени температуры плазмы, определенной как nT/n . Из этих рисунков следует, что быстрый нагрев плазмы происходил во время второго подъема диамагнитного сигнала.

Поскольку одновременно наблюдалось резкое возрастание ионного тока на боковой зонд, рис. 3 (b, d), это свидетельствовало о нагреве ионной компоненты плазмы. Момент начала второго подъема сильно зависел от давления нейтрального газа. Однако давление нейтрального газа не влияло на интервал плотностей, соответствующих второму подъему сигнала. Это позволило найти интервал плотностей, соответствующий нагреву ионной компоненты и определить зависимость этого интервала от магнитного поля (см. рис. 7). После прекращения нагрева ионов плотность плазмы продолжала возрастать, а так как диамагнитный сигнал изменялся мало, то температура плазмы спадала. Максимальное значение плотности зависело от давления нейтрального газа, т.е. рост плот-

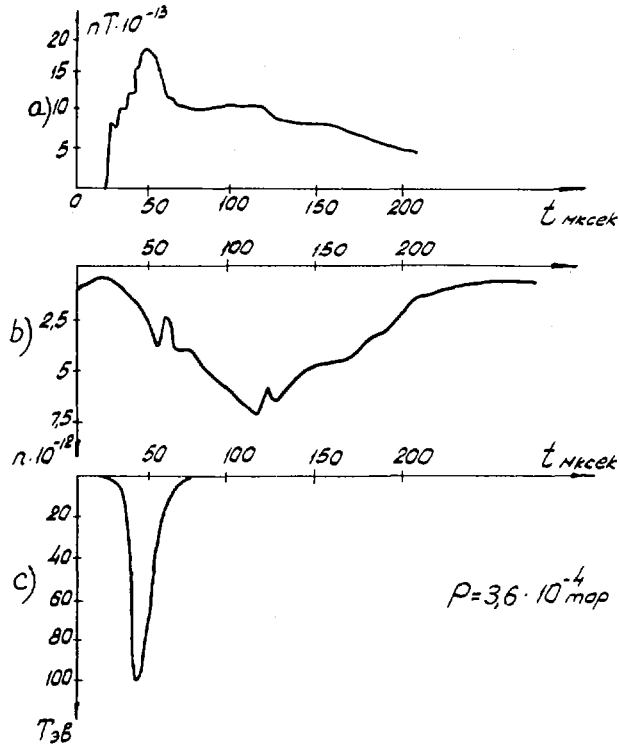


Рис. 4. Изменение во времени:
а) диамагнетизма, б) плотности, в) температуры плазмы, $H = 3$ кЭ.

ности после максимума объяснялся ионизацией нейтрального газа. Максимальная плотность равнялась 10^{13} см $^{-3}$, что свидетельствовало о высокой степени ионизации нейтрального газа при давлении $(1,6-3) \cdot 10^{-4}$ тор ($\sim 100\%$).

Распределение нагретых ионов по сечению плазменного столба изменялось при перемещении бокового зонда в направлении, перпендикулярном магнитному полю. Измерялись относительные величины токов в различные моменты времени при разных задерживающих потенциалах на собирающем электроде. При этом ионный ток из центральных областей всегда превышал ток из периферийных. Таким образом, нагрев ионного компонента происходил в центре столба. При подаче на собирающий электрод (коллектор) задерживающих ионы потенциалов измерялось распределение нагретых ионов по энергиям. Из-за наличия магнитного поля на коллектор могли попадать только ионы с энергией, превышающей некоторое предельное значение, что в наших экспериментах эквивалентно подаче на коллектор задерживающего потенциала 150-250 эВ. Поэтому распределение ионов по энергиям измерялось, начиная с этого предела. На рис. 5 приводятся кривые зависимости величин ионного тока от задерживающего потенциала при магнитных полях 2, 2,3 и 3 кЭ и давлении нейтрального газа $2,4 \cdot 10^{-4}$ тор. Пунктиром показана кривая задержки ионного тока

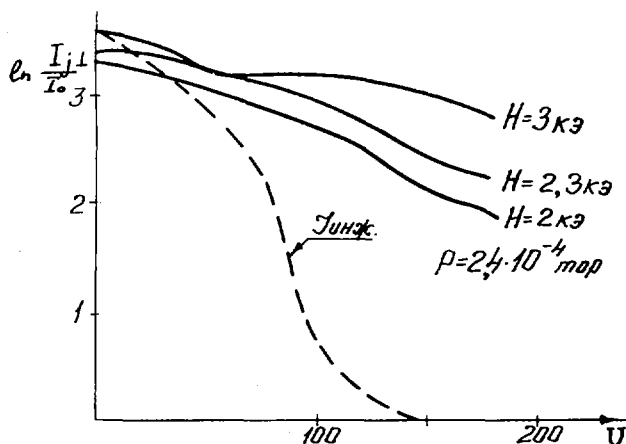


Рис. 5. Графики зависимости ионного тока на боковой зонд от задерживающего потенциала коллектора при различных потенциалах. Пунктирная кривая соответствует току инжектора при $H = 3$ кэ. Давление водорода — $2,4 \cdot 10^{-4}$ тор.

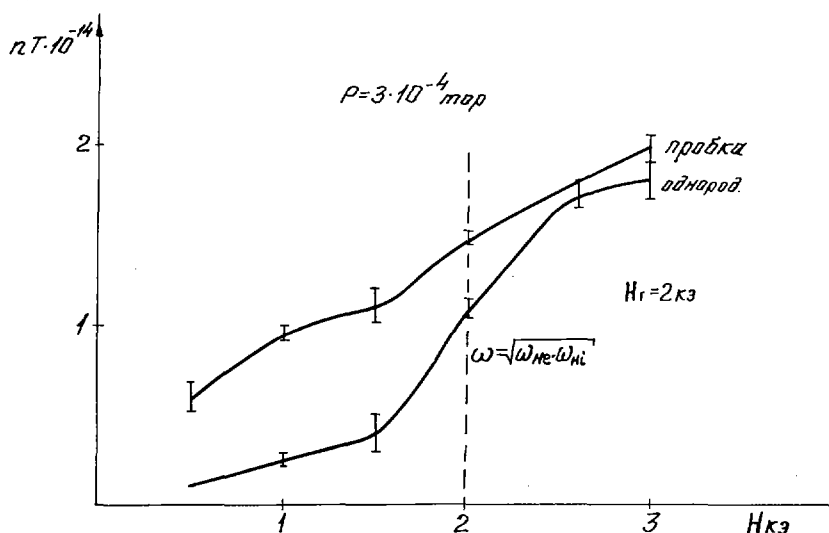


Рис. 6. Зависимость диамагнетизма плазмы от магнитного поля в однородном и пробочном поле при давлении $3 \cdot 10^{-4}$ тор.

СВЧ-инжектора. Если считать, что "поперечная температура" ионов $T_{\perp 1}$ соответствует спаду тока в "е" раз, то температура ионов в плазме инжектора равна 25-30 эВ. Температура нагретых ионов в момент максимума ионного тока больше 200 эВ, причем с увеличением магнитного поля средняя энергия ионов возрастала. При полях ≤ 2 кэ максимум ионной температуры наблюдался на некотором расстоянии от центра плазменного шнура. Существенной зависимости поперечной температуры от давления нейтрального газа не обнаружено. Это свидетельствовало о

том, что механизм поглощения ВЧ-энергии бесстолкновительный. В то же время, включение пробочного поля не оказало заметного влияния на энергию ионов. Измерения диамагнитного сигнала при различных магнитных полях показали, что поперечная энергия плазмы возрастала с увеличением поля в области "Н"-ввода. При магнитном поле меньше некоторого значения (1000 Э) нагрев плазмы сильно падал (см. рис. 6). Измерения, проведенные с помощью многосеточного зонда и электростатического анализатора, показали, что, наряду с поперечным, осуществлялся продольный нагрев плазмы. При перемещении многосеточного зонда по радиусу измерялось распределение электронов по энергиям. Если распределение электронного тока из плазмы, созданной инжектором, имеет максимум в центре, то максимальная средняя энергия нагретых электронов обнаружена в поверхностном слое плазмы. Средняя продольная энергия электронов плазмы инжектора и нагретых электронов в центре шнура равна 50-75 эВ и 100-120 эВ на расстоянии 15 мм от центра. В "пробочном" поле скин-характер нагрева электронов проявляется слабее. Продольная энергия ионов, измеренная многосеточным зондом, превышала 200 эВ.

С помощью электростатического анализатора, находившегося за областью рассеянного магнитного поля, измерялась полная (поперечная и продольная) энергия ионов, уходящих из плазмы. Обнаружены две группы ионов с энергией 100 и более 700 эВ. Поперечный и продольный уход частиц из плазмы происходил одновременно.

Результаты экспериментов свидетельствуют о том, что нагрев ионного компонента водородной плазмы поперек магнитного поля осуществлен до $T_{i\perp} \sim 100$ эВ и электронного компонента — до $T_{e\parallel} \sim 100$ эВ. Если предположить, что уход плазмы вдоль магнитного поля происходил за счет свободного течения, то мощность, уносимая плазмой, составляла ≈ 40 кВт. Это качественно согласуется с величиной мощности, вводимой от генератора в плазму (~ 100 кВт). По измерению добротности плазмы и вводимой ВЧ-мощности, а также с помощью магнитного зонда найдено, что напряженность переменного магнитного поля в плазме равнялась $\dot{H} \sim 20$ Э. Это соответствовало большому значению отношения давления плазмы к высокочастотному ($\beta = 8\pi r / \dot{H}^2 = 30$) и характеризовало высокую эффективность нагрева. Основные особенности нагрева заключались в следующем:

1. Бесстолкновительный характер нагрева. Время набора энергии плазмы, соответствующее второму подъему диамагнитного сигнала, составляло 5-7 мксек, что меньше характерных столкновительных времен. Нагрев улучшался при уменьшении давления нейтрального газа.

2. Сильное возрастание поперечной энергии плазмы наблюдалось только в магнитных полях, превышающих некоторое значение. Это значение близко к определяемому условием $\omega \sim \sqrt{\omega_{He} \omega_{H\parallel}}$.

3. Нагрев происходил только при плотности плазмы, лежащей в определенном интервале. Этот интервал плотностей близок к условию равенства частоты генератора ионной ленгмюровской частоте.

4. Поглощение энергии ионами происходило в центральных, а электронами — в периферийных областях плазменного столба. Измеренные экспериментально при разных магнитных полях интервалы плотностей плазмы, соответствующие ее быстрому нагреву, можно было сопоставить с теоретическими расчетами нагрева плазмы ионногибридными волнами, выполненными в работе [2]. Эти результаты даны на графиках рис. 7.

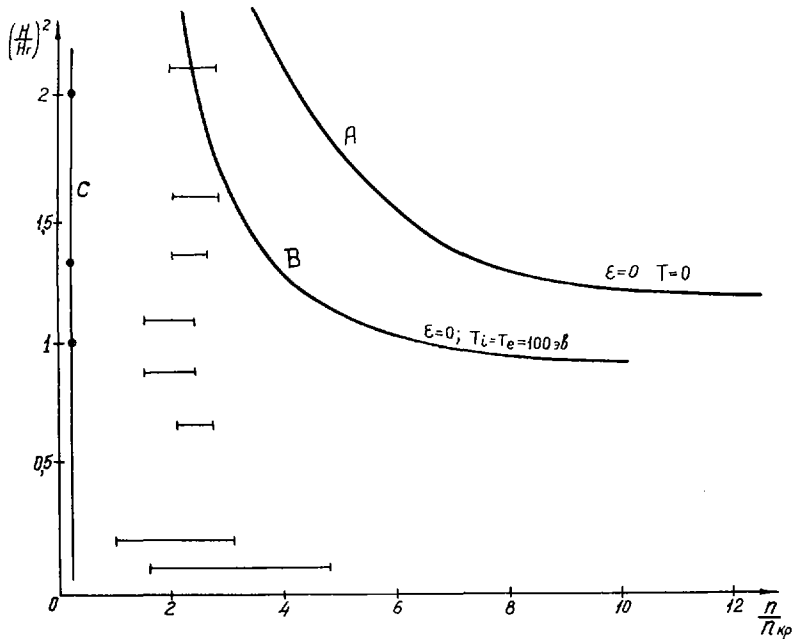


Рис. 7. Зависимость плотности плазмы от магнитного поля, соответствующие $\epsilon_{\parallel} = 0$ (кривая А), точкам трансформации в теплой плазме с ионной температурой 100 эВ (кривая В) и максимуму ионного поглощения (кривая С).

Кривая (А) соответствует гибричному резонансу холодной плазмы ($\epsilon_{\parallel} = 0$), кривая (В) — точкам трансформации электромагнитных волн в плазменные. Кривая (С) при $T = 100$ эВ дает значения плотностей, соответствующие максимуму поглощения плазменных волн. Найденные экспериментально интервалы изменения плотностей, соответствующие началу и концу нагрева ионов (второй подъем диамагнитного сигнала), изображены на рис. 7 горизонтальными отрезками прямых.

Зависимости даны в безразмерных параметрах:

1) $\omega_{0i}^2 / \omega^2 = n/n_{кр}$, где $n_{кр}\lambda^2 = 2,2 \cdot 10^{16} \text{ см}^{-1}$, причем плотность плазмы $n_{кр}$ отвечает условию $\omega = \omega_{0i}$, $\lambda = 2\pi c/\omega$;

2) $(\omega_{He} \omega_{Hi}) / \omega^2 = H^2 / H_1^2$, где $H_1 \lambda = 45,2 \cdot 10^4$ и H_1 находится из равенства $\omega = \sqrt{\omega_{He} \omega_{Hi}}$.

Из рис. 7 следует, что диапазон плотностей, при которых происходил нагрев, слабо зависел от магнитного поля. Этот результат хорошо согласуется с характером теоретической кривой максимального поглощения (С), хотя экспериментальные точки начала нагрева соответствуют большим значениям плотностей. В то же время нагрев наблюдался и в слабых магнитных полях, при которых, согласно расчету, полная трансформация (слияние плазменной и электромагнитной ветвей) отсутствует.

Наблюдавшийся в этих полях нагрев был более слабым (см. рис. 6) и может быть объяснен непосредственным возбуждением плазменных волн.

ВЫВОДЫ

1. Используя эффект нагрева на частоте, близкой к нижнему гибриднему резонансу, получена плазма с ионной температурой $T_{iL} \sim 100$ эВ и плотностью $2 \cdot 10^{12}$ см⁻³.

2. При больших магнитных полях ($H \geq H_T$) результаты экспериментов качественно согласуются с теорией распространения и поглощения ионно-гибридных волн в слабонеоднородном плазменном слое с учетом пространственной дисперсии, а именно:

а) максимальное поглощение ионами осуществляется в области $\omega \sim \omega_{oi}$;

б) максимальное электронное поглощение происходит при меньших плотностях плазмы, т.е. в поверхностном слое;

в) нагрев происходит эффективно только в магнитных полях, выше ~ 1000 Э.

3. При дальнейшей экспериментальной разработке (увеличение частоты генератора, мощности) метод нагрева может оказаться весьма перспективным для решения проблемы нагрева ионов плазмы с плотностью $\sim 10^{14}$ см⁻³ до температур 10-20 кэВ в крупных термоядерных установках с магнитным удержанием.

ЛИТЕРАТУРА

- [1] СТИКС, Т., "Теория плазменных волн", Госатомиздат, М., 1965.
- [2] ГЛАГОЛЕВ, В.М., Препринт Института атомной энергии им. И.В.Курчатова, № 1949, 1970; Plasma Physics (в печати).
- [3] ЗАСЛАВСКИЙ, Г.М., МОИСЕЕВ, С.С., САГДЕЕВ, Р.З., ДАН 15 6 (1964) 1295.
- [4] РУХАДЗЕ, А.А., САВОДЧЕНКО, В.С., ТРИГЕР, С.А., ПМТФ 6 (ноябрь-декабрь 1965) 58.
- [5] АЛИКАЕВ, В.В. и др. Plasma Physics and Controlled Nuclear Fusion Research, Vienna, IAEA, CN-24/J2, 2 1969.
- [6] ЛОБИКОВ, Е.А., НАСТЮХА, А.Н., ЖТФ 32 в.32.
- [7] АЛИНОВСКИЙ, Н.И., Сб. "Диагностика плазмы" вып. 2, Госатомиздат, М., 1968, стр.382.
- [8] ПИЛИЯ, А.Д., ФЕДОРОВ, В.Н., ЖЭТФ 57 (1969) 1198.

DISCUSSION

TO PAPERS IAEA-CN-28/L-4, L-5, L-6

P. K. KAW: In the experiment on heating near the lower hybrid frequency, was there any dependence of the absorption on the amplitude of the excited wave? If so, was it a threshold phenomenon?

K. N. STEPANOV: In the experiments carried out by Glagolev et al., the amplitude of the high-frequency field was large, and beam and parametric instabilities could be excited, so that turbulent heating of the ions took place. Experiments were also carried out with waves of small amplitude, and they too indicated the presence of strong damping. The absorption of low-amplitude waves is well explained by wave transformation under lower hybrid resonance conditions.

P. E. M. VANDENPLAS: I was very interested to note that the experimental results obtained by the Kharkov team in the MHz range depended strongly on the orientation of the loop with respect to the plasma torus — from a preponderantly transverse magnetic (TM) excitation to an excitation which has also an important transverse electric (TE) component. A recent general study performed by Messiaen and myself (Nucl. Fusion 11 (1971) 556) on a hot magnetized plasma column with $k_{\parallel} \neq 0$ predicts that the TE and TM behaviour will indeed differ considerably in this frequency domain.

I should like also to ask what are the exact differences in the experimental results obtained by Golant's group in Leningrad and Glagolev's group in Moscow for plasma heating in the lower hybrid region?

K. N. STEPANOV: I understand that the results are in good agreement. However, one cannot really make exact statements about differences between the two sets of results in view of their qualitative nature.

T. H. STIX: In the experiments on wave transformation, were any measurements made on the wavelength in the plasma beyond the point of transformation? If so, what were the wavelengths in terms of the gyro-radii of the particles?

K. N. STEPANOV: As far as I know, the length of the plasma waves was not measured.

J. P. GIRARD: In Paper L-8 is there a magnetic beach in the toroidal configuration? What is the ion containment time?

K. N. STEPANOV: The plasma heating experiments in Paper L-8 were carried out both with and without a magnetic beach. Heating was stronger with a beach. The longitudinal magnetic field was inhomogeneous ($\Delta H/H \sim 10\%$). There were no helical windings in this work. The plasma confinement time was apparently determined simply by the toroidal drift.

J. P. GIRARD: What is the heating efficiency in the experiments on heating at the lower hybrid frequency?

K. N. STEPANOV: A considerable amount of the generator energy was absorbed by the plasma.

ИССЛЕДОВАНИЕ ВЫСОКОЧАСТОТНОГО НАГРЕВА ПЛАЗМЫ

Л. И. ГРИГОРЬЕВА, А. В. ЛОНГИНОВ, А. И. ПЯТАК,
В. Л. СИЗОНЕНКО, Б. И. СМЕРДОВ, К. Н. СТЕПАНОВ,
В. В. ЧЕЧКИН

Физико-технический институт Академии наук
Украинской ССР, Харьков,
Союз Советских Социалистических Республик

Abstract-Аннотация

RESEARCH ON HIGH-FREQUENCY HEATING OF A PLASMA.

It is shown that the high-frequency method of plasma heating employing a collisionless wave absorption mechanism under the resonance conditions $\omega = K_{\parallel} v_{\parallel} + n \omega_{B\alpha}$ can ensure heating of a dense plasma of large dimensions to thermonuclear temperatures if the plasma confinement period is long enough. The absorption of the high-frequency energy is effected by resonance particles. The Coulomb collisions of these particles with the remaining particles of the plasma prevent the formation of a plateau in the distribution function and ensure heating of all the plasma. A theoretical investigation has been made of the turbulence of a plasma with a transverse current for the case in which the relative velocity of the electrons and ions "U" is considerably less than the electron thermal velocity. A review is given of cases of strongly non-isothermic plasma ($T_e \gg T_i$ and $T_e \ll T_i$) and of isothermic plasma ($T_e \approx T_i$). The case of hydrodynamic instability, where $u \gg \sqrt{(T_e + T_i)/m_i}$ is also considered. Estimates are given of the level of turbulence and the rate of electron and ion heating. Attention is also devoted to the nonpotential instability of a plasma with a transverse current under conditions of finite pressure. The results are presented of experiments on the investigation of turbulence and the heating of a hydrogen plasma with fast magneto-acoustic and ion-cyclotron waves of high amplitude. Measurements have been made of the spectra of turbulent pulses and the noise level, and the conditions have been determined in which preferential heating of electrons or ions occurs.

ИССЛЕДОВАНИЕ ВЫСОКОЧАСТОТНОГО НАГРЕВА ПЛАЗМЫ.

Показано, что ВЧ-методы нагрева плазмы, использующие бесстолкновительные механизмы поглощения волн, в условиях резонансов $\omega = K_{\parallel} v_{\parallel} + n \omega_{B\alpha}$ могут обеспечить нагрев плотной плазмы больших размеров до термоядерных температур, если время удержания плазмы достаточно велико. Поглощение ВЧ-энергии осуществляется резонансными частицами, кулоновские столкновения этих частиц с остальными частицами плазмы препятствуют образованию плато на функции распределения и обеспечивают нагрев всей плазмы. Теоретически исследовалась турбулентность плазмы с поперечным током в случае, когда относительная скорость электронов и ионов значительно меньше тепловой скорости электронов. Рассмотрены случаи сильно неизотермической плазмы ($T_e \gg T_i$ и $T_e \ll T_i$), изотермической плазмы ($T_e \approx T_i$), а также случаи гидродинамической неустойчивости, когда $u \gg \sqrt{(T_e + T_i)/m_i}$. Даны оценки уровня турбулентности и скорости нагрева электронов и ионов. Рассмотрена также непотенциальная неустойчивость плазмы с поперечным током в плазме конечного давления. Приведены результаты экспериментов по исследованию турбулентности и нагрева водородной плазмы быстрой магнитозвуковой и ионной циклотронной волнами большой амплитуды. Измерены спектры турбулентных пульсаций, уровень шумов и определены условия, при которых осуществляется преимущественный нагрев электронов или ионов.

В данном докладе рассматриваются следующие основные вопросы.

1. Исследование возможности применения различных высокочастотных методов нагрева плазмы до термоядерных температур в ловушках больших размеров за счет взаимодействия волна-частица в линейном режиме.
2. Исследование нагрева плазмы низкочастотными электромагнитными волнами большой амплитуды в турбулентном режиме. Получены

теоретические оценки для уровня турбулентных шумов и скорости нагрева электронов и ионов, и приведены результаты экспериментов по турбулентному нагреву плазмы свистами и ионными циклотронными волнами.

1. О ВЫСОКОЧАСТОТНОМ НАГРЕВЕ ПЛАЗМЫ БОЛЬШИХ РАЗМЕРОВ

Для осуществления ВЧ-нагрева плазмы необходимо обеспечить эффективный ввод и поглощение энергии ВЧ-поля в плазме. Энергия электромагнитных полей может передаваться частицам плазмы за счет следующих механизмов:

- 1) кулоновских парных столкновений между частицами плазмы (этот механизм, как правило, не эффективен, так как затухание волны пропорционально частоте столкновений, которая быстро убывает с ростом температуры);
- 2) взаимодействие волна-частица (черенковское и циклотронное затухание);
- 3) линейной и нелинейной трансформации в другие типы электромагнитных волн, поглощающихся частицами плазмы либо вследствие столкновений, либо вследствие взаимодействия волна-частица;
- 4) турбулентных механизмов, когда наличие электромагнитной волны приводит к возбуждению в плазме мелкомасштабных неустойчивостей, а рассеяние частиц плазмы на турбулентных пульсациях электрического поля приводит к их нагреву (турбулентное поглощение трудно осуществимо для неустойчивостей, для которых значение пороговой скорости — порядка тепловой скорости ионов, так как в этом случае необходимо возбуждение в плазме электромагнитных полей очень большой амплитуды).

В ловушках с достаточно большими размерами время удержания плазмы велико. Поэтому оказывается возможным нагрев плазмы до высоких температур высокочастотными методами, основанными на использовании черенковского и циклотронного поглощения энергии волн резонансными частицами в линейном режиме волнами малой амплитуды. Кулоновские столкновения в этом случае обеспечивают передачу энергии от резонансных остальных частицам плазмы, чем препятствуют образованию плато на функции распределения в узкой области, занимаемой резонансными частицами.

Рассмотрение возможности эффективного ввода и поглощения электромагнитных волн показывает, что целесообразно, на наш взгляд, применение следующих методов ВЧ-нагрева, анализ которых проводится ниже. Далее при оценках мы для определенности будем считать, что основные параметры плазмы равны по порядку величины $n_0 \sim 5 \cdot 10^{14} \text{ см}^{-3}$, $T_e \sim T_i \sim 10 \text{ кэВ}$, $B_0 \sim 50 \text{ кГс}$, малый радиус плазмы $a \sim 50 \text{ см}$ и время нагрева порядка времени удержания $\tau \sim 0,1 \text{ сек}$. В такой системе время обмена энергией между электронами и ионами $\lesssim \tau$, так что в принципе безразлично, какая компонента плазмы непосредственно получает энергию от ВЧ-поля. Необходимая для нагрева мощность на единицу длины плазменного цилиндра $W \sim 0,1 \text{ МВт/см}$.

Электронный циклотронный резонанс

В области высоких частот $\omega \gtrsim \omega_{pe}$, ω_{pe} , соответствующей миллиметровому диапазону, $\lambda \sim c/\omega < 1 \text{ мм}$, электромагнитные волны с частотой $\omega \approx n\omega_{pe}$ ($n = 1, 2, 3$) поглощаются на расстоянии l порядка [1, 2]:

$$l \lesssim \frac{\omega}{\gamma} \lambda \sim \frac{c^2}{\omega v_{Te}} \quad \left(\left| \frac{\omega - \omega_{Be}}{\omega} \right| \lesssim \frac{v_{Te}}{c} \right)$$

$$l \sim \frac{\omega}{\gamma} \lambda \sim \left(\frac{c}{v_{Te}} \right)^{2n-3} \frac{c}{\omega} \quad \left(\left| \frac{\omega - n\omega_{Be}}{\omega} \right| \lesssim \frac{v_{Te}}{c} \quad n = 2, 3 \right)$$

и даже для $n = 3$ длина затухания составляет всего несколько сантиметров. Для этого метода нагрева не существует проблемы ввода ВЧ-энергии в плазму, так как электромагнитные волны в этом диапазоне свободно проходят через плазму вне области поглощения.

В этом же диапазоне частот возможен метод нагрева [3], использующий трансформацию электромагнитных волн в плазменные волны в области верхнего гибридного резонанса, где $\omega = \sqrt{\omega_{pe}^2(r) + \omega_{Be}^2(r)}$. Точка резонанса может быть достигнута (область непрозрачности между точкой резонанса и границей плазмы отсутствует), если магнитное поле не однородно, при пропускании волны в направлении убывания магнитного поля. В этом случае между точкой гибридного резонанса и границей плазмы имеется точка циклотронного резонанса $r = r_{рез}$, где $\omega_{Be}(r) = \omega$. Если угол θ между направлением распространения волны и магнитным полем в этой точке близок к $\pi/2$, то циклотронное поглощение падающей волны при прохождении $r \approx r_{рез}$ может оказаться малым, в то же время циклотронное затухание коротковолновой плазменной волны ($k\rho_e \sim k r_D \sim 1$) в этой области может оказаться полным.

Нижний гибридный резонанс

Точка нижнего гибридного резонанса в неоднородной плазме достигается, если электромагнитная волна в плазме возбуждается при помощи замедляющей системы, создающей волну с фазовой скоростью вдоль магнитного поля, меньшей скорости света. При этом продольный показатель преломления должен быть больше некоторого критического значения [4]: $N_{||} = k_{||} c/\omega > N_{кр} \sim \sqrt{2(1 + \omega_{pe}^2/\omega_{Be}^2)} \sim 2 + 4$. В рассматриваемом случае частота $\omega \sim \sqrt{\omega_{Be} \omega_{Bi}} \sim 10^{10} \text{ сек}^{-1}$ и $\lambda = c/\omega \sim 3 \text{ см}$.

Поперечный показатель преломления волн с $\omega \ll \omega_{Be}$ определяется соотношением:

$$N_{\perp}^2 = \frac{1}{2\epsilon_1} \left\{ (\epsilon_1 + \epsilon_3)(\epsilon_1 - N_{||}^2) - \epsilon_2^2 \right. \\ \left. \pm \sqrt{[(\epsilon_1 + \epsilon_3)(N_{||}^2 - \epsilon_1) + \epsilon_2^2]^2 - 4\epsilon_1 \epsilon_3 [(N_{||}^2 - \epsilon_1)^2 - \epsilon_2^2]} \right\} \quad (1.1)$$

$$\epsilon_1 = 1 + \frac{\omega_{pe}^2}{\omega_{Be}^2} - \frac{\omega_{pi}^2}{\omega^2 - \omega_{Bi}^2} \quad \epsilon_2 = \frac{\omega_{pi}^2 \omega}{\omega_{Bi}(\omega_{Bi}^2 - \omega^2)} \quad \epsilon_3 = 1 - \frac{\omega_{pe}^2}{\omega^2} \quad (1.2)$$

Зависимость N_{\perp}^2 от плотности для двух типов волн (назовем одну из них медленной, другую — быстрой) показана на рис. 1. Для осуществления гибридного резонанса используется медленная волна (см. рис. 1 а), которая может распространяться ($N_{\perp}^2 > 0$) при $r < r_{01}$, где $\omega_{pe}(r_{01}) = \omega$. При линейной зависимости плотности от радиуса расстояние от границы плазмы $r = a$ до точки $r = r_{01}$ порядка:

$$\delta r_0 = a - r_{01} \sim a \frac{\omega^2}{\omega_{pe}^2} \Big|_{r=0} \lesssim 10^{-2} \text{ см}$$

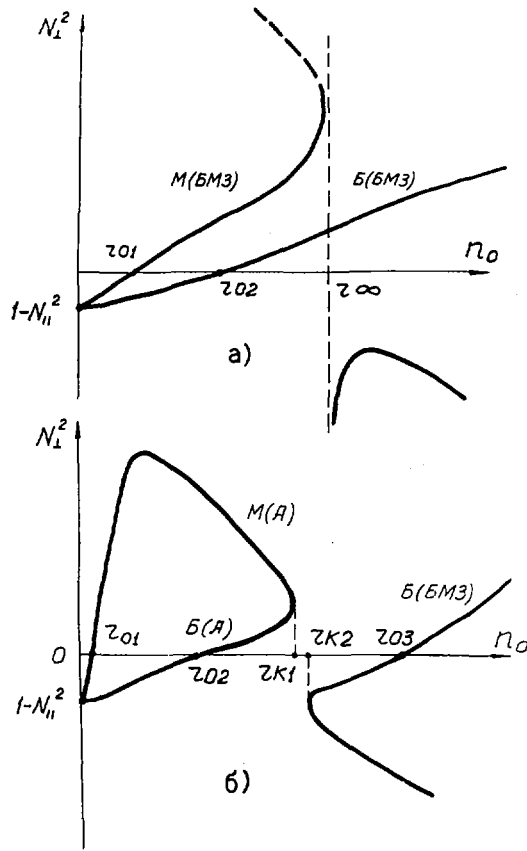


Рис. 1. Зависимость поперечного показателя преломления быстрой магнитозвуковой (БМЗ) и альфвеновской (А) волн от плотности:
 а) при $\omega_{В1} < \omega < \sqrt{\omega_{Вe} \omega_{В1}}$ и $N_{||} > N_{||кр}$ и
 б) при $\omega < \omega_{В1}$ и $N_{||} \gg 1$.

Отсюда следует, что ширина области непрозрачности $\delta r_{01} \ll c/\omega$, так что возбуждение этой волны при помощи замедляющей системы с $N_{||} \approx 2$, расположенной на границе плазменного шнура, не представляет существенных трудностей. Для медленной волны $N_1^2 \rightarrow \infty$ при $r = r_{\infty}$, где $\epsilon_1 = 0$. Однако в этой области выражение (1.1), полученное без учета пространственной дисперсии, не применимо, и необходимо пользоваться выражениями:

$$N_1^2 = \frac{1}{\delta \epsilon} \left[\epsilon_1 \pm \sqrt{\epsilon_1^2 + 4\delta \epsilon (\epsilon_3 N_{||}^2 + \epsilon_2^2)} \right] \quad (1.3)$$

где

$$\delta \epsilon \equiv 3 \frac{v_{T1}^2 \omega_{P1}^2}{c^2 \omega^2} + \frac{3}{4} \frac{v_{Te}^2 \omega_{Pe}^2 \omega^2}{c^2 \omega_{Be}^4} \quad (1.4)$$

Верхний знак в (1.3) относится к плазменной, а нижний — к медленной волне. В этой области для обеих волн:

$$N_{\perp} \sim \sqrt{\frac{2c m_i}{v_{Te} m_e}} \quad k_{\perp} \rho_e \sim \sqrt{\frac{v_{Te}}{c}} \quad (1.5)$$

График N_{\perp}^2 для плазменной волны показан на рис. 1 а пунктиром. При удалении от точки $r = r_{\infty}$ к периферии плазмы поперечное волновое число k_{\perp} плазменной волны, которая становится чисто продольной, увеличивается ($k_{\perp} \sim 1/\rho_e$). В этой области k_{\perp} определяется из уравнения:

$$\epsilon + i \epsilon' = 0 \quad (1.6)$$

где

$$\begin{aligned} \epsilon &= 1 + \frac{\omega_{pe}^2}{k^2 v_{Te}^2} \left[1 - e^{-k_{\perp}^2 \rho_e^2} I_0(k_{\perp}^2 \rho_e^2) \right] \\ &+ \frac{\omega_{pi}^2}{k_{\perp}^2 v_{Ti}^2} \left[\psi(z) - \sqrt{\pi} z e^{-z^2} \operatorname{ctg} \left(\pi \frac{\omega}{\omega_{Bi}} \right) \right] \\ \psi(z) &= 1 - 2z e^{-z^2} \int_0^z e^{t^2} dt \quad z = \frac{\omega}{\sqrt{2} k v_{Ti}} \\ \epsilon' &= \sqrt{\frac{\pi}{2}} \frac{\omega_{pi}^2 \omega}{k_{\perp}^2 k_{\parallel} v_{Ti}^3} \sum_{n=1}^{\infty} e^{-k^2 \rho_i^2} I_n(k_{\perp}^2 \rho_i^2) e^{-z_n^2} \quad z_n = \frac{\omega - n \omega_{Bi}}{\sqrt{2} k_{\parallel} v_{Te}} \end{aligned}$$

Циклотронное затухание, которое на высоких гармониках $n = \omega/\omega_{Bi} \sim \sqrt{m_i/m_e}$ чрезвычайно мало, может стать существенным для плазменной волны в области, где $k_{\perp} \approx n/\rho_i$. При приближении к этой области коэффициент затухания $\chi = \operatorname{Im} k_{\perp}$ становится равным

$$\frac{\chi}{|k_{\perp}|} = - \frac{\epsilon'}{k_{\perp} \frac{\partial \epsilon}{\partial k_{\perp}}} \sim \frac{1}{4} \frac{c}{v_{Ti}} \sqrt{\frac{m_e}{m_i}} e^{-z_n^2} \quad (1.7)$$

(Мы учли, что при $x \approx n e^{-x^2} I_n(x^2) \approx 1/4n$).

Таким образом, использование замедленной волны ($N_{\parallel} > N_{кр}$) для нагрева плазмы позволяет осуществить эффективный нагрев ионов путем трансформации этой волны в плазменные колебания в области нижнего гибридного резонанса и последующего циклотронного поглощения плазменных волн на гармониках ионной циклотронной частоты с высоким номером.

Кратный ионный циклотронный резонанс

Рассмотрим нагрев плазмы при использовании быстрой ветви колебаний (см. рис. 1 а), соответствующей быстрой магнитозвуковой волне с частотой $\omega \approx 2\omega_{Bi}$ (этот метод нагрева был предложен в [5]). Распространение этой волны возможно при $r < r_{02}$, где $N_A(r_{02}) = \sqrt{3} N_{\parallel}$,

$N_A(r) \equiv c/v_A(r) \equiv \omega_{pi}/\omega_{Bi}$. Показатель преломления этой ветви в области плотной плазмы имеет вид:

$$N_{\perp}^2 = \frac{(\epsilon_1 - N_{||}^2) - \epsilon_2^2}{\epsilon_1 - N_{||}^2} \quad (1.8)$$

Ширина слоя непрозрачности при линейном ходе плотности:

$$\delta r = (a - r_{02}) \approx 3a \frac{N_{||}^2}{N_A^2(r=0)}$$

Внутри плазменного шнура $N_{\perp} \sim N_A \sim 100$, $\lambda \sim 1$ см. Коэффициент затухания этой волны равен [5]:

$$\frac{\chi}{|k_{\perp}|} = \sqrt{\frac{\pi}{2}} \frac{N_A^2 v_{Ti}}{N_{||} c} e^{-z_2^2} \quad z_2 = \frac{\omega - 2\omega_{Bi}}{\sqrt{2} k_{||} v_{Ti}} \quad (1.9)$$

Коэффициент затухания (1.9) увеличивается при уменьшении $N_{||}$. Однако очень малые $N_{||}$ выбирать нецелесообразно, так как при малых $N_{||}$ в неоднородном магнитном поле область поглощения, где $|z_2| \lesssim 1$, будет очень узкой и поглощение волны окажется неполным. В случае неоднородного магнитного поля волна полностью поглощается на расстоянии:

$$\Delta r \sim a \frac{k_{||} v_{Ti}}{\omega_{Bi}} \cdot \frac{B_0}{\Delta B_0} \quad (1.10)$$

Для определения эффективности возбуждения БМЗ-волны в плазме рассмотрим задачу о падении плоской волны из полупространства, заполненного диэлектриком (замедляющая среда), с $\epsilon = \epsilon_0 > 1$, на границу плазмы с линейной зависимостью $N_{\perp}^2(r)$. При $N_{||}^2 \ll N_A^2(r=0)$ формирование волны будет происходить на расстоянии порядка нескольких δr_0 , в глубине плазмы будет применимо приближение геометрической оптики и отраженные волны будут отсутствовать из-за сильного циклотронного поглощения в резонансном слое. Поэтому задача о возбуждении колебаний в цилиндрическом плазменном шнуре хорошо аппроксимируется плоской задачей. При $\omega \approx 2\omega_{Bi}$ линейной зависимости N_{\perp}^2 от r соответствует зависимость n_0 от r незначительно отличающаяся от линейной. Графики величин $q = 1/(1 - |R|^2)$ и ψ , связанных с коэффициентом отражения $R = |R|e^{i\psi}$, в зависимости от параметров α и β , где

$$\alpha = \frac{\delta r}{2\pi} k_{||} \quad \beta = \frac{\delta r k_{\perp} g}{2\pi} \equiv \frac{\delta r}{2\pi} \sqrt{\frac{\omega^2}{c^2} \epsilon_0 - k_{||}^2}$$

показаны на рис. 2.

Если диэлектрик, окружающий плазму, имеет конечную толщину, то возбуждающая система будет представлять собой резонатор, энергия которого при $|R| \approx 1$ сосредоточена в основном в диэлектрике. В этом случае эффективность возбуждения волны в плазме характеризуется величиной добротности нагруженного резонатора, которая связана с величиной q соотношением:

$$Q = q(2\pi n - \psi) \quad (1.11)$$

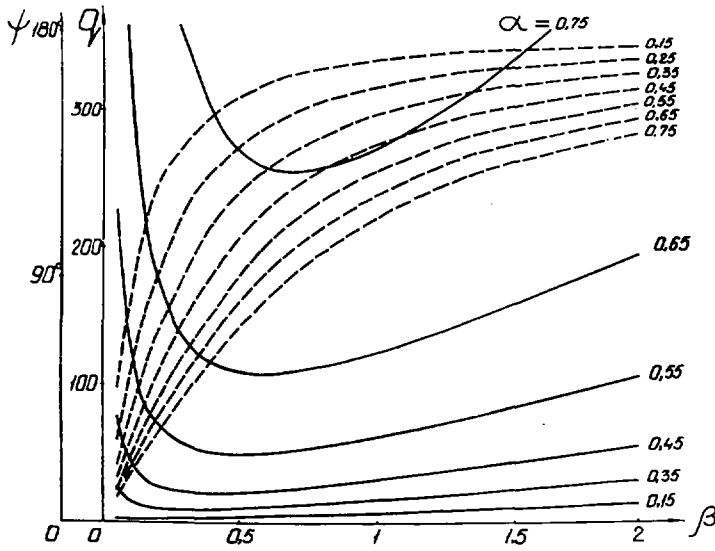


Рис. 2. Зависимость функций q и ψ от β для различных значений параметра α .

Из рис. 2 следует, что нецелесообразно выбирать значения параметра $\alpha > 0,5$, так как в этом случае из-за сильного затухания поля в области непрозрачности эффективность возбуждения волны в плазме будет низкой.

Задача о возбуждении и распространении БМЗ-волны в неоднородном плазменном цилиндре при $\omega \approx 2\omega_{Bi}$ была решена численно (при этом были использованы результаты [6]), где получены выражения для плотности тока в плазме при $\omega \approx 2\omega_{Bi}$.

На рис. 3 и рис. 4 приведены некоторые результаты этого расчета. Увеличение амплитуды поля и скорости роста температуры при малых значениях r обусловлено кумулятивным эффектом, связанным с сохранением потока энергии через поверхность цилиндра при больших значениях $k_{\perp}r$. Эти расчеты указывают, в соответствии с приведенными оценками, на сильное поглощение волны даже в случае сильно неоднородного магнитного поля.

Приведенное рассмотрение показывает, что резонанс $\omega = 2\omega_{Bi}$ может быть эффективно использован для нагрева больших плазменных систем в линейном режиме.

Ионные циклотронные волны

При $\omega < \omega_{Bi}$ зависимость N_{\perp}^2 от n_0 при $N_{\parallel} > 1$ показана на рис. 1 б. Ионной циклотронной волне [7] соответствует область $r_{02} > r > r_{k1}$. Для этой волны ширина области непрозрачности ($a - r_{02}$) и ширина области распространения ($r_{02} - r_{k1}$) — одного порядка (при линейной зависимости n_0 от r имеем $(a - r_{02}) \approx (r_{02} - r_{k1})$). Показатель преломления ИЦВ равен:

$$N_{\perp}^2(r) = \frac{2\epsilon_1 - N_{\parallel}^2}{N_{\parallel}^2 - \epsilon_1} N_{\parallel}^2 \quad \epsilon_1 = \frac{\omega_{Bi}^2}{\omega^2 - \omega_A^2} N_A^2(r) \quad (1.12)$$

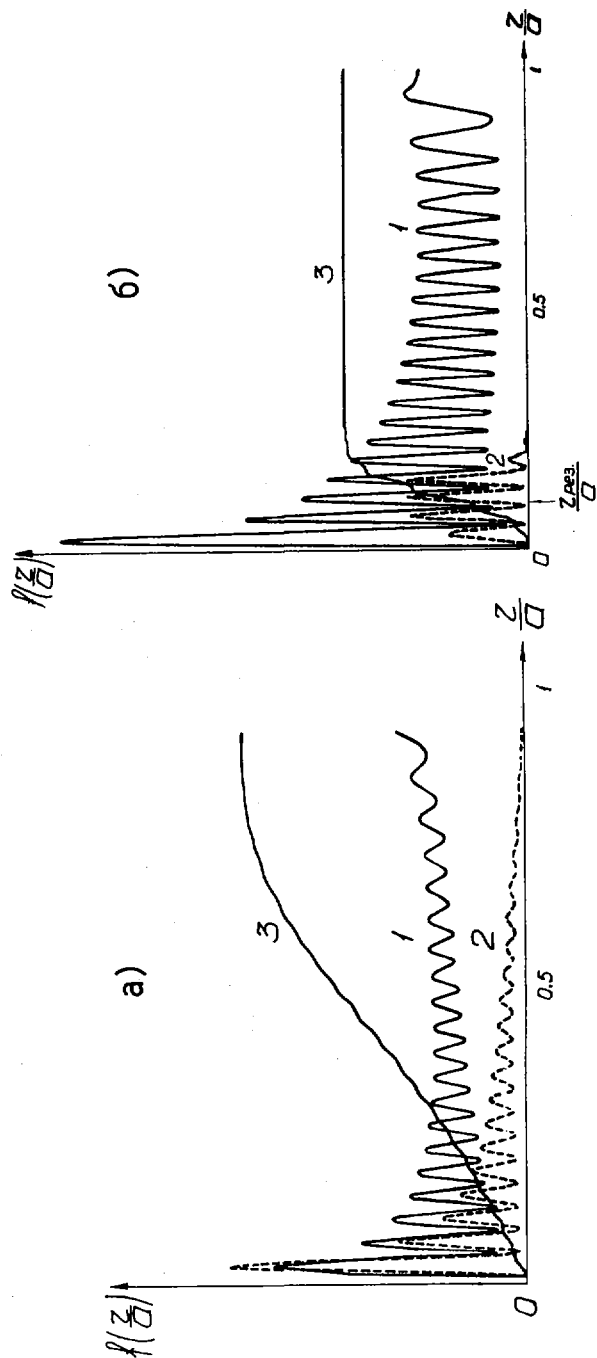


Рис. 3. Зависимость амплитуды поля (1), потока ВЧ-мощности через поверхность $r = \text{const}$ (3) и скорости увеличения температуры dT_1/dt (2) от радиуса. Функции $n_0(r/a)$ и $T_1(r/a)$ выбраны в виде $n_0(r/a) = n_0(0)(1 - r^2/a^2)$ и $T_1(r/a) = T_1(0)(1 - 0,65 r^2/a^2 - 0,25 r^3/a^3 - 0,15 r^4/a^4)$.
 Значения параметров: $N_A(0) = 100$, $N_0 = 10$, $v_{r1}(0) k_{II}/\omega = 10^{-3}$, $\omega/c N_0 a = 8,3$.
 а) магнитное поле однородно ($\omega_{BI} = \omega/2$)
 б) магнитное поле неоднородно ($\omega_{BI}(r/a) = \omega/2(0,99 + 0,1 r/a)$).

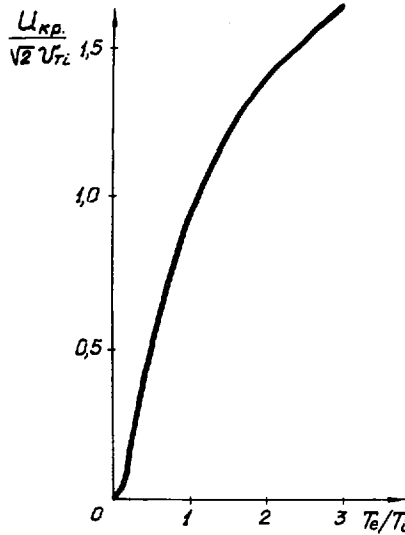


Рис. 4. Зависимость отношения $u_{кр}/v_{тi}$ от T_e/T_i .

При приближении к точке $\gamma_{k1} N_1$ резко возрастает, при этом также увеличивается и затухание этой волны, которое может быть обусловлено циклотронным резонансом на ионах из "хвоста" распределения, черенковским затуханием на электронах при $\omega < k_{||} v_{Te}$, а также турбулентными эффектами, которые могут появиться из-за возрастания поля E_r волны и увеличения относительной скорости ионов и электронов. Кроме того, возможна трансформация ИЦВ в медленную ветвь колебаний.

Однако использование ИЦВ в плазме с большими размерами для целей нагрева невозможно из-за трудностей непосредственного возбуждения этой волны внутри плазмы. Для того чтобы поле проникало в плазму, необходимо выбирать δr сравнимым с a . Полагая, например, $\delta r \approx a/3$ и учитывая, что для эффективного возбуждения волны в плазме необходимо выбирать $k_{||} \delta r \leq 2$ (это соответствует $\alpha = 0,5$ на рис. 2), получим соотношение, связывающее плотность в центре шнура и радиус плазмы, для которых эффективность возбуждения ИЦВ еще достаточно высока:

$$n_0(0) a^2 \sim 10 \frac{m_i c^2}{e^2} \frac{\omega_{Bi} - \omega}{\omega} \quad (1.13)$$

Например, при $n_0(0) \approx 10^{15} \text{ см}^{-3}$ и $\omega_{Bi} - \omega = 0,1 \omega$ получим, что $a \sim 5 \text{ см}$.

Магнитогидродинамические волны

В области МГД-волн ($\omega \ll \omega_{Bi}$) выражение (1.1) для показателя преломления принимает следующий вид:

$$N_{\perp}^2 = -N_i^2 + N_A^2(r) - \frac{\omega^2}{\omega_{Bi}^2} \frac{N_A^4(r)}{N_A^2(r) - N_{||}^2} \quad (1.14)$$

Длина волны в плазме $\lambda \sim v_A / \omega$ при $k_{\parallel} a \lesssim 1$ может быть порядка радиуса плазменного цилиндра a . В этом случае возможен эффективный ввод ВЧ-энергии в плазму с использованием резонансов раскачки. При этом поглощение волн будет осуществляться в узкой области, где $N_{\parallel} \approx N_A$ (в этой области МГД-волна трансформируется в сильнозатухающую, вследствие столкновительного или черенковского поглощения электронами, плазменную волну). Доля поглощаемой энергии — порядка ω^2 / ω_{Bi}^2 от мгновенного потока энергии [8]. Отсюда следует, что эффективный декремент затухания

$$\gamma \sim \left(\frac{\omega}{\omega_{Bi}} \right)^2 \omega \quad (1.15)$$

может быть достаточно большим, так что эти волны могут использоваться для нагрева плазмы больших размеров.

Магнитная накачка

При использовании низкочастотных ВЧ-полей с $\omega \ll \omega_{Bi}$ возможен эффективный нагрев ионной компоненты, если $\omega / k_{\parallel} \sim v_{Ti}$ (см. [9,10] и др.). В этом случае $N_{\perp}^2 \approx -N_{\parallel}^2$ и плазма оказывает малое влияние на распределение электромагнитного поля. Доля поглощаемой плазмой энергии — порядка $\gamma / \omega \sim 4\pi T_i / E_0^2$ от мгновенной мощности, т.е. поглощение энергии весьма эффективно. Поэтому магнитная накачка может быть с успехом использована для нагрева плазмы больших размеров.

В заключение отметим, что из рассмотренных выше методов ВЧ-нагрева использование низкочастотных методов (двойного ионного циклотронного резонанса, $f \sim 50 \div 100$ МГц, МГД-волн, $f \sim 1$ МГц, и магнитной накачки, $f \sim 50$ кГц) представляется более предпочтительным в настоящее время по сравнению с СВЧ-методами, так как создание источников ВЧ-энергии необходимой мощности не представляет особых трудностей.

2. НЕУСТОЙЧИВОСТЬ И ТУРБУЛЕНТНОСТЬ ПЛАЗМЫ С ПОПЕРЕЧНЫМ ТОКОМ

При движении электронов относительно ионов перпендикулярно магнитному полю в плазме возможно возникновение различных неустойчивостей пучкового типа (см. [11-21] и др.).

Поперечный ток может возникнуть при прохождении через плазму электромагнитных волн (например, быстрых магнитозвуковых волн или ионно-циклотронных волн), на фронте ударной волны, во вращающейся плазме, находящейся в скрещенных электрическом и магнитном полях, в плазменных сгустках, входящих в неоднородное магнитное поле, в плазменных пушках и т.д.

Рассеяние частиц плазмы на пульсациях электрического поля в состоянии с развитой турбулентностью плазмы с поперечным током может приводить к мощному нагреву электронов и ионов плазмы. В такой плазме может также наблюдаться сильная аномальная диффузия плазмы поперек магнитного поля. Эти эффекты детально исследовались в последние годы экспериментально. Турбулентные флуктуации плотности и электрического поля в плазме с поперечным током в последнее время обнаружены и исследованы экспериментально.

В данном разделе доклада рассматривается турбулентность плазмы с поперечным током, возникающая в результате развития ряда неустойчивостей. Мы ограничимся рассмотрением колебаний, для которых частота и инкремент нарастания значительно больше ионной циклотронной частоты, а длина волны значительно меньше ларморовского радиуса ионов с тепловой скоростью. В этом случае можно пренебречь влиянием магнитного поля на движение ионов в поле неустойчивых колебаний, т.е. считать ионы незамагниченными. Кроме того, будем считать, что время изменения невозмущенных значений скорости $\vec{u}_{e,i}$, температуры $T_{e,i}$ и плотности n_0 электронов и ионов значительно больше времени развития неустойчивости, а характерные размеры, на которых изменяются эти величины, значительно больше длины волны колебаний. В этом случае при рассмотрении колебаний можно плазму рассматривать как однородную среду, электроны и ионы которой движутся равномерно и прямолинейно. Тогда дисперсионное уравнение для продольных колебаний будет иметь следующий вид:

$$1 + \delta \epsilon_e + \delta \epsilon_i = 0 \tag{2.1}$$

где

$$\delta \epsilon_e = \frac{\omega_{pe}^2}{k^2 v_{Te}^2} \left[1 + i \sqrt{\pi} z_0 \sum_{n=-\infty}^{\infty} A_n(x) W(z_n) \right] \tag{2.2}$$

$$\delta \epsilon_i = \frac{\omega_{pi}^2}{k^2 v_{Ti}^2} \left[1 + i \sqrt{\pi} z_i W(z_i) \right] \tag{2.3}$$

$$W(z) = e^{-z^2} \left(1 + \frac{2i}{\sqrt{\pi}} \int_0^z e^{t^2} dt \right)$$

$$z_n = \frac{\omega - n\omega_{pe} - \vec{k} \vec{u}_e}{\sqrt{2} k_{||} v_{Te}} \quad z_i = \frac{\omega - \vec{k} \vec{u}_i}{\sqrt{2} k v_{Ti}}$$

$$A_n(x) = e^{-x} I_n(x) \quad x = k_{||}^2 \rho_e^2 \equiv \frac{k_{||}^2 v_{Te}^2}{\omega_{pe}}$$

Мы будем рассматривать только случай малых значений относительной скорости $u = |\vec{u}_e - \vec{u}_i| \ll v_{Te}$.

Критическое значение скорости $u = u_{кр}$, выше которого плазма неустойчива, получим из (2.1), учитывая, что $|\omega| \ll \omega_{pe}$ и что при $T_e \ll T_i$ неустойчивы колебания, для которых $k\rho_e < 1$. Тогда (2.1) примет вид:

$$k^2 r_{De}^2 + \frac{T_i}{T_e} \left[1 + i \sqrt{\pi} z_0 W(z_0) \right] + 1 + i \sqrt{\pi} z_i W(z_i) = 0 \tag{2.4}$$

где $\text{Im}\omega = 0$. Зависимость отношения $u_{кр}/v_{Ti}$ от T_e/T_i , полученная численным решением (2.4), показана на рис. 4 (см. также [18]).

Рассмотрим различные предельные случаи, при этом мы ограничимся рассмотрением плотной плазмы $\omega_{pe} \gg \omega_{Be}$.

Изотермическая плазма ($T_e \sim T_i$)

Если $T_e = T_i$, то $u_{кр} = 1,3 v_{Ti}$. Вблизи границы области устойчивости ($\Delta u = u - u_{кр} \ll u$) частота и инкремент нарастания и характерные значения волнового вектора равны:

$$\begin{aligned} \omega_R^2 &= 1,3 k_{||} v_{Te} \sim \sqrt{\omega_{Be} \omega_{Bi}} \left(\frac{\Delta u}{u}\right)^{3/2} & \gamma_k &\sim \sqrt{\omega_{Be} \omega_{Bi}} \left(\frac{\Delta u}{u}\right)^{5/2} \\ |k_{||}| &\sim \frac{1}{\rho_e} \sqrt{\frac{m_e}{m_i}} \left(\frac{\Delta u}{u}\right)^{3/2} & k_{\perp} &\sim \frac{1}{\rho_e} \left(\frac{\Delta u}{u}\right)^{1/2} \end{aligned} \quad (2.5)$$

Когда уровень шумов $W \equiv 1/8\pi \langle (\nabla\phi)^2 \rangle$ достигает значения порядка

$$W \sim \frac{m_e}{m_i} \frac{\omega_{Be}^2}{\omega_{pe}^2} \left(\frac{\Delta u}{u}\right)^5 n_0 T_e \quad (2.6)$$

движение электронов в электрическом поле колебаний становится сильно нелинейным. Оценки (2.5) и (2.6) справедливы по порядку величины и при $\Delta u/u \sim 1$. В этом случае рассеяние резонансных электронов и ионов на турбулентных пульсациях электрического поля приводит к их нагреву. Скорость изменения продольной температуры электронов и поперечной температуры ионов можно оценить по квазилинейной теории

$$\frac{\partial \ln T_{ne}}{\partial t} \sim \frac{\partial \ln T_{ni}}{\partial t} \sim \omega_{Bi} \sqrt{\frac{m_e}{m_i}} \quad (2.7)$$

При увеличении u в области $u \gg v_{Ti}$ возможна раскачка двух типов неустойчивостей: гидродинамической и кинетической. Для первой из них $k_{\perp} \rho_e \ll 1$, $|\vec{k} \vec{u}_e - \omega| \gg k_{||} v_{Te}$, $|\vec{k} \vec{u}_i - \omega| \gg kv_{Ti}$ и

$$\omega_k \sim \gamma_k \sim k_{\perp} u \sim \sqrt{\omega_{Be} \omega_{Bi}} \quad |\cos \theta| \sim \sqrt{\frac{m_e}{m_i}} \quad (2.8)$$

Эта неустойчивость может быть стабилизирована в режиме сильной нелинейности для электронов, когда нелинейный член в уравнениях движения ($\vec{u}_e \nabla$) \vec{u}_e становится порядка $\partial \vec{u}_e / \partial t$. Уровень шумов в этом случае равен:

$$W \sim n_0 m_e u^2 \frac{\omega_{Be}^2}{\omega_{pe}^2} \quad (2.9)$$

Вследствие сильной турбулентности характерное время корреляции $\tau_{корр}$ компонент Фурье будет мало ($\tau_{корр} \sim 1/\sqrt{\omega_{Be} \omega_{Bi}}$). Поэтому становится возможным стохастический нагрев ионов и электронов, обусловленный конечностью времени корреляции [26], при этом [21]

$$\frac{\partial T_{ne}}{\partial t} \sim \frac{\partial T_{ni}}{\partial t} \sim \omega_{Bi} \sqrt{\frac{m_e}{m_i}} m_i u^2 \quad (2.10)$$

Для кинетической неустойчивости при $u \gg v_{Ti}$ имеем

$$k_{\perp} \rho_e \sim 1 \quad z_0 \sim 1 \quad z_1 \sim 1$$

$$\omega_{\vec{k}} = \vec{k} \vec{u}_i + \Delta\omega \quad \Delta\omega \sim \gamma_{\vec{k}} \sim \sqrt{\omega_{Be} \omega_{Bi}} \quad |\cos \theta| \sim \frac{u}{v_{Te}} \gg \sqrt{\frac{m_e}{m_i}} \quad (2.11)$$

Уровень шумов для этой неустойчивости определяется, как и для гидродинамической неустойчивости, формулой (2.9). Скорость нагрева электронов и ионов можно оценить по квазилинейной теории:

$$\frac{\partial \ln T_{ie}}{\partial t} \sim \omega_{Be} \left(\frac{u}{v_{Te}} \right)^3 \quad \frac{\partial \ln T_{ii}}{\partial t} \sim \omega_{Be} \sqrt{\frac{m_e}{m_i}} \left(\frac{u}{v_{Te}} \right)^2 \quad (2.12)$$

Сравнение (2.10) и (2.12) показывает, что нагрев ионов на гидродинамических и кинетических пульсациях происходит с одинаковой скоростью, в то время как электроны нагреваются на кинетических ветвях колебаний значительно быстрее. В результате нагрева плазма становится сильно неизотермической ($T_e \gg T_i$).

Плазма с горячими электронами ($T_e \gg T_i$).

$$\text{В этом случае, как известно, } u_{кр} \approx v_s \left(\frac{m_i}{m_e} \frac{T_e^3}{T_i^3} \right)^{1/2} \exp\left(-\frac{T_e}{2T_i}\right).$$

При $|\cos \theta| \sim 1$ возбуждаются хорошо известные незамагниченные ионно-звуковые колебания.

Кроме того, при $|\cos \theta| \sim u/v_{Te}$ возникают коротковолновые колебания ($k_{\perp} \rho_e > 1$), для которых:

$$\omega_{\vec{k}} + i\gamma_{\vec{k}} = \vec{k} \vec{u}_i \pm \frac{\omega_{pi}}{\sqrt{1 + \delta \epsilon_e(\omega, \vec{k})}} \Big|_{\omega = \vec{k} \vec{u}_i} \quad (z_i \gg 1) \quad (2.13)$$

По порядку величины при $v_{Te}/u \geq k_{\perp} \rho_e \geq 1$, $k_{\perp} r_D \leq 1$ и $|\cos \theta| \sim u/v_{Te}$ имеем:

$$|\omega_{\vec{k}} - \vec{k} \vec{u}_i| \sim kv_s \quad \gamma_{\vec{k}} \sim \sqrt{\omega_{Be} \omega_{Bi}} \quad (2.14)$$

причем в этом случае в раскатке колебаний в условиях черенковского резонанса принимают участие электроны с $|v_{\parallel}| \sim v_{Te}$. При $k_{\perp} \rho_e \sim v_{Te}/u$ частота колебаний становится сравнимой с ω_{Be} и становится существенной раскатка колебаний с участием электронов с $|v_{\parallel}| \sim v_{Te}$ в условиях циклотронных резонансов $\omega - \vec{k} \vec{u}_i = n\omega_{Be} + k_{\parallel} v_{\parallel}$. Уровень шумов для неустойчивых колебаний (2.14) определяется соотношением [22]:

$$W \sim n_0 m_e u^2 \frac{\omega_{Be}^2}{\omega_{pe}^2} (k_{\perp} \rho_e)^2 \sim \begin{cases} n_0 T_e \frac{\omega_{Be}^2}{\omega_{pe}^2} & \text{при } \frac{v_{Te}}{u} \frac{\omega_{Be}}{\omega_{pe}} \ll 1 \\ n_0 m_e u^2 & \text{при } \frac{v_{Te}}{u} \frac{\omega_{Be}}{\omega_{pe}} \geq 1 \end{cases} \quad (2.15)$$

При рассеянии электронов на колебаниях (2.14) происходит нагрев электронов, скорость которого, оцененная по квазилинейной теории, определяется формулой (2.12). На этих колебаниях также возможен стохастический нагрев ионов, скорость которого, как и для случая гидродинами-

ческих неустойчивостей, определяется формулой (2.10). При этом электроны нагреваются быстрее, чем ионы

$$\frac{dT_{\perp e}}{dT_{\perp i}} \sim \frac{u}{v_s} > 1 \quad (2.16)$$

до тех пор, пока v_s не станет порядка u . (Соотношение (2.16) для немагнитного ионного звука было получено в [13]).

Отметим, что колебания с $k_{\perp} \rho_e \sim v_{Te}/u$ будут также приводить к увеличению $T_{\perp e}$, кроме того, рассеяние электронов на немагнитных ионно-звуковых пульсациях будет приводить к перекачке энергии из продольной в поперечные степени свободы, так что можно считать, что $T_{\perp e} \sim T_{\parallel e}$.

Плазма с горячими ионами ($T_i \gg T_e$)

В этом случае $u_{кр} \ll v_{Ti}$ и при $u < v_{Ti}$ возможно возбуждение электронного звука:

$$\omega_{\vec{k}} - \vec{k} \vec{u}_i \approx \frac{u}{2v_{Ti}} \sqrt{\omega_{Be} \omega_{Bi}} \quad \gamma_{\vec{k}} \approx 0,07 \left(\frac{u}{v_{Ti}} \right)^2 \sqrt{\omega_{Be} \omega_{Bi}} \quad |\cos \theta| \sim \frac{u}{\sqrt{2} v_{Ti}} \sqrt{\frac{m_e}{m_i}} \quad (2.17)$$

$$k_{\perp} \rho_e \sim \sqrt{\frac{T_e}{T_i}} \quad (\omega_{\vec{k}} - \vec{k} \vec{u}_i < \sqrt{2} k_{\perp} v_{Ti})$$

Стабилизация этих колебаний наступает при уровне шумов порядка (2.9). Рассеяние резонансных ионов на электронно-звуковых колебаниях будет приводить к их нагреву. При этом [20]:

$$\frac{\partial T_i}{\partial t} \sim m_i u^2 \omega_{Bi} \sqrt{\frac{m_e}{m_i}} \left(\frac{u}{v_{Ti}} \right)^2 \quad (2.18)$$

Кроме того, возможен стохастический нагрев электронов, обусловленный конечностью времени корреляции компонент Фурье электрического поля электронно-звуковых колебаний. Считая, что $\tau_{корр} \sim 1/\gamma_{\vec{k}}$, получим:

$$\frac{\partial T_{\perp e}}{\partial t} \sim 0,15 m_i u^2 \omega_{Bi} \sqrt{\frac{m_e}{m_i}} \left(\frac{u}{v_{Ti}} \right)^2 \quad (2.19)$$

Если $u \gg v_{Ti}$, то для колебаний с $\omega \ll \omega_{Be}$ и $z_0 \gg 1$ дисперсионное уравнение (2.1) примет вид:

$$\frac{T_i}{T_e} \left(k_{\perp}^2 \rho_e^2 - \frac{1}{2z_0^2} \right) + 1 + i \sqrt{\pi} z_i W(z_i) = 0 \quad (2.20)$$

Это уравнение при $|\vec{k} \vec{u}_i| \gg \sqrt{2} k_{\perp} v_{Ti}$ ($z_i \gg 1$) имеет решения, соответствующие гидродинамической неустойчивости (2.8). Кроме того, имеется еще кинетическая ветвь колебаний ($z_i \leq 1$). Действительно, полагая $\omega = \vec{k} \vec{u}_i + i\gamma$, получим при $k_{\perp}^2 \rho_e^2 \sim 1/2z_0^2$, что для

$$k_{\perp} v_{Ti} \sim \sqrt{\omega_{Be} \omega_{Bi}} \quad |\cos \theta| \leq \frac{u}{v_{Ti}} \sqrt{\frac{m_e}{m_i}} \quad z_0^2 \sim \frac{T_i}{T_e}$$

уравнение (2.20) имеет неустойчивые решения с

$$\gamma_k \sim k_{\perp} v_{Ti} \sim \sqrt{\omega_{Be} \omega_{Bi}} \quad (2.21)$$

Точное значение γ_k определяется из уравнения

$$1 - \sqrt{\pi} x e^{x^2} + 2x e^{x^2} \int_0^x e^{-t^2} dt = \frac{k_{\perp}^2 v_{Ti}^2}{\omega_{pi}^2} \left[\frac{\omega_{pe}^2}{(k_{\parallel} u)^2} \cos^2 \theta - \frac{\omega_{pe}^2}{\omega_{Be}^2} \right] \quad (2.22)$$

где $x \equiv \gamma_k / \sqrt{2} k_{\perp} v_{Ti}$.

В резонансном случае, когда правая часть (2.22) обращается в нуль, уравнение (2.20) принимает вид:

$$z_i + \eta [1 + i\sqrt{\pi} z_i W(z_i)] = 0 \quad \eta = \frac{T_e}{T_i} \frac{(k_{\parallel} u)^3}{2\sqrt{2} k_{\perp} k_{\parallel}^2 v_{Te}^2 v_{Ti}} \quad (2.23)$$

При $\eta \sim 1$ имеем $\text{Re } z_i \sim \text{Im } z_i \sim 1$, т.е.

$$\gamma_k \sim k_{\perp} v_{Ti} \sim \sqrt{\frac{u}{v_{Ti}} \omega_{Be} \omega_{Bi}} \quad |\cos \theta| \sim \sqrt{\frac{m_e}{m_i}} \left(\frac{u}{v_{Ti}} \right)^{3/2} \quad (2.24)$$

Условие $z_0 \gg 1$ выполняется в этом случае, если $u/v_{Ti} \ll T_i/T_e$. (При $u/v_{Ti} \geq T_i/T_e$ резонансный случай невозможен и возбуждаются только колебания с инкрементом (2.21)).

Уровень шумов в нерезонансном случае определяется, как и для гидродинамических колебаний, формулой (2.9). При рассеянии ионов на этих колебаниях происходит их нагрев, который обусловлен как черенковским механизмом, так и нелинейными эффектами конечного времени корреляции, при этом скорость нагрева ионов определяется формулой (2.10). Возможен также стохастический нагрев электронов, который происходит с той же скоростью, что и нагрев ионов. Поэтому при $u \gg v_{Ti}$ и $T_i \gg T_e$ в результате турбулентного нагрева неизотермичность плазмы будет уменьшаться ($T_{\parallel e}$ становится порядка $T_{\parallel i}$).

Кроме рассмотренных неустойчивостей, дисперсионное уравнение (2.1) при $k_{\perp} \rho_e \gg 1$ и $z_i \gg 1$ имеет решения, близкие к ω_{Be} [14,19]. Инкременты нарастания для этих колебаний могут быть заметно больше $\sqrt{\omega_{Be} \omega_{Bi}}$. Однако для этих колебаний уровень шумов оказывается чрезвычайно низким, так что их влиянием на нагрев плазмы, по-видимому, можно пренебречь.

Непотенциальные колебания

Рассмотренные выше колебания считались продольными ($\vec{E} = -\nabla \varphi$). При увеличении токовой скорости эти колебания становятся непотенциальными. Рассмотрим, например, как видоизменяется гидродинамическая неустойчивость при учете непотенциального характера колебаний. Считая, что $u \gg v_{Ti}$, v_s , $k_{\perp} \rho_e \ll 1$, $\omega \ll \omega_{Be}$, $\omega \gg k_{\parallel} v_{Te}$, получим вместо (2.1) следующее дисперсионное уравнение:

$$\left[\frac{\omega_{pe}^2}{\omega_{Be}^2} + \frac{\omega_{pe}^4}{\omega_{Be}^2 k^2 c^2} - \frac{\omega_{pi}^2}{(\omega - k_{\parallel} u)^2} \right] \left(1 + \frac{\omega_{pe}^2}{k^2 c^2} \right) - \frac{\omega_{pe}^2 \cos^2 \theta}{(\omega - k_{\parallel} u)^2} = 0 \quad (2.25)$$

При $\omega_{pe}/k c \ll 1$ это уравнение переходит в дисперсионное уравнение для продольных колебаний. Так как для последних $k_{\perp} u \sim \sqrt{\omega_{Be} \omega_{Bi}}$, то условие $\omega_{pe} \ll k c$ означает, что $u \ll v_A$. При $u \gg v_A$ рассматриваемая неустойчивость становится существенно непотенциальной. Для длинноволновых колебаний ($\omega_{pe} \gg k c$) уравнение (2.25) переходит в дисперсионное уравнение для "свистящих атмосфериков".

Отметим, что при получении (2.25) предполагалось, что $\lambda_{\parallel} = 1/k_{\parallel}$ значительно меньше характерных расстояний вдоль магнитного поля, на которых изменяются токовая скорость, плотность и само магнитное поле. При $u \sim v_A$ это условие не всегда выполняется, например в случае, когда поперечный ток создается ионной циклотронной или быстрой магнито-звуковой волнами с частотами порядка ω_{Bi} . В последнем случае при $u \sim v_A$ необходимо учитывать неоднородности, создаваемые волной.

При $|\cos \theta| \sim \sqrt{m_e/m_i}$ и $u \lesssim v_A$ для ω_k и γ_k получаем из (2.25) оценки (2.8), а для уровня шумов и для скорости стохастического нагрева электронов и ионов оценки (2.9) и (2.10). Эти колебания будут сопровождаться колебаниями магнитного поля. Амплитуда колебаний B^{\sim} порядка

$$B^{\sim} \sim \sqrt{\frac{m_e}{m_i} \frac{u^2}{v_A^2}} B_0 \quad (2.26)$$

В заключение этого раздела отметим, что неустойчивые колебания с $k_{\perp} \rho_e$ в плазме с поперечным током с характерными частотами порядка $\sqrt{\omega_{Be} \omega_{Bi}}$ были обнаружены в плазменном сгустке, входящем в магнитное поле соленоида [23], в плазме, находящейся в поле быстрой магнито-звуковой волны большой амплитуды [24] и в тэтапиче [25]. Частотные характеристики и уровень шумов, определяемый по величине колебаний потенциала двойного электрического зонда [23-25], а также по комбинационному рассеянию микрорадиоволн [25], хорошо соответствуют приведенным выше оценкам.

3. ЭКСПЕРИМЕНТЫ ПО ВЫСОКОЧАСТОТНОМУ ТУРБУЛЕНТНОМУ НАГРЕВУ

Экспериментальные исследования нагрева плазмы сильным переменным электрическим полем проводились на установке, подробное описание которой приведено в работе [27]. Плазма с плотностью $\sim 10^{13} - 10^{14} \text{ см}^{-3}$ создавалась импульсным разрядом с колеблющимися электронами в водороде при исходном давлении $\lesssim 10^{-3}$ мм рт.ст. Внутренний диаметр стеклянной разрядной трубы равнялся 6,6 см, расстояние между катодами — 88 см. Разряд находился в квазипостоянном магнитном поле, имевшем однородный участок на длине 70 см в средней части системы и пробки с пробочным отношением 1,4 в местах расположения катодов источника плазмы. ВЧ-поле генерировалось катушкой Стикса, охватывающей разрядную трубу и состоящей из восьми двухвитковых секций, соединенных попарно в противофазе. Аксиальный период такой системы равнялся 20 см. Катушка являлась индуктивностью ударного контура. Частота колебаний равнялась $\omega/2\pi = 7$ МГц, добротность без плазмы — 35. Продольное переменное магнитное поле B_z^{\sim} могло достигать 250 Э на оси системы в вакууме.

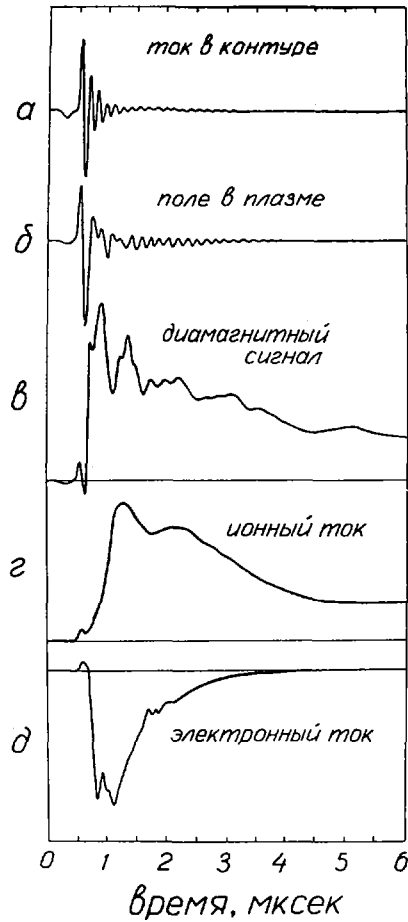


Рис. 5. Осциллограммы величин, характеризующих нагрев плазмы свистом большой амплитуды в резонансе возбуждения.

Средняя по радиусу плотность электронов плазмы измерялась с помощью микроволнового интерферометра. Радиальное распределение плотности определялось двойным ленточным зондом. Поперечная энергия плазмы определялась по сигналу диамагнетизма. Продольная энергия электронов и ионов, выходящих из плазмы вдоль постоянного магнитного поля, измерялась с помощью многосеточного электростатического анализатора с задерживающим потенциалом. Составляющие переменного магнитного поля B_z и B_ϕ в плазме измерялись с помощью миниатюрных зондов. Хаотические мелкомасштабные пульсации потенциала плазмы измерялись двойным симметричным электрическим зондом под плавающим потенциалом. Расстояние между штырьками зонда, имеющими контакт с плазмой, равнялось 0,2 см, их диаметр — 0,03 см, длина — 0,3 см. Эффективность передачи ВЧ-энергии из контура в плазму характеризуется

коэффициентом передачи α , равным отношению энергии, поглощаемой в контуре при наличии плазмы за вычетом омических потерь в самом контуре, к полной энергии, запасенной в конденсаторах контура перед его включением. Величина α определялась с помощью прибора для измерения декремента затухания [28].

Изучение нагрева плазмы проводилось в двух различных условиях. В одном случае плотность плазмы и постоянное магнитное поле подбирались так, чтобы реализовать условия возбуждения свиста ($\omega \gg \omega_{Bi}$, $\omega_{pe}^2 \gg \omega_{Be}^2$). В другом — плотность плазмы и магнитное поле соответствовали оптимальным условиям для нагрева плазмы в ионном циклотронном резонансе ($\omega \approx \omega_{Bi}$, $\epsilon \sim N_{ii}^2$).

При возбуждении свиста, как показано в [27,29], передача энергии из контура в плазму происходит наиболее эффективно ($\alpha \sim 70\%$) в резонансе возбуждения, когда аксиальный период поля, генерируемого катушкой, близок к продольной длине волны собственных колебаний плазменного цилиндра. При этом ВЧ-поле в плазме возрастает в 2-2,5 раза.

Основные экспериментальные данные, характеризующие нагрев плазмы свистом, представлены на рис. 5. ВЧ-поле включалось через несколько микросекунд после прекращения тока разряда, в момент, когда средняя по радиусу плотность электронов распадающейся плазмы уменьшалась до $3 \cdot 10^{13} \text{ см}^{-3}$, а температура электронов составляла $\leq 1 \text{ эВ}$. Приращение плотности плазмы, вследствие дополнительной ионизации после включения контура, не превышало $\sim 20\%$. Емкость контура заряжалась до напряжения 54 кВ, что соответствует запасаемой энергии 7,2 Дж. При этом максимальная амплитуда поля B_z в плазме на оси под секцией катушки в резонансе возбуждения ($B_0 \approx 800 \text{ Э}$) составляла 500 Э. Из рис. 5 следует, что после включения тока в контуре (рис. 5 а) поле B_z в плазме (рис. 5 б) сначала растет, что обусловлено резонансной раскачкой колебаний в плазме, и по достижении максимальной величины во втором полупериоде колебаний резко уменьшается, достигая в третьем полупериоде лишь $\sim 1/4$ от максимального значения. Одновременно с появлением сильного затухания ВЧ-поля начинается быстрый рост диамагнитного сигнала (рис. 5 в): время роста составляет примерно половину периода колебаний, т.е. 0,07 мксек.

Средняя по радиусу и максимальная во времени температура плазмы, вычисленная по сигналу диамагнетизма с учетом распределения плотности плазмы по радиусу, составила для рассмотренного случая 150 эВ. Для выяснения вопроса о том, как изменяются температуры ионов и электронов в отдельности, обратимся к рис. 5 г и д, на которых показаны осциллограммы тока ионов (г) и электронов (д) на коллектор анализатора при нулевом задерживающем потенциале. Из этих рисунков следует, что после включения ВЧ-поля происходит быстрое увеличение ионного и электронного токов, обусловленное, как и рост диамагнитного сигнала, нагревом электронов и ионов. При этом видно, что электроны начинают греться одновременно с резким уменьшением амплитуды ВЧ-поля в плазме и ростом диамагнитного сигнала.

Чтобы оценить температуру ионов, которая достигается в рассматриваемых условиях, можно воспользоваться тем, что в поздние моменты времени, когда ВЧ-поле в плазме уже мало, ток электронов на коллектор уменьшается быстрее, чем ионный ток, что говорит о более быстром остывании электронов. Из сопоставления рис. 5 в, 5 г и 5 д следует, что через 2-3 мксек после включения ВЧ-поля диамагнетизм плазмы обуслов-

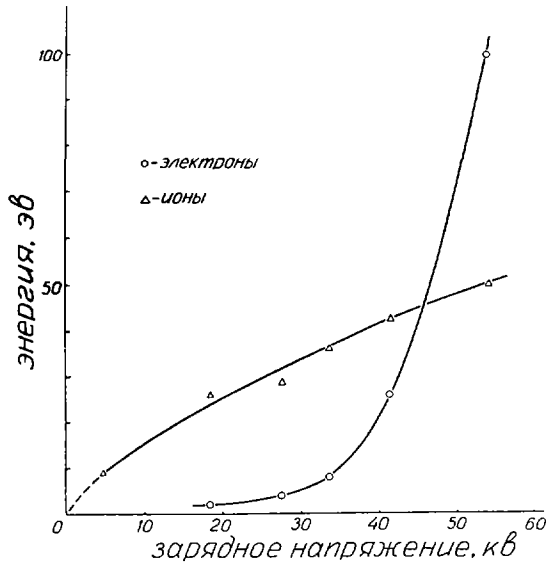


Рис. 6. Зависимости средней энергии электронов и ионов от амплитуды ВЧ-напряжения на контуре.

лен, главным образом, ионами. Отсюда температура ионов, определенная по диамагнитному сигналу, равна 30-40 эВ (в предположении, что плотность плазмы распределена по радиусу равномерно и равна $3 \cdot 10^{13} \text{ см}^{-3}$). Эта величина удовлетворительно согласуется с данными непосредственного измерения энергии ионов с помощью анализатора. Как следует из этих же измерений, проведенных при более высоких значениях V_0 , вне области резонатора возбуждения, где амплитуда ВЧ-поля в 2-2,5 раза меньше, энергия электронов не превышает нескольких электронвольт. Средняя же энергия ионов с увеличением V_0 растет до уровня ~ 100 эВ и остается на этом уровне всюду в исследованном диапазоне V_0 (до 3000 Э). При этом ларморовский радиус иона со средней энергией составляет $(0,3 \div 0,2) \text{ а} \sim 1 \text{ см}$ при всех значениях V_0 , как в области резонанса возбуждения, так и вне ее. По-видимому, именно этим обстоятельством и определяется верхний предел энергии ионов в рассмотренных условиях.

Отмеченная выше сильная зависимость энергии электронов от напряженности постоянного магнитного поля полностью согласуется с зависимостью средней энергии электронов от амплитуды ВЧ-поля или фиксированном значении V_0 . Такая зависимость для $V_0 = 900 \text{ Э}$ совместно с зависимостью средней энергии ионов изображена на рис. 6, где на горизонтальной оси отложено напряжение, до которого заряжалась емкость ударного контура. В рассматриваемых условиях амплитуда ВЧ-поля в плазме в первом периоде колебаний пропорциональна зарядному напряжению. Как и следовало ожидать, при уменьшении амплитуды ВЧ-поля в плазме энергия электронов уменьшается значительно быстрее, чем ионов.

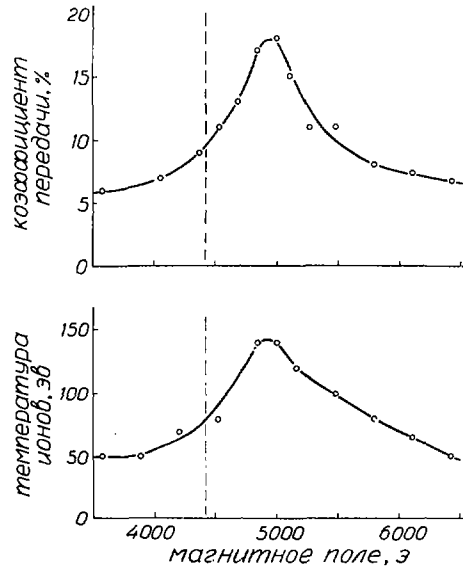


Рис. 7. Коэффициент передачи и температура ионов в функции B_0 при нагреве сильным ВЧ-полем в области ионного циклотронного резонанса.

В опытах по нагреву плазмы сильным ВЧ-полем в области ионного циклотронного резонанса использовались два источника плазмы. В одном случае плазма создавалась так же, как и в описанных выше опытах. При этом ВЧ-поле включалось в момент, когда плотность холодной ($T_{e,i} \leq 1$ эВ) распадающейся плазмы была порядка 10^{13} см $^{-3}$. Вследствие низкой проводимости такой плазмы, в ней не могла возбуждаться ионная циклотронная волна [7]. ВЧ-поле в плазме имело такую же величину, как и в вакууме (т.е. $B_z \approx 200$ Э), коэффициент передачи не превышал 20% (в рассматриваемых условиях α принимает максимальное значение при таком значении B_0 , когда скорость направленного движения ионов поперек магнитного поля в поле волны максимальна [29,30]). Зависимости коэффициента передачи и температуры ионов от B_0 представлены на рис. 7. Штриховыми линиями отмечено значение B_0 , соответствующее циклотронному резонансу на частоте контура. Температура ионов в максимуме поглощения достигает 150 эВ. Температура электронов не превышала нескольких электронвольт всюду в исследованном интервале B_0 . В рассмотренных условиях имел место аномально быстрый распад плазмы во время существования в ней ВЧ-поля. Природа этого распада, по-видимому, такая же, что и в работе [31].

Во втором случае в качестве источника плазмы использовался сильноточный прямой разряд, температура электронов в момент включения ВЧ-поля могла составлять несколько десятков электронвольт ($T_e \gg T_i$). В этих условиях, как и в работе [32], величина α могла достигать 60–70% в максимуме поглощения. При этом, как показали измерения с помощью многосеточного анализатора, имел место быстрый нагрев электронов до $T_e \geq 100$ эВ.

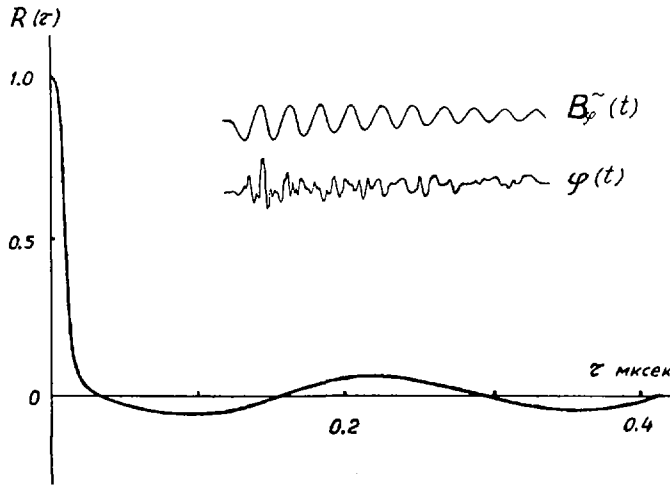


Рис. 8. Автокорреляционная функция шумов и осциллограммы шумов и соответствующего поля \tilde{B}_φ в случае свиста большой амплитуды ($B_0 = 900$ Э).

Сопоставим полученные экспериментальные результаты с теоретическими оценками, приведенными в предыдущем разделе. При возбуждении в плазме свиста величина токовой скорости, равная примерно дрейфовой скорости электронов в азимутальном направлении, при $B_z \sim 500$ Э на оси составляет $u \approx 5 \cdot 10^7$ см·сек⁻¹ на среднем радиусе $r = 1,6$ см. Направленная скорость ионов значительно меньше. Наблюдаемый быстрый нагрев электронов можно объяснить рассеянием электронов на турбулентных коротковолновых продольных колебаниях типа "замагниченного" ионного звука, см. формулу (2.14). Теоретическая оценка времени нагрева электронов при рассеянии на этих колебаниях (2.12) дает разумный порядок величины $\tau_e \sim 4 \cdot 10^{-8}$ сек (при $B_0 = 800$ Э, $u \sim 5 \cdot 10^7$ см/сек и $T_e \sim 100$ эВ). Эти колебания обеспечивают увеличение как продольной, так и поперечной температуры электронов.

Нагрев ионов может обеспечиваться стохастическим механизмом сбоя фаз в поле турбулентных пульсаций типа (2.14) или гидродинамических колебаний (2.8). В условиях резонанса возбуждения (рис. 5) такой нагрев будет иметь место после быстрого нагрева электронов и падения амплитуды свиста в ~ 4 раза, т.е. на последующей стадии медленного затухания свиста с малой амплитудой. Аналогичное явление имеет место и при уходе от резонанса возбуждения в сторону больших значений B_0 , где амплитуда свиста уменьшается, а время затухания колебаний в плазме увеличивается до значения ≥ 1 мксек.

В предположении, что нагрев ионов прекращается, когда их средний ларморовский радиус становится равным ($0,2 \div 0,3$) а, оценка времени нагрева ионов дает величину $1 \div 4$ мксек, что не противоречит экспериментальным данным. Нагрев же электронов при малых амплитудах ВЧ-поля может ограничиться потерями при неупругих столкновениях.

В случае возбуждения колебаний большой амплитуды вблизи ионного циклотронного резонанса наблюдаемый нагрев ионов может быть обусловлен их взаимодействием либо с турбулентными гидродинамическими или электронно-звуковыми пульсациями (в условиях возбуждения колебаний в холодной плазме), либо с гидродинамическими и "замагниченными" ионно-звуковыми пульсациями (в случае плазмы с предварительно нагретыми электронами). В последнем случае, как и в случае свиста, наблюдаемый нагрев электронов может быть обусловлен их расстоянием на колебаниях с частотой (2.14).

Эксперименты по исследованию шумов, возникающих в плазме при возбуждении в ней свистов большой амплитуды, описаны в [25]. С помощью описанного выше электрического зонда регистрировались флуктуационные электрические поля, направленные перпендикулярно к полю B_0 . Характерные частоты этих шумов были порядка $(\omega_{Be} \omega_{Bi})^{1/2}$ длина волны $\sim 0,4$ см. Зависимость амплитуды шумов от токовой скорости в поле свиста носит пороговый характер, причем вблизи порога $u \sim v_s = (T_e/m_i)^{1/2}$. Полученные данные позволяют отождествить эти шумы либо с гидродинамической неустойчивостью (2.8), либо с "замагниченными" ионно-звуковыми колебаниями. Автокорреляционная функция сигнала с электрического зонда совместно с осциллограммами самого сигнала и поля V_{ϕ} свиста (пропорционального радиальной токовой скорости u_r) приведена на рис. 8. Из рис. 8 следует, что время исчезновения корреляции наблюдаемых шумов — порядка 10^{-8} сек. Эта величина близка к $(\omega_{Be} \omega_{Bi})^{-1/2}$, т.е. плазма в процессе нагрева свистом большой амплитуды действительно находится в состоянии сильной турбулентности. В частности, подтверждается возможность стохастического нагрева ионов в поле гидродинамических или ионно-звуковых шумов.

ЛИТЕРАТУРА

- [1] СТЕПАНОВ, К.Н., ЖЭТФ 35 (1958) 283.
- [2] АХИЗЕР, А.А. и др., Коллективные колебания в плазме, Госатомиздат, М., 1964.
- [3] ГОЛАНТ, В.Е., ЛИЛИЯ, А.Д., Препринт № 270, ЛФТИ, Ленинград, 1970, М-09919.
- [4] СТИКС, Т., Теория плазменных волн, Госатомиздат, М., 1965.
- [5] СТЕПАНОВ, К.Н., Доклад на I конференции ФТИ АН УССР по физике плазмы, Харьков, 25 июня-2 июля 1959 г., в сб. Физика плазмы и проблемы управляемого термоядерного синтеза, вып. I, Изд-во АН УССР, 1962, стр. 45; ЖЭТФ 38 (1960) 265.
- [6] ДОЛГОПОЛОВ, В.В., СТЕПАНОВ, К.Н., в сб. Физика плазмы и проблемы управляемого термоядерного синтеза, вып. 4, Наукова думка, 1965, стр. 44.
- [7] STIX, T.H., Phys. Rev. 106 (1957) 1146.
- [8] ДОЛГОПОЛОВ, В.В., СТЕПАНОВ, К.Н., Ядерный синтез 5 (1965) 276; ЖТФ 36 (1966) 1003.
- [9] BERGER, J.M. et al., Physics Fluids 1 (1958) 301.
- [10] ДОЛГОПОЛОВ, В.В., СТЕПАНОВ, К.Н., Ядерный синтез 3 (1963) 205.
- [11] МИХАЙЛОВСКИЙ, А.Б., Теория плазменных неустойчивостей, Госатомиздат, М., 1 1970.
- [12] КАДОМЦЕВ, Б.Б., в сб. Физика плазмы и проблема управляемых термоядерных реакций, Изд-во АН СССР 4 1958, стр. 364.
- [13] SAGDEEV, R.Z., Proceedings of the Symposium on Electromagnetic and Fluid Dynamics of Gaseous Plasma, Polytechnic Institute of Brooklyn, Apr. 4-6, 1961.
- [14] КУРИЛКО, В.И., МИРОШНИЧЕНКО, В.И., в сб. Физика плазмы и проблемы управляемого термоядерного синтеза, вып. 3, Изд-во АН УССР, 1963, стр. 161.
- [15] БАБЫКИН, М.В. и др., ЖЭТФ 46 (1964) 511.
- [16] СТЕПАНОВ, К.Н., ЖТФ 34 (1964) 2146.

- [17] СИЗОНЕНКО, В.Л., СТЕПАНОВ, К.Н., Ядерный синтез 7 (1967) 131.
- [18] АРЕФЬЕВ, В.И., ЖТФ 39 (1969) 1937.
- [19] WONG, H.V., Physics Fluids 13 (1970) 757.
- [20] АРЕФЬЕВ, В.И. и др., Plasma Physics and Controlled Nuclear Fusion Research 2, IAEA, Vienna (1969) 165.
- [21] ДЕМЧЕНКО, В.В. и др., Препринт ХФТИ 70-62, Харьков, 1970.
- [22] ГРИГОРЬЕВА, Л.И. и др., Препринт ХФТИ, 70-64, Харьков, 1970.
- [23] ASHBY, D.E.T.F., RATON, A., Plasma Physics 9 (1967) 359.
- [24] ГРИГОРЬЕВА, Л.И. и др., Письма ЖЭТФ 8 (1968) 616; ЖЭТФ 58 (1970) 45.
- [25] АДАМОВ, И.Ю. и др., Укр. физ. журн. 15 (1970) 1384.
- [26] БАСС, Ф.Г. и др., ЖЭТФ 49 (1965) 329.
- [27] ВАСИЛЬЕВ, М.П. и др., ЖЭТФ 54 (1968) 1647.
- [28] ЛОНГИНОВ, А.В., ПТЭ, вып. 2 (1970) 149.
- [29] ГРИГОРЬЕВА, Л.И. и др., ЖЭТФ 58 (1970) 1234.
- [30] ВАСИЛЬЕВ, М.П. и др., ЖТФ 34 (1964) 974, 984.
- [31] ЧЕЧКИН, В.В. и др., Ядерный синтез 4 (1964) 145.
- [32] ДУБОВОЙ, Л.В., ФЕДЯКОВ, В.П., ЖЭТФ 53 (1967) 1278.

ЭКСПЕРИМЕНТЫ ПО ВЫСОКОЧАСТОТНОМУ НАГРЕВУ ПЛАЗМЫ В ТОРОИДАЛЬНОЙ ЛОВУШКЕ

С. С. ОВЧИННИКОВ, С. С. КАЛИНИЧЕНКО, П. И. КУРИЛКО,
О. М. ШВЕЦ, В. Т. ТОЛОК
Физико-технический институт Академии наук
Украинской ССР, Харьков,
Союз Советских Социалистических Республик

Доклад представлен К. Н. Степановым

Presented by K. N. Stepanov

Abstract—Аннотация

EXPERIMENTS ON HIGH-FREQUENCY HEATING OF A PLASMA IN A TOROIDAL TRAP.

A description is given of experiments devoted to the study of the excitation and propagation of low-frequency waves ($\omega^2 \ll \omega_{ci} \omega_{ce}$) in a high-density plasma ($\omega_{pe}^2 \gg \omega_{ci} \omega_{ce}$) contained in a toroidal trap. The plasma was produced by means of an electron beam. Conditions are found for the effective introduction of high-frequency power into the plasma by means of exciting devices arranged inside the conducting vacuum chamber. A study of the structure of the excited waves shows that axially asymmetric waves are those most effectively produced in a toroidal plasma. The possibility was experimentally investigated of heating the plasma ions to high energies with axially-asymmetric ion-cyclotron waves. The high-frequency power was introduced at high levels by an exciting device which creates in the plasma a spatial-periodic transverse high-frequency field. For recording of the plasma heating the diamagnetic signal was measured and the ion energy spectrum was analysed.

ЭКСПЕРИМЕНТЫ ПО ВЫСОКОЧАСТОТНОМУ НАГРЕВУ ПЛАЗМЫ В ТОРОИДАЛЬНОЙ ЛОВУШКЕ.

Описываются эксперименты по изучению возбуждения и распространения низкочастотных волн ($\omega^2 \ll \omega_{ci} \omega_{ce}$) в плазме большой плотности ($\omega_{pe}^2 \gg \omega_{ci} \omega_{ce}$), находящейся в тороидальной ловушке. Предварительное создание плазмы осуществлялось электронным пучком. Найдены условия эффективного ввода высокочастотной мощности в плазму возбуждающими устройствами, расположенными внутри проводящей вакуумной камеры. Изучение структуры возбуждаемых волн показало, что в тороидальной плазме наиболее эффективно возбуждаются аксиально-несимметричные волны. Экспериментально исследована возможность нагрева ионов плазмы аксиально-несимметричными ионно-циклотронными волнами до высоких энергий. Ввод высокочастотной мощности при больших уровнях осуществляется возбуждающим устройством, создающим в плазме пространственно-периодическое поперечное высокочастотное поле. Для регистрации нагрева плазмы производились измерения диамагнитного сигнала и анализ спектра ионов по энергиям.

Разрабатываемые сейчас методы ВЧ-нагрева плазмы можно разделить на две группы по характерным временам нагрева. Для быстрого нагрева требуются мощные генераторы, работающие в режиме коротких импульсов. Достоинство такого метода заключается в возможности быстрого (неадиабатического) прохождения опасных с точки зрения неустойчивостей значений параметров плазмы, а также в возможности нелинейной термализации энергии возбуждаемых волн [1,2].

Использование этого метода для быстрого нагрева плазмы большого объема будет связано с необходимостью введения в плазму очень больших мощностей.

Необходимые мощности уменьшаются обратно пропорционально времени нагрева, а инициируемая ВЧ-полями повышенная диффузия плазмы может оказаться меньшей, чем при быстром нагреве. Это — важное достоинство медленного нагрева. Можно ожидать, что медленный нагрев может позволить рационально, без внесения сильных возмущений в плазму, использовать длительные времена удержания плазмы, достигнутые сейчас на лучших установках. Разумеется, особенно важной может оказаться роль медленного нагрева в стационарных установках.

В данной работе изложены результаты исследований нагрева плазмы в замкнутой магнитной ловушке ВЧ-полями с характерными частотами порядка ионной циклотронной.

Экспериментально эффективность высокочастотного нагрева плазмы, находящейся во внешнем магнитном поле, изучалась ранее в работах [3-7], где наблюдалось возбуждение и термализация аксиально-симметричных ионно-циклотронных волн. В частности, в работах [5,6] описаны эксперименты по нагреву плотной плазмы, помещенной в камеру с проводящими стенками и находящейся в магнитной ловушке пробочной конфигурации. Термализация энергии волн происходила в "магнитном берегу". В экспериментах был осуществлен нагрев плотной плазмы ($n \sim 10^{14} \text{ см}^{-3}$) до сравнительно высоких энергий ($\sim 1 \text{ кэВ}$). Эта методика нагрева была применима для плазмы, находящейся в прямых магнитных системах. Эксперименты по ВЧ-нагреву плазмы в тороидальной магнитной ловушке с металлической камерой без диэлектрического участка до настоящего времени, насколько нам известно, еще не проводились.

Нагрев плазмы с помощью ионно-циклотронных волн изучался в замкнутой магнитной системе стелларатора-рейстрека модели С в Принстоне (США). Для нагрева использовались индукционные катушки Стикса.

Применение "магнитного берега" для хаотизации колебательной энергии частиц в ионно-циклотронной волне связано с необходимостью нарушения конфигурации удерживающего магнитного поля. В экспериментах на стеллараторе С [8], в области возбуждения волны (в месте расположения катушки Стикса), напряженность удерживающего магнитного поля была выше ионно-циклотронного значения. По этой причине в течение импульса ВЧ-нагрева, из-за отставания перераспределения поперечной энергии ионов в продольную, наблюдалось существенное уменьшение плотности плазмы под контуром. Это приводило к расстройке резонанса связи ВЧ-генератора с плазмой и уменьшению эффективности дальнейшего нагрева. При попытке возбудить волну во всем объеме плазмы (т.е. при отсутствии "магнитного берега") было обнаружено, что возбуждаемая на прямолинейном участке стелларатора С аксиально-симметричная волна не распространялась по криволинейным участкам. Причина этого явления в работе [8] точно не была установлена.

Целью данной работы являлось изучение особенностей ввода ВЧ-мощности в плазму, находящуюся в тороидальной ловушке в проводящей камере, а также осуществление нагрева плазмы при термализации энергии возбуждаемых волн в магнитном берегу.

В работе излагаются результаты комплекса исследований, включающего в себя изучение структуры волн, которые могут распространяться в тороидальной плазме, установление условий их возбуждения, разработку систем наиболее эффективного ввода ВЧ-мощности в плазму; разработку возбуждающих устройств, размещаемых внутри вакуумной камеры с целью увеличения их связи с плазмой.

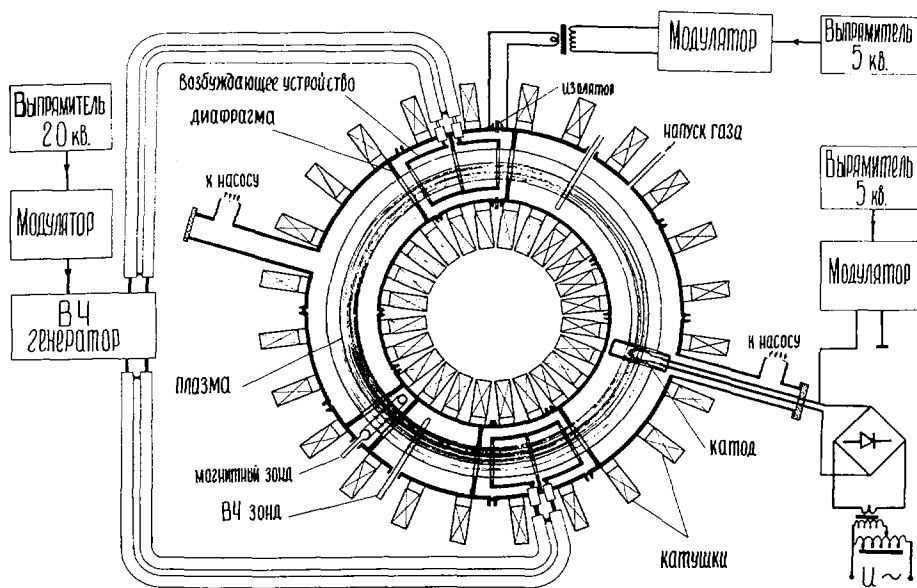


Рис. 1. Блок-схема установки "Омега".

1. ОПИСАНИЕ УСТАНОВКИ И МЕТОДОВ ИЗМЕРЕНИЙ

Приведенные в данной работе эксперименты были проведены на установке "Омега", блок-схема которой приведена на рис. 1.

Тороидальная вакуумная камера ($D = 800$ мм, $d = 200$ мм) помещена в стационарное магнитное поле, напряженность которого плавно регулируется от 0 до 10 кЭ. Камера изготовлена из меди и состоит из восьми секций, четыре из которых предназначены для расположения возбуждающих устройств. Для ограничения диаметра разряда и уменьшения бомбардировки стенок камеры частицами плазмы в камере установлены медные диафрагмы с внутренним диаметром 8 см.

Плазма создавалась ионизацией рабочего газа осциллирующими электронами, эмиттируемыми электронной пушкой. Плотность плазмы могла регулироваться в пределах $10^{12} \div 10^{14}$ см $^{-3}$ изменением давления рабочего газа и тока накала катода. Параметры плазмы при изменении магнитного поля в пределах $2 \div 10$ кЭ практически не изменялись.

Высокочастотная мощность от генератора ($f = 2 \div 10$ МГц, $P = 1,5$ МВт) к возбуждающим устройствам подается через согласующие четвертьволновые линии.

Для определения структуры полей волны в плазме использовались магнитные зонды. Газокинетическое давление nT измерялось диамагнитными зондами, размещенными в стеклянных торах, охватывающих плазму. Плотность плазмы определялась микроволновой диагностикой. Энергетический спектр ионов измерялся анализатором поперечной энергии с задерживающим потенциалом [5].

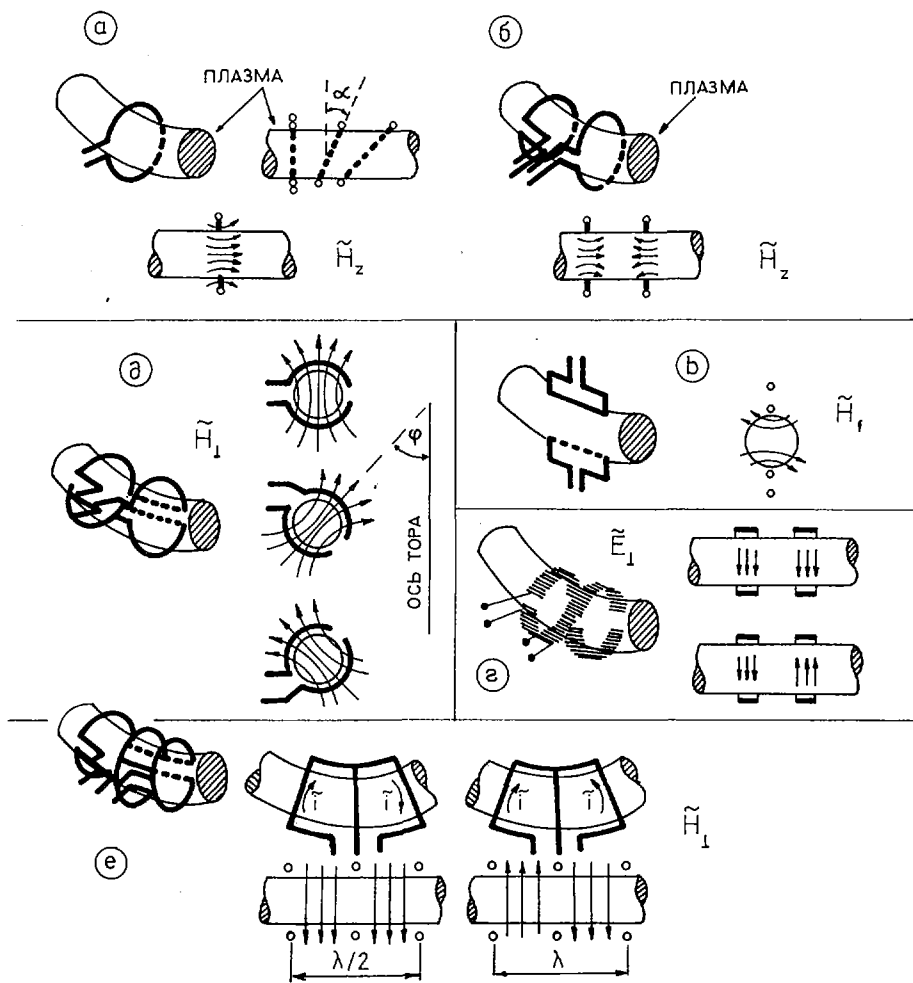


Рис. 2. Возбуждающие устройства.

II. ИССЛЕДОВАНИЕ ВОЛНОВЫХ СВОЙСТВ И КАРТИНЫ ВЫСОКОЧАСТОТНЫХ ПОЛЕЙ ВОЛН ПЛАЗМЕННОГО ТОРА

Для обеспечения эффективной связи источника высокочастотной мощности с плазмой требуется обеспечивать максимальное соответствие структуры высокочастотных полей (токов), создаваемых внешними возбуждающими устройствами, структуре полей возбуждаемой волны.

В настоящее время достаточно полной теории, описывающей волноводные свойства плазменного тора, не разработано. Поэтому необходимо было экспериментально выяснить, какого типа волны могут быть возбуждены и какие компоненты полей имеют наибольшую величину.

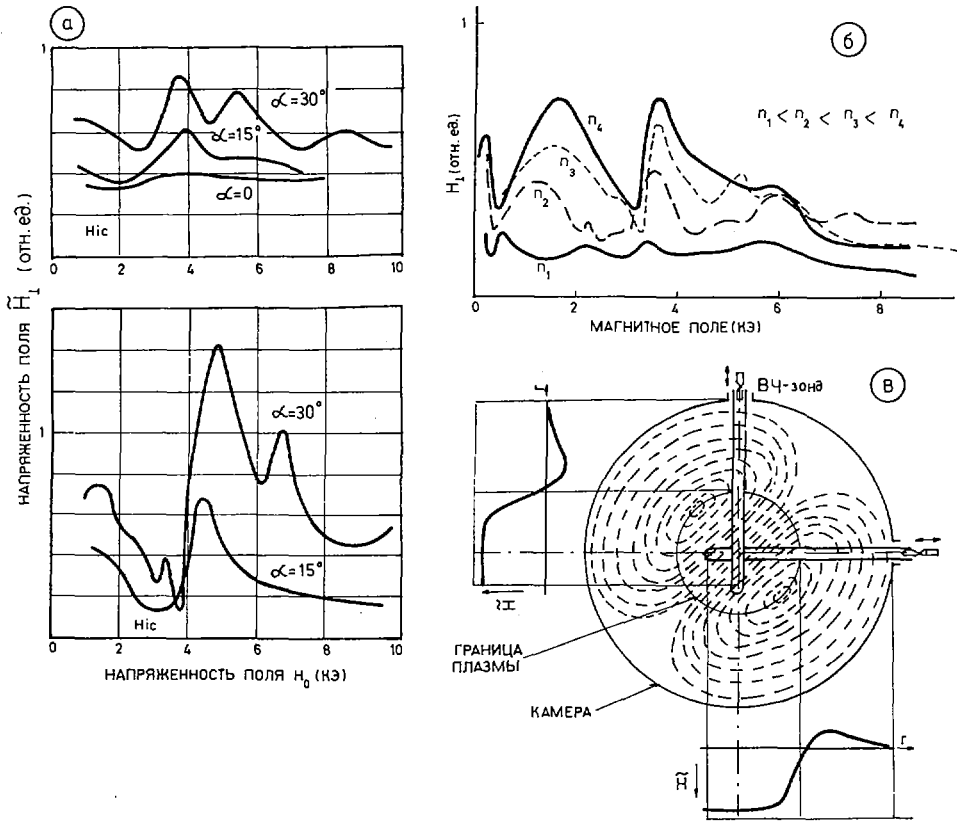


Рис. 3. (а) Зависимость напряженности ВЧ-поля в плазме от магнитного поля H_0 при различных углах наклона плоскости витка к оси плазмы. Рабочая частота 1,8 МГц и 4,2 МГц.

(б) То же при возбуждении поперечным магнитным ВЧ-полем, $f = 4,2$ МГц.

(в) Примерная картина магнитного ВЧ-поля в поперечном сечении камеры.

1. Исследование волноводных свойств плазменного тора для аксиально-несимметричных волн

Эксперименты, проведенные при вводе высокочастотной мощности в плазму аксиально-симметричными возбуждающими устройствами, изображенными на рис. 2 (а, б, в), показали, что эффективность возбуждения аксиально-симметричных волн в плазменном торе крайне низка.

Исследования волноводных свойств плазменного тора для аксиально-несимметричных волн проводились при небольших уровнях высокочастотных мощностей, подводимых к возбуждающему устройству. Для ввода высокочастотной мощности в плазму использовался виток, охватывающий плазму, подобный показанному на рис. 2 (а). Аксиальная несимметрия внешнего высокочастотного поля создавалась за счет накала плотности витка относительно оси плазмы на угол α (рис. 2 а), который мог изме-

няться в пределах от 0 до 30°. При $\alpha = 0$ полей волны в плазме не было обнаружено. Однако при наклоне плоскости витка зонды, расположенные на расстоянии 40 см и 100 см от возбуждающего устройства, показали, что в этом случае в плазме появляются высокочастотные поля. Зонды ориентировались на максимум сигнала.

На рис. 3 (а) приведены зависимости напряженности магнитной составляющей поля волны в плазме на расстоянии 100 см от возбуждающего устройства (ВУ) от напряженности удерживающего магнитного поля при различных углах наклона плоскости витка к оси плазмы. В области полей $H_0 > H_{ci}$ наблюдается возбуждение ионно-циклотронной волны, эффективность которого растет с увеличением угла α , т.е. с увеличением асимметрии внешнего высокочастотного поля. При увеличении угла величина поперечного поля возрастает, что соответствует росту напряженности поля возбуждаемой волны.

С целью увеличения аксиальной несимметрии внешнего высокочастотного поля на следующем этапе исследований для возбуждения ионных циклотронных волн использовались рамки с током (рис. 2 д), создающие в плазме поперечное магнитное поле. Эффективность возбуждения волны таким возбуждающим устройством оказалось более высокой, чем при возбуждении наклонно расположенным витком. На рис. 3 (б) приведены зависимости поля волны в плазме от напряженности удерживающего магнитного поля для нескольких значений плотности плазмы при рабочей частоте генератора 4,2 МГц. Видно, что такая система в магнитном поле $H_0 > H_{ic}$ возбуждает ионно-циклотронные волны.

Кроме того, в полях $H_0 < H_{ic}$ имеется еще два максимума напряженности высокочастотного поля в плазме. Максимум в полях 250-500 Э соответствует резонансному возбуждению быстрой магнитозвуковой волны, когда длина волны в плазме равна длине, навязываемой плазме возбуждающим устройством, т.е. λ внешнее = λ_g (в данном случае $1/2 \lambda$ внешнее = 12 см), второй максимум обусловлен возбуждением быстрой магнитозвуковой волны в области критической частоты¹.

Из приведенных измерений следует, что возбуждающее устройство с аксиальной несимметрией позволяют возбудить в плазменном торе ионно-циклотронные и быстрые магнитозвуковые волны.

2. Исследование картины поля аксиально-несимметричных волн

Исследование структуры поля волны в поперечном сечении тора производилось по радиусу камеры в одной плоскости во взаимноперпендикулярных направлениях. Зонды ориентировались таким образом, что могли измерять компоненты ВЧ-поля, параллельные удерживающему магнитному полю \check{H}_z , либо перпендикулярные ему \check{H}_\perp (\check{H}_\perp равняется векторной сумме полей \check{H}_r и \check{H}_φ). Измерения показали, что компонент \check{H}_z мал по сравнению с \check{H}_\perp , а максимум поля находится на оси плазмы. Из теории волноводных свойств плазменного цилиндра следует, что максимум \check{H}_\perp на оси плазмы может иметь только гармоника с одной вариацией по азимуту ($m = 1$). Поэтому из экспериментальных измерений мы делаем вывод, что в наших условиях возбуждается именно эта гармоника. На рис. 3 (в) показано расположение ВЧ-зондов в камере и примерная картина распределения магнитной составляющей поля волны в поперечном сечении камеры при возбуждении волны полем \check{H}_\perp (возбуждающим устрой-

¹ Частота определяется условием $v_\phi(\Omega_c) = \infty$ [9].

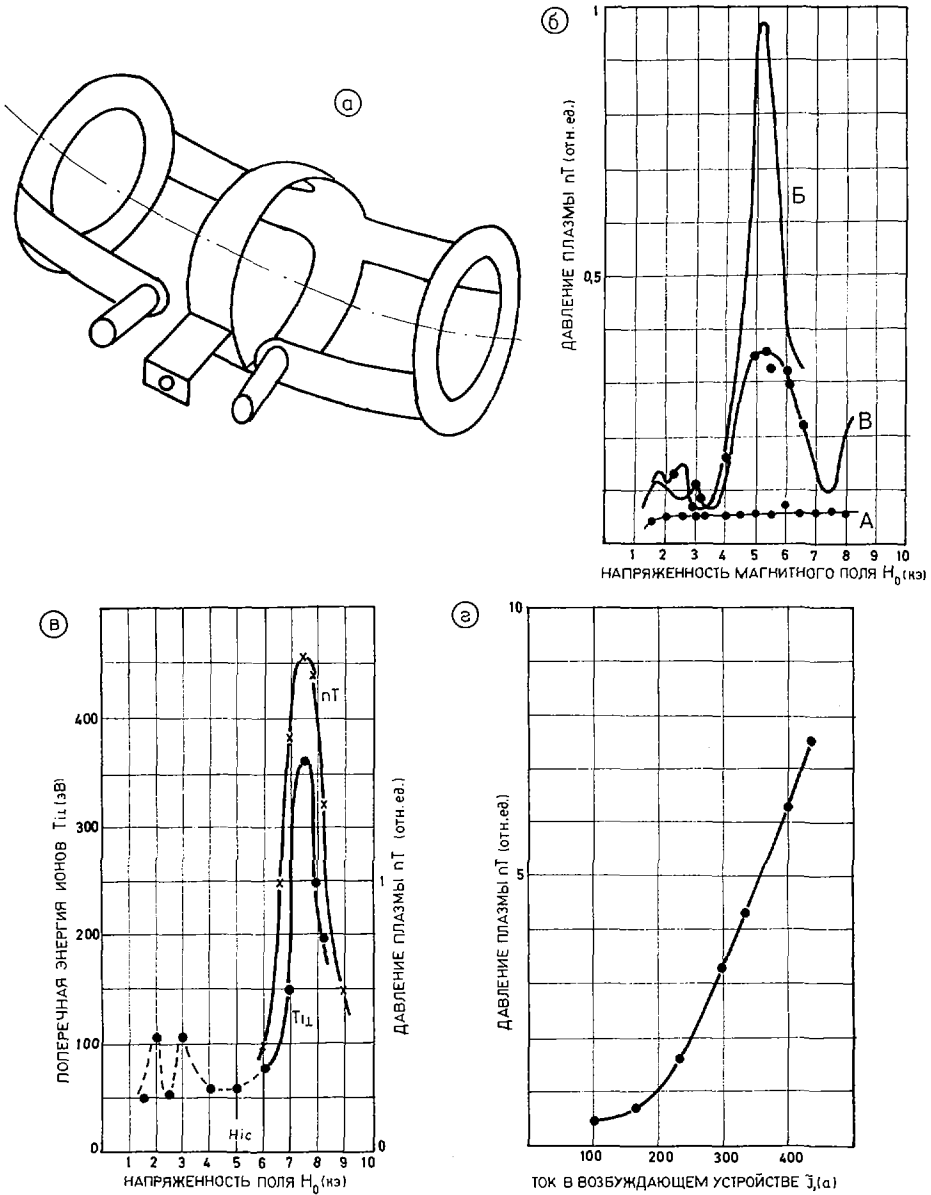


Рис.4.(а) Возбуждающее устройство, создающее в плазме пространственно-периодическое поперечное ВЧ-поле.

(б) Зависимость nT плазмы от магнитного поля: А - предварительно созданной плазмы, Б - при токе в возбуждающем устройстве $I_1 = 200$ А, В - то же без магнитного берега, рабочий газ - водород, $f = 4,45$ МГц.

(в) Зависимость поперечной энергии ионов и nT плазмы от магнитного поля, $f = 3,82$ МГц, $n = 5 \cdot 10^{13} \text{ см}^{-3}$, рабочий газ - дейтерий, $I_1 = 200$ А.

(г) Зависимость nT плазмы от тока в возбуждающем устройстве I_1 , рабочий газ - дейтерий, $f = 3,82$ МГц.

ством (ВУ), рис. 2 д). Поле \tilde{H}_L на оси плазмы направлено под углом $\varphi = 45^\circ$ к оси тора и имеет максимальное значение на оси плазмы. Такая же картина поля получена при возбуждении волны наклонным витком. Важно было выяснить влияние изменения угла между направлением внешнего ВЧ-поля и плоскостью тора на эффективность возбуждения волн. Для этой цели использовалось ВУ, показанное на рис. 2 д). Экспериментально было установлено, что амплитуда поля \tilde{H}_L максимальна при $\varphi = 45^\circ$, т.е. когда направление внешнего ВЧ-поля совпадает с направлением поля в волне.

На основании анализа проведенных исследований было изготовлено ВУ, создающее в плазме поперечное высокочастотное магнитное поле под углом $\varphi = 45^\circ$ к оси тора (рис. 4 а). Для обеспечения резонанса связи такое устройство создавало вдоль оси плазмы пространственно-периодическое поле. Изменением направления ВЧ-тока в рамках (внешним переключением) можно было изменять структуру поля вдоль плазмы. Изменением плотности плазмы (меняя ток накала катода электронной пушки и давление водорода в системе) можно было получить четко выраженный резонансное возбуждение ионно-циклотронной волны. В некоторых экспериментах для возбуждения волны использовалось поперечное электрическое поле, которое создавалось устройством, приведенным на рис. 2 г, и рамка с током, расположенная вблизи границы плазмы (рис. 4 в — одна петля, т.е. внешнее высокочастотное поле создавалось только на границе плазмы). В обоих случаях имеет место возбуждение ионно-циклотронных волн, а напряженность поля имела максимум на оси плазмы.

Таким образом, приведенные результаты исследований показали, что в плазменном торе можно резонансно возбуждать ионно-циклотронные и быстрые магнитозвуковые волны возбуждающими устройствами разнотипной конструкции. В условиях нашего эксперимента наибольший эффективностью обладало возбуждающее устройство, создающее в плазме пространственно-периодическое вдоль оси поперечное высокочастотное магнитное поле, направленное под углом 45° к оси тора.

III. ТЕОРИЯ

Методы решения граничных задач электродинамики для систем с тороидальной геометрией, особенно при наличии гиротронного заполнения, в настоящее время не разработаны. Поэтому для теоретической оценки дисперсионных свойств и картины поля аксиально-несимметричных волн в рассматриваемой установке мы будем исходить из простейшей модели плазменного цилиндра, для которой решение может быть получено в явном виде.

Итак, рассмотрим плазменный цилиндр радиуса a , заполненный однородной плазмой с плотностью n_p , помещенный в магнитное поле H_0 и окруженный проводящим кожухом радиуса b . Найдем фазовые скорости и картину поля волн, распространяющихся в такой системе в области частот порядка ионно-циклотронной. Так как в интересующей нас области параметров плазмы выполнены неравенства $\omega_{ci} \approx \omega \ll (\omega_{ci} \omega_{ce})^{1/2} \ll \omega_{pe}$, то решение уравнений Максвелла в плазме ($r < a$) можно искать приближенным методом, полагая в них $m_e \rightarrow 0$ ($|\epsilon_{zz}| \rightarrow \infty$) и $E_z \rightarrow 0$ [10].

Таким путем получены следующие выражения для полей в плазме:

$$\begin{aligned}
 H_z &= H_0 J_1(\lambda_\alpha r/a) \Phi_\alpha & \Phi_\alpha &\equiv \exp\{i\gamma_\alpha z + im\varphi - i\omega t\} \\
 H_r &= -\frac{i\gamma_\alpha a}{\lambda_\alpha} H_0 \left\{ J_1\left(\lambda_\alpha \frac{r}{a}\right) + \frac{\lambda_\alpha}{\Delta_\alpha + k^2 \epsilon_2 m} \cdot \frac{1}{ar} J_1\left(\lambda_\alpha \frac{r}{a}\right) \right\} \Phi_\alpha \\
 H_\varphi &= \frac{\gamma_\alpha a}{\lambda_\alpha} m H_0 \left\{ \frac{k^2 \epsilon_2 m}{\Delta_\alpha} J_0\left(\lambda_\alpha \frac{r}{a}\right) - \frac{\lambda_\alpha}{\Delta_\alpha + k^2 \epsilon_2 m} \cdot \frac{1}{ar} J_1\left(\lambda_\alpha \frac{r}{a}\right) \right\} \Phi_\alpha \\
 E_\varphi &= -\frac{k}{\gamma_\alpha} H_z & E_r &= \frac{k}{\gamma_\alpha} H_\varphi & |m| &= 1 \\
 \Delta_\alpha &\equiv \epsilon_1 k^2 - \gamma_\alpha^2 & \epsilon_1 &\equiv \epsilon_{zz} \equiv \epsilon_{\varphi\varphi} & \epsilon_2 &\equiv i\epsilon_{r\varphi} = -i\epsilon_{\varphi r}
 \end{aligned} \tag{1}$$

где $\alpha \equiv (m, n)$ — совокупность индексов, характеризующая тип волны — направление вращения по азимуту m и номер радиальной гармоники n . Здесь и ниже мы будем ограничиваться рассмотрением первой гармоники по азимуту ($|m| = 1$), поскольку только для нее поля H_φ и H_r не обращаются в нуль на оси.

При фиксированном значении поперечного волнового числа λ_α/a продольные волновые числа γ_α волн в плазме определяются соотношением:

$$\gamma_\alpha^2 = \epsilon_1 k^2 - \frac{\lambda_\alpha^2}{2a^2} \pm \sqrt{\epsilon_2^2 k^4 + \frac{\lambda_\alpha^4}{4a^4}} \tag{2}$$

в котором верхний знак соответствует ионно-циклотронной, а нижний — магнитозвуковым волнам. Спектр собственных чисел задачи определяется граничными условиями на поверхности плазменного цилиндра $r = a$, которые сводятся к требованию непрерывности тангенциальных компонент полных полей (и обращению в нуль тангенциальных компонент электрического поля на поверхности кожуха $r = b$). Поскольку внутри плазмы в рассматриваемых волнах продольная компонента электрического поля равна нулю, то вне плазмы достаточно ограничиться полем Н-волны. Таким образом, из условий непрерывности H_z и E_φ при $r = a$ получим следующее уравнение²:

$$\frac{1}{\lambda_\alpha} \left[1 + \frac{\epsilon_2 k^2 m}{\Delta_\alpha} - \frac{\lambda_\alpha J_0(\lambda_\alpha)}{J_1(\lambda_\alpha)} \right] = \frac{1}{\gamma_\alpha a} \left[\frac{1}{\gamma_\alpha a} - \frac{W_1(\gamma_\alpha)}{W_0(\gamma_\alpha)} \right] \tag{3}$$

$$W_s \equiv [I_s(\gamma_\alpha a) - (-1)^s p K_s(\gamma_\alpha a)] \quad p \equiv \frac{\gamma_\alpha b I_0(\gamma_\alpha b) - I_1(\gamma_\alpha b)}{\gamma_\alpha b K_0(\gamma_\alpha b) + K_1(\gamma_\alpha b)}$$

которое совместно с (2) полностью определяет спектр чисел λ_α рассматриваемого волновода.

Определяя λ_α из системы уравнений (2)-(3) и подставляя полученные таким образом решения в (2) и (1), найдем фазовые скорости рассматриваемых волн и соотношения между компонентами полей в них.

² Условие непрерывности при этом удовлетворяется автоматически.

Более полный анализ, учитывающий конечную величину продольной диэлектрической постоянной плазмы ϵ_{zz} , показывает, что рассматриваемое приближение применимо при не слишком больших значениях λ_α :

$$\lambda_\alpha^4 \ll 4 \frac{\epsilon_2^2 k^2 a^2}{|\epsilon_{zz}|} (\lambda_\alpha^2 + |\epsilon_{zz}| k^2 a^2) \quad (4)$$

Если это неравенство не выполнено, то гиротропией плазмы можно пренебречь, и рассматриваемые волны переходят, соответственно, в Н и Е-волны анизотропного плазменного волновода [11]. Ниже мы будем рассматривать волны с малыми поперечными волновыми числами, для которых неравенство (4) выполнено, поскольку в эксперименте возбуждались поля, слабо осциллирующие по радиусу. Наибольший интерес при этом представляет выяснение условий существования решения системы (2) и (3) в области $\lambda_\alpha^2 \ll 1$, поскольку в соответствующей волне поперечные компоненты поля слабо зависят от радиуса, а продольная компонента магнитного поля мала по сравнению с поперечными:

$$\left| \frac{H_z}{H_\varphi} \right| = \left| \frac{H_z}{H_r} \right| \approx \frac{2\lambda_\alpha^2}{\gamma_\alpha a} \ll 1 \quad (5)$$

как это имеет место в эксперименте.

Исследование системы (2)-(3) показывает, что решение $\lambda_\alpha^2 = 0$ действительно существует при $\epsilon_2 m > 0$ и параметрах плазмы, удовлетворяющих условию $\epsilon_1 k^2 a^2 = 8 (b - a \geq \lambda_g)$, что при расстройке $\omega_{ci} - \omega \approx 0,2 \omega_{ci}$ и радиусе плазмы $a = 4$ см соответствует плотности $n_p = 10^{13}$ см⁻³ и находится в удовлетворительном согласии с экспериментом. При меньших плотностях поля H_r и H_φ этой волны спадают от поверхности плазмы по экспоненциальному закону ($\lambda_\alpha^2 < 0$), а при больших — осциллируют, оставаясь конечными на оси.

Зависимость решений дисперсионного уравнения рассматриваемого волновода (2)-(3) и картины поля соответствующих волн (1) от направления распространения волн относительно магнитного поля $\text{Sgn } \epsilon_2 m$ указывает на возможность проявления эффекта невзаимности (зависимость потока энергии в волне от направления распространения). Для оценки ожидаемой величины этого эффекта была вычислена зависимость от плотности плазмы отношения

$$R \equiv S_{+1,1}/S_{-1,1}$$

$$S_\alpha \equiv \frac{c\gamma_\alpha}{4k} \left| \frac{H_0}{kD} \right|_\alpha^2 \left\{ -2(\Delta_\alpha - \epsilon_2 k^2 m)(1 - 2\Phi_\alpha) + [(\epsilon_2^2 k^4 + \Delta_\alpha^2)(\lambda_\alpha^2 + 2) - 4\Delta_\alpha \epsilon_2 k^2 m] J_0^2(\lambda_\alpha) + \lambda_\alpha^2 (\epsilon_2^2 k^4 + \Delta_\alpha^2) J_1^2(\lambda_\alpha) \right\}$$

где

$$D_\alpha \equiv 1/k^2 (\epsilon_2^2 k^4 - \Delta_\alpha^2), \quad \Phi_\alpha \equiv \int_0^{\lambda_\alpha} 1/x J_1^2(x) dx$$

потоков мощности первых радиальных гармоник циклотронной волны для простейшего случая полностью заполненного плазмой проводящего цилиндра $b \rightarrow a$.³

³ При этом амплитуды продольных компонент поля обеих гармоник ($m = \pm 1$) на поверхности проводника ($r = a$) считались равными.

Для того чтобы этот эффект проявился в условиях эксперимента, необходимо наличие бегущей волны тока в возбуждающем устройстве или же асимметрии параметров плазмы по азимуту. Последний эффект является, по-видимому, основной причиной наблюдавшейся в эксперименте асимметрии поглощения.

В заключение необходимо заметить следующее. Рассматриваемая выше модель плазменного цилиндра заведомо не может учесть всех особенностей экспериментальной установки, например эффектов, обусловленных тороидальностью и наличием градиентов плотности. Тем не менее, эта модель позволяет объяснить качественно, а в целом ряде случаев и количественно, основные результаты эксперимента. В частности, проведенное выше рассмотрение объясняет основные особенности картины поля возбуждаемой волны (отличие от нуля поперечных полей на оси и малую величину продольной компоненты магнитного поля ионно-циклотронной волны), пороговую зависимость сигнала ионно-циклотронной волны на ВЧ-зонде от плотности плазмы, эффект асимметрии нагрева в "магнитном берегу" (см. раздел IV), а также положение резонансных частот, соответствующих максимуму эффективности возбуждения быстрой магнитозвуковой волны.

IV. ВЫСОКОЧАСТОТНЫЙ НАГРЕВ

Для исследования возможности нагрева плазмы при больших уровнях вводимой мощности использовалось возбуждающее устройство, изображенное на рис. 4 (а).

Средний вывод подсоединяется к камере; крайние выводы через проходные изоляторы подсоединяются к генератору, либо в одинаковой фазе ($\lambda = 20$ см), либо в противофазе ($\lambda = 40$ см).

Для определения оптимальных условий возбуждения волны измерялась напряженность переменного магнитного поля \tilde{H}_\perp по радиусу камеры и напряжение \tilde{U}_2 на приемном контуре, конструктивно аналогичном ВУ и расположенном на диаметрально противоположной стороне камеры. При напряженности магнитного поля, ниже ионно-циклотронной, волны в плазме не возбуждаются и поле слабо проникает в плазму. При резонансном возбуждении ионно-циклотронных волн напряженность высокочастотного поля в плазме под ВУ возрастает и становится выше вакуумной. Измерения напряжения \tilde{U}_2 на приемном контуре позволили определить коэффициент связи между возбуждающим устройством и плазмой, который в условиях эксперимента при отсутствии магнитного берега достигал значения 0,25. Нагрузка на возбуждающее устройство при этом мало отличалась от вакуумной (эквивалентное последовательное сопротивление $r = 0,4$ Ом). При наличии магнитного берега глубиной 25% и длиной 30 см связь между приемным и возбуждающим устройствами, за счет затухания волны в берегу, уменьшалась, а нагрузка на ВУ увеличивалась до $r = 4$ Ом при резонансном возбуждении волны. Было замечено, что волны, распространяющиеся влево и вправо от возбуждающего устройства, вносят неодинаковый вклад в величину связи между возбуждающим и приемным устройствами. По-видимому, основной причиной асимметрии поглощения является асимметрия параметров плазмы по азимуту (см. раздел III).

При создании берега с провалом поля больше 25% и длиной 15 см ("крутой берег") нагрузка на возбуждающее устройство и передаваемая в плазму мощность уменьшались.

На рис. 4 (б) показаны зависимости давления плазмы nT , измеренные магнитным зондом в области магнитного берега. Зависимость A соответствует замерению nT плазмы, предварительно созданной электронным пучком, две другие — при высокочастотном нагреве: B — берег с уменьшением поля на 25% и B — при отсутствии берега. Наличие максимума при отсутствии берега объясняется затуханием волны в гофрах магнитного поля, которые имеют величину порядка 13%. Приведенные зависимости показывают, что величина nT при высокочастотном нагреве возрастает в несколько десятков раз по сравнению с начальным значением (плотность при наложении высокочастотного поля на предварительно созданную плазму практически не изменялась).

Следует отметить, что nT плазмы увеличивается только в области магнитного берега, так как в процессе термализации ионы, в основном, приобретают поперечную энергию и оказываются захваченными в локальной магнитной ловушке. Перераспределение поперечной энергии в продольную не успевает происходить из-за малого времени удержания плазмы в тороидальной ловушке без вращательного преобразования. В ряде экспериментов высокочастотная мощность подавалась на два ВУ, работающих одновременно. Это позволило увеличить вводимую в плазму мощность.

На рис. 4 (в) приведены зависимости nT и $T_{\perp i}$ (измеренные анализатором поперечной энергии) от напряженности поля H_0 . Высокочастотная мощность подается на два диаметрально противоположно расположенные возбуждающие устройства, рабочий газ — дейтерий. При более высоком уровне вводимой мощности измерения энергии ионов анализатором провести не удалось из-за сильного загрязнения плазмы. Однако при отсутствии анализатора в области разряда nT увеличивается с увеличением уровня вводимой мощности (рис. 4 г). Оценка средней энергии ионов, полученная из максимальных показаний диамагнитного зонда, дает значение порядка 2 кэВ. Следует отметить, что в распределении ионов по энергиям плотность ионов в области высоких энергий ниже соответствующей максвелловскому распределению из-за уменьшения времени жизни ионов в тороидальном поле при увеличении их энергии.

Проведенные исследования показали, что в тороидальной плазме, помещенной в проводящую камеру, возможно эффективное возбуждение аксиально-несимметричных ионно-циклотронных волн и их термализация.

Разработанные возбуждающие устройства обеспечивают высокую эффективность связи ВЧ-генератора с плазмой (коэффициент связи ВУ с плазмой $\approx 0,25$).

Проведенные эксперименты также показывают возможность возбуждения в плазме не только ионно-циклотронных, но и других типов волн, в частности быстрых магнитозвуковых и альфвеновских.

Показано, что аксиально-несимметричные волны могут использоваться для нагрева плотной плазмы ($n \approx 10^{14} \text{ см}^{-3}$ и выше) в тороидальной ловушке. Термализация этих волн в области магнитного берега в условиях эксперимента позволяет осуществлять нагрев ионов плазмы до высоких энергий.

Распределение напряженности поля волны по радиусу плазмы позволяет надеяться на возможность использования таких полей для нагрева плазмы большого поперечного сечения.

Авторы благодарят В.И. Курилко за ценные советы и помощь в процессе выполнения данной работы.

ЛИТЕРАТУРА

- [1] СТЕПАНОВ, К.Н., ЖТФ 34 (1964) 2146.
- [2] ВАСИЛЬЕВ, М.П., ГРИГОРЬЕВА, Л.И., ЛОНГИНОВ, А.В., СМЕРДОВ, Б.И., ЧЕЧКИН, В.В., ЖТФ 54 (1968) 1646.
- [3] НАЗАРОВ, Н.И., ЕРМАКОВ, А.И., ТОЛОК, В.Т., ЖТФ (1966) 37, 40, 612.
- [4] БАКАЕВ, Н.И., ЗАЛЕСКИЙ, Ю.Г., НАЗАРОВ, Н.И., УКРАИНСКИЙ, А.И., ТОЛОК, В.Т., Атомная энергия 15 (1963) 3.
- [5] ШВЕЦ, О.М., ТАРАСЕНКО, В.Ф., ОВЧИННИКОВ, С.С., ТОЛОК, В.Т., Plasma Physics and Controlled Nuclear Fusion Research, 2, IAEA, Vienna (1966) 913.
- [6] ШВЕЦ, О.М., ТАРАСЕНКО, В.Ф., ОВЧИННИКОВ, С.С., БРЖЕЧКО, Л.В., ПАВЛИЧЕНКО, О.С., ТОЛОК, В.Т., ЖТФ 36 (1966) 443.
- [7] STIX, T.H., PALLADINO, R.W., Physics Fluids 1 (1958) 446.
- [8] ROTHMAN, M.A., SINCLAIR, P.M., BROWN, I.G., ROSEA, I.C., Physics Fluids 12, 10 (1969) 2111.
- [9] КУРИЛКО, В.И., ШВЕЦ, О.М., Сб. "Взаимодействие заряженных частиц с плазмой", Изд. "Наукова думка", Киев, 1967.
- [10] СТИКС, Т., "Теория плазменных волн", Госатомиздат, М, 1965.
- [11] АХИЕЗЕР, А.И., ФАЙНБЕРГ, Я.Б., и др., в кн. "Труды II Международной конференции по мирному использованию атомной энергии" (Женева, 1958) Госатомиздат, М., 1959, стр. 184.
- [12] ШВЕЦ, О.М., КАЛИНИЧЕНКО, С.С., МИРОШНИЧЕНКО, Г.А., Письма в редакцию ЖТФ 8, вып. II (5 декабря 1968) 629.

SUMMARY OF THE CONFERENCE
(Session M)

Chairman: H. POSTMA

REVIEW OF THEORY

T. K. FOWLER
Lawrence Radiation Laboratory
Livermore, Calif.
United States of America

On behalf of all of us attending this Conference I would like to thank the University of Wisconsin and the local committee for their generous hospitality. Also, I would like to take this opportunity to acknowledge the role of these IAEA international Conferences in furthering progress in Controlled Fusion Research over the last decade.

Since of the roughly forty theoretical papers presented here, nearly half concerned Tokamaks, I will attempt to summarize these first.

Let me begin with classical transport. Much of the new work concerns trapped particles. These are the few particles trapped in the weak magnetic mirrors created by the gradient in the strong toroidal field. Though few in number they are readily displaced large radial distances by weak collisions. As Galeev and Sagdeev first showed, in the small-collision-frequency (or "banana") regime, this leads to a radial diffusion coefficient which is approximately given by

$$D_{\perp} = \left(\frac{a}{R}\right)^{\frac{1}{2}} \rho_{\theta}^2 \nu_c$$

Here a and R are the minor and major radii, ρ_{θ} is the gyro-radius in the poloidal field and ν_c is the 90° -collision frequency. Since this simple result gives a crude fit to experimental data, it has become important to calculate the classical transport coefficients as accurately as possible in order to distinguish non-classical effects. Results have been presented and expanded upon here by Galeev, Kovrizhnykh, Rosenbluth and others. The theory is fairly complete for axisymmetric tori. It includes the known trapped-particle effects. Besides diffusion, these include the trapped-particle pinch effect due to E_{\parallel} , discussed here by Ware, and the so-called "bootstrap" current to which we shall return. For lack of time, it is referred to the papers for discussions of ambipolar effects, rotation and viscosity calculated so far. I would like to turn now to some of the current applications.

Clear evidence of classical transport in the collisional and plateau regimes was presented, for example, in the Proto-Cleo paper including an improved fit to the data in the plateau regime using Stringer's very recent modifications of the theory.

The theory has also been applied at Princeton to an analysis of Tokamak data with, in the authors' opinion, encouraging success. There is still the difficulty that the theory predicts a skin effect not observed. Instabilities not contained in the theory would destroy the sheath, as suggested by several authors. Also, in the theory, the skin effect is enhanced by the unstable buildup of current at a hot spot where the conductivity is growing. Thus current tends to spring up first wherever it is initiated, and it shys away from regions kept cold by external influences such as an influx of neutrals.

Another electron anomaly is a possibly enhanced resistance, though this too might merely reflect high-Z impurities. Because of these difficulties, transient effects can be explained only by artifices simulating the missing physics. Furthermore, the data are not sufficient to discriminate among competing empirical fits; Ware contends that the trapped-particle pinch effect explains most of the facts. Nonetheless, I think that it must be significant that the final β_0 and T_e/T_i are given fairly closely by computations which did not resort to arbitrary constants but used the neoclassical coefficients derived from first principles.

While we are on the subject of fitting data, I think that the Conference prize for including the largest number of experimental results within one theoretical conjecture must surely go to Shoichi Yoshikawa. I refer to his paper on pseudo-classical diffusion enhanced by fluctuations, also proposed by Artsimovich. Concerning his graph of all toroidal experiments against pseudo-classical scaling, I can only say that the consistency is rather remarkable, even if one takes into account the well-known law that a semi-log plot can make a little bit of order out of any state of chaos.

Next I want to mention results concerning two questions concerning Tokamak as a reactor, namely, the upper limit on β and the necessity for pulsed operation. Now, while low β would imply an expensive container cost per kilowatt, here we have heard several papers indicating a higher β (up to $a/(q^2R)$) if the minor cross-section is shaped optimally to increase shear. Also we have heard experimental evidence that at higher T_e stability occurs at lower values of the "safety factor" q . This is in accord with the conclusion by Shafranov and others that the fact that the observed q is higher than the MHD-value is associated with resistive modes. Thus it appears that the β limit for Tokamaks will probably not be as low as was thought first. In fact, it has been suggested that β may be high enough that the heat load on the wall becomes the limiting problem.

As to pulsed operation, here we heard Kadomtsev describe a mode of Tokamak operation which is almost steady-state, an idea also put forward by Bickerton, Connor and Taylor. This utilizes the bootstrap current around the torus which is sustained by radial diffusion of the plasma. Again the trapped particles are involved to get the highest current; the current is a factor $(a/R)^{3/2}$ less in the collisional regime according to Stringer and Galeev. Since this current does not require the usual applied inductive electric field, the Tokamak configuration can be maintained in steady state if new ions are continually supplied, for example, as neutrals. There is possibly a problem at the axis, which might be solved by imparting momentum there by means of neutral beams as suggested by Ohkawa. In any case, it appears that essentially steady operation could be achieved, in principle.

The main question, of course, continues to be confinement. In this we are all encouraged by the generally improved confinement as the temperature is increased. But as theorists, we must look ahead to instability problems which might arise in the fully collisionless regime. Again the trapped particles seem to be the worst potential problem. The mode in question is the Kadomtsev-Pogutse trapped-particle interchange caused by unfavourable drift in the toroidal field gradient. So far, only collisions have been put forward as a stabilizing effect. This could explain the apparent absence of these effects in present experiments. The rough criterion requires that the ion collision frequency exceed the bounce frequency reduced by a factor of 10 or so, not known exactly. This would set a lower limit on

the circumference of the machine which would be very large assuming classical collisions. Coppi suggests that we look for stronger anomalous collisions due to mode coupling, but this remains an open question. Besides trapped particles, we also must not forget the temperature gradient mode which Kadomtsev introduced at the Culham meeting. This would determine a minimum minor radius.

As Yoshikawa discussed, a levitron or spherator configuration in which the internal ring conductor is replaced by an Astron-type relativistic electron layer would be free of trapped-particle instabilities within the minimum-B region inside the E-layer. Then the question is the stability of the E-layer. This configuration is created by adding a toroidal field to the Astron. Yoshikawa points out that the toroidal field would also produce helical electron orbits less subject to synchrotron radiation losses and may produce a force-free current distribution subject neither to the Lawson limit nor the Kruskal-Shafranov limit. Also, Christofilos reported experiments at this Conference in which the addition of a weak toroidal field improved E-layer injection and trapping, in part by suppressing the precessional mode in agreement with theory.

Let me now call your attention to two high- β results. At the Novosibirsk Conference we had heard that a theta pinch with an $\ell = 1$ winding would be stable to $m = 1$ MHD-modes, like Scyllac. It was known experimentally that only the $m = 1$ mode occurred, but MHD-theory could not account for suppression of higher modes. Freidberg reports that this has now been resolved. Vlasov theory predicts a slow growth rate for the $m = 2$ mode whereas MHD-theory predicted growth 3 times that for $m = 1$. The other high- β result I want to mention is Grad's conclusion that perturbations of a high- β plasma can generate magnetic islands.

Turning to mirror confinement, the theoretical picture is conceptually clear, though complicated in detail. The plasma supports a variety of waves which the ion loss-cone distribution can excite. As low densities, these are electron plasma oscillations which we damped by Landau damping. This was demonstrated in the Phoenix-II data, and earlier in Baseball II. But at higher densities ($\omega_{pi} > \omega_{ci}$), the main question is whether the waves can fit inside the plasma taking boundary conditions and inhomogeneities into account. Answers to these questions yield criteria as to the plasma length (in some cases the radius) required to set up the wave. The plasma is stable if it is shorter than this critical length. Considerable progress has been made since the Novosibirsk Conference, reported here by Berk.

The waves are of two basic types: convective and flute-like. An important prediction of the theory, not yet verified experimentally, is that the relatively gentle density profile produced by classical mirror losses will not appreciably reflect convective waves. (The sharp profiles do, of course, as in the Phoenix-II case, for example.) If this is correct, the shortest critical lengths for convective waves arise from resonances in the dispersion function due to variation of the ion gyrofrequency with position in a non-uniform field. For $\beta > m_e/m_i$, the critical length is

$$\frac{L}{a_i} < \frac{A}{\sqrt{\beta}}$$

Here A depends on the distribution function and is typically 10 or more, L is the magnetic scale length, not the plasma length. At lower β , replace

$\beta \rightarrow m_e/m_i$ in the formula. So far this prediction has not been tested experimentally. Existing experiments have been, at most, marginally unstable by this criterion. Also, the other class of modes dominates. There are the flute-like modes including impurity, or double-hump, modes; the modified negative mass; the DGH-mode caused by a narrow energy distribution; and the drift cyclotron loss cone mode (drift cone). As Berk reported, despite earlier ups and downs, the drift-cone mode insistently refuses to go away. Since none of these flute-like modes would be present at reactor parameters, they presently constitute a nuisance which must be overcome to get at the potentially important convective modes described above.

The last subject which I would like to discuss is beam-plasma interaction and turbulent heating. This subject now seems to be fairly well understood. This is mainly due to the impetus of experiments, I think, though we have to admit that luckily one has not yet had to ask the most detailed questions in order to find out the most important things.

One not so easy and very old question which seems to have been resolved is the origin of resistance due to current-driven ion acoustic and ion cyclotron waves, discussed here by Rudakov, Fried and others. In both cases the current excites waves of velocities much less than the electron thermal velocity. Since only the few resonant (or trapped) particles interact strongly, the conductivity due to all the rest is little affected. To account for resistance, we require non-linear coupling to a broad spectrum. Though there is no single answer for all cases, Rudakov now reports a number of candidate classes of electron cyclotron modes which would do it.

An overview of beam interaction is something like this. To avoid interaction, as in applications such as the Astron E-layer, the object is to create the bump-on-tail situation of a low-density beam in a high-density plasma. If the plasma oscillations are damped by collisions or otherwise, the beam can drive them only until the beam energy spreads enough to satisfy the "gentle-bump" criterion. One can obtain relatively mild interaction by applying not too strong electric fields, as in turbulent heating experiments. Interaction now occurs, but the gentle-bump situation is generally never reached, all electrons being accelerated. Either the accelerated electrons never reach the electron thermal speed, in which case ion acoustic or ion cyclotron resistance dominates, or with a larger electric field some electrons may try to run away. If so, their number is generally (not always) too great to satisfy what is essentially the gentle-bump criterion, so that plasma oscillations are excited, as pointed out in the MIT-paper. Finally, if a strong beam-plasma interaction is desired, a large beam not satisfying gentle-bump criteria is required and thermodynamic criteria such as those presented by Drummond apply. This was the theme of Rudakov's discussion of an electron-beam fusion concept. By the way, this was, I think, one of only two fundamentally new ideas at the Conference, the other being Dawson's laser heating scheme.

In trying to sum up my impressions of this Conference, I concluded that perhaps the most important thing was that this is the first IAEA fusion Conference with an entire session on fusion reactor systems. Perhaps this Conference will be remembered as sort of an engagement party between plasma containment and fusion reactors. Admittedly, the two seemed a little like strangers from time to time here. But this will change, for we have brought some valuable presents to this party, for example, the

number of new experiments we have heard about which are about to push on to the high temperatures and high densities where the real problems lie. As I have tried to outline here, the theoretical development is now such that critical questions are posed which these experiments can answer. I think that we shall really find out whether trapped particles are significant, whether mirrors have a critical length, and whether theta pinches can last for milliseconds. And when we do, even if at first some answers are disappointing, I am confident that we shall soon be on the road to building a fusion reactor.

REVIEW OF EXPERIMENTAL WORK

R.J. BICKERTON
UKAEA, Culham Laboratory,
Abingdon, Berks,
United Kingdom

In reviews of this kind it is customary first to look back at the situation as it was at the last meeting; in this case, three years ago when we met in Novosibirsk.

At that time the low- β toroidal experiments were still in the process of emerging from the bad years of Bohm diffusion. A group claiming plasma containment for longer than the Bohm time prepared their defences well for they knew that they would be subjected to instant critical attention. True, the Tokamak group were claiming 30 Bohm times in the T-3 machine. However, since the electron temperature was deduced from a complicated analysis of electrical signals while the discharge radius was uncertain, this claim was not entirely accepted. Indeed a minor industry was established devoted to the proposition that within experimental error the containment was, in fact, Bohm-like.

The linear theta-pinch work had reached a peak of sophistication in 1968, hot plasmas could regularly be produced, and the physical mechanisms were well understood. It was apparent that further improvements in the plasma life-time could only come by changing to toroidal, or closed geometry. As will be seen, theta-pinch groups have chosen various toroidal schemes, some symmetric such as the screw-pinch and diffuse pinch, some asymmetric such as the high- β stellarator.

In the field of stellarator research, the most powerful machine, the Princeton Model C, showed only a modest increase over Bohm. Even this was presented by the Princeton scientists with intense and proper scepticism. One experimental 'ray of hope' was the demonstration that single particles could be contained for many transits round a well-constructed stellarator. The other main excitement in this field concerned the discovery of various types of banana orbits and the resulting neo-classical diffusion theory then in its infancy.

In the study of open traps of the mirror type the neutral injection machines showed only a hint of plasma trapping and the density was limited by instability. The plasma injection mirrors showed, in the main, anomalously fast losses. At that time also crude Fokker-Planck calculations of the classical loss rate suggested that even the 'ideal' mirror confinement limited only by binary scattering would be inadequate for an economic mirror reactor.

In the general field of plasma physics, the results on turbulent heating and collisionless shocks excited the most interest.

Turning now to the progress in the last three years - in 1969 light-scattering experiments on the T-3 Tokamak in Moscow showed that the

plasma parameters were indeed as the Russian workers had earlier claimed. A rapid growth in Tokamak research outside Russia quickly followed. Thus there are now, at least, a dozen major Tokamak-type devices under construction outside the Soviet Union. Results from the first of these, the Princeton ST, were reported at this conference. Broadly speaking the American scientists find the same results as in the Soviet experiments. Electron temperatures ~ 1 keV are reached, with an energy containment time ~ 10 ms for a gas current ~ 50 kA. Consequently, most attention is now given to the differences in detail between the Soviet and United States results. The temperature in the Princeton machine is strongly peaked near the magnetic axis, the energy and particle containment times are about equal, and the electrical resistivity is classical when due allowance is made for the presence of impurities and for the effect of trapped particles. By contrast, the temperature profile in T-3 is flat, the particle containment time is substantially longer than that for the energy, and the resistivity is anomalous. Some of these differences may be more apparent than real in that they result from differences in the interpretation of measurements. As in the Soviet experiments, the Princeton workers find that the energy content per unit length of the discharge is proportional to the square of the current. The discharge can be said to satisfy the classic Bennett relation with " β poloidal" a constant, the value found being ~ 0.5 . The reason for this is not clearly understood, and we note in parenthesis here that a Tokamak reactor will require this parameter to be increased by nearly one order of magnitude. The effect of perturbing the axial symmetry of the Princeton machine has also been studied. When the toroidal magnetic field was increased locally by 30 per cent, the confinement time fell by 30 per cent. Clearly axisymmetry is not a vital feature under present operating conditions. This result is in accord with the neo-classical diffusion theory. However, at higher temperatures and longer mean free paths axisymmetry should be more important and some hint of this was seen in the effect on fast ions. Their relative population was depressed by the induced asymmetry.

Results from the T-4 Tokamak, which is an improved version of T-3, were presented. The toroidal magnetic field can be higher and the copper shell is nearer to the plasma than in the earlier machine. Regular stable operation with the safety factor q as low as 2 is found, and plasma currents of up to 200 kA have been achieved. The plasma parameters continue to follow the scaling laws established by the earlier studies. Thus the ion temperature as deduced from the neutron flux reaches 600 eV.

In other experiments both at Princeton and in Russia the residual hydromagnetic instabilities were studied. These have high mode number, and it seems that a detailed understanding of the phenomena will only be achieved when the radial distribution of poloidal field within the discharge can be measured.

This is just one of the many features of the Tokamak discharge which are not understood at present. The precise role of the limiter is unknown, the energy and particle containment times cannot be explained by classical processes alone. The importance of the trapped particle pinch effect is not clear. We do not know experimentally the maximum β which the system can confine. The wide range of new experiments of the Tokamak type coming into operation in the next few years will throw light on these questions. Particularly interesting will be those machines incorporating auxiliary heating methods.

Stellarator research has now been completely exported from the United States. Most of the experiments reported were with relatively small machines confining low-temperature and often weakly ionized plasma. The results are complex, and it is difficult to draw clear conclusions. Thus very detailed measurements on the Nagoya stellarator show the presence of a convective cell which transports plasma to the outer regions where strong drift wave fluctuations carry the plasma out of the separatrix. The containment time is one order shorter than the neo-classical value. The Culham stellarator with very similar machine parameters shows containment which agrees with the Pfirsch and Schlüter formula at high collision rates and with the neo-classical and superbanana theories over several decades of the collision parameter. However, the diffusion-driven current which should accompany this apparent neo-classical diffusion was not observed.

In low-shear machines, the minima in containment time associated with rational values of the transform were ascribed to island formation by the Lebedev group and to transitions to convective equilibria by the Garching experimenters.

Also at the Lebedev Institute a very careful series of measurements has shown the spinning of the stellarator plasma about the major axis due to the preferential loss of resonance particles.

At Kharkov, the containment of hot plasma is studied in the Uragan stellarator. The plasma is heated by turbulent heating, the electron temperature at the peak of the current pulse varies up to 400 eV; the energy containment time is found to increase with electron temperature up to a certain critical value and then to decrease. This critical value seems to be associated with the hydromagnetic instability of the discharge at that point since the current-produced rotational transform is then comparable with that due to the helical windings. The maximum energy containment time of 300 μ sec corresponds to a few Bohm times.

In all these stellarators the effective poloidal field is relatively small, and for example, in Uragan, the equivalent current is only ~ 7 kA.

The importance of the poloidal field for toroidal confinement has only gradually become recognized over the last decade. The first step in this direction was made by Pfirsch and Schlüter; then the neo-classical theory and now in ultimate form the quasi-classical hypothesis. Thus according to the present picture the toroidal field is only an auxiliary field, necessary in Tokamak to stabilize the current producing the poloidal field and in stellarators to create magnetic surfaces. Viewed in this light, the poor performance of stellarators relative to Tokamaks is simply because the product of poloidal field and minor radius is, at least, an order of magnitude lower.

In this connection the stellarators at present under construction at Culham and Garching which have equivalent currents of order 50 kA will be especially interesting.

In buried-ring devices the poloidal field is produced by currents in material conductors, the rings, inside the plasma. Consequently, they offer the hope of testing confinement ideas such as shear, average minimum B and the neo-classical theory in a controlled manner. In practice, many of the machines have proved to be far from ideal. Difficulties arise due to the time-dependent magnetic fields in induced-ring-current systems and to ring supports where they exist. Only the levitated superconducting devices completely avoid these problems. Methods of plasma production can also lead to further difficulties.

Nevertheless near-classical loss has been shown in the San Diego D.C. octopole but with loss due to field errors predominant at low densities. Similarly, the Princeton spherator, which has a levitated superconducting ring, exhibits classical behaviour with a microwave-produced plasma. These results are extremely encouraging since they show that classical containment in a torus is not just a figment of the theoretician's imagination.

At Livermore and Culham superconducting Levitrons with neutral injection will soon be coming into operation and one of these was described at this conference. However, neither these, nor the existing machines have the capability to explore the regime of direct relevance to Tokamak and Stellarators, namely, that in which the toroidal field is large compared with the poloidal field. It seems to me that a definitive test of the neo-classical diffusion theory in such a device would be a major contribution.

The high- β toroidal devices are the direct descendants of the linear theta pinches so numerous in earlier times. The present aim is usually to preserve the proven ability of theta pinches to produce dense hot plasmas in some form of toroidal system.

In the Culham experiment, the chosen configuration is the diffuse pinch. By programming several driving capacitor banks a variety of configurations was set up and their behaviour shown to be qualitatively in agreement with the predictions of hydromagnetic theory. However, the rate of energy input is limited in the diffuse pinch case since it must not be strongly compressed. Thus the electron temperature achieved is only ~ 10 eV and the configuration relaxes through resistive diffusion to an unstable one after $15 \mu\text{s}$.

Experiments on the screw pinch at Garching, Jutphaas and Culham have shown the containment of a central hot core with the temperature exceeding 100 eV, density $\sim 10^{16} \text{ cm}^{-3}$ for $\sim 20 \mu\text{s}$.

This configuration derives its equilibrium from the axial current in the outer cold plasma between the core and the wall. The rapid decay of this current seems to be the limiting factor in some experiments. However, in the Garching experiments maintaining this current by an external driving voltage did not extend the life of the discharge.

In the very large Scyllac machine at present under development at Los Alamos it is planned to provide a toroidal equilibrium through the use of combined $\ell = 0$ and $\ell = 1$ additional fields. Preliminary experiments on a 5-metre segment of the torus showed that these fields do indeed control the toroidal drift, at least, for the first 3 microseconds. The sudden loss of the plasma at that time is attributed to the finite length of the test section.

Two interesting experiments at Jülich and Garching are essentially high β , shaped cross-section Tokamaks; Tokamaks in the sense that the safety factor $q > 1$ and with strongly elliptical cross-sections for the plasma. The major axes of the ellipse and the torus are parallel in both cases. In the Jülich experiment the plasma with a relatively high β of 15 per cent has a life limited by the resistive decay of the toroidal current. Only very preliminary results were given for the Garching experiment: a streak picture appeared to show stable confinement for $75 \mu\text{s}$.

After more refined calculations of the scattering losses in mirror machines it is now clear that the reactor prospects for these systems depend on finding efficient and economic methods for recycling the plasma energy lost through the mirrors or for reducing the mirror loss by auxiliary means. Such schemes must surely fail if the end losses are enhanced by instabilities much above the classical level.

The two high-density mirror machines, PR6 in Moscow and 2X in Livermore, both showed loss rates which were initially only slightly faster than classical, but which subsequently increased to more than ten times the classical value. Evidence of radio frequency noise near the ion cyclotron frequency was found in both machines, but no definitive mode identification was made. Similarly, in the French Deca II machine the initial relaxation of the ion velocity distribution occurred at approximately the classical rate. However, in this machine the subsequent plasma decay is due to charge-exchange collisions.

In the Phoenix mirror machine, plasma trapping of the injected neutral beam is now very clearly seen. However, plasma exponentiation is inhibited by anomalous loss due to ion cyclotron instabilities.

It seems that stable mirror confinement, if it can be achieved, requires very careful control of the particle velocity distribution at all stages during the plasma build-up. The fact that the high-density machines appear not to relax into stable distributions seems to me to imply that this task will be an extremely difficult one.

Turning now to the Astron in which a magnetic bottle is to be created through the combination of external windings and current carried by a relativistic shell of electrons. The superposition of multiple bunches of injected electrons has been successfully demonstrated and gives a field reduction due to the electron ring of 7 per cent. With a single pulse focussed axially by a relatively strong toroidal magnetic field the field reduction is 15 per cent. The half-life of the E-layer is typically 10 milliseconds.

It is to be hoped that field reversal will be achieved before the next meeting so that plasma confinement studies can, at last, begin after these Herculean labours to construct the trap.

The study of the plasma focus continues to excite interest. As is well known these systems produce an extreme state of matter with kilovolt temperatures and densities between 10^{18} and 10^{20} cm^{-3} . In several devices two pinches are observed with the majority of the neutrons coming from the second pinch. Shadowgrams show the existence of Rayleigh-Taylor instabilities during the collapse phase. From light-scattering measurements the Limeil group deduces that the ion temperature in their device is 1 keV. In another experiment, highly stripped impurity ions are shown to have much higher energies than the deuterons. This is attributed, in part, to the implosion and in part to acceleration by fluctuating electric fields. The optimized neutron yield from one device reached 3×10^{11} neutrons/pulse in deuterium. Experimental analysis of the angular distribution of the neutrons and computer simulation suggest that both thermonuclear and accelerated-beam processes contribute to the yield.

Neutrons from laser-produced plasmas were reported from both Garching and Limeil. In the Garching case, there is evidence to suggest that the neutrons in their case have a non-thermal origin. The higher-power Limeil experiment gives $\sim 10^5$ neutrons/pulse and it seems likely that these have a truly thermonuclear origin.

In the work on collisionless shocks, very detailed information has been obtained concerning the turbulent spectrum of fluctuations in low-Mach-number, perpendicular shocks. As yet, there is no satisfactory theory with which to compare this data. The major uncertainty concerns the nature of the initial linear instability. There are two schools of thought — one holds it to be an electron cyclotron wave, while the other prefers an ion-acoustic mode.

Since electron cyclotron waves can only propagate in a narrow cone almost perpendicular to the magnetic field, this, in a sense, theological dispute is likely to be resolved by further measurements on the cone of turbulence in the shock.

The efficient shock heating of deuterium plasma to keV-temperatures was reported from both Jülich and Columbia. In the latter case, the shock wave involved is collisional.

In the closely related subject of turbulent heating, ordered particle motion produced by strong externally applied electric fields is rapidly thermalized to produce hot plasma. The character of the collective fluctuations responsible for this thermalization has been the subject of much of the research. From these studies, it is found that the turbulence in most experiments is of the ion-sound type. In that case, both electron and ion heating are seen, frequently to keV-temperatures. When the electron drift velocity is made very high the Bunemann-Budker instability is excited with consequent strong electron heating.

The main properties and parameter ranges of turbulent heating are now fairly well documented. Widespread application of the technique is delayed mainly by the technical difficulty of applying transient high voltages to containment systems and partly by uncertainty concerning possible skin effects in large plasmas.

The new technique reported at this meeting is that for producing pulsed relativistic electron beams. Beams of MeV electrons can now be produced with currents of ~ 100 kA lasting for ~ 100 ns. The anomalous absorption of this type of beam by a plasma was discussed in an experimental paper from Novosibirsk. At Cornell, a similar beam has been injected into a magnetic field to produce an Astron-type configuration with full field reversal. However, the life-time of the ring current was limited to 600 ns.

And now to conclude. Although much progress has been made it is clear that the confinement problem is still the most important one for fusion. The results from the mirror machines are not encouraging. As is well known, for effective confinement in these devices the level of instabilities must be very low indeed. One can only hope that the required quiescence will be found in one or both of the new machines at Livermore.

The work on toroidal high- β systems is still in its infancy. Encouraging preliminary results on the control of toroidal drift have been obtained. There is a substantial area of agreement between the predictions of hydromagnetic stability theory and the observations. At least, in most of these experiments there is no problem with the production of hot plasma. However, only the requirements of equilibrium and of stability against the simplest hydromagnetic modes are met by many of the experimental schemes. It remains to be seen whether the more subtle modes will appear as the confinement time is increased.

In the buried-ring devices classical diffusion has been demonstrated under some conditions. They have also shown what should be avoided; for example, field lines which close on themselves are found to be very susceptible to field errors. In future work we may hope for detailed comparison between the experiments and the massive catalogue of theoretical instabilities.

In the stellarator work containment times near the neo-classical value are claimed in several experiments. These experiments are in apparatus too small to allow wide parameter scaling, so that these claims must be viewed with caution. Only general rules can be given for the stellarator

designer. High shear not only helps to stabilize the drift modes, it also reduces the susceptibility of the configuration to field errors and removes the possibility of a rational transform over a large radial zone. Above all, the mean poloidal field should be as high as possible. A decisive comparison between stellarator and Tokamak can only be made when this latter parameter is comparable in the two machines.

The most exciting advances have been made in Tokamak research. The Princeton group have confirmed the earlier Russian results while the Russians themselves have gone on to obtain still higher temperatures with increased plasma current. The fruits of the rapid expansion in Tokamak research will only be apparent by the time of the next meeting. At present, and in the simplest terms, future progress apparently depends only on increasing the gas current and on applying auxiliary heating methods. There may well turn out to be insurmountable barriers across this golden road to riches; however, only by travelling along it will their presence or absence be discovered.

REVIEW OF REACTOR SYSTEMS

H. K. FORSEN
University of Wisconsin,
Madison, Wisconsin,
United States of America

In my opinion, it is significant that at this Fourth Conference on Plasma Physics and Controlled Nuclear Fusion Research the progress of research has come to the point where a session on reactor systems is held, at all. Let us hope that progress in the plasma physics will continue to give us encouragement that such reactor studies are meaningful and indeed required.

Let us now go into some detail. Because of the nature of plasma losses from mirror devices it appears essential to re-circulate this escaping plasma in order to ensure their competitive position in eventual fusion reactors. Two papers were presented with possible solutions to this problem. One from Livermore was reviewed by Post and gave results on the direct conversion of charged-particle kinetic energy to electricity.

This method of energy recovery has a potential efficiency of well over 90% and would work to the best advantage if all of the primary reaction products were charged such as in the D-³He cycle. Bench tests on such a direct conversion system have been conducted, and the efficiency was found to compare favourably with that calculated for the system of 83%. Scaling of such systems to handle the higher power densities and energies necessary for reactors remains to be explored, but if it is indeed possible and at a reasonable cost, it would be of significant benefit to mirror systems and even possibly to closed line systems.

Because of the higher efficiencies possible in such systems when operated at higher temperature, injection energies from 300 to over 500 keV are desirable. This reduces the current requirements for fuelling the reactors but puts a considerable burden on the injectors and charge-exchange cells. Here negative ion sources are found to be important.

A second method of handling the particle losses from mirror systems was suggested by the Culham group and described by Sweetman. In this system, the escaping ions are carried along the field lines to a region located at the centre of a spherical shell reactor. There the ions are allowed to exchange charge, leave the field lines and move outward toward the plasma confinement region where they are ionized and trapped.

Because of the charge-exchange requirement on the positive ions, a temperature close to 100 keV appears most desirable. This also reduces the burden on the ion source. So far, no experiments have been conducted to check this principle but from the point of view of cost and beam handling, such a system looks extremely attractive.

In any case, the various cycles considered for mirror systems must face the severe limitation of low calculated values of Q where Q is defined as the ratio of fusion power to injected power. Studies on this problem and how to optimize the system were also undertaken. The Livermore calculations show that for a given Q-value, the costs for a D-³He system are lower than those for a D-T system because of their favourable cost projections for

direct converters. On the other hand, for the extremely low Q -values now predicted for D- ^3He , the D-T system is perhaps the only possible system since the costs are not sensitive to modest changes in Q . Post also pointed out that the cost penalty for smaller reactor systems (below 1000 MWe) is not excessive for the projected direct-conversion scaling laws.

The Culham group finds similar results and is equally pessimistic about the relative merits and costs of D- ^3He compared to D-T. Their costs/kWe are compared in "notional pounds" but if converted to "notional dollars" they are similar to those of Livermore. That is, both groups find \$200.-300./kWe are reasonable brackets for D-T mirror systems. By using the Culham auto-injection method and injecting at 100 kV, it is possible to operate at the low end of this cost bracket and this seems quite promising.

Before leaving mirror reactors and D- ^3He cycles, I would like to explain that, in general, these systems are essentially D-D systems with ^3He produced as a reaction product and then re-circulated. Studies by both groups here used 15-20% ^3He with the remainder D. This is just about the amount of ^3He produced in the reactor.

Switching now to low- β toroidal systems, we heard several things to be encouraged about. The first is the possibility of using diffusion-driven currents to bootstrap Tokamaks to steady-state reactors. If this proves to be feasible in actual systems with no loss in the critical β , such reactor systems would be extremely attractive.

In a paper by the Culham group, considerations of such reactor systems were undertaken and compared with Stellarators. They concluded that such bootstrapping is probably not more restrictive on stability than the earlier criterion provided that for Tokamaks the stability factor (q) is greater than 3 or for Stellarators the aspect ratio is greater than 8.

They also point out the need for diverters in such systems and here Stellarators look easier than Tokamaks. However, in a paper by Jukes and Haas, it appeared that poloidal field diverters in Tokamaks may not affect the stability provided they are properly located.

It would seem that the need for diverters in toroidal systems because of wall effects is perhaps the most critical toroidal reactor problem.

An excellent paper was presented by the ORNL group on the engineering design of a superconducting magnet system for a Tokamak reactor. Their study suggests that large superconducting reactor systems will be practical, but in order to keep the costs down some compromises will have to be made. One stems from the large amount of refrigeration power needed if the initial cool down time is to be less than months. A second important point is made that if the first wall loading is reduced as well as the output power and toroidal magnetic field, the magnet forces, the power losses and the radiation damage can be significantly reduced. The use of a wall loading factor of 10-13 MW/m² may be too large in the face of the rest of the system performance. However, some benefit may be derived from using non-cylindrical blankets. This continues to point out the need for reactor system studies.

We can compare the cost analysis of the magnet system of the ORNL paper and the Culham paper. There are significant differences but happily the in-depth study by ORNL indicates that costs may be less, not greater than originally imagined, and also that Stellarators appear more expensive than Tokamaks because of the multipolar nature of the windings.

Moving to the problems of start up and heating of Tokamak reactors we find that several approaches appear to look attractive. Calculations on

neutral-beam heating were described in a paper from ORNL and similar results are suggested by Culham and the French research workers. Many groups are developing plasma sources capable of doing this and the Hall accelerator concept appears as a new hope for high currents at modest energies.

Some interesting prospects for ignition were given in papers outside the reactor session. These include the initial heating of a reactor by intense relativistic beams colliding with encased solid D-T fuel pellets as described by Rudakov and similar processes driven by short-pulse high-power lasers. These and other techniques for heating and ignition will be discussed at the working sessions on reactor technology at Oak Ridge at the beginning of July 1971. One of the other encouraging aspects brought out at this meeting is the fact that more groups are starting to undertake reactor studies. Papers from the Soviet Union, the Federal Republic of Germany and Japan reflect the broad interest by both plasma physicists and reactor engineers in the technology of controlled fusion reactors.

An interesting example of this fact was reflected in the paper on thermal control of fusion reactors. In this paper the authors (from JAERI in Japan) show that if either charged-particle or injection heated reactors are operated below a certain minimum critical temperature, a feedback mechanism is required to properly control the plasma temperature. Operation above this temperature can be self-regulating. The critical temperature is determined by the kind of diffusional loss under which the closed reactor system operates. Strangely enough, the simplest system to control in terms of a minimum operating temperature is one dominated by Bohm diffusion. Since it would appear at this time, at least, that low- β toroidal systems will require some form of external heating, injection heating and control by adjusting beam parameters appears straightforward.

Moving now to blanket problems in D-T reactors, we find the problem centred around the difficulty in handling the 14-MeV neutrons. These neutrons represent a large radiation damage problem to the first wall; again we shall hear about this at the Oak Ridge working sessions on reactor technology. The thermalization and capture of the neutrons in Li or Li-salt blankets does not appear to present significant difficulties as determined by several calculational methods, but, as yet, there are no bench marks to check the calculations. Some uncertainties in cross-sections will eventually have to be rectified.

Breeding ratios adequately larger than unity are possible using lithium or Li-salts. Whether there is a separate advantage in using the salts because of a smaller inventory or simpler recovery techniques remains to be seen, but this will strongly affect the fuel doubling time.

Separate calculations on the MHD-pumping power for pure Li systems where the Li must flow out of the blanket to a heat exchanger suggest that substantial fractions of the reactor power may be required in pumping power. This too may suggest the use of salts.

Because of the intense heat load on the first wall due to elastic collisions with the fast neutrons, the absorption of bremsstrahlung radiation from the plasma, and the backshine of gammas from neutron inelastic collisions on the blanket side of the wall, the first wall is again perhaps the most critical area in the reactor. Studies of heat removal from this wall and the reactor blanket were undertaken in a paper from Jülich. In this paper, several heat removal systems were evaluated and the most attractive ones appear to be

indirect cooling of Li by He or H₂O very similar to how fast-breeder reactor cooling is presently envisioned. Plant efficiencies of 42-46% are calculated for these systems without anything additional being done to handle the charged reaction products.

Since all large industrial complexes have some hazard potential associated with them, it is instructive to view the comparisons made by Steiner of fusion reactors with both thermal and fast-breeder reactors. He finds, in general, that fusion reactors present a lower hazard potential associated with radioactive inventories, lower nuclear power densities during operation and for significant periods after shut-down, no potential for reactivity insertions resulting from loss of coolant or melt-down, and significant advantages associated with radioactive waste disposal.

Studies which are not yet completed suggest that the use of vanadium instead of niobium for blanket structural and wall materials offer even greater possible advantages.

The point of this seems to be that reactor design studies have shown some problem areas to be circumvented, but insofar as reactor studies have been undertaken, there is nothing in the technology that is a fundamental limit to the success of fusion power. This says, at least, two things. The first is that our reactor studies should continue and expand to see if there is yet a fundamental technological problem, and second that we need to progress as rapidly as possible in our understanding of the plasma physics so that the reactor prospects of fusion can indeed be tested.

CHAIRMEN OF SESSIONS

Session A	M. GOTTLIEB	USA
Session B	C. M. BRAAMS	Netherlands
Session C	B. B. KADOMTSEV	USSR
Session D	B. BRUNELLI	Italy
Session E	J. B. TAYLOR	UK
Session F	B. LEHNERT	Sweden
Session G	M. TROCHERIS	France
Session H	G. VON GIERKE	Federal Republic of Germany
Session J	C. N. WATSON-MUNRO	Australia
Session K	E. P. VELIKHOV	USSR
Session L	K. HUSIMI	Japan
Session M	H. POSTMA	United States of America

SECRETARIAT

Scientific Secretary:	H. S. T. DRIVER	Division of Research and Laboratories, IAEA
Administrative Secretary:	C. DE MOL VAN OTTERLOO	Division of Scientific and Technical Information, IAEA
Editors:	R. SCHENIN J. W. WEIL	Division of Publications, IAEA
Records Officer:	D. J. MITCHELL	Division of Languages, IAEA

LIST OF PARTICIPANTS

ARAB REPUBLIC OF EGYPT

Husseiny, A. A. Faculty of Engineering, University of Alexandria,
Al-Hadara, Alexandria

AUSTRALIA

May, R.M. University of Sydney, Sydney, N.S.W. 2006

Watson-Munro, C. University of Sydney, Sydney, N.S.W. 2006

AUSTRIA

Cap, F.F. Institute of Theoretical Physics, University of Innsbruck,
52 Innrain, A-6020 Innsbruck

BELGIUM

Messiaen, A. M. A. Laboratoire de Physique des Plasmas,
Ecole Royale Militaire,
1040 Brussels

Vandenplas, P. E. M. Laboratoire de Physique des Plasmas,
Ecole Royale Militaire,
1040 Brussels

Verhoest, F. G. G. Seminarie voor Analytische Mechanica,
Plateaustraat 22, Rijksuniversiteit Gent,
B-9000 Gent

CANADA

Burkhardt, H. Center of Energy, I. N. R. S., University of Quebec,
C.P. 1020, Varennes, Quebec

Ehrman, J. B. Department of Applied Mathematics,
University of Western Ontario,
London 72, Ontario

Gregory, B. C. Center of Energy, I. N. R. S., University of Quebec,
C.P. 1020, Varennes, Quebec

Hoffmann, C. R. J. Accelerator Physics Branch, Applied Physics Division,
Atomic Energy of Canada Ltd.,
Chalk River, Ontario

Nodwell, R. A. University of British Columbia, Vancouver 8

Parbhakar, K.J.	Center of Energy, I.N.R.S., University of Quebec, C.P. 1020, Varennes, Quebec
Richard, C.	Institut de Recherche de l'Hydro-Quebec, Montée Ste-Julie, Varennes, Quebec

CHILE

Schaffer, M.J.	Universidad Técnica del Estado, Santiago
----------------	--

CHINA

Wei, C.-C.	Institute of Physics, National Tsing Hua University, Hsinchu, Taiwan
------------	---

CZECHOSLOVAK SOCIALIST REPUBLIC

Sunka, P.	Institute of Plasma Physics, Czechoslovak Academy of Sciences, Nademlynska 600, Prague 9
-----------	--

DENMARK

Jensen, V.O.	Danish AEC Research Establishment Risø, 4000 Roskilde
--------------	--

FRANCE

Bernard, A.M.J.	CEA, 29-33, rue de la Fédération, Paris 15
Bobin, J.L.	CEA, Centre d'Etudes de Limeil, B.P. No.27, 94 Villeneuve St. Georges
Breton, D.G.E.	CEA, 29-33, rue de la Fédération, Paris 15
Briffod, G.M.	CEN Grenoble, rue des Martyres, 38 Grenoble
Consoli, T.	CEN Grenoble, rue des Martyres, 38 Grenoble
Coutant, J.	Association EURATOM-CEA, B.P. No.6, 92 Fontenay-aux-Roses
Doucet, H.J.	Laboratoire de Physique des Milieux Ionisés, Ecole Polytechnique, 17, rue Descartes, Paris 5
Fabre, E.L.	Laboratoire de Physique des Milieux Ionisés, Ecole Polytechnique, 17, rue Descartes, Paris 5
Geller, R.	CEN Grenoble, rue des Martyres, 38 Grenoble
Girard, J.P.	CEA, B.P. No.6, 92 Fontenay-aux-Roses

Hubert, P.L.	Association EURATOM-CEA, B.P. No.6, 92 Fontenay-aux-Roses
Jablon, C.J.	Laboratoire de Physique des Plasmas, Faculté des Sciences, 91 Orsay
Launois, D.	CEA, B.P. No.6, 92 Fontenay-aux-Roses
Maschke, E.K.	Association EURATOM-CEA, B.P. No.6, 92 Fontenay-aux-Roses
Pellat, R.	CEN/FAR, B.P. No.6, 92 Fontenay-aux-Roses
Rebut, P.H.	CEN/FAR, B.P. No.6, 92 Fontenay-aux-Roses
Renaud, C.	CEN/FAR, B.P. No.6, 92 Fontenay-aux-Roses
Soubbaramayer	CEN/FAR, B.P. No.6, 92 Fontenay-aux-Roses
Trocheris, M.G.	CEN/FAR, B.P. No.6, 92 Fontenay-aux-Roses
Vermeersch, H.	CEA, Centre d'Etudes de Limeil, B.P. No.27, 94 Villeneuve St. Georges
Watteau, J.P.	CEA, 29-33, rue de la Fédération, Paris 15

GERMANY, FEDERAL REPUBLIC OF

Biskamp, D.	Max-Planck-Institut für Plasmaphysik, 8046 Garching bei München
Bohn, W.L.	DFVLR-Institut für Plasmadynamik, 7 Stuttgart-80, Pfaffenwaldring 38
Conrads, J.P.F.	Institut für Plasmaphysik, Kernforschungsanlage Jülich GmbH, Postf. 365, 5170 Jülich
Darvas, J.	Kernforschungsanlage Jülich GmbH, Postf. 365, 5170 Jülich
Derfler, H.	Max-Planck-Institut für Plasmaphysik, 8046 Garching bei München
Dippel, K.H.	Institut für Plasmaphysik, Kernforschungsanlage Jülich GmbH, Postf. 365, 5170 Jülich
Dum, C.T.	Max-Planck-Institut für Plasmaphysik, 8046 Garching bei München
Eckhardt, D.	Max-Planck-Institut für Plasmaphysik, 8046 Garching bei München
Feneberg, W.	Max-Planck-Institut für Plasmaphysik, 8046 Garching bei München
Förster, S.	Institut für Reaktorentwicklung, Kernforschungsanlage Jülich GmbH, Postf. 365, 5170 Jülich

Gierke, G.O.J. von	Max-Planck-Institut für Plasmaphysik, 8046 Garching bei München
Grieger, G.	Max-Planck-Institut für Plasmaphysik, 8046 Garching bei München
Henkes, W.	Kernforschungszentrum, Weber-Str. 5, 7500 Karlsruhe
Herold, H.	Max-Planck-Institut für Plasmaphysik, 8046 Garching bei München
Hintz, E.A.K.	Institut für Plasmaphysik, Kernforschungsanlage Jülich GmbH, Postf. 365, 5170 Jülich
Jordan, H.L.	Institut für Plasmaphysik, Kernforschungsanlage Jülich GmbH, Postf. 365, 5170 Jülich
Keilhacker, M.M.K.	Max-Planck-Institut für Plasmaphysik, 8046 Garching bei München
Klingelhöfer, R.P.W.	Institut für Kernverfahrenstechnik, Kernforschungszentrum Karlsruhe, 7500 Karlsruhe
Knobloch, A.F.	Max-Planck-Institut für Plasmaphysik, 8046 Garching bei München
Köhler, W.H.	Institut für Kernverfahrenstechnik, Kernforschungszentrum Karlsruhe, 7500 Karlsruhe
Köppendörfer, W.	Max-Planck-Institut für Plasmaphysik, 8046 Garching bei München
Lehner, G.	Max-Planck-Institut für Plasmaphysik, 8046 Garching bei München
Neuhauser, J.	Max-Planck-Institut für Plasmaphysik, 8046 Garching bei München
Noll, P.C.	Kernforschungsanlage Jülich GmbH, 5170 Jülich
Ohlendorf, W.	Max-Planck-Institut für Plasmaphysik, 8046 Garching bei München
Pfirsch, D.	Max-Planck-Institut für Plasmaphysik, 8046 Garching bei München
Schlüter, J.	Institut für Plasmaphysik, Kernforschungsanlage Jülich GmbH, 5170 Jülich
Schmitter, K.H.	Max-Planck-Institut für Plasmaphysik, 8046 Garching bei München
Sigel, R.	Max-Planck-Institut für Plasmaphysik, 8046 Garching bei München

Tasso, H. Max-Planck-Institut für Plasmaphysik,
8046 Garching bei München

Waelbroeck, F.G. Institut für Plasmaphysik, Kernforschungsanlage Jülich GmbH,
5170 Jülich

Wipf, S.L. Max-Planck-Institut für Plasmaphysik,
8046 Garching bei München

Witkowski, S. Max-Planck-Institut für Plasmaphysik,
8046 Garching bei München

Wobig, H. Max-Planck-Institut für Plasmaphysik,
8046 Garching bei München

Wolf, G.H. Max-Planck-Institut für Plasmaphysik,
8046 Garching bei München

Zehrfeld, H.P. Max-Planck-Institut für Plasmaphysik,
8046 Garching bei München

Zwicker, H. Max-Planck-Institut für Plasmaphysik,
8046 Garching bei München

INDIA

Kaw, P.K. Physical Research Laboratory,
Navrangpura, Ahmedabad 9

Varma, R. Physical Research Laboratory,
Navrangpura, Ahmedabad 9

ISRAEL

Cuperman, S. Department of Physics and Astronomy,
University of Tel Aviv,
Tel Aviv

ITALY

Brunelli, B. CNEN Laboratorio Gas Ionizzati,
00044 Frascati, Rome

Enriques, L. CNEN, Viale Regina Margherita, Rome

Fontanesi, M. CNEN, Laboratorio di Fisica del Plasma, Università,
Via Celoria 16, Milan

Mazzucato, E. CNEN, Viale Regina Margherita, Rome

Segre, S.E. CNEN, Viale Regina Margherita, Rome

Sestero, A. CNEN, Laboratorio Plasma, Via E. Fermi,
Frascati, Rome

Toschi, R. CNEN, C.P. 65, Frascati

JAPAN

Fujita, J.	Institute of Plasma Physics, Nagoya University, Nagoya
Husimi, K.	Institute of Plasma Physics, Nagoya University, Nagoya
Ichimaru, S.	Department of Physics, University of Tokyo, Bunkyo-ku, Tokyo 113
Kiyama, S.	Electrotechnical Laboratory, Tanashi, Tokyo
Miyamoto, K.	Institute of Plasma Physics, Nagoya University, Nagoya
Nakai, S.	Department of Electrical Engineering, Osaka University, Suita, Osaka
Ogawa, K.	Electrotechnical Laboratory, Tanashi, Tokyo
Ohta, M.	Japan Atomic Energy Research Institute, Tokai-Mura, Ibaraki-ken
Takeda, T.	Japan Atomic Energy Research Institute, Tokai-Mura, Ibaraki-ken
Uchida, T.	Institute of Plasma Physics, Nagoya University, Nagoya
Uo, K.U.	Plasma Physics Laboratory, Kyoto University, Gokasho, Uji, Kyoto
Yamamoto, K.	Japan Atomic Energy Research Institute, 1-1 Shinbashi, Minato-ku, Tokyo 105
Yoshikawa, M.	Japan Atomic Energy Research Institute, Tokai-Mura, Ibaraki-ken

MEXICO

de la Fuente-Viallarreal, H.	Instituto Politécnico Nacional, Departamento de Ingeniería Nuclear, Zacatenco, México 14, D.F.
Martin, J.G.	Instituto Politécnico Nacional, Departamento de Ingeniería Nuclear, Zacatenco, Mexico 14, D.F.
Vazquez Reyna, M.	Comisión Nacional de Energía Nuclear, Av. Insurgentes Sur 1079, Mexico 18, D.F.

NETHERLANDS

Bobeldijk, C.	FOM-Instituut voor Plasma-Fysica, Rijnhuizen, Jutphaas
---------------	--

Braams, C.M.	FOM-Instituut voor Plasma-Fysica, Rijnhuizen, Jutphaas
Brandt, H.B.	FOM-Instituut voor Plasma-Fysica, Rijnhuizen, Jutphaas
Goedbloed, J.P.	FOM-Instituut voor Plasma-Fysica, Rijnhuizen, Jutphaas
Kistemaker, J.	FOM-Stichting Fundamenteel Onderzoek Materie, Kruislaan 407, Amsterdam
Kluiver, H. de	FOM-Instituut voor Plasma-Fysica, Rijnhuizen, Jutphaas
Laan, P.C.T. van der	FOM-Instituut voor Plasma-Fysica, Rijnhuizen, Jutphaas
Minardi, E.	FOM-Instituut voor Plasma-Fysica, Rijnhuizen, Jutphaas
Ornstein, L.T.M.	FOM-Instituut voor Plasma-Fysica, Rijnhuizen, Jutphaas
Rem, J.	FOM-Instituut voor Plasma-Fysica, Rijnhuizen, Jutphaas
Rietjens, L.H.Th.	Technische Hogeschool, Eindhoven
Schram, D.C.	FOM-Instituut voor Plasma-Fysica, Rijnhuizen, Jutphaas
Weenink, M.P.H.	FOM-Instituut voor Plasma-Fysica, Rijnhuizen, Jutphaas

PHILIPPINES

Roque, R.	Center of Energy, I.N.R.S. University of Quebec, C.P. 1020 Varennes, Quebec
-----------	--

ROMANIA

Popescu, I.M.	Institut de Physique Atomique, P.O. Box 35, Bucarest
---------------	--

SOUTH AFRICA

Cilliers, W.A.	University of Cape Town, Rondebosch, Cape Province
Hellberg, M.A.	Department of Physics, University of Natal, Durban
Jacobsen, R.A.	Atomic Energy Board, Private Bag 256, Pretoria

SWEDEN

Bergström, J.B.	Royal Institute of Technology, Division of Plasmaphysics and Fusion Research, S-10044 Stockholm 70
Hörnqvist, N.G.	FOA 4, Research Institute of National Defense, Lindegatan 89, S-10450 Stockholm 80
Lehnert, B.P.	Royal Institute of Technology, Division of Plasmaphysics and Fusion Research, S-10044 Stockholm 70

SWITZERLAND

- Berney, A.P. Physics Department, University of British Columbia,
Vancouver
- Hofmann, F. Centre de Recherches en Physique des Plasmas,
21, av. des Bains, 1007 Lausanne
- Weibel, E.S. Centre de Recherches en Physique des Plasmas,
21, av. des Bains, 1007 Lausanne

UNION OF SOVIET SOCIALIST REPUBLICS

- Akulina, Mrs. Dina K. P.N. Lebedev Institute of Physics of the USSR
Academy of Sciences, Moscow
- Cheverev, N.S. State Committee for Utilization of Atomic Energy,
Moscow
- Galeev, A.A. Institute of High Temperatures of the USSR,
Academy of Sciences, Moscow
- Georgievsky, A.V. Physico-Technical Institute of the Academy of Sciences
of the Ukrainian SSR, Kharkov
- Grebenshchikov, S.E. P.N. Lebedev Institute of Physics of the USSR
Academy of Sciences, Moscow
- Kadomtsev, B.B. I.V. Kurchatov Institute of Atomic Energy, Moscow
- Kovrizhnykh, L.M. P.N. Lebedev Institute of Physics of the USSR
Academy of Sciences, Moscow
- Lominadze, D.G. Institute of Physics of the Academy of Sciences of
the Georgian SSR, Tbilisi
- Romanovsky, M.K. I.V. Kurchatov Institute of Atomic Energy, Moscow
- Rudakov, L.I. I.V. Kurchatov Institute of Atomic Energy, Moscow
- Savenkov, A.M. I.V. Kurchatov Institute of Atomic Energy, Moscow
- Shafranov, V.D. I.V. Kurchatov Institute of Atomic Energy, Moscow
- Skrebtsov, G.P. A.F. Joffe Physico-Technical Institute of the USSR
Academy of Sciences, Leningrad
- Stepanov, K.N. Physico-Technical Institute of the Academy of Sciences
of the Ukrainian SSR, Kharkov
- Strelkov, V.S. I.V. Kurchatov Institute of Atomic Energy, Moscow
- Velikhov, E.P. I.V. Kurchatov Institute of Atomic Energy, Moscow
- Voitsenya, V.S. Physico-Technical Institute of the Academy of Sciences
of the Ukrainian SSR, Kharkov
- Volosov, V.I. Institute of Nuclear Physics, Siberian Department of the
USSR Academy of Sciences, Novosibirsk

UNITED KINGDOM

Bickerton, R. J.	UKAEA, Culham Laboratory, Abingdon, Berks
Blow, S.	UKAEA, Harwell, Didcot, Berks
Bodin, H. A. B.	UKAEA, Culham Laboratory, Abingdon, Berks
Dangor, A. E.	Physics Department, Imperial College, London, S. W. 7
Dellis, A. N.	UKAEA, Culham Laboratory, Abingdon, Berks
Gibson, A.	UKAEA, Culham Laboratory, Abingdon, Berks
Haines, M. G.	Physics Department, Imperial College, London, S. W. 7
Hamberger, S. M. H.	UKAEA, Culham Laboratory, Abingdon, Berks
Hancox, R.	UKAEA, Culham Laboratory, Abingdon, Berks
Jukes, J. D.	UKAEA, Culham Laboratory, Abingdon, Berks
Motz, H.	Department of Engineering Science, Oxford University, Oxford
Paul, J. W. M.	UKAEA, Culham Laboratory, Abingdon, Berks
Peacock, N. J.	UKAEA, Culham Laboratory, Abingdon, Berks
Phelps, A. D. R.	Physics Department, Imperial College, London, S. W. 7
Potter, D. E.	Physics Department, Imperial College, London, S. W. 7
Reynolds, P.	UKAEA, Culham Laboratory, Abingdon, Berks
Robinson, D. C.	UKAEA, Culham Laboratory, Abingdon, Berks
Stott, P. E.	UKAEA, Culham Laboratory, Abingdon, Berks
Stringer, T. E.	UKAEA, Culham Laboratory, Abingdon, Berks
Sweetman, D. R.	UKAEA, Culham Laboratory, Abingdon, Berks
Taylor, J. B.	UKAEA, Culham Laboratory, Abingdon, Berks
Thompson, E.	UKAEA, Culham Laboratory, Abingdon, Berks
Wooding, E. R.	Physics Department, Royal Holloway College (University of London), Englefield Green Surrey

UNITED STATES OF AMERICA

Ahlstrom, H. G.	University of Washington, 98105 Seattle, Wash.
Alexeff, I.	Oak Ridge National Laboratory, P.O. Box Y, 37830 Oak Ridge, Tenn.

Anderson, O.A.	Lawrence Radiation Laboratory, University of California, 94551 Livermore, Calif.
Andrews, M.L.	Wright State University, 45400 Dayton, Ohio
Ard, W.B.	Oak Ridge National Laboratory, 37830 Oak Ridge, Tenn.
Asmussen J., Jr.	Michigan State University, 48823 East Lansing, Mich.
Auer, P.L.	Laboratory of Plasma Studies, Cornell University, 14850 Ithaca, N. Y.
Baker, D.A.	Los Alamos Scientific Laboratory, P.O. Box 1663, 87544 Los Alamos, N.Mex.
Baker, W.L.	Air Force Weapons Laboratory, Kirtland Air Force Base, 87117 Kirtland, N.Mex.
Baldwin, D.E.	Lawrence Radiation Laboratory, University of California, 94551 Livermore, Calif.
Bateman, R.G.	Courant Institute, New York University, 251 Mercer St., 10012 New York, N.Y.
Baum, P.J.	IGPP, Department of Physics, University of California, 92502 Riverside, Calif.
Beasley, C.O., Jr.	Oak Ridge National Laboratory, 37830 Oak Ridge, Tenn.
Beckner, E.H.	Sandia Laboratory, 87115 Albuquerque, N.Mex.
Bekefi, G.	MIT, Room 20A-112, 02139 Cambridge, Mass.
Bennett, W. H.	North Carolina State University, Box 5342, 26706 Raleigh, N. C.
Berk, H.L.	Lawrence Radiation Laboratory, University of California, 94551 Livermore, Calif.
Bernstein, I. B.	Yale University, New Haven, Conn.
Bernstein, M.J.	The Aerospace Corporation, P.O. Box 95085, 90045 El Segundo, Calif.
Berry, L.A.	Oak Ridge National Laboratory, 37830 Oak Ridge, Tenn.
Bers, A.	MIT, 02139 Cambridge, Mass.
Bestgen, R.	US Air Force Rocket Propulsion Laboratory, US Air Force, Flowards, Calif.
Beyer, J.	Department of EE, University of Wisconsin, 53706 Madison, Wis.

Bhatnagar, V.P. Electron Physics Laboratory, University of Michigan,
3505 Elec. Eng. Bldg.,
48104 Ann Arbor, Mich.

Birdsall, C.K. Department of Elec. Eng, University of California,
Berkeley, Calif.

Bol, K. Plasma Physics Laboratory, Princeton University,
98540 Princeton, N.J.

Boris, J.P. Naval Research Laboratory, Overlook Av.,
22304 Washington, D.C.

Bostick, W.H. Stevens Institute of Technology,
07030 Hoboken, N.J.

Bottoms, P.J. Los Alamos Scientific Laboratory,
87544 Los Alamos, N.Mex.

Boyd, D.A. Physics Department, Stevens Institute of Technology,
97030 Hoboken, N.J.

Briggs, R.J. MIT, Mass. Ave.,
02139 Cambridge, Mass.

Burger, J.M. Public Service Electric and Gas Co., 80 Park Place,
07101 Newark, N.J.

Burkhardt, L. Los Alamos Scientific Laboratory, P.O. Box 1663,
87544 Los Alamos, N.Mex.

Burnett, S.C. Los Alamos Scientific Laboratory,
87544 Los Alamos, N.Mex.

Butler, J.W. Argonne National Laboratory, 9700 So. Cass Ave.,
60439 Argonne, Ill.

Cairns, E. Argonne National Laboratory, 9700 So. Cass Ave.,
60439 Argonne, Ill.

Callen, J.D. MIT, 02139 Cambridge, Mass.

Carbon, M.W. Nuclear Engineering Department, University of Wisconsin,
53706 Madison, Wis.

Carpenter, J.P. Los Alamos Scientific Laboratory,
87544 Los Alamos, N.Mex.

Chang, T.S. North Carolina State University and MIT,
62139 Cambridge, Mass.

Chen, F.F. University of California,
90024 Los Angeles, Calif.

Chen, Y.G. Plasma Laboratory, Columbia University,
520 W. Main St., New York, N.Y.

Cheng, D.Y. University of Santa Clara, Santa Clara, Calif.

Christofilos, N.C.	Lawrence Radiation Laboratory, 94551 Livermore, Calif.
Chu, T.K.	Princeton University, 08540 Princeton, N.J.
Clarke, J.G.	Oak Ridge National Laboratory, 37830 Oak Ridge, Tenn.
Coengsen, F.H.	Lawrence Radiation Laboratory, P.O. Box 808, 94551 Livermore, Calif.
Colchin, R.J.	Oak Ridge National Laboratory, 38730 Oak Ridge, Tenn.
Cole, F.T.	National Exceclator Laboratory, P.O. Box 500, 60510 Batavia, Ill.
Cook, L.G.	Esso Corporation Research, P.O. Box 45, 07036 Linden, N.Y.
Cooper, W.C.	Lawrence Radiation Laboratory, University of California, 94720 Berkeley, Calif.
Coppi, B.	MIT, 02139 Cambridge, Mass.
Crawford, F.W.	Institute for Plasma Research, Stanford University, 94305 Stanford, Calif.
Creutz, E.C.	National Science Foundation, 1800 G. St., N.W., 20550 Washington, D.C.
Curtis, J.A.	Aerospace Research Laboratory, W-P Air Force Base, Ohio
Damm, C.C.	Lawrence Radiation Laboratory, P.O. Box 808, 94720 Berkeley, Calif.
Dandl, R.A.	Oak Ridge National Laboratory, 37830 Oak Ridge, Tenn.
Dardis, J.G.	Office of Naval Research, 22217 Arlington, Va.
Davidson, R.W.C.	University of Maryland, 20742 College Park, Md.
Davis, M.C.	University of Arizona, 85771 Tuscon, Ariz.
Davis, W.D., IV	University of Maryland, 20742 College Park, Md.
Dawson, J.M.	Plasma Physics Laboratory, Princeton University, 08540 Princeton, N.J.
Dean, S.O.	Naval Research Laboratory, 20390 Washington, D.C.

Dewar, R.L.	Physics and Astronomy Department, University of Maryland, 20742 College Park, Md.
DiMarco, J.N.	Los Alamos Scientific Laboratory, 87544 Los Alamos, N. Mex.
Dixon, R.H.	Naval Research Laboratory, Code 7721, 20390 Washington, D.C.
Dobrot, D.R.	New York University, 251 Mercer St., 10012 New York, N.Y.
Doggett, W.	Physics Department North Carolina State University, 27607 Raleigh, N.C.
Dolan, T.J.	University of Missouri
Dory, R.A.	Oak Ridge National Laboratory, P.O. Box Y, 37830 Oak Ridge, Tenn.
Dove, W.F.	University of Maryland, 20742 College Park, Md.
Draley, J.E.	Argonne National Laboratory, 60439 Argonne, Ill.
Dreicer, H.	Los Alamos Scientific Laboratory, P.O. Box 663, 87544 Los Alamos, N. Mex.
Drummond, W.F.	The University of Texas at Austin, and Austin Research Associates, Inc., 78712 Austin, Tex.
Düchs, D.F.	Naval Research Laboratory, 20390 Washington, D.C.
Dunlap, J.L.	Oak Ridge National Laboratory, P.O. Box Y, 37830 Oak Ridge, Tenn.
Dupree, T.H.	MIT, 02139 Cambridge, Mass.
Eastlund, B.J.	US Atomic Energy Commission, 20545 Washington, D.C.
Ellis, R.A.	Plasma Physics Laboratory, Princeton University, 08540 Princeton, N.J.
Ellis, W.R.	Los Alamos Scientific Laboratory, University of California, 87544 Los Alamos, N.M.
Elton, R.C.	Naval Research Laboratory, Code 7720, 20390 Washington, D.C.
Emmert, G.A.	Department of Nuclear Engineering, University of Wisconsin, Engineering Research Building, 53706 Madison, Wis.

England, A.C.	Oak Ridge National Laboratory, P.O. Box Y, 37830 Oak Ridge, Tenn.
Epstein, R.J.	Argonne National Laboratory, 977 So. Cass Ave., 60515 Argonne, Ill.
Erickson, C.W.	Honeywell Corporate Research Center, 55343 Hopkins, Minn.
Estabrook, K.G.	Oak Ridge National Laboratory, 37830 Oak Ridge, Tenn.
Fader, W.J.	United Aircraft Research Laboratory, 06108 East Hartford, Conn.
Farr, W.M.	University of Arizona, 85721 Tuscon, Ariz.
Ferber, R.R.	Westinghouse Electric Corporation, 15112 East Pittsburgh, Pa.
Fessenden, T.J.	Lawrence Radiation Laboratory, P.O. Box 808, 94551 Livermore, Calif.
Fleischmann, H.H.	Department of Applied Physics, Cornell University, 14850 Ithaca, N.Y.
Forman, P.	Los Alamos Scientific Laboratory, University of California, 87544 Los Alamos, N.Mex.
Forsen, H.K.	Department of Nuclear Engineering, University of Wisconsin, 53706 Madison, Wis.
Forslund, D.W.	Los Alamos Scientific Laboratory, University of California, 87544 Los Alamos, N.Mex.
Fowler, T.K.	Lawrence Radiation Laboratory, P.O. Box 808, 94550 Livermore, Calif.
Freeman, J.R.	Sandia Laboratories, Div. 5241 Sandia Base, 87115 Albuquerque, N.Mex.
Freidberg, J.P.	Los Alamos Scientific Laboratory, 87544 Los Alamos, N.Mex.
Freiwald, D.A.	Sandia Laboratories, 87115 Albuquerque, N.Mex.
Fried, B.D.	University of California, 90024 Los Angeles, Calif.
Friedrich, O.M., Jr.	Department of Electrical Engineering, University of Texas at Austin, 78712 Austin, Tex.

Frost, P.R.T.	Argonne National Laboratory, 9700 So. Cass Ave., 60439 Argonne, Ill.
Furth, H.P.	Princeton University, 08540 Princeton, N.J.
Futch, A.H., Jr.	Lawrence Radiation Laboratory, University of California, P.O. Box 808, 94550 Livermore, Calif.
Gajewski, R.	MIT, 02139 Cambridge, Mass.
Gary, S.P.	College of William & Mary, 23185 Williamsburg, Va.
Gerardo, J.B.	Sandia Laboratories, 87115 Albuquerque, N. Mex.
Gerber, R.A.	Sandia Laboratories, 87115 Albuquerque, N. Mex.
Gerwin, R.A.	Los Alamos Scientific Laboratory, 87544 Los Alamos, N. Mex.
Getty, W.D.	Department of Electrical Engineering, University of Michigan, 48104 Ann Arbor, Mich.
Goeler, S. von	Plasma Physics Laboratory, Princeton University, 08540 Princeton, N.J.
Goldman, L.M.	General Electric Co. Corporate Research and Development, P.O. Box 8, Schenectady, N.Y.
Gorman, J.B.	Plasma Physics Laboratory, Princeton University, P.O. Box 451, 08540 Princeton, N.J.
Gottlieb, M.B.	Plasma Physics Laboratory, Princeton University, P.O. Box 451, 08540 Princeton, N.J.
Gouch, W.C.	USAEC, Division of Research, 20545 Washington, D.C.
Gould, R.W.	USAEC, 20545 Washington, D.C.
Grad, H.	Courant Institute of Mathematical Sciences, New York University, 251 Mercer St., 87544 New York, N.Y.
Graves, G.A.	Los Alamos Scientific Laboratory, 87544 Los Alamos, N.M.
Gray, E.P.	Applied Physics Laboratory, John Hopkins University, 8881 Georgia Ave., 20904 Silver Spring, Md.
Greene, D.G.S.	Towson State College, Baltimore, Md.

Griem, H.R.	University of Maryland, 20742 College Park, Md.
Gross, R.A.	Columbia University, 10027 New York, N.Y.
Grove, D.J.	Plasma Physics Laboratory, Princeton University, P.O. Box 451, 08540 Princeton, N.J.
Gruen, D.M.	Argonne National Laboratory, 9700 So. Cass Ave., 60430 Argonne, Ill.,
Guest, G.E.	Oak Ridge National Laboratory, P.O. Box Y, 37830 Oak Ridge, Tenn.
Gullickson, R.L.	Air Force Weapons Laboratory, Kirtland AFB, 87117 Kirtland, N.Mex.
Haberstich, A.	Los Alamos Scientific Laboratory, University of California, 87501 Los Alamos, N.Mex.
Hagler, M.	Department of Electrical Engineering, Texas Technical University, 79409 Lubbock, Tex.
Hall, L.S.	Department of Applied Sciences, University of California, 94550 Livermore, Calif.
Hammel, J.E.	Los Alamos Scientific Laboratory, University of California, 87501 Los Alamos, N.Mex.
Hammer, D.A.	Naval Research Laboratory, 20390 Washington, D.C.
Harder, C.R.	Los Alamos Scientific Laboratory, University of California, 87544 Los Alamos, N.Mex.
Harrison, H.	AEC/NASA Space Nuclear Systems Office, USAEC, 20505 Washington, D.C.
Hartman, C.W.	Lawrence Radiation Laboratory, University of California, 94551 Livermore, Calif.
Harvey, R.J.	Stevens Institute of Technology, Castle Point Station, 07030 Hoboken, N.J.
Haste, G.R.	Oak Ridge National Laboratory, 37830 Oak Ridge, Tenn.
Hatch, A.J.	Argonne National Laboratory, 60439 Argonne, Ill.

Haught, A.F. United Aircraft Research Laboratories,
400 Main St.,
06108 East Hartford, Conn.

Hendel, H.W. Plasma Physics Laboratory, Princeton University,
08540 Princeton, N.J.

Henderson, D.B. Los Alamos Scientific Laboratory, P.O. Box 1663,
87544 Los Alamos, N.M.

Hendricks, C.D. Department of Electrical Engineering,
University of Illinois,
61801 Urbana, Ill.

Hickok, R.L., Jr. Plasma Physics Laboratory, Princeton University,
08540 Princeton, N.J.

Hieronymus, J. Department of Applied Physics, Cornell University,
14850 Ithaca, N. Y.

Higgins, T.J. University of Wisconsin,
53703 Madison, Wis.

Hinnov, E. Plasma Physics Laboratory, Princeton University,
08540 Princeton, N.J.

Hinton, F.L. University of Texas,
78712 Austin, Tex.

Hirose, A. Oak Ridge National Laboratory,
37830 Oak Ridge, Tenn.

Hirsch, R.L. USAEC, 20545 Washington, D.C.

Hiskes, J.R. Lawrence Radiation Laboratory, P.O. Box 808,
University of California,
94551 Livermore, Calif.

Hogan, J.T. Oak Ridge National Laboratory,
37830 Oak Ridge, Tenn.

Hohl, F. NASA, Langley Research Center,
23365 Hampton, Va.

Hooper, E.B., Jr. Lawrence Radiation Laboratory,
University of California,
94551 Livermore, Calif.

Horton, C.W. University of Texas,
78712 Austin, Tex.

Hosea, J.C. Plasma Physics Laboratory, Princeton University,
08540 Princeton, N.J.

Hurwitz, H., Jr. General Electric Co. Corporate Research and
Development,
12301 Schenectady, N.Y.

Ingraham, J.C.	Los Alamos Scientific Laboratory, P.O. Box 1663, 87544 Los Alamos, N.Mex.
Jahoda, F.C.	Los Alamos Scientific Laboratory, P.O. Box 1663, 87544 Los Alamos, N.Mex.
Jassby, D.L.	University of California, 90024 Los Angeles, Calif.
Jensen, T.H.	Gulf General Atomic, P.O. Box 608, 92112 San Diego, Calif.
Jobes, F.C.	Plasma Physics Laboratory, Princeton University, 08540 Princeton, N.J.
Johnson, L.C.	Princeton University, 08540 Princeton, N.J.
Kalman, G.	Boston College, 02167 Chestnut Hill, Mass.
Kaminsky, M.S.	Argonne National Laboratory, 9700 So. Cass Ave., 60430 Argonne, Ill.
Kammash, T.	University of Michigan 48105 Ann Arbor, Mich.
Kane, J.A.	USAEC, 20545 Washington, D.C.
Kaufmann, M.	Los Alamos Scientific Laboratory, University of California, 87544 Los Alamos, N.Mex.
Kelley, G.	Oak Ridge National Laboratory, 37830 Oak Ridge, Tenn.
Kerns, J.R.	AFWL, Kirtland Air Force Base, 87117 Kirtland, N.Mex.
Kerst, D.	Department of Physics, University of Wisconsin, 53706 Madison, Wis.
Killeen, J.	Lawrence Radiation Laboratory, University of California, 94550 Livermore, Calif.
Kolb, A.	Maxwell Laboratories, Inc., 9244 Balboa Ave., 92123 San Diego, Calif.
Kribel, R.E.	Drake University, 50311 Des Moines, Iowa
Kristiansen, M.	Department of Electrical Engineering, Texas Technical University, 79409 Lubbock, Tex.

Kulsrud, R.M.	Princeton University, P.O. Box 451, 08540 Princeton, N.J.
Kunkel, W.B.	Lawrence Radiation Laboratory, University of California, 94720 Berkeley, Calif.
Kuswa, G.W.	Sandia Laboratories, P.O. Box 5800, 87115 Albuquerque, N. Mex.
Lamborn, B.N.A.	Department of Physics, Florida Atlantic University, 33432 Boca Raton, Fla.
Lashinsky, H.	Institute for Fluid Dynamics and Applied Mathematics, University of Maryland, 20740 College Park, Md.
Laverick, C.	Argonne National Laboratory, 9700 So. Cass Ave., 60439 Argonne, Ill.
Lazar, N.H.	Oak Ridge National Laboratory, 37830 Oak Ridge, Tenn.
Lee, E.P.	Lawrence Radiation Laboratory, University of California, 94550 Livermore, Calif.
Lee, J.F.	Vanderbilt University, 37203 Nashville, Tenn.
Lee, R.E.	Naval Research Laboratory, 20390 Washington, D.C.
Leonard, Ellen M.	University of Michigan, 48104 Ann Arbor, Mich.
Leonard, P.R., Jr.	Battelle Northwest, P.O. Box 999, 99352 Richland, Wash.
Leonard, T.	University of Michigan, 48104 Ann Arbor, Mich.
Levine, M.	Air Force Cambridge Research Laboratory, 01730 Hanscom Field, Mass.
Lichtenberg, A.J.	Department of Electrical Engineering, University of California, 94720 Berkeley, Calif.
Lidsky, L.M.	MIT, 02139 Cambridge, Mass.
Linnebur, J.	Department of Nuclear Engineering, University of Michigan, 48104 Ann Arbor, Mich.
Lipinski, W.C.	Argonne National Laboratory, 9700 So. Cass Ave., 60439 Argonne, Ill.

Little, P.F.	Physics Department, University of Texas, 78712 Austin, Tex.
Liu, C.S.	University of California, (UCLA), 90024 Los Angeles, Calif.
Lohr, J.M.	University of Wisconsin, 53706 Madison, Wis.
Long, H.M.	Oak Ridge National Laboratory, 37830 Oak Ridge, Tenn.
Lonngren, K.E.	University of Iowa, 52240 Iowa City
Love, J.D.	Department of Physics, University of California, P.O. Box 109, 92037 San Diego, Calif.
Lovelace, R.V.E.	Naval Research Laboratory, 20390 Washington, D.C.
Lubell, M.S.	Oak Ridge National Laboratory, P.O. Box Y, 37830 Oak Ridge, Tenn.
Luce, J.S.	Berkeley Analytical Sciences Service, Inc. 1434 C North Main St., Walnut Creek, Calif.
Lyon, J.F.	Oak Ridge National Laboratory, P.O. Box Y, 37830 Oak Ridge, Tenn.
Ma, B.M.	Department of Nuclear Engineering, Iowa State University of Science and Technology, 261 Sweeney Hall 50010 Ames, Iowa
MacKenzie, K.R.	University of California, 90024 Los Angeles, Calif.
MacMahon, A.	Center for Plasma Physics and Thermonuclear Research, University of Texas, 78712 Austin, Tex.
Maroni, V.A.	Argonne National Laboratory, 9700 So. Cass Ave., 60430 Argonne, Ill.
Marshall, J.	Los Alamos Scientific Laboratory, 87544 Los Alamos, N. Mex.
Marshall, L.C.	Department of Technology, Southern Illinois University, 62901 Carbondale, Ill.
Martin, R.L.	Argonne National Laboratory, 60439 Argonne, Ill.
Mather, J.W.	Los Alamos Scientific Laboratory, University of California, 87544 Los Alamos, N. Mex.

Mawardi, O.K. Case Western Reserve University, University Circle,
44106 Cleveland, Ohio

Mayer, R.J. Case Western Reserve University, University Circle,
44106 Cleveland, Ohio

McLane, C.K. Department of Aerospace Engineering Sciences,
University of Colorado,
80302 Boulder, Colo.

McPherson, D.A. Georgia Institute of Technology,
School of Electrical Engineering,
30332 Atlanta, Ga.

Meade, D.M. Department of Physics, University of Wisconsin,
53706 Madison, Wis.

Meier, H. Oak Ridge National Laboratory,
37830 Oak Ridge, Tenn.

Meservey, E. Princeton University,
08540 Princeton, N.J.

Meyer, R.E. University of Wisconsin,
53706 Madison, Wis.

Miley, G.H. 221 NEL, University of Illinois,
61801 Urbana, Ill.

Miller, B. US Atomic Energy Commission,
20545 Washington, D.C.

Mills, R.G. Plasma Physics Laboratory, Princeton University,
08540 Princeton, N.J.

Mischke, G.J. Office of Naval Research, Power Program Code 473,
22217 Arlington, Va.

Moir, R.W. Lawrence Radiation Laboratory, P.O. Box 808,
University of California,
94550 Livermore, Calif.

Montgomery, D.C. Department of Physics and Astronomy,
University of Iowa,
52240 Iowa City, Iowa

Morgan, O.B., Jr. Oak Ridge National Laboratory,
37830 Oak Ridge, Tenn.

Morikawa, G.K. Courant Institute of Mathematical Sciences,
New York University, 251 Mercer St.,
10012 New York, N.Y.

Morse, R.L. Los Alamos Scientific Laboratory, P.O. Box 1663,
87544 Los Alamos, N.Mex.

Motz, H.T. Los Alamos Scientific Laboratory, P.O. Box 1663,
87544 Los Alamos, N.Mex.

Nardi, V.	Stevens Institute of Technology, 07030 Hoboken, N.J.
Nation, J.A.	Laboratory of Plasma Studies, Cornell University, 14850 Ithaca, N. Y.
Neidigh, R. V.	Oak Ridge National Laboratory, 37830 Oak Ridge, Tenn.
Nevitt, M. V.	Argonne National Laboratory, 9700 So. Cass. Ave., 60430 Argonne, Ill.
Nexsen, W.E.	Lawrence Radiation Laboratory, University of California, 94550 Livermore, Calif.
Nielsen, C.E.	Department of Physics, Ohio State University, 174 W. 18th Ave., 43210 Columbus, Ohio
Oakes, M.E.	University of Texas, 78712 Austin, Tex.
Oberman, C.	Plasma Physics Laboratory, Princeton University, 08540 Princeton, N.J.
Ohkawa, T.	Gulf General Atomic Co., P.O. Box 608, 92110 San Diego, Calif.
Okabayashi, M.	Plasma Physics Laboratory, Princeton University, 08540 Princeton, N.J.
O'Leary, T. F.	US Atomic Energy Commission, 20545 Washington, D.C.
Olson, C.	Sandia Laboratories, 87115 Albuquerque, N. Mex.
O'Neil, T.M.	University of California, San Diego, 92037 La Jolla, Calif.
Osher, J.E.	Lawrence Radiation Laboratory, P.O. Box 808, University of California, 94551 Livermore, Calif.
Palmagesso, P. J.	Goddard Space Flight Center, 20771 Greenbelt, Md.
Papadopoulos, K.	Naval Research Laboratory, 20390 Washington, D.C.
Parker, R.R.	MIT, 02139 Cambridge, Mass.
Pearlstein, L.D.	Lawrence Radiation Laboratory, University of California, 94550 Livermore, Calif.
Perkins, F.W., Jr.	Plasma Physics Laboratory, Princeton University, 08540 Princeton, N.J.

Persiani, P.J. Argonne National Laboratory,
9700 So. Cass Ave.,
60439 Argonne, Ill.

Petrick, M. Argonne National Laboratory,
9700 So. Cass Ave.,
60430 Argonne, Ill.

Petrie, B.R., Jr. Technical Analysis and Advisory Group, Pentagon,
20350 Washington, D.C.

Petrie, T.W. University of Illinois,
61801 Urbana, Ill.

Phillips, J.A. Los Alamos Scientific Laboratory,
University of California,
87544 Los Alamos, N.M.

Politzer, P.A. MIT, 02139 Cambridge, Mass.

Pollack, H.C. General Electric Company,
Corporate Research and Development,
12301 Schenectady, N.Y.

Porkolab, M. Plasma Physics Laboratory, Princeton University,
08540 Princeton, N.J.

Porter, G.D. Lawrence Radiation Laboratory,
University of California,
94550 Livermore, Calif.

Post, R.F. Lawrence Radiation Laboratory,
University of California,
94550 Livermore, Calif.

Postma, H. Oak Ridge National Laboratory, P.O. Box X,
37830 Oak Ridge, Tenn.

Prior, W.J. Stevens Institute of Technology,
Fifth and River Sts,
07030 Hoboken, N.J.

Pyle, R.V. Lawrence Radiation Laboratory,
University of California,
94705 Berkeley, Calif.

Quinn, W.E. Los Alamos Scientific Laboratory, P.O. Box 1664,
University of California,
87544 Los Alamos, N.Mex.

Raether, M.J. University of Illinois,
61801 Urbana, Ill.

Ribe, R.L. Los Alamos Scientific Laboratory, P.O. Box 1664,
University of California,
87544 Los Alamos, N.Mex.

Roberts, M. Oak Ridge National Laboratory,
37830 Oak Ridge, Tenn.

Robertson, H.S.	University of Miami, 33155 Coral Gables, Fla.
Robson, A.E.	Center for Plasma Physics, University of Texas, 78712 Austin, Tex.
Rose, D.J.	Oak Ridge National Laboratory, P.O. Box X, 37830 Oak Ridge, Tenn.
Rosenbluth, M.N.	Institute of Advanced Study, Princeton University, 08540 Princeton, N.J.
Rostenbach, R.E.	National Science Foundation, 20550 Washington, D.C.
Rostoker, N.	Cornell University, 14850 Ithaca, N.Y.
Roth, J.R.	NASA Lewis Research Center, Mail Stop 301-1, 44135 Cleveland, Ohio
Rutherford, P.H.	Plasma Physics Laboratory, Princeton University, 08540 Princeton, N.J.
Sahlin, H.L.	Lawrence Radiation Laboratory, University of California, 94550 Livermore, Calif.
Sakanaka, A.	Courant Institute of Mathematical Sciences, New York University, 251 Mercer St., 10012 New York, N.Y.
Samaras, D.G.	Air Force Office of Scientific Research, 1400 Wilson Blvd., 22209 Arlington, Va.
Sawyer, G.A.	Los Alamos Scientific Laboratory, University of California, 87544 Los Alamos, N.Mex.
Scharer, J.E.	University of Wisconsin, 53706 Madison, Wis.
Schmidt, G.	Department of Physics, Stevens Institute of Technology, 07030 Hoboken, N.J.
Schmidt, J.A.	Plasma Physics Laboratory, Princeton University, 08540 Princeton, N.J.
Schwirzke, F.R.	Naval Postgraduate School, 93940 Monterey, Calif.
Seidl, M.	Stevens Institute of Technology, Castle Point Station, 07030 Hoboken, N.J.
Self, S.A.	Institute for Plasma Research, Stanford University, 94305 Stanford, Calif.
Sen, A.	University of Tennessee, 37916 Knoxville, Tenn.

Shelby, C.F. Argonne National Laboratory,
9700 So. Cass Ave.,
60439 Argonne, Ill.
DePaul University,
1215 W. Fullerton Ave.,
60614 Chicago, Ill.

Shen, M.C. University of Wisconsin,
53706 Madison, Wis.

Sherwood, A.R. Los Alamos Scientific Laboratory, P.O. Box 1663,
87544 Los Alamos, N.M.

Shohet, J.L. Department of Electrical Engineering,
University of Wisconsin,
53706 Madison, Wis.

Siambis, J.G. Carnegie Institute of Technology,
Carnegie-Mellon University,
15213 Pittsburgh, Pa.

Siemon, R.E. Los Alamos Scientific Laboratory,
University of California,
87544 Los Alamos, N.Mex.

Sigmar, D.J. Research Laboratory of Electronics, MIT,
02139 Cambridge, Mass.

Simon, A. Department of Mechanics and Aero-Sciences,
University of Rochester,
14627 Rochester, N. Y.

Simonen, T.C. Lawrence Radiation Laboratory, P.O. Box 808,
University of California,
94550 Livermore, Calif.

Sinclair, R.M. National Science Foundation,
20550 Washington, D.C.

Sinnis, J. Plasma Physics Laboratory, Princeton University,
08540 Princeton, N.J.

Skiles, J.J. Department of Electrical Engineering,
University of Wisconsin,
53706 Madison, Wis.

Sloan, M.L. Austin Research Associates, Inc.,
600 W. 28th St.,
78705 Austin, Tex.

Smith, D.F. High Altitude Observatory,
80302 Boulder, Colo.

Smith, D.R. Sandia Laboratories, P.O. Box 5800,
87115 Albuquerque, N. Mex.

Snell, A.H. Oak Ridge National Laboratory, P.O. Box X,
37830 Oak Ridge, Tenn.

Soper, G.	US Air Force WPAFB, 45433 Ohio
Sprott, J.C.	Oak Ridge National Laboratory, P.O. Box Y, 37830 Oak Ridge, Tenn.
Steiner, D.	Oak Ridge National Laboratory, 37830 Oak Ridge, Tenn.
Stenzel, R.L.	University of California, 90024 Los Angeles, Calif.
Stewart, L.D.	Oak Ridge National Laboratory, 37830 Oak Ridge, Tenn.
Stix, T.H.	Princeton University, 08540 Princeton, N.J.
Stodiek, W.	Princeton University, 08540 Princeton, N.J.
Stone, A.M.	Applied Physics Laboratory, Johns Hopkins University, 8621 Georgia Ave., 20910 Silver Spring, Md.
Strauss, H.R.	University of Texas, 78712 Austin, Tex.
Sudan, R.N.	Naval Research Laboratory, Department of Applied Physics, Cornell University, Clarke Hall, 14850 Ithaca, N. Y.
Swanson, D.G.	Department of Electrical Engineering, University of Texas, 78712 Austin, Tex.
Symon, K.R.	University of Wisconsin, 53706 Madison, Wis.
Tamano, T.T.	Gulf General Atomic Corp., P.O. Box 608, 92110 San Diego, Calif.
Taschek, R.F.	Los Alamos Scientific Laboratory, University of California, 87544 Los Alamos, N. Mex.
Taylor, R.J.	MIT, 02139 Cambridge, Mass.
Teofilo, V.L.	State University of New York Maritime College, 10012 New York, N. Y.
Thomas, K.S.	Los Alamos Scientific Laboratory, University of California, P.O. Box 1663, 87544 Los Alamos, Calif.
Thomassen, K.I.	MIT, 20 B-120, 02139 Cambridge, Mass.

Thompson, J.R. Austin Research Associates, Inc.,
600 W. 28th St.,
87805 Austin, Tex.

Thompson, W.B. Department of Physics, University of California, San Diego,
92307 La Jolla, Calif.

Tidman, D.A. University of Maryland,
20742 College Park, Md.

Toepfer, A.J. Sandia Laboratories, Org. 5341, Sandia Base,
87109 Albuquerque, N.Mex.

Trivelpiece, A.W. Department of Physics, University of Maryland,
20742 College Park, Md.

Tuck, J.L. Los Alamos Scientific Laboratory,
University of California, P.O. Box 1663,
87544 Los Alamos, N.Mex.

Vlases, G.C. University of Washington,
98105 Seattle, Wash.

Waniek, R.W. Advanced Kinetics Inc.,
1231 Victoria St.,
92627 Costa Mesa, Calif.

Ware, A.A. University of Texas,
78731 Austin, Tex.

Ware, K.D. Los Alamos Scientific Laboratory,
University of California,
87544 Los Alamos, N.Mex.

Weitzner, H. Institute of Mathematical Sciences,
New York University,
251 Mercer St.,
10012 New York, N.Y.

Wells, D.R. University of Miami,
33124 Coral Gables, Fla.

Wharton, C.B. Laboratory of Plasma Studies, Cornell University,
14850 Ithaca, N.Y.

Williams, A.H. Los Alamos Scientific Laboratory,
University of California,
87544 Los Alamos, N.Mex.

Winsor, N.K. Plasma Physics Laboratory, Princeton University,
08540 Princeton, N.J.

Wong, H.V. University of Texas,
78712 Austin, Tex.

Woo, J.C. United Aircraft Research Laboratories,
06108 East Hartford, Conn.

Wright, T.P.	Sandia Laboratories, 87115 Albuquerque, N.Mex.
Yevick, G.J.	Stevens Institute of Technology, 07030 Hoboken, N.J.
Yoshikawa, S.	Plasma Physics Laboratory, Princeton University, 08540 Princeton, N.J.
Yu, M.Y.	University of Michigan, 48104 Ann Arbor, Mich.
Zimmermann, E.L.	Los Alamos Scientific Laboratory, University of California, 87544 Los Alamos, N.M.

ORGANIZATIONS

CCE

Cannobio, E.	Association EUR-CEA, CEN Grenoble, France
Fairclough, C.G.	CCE, 200, rue de la Loi, 1040 Brussels, Belgium
Lafleur, C.	CCE, 200, rue de la Loi, 1040 Brussels, Belgium
Linhart, J.G.	Laboratorio Gas Ionizzati, Frascati, Rome, Italy
Maisonnier, D.J.C.	Laboratorio Gas Ionizzati, Frascati, Rome, Italy
Palumbo, D.	CCE, 200, rue de la Loi, 1040 Brussels, Belgium
Poffé, J.P.	Association EUR-CEA, CEN Fontenay-aux-Roses, B.P. No.6, 92 Fontenay-aux-Roses, France

IAEA

Finkelstein, A.	IAEA, Kärntner Ring 11, 1010 Vienna, Austria
Seligman, H.	IAEA, Kärntner Ring 11, 1010 Vienna, Austria

IUPAP

Brown, S.C.	International Commission on Plasma Physics, MIT, 02139 Cambridge, Mass.
-------------	--

AUTHOR INDEX

Roman numerals are volume numbers. Arabic numerals underlined refer to the first page of a paper. Other Arabic numerals refer to a contribution to the discussions.

- Adam, J. C. : II 539
 Agafonov, V. I. : I 573
 Ahlstrom, H. G. : I 673
 Akiyama, R. : III 169
 Akulina, D. K. : III 21
 Aldcroft, D. A. : II 37
 Alexeff, I. : II 112, 221, 233
 Altyntsev, A. T. : II 309
 Anderson, D. V. : I 137
 Anderson, O. A. : I 103
 Andrews, M. L. : I 169
 Andryukhina, E. D. : III 21
 Anisimov, A. I. : III 543
 Ard, W. B. : II 619
 Arkhipenko, V. I. : III 525
 Artemenkov, L. I. : I 359
 Artsimovich, L. A. : I 443
 Aubert, A. E. : III 513
 Auer, P. : II 25
- Babykin, M. V. : I 635
 Baiborodov, Yu. T. : II 647
 Bakai, A. S. : II 113
 Baker, D. : I 335
 Baker, D. A. : I 203
 Baldwin, D. E. : II 735
 Baratov, D. G. : I 287
 Barnett, C. F. : I 347
 Barr, W. L. : III 315
 Beasley, C. O., Jr. : II 735
 Beaulieu, J. : III 251
 Becker, G. : I 277
 Beckner, E. H. : I 654
 Belikov, V. S. : III 411
 Belitz, H. J. : III 179
 Belyaeva, I. F. : I 573
 Benford, G. A. : I 137
 Berezhetsky, M. S. : III 49
 Berezin, A. B. : II 99; III 525
 Berezin, A. K. : II 113
 Berezina, G. P. : II 113
 Bergström, J. : I 59
- Berk, H. L. : II 735, 755
 Berkner, K. H. : II 707
 Bernard, A. : I 553
 Bernstein, M. J. : I 533, 572, 633
 Bernstein, W. : II 55
 Berry, L. A. : II 221
 Bers, A. : II 247
 Besshaposhnikov, A. A. : I 183
 Bickerton, R. J. : III 375, 409, 619
 Birdsall, D. H. : I 103
 Biskamp, D. : II 265, 291
 Blanken, R. A. : II 619
 Blow, S. : III 445
 Bobeldijk, C. : II 425
 Bobin, J. L. : I 657, 672
 Bocharov, V. N. : III 3
 Bodin, H. A. B. : I 216, 225,
 249, 265; II 423; III 200, 214
 Bogen, P. : III 277
 Bohn, Th. : III 469
 Bol, K. : I 465
 Bolotin, L. I. : II 113
 Bolton, R. A. E. : III 79
 Booth, N. : I 335
 Borgwaldt, H. : III 457
 Borisenko, A. G. : II 141
 Bortnikov, A. V. : II 663
 Bostick, W. H. : I 535, 672
 Bottiglioni, F. : II 585
 Bottoms, P. J. : I 561
 Boujot, J. P. : I 425
 Bowers, E. C. : II 393
 Breizman, B. N. : II 309
 Brettschneider, M. : I 137
 Breun, R. A. : I 3
 Brevnov, N. N. : II 663
 Brunelli, B. : I 572
 Büchl, K. : I 645
 Budnikov, V. N. : III 525
 Burchenko, P. Ya. : III 119
 Burdonsky, I. N. : I 601
 Bureš, M. : I 59

- Burkhardt, L.C.: I 203
 Burnett, S.C.: III 201
 Butenko, V.K.: I 359
 Butov, I.Ya.: I 183
 Butt, E.P.: I 225
- Callen, J.: II 451
 Canobbio, E.: III 491
 Cap, F.F.: II 219
 Carlson, G.A.: III 329
 Carpenter, J.P.: I 561
 Cavallo, A.J.: I 3
 Cesari, G.: I 553
 Chechkin, V.V.: III 573
 Chen, F.F.: I 335, 343, 686;
 III 61
 Chen, Y.G.: III 241
 Chkuaseli, Z.D.: I 183
 Chodura, R.: II 265; III 265
 Christofilos, N.C.: I 119;
 II 357
 Chu, C.K.: III 241
 Chu, T.K.: I 325; II 111
 Clarke, J.F.: I 347
 Coensgen, F.H.: II 721, 733
 Colchin, R.J.: II 619, 733
 Colé, H.C.: III 393
 Condit, W.C. Jr.: I 119
 Conrads, J.P.F.: I 533
 Cooper, W.S.: II 707
 Coppi, B.: I 25, 357, 449, 480;
 II 247, 449, 451, 477; III 130, 409
 Cordey, J.G.: II 689; III 353
 Coroniti, F.V.: II 55
 Coudeville, A.: I 553
 Coutant, J.: II 585
 Craig, A.D.: III 251
 Crow, J.E.: I 225
 Cummins, W.F.: II 721
- Dagazian, R.: II 451
 Damm, C.C.: II 707, 718
 Dandl, R.A.: II 607, 617
 Dangor, A.E.: I 621
 Daughney, C.C.: III 251
 Davis, R.C.: I 347
 Davis, W.D.: III 289
 Davitian, H.: I 169
 Dawson, J.M.: I 673, 686;
 II 393
 De Groot, B.: II 67
 De Kluiver, H.: II 67
- De La Fuente, H.V.: I 3
 Dellis, A.N.: I 25, 85
 De Mascureau, J.: I 553
 Demidov, B.A.: II 3
 Demirkhanov, R.A.: I 287
 De Pretis, M.: II 595
 Derfler, H.: III 524
 De Silva, A.W.: III 289
 Dietz, K.J.: III 277
 Diky, A.G.: III 151
 Dimarco, J.N.: I 203
 Dimock, D.: I 451
 Dippel, K.H.: III 277
 Dory, R.A.: I 347, 357
 Dove, W.F.: III 289
 Drake, J.R.: I 3
 Dreicer, H.: I 58, 449
 Drummond, W.E.: II 167, 219
 Dubovoy, L.V.: II 99
 Düchs, D.F.: I 369
 Dudley, J.M.: II 221
 Dum, C.T.: II 25
 Dunlap, J.L.: II 619
 Dupree, T.: II 247
 Dushin, L.A.: III 131
 Dyachenko, V.F.: I 573
- Eason, H.O.: II 607
 Eckhartt, D.: I 451
 Edmonds, P.H.: I 347;
 II 607
 Efferson, K.R.: III 433
 Egorov, A.M.: II 113
 Ehlers, K.W.: II 707
 Eidmann, K.: I 645
 Ellis, W.R.: III 201
 El-Nadi, A.: II 628
 England, A.C.: II 607
 Erokhin, N.S.: II 113, 195
 Eskov, A.G.: II 309
 Eslabrook, K.G.: II 221
 Eubank, H.: I 451, 465
 Evrard, P.: II 595
- Fainberg, Ya.B.: II 113, 195
 Fanchenko, S.D.: II 3
 Farr, W.M.: II 735
 Fedorov, V.I.: III 525
 Fedyanin, O.I.: III 21
 Fessenden, T.J.: I 119
 Filimonova, E.A.: II 679
 Filippov, N.V.: I 573

- Filippova, T.I.: I 573
 Finlayson, V.A.: II 721
 Fleischmann, H.H.: I 169
 Floux, F.: I 657
 Fois, M.: II 585
 Fomin, I.P.: III 131
 Forman, P.R.: I 203
 Forsen, H.K.: I 3, 347;
 III 627
 Forslund, D.: II 55
 Förster, S.: III 469
 Fowler, T.K.: III 613
 Fraas, A.P.: III 433
 Freeman, R.: I 27
 Freidberg, J.P.: III 215
 Freis, R.P.: III 315
 Fried, B.D.: I 398, 571, 633;
 II 55, 291; III 311
 Frieman, E.A.: I 495
 Fujiwara, M.: III 93
 Fünfer, E.: III 189
 Furth, H.P.: I 369, 397
 II 450, 553; III 432
 Futch, A.H.: II 706, 707
- Gajewski, R.: II 451, 527
 Galeev, A.A.: I 481, 493; II 381
 Galushkin, Yu.I.: II 407
 Gauster, W.F.: III 433
 Geller, R.: II 631
 Georgievsky, A.V.: III 107, 131
 Gervids, V.I.: II 407
 Gibson, A.: I 58, 450; II 381;
 III 48, 161, 214, 351, 375
 von Gierke, G.O.J.: I 58, 423;
 II 382
 Gilleland, J.R.: I 15
 Girard, J.P.: I 450; II 718;
 III 571
 Glagolev, V.M.: III 559
 Glukhov, A.V.: I 443
 Goedbloed, J.P.: I 217
 Golant, V.E.: III 525, 543
 Goldman, L.M.: III 410
 Golovin, T.N.: I 359; II 679
 Golubchikov, L.G.: I 573
 Gorbunov, E.P.: I 443; II 441
 Gorman, J.G.: III 151
 Gourlan, C.: I 523
 Grad, H.: III 229
 Gratreau, P.: I 511
- Grebenschchikov, S.E.: III 49,
 60, 77, 92, 130
 Greenwood, J.R.: I 3
 Gribkov, V.A.: I 573
 Grieger, G.: III 37, 60, 77
 Griem, H.R.: III 289
 Grigoreva, L.I.: III 573
 Gross, R.A.: III 241, 311
 Grove, D.J.: I 451, 465;
 II 425, 450
 Gruber, O.: I 277
 Gubarev, V.F.: I 359
 Guest, G.E.: II 607, 619
 Gullickson, R.L.: III 311
 Gvaladze, Yu.S.: I 183
- Haas, F.A.: II 491
 Haberstich, A.: I 203
 Haines, M.G.: I 611, 621, 633
 Hall, L.S.: II 629
 Halmoy, E.: III 241
 Hamberger, S.M.: II 37, 111
 Hamilton, G.W.: II 707
 Hammel, J.E.: I 97
 Hammer, C.F.: III 201
 Hammond, D.P.: III 393
 Hancox, R.: III 375, 444
 Harder, C.R.: III 201
 Harding, R.C.: II 735
 Harris, H.W.: III 201
 Harrison, H.: III 351, 409
 Hartman, C.W.: I 103; III 107
 Haste, G.R.: II 619
 Hatch, A.J.: III 524
 Hedrick, C.L.: II 607, 619
 Hellberg, M.A.: II 393
 Hendel, H.W.: I 325, 343
 Henins, I.: I 97
 Herold, H.: I 277
 Hertzberg, A.: I 673
 Hester, R.E.: I 119
 Hinnov, E.: I 451
 Hintz, E.: III 277, 311
 Hirose, A.: II 221
 Hirsch, R.L.: II 111
 Hobby, M.G.: I 537
 Hofmann, F.: I 267
 Hogan, J.I.: I 347; II 607
 Holmes, L.S.: III 251
 Hooper, E.B. Jr.: I 103
 Hosea, J.C.: I 450; II 425, 440
 Höthker, K.: III 277

- Hubert, P.L.: III 409
 Hugill, J.: III 79, 393
 Humphries, S.: I 119
 Husseiny, A.A.: III 432, 487
- Ichimaru, S.: II 373
 Iiyoshi, A.: III 109
 Imshennik, V.S.: I 573
 Inoue, N.: III 93
 Ioffe, M.S.: II 647
 Ipatov, V.A.: III 543
 Irons, F.E.: I 225
 Ishida, T.: III 109
 Itatani, R.: III 93
 Ivanov, A.A.: I 635
 Ivanov, B.I.: II 113
 Ivanov, V.D.: I 573
 Ivanovsky, M.A.: III 63
 Izmailov, A.N.: II 113
- Jacquinet, J.: II 595
 Jacquot, B.: II 631
 Jacquot, C.: II 631
 Jahoda, F.C.: III 201
 Jancarik, J.: II 37
 Janicke, L.: III 179
 Jassby, D.L.: I 335
 Jernigan, T.C.: I 3
 Johnson, L.C.: I 451
 Jolas, A.: I 553
 Jones, W.D.: II 221
 Jukes, J.D.: I 397; II 491, 527,
 Jungwirth, K.: II 155
 Junker, J.: I 225
- Kadomtsev, B.B.: II 479, 488
 Kagansky, M.G.: 543
 Kalinichenko, S.S.: III 597
 Kalinin, Yu.G.: II 3
 Kalmykov, S.G.: III 543
 Kanaev, B.I.: II 647
 Karchevsky, A.I.: II 325
 Karkhov, A.N.: II 75
 Karr, H.J.: I 203
 Kartashev, K.B.: II 679
 Kaufmann, M.: III 189
 Kaw, P.K.: I 343, 609, 672;
 II 165, 232; III 571
 Keen, B.E.: I 315
 Keilhacker, M.K.: I 313;
 III 265, 311
 Kelley, G.G.: I 347, 357
- Kennel, C.F.: II 55
 Kerst, D.W.: I 3, 14, 480
 Kesner, J.: II 575
 Kewish, R.W., Jr.: I 97
 Khautiev, E. Yu.: I 183
 Khmaruk, V.G.: II 141
 Kholnov, Yu.V.: III 21
 Kidder, R.E.: I 673
 Kilkenny, J.D.: I 621
 Killeen, J.: I 137
 Kindel, J.M.: II 55
 King, C.D.: I 85
 Kirichenko, G.S.: II 141
 Kirov, A.G.: I 287
 Kiselev, V.A.: II 113
 Kislyakov, A.I.: III 543
 Kivshik, A.F.: II 113
 Kiyama, S.: III 303
 Koechlin, F.: III 505
 Kogan, V.I.: II 407
 Köhler, W.H.: III 409, 457
 Kolesnichenko, Ya.I.: III 411
 Kolyada, Yu.E.: II 113
 Komin, A.V.: III 3
 Konoshima, Sh.: III 109
 Konovalov, V.G.: III 151
 Korn, P.: II 25
 Kornherr, M.: III 265
 Kornilov, E.A.: II 113
 Koroteev, V.I.: II 309
 Kossy, I.A.: III 49
 Kotsubanov, V.D.: III 151
 Kovpik, O.F.: II 113
 Kovrizhnykh, L.M.: I 399, 423,
 479, 495
 Kozlov, P.I.: I 359
 Krall, N.A.: III 289
 Krause, H.: I 251
 Kribel, R.E.: I 169
 Kristiansen, M.: I 687
 Krivoruchko, S.M.: II 113
 Krivov, N.A.: III 559
 Krlín, L.: II 155
 Krokhin, O.N.: I 573
 Kukhtenko, A.I.: I 359
 Kulsrud, R.: II 247
 Küppers, G.: II 529
 Kurilko, P.I.: III 597
 Kurilko, V.I.: II 113, 195
 Kurtmullaev, R.Kh.: II 309
 Kusse, B.R.: I 169
 Kvartskhava, I.F.: I 183

- Ladikov - Roev, Yu, P.: I 359
 Lashinsky, H.: III 373
 Launois, D.: II 575
 Laval, G.: II 507, 539
 Lazar, N.H.: II 619, 628
 Lecoustey, P.: II 575
 Lee, J.H.: I 534
 Lee, J.D.: III 329
 Lee, R.: I 169
 Lees, D.J.: III 79
 Lehnert, B.: I 59, 117, 398, 449,
 Leloup, C.: II 595
 Lencioni, D.E.: I 3
 Leonov, V.M.: II 441
 Levin, M.B.: II 195
 Levine, M.: I 250; II 381
 Lichtenberg, A.J.: I 687;
 II 617; III 77
 Liewer, P.C.: III 289
 Likhtenshtein, V.Kh.: II 75
 Linhart, J.G.: II 489
 Little, P.F.: II 111, 706
 Litvinov, A.P.: III 151
 Liu, C.S.: I 335
 Lominadze, D.G.: II 345
 Long, H.M.: III 433
 Longinov, A.V.: III 573
 Lotz, W.: III 189
 Lovelace, R.V.: I 169
 Lubell, M.S.: III 433, 444
 Lubin, M.J.: I 347
 Luc, H.: II 507
 Luton, J.N.: III 433
 Lutsenko, E.I.: II 113
 Luzzi, G.: I 511, 523
 Lyon, J.F.: II 619
 Lysenko, S.E.: I 443
 Lyubarsky, M.G.: II 195
 Lyublin, B.V.: II 99

 Ma, B.M.: II 718
 Mackenzie, K.: II 55
 Maisonnier, Ch.: I 511, 523, 533
 Malykh, N.I.: I 287
 Mann, L.W.: I 203
 Manzyuk, N.A.: II 85
 Marcus, F.B.: III 353
 Marshall, J.: I 97
 Maschke, E.K.: II 477, 507,
 527; III 61
 Mather, J.W.: I 561
 Matsiborko, N.G.: II 195

 Matsuda, S.: I 75
 Matveev, Yu.V.: I 183
 McCracken, G.M.: III 393
 McCune, J.E.: II 735
 McNally, J.R.: I 347
 Meade, D.M.: I 3, 117
 Megaw, J.H.P.C.: I 85
 Melikhov, P.I.: I 359
 Mercier, C.: I 425; II 507
 Merezhkin, V.G.: I 287
 Meservey, E.: I 451, 479
 Messiaen, A.M.: III 513
 Millar, W.: III 79
 Mills, R.G.: III 432
 Mirin, A.A.: I 137
 Mirnov, S.V.: I 443; II 401
 Mitin, L.A.: II 113
 Miyamoto, K.: III 48, 93, 107
 Mohri, A.: III 93, 169
 Moir, R.W.: III 315, 329
 Moiseev, S.S.: II 113, 195
 Moiseeva, M.P.: I 573
 Molvik, A.W.: I 3
 Montgomery, D.C.: II 219
 Morgan, O.B.: I 347
 Morgan, P.D.: I 537
 Mori, S.: I 75; III 423
 Moriette, P.: II 241
 Morse, R.L.: I 572, 655;
 II 291; III 214
 Mukhovatov, V.S.: II 441
 Mulser, P.: I 645
 Munger, R.H.: I 103
 Murakami, M.: I 347
 Murray, E.L.: III 251

 Nagashima, T.: I 75
 Nardi, V.: I 571
 Nation, J.A.: I 169; II 165
 Nechaev, Yu.I.: III 21
 Neidigh, R.V.: II 221
 Neuhauser, J.: III 189, 200
 Newcomb, W.A.: I 137
 Newton, A.A.: I 225
 Nexsen, W.E., Jr.: II 721
 Nicolas, M.: III 575
 Niedermeyer, H.: III 265
 Noll, P.: III 179
 Novik, K.M.: III 525

 Oberman, C.: I 442
 Obukhov, A.A.: III 525

- Ogawa, K.: III 303
 Ohkawa, T.: I 15, 25, 249, 266
 Ohlendorf, W.: III 37, 48
 Ohta, M.: III 423, 432
 Ohtsuka, H.: I 75
 Okabayashi, M.: I 27
 Olsen, J.N.: II 221
 Onishchenko, I.N.: II 195
 Oraevsky, V.N.: III 411
 Osher, J.E.: II 707
 Ovchinnikov, S.S.: III 597
 Ovsyannikov, V.A.: III 543
- Pacher, G.: I 27
 Pacher, H.D.: III 37
 Pakhomov, L.P.: III 543
 Panasyuk, V.M.: II 3
 Panov, D.A.: II 75
 Papadopoulos, K.: I 655
 Papagno, L.: I 523
 Parker, C.E.: III 433
 Pataraya, A.D.: II 345
 Paul, J.W.M.: III 251
 Pavlichenko, N.P.: III 151
 Peacock, N.J.: I 537, 571
 Pearlstein, L.D.: II 735
 Pecorella, F.: I 511, 523
 Pedenko, N.S.: II 113
 Pellat, R.: I 450, 493; II 507, 539
 Perepelkin, N.F.: III 151
 Pergament, M.I.: I 601
 Pergament, V.I.: II 663
 Petrov, M.P.: II 441
 Pfirsch, D.: II 529; III 163, 165
 Phillips, J.A.: I 203, 216
 Piekaar, H.W.: II 67
 Piffel, V.: II 155
 Piliya, A.D.: III 525
 Pistunovich, V.I.: II 679
 Plakhov, A.G.: II 3
 Plantikow, U.: III 179
 Platonov, V.V.: II 679
 Podushnikova, K.A.: III 543
 Poffé, J.P.: II 595
 Pogozhev, D.P.: III 131
 Ponomarenko, N.P.: III 151
 Popov, S.N.: III 63
 Popryadukhin, A.P.: II 63
 Porter, G.D.: I 119
 Post, R.F.: III 315, 329, 351, 372
 Potter, D.E.: I 611, 621, 633, 672
 Prater, R.: I 3
- Prentice, R.: I 85
 Prevot, F.: II 585
 Prior, W.J.: I 571
 Prono, D.: II 25
 Pyatak, A.I.: III 573
 Pyle, R.V.: II 707
- Quinn, W.E.: III 201
- Rabinovich, M.S.: III 63
 Rager, J.P.: I 511, 523
 Rawcliffe, A.S.: III 201
 Razmadze, N.A.: I 183
 Rebut, P.H.: I 686
 Rensink, M.E.: I 137
 Reva, N.I.: II 85
 Reynolds, P.: III 79, 92,
 Ribe, F.L.: I 249, 343;
 III 178, 199, 201, 214, 311,
 445
 Ripin, B.: I 27
 Riviere, A.C.: III 393
 Roberts, M.: I 347
 Robertson, S.: II 25
 Robinson, D.C.: I 225
 Robouch, B.V.: I 511, 523
 Roife, I.M.: I 305
 Romanovsky, M.K.: II 663;
 III 351
 Rose, D.J.: III 351, 444, 487
 Rosenbluth, M.N.: I 495; II 373,
 488, 553; III 165
 Roth, J.R.: I 14; II 233, 617
 Rudakov, L.T.: I 635, 643;
 II 3, 235
 Rudakov, V.A.: III 119
 Rudmin, J.W.: I 3
 Rumsby, P.T.: III 251
 Rusanov, V.D.: II 3
 Rutgers, W.R.: II 67
 Rutherford, P.H.: I 369, 495;
 II 553
 Ryutov, D.D.: II 293, 309
 Ryutov, V.D.: II 679
- Sagdeev, R.Z.: I 481; II 55, 293
 Salzmann, H.: I 645
 Samain, A.: III 505
 Samaras, D.G.: III 373
 Samoilenko, Yu.I.: I 359
 Samuelli, M.: I 511, 523
 Sand, F.: III 179

- Santini, F.: II 247
 Sato, K.: III 169
 Sato, M.: III 109
 Sawyer, G.A.: III 201
 Sbitnikova, I.S.: III 49
 Schlüter, A.: III 163
 Schlüter, J.: III 179
 Schmidt, G.: II 219
 Schmidt, J.A.: I 27, 58
 Schneider, S.: III 241
 Schofield, A.E.: I 203
 Schrijver, H.: II 67
 Schroeter, K.E.: II 457
 Schuurman, W.: I 217
 Schwirzke, F.R.: I 655; II 719
 Scott, F.R.: II 221
 Sellen, J.M., Jr.: II 55
 Semenov, I.B.: I 443; II 401
 Semenov, V.N.: II 309
 Sen, A.: II 735
 Serechenko, E.V.: I 305
 Shafranov, V.D.: II 423, 479, 519
 Shakhovets, K.G.: III 525, 543
 Shapiro, V.D.: II 113, 195
 Shapkin, V.V.: II 3
 Sharp, L.E.: II 37
 Sherwood, A.R.: I 97
 Shevchenko, V.I.: II 113, 195
 Shiina, T.: I 75
 Sholin, G.V.: II 3
 Shpigel, I.S.: III 49
 Shvets, O.M.: III 597
 Shvindt, N.N.: I 359
 Siemon, R.E.: III 201
 Siemsen, F.: III 277
 Sigel, R.: I 645, 654
 Sigmar, D.J.: II 451, 619, 755
 Simonen, T.C.: II 721
 Sinclair, R.M.: III 77, 107
 Sinitsina, L.D.: II 441
 Sinnis, J.: I 27
 Sizonenko, V.L.: III 119, 573
 Skibenko, A.I.: III 131
 Sklizkov, G.V.: I 573
 Skoryupin, V.A.: II 3
 Skosyrev, Yu.V.: III 559
 Sloan, M.L.: II 167
 Smerdov, B.I.: III 573
 Smolkin, G.E.: II 3
 Sobolev, R.I.: II 647
 Solodovchenko, S.I.: III 131
 Soubbaramayer: I 425, 442;
 II 450
 Soures, J.M.: I 347
 Sprott, J.C.: I 3; II 607
 Stallard, B.W.: I 119
 Steiner, D.: III 433, 447, 487
 Steinhauer, L.C.: I 673
 Stenzel, R.: I 335; II 55
 Stepanov, K.N.: III 119, 130, 571,
 573
 Steuer, K.-H.: III 265
 Stewart, L.D.: I 347
 Stirling, W.L.: I 347; II 221
 Stix, T.H.: III 571
 Stoddart, W.C.T.: III 433
 Stodiek, W.: I 465
 Stott, P.E.: I 315, 343
 Strakhov, Yu.I.: II 325
 Strauss, H.R.: II 527
 Strelkov, V.S.: I 357, 443, 449,
 479; II 440, 449
 Stringer, T.E.: II 383
 Sudan, R.N.: I 169, 643; II 219,
 291; III 311
 Sugawara, T.: I 75
 Sukhomlin, E.A.: II 85
 Summers, D.D.R.: III 251
 Sunka, P.: II 155, 165
 Suprunenko, V.A.: II 85; III 131,
 151
 Sweetman, D.R.: II 689, 733;
 III 353, 373, 393
 Tachon, J.: II 575
 Tamano, T.: I 15
 Tamura, S.: I 75
 Tasso, H.L.: II 423, 529, 571
 Taylor, C.E.: I 103; III 329
 Taylor, J.B.: I 495; II 488
 Taylor, R.J.: II 55, 111
 Tennfors, E.: I 59
 Terashima, Y.: III 93
 Ternopol, A.M.: II 85
 Thomas, K.S.: III 201
 Thomassen, K.I.: I 343
 Thompson, E.: II 718, 734; III 393
 Thompson, J.R.: II 167, 689, 706
 Tikhanov, E.K.: I 183
 Titov, A.V.: II 3
 Tolnas, E.: I 451
 Tolok, V.T.: II 85; III 131, 151, 597

- Tolstoluzhsky, A. P. : II 113, 195
 Tonkopryad, V. M. : III 151
 Tonon, G. : I 657
 Tuck, J. L. : I 265, 450, 490;
 II 423; III 373
 Tyulpanov, S. S. : III 543

 Uchida, T. : III 169, 178
 Ullschmied, J. : II 155
 Uo, K. U. : II 571; III 109

 Vandenplas, P. E. M. : I 423; II 513,
 524, 571
 Van der Laan, P. C. T. : I 217, 222
 Vasileva, R. P. : I 601
 Vasilevsky, M. A. : I 305
 Vekshtein, G. E. : II 293
 Velikhov, E. P. : I 609
 Vershkov, V. A. : I 443
 Vikhrev, V. V. : I 573
 Vinogradov, N. I. : III 543
 Vinogradova, N. D. : II 441
 Vlasenkov, V. S. : II 441
 Vlasses, G. C. : I 673
 Voitsenya, V. S. : III 131, 161
 Volkov, E. D. : III 119
 Volosov, V. I. : III 3
 Von Goeler, S. : I 465

 Waelbroeck, F. G. : I 265, 442;
 III 179
 Waidmann, G. : III 179
 Ware, A. A. : I 397, 411, 423; II 440
 Ware, K. D. : I 561
 Watkins, M. L. : I 621
 Watson, C. J. H. : III 353
 Watteau, J. P. : I 553
 Weiss, P. B. : I 119
 Weitzner, H. : III 223
 Werner, R. W. : III 329
 Wetherell, A. : II 37
 Wharton, C. : II 25, 111, 233
 White, R. : II 55

 Widner, M. M. : I 347; II 221
 Wilhelm, R. : I 251, 259
 Williams, A. H. : I 561
 Wilner, B. : I 59
 Wing, W. R. : II 221
 Winsor, N. K. : II 393, 571; III 107
 Witkowski, S. : I 645
 Wobig, H. : III 37
 Wolf, G. H. : I 222; III 37
 Wong, A. Y. : I 335, II 55
 Wong, H. V. : II 167
 Wright, T. P. : I 672

 Yamato, H. : I 75; III 423
 Yaroslavsky, A. I. : I 601
 Yatsu, K. : III 93
 Yevick, G. J. : I 249, 449, 571,
 654
 Yoshikawa, M. : I 15, 58, 75;
 II 527
 Yoshikawa, S. : I 27; II 357, 381;
 III 92, 108
 Yoshioka, Sh. : III 109
 Yudin, Yu. N. : II 3
 Yurchenko, E. I. : II 519
 Yushmanov, E. E. : II 647

 Zalkind, V. M. : III 151
 Zaveryaev, V. S. : I 443
 Zavoisky, E. K. : I 635; II 3
 Zeidlits, V. P. : II 113
 Zelenin, G. V. : III 151
 Zeyer, G. : III 277
 Zharikov, V. N. : I 287
 Zhdanov, V. A. : I 287
 Zhiltsov, V. A. : I 75
 Zhukovsky, V. G. : II 663
 Ziser, V. E. : III 131
 Zolotovskiy, O. A. : II 309
 Zukakishvili, G. G. : I 183
 Zwart, J. W. A. : I 217
 Zwicker, H. : I 223, 251, 259,
 265

TRANSLITERATION INDEX

Агафонов, В.И.	Agafonov, V.I.
Акулина, Д.К.	Akulina, D.K.
Алтынцев, А.Т.	Altyntsev, A.T.
Андрюхина, Э.Д.	Andryukhina, E.D.
Анисимов, А.И.	Anisimov, A.I.
Артеменков, Л.И.	Artemenkov, L.I.
Архипенко, В.И.	Arkhipenko, V.I.
Арцимович, Л.А.	Artsimovich, L.A.
Бабыкин, М.В.	Babykin, M.V.
Байбородов, Ю.Т.	Baiborodov, Yu.T.
Бакай, А.С.	Bakai, A.S.
Баратов, Д.Г.	Baratov, D.G.
Беликов, В.С.	Belikov, V.S.
Беляева, И.Ф.	Belyaev, I.F.
Бережецкий, М.С.	Berezhetsky, M.S.
Березин, А.Б.	Berezin, A.B.
Березин, А.К.	Berezin, A.K.
Березина, Г.П.	Berezina, G.P.
Бешапошников, А.А.	Besshaposchnikov, A.A.
Болотин, Л.И.	Bolotin, L.I.
Борисенко, А.Г.	Borisenko, A.G.
Бортников, А.В.	Bortnikov, A.V.
Бочаров, В.Н.	Bocharov, V.N.
Бревнов, Н.Н.	Brevnov, N.N.
Брейзман, Б.Н.	Breizman, B.N.
Будников, В.Н.	Budnikov, V.N.
Бурдонский, И.Н.	Burdonsky, I.N.
Бурченко, П.Я.	Burchenko, P.Ya.
Бутенко, В.К.	Butenko, V.K.
Бутов, И.Я.	Butov, I.Ya.
Васильева, Р.П.	Vasileva, R.P.
Василевский, М.А.	Vasilevsky, M.A.
Векштейн, Г.Е.	Vekshtein, G.E.
Велихов, Е.П.	Velikhov, E.P.
Вершков, В.А.	Vershkov, V.A.
Виноградов, Н.И.	Vinogradov, N.I.
Виноградова, Н.Д.	Vinogradova, N.D.
Власенков, В.С.	Vlasenkov, V.S.
Войцения, В.С.	Voitsenya, V.S.
Волков, Е.Д.	Volkov, E.D.
Волосов, В.И.	Volosov, V.I.
Галеев, А.А.	Galeev, A.A.
Галушкин, Ю.И.	Galushkin, Yu.I.
Гваладзе, Ю.С.	Gvaladze, Yu.S.

- Георгиевский, А.В.
Гервидс, В.И.
Глаголев, В.М.
Глухов, А.В.
Голант, В.Е.
Головин, И.Н.
Голубчиков, Л.Г.
Горбунов, Е.П.
Гребенщиков, С.Е.
Грибков, В.А.
Григорьева, Л.И.
Губарев, В.Ф.
Демидов, Б.А.
Демирханов, Р.А.
Дикий, А.Г.
Дубовой, Л.В.
Душин, Л.А.
Дьяченко, В.Ф.
Егоров, А.М.
Ерохин, Н.С.
Еськов, А.Г.
Жариков, В.Н.
Жданов, В.А.
Жильцов, В.А.
Жуковский, В.Г.
Заверьяев, В.С.
Завойский, Е.К.
Залкинд, В.М.
Зейдлиц, В.П.
Зеленин, Г.В.
Зисер, В.Е.
Золотовский, О.А.
Зукакишвили, Г.Г.
Иванов, А.А.
Иванов, Б.И.
Иванов, В.Д.
Ивановский, М.А.
Измайлов, А.Н.
Имшенник, В.С.
Иоффе, М.С.
Ипатов, В.А.
Кадомцев, Б.Б.
Каганский, М.Г.
Калинин, Ю.Г.
Калиниченко, С.С.
Калмыков, С.Г.
Канаев, Б.И.
Карташев, К.Б.
Кархов, А.Н.
Карчевский, А.И.
Кварцхава, И.Ф.
Кившик, А.Ф.
- Georgievsky, A.V.
Gervids, V.I.
Glagolev, V.M.
Glukhov, A.V.
Golant, V.E.
Golovin, I.N.
Golubchikov, L.G.
Gorbunov, E.P.
Grebenshchikov, S.E.
Gribkov, V.A.
Grigoreva, L.I.
Gubarev, V.F.
Demidov, B.A.
Demirkhanov, R.A.
Diky, A.G.
Dubovoy, L.V.
Dushin, L.A.
Dyachenko, V.F.
Egorov, A.M.
Erokhin, N.S.
Eskov, A.G.
Zharikov, V.N.
Zhdanov, V.A.
Zhiltsov, V.A.
Zhukovsky, V.G.
Zaveryaev, V.S.
Zavoisky, E.K.
Zalkind, V.M.
Zeidlits, V.P.
Zelenin, G.V.
Ziser, V.E.
Zolotovsky, O.A.
Zukakishvili, G.G.
Ivanov, A.A.
Ivanov, B.I.
Ivanov, V.D.
Ivanovsky, M.A.
Izmailov, A.N.
Imshennik, V.S.
Ioffe, M.S.
Ipatov, V.A.
Kadomtsev, B.B.
Kagansky, M.G.
Kalinin, Yu.G.
Kalinichenko, S.S.
Kalmykov, S.G.
Kanaev, B.I.
Kartashev, K.B.
Karkhov, A.N.
Karchevsky, A.I.
Kvartskhava, I.F.
Kivshik, A.F.

- Кириченко, Г.С.
Киров, А.Г.
Кисляков, А.И.
Ковпик, О.Ф.
Коврижных, Л.М.
Коган, В.И.
Козлов, П.И.
Колесниченко, Я.И.
Коляда, Ю.Е.
Комин, А.В.
Коновалов, В.Г.
Корнилов, Е.А.
Коротеев, В.И.
Коссий, И.А.
Коцубанов, В.Д.
Кривов, Н.А.
Криворучко, С.М.
Крохин, О.Н.
Курилко, В.И.
Курилко, П.И.
Куртмуллаев, Р.Х.
Кухтенко, А.И.
Ладиков-Роев, Ю.П.
Левин, М.Б.
Леонов, В.М.
Литвинов, А.П.
Лихтенштейн, В.Х.
Ломинадзе, Д.Г.
Лонгинов, А.В.
Луценко, Е.И.
Лысенко, С.Е.
Любарский, М.Г.
Люблин, Б.В.
Малых, Н.И.
Манзюк, Н.А.
Масалов, В.Л.
Матвеев, Ю.В.
Мациборко, Н.Г.
Мелихов, П.И.
Мережкин, В.Г.
Мирин, А.А.
Мирнов, С.В.
Моисеев, С.С.
Моисеева, М.П.
Муховатов, В.С.
Нечаев, Ю.И.
Новик, К.М.
Обухов, А.А.
Овсянников, В.А.
Овчинников, С.С.
Онищенко, И.Н.
Ораевский, В.Н.
- Kirichenko, G.S.
Kirov, A.G.
Kislyakov, A.I.
Kovpik, O.F.
Kovrizhnykh, L.M.
Kogan, V.I.
Kozlov, P.I.
Kolesnichenko, Ya.I.
Kolyada, Yu.E.
Komin, A.V.
Konovalov, V.G.
Kornilov, E.A.
Koroteev, V.I.
Kossy, I.A.
Kotsubanov, V.D.
Krivov, N.A.
Krivoruchko, S.M.
Krokhin, O.N.
Kurilko, V.I.
Kurilko, P.I.
Kurtmullaev, R.Kh.
Kukhtenko, A.I.
Ladikov-Roev, Yu.P.
Levin, M.B.
Leonov, V.M.
Litvinov, A.P.
Likhtenshtein, V.Kh.
Lominadze, D.G.
Longinov, A.V.
Lutsenko, E.I.
Lysenko, S.E.
Lyubarsky, M.G.
Lyublin, B.V.
Malykh, N.I.
Manzyuk, N.A.
Masalov, V.L.
Matveev, Yu.V.
Matsiborko, N.G.
Melikhov, P.I.
Merezhkin, V.G.
Mirin, A.A.
Mirnov, S.V.
Moiseev, S.S.
Moiseeva, M.P.
Mukhovatov, V.S.
Nechaev, Yu.I.
Novik, K.M.
Obukhov, A.A.
Ovsyannikov, V.A.
Ovchinnikov, S.S.
Onishchenko, I.N.
Oraevsky, V.N.

- | | |
|--------------------|---------------------|
| Павличенко, Н.П. | Pavlichenko, N.P. |
| Панасюк, В.М. | Panasyuk, V.M. |
| Панов, Д.А. | Panov, D.A. |
| Патарая, А.Д. | Pataraya, A.D. |
| Пахомов, Л.П. | Pakhomov, L.P. |
| Педенко, Н.С. | Pedenko, N.S. |
| Пергамент, В.И. | Perepelkin, N.F. |
| Пергамент, М.И. | Pergament, V.I. |
| Перепелкин, Н.Ф. | Pergament, M.I. |
| Петров, М.П. | Petrov, M.P. |
| Пилия, А.Д. | Piliya, A.D. |
| Пистуневич, В.И. | Pistunovich, V.I. |
| Платонов, В.В. | Platonov, V.V. |
| Плахов, А.Г. | Plakhov, A.G. |
| Подушникова, К.А. | Podushnikova, K.A. |
| Погожев, Д.П. | Pogozhev, D.P. |
| Пономаренко, Н.П. | Ponomarenko, N.P. |
| Попов, С.Н. | Popov, S.N. |
| Попрядухин, А.П. | Popryadukhin, A.P. |
| Пятак, А.И. | Pyatak, A.I. |
| Рабинович, М.С. | Rabinovich, M.S. |
| Размадзе, Н.А. | Razmadze, N.A. |
| Рева, Н.И. | Reva, N.I. |
| Ройфе, И.М. | Roife, I.M. |
| Романовский, М.К. | Romanovsky, M.K. |
| Рудаков, В.А. | Rudakov, V.A. |
| Рудаков, Л.И. | Rudakov, L.I. |
| Русанов, В.Д. | Rusanov, V.D. |
| Рютов, В.Д. | Ryutov, V.D. |
| Рютов, Д.Д. | Ryutov, D.D. |
| Сагдеев, Р.З. | Sagdeev, R.Z. |
| Самойленко, Ю.И. | Samoilenko, Yu.I. |
| Сбитникова, И.С. | Sbitnikova, I.S. |
| Семенов, В.Н. | Semenov, V.N. |
| Семенов, И.Б. | Semenov, I.B. |
| Середенко, Е.В. | Seredenko, E.V. |
| Сизоненко, В.Л. | Sizonenko, V.L. |
| Синицина, Л.Д. | Sinitsina, L.D. |
| Скибенко, А.И. | Skibenko, A.I. |
| Склизков, Г.В. | Sklizkov, G.V. |
| Скорюпин, В.А. | Skoryupin, V.A. |
| Скосырев, Ю.В. | Skosyrev, Yu.V. |
| Смердов, Б.И. | Smerdov, B.I. |
| Смолкин, Г.Е. | Smolkin, G.E. |
| Соболев, Р.И. | Sobolev, R.I. |
| Солодовченко, С.И. | Solodovchenko, S.I. |
| Степанов, К.Н. | Stepanov, K.N. |
| Страхов, Ю.И. | Strakhov, Yu.I. |
| Стрелков, В.С. | Strelkov, V.S. |
| Супруненко, В.А. | Suprunenko, V.A. |
| Сухомлин, Е.А. | Sukhomlin, E.A. |
| Тернопол, А.М. | Ternopol, A.M. |

Титов, А.В.	Titov, A.V.
Тиханов, Е.К.	Tikhanov, E.K.
Толок, В.Т.	Tolok, V.T.
Толстолужский, А.П.	Tolstoluzhsky, A.P.
Тонкопряд, В.М.	Tonkopryad, V.M.
Тюльпанов, С.С.	Tyulpanov, S.S.
Файнберг, Я.Б.	Fainberg, Ya.B.
Фанченко, С.Д.	Fanchenko, S.D.
Федоров, В.И.	Fedorov, V.I.
Федянин, О.И.	Fedyanin, O.I.
Филимонова, Е.А.	Filimonova, E.A.
Филиппов, Н.В.	Filippov, N.V.
Филиппова, Т.И.	Filippova, T.I.
Фомин, И.П.	Fomin, I.P.
Хаутиев, Э.Ю.	Khautiev, E.Yu.
Хмарук, В.Г.	Khmaruk, V.G.
Хольнов, Ю.В.	Kholnov, Yu.V.
Чечкин, В.В.	Chechkin, V.V.
Чкуасели, З.Д.	Chkuaseli, Z.D.
Шапиро, В.Д.	Shapiro, V.D.
Шапкин, В.В.	Shapkin, V.V.
Шафранов, В.Д.	Shafranov, V.D.
Шаховец, К.Г.	Shakhovets, K.G.
Швец, О.М.	Shvets, O.M.
Швиндт, Н.Н.	Shvindt, N.N.
Шевченко, В.И.	Shevchenko, V.I.
Шолин, Т.В.	Sholin, G.V.
Шпигель, И.С.	Shpigel, I.S.
Юдин, Ю.Н.	Yudin, Yu.N.
Юрченко, Е.И.	Yurchenko, E.I.
Юшманов, Е.Е.	Yushmanov, E.E.
Ярославский, А.И.	Yaroslavsky, A.I.

HOW TO ORDER IAEA PUBLICATIONS

Exclusive sales agents for IAEA publications, to whom all orders and inquiries should be addressed, have been appointed in the following countries:

UNITED KINGDOM Her Majesty's Stationery Office, P.O. Box 569, London S.E.1
UNITED STATES OF AMERICA UNIPUB, Inc., P.O. Box 433, New York, N.Y. 10016

In the following countries IAEA publications may be purchased from the sales agents or booksellers listed or through your major local booksellers. Payment can be made in local currency or with UNESCO coupons.

ARGENTINA Comisión Nacional de Energía Atómica, Avenida del Libertador 8250, Buenos Aires
AUSTRALIA Hunter Publications, 23 McKillop Street, Melbourne, C.1
BELGIUM Office International de Librairie, 30, avenue Marnix, Brussels 5
CANADA Information Canada, Ottawa
C.S.S.R. S.N.T.L., Spálená 51, Prague 1
Alfa, Publishers, Hurbanovo námestie 6, Bratislava
FRANCE Office International de Documentation et Librairie, 48, rue Gay-Lussac, F-75 Paris 5^e
HUNGARY Kultura, Hungarian Trading Company for Books and Newspapers, P.O.Box 149, Budapest 62
INDIA Oxford Book and Stationery Comp., 17, Park Street, Calcutta 16
Prakash Publishers, Film Colony, Chaura Rasta, Jaipur-3 (Raj.)
ISRAEL Heitiger and Co., 3, Nathan Strauss Str., Jerusalem
ITALY Agenzia Editoriale Commissionaria, A.E.I.O.U., Via Meravigli 16, I-20123 Milan
JAPAN Maruzen Company, Ltd., P.O.Box 5050, 100-31 Tokyo International
NETHERLANDS Martinus Nijhoff N.V., Lange Voorhout 9-11, P.O.Box 269, The Hague
PAKISTAN Mirza Book Agency, 65, The Mall, P.O.Box 729, Lahore-3
POLAND Ars Polona, Centrala Handlu Zagranicznego, Krakowskie Przedmiescie 7, Warsaw
ROMANIA Cartimex, 3-5 13 Decembrie Street, P.O.Box 134-135, Bucarest
SOUTH AFRICA Van Schaik's Bookstore, P.O.Box 724, Pretoria
Universitas Books (Pty) Ltd., P.O.Box 1557, Pretoria
SWEDEN C.E.Fritzes Kungl. Hovbokhandel, Fredsgatan 2, Stockholm 16
U.S.S.R. Mezhdunarodnaya Kniga, Smolenskaya-Sennaya 32-34, Moscow G-200
YUGOSLAVIA Jugoslovenska Knjiga, Terazije 27, Belgrade

Orders from countries where sales agents have not yet been appointed and requests for information should be addressed directly to:



Publishing Section,
International Atomic Energy Agency,
Kärntner Ring 11, P.O.Box 590, A-1011 Vienna, Austria

INTERNATIONAL
ATOMIC ENERGY AGENCY
VIENNA, 1971

PRICE: US \$ 20.00
Austrian Schillings 482,-
(£8.08; F.Fr.110,40 DM 66,40)

SUBJECT GROUP: III
Physics/Plasma Physics, Fusion